

BIOTECHNOLOGY: PHARMACEUTICAL ASPECTS

Drug Absorption Studies

In Situ, In Vitro and
In Silico Models

Edited by
Carsten Ehrhardt
Kwang-Jin Kim

 Springer



Drug Absorption Studies

Biotechnology: Pharmaceutical Aspects

Volume I: *Pharmaceutical Profiling in Drug Discovery for Lead Selection*

R.T. Borchardt, E.H. Kerns, C.A. Lipinski, D.R. Thakker,
B. Wang

Volume II: *Lypophilization of Biopharmaceuticals*

H.R. Constantino, M.J. Pikal

Volume III: *Methods for Structural Analysis of Protein Pharmaceuticals*

W. Jiskoot, D.J.A. Crommelin

Volume IV: *Optimizing the “Drug-Like” Properties of Leads in Drug Discovery*

R.T. Borchardt, E.H. Kerns, M.J. Hageman, D.R. Thakker,
J.L. Stevens

Volume V: *Prodrugs: Challenges and Rewards, Parts 1 and 2*

V.J. Stella, R.T. Borchardt, M.J. Hageman, R. Oliyai, H. Maag,
J.W. Tilley

Volume VI: *Solvent Systems and Their Selection in Pharmaceutics and Biopharmaceutics*

P. Augustijns, M.E. Brewster

Volume VII: *Drug Absorption Studies: In Situ, In Vitro and In Silico Models*

C. Ehrhardt, K.J. Kim

Carsten Ehrhardt
Editors

Kwang-Jin Kim

Drug Absorption Studies

In Situ, In Vitro and In Silico Models

 Springer

Editors

Carsten Ehrhardt
School of Pharmacy and
Pharmaceutical Sciences
Trinity College Dublin
Panoz Institute, Westland Row
Dublin 2, Ireland
Telephone: +353 1 896 2441
Fax: +353 896 2783
Email: ehrhardc@tcd.ie

Kwang-Jin Kim
Keck School of Medicine
University of Southern California
Room HMR-914, 2011 Zonal Avenue
Los Angeles, CA 90033, USA
Telephone: +1 323 442 1217
Fax: +1 323 442 2611
Email: Kwang.J.Kim@usc.edu

ISBN 978-0-387-74900-6

e-ISBN 978-0-387-74901-3

Library of Congress Control Number 2007937951

© 2008 American Association of Pharmaceutical Scientists

All rights reserved. This work may not be translated or copied in whole or in part without the written permission of the publisher (Springer Science+Business Media, LLC, 233 Spring Street, New York, NY 10013, USA), except for brief excerpts in connection with reviews or scholarly analysis. Use in connection with any form of information storage and retrieval, electronic adaptation, computer software, or by similar or dissimilar methodology now known or hereafter developed is forbidden.

The use in this publication of trade names, trademarks, service marks, and similar terms, even if they are not identified as such, is not to be taken as an expression of opinion as to whether or not they are subject to proprietary rights.

Printed on acid-free paper.

9 8 7 6 5 4 3 2 1

springer.com

Contents

Preface	xv
Contributors	xvii
Part 1 Perfused Organ Level/In Situ Techniques	
1. Models for Skin Absorption and Skin Toxicity Testing	3
<i>Ulrich F. Schaefer, Steffi Hansen, Marc Schneider, Javiana Luengo Contreras, and Claus-Michael Lehr</i>	
1.1 Introduction	4
1.2 Structure and Function of the Skin	4
1.2.1 Anatomical Structure of Human Skin	4
1.2.2 Biological Activity of the Skin	6
1.2.3 Skin Appendages	6
1.2.4 Skin Absorption Pathways	7
1.3 Strategies for Skin Invasion Testing Classified According to Their Resemblance of the In Vivo Situation	8
1.3.1 In Vivo Studies Using Pharmacodynamic Response	9
1.3.2 In Vivo Dermatopharmacokinetic Approach	9
1.3.3 In Vivo <i>Dermal Microdialysis</i>	10
1.3.4 Perfused Skin Models	11
1.3.5 In Vitro Skin Permeation Studies	12
1.3.6 In Vitro Skin Penetration Studies	16
1.4 Testing on Skin Toxicity	18
1.4.1 Skin Sensitization	18
1.4.2 Skin Irritation and Corrosion	21
1.4.3 Skin Phototoxicity	23
2. Models of the Small Intestine	34
<i>Brendan Griffin and Cairiona O'Driscoll</i>	
2.1 Introduction	35
2.2 Theoretical Models Describing the Gastrointestinal Absorption of Drugs	37
2.2.1 Estimating Drug Absorption Trends from Physiochemical Characteristics	37
2.2.2 General Model Describing Gastrointestinal Absorption	40
2.2.3 The Effective Permeability Coefficient	41
2.2.4 Estimating Effective Intestinal Permeability Coefficient Using a Mass Balance Approach	42
2.2.5 Using P_{eff} to Estimate the Extent of Absorption	44

2.3	In Situ Models	46
2.3.1	Intestinal Perfusion Techniques	46
2.3.2	Intestinal Perfusion with Venous Sampling Models	50
2.3.3	The Isolated and Vascularly Perfused Intestinal Models	53
2.3.4	Mesenteric Lymph Duct Cannulated Anaesthetised Rat Model	54
2.3.5	Anaesthetised Large Animal Model	55
2.4	In Vivo Models	55
2.4.1	Cannulated Conscious Rat Models	56
2.4.2	Cannulated Conscious Large Animal Model	57
2.4.3	Single-Pass Perfusion in Conscious Dog/Pig—Loc-I-Gut	59
2.4.4	Single-Pass Perfusion in Conscious Humans—Loc-I-Gut	60
2.5	Discussion	62
2.5.1	Standardisation and Validation Criteria in P_{eff} Determination	63
2.5.2	Choice of in Situ Versus in Vivo Models	63
2.5.3	Choice of Animal Species	65
3.	Drug Absorption from the Colon In Situ	77
	<i>Hiroaki Yuasa</i>	
3.1	Introduction	78
3.2	In Situ Rat Colon Model for Absorption Evaluation	79
3.3	Permeability Characteristics of the Rat Colonic Membrane	81
3.3.1	Carrier-Mediated Transport	81
3.3.2	Passive Transport	84
3.4	Concluding Remarks	86
4.	In Vivo and In Vitro Models for Assessing Drug Absorption Across the Buccal Mucosa	89
	<i>Joseph A. Nicolazzo and Barrie C. Finnin</i>	
4.1	Introduction	89
4.2	Structure and Environment of the Buccal Mucosa	90
4.2.1	Epithelial Organization	90
4.2.2	Organization of the Intercellular Domain	90
4.3	The Barriers of the Buccal Mucosa	91
4.3.1	Location of the Permeability Barrier	91
4.3.2	Chemical Nature of the Permeability Barrier	92
4.3.3	Other Permeability Barriers in the Buccal Mucosa	92
4.4	Mechanisms Involved in Oral Mucosal Absorption	94
4.4.1	Passive Diffusion	94
4.4.2	Carrier-Mediated Transport	94
4.5	Methods Employed to Assess the Permeability of the Buccal Mucosa	95
4.5.1	In Vivo Methods	96
4.5.2	In Vitro Methods	97
4.5.3	Buccal Cell Cultures	102
4.6	Concluding Remarks	103

5. In Situ and Ex Vivo Nasal Models for Preclinical Drug Development Studies	112
<i>Remigius U. Agu and Michael I. Ugwoke</i>	
5.1 Introduction	113
5.2 Advantages of Ex Vivo and in Situ Models for Drug Absorption and Metabolism Studies	114
5.3 Limitations of Ex Vivo and in Situ Models for Drug Absorption and Metabolism Studies	116
5.4 Specific Applications of in Situ Methods in Nasal Drug Delivery Studies	117
5.4.1 Permeability Studies	117
5.4.2 Metabolism Studies	118
5.4.3 Optimization of Drug Absorption Enhancement Strategies	119
5.4.4 Nasal Drug Irritation and Tolerance	121
5.5 Specific Applications of Ex Vivo Models in Nasal Drug Delivery Studies	121
5.5.1 Permeability Studies and Characterization of Drug Absorption Pathways	121
5.5.2 Metabolism Studies	125
5.5.3 Optimization of Formulation Parameters and Drug Absorption Enhancement Strategies	126
5.5.4 Nasal Drug Irritation and Tolerance	127
5.6 Correlation Between Nasal Drug Absorption Models	127
5.7 Conclusions	129
6. The Isolated Perfused Lung for Drug Absorption Studies	135
<i>Ann Tronde, Cynthia Bosquillon, and Ben Forbes</i>	
6.1 Respiratory Drug Delivery	136
6.1.1 Inhaled Drug Delivery	136
6.1.2 The Lung	137
6.1.3 Drug Administration to the Lung	141
6.1.4 Drug Absorption in the Lung	142
6.1.5 Lung Model Selection for Drug Absorption Studies	143
6.2 The Isolated Perfused Lung	146
6.2.1 Principles of the Preparation	146
6.2.2 Experimental Set-up	147
6.2.3 Drug Administration to the IPL	150
6.2.4 Drug Absorption Studies Using the Isolated Perfused Lung	151
6.2.5 Developments in the IPL	154
Part 2 Cellular Level—In Vitro Models of Epithelial and Endothelial Barriers	
7. In Vitro Models for Investigations of Buccal Drug Permeation and Metabolism	167
<i>Tanja Obradovic and Ismael J. Hidalgo</i>	
7.1 Introduction	167

7.2 In Vitro Studies	168
7.2.1 Isolated Buccal Tissue Mounted in Diffusion Cell Apparatus	168
7.2.2 Buccal Epithelial Cell Cultures	172
7.3 Concluding Remarks	176
8. In Vitro Screening Models to Assess Intestinal Drug Absorption and Metabolism	182
<i>Sven Deferme, Pieter Annaert, and Patrick Augustijns</i>	
8.1 Introduction	183
8.1.1 General Factors Influencing Intestinal Drug Absorption	183
8.1.2 The Intestinal Mucosa as a Physical and Biochemical Barrier to Drug Absorption	184
8.2 In Vitro Models to Study Intestinal Absorption	187
8.2.1 Membrane-Based Models (PAMPA)	187
8.2.2 Cell Culture-Based Models (Caco-2)	192
8.2.3 Ex Vivo Models (Ussing Chambers Technique)	201
8.2.4 Combination of Models	203
8.3 In Vitro Methods to Assess Intestinal Metabolism	204
8.4 Concluding Remarks	205
9. In Vitro Cellular Models for Nasal Drug Absorption Studies	216
<i>Dae-Duk Kim</i>	
9.1 Introduction	217
9.2 Structure and Physiology of the Nasal Cavity	218
9.2.1 Anatomy and Function	218
9.2.2 Physiology of Nasal Mucosa	219
9.3 Factors Affecting the Nasal Absorption	219
9.3.1 Physiological Factors	219
9.3.2 Physicochemical Characteristics of the Drugs	220
9.3.3 Effect of Formulation	220
9.4 Transport Routes of Nasal Epithelial Barrier	221
9.4.1 Transcellular Route	221
9.4.2 Paracellular Route	222
9.5 Models for Nasal Drug Transport and Absorption Studies	223
9.5.1 In Vivo Animal Models	223
9.5.2 In Vitro Excised Models	224
9.5.3 Cell Line Models	224
9.5.4 In Vitro Primary and Passaged Cell Culture Models	224
9.6 Conclusions	229
10. In Vitro Models of the Tracheo-Bronchial Epithelium	235
<i>Carsten Ehrhardt, Ben Forbes, and Kwang-Jin Kim</i>	
10.1 Introduction	236
10.1.1 Anatomy of the Lung Airways	236
10.1.2 Drug Delivery to the Tracheo-Bronchial Region	239
10.2 In Vitro Models of the Tracheo-Bronchial Epithelium	240
10.2.1 Primary Cell Cultures	240

10.2.2	Tracheo-Bronchial Epithelial Cell Lines	241
10.2.3	In Vitro Models of CF Airway Epithelium	242
10.3	Use of In Vitro Models of Tracheo-Bronchial Epithelial Barriers in Biopharmaceutical Research	243
10.3.1	Drug Absorption Studies	243
10.3.2	Drug Metabolism Studies Using Tracheo-Bronchial Epithelial Cells	245
10.4	Concluding Remarks	249
11.	In Vitro Models of the Alveolar Epithelial Barrier	258
	<i>Carsten Ehrhardt, Michael Laue, and Kwang-Jin Kim</i>	
11.1	Introduction	259
11.1.1	The Alveolar Epithelium	259
11.2	In Vitro Models of the Alveolar Epithelial Barrier for Drug Absorption Studies	266
11.2.1	In Vitro Models of the Alveolar Epithelial Barrier	266
11.2.2	The Use of Alveolar Epithelial Cells in Biopharmaceutical Research	269
11.3	Concluding Remarks	274
12.	Cell Culture Models of the Corneal Epithelium and Reconstructed Cornea Equivalents for In Vitro Drug Absorption Studies	283
	<i>Stephan Reichl and Ulrich Becker</i>	
12.1	Introduction	284
12.2	Anatomy and Physiology of Human Cornea	285
12.3	Transcorneal Drug Absorption into the Eye	289
12.4	Corneal Cell Culture Models	290
12.4.1	Primary Corneal Cell Cultures	290
12.4.2	Immortalized Continuous Cell Lines for Corneal Epithelial Cells	291
12.5	Organotypic Equivalents	294
12.6	Concluding Remarks	300
13.	The Conjunctival Barrier in Ocular Drug Delivery	307
	<i>Hovhannes J. Gukasyan, Kwang-Jin Kim, and Vincent H.L. Lee</i>	
13.1	Introduction to the Ocular Surface and the Relative Contribution of the Conjunctiva	308
13.2	Trans- and Sub-Conjunctival Ocular Drug Delivery	310
13.3	An Overview of Conjunctival Disorders	312
13.4	Models for Studying Conjunctival Transport Properties	313
13.4.1	Excised Conjunctival Tissues	313
13.4.2	Primary Culture Models of Conjunctival Epithelial Cell Layers	316
13.4.3	Conjunctival Disease Models	317
13.5	Summary and Conclusions	317
14.	Inner Blood–Retinal Barrier: Transport Biology and Methodology	321
	<i>Ken-ichi Hosoya and Masatoshi Tomi</i>	
14.1	Introduction	322

14.2	Conditionally Immortalized Cell Lines as a Novel in Vitro Inner Blood–Retinal Barrier Model (Uptake Studies)	324
14.3	In Vivo Blood-to-Retina Influx Transport	326
14.3.1	Integration Plot Analysis	326
14.3.2	Retinal Uptake Index Method	327
14.4	In Vivo Vitreous/Retina-to-Blood Efflux Transport (Microdialysis Study)	328
14.5	Ex Vivo Transporter Gene Expression Levels at the Inner Blood–Retinal Barrier (Magnetic Isolation of Retinal Vascular Endothelial Cells)	330
14.6	Mechanism of Drug Transport at the Inner Blood–Retinal Barrier	332
14.6.1	Blood-to-Retina Influx Transport	332
14.6.2	Retina-to-Blood Efflux Transport	334
14.7	Conclusions	334
15.	Regulation of Paracellular Permeability in Low-Resistance Human Vaginal-Cervical Epithelia	339
	<i>George I. Gorodeski</i>	
15.1	Introduction	340
15.2	The Ussing-Zerahn Model of Transepithelial Fluid Transport	341
15.3	Regulation of Paracellular Transport Across Secretory Epithelia	344
15.4	Regulation of Paracellular Permeability	345
15.5	Regulation of R_{TJ}	346
15.5.1	Role of Ca_o	346
15.5.2	Regulation of Assembled Tight Junctions by Extracellular ATP	349
15.5.3	Estrogen Regulation of R_{TJ}	349
15.5.4	Early Stages of Tight Junctional Disassembly	350
15.5.5	Claudin/Occludin Model of Regulation of the R_{TJ}	351
15.6	Regulation of the R_{LIS}	352
15.6.1	Estrogen Regulation of the R_{LIS}	353
15.6.2	Estrogen Regulation of Actin Polymerization	354
15.6.3	Modulation of Actin Polymerization: Estrogen vis-à-vis Aging Effects	354
15.6.4	Estrogen Regulation of Cortical Myosin	355
15.6.5	Composite Effects of Estrogen on Paracellular Permeability	356
15.7	Implications of the Data for Topical Drug Delivery	357
15.8	Concluding Remarks	357
16.	In Vitro Models and Multidrug Resistance Mechanisms of the Placental Barrier	368
	<i>Pallabi Mitra and Kenneth L. Audus</i>	
16.1	Introduction	369
16.2	Structure of the Placenta	370
16.3	Placental Transport Mechanisms	370

16.4 Available Model Systems	371
16.4.1 Perfused Placental Model	371
16.4.2 Trophoblast Tissue Preparations	372
16.4.3 Trophoblast Cultures	374
16.5 Multidrug Resistant Transporters of the Placenta	377
16.5.1 MDR1/P-Glycoprotein (ABCB1)	377
16.5.2 Multidrug Resistance-Associated Proteins	381
16.5.3 Breast Cancer Resistance Protein (BCRP/ABCG2)	383
16.6 Conclusions	386
17. In Vitro Models to Study Blood–Brain Barrier Function	397
<i>Gert Fricker</i>	
17.1 Introduction	398
17.1.1 Discovery of the Blood–Brain Barrier	398
17.2 Structure and Function of the Blood–Brain Barrier	399
17.3 Relevance of the Barrier for Drug Delivery	400
17.3.1 Rapid Transport Protein Modulation	403
17.3.2 Modulation of P-glycoprotein Transcription	404
17.4 Models to Study Blood–Brain Barrier Function	405
17.4.1 Isolated Cerebral Capillaries	406
17.4.2 Brain Capillary Endothelial Cell Culture	406
17.4.3 In Silico Methods	410
17.5 Perspectives	410
18. High-Throughput Screening Using Caco-2 Cell and PAMPA Systems	418
<i>Cheng Li, Sam Wainhaus, Annette S. Uss, and Kuo-Chi Cheng</i>	
18.1 Introduction	418
18.2 Caco-2 Cell Monolayer System	419
18.3 Parallel Artificial Membrane Permeability Assays	425
18.4 Combining Use of Caco-2 and PAMPA	426
18.5 Concluding Remarks	427
19. Instrumented In Vitro Approaches to Assess Epithelial Permeability of Drugs from Pharmaceutical Formulations	430
<i>Stephan A. Motz, Michael Bur, Ulrich F. Schaefer, and Claus-Michael Lehr</i>	
19.1 Introduction	431
19.2 Intestinal Permeability of Drugs Delivered as Solid Dosage Forms	431
19.2.1 Rationale for Connecting Dissolution and Permeation Measurements	431
19.2.2 Connecting Dissolution and Permeation Measurement in One Instrumented Setup	436
19.2.3 Critical Evaluation of the State of the Art and Further Needs	442
19.3 Permeability Assessment of Pulmonary Aerosol Formulations	443
19.3.1 Measuring Drug Transport Across Epithelial Barriers in Submersed Conditions: Ussing Chamber and Transwell®-Like Systems	445

19.3.2	Setups Allowing to Measure Drug Transport Across Pulmonary Epithelia Interfacing Air	446
19.3.3	Critical Evaluation of the State of the Art and Further Needs	450
Part 3 Bioinformatics—In Silico Tools to Predict Drug Absorption		
20.	Modeling Transdermal Absorption	459
	<i>Dirk Neumann</i>	
20.1	Introduction	460
20.2	The Skin Barrier	460
20.3	The Diffusion Equation	461
20.4	Data Analysis	461
20.4.1	QSPR Models	463
20.4.2	Non Steady-State Solutions and Morphological Models	477
20.5	Pharmacokinetic Models	478
20.6	Outlook	479
21.	Physiologically Based in Silico Models for the Prediction of Oral Drug Absorption	486
	<i>Fredrik Johansson and Ronnie Paterson</i>	
21.1	Introduction	487
21.2	Absorption Process	488
21.2.1	Overall Absorption Process	488
21.2.2	Drug Dissolution	489
21.2.3	Drug Absorption	490
21.3	Physiologically-Based Absorption Models	491
21.3.1	General Considerations	491
21.3.2	Mixing Tank Models	492
21.3.3	Mass Balance Models	494
21.3.4	Compartmental Absorption and Transit (CAT) Models	496
21.3.5	Other Models (PK-Map TM /PK-Sim [®])	499
21.4	The Use and Validation of Physiologically Based Simulation Models	500
21.4.1	How Predictive are the Models?	500
21.4.2	Situations Where Less Accurate Predictions Can Be Encountered	502
21.5	Summary	505
22.	In Silico Modeling for Blood–Brain Barrier Permeability Predictions	510
	<i>Prabha Garg, Jitender Verma, and Nilanjan Roy</i>	
22.1	Introduction	511
22.2	In Silico Methods Published for Prediction of BBB Permeability	512
22.3	Summary	544

Part 4 Molecular/Sub-Cellular Level—Mechanistic Tools

23. Impact of Drug Transport Proteins	559
<i>Tomohiro Terada and Ken-ichi Inui</i>	
23.1 Introduction	560
23.2 Determination and Classification of Drug Transporters	561
23.3 Characteristics of Major Drug Transporters	561
23.3.1 PEPT (SLC15)	561
23.3.2 OATP (SLCO)	563
23.3.3 OCT/OCTN/OAT/URAT (SLC22)	565
23.3.4 MATE (SLC47)	567
23.3.5 ABC Transporters	567
23.4 Conclusions and Perspectives	569
24. Cloning and Functional Heterologous Expression of Transporters	577
<i>Carsten Kneuer and Walther Honscha</i>	
24.1 Introduction	578
24.2 Cloning Techniques	578
24.2.1 Historical Overview and General Considerations	578
24.2.2 <i>Xenopus Laevis</i> Oocytes for Cloning of Drug Carrier	580
24.2.3 Complementation Cloning Strategies	584
24.2.4 Homology Cloning	585
24.3 Heterologous Expression Systems	588
24.3.1 Cell-Free Expression Systems	588
24.3.2 Bacterial Expression Systems	590
24.3.3 Yeast Expression Systems	591
24.3.4 <i>Xenopus Oocytes</i>	592
24.3.5 Insect Cell Lines	593
24.3.6 Mammalian Cell Lines	593
24.4 Concluding Remarks	596
25. The Pharmacology of Caveolae	598
<i>Stuart A. Ross, William V. Everson, and Eric J. Smart</i>	
25.1 Introduction	599
25.2 Action at Caveolae	602
25.3 Caveolae and Vesicular Drug Transport	602
25.3.1 Exploiting Caveolae for Drug Delivery	602
25.3.2 Caveolae-Linked Endocytosis and Non-Caveolae, Clathrin-Independent Endocytosis Offer Delivery of Drugs to Novel Intracellular Targets	603
25.4 Caveolae and Cancer	604
25.4.1 Caveolin Expression	604
25.4.2 A Caveolar Mechanism of Multidrug Resistance	605
25.4.3 A Gateway to Targeted Cancer Cell Ablation	606
25.4.4 Caveolae, Folate Receptor, Receptor Clustering, and Potocytosis	607
25.4.5 Folate Conjugates and Therapeutics	608
25.5 Pharmacology at Caveolae: Presentation, Presentation, Presentation	608

26. Immortalization Strategies for Epithelial Cells in Primary Culture	616
<i>David de Semir Frappart, Rosalie Maurisse, Esther H. Vock, and Dieter C. Gruenert</i>	
26.1 Introduction	617
26.2 Cell Transformation and Immortalization Strategies	618
26.2.1 Transformation Versus Immortalization	618
26.2.2 Selecting the Appropriate Cell Line	618
26.2.3 Human Epithelial Cells as a Model for Transformation and Immortalization	619
26.2.4 Strategies to Generate Transformed and/or Immortalized Epithelial Cells	619
26.3 Protocols	621
26.3.1 Generation, Isolation, and Characterization	621
26.4 Summary	626
27. Binding-Uptake Studies and Cellular Targeting	640
<i>Franz Gabor and Michael Wirth</i>	
27.1 Introduction	641
27.1.1 Design of Targeted Drug Delivery Systems	642
27.1.2 Cell Culture Models	643
27.1.3 Analytical Tools: Labeling and Detection of Targeted Drug Delivery Systems	643
27.2 The Cell–Target System Interaction	645
27.2.1 Cytoadhesion Assays	645
27.2.2 Specificity of Interaction	647
27.2.3 Binding Versus Uptake—Cytoinvasion Assays	648
27.2.4 Cytoevasion	650
27.2.5 Active or Passive Uptake?	650
27.2.6 Uptake and Intracellular Localization Within Acidic Compartments	651
27.3 Analytical Techniques	652
27.3.1 Flow Cytometry	652
27.3.2 Intracellular Localization by Means of Confocal Laser Scanning Microscopy	655
27.4 Concluding Remarks	659
Part 5 Regulatory Considerations	
28. Drug Permeability Studies in Regulatory Biowaiver Applications	665
<i>Donna A. Volpe</i>	
28.1 Biopharmaceutics Classification System	666
28.2 Regulatory Application of the BCS	667
28.3 Permeability Measurements	669
28.4 Method Suitability	672
28.5 Conclusions	676
Appendix: Lab Protocols (available online, updated semi-annually, as required)	681
Index	683

Preface

It all started on a day in summer of 2005, when Ms. Andrea Macaluso from Springer Publishers contacted us with an invitation to edit a book on preclinical models for drug absorption and related subjects. Later that year, when Kwang-Jin Kim visited Trinity College Dublin where Carsten Ehrhardt teaches and pursues his research, we went out for drinks after a hard day's work, followed by a dinner at an Italian trattoria in Sandymount. By the end of the dinner, the outline for the book was scribbled on several pieces of paper serviettes provided by the trattoria's patient staff. Consuming unknown amounts of wine, we enjoyed rather yummy Irish-Italian dishes and worked on the basic layout of the book, that is relevant topics and potential authors. Hence, if there is something that any reader might feel wrong about the present form(at) of the book, we strongly blame it on the Italian wine which we drank during the brainstorming session part of the working dinner.

Over the recent years, the impact of absorptive/secretive processes on a drug's bioavailability has been recognised, further evolving into the wish to predict the drug's fate at a preclinical stage during drug development. In vitro absorption models have revolutionised our understanding in this field and pushed our thinking more in terms of mechanisms beyond mere phenomenology. Moreover, the FDA Biowaiver based on the Biopharmaceutics Classification System (BCS) has further boosted the use of in vitro absorption models. This book is meant to provide an overview on what is available with regards to various experimental models for the studies of drug transport in general, with a brief synopsis of pertinent data generated for each model.

The book starts with chapters emphasising in situ and ex vivo techniques, which now appear to enjoy a renaissance in research, due to perhaps the central role played by such models in 'translational research', as some questions cannot be answered with certainty using simplistic in vitro models. We have tried to cover as many cell-based in vitro approaches as possible, for those originating from almost all known biological barriers of importance (i.e. from epithelium to endothelium, the skin to various epithelial tracts of respiratory, gastrointestinal and reproductive organs, the brain, the eye and so forth). So as to give the reader who may be keen on utilising New Age Science tools sans the biological tissues and cells altogether, we were able to come up with three chapters on cell-free systems, that is in silico models that have been established for several barriers in the very recent past. In short, we wanted to offer the reader a comprehensive overview of different models and approaches that can be utilised in the investigation and prediction of drug absorption via many biological barriers in the body. Moreover, we also included a section that

focuses on several techniques for the studies of drug transport mechanisms (i.e. transporter proteins or endocytotic processes), binding and uptake, and the generation of continuous cell lines, since the information on these techniques might be useful for the more advanced or more molecular biology-oriented users. We would like to make a note that a chapter focusing on regulatory considerations of using the absorption models and FDA Biowaiver implications is also included.

As a final twist, this book also features a ‘living appendix’, an idea born out of most likely too much vino flown down into our digestive tracts during the brainstorming session at the trattoria, in that the reader can print a respective protocol that she/he wants to use in the daily run of laboratory works, thus, alleviating the fear of the physical/chemical damage incurred on the expensive book at the laboratory bench side. It is our intention to urge the participating authors to make necessary updates/additions to their respective appendix materials, albeit on a voluntary basis as need arises. Hence, we expect that the appendices that are going to be available by the time the book is in print will always reflect the latest trends/techniques. We might also establish an online forum where readers/users can post pertinent questions or request specific protocol(s). The actual format and question and answer sessions may evolve as time goes by.

We the editors send our warmest regards to all the authors who had to put up with our constant nagging and repeated demands on several rounds of revisions. To some authors, it may have caused some anxiety attacks, for which we apologise and also commend them profusely for their patience and hard work. Last, but not the least, both Carsten Ehrhardt and Kwang-Jin Kim appreciate the expert review and digestion for the *in silico* chapters extended by their mutual friend, Ian Haworth, Ph.D., at the University of Southern California – School of Pharmacy. Finally, we also realise that the book is a live being that constantly requires updates and mending, as the science moves forward. Therefore, we can hardly wait for the next edition for that reason.

Contributors

Remigius U. Agu, Ph.D., College of Pharmacy, Dalhousie University, Burbridge Pharmacy Building, 5968 College Street, Halifax, Nova Scotia B3H 3J5, Canada, Telephone: +1 902 494 2092, Fax: +1 902 494 1396, E-mail: remigius.agu@dal.ca

Prof. Dr. Pieter Annaert, Laboratorium voor Farmacotechnologie en Biofarmacie, Departement Farmaceutische Wetenschappen, Katholieke Universiteit Leuven, O&N2, Gasthuisberg - bus 921, 3000 Leuven, Belgium, Telephone: +32 16 330 303, Fax: +32 16 330 305, E-mail: pieter.annaert@pharm.kuleuven.be

Kenneth L. Audus, Ph.D., Department of Pharmaceutical Chemistry, School of Pharmacy, The University of Kansas, 1251 Wescoe Hall Drive, 2056 Malott, Lawrence, KS 66045, USA, Telephone: +1 785 864 3591, Fax: +1 785 864 5265, E-mail: audus@ku.edu

Prof. Dr. Patrick Augustijns, Laboratorium voor Farmacotechnologie en Biofarmacie, Departement Farmaceutische Wetenschappen, Katholieke Universiteit Leuven, O&N2, Gasthuisberg - bus 921, 3000 Leuven, Belgium, Telephone: +32 16 330 301, Fax: +32 16 330 305, E-mail: patrick.augustijns@pharm.kuleuven.be

Dr. rer. nat. Ulrich Becker, Labtec GmbH, Raiffeisenstr. 4a, 40764 Langenfeld, Germany, Telephone: +49 2173 9735 25, Fax: +49 2173 9735 35, E-mail: ulrich.becker@labtec-pharma.com

Cynthia Bosquillon, Ph.D., School of Pharmacy, University of Nottingham, Boots Science Building Room D10, University Park, Nottingham NG7 2RD, Telephone: +44 115 8466078, E-mail: cynthia.bosquillon@nottingham.ac.uk

Dr. rer. nat. Michael Bur, Dipl. Pharm., Biopharmazie und Pharmazeutische Technologie, Universität des Saarlandes, Im Stadtwald, Gebäude A4 1, 66123 Saarbrücken, Germany, Telephone: +49 681 302 3140, Fax: +49 681 302 4677, E-mail: m.bur@mx.uni-saarland.de

K.-C. Cheng, Ph.D., Schering-Plough Research Institute, K-15-2-2700, 2015 Galloping Hill Road, Kenilworth, NJ 07033, USA, Telephone: +1 908 740 4056, Fax: +1 908 740 2916, E-mail: kuo-chi.cheng@spcorp.com

Sven Deferme, Ph.D., Pharma XL Comm.V., Strijderstraat 7, 3370 Boutersem, Belgium, Telephone: +32 16 39 47 96, Fax: +32 16 39 47 01, E-mail: sven.deferme@pharmaxl.net

Dr. rer. nat. Carsten Ehrhardt, School of Pharmacy and Pharmaceutical Sciences, Trinity College Dublin, Panoz Institute, Westland Row, Dublin 2, Ireland, Telephone: +353 1 896 2441, Fax: +353 896 2783, E-mail: ehrhardc@tcd.ie

William V. Everson, Ph.D., Department of Pediatrics, University of Kentucky, 423 Sanders-Brown, 800 Limestone Street, Lexington, KY 40536, USA, Telephone: +1 859 323-2852, Fax: +1 859 257 2120, E-mail: everson@uky.edu

Barrie C. Finnin, Ph.D., Department of Pharmaceutics, Victorian College of Pharmacy, Monash University, 381 Royal Parade, Parkville, Victoria 3052, Australia, Telephone: +61 3 9903 9520, Fax: +61 3 9903 9583, E-mail: barrie.finnin@vcp.monash.edu.au

Ben Forbes, Ph.D., King's College London, Pharmaceutical Science Division, Franklin Williams Building, 150 Stamford Street, London SE1 9NH, UK, Telephone: +44 207 848 4823, Fax: +44 207 848 4800, E-mail: ben.forbes@kcl.ac.uk

Prof. Dr. rer. nat. Gert Fricker, Abteilung für Pharmazeutische Technologie und Pharmakologie, Institut für Pharmazie und Molekulare Biotechnologie, Ruprecht-Karls- Universität Heidelberg, Im Neuenheimer Feld 366, 69120 Heidelberg, Germany, Telephone: +49 6221 54 8336, Fax: +49 6221 54 5971, E-mail: gert.fricker@uni-hd.de

Univ.-Prof. Dr. Franz Gabor, Department für Pharmazeutische Technologie und Biopharmazie, Universität Wien, Pharmaziezentrum, Althanstrasse 14, 1090 Vienna, Austria, Telephone: +43 1 4277 554 06, Fax: +43 1 4277 9 554, E-mail: franz.gabor@univie.ac.at

Prabha Garg, B.E., M.Tech., Ph.D., National Institute of Pharmaceutical Education & Research, Computer Centre, NIPER, Sector 67, S.A.S. Nagar, Punjab 160 062, India, Telephone: +91 172 2214682-87, Fax: +91 172 2214692, E-mail: prabhagarg@niper.ac.in

Prof. George I. Gorodeski, M.D., Ph.D., Departments of Reproductive Biology, Physiology and Biophysics, and Oncology, Case Western Reserve University (CWRU), and the Department of Obstetrics and Gynecology, University MacDonald Women's Hospital, University Hospitals of Cleveland, 11100 Euclid Avenue, Cleveland, Ohio 44106. Telephone: 216-844-5977. Fax: 216-983-0091. E-mail: gig@cwru.edu

Brendan Griffin, Ph.D., School of Pharmacy, University College Cork, Cavanagh Pharmacy Building, College Road, Cork, Ireland, Telephone: +353 21 490 1657, Fax: +353 21 490 1656, E-mail: brendan.griffin@ucc.ie

Dieter C. Gruenert, Ph.D., California Pacific Medical Center Research Institute, Room 224, Suite 220, 475 Brannan Street, San Francisco, CA 94107, USA, Telephone: +1 415 600 1362, Fax: +1 415 600 1725, E-mail: dieter@cpmcri.org

Hovhannes J. Gukasyan, Ph.D., Research Formulations, Science & Technology, Pfizer Global R&D, La Jolla Laboratories, Pfizer Inc., San Diego, CA 92121, USA, Telephone: +1 858 622 5998, Fax: +1 858 678 8185, E-mail: hovik.gukasyan@pfizer.com

Steffi Hansen, Dipl. Pharm., Biopharmazie und Pharmazeutische Technologie, Universität des Saarlandes, Campus, Gebäude A4 1, 66123 Saarbrücken, Germany, Telephone: +49 681 302 3140, Fax: +49 681 302 4677, E-mail: st.hansen@mx.uni-saarland.de

Ismael J. Hidalgo, Ph.D., Absorption Systems, Oaklands Corporate Center, 440 Creamery Way, Suite 300, Exton, PA 19341, USA, Telephone: +1 610 280 7300, Fax: +1 610 280 3779, E-mail: hidalgo@absorption.com

Prof. Dr. rer. nat. Walther Honscha, Institut für Pharmakologie, Pharmazie und Toxikologie, Universität Leipzig, An den Tierkliniken 15, 04103 Leipzig, Germany, Telephone: +49 341 9738 132, Fax: +49 341 9738 149, E-mail: honscha@vetmed.uni-leipzig.de

Ken-ichi Hosoya, Ph.D., Department of Pharmaceutics, Graduate School of Medical and Pharmaceutical Sciences, University of Toyama, 2630 Sugitani, Toyama 930-0194, Japan, Telephone: +81 76 434 7505, Fax: +81 76 434 5172, E-mail: hosoyak@pha.u-toyama.ac.jp

Ken-ichi Inui, Ph.D., Department of Pharmacy, Kyoto University Hospital, 54 Kawahara-cho, Shogoin, Sakyo-ku, Kyoto 606-8507, Japan, Telephone: +81 75 751 3577, Fax: +81 75 751 4207, E-mail: inui@kuhp.kyoto-u.ac.jp

Fredrik Johansson, Ph.D., Pharmaceutical and Analytical R&D, AstraZeneca R&D Lund, 221 87 Lund, Sweden, Telephone: +46 46 33 7671, Fax: +46 46 33 7128, E-mail: fredrik.fjo.Johansson@astrazeneca.com

Dae-Duk Kim, Ph.D., College of Pharmacy, Seoul National University, Seoul 151-742, South Korea, Telephone: +82 2 880 7870, Fax: +82 2 873 9177, E-mail: ddkim@snu.ac.kr

Kwang-Jin Kim, Ph.D., Will Rogers Institute Pulmonary Research Center, Keck School of Medicine, University of Southern California, Room HMR-914, 2011 Zonal Avenue, Los Angeles, CA 90033, USA, Telephone: +1 323 442 1217, Fax: +1 323 442 2611, E-mail: Kwang.J.Kim@usc.edu

Dr. rer. nat. Carsten Kneuer, Institut für Pharmakologie, Pharmazie und Toxikologie, Universität Leipzig, An den Tierkliniken 15, 04103 Leipzig, Germany, Telephone: +49 341 9738 142, Fax: +49 341 9738 149, E-mail: kneuer@vetmed.uni-leipzig.de

Dr. rer. nat. Michael Laue, Zentrum für Biologische Sicherheit 4 (ZBS4), Robert Koch-Institut, Nordufer 20, 13353 Berlin, Germany, Telephone: +49 1888 754 2326, Fax: +49 1888 754 2571, E-mail: lauem@rki.de

Vincent H.L. Lee, Ph.D., School of Pharmacy, Faculty of Medicine, Chinese University of Hong Kong, Room 626E, 6/F Choh-Ming Li Basic Medical Science Building, Shatin, New Territories, Hong Kong, Telephone: +852 2609 6862, Fax: +852 2603 5295, E-mail: vincent.lee@cuhk.edu.hk

Prof. Dr. rer. nat. Claus-Michael Lehr, Biopharmazie und Pharmazeutische Technologie, Universität des Saarlandes, Im Stadtwald, Gebäude A4 1, 66123 Saarbrücken, Germany, Telephone: +49 681 302 3039, Fax: +49 681 302 4677, E-mail: lehr@mx.uni-saarland.de

Cheng Li, Ph.D., Schering-Plough Research Institute, K-15-2-2700, 2015 Galloping Hill Road, Kenilworth, NJ 07033, USA, Telephone: +1 908 740 4363, Fax: +1 908 740 2916, E-mail: li.cheng@spcorp.com

Dr. rer. nat. Javiana Luengo Contreras, M.Sc., Departamento de Farmacia, Universidad de Concepción, Barrio Universitario s/n, Concepción, Chile, Telephone: +56 41 2203019, Fax: +56 41 2207086, E-mail: jluengo@udec.cl

Rosalie Maurisse, Ph.D., California Pacific Medical Center Research Institute, Suite 220, 475 Brannan Street, San Francisco, CA 94107, USA, Telephone: +1 415 600 1362, Fax: +1 415 600 1725, E-mail: rosalie.maurisse@gmail.com

Pallabi Mitra, M.Sc., Department of Pharmaceutical Chemistry, School of Pharmacy, The University of Kansas, 2095 Constant Avenue, 226 Simons Laboratories, Lawrence, KS 66047, USA, Telephone: +1 785 864 4138, Fax: +1 785 864 5736, E-mail: pmitra77@ku.edu

Dr. rer. nat. Stephan A. Motz, Ursapharm GmbH & Co. KG, Industriestraße, 66129 Saarbrücken, Germany, Telephone: +49 6805 9292 402, Fax: +49 6805 9292 88, E-mail: s.motz@ursapharm.de

Dr. rer. nat. Dirk Neumann, Zentrum für Bioinformatik, Universität des Saarlandes, Im Stadtwald, Gebäude E1 1, 66123 Saarbrücken, Germany, Telephone: +49 681 302 68610, Fax: +49 681 302 64719, E-mail: d.neumann@bioinf.uni-sb.de

Joseph A. Nicolazzo, Ph.D., Department of Pharmaceutics, Victorian College of Pharmacy, Monash University, 381 Royal Parade, Parkville, Victoria 3052, Australia, Telephone: +61 3 9903 9605, Fax: +61 3 9903 9583, E-mail: joseph.nicolazzo@vcp.monash.edu.au

Caitriona O'Driscoll, Ph.D., School of Pharmacy, University College Cork, Cavanagh Pharmacy Building, College Road, Cork, Ireland, Telephone: +353 21 490 1396, Fax: +353 21 490 1656, E-mail: caitriona.odriscoll@ucc.ie

Tanja Obradovic, Ph.D., Absorption Systems, Oaklands Corporate Center, 440 Creamery Way, Suite 300, Exton, PA 19341, USA, Telephone: +1 610 280 1406, Fax: +1 610 280 3779, E-mail: obradovic@absorption.com (current contact information - Merck & Co., Inc., 351 North Summeytown Pike, UG4D-80, North Wales, PA 19454-2505, Phone: +1 267 305 1576, Fax: +1 215-305-6428, Email: tanja_obradovic@merck.com)

Ronnie Paterson, Ph.D., Boston Scientific Ireland, R&D Galway, Ballybritt Business Park, Galway, Ireland, Telephone: +353 91 70 1128, Fax: +353 91 70 1395, E-mail: ronnie.paterson@bsci.com

Dr. rer. nat. Stephan Reichl, Institut für Pharmazeutische Technologie, Technische Universität Carolo-Wilhelmina zu Braunschweig, Mendelssohnstraße 1, 38106 Braunschweig, Germany, Telephone: +49 531 391 5651, Fax: +49 531 391 8108, E-mail: s.reichl@tu-braunschweig.de

Stuart A. Ross, Ph.D., Department of Pediatrics, University of Kentucky, 423 Sanders-Brown, 800 Limestone Street, Lexington, KY 40536, USA, Telephone: +1 859 323 6412, Fax: +1 859 257 2120, E-mail: ejsmart@email.uky.edu

Nilanjan Roy, Ph.D., National Institute of Pharmaceutical Education & Research, Department of Biotechnology, NIPER, Sector 67, S.A.S. Nagar, Punjab 160 062, India, Telephone: +91 172 2214682-87, Fax: +91 172 2214692, E-mail: nilanjanroy@niper.ac.in

Dr. rer. nat. Ulrich F. Schaefer, Biopharmazie und Pharmazeutische Technologie, Universität des Saarlandes, Campus, Gebäude A4 1, 66123 Saarbrücken, Germany, Telephone: +49 681 302 2019, Fax: +49 681 302 4677, E-mail: ufs@rz.uni-saarland.de

Prof. Dr. rer. nat. Marc Schneider, Pharmazeutische Nanotechnologie, Universität des Saarlandes, Campus, Gebäude A4 1, 66123 Saarbrücken, Germany, Telephone: +49 681 302 2438, Fax: +49 681 302 4677, E-mail: marc.schneider@mx.uni-saarland.de

David de Semir Frappart, Ph.D., UCSF Cancer Center, Department of Dermatology, University of California, San Francisco, Suite 471, 2340 Sutter Street, San Francisco, CA 94115, USA, Telephone: +1 415 502 5638, Fax: +1 415 502 8218, E-mail: ddesemir@cc.ucsf.edu

Eric J. Smart, Ph.D., Department of Pediatrics, University of Kentucky, 423 Sanders-Brown, 800 Limestone Street, Lexington, KY 40536, USA, Telephone: +1 859 323 6412, Fax: +1 859 257 2120, E-mail: ejsmart@email.uky.edu

Tomohiro Terada, Ph.D., Department of Pharmacy, Kyoto University Hospital, 54 Kawahara-cho, Shogoin, Sakyo-ku, Kyoto 606-8507, Japan, Telephone: +81 75 751 3586, Fax: +81 75 751 4207, E-mail: tomohiro@kuhp.kyoto-u.ac.jp

Masatoshi Tomi, Ph.D. Department of Pharmaceutics, Graduate School of Medical and Pharmaceutical Sciences, University of Toyama, 2630 Sugitani, Toyama 930-0194, Japan, Telephone: +81 76 434 7508, Fax: +81 76 434 5172, E-mail: tomimasatoshi@yahoo.co.jp

Ann Tronde, Ph.D., Clinical Development, AstraZeneca R&D Lund, S-221 87 Lund, Sweden, Telephone: +46 46 33 6482, Fax: +46 46 33 6666, E-mail: ann.tronde@astrazeneca.com

Michael I. Ugwoke, Ph.D., Disphar International bv, Tolweg 15, 3741 LM Baarn, The Netherlands, Tel: +31 35 5280 429, Fax: +31 35 5480 585, E-mail: ugwoke@disphar.com

Annette S. Uss, Ph.D., Schering-Plough Research Institute, K-15-2-2700, 2015 Galloping Hill Road, Kenilworth, NJ 07033, USA, Telephone: +1 908 740 3696, Fax: +1 908 740 2916, E-mail: annette.uss@spcorp.com

Jitender Verma, M.Sc. (Pharm.), National Institute of Pharmaceutical Education & Research, Pharmacoinformatics Division, NIPER, Sector 67, S.A.S. Nagar, Punjab 160 062, India, Telephone: +91 986 7589850, Fax: +91 172 2214692, E-mail: jeetu270@yahoo.co.in

Dr. sc. nat. Esther H. Vock, Boehringer Ingelheim Pharma GmbH & Co. KG, Non-Clinical Drug Safety, Birkendorfer Straße 88397 Biberach an der Riß, Germany, Telephone: +49 7351 54 97912, E-mail: esther.vock@bc.boehringer-ingelheim.com

Donna A. Volpe, Ph.D., Food and Drug Administration, 10903 New Hampshire Avenue, Silver Spring, MD 20993, USA, Telephone: +1 301 796 0014, Fax: +1 301 796 9816, E-mail: donna.volpe@fda.hhs.gov

Sam Wainhaus, Ph.D., Schering-Plough Research Institute, K-15-2-2700, 2015 Galloping Hill Road, Kenilworth, NJ 07033, USA, Telephone: +1 908 740 6587, Fax: +1 908 740 2916, E-mail: samuel.wainhaus@spcorp.com

Univ.-Prof. Dr. Michael Wirth, Department für Pharmazeutische Technologie und Biopharmazie, Universität Wien, Pharmaziezentrum, Althanstrasse 14, 1090 Wien, Österreich, Telephone: +43 1 4277 554 07, Fax: +43 1 4277 9 554, E-mail: michael.wirth@univie.ac.at

Hiroaki Yuasa, Ph.D., Department of Biopharmaceutics, Graduate School of Pharmaceutical Sciences, Nagoya City University, 3-1 Tanabe-dori, Mizuho-ku, Nagoya 467-8603, Japan, Telephone: +81 52 836 3423, Fax: +81 52 836 3426, E-mail: yuasa@phar.nagoya-cu.ac.jp

Models for Skin Absorption and Skin Toxicity Testing

Ulrich F. Schaefer, Steffi Hansen, Marc Schneider, Javiana Luengo Contreras, and Claus-Michael Lehr

Abstract This chapter includes information about models for skin absorption testing and skin toxicity testing in a condensed form. At first, the structure and function of human skin is described discussing the contribution of the different skin layers and skin appendages to skin absorption. Moreover, various skin absorption pathways are discussed. Particular attention is paid to the strategies used to test skin invasion. This chapter includes in vivo, ex vivo as well as in vitro experimental setups whose advantages and disadvantages are presented. Finally skin toxicity is addressed paying attention to skin sensitization, skin irritation and corrosion, and skin phototoxicity testing. Altogether an up-to-date status on techniques concerning skin invasion testing and skin toxicity testing is provided.

Keywords: Transdermal drug delivery; Skin toxicity; Microdialysis; In vitro permeation; In vitro penetration

Abbreviations

ATR-FTIR	Attenuated total-reflectance Fourier-transformation infrared spectroscopy
AUEC	Area under the effect curve
EC	European Commission
ECETOC	European Centre for Ecotoxicology and Toxicology of Chemicals
ECVAM	European Centre for the Validation of Alternative Methods
FCA	Freund's complete adjuvant
FDA	United States Food and Drug Administration
GPMT	Guinea pig maximization test
IPPSF	Isolated perfused porcine skin flap
LLNA	Local lymph node assay
MPE	Mean photo effect
MTT	3-[4,5-dimethylthiazol-2-yl]-2,5-diphenyltetrazolium bromide
NR	Neutral red
OECD	Organization for Economic Cooperation and Development
pHEMA	poly(2-hydroxyethyl methacrylate)

PIF	Photo irritation factor
SCCNFP	Scientific Committee on Cosmetic and Non-Food Products Intended for Consumers
TER	Transcutaneous electrical resistance
TEWL	Transepidermal water loss
TG	Test guideline
TTS	Transdermal therapeutic system

1.1. Introduction

The skin constitutes one of the largest interfaces between the body and the environment. On the one hand, the function of human skin is to protect our body against chemical, physical, and microbial injury, loss of water, and other endogenous substances; on the other hand, it is involved in the thermoregulation of the body and serves as an excretory organ. This bifunctional nature of the skin depends on its highly differentiated structure, with the main barrier function being located in the outermost skin layer, the *stratum corneum*. Understanding of skin absorption processes is needed for several reasons, such as assessment of the safety aspects of chemicals, other xenobiotics, and cosmetic formulations and utilizing the opportunity to deliver drug substances to the skin and further to the systemic circulation. Safety aspects of chemicals are particularly addressed in the European Union (EU) REACH (Registration, Evaluation, Authorisation and Restriction of Chemicals) REACH Regulation (EC) No 1907/2006 and Directive 2006/121/EC amending Directive 67/548/EEC were published in the official journal 30 December 2006. REACH program, requesting skin absorption data for toxicological examination. Moreover, for substance classification in the context of regulatory purposes, skin sensitization, skin corrosiveness, and skin phototoxicity data are needed. The latter ones are also requirements for cosmetically used formulations, additional to the knowledge of the invasive behavior of active ingredients in these preparations. In the field of pharmaceutical sciences, drug delivery to the skin is gaining more and more interest, owing to the high acceptance by patients. In this regard, two different cases have to be distinguished: local delivery to selected skin layers (e.g., antimycotics) and systemic delivery (e.g., hormones). In the context of bioavailability assessment, knowledge on the absorption behavior of the active compound is essential. For ethical reasons, fundamental skin absorption data can normally not be obtained by conducting *in vivo* studies. Therefore, other techniques must be used to obtain the desired information. One option to obtain these data is the use of *in vitro* penetration and permeation models. Some basic information on these techniques is provided in a number of documents, such as the Organization for Economic Cooperation and Development (OECD) guideline 428 [1] in combination with OECD guidance 28 [2], the Scientific Committee on Cosmetic and Non-Food Products Intended for Consumers (SCCNFP) guideline [3], a European Commission (EC) guide [4], and a United States Food and Drug Administration (FDA) guidance [5]. More detailed information is provided in this chapter.

1.2. Structure and Function of the Skin

1.2.1. Anatomical Structure of Human Skin

The multitude of different functions of the human skin can only be achieved by a unique anatomical structure of the different skin layers. These are as follows:

- Epidermis consisting of
 - *Stratum corneum* (outermost layer)
 - Viable epidermis
- Dermis
- Subcutis or subcutaneous fatty tissue

1.2.1.1. Epidermis

Because of practical reasons, the human epidermis can be generally divided into two main layers, the *stratum corneum* and the viable epidermis.

The *stratum corneum* consists of separated, nonviable, cornified, almost nonpermeable corneocytes embedded into a continuous lipid bilayer made of various classes of lipids, for example, ceramides, cholesterol, cholesterol esters, free fatty acids, and triglycerides [6]. Structurally, this epidermis layer is best described by the so-called brick-and-mortar model [7]. The *stratum corneum* is crucial for the barrier function of the skin, controlling percutaneous absorption of dermally applied substances and regulating fluid homeostasis. The thickness of the *stratum corneum* is usually 10–25 μm , with exceptions at the soles of the feet and the palms, and swells several-fold when hydrated. All components of the *stratum corneum* originate from the basal layer of the epidermis, the *stratum germinativum*.

The viable epidermis is made of several layers starting with the innermost layer called *stratum germinativum* (the basal layer), followed by the *stratum spinosum*, the *stratum granulosum*, and the *stratum lucidum*, which is present only at the palm of the hand and at the sole of the foot. Over the course of 28 days, cells originating from the *stratum germinativum* migrate to the skin surface, undergoing various states of differentiation. The cells in doing so lose their nuclei, get flattened, discharge lipids into the intercellular space (*stratum granulosum*), and are cornified, building up the unique *stratum corneum* structure. Furthermore, in the viable epidermis melanocytes, which produce melanin for light protection, and Langerhans cells, responsible for the immune response of the skin, are localized. It should be noted that in the viable epidermis no vascularization exists.

1.2.1.2. Dermis

Depending on the body site, the thickness of the dermis ranges from 3 to 5 mm. The dermis consists of a matrix of connective tissue composed of collagen, elastin, and reticulin, and is interspersed by skin appendages, such as sweat glands, pilosebaceous units, and hair follicles. Furthermore, nerves, lymphatic and blood vessels are located in this skin layer. Blood vessels are found directly beneath the *stratum germinativum* of the viable epidermis, supplying nutrients and removing metabolites. For systemic drug absorption, both the blood system and the lymphatic system are responsible, acting as sinks and hence keeping the drug concentration in the dermis low.

1.2.1.3. Subcutis, Subcutaneous Fatty Tissue

The subcutaneous fat layer acts mainly as a heat insulator and a mechanical cushion and stores readily available high-energy chemicals.

1.2.2. Biological Activity of the Skin

The human skin is active both biosynthetically and metabolically. For example, vitamin D and the skin lipids are synthesized in the skin, while various drugs, for example, testosterone [8] and benzoic acid [9], are metabolized. In general, all major enzymes, including aryl hydrocarbon hydroxylase, deethylases, hydrolases, monooxygenases, esterases, peptidases, and aminopeptidases, can be found in the skin; however, their activity seems somewhat reduced in comparison to the liver [10]. Therefore, a reduced first pass effect is often associated with transdermal drug delivery. To what extent biotransformation is affecting skin permeability and pharmacological effects is difficult to forecast, since our knowledge in this field is limited, particularly with regard to the location of metabolic enzymes. Moreover, concerning in vitro skin experiments, the activity of some enzymes may be reduced, due to the heating step which is used to separate dermis and epidermis [11]. A more detailed review on skin metabolism can be found in reference [12].

1.2.3. Skin Appendages

Skin appendages can be distinguished into hair follicles with their associated sebaceous glands, eccrine sweat glands, apocrine sweat glands, and nails.

1.2.3.1. Hair Follicles

Hair follicles with their associated sebaceous glands are present all over the skin surface with the exception of lips, palms, and soles. Furthermore, hair follicles intersperse down to the subcutis, offering permeation pathways deep into the skin. The density of hair follicles varies with species and body site; for example, Bronough [13] reported 11 ± 1 follicles/cm² for human abdominal skin and porcine skin from the back. In comparison, 289 ± 21 follicles/cm² can be found on the back of the rat, 658 ± 38 on the mouse, and 75 ± 6 on nude mice. These distinctions might explain the differing results across species obtained in skin permeation studies. In addition, the sebaceous glands produce the sebum, consisting mainly of squalene, wax esters, triglycerides, cholesterol, and free fatty acid. Sebum lubricates and protects the skin, and is involved in the regulation of the pH on the skin surface.

1.2.3.2. Eccrine Glands

Eccrine glands can be found on the entire body surface of humans, except for the lips, external ear canal, clitoris, and labia minora. These glands play an important role in thermoregulation, which is necessary for fluid and electrolyte homeostasis. They secrete a milky or oily odorless liquid which produces the characteristic body smell after metabolism through surface bacteria of the skin.

1.2.3.3. Apocrine Glands

Apocrine glands produce a viscous secretion that contains compounds related to communication between individuals of a species, by acting as a sex attractant or as territorial marker. In humans, these glands are located only in the axillary, pubic, and perianal region.

1.2.3.4. *The Nails*

The nails are composed of flattened, keratinized cells, fused into a dense and hard, yet slightly elastic plate. Their thickness varies from 0.5 to 1.0 mm. In contrast to the *stratum corneum* (10%), the total lipid content of the nails lies between 0.1% and 1%, and the keratin domain is harder, due to higher sulfur content (cystine). Moreover, the water content is only 7% to 12%, in comparison to 25% in the *stratum corneum*. The relative water gain may not exceed 25% at 100% relative humidity, in sharp contrast to 200–300% as found in the *stratum corneum*.

1.2.4. Skin Absorption Pathways

Skin absorption pathways can be divided into the transport (a) across the intact *stratum corneum* and (b) along using skin appendages. The physicochemical properties of the compound, as well as the used formulation, are the main factors influencing the choice of pathway.

1.2.4.1. *Transport Across the Intact Stratum Corneum*

Generally, the *stratum corneum* is considered to be the rate limiting layer of the skin with regard to transdermal drug absorption. However, for the invasion of very lipophilic compounds, the bottleneck moves from the *stratum corneum* down to the viable, very hydrophilic layer of the epidermis, due to substances' reduced solubility in this rather aqueous layer [14].

Originating from the structure of the *stratum corneum*, two permeation pathways are possible: (a) the intercellular route and (b) the transcellular route.

The intercellular route is considered to be the predominantly used pathway in most cases, especially when steady-state conditions in the *stratum corneum* are reached. In case of intercellular absorption, substance transport occurs in the bilayer-structured, continuous, intercellular lipid domain within the *stratum corneum*. Although this pathway is very tortuous and therefore much longer in distance than the overall thickness of the *stratum corneum*, the intercellular route is considered to yield much faster absorption due to the high diffusion coefficient of most drugs within the lipid bilayer. Resulting from the bilayer structure, the intercellular pathway provides hydrophilic and lipophilic regions, allowing more hydrophilic substances to use the hydrophilic and more lipophilic substances to use the lipophilic route. In addition, it is possible to influence this pathway by certain excipients in the formulation.

Under normal conditions, the transcellular route is not considered as the preferred way of dermal invasion, the reason being the very low permeability through the corneocytes and the obligation to partition several times from the more hydrophilic corneocytes into the lipid intercellular layers in the *stratum corneum* and vice versa. The transcellular pathway can gain in importance when a penetration enhancer is used, for example, urea, which increases the permeability of the corneocytes by altering the keratin structure.

1.2.4.2. *The Appendages Route*

The appendages route consists of the glandular and the follicular pathways, with the latter one being the more important. However, since appendages cover only 0.1% of the whole skin surface area, these pathways do not contribute significantly to dermal absorption during steady-state conditions of skin absorption. In contrast, in the initial stages of a skin absorption process and in the case of large hydrophilic compounds and ions, invasion through the

appendages may play a considerable role. Recent studies also report that the appendages route may be involved in the absorption of liposomes, nanoparticles, and cyclodextrin-inclusion complexes [15, 16].

1.3. Strategies for Skin Invasion Testing Classified According to Their Resemblance of the In Vivo Situation

Several official documents, provided by the European authorities and the FDA, are at the disposal of researchers in the field of skin research [1, 2, 17–19]. Where ambiguities and freedom of interpretation remain, advice, on how to practically apply this guidance to protocols in current use, is at hand [20].

In vivo skin absorption measurements are intrinsically rare, due to ethical, economical, and analytical concerns. Therefore, tremendous focus has been given to developing and validating alternative in vitro test methods [21–24]. A comprehensive compilation of literature data, comparing the permeability of chemicals across animal and human skin in vivo, as well as in vitro, has been published by the European Centre for Ecotoxicology and Toxicology of Chemicals (ECETOC) [18]. The diversity of existing in vitro and in vivo techniques shows the difficulties of comparing results between different methods, species, ages, as well as healthy and diseased skin. Howes et al. [19] introduced a hierarchy of frequently applied in vitro methods for measuring percutaneous absorption according to their resemblance of the in vivo situation (Figure 1.1). This knowledge is very helpful when comparing different results of skin absorption studies.

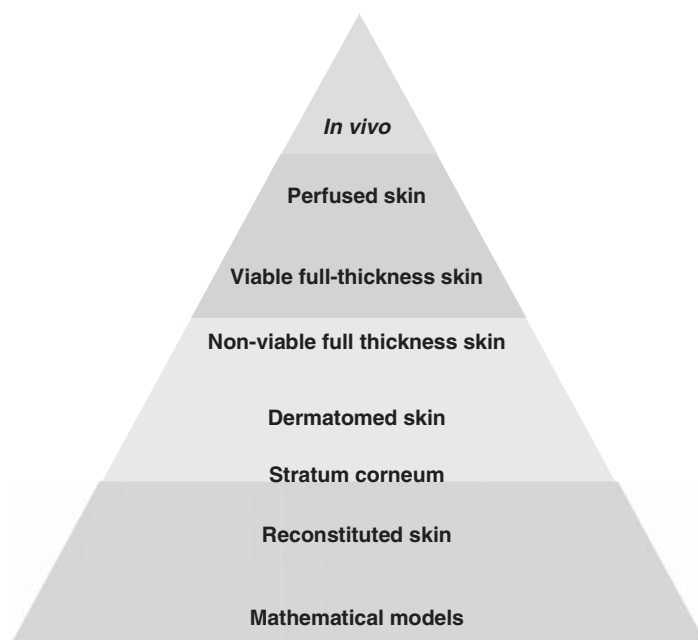


Figure 1.1 Hierarchy of frequently applied methods for measuring percutaneous absorption according to their resemblance of the in vivo situation (adapted from Howes et al. [19]).

After oral administration, drug and metabolite concentrations in blood, urine, and feces can easily be monitored. In contrast, topical application to the skin usually aims at a local treatment. Therefore, the main interest lies in determining the drug level within the skin, in order to evaluate the dermal bioavailability of compounds or assess the bioequivalence between different formulations. In the following sections, appropriate analytical techniques will be presented.

1.3.1. In Vivo Studies Using Pharmacodynamic Response

Only a limited number of chemicals evoke a local quantifiable pharmacodynamic response, for example, the concentration-dependent vasoconstriction effect of corticosteroids. In these experiments, resulting skin blanching is scored visually by one or more qualified investigators, using an ordinal data scale. The lack of instrumentation has been criticized, because of possible subjective errors [25]. However, approaches using the Chromameter device, although recommended by the FDA, have failed to return the desired precision [26, 27].

In addition to a single time-point measurement, skin blanching may be followed over a prolonged period of time. In doing so, depot formation and kinetics of substance removal due to local metabolic or systemic clearance may be observed. By plotting the magnitude of response against time and integrating the area under the effect curve (AUEC), different formulations can be compared. This is the method of choice to determine the bioequivalence of generic products, as described in the FDA guidance for industry on topical dermatologic corticosteroids [5]. The ventral forearm is recommended as the application site. A maximum of eight sites, each of an area of 1 cm² and spaced 2.5 cm from centre to centre, may be framed on each arm. If different formulations or doses are to be tested, these shall be administered randomly to one arm. On the second arm, the same preparations are applied; however, the formulations change their positions. It is encouraged to perform a pilot in vivo study in order to define appropriate parameters for the pivotal study. This includes defining the linear proportion of the sigmoidal dose–response curve, the half maximal effective dose ED₅₀, and assessing the lower limits of sensitivity and the maximum effect. The general study design described in this guidance document also sets the benchmarks for in vivo studies with compounds other than corticosteroids.

1.3.2. In Vivo Dermatopharmacokinetic Approach

1.3.2.1. Recovery Studies

Independent of any visible response, the extent of dermal absorption may be judged from the amount of substance missing within the recovered formulation after finishing incubation. However, this method keeps the researcher in the dark about the ultimate fate of the substance. In addition, recovery studies are not suitable for infinite dosing, as the recovery will always exceed 90%. Comprehensive mass balance including both drug and metabolite levels in the remaining formulation, washings, *stratum corneum*, blood, urine, and feces can provide a more detailed insight. According to OECD guideline 427 “Skin absorption: in vivo method” this technique is also to be favored for safety assessment of chemicals in in vivo animal studies [17].

1.3.2.2. Skin Segmentation Studies – Tape Stripping Method

Sampling from the *stratum corneum* is usually performed by tape-stripping single corneocyte layers (see the respective paragraph later in this chapter). Provided the test substance yields a unique infrared signal, distinguishable from surrounding tissue and formulation components, attenuated total-reflectance Fourier-transformation infrared (ATR-FTIR) spectroscopy is a fast, technically sophisticated, equipment-extensive method of quantification [28]. It has been used to monitor dermal absorption of model substances like 4-cyanophenol, to investigate depth-dependent changes in barrier properties or hydration of the *stratum corneum*, and investigate the effects of formulation excipients and penetration enhancers, such as oleic acid, on the *stratum corneum* barrier function [29–32]. It should be noted that with both tape-stripping and ATR-FTIR, the researcher's field of vision is limited to the nonviable part of the skin.

Comparative studies on the bioavailability of three different tretinoin gel formulations showed that the dimensions of the sampling area may play a critical role in determining the extent of dermal drug uptake [33, 34]. If, by lateral spreading, a substance is distributed over an area sufficiently larger than the sampling area, significant proportions of compound will not be recovered and hence permeability will be underestimated.

1.3.3. In Vivo Dermal Microdialysis

Originating from the neurosciences, the microdialysis technique has been used since several years to monitor drug absorption and disposition or the levels of endogenous substances in the extracellular space of different organs and fluids, such as bone, lung, liver, brain, and blood. The method has evolved from its use in different animal species to the human microdialysis during the late 80s [35].

The technique consists of a microdialysis probe, a thin hollow tube made of a semi-permeable membrane usually around 200–500 μm in diameter, which is implanted into the skin and perfused with a receiver solution that recovers the unbound permeant from the local area. In principle, the driving force of dialysis is the concentration gradient existing between two compartments separated by a semi-permeable membrane. For skin under in vivo conditions, these compartments represent the dermal or subcutaneous extracellular fluid (depending on the probe position) and an artificial physiological solution inside the probe [36–38].

Normally, diffusion microdialysis processes are mathematically described by Fick's second law relating the diffusion rate of the substance from the medium to the concentration gradient and the surface area of the membrane. One of the most important parameters to be considered is the flow rate of the perfusate (solution flowing into the probe), which is normally in the range of 0.1–5 $\mu\text{l}/\text{min}$, inversely related to the amount of drug recovered in the dialysate (solution flowing out of the probe). Other factors that strongly influence the drug recovery from the surrounding medium are the lipophilicity and the extent of protein binding of the substance, as these will decrease the recovery by aqueous perfusate media and the molecular size of the compound, which will limit the pass through the dialysis membrane according to its molecular cutoff. To improve the recovery of lipophilic drugs, strategies such as addition of

solvents (e.g., polyethylene glycol, cyclodextrins, proteins, and lipids) to the perfusate have been used [36, 38, 39].

The relative recovery (RR) of the probe, essential for data interpretation, is calculated using the retrodialysis method, which assumes that the net transport through the microdialysis membrane from the perfusate to the surrounding tissues equals the net transport from the tissues into the perfusate. The equation for calculation is represented as follows [39]:

$$RR = \left(\frac{C_{\text{perfusate}} - C_{\text{dialysate}}}{C_{\text{perfusate}}} \right) \quad (1.1)$$

with $C_{\text{perfusate}}$ and $C_{\text{dialysate}}$ being the compound concentration in the perfusate and in the dialysate. Among the techniques used to determine cutaneous availability, such as tape-stripping, biopsies, or imaging procedures, microdialysis has shown to be promising having several advantages for the assessment of in vivo drug pharmacokinetic profiles. The minimally invasive procedure ensures minor reversible trauma. It allows long-term sampling under physiological conditions in conscious individuals, and gives indication of tissue concentration with respect to time. With the other above mentioned techniques, this would require a large number of volunteers. Due to the relatively low molecular weight cutoff of the membrane, the obtained samples are protein free allowing analysis without any further purification steps and also avoiding an enzymatic degradation of the sample. Nevertheless, the small sample size is a disadvantage since it requires very sensitive analytical methods [39–41].

An increasing number of studies are using microdialysis of a wide range of drugs in animals and humans, supporting the potential of this technique for bioavailability and bioequivalence studies. Some examples of studies in vitro, as well as in vivo, involving different delivery systems and species are iontophoretic drug delivery in rats by Mathy et al. [42]; oral delivery and skin pharmacokinetics by Bielecka-Grzela and Klimowicz [43]; determination of salicylic compounds on rat skin by Simonsen et al. [44] and in human skin by Leveque et al. [45]; and anesthetic extended release products in human skin by Kopacz et al. [46]. For further details about dermal microdialysis, refer to the reviews published during the last few years by McCleverty et al. [35], Kreilgaard [39], Stahl et al. [47], Davies [37], and Elmquist and Sawchuck [48].

1.3.4. Perfused Skin Models

Perfused skin models are considered the missing link between in vivo and in vitro methods. Circumventing the potential harm of testing hazardous compounds in living humans or animals, as well as inconveniences connected to repeated sampling from the venous system or extensive biopsies, perfused skin models offer the benefits of living tissue with fully active microcirculation and metabolism [49, 50]. Ears of different animal origin, such as hairless mice, rabbits, or pigs, have been used. However, the exposed location of the ears and their involvement in thermoregulation implement a high degree of vascularization [51–53]. Because of their unusually high permeability, perfused ear models have been proposed to be predictive models of premature neonate skin [54].

Further specimens in use are the perfused cow udder, the porcine forelimb, and the isolated perfused porcine skin flap (IPPSF) [55–57]. While the first two require the sacrifice of the animal, the last one can be isolated surgically from the abdomen of the pigs, which afterwards can be returned to their prior disposition [49].

Basically, these models comprise a surgically prepared portion of animal skin including a continuous vascular circulation which can be cannulized, perfused with tissue-culture medium, and sampled for cutaneously applied chemicals or their metabolites. The easy sampling of substance levels within the vascular system itself allows analysis of systemically available drugs. Methods known from *in vivo* investigations, such as mass balance, including perfusate levels, surface washings, *stratum corneum* tape-stripping, and deeper skin layer biopsies, are easily transferable to the perfused skin. Wester et al. could show for five compounds with different physicochemical properties that the dose absorbed in the IPPSF after 8 h (i.e., the cumulative dose recovered from surface washings, skin, and perfusate) compared favorably to the percutaneous absorption after 7 days in man (i.e., urinary levels relative to intravenous application) [58]. For the perfused cow udder, such relationship still remains to be shown [59]. Nonetheless, the cow udder proved suitable for investigating skin irritation. Pittermann et al. tested the effects of a water-soluble coolant used in metal industry using sodium lauryl sulphate as positive control. The results showed the benefits of applying special skin protection formulations before contact with an irritant [60].

In a study using porcine forelimbs, Mahmoud et al. found similar metabolism rates of 17β -estradiol applied in ethanolic solution, gel, or transdermal therapeutic system (TTS), as found in human plasma of female patients undergoing transdermal hormone replacement therapy. However, studies by Wagner et al., analyzing the transdermal availability of estradiol and nitroglycerine from TTS, clearly showed that some work remains to be done before the porcine forelimb may be used for predicting *in vivo* percutaneous absorption in man [56]. Concerns about using animal skin as a surrogate for human risk assessment and dermal drug absorption are the same as expressed later for *in vitro* analyses employing membranes of animal origin.

1.3.5. In Vitro Skin Permeation Studies

Most publications in the field of skin permeation research are carried out using a large variety of setups and experimental protocols varying from laboratory to laboratory. This raises questions of standardization and regularization.

Both static and flow-through diffusion cells are approved by the authorities, and data are available on their relevance for predicting the *in vivo* situation [2, 61–64]. Basically, a donor and an acceptor compartment are separated by a membrane of either native skin or bioengineered materials. These materials can be of human, animal, or artificial origin. Sampling from the acceptor compartment is performed either continuously or at predetermined time intervals.

Dosing is possible in infinite (typically $>10 \mu\text{l}/\text{cm}^2$ or $10 \text{ mg}/\text{cm}^2$) or finite manner ($<10 \mu\text{l}/\text{cm}^2$ or $10 \text{ mg}/\text{cm}^2$). The donor chamber may either be left open or be occluded. Nonoccluded conditions permit an exchange with the environment, such as evaporation of volatile substances and drying of the skin surface. In contrast, a tight occlusion of the skin surface may lead to excessive

hydratization. For the determination of membrane integrity, transepidermal water loss (TEWL) measurements are recommended in many guidelines. However, Netzlaff et al. reported certain limitations in applying this method in vitro [65].

Temperature may be controlled by using a water jacket around each permeation cell, an external water bath, or warm air in a drying oven. Usually, experiments are carried out at 32°C, that is, the temperature of the skin surface, or else a temperature gradient may be applied: of 32°C at the skin surface to 37°C in the acceptor compartment, mimicking body temperature. Constant stirring of the acceptor phase ensures that diffusion is unhampered by the buildup of high local concentrations and provides sink conditions throughout the duration of the experiment.

Acceptor solutions preferably comprise buffer solutions of pH 7.4, spiked with preservatives, such as 0.05% sodium azide, if long-term incubation is desired. Low aqueous solubility of the compound in question may require the addition of solubilizers. Although suggested by the original OECD guidance document 28, ethanol:water (1:1) and BRIJ 98 were both found to interfere with membrane integrity and analytics [20]. To investigate metabolic processes, the viability of freshly excised skin may be sustained using tissue-culture medium as acceptor fluid. Further recommendations for experimental methods are available [2, 20].

1.3.5.1. Membranes

Various membrane types suitable for permeation experiments are listed below. More details are available in literature [66].

1.3.5.1.a. Membranes of Human Skin Origin: For all in vitro skin experiments, human skin is considered to be the “gold-standard.” Supply is usually provided from plastic surgery, amputations, or cadavers. While for in vivo studies the volar forearm is used, in vitro skin sources are mostly abdominal, back, leg, or breast skin. Much attention has been turned to assessing the degree and sources of variability [63, 67–70]. Nonetheless, large intra- and interindividual variations of up to 45% in vivo are documented. These may be due to differences in lipid composition, skin thickness, or hydration, which depend on body site and sex or are a consequence of skin diseases [71–75]. In an in vitro situation even larger variations have been reported, as excision, storage, and experimental manipulations may cause additional modifications [76].

After excision, the skin should quickly be freed from subcutaneous fat and stored deep frozen at –20°C to –30°C in tightly sealed plastic bags. It may then be stored for up to several months without impairing barrier function, provided that repeated thawing and freezing is avoided [77–79].

Special attention shall be drawn to the preparation of the excised skin prior to the experiment. Long lag-times encountered with hydrophilic substances, as well as an unfavorable partition of lipophilic compounds into viable skin layers, may require the further separation of the skin into its individual layers [80]. Furthermore, the absence of dermal blood flow in vitro may build up a significant hindrance to diffusion [81]. Reducing the membrane thickness will generally reduce experiment times and thus minimize the risk of bacterial contamination.

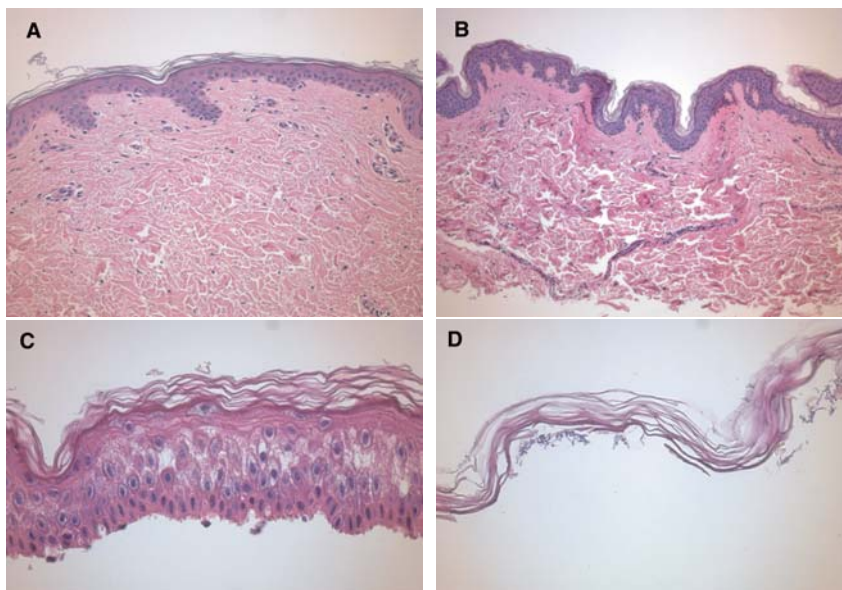


Figure 1.2 Cross sections of (A) full-thickness skin, $\times 100$; (B) dermatomed skin, $\times 100$; (C) heat-separated epidermis, $\times 400$; and (D) trypsin isolated *stratum corneum*, $\times 400$. (Images courtesy of Leon Muijs, Biopharmaceutics & Pharmaceutical Technology, Saarland University, Germany).

Figure 1.2 shows differently prepared skin membranes. The individual membranes were prepared from freshly excised human abdominal skin, originating from females undergoing reductive surgery. Samples were fixed with xylol, stained with hematoxylin/eosin, and embedded into paraffin. Cross sections with a thickness of $4\ \mu\text{m}$ were prepared using a microtome.

Dermatomed Skin or Split Skin The dermatomisation technique may be used for harvesting skin, as well as for reduction of the dermal thickness. Samples in the latter case comprise epidermis including *stratum corneum*, as well as part of the dermis. Care has to be taken to avoid any damage to the *stratum corneum* barrier. This may be achieved by protecting the skin surface with a piece of plastic [82]. The recommended thickness is $200\text{--}400\ \mu\text{m}$ and $400\text{--}700\ \mu\text{m}$ for human and pig skin, respectively [20]. Although the dermatome will cut through hair follicles, the holes will readily close during incubation in aqueous media, due to swelling of the tissue.

Epidermis Complete removal of the dermis may be achieved by several mechanical, thermal, and chemical techniques. Most commonly, the epidermal–dermal junction is split by heating the skin to $60\ \text{C}$ for $30\text{--}120\ \text{s}$ [83, 84]. Pitman et al. [85] could show that such a treatment does not impair the barrier function. The use of ethylene diamine tetraacetic acid, sodium bromide, or ammonia fumes has also been reported [80, 83, 86]. It may, however, be suspected that the use of sufficiently strong acids or bases may change the buffer capacity of skin, which would especially influence the penetration behavior of ionizable drugs.

Stratum Corneum The cornified skin layers may be isolated by digestion of the connective epidermal tissue using trypsin in buffer solutions of pH 7.4.

This may be achieved by complete immersion of full-thickness skin in trypsin solution or by placing the heat-separated epidermis for 24 h at 37°C on a filter paper soaked with the enzyme preparation [64, 83]. Other techniques, such as vacuum or chemically induced blistering, stretching, application of staphylococcal exfoliatin, or proteolytic digestion of viable cells, are seldom reported [74, 87–89].

Skin with Impaired Barrier Function (Dermis, Stripped Skin) In the course of studying the behavior of diseased, injured, or premature skin, it may be necessary to deliberately impair the skin's barrier function. As the rate limiting barrier for most compounds resides within the *stratum corneum*, removal of the outermost cornified layer will result in an increased permeability [74, 90]. This has been monitored by measuring the concomitant increase in TEWL and change in skin impedance [91]. Both tape-stripping and dermatomization seem to be suitable preparation techniques, since heat separation of epidermis at 60°C and trypsin-induced removal of the *stratum corneum* are likely to result in significant precipitation or digestion of dermal proteins [11].

Reconstructed Human Epidermis Equivalents Because of the limited availability of human skin, reconstructed human epidermis equivalents are under investigation to serve as membranes in permeation experiments. A summary on these replacement tools has been recently published by Netzlaff et al. [92]. First results of a German prevalidation study have shown the suitability of such bioengineered human epidermis equivalents in permeation studies [93].

1.3.5.1.b. Membranes of Animal Skin Origin: The limited availability of human skin, together with an increasing need to test the bioavailability of dermal products in pharmaceuticals and cosmetics, as well as risk assessment of chemicals, has promoted the search for alternative models. A switch to animal skin, therefore, seems obvious. Species currently in use are mouse, hairless rat, hamster (cheek pouch), snake (shed skin), pig (ear, flank, abdomen, or back), and cow (udder). However, differences in *stratum corneum* thickness, number of corneocyte layers, hair density, water content, lipid profile, and morphology cause animal skin to be more permeable than human skin, leading to an overemphasis of compound permeability [13]. When comparing results of several species, human skin finds its closest match in porcine tissue [13, 20, 94]. While animal skin is still mentioned in the OECD guidance document 28, the explicit use of human skin has later been demanded as the only acceptable surrogate in human risk assessment [2, 20]. In addition, a general testing, as well as marketing ban concerning the use of animals for testing cosmetics or their ingredients, will come into action in the EU in September 2009 [95]. Nonetheless, animal skin may still be suitable for specific, usually veterinary, applications [20].

1.3.5.1.c. Membranes of Nonskin Origin: The complexity of published setups ranges from the simple use of dialysis tubing and polymeric membranes, made up of regenerated cellulose, polycarbonate, polyethylene, or polydimethylsiloxane, to amphiphilic multilayer laminates and polymer networks [96–100]. Because of their negligible barrier-forming properties, simple porous membranes do not present a significant hindrance for drug absorption. They may, however, serve as tools for separation of formulation and acceptor compartment in drug release studies. Diffusion takes place via aqueous channels along the

tortuous pathway of the pores. Primary fields of application are formulation optimization, quality control, and comparison of pharmaceutical availability of different products. Polymeric membranes usually do not provide insight into the inherently complex mechanisms of skin absorption.

On the other hand, amphiphilic composite membranes made up of silicone and poly(2-hydroxyethyl methacrylate) (pHEMA) have been reported to form a significant barrier. Although their absolute permeability is usually higher than that of skin, the permeability coefficients of several test compounds correlated reasonably well to values found across rat skin [101–103]. For a set of compounds, mostly substituted phenols, Geinoz et al. [104] could further demonstrate similar structure–permeation relationships across silicone membranes and literature data on human epidermis. Lipophilicity and hydrogen-bond donor acidity are the main determinants for transport across silicone membranes. Accordingly, another group suggested silicone membranes as a simple model to study the impact of vehicle components on partition, permeability, and retention of drug molecules [105].

Of particular interest are membranes prepared of an inert porous support carrying natural or artificial lipids. These coatings may comprise a single component, such as isopropylmyristate or dodecanol [99, 106], or mixtures of comparable composition as the *stratum corneum* intercellular bilayer [107, 108]. Usually, synthetic lipids are used, due to an elaborate isolation procedure for *stratum corneum* lipids, with limited yield and the necessity of separation of triglycerides, originating from subcutaneous fatty tissue or skin care products [109].

By adjusting the lipid composition, a variety of problems can be addressed. Mechanistic studies employing wide- and small-angle X-ray diffraction, FT-IR spectroscopy, and neutron scattering have been used to show the contribution of the individual classes of skin lipids to barrier formation and the sandwich-like lipid organization within the intercellular bilayers of the *stratum corneum* [110–115]. Moreover, the mode of action of penetration enhancers, such as oleic acid [116, 117], the structure and hydration of *stratum corneum* lipids [118], and the degree of ionization of free fatty acids [119] were investigated. Lipid-coated membranes have also been applied as surrogates for skin absorption [120–122]. Jaekle et al. used an iterative method to examine the influence of formulation excipients on the diffusion of a model compound through lipid-coated membrane filter discs [107].

1.3.6. In Vitro Skin Penetration Studies

As described previously in this chapter, efforts have been made to develop methods for quantification of skin permeability, validation of diffusion cell setups, and correlation of in vitro data with the in vivo situation. However, the average drug permeation experiment does not provide insight into the temporal and local disposition within the tissue, that is, the skin penetration. The following discussion will give an overview of methods tackling this kind of problem.

Drug levels within the *stratum corneum* can be assessed by sampling single corneocyte layers with adhesive film. The drug is then extracted from the tape-strips and quantified by a suitable analytical method. Usually, scintillation counting (for radioactive compounds) or high performance liquid

chromatography analytics are employed. Results are reported as the *stratum corneum* drug amount absorbed per square cm of skin. In addition, correlating the local drug concentration with the skin depth will result in a detailed insight into the concentration gradient across the membrane, that is, the actual driving force for drug diffusion. Within the deeper skin layers, that is, the epidermis and dermis, analogous information can be obtained using biopsy punches. However, the invasive character of the sampling procedure practically restricts this technique to *in vitro* studies. After freezing, the punch biopsies may be segmented parallel to the surface, by means of a cryo-microtome. After substance extraction, the drug amount is determined using an appropriate analytical method, for example, high performance liquid chromatography.

The tape-stripping technique has been applied *in vivo*, as well as *in vitro*. The used *in vitro* incubation devices are the same as described for skin permeation studies. A specialized incubation device developed by Loth and coworkers, the “Saarbrücken penetration model,” allows investigation of skin penetration bypassing the normally occurring nonphysiological hydration of the dermis [64].

It has been observed that, especially with aqueous donor media, the generation of concentration-skin depth profiles is limited to a few hours of incubation. Excessive hydration progressively weakens the coherence of the corneocytes, which are then torn off by the tapes in large flaps instead of distinct layers. Particularly, the investigation of hydrophilic or high molecular weight compounds with long *stratum corneum* lag-times is affected. Mueller et al. proposed that incubation can be prolonged up to 48 h if the membrane is allowed to dry at room conditions for 30 min prior to tape-stripping [123]. Efforts have been made to correlate short time concentration gradients with steady-state flux. Pirot et al. correctly predicted the steady-state flux of 4-cyanophenol, by fitting the concentration gradient measured *in vivo* after a short time-exposure of 15 min, that is, approximately half the lag-time, to the solution of Fick’s second law of diffusion [124].

To show the substance distribution in the different skin layers, the allocation of the different removed skin segments, obtained either by a stripping procedure or by cryo-cutting, is essential.

In the following section, methods of assessing the thickness of *stratum corneum* removed per tape are summarized.

1.3.6.1. Determination of the stratum corneum depth by Tape-Strip Number

For untreated skin, repeated stripping may remove a constant amount of *stratum corneum*, independent of the number of strips already performed [125]. The momentary depth may thus be calculated by dividing the mean thickness of the overall *stratum corneum* by the total number of tapes necessary to remove it completely and multiplying with the number of strips already performed.

However, the validity of a similar assumption has to be questioned, in case the skin has previously been treated with a topically applied formulation [126]. Opinions differ, whether the distinct curvature of the steady-state *stratum corneum* concentration gradient, reported in literature, may be an artifact of a wrong depth scale, since such a behavior cannot be reasonably explained by the established diffusion theory.

1.3.6.2. Determination of the stratum corneum depth by Weight of Removed Tissue

A linearization of the steady-state concentration gradient could be demonstrated by relating the depth to the weight of the tissue, removed per piece of adhesive tape. However, large errors, especially, within the first tapes, cast doubt over these findings [127, 128]. The procedure is time-consuming and artifacts, due to absorption and desorption of moisture, formulation excipients, or sebaceous lipids, are likely.

1.3.6.3. Determination of the stratum corneum depth by Amount of Protein

A standard Lowry-based protein assay has been adjusted to the special conditions encountered with skin [126]. Basically, proteins reduce an alkaline solution of Cu(II)-tartrate to Cu(I) in a concentration-dependent manner. Then, the formation of a blue complex between Folin-Ciocalteu reagent (a solution of complex polymeric ions formed from phosphomolybdic and phosphotungstic heteropoly acids) and Cu(I) can be measured spectrophotometrically at 750 nm. A calibration curve can be obtained by dissolving known amounts of *stratum corneum* in 1 M sodium hydroxide. A piece of tape that has not been in contact with skin is subjected to an identical procedure and serves as negative control. The method was recently adapted to a 96-well plate format, notably reducing analysis times [129].

Assessing the depth by determining the protein amount removed per strip, Mueller et al. noted a nonlinear steady-state concentration gradient which they ascribed to an increased permeability of the cornified envelope within the *stratum disjunctum* [123].

1.3.6.4. Determination of the stratum corneum depth by Optical Spectroscopy in the Visible Range

Corneocytes adhered to a piece of adhesive tape will refract light by reflection, scattering, and diffraction, almost independent of the wavelength [128]. After stripping, the tape is transferred into a sample holder in a way that the rectangular beam of a specially designed double beam UV/Vis spectrophotometer penetrates the area carrying corneocytes. The absorbance is then measured at 430 nm, using an empty tape in the reference beam. As most compounds and excipients absorb light in the ultraviolet spectral range, an overlap of the signal by formulation components is unlikely.

1.4. Testing on Skin Toxicity

1.4.1. Skin Sensitization

Substances when applied to human skin might exert a sensitizing potential on the skin and need, therefore, to be evaluated and classified for their possible toxicity. Every substance that provokes immunologically mediated cutaneous reactions (i.e., skin sensitization or allergic contact dermatitis) is referred to as skin sensitizer. Several tests are recommended, but no single method is able to identify all potential substances capable of inducing sensitization of human skin. Widely used test methods for the investigation of skin sensitization, the so-called adjuvant and nonadjuvant tests, are described below.

1.4.1.1. Guinea Pig Maximization Test

The guinea pig maximization test (GPMT) is a preferred method for the detection of skin sensitizers. It belongs to the class of adjuvant-tests, where the substance will be applied in Freund's complete adjuvant (FCA). The test is based on the possible induction of an immune response of the skin during an induction period (at least 1 week). This pretreatment of the subject will eventually result in a hypersensitive reaction during a further exposure, the so-called challenging phase.

The dose used for the induction exposure is chosen in such a way that it is systemically well tolerated and causes only mild-to-moderate skin irritations. The dose during the challenging period should be the highest nonirritating dose. Both doses need to be determined in preliminary tests, in case no other information on the test substances is available.

The test is started with an intradermal and/or epidermal application of the test substance, using the induction dose on young adult guinea pigs of either gender. In the case of female animals, these have to be nulliparous and nonpregnant. For 5 days prior to the test, animals are kept at $(20 \pm 3)^\circ\text{C}$ with 30–70% relative humidity, conventional laboratory diet, and unlimited access to water. The induction dose is administered to the shoulder region and is followed by the induction period (10–14 days), in which the animals can rest and a possible immune response may develop. It should be noted that the location of the induction dose is kept occluded for the first 48 h after administration.

Thereafter, the animals are exposed for a second time at their flanks, using the challenging dose for 24 h under occlusive conditions. Twenty-one hours after removing the challenging dose patches, the area is cleaned and freed from hair, without abrasion of the skin. After an additional 3-h period (exactly 48 h after the challenging treatment), the skin is investigated in comparison to that in the control group that received sham treatment during the induction phase. A second investigation of the incubated area is performed a further 24 h later, and judgments are made according to the Magnusson/Kligman scheme (Table 1.1) [130].

Along with the testing of the materials of interest, control experiments with reference substances need to be performed. At least every 6 month, the control test needs to be carried out using mild-to-moderate skin sensitizers [recommended substances are α -hexylcinnamaldehyde, benzothiazole-2-thiol (mercaptobenzothiazole), and benzocaine] to evaluate the testing procedure.

The minimal number of animals to be investigated is 10 in the treatment group and 5 in the control group. If the findings indicate a nonsensitizing substance, the number of animals needs to be increased to a total of 20 and 10 for the treatment and the control groups, respectively.

Table 1.1 Magnusson/Kligman grading scale for the evaluation of challenge patch test reactions [130].

Observed skin reaction	Noted value
No visible change	0
Discrete or patchy erythema	1
Moderate or confluent erythema	2
Intense erythema and swelling	3

1.4.1.2. *Buehler Test*

The Buehler test [131] is the preferred nonadjuvant test method, even though it might be not as accurate as other tests [132]. Like the GPMT, the Buehler test consists of two successive phases, the induction treatment followed by the challenging exposure. The induction dose needs to be chosen in such a way that it is high enough to cause mild irritation on the skin, while the challenging dose should equal the highest nonirritating concentration of the investigated substance. Both doses have to be determined in a pilot study.

Guinea pigs of either sex can be used. If female animals are used, these have to be nonpregnant and nulliparous. A minimum of 20 animals for testing and at least 10 as control are recommended.

The test patches are brought in contact with hair-free areas on the flanks of the guinea pigs under occlusive conditions for 6 h. The control group (potentially a naive control) will be treated with the vehicle only, which is applied in a similar manner on hair-free guinea pig flanks. The same treatment is carried out on days 6–8 and again on days 13–15. On days 27–29 after the initial incubation, the challenging dose is applied under occlusive conditions to the, until then, not exposed flank of the guinea pigs (hair-free). These patches are also held in contact with the skin for 6 h.

Twenty-one hours after the end of the incubation, all hairs are again removed from the treated flanks (abrasions are to be avoided) and observation of the skin's reaction is made after a further 3 h. These are recorded according to the grades proposed by Magnusson and Kligman (Table 1.1) [130]. After an additional 24 h, the skin reactions are observed again and recorded following the same scale.

1.4.1.3. *Local Lymph Node Assay*

The murine local lymph node assay (LLNA) was developed as an alternative to the GPMT [133]. Even though it cannot fully replace the GPMT, fewer animals are necessary to perform the test. The LLNA enables the hazard classification of substances that induce allergic contact dermatitis, while offering animal welfare advantages, compared to the GPMT (elimination of pain and reduction in animal numbers required). Furthermore, the LLNA allows assigning substances into specific potency categories (classes 1–3) [134]. The LLNA has recently been accepted by the SCCNFP and is published as OECD test guideline (TG) 429 updated (2002) [135].

The test method is based on the fact that sensitizers induce a proliferation of lymphocytes in the lymph node draining the site of substance administration. The increased proliferation is proportional to the applied dose of the chemical and the potency of the allergen. Hence, the murine LLNA assesses proliferation in a dose–response manner, comparing it to the proliferation in a control group. The ratio of the proliferation after sensitizer application to the control group defines the Stimulation Index (SI).

$$SI = \frac{\text{sensitizer stimulated proliferation}}{\text{sensitizer – free proliferation}}$$

An $SI \geq 3$ is the minimum requirement to be met, before a chemical has to undergo further evaluation as a skin sensitizer. Radio labeling is a standard method to quantitatively assess the proliferation, but other analytical techniques exist. For all investigations, positive controls need to be performed. The

positive control should result in an $SI > 3$, but the substance should be chosen in such a way that it clearly does not cause excessive reactions (e.g., hexyl cinnamic aldehyde and mercaptobenzothiazole). Experiments shall be performed using young adult, nonpregnant, and nulliparous female mice (CBA/Ca or CBA/J strain). The mice shall be housed at $(22 \pm 3)^\circ\text{C}$ with relative humidity kept between 30% and 70%, at 12-h light–dark alterations, in individual cages at conventional diet and unlimited water supply. Male animals or other strains can be used, if enough data are generated to show parity in the LLNA.

The procedure goes over 6 days of which on days 1–3 the verum or just the vehicle (typical vehicles are acetone/olive oil mixtures, *N,N*-dimethylformamide, methyl ethyl ketone, propylene glycol, or dimethyl sulfide) are applied onto the ears of the animals, whereas the fourth and the fifth day are without treatment. On the sixth day, a suspension of lymph node cells is prepared for each mouse.

The LLNA is the preferred method when compared to the GPMT because (a) it can equivalently predict human contact dermatitis, (b) a dose–response can be obtained, and (c) it is in line with current animal welfare efforts. Nevertheless, several situations exist where the GPMT is advantageous, depending predominantly on the choice of test substances. The LLNA is known for less powerful detection of the sensitization potential of metallic compounds, high molecular weight proteins, strong irritants, and for substances with low adhesion to the skin surface (skin wettability is a prerequisite for the successful application of LLNA) [136–140].

The skin reaction observed after performing the GPMT should also be recorded analogous to the Magnusson/Kligman grading scale (Table 1.1).

1.4.2. Skin Irritation and Corrosion

Any application of substances onto the skin, for instance, cosmetic products, must not cause damage to human health when applied under normal conditions. Therefore, any compound considered for application on human skin needs to be tested for reversible disadvantageous effects (skin irritation) and irreversible skin damage (skin corrosion).

To test the irritancy potential of substances, two tests which can reliably distinguish between skin corrosives and noncorrosives are endorsed by the European Centre for the Validation of Alternative Methods (ECVAM). The testing procedures are based on the transcutaneous electrical resistance (TER) measurements of rat skin and on a human skin model. Both test systems [141–145] will be briefly outlined below. Nevertheless, these tests are not suited for the group of mild irritants which do not induce an acute effect on the barrier function. For those substances, new markers need to be evaluated. First results are available for heat shock protein 27 where higher levels were observed in skin models after exposure to mildly irritating chemicals [146, 147].

1.4.2.1. Rat Skin Transcutaneous Electrical Resistance

The rat skin TER assay enables to reliably discriminate between skin corrosives and noncorrosive substances [148]. The assay relies on the change in the bioelectrical properties of the skin in response to the application of test chemicals. For the measurements, small discs of rat skin are necessary onto which the substances are applied to the epidermal surface for up to 24 h. In

the case of a corrosive impact on the barrier, the TER value will fall below a threshold value of 5 k Ω [149]. This effect will only be observed for corrosive materials, due to the degradation of the barrier integrity, but not for irritant materials.

For the experiment, the dorsal skin of young rats (Wistar or a comparable strain) is shaved and washed with an antibiotic solution (containing, e.g., streptomycin, penicillin, chloramphenicol, and amphotericin in concentrations inhibiting bacterial growth). After skin excision, excess fat is peeled off and the skin is placed over the end of a polytetrafluoroethylene tube with the epidermal side in touch with the hollow cylinder. The skin is fixed with an O-ring and the tube interior is sealed. The side of the dermis is then submersed in a magnesium sulphate solution (154 mM). The samples are applied at 30°C to the epidermal side of the skin in such a way that the skin interface is fully covered. After the incubation time, the substances are removed with prewarmed water; the skin surface tension is decreased with ethanol which is subsequently replaced with magnesium sulphate solution (154 mM).

As positive control, 10 M hydrochloric acid (36%) is recommended; distilled water will work as a negative control.

In the case that TER values below 5 k Ω are measured for surfactants or neutral organics, an assessment of dye (sulforhodamine B) penetration can be carried out to determine false-positive results [150]. Preparation of the skin discs and the washing steps are known to be the critical steps.

The TER assay of rat skin is a fully accepted replacement method of animal tests for skin corrosion. Hence, in the EU the TER assay is mandatory for the evaluation of test substances. Investigation of animals to test the corrosivity of chemicals and/or other substances is not permitted [151].

In 2000, the TER assay has been included into “Annex V. Part B.40 on Skin Corrosion” of the “Directive 67/548/EEC on the Classification, Packaging and Labelling of Dangerous Substances” [152]. Moreover, at the 14th Meeting of the OECD National Coordinators for the TGs Programme, the draft TG 430 for the TER assay for testing in vitro skin corrosion was granted approval, which is the basis for a subsequent acceptance at the OECD level [153].

1.4.2.2. Human Skin Model Assay

The human skin model assay involves measuring the effects of corrosives on viable cells in a reconstituted human skin equivalent. To be accepted as a valid human skin model, several criteria must be met. The artificial skin must comprise a functional *stratum corneum* with an underlying layer of viable cells. Furthermore, the barrier function of the *stratum corneum*, as well as the viability of the epidermis, must be verified with appropriate experimental setups. The chemicals to be tested are applied up to 4 h as a liquid or a wet powder onto the skin model. Afterwards, careful washing has to be performed, followed by investigation of the cell viability [e.g., with a (MTT)] reduction assay).

The human skin model assay can provide further data on the degree of corrosiveness and allows ranking corrosives among each other. It is, therefore, accepted as a replacement method of animal tests for skin corrosion in the EU.

The following in vitro methods based on reconstructed human skin models are validated (by the ECVAM) for predicting skin corrosion—EPISKIN[®], EpiDerm[®], Corrositex[®]—and irritation: EPISKIN[®], EpiDerm[®], PREDISKIN[®], SIFT [142]. Additionally, the SkinEthic[™] was assessed and

concordance between the model and the accepted test of OECD TG 430 and TG 431 was obtained [93, 154, 155].

1.4.3. Skin Phototoxicity

This section will briefly focus on tests used to identify chemicals that lead to toxic responses after contact with skin and a subsequent exposure to light. This involves locally as well as systemically administered substances.

1.4.3.1. 3T3-Neutral Red Uptake

This test enables to identify compounds which show a phototoxic effect in vivo [156]. It allows inter alia assessing the photo irritancy potential of ultraviolet (UV) filter candidates after topical application and distribution to the skin [157]. The 3T3-neutral red uptake test, however, is unable to predict other adverse effects that might result from the combined interaction of chemicals with light.

The test is based on an in vitro assay of the uptake of the dye, neutral red (NR), in Balb/c 3T3 fibroblasts. It was developed to detect the phototoxicity induced by the combined interaction of the test substance and light of the wavelength range from 315 to 400 nm, the so-called UVA. The cytotoxicity is evaluated in the presence (+UVA) or absence (–UVA) of UVA light exposure, after application of a nontoxic dose of the compound. The cytotoxicological impact is assessed via the inhibition of the fibroblasts to take up the vital dye NR (NR is a weak cationic dye, penetrating easily into the cell membrane by a nonionic diffusion and accumulates in the lysosomes) one day after the initial treatment. Normally, healthy cells may incorporate and bind NR. Alterations of the cell surface or the lysosomal membranes, however, lead to a decreased uptake and binding of the dye.

For the in vitro test, the fibroblasts are allowed to form a half-confluent monolayer within 24 h. Different concentrations of the test chemical are then incubated for 1 h with two sets of cells in parallel (typically on 96-well plates, 10^4 cells per well, passage number <100). After the incubation with the test substances, one set is irradiated with a nontoxic dose of UVA light (5 J/cm^2), while the other set is kept in the dark. Twenty hours after irradiation, cell viability is evaluated by measuring the uptake of NR for 3 h. After the end of the absorption process, excess NR is removed and the cells are treated with an NR desorption solution (ethanol/acetic acid) to extract the dye taken up by the cells. Subsequently, the optical density of the NR solution is measured at 540 nm. As positive control, a test with chlorpromazine is performed.

For the evaluation of the results, the obtained concentration–response curves for +UVA and –UVA are compared. The photo irritation factor (PIF) is calculated, which allows to determine the phototoxic potential of a substance according to a numerical value. The PIF-value represents the ratio of the EC_{50} (effective cytotoxic concentration) (–UVA) and the EC_{50} (+UVA). A PIF-value above 5 indicates a phototoxic potential, whereas a PIF-value below 5 predicts no such potential. To overcome problems in the case of no phototoxicity up to the highest investigated concentration [no EC_{50} (–UVA) and/or no EC_{50} (+UVA)], a second measure was introduced, the so-called mean photo effect (MPE) [158], which can be calculated using a freeware program available at the Humboldt University in Berlin (Germany) from H.G. Holzhuetter.

1.4.3.2. Reconstructed Human Epidermis in Combination with MTT-Assay

A further option to investigate the phototoxic potential of substances is the use of reconstructed human skin models. The evaluation of the cell viability is based on the MTT-assay that is sensitive for the mitochondria activity in cells. Currently, these *in vivo* substitutes are still under validation and are not approved as full standard test methods for the investigation of the phototoxicity potency of a test chemical. However, several existing models are in use for prevalidation studies and are described elsewhere in more detail [92].

1.4.3.2.a. *SkinEthic*[®]: The *SkinEthic*[®] model has shown some relevance for the assessment of phototoxicity by comparing experimental *in vitro* data to *in vivo* data from tolerability studies. The model proved capable of discriminating between phototoxic and nonphototoxic compounds [159] following a protocol described by Liebsch et al. [160]

1.4.3.2.b. *EpiSkin*[®]: In studies to examine the suitability of the model for phototoxicity, the effects of several weak phototoxic substances were compared to the effect of chlorpromazine, a strongly phototoxic reagent. The substances were applied topically, and after 1 h of incubation, the *EpiSkin*[®] models were exposed to a noncytotoxic dose of UVA radiation. After a further 18 h of incubation, an MTT-assay was performed and the IL1 α released was quantified. The phototoxic compounds combined with UVA lead to an increase in cell mortality and a rise in IL1 α release, hence demonstrating the ability of the model to be used for identification of phototoxic substances [161].

1.4.3.2.c. *EpiDerm*[®]: Liebsch et al. adapted a test protocol for phototoxicity testing to the *EpiDerm*[®] model [160]. The test compounds were applied topically at five different concentrations and then the reaction to the irradiation with UVA/Vis light was evaluated 24 h later by MTT-assay. The *EpiDerm*[®] model was able to identify the phototoxic substance [160].

References

1. OECD. Test guideline 428: Skin Absorption: In Vitro Method, OECD, Paris, 2004.
2. OECD. Guidance document for the conduct of skin absorption studies. OECD Series on Testing and Assessment. No 28, Environment Directorate, Paris, 2004.
3. SCCNFP. Basic criteria for the in-vitro assessment of dermal absorption of cosmetic ingredients, 2003.
4. EC. Guidance document on dermal absorption, European Commission Health & Consumer Protection Directorate—General Directorate E—Food Safety: Plant health, animal welfare, international questions E1—Plant health, 2004.
5. FDA. Guidance for industry: SUPAC-SS In-vitro release testing and in-vivo bioequivalence documentation, Center for Drug Evaluation and Research (CDER), 1997.
6. P. W. Wertz and D. T. Downing. Stratum corneum: Biological and biochemical considerations. In J. Hadgraft and R. Guy (eds.), *Transdermal Drug Delivery*, Marcel Dekker, New York, Basel, 1989, pp. 1–22.
7. P. M. Elias. Epidermal lipids, barrier function, and desquamation. *J. Invest. Dermatol.* **80**: 44–49 (1983).
8. S. W. Collier, N. M. Sheikh, A. Sakr, J. L. Lichtin, R. F. Stewart, and R. L. Bronaugh. Maintenance of skin viability during in-vitro percutaneous absorption/metabolism studies. *Toxicol. Appl. Pharmacol.* **99**: 522–533 (1989).

9. D. Nathan, A. Sakr, J. L. Lichtin, and R. L. Bronaugh. In-vitro skin absorption and metabolism of benzoic acid, p-aminobenzoic acid, and benzocaine in hairless guinea pig. *Pharm. Res.* **7**: 1145–1151 (1990).
10. A. Pannatier, P. Jenner, B. Testa, and J. C. Etter. The skin as metabolising organ. *Drug Metab. Rev.* **8**: 319–343 (1978).
11. R. C. Wester, J. Christoffel, T. Hartway, N. Poblete, H. I. Maibach, and J. Forsell. Human cadaver skin viability for in vitro percutaneous absorption: Storage and detrimental effects of heat-separation and freezing. *Pharm. Res.* **15**: 82–84 (1998).
12. S. A. Hotchkiss. Dermal absorption. In M. Roberts and K. A. Walters (eds.), *Dermal Absorption and Toxicity Assessment*, Marcel Dekker, New York Basel, 1998, pp. 43–101.
13. R. L. Bronaugh, R. F. Stewart, and E. R. Congdon. Methods for in vitro percutaneous absorption studies. II. Animal models for human skin. *Toxicol. Appl. Pharmacol.* **62**: 481–488 (1982).
14. H. R. Moghimi, B. W. Barry, and A. C. Williams. Stratum corneum and barrier performance: A model lamellar structural approach. In R. L. Bronaugh and H. Maibach (eds.), *Percutaneous Absorption—Drugs, Cosmetics, Mechanisms, Methodology*, Marcel Dekker, New York, Basel, Hong Kong, 1999, pp. 515–553.
15. G. Blume. Cyclodextrine, vesicles and particles that really get under your skin. *COSSMA* **5**: 30–33 (2004).
16. J. Lademann, H. Richter, U. F. Schaefer, U. Blume-Peytavi, A. Teichmann, N. Otberg, and W. Sterry. Hair Follicles—A long-term reservoir for drug delivery. *Skin Pharmacol. Physiol.* **19**: 232–236 (2006).
17. OECD. Test guideline 427: Skin Absorption: In Vivo Method, OECD, Paris, 2004.
18. ECETOC. Monograph No. 20, Percutaneous Absorption, ECETOC (European Centre for Ecotoxicology and Toxicology of Chemicals), Brussels, 1993.
19. D. Howes, R. Guy, J. Hadgraft, J. Heylings, U. Hoeck, F. Kemper, H. Maibach, J.-P. Marty, H. Merk, J. Parra, D. Rekkas, I. Rondelli, H. Schaefer, U. Tauer, and N. Verbiese. Methods for assessing percutaneous absorption. The art and recommendations of ECVAM Workshop 13. *Altern. Lab. Anim.* **24**: 81–106 (1996).
20. H. Raabe, R. Curren, S. Ward, and J. Harbell. Report from an in vitro dermal absorption assay workshop, 2005 *In Vitro Percutaneous Absorption Expert Users Workshop*, Gaithersburg, USA, 2005.
21. S. T. K. Narishetty and R. Panchagnula. Transdermal delivery system for zidovudine: In vitro, ex vivo and in vivo evaluation. *Biopharm. Drug Dispos.* **25**: 9–20 (2004).
22. R. P. Moody, B. Nadeau, and I. Chu. In vitro dermal absorption of pesticides: VI. In vivo and in vitro comparison of the organochlorine insecticide ddt in rat, guinea pig, pig, human and tissue-cultured skin. *Toxicol. In vitro* **8**: 1225–1232 (1994).
23. X. Z. Yu, X. P. Jin, L. Yin, G. Z. Shen, H. F. Lin, and Y. L. Wang. Influence of in vitro methods, receptor fluids on percutaneous absorption and validation of a novel in vitro method. *Biomed. Environ. Sci.* **7**: 248–258 (1994).
24. R. C. Scott, P. L. Batten, H. M. Clowes, B. K. Jones, and J. D. Ramsey. Further validation of an in vitro method to reduce the need for in vivo studies for measuring the absorption of chemicals through rat skin. *Fundam. Appl. Toxicol.* **19**: 484–492 (1992).
25. W. P. Adams and G. J. P. Singh. Guidance: Topical dermatology corticosteroids: In vivo bioequivalents, Division of Bioequivalence, Office of Generic Drugs, Food and Drug Administration, 1995.

26. E. W. Smith, J. M. Haigh, and R. B. Walker. Analysis of chromameter results obtained from corticosteroid-induced skin blanching I: Manipulation of data. *Pharm. Res.* **15**: 280–285 (1998).
27. F. P. Schwarb, E. W. Smith, J. M. Haigh, and C. Surber. Analysis of chromameter results obtained from corticosteroid-induced skin blanching assay: Comparison of visual and chromameter data. *Eur. J. Pharm. Biopharm.* **47**: 261–267 (1999).
28. H. M. Klimisch and G. Chandra. Use of Fourier transform infrared spectroscopy with attenuated total reflectance for in vivo quantitation of polydimethylsiloxanes on human skin. *J. Soc. Cosmet. Chem. Jpn.* **37**: 73–87 (1986).
29. C. Curdy, A. Naik, Y. N. Kalia, I. Alberti, and R. H. Guy. Non-invasive assessment of the effect of formulation excipients on stratum corneum barrier function in vivo. *Int. J. Pharm.* **271**: 251–256 (2004).
30. M. B. Reddy, A. L. Stinchcomb, R. H. Guy, and A. L. Bunge. Determining dermal absorption parameters *in vivo* from tape strip data. *Pharm. Res.* **19**: 292–298 (2002).
31. V. H. W. Mak, R. O. Potts, and R. H. Guy. Oleic acid concentration and effect in human stratum corneum: Non-invasive determination by attenuated total reflectance infrared spectroscopy in vivo. *J. Control. Release* **12**: 67–75 (1990).
32. V. H. W. Mak, R. O. Potts, and R. H. Guy. Percutaneous penetration enhancement in vivo measured by attenuated total reflectance infrared spectroscopy. *Pharm. Res.* **7**: 835–841 (1990).
33. L. K. Pershing, J. L. Nelson, J. L. Corlett, S. P. Shrivastava, D. B. Hare, and V. P. Shah. Assessment of dermatopharmacokinetic approach in the bioequivalence determination of topical tretinoin gel products. *J. Am. Acad. Dermatol.* **48**: 740–751 (2003).
34. V. P. Shah. IV-IVC for topically applied preparations—A critical evaluation. *Eur. J. Pharm. Biopharm.* **60**: 309–314 (2005).
35. D. McCleverty, R. Lyons, and B. Henry. Microdialysis sampling and the clinical determination of topical dermal bioequivalence. *Int. J. Pharm.* **308**: 1–7 (2006).
36. F. Muhammad and J. E. Riviere. In vivo models. In J. E. Riviere (ed.), *Dermal Absorption in Toxicology and Pharmacology*, CRC Press, Taylor & Francis Group, Raleigh, North Carolina, 2006, pp. 49–70.
37. M. I. Davies. A review of microdialysis sampling for pharmacokinetic applications. *Anal. Chim. Acta* **379**: 227–249 (1999).
38. J. Kehr. A survey on quantitative microdialysis: Theoretical models and practical applications. *J. Neurosci. Methods* **48**: 251–261 (1993).
39. M. Kreilgaard. Assessment of cutaneous drug delivery using microdialysis. *Adv. Drug Deliv. Rev.* **54**: S99–S121 (2002).
40. K. R. Brain, K. A. Walters, and A. C. Watkinson. Methods for studying percutaneous absorption. In K. A. Walters (ed.), *Dermatological and Transdermal Formulations*, Vol. 119, Drugs and the Pharmaceutical Sciences, Marcel Dekker, Inc., New York, 2002, pp. 197–269.
41. F.-X. Mathy, A.-R. Denet, B. Vroman, P. Clarys, A. Barel, R. Verbeeck, and V. Pr at. In vivo tolerance assessment of skin after insertion of subcutaneous and cutaneous microdialysis probes in the rat. *Skin Pharmacol. Physiol.* **16**: 18–27 (2003).
42. F.-X. Mathy, C. Lombry, R. Verbeeck, and V. Pr at. Study of percutaneous penetration of flubiprofen by cutaneous and subcutaneous microdialysis after iontophoretic delivery in rat. *J. Pharm. Sci.* **94**: 144–152 (2005).
43. S. Bielecka-Grzela and A. Klimowicz. Application of cutaneous microdialysis to evaluate metronidazole and its main metabolite concentrations in the skin after a single oral dose. *J. Clin. Pharm. Ther.* **28**: 465–469 (2003).

44. L. Simonsen, A. Jorgensen, E. Benfeldt, and L. Groth. Differentiated in vivo skin penetration of salicylic compounds in hairless rats measured by cutaneous microdialysis. *Eur. J. Pharm. Sci.* **21**: 379–388 (2004).
45. N. Leveque, S. Makki, J. Hadgraft, and P. Humbert. Comparison of Franz cells and microdialysis for assessing salicylic acid penetration through human skin. *Int. J. Pharm.* **269**: 323–328 (2004).
46. D. J. Kopacz, C. M. Bernards, H. W. Allen, C. Landau, P. Nandy, D. Wu, and P. G. Lacouture. A model to evaluate the pharmacokinetic and pharmacodynamic variables of extended-release products using in vivo tissue microdialysis in humans: Bupivacaine-loaded microcapsules. *Anaesth. Analg.* **97**: 124–131 (2003).
47. M. Stahl, R. Bouw, A. Jackson, and V. Pay. Human microdialysis. *Curr. Pharm. Biotechnol.* **3**: 165–178 (2002).
48. W. F. Elmquist and R. J. Sawchuck. Application of microdialysis in pharmacokinetic studies. *Pharm. Res.* **14**: 267–288 (1997).
49. J. E. Riviere. Perfused skin models. In J. E. Riviere (ed.), *Dermal Absorption Models in Toxicology and Pharmacology*, Taylor & Francis Group, Boca Raton, 2006.
50. J. E. Riviere, K. F. Bowman, and N. A. Monteiro-Riviere. On the definition of viability in isolated perfused skin preparations. *Br. J. Dermatol.* **116**: 739–741 (1987).
51. J. G. M. VanRooij, E. Vinke, J. De Lange, P. L. B. Bruijnzeel, M. M. Bodelier-Bade, J. Noordhoek, and F. J. Jongeneelen. Dermal absorption of polycyclic aromatic hydrocarbons in the blood-perfused pig ear. *J. Appl. Toxicol.* **15**: 193–200 (1995).
52. L. Celesti, C. Murratzu, M. Valoti, G. Sgaragli, and P. Corti. The single-pass perfused rabbit ear as a model for studying percutaneous absorption of clonazepam. I. General characteristics. *Methods Find. Exp. Clin. Pharmacol.* **14**: 701–709 (1992).
53. J. H. Barker, F. Hammersen, I. Bondar, T. J. Galla, M. D. Menger, W. Gross, and K. Messmer. Direct monitoring of nutritive blood flow in a failing skin flap: The hairless mouse ear skin-flap model. *Plast. Reconstr. Surg.* **84**: 303–313 (1989).
54. N. Sekkat, Y. N. Kalia, and R. Guy. Porcine ear skin as a model for the assessment of transdermal drug delivery to premature neonates. *Pharm. Res.* **21**: 1390–1397 (2004).
55. M. Kietzmann, W. Loscher, D. Arens, P. Maass, and D. Lubach. The isolated perfused bovine udder as an in vitro model of percutaneous drug absorption of dexamethasone, benzoyl peroxide, and etofenamate. *J. Pharm. Toxicol. Meth.* **30**: 75–84 (1993).
56. S. M. Wagner, A. C. Nogueira, M. Paul, D. Heydeck, S. Klug, and B. Christ. The isolated normothermic hemoperfused porcine forelimb as a test system for transdermal absorption studies. *J. Artif. Organs* **6**: 183–191 (2003).
57. J. E. Riviere, K. F. Bowman, and N. A. Monteiro-Riviere. The isolated perfused porcine skin flap (IPPSF). I. A novel in vitro model for percutaneous absorption and cutaneous toxicology studies. *Fundam. Appl. Toxicol.* **7**: 444–453 (1986).
58. R. C. Wester, J. L. Melendres, and H. I. Maibach. In vivo percutaneous absorption of acetochlor in the rhesus monkey: Dose-response and exposure risk assessment. *Food Chem. Toxicol.* **34**: 979–983 (1996).
59. A. M. Ehinger and M. Kietzmann. Studying the tissue distribution of antibiotics in the udder—Comparison of the situation in vivo with the isolated perfused bovine udder. *Deutsche Tierärztliche Wochenschrift* **108**: 195–200 (2001).
60. W. F. Pittermann and M. Kietzmann. Bovine udder skin (BUS): Testing of skin compatibility and skin protection. *ALTEX* **23**: 65–71 (2006).

61. S. A. Hotchkiss, P. Hewitt, J. Caldwell, W. L. Chen, and R. R. Rowe. Percutaneous absorption of nicotinic acid, phenol, benzoic acid and triclopyr butoxyethyl ester through rat and human skin in vitro: Further validation of an in vitro model by comparison with in vivo data. *Food Chem. Toxicol.* **30**: 891–899 (1992).
62. S. A. Hotchkiss, M. A. Chidgey, S. Rose, and J. Caldwell. Percutaneous absorption of benzyl acetate through rat skin in vitro. I. Validation of an in vitro model against in vivo data. *Food Chem. Toxicol.* **28**: 443–447 (1990).
63. R. H. Larsen, F. Nielsen, J. A. Sorensen, and J. B. Nielsen. Dermal penetration of fentanyl: Inter- and intraindividual variations. *Pharmacol. Toxicol.* **93**: 244–248 (2003).
64. H. Wagner, K. H. Kostka, C. M. Lehr, and U. F. Schaefer. Drug distribution in human skin using two different in vitro test systems: Comparison with in vivo data. *Pharm. Res.* **17**: 1475–1481 (2000).
65. F. Netzlaff, K.-H. Kostka, C.-M. Lehr, and U. F. Schaefer. TEWL measurements as a routine method for evaluating the integrity of epidermis sheets in static Franz type diffusion cells in vitro. Limitations shown by transport data testing. *Eur. J. Pharm. Biopharm.* **63**: 44–50 (2006).
66. J. M. Haigh and E. W. Smith. The selection and use of natural and synthetic membranes for in vitro diffusion experiments. *Eur. J. Pharm. Sci.* **2**: 311–330 (1994).
67. R. C. Scott, M. A. Corrigan, F. Smith, and H. Mason. The influence of skin structure on permeability: An intersite and interspecies comparison with hydrophilic penetrants. *J. Invest. Dermatol.* **96**: 921–925 (1991).
68. P. Liu, A. S. Nightingale, and T. Kurihara-Bergstrom. Variation of human skin permeation in vitro: Ionic vs. neutral compounds. *Int. J. Pharm.* **90**: 171–176 (1993).
69. P. W. Wertz, D. C. Swartzendruber, and C. A. Squier. Regional variation in the structure and permeability of oral mucosa and skin. *Adv. Drug Deliv. Rev.* **12**: 1–12 (1993).
70. J. C. Tsai, C. Y. Lin, H. M. Sheu, Y. L. Lo, and Y. H. Huang. Noninvasive characterization of regional variation in drug transport into human stratum corneum in vivo. *Pharm. Res.* **20**: 632–638 (2003).
71. M. A. Lampe, A. L. Burlingame, and J. A. Whitney. Human stratum corneum lipids: Characterization and regional variations. *J. Lipid Res.* **24**: 120–130 (1983).
72. A. P. M. Lavrijsen, J. A. Bouwstra, G. S. Gooris, A. Weerheim, H. E. Bodde, and M. Ponc. Reduced skin barrier function parallels abnormal stratum corneum lipid organization in patients with lamellar ichthyosis. *J. Invest. Dermatol.* **105**: 619–624 (1995).
73. G. S. K. Pilgram, D. C. J. Vissers, H. Van der Meulen, S. Pavel, S. P. M. Lavrijsen, J. A. Bouwstra, and H. K. Koerten. Aberrant lipid organization in stratum corneum of patients with atopic dermatitis and lamellar ichthyosis. *J. Invest. Dermatol.* **117**: 710–717 (2001).
74. P. M. Elias, E. R. Cooper, A. Korc, and B. E. Brown. Percutaneous transport in relation to stratum corneum structure and lipid composition. *J. Invest. Dermatol.* **76**: 297–301 (1981).
75. J. Sandby-Møller, T. Poulsen, and H. C. Wulf. Epidermal Thickness at different body sites: Relationship to age, gender, pigmentation, blood content, skin type and smoking habits. *Acta Derm. Venereol.* **83**: 410–413 (2003).
76. D. Southwell, B. W. Barry, and R. Woodford. Variations in permeability of human skin within and between specimens. *Int. J. Pharm.* **18**: 299–309 (1984).
77. J. Swarbrick, G. Lee, and J. Brom. Drug permeation through human skin: I. Effect of storage conditions of skin. *J. Invest. Dermatol.* **78**: 63–66 (1982).
78. S. M. Harrison, B. W. Barry, and P. H. Dugard. Effects of freezing on human skin permeability. *J. Pharm. Pharmacol.* **36**: 261–262 (1984).

79. U. Schaefer, M. Szayna, W. P. Kuhn, and H. Loth. NMR-microscopy of human skin in vivo and in vitro. *Proc. Control Release Soc.* 626–627 (1995).
80. R. C. Scott, M. Walker, and P. H. Dugard. In vitro percutaneous absorption experiments: A technique for the production of intact epidermal membranes from rat skin. *J. Soc. Cosmet. Chem. Jpn.* **37**: 35–41 (1986).
81. S. E. Cross, B. M. Magnusson, G. Winckle, Y. Anissimov, and M. S. Roberts. Determination of the effect of lipophilicity on the in vitro permeability and tissue reservoir characteristics of topically applied solutes in human skin layers. *J. Invest. Dermatol.* **120**: 759–764 (2003).
82. K. R. Brain, K. A. Walters, and A. Watkinson. Investigation of skin permeation in vitro. M. Roberts and K. A. Walters (eds.), *Dermal Absorption and Toxicity Assessment*. Vol. 91, Marcel Dekker, New York: 161–187 (1998).
83. A. M. Kligman and E. Christophers. Preparation of isolated sheets of human stratum corneum. *Arch. Dermatol.* **88**: 702–705 (1963).
84. H. Durrheim, G. L. Flynn, W. I. Higuchi, and C. R. Behl. Permeation of hairless mouse skin. I: Experimental methods and comparison with human epidermal permeation by alkanols. *J. Pharm. Sci.* **69**: 781–786 (1980).
85. I. H. Pitman and S. J. Rostas. A comparison of frozen and reconstituted cattle and human skin as barriers to drug penetration. *J. Pharm. Sci.* **71**: 427–430 (1982).
86. G. Lee and P. Parlicharla. An examination of excised skin tissues used for in vitro membrane permeation studies. *Pharm. Res.* **3**: 356–359 (1986).
87. P. Agache, J. P. Boyer, and R. Laurent. Biomechanical properties and microscopic morphology of human stratum corneum incubated on a wet pad in vitro. *Arch. Dermatol. Res.* **246**: 271–283 (1973).
88. P. J. Frosch and A. M. Kligman. Rapid blister formation in human skin with ammonium hydroxide. *Br. J. Dermatol.* **96**: 461–473 (1977).
89. T. Shukuwa, A. M. Kligman, and T. J. Stoudemayer. A new model for assessing the damaging effects of soaps and surfactants on human stratum corneum. *Acta Derm. Venereol.* **77**: 29–34 (1997).
90. G. L. Flynn, H. Durrheim, and W. I. Higuchi. Permeation of hairless mouse skin II: Membrane sectioning techniques and influence on alkanol permeabilities. *J. Pharm. Sci.* **70**: 52–56 (1981).
91. Y. N. Kalia, F. Pirot, and R. H. Guy. Homogeneous transport in a heterogeneous membrane: Water diffusion across human stratum corneum in vivo. *Biophys. J.* **71**: 2692–2700 (1996).
92. F. Netzlaff, C.-M. Lehr, P. W. Wertz, and U. F. Schaefer. The human epidermis models EpiSkin[®], SkinEthic[®] and EpiDerm[®]: An evaluation of morphology and their suitability for testing phototoxicity, irritancy, corrosivity, and substance transport. *Eur. J. Pharm. Biopharm.* **60**: 167–178 (2005).
93. M. Schaefer-Korting, U. Bock, A. O. Gamer, A. Haberland, E. Haltner-Ukomadu, M. Kaca, M. Kietzmann, H. C. Korting, H.-U. Kraechter, C. M. Lehr, M. Liebsch, A. Mehling, F. Netzlaff, F. Niedorf, M. K. Ruebbelke, U. F. Schaefer, E. Schmidt, S. Schreiber, K.-R. Schroeder, H. Spielmann, and A. Vuia. Reconstructed human epidermis for skin absorption testing: Results of the German prevalidation study. *Altern. Lab. Anim.* **34**: 283–294 (2006).
94. F. P. Schmoock, J. G. Meingassner, and A. Billich. Comparison of human skin or epidermis models with human and animal skin in in-vitro percutaneous absorption. *Int. J. Pharm.* **215**: 51–56 (2001).
95. M. Ruet Rossignol. The 7th Amendment to the Cosmetics Directive. *Altern. Lab. Anim.* **33**(Suppl. 1): 19–20 (2005).
96. R. Hermes and K. H. Bauer. Preparation and characterization of amphiphilic membranes with lyotropic mesophases for simulation of skin permeation resistance. *Pharmazie* **50**: 481–486 (1995).

97. P. R. Rege, V. D. Vilivalam, and C. C. Collins. Development in release testing of topical dosage forms: Use of the Enhancer Cell(TM) with automated sampling. *J. Pharm. Biomed. Anal.* **17**: 1225–1233 (1998).
98. C. B. Lalor, G. L. Flynn, and N. Weiner. Formulation factors affecting release of drug from topical formulations. I. Effect of emulsion type upon in vitro delivery of ethyl p-aminobenzoate. *J. Pharm. Sci.* **83**: 1525–1528 (1994).
99. H. Loth and A. Holla-Benninger. Investigation of drug release from ointments. *Pharm. Ind.* **40**: 256–261 (1978).
100. H. Loth, A. Holla-Benninger, and M. Hailer. Studies of the release of active agents from ointments. II. Effects of the quality of water-free ointment bases on the release of active agents from suspension ointments. *Pharm. Ind.* **41**: 789–796 (1979).
101. Y. Yamaguchi, T. Usami, H. Natsume, T. Aoyagi, Y. Nagase, K. Sugibayashi, and Y. Morimoto. Evaluation of skin permeability of drugs by newly prepared polymer membranes. *Chem. Pharm. Bull.* **45**: 537–541 (1997).
102. T. Hatanaka, M. Inuma, K. Sugibayashi, and Y. Morimoto. Prediction of skin permeability of drugs. II. Development of composite membrane as a skin alternative. *Int. J. Pharm.* **79**: 21–28 (1992).
103. T. Hatanaka, M. Inuma, K. Sugibayashi, and Y. Morimoto. Prediction of skin permeability of drugs. I. Comparison with artificial membrane. *Chem. Pharm. Bull.* **38**: 3452–3459 (1990).
104. S. Geinoz, S. Rey, G. Boss, A. L. Bunge, R. H. Guy, P.-A. Carrupt, M. Reist, and B. Testa. Quantitative structure—Permeation relationships for solute transport across silicone membranes. *Pharm. Res.* **19**: 1622–1629 (2002).
105. S. E. Cross, W. J. Pugh, J. Hadgraft, and M. S. Roberts. Probing the effect of vehicles on topical delivery: Understanding the basic relationship between solvent and solute penetration using silicone membranes. *Pharm. Res.* **18**: 999–1005 (2001).
106. S. Proniuk, S. E. Dixon, and J. Blanchard. Investigation of the utility of an in vitro release test for optimizing semisolid dosage forms. *Pharm. Dev. Technol.* **6**: 469–476 (2001).
107. E. Jaeckle. Stratum Corneum analoge Lipidmischungen als Diffusionsmedien, ihre Eigenschaften und deren Beeinflussung durch Salbengrundlagen, Saarland university, Saarbrücken, 1996.
108. T. Kai, T. Isami, Y. Kurosaki, T. Nakayama, and T. Kimura. Keratinized epithelial transport of beta-blocking agents. II. Evaluation of barrier property of stratum corneum by using model lipid systems. *Biol. Pharm. Bull.* **16**: 284–287 (1993).
109. J. A. Bouwstra, G. S. Gooris, K. Cheng, A. Weerheim, W. Bras, and M. Ponec. Phase behavior of isolated skin lipids. *J. Lipid Res.* **37**: 999–1011 (1996).
110. M. W. De Jager, G. S. Gooris, I. P. Dolbnya, W. Bras, M. Ponec, and J. A. Bouwstra. The phase behaviour of skin lipid mixtures based on synthetic ceramides. *Chem. Phys. Lipids* **124**: 123–134 (2003).
111. M. W. de Jager, G. S. Gooris, I. P. Dolbnya, W. Bras, M. Ponec, and J. A. Bouwstra. Novel lipid mixtures based on synthetic ceramides reproduce the unique stratum corneum lipid organization. *J. Lipid Res.* **45**: 923–932 (2004).
112. M. De Jager, G. Gooris, M. Ponec, and J. Bouwstra. Acylceramide head group architecture affects lipid organization in synthetic ceramide mixtures. *J. Invest. Dermatol.* **123**: 911–916 (2004).
113. M. W. De Jager, G. S. Gooris, I. P. Dolbnya, M. Ponec, and J. A. Bouwstra. Modelling the stratum corneum lipid organisation with synthetic lipid mixtures: The importance of synthetic ceramide composition. *Biochim. Biophys. Acta Bio-membr.* **1664**: 132–140 (2004).

114. M. W. De Jager, G. S. Gooris, M. Ponec, and J. A. Bouwstra. Lipid mixtures prepared with well-defined synthetic ceramides closely mimic the unique stratum corneum lipid phase behavior. *J. Lipid Res.* **46**: 2649–2656 (2005).
115. J. Bouwstra, G. Pilgram, G. Gooris, H. Koerten, and M. Ponec. New aspects of the skin barrier organization. *Skin Pharmacol. Appl. Skin Physiol.* **14**: 52–62 (2001).
116. A. C. Rowat, N. Kitson, and J. L. Thewalt. Interactions of oleic acid and model stratum corneum membranes as seen by ²H NMR. *Int. J. Pharm.* **307**: 225–231 (2006).
117. R. Lieckfeldt, J. Villalain, J.-C. Gomez-Fernandez, and G. Lee. Influence of oleic acid on the structure of a mixture of hydrated model stratum corneum fatty acids and their soaps. *Colloids Surf.* **90**: 225–234 (1994).
118. M. A. Kiselev, N. Y. Ryabova, A. M. Balagurov, S. Dante, T. Hauss, J. Zbytovska, S. Wartewig, and R. H. H. Neubert. New insights into the structure and hydration of a stratum corneum lipid model membrane by neutron diffraction. *Eur. Biophys. J.* **34**: 1030–1040 (2005).
119. R. Lieckfeldt, J. Villalain, J.-C. Gomez-Fernandez, and G. Lee. Apparent pK(a) of the fatty acids within ordered mixtures of model human stratum corneum lipids. *Pharm. Res.* **12**: 1614–1617 (1995).
120. R. Lange-Lieckfeldt and G. Lee. Use of a model lipid matrix to demonstrate the dependence of the stratum corneum's barrier properties on its internal geometry. *J. Control. Release* **20**: 183–194 (1992).
121. R. Lieckfeldt, J. Villalain, J. C. Gomez-Fernandez, and G. Lee. Diffusivity and structural polymorphism in some model stratum corneum lipid systems. *Biochim. Biophys. Acta Biomembr.* **1150**: 182–188 (1993).
122. K. Miyajima, S. Tanikawa, M. Asano, and K. Matsuzaki. Effects of absorption enhancers and lipid composition on drug permeability through the model membrane using stratum corneum lipids. *Chem. Pharm. Bull.* **42**: 1345–1347 (1994).
123. B. Mueller, Y. G. Anissimov, and M. S. Roberts. Unexpected clobetasol propionate profile in human stratum corneum after topical application in vitro. *Pharm. Res.* **20**: 1835–1837 (2003).
124. F. Pirot, Y. N. Kalia, A. L. Stinchcomb, G. Keating, A. Bunge, and R. H. Guy. Characterization of the permeability barrier of human skin in vivo. *Proc. Natl. Acad. Sci. USA* **94**: 1562–1567 (1997).
125. J.-C. Tsai, M. J. Cappel, N. D. Weiner, G. L. Flynn, and J. Ferry. Solvent effects on the harvesting of stratum corneum from hairless mouse skin through adhesive tape stripping in vitro. *Int. J. Pharm.* **68**: 127–133 (1991).
126. F. Dreher, A. Arens, J. J. Hostýnek, S. Mudumba, J. Ademola, and H. I. Maibach. Colorimetric method for quantifying human stratum corneum removed by adhesive-tape-stripping. *Acta Derm. Venereol.* **78**: 186–189 (1998).
127. N. Higo, A. Naik, D. B. Bommaman, R. O. Potts, and R. H. Guy. Validation of reflectance infrared spectroscopy as a quantitative method to measure percutaneous absorption in vivo. *Pharm. Res.* **10**: 1500–1506 (1993).
128. H.-J. Weigmann, J. Lademann, H. Meffert, H. Schaefer, and W. Sterry. Determination of the horny layer profile by tape stripping in combination with optical spectroscopy in the visible range as a prerequisite to quantify percutaneous absorption. *Skin Pharmacol. Appl. Skin Physiol.* **12**: 34–45 (1999).
129. F. Dreher, B. S. Modjtahedi, S. P. Modjtahedi, and H. I. Maibach. Quantification of stratum corneum removal by adhesive tape stripping by total protein assay in 96-well microplates. *Skin Res. Technol.* **11**: 97–101 (2005).
130. B. Magnusson and A. M. Kligman. The identification of contact allergens by animal assay. The guinea pig maximization test. *J. Invest. Dermatol.* **52**: 268–276 (1969).
131. L. V. Buehler. Occlusive patch method for skin sensitization in guinea pigs: The Buehler method. *Food Chem. Toxicol.* **32**: 97–101 (1994).

132. S. Frankild, A. Volund, J. E. Wahlberg, and K. E. Andersen. Comparison of the sensitivities of the Buehler test and the guinea pig maximization test for predictive testing of contact allergy. *Acta Derm. Venereol.* **80**: 256–262 (2000).
133. D. A. Basketter, G. F. Gerberick, I. Kimber, and S. E. Loveless. The local lymph node assay: A viable alternative to currently accepted skin sensitization tests. *Food Chem. Toxicol.* **34**: 985–997 (1996).
134. D. Basketter, S. Casati, G. F. Gerberick, P. Griem, B. Philips, and A. Worth. Skin sensitisation. *Altern. Lab. Anim.* **33**(Suppl. 1): 83–103 (2005).
135. Alternatives to Animal testing, Colipa, <http://www.colipa.com/site/index.cfm?SID=15588&OBJ=15793>.
136. D. A. Basketter, G. F. Gerberick, and I. Kimber. Strategies for identifying false positive responses in predictive skin sensitization tests. *Food Chem. Toxicol.* **36**: 327–333 (1998).
137. M. Chamberlain and D. A. Basketter. The local lymph node assay: Status of validation. *Food Chem. Toxicol.* **34**: 999–1002 (1996).
138. D. A. Basketter, L. Blaikie, R. J. Dearman, I. Kimber, C. A. Ryan, G. F. Gerberick, P. Harvey, P. Evans, I. R. White, and R. J. G. Rycroft. Use of the local lymph node assay for the estimation of relative contact allergenic potency. *Contact Dermatitis* **42**: 344–348 (2000).
139. A. Suda, M. Yamashita, M. Tabei, K. Taguchi, H.-W. Vohr, N. Tsutsui, R. Suzuki, K. Kikuchi, K. Sakaguchi, K. Mochizuki, and K. Nakamura. Local lymph node assay with non-radioisotope alternative endpoints. *J. Toxicol. Sci.* **27**: 205–218 (2002).
140. G. Ehling, M. Hecht, A. Heusener, J. Huesler, A. O. Gamer, H. Van Loveren, T. Maurer, K. Riecke, L. Ullmann, P. Ulrich, R. Vandebriel, and H.-W. Vohr. An European inter-laboratory validation of alternative endpoints of the murine local lymph node assay: First round. *Toxicology* **212**: 60–68 (2005).
141. J. H. Fentem, G. E. B. Archer, M. Balls, P. A. Botham, R. D. Curren, L. K. Earl, D. J. Esdaile, H.-G. Holzhuetter, and M. Liebsch. The ECVAM international validation study on in vitro tests for skin corrosivity. II. Results and evaluation by the management team. *Toxicol. In vitro* **12**: 483–524 (1998).
142. J. H. Fentem and P. A. Botham. Update on the validation and regulatory acceptance of alternative tests for skin corrosion and irritation. *Altern. Lab. Anim.* **32**: 683–688 (2004).
143. OECD. Test guideline 430: In Vitro Skin Corrosion: Transcutaneous Electrical Resistance, OECD, Paris, 2004.
144. OECD. Test guideline 431: In Vitro Skin Corrosion: Human Skin Model Test, OECD, Paris, 2004.
145. ECVAM. News and Views. Statement on the scientific validity of the rat skin transcutaneous electrical resistance (TER) test (an in vitro test for skin corrosivity). *ATLA* **26**: 275–280 (1998).
146. I. L. A. Boxman, P. J. Hensbergen, R. C. Van Der Schors, D. P. Bruynzeel, C. P. Tensen, and M. Ponc. Proteomic analysis of skin irritation reveals the induction of HSP27 by sodium lauryl sulphate in human skin. *Br. J. Dermatol.* **146**: 777–785 (2002).
147. C.-M. Huang, H. Xu, C.-C. Wang, and C. A. Elmets. Proteomic characterization of skin and epidermis in response to environmental agents. *Expert Rev. Proteomics* **2**: 809–820 (2005).
148. A. Barlow, R. A. Hirst, M. A. Pemeberton, T. J. Hall, P. A. Botham, and G. J. A. Oliver. Refinement of an in vitro test for the identification of skin corrosive chemicals. *Toxicol. Methods* **1**: 106–115 (1991).
149. P. A. Botham, T. J. Hall, R. Dennett, J. C. McCall, D. A. Basketter, E. Whittle, M. Cheeseman, D. J. Esdaile, and J. Gardner. The skin corrosivity test in vitro. Results of an inter-laboratory trial. *Toxicol. In vitro* **6**: 191–194 (1992).

150. A. P. Worth, J. H. Fentem, M. Balls, P. A. Botham, R. D. Gurren, L. K. Earl, D. J. Esdaile, and M. Liebsch. An evaluation of the proposed OECD testing strategy for skin corrosion. *Altern. Lab. Anim.* **26**: 709–720 (1998).
151. ECVAM. ECVAM News & Views. *Altern. Lab. Anim.* **26**: 275–280 (1998).
152. Anon. Commission Directive 2000/33/EC of 25 April 2000 adapting to technical progress for the 27th time Council Directive 67/548 EEC on the classification, packaging and labelling of dangerous substances. *Off. J. Eur. Communities* **L136**: 90–107 (2000).
153. Anon. *14th Meeting of the OECD National Coordinators for the Test Guidelines Programme, Paris 29–31 May 2002 for the approval of Draft Test Guidelines*, Paris, 2002.
154. H. Kandárová, M. Liebsch, E. Schmidt, E. Genschow, D. Traue, H. Spielmann, K. Meyer, C. Steinhoff, C. Tornier, B. De Wever, and M. Rosdy. Assessment of the skin irritation potential of chemicals by using the SkinEthic reconstructed human epidermal model and the common skin irritation protocol evaluated in the ECVAM skin irritation validation study. *Altern. Lab. Anim.* **34**: 393–406 (2006).
155. H. Kandárová, M. Liebsch, H. Spielmann, E. Genschow, E. Schmidt, D. Traue, R. Guest, A. Whittingham, N. Warren, A. O. Gamer, M. Remmele, T. Kaufmann, E. Wittmer, B. De Wever, and M. Rosdy. Assessment of the human epidermis model SkinEthic RHE for in vitro skin corrosion testing of chemicals according to new OECD TG 431. *Toxicol. In vitro* **20**: 547–559 (2006).
156. E. Borenfreund and J. A. Puerner. Toxicity determined in vitro by morphological alterations and neutral red absorption. *Toxicol. Lett.* **24**: 119–124 (1985).
157. H. Spielmann, M. Balls, J. Dupuis, W. J. W. Pape, O. De Silva, H.-G. Holzhuetter, F. Gerberick, M. Liebsch, W. W. Lovell, and U. Pfannenbecker. A study on UV filter chemicals from annex VII of European Union Directive 76/768/EEC, in the in vitro 3T3 NRU phototoxicity test. *Altern. Lab. Anim.* **26**: 679–708 (1998).
158. H.-G. Holzhütter. A general measure of in vitro phototoxicity derived from pairs of dose-response curves and its use for predicting the in vivo phototoxicity of chemicals. *ATLA* **25**: 445–462 (1997).
159. F.-X. Bernard, C. Barrault, A. Deguercy, B. De Wever, and M. Rosdy. Development of a highly sensitive in vitro phototoxicity assay using the SkinEthic(TM) reconstructed human epidermis. *Cell Biol. Toxicol.* **16**: 391–400 (2000).
160. M. Liebsch, C. Barrabas, D. Traue, and H. Spielmann. Development of a new in vitro test for dermal phototoxicity using a model of reconstituted human epidermis. *ALTEX* **14**: 165–174 (1997).
161. P. Portes, M. J. Pygmalion, E. Popovic, M. Cottin, and M. Mariani. Use of human reconstituted epidermis Episkin(R) for assessment of weak phototoxic potential of chemical compounds. *Photodermatol. Photoimmunol. Photomed.* **18**: 96–102 (2002).

2

Models of the Small Intestine

Brendan Griffin and Caitriona O’Driscoll

Abstract Predicting the extent of oral drug absorption can be an important aspect to lead candidate selection during the drug development process. Drug absorption from the intestine is the culmination of a number of steps, including drug dissolution in the gastrointestinal tract (GIT), uptake through the intestinal mucosa, followed by delivery into the systemic circulation. In order to predict the in vivo performance of a drug after oral administration, it is essential that the physiochemical and physiological factors affecting drug absorption are established. The Biopharmaceutical Classification System (BCS) has identified that drug solubility and intestinal permeability are the key biopharmaceutical characteristics impacting on drug uptake from the GIT [3]. The current chapter outlines the theoretical basis for the relationship between intestinal permeability estimates (P_{eff}) and the fraction of dose absorbed in humans (f_a), and the intestinal perfusion models used for determination of intestinal permeability. In addition, a number of alternative in situ/in vivo intestinal absorption models, which facilitate a more mechanistic evaluation of the impact of intestinal versus hepatic first-pass extraction on limiting the oral bioavailability of drugs, are described.

Keywords: Oral absorption; Bioavailability; Models of small intestine; Intestinal permeability; Intestinal perfusion techniques; Intestinal versus hepatic first-pass metabolism

Abbreviations

ABL	Aqueous boundary layer
AP	Absorption potential
BCS	Biopharmaceutics Classification System
CAT	Compartmental absorption and transit model
D_{aq}	Aqueous diffusion coefficient
GIT	Gastrointestinal tract
IVAP	Intestinal and vascular access port
$\log P$	Octanol/water partition coefficient
P_{app}	Apparent permeability coefficient
P_{aq}	ABL permeability

P_{eff}	Effective permeability coefficient
P-gp	P-glycoprotein
P_m	Membrane permeability
PSA	Polar surface area
P_{trans}	Apparent trans-cellular permeability

2.1. Introduction

Oral drug administration is the most common and convenient route for chronic drug therapy [1]. Bioavailability is the term used to define both the extent and the rate at which unchanged drug proceeds from the site of administration to the site of measurement within the body [2]. Oral bioavailability is directly related to the kinetic processes whereby drug passes from the gastrointestinal tract (GIT) through the apical membrane of the epithelial cells (i.e. enterocytes), through the enterocyte cells into pre-hepatic blood vessels, which collect in the portal vein prior to passage through the liver, before reaching the systemic circulation (Figure 2.1). The bioavailability of a drug compound after oral administration is described by the following general relationship (Eq. 2.1):

$$F = f_a \times f_g \times f_h \quad (2.1)$$

where f_a is the fraction of active absorbed from the intestine; f_g is the fraction of intact drug that escapes intestinally mediated metabolism; and f_h is the fraction that escapes hepatically mediated first-pass metabolism. f_g and f_h may be further defined in terms of the extraction ratios of the intestinal-based metabolism (E_g) and hepatic-based metabolism (E_h):

$$F = f_a(1 - E_g)(1 - E_h) \quad (2.2)$$

Understanding the factors influencing drug absorption and in particular predicting these values on the basis of pre-clinical in vitro and in situ experiments remains crucial to bringing safe and effective drugs to the market [3].

The advent of combinatorial synthesis and high throughput screening has resulted in the rapid identification of potential lead candidates with optimum pharmacodynamic properties. Coincident with the increasing use of these technologies, however, has been the greater need for methods that can rapidly and efficiently assess pharmacokinetic properties of lead candidates. In particular, in terms of developing an oral dosage form, the ability to screen candidates for effective bioavailability is paramount. The challenge to balance idealised pharmacodynamic and pharmacokinetic properties is even further complicated by the realisation that attributes which tend to provide optimised drug-receptor binding characteristics tend to result in pharmacokinetic properties that are far from ideal. For example, high molecular weight lipophilic candidates tend to display poor solubility, susceptibility to efflux transporters in the gastrointestinal membrane, and rapid hepatic extraction. Oral formulation of such candidate drugs thus presents considerable challenges to the pharmaceutical scientist. Hence the focus of drug design is not solely on optimising pharmacodynamic activity but also to ensure adequate pharmacokinetic properties (i.e. absorption, distribution, metabolism, and elimination) to enable suitable dosage forms/regimens to be developed.

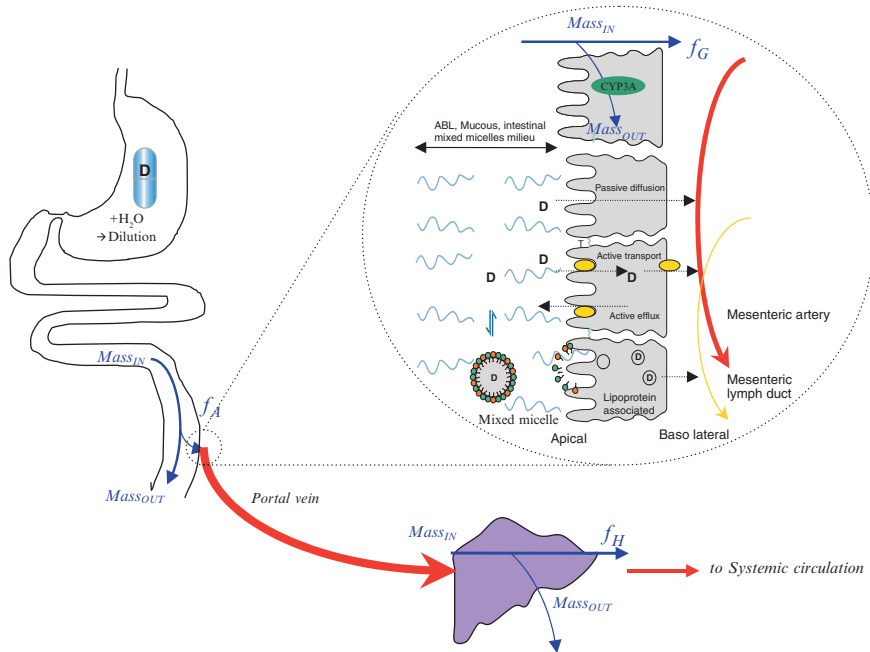


Figure 2.1 Oral drug absorption process from the gastrointestinal tract (GIT). Schematic depicting the three major processes (f_a , f_g , and f_h) affecting absorption of drug from the site of administration to the systemic circulation, that is oral bioavailability. f_a , f_g , and f_h can be estimated from the general relationship provided in Eq. 2.3:

$$f_a, f_g, \text{ or } f_h = \frac{\text{Mass}_{\text{IN}} - \text{Mass}_{\text{OUT}}}{\text{Mass}_{\text{IN}}} \quad (2.3)$$

(See also color insert.)

Two fundamental reasons for developing predictive oral drug delivery models are (a) to make reasonable estimates of drug absorption without the need for human studies and (b) to gain a better understanding of the rate-limiting processes affecting drug absorption so that oral drug delivery strategies can be developed [4]. Absorption is a complex kinetic process that is dependent on numerous physiological, physiochemical, and dosage form factors (Table 2.1). Ho et al. [5] stated that the absorption characteristics of a drug are dictated by (a) the physiochemical properties of the drug and (b) the biophysiochemical properties of the gastrointestinal barrier membrane. These fundamental principles have been extensively explored over the ensuing years, ultimately leading to the establishment of a Biopharmaceutical Classification System (BCS), where drug absorption characteristics are categorised on the basis of solubility and membrane permeability (P_m) characteristics [3]. The development of the BCS and its adoption by regulatory authorities in decisions relating to waivers of *in vivo* bioavailability studies (i.e. biowaivers) has renewed interest in methods for obtaining estimates of drug permeability.

There are a variety of methods available for studying intestinal absorption as will be outlined in this chapter. Given the complexity of the absorption process, each individual model will differ in terms of merits and inherent assumptions. The key advantage of *in situ/in vivo* models will be the intact blood supply and

Table 2.1 Factors influencing gastrointestinal absorption of drugs.

Physiochemical factors of drug substances	Physiological factors of GIT	Dosage form and formulation factors
Solubility	Stomach emptying rate	Dissolution rate
$\log P$	Intestinal motility/flow rate	Disintegration rate
pK_a	Membrane surface area	Drug release mechanisms
H-bonding potential	Intestinal metabolism	Excipient effects
Molecular weight/size	Transport mechanisms	
PSA	Native surfactants	
	Intestinal secretions, e.g. mucous, enzymes	
	Intestinal blood/lymph flow	

GIT: gastrointestinal tract; PSA: polar surface area; $\log P$: octanol/water partition coefficient.

the ability to perform a mechanistic evaluation of the absorption process under controlled and semi-conscious conditions.

2.2. Theoretical Models Describing the Gastrointestinal Absorption of Drugs

2.2.1. Estimating Drug Absorption Trends from Physiochemical Characteristics

Numerous efforts exist to relate the use of physiochemical descriptors of drug molecules to the passive diffusion of drugs through biological membranes and therein predict the extent of absorption from the GIT. The pH partition hypothesis, originally proposed by Overton [6], was devised to predict the extent of absorption of an ionisable drug substrate through a lipoidal membrane on the basis of the pK_a and the pH at the absorption site. The basic premise of this hypothesis is that only the un-ionised form of the drug will diffuse through a lipophilic membrane. While correlations between absorption rates and pK_a were found to be consistent with this theory, deviations, however, are often reported, and this is now generally viewed as an over-simplification of the drug absorption process [7, 8].

Ho et al. [5] presented a theoretical model for gastrointestinal absorption of drugs (Figure 2.2), which described the biomembrane as a series of lipoidal and aqueous pores in parallel.

It was postulated that the aqueous pores are available to all molecular species, both ionic and non-ionic, while the lipoidal pathway is accessible only to un-ionised species. In addition, Ho and co-workers introduced the concept of the aqueous boundary layer (ABL) [9, 10]. The ABL is considered a stagnant water layer adjacent to the apical membrane surface that is created by incomplete mixing of luminal contents near the intestinal cell surface. The influence of drug structure on permeability in these domains will be different; for example ABL permeability (P_{aq}) is inversely related to solute size, whereas membrane permeability (P_m) is dependent on both size and charge. Using this model, the apparent permeability coefficient (P_{app}) through the biomembrane may therefore be expressed as a function of the resistance of the ABL and

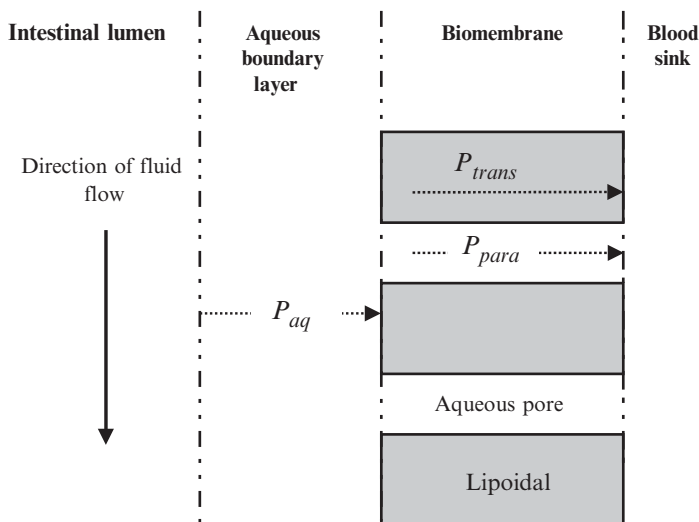


Figure 2.2 Schematic diagram of the physical model for passive transport of solutes across the intestinal membrane. The bulk aqueous solution with an aqueous boundary layer (ABL) on the mucosal side is followed by a heterogeneous membrane consisting of lipoidal and aqueous channel pathways and thereafter by a sink on the serosal side. (Adapted from Ho et al. [5]).

membrane resistance in series as expressed in

$$P_{\text{app}} = \frac{1}{1/P_{\text{aq}} + 1/P_{\text{m}}} \quad (2.4)$$

where P_{m} and P_{aq} are the permeability coefficients of the epithelial biomembrane and the ABL, respectively. The individual permeability coefficients can be further defined in terms of the aqueous diffusion coefficient (D_{aq}), thickness of the ABL (h), fraction of un-ionised drug (X_{s}), apparent trans-cellular permeability (P_{trans}), and apparent paracellular permeability (P_{para}) (Eqs. 2.5 and 2.6).

$$P_{\text{aq}} = \frac{D_{\text{aq}}}{h} \quad (2.5)$$

$$P_{\text{m}} = P_{\text{trans}} \cdot X_{\text{s}} + P_{\text{para}} \quad (2.6)$$

Because of the lipid nature of biological membranes, drug lipophilicity has long been considered an important determinant of absorption [11, 12]. The octanol/water partition coefficient ($\log P$) and/or the octanol/buffer partition coefficient at a selected pH ($\log D$) are key indicators of lipophilicity, and are widely used to predict drug permeation through the gastrointestinal membrane. Higuchi and co-workers demonstrated a sigmoid relationship between apparent n-octanol/water partition coefficient and fraction absorbed through an intestinal segment for a group of structurally similar compounds [5]. It was proposed that if the permeating substance has a high partition coefficient, the membrane resistance becomes negligible as compared to the ABL resistance resulting in an ABL-controlled situation. Conversely, for hydrophilic solutes, membrane resistance tends to be higher than ABL resistance, resulting in a membrane controlled situation. This relationship led to a model for structure-absorptivity relationship for passive absorption (Figure 2.3). As the lipophilicity of the molecule increases, the propensity to partition through a lipoidal membrane also increases. This increase in permeability will approach a plateau value beyond which further increases in partition coefficient do not result in increased

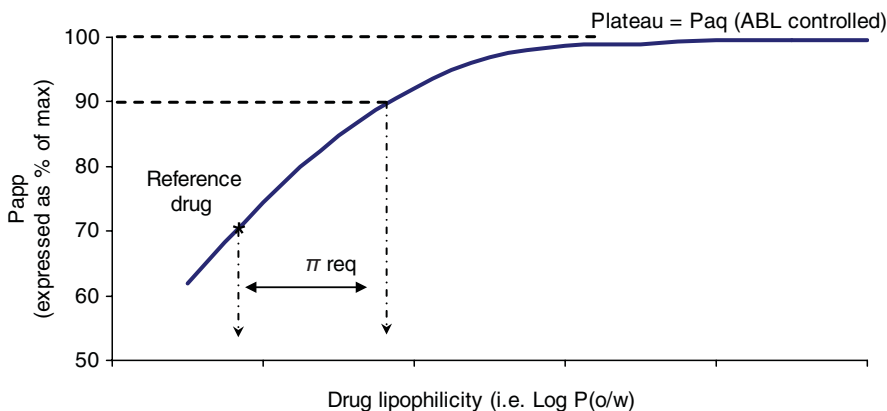


Figure 2.3 Schematic diagram of the method approach in optimising the drug design for passive absorption by determining the additional lipophilicity required to raise the absorption rate constant of the lead candidate in dilute solution to >90% of the maximum (Adapted from Ho et al. [5]).

permeability, that is ABL controlled. They developed a theoretical calculation for a π_{req} parameter to define the lipophilicity required to raise the absorption rate constant of the lead drug to within 10% of the maximum P_{app} . In essence, the lipophilicity of the drug can be tailored to improve absorption by means of synthetic structural analogues or derivatives. However, the relationship between $\log P$ and P_{app} has generally been demonstrated only for a group of structurally similar compounds. For compounds that are not passively absorbed, a simple relationship between P_{app} and partition coefficient is not expected.

Dressman et al. [13] developed a dimensionless ‘absorption potential (AP)’ model based on the concept that the fraction of dose absorbed, assuming negligible luminal instability and first-pass metabolism, is a function of drug lipophilicity ($\log P_{\text{o/w}}$), solubility (S_w), and dose (D), as defined in Eq. 2.7.

$$AP = \log \left(P_{\text{o/w}} \cdot F_{\text{non}} \frac{S_w V_L}{D} \right) \quad (2.7)$$

where F_{non} is the fraction of un-ionised form at gastrointestinal pH (i.e. 6.5) and V_L is the volume of luminal contents (generally assumed to be 250 ml). Negative values of AP correspond to poor absorption while values greater than one indicates complete absorption, which implies no limitation on absorption by equilibrium physiochemical factors. A number of studies have validated this approach by confirming a strong relationship between the value of AP and the fraction absorbed for a structurally similar group of compounds [13–16]. In general, the AP is an empirical correlation that is satisfactory for drugs where the aqueous to membrane permeability is proportional to octanol/water partition coefficient (i.e. passive diffusion). However, for drugs which are absorbed via active transport and/or paracellular transport routes, such correlations are unlikely to exist.

More recently the H-bonding potential (an estimate of hydrophilicity) and surface charge characteristics of a molecule have been used as predictors of passive P_m and intestinal absorption [17, 18]. Theoretical models based on the determination of polar surface area (PSA) have been utilised to reasonable

success to predict human intestinal absorption [19]. PSA can be described in numerous ways, depending on the kind of molecular surface area used and atoms considered to be polar, but is generally defined as the area occupied by nitrogen and oxygen atoms, and hydrogen atoms attached to these heteroatoms [20–22]. A sigmoid relationship was established between the absorbed dose in humans and the PSA for 20 drugs ($r^2 = 0.94$). However, the prediction for a larger set of drugs was less impressive [23].

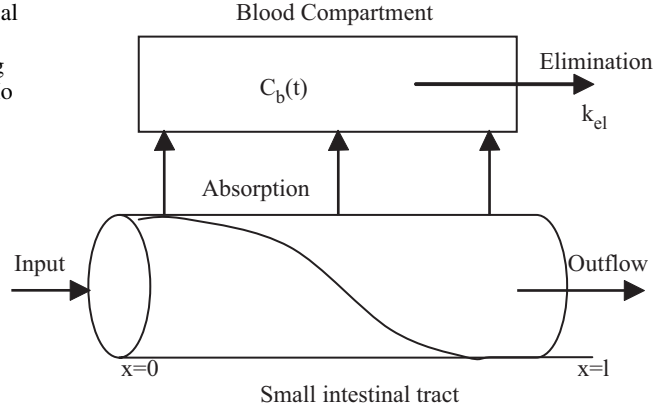
The quasi-equilibrium models, defined by Yu et al. [24] as models based solely on physicochemical properties and/or molecular descriptors, provide a basic guideline for understanding drug absorption trends and are useful for the purpose of early stage library design and lead optimisation. Lipinski's rule of five, in particular, has been widely proposed as a qualitative predictive model for oral absorption trends [25]. It established limits on properties such as $\log P$, Mw, and number of hydrogen donors and acceptors, beyond which oral absorption is predicted to be poor. Recently, Yalkowsky et al. [16] proposed a 'Rule of unity' model, based on a modification of the AP concept and derived from $\log P$, melting point, pK_a , and dose, which may in fact be a more reliable predictor of drug absorption trends. More quantitative structure–bioavailability relationships [26] and/or quantitative structure–permeability relationships [27, 28] have been developed to predict the drug absorption on the basis of equilibrium physicochemical descriptors. However, the difficulty inherent with all these types of approaches, based solely on physicochemical descriptors, is that they either predict drug absorption qualitatively or are based on a limited set of compounds. The complex physiological factors that influence the rate of drug presentation at the intestinal surface, the trans-membranal transport process, and finally release into the systemic circulation (e.g. portal vein) require more than simplified empirical relationships. Techniques for determining these kinetic rate constants and identification of the rate-limiting steps within the in vivo physiological conditions of the GIT are essential in predicting drug absorption from the GIT.

2.2.2. General Model Describing Gastrointestinal Absorption

A basic starting point in the development of predictive absorption models is to review the mathematical descriptions of rate and extent of drug absorption. A physical model for simultaneous fluid flow and intestinal absorption that applies broadly to idealised simulation experiments, animal studies, and in vivo studies in humans has been described by Ho et al. [30] and is depicted in Figure 2.4.

The change in blood levels of drug with time will be the result of non-steady-state drug appearance kinetics within a defined length of intestine and the rate of elimination from the blood. As drug from the stomach is infused into a flowing liquid within the small intestine, there occurs a non-steady-state concentration gradient along the intestinal tract, and the concentration is a function of both distance and time. The concentration gradient will be influenced by a number of factors: stomach emptying rate, intestinal fluid flow, absorption rates, and the extent of spreading of solute along the tract. Ni et al. [29], using a differential mass balance approach, derived Eq. 2.8 to describe simultaneous fluid flow and drug absorption at a non-steady state of

Figure 2.4 Schematic diagram of the physical model relating non-steady-state intestinal absorption and blood level kinetics with drug infusion from the stomach. (Adapted from Ho et al. [30]).



drug perfusion through the intestine as follows:

$$\frac{dC(x, t)}{dt} = \alpha \left(\frac{d^2C(x, t)}{dx^2} \right) - \beta \left(\frac{dC(x, t)}{dx} \right) - k_a C(x, t) \quad (2.8)$$

i.e. [change in concentration with distance and time] = [longitudinal spreading] – [flow] – [absorption], where $C(x, t)$ is the drug concentration at any distance along the intestine at time t (mass/cm³), α is the longitudinal spreading coefficient (cm²/s), β is the linear flow velocity (cm/s) and k_a is the apparent first-order absorption rate constant (per second).

This model, which has also been referred to as the dispersion model, has been utilised to simulate oral drug absorption [24, 30]. It has also been useful in establishing the anatomical reserve length concept, and predicting the effect of bile salt sequestrants on human bile salt excretion [31]. Solving this equation or estimating the extent of absorption in a non-steady-state, experimental setting can be quite complex [24, 29, 32]. However, the model and equation is a good starting point for understanding some of the key physiological variables affecting the kinetics of oral absorption and lays the foundations for understanding the mass balance approach to estimating intestinal permeability.

2.2.3. The Effective Permeability Coefficient

The first-order absorption rate constant introduced above may be directly related to the effective permeability coefficient (P_{eff}) using

$$k_a = \frac{A}{V} P_{\text{eff}} \quad (2.9)$$

where P_{eff} is the effective intestinal permeability coefficient through a cylindrical intestinal segment of radius r and length L , A represents the surface area available ($2\pi rL$), and V represents the volume (πr^2L). The intestinal permeability (P_{eff}) is one of the key biopharmaceutical parameters that determine the rate (Eq. 2.9) and extent of intestinal drug absorption. P_{eff} is derived from Fick's law (Eq. 2.10), which defines the relationship between the net flux (J_{wall} or mass per unit area per unit time) through a membrane wall and the drug concentration drop (ΔC) across the membrane surface.

$$J_{\text{wall}} = P_{\text{eff}} \Delta C \quad (2.10)$$

Factors which will affect P_{eff} include physiochemical properties of the drugs such as lipophilicity, molecular size, hydrogen bonding capacity, PSA, and also physiological factors in the membrane such as passive versus active transport and location in the GIT. As drug in solution passes through the intestine, the concentration of drug in the lumen decreases due to absorption. The transport rate of drug across the entire intestinal segment (absorbed mass) can be defined by Fick's law where net flux is expressed as the mass per unit area per unit time (Eqs. 2.11 and 2.12):

$$J_{\text{wall}} = \frac{dM}{dt} \cdot \frac{1}{A} \quad (2.11)$$

$$\frac{dM}{dt} = A \cdot P_{\text{eff}} \left(C_{\text{lumen}}^{\text{ref}} - C_{\text{blood}}^{\text{ref}} \right) \quad (2.12)$$

This can be further simplified if it is assumed that there is no accumulation of drug on the blood side (i.e. $C_{\text{blood}}^{\text{ref}} \ll C_{\text{lumen}}^{\text{ref}}$) or the portal blood is considered to be under sink conditions. Lennernäs et al. [33] reported that concentrations in the plasma are generally more than several orders of magnitude below the intestinal lumen in humans, thus demonstrating the validity of this assumption. Hence the drug absorption rate is dependent on the area exposed, the permeability coefficient, and the concentration at the membrane surface as follows:

$$\frac{dM}{dt} = A \cdot P_{\text{eff}} \cdot C_{\text{lumen}}^{\text{ref}} \quad (2.13)$$

More generally, this relationship is used to define the overall rate of absorption along the entire GIT as per

$$\text{Rate:} \quad \frac{dM}{dt} = \iint_A P_{\text{eff}} \cdot C_{\text{lumen}}^{\text{ref}} dA \quad (2.14)$$

where the double integral is over the entire absorbing surface and the mass absorbed at any time (i.e. extent) is given in

$$\text{Extent:} \quad M(t) = \int_t \iint_A P_{\text{eff}} \cdot C_{\text{lumen}}^{\text{ref}} dA dt \quad (2.15)$$

where the permeability and concentration are position-dependent and time-dependent [3].

2.2.4. Estimating Effective Intestinal Permeability Coefficient Using a Mass Balance Approach

A physical model for simultaneous bulk fluid flow and absorption in the intestinal tract under steady-state conditions is presented in Figure 2.5.

At steady state, the following mass balance can be applied across a perfused segment of the intestine. The rate of mass entering and exiting the intestinal segment (i.e. cylindrical tube) is the product of the volumetric flow rate (Q) and either inlet concentration (C_{in}) or outlet concentration (C_{out}), respectively. Assuming that mass is lost from the tube only by absorption into the blood, the mass absorbed per unit time is the difference between the rates of mass flow in and out of the tube as follows:

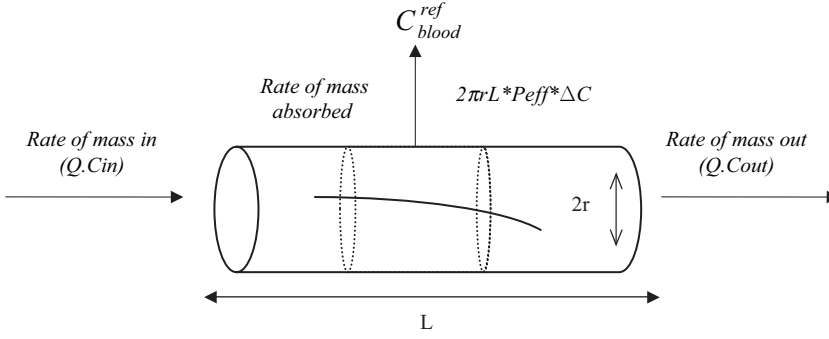


Figure 2.5 Mass balance model for intestinal perfusion experiments at steady state (Adapted from Johnson and Amidon [129]).

Rate of mass in – Rate of mass out = Rate of mass absorbed

$$Q \cdot C_{in} - Q \cdot C_{out} = A \cdot P_{eff} \cdot C_{lumen}^{ref}$$

$$P_{eff} = \frac{Q}{A} \cdot \frac{(C_{in} - C_{out})}{C_{lumen}^{ref}} \quad (2.16)$$

Estimating the term C_{lumen}^{ref} (i.e. bulk drug concentration profile in an intestinal segment) is dependent on the flow dynamics in the intestine. Several mathematical models have been proposed to define this [34, 35]. The two most frequently models are described here [4]. The simplest model is the mixing tank or well-stirred model, where complete mixing (i.e. axial and radial) is achieved within the intestine and as such there is a uniform concentration within the intestine. The model assumes an instantaneous dilution of the inlet stream occurring in the intestinal segment. The term C_{lumen}^{ref} can thus be approximated with the C_{out} concentration and P_{eff} calculated as follows:

$$P_{eff} = \frac{Q}{A} \cdot \left(\frac{C_{in} - C_{out}}{C_{out}} \right) \quad (2.17)$$

[Well-stirred model (i.e. mixing tank model)]

An alternative model is the complete radial mixing or parallel tube model which considers a constant fluid flow down a cylinder. It is also referred to as an ‘open’ system, where the perfusion solution, containing a drug, flows down a cylindrical segment and at steady state a constant concentration gradient is established along the length of the segment. The concentration profile is considered to be constant radially but not axially. Hence, the concentration profile will decrease in an exponential fashion, assuming first-order absorption. The term C_{lumen}^{ref} can be approximated as the logarithmic mean concentration ($\langle C \rangle$) in the intestine [i.e. $\langle C \rangle = (C_{out} - C_{in}) / \ln(C_{out}/C_{in})$], substituting this into Eq. 2.16 yields the following:

$$P_{eff} = -\frac{Q}{A} \cdot \ln \left(\frac{C_{out}}{C_{in}} \right) \quad (2.18)$$

[Parallel tube model (i.e. complete radial mixing model)]

2.2.5. Using P_{eff} to Estimate the Extent of Absorption

The fraction of drug remaining in the intestine (unabsorbed) at steady state is defined as ratio of inlet to outlet concentrations and can be calculated by rearranging Eq. 2.18 as follows:

$$\frac{C_{\text{out}}}{C_{\text{in}}} = e^{\left\{\frac{-A}{Q} P_{\text{eff}}\right\}} \quad (2.19)$$

A key assumption of this steady-state model is that complete transfer of drug occurs from the lumen to the portal vein (i.e. mass of drug loss reflects mass of drug appearing in blood). Therefore, the fraction of drug absorbed (f_a) can be thus defined as per Eqs. 2.20 and 2.21:

$$f_a = 1 - \left(\frac{C_{\text{out}}}{C_{\text{in}}}\right) \quad (2.20)$$

$$f_a = 1 - e^{\left\{\frac{-A}{Q} P_{\text{eff}}\right\}} \quad (2.21)$$

Hence, the fraction of drug absorbed may be predicted by P_{eff} values, assuming the area and flow rate through the intestine is known. The steady-state physical model described above (i.e. complete radial mixing) may also be derived using dimensionless analysis. The Graetz number, Gz , represents the ratio of the time required for fluid flowing in the centre of the lumen to transverse the gut ($\pi r^2 L/2Q$) and the time required for a solute in the centre of the lumen to diffuse out to the brush border membrane (r^2/D) (Eq 2.22). Since the radius cancel out, the Gz is independent of radius.

$$Gz = \frac{\pi DL}{2Q} \quad (2.22)$$

where D is the solute diffusivity in the perfusion fluid. The dimensionless effective permeability coefficient, (P_{eff}^*) may be defined in terms of the individual dimensionless permeability coefficients for permeation through the bio-membrane (P_m) and through the ABL (P_{aq}) as follows:

$$P_{\text{eff}}^* = \frac{1}{1/P_{\text{aq}}^* + 1/P_m^*}$$

$$\text{where: } P_m^* = P_m \cdot \frac{r}{D} \text{ and } P_{\text{aq}}^* = P_{\text{aq}} \cdot \frac{r}{D} \quad (2.23)$$

Using this dimensionless analysis approach, the fraction absorbed can be predicted from Eq. 2.21 on the basis of two dimensionless variables as follows:

$$f_a = 1 - e^{-4GzP_{\text{eff}}^*} \quad (2.24)$$

The Graetz number of the human intestine can be estimated to be about 0.5 using an intestinal length of 500 cm, a flow rate of 0.5 ml/min and a diffusivity of $5 \times 10^{-6} \text{ cm}^2/\text{s}$. Consequently, Eq. 2.24 becomes

$$f_a = 1 - e^{-2P_{\text{eff}}^*} \quad (2.25)$$

The fundamental relationship hypothesised by Eq. 2.25 was first validated by comparing the extent of absorption reported from humans and P_{eff} calculated

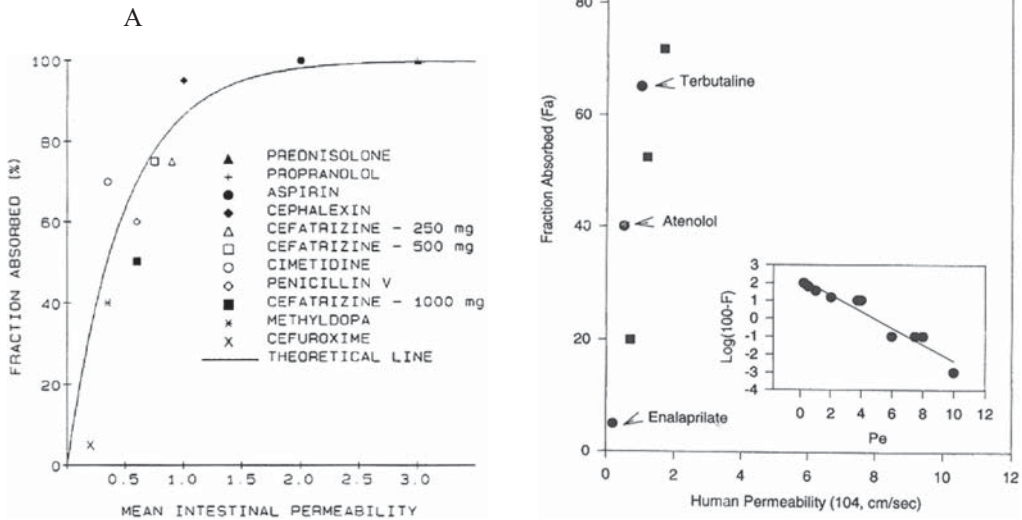


Figure 2.6 (A) Fraction absorbed in humans versus intestinal rat permeability [36] and (B) fraction absorbed in humans versus human intestinal permeability [3].

from rat small intestine for nine compounds [36] (Figure 2.6A). The correlation indicated that a dimensionless permeability (P_{eff}^*) of >1 , or $\sim 25 \times 10^{-4}$ cm/min, assuming an average aqueous drug diffusivity of 5×10^{-4} cm²/min, corresponded to a well-absorbed drug. Rather importantly, and unlike much of the models referred to in Sect. 2.2.1, the relationship was independent of the drug's structural class or absorption mechanism. These findings represented a major paradigm shift away from traditional physiochemical predictors of absorption (e.g. pK_a , $\log P$, and AP) to recognise P_{eff} as the fundamental absorption parameter of interest. Later a direct comparison of effective permeability values in humans and the extent of absorption was performed [3]. A key characteristic of the relationship identified (Figure 2.6B) is that the P_{eff} value of >2 in humans represents complete absorption, whereas <2 represents incomplete absorption [3].

Further predictions of *in vivo* drug absorption could be obtained by using fundamental dimensionless groups such as Do (dose number), Dn (dissolution number), and An (absorption number). The three dimensionless numbers are combinations of physiochemical and physiological parameters and represent the most fundamental view of GIT drug absorption and are the foundation principles of the BCS [3]. Do is calculated using Eq. 2.26:

$$Do = \frac{(M_0/V_0)}{C_s} \quad (2.26)$$

where M_0 is the highest dose strength, C_s is the saturation solubility, and V_0 is the volume of water taken with the dose. The dissolution number is the ratio of

the residence time (T_{si}) to the dissolution time (T_{diss}) and is defined as per

$$Dn = \frac{\langle T_{si} \rangle}{\langle T_{diss} \rangle} = \left(\frac{3D}{r^2} \right) \left(\frac{C_s}{\rho} \right) \langle T_{si} \rangle \quad (2.27)$$

where D is the diffusivity, ρ is the density, and r is the initial particle radius. An is defined as the ratio of the radial absorption rate (i.e. $P_{eff} \times \pi rL$) to the axial convection rate (i.e. Q). Eq. 2.21 can be redefined using this parameter as illustrated below:

$$f_a = 1 - e^{-2An} \quad (2.28)$$

Refinement and expansion of these steady-state mass balance approaches has led to the development of dynamic models which allow for estimation of the fraction absorbed as a function of time and can therefore be used to predict the rate of drug absorption [37]. These compartmental absorption and transit models (CAT) models have subsequently been used to predict pharmacokinetic profiles of drugs on the basis of in vitro dissolution and permeability characteristics and drug transit times in the intestine [38].

2.3. In Situ Models

Many variations of intestinal perfusion methods have been used as absorption models over the years. In situ methods offer advantages over in vitro models. Although the animal has been anaesthetised and surgically manipulated, neural, endocrine, lymphatic, and mesenteric blood supplies are intact and therefore all the transport mechanisms present in a live animal should be functional. As a result absorption rates from these methods may be more realistic in magnitude than those determined from in vitro techniques.

2.3.1. Intestinal Perfusion Techniques

The development of stable, vascularly perfused preparations of the small intestine has proved a powerful research tool for the investigation of intestinal drug transport and metabolism. Since originally proposed by Schanker et al. [39], this model has gained widespread use and application, owing to its relative simplicity, relative ease of surgical techniques, and low cost. In this approach, the abdominal cavity of an anaesthetised animal is exposed by laparotomy. A number of modifications to the original method have been developed. The intestinal segment into which drug is introduced can be either 'closed' or 'open'. In closed loop experiments (Sect. 2.3.1.1), described by Doluisio et al. [40], a drug solution is placed in an isolated segment of the intestine and the resultant luminal solution is analysed at pre-determined time points. In the open loop or 'through and through' perfusion techniques (Sect. 2.3.1.2), originally proposed by Higuchi and co-workers, continuous fluid flow is maintained down the intestine, and intestinal permeability is estimated via the concentration difference in inlet and outlet perfusate at steady state [41].

An additional consideration when using in situ techniques is the volume of the luminal drug solution as water absorption and secretion during the perfusion may introduce errors in the luminal concentrations and therefore in the calculated absorption. Various water flux correction methods have been published [42] including the co-perfusion of a 'non-absorbed' marker such

as phenol red, inulin, or ^{14}C PEG 4000 (Eq. 2.29). Alternatively, a simpler gravimetric method may also be applied using Eq. 2.30:

$$C_{\text{out}}^{\text{corrected}} = C_{\text{out}} \cdot \frac{[\text{Concentration of Marker}_{\text{in}}]}{[\text{Concentration of Marker}_{\text{out}}]} \quad (2.29)$$

$$C_{\text{out}}^{\text{corrected}} = C_{\text{out}} \cdot \frac{Q_{\text{out}}}{Q_{\text{in}}} \quad (2.30)$$

where Q_{in} and Q_{out} are the measure flow rates entering and exiting the intestinal segment. Sutton et al. [42] reported that the gravimetric method may in fact be as accurate as the ‘marker’ methods based on non-absorbable markers, with the additional advantages of avoiding the risk of interactions between drug and marker (e.g. analytical) and/or the possible effects of markers on membrane function.

2.3.1.1. Closed Loop Intestinal Perfusion Technique

In the closed loop experiments, the rats weighing 250–350 g are typically fasted overnight and allowed access to water *ad libitum*. It is considered good practice to allow animals to acclimatise for typically 1 week prior to experiment. The rats are anaesthetised, placed on a heating pad to maintain a constant body temperature of 37 °C, and a laparotomy is performed to identify the small intestine. Two L-shaped cannulas are inserted through small slits at the duodenal and ileal ends. Efforts are made to minimise handling of the small intestine and to reduce surgery to a minimum in order to maintain an intact blood supply. The cannulas are secured by ligature. Four-centimetre segments of polyethylene tubing are attached to the exposed ends of both cannulas, and a 30-ml hypodermic syringe fitted with a three-way stopcock and containing perfusion solution, warmed to 37 °C, is attached to the duodenal cannula. The perfusion solution is then passed through the segment to clear intestinal contents and effluent discarded until running clear. The remaining perfusion solution is then carefully expelled, by means of air pumped through the intestine, 10 ml of drug solution is introduced into the isolated intestinal segment, and a second hypodermic syringe is attached to the ileal cannula. At pre-determined time intervals (e.g. 5-min intervals for 30 min), the lumen solution is sampled by pumping it into either the duodenal or the ileal syringe, removing ~0.1 ml solution, and returning the lumen solution within 10–15 s. The method may be modified by the addition of an in-line peristaltic pump which facilitates constant and gradual mixing of the medium in the lumen, without the mechanical trauma likely to be exerted upon the intestine each time the syringe contents are alternated (i.e. recirculation apparatus). Assuming sink conditions prevail, drug concentration in the ‘closed’ intestinal segment is assumed to decrease in a first-order fashion with time, t , as defined in

$$C = C_0 e^{-k_a \cdot t} \quad (2.31)$$

where C_0 is the initial drug concentration. Hence a plot of drug concentration remaining versus time may be fitted to a first-order equation, to define k_a , the apparent first-order absorption rate constant. P_{eff} can hence be calculated from Eq. 2.9.

2.3.1.2. Single Pass Intestinal Perfusion Technique

For the quantitative estimation of absorption parameters, the Doluisio method has suffered from the potential drawback that the drug is exposed to the entire surface area of the intestinal segment throughout the study, which does not reflect the true in vivo situation (i.e. single-pass intestinal fluid flow). The single-pass perfusion or 'through and through' model, originally proposed by Higuchi and co-workers, is designed to estimate drug absorption properties with continuous fluid flow through the intestine. It is generally considered superior to the Doluisio method giving better control of the hydrodynamics and increased surface area [30, 43]. In general, P_{eff} values obtained from both models tend to be similar when normalised for the perfused volumes and intestinal lengths; however, the single-pass perfusion has been reported to give more reproducible absorption rate and lower variance within experiments [44].

The experimental set-up and cannulation of the intestinal segment is similar to that described in section 2.3.1.1. The drug solution is perfused continuously (via an infusion pump) down a set length of intestine through the duodenal-end cannula and perfusate collected from the ileal-end cannula, at flow rates of between 0.1 and 0.3 ml/min. The samples collected at outflow are assayed for drug content. In some experiments, to prevent entero-hepatic recycling the bile duct may be closed before perfusion. Estimation of the effective intestinal permeability (P_{eff}) is determined by calculating the concentration difference between inlet and outlet fluids, once steady state has been achieved (i.e. when the outlet concentrations of the compound are stable over time), using the parallel tube model (Eq. 2.18). A comparison of both open and closed methods is presented in Table 2.2.

The choice of flow rates in perfusion experiments is an important consideration as it may affect hydrodynamics [35], ABL thickness [30], intestinal radius [34], intestinal surface area [45], and time to reach steady-state conditions [32], all of which can impact on P_{eff} estimates. The intestinal radius has implications for the estimation of the permeability coefficient. The most widely used estimate for the rat intestinal radius is 0.18 cm [34]. These authors found that there was a small change in intra-luminal pressure with an increase in flow

Table 2.2 Comparison of closed loop and single-pass (open loop) intestinal perfusion models.

	Closed loop	Open loop
Theoretical basis	Determining decrease in drug concentration for segment of intestine over time	Determining concentration drop between inlet and outlet concentration at steady state
Fluid volumes	5–10 ml static over ~30 min	3–100 ml continuous flow over ~30 min
Hydrodynamics	Well-stirred model, i.e. uniform concentration inside intestine	Parallel tube model, i.e. concentration decrease exponentially down the length of the intestine
Intestinal set-up	Intestine is removed initially and may be returned to intestine during perfusion	Intestine is generally located outside the abdomen during perfusion.

rate from 0.25 to 0.5 ml/min but that this was without any apparent change in the distension to the intestinal lumen.

The advantages of the *in situ* techniques include an intact blood supply; multiple samples may be taken, thus enabling kinetic studies to be performed. A fundamental point regarding the *in situ* intestinal perfusion method is that the rat model has been demonstrated to correlate with *in vivo* human data [46–49]. Amidon et al. [36] have demonstrated that it can be used to predict absorption for both passive and carrier-mediated substrates. However, the intestinal luminal concentrations used in rat experiments should reflect adequately scaled and clinically relevant concentrations to ensure appropriate permeability determinations [50]. There are limitations of the *in situ* rat perfusion models. The assumption involved in derivation of these models that all drug passes into portal vein, that is drug disappearance reflects drug absorption, may not be valid in some circumstances as discussed below.

If the drug under study is metabolised by enterocytes, drug disappearance from the lumen will not reflect drug appearance into the blood. Conventional teaching of drug metabolism has tended to focus on hepatic metabolism, whereas the influence of intestinal bio-transformations has traditionally been considered a minor factor. However, since Watkins et al. [51] reported that a major cytochrome P450 enzyme, CYP3A4, is relatively abundant in the intestinal mucosa, the potential of the intestinal enzyme system to significantly reduce oral bioavailability has been a major topic for discussion [52]. Watkins [53] proposed that despite the relatively small amount of P450 in the intestinal mucosa relative to the liver (i.e. mean microsomal CYP3A4 contents are reported to be ~50% of the levels found in human liver) the intestine plays a major role in drug metabolism. The location of the P450, just below the microvillus border, maximises drug metabolism as it traverses the intestinal wall. In addition, Watkins [53] suggested that the exposure of enterocytes to high drug concentrations increase the relative importance of intestinal metabolism, since CYP3A4 is a low affinity, high capacity enzyme. The high level of specific CYP P450 becomes of even greater importance when it is recognised that more than 50% of drugs, for human administration, may be substrates for this enzyme [54]. Hence the model assumption that metabolism in intestinal cells is not significant may in many circumstances be untrue.

Similarly, intestinal perfusion models based on disappearance kinetics from the intestine segment assume drug transport into the enterocyte (i.e. through the apical membrane) is rate limiting [55]. This view is most likely true in the case of passively absorbed compounds but exceptions to this would include drugs which are actively transported through the baso-lateral membrane. For example, considering the rapid transport of di- and tripeptides through the oligopeptide carrier, it seems likely that the baso-lateral membrane is the slowest step in the overall transport from lumen to portal blood [50, 56]. Similarly if a drug is transported via the intestinal lymphatics (e.g. lipophilic drugs), association with intra-cellularly produced lipoproteins appears to be the critical rate-limiting step for access to the systemic circulation [57, 58].

In general, the intestinal perfusion technique has proved a powerful research tool, despite these shortcomings. Its primary application has been in the estimation of P_{eff} ; the model also lends itself to comparing permeability differences from one site to another along the intestine, an essential prerequisite for accurately classifying controlled release products [59]. Cross-over experiments tend

to be impractical, given the animal is anaesthetised, and as such the experimental numbers tend to be quite high to demonstrate significance outside of inter-animal variability. In addition, the model can be used to examine concentration-dependent saturable transport processes, as well as overall contribution of paracellular transport to drug absorption [60, 61]. It is also relatively robust when compared to cell culture lines such as Caco 2 cells [49].

There have been some useful modifications of the original method, particularly when investigating carrier-mediated drug transport in drug absorption. Carrier-mediated transport processes can be demonstrated by comparing P_{eff} values at increasing drug concentration in the perfusate, where a reduction in P_{eff} suggests saturation of carrier-mediated influx [62] and an increasing P_{eff} values suggests saturation of efflux transporters [63]. Co-administration of modulators of enterocyte-based metabolism and/or efflux is required to provide a more specific insight into the type of transport/elimination processes involved. The metabolite profile in intestinal perfusate may be assessed to demonstrate intestinally mediated metabolism/efflux and also the impact of serosal to mucosa efflux following IV administration [64]. Sandström et al. [65] reported that efflux of R/S-nor-verapamil was high after IV administration of R/S verapamil, suggesting extensive metabolism of parent drug in the enterocyte. The efflux of metabolite into the lumen was reduced following administration of chlorpromazine (a CYP3A4 substrate), suggesting inhibition of enterocyte metabolism and/or efflux. The closed loop technique may in fact offer advantages versus the single-pass technique in the investigation of low permeability (i.e. high efflux) compounds, given that the entire contents of the solution are in contact with the lumen for the duration of the experiment and hence disappearance rates (i.e. absorption rates) are higher. It also facilitates a more precise control of concentrations of drug and/or inhibitor within the intestinal segment [66].

2.3.2. Intestinal Perfusion with Venous Sampling Models

The intestinal perfusion techniques described in Sect. 2.3.1 facilitate a direct determination of fraction of dose absorbed on the basis of disappearance kinetics from an intestinal segment. However, the model is limited by the fact that the drug absorption is predicted by quantifying net drug uptake into enterocyte cells and not net flux through the cell. By applying a plasma sampling technique, drug absorption through the enterocytes can be quantified on the basis of appearance kinetics in pre-hepatic blood (Figure 2.7). The major advantage of this experimental technique therefore is that it facilitates both a quantification of steady-state disappearance kinetics from the intestinal lumen and concurrent appearance kinetics into pre-hepatic blood. Permeability estimates on the basis of drug appearance in pre-hepatic blood therefore reflect the net effect of (a) drug absorption into the apical membrane (i.e. f_a) and (b) drug flux through the enterocyte (i.e. f_g).

This technique, also referred to as the 'auto-perfused' method after experiments by Windmuller and Spaeth [67] involves cannulation and drainage of a vein from an intestinal segment and donor blood replacement via a sustainable blood vessel (e.g. jugular vein). The most commonly reported site of cannulation is the mesenteric vein. Cannulation is performed as follows. A midline incision of ~4 cm is made and an 8–12-cm segment of the ileum is located to

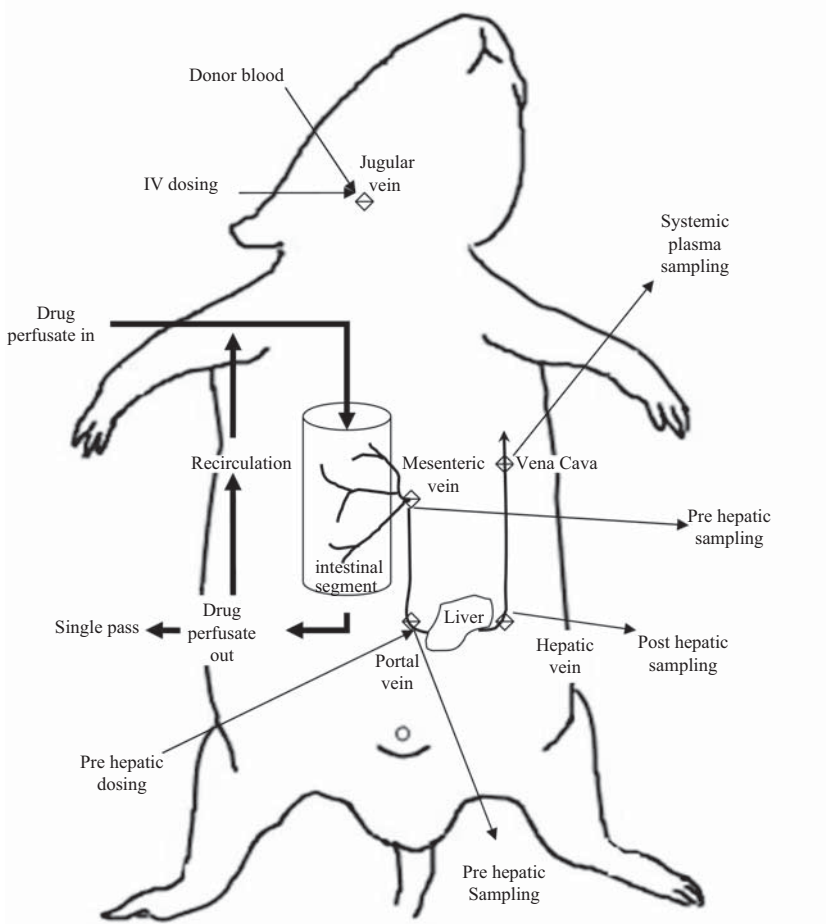


Figure 2.7 Illustration of the experimental procedures for intestinal perfusion with possible sites for vascular cannulation.

facilitate an examination of the entire mesenteric blood flow from the intestinal segment and to facilitate an optimal site for mesenteric cannulation. A segment of the intestine is cannulated as before. After this, the tissue covering the mesenteric venules draining blood out of the isolated ileal segment is gently removed. A 4-0 silk suture is carefully passed below the mesenteric vein at the site of cannulation. The mesenteric vein is cannulated using a 24-gauge catheter in which the top 1 cm bevelled tip is cut such that this 1-cm tip remains in the mesenteric vein, and the 4-0 silk suture passed earlier below the mesenteric vein is tied around the cannula and mesenteric vein, thus occluding blood flow to the systemic circulation. The cannula is secured in place using cyanoacrylate glue and connected to a flexible silastic tubing to facilitate blood collection. Once blood flow from the mesenteric vein is established, donor blood is infused at an equal rate via infusion through a jugular vein cannula ($\sim 0.3\text{--}0.5$ ml/min) [68]. Any mesenteric venules that do not originate from the isolated intestinal segment to be cannulated are occluded. In another similar experimental set-up, portal vein cannulation is accomplished using a 22-gauge

IV catheter [69]. In this case, periodic samples are taken from the portal vein (200 μ l) and withdrawn blood is replaced with heparinised saline.

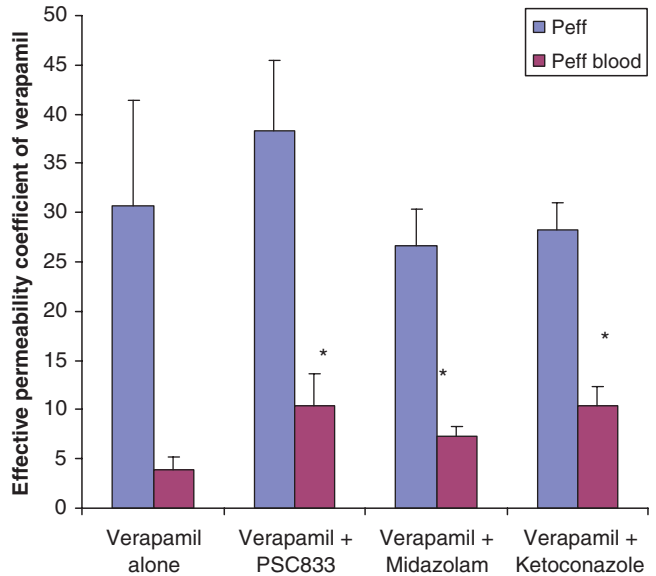
The intestinal permeability may be determined from the rate of drug appearance in mesenteric blood (i.e. dM/dt) at steady state, using Eq. 2.12. Estimating the term $C_{\text{lumen}}^{\text{ref}}$ will again depend on the flow dynamics of the model chosen. The most commonly used experimental procedure is the single-pass perfusion (i.e. parallel tube model) and the luminal concentration can be estimated using the logarithmic mean of inlet and outlet concentrations (i.e. $\langle C \rangle$).

Singhal et al. [68] compared P_{eff} (disappearance from lumen) to $P_{\text{eff}}^{\text{blood}}$ (appearance into pre-hepatic blood) for 2'-3'-dideoxyinosine (ddI) and a series of prodrugs. It was demonstrated that for the parent compound P_{eff} and $P_{\text{eff}}^{\text{blood}}$ were essentially similar, suggesting minimal intestinal first-pass metabolism, whereas for a more lipophilic pro-drug form the $P_{\text{eff}}^{\text{blood}}$ was 4.5-fold lower than the P_{eff} , which indicated extensive metabolism of the pro-drug during intestinal transport. The study clearly demonstrates that high P_{eff} values merely demonstrate high drug uptake into enterocytes (i.e. f_a), whereas $P_{\text{eff}}^{\text{blood}}$ values must be used to assess overall drug flux through the intestinal cells (i.e. f_g).

Cummins et al. [136] assessed the impact of co-administered anti-metabolites/efflux inhibitors on the degree of intestinal metabolism and/or efflux of K77 in the in situ rat intestinal perfusion model with pre-hepatic sampling. K77 is a substrate for intestinal CYP3A and is also actively transported by the apically polarised efflux protein P-glycoprotein (P-gp). P-gp has attracted much attention as a possible physiological determinant of the poor oral absorption; in particular, since the substrates of P-gp and CYP 3A4 are mutually overlapping. Benet and co-workers have proposed that these proteins act synergistically to present a barrier to absorption from the small intestine [54, 70]. It is hypothesised that P-gp has the effect of recycling the substrate, increasing enterocyte residence time and therein increasing susceptibility to metabolism by CYP 3A4. The P_{eff} based on lumen disappearance rate was 20-fold higher than $P_{\text{eff}}^{\text{blood}}$ estimated from mesenteric blood, reflecting the high degree of intestinal metabolism/loss of K77 on passage through the absorptive cells. The $P_{\text{eff}}^{\text{blood}}$ of K77 was significantly increased following co-administration of GG918, a selective P-gp inhibitor, confirming the impact of P-gp on limiting drug transport through intestinal enterocytes. In addition, the fraction of K77 metabolised after P-gp inhibition was reduced, which supports the hypothesis that P-gp was increasing the extent of metabolism of drug when it was active, through repeated cycles of absorption and efflux. The study therefore demonstrates the impact of P-gp on limiting drug uptake into intestinal cells (i.e. f_a) and also supports a role for P-gp in modulating the extent of intestinal metabolism (i.e. f_g) by controlling drug access to enterocyte enzymes.

Johnson et al. [71] performed a similar study on verapamil permeability, absorption, efflux, and metabolism. Verapamil is metabolised by CYP450 enzymes, and in this in situ rat model significant differences in the permeability estimates on the basis of disappearance or appearance were obtained, confirming the impact of intestinally mediated metabolism on verapamil. The impact of co-administering modulators of intestinal membrane function on verapamil uptake was also assessed. The study clearly demonstrates that inhibition of intestinal P-gp/CYP did not significantly affect the P_{eff} of verapamil based on

Figure 2.8 Effective permeability coefficients (P_{eff}) ($\times 10^{-6}$) of verapamil calculated from appearance in venous blood ($P_{\text{eff}}^{\text{blood}}$) and disappearance from lumen (P_{eff}) in the presence and absence of PSC833, midazolam, or ketoconazole in the vascularly perfused intestinal. (Adapted from Johnson et al. [71]) (* Significant difference compared with control permeability $p < 0.025$).



luminal disappearance (Figure 2.8); however, significant increases in $P_{\text{eff}}^{\text{blood}}$ values based on appearance kinetics were obtained. Blood and intestinal perfusate samples were analysed for metabolites of the parent compound. In addition, a compartmental modelling analysis of the metabolism kinetics was also performed. As expected the rate of verapamil metabolism was reduced following co-administration of CYP inhibitors (i.e. midazolam and ketoconazole), clearly demonstrating the impact of intestinal CYP on limiting drug flux through intestinal cells. Similarly, selective inhibition of intestinal P-gp, using PSC833, resulted in an increased rate of appearance of verapamil in the blood. Interestingly, despite the increased flux of verapamil through the cell, the rate of metabolite formation appeared unchanged. The study therefore suggests that inhibition of P-gp serves predominately to increase the rate of transport of verapamil through the cell rather than any change in the rate of intra-cellular metabolism.

2.3.3. The Isolated and Vascularly Perfused Intestinal Models

These techniques involve isolating and cannulation of an intestinal segment, and, in addition, cannulation of a major supply artery (e.g. mesenteric artery) and drainage vein (mesenteric vein) of the intestinal segment [72–75]. The experimental set-up facilitates a quantification of intestinal-mediated extraction (f_g) by comparing perfusate profiles following input via either the lumen versus arterial supply. Generally, the animal is sacrificed after the start of the perfusion and the success of organ perfusion techniques is very dependent on maintaining a suitable oxygen/glucose supply to the intestinal segment [43, 76]. Another type of experimental set-up is the isolated and vascularly perfused rat intestine-liver technique [77, 78]. Two rats are used for each experiment, one as the intestinal donor and the other as the liver donor. The superior mesenteric artery and hepatic artery are cannulated for perfusate inflow to the intestine and liver, respectively. The pyloric vein is cannulated for portal sampling and systemic sampling is performed via the hepatic vein.

The technique allows for single-pass or re-circulating experiments involving systemic and luminal drug administration. The intestine and liver may be kept viable for up to 2 h, using an oxygen exchange chamber to re-oxygenate perfusate (95% O₂/5% CO₂). Tissue viability can be assessed by monitoring oxygen and glucose consumption, perfusate pH, active transport of glucose, and exclusion of macromolecular markers, in addition to histological or morphological examination. The technique is particularly useful in examining the relative contribution of intestinal versus hepatic first-pass metabolism in a controlled experimental setting. However, the major drawbacks of isolated tissue models will be the impact of humoral/neurogenic removal on tissue viability and the highly specialised surgical procedures involved.

2.3.4. Mesenteric Lymph Duct Cannulated Anaesthetised Rat Model

Studies of the uptake and transport of drugs into the body via the intestinal lymphatics have received increasing attention in recent years [79, 80]. Gastrointestinal absorption may occur via two principle routes: portal uptake or transport through the intestinal lymphatics. The intestinal lymphatics are responsible for the gastrointestinal uptake of dietary lipid and lipophilic nutrients and may contribute to the fraction of drug absorbed from the intestine, particularly for lipophilic drug substances. While the exact mechanisms by which a drug is transported by the intestinal lymphatic system are not fully elucidated, it is widely reported that lipophilic drugs with $\log P > 5$ and a lipid solubility >50 mg/ml are potentially good candidates [81].

Numerous experimental protocols have been reported for assessing intestinal lymphatic drug transport [82]. The most frequent of which involves a triple cannulation technique, involving cannulation of the carotid artery for the collection of systemic blood samples, the mesenteric lymph duct for the collection of the mesenteric lymph, and the duodenum for the administration of drug. The mesenteric intestinal lymph duct, rather than the thoracic lymphatic duct, is the preferred site of cannulation as all the lymph draining from the intestine collects in the mesenteric lymph duct. In contrast, lymph appearing in the thoracic duct may also be derived following redistribution of lymph flow throughout the body [83].

Cannulation of the mesenteric lymph duct is performed as follows: The rat is anaesthetised and a laparotomy is performed. The intestines are gently pushed to the left side (into the body cavity). A pair of 4-inch pointed forceps is then placed into the fat pad beneath the right kidney. The forceps, with tips together, are gently pushed through the fat, under the vena cava, raising the peritoneal membrane on the other side of the vena cava. Once the peritoneal membrane had been raised, it is cut to leave the mesenteric artery and the mesenteric lymph duct exposed. While the forceps are under the vena cava, the lymphatic cannula can be pulled through. A syringe filled with heparinised saline (1000 IU/ml) is used to flush the cannula to prevent lymph clotting. Taking great care, the top of the lymph duct is cut. The polyethylene end of the cannula is inserted 3–4 mm into the lymph duct. Any auxiliary lymph ducts to the right of the artery are cut to ensure all the lymph flow is into the main mesenteric duct. A 5 × 5 mm of muscle tissue which had been

cut from the abdominal wall is placed over the cannula and secured with cyanoacrylate glue to help secure the cannula and to prevent adhesions of the intestines.

To date much of the research on lymphatic transport has been performed in anaesthetised rats and the maximum percentage transported in the lymph for highly lipophilic drugs ($\log P > 5$), administered with lipid-based delivery systems, tends to be limited to $\sim 15\text{--}20\%$ of the administered dose [84]. However, a study in a conscious dog model, using the lipophilic drug halofantrine (Hf), showed much higher levels (54%) of lymphatic transport in the fed state [85] (Sect. 2.4.2). These studies, in the more physiologically relevant dog model, have indicated a greater capacity for this route of transport than was previously thought possible. This, coupled with the increasing trend towards highly potent, lipophilic drug candidates in drug development programs, has resulted in renewed interest in quantifying intestinal lymphatic transport [79].

2.3.5. Anaesthetised Large Animal Model

Recently, Petri et al. [86] described a novel pig model involving jejunal single-pass perfusion, with blood sampling from both portal vein and superior cava vein, in addition to bile duct collection. The combined perfusion and hepatobiliary sampling method was a useful method to quantitatively compare intestinal versus hepatic versus hepatobiliary-mediated elimination of the low permeability compound, fexofenadine. The value for P_{eff} for fexofenadine was similar to that reported for humans in vivo. However, the P_{eff} in pigs for two high permeability compounds verapamil and antipyrine were sixfold to eightfold lower than corresponding values in humans. A plausible explanation for the lower P_{eff} values seen in the pig model is differences in the effective absorptive area within the perfused segment induced by surgery and/or the anaesthesia applied. It may also be explained by species-related differences in physiology affecting partitioning into the membrane, diffusion coefficient, and/or diffusion distance [46, 47].

2.4. In Vivo Models

The key advantage of conscious animal models over in situ techniques is the avoidance of the non-physiological conditions of anaesthesia and surgical trauma which may affect absorption kinetics. However, as the complexity of the absorption model increases, an increasing number of factors influencing drug absorption come into play, which can complicate the interpretation of results. In addition, establishment of these techniques requires specialised surgical skills and very intensive animal husbandry, and are therefore generally not suitable for routine screening purposes.

2.4.1. Cannulated Conscious Rat Models

Poelma and Tukker [130] developed the chronically isolated intestinal loop method which allows absorption to be studied in the absence of surgical trauma and anaesthesia. The model also facilitates cross-over experimental schemes. A major segment of the intestine is identified and surgically isolated under initial anaesthesia. The loop remains in the peritoneal cavity, with intact blood supply

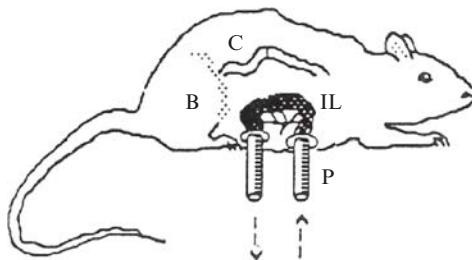


Figure 2.9 The chronically isolated intestinal loop model. Key: (B) blood catheter; (C) head-to-tail connection of the intestine; (IL) internal loop with intact blood supply and innervation; and (P) perfusion tubes (Adapted from Poelma and Tukker [130]).

and innervation but is externalised to the abdominal wall via two permanent cannulas (6–8 cm) (Figure 2.9). The severed ends of the gut are then rejoined to allow ‘normal’ digestion and absorption. Animals must be placed in restraining cages, with food/water access. The loop may be connected, via the two external cannulas, to a perfusion pump. The rats are allowed 2–4 days to recover from the surgery before starting the perfusion studies. The single-pass perfusion is performed at a rate of 1.0 ml/min. Usually, blood sampling is also performed via catheterisation of the inferior vena cava. Hence a complete mass balance of drug disappearance from the perfusion solution and appearance rate in the blood can be established. The model also lends itself to studying site-dependent absorption characteristics where different segments of the intestine were isolated and externalised [87]. In this study the absorption rates of lipophilic model compounds from the jejunum, ileum, and colon were comparable; in contrast, the absorption rates for hydrophilic model compounds were higher in the proximal parts of the intestine, suggesting preferential absorption in the upper small intestine. The differences in the absorption characteristics were explained by anatomical differences in the GIT [88].

Lu et al. (1992) performed a comparison of water and solute uptake in the *in situ* single-pass perfusion model and the isolated loops conscious rat model. Water flux in both experimental set-ups was found to be comparable. It was found that the solute (i.e. acetaminophen and phenytoin) membrane permeabilities (P_m) were consistently higher in the chronically isolated loops compared to the *in situ* perfusion. It was suggested that this was as a result of greater luminal fluid mixing in the *in vivo* system. A key advantage of the *in vivo* approach was that each animal can act as its own control for drug absorption studies.

A number of cannulated conscious rat models involving insertion of a duodenal cannula for intra-duodenal dosing, portal vein cannulation for pre-hepatic dosing/sampling, and systemic vein (e.g. vena cava) cannulation for post-hepatic sampling or *i.v.* dosing have been described [89–91]. Cannulation of the portal vein facilitates determination of the fraction of drug removed by the liver (E_h) by comparison of dose normalized plasma profiles following either pre-hepatic dosing (i.e. . . . intra-portal vein (*i.p.v.*)) or post-hepatic dosing (i.e. intravenous (*i.v.*)). These models generally do not involve chronically isolating an intestinal segment, and as such do not facilitate a mechanistic examination of the drug absorption process, that is cannot be used to estimate f_a directly.

With this experimental set-up, absolute bioavailability and hepatic extraction ratio (E_h) can be directly calculated as per Eqs. 2.32 and 2.33:

$$F = \frac{AUC_{i.d.}/Dose_{i.d.}}{AUC_{i.v.}/Dose_{i.v.}} \quad (2.32)$$

$$1 - E_h = \frac{AUC_{i.p.v.}/Dose_{i.d.}}{AUC_{i.v.}/Dose_{i.v.}} \quad (2.33)$$

where $AUC_{i.d.}$, $AUC_{i.p.v.}$, and $AUC_{i.v.}$ are the systemic AUC values after i.d., i.p.v., and i.v. administration. E_g may then be calculated from Eq. 2.2 assuming f_a is known. These models generally do not involve chronically isolating an intestinal segment, and as such cannot be used to estimate f_a .

Using an alternative method, generally referred to as an indirect method, E_g may also be estimated following i.d. dosing alone and sampling portal blood and the systemic circulation concurrently. The mass of drug appearing in the portal vein (Ma) is defined as follows:

$$Ma = Dose_{i.d.} \cdot f_a(1 - E_g) \quad (2.34)$$

Ma may also be estimated from the absorption flux of drug in the portal vein as follows:

$$Ma = \int (\text{Absorption flux}) dt = \int Q_{p.v.} (C_{p.v.} - C_{sys}) dt \quad (2.35)$$

where $Q_{p.v.}$, $C_{p.v.}$, and C_{sys} are the portal blood flow, blood concentration in portal vein, and blood concentration in systemic circulation respectively. Therefore, E_g may be calculated using Eq. 2.36, assuming f_a and $Q_{p.v.}$ are known.

$$1 - E_g = \frac{\int Q_{p.v.} (C_{p.v.} - C_{sys}) dt}{Dose_{i.d.} \cdot f_a} \quad (2.36)$$

Direct determination of portal blood flow rate is difficult and would generally require placement of an electronic flow probe in each animal. However the technique proposed by Hoffman et al. utilised tritiated water as an absorption probe (i.e. internal standard) [89]. By dosing and sampling drug/ absorption probe concurrently, factors such as variable portal blood flow rate are normalised between experiments.

2.4.2. Cannulated Conscious Large Animal Model

Sinko et al. [92] established an Intestinal and Vascular Access Port (IVAP) model where dogs were fitted with three intestinal catheters for site-specific administration to various section of the intestine (i.e. duodenum, ileum, and colon), one vascular catheter for access to the portal vein, and a peripheral vein (e.g. branchial) for IV access. The animals were allowed to recover for 2 weeks prior to initiation of studies. The extent of intestinal versus hepatic first-pass metabolism was determined by comparing blood levels following intra-duodenal ($AUC_{i.d.}$) versus portal ($AUV_{i.p.v.}$) versus intravenous ($AUC_{i.v.}$) administration. The model also lends itself to a comparison of the impact of site-specific preferential absorption, and hence a determination of the optimal site for intestinal delivery.

The pharmacokinetics of verapamil was studied using this technique [93]. There were no significant differences in bioavailability following i.d. and i.p.v. administration, confirming that f_a and f_g are $\sim 100\%$ in the dog model. The fraction escaping hepatically mediated first-pass metabolism (f_h) was estimated to be 21% and was significantly increased by co-administration of the CYP3A inhibitor, ritonavir. The lack of an appreciable enterocyte-based metabolism of verapamil in the dog model was unexpected given that verapamil is a substrate for CYP3A and studies in humans indicate a substantial intestinal first-pass effect (i.e. $E_g > 0.50$) [94]. This may reflect inter-species differences in verapamil pharmacokinetics, and indeed a more recent similar study by this group in an IVAP rabbit model identified substantial intestinally based metabolism [95]. However, the discrepancy between the dog and humans data may also reflect alternative approaches to determination of E_g in the different models. The current dog study is a direct method, whereby E_g is estimated using equation 2.2 by firstly determining E_h and F following administration via i.d. and via i.p.v. (i.e. Eqs. 2.32 and 2.33) and assuming f_a for verapamil is known (~ 1). As AUC profiles were similar following i.d. and i.p.v. administration, E_g were estimated to be ~ 0 . Using the 'indirect' method (eq. 2.36) and assuming a portal blood flow rate of 30 ml/min/kg, E_g can be estimated to be 0.38. There are numerous other reports in the literature where E_g estimated by 'direct' method is substantially lower than that determined using the 'indirect' method, for example nifedipine [96] and midazolam [97]. Possible reasons for these apparent inconsistencies between the different methods have been reviewed [95, 98] and further studies are required to explore the differing findings.

Charman and co-workers have developed a triple cannulated conscious dog model whereby lymphatic drug transport is determined via collection of thoracic lymph directly, and portal and systemic blood is sampled for the assessment of non-lymphatic drug absorption and possible enterocyte-based metabolism [85]. The model was used to delineate the mechanisms associated with a 12-fold increase in the extent of bioavailability in the fed versus fasted state for the lipophilic anti-malarial drug, Hf in beagle dogs [99]. Furthermore, administration in the fed state appeared to alter the metabolite profile in plasma. Hf is predominately metabolised to desbutyl halofantrine (Hfm), by CYP3A4, which is present in the liver and intestinal epithelium [52]. The ratio of Hfm:Hf in plasma was significantly reduced in the post-prandial state, suggesting a reduced rate of metabolite formation. Possible reasons for the increased bioavailability and reduced metabolite ratio in the fed state include the multiple effects of food constituents, and in particular lipid digestion products, on enhancing drug dissolution/solubilisation in the GIT, increasing drug transport through enterocytes, and/or modulating enterocyte-based metabolism. In the lymph cannulated dog model, the lymphatic transport of Hf increased from 1.3% to 53.9% of the administered dose in fed versus fasted dogs, respectively, whereas portal concentrations of Hf were similar in both fed and fasted states. In addition, a comparison of portal and systemic plasma concentrations confirmed that the proportion of Hf metabolised to Hfm was unaffected by post-prandial administration. Hence, it was concluded that the increased bioavailability and the decreased metabolite ratio is largely a consequence of significant post-prandial intestinal lymphatic transport (which bypasses hepatic metabolism) and not as a

result of lipid/formulation-mediated modulation of CYP3A-mediated first-pass metabolism.

In summary, large animal models such as these allow for oral administration of clinically relevant human dosage forms in representative fed and fasted states. Larger animal models have the advantage of gastric transit and biliary secretion profiles that more closely resemble the human situation. In addition cannulation of primary absorption routes (e.g. portal vein, thoracic lymph duct) affords a unique mechanistic assessment of the drug absorption/elimination processes, which is not feasible and/or possible with smaller animal models or human studies. However these models are expensive to set up and monitor, and are therefore impractical for initial screening of drug candidate molecules.

2.4.3. Single-Pass Perfusion in Conscious Dog/Pig–Loc-I-Gut

Although more widely quoted for testing in humans, the Loc-I-Gut technique has also been applied to large animal models (Figure 2.10). Lipka et al. [100] intubated beagle dogs in a standing position, using a wooden bite with a centre opening to prevent the dog chewing on the tube. The tube is passed slowly into the upper SI and the position verified by X-ray. The two end balloons are then inflated to facilitate controlled sampling and infusion in the intestinal segment. At a flow rate of 1.9 ml/min, and collecting the out flowing perfusate at 10-min intervals, steady state was achieved after ~30 min. P_{eff} values can then be estimated using the well-mixed tank model. This model again lends itself to a cross-over design, and dosing a different drug concentration which may be particularly useful in examining non-linear absorption kinetics. It also allows the effects to be examined in the absence of bile flow/gastric effluent. Four dogs were used in this study, which was performed according to a randomised cross-over design with a minimum 1-week washout between each treatment group. The model was used to demonstrate a concentration-dependent increase in the P_{eff} of S-celiprolol, indicative of a non-linear absorption mechanism and possibly a saturable intestinal efflux mechanism.

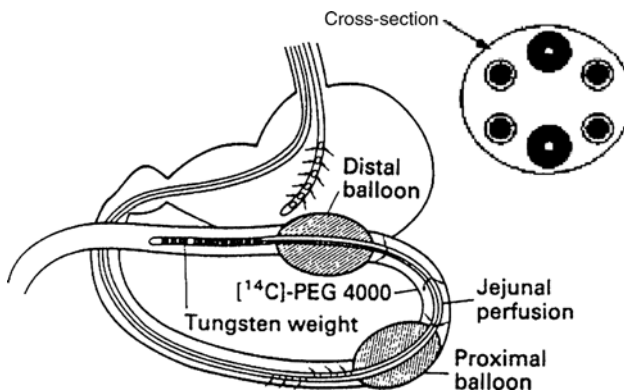


Figure 2.10 The Loc-I-Gut instrument allowing segmental intestinal perfusion in humans. The balloons are filled with air when the proximal balloon has passed the ligament of Treitz. The six-channel tube facilitates infusion of drug and marker, aspiration of perfusate and gastric drainage, and inflation of the two balloons [60].

2.4.4. Single-Pass Perfusion in Conscious Humans—Loc-I-Gut

Traditionally the most common way to evaluate drug absorption and bioavailability of drugs has been de-convolution techniques of plasma profiles from oral bioavailability studies. Methods of determining the rate and extent of absorption include the mass balance methods (Wagner Nelson, Loo reigleman), residual methods for k_a determination, and C_{\max} and t_{\max} [2]. However, these traditional methods are based on establishing plasma concentration versus time data and cannot be used to explicitly investigate transport rate across intestinal epithelium in vivo. There are a number of isolated intestinal perfusion techniques reported in humans, including open, semi-open, or closed perfusion of an intestinal segment, perfusion of a tied loop during surgery, colorectal perfusion, and colonic load via endoscope [33, 101–104].

The most commonly used intestinal perfusion technique utilises the Loc-I-Gut device, a sterile polyvinyl multi-lumen tube (external diameter 5.3 mm). The multi-channel tube (~175 cm long) contain six channels: two channels to the two latex balloons, one for infusion of drug solution, and one for sampling intestinal fluid. The two other tubes are for administration of marker (e.g. phenol red to detect leakage/drainage) (Figure 2.10). A 10-cm long segment is created between the balloons, enabling perfusion of a defined and closed section of the intestine. The occluding balloon provides a 'closed' set-up which has advantages over alternative open or semi-open perfusion techniques in that the closed system results in less contamination with luminal fluids from both proximal and distal leakage and provides better control of the hydrodynamic conditions within the segment. The tube is inserted and positioned in the human proximal jejunum under the guidance of a fluoroscopic technique. Subjects are fasted for a minimum of 10 h prior to positioning the tube, which takes ~1 h. Once in place, the latex balloons are inflated with air and a perfusion of phosphate buffer (70 mM) is initiated (2–3 ml/min). Phenol red is used as a marker in the stomach to detect proximal leakage. Given the two balloon set-up provides a 'closed' system, the hydrodynamics in the perfused segment are best described by the well-stirred model (Eq. 2.17). Furthermore Lennernäs et al. [105] performed a study on residence time distribution analysis to demonstrate that the hydrodynamics of this experimental set-up were best described using the well-stirred model. Drug absorption is calculated from the rate of disappearance of the drug from the perfused segment. Blood sampling from peripheral sites (e.g. forearms) is usually also performed to facilitate IV dosing and absolute bioavailability measurements.

Lennernäs's group at Uppsala has performed extensive studies to confirm the validity of this in vivo experimental set-up at assessing the rate and the extent of drug absorption. Recovery of PEG 4000 (a non-absorbable marker) is more than 95%, which indicates that the absorption barrier is intact. In addition, maintenance of functional viability of the mucosa during perfusion has been demonstrated by the rapid transmucosal transport of D-glucose and L-leucine. Estimation of absorption half-lives from the measured P_{eff} agree well with half-lives derived from oral dose studies in humans (i.e. physiologically realistic half-lives). Human P_{eff} estimates are well correlated with the fraction absorbed in humans, and served as the basis for BCS development, and hence the technique is ultimately the benchmark by which other in situ intestinal perfusion techniques are compared. The model has been extensively used to

assess both the impact of the ABL and paracellular route on drug absorption in humans [55]. Data from *in vivo* studies tend to indicate that the resistance of the ABL (i.e. P_{aq} in equation 2.4) to intestinal absorption of drugs can be generally considered to be negligible, and for both low and high permeability drugs, membranal resistance (i.e. P_m) appears to be rate-limiting step [106]. In addition, the contribution of paracellular transport in humans appears to be limited to small molecular weight hydrophilic drug compounds, and as such trans-cellular transport appears to be the major drug transport barrier for drug compounds >200 Da [60, 61, 107]. However, given the complexity of the model and the costs/ethical issues associated with human studies, the technique is generally considered a reference technique and it cannot be used routinely during drug development. A more detailed description of the technique, and in particular the applications of this technique to quantify *in vivo* dissolution and *in vivo* intestinal first-pass metabolism effects, is provided by Lennernäs [50].

The application of this model is currently best served in elucidating the interplay of various efflux transporters and/or first-pass metabolism on drug absorption. The technique has been successfully used to demonstrate increased intestinal permeability of verapamil with increasing jejunal concentrations, reflecting saturation of an active efflux transporter (presumed to be P-gp) at higher drug concentrations [94]. This effect has previously been demonstrated in the *in vitro* cell lines; however, in the human model the overall value of P_{eff} is high enough to suggest complete absorption, implying that passive diffusion in the apical to baso-lateral direction appears to dominate. In addition, a complete evaluation of the oral absorption process was accomplished by quantifying f_a , f_g , and f_h (estimated to be 0.58 ± 0.08 , 0.51 ± 0.18 , and 0.37 ± 0.14 for R-verapamil, respectively). Co-administration of ketoconazole, a potent CYP3A and modulator of P-gp, was found to increase overall bioavailability whereas the P_{eff} was unaffected [108]. Hence, intestinal and/or hepatic-mediated metabolism, and not susceptibility to P-gp efflux in the intestine, appears to be the major determinant of the overall amount of verapamil reaching the systemic circulation.

A more recent example of this technique has been the study on human absorption characteristics of fexofenadine [109]. Fexofenadine has been shown to be a substrate for P-gp in the *in vitro* cell lines; its disposition is altered in knockout mice lacking the gene for MDR1a, and co-administration of P-gp inhibitors (e.g. ketoconazole and verapamil) was shown to increase the oral bioavailability of fexofenadine [110–113]. Hence, it is suggested that the pharmacokinetics of fexofenadine appears to be determined by P-gp activity. In the human model, the intestinal permeability estimated on the basis of disappearance kinetics from the jejunal segment is low, and the fraction absorbed is estimated to be 2% [114]. Co-administration of verapamil/ketoconazole did not affect the intestinal permeability estimates; however, an increased extent of absorption (determined by de-convolution) was demonstrated. The increased absorption of fexofenadine was not directly related to inhibition of P-gp-mediated efflux at the apical membrane of intestinal cells as intestinal P_{eff} was unchanged. Furthermore, the effect cannot be explained by inhibition of intestinal based metabolism, as fexofenadine is not metabolised to any major extent. It was suggested that this may reflect modulation of efflux transporters in hepatocyte cells, thereby reducing hepatobiliary extraction of fexofenadine.

This theory was further explored in an anaesthetised pig model, which facilitated portal vein and bile sampling [86]. However, the hepatic extraction ratio and the biliary clearance of fexofenadine were unaffected by verapamil in the pig model. The question as to why verapamil/ketoconazole increase the fraction absorbed (i.e. based on appearance kinetics) and yet the fraction absorbed estimated on the basis of disappearance kinetics (i.e. P_{eff}) for the intestinal segment appears unchanged remains to be explored and most likely reflect multiple interplay between absorptive and efflux drug transporters in the intestinal tissue.

2.5. Discussion

Ultimately, the goal of the experimental models outlined is to demonstrate the benefit of direct in situ/in vivo investigations of important biopharmaceutical/pharmacokinetic properties, such as in vivo permeability, transport processes, and pre-systemic metabolism to oral drug development programs. The success of drug design and development programs represents a balance in optimising pharmacodynamic and pharmacokinetic properties of lead candidates to ensure adequate dosage form/dosage regimen design. In oral drug development programs, much of the focus centres on screening candidates for oral absorption characteristics, and in particular in selecting candidates with optimal intestinal permeability characteristics. A major success in terms of predicting optimal pharmacokinetic properties has been the derivation of the theoretical model whereby intestinal permeability P_{eff} can be used to predict fraction absorbed in humans. Hence estimates of fraction absorbed could be rapidly determined using an in situ rat perfusion technique, and indeed more rapid in vitro cell culture techniques have been similarly employed to provide less quantitative estimates of P_{eff} . Data from the rat perfusion system does not appear to be biased with respect to carrier-mediated or paracellular transport. While P_{eff} estimates using Caco-2 cells systems also show sufficient predictability for passively absorbed compounds [115], the P_{eff} for carrier-mediated and paracellularly transported compounds are generally poorly correlated to in vivo data, possibly reflecting differing morphological characteristics of colon cell culture models versus the in situ small intestine. For example, the overall lower effective permeability in Caco-2 model for small hydrophilic molecules reflects impaired paracellular transport due to tighter tight junctions in the in vitro model. Similarly, the importance of efflux carriers on intestinal absorption process may be overrated based on comparisons between Caco-2 cell data and human data [1, 109]. Therefore, despite lower throughput versus in vitro screening, the rat in situ perfusion model provide experimental conditions closer to the true in vivo situation and can therefore be considered favourable for preliminary BCS screening. Stewart et al. [115] recommend corroboration of permeabilities with an in vitro model (e.g. Caco-2, Ussing chamber) to provide the most useful insight into drug absorption characteristics in pre-clinical development.

2.5.1. Standardisation and Validation Criteria in P_{eff} Determination

As permeability predictions are required for defining the BCS classification of a drug, it is important to ensure that the conditions chosen should be carefully

set and standardised using the different absorption models. Conditions such as drug stability in intestinal perfusate, drug adsorption to apparatus, pH and osmolarity of buffer solutions, and the use of clinically relevant drug concentrations should be carefully considered to avoid potential errors in P_{eff} estimates. The functional viability of the intestinal tissue is always crucial when in situ models for intestinal membrane transport are used. The most commonly recommended standardisation criteria are listed in Table 2.3. The importance of standardising conditions was highlighted by Fagerholm et al. [46, 47] where in one set of experiments, the extent of recovery of PEG 4000 was >30%, which was indicative of un-physiological intestinal leakage.

To facilitate a standardisation of inter-laboratory results of permeability, it is now common practice to include a range of model drugs as internal standards in initial validation (i.e. method suitability) of intestinal perfusion techniques [116]. A list of 20 model drugs has been reported by the FDA for the standardisation of the in situ intestinal perfusion experiment, whereas six drugs are recommended for human studies. Once the method has been

Table 2.3 Standardisation criteria used to establish an intestinal perfusion model for use in a BCS context.

Condition	Criteria
Osmolarity of perfusate solution	The buffer osmolarity should be standardised to facilitate estimation of P_{eff} values. Generally adjusted to physiological conditions of ~290 mOsm/kg. (70 mM phosphate buffer) with 5.4 mM potassium chloride, 48 mM sodium chloride, 35 mM mannitol, and 10 mM D-glucose. Lane et al. [131] demonstrated the effect of hypersomolar perfusion on P_{app} of ibuprofen in the in situ rat gut technique. Hypersomolar solutions tended to decrease P_{eff} values, attributable to a reversed solvent drag effect.
Internal standards	Used to demonstrate method reproducibility. Reference materials, such as the low permeability markers mannitol and atenolol and the high permeability markers metoprolol and ketoprofen, may be used to compare values between laboratories [3, 50]
Clinically relevant drug concentrations	Linear absorption characteristics at clinically relevant concentrations should be demonstrated. Lack of effect of concentration on P_{eff} determined in a range of physiologically relevant concentrations can be used to demonstrate lack of a saturable absorption mechanism (i.e. carrier mediated). Concentrations used in experiment should represent clinically relevant concentrations [132]
pH	Generally adjusted to physiological conditions, e.g. 6.5. Levis et al. [133] assessed the impact of a range of physiological buffers on P_{eff} of ibuprofen. The perfusate pH affected the P_{eff} significantly, thereby underlining the importance of taking into account the effect of pH, particularly for ionisable drug compounds
Drug stability in experimental set-up.	Demonstrate minimal degradation of drug substance in buffer and also adsorption onto experimental apparatus

Table 2.4 Compounds used to assess viability and/or modulate physiological functions in intestinal perfusion techniques.

Compound	Function	Criteria
^{14}C PEG4000	Non-absorbable marker or zero permeability marker	Extent of recovery >95–99% indicates that the intestinal mucosa is intact, also used as markers for transmucosal water flux
^3H D-glucose	Actively transported via the Na^+ /D-glucose co-transporter	Steady-state permeability values for D-glucose indicate that active transport processes are operational (typically at concentration >100 mM). At low concentrations (e.g. 1 mM), absorption is assumed to be ABL controlled and hence at these concentration can serve as marker for resistance of the ABL
Antipyrine	Passively transported compound	Steady-state permeability values for antipyrine indicate that passive transport processes are operational. Stable transmucosal transport of antipyrine during the experiment indicates that the mesenteric blood flow is stable [33, 60]
$^3\text{H}_2\text{O}$	Blood flow at absorption site	The intestinal absorption of $^3\text{H}_2\text{O}$ is reported to be blood flow limited and serves as a marker for blood flow at the absorption site [89, 118]
Verapamil/Digoxin	Efflux pump substrate/inhibitor	Co-administration of verapamil/digoxin can be used to demonstrate the impact of efflux transporters on permeability [134]
Ketoconazole	Efflux pump modulator and/or CYP inhibitor	Can be used to demonstrate the impact of intestinally mediated efflux/metabolism on permeability estimates [114].
Rifampicin	CYP inducer	Pre-treatment of rats with Rifampicin for up to 2 weeks pre-experiment can be used to assess the effect of induction of intestinal metabolism on P_{eff} values [135]

ABL: aqueous boundary layer.

validated, it is common to include three compounds in perfusion experiments (a zero, low, and high permeability model compound) as internal standards. A zero permeability marker may be used to correct for volume changes; a low permeability internal standard is suggested to provide assurance of membrane integrity, and in addition to the high permeability standard, verify method reproducibility (Table 2.4)

2.5.2. Choice of in Situ Versus in Vivo Models

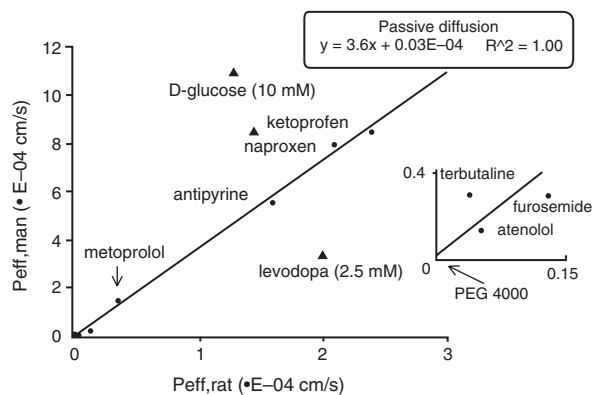
In situ techniques suffer the disadvantage that the animal is anaesthetised for the duration of the experiment. Surgery and anaesthesia change several physiological factors that can alter drug absorption characteristics. Anderson et al. [117] found the ABL thickness in laparotomised rats to be higher than in conscious non-laparotomised rats. Yuasa et al. [118] reported that

the combined effect of laparotomy and anaesthesia appears to increase ABL resistance, possibly as a result of reduced gut motility and luminal mixing, providing a greater barrier to absorption of lipophilic drugs. Indeed, in studies on intestinal amino acid and xylose absorption, intestinal absorptive function was not fully returned to normal levels until 2–3 days post-operative [90, 119]. Urethane and phenobarbital are the most widely used anaesthetic regimens in intestinal absorption studies. Whereas urethane may offer advantages in terms of longer and more stable anaesthesia, phenobarbital appeared to have less of an impact on the absorption process. However, a study by Ueda et al. [120] found that bioavailability of oxacillin was increased in phenobarbital-induced anaesthetised rats versus conscious rats and this was mainly due to a decrease in hepatic metabolic extraction. Ketamine/midazolam appears to diminish the active transport of glucose and increase intestinal blood flow and as such is not favoured in intestinal absorption studies [118]. Uhing et al. [91] studied the effect of surgery/anaesthesia on CYP3A activity and portal venous blood flow in acute (i.e. 4 h post-surgery) and chronic (i.e. 3 days post-surgery) groups of rats. Ketamine/xylazine anaesthetic significantly reduced hepatic CYP3A activity and portal venous blood flow in the acute group. Ketamine/midazolam also appears to diminish the active transport of glucose and as such is not favoured in intestinal absorption studies [118]. Hence, while in situ methods facilitate a more mechanistic evaluation under controlled conditions, and are generally cheaper to establish, the interpretation of in situ experimental results should carefully address the impact of anaesthesia and/or surgical trauma.

2.5.3. Choice of Animal Species

Fagerholm et al. [46, 47] demonstrated that the rat and the human jejunum P_{eff} estimates of passively transported compounds correlate highly (Figure 2.11) and both can be used to predict in vivo oral absorption in man, therein supporting the utility of the rat in predicting f_a in humans. The human P_{eff} estimates for a range of passively absorbed compounds were on average 3.6 times higher than in the rat irrespective of BCS classification. Possible reasons for the lower value in the rat model versus human data are differences in effective absorptive area of the perfused segment. Species differences affecting partitioning into the membrane may also be a factor for certain actively transported compounds. Carrier-mediated transported compounds (such as L-dopa and D-glucose) deviate from the linear relationship (Figure 2.11). P_{eff} for D-glucose was ~ 10 times

Figure 2.11 A comparison between human and rat effective intestinal permeability coefficients (P_{eff}). The equation describes the correlation for passive diffusion. The inset shows the P_{eff} values in the lower range (\bullet = passive absorption; Δ = carrier-mediated absorption) [46, 47].



lower in the in situ rat compared to that in humans, which most likely reflects anaesthesia-induced reduction in D-glucose. Similarly, Cao et al. [121] found a high degree of correlation (>0.8) between P_{eff} estimates in rats and humans for 16 compounds encompassing both passive and carrier-mediated substrates; verapamil, a substrate for P-gp, however, did not appear to fit the trend as well as the other compounds. Hence, for certain carrier-mediated transport drugs, scaling between models may be required, since the transport maximum and/or substrate specificity might differ [46, 47].

While the primary objective of the BCS was to assist in the prediction of oral absorption characteristics, it should be remembered that the fraction absorbed predicted from intestinal permeability estimates is not synonymous with bioavailability (i.e. rate and extent of absorption). In particular, quantifying the impact of intestinally mediated efflux/elimination and hepatic-mediated metabolism on the fraction of drug reaching the systemic circulation has become a new focus. Hence, for drugs where f_g and f_h are significant, perfusion techniques with concomitant plasma sampling are required to delineate the relative contributions of intestinal and hepatic-mediated extraction. The success of the rat model in terms of predicting human absorption characteristics data undoubtedly lies in the correlation between the permeability characteristics of the rat and the human tissue. However, the debate as to the utility of rat to predict f_g and f_h in humans is still unresolved. Chiou and Barve [48] reported that the bioavailability of 64 drugs in rats was highly correlated with the bioavailability obtained in humans ($r^2 > 0.97$). The range of drugs studied was all considered non-solubility rate limited, varied widely in physiochemical properties, and display both passive and active absorption mechanisms.

In contrast a recent paper by Cao et al. [121] identified that the rat model may not be a good predictor of human oral bioavailability. No correlation was found in terms of bioavailability in rats and bioavailability in humans. A correlation of >0.8 was obtained for a comparison of rat and human permeability for a range of drugs with both carrier-mediated and passive diffusion mechanisms, confirming that the rat is a good predictor of the fraction absorbed in humans. The reasons for these differences reflect the inter-species differences in f_a , f_g , and f_h and these were further explored by comparing expression profiles of transporters and metabolising enzymes in rats and humans. Gene expression profiles were measured using gene-chip analysis. The correlation between transport and metabolising enzymes are presented in Figure 2.12.

The authors suggest that the transport expression profiles displayed a moderate correlation ($r^2 = 0.57$) obtained in the SI. No correlation was found for the expression of metabolising enzymes between the rat and the human intestine, which indicates the difference in drug metabolism in the two different species and the challenges in predicating f_g and f_h from rat to human. These findings suggest therefore that the rat model can be used for predicting f_a in humans, but not to predict the first-pass metabolism (i.e. f_g and f_h) and/or bioavailability (F) in humans. This study highlights the need for further mechanistic studies in both human and animal models to identify inter-species commonalities in transporter and/or metabolic profiles.

Large animal models represent a more costly yet valuable tool in the evaluation of the gastrointestinal absorption of oral dosage forms. The dog has been considered by many groups as a popular model, despite considerable differences in physiology of the GIT compared to humans (Gardner et al.

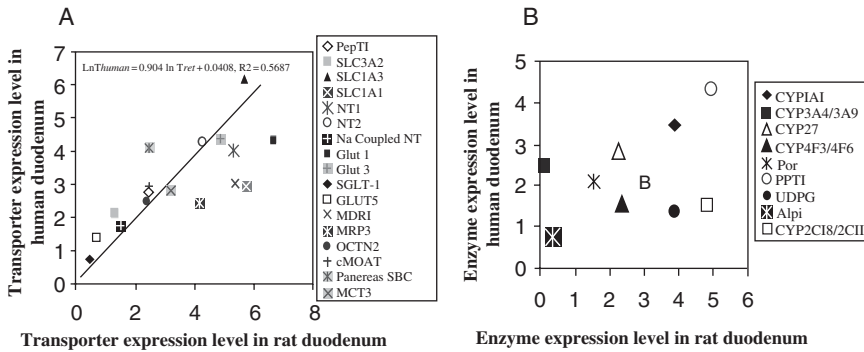


Figure 2.12 Correlation plots of (A) transporter expression and (B) metabolic enzyme expression in duodenum between rat and human. The expression levels of transporters and metabolic enzymes are normalised by GADPH expression, transformed by natural logarithm and absolute values were used in the correlation analysis [121].

[137]). Chiou et al. [122] completed a comparison of bioavailability of 43 drugs in dogs and humans, and reported a poor correlation between the two species ($r^2 = 0.512$). Monkey may be a good model for predicting oral absorption in humans, but are very expensive models. Chiou and Buehler [123] found absorption values in monkeys were similar to those in humans. Similar t_{\max} values were found in monkeys and humans at comparable doses, indicative of similar absorption kinetics between the two species. The pig is considered to be the most suitable non-primate animal model since it resembles the human better than any other non-primate animal species with regard to eating behaviour, anatomy, and physiology of the GIT [124, 125]. In the pig, each segment of the GIT is considered to be comparable to man. Moreover, the bacterial flora of the colon and the digestion characteristics of the small intestines are considered to be similar to man [126]. The pig has been extensively used as a model of physiological studies of the digestive system and has recently received increased attention as a model for investigations of the impact of intestinal absorption and first-pass metabolism of drugs [86, 127, 128]. However, the expression and functional activity of membrane transporters/enzymes in intestinal and hepatic membranes is less explored than in rats.

In this regard the study by Cao et al. [121] provided a useful means for evaluating suitability of animal species for pre-clinical studies by comparing gene expression profiles of the major intestinally based efflux transporters and metabolising enzymes between species. For example in this study drug transporters expression profiles in rats and humans were generally similar with higher expression levels in the small intestine for both species. An interesting exception to this, however, is the MDR1 expression which codes for P-gp. In humans MDR1 expression is 2.7-fold greater in duodenum than in the colon (Figure 2.13a). These findings suggest that in the humans P-gp-mediated efflux activity is greater in the duodenum relative to the colon, whereas in the rat the opposite appears to be true. CYP3A4 in humans corresponds to the ortholog CYP3A9 in rat, based on unigene analysis. While expression levels are higher in the small intestine for both rat and human, interestingly the

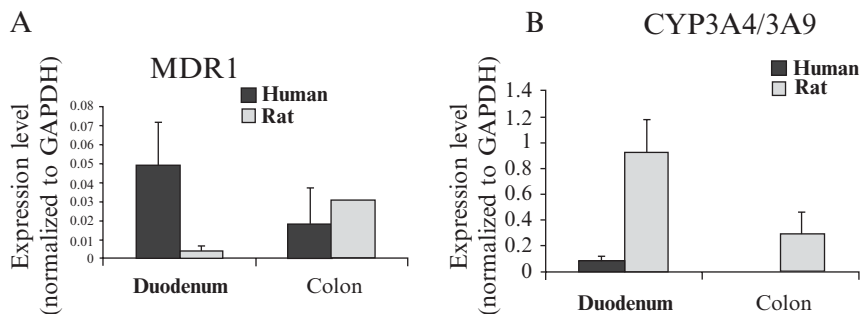


Figure 2.13 Comparison of gene expression levels for (A) MDR1 (i.e. P-gp) and (B) human CYP3A4 and the homology in rat (CYP3A9), in duodenum and colon of human and rat intestine. The expression levels of transporters and metabolic enzymes are normalised by GAPDH expression, transformed by natural logarithm and absolute values were used in the correlation analysis [121].

rat intestine appears to display significantly higher CYP levels—suggesting a superior capacity of rat intestine to metabolise drug compared to human intestine (Figure 2.13b). The implications for the differing regional expression profiles between the species may shed some light on discrepancies between in situ and in vivo observations and direct researchers into appropriate species selection.

In summary, the approaches to predicting oral drug absorption have been summarised. The key role of in situ models for determination of intestinal permeability characteristics and its application in defining oral absorption characteristics and BCS classification were outlined. Despite lower throughput versus in vitro cell culture techniques, the in situ rat intestinal perfusion model remains a crucial pre-clinical screening tool, offering clear advantages in terms of predicting human permeability characteristics of both passive and carrier-mediated compounds. However, elucidating the factors defining intestinal versus hepatically mediated first-pass metabolism continues to offer an exciting research challenge, aimed ultimately at providing a clearer understanding of the factors determining the rate and the extent of drug presentation to the systemic circulation. Further in situ and in vivo studies are required to provide greater insight into the overall contribution of intestinal-based first-pass metabolism and the relative contribution of the various drug efflux transporters on drug uptake and extraction. To this end, large animal models, and in particular the pig, involving direct determination of f_a (intestinal perfusion), f_g (pre-hepatic sampling), and f_h (post-hepatic sampling), may offer distinct advantages in terms of providing a more complete mechanistic evaluation of oral drug absorption process and therein predict the oral bioavailability in humans.

References

1. Lennernäs H and Abrahamsson B (2005) The Use of Biopharmaceutic Classification of Drugs in Drug Discovery and Development: Current Status and Future Extension. *J Pharm Pharmacol* **57**: pp 273–285.
2. Roland M and Tozer TN (1995) *Clinical Pharmacokinetics: Concepts and Applications*. 3rd Edn. Lippincott, Williams & Wilkins.

3. Amidon GL, Lennernäs H, Shah VP and Crison JR (1995) A Theoretical Basis for a Biopharmaceutical Drug Classification: The Correlation In Vitro Drug Product Dissolution and In Vivo Bioavailability. *Pharm Res* **12**: pp 413–420.
4. Sinko PJ, Leesman GD and Amidon GL (1991) Predicting Fraction Dose Absorbed in Humans Using a Macroscopic Mass Balance Approach. *Pharm Res* **8**: pp 979–988.
5. Ho NF, Park JY, Morozowich W and Higuchi WI (1977) Physical Model Approach to the Design of Drugs With Improved Intestinal Absorption. In: EB Roche (Ed.), Design of Biopharmaceutical Properties Through Prodrugs and Analogs. Washington, D.C., AAPS Vol. 8: pp 136–227.
6. Overton E (1899) Ueber Die Allgemeinen Osmotischen Eigenschaften Der Zelle, Ihre Vermutlichen Ursachen Und Ihre Bedeutung Fur Die Physiologie. *Vjschr Naturforsch Ges Zurich* **44**: pp 88.
7. Gibaldi M (1991) Biopharmaceutics and Clinical Pharmacokinetics. 4th Edn. Lea and Febiger.
8. Ashford M (2002) Bioavailability—Physicochemical and Dosage Form Factors: In Pharmaceutics the Science of Dosage Form Design. In: M Aulton (Ed.), Pharmaceutics. The Science of Dosage Form Design. 2nd Ed. Churchill Livingstone, pp 234–252.
9. Suzuki A, Higuchi WI and Ho NF (1970a) Theoretical Model Studies of Drug Absorption and Transport in the Gastrointestinal Tract. I. *J Pharm Sci*. **59**: pp 644–651.
10. Suzuki A, Higuchi WI and Ho NF (1970b) Theoretical Model Studies of Drug Absorption and Transport in the Gastrointestinal Tract. II. *J Pharm Sci* **59**: pp 651–659.
11. Leo A, Hansch C and Elkins D (1971) Partition Coefficients and Their Uses. *Chem Rev* **71**: pp 525.
12. Hansch C and Dunn WJ (1972) Linear Relationships Between Lipophilic Character and Biological-Activity of Drugs. *J Pharm Sci* **61**: pp 1–19.
13. Dressman JB, Amidon GL and Fleisher D (1985) Absorption Potential—Estimating the Fraction Absorbed for Orally-Administered Compounds. *J Pharm Sci* **74**: pp 588–589.
14. Macheras PE and Symillides MY (1989) Toward a Quantitative Approach for the Prediction of the Fraction of Dose Absorbed Using the Absorption Potential Concept. *Biopharm Drug Dispos* **10**: pp 43–54.
15. Sanghvi T, Ni N and Yalkowsky SH (2001) A Simple Modified Absorption Potential. *Pharm Res* **18**: pp 1794–1796.
16. Yalkowsky SH, Johnson JL, Sanghvi T and Machatha SG (2006) A ‘Rule of Unity’ for Human Intestinal Absorption. *Pharm Res* **23**: pp 2475–2481.
17. Diamond JM and Wright EM (1969) Molecular Forces Governing Non-Electrolyte Permeation Through Cell Membranes. *Proc. R. Soc. London Ser. B-Biol. Sci.* **172**: pp 273–316.
18. Conradi RA, Burton PS and Borchardt RT (1996) Physicochemical and Biological Factors That Influence a Drug’s Cellular Permeability by Passive Diffusion. In: V Pliska, B Testa, H Van De Waterbeemd (Eds.), Lipophilicity in Drug Action and Toxicology. Weinheim, VCH, pp 233–252.
19. Palm K, Stenberg P, Luthman K and Artursson P (1997) Polar Molecular Surface Properties Predict the Intestinal Absorption of Drugs in Humans. *Pharm Res* **14**: pp 568–571.
20. Palm K, Luthman K, Ungell AL, Strandlund G and Artursson P (1996) Correlation of Drug Absorption with Molecular Surface Properties. *J Pharm Sci* **85**: pp 32–39.
21. Winiwarter S, Ax F, Lennernäs H, Hallberg A, Pettersson C and Karlen A (2003) Hydrogen Bonding Descriptors in the Prediction of Human In Vivo Intestinal Permeability. *J Mol Graph Model* **21**: pp 273–287.

22. Zhao YH, Abraham MH, Hersey A and Luscombe CN (2003) Quantitative Relationship Between Rat Intestinal Absorption and Abraham Descriptors. *Eur J Med Chem* **38**: pp 939–947.
23. Clark DE (1999) Rapid Calculation of Polar Molecular Surface Area and Its Application to the Prediction of Transport Phenomena. 1. Prediction of Intestinal Absorption. *J Pharm Sci* **88**: pp 807–814.
24. Yu LX, Lipka E, Crison JR and Amidon GL (1996b) Transport Approaches to the Biopharmaceutical Design of Oral Drug Delivery Systems: Prediction of Intestinal Absorption. *Adv Drug Deliv Rev* **19**: pp 359–376.
25. Lipinski CA, Lombardo F, Dominy BW and Feeney PJ (1997) Experimental and Computational Approaches to Estimate Solubility and Permeability in Drug Discovery and Development Settings. *Adv Drug Deliv Rev* **23**: pp 3–25.
26. Andrews CW, Bennett L and Yu LX (2000) Predicting Human Oral Bioavailability of a Compound: Development of a Novel Quantitative Structure-Bioavailability Relationship. *Pharm Res* **17**: pp 639–644.
27. Winiwarter S, Bonham NM, Ax F, Hallberg A, Lennernäs H and Karlen A (1998) Correlation of Human Jejunal Permeability (in Vivo) of Drugs With Experimentally and Theoretically Derived Parameters: A Multivariate Data Analysis Approach. *J Med Chem* **41**: pp 4939–4949.
28. Jung SJ, Choi SO, Um SY, Kim JI, Choo HY, Choi SY and Chung SY (2006) Prediction of the Permeability of Drugs Through Study on Quantitative Structure-Permeability Relationship. *J Pharm Biomed Anal* **41**: pp 469–475.
29. Ni PF, Ho NF, Fox JL, Leuenberger H and Higuchi WI (1980) Theoretical Model Studies of Intestinal Drug Absorption 5. Non-Steady-State Fluid Flow and Absorption. *Int J Pharm* **5**: pp 33–48.
30. Ho NF, Merkle HP and Higuchi WI (1983a) Quantitative, Mechanistic and Physiologically Realistic Approach to the Biopharmaceutical Design of Oral-Drug Delivery Systems. *Drug Dev Ind Pharm* **9**: pp 1111–1184.
31. Leipold RJ (1995) Description and Simulation of a Tubular, Plug Flow Model to Predict the Effect of Bile Sequestrants on Human Bile Excretion. *J Pharm Sci* **84**: pp 670–672.
32. Corrigan OI, Gubbins RH and O'Driscoll CM (2003) Estimation of Absorption Parameters from the Non-Steady-State Phase in the Rat Gut Perfusion Model. *J Pharm Pharmacol* **55**: pp 487–493.
33. Lennernäs H, Ahrenstedt O, Hallgren R, Knutson L, Ryde M and Paalzow LK (1992) Regional Jejunal Perfusion, a New In vivo Approach to Study Oral-Drug Absorption in Man. *Pharm Res* **9**: pp 1243–1251.
34. Komiya I, Park JY, Kamani A, Ho NF and Higuchi WI (1980) Quantitative Mechanistic Studies in Simultaneous Fluid Flow and Intestinal Absorption Using Steroids As Model Solutes. *Int J Pharm* **4**: pp 249–262.
35. Amidon GL, Kou J, Elliott RL and Lightfoot EN (1980) Analysis of Models for Determining Intestinal Wall Permeabilities. *J Pharm Sci* **69**: pp 1369–1373.
36. Amidon GL, Sinko PJ and Fleisher D (1988) Estimating Human Oral Fraction Dose Absorbed—A Correlation Using Rat Intestinal-Membrane Permeability for Passive and Carrier-Mediated Compounds. *Pharm Res* **5**: pp 651–654.
37. Yu LX, Crison JR and Amidon GL (1996a) Compartmental Transit and Dispersion Model Analysis of Small Intestinal Transit Flow in Humans. *Int J Pharm* **140**: pp 111–118.
38. Yu LX and Amidon GL (1999) A Compartmental Absorption and Transit Model for Estimating Oral Drug Absorption. *Int J Pharm* **186**: pp 119–125.
39. Schanker LS, Tocco DJ, Brodie BB and Hogben CA (1958) Absorption of Drugs from the Rat Small Intestine. *J Pharmacol Exp Ther* **123**: pp 81–88.

40. Doluisio JT, Billups NF, Dittert LW, Sugita ET and Swintosky JV (1969) Drug Absorption.I. An In Situ Rat Gut Technique Yielding Realistic Absorption Rates. *J Pharm Sci* **58**: pp 1196–1200.
41. Ho NF and Higuchi WI (1974) Theoretical Model Studies of Intestinal Drug Absorption IV. *J Pharm Sci* **63**: pp 686–690.
42. Sutton SC, Rinaldi MT and Vukovinsky KE (2001) Phenol Red and Comparison of the Gravimetric 14c-Peg-3350 Methods to Determine Water Absorption in the Rat Single-Pass Intestinal Perfusion Model. *AAPS Pharm Sci* **3**: pp 1–5.
43. Stewart BH, Chan HO, Kezyk N and Fleisher D (1997) Discrimination Between Drug Candidates Using Models for Evaluation of Intestinal Absorption. *Adv Drug Deliv Rev* **23**: pp 27–45.
44. Schurgers N, Bijdendijk J, Tukker JJ and Crommelin DJ (1986) Comparison of Four Experimental Techniques for Studying Drug Absorption Kinetics in the Anaesthetized Rat in Situ. *J Pharm Sci* **75**: pp 117–119.
45. Scott-Harris M, Kennedy JG, Siegesmund KA and Yorde DE (1988) Relationship Between Distension and Absorption in Rat Intestine.1. Effect of Luminal Volume on the Morphology of the Absorbing Surface. *Gastroenterology* **94**: pp 1164–1171.
46. Fagerholm U, Johansson M and Lennernäs H (1996a) Comparison Between Permeability Coefficients in Rat and Human Jejunum. *Pharm Res* **13**: pp 1336–1342.
47. Fagerholm U, Lindahl A and Lennernäs H (1996b) Regional Intestinal Permeability for Compounds with Different Physico-Chemical Properties and Transport Mechanisms in Rats. *Eur J Pharm Sci* **4**: pp 153.
48. Chiou WL and Barve A (1998) Linear Correlation of the Fraction of Oral Dose Absorbed of 64 Drugs Between Humans and Rats. *Pharm Res* **15**: pp 1792–1795.
49. Salphati L, Childers K, Pan L, Tsutsui K and Takahashi L (2001) Evaluation of a Single-Pass Intestinal-Perfusion Method in Rat for the Prediction of Absorption in Man. *J Pharm Pharmacol* **53**: pp 1007–1013.
50. Lennernäs H (2000) Animal Perfusion Studies. In: JB Dressman, H Lennernas (Eds.), *Oral Drug Absorption: Prediction and Assessment*. New York, NY, Dekker, Inc. pp 73–98.
51. Watkins PB, Wrighton SA, Schuetz EG, Molowa DT and Guzelian PS (1987) Identification of Glucocorticoid-Inducible Cytochromes P-450 in the Intestinal Mucosa of Rats. *J Clin Invest* **80**: pp 1029–1036.
52. Kolars JC, Stetson PL, Rush BD, Ruwart MJ, Schmiedlin-Ren P and Duell EA (1992) Cyclosporin Metabolism by P450III A in Rat Enterocytes. *Transplantation* **53**: pp 596–602.
53. Watkins PB (1992) Drug Metabolism by Cytochromes P450 in the Liver and Small Bowel. *Gastroenterol Clin North Am* **21**: pp 511–526.
54. Benet LZ, Wu CY, Hebert MF and Wachter VJ (1996) Intestinal Drug Metabolism and Anti-Transport Processes: A Potential Paradigm Shift in Oral Drug Delivery. *J Control Release* **39**: pp 139–143.
55. Lennernäs H (1998) Human Intestinal Permeability. *J Pharm Sci* **87**: pp 403–410.
56. Meredith D and Boyd CA (1995) Oligopeptide Transport by Epithelial Cells. *J Membr Biol* **145**: pp 1–12.
57. Porter CJ and Charman WN (2001) Intestinal Lymphatic Drug Transport: An Update. *Adv Drug Deliv Rev* **50**: pp 61–80.
58. Griffin BT and O'Driscoll CM (2006) A Comparison of Intestinal Lymphatic Transport and Systemic Bioavailability of Saquinavir from Three Lipid-Based Formulations in the Anaesthetised Rat Model. *J Pharm Pharmacol* **58**: pp 917–925.
59. Ungell AL, Nylander S, Bergstrand S, Sjoberg A and Lennernäs H (1998) Membrane Transport of Drugs in Different Regions of the Intestinal Tract of the Rat. *J Pharm Sci* **87**: pp 360–366.

60. Nilsson DA, Fagerholm U and Lennernäs H (1994) The Influence of Net Water Absorption on the Permeability of Antipyrine and Levodopa in the Human Jejunum. *Pharm Res* **11**: pp 1540–1544.
61. Lennernäs H (1995) Does Fluid Flow Across the Intestinal Mucosa Affect Quantitative Oral Drug Absorption? Is It Time for a Re-Evaluation? *Pharm Res* **12**: pp 1573–1582.
62. Munoz MJ, Merino-Sanjuan M, Lledo-Garcia R, Casabo VG, Manez-Castillejo F and Nacher A (2005) Use of Nonlinear Mixed Effect Modeling for the Intestinal Absorption Data: Application to Ritonavir in the Rat. *Eur J Pharm Biopharm* **61**: pp 20–26.
63. Rodriguez-Ibanez M, Sanchez-Castano G, Montalar-Montero M, Garrigues TM, Bermejo M and Merino V (2006) Mathematical Modelling of In Situ and In Vitro Efflux of Ciprofloxacin and Grepafloxacin. *Int J Pharm* **307**: pp 33–41.
64. Lindahl A, Sandström R, Ungell AL and Lennernäs H (1998) Concentration- and Region-Dependent Intestinal Permeability of Fluvastatin in the Rat. *J Pharm Pharmacol* **50**: pp 737–744.
65. Sandström R, Karlsson A and Lennernäs H (1998b) The Absence of Stereoselective P-Glycoprotein-Mediated Transport of R/S-Verapamil Across the Rat Jejunum. *J Pharm Pharmacol* **50**: pp 729–735.
66. Ruiz-Balaguer N, Nacher A, Casabo VG and Sanjuan MM (2002) Intestinal Transport of Cefuroxime Axetil in Rats: Absorption and Hydrolysis Processes. *Int J Pharm* **234**: pp 101–111.
67. Windmuller HG and Spaeth AE (1981) Vascular Autoperfusion of the Rat Small Intestine In-Situ. *Methods Enzymol* **77**: pp 120–129.
68. Singhal D, Ho NF and Anderson BD (1998) Absorption and Intestinal Metabolism of Purine Dideoxynucleosides and an Adenosine Deaminase-Activated Prodrug of 2',3'-Dideoxyinosine in the Mesenteric Vein Cannulated Rat Ileum. *J Pharm Sci* **87**: pp 569–577.
69. Pithavala YK, Soria I and Zimmerman CL (1997) Use of the Deconvolution Principle in the Estimation of Absorption and Pre-Systemic Intestinal Elimination of Drugs. *Drug Metab Dispos* **25**: pp 1260–1265.
70. Wachter VJ, Wu CY and Benet LZ (1995) Overlapping Substrate Specificities and Tissue Distribution of Cytochrome-P450 3a and P-Glycoprotein—Implications for Drug-Delivery and Activity in Cancer-Chemotherapy. *Mol Carcinog* **13**: pp 129–134.
71. Johnson BM, Chen WQ, Borchardt RT, Charman WN and Porter CJ (2003) A Kinetic Evaluation of the Absorption, Efflux, and Metabolism of Verapamil in the Autoperfused Rat Jejunum. *J Pharmacol Exp Ther* **305**: pp 151–158.
72. Miyazaki K, Sunada K, Iseki K and Arita T (1986) Simultaneous Vascular and Luminal Perfusion of Rat Small-Intestine. *Chem Pharm Bull* **34**: pp 3830–3835.
73. Devries MH, Rademaker CM, Geerlings C, Vandijk A and Noordhoek J (1989) Pharmacokinetic Modeling of the Effect of Activated-Charcoal on the Intestinal Secretion of Theophylline, Using the Isolated Vascularly Perfused Rat Small-Intestine. *J Pharm Pharmacol* **41**: pp 528–533.
74. Kavin H, Levin NW and Stanley MM (1967) Isolated Perfused Rat Small Bowel—Technic Studies of Viability Glucose Absorption. *J Appl Physiol* **22**: pp 604–611.
75. McMaster D, Steel L and Love AH (1983) The Isolated, Vascularly Perfused, Small-Intestine of the Rat—A Useful Tool for the Study of Absorption in Nutritional Deficiency. *Ir J Med Sci* **152**: pp 329–335.
76. Stretch GL, Nation RL, Evans AM and Milne RW (1999) Organ Perfusion Techniques in Drug Development. *Drug Develop Res* **46**: pp 292–301.

77. Pang KS, Cherry WF and Ulm EH (1985) Disposition of Enalapril in the Perfused Rat Intestine-Liver Preparation—Absorption, Metabolism and 1st-Pass Effect. *J Pharmacol Exp Ther* **233**: pp 788–795.
78. Cong D, Fong AK, Lee R and Pang KS (2001) Absorption of Benzoic Acid in Segmental Regions of the Vascularly Perfused Rat Small Intestine Preparation. *Drug Metab Dispos* **29**: pp 1539–1547.
79. O’Driscoll C (2003) Intestinal Lymphatic Targeting of Drugs. *STP Pharma Sci* **13**: pp 17–25.
80. Porter CJ, Treviskis NL and Charman WN (2007) Lipids and Lipid-Based Formulations: Optimizing the Oral Delivery of Lipophilic Drugs. *Nat Rev Drug Discov* **6**: pp 231–248.
81. Charman WN and Stella VJ (1986) Estimating the Maximal Potential for Intestinal Lymphatic Transport of Lipophilic Drug Molecules. *Int J Pharm* **34**: pp 175–178.
82. Edwards GA, Porter CJ, Caliph SM, Khoo SM and Charman WN (2001) Animal Models for the Study of Intestinal Lymphatic Drug Transport. *Adv Drug Deliv Rev* **50**: pp 45–60.
83. O’Driscoll CM (1992) Anatomy and Physiology of the Lymphatics. In: WN Charman, VJ Stella (Eds.), *Lymphatic Transport of Drugs*. Boca Raton, CRC Press.
84. Porter CJ and Charman WN (1997) Uptake of Drugs into the Intestinal Lymphatics After Oral Administration. *Adv Drug Deliv Rev* **25**: pp 71–89.
85. Khoo SM, Shackelford DM, Porter CJ, Edwards GA and Charman WN (2003) Intestinal Lymphatic Transport of Halofantrine Occurs After Oral Administration of a Unit-Dose Lipid-Based Formulation to Fasted Dogs. *Pharm Res* **20**: pp 1460–1465.
86. Petri N, Bergman E, Forsell P, Hedeland M, Bondesson U, Knutson L and Lennernäs H (2006) First-Pass Effects of Verapamil on the Intestinal Absorption and Liver Disposition of Fexofenadine in the Porcine Model. *Drug Metab Dispos* **34**: pp 1182–1189.
87. Tukker JJ and Poelma FG (1988a) Site Dependent Absorption in the Rat Intestine. Abstract, Third Int. Conf. on Drug Absorption, Edinburgh, P45.
88. Tukker JJ and Poelma FG (1988b) Site-Dependent Absorption in the Intestine of the Rat—Variation in Absorption Between Lipophilic and Hydrophilic Compounds. *Pharmac Weekblad-Sci Ed* **10**: pp 183.
89. Hoffman DJ, Seifert T, Borre A and Nellans HN (1995) Method to Estimate the Rate and Extent of Intestinal-Absorption in Conscious Rats Using an Absorption Probe and Portal Blood-Sampling. *Pharm Res* **12**: pp 889–894.
90. Uhing MR and Arango V (1997) Intestinal Absorption of Proline and Leucine in Chronically Catheterized Rats. *Gastroenterology* **113**: pp 865–874.
91. Uhing MR, Beno DW, Jiyamapa-Serna VA, Chen Y, Galinsky RE, Hall SD and Kimura RE (2004) The Effect of Anesthesia and Surgery on CYP3A Activity in Rats. *Drug Metab Dispos* **32**: pp 1325–1330.
92. Sinko PJ, Lee YH, Makhey V, Leesman GD, Sutyak JP, Yu H, Perry B, Smith CL, Hu P, Wagner EJ, Falzone LM, Mcwhorter LT, Gilligan JP and Stern W (1999) Biopharmaceutical Approaches for Developing and Assessing Oral Peptide Delivery Strategies and Systems: In Vitro Permeability and In Vivo Oral Absorption of Salmon Calcitonin (Sct). *Pharm Res* **16**: pp 527–533.
93. Lee YH, Perry BA, Lee HS, Kunta JR, Sutyak JP and Sinko PJ (2001) Differentiation of Gut and Hepatic First-Pass Effect of Drugs: 1. Studies of Verapamil in Ported Dogs. *Pharm Res* **18**: pp 1721–1728.
94. Sandström R, Karlsson A, Knutson L and Lennernäs H (1998a) Jejunal Absorption and Metabolism of R/S-Verapamil in Humans. *Pharm Res* **15**: pp 856–862.

95. Kunta JR, Lee SH, Perry BA, Lee YH and Sinko PJ (2004) Differentiation of Gut and Hepatic First-Pass Loss of Verapamil in Intestinal and Vascular Access-Ported (IVAP) Rabbits. *Drug Metab Dispos* **32**: pp 1293–1298.
96. Kleinbloesem CH, Vanharten J, Wilson JP, Danhof M, Vanbrummelen P and Breimer DD (1986) Nifedipine—Kinetics and Hemodynamic-Effects in Patients with Liver-Cirrhosis After Intravenous and Oral-Administration. *Clin Pharmacol Ther* **40**: pp 21–28.
97. Paine MF, Shen DD, Kunze KL, Perkins JD, Marsh CL, Mcvicar JP, Barr DM, Gillies BS and Thummel KE (1996) First-Pass Metabolism of Midazolam by the Human Intestine. *Clin Pharmacol Ther* **60**: pp 14–24.
98. Lin JH, Chiba M and Baillie TA (1999) Is the Role of the Small Intestine in First-Pass Metabolism Overemphasized? *Pharmacol Rev* **51**: pp 135–157.
99. Humberstone AJ, Porter CJ and Charman WN (1996) A Physicochemical Basis for the Effect of Food on the Absolute Oral Bioavailability of Halofantrine. *J Pharm Sci* **85**: pp 525–529.
100. Lipka E, Spahn-Langguth S, Mutschler E and Amidon GL (1998) In Vivo Non-Linear Intestinal Permeability of Celiprolol and Propranolol in Conscious Dogs: Evidence for Intestinal Secretion. *Eur J Pharm Sci* **6**: pp 75–81.
101. Ewe K, Wanitscke R and Staritz M (1984) Intestinal Permeability Studies in Humans. In: TZ Csaky (Ed.), *Pharmacology of Intestinal Permeation II*. New York, Springer-Verlag, pp 535–571.
102. Knutson L, Olind B and Hallgren R (1989) A New Technique for Segmental Jejunal Perfusion in Man. *Am J Gastroenterol* **84**: pp 1278–1284.
103. Raab Y, Hällgren R, Knutson L, Krog M and Gerdin B (1992) A Technique for Segmental Rectal and Colonic Perfusion in Humans. *Am J Gastroenterol* **10**: pp 1453–1459.
104. Lennernäs H (1997) Human Jejunal Effective Permeability and Its Correlation with Preclinical Drug Absorption Models. *J Pharm Pharmacol* **49**: pp 627–638.
105. Lennernäs H, Lee I, Fagerholm U and Amidon GL (1997) A Residence-Time Distribution Analysis of the Hydrodynamics Within the Intestine in Man During a Regional Single-Pass Perfusion With Loc-I-Gut: In-Vivo Permeability Estimation. *J Pharm Pharmacol* **49**: pp 682–686.
106. Fagerholm U and Lennernäs H (1995) Estimation of the Unstirred Water Layer Thickness in the Human Small Intestine, and Its Importance in Oral Drug Absorption. *Eur J Pharm Sci* **3**: pp 247–253.
107. Lennernäs H, Ahrenstedt O and Ungell AL (1994) Intestinal Drug Absorption During Induced Net Water Absorption in Man; a Mechanistic Study Using Antipyrine, Atenolol and Enalaprilat. *Br J Clin Pharmacol* **37**: pp 589–596.
108. Sandström R, Knutson TW, Knutson L, Jansson B and Lennernäs H (1999) The Effect of Ketoconazole on the Jejunal Permeability and CYP3A Metabolism of (R/S)-Verapamil in Humans. *Br J Clin Pharmacol* **48**: pp 180–189.
109. Lennernäs H (2003) Intestinal Drug Absorption and Bioavailability: Beyond Involvement of Single Transport Function. *J Pharm Pharmacol* **55**: pp 429–433.
110. Cvetkovic M, Leake B, Fromm MF, Wilkinson GR and Kim RB (1999) OATP and P-Glycoprotein Transporters Mediate the Cellular Uptake and Excretion of Fexofenadine. *Drug Metab Dispos* **27**: pp 866–871.
111. Soldner A, Christians U, Susanto M, Wachter VJ, Silverman JA and Benet LZ (1999) Grapefruit Juice Activates P-Glycoprotein-Mediated Drug Transport. *Pharm Res* **16**: pp 478–485.
112. Simpson K and Jarvis B (2000) Fexofenadine—a Review of Its Use in the Management of Seasonal Allergic Rhinitis and Chronic Idiopathic Urticaria. *Drugs* **59**: pp 301–321.

113. Petri N, Tannergren C, Rungstad D and Lennernäs H (2004) Transport Characteristics of Fexofenadine in the Caco-2 Cell Model. *Pharm Res* **21**: pp 1398–1404.
114. Tannergren C, Knutson T, Knutson L and Lennernäs H (2003) The Effect of Ketoconazole on the In Vivo Intestinal Permeability of Fexofenadine Using a Regional Perfusion Technique. *Br J Clin Pharmacol* **55**: pp 182–190.
115. Stewart BH, Chan OH, Lu RH, Reyner EL, Schmid HL, Hamilton HW, Steinbaugh BA and Taylor MD (1995) Comparison of Intestinal Permeabilities Determined in Multiple In-Vitro and In-Situ Models—Relationship to Absorption in Humans. *Pharm Res* **12**: pp 693–699.
116. Centre for Drug Evaluation FDA (2000). Waiver of In Vivo Bioavailability and Bioequivalence Studies for Immediate Release Solid Oral Dosage Forms Based on a Biopharmaceutical Classification System. Guidance for industry. 2000.
117. Anderson BW, Levine AS, Levitt DG, Kneip JM and Levitt MD (1988) Physiological Measurement of Luminal Stirring in Perfused Rat Jejunum. *Am J Phys* **254**: pp G843–G848.
118. Yuasa H, Matsuda K and Watanabe J (1993) Influence of Anesthetic Regimens on Intestinal-Absorption in Rats. *Pharm Res* **10**: pp 884–888.
119. Singh G, Chaudry KL, Chudler LC, Oneill PJ and Chaudry IH (1991) Measurement of D-Xylose Gut Absorptive-Capacity in Conscious Rats. *Am J Physiol* **261**: pp R1313–R1320.
120. Ueda S, Yamaoka K and Nakagawa T (1999) Effect of Pentobarbital Anaesthesia on Intestinal Absorption and Hepatic First-Pass Metabolism of Oxacillin in Rats, Evaluated by Portal-Systemic Concentration Difference. *J Pharm Pharmacol* **51**: pp 585–589.
121. Cao XH, Gibbs ST, Fang LY, Miller HA, Landowski CP, Shin HC, Lennernäs H, Zhong YQ, Amidon GL, Yu LX and Sun DX (2006) Why Is It Challenging to Predict Intestinal Drug Absorption and Oral Bioavailability in Human Using Rat Models. *Pharm Res* **23**: pp 1675–1686.
122. Chiou WL, Jeong HY, Chung SM and Wu TC (2000) Evaluation of Using Dog As an Animal Model to Study the Fraction of Oral Dose Absorbed of 43 Drugs in Humans. *Pharm Res* **17**: pp 135–140.
123. Chiou WL and Buehler PW (2002) Comparison of Oral Absorption and Bioavailability of Drugs Between Monkey and Human. *Pharm Res* **19**: pp 868–874.
124. Kararli TT (1995) Comparison of the Gastrointestinal Anatomy, Physiology, and Biochemistry of Humans and Commonly Used Laboratory-Animals. *Biopharm Drug Dispos* **16**: pp 351–380.
125. Davis SS, Illum L and Hinchcliffe M (2001) Gastrointestinal Transit of Dosage Forms in the Pig. *J Pharm Pharmacol* **53**: pp 33–39.
126. Dressman JB and Yamada K (1991) Animal Models for Oral Absorption. In: PG Welling, FLS Tse, SV Dinghe (Eds.), *Pharmaceutical Bioequivalence*, VI 48. New York, Dekker, pp 727–739.
127. Goh LB, Spears KJ, Yao DG, Ayrton A, Morgan P, Wolf CR and Friedberg T (2002) Endogenous Drug Transporters in In Vitro and In Vivo Models for the Prediction of Drug Disposition in Man. *Biochem Pharmacol* **64**: pp 1569–1578.
128. Tannergren C, Evilevitch L, Pieczynowski S, Piedra JV, Westrom B, Erlwanger K, Tatara M and Lennernäs H (2006) The Effect of Pancreatic and Biliary Depletion on In Vivo Pharmacokinetics of Digoxin in Pigs. *Eur J Pharm Sci* **29**: pp 198–204.
129. Johnson DA and Amidon GL (1988) Determination of Intrinsic Membrane Transport Parameters from Perfused Intestine Experiments a Boundary Layer Approach to Estimating the Aqueous and Unbiased Membrane Permeabilities. *J Theor Biol* **131**: pp 93–106.
130. Poelma FGJ and Tukker JJ (1987) Evaluation of a Chronically Isolated Internal Loop in the Rat for the Study of Drug Absorption Kinetics. *J Pharm Sci* **76**: pp 433–436.

131. Lane ME, Levis KA and Corrigan OI (2006) Effect of Intestinal Fluid Flux on Ibuprofen Absorption in the Rat Intestine. *Int J Pharm* **309**: pp 60–66.
132. Berggren S, Hoogstraate J, Fagerholm U and Lennernäs H (2004) Characterization of Jejunal Absorption and Apical Efflux of Ropivacaine, Lidocaine and Bupivacaine in the Rat Using In Situ and In Vitro Absorption Models. *Eur J Pharm Sci* **21**: pp 553–560.
133. Levis KA, Lane ME and Corrigan OI (2003) Effect of Buffer Media Composition on the Solubility and Effective Permeability Coefficient of Ibuprofen. *Int J Pharm* **253**: pp 49–59.
134. Salphati L and Benet LZ (1998) Effects of Ketoconazole on Digoxin Absorption and Disposition in Rat. *Pharmacology* **56**: pp 308–313.
135. Sandström R and Lennernäs H (1999) Repeated Oral Rifampicin Decreases the Jejunal Permeability of R/S-Verapamil in Rats. *Drug Metab Dispos* **27**: pp 951–955.
136. Cummins CL, Salphati L, Reid MJ and Benet LZ (2003) In vivo modulation of Intestinal CYP3A by P-Glycoprotein: Studies using the rat single pass intestinal perfusion model. *J Pharmacol Exp Ther* **305**: pp 306–314.
137. Gardner N, Haresign W, Spiller R, Farraj N, Wiseman J, Norbury H, Illum L (1996) Development and validation of a pig model for colon-specific drug delivery. *J. Pharm. Pharmacol* **48**: pp 689–693.

Drug Absorption from the Colon In Situ

Hiroaki Yuasa

Abstract Recent advances in controlled-release techniques have allowed the delivery of drugs to the colon, that is, the lower part of the gastrointestinal tract, following oral administration, and this has raised the general interest in colonic drug absorption. Although the colon cannot match the small intestine in many of its morphological and functional aspects related to drug absorption, it notably has several carrier-mediated transport systems that might be used as drug targets for colonic absorption, and it is as permeable as the small intestine to some lipophilic drugs. In situ rat colon models are important in preclinical investigations to assess fundamental permeability issues and also to explore colonic drug delivery strategies. For absorption evaluation using these models, the closed loop method is usually the recommended choice as it is more suitable for relatively slow absorption, which is often the case in the colon, than perfusion methods. These methods of absorption evaluation are reviewed in this chapter together with permeability characteristics of the colonic membrane.

Keywords: Colon; Controlled release; Sustained release; Rat; Single-pass perfusion; Recirculation; Closed loop; Carrier-mediated transport; Passive transport; Membrane permeability; P-glycoprotein; Paracellular pathway; Transcellular pathway

Abbreviations

BCRP	Breast cancer resistance protein
CYP	Cytochrome P450
MRP	Multidrug resistance-associated protein
MW	Molecular weight
P-gp	P-glycoprotein/Multidrug resistance protein-1
SCFA	Short-chain fatty acid
SI	Small intestine

3.1. Introduction

The colon generally plays only a secondary role in systemic drug absorption, since many orally administered drugs from conventional rapid-release formulations are already absorbed during their passage through the small intestine, before even reaching the lower part of the gastrointestinal tract, that is, the colon. The small intestine, composed of duodenum, jejunum, and ileum, is undoubtedly the main site of drug absorption, due to its anatomical location right after the stomach. Because of its morphological features, such as its length and large surface area, the small intestine is perfectly designed for solute absorption. Furthermore, it features various carrier-mediated transport systems for nutrient absorption which can also be helpful in absorbing drugs that are structurally analogous to nutrients. The colon cannot match the small intestine in any of these aspects and has, therefore, attracted less attention as a site of drug absorption. Recent advances in controlled-release techniques, however, allow for delivery of drugs to the lower part of the gastrointestinal tract and thus, the general interest in colonic drug absorption has been raised [1].

To devise and achieve successful colonic drug delivery, it is important to understand the characteristics of the colonic epithelium as the barrier to drug absorption, and also the physiological characteristics of the colon, including its luminal environment. The colonic lumen is maintained low with water content, due to continued water absorption as a process of fecal formation, and slightly acidic, due to production of short-chain fatty acids (SCFA) by the abundant bacterial fauna. Colonocytes can take SCFA up efficiently and in part utilize them as nutritional sources. Intracellular pH is, however, maintained homeostatically, avoiding unwanted acidification by absorbed SCFA. It is notable that several carrier-mediated transport systems are involved in such a homeostatic pH regulation and also in the uptake of SCFA. However, although the bacterial flora in the lumen of the colon is by far more numerous than that of the small intestine, it has been suggested that the peptidase activity in the colon is much lower than that of the small intestine [2, 3]. In addition, the activities of several other enzymes involved in drug metabolism, such as cytochrome P450 (CYP) 3A [4], esterases [5], UDP glucosyltransferases, and sulfotransferases [6], have been suggested to be lower in the colon. Therefore, for drugs that are prone to presystemic degradation, colonic delivery may be an advantageous option. One example being peptide drugs that are degraded by peptidases in the small intestine, but may be delivered more efficiently via the colon, using colon-specific delivery techniques. Colonic absorption can also be beneficial in enhancing the performance of sustained release formulations. Materials that have reached the colon stay there for quite a long time. The colonic transit time can be, though variable and difficult to estimate, as long as 8 h or longer [2, 7], while the small intestinal transit time is shorter in a range of about 2–5 h [2, 8]. Therefore, delayed release in the colon could be effective in further sustaining absorption. However, it is fundamental and prerequisite that drugs are permeable across the colonic epithelium at an appreciable level for successful colonic delivery, including the possible examples mentioned above.

An increasing number of preclinical and clinical studies have been conducted in recent years aiming to clarify the barrier function of the colonic epithelium in more detail and to devise drug delivery strategies, for example, by modulating factors limiting colonic drug absorption. For preclinical

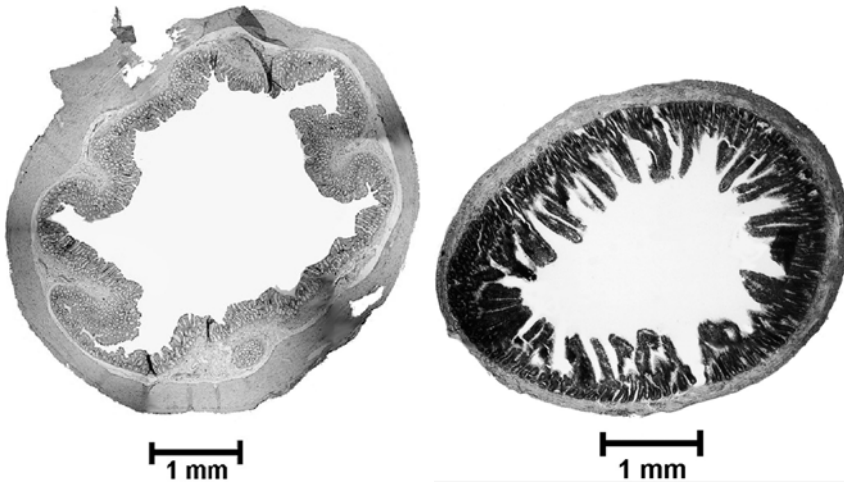


Figure 3.1 Cross section of the rat colon (A) in comparison to small intestine (B). Tissues were fixed with 10% formalin, stained with 0.125% hematoxylin and 0.25% eosin, and observed with a microscope ($\times 20$).

evaluation of colonic drug absorption, the rat is the most widely used animal, as is often the case for pharmacokinetic and drug disposition studies.

3.2. In Situ Rat Colon Model for Absorption Evaluation

The colon of male adult rats of about 300 g, which are regularly used for this type of studies, is about 10 cm in length. This is roughly one-tenth the length of the small intestine. The wet weight of colonic tissue is about 150 mg/cm and thereby about 30% higher than that of the small intestine [9]. The main reason for this significant difference can be found in the thicker tissue layer, although the colon has a moderately larger outer circumference than the small intestine. The anatomical architecture of the cross section of the colon is compared with that of the small intestine in Figure 3.1. The approximated cylindrically luminal radius of the rat colon is comparable with that of the small intestine (0.2–0.25 cm), and hence the colon can accommodate the same volume of solution per unit length (about 100 $\mu\text{l}/\text{cm}$) in absorption experiments. However, the luminal surface of the colon does not have the villous structure of the small intestine and therefore its mucosal surface area (2.2 cm^2) for unit length is about one-fourth to one-half in comparison (8.2, 8.5, 6.3, and 4.4 cm^2 , respectively, for duodenum, jejunum, midgut, and ileum) [10, 11]. Furthermore, although colonic enterocytes do have microvilli, those are less closely packed. In summary, it is evident that the surface of the colon is morphologically less well equipped for water and solute absorption than that of the small intestine.

Because of fermentation processes, the luminal environment of the colon is slightly acidic at a pH value around 6.6 [2]. Similar pH values can be found in the upper small intestine (pH 6.5 and pH 6.7, in the duodenum and jejunum, respectively), whereas in the ileum the pH is slightly higher at a neutral to alkaline pH value around 7.1 [2]. Therefore, the slightly acidic solutions, which are generally used for maintaining physiologically relevant luminal conditions

in situ absorption experiments involving the small intestine, can be also used as standard solutions in the colon.

Experimental methods for in situ absorption evaluation used in the colon are similar to those used for the small intestine. The colonic lumen can be perfused by a single-pass manner (single-pass perfusion method), perfused in a recirculated manner (recirculation method), or filled with drug solution (closed loop method). Absorption can then be measured from the amount of drug that disappeared from the lumen. Alternatively or supplementarily, it can also be evaluated by the amount that appears in the mesenteric blood or the systemic circulation. However, perfusion experiments are slightly more difficult to conduct in the colon, compared to the small intestine. The reason is that the colonic absorption is often too slow to achieve a significant absorptive extraction after a single passage of drug solution through the perfused segment. The extraction can in theory be increased by using a longer segment or by reducing the flow rate. However, manipulating such experimental parameters is not very helpful to overcome the problem, because the total length of the colon is limited and a certain flow rate is required to maintain the flow stable. In a typical setting of an absorption study using the small intestine, a 10-cm segment is perfused at a flow rate of at least 0.15 ml/min. Since the total length of the rat colon is only 10 cm, using a longer part is out of the question; on the other hand, it is difficult to maintain a stable flow at even lower flow rates. The situation is similar when the perfusion solution is recirculated through a reservoir. It generally takes a longer time to achieve a detectable reduction in the drug concentration in the reservoir for the colon than for the small intestine. Consequently, the closed loop method is usually the recommended choice for absorption evaluation in the colon in situ. In this method, a drug solution is introduced into a segment of colon, of which the both ends are closed by ligation, and the luminal solution is obtained at an appropriate time to determine the amount of remaining drug and evaluate its absorptive loss. This method is similar to the recirculation method in the way that absorption is evaluated from the disappearance of drugs as a function of time. The volume of drug solution is minimized to the luminal volume, without an external reservoir, so that the fractional rate of absorption is maximized and absorptive loss can be detected very easily.

Absorption evaluation from luminal disappearance of drugs has been widely employed as a simple and easy method. Although the appearance of drugs in the mesenteric blood can provide a more sensitive way that enables to detect lower levels of absorption, it is technically more complicated, especially due to the colon's anatomical and morphological configuration. Another alternative for absorption evaluation is to measure drugs that appear in the systemic circulation, although this method cannot provide a direct measure of membrane permeability.

In situ models are to evaluate absorption or membrane permeability under the physiologically relevant tissue condition. While the luminal environment can be modulated by the administered solution, the tissue condition is physiologically controlled. The estimated membrane permeability can be, in most cases, assumed to represent the transport across the epithelial cell layer at steady state or quasisteady state. However, one needs to be aware that the involvement of metabolic degradation, which may occur at the cellular surface or within the cytosol, can be a factor leading to biased estimates of membrane permeability and erroneous interpretation of the transport process. Particularly,

metabolic degradation at the epithelial surface can contribute to luminal disappearance, based on which absorption is generally evaluated.

3.3. Permeability Characteristics of the Rat Colonic Membrane

3.3.1. Carrier-Mediated Transport

Although the colon is not a major organ for absorption of nutrients and drugs, the colonic epithelium is highly active in absorbing water, Na^+ , and other minerals [2]. SCFA, which typically include acetic, propionic, and butyric acid produced by colonic bacteria, are also well absorbed [2]. Such absorptive functions, which are important in maintaining the colonic environment, are largely supported by various carrier-mediated transport systems. Thus, while many carrier-mediated transport systems for important nutrients, such as D-glucose, are absent or present only at low levels, it has been known that several carrier-mediated transport systems, such as Na^+/H^+ exchangers and monocarboxylate/ H^+ cotransporters, are present in the colon and play physiologically important roles [12–14]. It is, therefore, of interest to study the characteristics of the colonic membrane and compare them with those of the small intestinal membrane, with regard to solute permeation by carrier-mediated transport, as well as passive transport. It is of particular interest to examine if any of the carrier-mediated transport systems that have been identified in the small intestine, or similar ones, may exist in the colon, since they might be possibly used as drugs' targets for colonic absorption, in addition to absorption in the small intestine. Alternatively, those transport systems might be important for absorption processes of drugs released from sustained-release formulations.

The carrier for riboflavin (vitamin B₂) is an example of a highly active one found to be functionally present in the rat colon in situ [15]. The apparent membrane permeability of riboflavin is markedly lower at a higher concentration (Table 3.1), indicating the involvement of saturable transport by the carrier. The apparent membrane permeability for carrier-mediated transport is as much as about half of that in the small intestine at the lower concentration, where carrier-mediated transport is highly efficient (Table 3.2). As demonstrated by an in vitro study using everted sacs of intestinal tissue, the carrier-mediated riboflavin transport system in the colon is Na^+ -dependent, similarly to the one in the small intestine [16]. Inhibition by lumiflavin, an analogue of riboflavin, and several tricyclic-type drugs, which are structurally analogous to riboflavin, for example, chlorpromazine and methylene blue, can be observed similarly in both intestinal sites. The Michaelis constant (K_m) of carrier-mediated riboflavin transport is, however, lower in the colon ($0.13 \mu\text{M}$) than in the small intestine ($0.57 \mu\text{M}$), indicating that the carrier in the colon has a higher affinity to riboflavin. Thus, although the riboflavin carrier in the colon may not be identical with the one in the small intestine, both seem to be quite similar in terms of substrate specificity and regulation mechanism. Although the physiological role of the carrier in the colon is mostly unclear, it can be hypothesized that it assists in the efficient uptake of low levels of riboflavin produced by luminal bacteria for local nutrition of colonocytes [17].

Table 3.1 Saturable transport in the rat colon of selected compounds which are typically absorbed by carrier-mediated transport in the small intestine.

Compound	Concentration (mM)	CL _{app} (μl/min/cm)	References
Riboflavin	0.1 × 10 ⁻³	1.76 ± 0.37	[15]
	0.2	0.12 ± 0.03 ^a	
D-Glucose	0.001	0.99 ± 0.15	[18]
	0.1	1.02 ± 0.15	
	0.5	0.75 ± 0.10	
	1	0.37 ± 0.08 ^a	
	2	0.22 ± 0.10 ^a	
	10	ND	
Taurocholate	0.1 × 10 ⁻³	1.11 ± 0.036	[18]
	0.001	0.99 ± 0.07	
	0.1	0.23 ± 0.02 ^a	
	4	0.07 ± 0.004 ^a	
Glycerol	0.002	0.55 ± 0.03	[19]
	1	0.22 ± 0.02 ^a	
	40	0.08 ± 0.03 ^a	

Note: Data represent the mean ± S.E. ($n = 3$). CL_{app}, apparent membrane permeability clearance; ND, not detected. Absorption was evaluated in our laboratory using the closed loop of the rat colon in situ (urethane anesthesia, 1.125 g/4.5 ml/kg, i.p.) in 60 min for riboflavin and 30 min for the others.

^a $p < 0.05$ compared with the value for the lowest concentration.

Saturable transport indicating the involvement of carriers in the rat colon in situ, although less efficient than the one for riboflavin, has also been described for D-glucose, taurocholate, and glycerol (Tables 3.1 and 3.2) [18–20]. The apparent membrane permeability for carrier-mediated transport in the colon is less than 20% of that in the small intestine, as evaluated at concentrations where carrier-mediated transport is highly efficient. For the carriers for D-glucose and taurocholate in the colon, although functional levels are low, Na⁺-dependent nature can be observed in situ [18] and also in everted sacs in vitro [21]. This is similar to the respective counterparts in the small intestine. Interestingly, the K_m is smaller in the colon by a factor of about 18

Table 3.2 Comparison of apparent membrane permeabilities of carrier-mediated transport between colon and small intestine of the rat.

Compound	Concentration (μM)	CL _{app,c} (μl/min/cm)			References
		Colon	SI	Colon/SI	
Riboflavin	0.1	1.64	3.8	0.43	[15]
D-Glucose	1	0.99	11.0 ^a	0.090	[18, 20]
Taurocholate	0.1	1.11	6.5 ^a	0.17	[18, 20]
Glycerol	2	0.47	4.2	0.11	[19]

Note: CL_{app,c}, apparent membrane permeability clearance for carrier-mediated transport component at lower concentrations where it is highly efficient; SI, small intestine; ileum for taurocholate and midgut for the others. Absorption was evaluated in our laboratory using the closed loop of the rat intestine in situ (urethane anesthesia, 1.125 g/4.5 ml/kg, i.p.) in 60 min for riboflavin and 30 min for the others.

^a Apparent J_{max}/K_m by single-pass perfusion experiments, where J_{max} is the maximum transport rate and K_m is the Michaelis constant [20].

Table 3.3 Unsaturable transport in the rat colon of selected compounds which are absorbed by carrier-mediated transport in the small intestine.

Compound	Concentration (mM)	CL _{app} (μ l/min/cm)	References
L-Carnitine	0.01	0.054 \pm 0.036	[23]
	10	0.052 \pm 0.024	
Methotrexate	0.1 $\times 10^{-3}$	0.059 \pm 0.032	[18]
	0.02	0.050 \pm 0.046	
Cephadrine	0.1	0.39 \pm 0.02	[18]
	40	0.23 \pm 0.15	
5-Fluorouracil	0.02 $\times 10^{-3}$	0.90 \pm 0.09	[18]
	10	0.64 \pm 0.02	

Note: Data represent the mean \pm S.E. ($n = 3$). CL_{app}, apparent membrane permeability clearance. Absorption was evaluated in our laboratory using the closed loop of the rat colon in situ (urethane anesthesia, 1.125 g/4.5 ml/kg, i.p.) in 60 min for L-carnitine and 30 min for the others.

and 67, for D-glucose and taurocholate, respectively [22]. Thus, the colonic carrier-mediated transport systems for D-glucose and taurocholate, as well as that for riboflavin, have consistently higher affinity than their respective counterparts in the small intestine. The common feature of these carriers may be their role in an effective absorption of low levels of nutrients, which have not already been absorbed in the small intestine but managed to reach the colon.

On the other hand, several probe substrates of carrier-mediated transport systems in the small intestine have been reported to be not absorbed by carrier-mediated mechanism in the rat colon in situ. Those include L-carnitine [23], methotrexate [18], cephradine [18], and 5-fluorouracil [18], as substrates of the L-carnitine carrier, folate carrier, peptide carrier, and pyrimidine carrier, respectively (Table 3.3). It is based on the nonsaturable nature of their transport. Particularly, the apparent membrane permeabilities of L-carnitine and methotrexate are negligibly low, suggesting that these compounds are practically unabsorbable from the colon. In the case of 5-fluorouracil, Na⁺-independence of transport was observed in situ [18] and also in everted sacs in vitro in the colon [21], while its carrier in the small intestine is known to be Na⁺-dependent. Furthermore, for ascorbate and nicotinate, as described in everted sacs in vitro [21], and L-dopa, as described in situ [24], carrier-mediated transport cannot be observed in the rat colon.

Carrier-mediated efflux from the epithelial cells is an important factor limiting absorption. It has been suggested that the expression of P-glycoprotein (P-gp), probably the most important efflux pump in the body, is to some extent higher in the colon than in the small intestine [25]. However, P-gp is functionally not more active, as suggested by the fact that the apparent membrane permeability of rhodamine 123, a typical substrate of P-gp, in the rat colon in situ is comparable with that in the small intestine [26]. Similar findings are described for verapamil [27] and DMP728 cyclic peptide [28] in studies using the rat intestinal tissue in vitro. A number of other secretory carriers have been found recently, for example, breast cancer resistance protein (BCRP) and multidrug resistance-associated protein-2 (MRP2), but their

functional expression levels in the colon have only been perfunctory studied to date.

3.3.2. Passive Transport

Absorption profiles and physicochemical properties of several passively transported hydrophilic compounds across the rat intestine *in situ* are summarized in Table 3.4 [15, 18, 19, 23, 29, 30]. Urea, the smallest molecule listed, shows much higher apparent membrane permeability than glycerol, the second smallest one, in the colon, even though they are similar in lipophilicity. This may be because transport through the paracellular (or channel) pathway is prevailing in the colonic absorption of urea and the pathway may be tight or selective enough to exclude molecules of the size of glycerol and above. However, among the other, bigger molecules, riboflavin, cephradine, and 5-fluorouracil are more permeable than glycerol, while D-mannitol, D-xylose, and L-carnitine are permeable, but as poorly as glycerol. Especially, 5-fluorouracil is more permeable than even urea. Since the lipophilicity of 5-fluorouracil is much higher than that of urea and other compounds with very low apparent membrane permeability, passive transcellular transport may be prevailing in its colonic absorption. This may also be the case for riboflavin and cephradine.

Based on morphological surface area consideration, the apparent membrane permeability for passive transport in the colon should be about 30% of that in the midgut area of the small intestine. The colon-to-SI (small intestine) ratios of the apparent membrane permeability for hydrophilic solutes are, however, highly variable as shown in Table 3.4. While the colon-to-SI ratios for D-mannitol, riboflavin, and cephradine are relatively close to the value of 30%, the ratios for D-xylose and glycerol are an order of magnitude lower. It is also interesting to note that glycerol is more permeable than urea in the small intestine, while it is opposite in the colon. This may be because of the presence of a channel that is more selective for glycerol, but is present only in the small intestine. It may also explain in part the very small colon-to-SI ratio for glycerol. The colon-to-SI ratio for urea is also relatively small, being about one-half of what would be expected. The reason for this might be looser (or abundant) paracellular (or channel) pathways in the small intestine. D-Xylose, a five-carbon monosaccharide, is another compound showing a very small colon-to-SI ratio, particularly compared with D-mannitol, which is a six-carbon monosaccharide and quite similar to D-xylose in terms of physicochemical properties. A possible explanation is that D-xylose has some affinity to the D-glucose carrier, though very weak and unsaturable at a wide range of concentration. This glucose carrier is more abundant in the small intestine.

Thus, the apparent membrane permeability characteristics of hydrophilic compounds listed in Table 3.4 indicate that colonic epithelium is different from small intestinal epithelium in selectivity, or size or density distribution of the paracellular pathway. This is further complicated because of the possible involvement of unidentified carriers or channels for some compounds, as suggested for glycerol and D-xylose. However, the colon-to-SI ratios of the apparent membrane permeability are generally comparable with (or lower than) those calculated considering the morphological surface area, suggesting that such factors are not in favor for colonic absorption in most cases. Matching

Table 3.4 Absorption profiles of hydrophilic compounds absorbed by passive transport in the rat intestine.

Compound	MW	log $P_{o/w}$	Concentration (mM)		Fraction absorbed (%)		CL _{app} (μ l/min/cm)			Reference
			Colon	SI	Colon	SI	Colon	SI	Colon/SI	
Urea	60	-2.75	11.4 ± 1.4	62.3 ± 0.6	0.40 ± 0.05	3.25 ± 0.05	0.12			[19]
Glycerol	92	-2.56	2.5 ± 0.9	73.1 ± 0.2	0.08 ± 0.03	4.38 ± 0.03	0.018			[19]
Riboflavin	376	-1.14	6.9 ± 1.5	20.6 ± 1.8	0.12 ± 0.03	0.39 ± 0.04	0.31			[15]
Cephradine	349	NA	6.7 ± 4.0	NA	0.23 ± 0.15	0.83 ± 0.05 ^a	0.28			[18, 29]
5-Fluorouracil	130	-0.95	17.4 ± 0.6	65.7 ± 6.8	0.64 ± 0.02	3.70 ± 0.66	0.17			[18]
D-Mannitol	182	-3.10	0.30 ± 0.08	0.74 ± 0.31	0.010 ± 0.003	0.025 ± 0.010	0.40			NA ^b
D-Xylose	150	-2.44	0.93 ± 0.09	12.6 ± 1.8	0.031 ± 0.003	0.49 ± 0.08	0.063			NA ^b
L-Carnitine	162	NA	3.1 ± 1.4	13.8 ± 2.3	0.052 ± 0.024	0.25 ± 0.05	0.21			[23]

Note: Data represent the mean ± S.E. ($n = 3$). MW, molecular weight; $P_{o/w}$, octanol-to-water partition coefficient; CL_{app}, apparent membrane permeability clearance; SI, midgut area of the small intestine; NA, not available or applicable. Absorption was evaluated in our laboratory using the closed loop of the rat intestine in situ (urethane anesthesia, 1.125 g/4.5 ml/kg, i.p.) in 60 min for riboflavin and L-carnitine and 30 min for the others. For those that are transported by carriers in part (riboflavin and glycerol in both colon and SI, and L-carnitine, 5-fluorouracil, and cephradine in SI), absorption was evaluated at higher concentrations where the contribution of carrier-mediated transport is negligible. Values of $P_{o/w}$ were obtained from a report by Leo et al. [30] except for that of D-xylose, which was determined in our laboratory.

^a Data by single-pass perfusion experiments.

^b Unpublished data from our laboratory.

colon-to-SI ratios have also been reported for atenolol (0.33) and metoprolol (0.27) in a study using the rat intestine in situ [24]. It is known, on the other hand, that lipophilic drugs tend to show higher colon-to-SI ratios. It is notable that naproxen [24] and indomethacin [31] are highly and almost equally permeable in the colon and small intestine, according to studies using the rat intestine in situ. However, there is no theoretical basis established for this observation beyond the suggestion that lipophilicity may be a factor.

3.4. Concluding Remarks

Recent advances in controlled-release techniques have allowed the delivery of drugs to the colon, that is, the lower part of the gastrointestinal tract, following oral administration and this has raised the general interest in colonic drug absorption. While various colonic drug delivery strategies have been explored, it is fundamentally important to understand the permeability characteristics of the colonic membrane. In situ rat colon is an important model used in preclinical studies to address the issue. Studies using the rat colon in situ model have established that while many carrier-mediated transport systems for nutrients are absent or present only marginally, the carrier for riboflavin is expressed functionally in the colon at a level comparable with that in the small intestine. Although the colonic membrane is less permeable to passive transport than the small intestinal membrane in general, it is notable that some lipophilic drugs are highly or equally permeable across both intestinal sites. Thus, it may be possible to utilize the colon, although not for all drugs, as a site of absorption by both carrier-mediated and passive mechanisms.

References

1. Rouge N, Buri P, Doelker E (1996) Drug absorption sites in the gastrointestinal tract and dosage forms for site-specific delivery. *Int J Pharm* 136:117–139
2. Kararli TT (1995) Comparison of the gastrointestinal anatomy, physiology, and biochemistry of humans and commonly used laboratory animals. *Biopharm Drug Dispos* 16:351–380
3. Ritschel WA (1991) Microemulsions for improved peptide absorption from the gastrointestinal tract. *Meth Find Exp Clin Pharmacol* 13:205–220
4. Krishna DR, Klotz U (1994) Extrahepatic metabolism of drugs in humans. *Clin Pharmacokinet* 26:144–160
5. Augustijns P, Annaert P, Heylen P, Mooter GV, Kinget R (1998) Drug absorption studies of prodrug esters using the Caco-2 model: evaluation of ester hydrolysis and transepithelial transport. *Int J Pharm* 166:45–53
6. Lin JH, Chiba M, Baillie TA (1999) Is the role of the small intestine in first-pass metabolism overemphasized? *Pharmacol Rev* 51:135–157
7. Bungay PM, Dedrick RL, Matthews HB (1981) Enteric transport of chlordecone (Kepone®) in the rat. *J Pharmacokin Biopharm* 9:309–341
8. Lorenzo CD, Dooley CP, Valenzuela JE (1991) Role of fasting gastrointestinal motility in the variability of gastrointestinal transit time assessed by hydrogen breath test. *Gut* 32:1127–1130
9. Yuasa H, Matsuda K, Kimura Y, Soga N, Watanabe J (1997) Comparative assessment of intestinal transport of hydrophilic drugs between small intestine and large intestine. *Drug Deliv* 4:269–272

10. Wood HO (1944) The surface area of the intestinal mucosa in the rat and in the cat. *J Anat* 78:103–105
11. Permezel NC, Webling DD (1971) The length and mucosal surface area of the small and large gut in young rats. *J Anat* 108:295–296
12. Binder HJ, Sandle GI (1987) Electrolyte absorption and secretion in the mammalian colon. In: Johnson LR (ed.) *Physiology of the Gastrointestinal Tract*, 2nd edn., Raven Press, New York, pp 1389–1418
13. Chu S, Montrose MH (1995) An Na⁺-independent short-chain fatty acid transporter contributes to intracellular pH regulation in murine colonocytes. *J Gen Physiol* 105:589–615
14. Ritzhaupt A, Wood IS, Ellis A, Hosie KB, Shirazi-Beechey SP (1998) Identification and characterization of a monocarboxylate transporter (MCT1) in pig and human colon: Its potential to transport L-lactate as well as butyrate. *J Physiol* 513:719–732
15. Yuasa H, Hirobe M, Tomei S, Watanabe J (2000) Carrier-mediated transport of riboflavin in the rat colon. *Biopharm Drug Dispos* 21:77–82
16. Tomei S, Yuasa H, Inoue K, Watanabe J (2001) Transport functions of riboflavin carriers in the rat small intestine and colon: Site difference and effects of tricyclic-type drugs. *Drug Deliv*. 8:119–124
17. Rose RC (1987) Intestinal absorption of water-soluble vitamins. In: Johnson LR (ed.) *Physiology of the Gastrointestinal Tract*, 2nd edn., Raven Press, New York, pp 1581–1596
18. Yuasa H, Torimoto M, Tomei S, Watanabe J (2000) Carrier-mediated drug transport in the colon: implications in designing drugs for sustained release formulations. *Millennial World Congress of Pharmaceutical Sciences*, San Francisco, California, USA, Abstracts: p 77
19. Yuasa H, Hamamoto K, Dogu S, Marutani T, Nakajima A, Kato T, Hayashi Y, Inoue K, Watanabe J (2003) Saturable absorption of glycerol in the rat intestine. *Biol Pharm Bull* 26:1633–1636
20. Yuasa H, Miyamoto Y, Iga T, Hanano M (1986) Determination of kinetic parameters of a carrier-mediated transport in the perfused intestine by two-dimensional laminar flow model: Effects of the unstirred water layer. *Biochim Biophys Acta* 856:219–230
21. Tomei S, Hayashi Y, Inoue K, Torimoto M, Ota Y, Morita K, Yuasa H, Watanabe J (2003) Search for carrier-mediated transport systems in the rat colon. *Biol Pharm Bull* 26:274–277
22. Tomei S, Torimoto M, Hayashi Y, Inoue K, Yuasa H, Watanabe J (2003) Kinetic characterization of carrier-mediated transport systems for D-glucose and taurocholate in the everted sacs of the rat colon. *Biol Pharm Bull* 26:899–901
23. Matsuda K, Yuasa H, Watanabe J (1998) Fractional absorption of L-carnitine after oral administration in rats: Evaluation of absorption site and dose dependency. *Biol Pharm Bull* 21:752–755
24. Fagerholm U, Lindahl A, Lennernäs H (1997) Regional intestinal permeability in rats of compounds with different physicochemical properties and transport mechanisms. *J Pharm Pharmacol* 49:687–690
25. Fojo AT, Ueda K, Slamon DJ, Poplack DG, Gottesman MM, Pastan I (1987) Expression of a multidrug-resistance gene in human tumors and tissues. *Proc Natl Acad Sci USA* 84:265–269
26. Iida A, Tomita M, Hayashi M (2005) Regional difference in P-glycoprotein function in rat intestine. *Drug Metab Pharmacokinet* 20:100–106
27. Saitoh H, Aungst BJ (1995) Possible involvement of multiple P-glycoprotein-mediated efflux systems in the transport of verapamil and other organic cations across rat intestine. *Pharm Res* 12:1304–1310

28. Aungst BJ, Saitoh H (1996) Intestinal absorption barriers and transport mechanisms, including secretory transport, for a cyclic peptide, fibrinogen antagonist. *Pharm Res* 13:114–119
29. Yuasa H, Soga N, Kimura Y, Watanabe J (1997) Effect of aging on the intestinal transport of hydrophilic drugs in the rat small intestine. *Biol Pharm Bull* 20:1188–1192
30. Leo A, Hansch C, Elkins D (1971) Partition coefficients and their uses. *Chem Rev* 71:525–616
31. Kimura T, Sudo K, Kanzaki Y, Miki K, Takeichi Y, Kurosaki Y, Nakayama T (1994) Drug absorption from large intestine: physicochemical factors governing drug absorption. *Biol Pharm Bull* 17:327–333

In Vivo and In Vitro Models for Assessing Drug Absorption Across the Buccal Mucosa

Joseph A. Nicolazzo and Barrie C. Finnin

Abstract The buccal mucosa serves as an attractive site for the systemic delivery of many drugs, including peptides and proteins, because of its inherent permeability and the avoidance of intestinal and hepatic first-pass effects. In order to assess the potential of the buccal mucosa to act as a site of drug absorption in preclinical drug discovery and development, various models have been used. This chapter focuses on the in vivo and in vitro methods that are available to assess buccal mucosal drug absorption, with an emphasis on the advantages and limitations associated with each of the models available and the issues associated with choice of animal tissue used in preclinical drug absorption studies. Most of our work in this field has been performed using porcine buccal mucosa in modified Ussing chambers, and the reader is referred to the appendix (available online) for a comprehensive protocol on this technique.

Keywords: Buccal mucosa; Permeability barrier; Passive diffusion; Excised tissue; Nonkeratinized epithelium; Diffusion chamber

4.1. Introduction

Most drugs are delivered to the systemic circulation by the conventional oral route; however, the systemic absorption of certain drugs can be significantly hindered by the environment of the gastrointestinal tract. Drugs that are susceptible to acid hydrolysis, are substrates for the various efflux mechanisms present in the intestinal wall, or have significant intestinal or hepatic metabolism may exhibit poor bioavailability when administered via the oral route [8]. With the advent of the biotechnology era, drug candidates with such properties are emerging, and so alternative routes of drug administration are becoming more necessary.

The buccal mucosa, which lines the inside of the cheek, has been investigated as an alternative route for drug delivery, especially for proteins and peptides. There are many advantages associated with the use of the buccal mucosa as a site for the delivery of drugs into the systemic circulation. Since blood flow from the buccal epithelium drains directly into the internal jugular

vein [66, 75], first-pass metabolism in the liver and intestine can be avoided. Additionally, the mucosa lining the oral cavity is easily accessible, which ensures that a discrete dosage form can be applied to the required site and can be removed easily in the case of an emergency [27, 96, 103]. However, like the skin, the buccal mucosa acts as a barrier to the absorption of xenobiotics, and may hinder the absorption of drugs into the systemic circulation. Consequently, preclinical permeation studies can be used to elucidate whether a compound can be successfully delivered systemically via the buccal route.

4.2. Structure and Environment of the Buccal Mucosa

4.2.1. Epithelial Organization

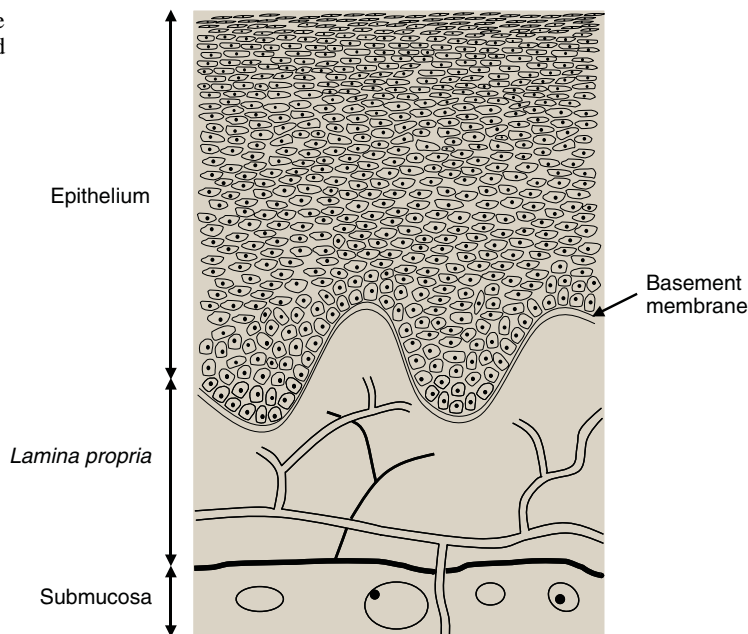
Given that the primary role of the buccal mucosa, like the skin, is to protect underlying tissues and organs from foreign agents, it is not surprising that this tissue is highly structured. The surface of the buccal mucosa consists of a stratified squamous epithelium which is separated from the underlying connective tissue (*lamina propria* and submucosa) by an undulating basement membrane (a continuous layer of extracellular material $\sim 1\text{--}2\ \mu\text{m}$ in thickness) [95]. This stratified squamous epithelium consists of differentiating layers of cells (keratinocytes), whose size, shape, and content change as the cells travel from the basal region to the superficial region [21]. The superficial cells of the nonkeratinized buccal mucosa, unlike corneocytes of the *stratum corneum*, retain their nuclei and some cytoplasmic function, and are surrounded by a cross-linked protein envelope [125]. There are $\sim 40\text{--}50$ cell layers in the buccal mucosa, resulting in a tissue with a thickness of $500\text{--}600\ \mu\text{m}$ [37, 42, 100]. While the epithelium serves as a mechanical barrier, the *lamina propria* provides mechanical support and carries the blood vessels and nerves, which supply nutrition and innervation to the epithelium, respectively. The general structure of the buccal mucosa is shown in Figure 4.1.

4.2.2. Organization of the Intercellular Domain

As cells migrate to the upper third of the epithelium, membrane-coating granules become evident at the superficial aspect of the cells. While the appearance of membrane-coating granules in the epidermis has been well characterized [43, 74, 90,], less is known about their nature in nonkeratinized epithelia, albeit their existence has been demonstrated [120, 121]. The membrane-coating granules are small cytoplasmic granules, $\sim 2\ \mu\text{m}$ in diameter, which appear in the Golgi region of the prickle cell layer, migrate to the superficial region of cells at the midlevel of the epithelium, and apparently fuse with the cell membrane in the upper third-quarter of the epithelium [120]. It is upon fusion with the cell membrane that the contents of the membrane-coating granules are extruded into the intercellular spaces of the epithelium [68].

The membrane-coating granules in keratinized epithelia contain electron-dense lipid lamellae [68, 77], and therefore, the intercellular spaces of the *stratum corneum* are filled with short stacks of lipid lamellae [67, 132]. Most of the membrane-coating granules in nonkeratinized epithelia consist of amorphous material [120]; however, some studies have shown that a small number of these granules in nonkeratinized epithelia contain lamellae [151]. Therefore,

Figure 4.1 General structure of the buccal mucosa. Taken and modified with permission from Harris et al. [42].



the intercellular spaces of the superficial layer of nonkeratinized epithelia contain electron lucent material, which may represent nonlamellar liquid phase lipid, with occasional short stacks of lipid lamellae [69]. It is this absence of organized lipid lamellae in the intercellular spaces of the buccal mucosa which results in a greater permeability to exogenous compounds, compared with keratinized epithelia [123].

4.3. The Barriers of the Buccal Mucosa

4.3.1. Location of the Permeability Barrier

The upper one-third to one-quarter of the buccal epithelium is generally responsible for the barrier properties of the buccal mucosa. This was originally reported in 1973, when it was demonstrated that horseradish peroxidase could not penetrate the top 1–3 cell layers of the oral mucosa of monkeys, rabbits, and rats, when applied topically to these surfaces [119]. When applied subepithelially, horseradish peroxidase was found in the connective tissue and extended through the intercellular spaces of the epithelium, up to the region which coincided with the appearance of membrane-coating granules [119]. This led to the suggestion that the permeability barrier of the buccal mucosa may be attributed to the materials extruded from the membrane-coating granules. These experiments were repeated using lanthanum salts, to ensure that this region was also the main barrier to the permeation of smaller molecules, and identical results were obtained [122]. Further evidence to suggest that the barrier properties of the buccal mucosa are due to the extruded materials of the membrane-coating granules comes from studies assessing the permeability of tissues lacking such granules. An example of such tissue is the junctional

epithelium which attaches the gingival stratified squamous epithelium to the tooth surface [100]. When horseradish peroxidase and microperoxidase were applied to the epithelial surface of this tissue or injected subepithelially, both proteins penetrated through the intercellular spaces of the entire epithelium [97, 133], giving evidence that the lipids extruded by these membrane-coating granules are the major hindrance to permeability across the buccal mucosa.

4.3.2. Chemical Nature of the Permeability Barrier

It is generally accepted that the barrier of the nonkeratinized oral epithelium is composed of lipid material, since treatment of oral mucosa with chloroform/methanol mixtures has resulted in a reduced barrier function [126]. To verify the chemical nature of these lipids, various regions of porcine oral cavity have been separated and the lipids present in each region have been extracted and identified by thin-layer chromatography [69, 126, 127, 129, 152,]. Similar to porcine epidermis, the keratinized palatal and gingival mucosae contained high quantities of ceramides and cholesterol, and a low proportion of cholesterol esters and glycosylceramides. In contrast, the buccal and sublingual mucosae, both of which are nonkeratinized, contained higher quantities of the more polar phospholipids, cholesterol esters, and glycosylceramides, and minimal amounts of ceramides. Histochemical staining suggested that the polar lipids were localized in the intercellular spaces of the nonkeratinized oral epithelium [129]. Therefore, the intercellular lipids of the nonkeratinized regions of the oral cavity are of a more polar nature than the lipids of the epidermis, palate, and gingiva, and this difference in the chemical nature of the lipids may in part contribute to the differences in permeability observed between these tissues [126].

4.3.3. Other Permeability Barriers in the Buccal Mucosa

In addition to the intercellular lipids of the buccal mucosa, there appear to be other barriers which may reduce the ability of an exogenous compound to permeate the buccal mucosa. These include the salivary film and mucus layer, the basement membrane, and a metabolic barrier.

4.3.3.1. Salivary Film and Mucus Layer

Unlike the skin, the mucosae of the oral cavity are constantly maintained moist by the continual secretion of saliva from the three major salivary glands (submandibular, parotid, and sublingual) and the minor salivary glands located in or beneath the mucosae. The thickness of the salivary film (pellicle) has been calculated to be between 70 μm and 100 μm [23]; however, both the composition and amount of saliva produced can vary between individuals, with time of day, disease states, and drug therapy [33], all of which must be taken into account when considering the oral cavity as a site for drug delivery.

The function of the mucosal pellicle is to serve as a barrier between the oral epithelial surface and the external environment, and so it may also act as a barrier to drug delivery. However, there are limited studies assessing the role of the mucus layer in buccal permeability. In one study, treatment of the oral mucosa with anticholinergic agents resulted in an increased permeability of certain compounds, and it was suggested that the reduced salivary flow may have been responsible for the reduced barrier properties of the tissue [113]. In

another study, addition of human submandibular saliva to the surface of rabbit oral mucosa reduced the initial rate of transport of tritiated water; however this effect was transitory [1]. Therefore, the role of mucus in the overall permeability barrier of the buccal mucosa is not clear, and any hindrance provided by the mucus layer may be negligible relative to the inherent barrier nature of the epithelium. The presence of mucins in the mucosal pellicle may also be exploited by the formulation scientist for mucoadhesive purposes, and this advantage may outweigh any slight improvement in permeability achieved by removing or manipulating this layer.

4.3.3.2. Basement Membrane

While the superficial layers of the buccal mucosa represent the primary barrier to exogenous compounds, there is evidence to suggest that the basement membrane may be important in limiting the transport of some agents from the epithelium into the underlying connective tissue. The basement membrane may act as a barrier to the transport of large molecules, including immune complexes [135] and proteins [4]; however, there is no clear relationship between the size of permeant and the hindrance provided by the basement membrane. This was shown in a study where the basement membrane acted as a major barrier to inulin (5,000 Da) and dextran 70 (70,000 Da) but not to dextran 20 (20,000 Da) [5]. Additionally, the basement membrane has been shown not to limit the transport of the large protein, horseradish peroxidase [119], but restricts the absorption of smaller β -adrenoceptor-blocking agents and the nucleoside reverse transcriptase inhibitor, 2', 3'-dideoxycytidine [28, 153]. This suggests that the charge on molecules may be important in nonspecific binding to components of the basal lamina [125], rather than the basal lamina having a simple sieving function. Although the basement membrane may provide some resistance to the permeability of some compounds, a greater body of evidence suggests that the superficial layers of the buccal epithelium are largely responsible for the barrier properties of the buccal mucosa [119, 122–124].

4.3.3.3. Metabolic Barrier

Although the buccal mucosa is an alternative route for compounds which undergo extensive hepatic metabolism, there is some potential for biotransformation in the oral cavity, particularly for peptides and proteins. Proteolytic activity has been identified in buccal tissue homogenates from various species and a number of peptides have been shown to undergo degradation in such homogenates [56, 86, 156]. However, as the location of the peptidase (intracellular or extracellular) cannot be determined from these experiments, it is difficult to assess whether these enzymes will come into contact with proteins and affect their subsequent penetration across the mucosa. To assess this, the permeability of insulin in the presence of an enzyme inhibitor was investigated. While the degradation of insulin in rabbit buccal homogenate was strongly inhibited by the serine protease inhibitor aprotinin [156], the enzyme inhibitor had no effect on the buccal absorption of insulin in vivo [9]. Because of the large molecular weight of insulin, it is unlikely to enter the epithelial cells of the mucosa as it traverses the tissue, and since the transport of insulin was not affected by aprotinin, this suggested that the protease was present intracellularly. It is therefore unlikely that these proteases will act as a significant barrier

to compounds which do not enter epithelial cells as they permeate the buccal mucosa.

A recent study, however, has shown that aminopeptidase activity is present on the surface of porcine buccal mucosa, and that various aminopeptidase inhibitors, including amastatin and sodium deoxycholate, reduce the mucosal surface degradation of the aminopeptidase substrate, leucine-enkephalin [149]. Since the peptidases are present on the surface of the buccal mucosa, they may act as a significant barrier to the permeability of compounds which are substrates for the enzyme. In addition to proteolytic enzymes, there exist some esterases, oxidases, and reductases originating from buccal epithelial cells, as well as phosphatases and carbohydrases present in saliva [154], all of which may potentially be involved in the metabolism of topically applied compounds.

4.4. Mechanisms Involved in Oral Mucosal Absorption

Substances can be transported across epithelial membranes by simple passive diffusion, carrier-mediated diffusion, and active transport, in addition to other specialized mechanisms, including endocytosis.

4.4.1. Passive Diffusion

The major mechanism involved in the transfer of a drug across the oral mucosa is described by simple Fickian or passive diffusion of the un-ionized form of the drug in accordance with the pH-partition hypothesis [75, 117]. This was first demonstrated for buccal absorption with a series of amphetamines [13]. In this study, drug transport appeared to be a passive diffusion process since optical isomers of a drug were absorbed to the same extent; absorption was dependent on the concentration of un-ionized lipid-soluble form of the drug; and no difference in the percentage absorption of the drug at any given pH value was observed when the drug was given separately or as a mixture with other drugs. Since this initial finding, there have been many studies demonstrating the passive nature of transfer across the oral mucosa [6, 14–17, 20, 22, 25, 26, 44, 94, 101, 110, 130]. Under these conditions of passive diffusion, the physicochemical properties of the membrane and the drug dictate the transport rate across the biological membrane [96].

4.4.2. Carrier-Mediated Transport

Although passive diffusion is the major transport mechanism for drug permeation across the buccal mucosa, the absorption of certain nutrients from the oral cavity has been shown to involve carrier systems. The absorption of D-glucose and L-arabinose across the buccal mucosa was shown to be both saturable and stereospecific [73]. This indicated the presence of a carrier-mediated transport system for these sugars, since saturation and stereospecificity are not characteristics of a passive diffusion process. Additionally, the absorption of D-glucose, galactose, and 3-*O*-methyl-D-glucose was at least partly dependent on the presence of sodium ions, and the transport of D-glucose was inhibited by galactose and 3-*O*-methyl-D-glucose, suggesting that there was at least one common carrier system in the buccal mucosa [73]. Such a specialized

mechanism for D-glucose transport was also observed in a cultured stratified cell layer of human oral mucosal cells [57]. In another study assessing the absorption of D-glucose at various sites in the oral cavity, absorption was found to be saturable only in the dorsum of the tongue, and these authors suggested that a specialized transport system for D-glucose existed only at this site [60]. However, using Western blot analysis, various glucose transporters have been identified in cells of the buccal mucosa as well as the dorsum of the tongue and the buccal mucosa [92]. Therefore, greater clarification is required in this area.

In addition to sugars, the absorption of various vitamins, including L-ascorbic acid, nicotinic acid, and nicotinamide, have been shown to be dependent on the presence of sodium ions, indicating absorption from the oral cavity by carrier-mediated processes [35, 99]. When the absorption of thiamine was investigated *in vivo*, absorption rates showed saturation at high concentrations of the vitamin [34], giving further support to the finding that carrier-mediated processes are involved in the oral mucosal absorption of some nutrients. Recent investigations have also indicated the existence of an energy-dependent carrier-mediated monocarboxylic acid transporter system in primary cultures of rabbit and hamster oral mucosal cells, and in hamsters *in vivo* [141, 140]. Such carrier-mediated systems may be important in the transport of certain drugs, such as salicylic acid. It has also been shown that the absorption of cefadroxil, an aminocephalosporin antibiotic, is absorbed in the human oral cavity via a specialized transport mechanism, since its absorption demonstrated saturation phenomena and was inhibited in the presence of another aminocephalosporin, cephalexin [65]. Therefore, evidence is building to suggest that passive diffusion of compounds may not be the only mechanism by which compounds permeate the buccal mucosa.

There has also been a report regarding the active transport of antibacterial agents in oral mucosa. In a cell line derived from oral epithelium, the uptake of ciprofloxacin and minocycline was not only saturable and inhibited in the presence of other compounds, but the intracellular levels of both antibiotics were 8–40-fold higher than the extracellular levels as well, demonstrating an active transport process [18]. Whether the permeability of these compounds across the entire oral mucosa occurs via an active transport process, however, remains to be determined.

4.5. Methods Employed to Assess the Permeability of the Buccal Mucosa

There have been a range of models used in the preclinical setting to assess the permeability of compounds across the buccal mucosa. While *in vivo* methods are often more appropriate in terms of assessing bioavailability via this route, *in vitro* and *in situ* methods have been instrumental for preclinical compound screening, elucidating mechanisms of transport across the buccal mucosa, and assessing the potential of chemical penetration enhancers for improvement of buccal transport. While this chapter mainly focuses on the *in vivo* and *in vitro* models available for assessing drug permeability across the buccal mucosa, novel cell culture techniques will also be briefly discussed.

4.5.1. In Vivo Methods

4.5.1.1. Buccal Absorption Test

One of the most common in vivo methods used to assess the permeability of the buccal mucosa is the buccal absorption test of Beckett and Triggs [13]. In this test, a known volume of a drug solution is introduced into the oral cavity of a subject, who swirls it around for a specified period of time and then expels it. The subject then rinses his or her mouth with an aliquot of distilled water or buffer solution, and the expelled drug solution and rinse are combined and analyzed for drug content. The difference between the initial and final drug concentration in the solution is assumed to be the amount of drug taken up into the oral mucosa.

The buccal absorption test of Beckett and Triggs has been modified slightly by various investigators. To account for the production of saliva throughout the test, a correction factor was included by Dearden and Tomlinson [29]. Others have added a marker compound into the swirling solution, such as phenol red or polyethylene glycol, to account for salivary dilution and accidental swallowing of the solution [6, 101, 137]. Since kinetic profiles cannot be determined using the original buccal absorption test, Tucker modified the test by taking small samples of the swirled solution from the oral cavity every few minutes without removing the entire test solution [137]. The major benefit of this is that the absorption kinetics of a drug may be studied in a single subject in a simple 15–20-min test.

Although the original and modified buccal absorption tests are easy to perform, do not require blood sampling, and allow for both the rate and the extent of drug loss from the oral cavity to be determined, there are some drawbacks to the method. One of the major disadvantages of this technique is that only the concentration of drug remaining in the oral cavity (swirling solution) is measured, and blood samples are not determined. The amount of drug which disappears from the swirling solution cannot be equated to the amount entering the systemic circulation, due to other factors including membrane storage, potential metabolism, and swallowing of the drug [45, 46]. Since the solution is swirled around the oral cavity, absorption of compound may also occur through all surfaces within the oral cavity, and so the degree to which absorption occurs across a specific site (e.g., buccal and sublingual) remains unknown.

4.5.1.2. Perfusion Cells

To overcome the limitation of nonspecific absorption across all surfaces of the oral cavity and to study regional variation in drug absorption, various absorption or perfusion cells have been designed which can be clamped or attached to particular mucosae within the oral cavity of both animals and humans [12, 59, 60, 91, 93, 94, 155, 158, 159]. In this method, a drug solution is perfused through the cell and the drug absorption is again calculated by drug disappearance from the perfusate. The major drawback with the perfusion cell technique is leakage and large intersubject variation [37]; however, these devices are a major advance in assessing the absorption characteristics of a particular region within the oral cavity, and would be most informative if the appearance of drug in the plasma was simultaneously monitored.

In particular cases where plasma cannot be simultaneously assayed, and there is information available relating the concentration of drug in saliva to the concentration in plasma, it is possible to collect saliva as a surrogate for plasma. Following collection and analysis, an appropriate multiplication factor is incorporated for extrapolation to plasma concentrations. Such a method was recently used to assess the buccal absorption of nicotine in humans [3]. In this study, the disappearance of nicotine from the perfusion solution was used to determine the rate of nicotine absorption, and saliva was simultaneously collected directly from the parotid gland using a modified Carlson-Crittenden cup [11] as a surrogate for plasma. While salivary concentrations increased as perfusion concentrations decreased, it is unknown whether this actually related to an increase in plasma concentrations. Consequently, it is important to determine whether there is a correlation between plasma concentrations and salivary concentrations, if this technique is to be successfully used as a predictor of systemic buccal absorption. However, as informative as such techniques may be, they may not be suitable in the preclinical setting, where high throughput permeability screening is required.

4.5.2. In Vitro Methods

In vitro permeability models are often employed to determine the barrier nature of a particular biological tissue because the diffusion of drugs can be studied in an environment where variables such as temperature, pH, and osmolarity can be easily controlled [157]. When using an in vitro method to predict the absorption of compounds across the human buccal mucosa, an appropriate animal model must be chosen on the basis of its similarity in structure and permeability to the human buccal mucosa. Using the buccal mucosa of an appropriate animal model, in vitro permeability studies are then commonly conducted in diffusion cells. The advantage of in vitro diffusion cells is that the amount of drug that has actually diffused across the tissue can be determined over time, and thus the kinetics of tissue transport may be assessed. There are various diffusion cells that are used in the preclinical screening of compound permeability, including Franz-type diffusion cells, flow-through cells, and modified Ussing chambers.

4.5.2.1. Animal Models

Because of the limited availability of the human buccal mucosa, it is often necessary to use freshly excised mucosa from an alternative animal species. If the role of in vitro studies is to assess the potential of the buccal mucosa as an alternative route for drug delivery in humans, then the buccal mucosa from the animal species chosen should be similar to the human buccal mucosa in terms of permeability, biochemistry, and morphology. While many research groups have used the oral mucosa of rats [10, 115] and hamsters [25, 39, 58, 61–64, 131, 136, 138], these surfaces are keratinized, and so may not be an appropriate model of the nonkeratinized human buccal mucosa. Rabbit buccal mucosa is nonkeratinized and has been used in many in vitro studies assessing the mucosal permeability of compounds [32, 36, 78, 116]; however, the small area of available nonkeratinized tissue often limits its use [125]. The buccal mucosa of dogs and monkeys is nonkeratinized and therefore may be used as a model for the human buccal mucosa; however, the epithelium of the mucosa in these animals is much thinner, and consequently, more permeable than that of

Table 4.1 Epithelial thickness and permeability coefficient (P) for tritiated water through the buccal mucosa of different species together with epithelial thickness.

Species	$P \times 10^{-7}$ (cm/min)	Epithelial thickness (μm)
Human	579 \pm 122	580 \pm 90
Pig	634 \pm 60	772 \pm 150
Monkey	1,025 \pm 154	271 \pm 50
Dog	1,045 \pm 37	126 \pm 20

Data are presented as mean \pm SD.

Table taken from Squier et al. 1996 [125]. Copyright (1996) From: Oral Mucosal Drug Delivery, by Michael J. Rathbone (Ed.). Reproduced by permission of Routledge/Taylor & Francis Group, LLC.

humans [2, 76, 87, 114, 125]. The comparative permeability of tritiated water through various animal species and humans is shown in Table 4.1. In addition, the thickness of the buccal epithelium in each species is shown.

Because of the physiologic, anatomic, nutritional, and metabolic similarities between humans and pigs [31], the pig has become a widely used and important animal model for research on human disease. The buccal mucosa of pigs is nonkeratinized and has a similar structure, morphology, and composition to the human buccal mucosa [24, 123, 126]. Additionally, as shown in Table 4.1, the thickness of the epithelia in human and porcine buccal mucosa is fairly similar. While structure and morphology are important determinants in the comparative process, the permeability characteristics of the model tissue must reflect the barrier nature of the human buccal mucosa. The permeability of tritiated water through porcine buccal mucosa has been shown to be very similar to that of the human buccal mucosa [72], and more recently, no significant differences were observed in the permeability of mannitol or testosterone through the porcine and the human buccal mucosa [87]. Because of the large amounts of pig oral mucosa available from slaughterhouses and the similar structure and permeability to human tissue, most laboratories use porcine buccal mucosa when assessing mucosal permeability and the effect of various chemical penetration enhancers on mucosal drug delivery [7, 20, 28, 30, 38, 41, 47, 48, 54, 70, 79, 80–84, 104, 105, 108, 110, 112, 130, 147, 148, 153]. It is therefore recommended that preclinical evaluation of compound permeability across the buccal mucosa be performed with porcine buccal mucosa, as a result of its similar structure and permeability characteristics to that seen in the human buccal mucosa.

4.5.2.2. Franz-Type Diffusion Cells

While Franz-type diffusion cells are commonly used to assess in vitro penetration of compounds across the skin, they have also been used for the assessment of compound permeability across the buccal mucosa [19, 71, 104]. In this system, buccal mucosa is sandwiched between two chambers, and compound solution is added to the donor chamber with compound-free buffer in the receptor chamber. The receptor chamber is then periodically sampled to assess the amount of compound that has permeated the tissue over time.

4.5.2.3. Flow-Through Diffusion Cells

Although more commonly used in permeation experiments for skin, there have been some research groups who use flow-through diffusion cells to assess

buccal permeability of compounds [128, 142–146, 153]. This technique is very similar to the Franz-type diffusion cells; however, the buccal mucosal surface is exposed to air (as there is no closed donor chamber) which can result in drying of tissue and potentially tissue death. In addition, the receptor solution flows underneath the buccal mucosa, which ensures that there is no accumulation of compound in the receptor compartment, which can often occur when using the Franz-type diffusion cells. The receptor solution, which flows underneath the tissue, collects any compound which has permeated through the tissue, and is periodically collected and analyzed to determine compound concentration.

4.5.2.4. Modified Ussing Chambers

Modified Ussing chambers have been commonly used to assess the transport of many compounds across the buccal mucosa [7, 28, 30, 41, 47, 48, 80–84, 106, 107]. The Ussing chamber, first described for investigating the transport of ions across isolated frog skin [139], has undergone a number of recent modifications, enabling convenient and rapid assessment of tissue permeability [40, 118]. This is the model which our laboratory has extensively used for assessment of buccal permeability [80–84], and it has been useful for assessing the potential of agents in enhancing permeability across the buccal mucosa. An illustration of the modified Ussing chamber commonly used in buccal mucosal permeation studies is shown in Figure 4.2.

As shown in Figure 4.2, the modified Ussing chamber system consists of two half chambers which when clamped together are separated by a piece of

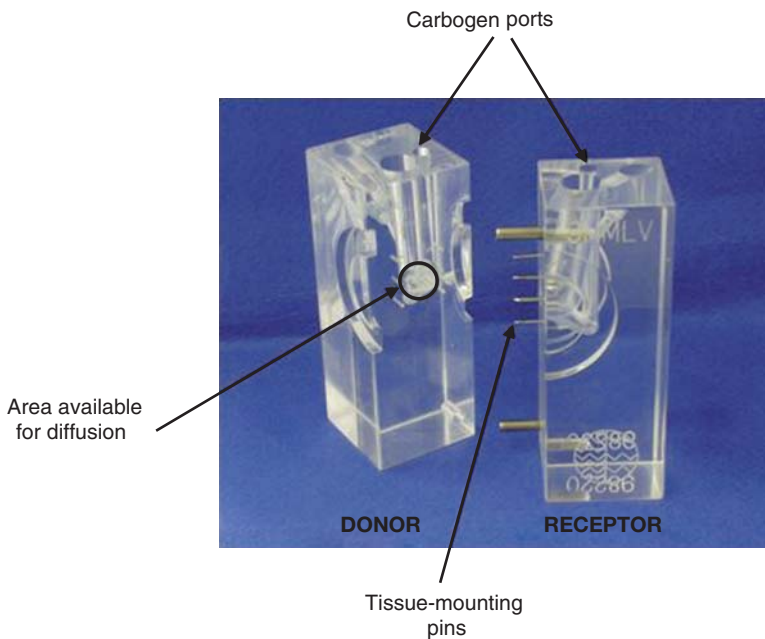


Figure 4.2 The modified Ussing chamber consisting of a donor and a receptor chamber which when clamped together are separated by a piece of tissue (intestinal, nasal, buccal, etc). The available area for diffusion (highlighted in a green circle to enhance visibility) is 0.64 cm^2 and the volume of solution applied to each chamber is 1.5 ml. The applied solution is bubbled with carbogen gas (95% O_2 + 5% CO_2) that enters the chambers through the gas ports (See also Color Insert.)

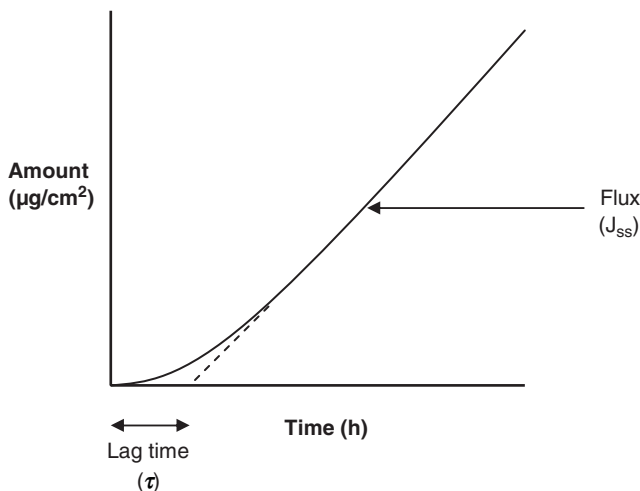


Figure 4.3 Representation of amount of drug appearing in the receptor chamber over time, where the steady-state flux (J_{ss}) is calculated from the gradient of the linear portion of the curve and the lag time (τ) is the time required for steady-state flux to be achieved.

biological tissue. A solution of drug in physiological buffer is then applied to the donor chamber and the same volume (1.5 ml) of physiological buffer is placed in the receptor chamber. The advantage of the modified Ussing chamber over the Franz-type diffusion cell and flow-through diffusion cell is that the donor and receptor chambers are provided with carbogen gas (95% O_2 + 5% CO_2), which not only provides stirring but also helps to maintain the viability of the buccal tissue [46]. The transport of compound from the donor chamber to the receptor chamber is monitored over a specified period of time, by periodic sampling of the receptor chamber. The concentration of drug appearing in the receptor chamber can then be analyzed by an appropriate detection method, and the amount of drug permeating into the receptor chamber may be plotted as a function of time, as shown in Figure 4.3.

The appropriate calculations for determining the flux and permeability coefficient across the buccal mucosa using this approach are detailed in the appendix containing the detailed method used in our laboratory for assessing buccal permeation.

4.5.2.5. Issues Associated With In Vitro Permeability Assessment

While the transport of compounds across the buccal mucosa may be assessed in a controlled environment with in vitro techniques, the ability to correlate the results obtained from the in vitro to the in vivo situation is often limited. It is thus necessary to consider the in vitro conditions and minimize, where possible, artifacts that may not be representative of the in vivo situation. This becomes particularly important when deciding on the thickness of the tissue to use in in vitro permeability experiments. When excising the buccal mucosa (as detailed in the appendix to this chapter), it is possible to use either full-thickness tissue (containing the buccal epithelium and underlying connective tissue) or buccal epithelium alone. In studies in our laboratory using both full-thickness and epithelial tissue, the presence of connective tissue significantly reduced the buccal permeation of the hydrophilic marker caffeine and the lipophilic marker estradiol [80]. However, it was observed that the difference in permeability was greater for estradiol than for caffeine, which may have been a result of the more hydrophilic nature of the connective tissue, which acts

as a greater barrier for lipophilic compounds than for hydrophilic compounds [28]. Given the blood vessels are located directly beneath the epithelial surface *in vivo*, we suggest using epithelial tissue in place of full-thickness tissue, avoiding the artificial barrier created by connective tissue in the absence of circulation.

Integrity markers are often used in *in vitro* permeability experiments to ensure that the model membrane is intact and that the observed permeability profiles of model compounds are not a result of compromised tissue integrity. One common method of assessing tissue integrity is to include a nonabsorbable marker at the completion of a permeability experiment. Our laboratory uses the high molecular weight fluorescein isothiocyanate (FITC)-labeled dextran with a molecular weight of 20 kDa as a marker of tissue integrity [80], on the basis that studies investigating the permeability of FITC-dextran have revealed that passage of such hydrophilic compounds through porcine buccal epithelium is restricted to permeants with a molecular weight less than 20 kDa [47, 48, 55]. We have demonstrated that such a high molecular weight dextran appears only in the receptor chamber following intentional tissue damage, and this was accompanied by an increase in the permeability of caffeine [80].

Because of the possible effects of active and carrier-mediated processes and metabolic biotransformation, the issue of tissue viability is important for *in vitro* buccal mucosal experiments. The barrier nature of the buccal mucosa resides in the upper layers of the epithelium, where unlike in the stratum corneum, the cells contain a variety of functional organelles [119, 122, 125, 150], and so tissue viability may be an important component of the barrier function of the tissue. Various methods have been employed to assess the viability of excised buccal mucosa, including measurement of biochemical markers, microscopic methods, and linearity of transport data [42]. While biochemical methods, including measurement of adenosine 5'-triphosphate (ATP) levels and utilization of glucose, provide information on the metabolic activity of the tissue, this does not necessarily relate to the barrier function of the tissue. In excised rabbit buccal mucosa, levels of ATP were measured and found to decline by 40% in 6 h, and this correlated well with transmission electron microscopic evaluation of the tissue (intact superficial cells) [32]. In addition, the permeability of a model peptide was unaltered up to 6 h postmortem, but at 8 h, a significant change in permeability was observed [32]. These investigators therefore claimed that excised rabbit buccal mucosa could be used for diffusion studies for ~6 h.

Recently it has been claimed that the tissue can be considered viable if the drug permeability does not change over the course of the experiment, and thus the actual permeability experiments themselves may provide insight into the viability of the tissue [109, 157]. This method was employed in permeation experiments using porcine buccal mucosa, where the permeability of compounds was assessed in two consecutive permeability experiments to ensure the nature of the barrier was not compromised [111, 112]. While this demonstrates that the barrier nature of the tissue was unaltered between the permeation experiments, the tissue may have already undergone tissue death in the time between the excision and the commencement of the initial permeation experiment, and thus the permeability rate obtained *in vitro* may not be representative of the *in vivo* situation. Therefore, more studies assessing the dependence of the barrier nature of the buccal mucosa on tissue viability are

required, especially since the role of specialized transport processes in oral mucosal permeability is becoming more appreciated.

In our laboratory, the viability of excised porcine buccal mucosa was assessed using histological evaluation and a 3-[4,5-dimethylthiazol-2-yl]-2,5-diphenyltetrazolium bromide (MTT) biochemical assay which has previously been used in assessing the viability of excised buccal mucosa and cornea [49, 50]. Histological evaluation of tissue demonstrated that the buccal epithelium appeared viable up to 9 h postmortem, and this was supported by the MTT biochemical assay, which indicated that viability was maintained for up to 12 h [80]. Therefore, we recommend that all permeation experiments using porcine buccal mucosa be performed within 9–12 h of animal death.

While there are limitations associated with the use of an *in vitro* permeability model for assessing the transport of compounds across the buccal mucosa, it can still be useful in assessing and comparing the permeability of compounds under different conditions, such as pH, temperature, and osmolarity, which provide valuable information on the mechanisms involved in drug transport. Additionally, the preliminary effects of potential chemical penetration enhancers or formulation excipients may be assessed, and these may provide a substantial rationale for subsequently assessing the effect of these agents in man.

4.5.3. Buccal Cell Cultures

The use of buccal cell cultures for assessing the permeability of the buccal mucosa has attracted recent attention (see Chap. 7 for a more extensive summary). In order to culture buccal epithelial cells, the cells must be harvested from an appropriate source and cultured under specific conditions using an appropriate growth medium, temperature, and humidity [46]. Cell cultures have been successfully grown from hamster cheek pouch. These cultured cells, however, did not differentiate to form a complete keratinized surface as seen in the normal hamster cheek pouch, and they consequently displayed a greater permeability to compounds when compared with keratinized hamster cheek pouch mucosa [134]. Therefore, the cultured hamster cheek cells more closely mimicked the human buccal mucosa due to their lack of keratinization, and so this may be an appropriate model for predicting permeability through the human buccal mucosa.

Another cell culture model which has been proposed as a model of the human buccal epithelium is the TR146 cell line [51, 52, 85–87]. The TR146 cells originate from a human buccal carcinoma [98], and when cultured, they form an epithelium resembling that of the buccal mucosa [52], with the appropriate differentiation patterns seen in human nonkeratinized epithelium [53]. However, the TR146 cell culture model has less of a barrier nature when compared to human and porcine buccal epithelium, as demonstrated by a significantly greater permeability to tritiated water, mannitol, testosterone, dextrans, and nicotine [85, 87–89], and this may be due to the cancerous nature of the original cells.

Recently, a cell culture derived from biopsies of healthy human buccal mucosa has been developed with remarkably similar morphology, membrane-coating granule structure and appearance, and lipid composition to intact buccal tissue [102]. The barrier nature of this cell culture model is similar to intact buccal mucosa, and so this cell culture may be an alternative model to the

TR146 cell culture. With the development of tissue culture techniques, it is anticipated that various cell culture models may be developed with similar morphological and barrier properties to normal intact buccal mucosa. Such models may be very useful in assessing the buccal permeability and metabolism of many compounds.

4.6. Concluding Remarks

The buccal mucosa does serve as an alternative route for administering compounds systematically; however, to ensure particular compounds are candidates for delivery across this biological tissue, preclinical screening is essential. While in vivo human permeability studies are ideal, due to their costs and associated issues, it is necessary to perform such screening in vitro. Assessment of compound permeability across porcine buccal mucosa has been widely used and can provide the preclinical biopharmaceutical scientist with much information relating to permeability, routes of transport, and effects of various chemical penetration enhancers.

References

1. Adams D (1975) The mucin barrier and absorption through oral mucosa. *J Dent Res* 54:B19–B26
2. Addy M (1980) The oral mucosal absorption and tissue distribution of triamcinolone acetonide in the dog studied by autoradiography. *Arch Oral Biol* 25: 809–817
3. Adrian CL, Olin HB, Dalhoff K, Jacobsen J (2006) In vivo human buccal permeability of nicotine. *Int J Pharm* 311:196–202
4. Alfano MC, Drummond JF, Miller SA (1975) Localization of rate-limiting barrier to penetration of endotoxin through nonkeratinized oral mucosa in vitro. *J Dent Res* 54:1143–1148
5. Alfano MC, Chasens AI, Masi CW (1977) Autoradiographic study of the penetration of radiolabelled dextrans and inulin through non-keratinized oral mucosa in vitro. *J Periodontal Res* 12:368–377
6. Arbab AG, Turner P (1971) Influence of pH on absorption of thymoxamine through buccal mucosa in man. *Br J Pharmacol* 43:479P–480P
7. Artusi M, Santi P, Colombo P, Junginger HE (2003) Buccal delivery of thiocholchicoside: In vitro and in vivo permeation studies. *Int J Pharm* 250:203–213
8. Aungst BJ (2000) Intestinal permeation enhancers. *J Pharm Sci* 89:429–442
9. Aungst BJ, Rogers NJ (1988a) Site dependence of absorption-promoting actions of laurth-9, Na salicylate, Na₂EDTA, and aprotinin on rectal, nasal, and buccal insulin delivery. *Pharm Res* 5:305–308
10. Aungst BJ, Rogers NJ, Shefter E (1988b) Comparison of nasal, rectal, buccal, sublingual and intramuscular insulin efficacy and the effects of a bile salt absorption promoter. *J Pharmacol Exp Ther* 244:23–27
11. Bardow A, Madsen J, Bauntofte B (2000) The bicarbonate concentration in human saliva does not exceed the plasma level under normal physiological conditions. *Clin Oral Invest* 4:245–253
12. Barsuhn CL, Olanoff LS, Gleason DD, Adkins EL, Ho NFH (1988) Human buccal absorption of flurbiprofen. *Clin Pharmacol Ther* 44:225–231
13. Beckett AH, Triggs EJ (1967) Buccal absorption of basic drugs and its application as an in vivo model of passive drug transfer through lipid membranes. *J Pharm Pharmacol* 19:31S–41S

14. Beckett AH, Moffat AC (1969) Correlation of partition coefficients in n-heptane-aqueous systems with buccal absorption data for a series of amines and acids. *J Pharm Pharmacol* 21:144S–150S
15. Beckett AH, Boyes RN, Triggs EJ (1968) Kinetics of buccal absorption of amphetamines. *J Pharm Pharmacol* 20:92–97
16. Bergman S, Siegel IA, Ciancio S (1968) Absorption of carbon-14 labeled lidocaine through the oral mucosa. *J Dent Res* 47:1184
17. Bergman S, Kane D, Siegel IA, Ciancio S (1969) In vitro and in situ transfer of local anaesthetics across the oral mucosa. *Arch Oral Biol* 14:35–43
18. Brayton JJ, Yang Q, Nakkula RJ, Walters JD (2002) An in vitro model of ciprofloxacin and minocycline transport by oral epithelial cells. *J Periodontol* 73:1267–1272
19. Ceschel GC, Maffei P, Sforzini A, Lombardi Borgia S, Yasin A, Ronchi C (2002) In vitro permeation through porcine buccal mucosa of caffeic acid phenetyl ester (CAPE) from a topical mucoadhesive gel containing propolis. *Fitoterapia* 73 Suppl. 1:S44–S52
20. Chen LL, Chetty DJ, Chien YW (1999) A mechanistic analysis to characterize oramucosal permeation properties. *Int J Pharm* 184:63–72
21. Chen SY, Squier CA (1984) The ultrastructure of the oral epithelium. In: Meyer J, Squier CA, Gerson SJ (eds.) *The Structure and Function of Oral Mucosa*. Pergamon Press, Oxford, pp 7–30
22. Chetty DJ, Chen LH, Chien YW (2001) Characterization of captopril sublingual permeation: Determination of preferred routes and mechanisms. *J Pharm Sci* 90:1868–1877
23. Collins LMC, Dawes C (1987) The surface area of the adult human mouth and thickness of the salivary film covering the teeth and oral mucosa. *J Dent Res* 66:1300–1302
24. Collins P, Laffoon J, Squier CA (1981) Comparative study of porcine oral epithelium. *J Dent Res* 60:543
25. Coutel-Egros A, Maitani Y, Veillard M, Machida Y, Nagai T (1992) Combined effects of pH, cosolvent and penetration enhancers on the in vitro buccal absorption of propranolol through excised hamster cheek pouch. *Int J Pharm* 84: 117–128
26. Davis BJ, Johnston A (1979) Buccal absorption of verapamil—evidence for membrane storage. *Br J Clin Pharmacol* 65:434P
27. de Vries ME, Boddé HE, Verhoef JC, Junginger HE (1991a) Developments in buccal drug delivery. *Crit Rev Ther Drug Carrier Syst* 8:271–303
28. de Vries ME, Boddé HE, Verhoef JC, Ponec M, Crane WIHM, Junginger HE (1991b) Localization of the permeability barrier inside porcine buccal mucosa: A combined in vitro study of drug permeability, electrical resistance and tissue morphology. *Int J Pharm* 76:25–35
29. Dearden JC, Tomlinson E (1971) Correction for effect of dilution on diffusion through a membrane. *J Pharm Sci* 60:1278–1279
30. Deneer VHM, Drese GB, Roemelé PEH, Verhoef JC, Lie-A-Huen L, Kingma JH, Brouwers JRBJ, Junginger HE (2002) Buccal transport of flecainide and sotalol: Effect of a bile salt and ionization state. *Int J Pharm* 241:127–134
31. Dodds WJ (1982) The pig model for biomedical research. *Fed Proc* 41:247–256
32. Dowty ME, Knuth KE, Irons BK, Robinson JR (1992) Transport of thyrotropin releasing hormone in rabbit buccal mucosa in vitro. *Pharm Res* 9: 1113–1122
33. Edgar WM (1992) Saliva: Its secretion, composition and functions. *Br Dent J* 172:305–312
34. Evered DF, Mallett C (1983) Thiamine absorption across human buccal mucosa in vivo. *Life Sci* 32:1355–1358

35. Evered DF, Sadoogh-Abasian F, Patel PD (1980) Absorption of nicotinic acid and nicotinamide across human buccal mucosa in vivo. *Life Sci* 27: 1649–1651
36. Gandhi R, Robinson J (1992) Mechanisms of penetration enhancement for trans-buccal delivery of salicylic acid. *Int J Pharm* 85:129–140
37. Gandhi RB, Robinson JR (1994) Oral cavity as a site for bioadhesive drug delivery. *Adv Drug Del Rev* 13:43–74
38. Ganem-Quintanar A, Quintanar-Guerrero D, Falson-Rieg F, Buri P (1998) Ex vivo oral mucosal permeation of lidocaine hydrochloride with sucrose fatty acid esters as absorption enhancers. *Int J Pharm* 173:203–210
39. Garren KW, Repta AJ (1989) Buccal drug absorption. II: In vitro diffusion across the hamster cheek pouch. *J Pharm Sci* 78:160–164
40. Grass GM, Sweetana SA (1988) In vitro measurement of gastrointestinal tissue permeability using a new diffusion cell. *Pharm Res* 5:372–376
41. Hansen LB, Christrup LL, Bundgaard H (1992) Enhanced delivery of ketobemidone through porcine buccal mucosa in vitro via more lipophilic ester prodrugs. *Int J Pharm* 88:237–242
42. Harris D, Robinson JR (1992) Drug delivery via the mucous membranes of the oral cavity. *J Pharm Sci* 81:1–10
43. Hayward AF (1976) Ingestion of colloid in a keratinized epithelium and its localization in membrane-coating granules. *J Anat* 121:313–321
44. Henry JA, Ohashi K, Wadsworth J, Turner P (1980) Drug recovery following buccal absorption of propranolol. *Br J Clin Pharmacol* 10:61–65
45. Ho NFH (1993) Biophysical kinetic modeling of buccal absorption. *Adv Drug Del Rev* 12:61–97
46. Hoogstraate AJ, Boddé HE (1993) Methods for assessing the buccal mucosa as a route of drug delivery. *Adv Drug Del Rev* 12:99–125
47. Hoogstraate AJ, Senel S, Cullander C, Verhoef J, Junginger HE, Boddé HE (1996) Effects of bile salts on transport rates and routes of FITC-labelled compounds across porcine buccal epithelium in vitro. *J Control Release* 40: 211–221
48. Hoogstraate AJ, Cullander C, Nagelkerke JF, Senel S, Verhoef JC, Junginger HE, Boddé HE (1994) Diffusion rates and transport pathways of fluorescein isothiocyanate (FITC)-labeled model compounds through buccal epithelium. *Pharm Res* 11:83–89
49. Imbert D, Cullander C (1997) Assessment of cornea viability by confocal laser scanning microscopy and MTT assay. *Cornea* 16:666–674
50. Imbert D, Cullander C (1999) Buccal mucosa in vitro experiments I. Confocal imaging of vital staining and MTT assays for the determination of tissue viability. *J Control Release* 58:39–50
51. Jacobsen J, Pedersen M, Rassing MR (1996) TR146 cells as a model for human buccal epithelium: II. Optimisation and use of a cellular sensitivity MTS/PMS assay. *Int J Pharm* 141:217–225
52. Jacobsen J, van Deurs B, Pedersen M, Rassing MR (1995) TR146 cells grown on filters as a model for human buccal epithelium: I. Morphology, growth, barrier properties, and permeability. *Int J Pharm* 125:165–184
53. Jacobsen J, Brøndum-Nielsen K, Christensen ME, Olin H-BD, Tommerup N, Rassing MR (1999) Filter-grown TR146 cells as an in vitro model of human buccal epithelial permeability. *Eur J Oral Sci* 107:138–146
54. Jasti BR, Zhou S, Mehta RC, Li X (2000) Permeability of antisense oligonucleotides through porcine buccal mucosa. *Int J Pharm* 208:35–39
55. Junginger HE, Hoogstraate JA, Verhoef JC (1999) Recent advances in buccal drug delivery and absorption—in vitro and in vivo studies. *J Control Release* 62: 149–159

56. Kashi SD, Lee VH (1986) Enkephalin hydrolysis in homogenates of various absorptive mucosae of the albino rabbit: Similarities in rates and involvement of aminopeptidases. *Life Sci* 38:2019–2028
57. Kimura T, Yamano H, Tanaka A, Matsumura T, Ueda M, Ogawara K, Higaki K (2002) Transport of D-glucose across cultured stratified cell layer of human oral mucosal cells. *J Pharm Pharmacol* 54:213–219
58. Kitano M, Maitani Y, Takayama K, Nagai T (1998) Buccal absorption through golden hamster cheek pouch in vitro and in vivo of 17β -estradiol from hydrogels containing three types of absorption enhancers. *Int J Pharm* 174:19–28
59. Kurosaki Y, Yano K, Kimura T (1997) Perfusion cells for studying regional variation in oral-mucosal permeability in humans. I: Kinetic aspects in oral-mucosal absorption of alkylparabens. *Pharm Res* 14:1241–1245
60. Kurosaki Y, Yano K, Kimura T (1998) Perfusion cells for studying regional variation in oral mucosal permeability in humans. 2. A specialized transport mechanism in D-glucose absorption exists in dorsum of tongue. *J Pharm Sci* 87:613–615
61. Kurosaki Y, Hisaichi S, Nakayama T, Kimura T (1989a) Enhancing effect of 1-dodecylazacycloheptan-2-one (Azone) on the absorption of salicylic acid from keratinized oral mucosa and the duration of enhancement in vivo. *Int J Pharm* 51:47–54
62. Kurosaki Y, Hisaichi S, Hamada C, Nakayama T, Kimura T (1988a) Effects of surfactants on the absorption of salicylic acid from hamster cheek pouch as a model of keratinized oral mucosa. *Int J Pharm* 47:13–19
63. Kurosaki Y, Takatori T, Kitayama M, Nakayama T, Kimura T (1988b) Application of propranolol to the keratinized oral mucosa: Avoidance of first-pass elimination and the use of 1-dodecylazacycloheptan-2-one (Azone) as an absorption enhancer of bioadhesive film-dosage form. *J Pharmacobiodyn* 11:824–832
64. Kurosaki Y, Hisaichi SI, Hong LZ, Nakayama T, Kimura T (1989b) Enhanced permeability of keratinized oral-mucosa to salicylic acid with 1-dodecylazacycloheptan-2-one (Azone): In vitro studies in hamster cheek pouch. *Int J Pharm* 49:47–55
65. Kurosaki Y, Nishimura H, Terao K, Nakayama T, Kimura T (1992) Existence of a specialized absorption mechanism for cefadroxil, an aminocephalosporin antibiotic, in the human oral cavity. *Int J Pharm* 82:165–169
66. Lamey PJ, Lewis MAO (1990) Buccal and sublingual delivery of drugs. In: Florence AT, Salole EG (eds.) *Routes of Drug Administration*. Butterworth & Co. (Publishers) Ltd., Norfolk, pp 30–47
67. Landmann L (1986) Epidermal permeability barrier: Transformation of lamellar granule-disks into intercellular sheets by a membrane-fusion process, a freeze-fracture study. *J Invest Dermatol* 87:202–209
68. Lavker RM (1976) Membrane coating granules: The fate of the discharged lamellae. *J Ultrastruct Res* 55:79–86
69. Law S, Wertz PW, Swartzendruber DC, Squier CA (1995) Regional variation in content, composition and organization of porcine epithelial barrier lipids revealed by thin-layer chromatography and transmission electron microscopy. *Arch Oral Biol* 40:1085–1091
70. Le Brun PPH, Fox PLA, de Vries ME, Boddé HE (1989) In vitro penetration of some β -adrenoceptor blocking drugs through porcine buccal mucosa. *Int J Pharm* 49:141–145
71. Lee J, Kellaway IW (2000) Combined effect of oleic acid and polyethylene glycol 200 on buccal permeation of [D-ala², D-leu⁵]enkephalin from a cubic phase of glyceryl monooleate. *Int J Pharm* 204:137–144
72. Lesch CA, Squier CA, Cruchley A, Williams DM, Speight P (1989) The permeability of human oral mucosa and skin to water. *J Dent Res* 68:1345–1349

73. Manning AS, Evered DF (1976) The absorption of sugars from the human buccal cavity. *Clin Sci Mol Med* 51:127–132
74. Matoltsy AG, Parakkal PF (1965) Membrane-coating granules of keratinizing epithelia. *J Cell Biol* 24:297–307
75. McElnay JC (1990) Buccal absorption of drugs. In: Swarbrick J, Boylan JC (eds.) *Encyclopedia of Pharmaceutical Technology*. Marcel Dekker, New York, pp 189–211
76. Mehta M, Kempainen BW, Stafford RG (1991) In vitro penetration of tritium-labelled water (THO) and [³H]PbTx-3 (a red tide toxin) through monkey buccal mucosa and skin. *Toxicol Lett* 55:185–194
77. Meyer W, Schlesinger C, Neurand K (1987) Membrane-coating granules (MCGs) in porcine epidermis. *Schweiz Arch Tierheilkd* 129:133–137
78. Nair M, Chien YW (1993) Buccal delivery of progestational steroids: I. Characterization of barrier properties and effect of penetrant hydrophilicity. *Int J Pharm* 89:41–49
79. Nair MK, Chetty DJ, Ho H, Chien YW (1997) Biomembrane permeation of nicotine: Mechanistic studies with porcine mucosae and skin. *J Pharm Sci* 86: 257–262
80. Nicolazzo JA, Reed BL, Finnin BC (2003) The effect of various in vitro conditions on the permeability characteristics of the buccal mucosa. *J Pharm Sci* 92: 2399–2410
81. Nicolazzo JA, Reed BL, Finnin BC (2004a) Assessment of the effects of sodium dodecyl sulfate on the buccal permeability of caffeine and estradiol. *J Pharm Sci* 93:431–440
82. Nicolazzo JA, Reed BL, Finnin BC (2004b) Modification of buccal drug delivery following pretreatment with skin penetration enhancers. *J Pharm Sci* 93: 2054–2063
83. Nicolazzo JA, Reed BL, Finnin BC (2005a) Enhanced buccal mucosal retention and reduced buccal permeability of estradiol in the presence of padimate O and Azone[®]—a mechanistic study. *J Pharm Sci* 94: 873–882
84. Nicolazzo JA, Reed BL, Finnin BC (2005b) Enhancing the buccal mucosal uptake and retention of triamcinolone acetonide. *J Control Release* 105: 240–248
85. Nielsen HM, Rassing MR (1999a) TR146 cells grown on filters as a model of human buccal epithelium: III. Permeability enhancement by different pH values, different osmolality values, and bile salts. *Int J Pharm* 185: 215–225
86. Nielsen HM, Rassing MR (2000a) TR146 cells grown on filters as a model of human buccal epithelium: V. Enzyme activity of the TR146 cell culture model, human buccal epithelium and porcine buccal epithelium, and permeability of leu-enkephalin. *Int J Pharm* 200:261–270
87. Nielsen HM, Rassing MR (2000b) TR146 cells grown on filters as a model of human buccal epithelium: IV. Permeability of water, mannitol, testosterone and β -adrenoceptor antagonists. Comparison to human, monkey and porcine buccal mucosa. *Int J Pharm* 194:155–167
88. Nielsen HM, Rassing MR (2002) Nicotine permeability across the buccal TR146 cell culture model and porcine buccal mucosa in vitro: Effect of pH and concentration. *Eur J Pharm Sci* 16:151–157
89. Nielsen HM, Verhoef JC, Ponec M, Rassing MR (1999b) TR146 cells grown on filters as a model of human buccal epithelium: Permeability of fluorescein isothiocyanate-labelled dextrans in the presence of sodium glycocholate. *J Control Release* 60:223–233
90. Odland GF (1960) A submicroscopic granular component in human epidermis. *J Invest Dermatol* 34:11–15

91. Oh CK, Ritschel WA (1990) Biopharmaceutic aspects of buccal absorption of insulin. *Methods Find Exp Clin Pharmacol* 12:205–212
92. Oyama Y, Yamano H, Ohkuma A, Ogawara K, Higaki K, Kimura T (1999) Carrier-mediated transport systems for glucose in mucosal cells of the human oral cavity. *J Pharm Sci* 88:830–834
93. Rathbone MJ (1991a) Human buccal absorption. I. A method for estimating the transfer kinetics of drugs across the human buccal membrane. *Int J Pharm* 69:103–108
94. Rathbone MJ (1991b) Human buccal absorption. II. A comparative study of the buccal absorption of some parahydroxybenzoic acid derivatives using the buccal absorption test and a buccal perfusion cell. *Int J Pharm* 74:189–194
95. Rathbone MJ, Hadgraft J (1991) Absorption of drugs from the human oral cavity. *Int J Pharm* 74:9–24
96. Rathbone MJ, Drummond BK, Tucker IG (1994) The oral cavity as a site for systemic drug delivery. *Adv Drug Del Rev* 13:1–22
97. Romanowski AW, Squier CA, Lesch CA (1989) Permeability of rodent junctional epithelium to exogenous protein. *J Periodontal Res* 23:81–86
98. Rupniak HT, Rowlatt C, Lane EB, Steele JG, Trejdosiwicz LK, Laskiewicz B, Povey S, Hill BT (1985) Characteristics of four new human cell lines derived from squamous cell carcinomas of the head and neck. *J Natl Cancer Inst* 75:621–635
99. Sadoogh-Abasian F, Evered DF (1979) Absorption of vitamin C from the human buccal cavity. *Br J Nutr* 42:15–20
100. Schroeder HE (1981) Differentiation of Human Oral Stratified Epithelia. Karger, Basel, pp 35–152
101. Schürmann W, Turner P (1978) Membrane model of the human oral mucosa as derived from buccal absorption performance and physicochemical properties of the beta-blocking drugs atenolol and propranolol. *J Pharm Pharmacol* 30:137–147
102. Selvaratnam L, Cruchley AT, Navsaria H, Wertz PW, Hagi-Pavli EP, Leigh IM, Squier CA, Williams DM (2001) Permeability barrier properties of oral keratinocyte cultures: A model of intact human oral mucosa. *Oral Dis* 7:252–258
103. Senel S, Kremer M, Nagy K, Squier C (2001) Delivery of bioactive peptides and proteins across oral (buccal) mucosa. *Curr Pharm Biotechnol* 2:175–186
104. Senel S, Duchêne D, Hincal AA, Capan Y, Ponchel G (1998) In vitro studies on enhancing effect of sodium glycocholate on transbuccal permeation of morphine hydrochloride. *J Control Release* 51:107–113
105. Senel S, Kremer MJ, Kas S, Wertz PW, Hincal AA, Squier CA (2000) Enhancing effect of chitosan on peptide drug delivery across buccal mucosa. *Biomaterials* 21:2067–2071
106. Senel S, Hoogstraate AJ, Spies F, Verhoef JC, Bos-van Geest A, Junginger HE, Boddé HE (1994) Enhancement of in vitro permeability of porcine buccal mucosa by bile salts: Kinetic and histological studies. *J Control Release* 32:45–56
107. Senel S, Capan Y, Sargon MF, İkinci G, Solpan D, Güven O, Boddé HE, Hincal AA (1997) Enhancement of transbuccal permeation of morphine sulfate by sodium glycodeoxycholate in vitro. *J Control Release* 45:153–162
108. Shin SC, Kim JY (2000) Enhanced permeation of triamcinolone acetoneidone through the buccal mucosa. *Eur J Pharm Biopharm* 50:217–220
109. Shojaei AH (1998) Buccal mucosa as a route for systemic drug delivery: A review. *J Pharm Pharmaceut Sci* 1:15–30
110. Shojaei AH, Berner B, Xiaoling L (1998a) Transbuccal delivery of acyclovir: I. In vitro determination of routes of buccal transport. *Pharm Res* 15:1182–1188
111. Shojaei AH, Zhou S, Li X (1998b) Transbuccal delivery of acyclovir (II): Feasibility, system design, and in vitro permeation studies. *J Pharm Pharmaceut Sci* 1:66–73

112. Shojaei AH, Khan M, Lim G, Khosravan R (1999) Transbuccal permeation of a nucleoside analog, dideoxycytidine: Effects of menthol as a permeation enhancer. *Int J Pharm* 192:139–146
113. Siegel IA (1984) Permeability of the oral mucosa. In: Meyer J, Squier CA, Gerson SJ (eds.) *The Structure and Function of Oral Mucosa*. Pergamon Press, Oxford, pp 95–108
114. Siegel IA, Gordon HP (1985a) Effects of surfactants on the permeability of canine oral mucosa in vitro. *Toxicol Lett* 26:153–157
115. Siegel IA, Gordon HP (1985b) Surfactant-induced increases of permeability of rat oral mucosa to non-electrolytes in vivo. *Arch Oral Biol* 30:43–47
116. Siegel IA, Gordon HP (1986) Surfactant-induced alterations of permeability of rabbit oral mucosa in vitro. *Exp Mol Path* 44:132–137
117. Siegel IA, Hall SH, Stambaugh R (1971) Permeability of the oral mucosa. In: Squier CA, Meyer J (eds.) *Current Concepts of the Histology of Oral Mucosa*. Thomas, Springfield, pp 274–286
118. Smith PL (1996) Methods for evaluating intestinal permeability and metabolism in vitro. In: Borchardt RT, Smith PL, Wilson G (eds.) *Models for Assessing Drug Absorption and Metabolism*. Plenum Press, New York, pp 13–34
119. Squier CA (1973) The permeability of keratinized and nonkeratinized oral epithelium to horseradish peroxidase. *J Ultrastruct Res* 43:160–177
120. Squier CA (1977) Membrane coating granules in nonkeratinizing oral epithelium. *J Ultrastruct Res* 60:212–220
121. Squier CA (1982) Zinc iodide-osmium staining of membrane-coating granules in keratinized and non-keratinized mammalian oral epithelium. *Arch Oral Biol* 27:377–382
122. Squier CA, Rooney L (1976) The permeability of keratinized and nonkeratinized oral epithelium to lanthanum in vivo. *J Ultrastruct Res* 54:286–295
123. Squier CA, Hall BK (1985a) The permeability of skin and oral mucosa to water and horseradish peroxidase as related to the thickness of the permeability barrier. *J Invest Dermatol* 84:176–179
124. Squier CA, Hall BK (1985b) In-vitro permeability of porcine oral mucosa after epithelial separation, stripping and hydration. *Arch Oral Biol* 30:485–491
125. Squier CA, Wertz PW (1996) Structure and function of the oral mucosa and implications for drug delivery. In: Rathbone MJ (ed.), *Oral Mucosal Drug Delivery*. Marcel Dekker, New York, pp 1–26
126. Squier CA, Cox P, Wertz PW (1991a) Lipid content and water permeability of skin and oral mucosa. *J Invest Dermatol* 96:123–126
127. Squier CA, Wertz PW, Cox P (1991b) Thin-layer chromatographic analyses of lipids in different layers of porcine epidermis and oral epithelium. *Arch Oral Biol* 36:647–653
128. Squier CA, Kremer M, Wertz PW (1997) Continuous flow mucosal cells for measuring the in-vitro permeability of small tissue samples. *J Pharm Sci* 86: 82–84
129. Squier CA, Cox PS, Wertz PW, Downing DT (1986) The lipid composition of porcine epidermis and oral epithelium. *Arch Oral Biol* 31:741–747
130. Squier CA, Kremer MJ, Bruskin A, Rose A, Haley JD (1999) Oral mucosal permeability and stability of transforming growth factor beta-3 in vitro. *Pharm Res* 16:1557–1563
131. Sveinsson SJ, Mezei M (1992) In vitro oral mucosal absorption of liposomal triamcinolone acetonide. *Pharm Res* 9:1359–1361
132. Swartzendruber DC (1992) Studies of epidermal lipids using electron microscopy. *Semin Dermatol* 11:157–161
133. Tanaka T (1984) Transport pathway and uptake of microperoxidase in the junctional epithelium of healthy rat gingiva. *J Periodontal Res* 19:26–39

134. Tavakoli-Saberi MR, Audus KL (1989) Cultured buccal epithelium: An in vitro model derived from the hamster pouch for studying drug transport and metabolism. *Pharm Res* 6:160–166
135. Tolo K (1974) Penetration of human albumin through the oral mucosa of guinea-pigs immunized to this protein. *Arch Oral Biol* 19:259–263
136. Tsutsumi K, Obata Y, Takayama K, Isowa K, Nagai T (1999) Permeation of several drugs through keratinized epithelial-free membrane of hamster cheek pouch. *Int J Pharm* 177:7–14
137. Tucker IG (1988) A method to study the kinetics of oral mucosal drug absorption from solutions. *J Pharm Pharmacol* 40:679–683
138. Ungphaboont S, Maitani Y (2001) In vitro permeation studies of triamcinolone acetamide mouthwashes. *Int J Pharm* 220:111–117
139. Ussing HH (1949) Active ion transport through the isolated frog skin in the light of tracer studies. *Acta Physiol Scand* 17:1–37
140. Utoguchi N, Watanabe Y, Takase Y, Suzuki T, Matsumoto M (1999) Carrier-mediated absorption of salicylic acid from hamster cheek pouch mucosa. *J Pharm Sci* 88:142–146
141. Utoguchi N, Watanabe Y, Suzuki T, Maehara J, Matsumoto Y, Matsumoto M (1997) Carrier-mediated transport of monocarboxylic acids in primary cultured epithelial cells from rabbit oral mucosa. *Pharm Res* 14:320–324
142. van der Bijl P, van Eyk AD, Thompson IO (1998a) Effect of freezing on the permeability of human buccal and vaginal mucosa. *S Afr J Sci* 94:499–502
143. van der Bijl P, van Eyk AD, Thompson IO (1998b) Penetration of human vaginal and buccal mucosa by 4.4-kd and 12-kd fluorescein-isothiocyanate-labeled dextrans. *Oral Surg Oral Med Oral Pathol Oral Radiol Endod* 85:686–691
144. van der Bijl P, van Eyk AD, Thompson IO (1998c) Permeation of 17β -estradiol through human vaginal and buccal mucosa. *Oral Surg Oral Med Oral Pathol Oral Radiol Endod* 85:393–398
145. van der Bijl P, van Eyk AD, Thompson IO, Stander IA (1998d) Diffusion rates of vasopressin through human vaginal and buccal mucosa. *Eur J Oral Sci* 106:958–962
146. van der Bijl P, Gluckman HL, van Eyk AD, Thompson IO (1998e) Permeability of lichen planus lesions and healthy buccal mucosa to water. *SADJ* 53:493–496
147. Veuillez F, Ganem-Quintanar A, Deshusses J, Falson-Rieg F, Buri P (1998) Comparison of the ex vivo oral mucosal permeation of tryptophan-leucine (Trp-Leu) and its myristoyl derivative. *Int J Pharm* 170:85–91
148. Veuillez F, Falson-Rieg F, Guy RH, Deshusses J, Buri P (2002) Permeation of a myristoylated dipeptide across the buccal mucosa: Topological distribution and evaluation of tissue integrity. *Int J Pharm* 231:1–9
149. Walker GF, Langoth N, Bernkop-Schnürch A (2002) Peptidase activity on the surface of the porcine buccal mucosa. *Int J Pharm* 233:141–147
150. Wertz PW, Squier CA (1991) Cellular and molecular basis of barrier function in oral epithelium. *Crit Rev Ther Drug Carrier Syst* 8:237–269
151. Wertz PW, Swartzendruber DC, Squier CA (1993) Regional variation in the structure and permeability of oral mucosa and skin. *Adv Drug Del Rev* 12:1–12
152. Wertz PW, Cox PS, Squier CA, Downing DT (1986) Lipids of epidermis and keratinized and nonkeratinized oral epithelia. *Comp Biochem Physiol B* 83:529–531
153. Xiang J, Fang X, Li X (2002) Transbuccal delivery of 2',3'-dideoxycytidine: In vitro permeation study and histological investigation. *Int J Pharm* 231:57–66
154. Yamahara H, Lee VHL (1993) Drug metabolism in the oral cavity. *Adv Drug Del Rev* 12:25–40
155. Yamahara H, Suzuki T, Mizobe M, Noda K, Samejima M (1990) In situ perfusion system for oral mucosal absorption in dogs. *J Pharm Sci* 79:963–967

156. Yamamoto A, Hayakawa E, Lee VH (1990) Insulin and proinsulin proteolysis in mucosal homogenates of the albino rabbit: Implications in peptide delivery from nonoral routes. *Life Sci* 47:2465–2474
157. Zhang H, Robinson JR (1996) In vitro methods for measuring permeability of the oral mucosa. In: Rathbone MJ (ed.), *Oral Mucosal Drug Delivery*. Marcel Dekker, New York, pp 85–100
158. Zhang J, Niu S, McJames S, Stanley T (1991a) Buccal absorption of insulin in an in vivo dog model—evidence of mucosal storage. *Pharm Res* 8:S–155
159. Zhang J, Niu S, Maland LJ, Barrus BK, Freimann VR, Hague BI (1991b) Buccal permeability of oral transmucosal fentanyl citrate (OTFCTM) in a dog model. *Pharm Res* 8:S–155

5

In Situ and Ex Vivo Nasal Models for Preclinical Drug Development Studies

Remigius U. Agu and Michael I. Ugwoke

Abstract Advances in drug delivery research are to a reasonable extent dependent on the use of innovative experimental models. As a result of many experimental, methodological, and ethical limitations associated with the use of the human species, animal models are routinely used for drug delivery studies, especially during early stages of drug development. The use of excised and cultured human or animal tissues as *in vitro* models to study nasal drug absorption and metabolism is growing in popularity. Based on the difficulties in obtaining human tissues or maintaining them in culture, most reported *in vitro* nasal drug transport and metabolism studies are based on animal tissues. A comparative treatise of various *in situ* and *ex vivo* nasal models is presented in this chapter. The advantages, limitations, specific applications of the various models in preclinical drug development, and *in vivo/in vitro* correlations are highlighted.

Keywords: Nasal drug delivery; Preclinical drug development; *In situ*; *Ex vivo*; Drug metabolism; Drug transport

Abbreviations

AMC	7-amido-4-methylcoumarin
ATP	Adenosine triphosphate
bis-THA	Bis-9-amino-1,2,3,4-tetrahydroacridine
BL-9	Polyoxyethylene-9-lauryl ether
DC	Sodium deoxycholate
DNP	Dinitrophenol
DTLE	des-tyrosine leucine enkephalin
EDTA	Ethylenediaminetetraacetic acid
GC	Sodium glycocholate
hCT	Human calcitonin
HPBCD	Hydroxypropyl- β -cyclodextrin
LDH	Lactate dehydrogenase
LPC	Lysophosphatidylcholine
MRP	Multidrug resistance protein
MTT	3-[4,5-dimethylthiazol-2-yl]-2,5-diphenyltetrazolium bromide

P_{app}	Apparent permeability
PEG-4000	Polyethylene glycol-4000
rHV2	Recombinant hiridin-2
SDS	Sodium dodecyl sulfate
STDHF	Sodium taurodihydrofusidate
TC	Sodium taurocholate

5.1. Introduction

Interest in nasal drug delivery has grown unabatedly the last 15 years. This is due to the several advantages the nose presents with respect to drug delivery, some of which include [1] the following:

- A relatively large surface area (epithelium covered with microvilli) available for drug absorption
- A thin, “porous,” and highly vascularized epithelium with high total blood flow per cubic centimeter, which ensures rapid absorption and onset of therapeutic action
- A porous endothelial basement membrane
- The direct transport of absorbed drugs into systemic circulation, effectively by-passing the first-pass effect of the liver and gastrointestinal tract
- Lower enzymatic activity compared to the gastrointestinal tract or liver
- Amenability to self-medication, which increases patient compliance
- Possibility of pulsatile delivery of some drugs to simulate the biorhythmic release of these drugs
- Lower risk of overdosage
- Achievement of controlled release

These attributes have led to several nasal formulations progressing to the market, not only for local but also for systemic administration. Granted that several types of studies (pharmacokinetics, pharmacodynamics, etc.) are only possible in vivo, fundamental understanding of drug transport and metabolism is frequently confounded by a lot of other factors. Determination of drug permeability (i.e., rate and extent of absorption and metabolism) across a specific mucosal epithelium plays a very crucial role in selection of drug candidates early in research and development. In addition, it is also highly desirable to screen permeation enhancement and toxicity of several investigational compounds and test formulations. This is because several factors affect drug permeability and absorption in vivo. These are related to the factors described in Table 5.1. In vitro techniques utilizing cell cultures and excised tissues have been used to study drug permeation, metabolism, and toxicity. The former is in detail described in Chap. 9. Therefore, this chapter will focus on in situ and ex vivo models used for drug absorption, metabolism, and toxicity investigations.

In the context of biopharmaceutical drug delivery “in situ” means the investigation of different aspects of drug delivery while the target site or organ remains a part of the intact animal. This is often achieved by perfusing the target organ with drug solutions that are under investigation. This experimental setup may be considered as a hybrid between in vivo (inside a living organism)

Table 5.1 Some factors that affect nasal drug absorption in vivo [2].

Biological	Formulation
1. Structural features	1. Physicochemical properties of the drug:
2. Biochemical changes	– Molecular weight
3. Physiological factors:	– Solubility
– Blood supply and neuronal regulation	– Lipophilicity
– Nasal secretions	– Dissociation and partition constants
– Nasal cycle	2. Physicochemical properties of the formulation:
– pH of the nasal cavity	– pH and mucosal irritancy
– Mucociliary clearance	– Osmolarity
4. Pathological conditions	– Viscosity and density
5. Environmental factors:	– Drug distribution
– Temperature	– Area of nasal mucosa exposed
– Humidity	– Amount of formulation applied
	– Type of dosage form
	3. Device-related factors:
	– Particle size of droplet/powder
	– Site and pattern of deposition

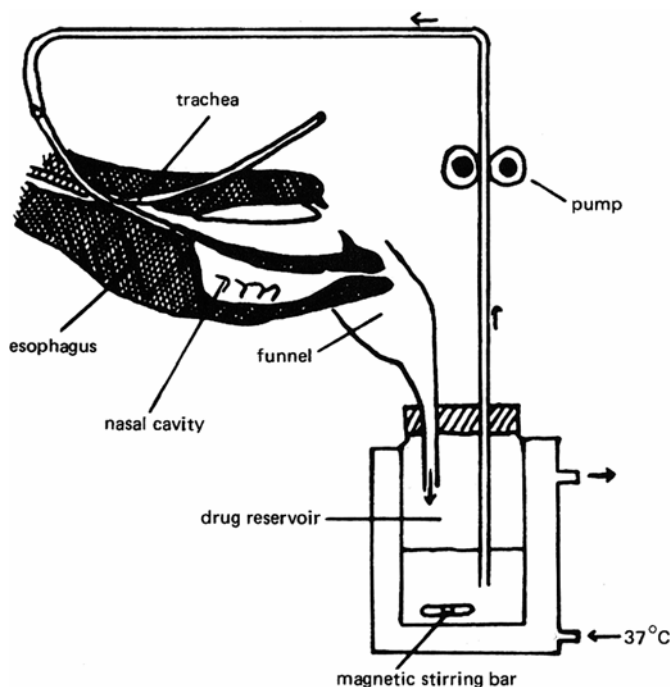
and in vitro (outside a living organism). Figure 5.1 depicts a typical experimental setup for in situ nasal perfusion studies.

Ex vivo refers to the application of living tissues for experimental research outside the intact organism. Therefore, the term may sometimes be used as synonym to “in vitro” (in glass—meaning in a test tube). For the purpose of this chapter, ex vivo models refer to nasal tissues harvested from different animals (rabbit, pig, cattle, sheep, rat, and human) for the purpose of investigating various aspects of nasal drug absorption in a standardized environment outside an intact living organism. Studies with excised tissues or cultured nasal cells are useful tools to obtain information on (a) the effect of enhancers on the flux and the concentration dependency of this effect, (b) the reversibility and recovery time of the enhancement, (c) the extent of tissue damage by histological examination, (d) the respective mechanisms involved, and (e) the effect on the ciliary beat frequency [3]. Therefore, it is important to emphasize that the usefulness of the models is not their predictive capability with respect to human nasal drug absorption, but their ability to use them to understand solute transport across the nasal epithelium and the various strategies to improve mucosal drug absorption.

5.2. Advantages of Ex Vivo and in Situ Models for Drug Absorption and Metabolism Studies

The ex vivo techniques of drug permeability using the Ussing chamber has extensively developed in the last few decades. It is very easy to monitor and therefore to maintain tissue viability throughout the study. This is ensured by monitoring the transepithelial potential difference and short-circuits current

Figure 5.1 Experimental setup for ex vivo nasal perfusion studies [4] (Reproduced with kind permission from Elsevier B.V.).



concurrently while the study is being performed. Several examples of media solutions together with CO₂/O₂ bubbling have been used to maintain tissue viability up to 6 h [3, 5, 6]. This time period is quite sufficient to allow conducting all types of relevant studies.

Compared to in vivo or cell culture methods, the availability of animal tissues for experimental use is better with respect to ex vivo techniques. Typically, tissues from rabbits, pigs, cows, and sheep are most frequently used. Because not only the ethical issues of using great numbers of animals in experimentations are avoided, but also nasal epithelium is very readily available from local slaughterhouses. This means that no animal is sacrificed only to obtain these tissues. In addition, the high quality of these tissues can be ensured, since diseased animals are not slaughtered anyway, and the snouts are immediately placed in ice after the slaughter. It is possible to obtain sufficient nasal epithelial tissues from one animal (typically from big animals like cow, sheep, and pig) for a complete six-chamber set Ussing study. This reduces variability of the resultant experimental data.

The ex vivo methods lend themselves easily for the performance of mechanistic investigations. In order to optimize selection of drug candidates prior to further clinical development, it is important to decipher the contributive roles of permeation, metabolism, efflux, and toxicity. This will then make it possible to properly channel the optimization process, for instance, by permeation enhancement, mucoadhesion, modification of the physicochemical characteristics of the drug, or even change in the route of administration in case the drug and/or formulation turns out to be too toxic. Regarding permeability studies, it is possible not only to quantify passive diffusion but also to identify and characterize (compound)-specific carrier-mediated transport routes. These tools have been used to identify and characterize the relative contribution of

the following active/carrier-mediated transport mechanisms [1]: Na/K-ATPase-dependent route, [2] endocytosis, and [3] multidrug resistance protein (MRP1) [3, 7]. Next to active transport through the mucosal-to-serosal direction, efflux pumps have been identified in the nasal mucosa as well [7]. Furthermore, the simplicity of these systems makes it possible to devise strategies to overcome the efflux pump actions. This increases the predictive power of these models for *in vivo* drug absorption. Indeed, this has been proven by Wadell et al. [8] where reasonable correlation with *in vivo* results was found for several compounds.

Even though the Ussing chamber method is used mostly to study drug permeability in liquid–liquid interphase, it has been demonstrated by Osth et al. [9] to be adaptable for air–mucosa interphase experiments. This simulates the *in vivo* situation more accurately. This air–mucosa interphase setup uses an even more limited amount of drug substance, which is an added advantage. The *ex vivo* models are very suitable for studying nasal toxicity of drugs, formulations, and excipients. Although not mounted in Ussing chambers, the chicken embryo trachea has been extensively used to study formulations toxicities [10]. Frequently, histopathological examinations of tissues reveal invaluable information on their toxicities [11]. The ability to screen various formulations quickly for both ciliotoxicity and other forms of epithelial toxicities is a strong positive attribute of the *ex vivo* models. Furthermore, advanced techniques such as confocal laser scanning microscopy can be used to study the drug permeation pathways of these tissues [12].

Although this section deals mainly with the advantages of excised tissues with respect to nasal drug delivery studies, it is important to highlight some important attributes of nasal *in situ* perfusion model. Although this method does not provide data on systemic absorption, it enables study of the interactions of nasal mucosal enzymes, peptide substrates, and metabolic inhibitors and their implications for nasal drug absorption [13]. It also enables the rate of nasal drug absorption to be determined.

5.3. Limitations of Ex Vivo and in Situ Models for Drug Absorption and Metabolism Studies

In spite of the numerous advantages of *ex vivo* models for nasal drug delivery experimentation which have made it indispensable to use them, they have a number of limitations as well. It is very important to realize these limitations and take them into consideration during interpretation and employment of the results obtained regarding *in vivo* situations. The thicknesses of nasal epithelial tissues differ per animal species, and this is further complicated by the amount of connective tissue left on the serosal side of the epithelium after tissue preparation. Since these factors have significant impact on the observed permeability, it becomes difficult not only to extrapolate the results to *in vivo* situation but also to compare *ex vivo* results of different researchers/groups. Another factor that complicates comparison of results is the current lack of standardization of experimental conditions with respect to temperature (28°C versus 37°C), gas perfusion (composition and rate), tissue incubation medium (including the often neglected influence of medium on solubility, dissociation of the drug substance), and stirring conditions (magnetic stirring versus air bubble lifting of solution). It has been argued that *in vivo*, 28°C is more

relevant than 37°C, since the nasal mucosa is in direct contact with ambient air temperature [3].

Migration of the drug into the perspex body of the Ussing chambers has been shown to occur at significant rates [9] and should be taken into account. Use of liquid–mucosa interphase compared to air–mucosa interphase can contradict the *in vivo* situation. Furthermore, the absence of mucus layer and ciliary clearance mechanisms complicates the situation. Both of these are important *in vivo* parameters with significant effect on total drug absorption. While the mucus lining increase the diffusion path length, the ciliary clearance limits the time available for drug absorption. Metabolic enzymes present in the nasal epithelium differ among various species not only in type but also in metabolic capacity [14]. This complicates *ex vivo*–*in vivo* correlations of metabolic activity. Some carrier-mediated transport systems are also human-specific and cannot be simulated *in vitro* using these models. Finally, it has to be mentioned that the Bovine Spongiform Encephalopathy (BSE) issue adds another dimension to the safety issues involved with executing these experiments [15]. It can affect availability of tissues from bovine origin, while putting the researcher at some risk.

The major limitation of the *in situ* nasal perfusion model is the significant differences in the experimental conditions of this model in comparison to nasal drug administration in humans. In this model perfusing the nasal mucosa with significant volumes (≥ 5 ml) of drug for a long period (90–120 min) will certainly result in the overestimation of the rate of nasal drug absorption, as well as the mucosal toxicity of the drug. This is expected considering that a volume of ~ 100 μ l is administered nasally to humans and this amount is rapidly removed by the mucociliary clearance in a span of 20–30 min.

5.4. Specific Applications of *in Situ* Methods in Nasal Drug Delivery Studies

Several nasal drug delivery studies have been conducted over the past two decades using this method. Although rabbits may be used, most of the studies reported in literature were conducted with rats. Therefore, studies performed using the rat model will be the focus of this chapter. The method simply involves circulating a buffered solution containing the drug under investigation through the rat or rabbit nasal mucosa and back into the test solution. The amount of drug absorbed is estimated by measuring the concentration of drug remaining at specified time intervals. The consideration of other potential sources of drug loss other than absorption (e.g., physical, chemical, and enzymatic degradation) is very important when using this method to investigate nasal drug absorption. The *in situ* nasal perfusion method has been used to investigate nasal drug permeation, metabolism, and irritation and for the optimization of formulation and absorption enhancement strategies. These specific applications are discussed in detail below.

5.4.1. Permeability Studies

A number of drugs, including digoxin [16], midazolam [17], sumatriptan [18], and tyrosine-linked drug [19] molecules, have been studied using the rat in

situ perfusion model. Kato et al. [16] used this model to show that digoxin disappeared from nasal perfusate via passive diffusion. The study also showed that the nasal absorption rate of digoxin decreased with an increase in perfusion volume from 5 to 20 ml, thus highlighting the importance of perfusion volume selection when using the method. In a similar study, midazolam diffusion across the rat nasal mucosa was shown to be partly pH-dependent, which is in agreement with the pH partition theory [17]. This means that the permeation of ionized form of the drug across the nasal mucosa was limited, but the nonionized form with higher lipid solubility had no problem crossing the nasal membrane. Additional contribution of hypoosmolarity to the nasal absorption of the compound was also investigated with the model. The absorption rates observed for hypoosmotic unbuffered solution were twice the values obtained with solution stabilized at pH 5.5 or 7.4 that were isoosmotic. The increased nasal absorption due to altered solution osmolarity was ascribed to epithelial swelling and the recruitment of the paracellular pathway for midazolam absorption. The results of these studies are clear indications that this model may be used to optimize formulation parameters for nasal drug delivery. In another study, Yang and Mitra [19] investigated the hypothesis that poorly permeable drugs will be absorbed significantly through the nasal route when linked to a tyrosine molecule. The assumption was that the tyrosine molecule will be recognized as a substrate by nasally expressed amino acid transporters. The hypothesis was confirmed based on the observation that the parent drug, which had different octanol–water partition coefficients were not absorbed, but when absorption occurred, it was by simple diffusion [19], while the absorption of tyrosine-linked compounds was concentration-dependent.

5.4.2. Metabolism Studies

Presystemic drug degradation, especially at mucosal sites, may significantly limit the bioavailability of a drug. This is particularly important for proteins and peptides that can easily be cleaved at specific amino acid sites. The rat perfusion models have been demonstrated to be a useful tool to screen nasal mucosal metabolism and absorption of peptides and proteins. This is very important because poor bioavailability of these compounds may be due to metabolism of the peptide at the absorption site, poor permeation through the membrane, or both of these mechanisms [20]. To investigate the utility of the intranasal administration of peptides for systemic medication, the nasal absorption of a model peptide, leucine enkephalin (Tyr-Gly-Gly-Phe-Leu), was studied in the rat [21]. According to the study, hydrolysis rather than polarity of the pentapeptide was responsible for limiting the nasal absorption of the peptide. In a closely related study, a series of enkephalin analogues with varying amino acids on the N-terminus were also evaluated using the rat *in situ* model for their hydrolytic stability and absorption following nasal absorption [20]. The amino acids on the N-terminus were tyrosine (Y), alanine (A), serine (S), lysine (K), and aspartic acid (D). Among these peptides, only the peptide carrying aspartic acid on the N-terminus was stable. The rank order of degradation rates was YGGFL > AGGFL > SGGFL, KGGFL > DGGFL. These results implied that there are relatively high activities of aminopeptidases N and B and relatively low activity of aminopeptidase A in the rat nasal mucosa. The study was found

to be in good agreement with low aminopeptidase A activity reported in rabbit nasal homogenates [22]. The rank order for peptide degradation in rabbit was YGGFL > AGGFL > SGGFL, KGGFL > > DGGFL. For systemic delivery of peptides through the human nasal mucosa, it is important to compare the amino peptidase activities in animal species (e.g., rat, rabbit, and pig) with that of the human nasal mucosa. This is very important for the interpretation of results based on animal studies and for subsequent data extrapolation to human species. Ohkubo et al. investigated different types of aminopeptidases expressed in human nasal epithelium. In their study aminopeptidase activities were defined by (a) substrate specificity with leucine enkephalin and alanine-nitroanilide, (b) inhibitor studies with puromycin and bestatin, (c) enzyme activity histochemistry (zymography), (d) immunohistochemistry, and (e) gel electrophoresis [23]. The study concluded that the predominant aminopeptidase in human nasal epithelial and submucosal gland cells was membrane-bound puromycin-resistant aminopeptidase. In another study with nasal lavages from patients with allergies and those without allergies, no aminopeptidase A-like activity was present—either before or after allergy challenge—as demonstrated by the complete absence of detectable amino acid conjugated to 7-amido-4-methylcoumarin (Glu-AMC) hydrolysis. In contrast, aminopeptidase M-like activity, determined by hydrolysis of Leu-AMC, was detected in all samples tested [24]. These studies indicate that the expression of different aminopeptidases in rat, rabbit, and human nasal epithelium are comparable, thus supporting the use of these animal species for preclinical drug delivery studies. A clear understanding of the presystemic metabolic pattern of peptides and corresponding metabolism inhibition strategies using the in situ or ex vivo animal models is very important for improving the bioavailability of this class of compounds. For instance, the use of specific inhibitors of aminopeptidases to achieve higher peptide stability and increased nasal absorption in animals (rabbit and rat) may reasonably reflect the absorption potential of a particular peptide when nasally administered to humans.

In addition to peptide-based studies, degradation and absorption kinetics of a homologous series of acyclovir ester prodrugs have been studied using the in situ perfusion model [25, 26]. The studies showed that due to high esterase activity of the rat nasal mucosa (96% disappearance of hexanoate prodrug of acyclovir in 960 min), the rat in situ model is an acceptable model to screen the nasal absorption of prodrugs.

5.4.3. Optimization of Drug Absorption Enhancement Strategies

The major strategies to enhance transmucosal peptide and other drug absorption include (a) coadministration with protease inhibitors, (b) the use of membrane permeation enhancers, (c) coadministration with a combination of absorption enhancers and protease inhibitors, (d) modification of peptide structure to improve metabolic stability or membrane permeation, and (e) use of nano- or microparticles [27]. Some of these strategies have been investigated using the in situ rat model.

Faraj et al. [28] studied the effects of different concentrations of leucine enkephalin, peptidase inhibitors, and sodium glycocholate (GC) on the stability and absorption of leucine enkephalin in nasal cavities of rats. Based on the study, the rate and extent of formation of des-tyrosine leucine enkephalin

(DTLE) were dependent on the concentration of leucine enkephalin administered and presence of GC. Therefore, both high peptide concentration and glycocholate reduced the rate of DTLE formation via enzyme saturation and inhibition, respectively. The study inferred that the *in vivo-in situ* perfusion technique yields more realistic data than the *in situ* method. The *in situ* perfusion with an *in vivo* component utilizes small volumes of solution to simulate the use of nose drops. The idea of using the *in situ-in vivo* approach was to correct the effect of perfusion volume on nasal drug absorption when using the *in situ* model alone. However, a comparison of nasal peptide delivery published by other authors showed that the results of enzyme inhibition with GC or saturation of peptide metabolism are comparable with results obtained using other methods [29, 30]. This does not mean that the effect of perfusion volume of drug absorption should not be taken seriously during nasal perfusion experiments.

Nasal absorption enhancement strategies using different excipients and formulations including lipid emulsions, chitosans, aminated gelatins, bile-salt-fatty acid mixed micelles, sodium deoxycholate (DC), hydroxyl-propyl- β -cyclodextrin, sodium caprate, sodium tauroglycocholate, and ethylenediaminetetraacetic acid (EDTA) were studied with the *in situ* nasal perfusion method. Mitra et al. studied the use of lipid emulsion-based formulations for insulin nasal absorption enhancement [31]. The nasal absorption of the compound was improved, especially when the insulin was incorporated into the continuous aqueous phase of an *o/w* emulsion. The presence of a small fraction of oil droplets along with the insulin in the aqueous phase favored its absorption [31]. Although this enhancement strategy based on the *in situ* perfusion model was cross-validated with *in vivo* rat model in the study, the possibility of lipo-pneumonia due to the oil droplets in the formulation implies that safer absorption enhancing approaches may be preferred for nasal insulin administration. In another study, Tengamnuay et al. showed the usefulness of free amine chitosans and soluble chitosans as absorption enhancers for peptides using the *in situ* perfusion model [32]. At 0.5% concentration, all the chitosans tested were effective in enhancing the nasal absorption of [D-Arg²]-kyotorphin, an opioid peptide. The enhancing effect of the free amine chitosans was pH-dependent and increased with decreasing pH. The application of aminated gelatin as absorption enhancer for insulin was studied using the *in situ* method [33]. The absorption enhancing effect of the gelatin was dependent on molecular weight, charge, and other physicochemical properties of the gelatin. The scope of applications of the *in situ* models also includes studies with prodrugs. The method was used to investigate the nasal absorption enhancement strategies for acyclovir and its prodrugs using bile-salt-fatty acid mixed micelles, bile-salt acylcarnitine, DC, hydroxyl-propyl- β -cyclodextrin, sodium caprate, sodium tauroglycocholate, and EDTA [25, 26, 34]. For the studies with prodrugs, the enhanced nasal absorption with the enhancers was due to reduction in epithelial membrane resistance. In the studies with bile-salt acylcarnitine mixed micelles, the effect of the micellar solutions was synergistic. The enhancement factor was higher with mixed micelles than with a single enhancer. This observation could be because of micellar solubilization of acylcarnitines by glycocholate. The order of increasing absorption enhancement of acyclovir by the enhancers was hydroxypropyl- β -cyclodextrin (HPBCD) > DC > sodium caprate > sodium tauroglycocholate > EDTA.

5.4.4. Nasal Drug Irritation and Tolerance

Following nasal drug administration, the major toxicity concerns include local irritation of the mucosa, impairment of the mucociliary clearance, epithelial damage, and the recovery rate of the damaged mucosa [35]. Although the usefulness of the in situ model for screening the toxicity of drugs remains controversial, due to the unrealistic drug exposure time and perfusion volume compared to the in vivo setting [36], several studies reported the use of this model for screening nasal toxicity of drugs and excipients. Tengamnuay et al. [32] investigated the effects of free amine and soluble chitosan salts on rat nasal mucosa using protein, phosphorous, and lactate dehydrogenase (LDH) release as toxicity indices after continuous perfusion of the nasal epithelium with formulations containing the excipients. At concentrations ranging between 0.1% and 0.5%, the excipients caused minimal release of protein, phosphorous, and LDH. The effects were comparable to the results obtained with tissue exposure to 5% HPBCD and 1.25% dimethyl- β -cyclodextrin. In a similar study, the potential deleterious effect of aminated gelatin on rat nasal mucosa was investigated by measuring LDH release. The amount of LDH release caused by 0.1–0.4% aminated gelatin was less than that caused by an equal concentration of chitosan. The lower toxicity of the enhancer was considered to be due to its high molecular weight and poor penetration into the nasal mucosa [37]. In as much as the in situ method is not the best approach to screen potential nasal toxicity by drugs and formulation excipients, the method is potentially useful for gathering toxicity data during permeation experiments. The most important thing when using the model for this purpose is to appropriately interpret the results of the study.

5.5. Specific Applications of Ex Vivo Models in Nasal Drug Delivery Studies

During preclinical drug development the following basic physicochemical properties need to be determined in order to develop a successful formulation: (a) solubility, (b) compatibility, (c) polymorphism, and (d) stability [38]. For nasal drug delivery, it is also important to investigate other factors that may affect the rate and extent of drug absorption. Such factors include drug permeation mechanisms, metabolic stability, formulation parameters, and the need for absorption enhancers. Excised tissues from different animal species have played an important role in investigating these factors.

5.5.1. Permeability Studies and Characterization of Drug Absorption Pathways

The extent of drug absorption following nasal administration depends to a reasonable extent on the ease with which a drug molecule crosses the nasal epithelium without degradation or rapid clearance by the mucociliary clearance system. The effects of these two elimination components are more pronounced for proteins and peptides. The nasal administration of drugs, especially proteins and peptides, as well as other molecules has been studied with excised tissues harvested from rabbit, cow, sheep, and pig species (Table 5.2). A

Table 5.2 Apparent permeability coefficients (P_{app}) of low and high molecular weight compounds across the nasal mucosa of tissues excised from different animal species.

	Molecular weight (g/mol)	P_{app} ($\times 10^6 \text{ cm}\cdot\text{s}^{-1}$)	Animal species
Nonpeptides			
Amino diether	251	49	Pig
Lidocaine	236	52.0	Pig
Melagatran	430	6.2	Pig
Nicotine	162	128.0	Pig
Polyethylene glycol	4,000	13.0	Pig
Propranolol	259	20.0	Pig
		25.5	Pig
Sumatriptan	295	14.3	Pig
Testosterone		32.2	Pig
Peptides			
Thyrotropin-releasing hormone	362	4.9	Rabbit
Thymotrinan (TP3)	417	15.7	Cattle
Thymocartin (TP4)	517	17.0	Cattle
Thymopentin (TP5)	680	9.2	Cattle
Octreotide	1,072	43	Cattle
Sandostatin		5	Human
Angiopeptin	1,156	0.91	Rabbit
Gonadorelin, LHRH	1,182	1.86	Cattle
Buserelin	1,239	14.7	Cattle
Hoe013	1,511	16.3	Cattle
[1,7 Asu]eel calcitonin	3,362	0.38	Rabbit
Human calcitonin	3,418	20.1	Cattle
Salmon calcitonin	3,432	19.2	Cattle
Insulin	5,600	0.24	Rabbit
		0.72	Rabbit
		0.95	Rabbit

Source: Data were modified from Schmidt et al.[3], Kubo et al. [45], Wadell et al. [52], and Hershey et al. [62].

summary of some of the studies conducted with each species is highlighted in the following sections.

5.5.1.1. Rabbit Tissues

Cremschi et al. [39] investigated transepithelial pathways of eel calcitonin, corticotrophin, sucrose, and polyethylene glycol-4000 (PEG-4000) transport across the nasal epithelium using rabbit nasal mucosa mounted on Ussing chamber that was maintained at 27°C. The electrical parameters of the tissues were those of leaky epithelium that allow macromolecules to permeate paracellularly; their observation was similar to the finding made by McMartin et al. [40] in which the authors described the nasal epithelium as leaky with

transepithelial resistance in the range 60–70 ohms·cm². Although it is important to conduct nasal permeation of macromolecules using leaky epithelia, comparable permeation profiles may also be observed when using less leaky epithelia (e.g., excised tracheal cells or cultured nasal epithelial cells showing resistances of 200–700 ohms·cm²). The comparable results may be explained by the involvement of active transport processes for nasal absorption of peptides. This hypothesis was confirmed in a study that examined the transport of eel calcitonin adsorbed onto microspheres [41] across the rabbit nasal epithelium. Different endocytosis inhibitors including cytochalasin B, colchicine, aluminum fluoride, and monensin were used for the study [42]. The most interesting aspect of the observed active transport phenomenon was that maximum transport occurs within 30 min, followed by progressive decrease in subsequent 90 min. The nature of the transport, its small entity, and transient duration suggested that the active transport processes did not evolve to massively absorb materials but to transfer chemical messages from nasal lumen to blood. As the transport relates to polypeptides, it might be involved in antigen sampling from the lumen at the entry of the airways [43]. This active and specific polypeptide transcytosis is correlated to the volume of lymphoid aggregates present in the mucosa. Both active and passive transport-mediated permeation of polypeptides in rabbit nasal tissues was also observed for recombinant hirudin-2 (rHV2) [44]. The permeation of the compound was inhibited by low temperature, 1 mM dinitrophenol (DNP) (uncoupler of oxidative phosphorylation), 10 mM NaN₃ (mitochondrial respiratory inhibitor), as well as by 0.1 mM colchicine (inhibitor of microtubular assembly). These findings implied that the transport of rHV2 was energy-dependent and involved adenosine triphosphate (ATP) production via oxidative phosphorylation. Lack of saturation, as well as absence of obvious differences in transport direction, also implicated passive diffusion as a mechanism for the rHV2 transport across the nasal epithelium. Permeation studies reported in literature involving rabbit nasal tissues, however, are not limited to proteins and peptides. Studies with other drug molecules, such as disodium cromoglycate or fluorescein isothiocyanate-dextran of different molecular weights, have also been reported [45].

5.5.1.2. Cow (Bovine) Tissues

Apart from a single study that investigated the transport of drug molecules across the olfactory mucosa [46], all other published studies were based on tissues harvested from the turbinates. Schmidt et al. [47] validated the use of excised bovine mucosa for drug permeation and metabolism studies using the following parameters: (a) positive viability staining, (b) constant transepithelial electrical resistance, (c) constant rates of metabolic turnover, and (d) linear permeation profiles of therapeutic peptides and 3H-mannitol. Using 1-leucine-4-methoxy-2-naphthylamide as a model substrate, the study showed no difference between bovine and human nasal aminopeptidase activities. Also, by employing a series of therapeutic peptides, no direct correlation was found between their effective permeability coefficients (ranging from $0.1 \times 10^{-5} \text{ cm}\cdot\text{s}^{-1}$ to $5 \times 10^{-5} \text{ cm}\cdot\text{s}^{-1}$) and their respective molecular masses (417–3,432 Da), indicating that other factors than permeability alone control peptide absorption across the nasal mucosa. According to this study, the permeability of metabolically labile peptides was concentration-dependent and saturable, as demonstrated for two short thymopoietin fragments, Arg-Lys-Asp

(thymotriganin, TP3) and Arg-Lys-Asp-Val (thymocartin, TP4) [48]. This is an interesting study because it provided the basic scientific foundation based on validation for the application of the bovine tissues for drug delivery studies. Although numerous studies have been reported using rabbit nasal tissues, we were unable to locate specific articles that used a methodological approach to validate the use of the tissues for drug absorption studies. For the application of bovine tissue for peptide-related drug delivery studies, Lang et al. [48] investigated the transport and metabolic pathway of TP4, the 32–35 fragment of thymopoietin (naturally occurring thymic factor), using side-by-side diffusion chambers. Based on the study, the metabolic pathway of the compound followed typical aminopeptidase cleavage pattern with formation of lys-asp-val and asp-val, respectively. Saturating the nasal aminopeptidases with high concentrations of TP4 increased the rate of peptide permeation. Similarly, Koushik and Kompella showed that deslorelin transport across excised bovine nasal mucosa was vectorial, temperature- and energy-dependent, and exhibits regional variation [49]. The regional differences in serosal to mucosal transport may be due to differences in the passive transport pathways in tissues from different sites. Differences in mucosal to serosal versus serosal to mucosal flux ratios may also be due to differential expression of active carriers. The study showed that in addition to tissues harvested from the rabbit nasal mucosa, bovine tissues may be used to investigate active drug transport across the nasal mucosa. In another study, Machova et al. [50] investigated cellular internalization of enhanced green fluorescent protein ligated to human calcitonin (hCT)-based carrier peptide using bovine nasal tissues. The internalization process was pH-dependent with better results at pH 5.5–6.5 as opposed to pH 7.4. In order to understand the nature of the interaction between hCT and nasal epithelium, Wagner et al. [51] studied the interaction between hCT fragments 9-32 with different phospholipids. The results showed that hCT (9-32) preferentially interacts with negatively charged phospholipids and does not insert spontaneously into lipid bilayers. This supports a nonreceptor-mediated endocytotic internalization pathway.

5.5.1.3. Pig (Porcine) and Sheep (Ovine) Tissues

An important attribute of an acceptable ex vivo tissue model for nasal drug delivery studies is data availability on validated use of the model with emphasis on morphological similarities, comparable solute transport, and metabolic characteristics of the excised tissues in comparison with the human nasal epithelium. This is very important as it serves as a reference point on which to interpret the results of a particular study. Wadell et al. recognized this fact when they reported the development and evaluation of porcine nasal mucosa for permeation studies [52]. According to the authors the choice of this model was based on the similarities in terms of anatomy, physiology, as well as histological and biochemical similarities when compared to the human nasal mucosa. The yardsticks for the validation were electrophysiological assessment, determination of permeability coefficients of radio-labeled molecules, histological evaluation, and colorimetric assay of 3-[4,5-dimethylthiazol-2-yl]-2,5-diphenyltetrazolium bromide (MTT) cytotoxicity as an index of biochemical suitability for metabolism studies. The different methods used were cross-validated with each other, showing that the viability and integrity of the

epithelium was maintained during several hours of diffusion chamber studies. The permeability of the mucosa to the tested markers correlated well with the electrophysiological interpretation of mucosal viability. In a related study, Osth et al. [9] described in detail the use of Ussing chambers in conjunction with the pig nasal mucosa to study the transport of testosterone and mannitol under immersion and air–liquid interface conditions. They found no significant differences in either the bioelectrical parameters (transmucosal electrical resistance, potential difference, and short circuit current) or the apparent permeability (P_{app}) of the mucosa to testosterone or mannitol between the liquid– and air–interface experiments. The usefulness of the porcine model was further highlighted in studies involving systemic delivery of an Alzheimer drug [53] and controlled release formulations [54] of dihydroalprenolol, hydrocortisone, and testosterone. The permeation kinetics of a bis-tacrin analog (bis-THA) indicated that the nasal mucosa is a possible route for systemic delivery of the drug. Delipidization studies suggested that the lipophilic components in the absorptive mucosa could play an important role in the permeation of bis-THA.

Although several results of in vivo nasal pharmacokinetic studies using sheep have been published, few authors reported the use of tissues harvested from the animal for ex vivo studies. Wheatley et al. [55] showed that sheep nasal mucosa mounted in Ussing chambers exhibits normal electrophysiology and histology. The transepithelial transport of inulin, mannitol, and propranolol across the mucosa occurred by passive diffusion. The model has been used to study the permeation of a wide range of compounds including growth hormone releasing peptide, mannitol, Lucifer yellow, and hCT [56, 57].

5.5.2. Metabolism Studies

Although valuable insights into the mechanisms of nasal drug metabolism and absorption can be obtained using animal models, their predictive power, which allows an extrapolation to nasal drug administration in humans, remains a controversial issue, due to species-dependent differences in the expression of various enzymes and their isoforms. Nevertheless, tissues isolated from various animal species are at the forefront in preclinical drug development for screening the effects of nasally expressed enzymes on drug metabolism and absorption. Such studies are important, because the enzymatic barrier plays a critical role in nasal delivery of some protein- and peptide-based drugs. Various drug-metabolizing enzymes have been identified in the nasal mucosa and they include oxidative phase I enzymes, conjugative phase II enzymes, and proteolytic enzymes [14]. The proteolytic enzymes play probably the most important role with respect to nasal drug delivery. These enzymes consist of exopeptidases, which are restricted to the hydrolysis of peptides at/or near the N- or C-terminal of the peptide or protein molecule, and endopeptidases, which hydrolyze internal peptide bonds within a peptide chain [58]. Jørgensen et al. estimated the stability of thyrotropin-releasing hormone against nasal enzymes using nasal washing and rat nasal homogenates [59]. While no degradation occurred in the human nasal washing, the degradation rate in the rat nasal homogenate was $0.5 \mu\text{g}/\text{h}$. This clearly shows the major limitation of tissue homogenates. In a study with intact tissues, the transport and metabolism of TP4 was studied in excised bovine mucosa [48]. The metabolic pathway of

TP4 in the nasal mucosa was classical for aminopeptidase-based cleavage. At the lower concentration range investigated, the transport of TP4 across the nasal mucosa was controlled by metabolism, while at the higher concentration range, diffusion control became more important, due to enzyme saturation. In a similar study, the susceptibility of hCT and salmon calcitonin to nasal mucosal enzymes was assessed by in-and-out reflection kinetics experiments [57]. Both compounds were readily metabolized by nasal mucosal enzymes. In the concentration range studied, metabolic rates were higher with hCT than with the salmon-derived protein. The presence of endopeptidase activities in the nasal mucosa resulted in the cleavage of both calcitonins in the central domain of the molecules. It is interesting to note that the metabolic pathway of the compounds in homogenized rat mucosa yielded additional pathways—at Leu⁹-Gly¹⁰, Thr²⁰-Tyr²¹, and Arg²³-thr²⁴. Such cleavage positions are indicative of chymotryptic endopeptidase activity. The differences in the cleavage pattern and in the number of cleavage positions in salmon calcitonin may be due to differences in experimental setup (homogenates versus intact tissues, exposure duration) and animal species used for the study. This observation emphasizes the need to confirm the metabolic breakdown of peptides using human nasal tissues or cell culture models. In as much as human-based tissues are important to identify particular fragments expected in vivo, tissues harvested from animals have helped in identifying major peptidases [60].

5.5.3. Optimization of Formulation Parameters and Drug Absorption Enhancement Strategies

Factors affecting nasal drug absorption, such as physicochemical properties of drugs, drug absorption mechanism, and the need for absorption enhancer, have been elaborately studied using isolated tissues. As the nasal epithelial tight junctions are the dominant factor regulating the permeation of hydrophilic macromolecules across the nasal mucosa, it is important to study the uptake and transport mechanism of these compounds using excised tissues as a forerunner for successful performance of delivery systems targeted to the nasal route [44]. The focus and need for the use of absorption enhancers are particularly important because of the high molecular weight and hydrophilic nature of proteins and peptides. Zhang et al. [44] used tissues excised from rabbits to investigate the effects of multiple absorption enhancers on the permeation of rHV2 across the rabbit nasal epithelium. Chitosan was effective in significantly improving permeation of the compound. When formulated in combination with other enhancers, such as sodium dodecylsulfate, brij35, tween 80, menthol, glycyrrhizic acid monoammonium salt, and azone, significant improvement in absorption was observed. The enhancement ratio for these excipients ranged from 7 to 33. The practical aspect of using these enhancers for further development, however, is doubtful considering that the study did not provide any information on the effects of the excipients on epithelial morphology. In another study, Hosoya et al. used the rabbit nasal tissues in combination with Ussing chambers to investigate the potential usefulness of sodium taurodihydrofusidate (STDHF), DC, polyoxyethylene-9-lauryl ether (BL-9), lysophosphatidylcholine (LPC), sodium dodecyl sulfate (SDS), GC, sodium taurocholate (TC), and EDTA as nasal absorption

enhancer [61]. The permeation of fluorescein isothiocyanate-labeled dextran (9,400 Da) across the nasal mucosa was higher in the presence of these enhancers. Their enhancement ratio was found to be in the order: BL-9 > STDHF > SDS > LPC > DC > EDTA > GC > TC. Apart from tissues harvested from rabbits, other animal sources, such as dog [62], cow [47], sheep [56], and pig [5], have been used to study nasal drug absorption enhancement. In addition to simple drug enhancement studies with absorption enhancers, isolated nasal tissues have been found to be useful for studying the permeation of special formulations (e.g., microspheres, cyclodextrin-based inclusion complexes, mucoadhesive gel formulations, and liposome entrapped drugs) across the nasal mucosa [63–66].

5.5.4. Nasal Drug Irritation and Tolerance

Drugs administered through the nasal route may compromise the nasal epithelial integrity or alter the mucociliary clearance. Therefore, investigating the effects of drugs and excipients used in formulating them on the nasal mucosa and mucociliary clearance is an important aspect of preclinical drug delivery studies. A highlight of the relevance of non-in vivo models of nasal epithelium as screening tools to assess the effects of drugs, excipients, and formulation variables on nasal mucosal tolerance, ciliotoxicity, and mucociliary clearance may be found in our previous work [35]. Emphasis in this section will be on the application of excised tissues in conjunction with Ussing chambers to screen the effects of drugs and excipients on epithelial integrity. Toxicity endpoints for these studies include the assessment of the effects of the drug on bioelectrical parameters (transmucosal electrical resistance, potential difference, and short circuit current), permeability of paracellular markers (e.g., mannitol and sodium fluorescein), leaching of membrane substances (LDH, MTT, proteins), and histological examination of tissues (necrosis) following the end of permeation studies. Although this approach is generally used, it is important to point out the fact that results from such studies may not represent the expected observations under in vivo setting. This is because the olfactory, respiratory, squamous, transitional, and lymphoepithelial nasal epithelium may be injured by an inhaled toxicant. Toxicant-induced epithelial lesions in the nasal passages of laboratory animals (and humans) are often site-specific and dependent on the intranasal regional dose of the inhaled chemical and the sensitivity of the nasal epithelial tissue to the specific chemical [67]. This important point cannot be reproduced in vitro when using excised tissues for toxicity screening.

5.6. Correlation Between Nasal Drug Absorption Models

During the last decade several in vitro models using excised mucosal segments and monolayers of epithelial cells have been established, providing an opportunity to predict nasal drug absorption in vivo while avoiding problems associated with more complex whole animals [8].

An evaluation of the various studies reported in the literature for preclinical assessment of drugs for nasal administrations indicated the usefulness of in situ, ex vivo, and in vivo approaches. Evidence from the literature also indicates that the choice of a particular model or animal species by different

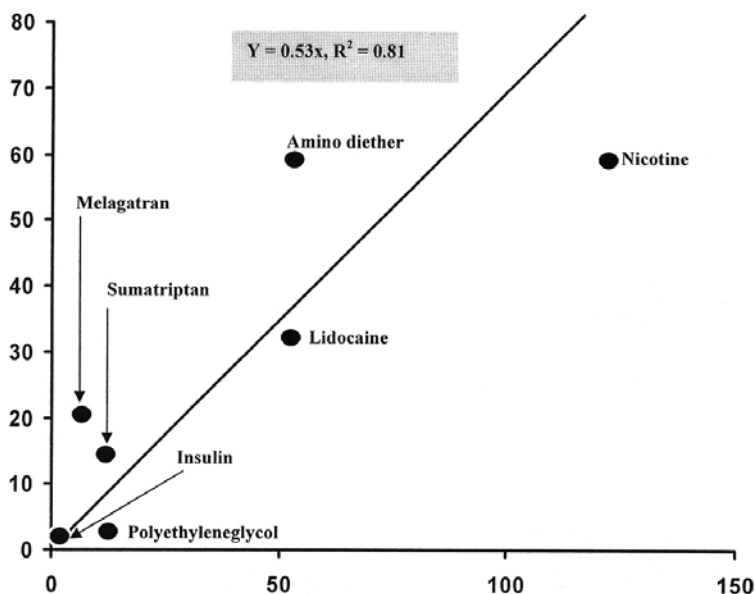


Figure 5.2 Literature data on fraction of drugs absorbed (in percent) after human nasal administration versus apparent permeability (P_{app}) data from Ussing chamber studies on porcine nasal mucosa (Reprinted with permission from Elsevier B.V.).

authors was generally not based on morphological, functional, or biochemical comparison of the model to the human nasal mucosa, but rather on the availability of tissues and expertise in a particular method. It is of utmost importance to consider the aim of nasal absorption studies before selecting the experimental model to use [54]. In order to increase the value of animal experiments, it is important to establish a correlation of nasal bioavailability between animal species and man and between flux of compounds across animal tissues and in vivo bioavailability [8, 68]. According to Gizurarson [69], rabbits, dogs, monkeys, and sheep are ideal animal models for nasal pharmacokinetic studies. Following this clue, Lindhardt et al. [70] investigated the correlation between the bioavailability of buprenorphine and diazepam in sheep, rabbit, and man. According to the studies, the correlation of bioavailability was not optimal between sheep, man, and rabbit with differences in both rate and extent of absorption. The observed discrepancy in absorption may be due to anatomical differences, method of drug sampling, and dosimetry-related issues, such as the site and the volume of drug deposition in the nasal mucosa. Having this in mind, one may wonder what level of correlation is possible to achieve comparing results of permeation studies with excised tissues and drug bioavailability in humans following nasal drug administration (Figure 5.2). Wadell et al. addressed this issue in a study that compared the permeability of porcine nasal mucosa with human nasal absorption [8]. Eight drug molecules with different physicochemical properties (insulin, lidocaine, nicotine, PEG-4000, propranolol, sumatriptan, melagatran, and an amino diether) were used for the study. A reasonable correlation was found ($r^2 = 0.81$ at the 95% confidence level). The authors considered the correlation coefficient to be low and suggested that the value may be due to the limited number of substances available for comparative studies and the possible involvement of active transport mechanisms for some drugs. Another reason cited for the calculated correlation coefficient based on the study is decreased tissue viability ex vivo with increased permeability as a consequence.

Table 5.3 Factors affecting pharmacokinetics of nasal absorption [40].

Physiological factors	Dosage form-related factors	Administration-related factors
– Rate of mucociliary clearance	– Concentration of active ingredient	– Type of dosage form (liquid, aerosol, powder)
– Presence of infection or allergy	– Physicochemical properties of drug	– Aerosol droplet size
– Atmospheric conditions	– Viscosity of formulation	– Mechanical drug loss to the esophagus
	– pH of dosage form	– Mechanical drug loss to other regions of the nose
	– Toxicity of dosage form	– Mechanical loss anteriorly from the nose
	– Nature of excipients used	

Generally speaking, it is extremely difficult to expect a very high correlation between *in vitro* and *in vivo* nasal absorption studies based on the reasons summarized in Table 5.3. Therefore, when using excised tissues for preclinical drug development studies, emphasis should not be placed on the ability of a model to be used to predict the rate and the extent of nasal drug absorption. The excised tissue models are more important for conducting mechanistic studies on factors and strategies for improving nasal drug absorption. Instead of worrying too much about *in vitro*–*in vivo* correlation, emphasis should in fact be on correlation between various *in vitro* models used for preclinical nasal drug absorption studies.

5.7. Conclusions

The advent of potent biotherapeutics and other drugs, frequently in limited supply during drug development, together with both societal and financial pressures on the pharmaceutical industry, will continue to spur innovative ways of formulating and administering these drugs. The use of *in situ* nasal perfusion, excised human or animal tissues (e.g., rabbit, ovine, canine, and bovine), and cultured cells as drug screening models is growing in popularity. Excised tissues are very attractive for drug delivery studies, especially during the early stages of drug development, because of difficulties in obtaining human tissues, and methodological and ethical limitations associated with the use of those tissues for research. The leaky nature of excised tissues (comparable to the *in vivo* situation) is also an important attribute. Despite the usefulness of *ex vivo* models in drug delivery studies, important factors, such as tissue viability and differences in activity of different nasal enzymes between various species, should be taken into account during experimental data interpretation and extrapolation to the human situation. Although the use of *in situ* nasal perfusion model is not favored by many researchers, because of some shortcomings of this method, the model may still be used, provided

some variables (e.g., perfusion volume/duration) are carefully selected and monitored. It is important to emphasize that attempts to replace or augment in vivo nasal drug delivery study approaches with in vitro or ex vivo alternatives should be guided by available information on the suitability, the validation, and the economic relevance of using such models. Presently, in vitro models may not replace in vivo methods, but are important complementary tools that will facilitate drug absorption enhancement strategies and toxicity screening. The nasal route is uniquely qualified for drug administration and the available methods described in this chapter facilitate fundamental research on drug permeability, metabolism, and toxicity. Continued research efforts are required to further perfect ex vivo–in vivo or in situ–in vivo or ex vivo–in situ correlation of the data obtained.

References

1. Ugwoke MI, Verbeke N, Kinget R (2001) The biopharmaceutical aspects of nasal mucoadhesive drug delivery. *J Pharm Pharmacol* 53:3–21.
2. Arora P, Sharma S, Garg S (2002) Permeability issues in nasal drug delivery. *Drug Discovery Today* 7:967–975.
3. Schmidt MC, Peter H, Lang SR, Ditzinger G, Merkle HP (1998) In vitro cell models to study nasal mucosal permeability and metabolism. *Adv Drug Del Rev* 29: 51–79.
4. Chien YW (1985) *Transnasal systemic medications*. Elsevier, Amsterdam/ Oxford/ NY/ Tokyo.
5. Osth K, Paulsson M, Bjork E, Edsman K (2002) Evaluation of drug release from gels on pig nasal mucosa in a horizontal Ussing chamber. *J Control Rel* 83:377–388.
6. Richter T, Keipert S (2004) In vitro permeation studies comparing bovine nasal mucosa, porcine cornea and artificial membrane: androstenedione in micro-emulsions and their components. *Eur J Pharm Biopharm* 58:137–143.
7. Kandimalla KK, Donovan MD, Carrier (2003) Mediated transport of chlorpheniramine and chlorcyclizine across bovine olfactory mucosa: Implications on nose-to-brain transport. *J Pharm Sci* 94: 613–624.
8. Wadell C, Bjork E, Camber O (2003) Permeability of porcine nasal mucosa correlated with human nasal absorption. *Eur J Pharm Sci* 18:47–53.
9. Osth K, Grasjo J, Bjork E (2002) A new method for drug transport studies on pig nasal mucosa using a horizontal Ussing chamber. *J Pharm Sci* 91:1259–1273.
10. Merkus P, Romeijn SG, Verhoef JC, Merkus FW, Schouwenburg PF (2001) Classification of cilio-inhibiting effects of nasal drugs. *Laryngoscope* 111:595–602.
11. Ugwoke MI, Agu RU, Jorissen M, Augustijns P, Sciot R, Verbeke N, Kinget R 2000 Toxicological investigations of the effects carboxymethylcellulose on ciliary beat frequency of human nasal epithelial cells in primary suspension culture and in vivo on rabbit nasal mucosa. *Int J Pharm* 205:43–51.
12. Ohtake K, Maeno T, Ueda H, Ogihara M, Natsume H, Morimoto Y (2003) Poly-L-arginine enhances paracellular permeability via serine/threonine phosphorylation of ZO-1 and tyrosine dephosphorylation of occludin in rabbit nasal epithelium. *Pharm Res* 20:1838–1845.
13. Hussain MA, Koval CA, Shenvi AB, Aungst BJ (1990) Recovery of rat nasal mucosa from the effects of aminopeptidase inhibitors. *J Pharm Sci* 79: 398–400.
14. Sarkar M.A. (1992) Drug metabolism in the nasal mucosa. *Pharm Res* 9: 1–9.

15. Konold T, Sivam SK, Ryan J, Gubbins S, Laven R, Howe MJ (2006) Analysis of clinical signs associated with bovine spongiform encephalopathy in casualty slaughter cattle. *Vet J* 171:438–444.
16. Kato Y, Yagi N, Yamada S, Sato M, Kimura R (1992) Nasal absorption of digoxin in rats. *J Pharmacobiodyn* 15:1–6.
17. Olivier JC, Djilani M, Fahmy S, Couet W (2001) In situ nasal absorption of midazolam in rats. *Int J Pharm* 213:187–192.
18. Chavanpatil MD, Vavia PR (2005) Nasal drug delivery of sumatriptan succinate. *Pharmazie* 60:347–349.
19. Yang C, Mitra AK (2001) Nasal absorption of tyrosine-linked model compounds. *J Pharm Sci* 90:340–347.
20. Hussain MA, Seetharam R, Wilk RR, Aungst BJ, Kettner CA (1995) Nasal mucosal metabolism and absorption of pentapeptide enkephalin analogs having varying N-terminal amino acids. *J Pharm Sci* 84:62–64.
21. Hussain A, Faraj J, Aramaki Y, Truelove JE (1985) Hydrolysis of leucine enkephalin in the nasal cavity of the rat- a possible factor in the low bioavailability of nasally administered peptides. *Biochem Biophys Res Commun* 133: 923–928.
22. Huang CH, Kimura R, Nassar RB, Hussain A (1985) Mechanism of nasal absorption of drugs I: Physicochemical parameters influencing the rate of in situ nasal absorption of drugs in rats. *J Pharm Sci* 74:608–611.
23. Ohkubo K, Baraniuk JN, Hohman R, Merida M, Hersh LB, Kaliner MA (1998) Aminopeptidase activity in human nasal mucosa. *J Allergy Clin Immunol* 102:741–750.
24. Proud D, Baumgarten CR, Naclerio RM, Ward PE (1987) Kinin metabolism in human nasal secretions during experimentally induced allergic rhinitis. *J Immunol* 138:428–434.
25. Shao Z, Park GB, Krishnamoorthy R, Mitra AK (1994) The physicochemical properties, plasma enzymatic hydrolysis, and nasal absorption of acyclovir and its 2'-ester prodrugs. *Pharm Res* 11:237–242.
26. Shao Z, Mitra AK (1994) Bile salt-fatty acid mixed micelles as nasal absorption promoters. III. Effects on nasal transport and enzymatic degradation of acyclovir prodrugs. *Pharm Res* 11:243–250.
27. Agu RU, Vu Dang H, Jorissen M, Willems T, Kinget R, Verbeke N (2002) Nasal absorption enhancement strategies for therapeutic peptides: an in vitro study using cultured human nasal epithelium. *Int J Pharm* 237:179–191.
28. Faraj JA, Hussain AA, Aramaki Y, Iseki K, Kagoshima M, Dittert LW (1990) Mechanism of nasal absorption of drugs. III: Nasal absorption of leucine enkephalin. *J Pharm Sci* 79:698–702.
29. Hayakawa E, Yamamoto A, Shoji Y, Lee VH (1989) Effect of sodium glycocholate and polyoxyethylene-9-lauryl ether on the hydrolysis of varying concentrations of insulin in the nasal homogenates of the albino rabbit. *Life Sci* 45:167–174.
30. Schmidt MC, Rubas W, Merkle HP (2000) Nasal epithelial permeation of thymotrinan (TP3) versus thymocartin (TP4): competitive metabolism and self-enhancement. *Pharm Res* 17:222–228.
31. Mitra R, Pezron I, Chu WA, Mitra AK (2000) Lipid emulsions as vehicles for enhanced nasal delivery of insulin. *Int J Pharm* 205:127–134.
32. Tengamnuy P, Sahamethapat A, Sailasuta A, Mitra AK (2000) Chitosans as nasal absorption enhancers of peptides: comparison between free amine chitosans and soluble salts. *Int J Pharm* 197:53–67.
33. Seki T, Kanbayashi H, Nagao T, Chono S, Tomita M, Hayashi M, Tabata Y, Morimoto K (2005) Effect of aminated gelatin on the nasal absorption of insulin in rats. *Biol Pharm Bull* 28:510–514.

34. Yang C, Gao H, Mitra AK (2001) Chemical stability, enzymatic hydrolysis, and nasal uptake of amino acid ester prodrugs of acyclovir. *J Pharm Sci* 90:617–624.
35. Agu RU, Jorissen M, Kinget R, Verbeke N, Augustijns P (2002) Alternatives to in vivo nasal toxicological screening for nasally-administered drugs. *STP Pharma Sci* 12:13–22.
36. Merkus FWHM, Marttin E, Romeijn SG, Verhoef J (1996) In situ perfusion is an unrealistic approach to assess the effects of absorption enhancers on nasal epithelium. *Eur J Pharm Biopharm* 42:159.
37. Wang J, Sakai S, Deguchi Y, Bi D, Tabata Y, Morimoto K (2002) Aminated gelatin as a nasal absorption enhancer for peptide drugs: evaluation of absorption enhancing effect and nasal mucosa perturbation in rats. *J Pharm Pharmacol* 54:181–188.
38. Chien YW, Su KSE, Chang S (ed) (1989) *Nasal systemic drug delivery*, vol 59. Marcel Dekker Inc, pp 39–78.
39. Cremaschi D, Rossetti C, Draghetti MT, Manzoni C, Aliverti V (1991) Active transport of polypeptides in rabbit nasal mucosa: possible role in the sampling of potential antigens. *Pflugers Arch* 419:425–432.
40. McMartin C, Hutchinson LE, Hyde R, Peters GE (1987) Analysis of structural requirements for the absorption of drugs and macromolecules from the nasal cavity. *J Pharm Sci* 76:535–540.
41. Cremaschi D, Porta C, Ghirardelli R (1996) The active transport of polypeptides in the rabbit nasal mucosa is supported by a specific vesicular transport inhibited by cytochalasin D. *Biochim Biophys Acta* 1283:101–105.
42. Cremaschi D, Porta C, Ghirardelli R, Manzoni C, Caremi I (1996) Endocytosis inhibitors abolish the active transport of polypeptides in the mucosa of the nasal upper concha of the rabbit. *Biochim Biophys Acta* 1280:27–33.
43. Cremaschi D, Ghirardelli R, Porta C (1998) Relationship between polypeptide transcytosis and lymphoid tissue in the rabbit nasal mucosa. *Biochim Biophys Acta* 1369:287–294.
44. Zhang Y, Zhang Q, Sun Y, Sun J, Wang X, Chen M (2005) Nasal recombinant hirudin-2 delivery: absorption and its mechanism in vivo and in vitro studies. *Biol Pharm Bull* 28:2263–2267.
45. Kubo H, Hosoya K, Natsume H, Sugibayashi K, Morimoto Y (1994) In vitro permeation of several model drugs across rabbit nasal mucosa. *Int J Pharm* 103:27–36.
46. Kandimalla KK, Donovan MD (2005) Transport of hydroxyzine and triprolidine across bovine olfactory mucosa: role of passive diffusion in the direct nose-to-brain uptake of small molecules. *Int J Pharm* 302:133–144.
47. Schmidt MC, Simmen D, Hilbe M, Boderke P, Ditzinger G, Sandow J, Lang S, Rubas W, Merkle HP (2000) Validation of excised bovine nasal mucosa as in vitro model to study drug transport and metabolic pathways in nasal epithelium. *J Pharm Sci* 89:396–407.
48. Lang S, Langguth P, Oschmann R, Traving B, Merkle HP (1996) Transport and metabolic pathway of thymocartin (TP4) in excised bovine nasal mucosa. *J Pharm Pharmacol* 48:1190–1196.
49. Koushik KN, Kompella UB (2004) Transport of deslorelin and LHRH agonist is vectorial and exhibits regional variation in excised bovine nasal tissue. *J Pharm Pharmacol* 56:861–868.
50. Machova Z, Muhle C, Krauss U, Trehin R, Koch A, Merkle HP, Beck-Sickinger AG (2002) Cellular internalization of enhanced green fluorescent protein ligated to a human calcitonin-based carrier peptide. *Chem Biochem* 3:672–677.

51. Wagner K, Van Mau N, Boichot S, Kajava AV, Krauss U, Le Grimellec C, Beck-Sickinger A, Heitz F (2004) Interactions of the human calcitonin fragment 9–32 with phospholipids: a monolayer study. *Biophys J* 87:386–895.
52. Wadell C, Bjork E, Camber O (1999) Nasal drug delivery-evaluation of an in vitro model using porcine nasal mucosa. *Eur J Pharm Sci* 7:197–206.
53. Patani GA, Pang YP, Chien YW (2005) A potent and selective tacrine analog-biomembrane permeation and physicochemical characterization. *Pharm Dev Technol* 10:525–538.
54. Osth K, Paulsson M, Bjork E, Edsman K (2002) Evaluation of drug release from gels on pig nasal mucosa in a horizontal Ussing chamber. *J Control Rel* 83:377–388.
55. Wheatley MA, Dent J, Wheeldon E B Smith P L (1988) Nasal drug delivery: An in vitro characterization of transepithelial electrical properties and fluxes in the presence or absence of enhancers. *J Control Release* 8:167–177.
56. Reardon PM, Gochoco CH, Audus KL, Wilson G, Smith PL (1993) In vitro nasal transport across ovine mucosa: effects of ammonium glycyrrhizinate on electrical properties and permeability of growth hormone releasing peptide, mannitol, and lucifer yellow. *Pharm Res* 10:553–561.
57. Lang SR, Staudenmann W, James P, Manz HJ, Kessler R, Galli B, Moser HP, Rummelt A, Merkle HP (1996) Proteolysis of human calcitonin in excised bovine nasal mucosa: elucidation of the metabolic pathway by liquid secondary ionization mass spectrometry (LSIMS) and matrix assisted laser desorption ionization mass spectrometry (MALDI). *Pharm Res* 13:1679–1685.
58. Hoang VD, Uchenna AR, Mark J, Renaat K, Norbert V (2002) Characterization of human nasal primary culture systems to investigate peptide metabolism. *Int J Pharm* 238:247–256.
59. Jørgensen L, Bechgaard E (1994) Intranasal permeation of thyrotropin-releasing hormone in vitro study of permeation and enzymatic degradation. *Int J Pharm* 107:231–237.
60. Chun IK, Chien YW (1993) Transmucosal delivery of methionine enkephalin. I: Solution stability and kinetics of degradation in various rabbit mucosa extracts. *J Pharm Sci* 82:373–378.
61. Hosoya K, Kubo H, Natsume H, Sugibayashi K, Morimoto Y (1994) Evaluation of enhancers to increase nasal absorption using Ussing chamber technique. *Biol Pharm Bull* 17:316–322.
62. Hersey SJ, Jackson RT (1987) Effect of bile salts on nasal permeability in vitro. *J Pharm Sci* 76:876–879.
63. Gavini E, Rasso G, Sanna V, Cossu M, Giunchedi P (2005) Mucoadhesive microspheres for nasal administration of an antiemetic drug, metoclopramide: in-vitro/ex-vivo studies. *J Pharm Pharmacol* 57:287–294.
64. Leitner VM, Guggi D, Bernkop-Schnurch A (2004) Thiomers in noninvasive polypeptide delivery: in vitro and in vivo characterization of a polycarbophil-cysteine/glutathione gel formulation for human growth hormone. *J Pharm Sci* 93:1682–1691.
65. Ventura CA, Giannone I, Musumeci T, Pignatello R, Ragni L, Landolfi C, Milanese C, Paolino D, Puglisi G (2006) Physico-chemical characterization of disoxaril-dimethyl-beta-cyclodextrin inclusion complex and in vitro permeation studies. *Eur J Med Chem* 41:233–240.
66. Maitani Y, Asano S, Takahashi S, Nakagaki M, Nagai T (1992) Permeability of insulin entrapped in liposome through the nasal mucosa of rabbits. *Chem Pharm Bull* 40:1569–1572.
67. Harkema JR, Carey SA, Wagner (2006) The nose revisited: a brief review of the comparative structure, function, and toxicologic pathology of the nasal epithelium. *Toxicol Pathol* 34:252–269.

68. Lindhardt K, Olafsson DR, Gizurarson S, Bechgaard E (2002) Intranasal bioavailability of diazepam in sheep correlated to rabbit and man. *Int J Pharm* 231: 67–72.
69. Gizurarson S (1990) Animal models for intranasal drug delivery studies. *Acta Pharm Nord* 2:105–122.
70. Lindhardt K, Bagger M, Andreasen KH, Bechgaard E (2001) Intranasal bioavailability of buprenorphine in rabbit correlated to sheep and man. *Int J Pharm* 217:121–126.

The Isolated Perfused Lung for Drug Absorption Studies

Ann Tronde, Cynthia Bosquillon, and Ben Forbes

Abstract Over the past 20 years, the isolated perfused lung (IPL) technique has been developed for the evaluation of pulmonary drug absorption and disposition. The procedure for establishing the model requires a skilled operator, a validated technique for intra-tracheal drug delivery and a system for maintenance and monitoring of the preparation. Most absorption studies to date have utilised the ex vivo rat lung maintained by ventilation and perfusion in an artificial thorax. Techniques for delivery of drugs into the airspaces of the IPL have been developed and the drug transfer (air-to-perfusate) profiles of a variety of actively and passively transported compounds have been measured. Recent developments include the reporting of in vitro–in vivo correlation for air-to-perfusate transfer in the IPL with pulmonary absorption in the rat in vivo, the use of the IPL to model active transport mechanisms and the use of a human lung reperfusion model. The value of the IPL is in discerning lung-specific drug absorption and disposition kinetics that may be difficult to interpolate from in vivo data and cannot be modelled with physiological relevance using reductive in vitro techniques such as cell culture.

Keywords: Isolated perfused lung; Absorption; Permeability; Instillation; Aerosolisation; Drug disposition; In vitro–in vivo correlation

Abbreviations

ADME	Absorption, distribution, metabolism and elimination
BCRP	Breast cancer resistance protein
BDP	Beclomethasone dipropionate
17-BMP	Beclomethasone-17-propionate
BSA	Bovine serum albumin
COPD	Chronic obstructive pulmonary disease
CYP	Cytochrome P450
DPI	Dry powder inhaler
DTPA	Diethylene triamine penta-acetate
IgG	Immunoglobulin G
IPL	Isolated perfused lung

K_a	Absorption coefficient
MRP	Multidrug resistance-associated protein
OCT	Organic cation transporter
P_{app}	Apparent permeability coefficient
P-gp	P-glycoprotein
PK/PD	Pharmacokinetic-pharmacodynamic
pMDI	Pressurised metered-dose inhaler
PSA	Polar surface area
rFcRn	Neonatal constant region fragment receptor
%PSA	Percent polar surface area of the total molecular surface area

6.1. Respiratory Drug Delivery

The first section of this chapter provides an introduction to respiratory drug delivery with a focus on the experimental research methods used to evaluate drug absorption from the lung. The factors that influence drug absorption and disposition are reviewed along with the design and interpretation of pulmonary drug absorption experiments. An overview of preclinical models for pulmonary drug absorption research is provided.

6.1.1. Inhaled Drug Delivery

The therapeutic benefits of drug inhalation for the treatment of respiratory diseases, such as asthma, chronic obstructive pulmonary disease (COPD), cystic fibrosis and pulmonary infections, have been appreciated for several decades [3, 12, 16, 23, 47]. Direct targeting of locally acting drugs to the lungs delivers a high local concentration of the drugs at the target site, rapid onset of drug action, low systemic exposure and consequently reduced side-effects [76, 147].

The use of the inhaled route for the systemic administration of drugs with poor systemic bioavailability after oral administration is less well established, but is attracting increasing attention on account of the favourable drug absorption features of the lung. These include the large absorptive surface area, thin air-to-blood barrier, relatively low enzymatic activity in the lung and the extensive vascularisation of the respiratory mucosa [4, 103, 152]. For instance, the inhalation of several agents which are subject to poor enzymatic stability and low permeation across biological membranes has been reported, including therapeutic peptides, proteins, oligonucleotides and vaccines [73, 95, 114, 132, 8, 104]. The first such product to market, inhaled insulin, has recently been approved in USA and Europe. Pulmonary delivery may also be beneficial for analgesic drugs such as morphine, for which a rapid onset of drug action is of therapeutic importance [26].

Although pulmonary delivery appears to provide an opportunity for the systemic delivery of drugs with a wide range of physicochemical properties, exploitation of this route is challenged by the experimental complexity in studying pulmonary drug delivery. Recent developments in the use of the isolated perfused lung (IPL) address some of these difficulties, including quantifying the delivered dose, regional deposition, use of relevant formulations, availability of preclinical models, lung lumen access and in vitro–in vivo correlation.


	Generation		Diameter (cm)	Length (cm)	Number	Total cross sectional area (cm ²)	
Conducting zone	trachea		0	1.08	12.0	1	2.54
	bronchi		1	1.22	4.8	2	2.33
			2	0.83	1.9	4	2.13
			3	0.56	0.8	8	2.00
	bronchioles		4	0.45	1.3	16	2.48
	terminal bronchioles		5	0.35	1.07	32	3.11
Transitional and respiratory zones		16	0.06	0.17	6·10 ⁴	180.0	
	respiratory bronchioles	17	↓	↓	↓	↓	
		19	0.05	0.10	5·10 ⁵	10 ³	
	alveolar ducts	20	↓	↓	↓	↓	
		22	↓	↓	↓	↓	
	alveolar sacs	23	0.04	0.05	8·10 ⁶	10 ⁴	

Figure 6.1 Structure of the human respiratory tract according to the model of Weibel [153].

Even though the pulmonary route provides opportunities for the absorption of drugs with a wide range of physicochemical properties, there are limitations in the use of the pulmonary delivery. Most existing inhalation devices cannot deliver conveniently more than about 5–10 mg of drug to the lung. Thus, the ideal inhaled drug should be highly potent to allow the administration of the dose by one or two inhalations.

6.1.2. The Lung

6.1.2.1. Structure and Function of the Lung

The principal physiological function of the lung is to distribute inspired air and pulmonary blood to ensure efficient gas exchange, that is oxygenation of the blood and removal of carbon dioxide from the body. Optimal matching of the ventilation to the blood perfusion is required to accomplish the gas exchange at a minimal energy cost. The human respiratory system can be divided into two functional regions: the conducting airways and the respiratory region. About 6–10% of the total lung volume consists of the conducting airways (bronchi and bronchioles) and about 85% is the gas exchange parenchyma (alveolar ducts, alveoli and alveolar capillary network).

The conducting airways filter and condition the inspired air and are composed of the nasal cavity and associated sinuses, the pharynx, larynx, trachea, bronchi and bronchioles. From trachea to the periphery of the airway tree, the airways repeatedly branch dichotomously into two daughter branches with smaller diameters and shorter length than the parent branch [154]. For each new generation of airways, the number of branches is doubled and the cross-sectional area increases exponentially. The conducting region of the airways is generally regarded as constituting generations 0 (trachea) to 16 (terminal bronchioles). The respiratory region, where gas exchange takes place, includes generation 17–23 and is composed of respiratory bronchioles, alveolar ducts and the alveolar sacs (Figure 6.1). The number of times the bronchial tree

branches before the gas exchange area is reached can vary from as few as 6 to as many as 28–30 [106].

Two different circulatory systems, the bronchial and the pulmonary, supply the lungs with blood [133]. The bronchial circulation is a part of the systemic circulation and is under high pressure. It receives about 1% of the cardiac output and supplies the conducting airways, pulmonary blood vessels and lymph nodes [133]. It is important for the distribution of systemically administered drugs to the airways and to the absorption of inhaled drugs from the airways [18]. The pulmonary circulation comprises an extensive low-pressure vascular bed, which receives the entire cardiac output. It perfuses the alveolar capillaries to secure efficient gas exchange and supplies nutrients to the alveolar walls. Anastomoses between bronchial and pulmonary arterial circulations have been found in the walls of medium-sized bronchi and bronchioles [18, 65, 67].

6.1.2.2. The Respiratory Mucosa

Lung Lining Fluid: Although the lung is an air-filled organ, the mucosa is covered by a film of lining fluid. The total volume of this fluid is small, but it covers an extensive surface area and generates a humidity of nearly 100% in the lung [157]. The thickness of the lining fluid in the airways is estimated to be 5–10 μm and gradually decreases along the airway generations until the alveoli, where the thickness is estimated to be about 0.05–0.08 μm [103]. The airway and alveolar lining fluids are covered by at least a monolayer of lung surfactant, orientated with the fatty acid tails projecting into the airspace [103]. The lung surfactant is synthesised and secreted by the alveolar type II cells and comprises a unique mixture of phospholipids and surfactant-specific proteins [133]. By reducing the surface tension in the alveoli, the lung surfactant stabilises the extensive alveolar air–liquid interface, promotes lung expansion on inspiration and prevents lung collapse on expiration [133]. Interaction between the phospholipids in the lung surfactant and inhaled drugs (e.g. glucocorticosteroids, polypeptides and antibiotics) has been reported to affect the solubility, absorption, retention and clearance of drugs in the lung [86, 149, 150, 157].

The Respiratory Epithelium: The cellular composition of the epithelium varies according to the airway generation (Figure 6.1) and is described in detail in the chapters on airway and alveolar epithelial cell culture. Briefly, the lining of the tracheo-bronchial airways is composed of several cell types, including basal cells, goblet cells, ciliated cells, brush cells, serous cells, Clara cells and neuroendocrine cells [106]. A variety of migratory cells such as lymphocytes, leukocytes, and mast cells are also present in the epithelium [106]. In the terminal bronchioles, the epithelium is composed of ciliated cells and Clara cells [106]. In the alveolar region, epithelial type I and II cells, alveolar brush cells (type III) and alveolar macrophages are present [79, 106]. The squamous type I cell covers approximately 96% of the alveolar surface area and has an average cell thickness of 0.26 μm . About 3% of the alveolar surface is covered by the much smaller cuboidal type II cells, which synthesise and secrete surface-active materials [83]. The heterogenous composition of the lung epithelium results in a large variation of tight junctional forms with variable tightness [46, 129].

The Endothelium and Lymphatics: The capillary endothelial surface of the lung is the largest in the body [131]. The alveolar-capillary endothelium has

specialised organelle-free domains to provide a particularly thin (from 200 nm down to 30–35 nm) barrier for gas exchange [131]. The endothelial cells are joined by tight junction with few parallel arrays of contacts, which renders the junctions leaky when the hydrostatic pressure increases [106, 131]. The interstitium of the lung, that is the extracellular and extravascular space between cells in the tissue, contains a variety of cells (e.g. fibroblasts, myofibroblasts, pericytes, monocytes, lymphocytes and plasma cells), collagen, elastic fibers and interstitial fluid [106]. The main drainage pathway for the interstitial fluid, between the epithelial and endothelial basement membranes, is via the lymphatic vessels [154].

6.1.2.3. Non-Absorptive Clearance from the Lung

A sophisticated respiratory host defence system has evolved to clear airborne particles and potential pathogens in inspired air [106, 143]. The system comprises mechanical (i.e. air filtration, cough, sneezing and mucociliary clearance), chemical (antioxidants, antiproteases and surfactant lipids) and immunological defence mechanisms and is tightly regulated to minimise inflammatory reactions [92, 143].

From a drug delivery perspective, the components of the host defence system comprise barriers that must be overcome to ensure efficient drug deposition as well as retention in and absorption from the respiratory tract. Important non-absorptive clearance mechanisms include mucociliary clearance, alveolar macrophages and metabolism (Figure 6.2).

Mucociliary Clearance: Mucociliary clearance operates by the coordinated movements of cilia, which sweep mucus out of the lungs towards the pharynx where it is swallowed. There is an inverse relationship between mucus velocity and airway generation, which relates to the lower percentage of ciliated cells, shorter cilia, lower ciliary beat frequency and lower number of secretory cells in the peripheral airways [121]. The reported tracheal mucociliary clearance

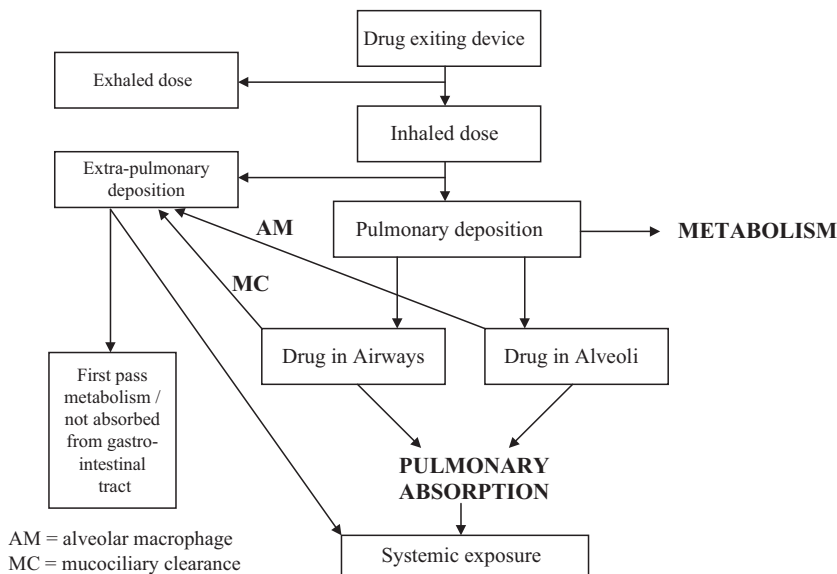


Figure 6.2 Schematic illustration of the fate of an inhaled drug. (Modified from Tronde [139]).

rate in young healthy subjects ranges from 4 mm/min to 20 mm/min [121]. The residence time of an inhaled drug particle in the lungs will depend on the site of deposition, which may vary with state of disease and inhalation device and the solubility/dissolution rate of the drug [31].

Alveolar Macrophages: Alveolar macrophages are found on the alveolar surface. These phagocytic cells play important roles in the defence mechanisms against inhaled bacteria and particles that have reached the alveoli [51]. Particles deposited in the lungs of rabbits and rats have been demonstrated to be phagocytised by alveolar macrophages within a few hours [11, 135]. Macromolecules with long residence time are also cleared from the lung by macrophages [77]. Macrophages are cleared from the alveoli to the bronchioles by the lining fluid, and then from the airways by the mucociliary escalator [59].

Metabolism: Generally, most of the metabolising enzymes found in the liver are also present in the lung, although in lesser amounts [79] and the lung does not express the full range of isoenzymes present in the liver [145]. For example, whereas CYP3A4 is the main cytochrome P450 (CYP) form in human liver, expression of the isozyme in the lung was found in only 20% of the investigated subjects [4]. The level of CYP in the lung shows approximately tenfold species variation and is 5–20 times lower than that of the liver [79]. However, the lung is the only organ through which the entire cardiac output passes; because of this high pulmonary blood flow, the metabolic capacity of the lung should not be ignored [79]. The lung is generally thought to have a lower proteolytic activity than many other organs [56, 151, 163] and the activity of the proteases is balanced by the release of antiproteases [79]. However, this balance may be disturbed in the diseased lung.

6.1.2.4. Pathophysiological and Physiological Influences

Pathophysiological changes in the lung may be induced by inflammatory lung diseases, such as COPD and asthma, or by repeated mucosal injury, for instance by allergens, viruses and chemical toxicants (e.g. tobacco smoke, pollutants and insoluble particles). These may result in chronic structural changes to the airways, such as subepithelial fibrosis, hyperplasia of smooth muscle and goblet cells, hypersecretion of mucus, epithelial disruption and plasma exudation [110, 121], collectively referred to as airway remodelling. These pathophysiological changes can severely affect the airway deposition pattern of inhaled therapeutic aerosols [113], mucociliary clearance [31, 72, 122], the properties of the epithelial and endothelial barriers and thus the permeability of drugs [39, 48, 55, 58, 98, 105], disposition of drugs in the lung tissue [6, 100] and altered expression and function of drug transporters [75, 148].

An increased epithelial permeability of hydrophilic compounds, that is terbutaline (Mw 225 Da), ^{99m}Tc-labelled diethylene triamine penta-acetate (^{99m}Tc-DTPA; Mw 492 Da), ^{113m}In-labelled biotinylated DTPA (Mw 1,215 Da) and insulin, has been demonstrated in smokers as compared to non-smokers [8, 62, 84, 127, 159].

A higher concentration of red blood cells, total protein and leukotriene B₄ has been measured in the lungs of athletes during severe exercise (i.e. high levels of pulmonary capillary pressures) compared to controls, indicating an altered integrity of the air-to-blood barrier [155]. In addition, an increased absorption rate and plasma C_{\max} of inhaled terbutaline during submaximal

exercise compared to the resting state has been reported [128], which may indicate a more subtle change in the integrity of the air-to-blood barrier.

6.1.3. Drug Administration to the Lung

6.1.3.1. Particle Deposition

The respiratory tract can be considered as a filter that removes particles from the inspired air [53]. The effectiveness of the filter depends on particle properties such as size, shape, density and charge, respiratory tract morphology and breathing pattern, for example airflow rate and tidal volume [53]. These parameters determine not only the quantity of particles that are deposited but also their regional deposition. Drug distribution in the lung depends upon the predominant particle deposition mechanisms, inertial impaction, sedimentation and diffusion. Regional deposition is an important determinant of drug disposition and absorption, both in preclinical research and clinically.

6.1.3.2. Dosing in Preclinical Studies

Liquid instillation and nebulised aerosols are the most common methods for pulmonary administration to experimental animals [22, 54, 109, 134]. The use of pressurised metered dose inhaler (pMDIs) and dry powder inhaler (DPIs) in preclinical studies is limited by the need for formulation development, which often cannot be performed in early drug discovery due to short supply of test materials. A number of alternative techniques for intra-tracheal administration of coarse sprays and powder formulations have been described [9, 15, 21, 36, 71, 80, 99, 138].

Intra-tracheal instillation of liquid formulations offers rapid delivery of defined doses, but mainly results in central, patchy and inhomogeneous lung distribution [10, 40]. To obtain reliable dosing, the liquid must be carefully instilled in order not to cause airway obstruction or disturb the normal breathing pattern. Although there are differences in the distribution, clearance and retention of test material when administered by instillation compared to inhalation [30], the instillation procedure has been applied in many pharmacokinetic and pharmacodynamic investigations [41, 125, 136]. When the method is applied to rats, the typical instillation volume is about 0.1–0.5 ml (1–2 ml/kg body weight). This volume corresponds up to a third of the average tidal volume of the rat and has thus been pointed out as being non-physiological [30]. Another concern regarding instillation is the influence of the vehicle in which the drug is suspended or dissolved. If it alters the physicochemical nature of the drug, it may alter the effect of the drug in the lungs and affect the physiological barriers of the lung [30].

Aerosol inhalation results in a more uniform lung distribution, compared to liquid instillation, and gives a more effective distribution into the alveolar region [10, 40]. In experiments comparing pulmonary drug absorption characteristics, it is important to secure a reproducible lung distribution profile of the administered drug via the administration procedures. Regional physiological differences in the respiratory barrier may influence the rate and extent of absorption of drugs delivered to the respiratory tract [103]. A higher absorption rate or systemic bioavailability or both have been demonstrated for various small compounds [125] as well as for peptides and proteins after aerosol inhalation compared to liquid instillation [19, 20, 40, 68, 95]. The use of a pulmonary delivery method that mimics the methods used in clinical therapy

Table 6.1 Factors That May Affect Pulmonary Drug Absorption and Disposition (Modified from Tronde [139]).

Physiology	Device and formulation	Drug
Breathing pattern	Particle properties	Dissolution rate
Blood flow	(size, density, shape, charge)	Solubility
Airway morphology	Deposition pattern	Lipophilicity
Surface area	Excipients	Molecular weight
Mucociliary clearance	Concentration	Molecular polar surface area
Lung surfactant	Osmolarity	Charge
Alveolar macrophages	Viscosity	Hydrogen bonding potential
Epithelial permeability	pH	Aggregation/complex binding
Endothelial permeability	Dose size/volume	Conformation
Transporter proteins		Chemical stability
Enzymatic/metabolic activity		Enzymatic stability
Disease		
Tissue composition (drug sequestration)		

may, therefore, be important for preclinical investigations of pulmonary drug absorption. As a result, a number of aerosol techniques have been developed for the administration of solutions and powder aerosols to the IPL (Sect. 6.2.3).

6.1.4. Drug Absorption in the Lung

The efficacy of an inhaled drug is determined by its absorption across the lung epithelial barrier to the location of its pharmacological site of action. For locally acting drugs, absorption into the systemic circulation may imply the removal and consequently the termination of action of the drug in the lung. On the other hand, for systemically acting drugs, the absorption profile of the drug from the lung will determine the onset, intensity and duration of action of the drug [137]. Although inhalation is a well-established means of drug administration, drug absorption kinetics in the lung have not been extensively researched. Understanding the determinants of pulmonary absorption and disposition of inhaled drugs in relation to their molecular properties is important to aid the design of new inhaled products for local and systemic action (Table 6.1).

In the 1970s and 1980s, Schanker and co-workers conducted a series of studies on the disappearance rate of miscellaneous compounds from the rat lungs after intra-tracheal instillation and aerosol inhalation. Their studies showed that most compounds were absorbed by passive diffusion and that the rate of absorption increased with an increase in lipophilicity for compounds with partition coefficients in chloroform/buffer pH 7.4 ranging from -3 to 2 [13, 124]. Recently, systematic generation of *in vitro* and *in vivo* pharmacokinetic (PK) data on the absorption of drugs across the rat lung barrier after aerosol delivery has revealed that lipophilicity, molecular polar surface area (PSA), percent polar surface area of the total molecular surface area (%PSA) and hydrogen bonding potential are the most influential physicochemical properties for pulmonary absorption of structurally diverse low molecular weight

compounds with $\log D_{7.4}$ ranging from -4 to 3 [139]. In contrast to the intestinal mucosa and the blood–brain barrier, the pulmonary epithelium was shown to be highly permeable to drugs with a high molecular PSA and %PSA [139].

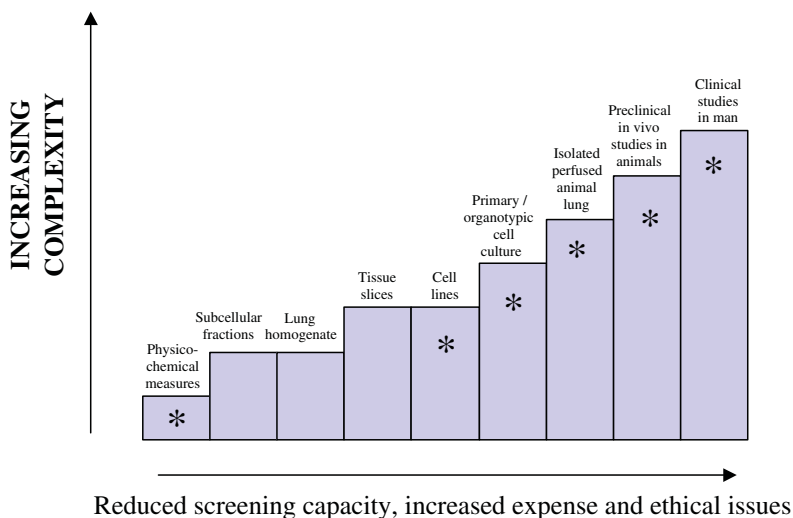
The absorption of lipophilic compounds is generally considered to occur by membrane diffusion [32], whereas hydrophilic solutes appear to be absorbed by passive diffusion through intercellular junction pores [130]. Most exogenous macromolecules with a molecular weight less than 40 kDa are thought to be absorbed from the airspace through tight junctions by passive diffusion [52, 85, 103]. The absorption rate of hydrophilic compounds is inversely related to the molecular weight (range 60–75 kDa) [123]. However, for compounds weighing less than 1,000 Da, the effect of molecular weight on the absorption rate appears to be negligible [94]. Drug transporters, such as peptide transporters [49, 50], P-glycoprotein (P-gp), breast cancer resistance protein (BCRP) and multidrug resistance-associated protein (MRPs) [75, 126, 148] and the organic cation transporter (OCT) [33, 57] have been identified in the lung, although a greater understanding of transporter impact on drug absorption from the lung is required. For example, the high systemic bioavailability after pulmonary administration of the efflux transporter substrates talinolol (81%) and losartan (92%) provides functional evidence that efflux transporters in the rat lung may not play a quantitatively important role in limiting substrate absorption [139].

The pulmonary lymphatic system contributes to the clearance of fluid and protein from the lung tissue interstitium and helps to prevent fluid accumulation in the lungs [108]. The lymphatic endothelium allows micron-sized particles (e.g. lipoproteins, plasma proteins, bacteria and immune cells) to pass freely into the lymph fluid [103]. After administration of aerosolised ultrafine particles into rats, particles were found in the alveolar walls and in pulmonary lymph nodes [135], which suggests that drainage into the lymph may contribute to the air-to-blood transport of the inhaled particles.

6.1.5. Lung Model Selection for Drug Absorption Studies

The inhaled drugs currently on the market are dominated by two compound classes: the corticosteroids and the beta-2-adrenoceptor agonists. As new targets are explored for the treatment of respiratory diseases and for systemic delivery via the pulmonary route, new compound classes require evaluation for administration via inhalation. Thus, experimental and computational models are required that can estimate and predict pulmonary drug absorption, distribution, metabolism and elimination (ADME). In the absence of much human lung absorption data, there is a need for accurate pharmacokinetic *in vivo* investigations in animals to establish reliable *in vitro*–*in vivo* correlations and drug structure–permeability relationships to guide drug discovery and development programmes.

Several models are available for preclinical investigations of pulmonary drug absorption and disposition. The complexity of the models increases from *in silico* permeability predictions and permeability screening experiments in cell culture models to *in vivo* pharmacokinetic analyses in animals or human tissue (Figure 6.3). The design of the experiments comprises selection of the most relevant biological model, selection of a suitable formulation and drug concentration and the selection of a drug administration technique that



* Can be used to study drug absorption / permeability

Figure 6.3 Simple schematic to illustrate the hierarchy of complexity of systems used for preclinical absorption and disposition investigations of inhaled drug products. Interspecies variation should be considered. In silico modelling based on human data and use of the human perfused lungs can provide complex information regarding human absorption and disposition data.

is appropriate for the amount of test material available and that can selectively deposit a defined dose of the drug to the intended lung region. A combination of in vitro and in vivo models is needed to elucidate the mechanism as well as the rate and extent of drug absorption after pulmonary administration.

6.1.5.1. In Vivo Animal Models

In vivo pharmacokinetic experiments in animals provide data on the fate of a drug and its metabolites in the body by assessment of the drug concentration in plasma or tissues. For determination of the pulmonary absorption rate and systemic bioavailability, plasma is sampled at predetermined time points after pulmonary drug administration and analysed for drug content [1, 68, 136]. An intravenous dose may be administered as reference. For investigations of the retention of the drug in the lung tissue or first-pass pulmonary uptake, or both, drug concentrations in lung tissue are assessed [13, 29, 60]. The pulmonary administration procedure should be selected to deliver the dose with precision of dose quantity and deposition pattern [68]. The effect of anaesthesia on physiological functions should thus be considered in the design of the experiments. For instance, volatile anaesthetics have been demonstrated to increase alveolar epithelial permeability [17, 161], destabilise surfactant [35, 161] and impair mucociliary clearance [102].

6.1.5.2. Ex Vivo Models

Ex Vivo Isolated Perfused Lung: The use of the IPL allows lung-specific pharmacokinetics to be investigated without the contribution of systemic ADME. In the IPL, the structural and cellular integrity of the lung tissue, the permeability barriers and interaction between different cell types and biochemical activity

are maintained [88]. Procedures for lung perfusion have been described for rats [115, 144], guinea pigs [61, 66, 115], rabbits [2], mice [63, 146], dogs [89] and humans [74, 89]. Compared to in vivo models, the IPL provides advantages such as careful control of the ventilation and perfusion of the lung, facilitated administration of drugs to the airway lumen or vascular circulation, easy sampling of perfusate and lavage fluid and ready determination of mass balance. Since multiple perfusate samples can be taken after drug administration to the IPL, the absorptive profile from a single lung is measured rather than the profile being compiled from absorption in individual animals that are sacrificed at different single time points after dosing. The IPL, therefore, has the ethical advantage of markedly reducing animal usage and also avoids the problem of inter-animal differences in drug administration. IPL experiments can be designed to address specific issues such as pharmacological effect [61], physiological phenomena [97], drug dissolution and absorption [96, 139], mechanisms of absorption [118], metabolism [28, 45, 78, 116, 138], tissue disposition [5, 82, 117] and retention [67, 117]. The main drawback of the IPL is the viability of the preparation, which is limited to a maximum of 5 h [7, 37] and prevents investigations of slow pharmacokinetic processes.

Lung Tissue Preparations: Lung tissue slices, which are thinly cut sections of the lung and contain all the pulmonary cell types, have been widely used for drug metabolism, tissue binding, pharmacological and toxicological studies, but cannot evaluate drug absorption [91, 160, 112, 25]. Tissue strips or rings from the tracheo-bronchial regions have been used in tissue baths and Ussing chambers to investigate drug permeability [156]. Size constraints mean that these tissue preparations are only available for the large airways, which is a major limitation in modelling lung absorption.

6.1.5.3. Cell Culture Models

The inaccessibility and cellular heterogeneity of the respiratory epithelium makes it difficult to study drug transport mechanisms in vivo or in ex vivo tissues. Therefore, a variety of airway and alveolar epithelial cell culture models of animal and human origin have been established as in vitro absorption models [34, 42, 90, 158, 162]. The advantage of these models is that drug transport mechanisms can be explored in systems with precise dosing and sampling, defined local drug concentration and surface area of exposure. Both cell line (airway) and primary cell culture (airway and alveolar) models and their application to pulmonary drug absorption are described in detail in subsequent chapters.

6.1.5.4. In Silico Models

The development of combinatorial chemistry and high throughput screening programmes has stimulated efforts to find experimental and computational models to estimate and predict drug absorption, distribution, metabolism and elimination based on drug physicochemical properties.

Recent systematic in vitro and in vivo pharmacokinetic data on absorption of drugs from the lungs and refined analysis of the absorption characteristics of the lung barrier in relation to drug physicochemical properties provide some guidance on important properties of inhaled drugs [139]. The lipophilicity, molecular PSA, %PSA and hydrogen bonding potential were shown to be the most influential physicochemical properties for the pulmonary absorption of

structurally diverse low molecular weight drugs. In addition, drug permeability in Caco-2 cell monolayers and 16HBE14o- cell monolayers have been demonstrated to correlate with the absorption rate constant in the rat lung [81, 139]. A log-linear model for prediction of the pulmonary drug absorption rate from the descriptors $\log P_{\text{app}}$ (Caco-2), %PSA and cLogD(7.4) was suggested [139]. The generation of such drug structure–permeability relationships based on systematically generated pharmacokinetic data may contribute to establish reliable prediction models of pulmonary drug absorption useful in the development of new inhaled drugs for local and systemic action.

6.2. The Isolated Perfused Lung

The IPL technique was developed during the middle of the last century for physiological investigations of lung function such as pressure–flow dynamics in the pulmonary circulation and ventilatory mechanics. Interest in the use of the model for pharmacological studies of endogenous and exogenous substances saw a number of variations of the IPL reported for this purpose in the 1970s. The advantages of the model for the study of drug metabolism and pulmonary pharmacology and toxicology were also recognised [7, 38, 61, 88, 93]. Over the past 20 years, the potential of the IPL to measure absorptive transport following airway drug administration has been demonstrated [14, 44, 119, 139].

6.2.1. Principles of the Preparation

The IPL is essentially an isolation of the lungs from the systemic circulation by establishing a perfusion through the pulmonary circulation of the lungs with blood or artificial media. The advantages of the IPL compared to experiments conducted *in vivo* include definitive evaluation of the role of the lung in the absorption and disposition of drugs administered to the lung, control of perfusion and the use of wide ranges of drug and inhibitor concentrations, accurate mass balance of exogenous compounds and metabolites and multiple and frequent sampling. Compared to simpler lung models (Figure 6.3), the clear advantage of the IPL is maintenance of the structural and functional integrity of the organ. The research niche of the IPL is in discerning lung-specific drug absorption and disposition kinetics that may be difficult to interpolate from *in vivo* data and cannot be modelled with physiological relevance using reductive *in vitro* techniques, such as cell culture.

The major limitation of the IPL is the short period for which viability may be maintained. This is in the order of a maximum of 3–5 h. Furthermore, the surgery to isolate the lung severs the bronchial circulation which serves the higher bronchi and trachea. Thus, the results of absorption and disposition experiments are thought to represent predominately the contribution of those parts of the lung served by the pulmonary circulation, although the presence of bronchial anastomoses has been suggested to provide a pathway to the higher airways [65, 67]. A practical limitation to wider use of the model might be that the surgery and maintenance of the preparation require skilled personnel trained in the technique and who regularly perform the experiments according to strict protocols.

Most systems used to study drug absorption to date have been sophisticated systems for drug delivery and preparation maintenance, such as that

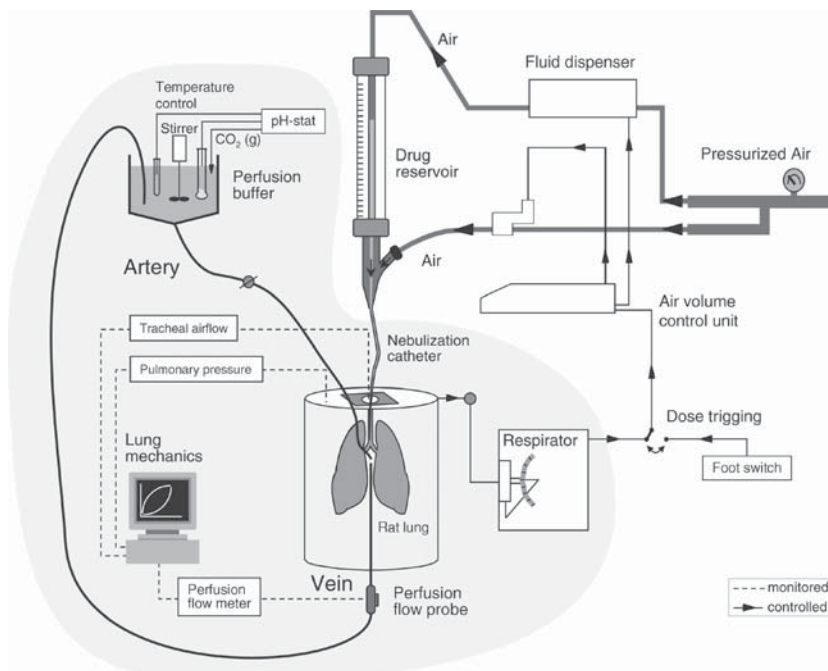


Figure 6.4 Experimental set-up for maintenance and monitoring of the isolated perfused lung [139].

described by Tronde and co-workers (Appendix: Lab Protocols [available online]; Figure 6.4). An alternative approach used at King's College London, UK, has been to evaluate the minimum requirements, that is the simplest system for the preparation that will yield useful drug absorption data (Appendix: Lab Protocols [available online]).

6.2.2. Experimental Set-up

6.2.2.1. Surgical Procedures

The surgery to isolate the lung is intricate and should be completed within 10–15 min with minimal interruption to ventilation and perfusion in order to obtain a viable and stable preparation. Contact with the delicate lung tissue during the surgical procedure should be avoided and care should be taken not to introduce air bubbles into the circulation. For isolation of rat and guinea-pig lungs, the following general procedure can be applied (more detailed stepwise procedures are provided in Appendix: Lab Protocols [available online]).

Generally, after induction of terminal systemic anaesthesia, via an intraperitoneal injection, heparin is injected into the jugular vein to prevent thrombosis. The first surgical step is to carefully cannulate the trachea and provide positive pressure respiratory support, using a small animal ventilator, to prevent lung collapse when the thoracic cavity is opened. The cannula should be carefully inserted into the trachea and tied firmly. The rats are then exsanguinated by cutting the abdominal aorta, the chest is opened and the pulmonary artery is cannulated through the right ventricle of the heart. After making an incision in the left ventricle of the heart, the lungs are carefully perfused with a buffered artificial medium, for example modified Krebs-Ringer buffer (37°C) supplemented with glucose and albumin and equilibrated with oxygen and carbon

dioxide to clear the tissue of blood. The lungs, which have a pink appearance before perfusion, become a uniform white colour once perfusion is established. The perfusion is then stopped, the pulmonary vein is cannulated through the incision in the left ventricle of the heart and carefully perfused once again. The perfusion is then stopped and the lungs are carefully dissected free together with the heart, and suspended by the trachea in a humidified jacketed glass chamber, 'artificial thorax', maintained at 37°C. Measures should then be taken to position the preparation and cannulas in the chamber such that perfusion and ventilation can be performed smoothly without tissue restrictions. The ventilation should then be immediately started and the lung preparation allowed to stabilize during single-pass perfusion for 10–15 min before start of the drug absorption/disposition experiments.

The lung is typically suspended vertically from the tracheal cannula [7, 38, 82, 88, 141]. It has been suggested that horizontal suspension from a rod that is threaded through the oesophagus provides a more physiological orientation for the lungs of small mammals [14, 119]. However, to the best of the authors' knowledge there is no data reported showing any difference in viability of the preparation or drug absorption characteristics dependent on the orientation of the preparation.

6.2.2.2. Apparatus and Maintenance Conditions

The basic principles to consider in establishing an experimental system for lung perfusion experiments are considered with regard to the apparatus and the mode of ventilation and perfusion.

Apparatus: The conditions for maintaining the isolated lung preparation *ex vivo* range from relatively simple methods with the lungs suspended from the tracheal cannula and perfused under a hydrostatic gradient by artificial medium [7] through to much more sophisticated techniques that are aimed at mimicking physiological conditions and prolonging preparation viability [66, 97, 144]. The apparatus for IPL maintenance and monitoring that are available commercially reflect this and include a system for the 'simplified isolated lung system with constant pressure non-recirculating perfusate' from Kent Scientific (USA) and a comprehensive system from Hugo-Sachs Elektronik, Harvard Apparatus (Germany) including software systems which will satisfy the most sophisticated adaptations described below. However, none of the adaptations reported extend the viability of the preparation beyond 5 h, with most practitioners accepting experimental durations of 2–3 h.

Ventilation: Two different mechanisms of ventilating the lungs are used: positive pressure ventilation to push bolus volumes of air into the lung and negative pressure ventilation (which is the physiological mechanism) under which the pressure in the chamber surrounding the lung is reduced, thereby inducing lung inflation. Most IPL systems used for drug absorption and disposition experiments employ negative pressure ventilation. The main reasons are (a) improved viability (i.e. reduced risk of oedema formation) [93] and (b) convenient drug administration to the airways without interruption of the ventilation, simulating *in vivo* conditions [14, 139].

Ventilation rates are generally sub-physiological to prevent excess barometric pressure on the lung, for example 1.5–2 ml volume at a rate of 30–80 min⁻¹ for the rat. Periodic hyperinflation (sometimes described as a 'sigh'

Table 6.2 Physiological Parameters in Mouse, Rat, Rabbit and Human of Relevance to the Isolated Perfused Lung Preparation (Data from Davies and Morris, [24]). Respiratory Tidal Volume Can Be Calculated by Dividing Total Ventilation by Respiratory Rate.

Parameter	Mouse (0.02 kg)	Rat (0.25 kg)	Rabbit (2.5 kg)	Human (70 kg)
Lung weight (g)	0.12	1.5	18	1,000
Lung volume (ml)	0.1	2.1	17	1,170
Respiratory rate (min ⁻¹)	163	85	51	12
Total ventilation (l/min)	0.025	0.12	0.8	8.0
Blood volume (ml)	1.7	13.5	165	5,200
Cardiac output (ml/min)	8.0	74	530	5,600

or augmented breath) has been suggested as a viability-enhancing procedure which will prevent the formation of focal areas of atelectasis (lung airspace closure) and promote even distribution of surfactant over the lung epithelial surface. The ventilating gas used for the preparation is usually 5% CO₂ in air. High oxygenation is important to maintain a highly viable preparation, that is minimise oedema formation, and to maintain an intact alveolar endothelial and epithelial permeability to water and macromolecules [27].

Perfusion: The perfusion medium may be either physiological buffers with or without red cells or autologous blood. The lung preparation can be perfused by either constant flow rate (pulsatile flow under a peristaltic pump) or constant pressure perfusion (continuous flow under hydrostatic gradient). Although the constant flow rate perfusion may mimic the physiological conditions more closely, it has the disadvantage of inducing hydrostatic oedema in the preparation during vasoconstriction. To minimise the risk of oedema formation in the lung preparation during drug absorption experiments, the constant pressure perfusion may be preferred. Despite this, constant flow perfusion is often employed.

The perfusion medium may either be administered as a single-pass system, which requires higher volumes of perfusate, or recirculated, which increases analytical sensitivity. The method of choice depends upon the kinetic issue to be investigated as well as the type of medium required for the investigation. Artificial media are more readily available and economic to use in greater quantities and are generally used for drug absorption applications. Important features for artificial media are to be buffered for neutral pH, to contain glucose and to provide a suitable oncotic pressure [e.g. with bovine serum albumin (BSA) 4–5% w/v]. If a recirculating medium is used, the pH should be maintained at 7.35–7.45 by adding CO₂. A single-pass system may be preferred for drug transport studies if a lung-metabolised, lung-sequestered (i.e. tissue retained), or rapidly absorbed drug is under investigation. The flow rate of 12–15 ml/min for a rat is lower than the physiological rate (Table 6.2) and is aimed at mitigating the tendency towards a hydrostatic oedema. On a practical note, it is wise to include a bubble trap to prevent gas bubble entry into and occlusion of the pulmonary circulation.

6.2.2.3. Preparation Viability

A viable preparation will have a uniform white appearance and inflates and deflates with normal elasticity. Visual inspections of the preparation should be

performed before start of any experiments to ensure absence of any local areas with slow blood washout or translucent areas in the pulmonary parenchyma (oedema), which both indicate non-viability of the preparation and hence changes in the integrity of the air-to-perfusate barrier.

Preparation viability can be maximised by careful surgical procedures, matching ventilation to perfusion and reducing the perfusion flow rate/vascular pressure below the physiological value, as well as ensuring a suitable oncotic potential in the perfusate composition. During experiments, visual inspections for signs of oedema formation and careful supervision of real-time lung mechanics (i.e. tidal volume, dynamic compliance and airway conductance), perfusion flow rate and hydrostatic pressure at the arterial level at consecutive time points are all indicators that the preparation remains viable and to ensure uniform quality of lung preparations in a series of experiments. For drug absorption experiments, validation of the IPL model using permeability markers is recommended to ensure an intact air-to-perfusate barrier with permeability corresponding to the permeability *in vivo* [139] and disposition relevant to the *in vivo* situation [111].

The mechanism of oedema formation in the IPL begins with fluid accumulation in the interstitial spaces which then ‘leaks’ into the airspaces. In the final stages, the lung appears engorged, no longer inflates normally and may efflux frothy fluid at the tracheal cannula. Oedema is an early marker of lung disruption and a more sensitive marker of viability than metabolic markers, such as glucose utilisation [38]. As such, the absence of oedema provides a simple indication of the success of a preparation. Monitoring lung weight provides an objective measure to indicate the absence of fluid accumulation.

6.2.2.4. Species Selection

Availability, ethics and cost of animals and maintenance are basic considerations. It may be desirable to evaluate lung absorption and disposition in the same species as used for pharmacodynamic (PD) and toxicological studies to explore PK/PD relationships and establish *in vitro*–*in vivo* correlations. The use of the mouse lung makes the possibility of using knockout mice to study the effect of specific gene deletions attractive, for example the use of MDR1 P-gp knockout mice in the case of drug absorption. Although there are differences between the lungs of human and those of laboratory species, including the arrangement of the lung lobes, the branching pattern and diameter of the airways, rats (followed by rabbits and guinea pigs) have emerged as the most popular laboratory species for the IPL [88]. In practice, mouse lungs may be too small for most applications including drug absorption studies, whereas the lungs of species such as dogs or monkey are excessive in size, uneconomic and less justifiable ethically. The isolation and perfusion of human lung lobes has been described [43, 74]. For reference, the normal physiological values for species that have been used to study drug absorption in the IPL are presented in Table 6.2.

6.2.3. Drug Administration to the IPL

Administration to the airspaces of the IPL can be achieved by instillation, forced sprays and aerosol inhalation. These can achieve regional targeting and should be considered carefully and validated at the beginning of experimental programmes. Drugs can also be administered to the lung via the

perfusate, which has relevance to systemic administration and lung uptake. Administration via the perfusate has also been used to measure perfusate-to-air solute transfer [156].

For preclinical investigations, the use of drug formulations and a dosing method generating a lung deposition pattern that mimic methods used in clinical therapy is important. Validation of the administration technique to be used should include quantification of the distribution in the lung (i.e. proportion of peripheral vs. airways deposition) and recovery of administered material. Methods for delivering defined doses accurately into the lung have been reported and used to study drug absorption and disposition in the IPL. A method of 'forced solution instillation' is established in-house by the group of Byron and co-workers for the purpose of administering drug to the lung to study the disposition of inhaled compounds [15, 119]. This method uses propellant to expel a solution, typically 100 μl , into the isolated perfused rat lung, which is simultaneously inflated. This technique results in high levels of peripheral penetration (65%) and relies on careful selection of the fluorocarbon propellant to control lung inflation [15], which is important as this could affect permeability.

Miniaturised nebulisation catheters have been validated for their delivery of defined doses to the isolated perfused rat lung. The AeroProbeTM nebulisation catheter was shown to deliver 38% of a delivered dose of 20 μl (in ten actuations) to the lung parenchyma [139]. In addition to delivery of drugs to the ex vivo rat lung to study drug disposition [141], this technique has been successfully adapted for the delivery of aerosol sprays to the mouse lung [64] and rat lungs in vivo [142]. It is noteworthy that this technique also has the potential for use with gene knockout mouse lung preparations (Sect. 6.2.4).

The DustGun aerosol generator, which has been reported for the delivery of aerosol particles to the IPL for toxicological evaluations [36], is another delivery technique which could be utilised for the evaluation of drug disposition after the delivery of pharmaceutical powder aerosols to the IPL.

6.2.4. Drug Absorption Studies Using the Isolated Perfused Lung

The following sections provide an overview of the application of the IPL for the study of drug absorption. Examples are provided to illustrate the use of the IPL to study drug permeability, absorption profiles, transport mechanisms and the effects of inhaled dose formulation on drug disposition.

6.2.4.1. Permeability of the Lung

The earliest studies of solute transfer in the IPL were performed with the aim of measuring the permeability of the lung [156]. These studies utilised the simplest form of the IPL in which the lungs can be fluid-filled rather than naturally air-filled, and measured the permeability of the lungs of a variety of species to mannitol and sucrose [156]. The permeability of these small hydrophilic compounds in the fluid-filled IPL, which is thought to measure predominately alveolar permeability, was markedly lower than permeability in ex vivo airway tissue.

Permeability in the IPL has generally been measured by solute flux in the airway to perfusate direction. The flux of solutes in the perfusate to luminal fluid direction compared to absorptive flux [87] revealed a consistent disparity for a series of six hydrophilic compounds, which was suggested to be due to

different effective surface areas available when the solutes are presented via the airspaces versus perfusate. Thus, efforts to optimise the recovery from the airspaces and use the IPL for direct comparison of bidirectional fluxes have proven difficult.

An advantage of using the fluid-filled lung is the accuracy of dosimetry and the even distribution of solute throughout the lung. This ensures that permeability is measured across the entire area of the respiratory epithelium. A concern, however, is that the IPL in which the airspaces are flooded with the donor solution may suffer distension of the epithelium leading to increased permeability.

6.2.4.2. Drug Absorption and Disposition

The use of the IPL to study the disposition of drugs administered to the lung via airway and in the perfusate was pioneered by Ryrfeldt and co-workers using isolated perfused rat and guinea-pig lungs. This technique has, for instance, been used to measure the uptake and biotransformation of ibutero, terbutaline [115], lidocaine [107], bambuterol [116], xanthines [67] and budesonide [117]. The IPL has also been optimised to study the pharmacodynamic activity of drugs delivered via the perfusate [66], and after aerosol inhalation of the long acting beta-2-adrenoceptor agonists salmeterol and formoterol compared to terbutaline [61].

The group of Byron and co-workers established an IPL model specifically to study drug deposition and absorption [14], and reported a novel technique for drug administration [15] and described the absorption of a variety of test compounds. The studies conducted in this model have been reviewed recently, along with a pharmacokinetic model developed to describe the disposition of the drugs administered via this route [119].

For passively absorbed compounds, the kinetic model resolves the proportion of lung dose that is not absorbed [119]. Absorption and non-absorptive clearance via mucociliary transport, phagocytosis and metabolism are accounted for and first-order kinetics are assumed for all of these processes. Dose deposited in the upper tracheo-bronchial region is regarded as non-absorbed on account of the bronchial circulation being incomplete. Mucociliary transfer of drug to this region is considered to render drug unavailable. Using this model, sodium fluorescein and FITC-dextran 4000 absorption profiles were found to be dose independent and typical of those expected for solutes of their respective molecular weights.

The disposition of insulin was shown to be susceptible to non-absorptive losses to metabolism and mucociliary clearance. Modification of the deposition profile of insulin in the lung showed that higher absorption rates were obtained for more peripheral deposition and co-administration of a metabolic inhibitor reduced losses to exopeptidase metabolism [101]. It is acknowledged by the investigators that the IPL technique and the dosing technique of Byron and co-workers are not widely accessible and have therefore not been widely adopted [119]. Active absorption has also been studied in this system as described in Sect. 6.2.4.3.

The pulmonary absorption and metabolism of an opioid tetrapeptide was investigated in the IPL and in rats *in vivo* by Tronde and co-workers [68, 140]. The lung metabolism, compared after airway and vascular delivery, was consistently showed to be higher after airway delivery indicating some first-pass

metabolism in the airways. Furthermore, the metabolic ratio obtained in the IPL (%metabolite/% parent compound, recovered in the perfusate) was quantitatively consistent with that observed in vivo (AUC_{metabolite}/AUC_{parent compound}; AUC – area under the plasma concentration time curve). These results illustrate an example of the validity of the IPL to investigate first-pass metabolism in the lung from a qualitative as well as a quantitative point of view. The first-pass metabolism after pulmonary delivery was, however, low compared to oral delivery and a high bioavailability was obtained. In total, the air-to-perfusate transfer of nine low molecular weight and physicochemically diverse drug compounds (Mw 225–430 Da) was systematically measured in this IPL system (Figure 6.4) to evaluate the influence of drug physicochemical properties on the pulmonary absorption. A strong correlation was found between the drug absorption rate in the IPL and the lipophilicity, PSA, %PSA, and the hydrogen bonding potential [139].

6.2.4.3. Evaluation of Active Transport Mechanisms

The kinetic model described above has been adapted for actively absorbed compounds including fluorescently labelled poly- α,β -[N(2-hydroxyethyl)-D,L-aspartamide (F-PHEA) and immunoglobulin G (IgG) [120] by adding an active absorption component with Michaelis-Menton kinetics (i.e. maximum rate, V_{\max} and affinity, K_m). This was used to explain the unexpectedly rapid absorption of PHEA in the IPL [118]. It was suggested that the transport mechanism involved a transcytotic mechanism on the basis of observations at lower temperature (25°C compared to 37°C) and in the presence of transcytosis inhibitors. The absorption of human IgG (0.3–2.5 mg/ml) was found to be slow (maximum 80 ng/h) and saturable by an excess of rat IgG, indicating a competitive transport process thought to be neonatal constant region fragment receptor (rFcRn) mediated [120].

Less direct evidence for active transport mechanisms includes the high degree of absorption of the P-gp substrate losartan in the isolated perfused rat lung, which indicated an absence of any absorption-retarding effect of P-gp [139]. Evidence to the contrary includes an increase in the uptake of idarubicin when administered to the IPL via the perfusate in the presence of P-gp inhibitors [70].

6.2.4.4. In Vitro–in Vivo Correlation

The potential for the isolated perfused rat lung to be used to predict drug absorption from the in vivo rat lung has been demonstrated by the relationship between the absorption of compounds in the IPL and absorption from the lung in vivo [142]. The air-to-perfusate absorption half-life of five low molecular weight physicochemically diverse drugs was measured in this system and was found to be linearly related to the logarithm of in vivo absorption half-life in the rat, with a correlation coefficient of $r = 0.96$ (Figure 6.5).

The solutes for which transport was evaluated in the IPL were also assayed for their transport in epithelial cell culture models. Permeability in the Caco-2 intestinal cell culture model [141] and the 16HBE14o- airway cell culture model [81] correlated with the rate of absorption in the IPL, with correlation coefficients of $r = 0.96$ and $r^2 = 0.78$ respectively.

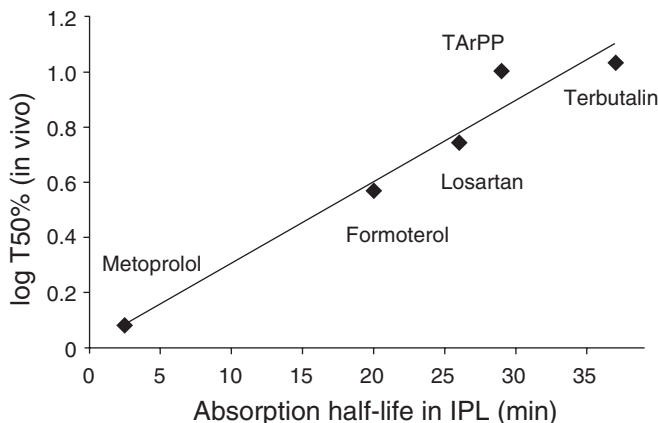


Figure 6.5 Relationship between drug absorption in vivo and airspace to perfusate transfer in the isolated perfused lung [142].

6.2.4.5. Drug Transfer in the Human IPL after Delivery by Metered Dose Inhaler

Early IPL studies focused mostly on the metabolism of the bronchodilators and corticosteroids or the pharmacological activity of bronchodilators on the ex vivo preparation. Recently, the absorptive transfer of beclomethasone dipropionate (BDP) has been measured following administration to the human lung reperfusion model by two different commercially available inhalers for which human pharmacokinetic data are available for comparison [43].

The ventilated and perfused human lung lobe was used as described by Linder and co-workers [74]. A twofold difference in the appearance of drug and metabolites in the perfusate was found for the two formulations. Small fractions of the applied dose of BDP were immediately detectable in the perfusate and the amount of the major metabolite, beclomethasone-17-propionate (17-BMP), increased over the experimental period. These observations were similar to the clinical observations that BDP is detected rapidly in the plasma after inhalation and that the appearance of the active metabolite 17-BMP occurs rapidly. The kinetic differences between the formulations were explained on the basis of particle size effects with the conclusion that the discriminatory value of this system to examine the lung pharmacokinetics of inhaled medicines in the absence of systemic effects such as hepatic metabolism was apparent.

6.2.5. Developments in the IPL

The IPL is finding increasingly application for drug absorption studies. There is interest in the potential of the method as a screening tool to evaluate drug absorption and disposition in the lung for new inhaled drug candidates. The technique also offers the opportunity to perform mechanistic studies by measuring drug air-to-perfusate and vice versa transfer independently of extrapulmonary influences. Use of the IPL to measure drug transport mechanisms and understand active transport in the lung have been reported recently. The IPL provides a complementary method to epithelial cell culture for such studies. Developments in the use of the technique and interpretation of the data generated may be expected to lead to wider application of the IPL as a tool for the evaluation of the biopharmaceutics of drugs targeted to the lungs either

via inhalation or via systemic delivery. Recently developed tools for inhalation research, such as the Dust-Gun for the delivery of drugs in relevant pharmaceutical form (i.e. powder aerosols) and dosing systems suitable for absorption studies in the mouse lung (allowing studies in genetic knockout lungs), may be adopted for use with the IPL and widen the scope of the preparation's current drug delivery applications.

References

1. Adjei A, Sundberg D, Miller J, Chun A (1992) Bioavailability of leuprolide acetate following nasal and inhalation delivery to rats and healthy humans. *Pharm Res* 9:244–249.
2. Anderson MW, Orton TC, Pickett RD, Eling TE (1974) Accumulation of amines in the isolated perfused rabbit lung. *J Pharmacol Exp Ther* 189:456–466.
3. Munch N and Rewell RE (1945) Penicillin by inhalation. *Lancet* 245:650–652.
4. Anttila S, Hukkanen J, Hakkola J, Stjernvall T, Beaune P, Edwards RJ, Boobis AR, Pelkonen O, Raunio H (1997) Expression and localization of CYP3A4 and CYP3A5 in human lung. *Am J Respir Cell Mol Biol* 16:242–249.
5. Audi SH, Dawson CA, Linehan JH, Krenz GS, Ahlf SB, Roerig DL (1998) Pulmonary disposition of lipophilic amine compounds in the isolated perfused rabbit lung. *J Appl Physiol* 84:516–530.
6. Audi SH, Roerig DL, Ahlf SB, Lin W, Dawson CA (1999) Pulmonary inflammation alters the lung disposition of lipophilic amine indicators. *J Appl Physiol* 87:1831–1842.
7. Bassett DJP, Roth RA (1992) The isolated perfused lung preparation. In: Watson RR (ed.) *In Vitro Methods of Toxicology*. Boca Raton, CRC Press, Florida, pp 143–155.
8. Becker RHA, Sha S, Frick AD, Fountaine RJ (2006) The effect of smoking cessation and subsequent resumption on absorption of inhaled insulin. *Diabetes Care* 29:277–282.
9. Ben-Jebria A, Eskew ML, Edwards DA (2000) Inhalation systems for pulmonary aerosol delivery in rodents using large porous particles. *Aerosol Sci Technol* 32:421–433.
10. Brain JD, Knudson DE, Sorokin SP, Davis MA (1976) Pulmonary distribution of particles given by intratracheal instillation or by aerosol inhalation. *Environ Res* 11:13–33.
11. Brain JD, Bloom SD, Valberg PA, Gehr P (1984) Correlation between the behavior of magnetic iron oxide particles in the lungs of rabbits and phagocytosis. *Exp Lung Res* 6:115–131.
12. Brewis RAL, Corrin B, Geddes DM, Gibson GJ (1995) *Respiratory Medicine*, second edition. WB Saunders Company Ltd, London.
13. Brown RA, Schanker LS (1983) Absorption of aerosolized drugs from the rat lung. *Drug Metab Dispos* 11:355–360.
14. Byron PR, Sian N, Roberts R, Clark AR (1986) An isolated perfused rat lung preparation for the study of drug deposition and absorption. *J Pharm Sci* 75:168–171.
15. Byron PR, Niven RW (1988) A novel dosing method for drug administration to the airways of the isolated perfused rat lung. *J Pharm Sci* 77:693–695.
16. Camps PWL (1929) A note on the inhalation treatment of asthma. *Guys Hosp Rep* 79:496–498.
17. ChangLai SP, Hung WT, Liao KK (1999) Detecting alveolar epithelial injury following volatile anesthetics by ^{99m}Tc DTPA radioaerosol inhalation lung scan. *Respiration* 66:506–510.

18. Chediak AD, Wanner A (1990) The circulation of the airways: anatomy, physiology and potential role in drug delivery to the respiratory tract. *Adv Drug Deliv Rev* 5:11–18.
19. Colthorpe P, Farr SJ, Taylor G, Smith IJ, Wyatt D (1992) The pharmacokinetics of pulmonary delivered insulin: a comparison of intratracheal and aerosol administration to the rabbit. *Pharm Res* 9:764–768.
20. Colthorpe P, Farr SJ, Smith IJ, Wyatt D, Taylor G (1995) The influence of regional deposition on the pharmacokinetics of pulmonary delivered human growth hormone in rabbits. *Pharm Res* 12:356–359.
21. Concessio NM, Oort MMV, Knowles M, Hickey AJ (1999) Pharmaceutical dry powder aerosols: correlation of powder properties with dose delivery and implications for pharmacodynamic effect. *Pharm Res* 16:833–839.
22. Dahlbäck M, Eirefelt S, Nerbrink O (1996) Aerosol delivery to the respiratory tract in experimental animals. In: Marijnissen JCM, Gradon L (eds.) *Aerosol Inhalation: Recent Research Frontiers*. Kluwer academic publishers, Netherlands, pp 235–246.
23. Dale O, Brown BRJ (1987) Clinical pharmacokinetics of the inhalation anaesthetics. *Clin Pharmacokinet* 12:145–167.
24. Davies B, Morris T (1993) Physiological parameters in laboratory animals and humans. *Pharm Res* 10:1093–1095.
25. Delmotte P, Sanderson MJ (2006) Ciliary beat frequency is maintained at a maximal rate in the small airways of mouse lung slices. *Am J Respir Cell Mol Biol* 35:110–117.
26. Dershwitz M, Walsh JL, Morishige RJ, Connors PM, Rubsamén RM, Shafer SL, Rosow CE (2000) Pharmacokinetics and pharmacodynamics of inhaled versus intravenous morphine in healthy volunteers. *Anesthesiology* 93: 619–628.
27. Dehler M, Zessin E, Bartsch P, Mairbaur H (2006) Hypoxia causes permeability oedema in the constant pressure perfused rat lung. *Eur Respir J* 27: 600–606.
28. Dollery CT, Junod AF (1976) Concentration of (\pm)-propranolol in isolated, perfused lungs of rat. *Br J Pharmacol* 57:67–71.
29. Drew R, Siddik Z, Mimnaugh EG, Gram TE (1981) Species and dose differences in the accumulation of imipramine by mammalian lungs. *Drug Metab Dispos* 9:322–326.
30. Driscoll KE, Costa DL, Hatch G, Henderson RF, Oberdörster G, Salem H, Schlesinger RB (2000) Intratracheal instillation as an exposure technique for the evaluation of respiratory tract toxicity: uses and limitations. *Toxicol Sci* 55: 24–35.
31. Edsbäcker S, Johansson C-J (2006) Airway selectivity: an update of pharmacokinetic factors affecting local and systemic disposition of inhaled steroids. *Basic Clin Pharmacol Toxicol* 98:525–536.
32. Effros RM, Mason GR (1983) Measurements of epithelial permeability *in vivo*. *Am Rev Respir Dis* 127:S59–S65.
33. Ehrhardt C, Kneuer C, Bies C, Lehr C-M, Kim K-J, Bakowsky U (2005) Salbutamol is actively absorbed across human bronchial epithelial cell layers. *Pulm Pharmacol Ther* 18:165–170.
34. Elbert KJ, Schäfer UF, Schäfers HJ, Kim KJ, Lee VHL, Lehr C-M (1999) Monolayers of human alveolar epithelial cells in primary cultures for pulmonary drug delivery and transport studies. *Pharm Res* 16:601–608.
35. Evander E, Wollmer P, Jonson B, Lachmann B (1987) Pulmonary clearance of inhaled ^{99m}Tc DTPA: effects of surfactant depletion by lung lavage. *J Appl Physiol* 62:1611–1614.

36. Ewing P, Blomgren B, Ryrfeldt Å, Gerde P (2006) Increasing exposure levels cause an abrupt change in the absorption and metabolism on acutely inhaled benzo(a)pyrene in the isolated, ventilated and perfused lung of the rat. *Toxicol Sci* 91:332–340.
37. Fisher AB, Dodia C, Linask J (1980) Perfusate composition and edema formation in isolated rat lungs. *Exp Lung Res* 1:13–21.
38. Fisher AB (1985) The isolated perfused lung. *Handb Exp Pharmacol* 75:149–179.
39. Folkesson HG, Weström BR, Pierzynowski SG, Karlsson BW (1991) Lung to blood passage of different-sized molecules during inflammation in the rat. *J Appl Physiol* 71:1106–1111.
40. Folkesson HG, Weström BR, Dahlbäck M, Lundin S, Karlsson BW (1992) Passage of aerosolized BSA and the nona-peptide dDAVP via the respiratory tract in young and adult rats. *Exp Lung Res* 18:595–614.
41. Folkesson HG, Weström BR, Karlsson BW (1998) Effects of systemic and local immunization on alveolar epithelial permeability to protein in the rat. *Am J Respir Crit Care Med* 157:324–327.
42. Foster KA, Avery ML, Yazdanian M, Audus KL (2000) Characterization of the Calu-3 cell line as a tool to screen pulmonary drug delivery. *Exp Cell Res* 243:359–366.
43. Freiwald M, Valotis A, Kirschbaum A, McClellan M, Murdter T, Fritz P, Friedel G, Thomas M, Hogger P (2005) Monitoring the initial pulmonary absorption of two different beclomethasone dipropionate aerosols employing a human lung reperfusion model. *Respir Res* 24:6–21.
44. French MC, Wishart GN (1985) Isolated perfused rabbit lung as a model to study the absorption of organic aerosols. *J Pharmacol Methods* 13:241–248.
45. Gillespie MN, Krechniak JW, Crooks PA, Altieri RJ, Olson JW (1985) Pulmonary metabolism of exogenous enkephalins in isolated perfused rat lungs. *J Pharmacol Exp Ther* 232:675–681.
46. Godfrey RW (1997) Human airways epithelial tight junctions. *Microsc Res Tech* 38:488–499.
47. Graeser JB, Rowe AH (1935) Inhalation of epinephrine for relief of asthmatic symptoms. *J Allergy* 6:415–420.
48. Greiff L, Andersson M, Svensson J, Wollmer P, Lundin S, Persson CGA (2002) Absorption across nasal airway mucosa in house dust mite perennial allergic rhinitis. *Clin Physiol Funct Imaging* 22:55–57.
49. Groneberg DA, Nickolaus M, Springer J, Doring F, Daniel H, Fisher A (2001) Localisation of the peptide transporter PEPT2 in the lung—implications for pulmonary oligopeptide uptake. *Am J Pathol* 158:707–714.
50. Groneberg DA, Eynott PR, Doring F, Dinh QT, Oates T, Barnes PJ, Chung KF, Daniel H, Fisher A (2002) Distribution and function of the peptide transporter PEPT2 in normal and cystic fibrosis human lung. *Thorax* 57:55–60.
51. Haley PJ, Muggenburg BA, Weissman DN, Bice DE (1991) Comparative morphology and morphometry of alveolar macrophages from six species. *Am J Anat* 191:401–407.
52. Hastings RH, Grady M, Sakuma T, Matthay MA (1992) Clearance of different-sized proteins from alveolar spaces in humans and rabbits. *J Appl Physiol* 73:1310–1317.
53. Heyder J, Svartengren MU (2002) Basic principles of particle behavior in the human respiratory tract. In: Bisgaard H, O'Callaghan C, Smaldone GC (eds.) *Drug Delivery to the Lung*. Marcel Dekker Inc, New York.
54. Hickey AJ, Carcia-Contrenas L (2001) Immunological and toxicological implications of short-term studies in animals of pharmaceutical aerosol delivery to the lungs: relevance to humans. *Crit Rev Ther Drug Carrier Syst* 18:387–431.

55. Hogg JC (1981) Bronchial mucosal permeability and its relationship to airways hyperreactivity. *J Allergy Clin Immunol* 67:421–425.
56. Hoover JL, Rush BD, Wilkinson KF, Day JS, Burton PS, Vidmar TJ, Ruwart MJ (1992) Peptides are better absorbed from the lung than the gut in the rat. *Pharm Res* 9:1103–1106.
57. Horvath G, Schmid N, Fragoso MA, Schmid A, Conner GE, Salathe M, Wanner A (2007) Epithelial organic cation transporters ensure pH dependent drug absorption in the airway. *Am J Respir Cell Mol Biol* 36:53–60.
58. Ilowite JS, Bennet WD, Sheetz WS, Groth ML, Nierman DM (1989) Permeability of the bronchial mucosa to ^{99m}Tc -DTPA in asthma. *Am Rev Respir Dis* 139:1139–1143.
59. Jeffrey PK (1995) Microscopic structure of normal lung. In: Brewis RAL, Corrin B, Geddes DM, Gibson GJ (eds.) *Respiratory Medicine*. WB Saunders Company Ltd, London.
60. Jendbro M, Johansson C-J, Strandberg P, Falk-Nilsson H, Edsbäcker S (2001) Pharmacokinetics of budesonide and its major ester metabolite after inhalation and intravenous administration of budesonide in the rat. *Drug Metab Dispos* 29:769–776.
61. Jeppsson A-B, Nilsson E, Waldeck B (1994) Formoterol and salmeterol are both long acting compared to terbutaline in the isolated perfused and ventilated guinea-pig lung. *Eur J Pharmacol* 257:137–143.
62. Jones JG, Minty BD, Lawler P, Hulands G, Crawley JC, Veall N (1980) Increased alveolar epithelial permeability in cigarette smokers. *Lancet* 1:66–68.
63. Kanekal S, Plopper C, Morin D, Buckpitt A (1991) Metabolism and cytotoxicity of naphthalene oxide in the isolated perfused mouse lung. *J Pharmacol Exp Ther* 256:391–401.
64. Köping-Höggård M, Issa MM, Köhler T, Tronde A, Vårum KM, Artursson P (2005) A miniaturized nebulization catheter for improved gene delivery to the mouse lung. *J Gene Med* 7:1215–1222.
65. Kröll F, Karlsson JA, Persson CGA (1987) Tracheobronchial microvessels perfused via the pulmonary artery in guinea-pig isolated lungs. *Acta Physiol Scand* 129:445–446.
66. Kröll F, Karlsson JA, Nilsson E, Persson CG, Ryrfeldt Å (1986) Lung mechanics of the guinea-pig isolated perfused lung. *Acta Physiol Scand* 128:1–8.
67. Kröll F, Karlsson J-A, Nilsson E, Ryrfeldt Å, Persson CGA (1990) Rapid clearance of xanthines from airway and pulmonary tissues. *Am Rev Respir Dis* 141:1167–1171.
68. Krondahl E, Tronde A, Eirefelt S, Forsmo-Bruce H, Ekström G, Lennernäs H (2002) Regional differences in bioavailability of an opioid tetrapeptide agonist *in vivo* in rats after administration to the respiratory tract. *Peptides* 23:479–488.
69. Krondahl E, von Euler-Chelpin H, Orzechowski A, Ekström G, Lennernäs H (2001) *In vitro* metabolism of opioid tetrapeptide agonists in various tissues and subcellular fractions from rats. *Peptides* 22:613–622.
70. Kuhlmann O, Hofmann HS, Muller SP, Weiss M (2003) Pharmacokinetics of idarubicin in the isolated perfused rat lung: effect of cinchonine and rutin. *Anti-cancer Drugs* 14:411–416.
71. Leong BKJ, Coombs JK, Sabaitis CP, Rop DA, Aaron CS (1998) Quantitative morphometric analysis of pulmonary deposition of aerosol particles inhaled via intratracheal nebulization, intratracheal instillation or nose-only inhalation in rats. *J Appl Toxicol* 18:149–160.
72. Lethem MI (1993) The role of tracheobronchial mucus in drug administration to the airways. *Adv Drug Deliv Rev* 11:271–298.
73. LiCalsi C, Christensen T, Bennett JV, Phillips E, Witham C (1999) Dry powder inhalation as a potential delivery method for vaccines. *Vaccine* 17:1796–1803.

74. Linder A, Friedel G, Fritz P, Kivistö KT, McClellan M, Toomes H (1996) The *ex-vivo* isolated, perfused human lung model: description and potential applications. *Thorac Cardiovasc Surg* 44:140–146.
75. Lips KS, Volk C, Schmitt BM, Pfeil U, Arndt P, Miska D, Ermert L, Kummer W, Koepsell H (2005) Polyspecific cation transporters mediate luminal release of acetylcholine from bronchial epithelium. *Am J Respir Cell Mol Biol* 33:79–88.
76. Lipworth BJ (1996) Pharmacokinetics of inhaled drugs. *Br J Clin Pharmacol* 42:697–705.
77. Lombry C, Edwards DA, Preat V, Vanbever R (2004) Alveolar macrophages are a primary barrier to pulmonary absorption of macromolecules. *Am J Physiol* 286:L1002–1008.
78. Longmore WJ (1982) The isolated perfused lung as a model for studies of lung metabolism. In: Farrel PM (ed.) *Lung Development: Biological and Clinical Perspectives*. Academic Press Inc, New York, pp 101–110.
79. Ma J, Bhat M, Rojanasakul Y (1996) Drug metabolism and enzyme kinetics in the lung. In: Hickey AJ (ed.) *Inhalation Aerosols*. Marcel Dekker Inc, New York.
80. MacIntyre NR (2001) Intratracheal catheters as drug delivery systems. *Respir Care* 46:193–197.
81. Manford F, Tronde A, Jeppson A-B, Patel N, Johansson F, Forbes B (2005) Drug permeability in 16HBE14o- airway cell layers correlates with absorption from the isolated perfused rat lung. *Eur J Pharm Sci* 26:414–420.
82. Martínéz Martínéz MS, Colino Gandarillas CI, Martínéz Lanao J, Sánchez Navarro A (2005) Comparative study of the disposition of levofloxacin, netilmicin and cefepime in the isolated rat lung. *J Pharm Pharmacol* 57:861–867.
83. Mason RJ, Crystal RG (1998) Pulmonary cell biology. *Am J Respir Crit Care Med* 157:S72–S81.
84. Mason GR, Peters AM, Bagdades E, Myers MJ, Snooks D, Hughes JMB (2001) Evaluation of pulmonary alveolar epithelial integrity by the detection of restriction to diffusion of hydrophilic solutes of different molecular sizes. *Clin Sci* 100:231–236.
85. Matsukawa Y, Lee VHL, Crandall ED, Kim K-J (1997) Size-dependent dextran transport across rat alveolar epithelial cell monolayers. *J Pharm Sci* 86: 305–309.
86. McAllister SM, Alpar HO, Teitelbaum Z, Bennett DB (1996) Do interactions with phospholipids contribute to the prolonged retention of polypeptides within the lung? *Adv Drug Deliv Rev* 19:89–110.
87. McLaughlin GE, Kim KJ, Berg MM, Agoris P, Lubman RL, Crandall ED (1993) Measurement of solute fluxes in isolated rat lungs. *Respir Physiol* 91:321–334.
88. Mehendale HM, Angevine LS, Ohmiya Y (1981) The isolated perfused lung—A critical evaluation. *Toxicology* 21:1–36.
89. Minchin RF, Johnston MR, Aiken MA, Boyd MR (1984) Pharmacokinetics of doxorubicin in isolated lung of dogs and humans perfused *in vivo*. *J Pharmacol Exp Ther* 229:193–198.
90. Morimoto K, Yamahara H, Lee VH, Kim K-J (1993) Dipeptide transport across rat alveolar epithelial cell monolayers. *Pharm Res* 10:1668–1674.
91. Nave R, Fisher R, Zech K (2006) *In vitro* metabolism of ciclesonide in human lung and liver precision-cut tissue slices. *Biopharm Drug Dispos* 27:197–207.
92. Nicod LP (1999) Pulmonary defence mechanisms. *Respiration* 66:2–11.
93. Niemeier RW, Bingham E (1972) An isolated perfused lung preparation for metabolic studies. *Life Sci II* 11:807–820.
94. Niven RW (1992) Modulated drug therapy with inhalation aerosols. In: Hickey AJ (ed.) *Pharmaceutical Inhalation Aerosol Technology*. Marcel Dekker Inc, Chicago, pp 321–359.
95. Niven RW (1995) Delivery of biotherapeutics by inhalation aerosol. In: Bruck SD (ed.) *Crit Rev Ther Drug Carrier Syst*. Begell House Inc, New York, pp 151–231.

96. Niven RW, Byron PR (1988) Solute absorption from the airways of the isolated rat lung. I. The use of absorption data to quantify drug dissolution or release in the respiratory tract. *Pharm Res* 5:574–579.
97. Nyhlén K, Rippe B, Hultkvist-Bengtsson U (1997) An isolated blood-perfused guinea-pig lung model for simultaneous registration of haemodynamic, microvascular and respiratory variables. *Acta Physiol Scand* 159:293–302.
98. O’Byrne PM, Dolovich M, Dirks R, Roberts RS, Newhouse MT (1984) Lung epithelial permeability: relation to non-specific airway responsiveness. *J Appl Physiol* 57:77–84.
99. Okamoto H, Aoki M, Danjo K (2000) A novel apparatus for rat *in vivo* evaluation of dry powder formulations for pulmonary administration. *J Pharm Sci* 89: 1028–1035.
100. Pang JA, Butland RJA, Brooks N, Cattell M, Geddes DM (1982) Impaired lung uptake of propranolol in human pulmonary emphysema. *Am Rev Respir Dis* 125:194–198.
101. Pang Y, Sakagami M, Byron PR (2005) The pharmacokinetics of pulmonary insulin in the *in vitro* isolated perfused rat lung: implications of metabolism and regional deposition. *Eur J Pharm Sci* 25:369–378.
102. Patrick G, Stirling C (1977) Measurement of mucociliary clearance from the trachea of conscious and anaesthetized rats. *J Appl Physiol* 42:451–455.
103. Patton JS (1996) Mechanisms of macromolecule absorption by the lungs. *Adv Drug Deliv Rev* 19:3–36.
104. Patton JS, Byron PR (2007) Inhaling medicines: delivering drugs to the body through the lungs. *Nat Rev Drug Discov* 6:67–74.
105. Persson CGA, Erjefält JS (1997) Airway epithelial restitution after shedding and denudation. In: Crystal RG, West JB (eds.) *The Lung*. Lippincott-Raven Publishers, Philadelphia, pp 2611–2627.
106. Plopper CG (1996) Structure and function of the lung. In: Jones TC, Dungworth DL, Mohr U (eds.) *Respiratory System*. Springer Verlag, Berlin, pp 135–150.
107. Post C, Andersson RG, Ryrfeldt Å, Nilsson E (1978) Transport and binding of lidocaine by lung slices and perfused lung of rats. *Acta Pharm Toxicol* 43: 156–163.
108. Puchelle E, Girod de Bentzmann S, Higenbottam T (1995) Airway secretion and lung liquids. In: Brewis RAL, Corrin B, Geddes DM, Gibson GJ (eds.) *Respiratory Medicine*. WB Saunders Company Ltd, London, pp 97–111.
109. Raeburn D, Underwood SL, Villamil ME (1992) Techniques for drug delivery to the airways and the assessment of lung function in animal models. *J Pharmacol Toxicol Methods* 27:143–149.
110. Redington AE (2001) Airway remodeling in asthma. *CME Bull Respir Med* 3: 37–40.
111. Reinoso RF, Sánchez-Navarro A, Lanao JM (1999) Distribution of ciprofloxacin in the isolated rat lung in the presence and absence of tissue oedema. *Eur J Pharm Sci* 8:203–209.
112. Ressmeyer AR, Larsson AK, Vollmer E, Dahlen SE, Uhlig S, Martin C (2006) Characterisation of guinea pig precision-cut lung slices: comparison with human tissues. *Eur Respir J* 28:603–611.
113. Rubin BK (1996) Therapeutic aerosol and airway secretions. *J Aerosol Med* 9:123–130.
114. Russell KE, Read MS, Bellinger DA, Leitermann K, Rup BJ, McCarthy KP, Keith JC, Khor SP, Schaub RG, Nicholls TC (2001) Intratracheal administration of recombinant human factor IX (BeneFixTM) achieves therapeutic levels in hemophilia B dogs. *Thromb Haemost* 85:445–449.

115. Ryrfeldt Å, Nilsson E (1978) Uptake and biotransformation of ibuterol and terbutaline in isolated perfused rat and guinea pig lungs. *Biochem Pharmacol* 27: 301–305.
116. Ryrfeldt Å, Nilsson E, Tunek A, Svensson LA (1988) Bambuterol: uptake and metabolism in guinea pig isolated lungs. *Pharm Res* 5:151–155.
117. Ryrfeldt Å, Persson G, Nilsson E (1989) Pulmonary disposition of the potent glucocorticoid budesonide, evaluated in an isolated and perfused rat lung model. *Biochem Pharmacol* 38:17–22.
118. Sakagami M, Byron PR, Rypacek F (2002) Biochemical evidence for transcytotic absorption of polyaspartamide from the rat lung: effects of temperature and metabolic inhibitors. *J Pharm Sci* 91:1958–1968.
119. Sakagami M (2006) *In vivo*, *in vitro* and *ex vivo* models to assess pulmonary absorption and disposition of inhaled therapeutics for systemic delivery. *Adv Drug Deliv Rev* 58:1030–1060.
120. Sakagami M, Omidji Y, Campbell L, Kandalaf LE, Moris CJ, Barar J, Gumbleton M (2006) Expression and transport functionality of FcRn within rat alveolar epithelium: a study in primary cell culture and in the isolated perfused lung. *Pharm Res* 23:270–279.
121. Salathé M, O’Riordan TG, Wanner A (1997) Mucociliary clearance. In: Crystal RG, West JB (eds.) *The Lung: Scientific Foundations*. Lippincott-Raven Publishers, Philadelphia, pp 2295–2308.
122. Samet JM, Cheng P-W (1994) The role of the airway mucus in pulmonary toxicology. *Environ Health Perspect* 102:89–103.
123. Schanker LS, Burton JA (1976) Absorption of heparin and cyanocobalamin from the rat lung. *Proc Soc Exp Biol Med* 152:377–380.
124. Schanker LS, Hemberger JA (1983) Relation between molecular weight and pulmonary absorption rate of lipid-insoluble compounds in neonatal and adult rats. *Biochem Pharmacol* 32:2599–2601.
125. Schanker LS, Mitchell EW, Brown RA, Jr (1986) Species comparison of drug absorption from the lung after aerosol inhalation or intratracheal injection. *Drug Metab Dispos* 14:79–88.
126. Scheffer GL, Pijnenborg ACLM, Smit EF, Müller M, Postma DS, Timens W, van der Valk P, de Vries EGE, Scheper RJ (2002) Multidrug resistance related molecules in human and murine lung. *J Clin Pathol* 55:332–339.
127. Schmekel B, Borgström L, Wollmer P (1991) Difference in pulmonary absorption of inhaled terbutaline in healthy smokers and non-smokers. *Thorax* 46:225–228.
128. Schmekel B, Borgström L, Wollmer P (1992) Exercise increases the rate of pulmonary absorption of inhaled terbutaline. *Chest* 101:742–745.
129. Schneeberger EE (1980) Heterogeneity of tight junction morphology in extrapulmonary and intrapulmonary airways in the rats. *Anat Rec* 198:193–208.
130. Schneeberger EE (1991) Airway and alveolar tight junctions. In: Crystal RG, West JB (eds.) *The Lung: Scientific Foundations*. Raven Press, New York, pp 205–214.
131. Simionescu M (1991) Lung endothelium: structure-function correlates. In: Crystal RG, West JB (eds.) *The Lung: Scientific Foundations*. Raven Press, New York, pp 301–312.
132. Skyler JS, Cefalu WT, Kourides IA, Landschulz WH, Balagtas CC, Cheng S-L, Gelfand RA (2001) Efficacy of inhaled human insulin type a diabetes mellitus: a randomized proof-of-concept study. *Lancet* 357:331–335.
133. Staub NC (1991) *Basic Respiratory Physiology*. Churchill Livingstone Inc, New York.
134. Sweeney TD, Brain JD (1991) Pulmonary deposition: determinants and measurement techniques. *Toxicol Pathol* 19:384–397.

135. Takenaka S, Karg E, Roth C, Schulz H, Ziesenis A, Heinzmann U, Schramel P, Heyder J (2001) Pulmonary and systemic distribution of inhaled ultrafine silver particles in rats. *Environ Health Perspect* 109:547–551.
136. Taljanski W, Pierzynowski SG, Lundin PD, Weström BR, Eirefelt S, Podlesny J, Dahlbäck M, Siwinska Golebiowska H, Karlsson BW (1997) Pulmonary delivery of intratracheally instilled and aerosolized cyclosporine A to young and adult rats. *Drug Metab Dispos* 25:917–920.
137. Taylor G (1990) The absorption and metabolism of xenobiotics in the lung. *Adv Drug Deliv Rev* 5:37–61.
138. Tronde A, Baran G, Eirefelt S, Lennernäs H, Bengtsson UH (2002) Miniaturized nebulization catheters: a new approach for delivery of defined aerosol doses to the rat lung. *J Aerosol Med* 15:289–296.
139. Tronde A (2002) Pulmonary drug absorption: *in vitro* and *in vivo* investigations of drug absorption across the lung barrier and its relation to drug physicochemical properties. Doctoral dissertation, Faculty of Pharmacy, Uppsala University, Uppsala Sweden ISSN0282-7484, ISBN 91-554-5373-2, (<http://publications.uu.se/theses/fulltext/91-554-5373-2.pdf>).
140. Tronde A, Kron Dahl E, von Euler-Chelpin H, Brunmark P, Bengtsson UH, Ekstrom G, Lennernäs H (2002) High airway-to-blood transport of an opioid tetrapeptide in the isolated rat lung after aerosol delivery. *Peptides* 23:469–478.
141. Tronde A, Norden B, Jeppson AB, Brunmark P, Nilsson E, Lennernäs H, Bengtsson UH (2003) Drug absorption from the isolated perfused rat lung—correlation with drug physicochemical properties and epithelial permeability. *J Drug Target* 11:61–74.
142. Tronde A, Norden B, Marchner H, Wendel AK, Lennernäs H, Bengtsson UH (2003) Pulmonary absorption rate and bioavailability of drugs *in vivo* in rats: structure-absorption relationships and physicochemical profiling of inhaled drugs. *J Pharm Sci* 92:1216–1233.
143. Twigg HL (1998) Pulmonary host defenses. *J Thorac Imaging* 13:221–233.
144. Uhlig S, Wollin L (1994) An improved setup for the isolated perfused rat lung. *J Pharmacol Toxicol Methods* 31:85–94.
145. Upton RN, Doolette DJ (1999) Kinetic aspects of drug disposition in the lung. *Clin Exp Pharmacol Physiol* 26:381–391.
146. Von Betham AN, Brasch F, Nusing R, Vogt K, Muller KM, Wendel A, Uhlig S (1998) Hyperventilation induces release of cytokines from perfused mouse lung. *Am J Respir Crit Care Med* 157:263–272.
147. Van den Bosch JMM, Westermann CJJ, Aumann J, Edsbäcker S, Tönneson M, Selroos O (1993) Relationship between lung tissue and blood plasma concentrations of inhaled budesonide. *Biopharm Drug Dispos* 14:455–459.
148. Van der Deen M, de Vries EGE, Timens W, Scheper RJ, Timmer-Bosscha H, Postma DS (2005) ATP-binding cassette (ABC) transporters in normal and pathological lung. *Respir Res* 6:59.
149. Van't Veen A, Gommers D, Verbrugge SJC, Wollmer P, Mouton JW, Kooij PPM, Lachmann B (1999) Lung clearance of intratracheally instilled Tc-99m-tobramycin using pulmonary surfactant as vehicle. *Br J Pharmacol* 126:1091–1096.
150. Van't Veen A, Mouton JW, Gommers D, Kluytmans JAJ, Dekkers P, Lachmann B (1995) Influence of pulmonary surfactant on *in vitro* bactericidal activities of amoxicillin, ceftazidime, and tobramycin. *Antimicrob Agents Chemother* 39:329–333.
151. Wall DA (1995) Pulmonary absorption of peptides and proteins. *Drug Deliv* 2:1–20.
152. Wall DA, Lanutti AT (1993) High levels of exopeptidase activity are present in rat and canine bronchoalveolar lavage fluid. *Int J Pharm* 97:171–181.

153. Weibel ER (1963) *Morphometry of the Human Lung*. Springer, Heidelberg.
154. Weibel ER (1991) Design of airways and blood vessels considered as branching trees. In: Crystal RG, West JB (eds.) *The Lung: Scientific Foundations*. Raven Press, New York, pp 711–720.
155. West JB (2006) Vulnerability of pulmonary capillaries during severe exercise. *Br J Sports Med* 40:821.
156. Widdicombe J (1997) Airway and alveolar permeability and surface liquid thickness: theory. *J Appl Physiol* 82:3–12.
157. Wiedmann TS, Bhatia R, Wattenberg LW (2000) Drug solubilization in lung surfactant. *J Control Release* 65:43–47.
158. Winton HL, Wan H, Cannell MB, Gruenert DC, Thompson PJ, Garrod DR, Stewart GA, Robinson C (1998) Cell lines of pulmonary and non-pulmonary origin as tools to study the effects of house dust mite proteinases on the regulation of epithelial permeability. *Clin Exp Allergy* 28:1273–1285.
159. Wise S, Chien J, Yeo K, Richardson C (2006) Smoking enhances absorption of insulin but reduces glucodynamic effects in individuals using the Lilly-Dura inhaled insulin system. *Diabet Med* 23:510–515.
160. Wohlsen A, Martin C, Vollmer E, Branscheid D, Magnussen H, Becker W-M, Lepp U, Uhlig S (2003) The early allergic response in small airways of human precision-cut lung slices. *Eur Respir J* 21:1024–1032.
161. Wollmer P, Schainer W, Bos JA, Bakker W, Krenning EP, Lachmann B (1990) Pulmonary clearance of ^{99m}Tc -DTPA during halothane anesthesia. *Acta Anaesthesiol Scand* 34:572–575.
162. Yamashita F, Mathias NR, Kim K-J, Lee VHL (1996) Dipeptide transport properties of rabbit tracheal epithelial cell monolayers cultured at an air-liquid interface. *Pharm Res* 15:979–983.
163. Yang X, Ma JKA, Malanga CJ, Rojanasakul Y (2000) Characterization of proteolytic activities of pulmonary alveolar epithelium. *Int J Pharm* 195:93–101.

In Vitro Models for Investigations of Buccal Drug Permeation and Metabolism

Tanja Obradovic and Ismael J. Hidalgo

Abstract Buccal drug delivery across mucosal lining of the cheek offers a clear advantage over the peroral dosing route by avoidance of intestinal and hepatic first-pass metabolism. However, despite offering the possibility of improved systemic drug delivery, buccal administration has been utilized for relatively few pharmaceutical products so far. One of the reasons is costly preclinical development, which includes laborious pharmacokinetic evaluation in animal models. Utilization of in vitro methodology can greatly aid in early development by offering a significant increase in the number of compounds and/or formulations that can be evaluated for their potential for buccal absorption. Currently, in vitro models used for the assessment of buccal drug delivery utilize freshly isolated animal buccal mucosa as well as human buccal tissue cultures. This chapter describes the different in vitro techniques used for the evaluation of buccal drug absorption and indicates their advantages and disadvantages.

Keywords: Buccal; Mucosa; In vitro; Absorption; Permeability; Culture

7.1. Introduction

Buccal drug delivery offers several advantages over the peroral route. These advantages include avoidance of presystemic drug elimination within the gastrointestinal tract and/or during the hepatic first-pass metabolism, and independence from the potential variability of absorption caused by the gastric emptying rate, or the presence of food in the upper region of the gastrointestinal tract [1]. In addition, the buccal mucosa is relatively permeable with a rich blood supply and has a substantial resistance to irritation or damage [1–3]. Structurally, the human buccal mucosa is a multistratified, nonkeratinized, squamous epithelium lining the cheek area of the oral cavity [4]. Drug permeation across buccal epithelium has been suggested, like for other mucosal barriers, to involve paracellular (between the cells) and transcellular (through the cells) routes [5]. Hydrophilic compounds predominantly permeate via the paracellular route, whereas hydrophobic compounds do so via the transcellular route [6]. Numerous compounds with diverse physicochemical properties have

been developed for buccal application targeting local or systemic delivery including proteins such as insulin [7–13]. Since buccal administration is an attractive way to deliver drugs, the feasibility of this route for a candidate compound is investigated by *in vivo* or *in vitro* methodologies of buccal drug permeation properties. This chapter will provide an insight into often employed *in vitro* methodologies for the assessment of drug absorption potential across buccal mucosa.

7.2. In Vitro Studies

7.2.1. Isolated Buccal Tissue Mounted in Diffusion Cell Apparatus

Currently, the most widely used *in vitro* methodology for assessing drug permeation across buccal mucosa is by testing drug permeation across isolated buccal tissue mounted in diffusion chambers. Chapter 4 of this book focuses exclusively on the available *in vivo* and *ex vivo* methods; thus, these will be discussed only in brief in the context of this chapter. Human buccal mucosa is scarcely available and if obtained, the size of the tissue available from one donor is not sufficient for conducting a large number of *in vitro* experiments. Therefore, most research efforts relied on the use of isolated animal buccal tissue. Because of species differences in physiology and anatomy of buccal mucosa, caution must be exercised during the process of selection of animal species to be used in this type of studies. The only laboratory animal with a nonkeratinized surface layer of the buccal mucosa similar to human tissue that has been used in buccal absorption studies is the rabbit [14, 15]. However, in the rabbit, the nonkeratinized area of the buccal tissue has a sudden transition to keratinized regions, which limits the amount of suitable tissue available and makes isolation of the desired region unreliable [16]. Therefore, buccal tissue from other animal species tends to be used more often than that from rabbits. In particular, the buccal mucosa of monkeys [17], dogs [17–21], and pigs [22–25] has been extensively used for *in vitro* drug permeability studies. The porcine buccal tissue is the most frequently utilized model due to relative similarity to human tissue [3], and a low cost associated with tissue acquisition.

For *in vitro* experiments using isolated animal buccal mucosa, different types of diffusion cells have been used for mounting tissue. The use of diffusion cells makes it possible to determine the actual amount of drug that diffuses across the mucosal barrier as well as the rate of drug diffusion. Various types of diffusion cells are available. Among them is the Franz-type diffusion chamber that was first utilized for the determination of buccal permeation by Kurosaki et al. [26]. The Franz-type diffusion chamber is a static, one-chamber diffusion cell where compound in neat solution or in formulated form is applied to the mucosal apical surface, which faces the air through the open cell-cap that constitutes the donor compartment (Figure 7.1). The receiver chamber volume is typically 6–8 ml and a stirring bar maintains homogeneous temperature and mixes the solution in the receiver compartment. The temperature of the apparatus is maintained at 37°C by placing the diffusion cell into a heated water bath. Samples from the receiver solution are taken via the side port on the diffusion cell typically for up to 180 min, a time interval much shorter (few hours) than

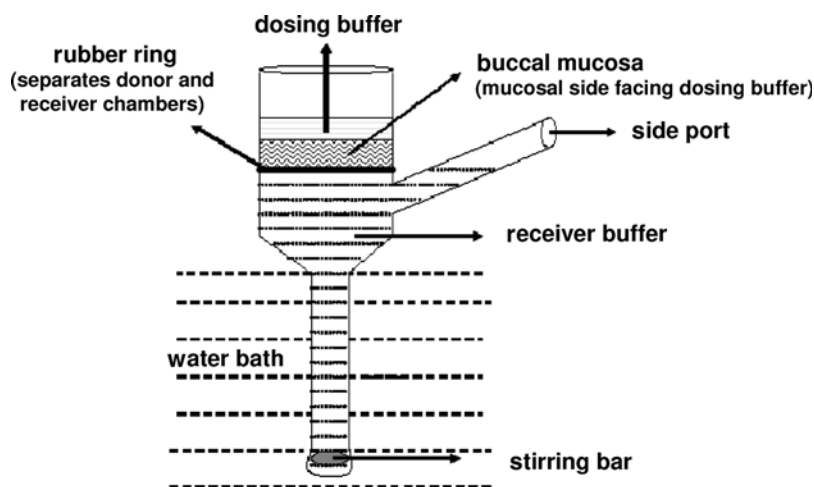


Figure 7.1 Schematic of a Franz-type diffusion cell.

that at which isolated buccal mucosa preparation is viable in this system [27]. In addition, the buccal tissue used in permeation studies should be fresh because freezing and thawing has been shown to alter significantly the permeability properties of porcine oral mucosa [28].

Figure 7.2 presents permeation across freshly isolated porcine buccal mucosa of caffeine and atenolol. Caffeine and atenolol are compounds with complete and poor human buccal absorption *in vivo*, respectively [10, 29],

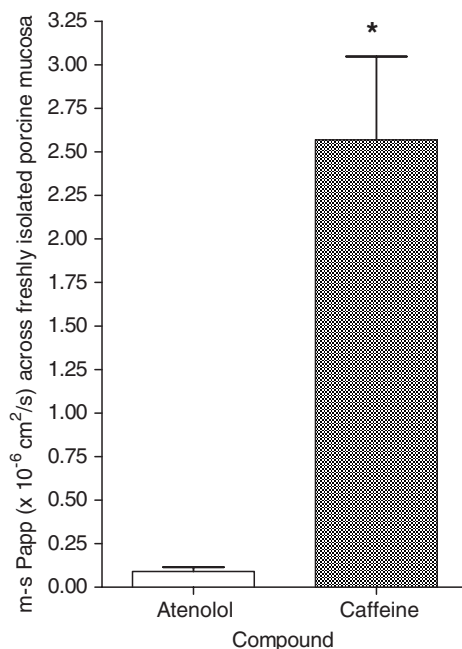


Figure 7.2 Mucosal-to-submucosal (m-s) P_{app} values of atenolol and caffeine obtained in freshly isolated porcine buccal mucosa from ten animals (average \pm SEM). * (Asterisk) significantly higher than atenolol value (*t*-test, $p < 0.005$). Results are from Ref. [42].

Table 7.1 Examples of atenolol and caffeine mucosal-to-submucosal (m-s) permeation across freshly isolated porcine buccal mucosa.

Porcine	Atenolol m-s P_{app} ($\times 10^{-6}$ cm/s)	Caffeine m-s P_{app} ($\times 10^{-6}$ cm/s)
1	0.01	1.89
2	0.02	2.46
3	0.04	1.56
4	0.04	1.61
5	0.07	4.31
6	0.22	5.90
7	0.05	1.97
8	0.10	1.14
9	0.12	1.53
10	0.23	3.32
Average (SD)	0.09 (0.08)	2.57 (1.51)

which correlates well with significantly higher caffeine than atenolol permeation across porcine buccal epithelium in vitro (Figure 7.2). The transport of caffeine and atenolol showed a significant difference in apparent permeability coefficient (P_{app}) values of at least an order of magnitude in each of ten animal tissue donors (Table 7.1). A clear difference existed between atenolol and caffeine P_{app} in each donor, despite a large variability between different animals (Table 7.1). The interindividual and intertissue variability in the buccal epithelium thickness observed histologically may be a significant factor contributing to the P_{app} variability shown in Table 7.1.

Squier and Hall [30, 31] have found that the thickness of the upper third of the buccal epithelium, which contains membrane-coating granules, plays a major role in limiting the drug permeation of hydrophilic compounds. In addition, a recent study by Giannola et al. [32] demonstrated an extensive effect of epithelial thickness on buccal in vitro permeation of carbamazepine, a relatively lipophilic compound ($c \log P$ 2.7). Therefore, the determination of statistically significant differences in permeation for compounds that have relatively close rates of buccal permeation may be difficult in diffusion cells due to large interanimal variability and it may require a large number of animal tissue samples [33].

In general, drug permeability across buccal tissue, or any other mucosal barrier, is dependent on physicochemical properties of the drug, such as lipophilicity, molecular weight, and degree of ionization at physiological pH (pH 6.8–7.4 for buccal tissue). Regardless of the transport route, small molecules tend to be absorbed faster. In addition, a positive relationship between lipophilicity and buccal in vitro permeability has been found on a set of acetanilides [34]. McElnay et al. [35] reported pH dependence of buccal captopril absorption with good correlation between in vitro results and in vivo human absorption. Current efforts to develop suitable drug delivery systems include permeation enhancers and controlled release systems for local or systemic therapy that rely substantially on the utilization of in vitro buccal tissue assays [36]. Only

a few studies have shown a correlation between in vitro and in vivo buccal drug absorption and most of them examined the effect of permeation enhancers or release rate-modifying excipients [37]. For example, a good correlation between in vitro permeation across porcine buccal mucosa and bioavailability enhancement in rabbits has been observed with a triamcinolone acetonide gel formulated with the permeability enhancer sodium deoxycholate [38, 39]. In addition, Degim et al. [40] recently observed good correlation between effective delivery of acyclovir following buccal tablet dosing in dogs and the acyclovir pH-dependant permeation profile across buccal tissue in vitro. In contrast, a poor correlation was found between in vitro permeation across porcine buccal epithelium and bioavailability in pigs of fluorescein isothiocyanate (FITC)-labeled dextrans, commonly used model compounds for peptides [41]. Therefore, caution needs to be exercised when extrapolating in vitro results to in vivo absorption, including delivery in humans.

As noted earlier, the choice of species for experimentation is critical due to anatomical differences and it may also reflect species, as well as individual, differences in the expression/activity of transporter and metabolic proteins [43, 44]. Since the fraction absorbed across buccal mucosa in vivo is not established for many compounds in different species including humans, the potential existence of a correlation between in vitro permeability coefficients in freshly isolated pig, dog, monkey, and human buccal mucosa was investigated (Figure 7.3). The correlation coefficient obtained for porcine and canine tissue was poor (0.65 and 0.67, respectively, at the 95% confidence level). Results for relatively high permeability compounds in porcine tissue resemble those previously reported where permeability coefficients were by an order of magnitude

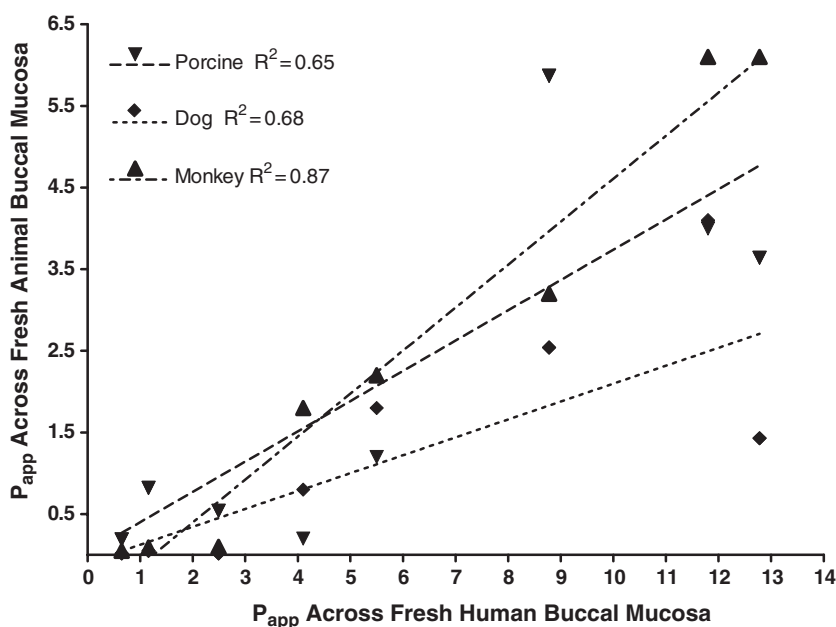


Figure 7.3 Correlation analysis for P_{app} values across freshly isolated animal buccal mucosa and freshly isolated human buccal mucosa of Lucifer yellow, enalaprilat, atenolol, caffeine, sumatriptan, and fentanyl. Results from internal study by Absorption Systems Company.

lower across porcine buccal mucosa mounted in the Franz-type chamber than across reconstituted human oral epithelium [32]. In addition, porcine buccal mucosa showed consistently lower permeability than human tissue toward compounds of hydrophilic and hydrophobic nature *in vitro* [45], which is in line with observations for atenolol and caffeine (Tables 7.1 and 7.2). These findings indicate that pig buccal tissue has a higher barrier property to drug permeation than do human buccal mucosa. The strongest correlation observed was that between permeation across monkey and human buccal mucosa (correlation coefficient 0.87 at the 95% confidence level). These observations, obtained on a small set of passively transported compounds with different physicochemical properties, indicate that *in vitro* permeability determined using buccal tissue mounted in the Franz-type cell varies across species. Observed correlation results likely reflect physiological and anatomical differences between the species [16], which also may contribute to the contradictory results between *in vitro* experiments with animal buccal tissue and *in vivo* human studies [46]. Other factors that can cause an underestimation of the drug buccal penetration potency *in vitro* include the lack of blood flow [47] and the existence of an unstirred water layer on the mucosal surface that may pose a substantial diffusion barrier especially for lipophilic compounds [26, 43].

In spite of the limitations associated with using the *in vitro* buccal tissue system, this model appears to be a useful tool for evaluating drug permeation across buccal mucosa. The main advantages include (1) assessment of buccal delivery at the intended application site where, unlike the *in vivo* situation, there is no compound loss due to swallowing; (2) tissue resistance to irritation and loss of integrity, which allows for a wide-range of excipient testing; and (3) the possibility to obtain *in vitro* animal buccal tissue data that can be correlated to *in vivo* animal results prior to human testing.

7.2.2. Buccal Epithelial Cell Cultures

Although isolated animal buccal mucosa mounted in diffusion chambers is the most used technique to estimate buccal absorption, this tissue model has several practical disadvantages. These include a limited surface area, presence of tissue damage from mastication, laborious and time-consuming excision procedure, minimal potential for assay automatization, and large variability in permeation results among replicates. These disadvantages make it impractical to use the tissue model for testing large numbers of compounds and/or compound formulations. For these reasons, attempts have been made to establish suitable *in vitro* buccal epithelial cell culture models for testing drug permeation and metabolism. Tavkoli-Saberi et al. [48] developed the hamster pouch epithelium culture. In addition, a TR146 cell culture derived from human buccal metastasis has been used to assess drug transport and metabolism [33, 49]. However, the effect of parameters that can affect drug transport, such as the control of culture growth rate, number of differentiated cell layers, lipid composition, and optimum day(s) in culture, is still not well characterized in these models. Therefore, these cultures have not been extensively used in the development of drug candidates for buccal delivery. Recently, a new cultured human buccal epithelium model EpiOral[®] has become commercially available (MatTek, Ashland, MA). This tissue model consists of normal human keratinocytes cultured to form a three-dimensional differentiated tissue that histologically

Table 7.2 Examples of atenolol and caffeine mucosal-to-submucosal (m-s) permeation across cultured buccal epithelium.

Batch	Atenolol m-s P_{app} ($\times 10^{-6}$ cm/s)	Caffeine m-s P_{app} ($\times 10^{-6}$ cm/s)
	Average \pm SD, $N = 3$	Average \pm SD, $N = 3$
1	1.89 \pm 0.23	17.7 \pm 1.1
2	2.02 \pm 0.31	17.2 \pm 0.5
3	1.67 \pm 0.19	15.6 \pm 0.9
Average (SD)	1.86 \pm 0.18*	16.8 \pm 1.1*

* Corresponding P_{app} value for atenolol and caffeine across freshly isolated human buccal mucosa mounted in Franz-type cell is 1.16 (0.25) and 14.5 (1.6), respectively.

and biochemically resembles human buccal tissue [50]. So far, this model has shown good correspondence to human buccal mucosa in terms of structure, protein expression, and lipid content with good reproducibility of the tissue cultures [51]. Also, a good correlation between the permeation of fentanyl across cultured buccal epithelium, applied in different tablet formulations, and bioavailability in humans has been found [52–54]. The P_{app} of atenolol (poorly absorbed reference) and caffeine (highly absorbed reference), across different cultured batches, are presented in Table 7.2. Results indicate that the barrier function of this in vitro model appears reproducible across batches. In addition, a relatively good correlation between drug permeabilities across freshly isolated human buccal mucosa and human buccal culture is observed (Figure 7.4, correlation coefficient 0.96 at the 95% confidence level). These results indicate that human buccal epithelial culture may be a better predictor of permeation across human buccal mucosa than animal buccal tissue models (Figure 7.3).

However, the number of compounds tested in vitro on human EpiOral[®] buccal culture is currently very limited [50]. Therefore, further studies are needed to better evaluate usefulness of this novel model in testing drug buccal delivery potential.

Of particular interest is a possible use of EpiOral[®] human buccal culture for evaluation of drug metabolism and its effect on buccal drug permeation. The use of previously frozen human mucosal specimens is an often-employed method in the investigation of drug metabolism [55, 56]. However, the loss of enzymatic activity in this tissue due to storage can be a limiting factor in accurately determining drug metabolism. On the other hand, metabolism in fresh human buccal tissue cannot be easily addressed due to lack of readily available fresh mucosa in sufficient quantities for in vitro testing. So far, the metabolic fate of drugs in the human buccal mucosa is predominantly investigated in tissue homogenates obtained from the oral cavity of different animal species [57–59]. However, due to well-known interspecies differences in enzyme expression [44, 60], results in animals can differ from human metabolism. The knowledge of drug enzymatic degradation in the human buccal mucosa is very limited including the roles of Cytochrome P450 enzymes (CYPs). The CYP enzymes are responsible for oxidative metabolism in the liver and extrahepatic tissues including buccal tissue [61, 62]. CYP3A4, CYP2C9, and CYP2D6 are the major human liver CYPs that are known to limit bioavailability of numerous drugs [63]. The functionality of these CYP enzymes in the EpiOral[®] human buccal culture was

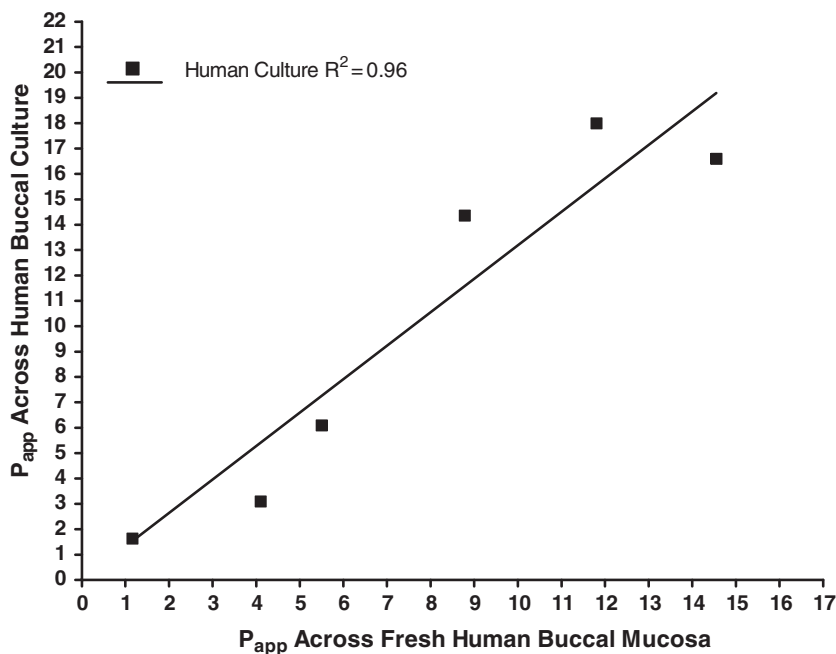


Figure 7.4 Correlation analysis for P_{app} values across cultured human buccal epithelium and freshly isolated human buccal mucosa of Lucifer yellow, enalaprilat, atenolol, caffeine, sumatriptan, and fentanyl. Results from internal study by Absorption Systems Company.

evaluated by determining the permeability of the marker substrates midazolam (CYP3A4), tolbutamide (CYP2C9), and bufuralol (CYP2D6) in the absence and presence of specific inhibitors (Figure 7.5). Results indicate a lack of CYP3A4, CYP2C9, and CYP2D6 effect on drug transport across human buccal tissue culture since permeation of marker substrates was not enhanced by CYP inhibition.

In addition, CYP substrates had permeation rates comparable to that of caffeine, a high-permeability, nonmetabolized, and completely absorbed

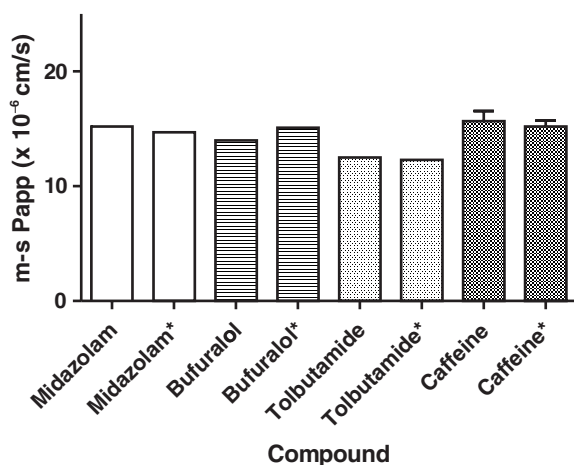
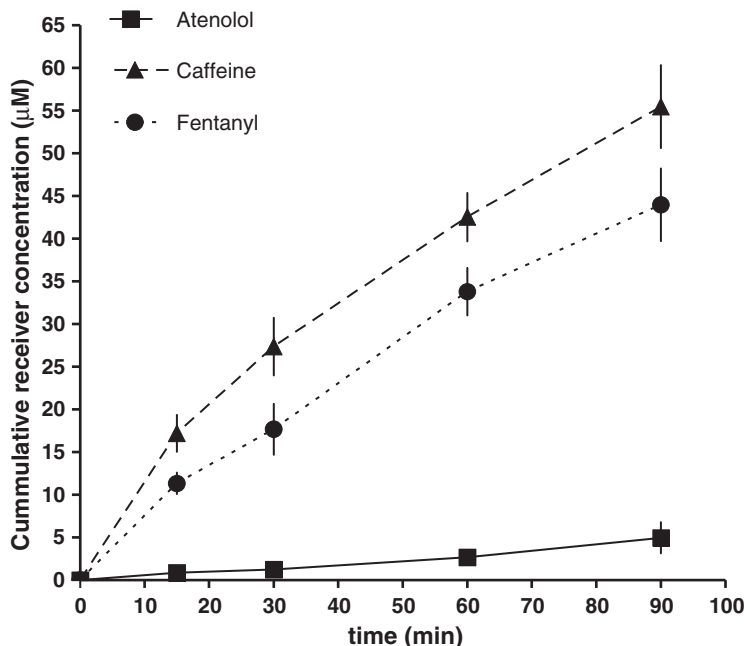


Figure 7.5 Mucosal-to-submucosal (m-s), P_{app} values across human buccal culture of midazolam (CYP3A4 substrate), bufuralol (CYP2D6 substrate), tolbutamide (CYP2C9 substrate), and the nonmetabolized, high-permeability control compound caffeine (average \pm SEM, $N = 1 - 3$ replicates). * (Asterisk) in the presence of CYP inhibitors (CYP3A4-ketoconazole; CYP2D6-quinidine; CYP2C9-suphaphenazole). In all treatments integrity of the culture was verified by permeation of Lucifer yellow ($< 2.0 \times 10^{-6}$ cm/s). Results from internal study by Absorption Systems Company.

Figure 7.6 Cumulative receiver concentrations of fentanyl, caffeine, and atenolol vs time across cultured human buccal tissue (average \pm SD, $N = 3$). Results from internal study by Absorption Systems Company.



compound in vivo. These results corroborate the findings of Vondracek et al. [64] where, on a large set of human donors, buccal epithelium expression and catalytic activity of CYP3A4, CYP2C9, and CYP2D6 was minimal or nonexistent despite mRNA expression. Therefore, for compounds that may be substantially degraded by CYP3A4, CYP2C9, and CYP2D6 following peroral administration, a buccal route of delivery may be advantageous. For example, fentanyl is a compound with very low oral bioavailability due to a high first-pass metabolism that is mediated by CYP3A4 in the liver and intestine [65]. Fentanyl permeation across cultured human buccal epithelium is high (Figure 7.6), which is in accordance with similar fentanyl and caffeine permeation in this model when fentanyl flux from the tablet form was tested [52]. Furthermore, these results are in agreement with reported rapid and complete fentanyl absorption when applied buccally in humans [53, 54]. Although buccal mucosa appears to have low basal CYP activity [50, 64], other non-CYP metabolic processes in this tissue have also been reported (Table 7.3). Among them, different types of peptidases and esterases have been identified in either human or animal buccal specimens [34, 49, 57, 66, 67]. In addition, the buccal metabolism of drugs that are subjected to peptidase and/or esterase-mediated degradation has been found to have substantial effect on their delivery through the buccal route [49, 68, 69]. Therefore, buccal administration of compounds that may be liable to these enzymatic processes may present a challenge.

Currently, most strategies for buccal delivery of peptide drugs have focused on the application of excipients that would shorten the time of absorption and adhere drugs to a local site on the mucosa, thus decreasing exposure to proteolytic degradation and possible release of drug back into the mouth cavity. This strategy has been utilized in the buccal delivery of insulin, enkephalin, and testosterone [37, 70].

Table 7.3 Enzymes present in the buccal mucosa.

Species	Enzyme
Human	Aminopeptidase ^{a, b}
	Carboxypeptidase ^b
	Esterase ^b
	Dehydrogenase ^c
	CYP1A1, 1A2, 2C, 2D6, 2E1, 3A4/7, 3A5 ^d
	Aminopeptidase ^b
Pig	Carboxypeptidase ^b
	Esterases ^b
	Aminopeptidase ^e
Rabbit	Carboxypeptidase ^f
	Protease ^g
	Aminopeptidase ^h
Rat	Carboxypeptidase ^f
	Esterase ⁱ

^a Ref. [71]; ^b Ref. [49]; ^c Ref. [72]; ^d Ref. [64]; ^e Ref. [73];

^f Ref. [74]; ^g Ref. [75]; ^h Ref. [66]; ⁱ Ref. [58].

7.3. Concluding Remarks

Considering the substantial use of excipients in buccal delivery systems, it is important to use a suitable *in vitro* model that correlates well with human results *in vivo*. Experiments on isolated animal buccal tissue provided sufficiently predictive results of excipient effect on *in vivo* buccal absorption for many drugs including many small molecules as well as peptides [37; 41]. Currently, buccal cell cultures have been utilized very scarcely to evaluate the effect of formulation excipients on drug transport intended for transbuccal delivery. So far, enhancing effects of chitosan [76], sodium glycocholate [77], and bile salts [78] on drug permeation across TR146 buccal cell culture have been reported while excipient effects in the EpiOral[®] model have not been investigated. In general, cell culture models tend to be less suitable than isolated mucosal tissue for excipient testing because cultured cells are more susceptible to formulation excipient effects on cell viability and functional integrity [79–81]. Therefore, studies on the effects of permeation enhancers and other excipients on the physical and biochemical integrity of cultured buccal epithelium are needed in order to evaluate the potential utility of this model to estimate buccal drug absorption under relevant conditions. Furthermore, such studies may address the potential of excipients/enhancers to cause irritation in humans.

At present, despite the advantages offered by the buccal delivery route, such as the bypass of intestinal and hepatic first-pass metabolism for systemic delivery, very few pharmaceutical products employ this route of administration. The reasons that contribute to this situation include (1) high costs associated with development, (2) lack of standardized tests to identify drug candidates suitability for this route, (3) the limited understanding of the impact of metabolism and/or transporters found in the oral cavity mucosa on buccal delivery, and (4) the relatively small number of reports describing the usefulness and safety of excipients/permeation enhancers in humans [82, 83]. Therefore, the

development of an in vitro screening model derived from human tissue that can address these issues may provide a useful tool in overcoming challenges during preclinical development of candidates intended for buccal delivery.

References

1. Rathbone M, Drummond B, and Tucker I (1994) The oral cavity as a site for systemic drug delivery. *Adv. Drug Deliv. Rev.* 13: 1–22.
2. Goodman CH, and Squier CA (1988) Blood flow in the oral mucosa of normal and arteriosclerotic rhesus monkeys. *J. Oral Path.* 17: 34–38.
3. Squier CA (1991) The permeability of oral mucosa. *Crit. Rev. Oral. Biol. Med.* 2: 13–32.
4. Squier CA and Finkelstein MW (1989) In: *Oral Histology, Development, Structure and Function*. A. R. Ten Cate (Ed.), C. V. Mosby, St. Louis, pp 345–385.
5. Zhang H, and Robinson JR (1996) In vitro methods for measuring permeability of the oral mucosa, In: *Oral Mucosa Drug Delivery*, Marcel Dekker, Inc., NY, pp 85–100.
6. Wertz PW, and Squier CA (1991) Cellular and molecular basis of barrier function in oral epithelium. *Crit. Rev. Ther. Drug Carrier Syst.* 8: 237–269.
7. Oh CK, and Ritschel WA (1990) Biopharmaceutical aspects of buccal absorption of insulin. *Methods Find. Exp. Clin. Pharmacol.* 12: 205–209.
8. Bray CL, Jain S, Faragher EB, Myers A, Myers P, MacIntyre P, Rae A, Goldman M, and Alcorn M (1991) A comparison of buccal nitroglycerin and sublingual nitroglycerin in the prophylaxis and treatment of exertional (situation-evoked) angina pectoris. *Eur. Heart J.* 12 Suppl A: 16–20.
9. Venugopalan P, Sapre A, Venkatesan N, and Vyas SP (2001) Pelleted bioadhesive polymeric nanoparticles for buccal delivery of insulin: Preparation and characterization. *Pharmazie* 56: 217–219.
10. Kamimori GH, Karyekar CS, Otterstetter R, Cox DS, Balkin TJ, Belenky GL, and Eddington ND (2002) The rate of absorption and relative bioavailability of caffeine administered in chewing gum versus capsules to normal healthy volunteers. *Int. J. Pharm.* 234: 159–167.
11. Attia MA, El-Gibaly I, Shaltout SE, and Fetih GN (2004) Transbuccal permeation, anti-inflammatory activity and clinical efficacy of piroxicam formulated in different gels. *Int. J. Pharm.* 276: 11–28.
12. Cernea S, Kidron M, Wohlgelemler J, and Raz I (2005) Dose-response relationship of an oral insulin spray in six patients with type 1 diabetes: A single-center, randomized, single-blind, 5-way crossover study. *Clin. Ther.* 27: 1562–1570.
13. Mystakidou K, Katsouda E, Parpa E, Vlahos L, and Tsitais ML (2006) Oral transmucosal fentanyl citrate: Overview of pharmacological and clinical characteristics. *Drug Deliv.* 13: 269–276.
14. Siegel IA, and Gordon HP (1986) Surfactant-induced alterations of permeability of rabbit oral mucosa in vitro. *Exp. Mol. Path.* 44: 132–137.
15. Dowty ME, Knuth KE, Irons BK, and Robinson JR (1992) Transport of tyrotropin releasing hormone in rabbit buccal mucosa in vitro. *Pharm. Res.* 9: 1113–1122.
16. Squier CA, and Wertz PW (1996) Structure and function of the oral mucosa and implications for drug delivery. In: *Oral Mucosal Drug Delivery*, Marcel Dekker, Inc., NY, pp. 1–26.
17. Mehta M, Kempaininen BW, and Stafford RG (1991) In vitro penetration of tritium-labeled water (THO) and [3H]PbTx-3 (a red tide toxin) through monkey buccal mucosa and skin. *Tox. Lett.* 55: 185–194.
18. Ishida M, Machida Y, Nambu N, and Nagai T (1981) New mucosal dosage form of insulin. *Chem. Pharm. Bull.* 29: 810–816.
19. Nagai T (1985) Adhesive topical drug delivery system. *J. Control. Rel.* 2: 121–134.

20. Veillard MM, Longer MA, Martens TW, and Robinson JR (1987) Preliminary studies of oral mucosal delivery of peptide drugs. *J. Control. Rel.* 6: 123–131.
21. Barsuhn CL, Olanoff LS, Gleason DD, Adkins EL, and Ho NFH (1988) Human buccal absorption of flubriprofen. *Clin. Pharmacol. Ther.* 44: 225–231.
22. Lesch CA, Squier CA, Crunchley A, Williams DM, and Speight P (1989) The permeability of human oral mucosa and skin to water. *J. Dent. Res.* 68: 1345–1349.
23. Hoogstraate AJ, Senel S, Cullander C, Verhoef J, Juninger HE, and Bodde HE (1996) Effects of bile salts on transport rates and routes of FTIC-labelled compounds across porcine buccal epithelium in vitro. *J. Control. Rel.* 40: 211–221.
24. Mashru R, Sutariya V, Sankalia M, and Sankalia J (2005) Transbuccal delivery of lamotrigine across porcine buccal mucosa: In vitro determination of routes of buccal transport. *J. Pharm. Pharm. Sci.* 28: 54–62.
25. Sandri G, Poggi P, Bonferoni MC, Rossi S, Ferrari F, and Caramella C (2006) Histological evaluation of buccal penetration enhancement properties of chitosan and trimethyl chitosan. *J. Pharm. Pharmacol.* 58: 1327–1336.
26. Kurosaki Y, Hisaichi S, Hamada C, Nakayama T, and Kimura T (1987) Studies on drug absorption from oral cavity. II. Influence of the unstirred water layer on absorption from hamster cheek pouch in vitro. *J. Pharmacobiodyn.* 10: 180–187.
27. Imbert D, and Cullander C (1999) Buccal mucosa in vitro experiments. I. Confocal imaging of vital staining and MTT assays for the determination of tissue viability. *J. Control. Rel.* 58: 39–50.
28. van Eyk AD, and van der Biijl P (2006) Comparative permeability of fresh and frozen/thawed porcine buccal mucosa towards various chemical markers. *SADJ* 61: 200–203.
29. Schurmann W, and Turner P (1977) The buccal absorption of atenolol and propranolol, and their physicochemical characteristics. *Br. J. Clin. Pharmacol.* 4: 655P–656P.
30. Squier CA, and Hall BK (1985a) In vitro permeability of porcine oral mucosa after epithelial separation, stripping and hydration. *Arch. Oral Biol.* 30: 485–491.
31. Squier CA, and Hall BK (1985b) The permeability of skin and oral mucosa to water and horseradish peroxidase as related to the thickness of the permeability barrier. *J. Invest. Dermatol.* 84: 176–179.
32. Giannola LI, De Caro V, Giandalia G, Siragusa MG, D'Angelo M, Lo Muzio L, and Campisi G (2006) Transbuccal tablets of carbamazepine: Formulation, release and absorption pattern. *Int. J. Immunopathol. Pharmacol.* 19: 21–31.
33. Nielsen HM, and Rassing MR (2000a) TR146 cells grown on filters as a model of human buccal epithelium: IV. Permeability of water, mannitol, testosterone, and beta-adrenoceptor antagonists. Comparison to human, monkey and porcine buccal mucosa. *Int. J. Pharm.* 194: 155–167.
34. Garren K, and Repta A (1988) Buccal drug absorption: Comparative levels of esterase and peptidase activities in rat and hamster buccal and intestinal homogenates. *Int. J. Pharm.* 48: 189–194.
35. McElnay JC, al-Furaih TA, Hughes CM, Scott MG, Elborn JS, and Nichols DP (1995) The effect of pH on the buccal and sublingual absorption of captopril. *Eur. J. Clin. Pharmacol.* 48: 373–379.
36. Hao J, and Heng WS (2003) Buccal Delivery Systems. *Drug Dev. Ind. Pharm.* 29: 821–832.
37. Birudaraj R, Mahalingam R, Li X, and Jasti BR (2005) Advances in buccal drug delivery. *Crit. Rev. Ther. Drug Carrier Syst.* 22: 295–330.
38. Shin SC, and Kim JY (2000) Enhanced permeation of triamcinolone acetonide through the buccal mucosa. *Eur. J. Pharm. Biopharm.* 50: 217–220.

39. Shin SC, Bum JP, and Choi JS (2000) Enhanced bioavailability by buccal administration of triamcinolone acetonide from the bioadhesive gels in rabbits. *Int. J. Pharm.* 209: 37–43.
40. Degim T, Eglen B, and Ocak O (2006) A sustained release dosage form of acyclovir for buccal application: An experimental study in dogs. *J. Drug Target* 14: 35–44.
41. Junginger HE, Hoogstraate JA, and Verhoef JC (1999) Recent advances in buccal delivery and absorption: In vitro and in vivo studies. *J. Control. Rel.* 62: 149–159.
42. Obradovic T, Huynh T, Shingaki T, Strab B, Peck B, and Hidalgo JI (2005) Permeation across porcine buccal mucosa is correlated with absorption across human buccal mucosa. *American Association Pharm. Sci. Abs.* W4101.
43. Lennernas H, Nylander S, and Ungell AL (1997) Jejunal permeability: A comparison between the Ussing chamber technique and the single-pass perfusion in humans. *Pharm. Res.* 14: 667–671.
44. Ioannides C (2006) Cytochrome P450 expression in the liver of food-producing animals. *Curr. Drug Metab.* 7: 335–348.
45. Van Eyk AD, and Van der Bijl P (2004) Comparative permeability of various chemical markers through human vaginal and buccal mucosa as well as porcine buccal and mouth floor mucosa. *Arch. Oral Biol.* 49: 387–392.
46. Wadell C, Bjork E, and Camber, O (2003) Permeability of porcine nasal mucosa correlated with human nasal absorption. *Eur. J. Pharm. Sci.* 18: 47–53.
47. Ungell A L (1997) In vitro absorption studies and their relevance to absorption from the GI tract. *Drug Dev. Ind. Pharm.* 23: 879–892.
48. Tavakoli-Saberi MR, and Audus KL (1989) Cultured buccal epithelium: An in vitro model derived from the hamster pouch for studying transport and metabolism. *Pharm. Res.* 6: 160–166.
49. Nielsen HM, and Rassing MR (2000b) TR146 cells grown on filters as a model of human buccal epithelium: V. Enzyme activity of the TR146 cell culture model, human buccal epithelium and porcine buccal epithelium, and permeability of leu-enkephalin. *Int. J. Pharm.* 200: 261–270.
50. Walle T, Walle UK, Sedmera D, and Klausner, M (2006) Benzo[A]pyrene-induced oral carcinogenesis and chemoprevention: Studies in bioengineered human tissue. *Drug Metab. Dispos.* 34: 346–350.
51. Kubilus J, Aychunie S, Breyfogle B, Dale DA, Kimball J, Wertz P, Klausner M (2006) Characterization and testing of new buccal and gingival tissue models. *American Association of Dental Res. Meeting* 399.
52. Agarwal V, Habib W, and Moe D (2005) Effervescent mediated transmucosal enhancement of fentanyl permeability: Comparison across ex vivo porcine buccal mucosa and in vitro cultured human buccal epithelium test. *American Association Pharm. Sci. Abs.* T2126.
53. Darwish M, Kirby M, Robertson P, Tracewell W, and Jiang JG (2006) Pharmacokinetic properties of fentanyl effervescent buccal tablets: A phase I, open-label, crossover study of single dose 100, 200, 400, and 800 micrograms in healthy adult volunteers. *Clin. Ther.* 28: 707–714.
54. Portenoy RK, Taylor D, Messins J, and Tremmel L (2006) A randomized, placebo-controlled study of fentanyl buccal tablet for breakthrough pain in opioid-treated patients with cancer. *Clin. J. Pain* 22: 805–811.
55. Wynalda MA, Hutzler JM, Koets MD, Podoll T, and Wienkers LC (2003) In vitro metabolism of clindamycin in human liver and intestinal microsomes. *Drug Metab. Disp.* 31: 878–887.
56. Godoy W, Albano RM, Moraes EG, Pinho PRA, Nunes RA, Saito EH, Higa C, Filho IM, Pinto Krueel CD, Schirmer CC, Gurski R, Lang MA, and Ribeiro Pinto LF (2002) CYP2A6/2A7 and CYP2E1 expression in human oesophageal mucosa: Regional and inter-individual variation in expression and relevance to nitrosamine metabolism. *Carcinogenesis* 23: 611–616.

57. Kashi DS, and Lee VHL (1986) Enkephalin hydrolysis in homogenates of various absorptive mucosal of the albino rabbit: Similarities in rates and involvement of aminopeptidases. *Life Sci.* 38: 2019–2028.
58. Garren KW, and Repta AJ (1989) Buccal drug absorption. II: In vitro diffusion across the hamster cheek pouch. *J. Pharm. Sci.* 78: 160–164.
59. Takagi Y, Kriehubner E, Imokawa G, Elias G, and Holleran WM (1999) β -Glucocerebrosidase activity in mammalian stratum corneum. *J. Lipid Res.* 40: 861–869.
60. Nelson DR, Koymans L, Kamataki T, Stegman JJ, Feyerisen R, Waxman DJ, Waterman MR, Gotoh O, Estabrook RW, Gunsalus IC, et al., (1996) P450 supefamily: Update on new sequences, gene mapping, accession numbers and nomenclature. *Pharmacogenetics* 6: 1–42.
61. Port JL, Yamaguchi K, Du BK, DeLorenzo M, Chang M, Heerdt OM, Kopelovich L, Marcus CB, Altoki NK, Subbaramaiah K, et al., (2004) Tobacco smoke induces CYP1B1 in the aerodigestive tract. *Carcinogenesis* 25: 2275–2281.
62. Wen X, and Walle T (2005) Preferential induction of CYP1B1 by benzo[a]pyrene in human oral epithelial cells: Impact on DNA adduct formation and prevention by polyphenols. *Carcinogenesis* 26: 1774–1781.
63. Rendic S (2002) Summary of information on human CYP enzymes: Human P450 metabolism data. *Drug Metab. Rev.* 34: 83–448.
64. Vondracek M, Xi Z, Larson P, Baker V, Mace K, Pfeifer A, Tjalve H, Donato MT, Gomez-Lechon MJ, and Grafstrom C (2001) Cytochrome P450 expression and related metabolism in human buccal mucosa. *Carcinogenesis* 22: 481–488.
65. Kharasch ED, Whittington D, and Hoffer C (2004) Influence of hepatic and intestinal cytochrome P4503A activity on the acute disposition and effects of oral transmucosal fentanyl. *Anesthesiology* 101: 729–737.
66. Harris D, and Robinson JR (1992) Drug delivery via mucous membranes of the oral cavity. *J. Pharm. Sci.* 81: 1–10.
67. Robinson DA, Bogdanoff MS, and Reed CJ (2002) Histochemical localization of carboxylesterase activity in rat and mouse oral cavity mucosa. *Toxicology* 180: 209–220.
68. Ho NF, Barshun CL, Burton SP, and Merkle HP (1992) Mechanistic insights to buccal delivery of proteinaceous substances. *Adv. Drug Deliv. Rev.* 8: 197–235.
69. Veuillez F, Kalia YN, Jacques Y, Deshusses J, and Buri PA (2001) Factors and strategies for improving buccal absorption of peptides. *Eur. J. Pharm. Biopharm.* 51: 93–109.
70. Wang C, Swerdloff R, Kipnes M, Matsumoto AM, Dobs AS, Cunningham G, Katznelson L, Weber TJ, Friedman TC, Snyder P, and Levine HL (2004) New testosterone buccal system (Striant) delivers physiological testosterone levels: Pharmacokinetics study in hypogonadal men. *J. Clin. Endocrinol. Metab.* 89: 3821–3829.
71. Audus KL, Williams A, and Tavakoli-Saberi MR (1991) A comparison of aminopeptidases from excised human buccal epithelium and primary cultures of hamster pouch buccal epithelium. *J. Pharm Pharmacol.* 43: 363–365
72. Hedberg JJ, Hoog J-O, Nilsson JA, Xi Z, Elfving A, and Graftstrom RC (2000) Expression of alcohol dehydrogenase 3 in tissue and cultured cells from human oral mucosa. *Am. J. Pathol.* 157: 1745–1754.
73. Stratford RE, and Lee VHL (1986) Aminopeptidase activity in homogenates of various absorptive mucosae in the albino rabbit: Implications in peptide delivery. *Int. J. Pharm.* 30: 73–82.
74. Wearly LL (1991) Recent progress in protein and peptide delivery by non-invasive routes. *Crit. Rev. Ther. Drug Carrier* 8: 331–394.

75. Yamamoto A, Hayakawa E, and Lee VH (1990) Insulin and proinsulin proteolysis in mucosal homogenates of the albino rabbit: Implications in peptide delivery from nonoral routes. *Life Sci.* 47: 2465–2474.
76. Portero A, Remunan-Lopez C, and Nielsen HM (2002) The potential of chitosan in enhancing peptide and protein absorption across the TR146 cell culture model—An in vitro model of the buccal mucosa. *Pharm. Res.* 19: 169–174.
77. Nielsen HM, Verhoef JC, Ponec M, and Rassing MR (1999) TR146 cells grown on filters as a model of human buccal epithelium: Permeability of fluorescein isothiocyanate-labelled dextrans in the presence of sodium glycocholate. *J. Control. Release* 60: 223–233.
78. Nielsen HM, and Rassing MR (1999) TR146 cells grown on filters as a model of human buccal epithelium: Permeability enhancement by different pH values, different osmolarity values, and bile salts. *Int. J. Pharm.* 185: 215–225.
79. Thanou M, Verhoef JC, and Junginger HE (2001) Chitosan and its derivatives as intestinal absorption enhancers. *Adv. Drug Deliv.Rev.* 50: S91–S101.
80. Sethia S, and Squillante E (2004) In vitro-in vivo evaluation of supercritical processed solid dispersions: Permeability and viability assessment in Caco-2 cells. *J. Pharm. Sci.* 93: 2985–2993.
81. Cano-Cebrian MJ, Zornoza T, Granero L, and Polache A (2005) Intestinal absorption enhancement via the paracellular route by fatty acids, chitosans and others: A target for drug delivery. *Curr. Drug Deliv.* 2: 9–22.
82. Zhang H, Zhang J, and Streisand JB (2002) Oral mucosal drug delivery: Clinical pharmacokinetics and therapeutic applications. *Clin. Pharmacokinet.* 41: 661–680.
83. Smart JD (2005) Buccal drug delivery. *Expert Opin. Drug Deliv.* 2: 507–517.

8

In Vitro Screening Models to Assess Intestinal Drug Absorption and Metabolism

Sven Deferme, Pieter Annaert, and Patrick Augustijns

Abstract Compounds intended for oral administration must have adequate biopharmaceutical properties in order to achieve therapeutic concentrations at the targeted site of action. Different models have been established for the parallel screening of these biopharmaceutical properties, including membrane-based models (PAMPA), cell culture-based models (such as Caco-2 and MDCK cell lines), and the Ussing chambers technique. In this chapter, the strengths and the drawbacks of these models are discussed, while examples of applications for these different models and suggestions to improve the models are provided. Finally, different in vitro methods for studying the intestinal metabolism are also described. As the intestinal absorption process depends on a multitude of parameters, a single universal model accounting for all these parameters does not exist. Therefore, combination of different in vitro models should be considered in order to obtain better insights in intestinal drug absorption in the different phases of drug discovery and development.

Keywords: Intestinal drug absorption; Intestinal metabolism; Cell culture-based models; Membrane-based models; Ex vivo models

Abbreviations

ABC	ATP-binding cassette protein
A-to-B	Apical to basolateral
BCRP	Breast cancer resistance protein
BCS	Biopharmaceutics classification system
BSA	Bovine serum albumin
CyA	Cyclosporin A
CYP	Cytochrome P450 enzyme
DMSO	Dimethyl sulfoxide
DOPC	Dioleoylphosphatidylcholine
FaSSIF	Fasted state simulated intestinal fluid
FeSSIF	Fed state simulated intestinal fluid
GI	Gastrointestinal
IBD	Inflammatory bowel disease
LDH	Lactate dehydrogenase

MDCK	Madin-Darby canine kidney cells
MDR	Multidrug resistance
MRP	Multidrug resistance-associated protein
MTT	3-(4,5-dimethylthiazol-2-yl)-2,5-diphenyltetrazolium bromide
NMP	<i>N</i> -methyl-2-pyrrolidone
NRU	Neutral red uptake
PAMPA	Parallel artificial membrane permeation assay
PC	Phosphatidylcholine
PD	Potential difference
PE	Phosphatidylethanolamine
PEG	Polyethyleneglycol
P-gp	P-glycoprotein
PI	Phosphatidylinositol
SCC	Short circuit current
TEER	Trans epithelial electrical resistance
UWL	Unstirred water layer

8.1. Introduction

8.1.1. General Factors Influencing Intestinal Drug Absorption

Despite tremendous innovations in the field of drug delivery technology, oral intake remains the preferred route of drug administration, for reasons of patient convenience and therapy compliance. Compounds intended for oral administration must have adequate biopharmaceutical properties in order to achieve therapeutic concentrations at the targeted site of action.

The *in vivo* absorption process is the outcome of a complex series of events and depends on a multitude of parameters related to drug characteristics as well as to physiological aspects of the gastrointestinal (GI) tract [93]. A summary of the most important factors influencing the rate and extent of intestinal absorption is given in Table 8.1.

The parallel screening of drug candidates for their pharmacological activity and for their physicochemical and biopharmaceutical properties has become a major challenge in drug development and is performed at very early stages

Table 8.1 Overview of the main factors influencing the extent and rate of intestinal drug absorption.

Physicochemical factors	Physiological factors	Formulation factors	Biochemical factors
Aqueous solubility	Stomach emptying	Dosage form	Metabolism
Molecular size and weight	time	Drug release	Efflux
Aggregation/Complexation	Intestinal motility	Absorption enhancers	transporters
Charge (pK_a)	Membrane permeability		Active uptake transporters
H-bonding potential	Intestinal pH		
Molecular surface area	Disease state		
Drug hydrophobicity	Blood flow		
Crystal lattice energy	Luminal content and composition (including bile salts)		

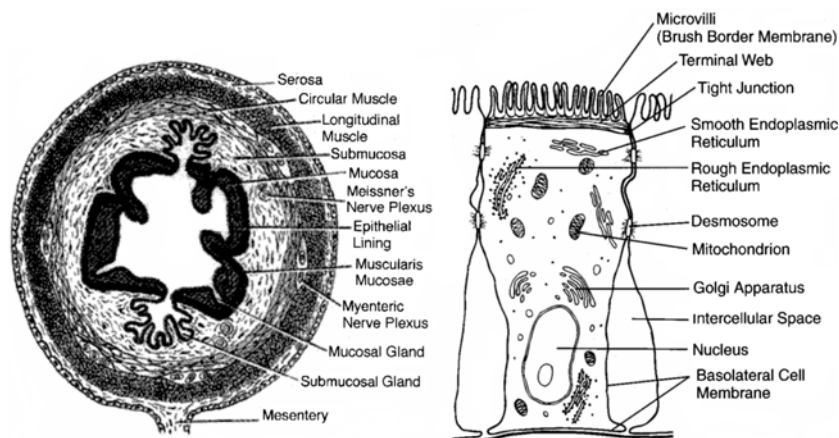


Figure 8.1 (A) Cross-sectional view of the organization of the small intestine, illustrating the serosa, the longitudinal and circular muscle layers (=muscularis externa), the submucosa, and the intestinal mucosa. The intestinal mucosa consists of four layers, the inner surface cell monolayer of enterocytes, the basal membrane, the *lamina propria* (connective tissue, blood capillaries), and the *muscularis mucosae*; (B) Schematic representation of an enterocyte (small intestinal epithelial cell); (according to Tso and Crissinger [151], with permission).

in drug development [50]. Numerous efforts have been made by the pharmaceutical industry and academia to identify the various molecular features that are important for drug absorption and to implement appropriate, high-capacity, and cost-effective screening models that are predictive for in vivo intestinal absorption. It should be noted that the intestinal absorption process is the result of interplay of various physicochemical, physiological, and biochemical properties. Therefore, no single in vitro model will mimic the complexity of the in vivo absorption process [22].

8.1.2. The Intestinal Mucosa as a Physical and Biochemical Barrier to Drug Absorption

8.1.2.1. Physical Barrier Function

The small intestinal wall (Figure 8.1) consists of the serosa, the *muscularis externa* (longitudinal and circular muscle layers), the submucosa, and the intestinal mucosa. The latter forms the main barrier that controls drug and nutrient uptake after dissolution in the luminal contents. The mucosa consists of four layers: a surface monolayer, the basal membrane, the *lamina propria* (containing connective tissue, nerves, lymphocytes, blood vessels, lymphatic vessels, macrophages, and mast cells), and the *lamina muscularis mucosa* (smooth muscle cells). The surface layer is a monolayer of columnar epithelial cells (enterocytes; see Figure 8.1) and also contains mucus-producing cells, lymphocytes, and microfold cells (M-cells) [134]. Because of the presence of tight junctions, the intercellular space is reduced to 0.8 nm (human jejunum) and 0.3 nm (human colon) [8]. Only small, hydrophilic, and polar molecules are able to cross the epithelial monolayer through the paracellular space [8, 104]. The paracellular route (see Figure 8.2) generally results in low oral absorption, due to the limited surface area. More lipophilic drugs will distribute into the cell membrane and cross the epithelial monolayer by the

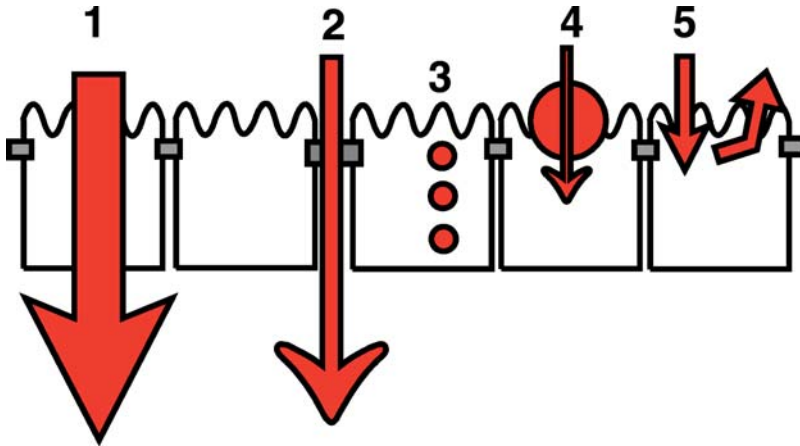


Figure 8.2 Possible drug transport pathways across the intestinal mucosa, illustrating transcellular (1) and paracellular (2) modes of passive transport, transcytosis (3), carrier-mediated transport (4), and efflux transport (5). A combination of these routes often defines the overall transepithelial transport rate of nutrients and drugs.

passive transcellular route [10]. The rate of transport through the epithelium depends on the concentration gradient and the permeation characteristics of the compound through the unstirred water layer at the luminal surface boundary of the epithelium and through the apical and basolateral membranes. Transcytosis, a form of transport in which the nutrient/drug is transported through the enterocyte by small vesicles, is a third transport pathway across the intestinal epithelium. Especially proteins and small nucleotides are believed to cross the intestine in this way [155]. Some compounds are essential for the functionality of the human body (e.g., glucose, amino acids) and can be actively taken up from the intestinal lumen by specific carriers present in the apical membrane of enterocytes. This carrier-mediated transport also follows an electrochemical concentration gradient. Several drugs, such as dopamine, cephalosporins, and angiotensin-converting enzymes (ACE)-inhibitors, are actively absorbed by the enterocytes. Finally, efflux-mediated transport represents a fifth form of transport. In this case, drugs that entered the enterocytes by passive diffusion are being actively pumped out of the enterocytes, back into the intestinal lumen. During this transport process, an energy source such as ATP, electron transport, or an electrochemical gradient of another ion is required to move ions or molecules against their electrochemical potential gradients [155].

8.1.2.2. Biochemical Barrier Function

8.1.2.2.1. Intestinal Metabolism: Intestinal drug metabolism can occur by microflora present in the gut lumen, as well as by enzymes present in luminal fluids and in the intestinal mucosa [166]. Metabolism of xenobiotics by gut microflora is low in comparison to metabolism by the gut mucosa and liver [62]. However, the intestinal microflora (e.g., *Bacteroides* and *Bifidobacteria*) may play an important role in the first-pass metabolism of compounds that are poorly or incompletely absorbed by the gut mucosa, especially in the lower parts of the intestine. This bacterial metabolism is largely degradative,

hydrolytic, and reductive, in contrast to the predominantly oxidative and conjugative metabolism that occurs in the intestinal mucosa.

Phase I metabolism by intestinal cytochrome P450 enzymes (CYP) has long been considered a relatively minor determinant of oral drug absorption, because concentrations normalized for the entire intestine are estimated to be ~20- to 200-fold lower than those found in the liver [20]. However, enzymes of the CYP3A subfamily, considered the major phase I drug metabolizing enzymes in humans, have been described to be expressed at high levels in the mature villus tip enterocytes of the small intestine [94, 73]. CYP3A4, accounting for ~70% of the CYP content in human enterocytes, and CYP3A5 are the major CYPs expressed in human intestine, whereas much lower levels of CYP1A1, CYP2C8, CYP2C9, CYP2C10, CYP2D6, and CYP2E1 could be detected [166]. Expression levels of intestinal CYP3A4 can be induced by drugs and food components [170, 76]. CYP3A5 does not seem to be inducible and, although it has similar substrate specificity to CYP3A4, demonstrates significantly different catalytic activities [127].

Esterases form another important group of metabolizing enzymes. These enzymes are characterized by a broad tissue distribution and play a role in the biotransformation of a vast number of structurally diverse drugs (e.g., ester- and amide-containing drugs). Besides arylesterases, lipases, acylesterases, and pancreatic hydrolases, the class of the carboxylesterases forms an important group of esterases present in the gut. Carboxylesterases are often considered to be the main esterases responsible for the activation of ester prodrugs, which are mainly used to overcome the poor membrane permeability of a pharmacologically active compound. After absorption by the intestine, the prodrug can be hydrolyzed by esterases to restore the parent drug in the bloodstream [163]. However, the luminal and mucosal esterase activity may cause a presystemic activation and thus a decreased absorption of the lipophilic prodrug.

The example of amprenavir, an HIV-1 protease inhibitor, shows that intestinal metabolism can also be used as a strategy to enhance the bioavailability of compounds. In the biopharmaceutics classification system (BCS), amprenavir can be categorized as a class II compound: it is poorly soluble but highly permeable [51]. Fosamprenavir, the water-soluble phosphate salt of amprenavir, on the other hand, shows poor transepithelial transport. However, after oral administration of fosamprenavir, this compound is metabolized into amprenavir in the intestinal lumen and in the enterocytes mainly by alkaline phosphatases, resulting in an increased intestinal absorption [51, 174].

Other drug-metabolizing enzymes of interest include monoamine oxidase and a wide range of hydrolytic and phase II enzymes (e.g., acetyltransferases, glutathione-S-transferases, methyltransferases, sulfotransferases, and UDP-glucuronosyltransferases) [62, 79]. An interesting example of intestinal metabolism can be found in a study on dietary flavonoids [91]. The results of this study indicate considerable differences among the various types of dietary flavonoids. Small intestinal absorption ranged from 0% to 60% of the dose, and elimination half-lives ranged from 2 to 28 h. Absorbed flavonoids underwent extensive first-pass phase II metabolism in the small intestinal epithelial cells and in the liver. It was concluded that the most abundant flavonoids in the diet

did not necessarily produce the highest concentration of flavonoids (or their metabolites) in vivo [91].

8.1.2.2.2. Intestinal Efflux: In addition to metabolism, intestinal efflux is a limiting factor to the absorption of a variety of structurally unrelated compounds. The intestinal efflux component is responsible for an active secretion from the epithelial cells to the luminal side, or, in some cases, to the serosal side. Different efflux transporters have been identified and have been classified as ATP-binding cassette (ABC) proteins [74]. While P-glycoprotein (P-gp, MDR1, ABCB1) is the most extensively studied ABC efflux transporter that acts as a biological barrier by extruding toxic substances and xenobiotics out of the cell, it was demonstrated that BCRP (breast cancer resistance protein; ABCG2) and MRP2 (ABCC2) are more extensively expressed in human jejunum than P-gp [141]. The in vivo effect of efflux proteins in modulating the oral absorption of drugs is not fully understood. A study in man with 13 drugs that were all substrates for intestinal efflux transporters, such as P-gp, showed no significant influence of efflux transport on the in vivo absorption of the drugs [37]. However, other reports suggest that the role of intestinal efflux transporters in modulating oral drug absorption can be important and especially relevant for dual CYP3A/efflux transporter substrates. In such cases, the metabolism and efflux-affinity can severely influence intestinal absorption [28, 29, 42].

Different food components (e.g., fruit extracts) and commonly used pharmaceutical excipients (e.g., Tween 80) can interfere with secretory transport systems, leading to drug–food interactions [31, 43, 46, 167]. As for CYPs, inhibition and induction of efflux transporters have been reported as possible causes for drug–drug interactions [88].

8.2. In Vitro Models to Study Intestinal Absorption

As oral intake remains the preferred route of drug administration, it is important to have a good understanding of the intestinal absorption characteristics of drug candidates in an early stage of their development. Clearly, whole animal studies cannot be used as a screening tool in an early development stage; therefore, in vitro models of intestinal absorption have been developed [33]. Each of these models has its advantages and disadvantages, which are summarized in Table 8.2. This overview confirms that there is no perfect absorption model and stresses the importance of using and combining different absorption models.

In this chapter, the focus will be on membrane-based, cell culture-based, and ex vivo models that are currently used in the industry to predict intestinal absorption of new compounds.

8.2.1. Membrane-Based Models (PAMPA)

8.2.1.1. Background

The use of artificial membranes to investigate passive permeation processes has a long history, going back more than 40 years [68]. The parallel artificial membrane permeation assay (PAMPA) is an application of the filter-supported lipid membrane system [149] and was first introduced by Kansy and

Table 8.2 Strengths and weaknesses of models to study intestinal drug absorption [157, 25, 154, 33, 159, 69, 70, 171].

Absorption model	Strengths	Limitations
In silico	No animals required Prediction of intestinal absorption before synthesis of compound	Difficult to model active processes Difficult to model complex interplay of a multitude of factors
Physicochemical methods (e.g., log P, log D)	No animals required Easy, fast, and inexpensive	Only predictive for transcellular pathway Low predictive value
Brush border membrane vesicles IAM	Both animal and human tissue can be used Useful for mechanistic studies	Nonspecific binding Only predictive for a part of absorption process
Artificial membranes (e.g., PAMPA technique)	High throughput Relatively inexpensive Different lipid compositions available Good predictability	Only predictive for a part of absorption process Membrane retention of lipophilic compounds Dependent on lipid composition and pH
Isolated intestinal cells	Animal or human origin Relatively easy to perform	Important intervariability in preparation of cells Need for radiolabeled or fluorescent compound Limited viability of primary cells
Everted intestinal rings/sacs	Easy and inexpensive to perform Both animal and human tissue can be used Any segment of intestine Useful for mechanistic studies	Nonspecific binding Viability of tissue (<30 min) Suboptimal stirring conditions
Caco-2 cell system	Good screening model No bioanalysis (simple salt buffer solutions) Evaluation of transport mechanisms (e.g. polarity in transport) Evaluation of absorption enhancing strategies on a mechanistic basis Evaluation of toxicity of compounds Reduction in the number of laboratory animals Techniques available to increase biorelevance of model Human origin	Lack of mucus secreting cells resulting in absence of a mucus layer Presence of a thicker unstirred water layer compared to human small intestine Cancer cells, with different or no expression of metabolic enzymes (e.g., absence of CYPs) "Tighter" monolayer compared to human small intestine Inter- and intralaboratory variability of permeability data Long differentiation period Low expression of uptake transporters Static model

(cont.)

Table 8.2 (Continued)

Absorption model	Strengths	Limitations
Ussing chambers (Diffusion chambers)	Good screening model Good correlation with in vivo permeability data No bioanalysis (simple salt buffer solutions) Possibility to evaluate different regions of the gastrointestinal tract Evaluation of transport mechanisms (e.g., polarity in transport) Evaluation of absorption enhancing strategies on a mechanistic basis Well-defined absorptive area Good oxygenation	Tissue viability Presence of circular muscle layers during transport studies, resulting in possible under-estimation of the permeability Difficulties with unstirred water layer Tissue availability (human)
In situ intestinal perfusion	Closest model to in vivo situation Evaluation of intestinal absorption without influence of hepatic first-pass metabolism Intact blood flow	Implies anesthesia and surgery No screening tool More difficult analysis due to biological media (e.g., blood) Laborious and time-consuming Relevance for human situation not always clear

coworkers as a rapid in vitro assay of transcellular permeation [67]. To make lipid membranes, phospholipids and other membrane constituents are added to the filter support as a solution in an organic solvent. In this first setup, a 96-well microtiter plate was completely filled with aqueous buffer solutions (pH 7.4/6.5) and was covered with a microtiter filterplate in a sandwich construction [67]. In the initial PAMPA experiments, the phospholipid composition of mammalian membranes was mimicked by using a 10% dodecane solution of egg lecithin [a mixed lipid containing phosphatidylcholine (PC), phosphatidylethanolamine (PE), phosphatidylinositol (PI), and cholesterol] [16]. Kansy and coworkers were able to relate their measured fluxes to human absorption values with a hyperbolic curve, resembling very much the relationship obtained in Caco-2 screening [67]. However, they experienced difficulties with polar compounds ($M_w < 250$) that are transported via the paracellular pathway and with actively transported compounds. Another disadvantage was the strong dependency of the membrane permeability on pH, especially with compounds having pK_a values near the pH of the incubation buffer used [67]. Additionally, the permeability of some basic compounds at pH 6.5 was underestimated.

8.2.1.2. Lipid Composition

As different tissues have different lipid compositions [112], several groups have worked on the composition of the lipid solutions to overcome these initial PAMPA issues. Sugano and coworkers investigated the influence of the chain length of the organic solvent on the permeability of a small set of compounds over a PC membrane [136]. They reported an enhanced permeability with

shorter chain alkyldienes, probably due to their lower viscosity. They also added an anionic compound to the lipid composition in order to mimic the intestinal lipid membrane, thus increasing the affinity of basic compounds to the membrane [136]. The best-performing lipid composition consisted of PC (0.8%), PE (0.8%), phosphatidylserine (0.2%), PI (0.2%), and cholesterol (1.0%). Sphingomyelin, one of the main constituents of the intestinal membrane, could not be added, due to its low solubility in 1,7-octadiene. This setup allowed performing the permeability measurements at pH 6.5 only, while obtaining a better prediction of oral drug absorption [136]. In a further study, the group of Sugano investigated the influence of pH conditions and cosolvents in their PAMPA setup [137].

In a second approach, Sugano et al. [138] tried to consider paracellular transport in addition to transcellular permeation. The prediction of the paracellular transport potential was based on size and charge parameters together with artificial membrane permeability in relation to known human absorption values. Other groups have focused on the paracellular route by modification of the assay [26].

Wohnsland and Faller ([175] performed measurements using a thin (9–10 μm) supported, phospholipid-free hexadecane layer. To validate their model, they used 32 well-characterized chemically diverse compounds. The permeability values obtained with their model could be correlated with known human absorption values if the maximum permeability obtained at different pH was taken into account. However, several disadvantages are related to this method. For hydrophilic drugs, hexadecane by itself has an increased barrier function in comparison with membranes. In addition, the hexadecane layers are not very stable, which makes this assay difficult to apply as a routine screening method. The advantage of this PAMPA setup is that it appears to be a satisfactory substitute for obtaining alkane–water partition coefficients, which are usually very difficult to measure directly, due to the poor solubility of drug molecules in alkanes.

Zhu and coworkers used hydrophilic filters (low protein binding PVDF) in their model [179]. This change in the setup resulted in a significant transport time reduction to 2 h (compared with more than 10 h for a hydrophobic filter) without loss of information for low permeability compounds.

Recently, the effect of the lipid composition on the permeability in PAMPA was investigated [129]. By varying the phosphate head group and the saturation degree of the acyl chain, differences in transport were observed for a set of five model compounds, which was due to changes in membrane fluidity and ion pairing [129].

Avdeef and coworkers continuously introduce new ideas to optimize and extend the original PAMPA method [15, 119, 103, 17, 18, 19]. The commercially available system reported by Avdeef and coworkers [13, 15, 16] is an extension of the original approach by Kansy [68]. In this PAMPA assay, a sandwich is formed from a 96-well microtiter plate and a 96-well microfilter plate, such that each composite well is divided into two chambers: donor at the bottom and acceptor at the top, separated by a 125- μm thick microfilter disc (with 0.45 μm pores), coated with a 2% dodecane solution of dioleoylphosphatidylcholine (DOPC), under conditions that multilamellar bilayers form inside the filter channels when the system contacts an aqueous buffer solution.

8.2.1.3. Applications of PAMPA

PAMPA can quickly provide information about passive-transport permeability that is not complicated by other mechanisms (e.g., active transport, paracellular transport, and metabolism) [103]. The procedure is used increasingly in pharmaceutical research in major pharmaceutical companies as well as in CROs [13, 137, 175, 179, 165, 119, 70]. However, it should be stated that PAMPA to date comprises numerous methods applied in various laboratories using different membrane constituents, sink conditions, permeation times, etc., which makes interlaboratory comparison extremely difficult. Therefore, standardization and validation methods of this technique should be introduced.

The assay is generally carried out in the 96-well format using the sandwich construction. As PAMPA focuses on high throughput, the concentration of the analytes in the acceptor wells after incubation is determined by rapid UV measurements at various wavelengths using a UV plate reader. However, for compounds lacking a UV chromophore or with a low UV extinction coefficient, LC/MS has been introduced as a detection method for determination of PAMPA permeability values [89, 95]. LC/MS detection offers greater sensitivity and selectivity as compared to UV-VIS detection for the PAMPA assay. This application is very useful when determining permeability of poorly soluble compounds in combination with solubilizer interfering with UV-VIS detection [89].

PAMPA is often used at various pH values in order to measure the permeability pH profiles, as the permeability of ionizable compounds depends heavily on the pH of the buffer. Since the pH range of the intestinal tract varies between pH 6 and 8, this is the range of pH values most often used. Kerns recommended to measure in a range from pH 4 to pH 7.4, in order to predict both bases and acids correctly [72]. Ruell and colleagues used permeation pH profiles from pH 4 to pH 9, together with the pK_a values of the compounds under investigation, to establish the optimum pH value for a single pH PAMPA measurement [119]. The Double-sinkTM conditions are offered commercially by pION. This method combines pH gradients between donor and acceptor compartments, depending on the acid/base properties of the analytes, with the use of a surfactant in the acceptor compartment, mimicking serum albumin and trapping mainly neutral compounds [18].

8.2.1.4. Modifications to Further Optimize PAMPA

A major problem that is encountered with different absorption models is membrane retention [173, 124, 13]. This phenomenon occurs especially with lipophilic compounds, which represent an increasing collection of compounds in current drug discovery programs. Unfortunately, this problem is often not taken into account [177]. A simple method to correct for membrane retention was introduced by Youdim and colleagues [177]. They suggested calculating the mass of the compound lost in cells or membranes from the difference between the total starting amount and the amounts in donor and receiver compartments at the end of the experiment. However, this methodology can be applied only for stable compounds. Compound degradation and compound retention to filters and plastic would then affect the accuracy of the permeability calculation. Additional experiments and analysis would be required to reduce these errors and the use of plastics and filters should be consistent and well-characterized.

Problems with highly lipophilic compounds ($\log D_{\text{pH}7.4} > 2.5$) might also be related to reduced solubility and variable sink conditions [124]. Sink conditions can hardly be achieved for lipophilic compounds because of the difficulty to abolish the back-flux from the acceptor to the donor compartment. Different strategies have been explored to overcome these problems. Addition of glycocholic acid to the donor solution in concentrations below the critical micelle concentration has been evaluated [68]. However, the observed permeabilities were only slightly altered by the inclusion of glycocholic acid in the test medium. This was probably due to solubilization effects as well as the formation of poorly absorbable drug-bile complexes [68]. Similar results were obtained for very lipophilic compounds in the 2% DOPC—dodecane lipid set-up [15]. Addition of taurocholic acid to the donor solution was observed to significantly increase permeabilities, but addition of sodium lauryl sulfate arrested membrane transport for cationic surface active drugs [15]. Sugano and coworkers studied the effect of PEG-400, dimethyl sulfoxide (DMSO), and ethanol in PAMPA [137]. DMSO and PEG-400 dramatically reduced the permeability of several of the molecules studied. The use of ethanol as a cosolvent resulted in increased permeabilities for some compounds and reduced permeabilities for other compounds. This effect of ethanol is probably due to a combination of two events: (1) the lower membrane-medium partition coefficient of water–cosolvent mixtures and (2) the decreased dielectric constants of the cosolvent–water mixture resulting in a higher proportion of the ionizable molecule in the uncharged state [137]. Another strategy is to use micelles to trap compounds in the acceptor compartment [16]. The application of sink conditions can also reduce membrane trapping by more than 50% for highly lipophilic compounds [16]. Sink conditions can also be created by applying serum proteins, usually bovine serum albumin (BSA), in the acceptor compartment in a concentration range of 0.1–3% [69].

Another important aspect is the presence of the unstirred water layer (UWL). Especially for lipophilic compounds, this UWL can function as the rate-limiting barrier when assessing their permeability. In human intestinal tissue, the thickness of the UWL has been estimated to be 30–100 μm [84]. However, in unstirred PAMPA assays, a value of 1900–3800 μm has been estimated, depending on the type of experimental conditions used [103]. The first attempts to reduce the thickness of the UWL in PAMPA did not work out [14]. When the PAMPA sandwich was shaken at a rate of 50–100 rpm, the thickness was reported to be 300 μm [175]. However, using another measuring technique, the estimated UWL thickness was 500–1200 μm at 75 rpm [103]. By introducing individual-well magnetic stirring, Avdeef and coworkers could reduce the size of the UWL in PAMPA to the *in vivo* range [17]. At a stirring speed of 622 rpm, the thickness of the UWL was reduced to only 13 μm . By applying this technique, the effective permeability of lipophilic compounds was spectacularly increased and the assay time could be reduced from 15 h to 15 min [17].

8.2.2. Cell Culture-Based Models (Caco-2)

As primary cultures of enterocytes fail to form a polarized epithelial monolayer and therefore, do not display an apical and basolateral surface, continuously growing (tumor) cell cultures can be used to investigate the permeation and

Table 8.3 Cell culture models commonly used for permeability assessments [81, 23, 122].

Cell line	Species or origin	Specific characteristics
Caco-2	Human colon adenocarcinoma	Well-established cell model Differentiates spontaneously and expresses some relevant efflux transporters (e.g., P-gp, MRP1–2, BCRP) Interlaboratory differences
MDCK	Dog kidney epithelial cells	Polarized cells with low intrinsic expression of transporters Suitable cell line for transfections
LLC-PK1	Pig kidney epithelial cells	Polarized cells with low intrinsic expression of transporters Suitable cell line for transfections
2/4/A1	Rat fetal intestinal epithelial cells	Temperature-sensitive differentiation More suited to study paracellular transport (leakier pores) than Caco-2
TC7	Caco-2 subclone	High taurocholic acid transport Stable expression of CYP3A4 Expression of CYP3A5 Low expression of P-gp
HT29	Human colon	Co-culture containing mucus-producing goblet cells

transport of drugs across the intestinal barrier. An overview of cell culture-based models commonly used for permeability assessment can be found in Table 8.3.

The Caco-2 cell model (derived from a human colon adenocarcinoma) has been the most popular and the most extensively characterized cell-based model in examining the permeability of drugs in the pharmaceutical industry and in academia [24]. Caco-2 cells undergo spontaneous enterocytic differentiation in culture to become polarized cells (i.e., having an apical and basolateral surface) with well-established tight junctions, and exhibit many functions of normal enterocytes. They express many brush border enzymes, some CYP isoenzymes (but not CYP3A), and phase II enzymes, including glutathione S-transferase and sulfotransferase [33]. Many active transport systems found in small intestinal enterocytes have been characterized in Caco-2 cells, including transport systems for glucose, peptides, amino acids, bile acids, and monocarboxylic acids, as well as transport proteins for organic anions and cations, P-gp, and MRPs [48, 91, 30].

Evaluation of the epithelial integrity can be performed by measuring the transepithelial electrical resistance (TEER). TEER values ranging from 150 ohms.cm² up to 600 ohms.cm² have been reported. An alternative method for assessing the monolayer integrity is to monitor the flux of hydrophilic marker molecules that pass the monolayers by the paracellular route (e.g., mannitol, Na-fluorescein, or atenolol).

8.2.2.1. Applications of Caco-2 Cells in Drug Discovery and Development

8.2.2.1.1. (High-Throughput) Screening of Drugs: Cell culture models have been employed in the screening of the intestinal permeability of libraries of new drug entities that have been generated through combinatorial chemistry

and high-throughput pharmacological screening [9]. The biggest challenge lies in accurately screening a large number of compounds in a short period of time. This can be achieved by cassette dosing (i.e., simultaneous testing of different compounds in 1 mixture, $N > 1$). The cassette dosing method can save valuable time, money, and resources, and can be used to achieve structure–permeability relationships, which can be useful in the design of bioavailable drugs. However, care should be taken to avoid drug–drug interactions during the coinubation and analysis. Another often applied technique is that of cassette analysis: the permeability screening of the compounds is performed separately, but after the screening experiment samples are pooled and the compounds are analyzed together. Automation, miniaturization, shorter cell culturing time, and analytical advances have also enabled the exploration of cassette dosing in cell culture models to drive the efficiencies even higher (see further).

8.2.2.1.2. Evaluation of Prodrugs for Enhanced Oral Absorption: Prodrug synthesis is one of the methods to enhance drug absorption of low permeability compounds. Evaluation of the use of prodrugs in an *in vivo* model is difficult and resource-intensive. Therefore, Caco-2 cells have been extensively used to assess the relative ability of various prodrugs to enhance the transport of drugs across the intestinal epithelium. In our laboratory, Caco-2 cells have been used to investigate the absorption of antiviral prodrugs and to evaluate strategies to enhance the absorption of esterase-sensitive prodrugs [11, 162, 6]. The addition of fruit extracts containing various esters resulted in a threefold increase in the transport of tenofovir disoproxil across Caco-2 monolayers [162]. Compared with the transport of the active parent compound adefovir, the use of an ester prodrug, adefovir dipivoxil, resulted in a 100-fold increase in transport of adefovir in the Caco-2 model [6].

8.2.2.1.3. Evaluation and Selection of Absorption Enhancers: The Caco-2 model is routinely used for assessing the impact of excipients used in drug delivery systems to enhance bioavailability and for mechanistic absorption-enhancer studies. The effects of several excipients, including Cremophor EL, Tween 80, and PEG-300, on the bidirectional transport of taxol were evaluated in the Caco-2 system [59]. After inclusion of the excipients, an increase in absorptive transport and a decrease in secretory transport of taxol could be observed, which was due to the (partial) inhibition of P-gp [59]. In another study, the effect of four different permeation enhancers (palmitoyl-DL-carnitine chloride, *N*-trimethyl chitosan chloride, sodium caprate, and EGTA) on the transport of clondronate was evaluated [114]. The addition of several of these permeation enhancers to the transport medium led to an increased transport of clondronate without reducing the viability of the cells. Other examples of compounds that have been evaluated for their absorption-enhancing properties in the Caco-2 system can be found in literature [115, 143, 110, 109].

8.2.2.1.4. Assessment of Drug–Drug, Drug–Food, and Drug–Excipient Interaction at the Level of Transporters: Carrier-mediated transport (influx and efflux), which influences the absorption of drug molecules, is generally a saturable process. This raises the possibility of competition for an enzyme or transporter during coadministration of a drug and an excipient. Drug interactions result in higher or lower exposure to drugs than would be predicted on the basis of the absorption kinetics of the single agents. Since Caco-2 cells

express different transporters, they can be used as an experimental tool for drug–drug, drug–food, and drug–excipient interaction studies at the level of transporters. Several examples of the interaction between P-gp substrates and P-gp inhibitors are known in the literature [111, 166, 167, 106], as well as between the substrates and inhibitors for other efflux mechanisms including MRP1 (ABCC1), MRP2 (ABCC2), and BCRP (ABCG2) [1, 60, 96, 126, 148]. In our laboratory, we have used the Caco-2 cell model to screen for the possible inhibitory effect of fruit extracts on P-gp-related efflux carriers [43]. In the first phase, the Caco-2 model was used to assess the effect of 68 fruit extracts on the secretory transport of cyclosporin A (CyA), a well-known P-gp substrate. In the second phase, nine extracts were retained to investigate their effect on the bidirectional transport of CyA, showing that strawberry, orange, apricot, and mint extract exert an inhibitory effect on intestinal P-gp-related functionality without compromising the viability of the Caco-2 cells [43, 44]. The results of this study suggested that coadministration of fruit extracts might be a conceptually safe and useful strategy to enhance the intestinal absorption of P-gp substrates.

Rege and colleagues have studied the effect of nonionic surfactants (e.g., Cremophor EL, Tween 80, and TPGS) on membrane transporters [116]. Similar results for vitamin E TPGS using talinolol and rhodamine 123 as P-gp substrates have been reported by Bogman et al. ([32] and Collnot and coworkers [40], respectively.

8.2.2.1.5. Prediction of a Dissolution–Absorption Relationship: Instrumented approaches for the assessment of drug transport across epithelial barriers are discussed in detail in Chapter 19. Therefore, only a brief outlook on the subject is given here. To predict dissolution–absorption relationships and the contributions of dissolution and intestinal permeation to overall drug absorption, Ginski and coworkers developed an integrated dissolution/Caco-2 system [52]. This integrated system consists of two steps. In the first step, a dosage form is dissolved in a dissolution vessel and the resulting solution is transferred to the Caco-2 system by a peristaltic pump. In the second step, the drug is transported from the apical to the basolateral (A-to-B) chamber of the Caco-2 system. This system showed a good correlation with data obtained from clinical studies. However, the system does not take into account the pH change along the GI tract. The system developed by Kobayashi and colleagues takes into account the solid drug dissolution and pH change in the GI tract [75]. In this new system, a dosage form is added into a drug-dissolving vessel filled with a solution at pH 1.0. In the second step, the dissolved drug is transferred to a pH adjustment vessel (pH 6.0) after which the drug solution is transferred to the apical surface of a Caco-2 monolayer to determine the permeation rate of the drug. A similar model was used to evaluate the pH-related changes in drug absorption [54] and to evaluate the oral absorption of pH-independent controlled-release preparations [139]. The integrated dissolution/Caco-2 system is useful for the determination of the influence of dissolution and permeability on overall drug absorption in humans. The system may prove to be a valuable tool in the biopharmaceutical characterization of oral solid dosage forms.

8.2.2.1.6. Cytotoxicity Studies: Cell culture models have been employed to determine the cytotoxicity of new chemical entities, drug delivery systems, and excipients. Various techniques are available to assess cytotoxicity and cell

viability, including TEER measurements, transport of trans- and paracellular markers, confocal laser scanning microscopy, release of lactate dehydrogenase (LDH), trypan blue exclusion assay, NRU (neutral red uptake), and MTT ((3-(4,5-Dimethylthiazol-2-yl)-2,5-diphenyltetrazolium bromide) assay. Very often researchers use only the TEER values to estimate the possible cytotoxic effects of the compound/excipient under investigation. However, the relationship between TEER and cytotoxicity is not very clear and nonlinear: above a certain level of TEER, very small increases in junctional permeability may produce large decreases in resistance, while at low-resistance values relatively large changes in transjunctional flux of tracer will often be associated with very modest changes in TEER [121]. Additionally, a decrease in TEER is not necessarily predictive for a cytotoxic effect as this decrease can be reversible. Kotze and colleagues reported that chitosan hydrochloride, chitosan glutamate, and *N*-trimethyl chitosan chloride are able to decrease TEER in a reversible manner [78]. Sandri and coworkers demonstrated that the absorption-enhancing properties, resulting in TEER decrease, of three grades of hyaluronic acid were not accompanied by cellular toxicity [123]. Therefore, the best way to assess cytotoxicity is to combine different techniques. For example, to evaluate the compatibility of FaSSIF (Fasted state simulated intestinal fluid) and FeSSIF (Fed state simulated intestinal fluid) with the Caco-2 model, a combination of TEER measurement, MTT assay, and histological examination was used [63].

8.2.2.2. Limitations and Drawbacks

8.2.2.2.1. Analytical Limitations: A major challenge of cell-based permeability models is the analysis. To meet the requirement of the analysis of a significant number of samples generated in discovery, high-throughput, sensitive, and accurate methods with a short analysis time are necessary. The high salt content of phosphate-buffered transport media interferes with ionization, thus complicating the development of LC/MS methods [23]. Traditional methods might not be optimal when special solubilizers and additives are used in the transport medium. Analytical methods with the speed of a UV-plate reader and the sensitivity of LC/MS would be ideal for preventing the bottleneck at the analytical end of permeability studies. Modifications to an analytical method that simultaneously quantifies marker compounds (e.g., atenolol, propranolol, and talinolol as marker compounds for paracellular, transcellular, and P-gp-mediated efflux, respectively) and discovery compounds can improve the efficiency of the analysis, as well as the quality of cell-based data [12].

8.2.2.2.2. Cacophilicity and Nonspecific Binding: Similar to the PAMPA model, the unstirred water layer can become rate-limiting for the transport of rapidly absorbed compounds, especially lipophilic compounds. Therefore, stirring the plates during transport experiments is recommended to reduce the effect of the UWL [55]. Besides the UWL, membrane retention, and perhaps more important, nonspecific binding to the plastic and to the filter support are significant factors to be considered when performing Caco-2 transport experiments. These effects can lead to a physical loss of the compound, resulting in a reduced concentration in the donor compartment (driving force) and a reduction of the concentration in the receiver compartment. This will result in an underestimation of transport across the monolayers and to false negatives. Therefore, a mass balance is required to correctly interpret the outcome of the experiments. A few approaches may be able to minimize nonspecific binding.

Rather than using the initial donor concentration, the final donor concentration at the termination of incubation can be used. Another approach to reduce non-specific binding involves the addition of serum proteins [80, 120] or micelle-forming excipients, such as Gelucire 44/14, Cremophor EL, or TPGS, [45] to the receiver compartment, leading to an improved assay recovery and better predictability of the model [64].

8.2.2.2.3. Low-Solubility Compounds: A significant percentage of new drug candidates cannot be evaluated in permeability models due to their poor aqueous solubility. Addition of organic cosolvents (e.g., DMSO, propylene glycol, *N*-methyl-2-pyrrolidone, NMP) to the donor solution is a possible way to overcome this problem. However, as the tight junctions are easily compromised, even at low concentrations of cosolvents (<1%), this creates only a limited solution. Inclusion of other solubility improving agents, such as cyclodextrins or bile acids, can be another strategy to work around this issue [64].

8.2.2.2.4. Expression of Transporters: Although pharmaceutically important (uptake) transporters, including peptide transporters, organic cation transporter, and organic anion transporter, are expressed in Caco-2 cells, they are quantitatively underexpressed compared to the *in vivo* situation [140]. Several β -lactam inhibitors and ACE inhibitors, which are known to be substrates of dipeptide transporters, show a poor permeability across Caco-2 monolayers despite being completely absorbed *in vivo* [38]). In addition to the lack of expression of various uptake transporter proteins, another issue is the different expression levels of efflux transporters in Caco-2 cells compared to human small and large intestine [141, 4, 128]. For instance, BCRP (ABCG2) exhibited a 100-fold lower transcript level in Caco-2 cells compared with jejunum [141].

8.2.2.2.5. Other Limitations: The small intestine is a very dynamic environment: the pH of the medium changes, the intestinal content is propelled by muscular contractions, food and xenobiotics are being digested by different enzymes and after absorption of compounds by the enterocytes, these compounds reach the blood vessels to be transported throughout the body. In contrast to the *in vivo* situation, the Caco-2 model is a static model consisting of one single cell type which is unable to secrete mucus. The unstirred water layer is thicker than the one *in vivo* and for some compounds it is difficult to work under sink conditions.

Another drawback is the lack of correlation for paracellularly transported compounds. For example, some low molecular weight hydrophilic compounds (e.g., ranitidine, atenolol, furosemide, and metformin) showed poor permeability in the Caco-2 model despite an absorption larger than 50% in humans [168]. This is due to the smaller size of the paracellular channels (controlled by tight junctions) in the Caco-2 model compared to human small intestine [146].

8.2.2.3. Improvements

8.2.2.3.1. Reduced Culture Time: Caco-2 cells are usually grown for at least 20 days to form differentiated monolayers on a porous filter support, forming an apical and a basolateral compartment. The 20-day culture time is required to obtain tight junctions, cell polarity, and an adequate expression of drug efflux mechanisms. For economical reasons, various attempts have

been made to reduce culture time [39, 86]. Fast growth of the Caco-2 cells can be obtained by altering the filter support, the filter coating, the seeding density, and the cell culture medium [23, 39]. After growing the cells for 3 days using the Biocoat[®] technique, the permeability of 18 passively absorbed compounds was found to correlate well with the extent of absorption in man [39]. However, due to the short culturing time, the expression of efflux transporters, such as P-gp, was significantly lower than in the original model, making the model not suitable for mechanistic and bidirectional studies.

8.2.2.3.2. Physiological Buffer Systems: Recently, a lot of efforts have been made on how to increase the biorelevance of the Caco-2 model [63, 47, 64, 65, 105]. Historically, the media used for Caco-2 experiments were buffered at pH 7.4 on both sides of the monolayer. The pH in the cellular interstice and blood compartment is known to be 7.4. However, the pH in the upper GI tract under fasted conditions ranges from 5.0 to 6.5, with an acidic microclimate existing just above the epithelial cell layer estimated to be between 5.8 and 6.3 [90]. The pH of the apical medium can have a critical effect on the transport of drugs, especially for drugs with a pK_a close to 7, or when pH-dependent transporters are involved.

Although useful for standard screening tests, the utility of a pH-gradient setup can be questioned when performing mechanistic studies in the Caco-2 system. Donor and acceptor solvents should indeed be similar or identical when determining bidirectionality of transport in order to avoid bias from external parameters [64]. Neuhoff and coworkers demonstrated the impact of a pH gradient when performing bidirectional transport experiments of weak bases and acids [101, 102]. The change of the unionized/ionized fraction of the drugs in the presence of a pH-gradient may alter the observed transport of the compounds by a “false” efflux component [101, 102]. Therefore, it has been suggested to use the pH-gradient setup when performing standard screening experiments for the absorptive ranking of compounds and to use an iso-pH setup when performing mechanistic efflux studies or when compounds are moving forward through the later development stages [64].

The inclusion of bile salts into the apical compartment has been proposed to enhance the solubility of drug compounds, as well as to increase the physiological relevance of the model. More complex media containing bile salts, such as FaSSIF, have also been evaluated in the Caco-2 model [63, 65]. In a study with 19 model compounds, no effect of FaSSIF was observed on the total predictability of the model [65]. However, an impact was demonstrated on the bidirectional transport of actively transported drugs and on the recovery, permeability, and solubility of poorly water-soluble drugs [65]. The observed differences were attributed to a P-gp inhibitory effect of sodium taurocholate, micellar encapsulation, and/or increase of the solubility of lipophilic drugs. When evaluating the possibility to use human intestinal fluid as a biorelevant medium in the Caco-2 model, an important P-gp attenuating effect of human intestinal fluid was observed [47].

8.2.2.3.3. Miniaturization: Currently, permeability studies using cell monolayers are conducted in automation-friendly 12- or 24-well multiwell plates. Unfortunately, further miniaturization (96- or 384-well cell models) has been technically difficult to achieve because of the small surface area of the

monolayer. Recently, there have been reports of the successful implementation of Caco-2 cells in 96-well plate format for both permeability and P-gp interaction studies [2, 92]. This will result in an increased throughput of the assay, reduced cost, and a decrease in the amount of compound required for permeability assessments.

8.2.2.3.4. Standardization: Despite the use of similar transport study protocols, permeability values obtained with the Caco-2 model in different laboratories differ [168, 35]. Small differences in culturing conditions (seeding density, composition of culturing media), experimental conditions (composition and pH of transport media, washing steps), and age of the cells (passage number and culture duration) can generate significant interlaboratory differences [122]. The expression level of P-gp and other transport proteins is known to vary significantly with the age of cell cultures [35, 3, 27, 128]. An improved scenario would be if each laboratory incorporated a set of standard internal reference compounds as controls and provided acceptance criteria for their cell culture models [64]. Therefore, standardization of cell culture procedures and protocols across all laboratories is required. A recent study has addressed these problems and has produced standard operating procedures for passive permeability testing (European Commission-Joint Research Centre, IHCP, ECVAM, study contract "Development and refinement of a Caco-2 cell in vitro model of intestinal barrier function," contract ISS/ECVAM 17299–2000–12 FIED ISP IT). This report is available upon request at <http://ecvam.jrc.it/index.htm>. Parts of this report can also be found in a publication by Le Ferrec and colleagues [81]. FDA recommends the use of compounds with high, low, and zero permeability, passive and active transport, and use of efflux markers for this purpose. A list of suggested internal standards can be found on <http://www.fda.gov/cder/guidance/3618fnl.pdf> (Guidance for Industry Waiver of In Vivo Bioavailability and Bioequivalence Studies for Immediate-Release Solid Oral Dosage Forms Based on a Biopharmaceutics Classification System). The simultaneous use of model compounds requires that they do not express cytotoxicity, do not interact with each other during permeation, and that they are easily detected. Therefore, the use of different sets of model compounds has to be validated before the actual experiments with drug candidates can be performed.

8.2.2.4. Alternative Cell Lines to Caco-2

8.2.2.4.1. MDCK: Madin-Darby canine kidney (MDCK) cells have received attention as an alternative to Caco-2 cells for permeability measurements. When grown under standard culture conditions, MDCK cells develop tight junctions and form monolayers of polarized cells. The main advantage over Caco-2 cells is the shorter culture time to confluence (3–5 days). The transepithelial electrical resistance of MDCK cells is lower than that of Caco-2 cells and thus, closer to the TEER of the small intestine in vivo. The permeability coefficients of hydrophilic compounds are usually lower in Caco-2 cells than in MDCK cells, which is consistent with the lower TEER values for MDCK cell monolayers. The nonhuman (canine) and nonintestinal (renal) origin of MDCK cells is considered as a disadvantage. They have low expression levels of transporter proteins and low metabolic activity [34]. MDCK cells that are stably transfected with P-gp/MDR1 are often proposed as an alternative for Caco-2 cells to study bidirectional transport of compounds and, more

particularly, to evaluate the influence of P-gp on drug transport. However, it has been suggested that the apparent kinetics, constants, and affinities of substrates determined in the MDCK-MDR1 cell model may be different than the values obtained in Caco-2 cells. These differences in substrate activity could result from differences in the relative expression levels of total P-gp in Caco-2 and MDCK-MDR1 cells and/or differences in the partitioning of substrates into these two cell membrane bilayers [144].

8.2.2.4.2. *LLC-PK1*: Cells derived from pig kidney epithelial cells (LLC-PK1) have been used as an alternative to Caco-2 cells for assessing the permeability for test compounds [153, 85]. LLC-PK1 cells are more easily transfected than Caco-2 cells. Especially the LLC-PK1 line stably transfected with P-gp/MDR1 has been reported as a tool to study bidirectional transport of compounds [142, 58, 180].

8.2.2.4.3. *TC7*: Clonal selection has been used to obtain Caco-2 cells with stronger metabolic competence [36]. The TC7 subclone has been characterized for its ability to transport and metabolize endogenous compounds and xenobiotics. After exposure to methotrexate, the TC7 subclone was shown to acquire a stable expression of CYP3A4, the major small intestinal CYP3A isoform [36]. A direct comparison of CYP3A isoforms mRNA expression in parental Caco-2 cells and in TC7 cells, in the absence of specific inducers, showed that TC7 cells expressed both CYP3A4 and CYP3A5 while the parental Caco-2 cells expressed only CYP3A5 [113, 49]. It was therefore suggested that the metabolic competence of TC7 cells makes this clone a valid alternative for the parental cell line, particularly suitable for drug transport and biotransformation studies [81]. However, the degree of expression of CYP3A in TC7 cells still remains lower than the expression level in human enterocytes.

8.2.2.4.4. *2/4/A1*: An interesting cell model is 2/4/A1 which originates from fetal rat intestine. This model might better mimic the permeability of the human small intestine, particularly with regard to passive paracellular transport [145–147]. The paracellular pore radius of 2/4/A1 was estimated to be 9.0 ± 2.0 Å, which is similar to the pores in the human small intestine (pore size in Caco-2 is estimated to be 3.7 ± 0.1 Å) [146]. The transport rate of poorly permeable compounds in 2/4/A1 monolayers was comparable with that in the human jejunum and was up to 300-fold higher than that in the Caco-2 cell monolayers. The transport of drugs with high permeability was comparable in both models [146].

8.2.2.4.5. *HT29*: Wild-type HT29 cells form multilayers of undifferentiated cells, which are not useful for intestinal permeability studies. Culturing wild-type HT29 cells in media containing galactose instead of glucose, however, leads to the selection of a subclone of HT29 that forms monolayers of polarized cells [56]. Several HT29 clones differentiate into enterocytic cells or mucus-secreting goblet cells. Two HT29 clones that secrete mucus are HT29-H and HT29-MTX [71, 36]. To increase the biorelevance of the Caco-2 model, cocultures with HT29-MTX and HT29-H cells have been developed [172, 57]. However, the expression of carriers involved in intestinal uptake of nutrients and drugs is significantly lower in these cocultures compared to the Caco-2 culture [57].

8.2.3. Ex Vivo Models (Ussing Chambers Technique)

8.2.3.1. Background

The Ussing chambers technique was originally developed by Ussing and Zerahn [160] and has since been used frequently in physiological studies concerning pharmacology and physiology of ion and water transport. Chapter 3 discusses available in situ and ex vivo models for the assessment of intestinal drug absorption in more detail. The original setup was further refined for GI permeability determinations by Grass and Sweetana [53]. The method utilizes excised intestinal segments (in some cases stripped of the serosa and the muscle layers), which are mounted between two diffusion cell compartments [157]. The serosal and the mucosal compartments are usually supplied with Krebs-Ringer bicarbonate buffer, which can be supplemented with additional elements including glucose, glutamate, fumarate, and pyruvate [44]. The buffer solution is continuously gassed with an O₂:CO₂ (95:5, carbogen) mixture to provide sufficient oxygen tension for maintaining tissue viability. Additionally, this gas lift [53] creates a fluid circulation in both compartments, thereby reducing the effect of the unstirred water layer on transport of lipophilic compounds. In order to avoid sometimes annoying foaming, especially when high amounts of proteins or surfactants are used in the buffer solutions, a stirring rotor system can be employed [156]. The test compound is added either to the mucosal or serosal side of the tissue to study transport in the absorptive or secretory direction, respectively.

8.2.3.2. Viability

The viability and integrity of the intestinal tissue mounted in the Ussing chambers remain controversial. Although drug transport in the Ussing chambers is usually followed for up to 150 or 180 min, intestinal edema and disruption of the villi have been reported to occur after only 20 min of incubation [107]. The phenomenon of edge damage might be an important factor in the loss of tissue viability [21], especially in chambers with a small exposed tissue area [135]. Polentarutti and coworkers monitored different sections of rat small intestine (duodenum, jejunum, ileum, and colon) over a time period of 180 min looking at the permeability of propranolol and mannitol in combination with the evolution of the electrical parameters and some morphological parameters [108]. They showed that permeability coefficients for propranolol and mannitol were significantly influenced by the duration of the experiment and that these time-dependent changes were related to changes in bioelectrical parameters and morphological alterations. However, other studies have demonstrated active transport of glucose for at least 120 min combined with limited transport of paracellular leakage markers, and a preserved ultrastructure [53, 132].

Electrophysiological parameters are widely accepted for monitoring the viability and integrity of intestinal segments in the Ussing chambers. In general, the potential difference (PD) is said to reflect the voltage gradient generated by the tissue, the transepithelial resistance (TEER or R_T) reflects the tissue integrity, and the short circuit current (SCC or I_{SC}) reflects the ionic fluxes across the epithelium [108]. Excluding tissue for experimental use by measuring the bioelectrical parameters of the intestinal segment before initiating transport studies is a common strategy to ensure sufficient quality of the tissue and to reduce variability [83, 158, 44, 152]. The bioelectrical parameters,

and therefore the tissue viability and integrity, are dependent on the overall prechamber treatment from the anesthesia of the rats to the mounting of the intestinal segments in the Ussing chambers.

Extracellular marker molecules, such as mannitol, inulin, Na-fluorescein, and PEG-400, have been used to verify a tight epithelium; they have also been used for testing the effects of enhancers and increased fluid absorption [159].

The more viable the segment is the better is the quality of the results. Based on the tissue viability data, extremes in permeability values can be discarded from the data set, resulting in better and more reliable results and a better overall understanding of drug transport [108].

In an attempt to increase the biorelevance of the Ussing chambers technique even further, the use of simulated intestinal fluids (FaSSIF and FeSSIF) as transport media was recently evaluated [105]. However, the potential difference collapsed to zero after 120 min when exposed to FaSSIF solution and permeability for mannitol was increased twofold. Electron micrographs revealed erosion of the villi tips and substantial denudation of the microvilli after exposure of the ileal tissue to FaSSIF and FeSSIF [105].

8.2.3.3. Applications of Ussing Chambers Technique

The major strength of the Ussing chambers technique is that it can be used for multiple purposes, as shown by several examples in the literature. The technique allows to determine transepithelial drug transport in combination with intestinal metabolism [117, 131, 6], to study regional differences in intestinal absorption, [91, 158, 100, 61, 21] or to study interspecies differences in intestinal absorption [118, 100]. Ussing chambers have also been used to assess the role of drug transporters in intestinal absorption. The functionality of several efflux transporters including P-gp, organic cation transporters, and MRPs in intestinal segments has been explored using the Ussing chambers technique [99, 44, 97, 130, 178]. Investigation of the influence of surfactants and excipients on the integrity of the tissue and on the permeability for compounds is another application of the Ussing chambers technique [77, 7, 130]. However, it must be stated that surfactants can be used only at low concentrations in systems equipped with the gas lift, due to foaming in the chambers.

The major drawback of the system is the possible underestimation of drug transport across the intestinal tissue due to membrane retention, which occurs especially for lipophilic compounds [176]. On the other hand, Ussing chambers are available which are manufactured from glass, which at least decreases drug adsorption on the chambers' walls. In the Ussing chambers, the transport of the compound across the whole intestinal tissue is assessed, including the muscle layers. This can be partly resolved by stripping the serosal muscle layer of the intestinal segment before mounting.

Similar to the PAMPA and the Caco-2 models, the experimental pH of the buffer solution can be changed in the Ussing chambers model. However, it seems that the impact of changing the pH of the mucosal (= apical) buffer solution is lower than for the other two systems [82]. This is probably due to the presence of the mucus layer retaining the microclimate pH regardless of the luminal pH using the Ussing chambers technique [82].

Recently, more importance is given to the link between the integrity of the mucosal epithelium on one side and the immune system on the

other. Intestinal models used to study the local changes in permeability and the barrier function related to different diseases, such as Crohn's disease and inflammatory bowel disease (IBD), are mainly in vivo models pre-treated with an immunological challenge. However, ex vivo animal models such as the Ussing chambers technique appear particularly useful to obtain insights in altered intestinal permeability to macromolecules including proteins [133].

8.2.3.4. In Vitro-In Vivo Correlations

Only a few studies on the correlation between data obtained with rat intestinal tissue in the Ussing chambers system and human absorption data have been performed [83, 158, 100, 169]. In a first report, the permeability of 12 passively transported compounds was compared using the Ussing chambers technique with rat intestinal tissue and single-pass perfusion in human jejunum [83]. Although very similar rank orders were obtained with both techniques, permeability values were fivefold higher in humans compared to rats. However, in a direct comparison of porcine, rat, and human intestinal tissue with the Ussing chambers technique, Nejdfor and coworkers found a higher permeability in rat compared to human intestinal tissue [100]. Watanabe and colleagues used the Ussing chambers method with rat intestinal tissue to predict the absorption of poorly water-soluble drugs in man [169]. Another study with 19 selected drug compounds with a wide range of physicochemical properties showed that the Ussing chambers model using rat intestinal segments was a very useful method to classify compounds with high and low permeability according to the BCS [158].

8.2.3.5. Concluding Remarks

The Ussing chambers technique is not designed as a high-throughput screening tool. However, when correctly used as a mechanistic secondary screening tool, well-suited for evaluation of new drug candidates, data from the Ussing chambers technique are more closely related to the in vivo situation than many of the other biological models available [159]. Clearly, none of the models discussed above will qualify individually as a universally applicable drug absorption screening tool.

8.2.4. Combination of Models

After discussing different models to predict the intestinal permeability, it is clear that a universal model which includes all parameters does not exist. Therefore, a combination of different in vitro models is generally required to predict intestinal drug absorption. Often a tiered approach is applied, which involves high-throughput (but less predictive) models for primary screening followed by low-throughput (but more predictive) models for secondary screening and mechanistic studies. To obtain the maximum permeability/absorption information in the least amount of time with minimal use of resources, a combination of PAMPA along with unidirectional Caco-2 experiments (A-to-B permeability) is becoming increasingly popular [72, 24]. Kerns and colleagues made suggestions for a tiered approach: during early drug discovery all compounds can be rapidly screened using PAMPA at a low and neutral pH in order to assess passive diffusion permeability as a potential for GI and cell assay permeation. During lead identification and optimization

phase, selected compounds can be additionally assayed by A-to-B Caco-2 experiments, which, in combination with PAMPA data, indicate susceptibility to additional permeation mechanisms (secretory and/or absorptive). Multiple directional Caco-2 experiments including the use of transporter inhibitors for complete characterization of permeation mechanisms can be conducted during late phase discovery to examine the selected candidates [72]. Balimane and colleagues recently recommended to simultaneously performing PAMPA and A-to-B Caco-2 experiments [24]. Based on the outcome of this set of experiments, a prioritization can be made for the compounds: if both PAMPA and A-to-B Caco-2 cell permeability values are low, then the compound will have a low intrinsic permeability and it is likely to show poor intestinal absorption in man. However, if the A-to-B Caco-2 cell permeability is low, but PAMPA values are high, then the compound is likely to be a substrate of an efflux transporter and not necessarily a poorly permeable compound in vivo [24]. Therefore, the parallel combination assessment of PAMPA and A-to-B Caco-2 cell permeability followed by more detailed bidirectional Caco-2 cell assays might be a path for research programs.

8.3. In Vitro Methods to Assess Intestinal Metabolism

Drugs can be metabolized either in the intestinal lumen or in the intestinal wall. The most common approach to determine drug metabolism in the intestinal lumen is by direct incubation with bacterial preparations, which can be gut content or pure culture of organisms of the GI tract of various mammalian species [62].

To determine the drug metabolism in the intestinal wall, a multitude of methods is available. The simplest and probably most widely used preparations for studying metabolic reactions are tissue homogenates and subcellular fractions. They provide data on pathways of intestinal xenobiotic metabolism and are eminently suited to screening new drug compounds for pre-systemic metabolism. This technique can also be used to gain information on the subcellular localization of enzymes. In a study in our laboratory, intestinal homogenates of different species were used in order to select a species for drug absorption studies of ester prodrugs and to identify a possible absorption window with low esterase activity [164]. A site-specific and species-dependent degradation was observed. It was shown that rat ileum is a suitable model to evaluate the influence of esterase activity on the oral absorption of the ester prodrug. Alternative, albeit less preferred models to study intestinal metabolism include tissue slices, isolated intestinal mucosal cells, and everted intestinal sacs.

Despite the lack of CYP enzymes in the parent, untreated Caco-2 cell line, activity of other drug metabolizing enzymes including peptidases and esterases has been demonstrated [5, 125, 162, 164]. Different attempts have been made to up-regulate the expression of CYP3A4 enzymes in the Caco-2 cells. Addition of 1α -25-dihydroxy-vitamin D₃ to the culture medium for 2 weeks post-confluence led to an increased expression of CYP3A4 [125, 150]. Another strategy to up-regulate CYP3A4 expression consisted in transfecting the CYP gene and subsequent stimulation with butyrate to provide the added CYP3A4 activity [41].

The Ussing chambers technique provides an excellent *ex vivo* model to study intestinal drug absorption in combination with intestinal metabolism. In this model, all the different enzymes are present at their normal expression levels. It has been used to assess segmental differences in intestinal metabolic activity [98], to explore the dynamic relationship between CYP3A and P-gp [66], to investigate human intestinal metabolism [132], and to investigate the effect of fruit extracts on the absorption/metabolism of sulfasalazine [97]. Recently, the metabolic activity of human small intestinal slices was compared with the metabolic activity of human intestinal segments using the Ussing chambers technique [161]. Similar metabolic rates, which were more than 2-fold higher than published microsomal data, were observed for phase I and phase II metabolism. The tissue remained viable and metabolically active for up to 4 h in both set-ups.

8.4. Concluding Remarks

Although a lot of effort is currently being put in optimization and improvement of different models to assess intestinal drug absorption, such as increasing the biorelevance of the models, it is clear that the ideal model does not exist. Based upon the goal of the study (e.g., screening, mechanistic study), the development stage of the compound under investigation, and the available resources, a choice has to be made between different models, taking into account the strengths and limitations of every model. In order to be able to draw the correct conclusions, a combination of different models should be considered. To increase the quality of the data obtained and to improve the intra- and interlaboratory comparison of these data, additional efforts are still required on the standardization and validation of the different models.

References

1. Allen JD, Schinkel AH (2002) Multidrug resistance and pharmacological protection mediated by the breast cancer resistance protein (BCRP/ABCG2). *Mol Cancer Ther* 1:427–434.
2. Alsenz J, Haenel E (2003) Development of a 7-day, 96-well Caco-2 permeability assay with high-throughput of P-gp screening in drug discovery. *Eur J Pharm Biopharm* 58:99–105.
3. Anderle P, Rakhmanova V, Woodford K, Zerangue N, Sadee W (2003) Messenger RNA expression of transporter and ion channel genes in undifferentiated and differentiated Caco-2 cells compared to human intestines. *Pharm Res* 20:3–15.
4. Anderle P, Huang Y, Sadee W (2004) Intestinal membrane transport of drugs and nutrients: Genomics of membrane transporters using expression microarrays. *Eur J Pharm Sci* 21:17–24.
5. Annaert P, Kinget R, Naesens L, de Clercq E, Augustijns P (1997) Transport, uptake, and metabolism of the bis(pivaloyloxymethyl)-ester prodrug of 9-(2-phosphonylmethoxyethyl)adenine in an *in vitro* cell culture system of the intestinal mucosa (Caco-2). *Pharm Res* 14:492–496.
6. Annaert P, Tukker JJ, Van Gelder J, Naesens L, de Clercq E, Van den Mooter G, Kinget R, Augustijns P (2000) *In vitro*, *ex vivo*, and *in situ* intestinal absorption characteristics of the antiviral ester prodrug adefovir dipivoxil. *J Pharm Sci* 89:1054–1062.

7. Araya H, Tomita M, Hayashi M (2006) The novel formulation design of self-emulsifying drug delivery systems (SEDDS) type O/W microemulsion III: The permeation mechanism of a poorly water soluble drug entrapped O/W microemulsion in rat isolated intestinal membrane by the Ussing chamber method. *Drug Metab Pharmacokinet* 21:45–53.
8. Artursson P, Ungell AL, Löfroth JE (1993) Selective paracellular permeability in two models of intestinal absorption: cultured monolayers of human intestinal epithelial cells and rat intestinal segments. *Pharm Res* 10:1123–1129.
9. Artursson P, Borchardt RT (1997) Intestinal drug absorption and metabolism in cell cultures: Caco-2 and beyond. *Pharm Res* 14:1655–1658.
10. Artursson P, Palm K, Luthman K (2001) Caco-2 monolayers in experimental and theoretical predictions of drug transport. *Adv Drug Deliv Rev* 46:27–43.
11. Augustijns P, Annaert P, Heylen P, Van den Mooter G, Kinget R (1998) Drug absorption studies of prodrug esters using the Caco-2 model: Evaluation of ester hydrolysis and transepithelial transport. *Int J Pharm* 166:45–53.
12. Augustijns P, Mols R (2004) HPLC with programmed wavelength fluorescence detection for the simultaneous determination of marker compounds of integrity and P-gp functionality in the Caco-2 intestinal absorption model. *J Pharm Biomed Anal* 34:971–978.
13. Avdeef A (2001) Physicochemical profiling (solubility, permeability, and charge state). *Curr Top Med Chem* 1:277–351.
14. Avdeef A, Stafford M, Block E, Balogh MP, Chambliss W, Kahn I (2001) Drug absorption in vitro model: Filter-immobilized artificial membranes. 2. Studies of the permeability properties of lactones in piper methysticum forst. *Eur J Pharm* 14:271–280.
15. Avdeef A (2002) High-throughput measurement of permeability profiles. In: Van de Waterbeemd H, Lennernäs H, Artursson P (Eds) *Drug Bioavailability—Estimation of Solubility, Permeability and Absorption*. Wiley-VCH, Weinheim, pp 46–70.
16. Avdeef A (2003) *Absorption and Drug Development: Solubility, Permeability and Charge State*. Wiley-Interscience, Hoboken pp 128–137.
17. Avdeef A, Nielsen PE, Tsinman O (2004) PAMPA—a drug absorption in vitro model 11. Matching the in vivo unstirred water layer thickness by individual-well stirring in microtitre plates. *Eur J Pharm Sci* 22:365–374.
18. Avdeef A, Artursson P, Neuhoff S, Lazorova L, Grasjö J, Tavelin S (2005) Caco-2 permeability of weakly basic drugs predicted with the double-sink PAMPA pK_a^{flux} method. *Eur J Pharm Sci* 24:333–349.
19. Avdeef A, Tsinman O (2006) PAMPA—a drug absorption in vitro model 13. Chemical selectivity due to membrane hydrogen bonding: In combo comparisons of HDM-, DOPC-, and DS-PAMPA models. *Eur J Pharm Sci* 28:43–50.
20. Back DJ, Rogers SM (1987) First-pass metabolism by gastrointestinal mucosa. *Aliment Pharmacol Ther* 1:339–357.
21. Bajka BH, Gillespie CM, Steeb CB, Read LC, Howarth GS (2003) Applicability of the Ussing chamber technique to permeability determinations in functionally distinct regions of the gastrointestinal tract in the rat. *Scand J Gastroenterol* 38:732–741.
22. Balimane PV, Chong S, Morrison RA (2000) Current methodologies used for evaluation of intestinal permeability and absorption. *J Pharmacol Toxicol Methods* 44:301–312.
23. Balimane PV, Chong S (2005) Cell culture-based models for intestinal permeability: A critique. *Drug Discov Today* 10:335–343.
24. Balimane PV, Han YH, Chong S (2006) Current industrial practices of assessing permeability and P-glycoprotein interaction. *AAPS J* 8:E1–E13.

25. Barthe L, Woodley J, Houin G (1999) Gastrointestinal absorption of drugs: Methods and studies. *Fundam Clin Pharmacol* 13:154–168.
26. Batzl-Hartmann C, Hurst L, Maas R (2002) Method for the improvement of parallel artificial membrane permeation assay (PAMPA) by using an additional hydrophilic membrane. German Patent Application 4.
27. Behrens I, Kissel T (2003) Do cell culture conditions influence the carrier-mediated transport of peptides in Caco-2 cell monolayers? *Eur J Pharm Sci* 19:433–442.
28. Benet LZ, Izumi T, Zhang Y, Silverman JA, Wacher VJ (1999) Intestinal MDR transport proteins and P-450 enzymes as barriers to oral drug delivery. *J Control Release* 62:25–31.
29. Benet LZ, Cummins CL (2001) The drug efflux-metabolism alliance: Biochemical aspects. *Adv Drug Deliv Rev* 50:S3–S11.
30. Bleasby K, Chauhan S, Brown C (2000) Characterization of MPP + secretion across human intestinal Caco-2 cell monolayers: Role of P-glycoprotein and a novel Na(+)-dependent organic cation transport mechanism. *Br J Pharmacol* 129:619–625.
31. Bogman K, Erne-Brand F, Alsenz J, Drewe J (2003) The role of surfactants in the reversal of active transport mediated by multidrug resistance proteins. *J Pharm Sci* 92:1250–1261.
32. Bogman K, Zysset Y, Degen L, Hopfgartner G, Gutmann H, Alsenz J, Drewe J (2005) P-glycoprotein and surfactants: effect on intestinal talinolol absorption. *Clin Pharmacol Ther* 77:24–32.
33. Bohets H, Annaert P, Mannens G, van Beijsterveldt L, Anciaux K, Verboven P, Meuldermans W, Lavrijsen K (2001) Strategies for absorption screening in drug discovery and development. *Curr Top Med Chem* 1:367–383.
34. Braun A, Hammerle S, Suda K, Rothn-Rutishauer B, Guthert M, Kramer SD, Wunderli-Allenspach H (2000) Cell cultures as tools in biopharmacy. *Eur J Pharm Sci* 11:S51–S60.
35. Briske-Anderson MJ, Finley JW, Newman SM (1997) The influence of culture time and passage number on the morphological and physiological development of Caco-2 cells. *Proc Soc Exp Biol Med* 214:248–257.
36. Carriere V, Lesuffleur T, Barbat A, Rousset M, Dussaulx E, Costet P, de Waziers I, Beaune P, Zweibaum A (1994) Expression of cytochrome P-450 3A in HT29-MTX and Caco-2 clone TC7. *FEBS Lett* 355:247–250.
37. Chiou WL, Chung SM, Wu TC, Ma C (2001) A comprehensive account on the role of efflux transporters in the gastrointestinal absorption of 13 commonly used substrate drugs in humans. *Int J Clin Pharmacol Ther* 39:93–101.
38. Chong S, Dando SA, Soucek KM, Morrison RA (1996) In vitro permeability through caco-2 cells is not quantitatively predictive of in vivo absorption for peptide-like drugs absorbed via the dipeptide transporter system. *Pharm Res* 13:120–123.
39. Chong S, Dando SA, Morrison RA (1997) Evaluation of Biocoat intestinal epithelium differentiation environment (3-day cultured Caco-2 cells) as an absorption screening model with improved productivity. *Pharm Res* 14:1835–1837.
40. Collnot EM, Baldes C, Wempe MF, Hyatt J, Navarro L, Edgar KJ, Schaefer UF, Lehr CM (2006) Influence of vitamin E TPGS poly(ethylene glycol) chain length on apical efflux transporters in Caco-2 cell monolayers. *J Control Release* 111:35–40.
41. Cummins CL, Mangravite LM, Benet LZ (2001) Characterizing the expression of CYP3A4 and efflux transporters (P-gp, MRP1, MRP2) in CYP3A4-transfected Caco-2 cells after induction with sodium butyrate and the phorbol ester 12-O-tetradecanoylphorbol-13-acetate. *Pharm Res* 18:1102–1109.

42. Cummins CL, Jacobsen W, Benet LZ (2002) Unmasking the dynamic interplay between intestinal P-glycoprotein and CYP3A4. *J Pharmacol Exp Ther* 300:1036–1045.
43. Deferme S, Van Gelder J, Augustijns P (2002a) Inhibitory effects of fruit extracts on P-glycoprotein-related efflux carriers: An in-vitro screening. *J Pharm Pharmacol* 54:1–7.
44. Deferme S, Mols R, Van Driessche W, Augustijns P (2002b) Apricot extract inhibits the P-gp mediated efflux of talinolol. *J Pharm Sci* 91:2539–2548.
45. Deferme S, Van Gelder J, Ingels F, Van den Mooter G, De Buck S, Balzarini J, Naesens L, De Clercq E, Kinget R, Augustijns A (2002c) Intestinal absorption characteristics of the low solubility thiocarboxanilide UC-781. *Int J Pharm* 234:113–119.
46. Deferme S, Augustijns P (2003) The effect of food components on the absorption of P-gp substrates: A review. *J Pharm Pharmacol* 55:153–162.
47. Deferme S, Tack J, Lammert F, Augustijns P (2003) P-glycoprotein attenuating effect of human intestinal fluid. *Pharm Res* 20:900–903.
48. Delie F, Rubas W (1997) A human colonic cell line sharing similarities with enterocytes as a model to examine oral absorption: Advantages and limitations of the Caco-2 model. *Crit Rev Ther Drug Carrier Syst* 14:221–286.
49. Engman HA, Lennernäs H, Taipalensuu J, Otter C, Leidvik B, Artursson P (2001) CYP3A4, CYP3A5, and MDR1 in human small and large intestinal cell lines suitable for drug transport studies. *J Pharm Sci* 90:1736–1751.
50. Fiese EF (2003) General pharmaceuticals—The new physical pharmacy. *J Pharm Sci* 92:1331–1342.
51. Furfine ES, Baker CT, Hale MR, Reynolds DJ, Salisbury JA, Searle AD, Stenberg SD, Todd D, Tung RD, Spaltenstein A (2004) Preclinical pharmacology and pharmacokinetics of GW433908, a water-soluble prodrug of the human immunodeficiency virus protease inhibitor amprenavir. *Antimicrob Agents Chemother* 48:791–798.
52. Ginski MJ, Polli JE (1999) Prediction of dissolution-absorption relationships from a dissolution/Caco-2 system. *Int J Pharm* 177:117–125.
53. Grass GM, Sweetana SA (1988) In vitro measurement of gastrointestinal tissue permeability using a new diffusion cell. *Pharm Res* 5:372–376.
54. He X, Kadomura S, Takekuma Y, Sugawara M, Miyazaki K (2004) A new system for the prediction of drug absorption using a pH-controlled Caco-2 model: Evaluation of pH-dependent soluble drug absorption and pH-related changes in absorption. *J Pharm Sci* 93:71–77.
55. Hidalgo IJ, Hillgren KM, Grass GM, Borchardt RT (1991) Characterization of the unstirred water layer in Caco-2 cell monolayers using a novel diffusion apparatus. *Pharm Res* 8:222–227.
56. Hidalgo IJ (2001) Assessing the absorption of new pharmaceuticals. *Curr Top Med Chem* 1:385–401.
57. Hilgendorf C, Spahn-Langguth H, Regardh CG, Lipka E, Amidon GL, Langguth P (2000) Caco-2 versus Caco-2/HT29-MTX co-cultured cell lines: Permeability via diffusion, inside- and outside-directed carrier-mediated transport. *J Pharm Sci* 89:63–75.
58. Hochman JH, Pudvah N, Qiu J, Yamazaki M, Tang C, Lin JH, Prueksaritanont T (2004) Interactions of human P-glycoprotein with simvastatin, simvastatin acid, and atorvastatin. *Pharm Res* 21:1686–91.
59. Hugger ED, Novak BL, Burton PS, Audus KL, Borchardt RT (2002) A comparison of commonly used polyethoxylated pharmaceutical excipients on their ability to inhibit P-glycoprotein activity in vitro. *J Pharm Sci* 91:1991–2002.

60. Huisman MT, Chhatta AA, van Tellingen O, Beijnen JH, Schinkel AH (2005) MRP2 (ABCC2) transports taxanes and confers paclitaxel resistance and both processes are stimulated by probenecid. *Int J Cancer* 116:824–829.
61. Hwang KK, Jiang L, Ren Y, Martin LL, Martin NF (2002) Site-specific absorption of M100240 and MDL 100,173 in rats evaluated using Sweetana-Grass diffusion chamber technology. *J Pharmacol Toxicol Methods* 48:97–101.
62. Ilett KF, Tee LB, Reeves PT, Minchin R (1990) Metabolism of drugs and other xenobiotics in the gut lumen and wall. *Pharmac Ther* 46:67–93.
63. Ingels F, Deferme S, Destexhe E, Oth M, Van den Mooter G, Augustijns P (2002) Simulated intestinal fluid as transport medium in the Caco-2 cell culture model. *Int J Pharm* 232:183–192.
64. Ingels FM, Augustijns PF (2003) Biological, pharmaceutical, and analytical considerations with respect to the transport media used in the absorption screening system, Caco-2. *J Pharm Sci* 92:1545–58.
65. Ingels F, Beck B, Oth M, Augustijns P (2004) Effect of simulated intestinal fluid on drug permeability estimation across Caco-2 monolayers. *Int J Pharm* 274:221–232.
66. Johnson BM, Charman WN, Porter CJH (2003) Application of compartmental modelling to an examination of in vitro intestinal permeability data: Assessing the impact of tissue uptake, P-glycoprotein, and CYP3A. *Drug Metab Dispos* 31:1151–1160.
67. Kansy M, Senner F, Gubernator K (1998) Physicochemical high-throughput screening: Parallel artificial membrane permeation assay in the description of passive absorption processes. *J Med Chem* 41:1007–1010.
68. Kansy M, Fischer H, Kratzat K, Senner F, Wagner B, Parrilla I (2001) High-throughput artificial membrane permeability studies in early lead discovery and development. In: Testa B, Van de Waterbeemd H, Folkers G, Guy R (Eds) *Pharmacokinetic Optimization in Drug Research. Biological, Physicochemical and Computational Strategies*. Wiley-Interscience, Hoboken, pp 447–464.
69. Kansy M, Avdeef A, Fischer H (2004a) Advances in screening for membrane permeability: High-resolution PAMPA for medicinal chemists. *DDT:Technologies* 1:349–355.
70. Kansy M, Fischer H, Bendels S, Wagner B, Senner F, Parrilla I, Micallef V (2004b) Physicochemical methods for estimating permeability and related properties. In: Borchardt RT, Kerns EH, Lipinski CA, Thakker DR, Wang B (Eds) *Biotechnology: Pharmaceutical Aspects Vol I: Pharmaceutical Profiling in Drug Discovery for Lead Selection*. AAPS Press, Arlington, pp 197–216.
71. Karlsson J, Wikman A, Artursson P (1993) The mucus layer as a barrier to drug absorption in monolayers of human intestinal epithelial HT29-H goblet cells. *Int J Pharm* 99:209–218.
72. Kerns EH, Di L, Petusky S, Farris M, Ley R, Jupp P (2004) Combined application of parallel artificial membrane permeability assay and Caco-2 permeability assays in drug discovery. *J Pharm Sci* 93:1440–1453.
73. Kivistö KT, Bookjans G, Fromm MF, Griese E-U, Münzel P, Kroemer HK (1996) Expression of CYP3A4, CYP3A5 and CYP3A7 in human duodenal tissue. *Br J Clin Pharmacol* 42:387–389.
74. Klein I, Sardaki B, Varadi A (1999) An inventory of the human ABC proteins. *Biochim Biophys Acta* 1461:237–262.
75. Kobayashi M, Sada N, Sugawara M, Iseki K, Miyazaki K (2001) Development of a new system for prediction of drug absorption that takes into account drug dissolution and pH change in the gastro-intestinal tract. *Int J Pharm* 221:87–94.
76. Kolars JC, Schmiedlin-Ren P, Schuetz JD, Fang C, Watkins PB (1992) Identification of rifampin-inducible P450III_A4 (CYP3A4) in human small bowel enterocytes. *J Clin Invest* 90:1871–1888.

77. Koga K, Kawashima S, Murakami M (2002) In vitro and in situ evidence for the contribution of Labrasol and Gelucire 44/14 on transport of cephalexin and cefoperazone by rat intestine. *Eur J Pharm Biopharm* 54:311–318.
78. Kotze AF, Leeuw BJ, Luessen HL, Boer AG, Verhoef JC, Junginger HE (1998) Comparison of the effect of different chitosan salts and N-trimethyl chitosan chloride on the permeability of intestinal epithelial cells (Caco-2). *J Control Release* 51:35–46.
79. Krishna DR, Klotz U (1994) Extrahepatic metabolism of drugs in humans. *Clin Pharmacokinet* 25:300–328.
80. Krishna G, Chen K, Lin C, Nomeir A (2001) Permeability of lipophilic compounds in drug discovery using in vitro human absorption model, Caco-2. *Int J Pharm* 222:77–89.
81. Le Ferrec E, Chesne C, Artursson P, Brayden D, Fabre G, Gires P, Guillou F, Rousset M, Rubas W, Scarino ML (2001) In vitro models of the intestinal barrier. The report and recommendations of ECVAM Workshop 46. European Centre for the Validation of Alternative methods. *Altern Lab Anim* 29:649–668.
82. Lee KJ, Johnson N, Castelo J, Sinko PJ, Grass G, Holme K, Lee YH (2005) Effect of experimental pH on the in vitro permeability in intact rabbit intestines and Caco-2 monolayer. *Eur J Pharm Sci* 25:193–200.
83. Lennernäs H, Nylander S, Ungell AL (1997) Jejunal permeability: A comparison between the Ussing chamber technique and the single-pass perfusion in humans. *Pharm Res* 14:667–671.
84. Lennernäs H (1998) Human intestinal permeability. *J Pharm Sci* 87:403–410.
85. Li H, Chung SJ, Shim CK (2002) Characterization of the transport of uracil across Caco-2 and LLC-PK1 cell monolayers. *Pharm Res* 19:1495–1501.
86. Liang E, Chessic K, Yazdananian M (2000) Evaluation of an accelerated Caoc-2 cell permeability model. *J Pharm Sci* 89:336–345.
87. Lin JH, Yamazaki M (2003) Role of P-glycoprotein in pharmacokinetics: clinical implications. *Clin Pharmacokinet* 42:59–98.
88. Liu H, Sabus C, Carter GT, Du C, Avdeef A, Tischler M (2003) In vitro permeability of poorly aqueous soluble compounds using different solubilizers in the PAMPA assay with liquid chromatography/mass spectrometry detection. *Pharm Res* 20:1820–1826.
89. Lucas M (1983) Determination of acid surface pH in vivo in rat proximal jejunum. *Gut* 24:734–739.
90. Makhey VD, Guo A, Norris DA, Hu P, Yan J, Sinko PJ (1998) Characterization of the regional intestinal kinetics of drug efflux in rat and human intestine and in Caco-2 cells. *Pharm Res* 15:1160–1167.
91. Manach C, Donovan JL (2004) Pharmacokinetics and metabolism of dietary flavonoids in humans. *Free Radic Res* 38:771–785.
92. Marino AM, Yarde M, Patel H, Chong S, Balimane PV (2005) Validation of the 96 well Caco-2 cell culture model for high throughput permeability assessment of discovery compounds. *Int J Pharm* 297:235–241.
93. Mayersohn M (1996) Principles of drug absorption. In: Banker GS, Rhodes CT (Eds) *Modern Pharmaceuticals*, 3rd ed., Marcel Dekker, New York, pp 21–74.
94. McKinnon RA, Burgess WM, Hall P, Roberts-Thomson SJ, Gonzalez FJ, McManus ME (1995) Characterization of CYP3A gene subfamily expression in human gastrointestinal tissues. *Gut* 36:259–267.
95. Mensch J, Noppe M, Adriaensen J, Melis A, Mackie C, Augustijns P, Brewster ME (2007) Novel generic UPLC/MS/MS method for high throughput analysis applied to permeability assessment in early Drug Discovery. *J Chromatogr B Analyt Technol Biomed Life Sci* 847:182–187.
96. Merino G, Alvarez AI, Pulido MM, Molina AJ, Schinkel AH, Prieto JG (2006) Breast cancer resistance protein (BCRP/ABCG2) transports fluoroquinolone

- antibiotics and affects their oral availability, pharmacokinetics, and milk secretion. *Drug Metab Dispos* 34:690–695.
97. Mols R, Deferme S, Augustijns P (2005) Sulfasalazine transport in in-vitro, ex-vivo and in-vivo absorption models: contribution of efflux carriers and their modulation by co-administration of synthetic nature-identical fruit extracts. *J Pharm Pharmacol* 57:1565–1573.
 98. Narawane M, Podder SK, Bundgaard H, Lee VHL (1993) Segmental differences in drug permeability, esterase activity and ketone reductase activity in the albino rabbit intestine (1993). *J Drug Target* 1:29–39.
 99. Naruhashi K, Tamai I, Inoue N, Muraoka H, Sai Y, Suzuki N, Tsuji A (2001) Active intestinal secretion of new quinolone antimicrobials and the partial contribution of P-glycoprotein. *J Pharm Pharmacol* 53:699–709.
 100. Nejdors P, Ekelund M, Jeppsson B, Weström BR (2000) Mucosal in vitro permeability in the intestinal tract of the pig, the rat, and man: Species- and region-related differences. *Scand J Gastroenterol* 5:501–507.
 101. Neuhoff S, Ungell AL, Zamora I, Artursson P (2003) pH-dependent bidirectional transport of weakly basic drugs across Caco-2 monolayers: Implications for drug-drug interactions. *Pharm Res* 20:1141–1148.
 102. Neuhoff S, Ungell AL, Zamora I, Artursson P (2005) pH-Dependent passive and active transport of acidic drugs across Caco-2 cell monolayers. *Eur J Pharm Sci* 25:211–220.
 103. Nielsen PE, Avdeef A (2004) PAMPA—a drug absorption in vitro model 8. Apparent filter porosity and the unstirred water layer. *Eur J Pharm Sci* 22:33–41.
 104. Pade V, Stavchansky S (1997) Estimation of the relative contribution of the transcellular and paracellular pathway to the transport of passively absorbed drugs in the Caco-2 cell culture model. *Pharm Res* 14:1210–1215.
 105. Patel N, Forbes B, Eskola S, Murray J (2006) Use of simulated intestinal fluids with Caco-2 cells and rat ileum. *Drug Dev Ind Pharm* 32:151–161.
 106. Perloff MD, von Moltke LL, Greenblatt DJ (2002) Fexofenadine transport in Caco-2 cells: Inhibition with verapamil and ritonavir. *J Clin Pharmacol* 42:1269–1274.
 107. Plumb JA, Burston D, Baker TG, Gardner MLG (1987) A comparison of the structural integrity of several commonly used preparations of rat small intestine in vitro. *Clin Sci* 73:53–59.
 108. Polentarutti BI, Peterson AL, Sjöberg AK, Anderberg EKI, Utter LM, Ungel ALB (1999) Evaluation of excised rat intestinal segments in the Ussing chamber: Investigation of morphology, electrical parameters and permeability characteristics. *Pharm Res* 16:446–454.
 109. Potluri P, Betageri GV (2006) Mixed-micellar proliposomal systems for enhanced oral delivery of progesterone. *Drug Deliv* 13:227–232.
 110. Prabhu S, Ortega M, Ma C (2005) Novel lipid-based formulations enhancing the in vitro dissolution and permeability characteristics of a poorly water-soluble model drug, piroxicam. *Int J Pharm* 301:209–216.
 111. Profit L, Eagling VA, Back DJ (1999) Modulation of P-glycoprotein function in human lymphocytes and Caco-2 cell monolayers by HIV-1 protease inhibitors. *AIDS* 13:1623–1627.
 112. Proulx P (1996) Membrane vesicles. *Adv Food Nutr Res* 40:197–206.
 113. Raeissi S, Hidalgo I, Segura-Aguilar J, Artursson P (1999) Interplay between CYP3A-mediated metabolism and polarized efflux of terfenadine and its metabolism in intestinal epithelial cells Caco-2 (TC7) cell monolayers. *Pharm Res* 16:625–632.
 114. Raiman J, Tormalehto S, Yritys K, Junginger HE, Monkkonen J (2003) Effects of various absorption enhancers on transport of clodronate through Caco-2 cells. *Int J Pharm* 261:129–136.

115. Rege BD, Yu LX, Hussain AS, Polli JE (2001) Effect of common excipients on Caco-2 transport of low-permeability drugs. *J Pharm Sci* 90:1776–1786.
116. Rege BD, Kao JPY, Polli JE (2002) Effects of nonionic surfactants on membrane transporters in Caco-2 cell monolayers. *Eur J Pharm Sci* 16:237–246.
117. Rogers SM, Back DJ, Orme MLE (1987) Intestinal metabolism of ethinylestradiol and paracetamol in vitro: studies using Ussing chambers. *Br J Clin Pharmacol* 23:727–734.
118. Rubas W, Jezyk N, Grass GM (1993) Comparison of the permeability characteristics of a human colonic epithelial (Caco-2) cell line to colon of rabbit, monkey and dog intestine and human drug absorption. *Pharm Res* 10:113–118.
119. Ruell JA, Tsinman KL, Avdeef A (2003) PAMPA—a drug absorption in vitro model. 5. Unstirred water layer in iso-pH mapping assays and pK_a^{flux} —optimized design (pOD-PAMPA). *Eur J Pharm Sci* 20:393–402.
120. Saha P, Kou J (2002) Effect of bovine serum albumin on drug permeability estimation across Caco-2 monolayers. *Eur J Pharm Biopharm* 54:319–324.
121. Sambuy Y, Ferruzza S, Ranaldi G, De Angelis I (2001) Intestinal cell culture models. Applications in toxicology and pharmacology. *Cell Biol Toxicol* 17:301–317.
122. Sambuy Y, De Angelis I, Ranaldi G, Scarino ML, Stamatii A, Zucco F (2005) The Caco-2 cell line as a model of the intestinal barrier: Influence of cell and culture-related factors on Caco-2 cell functional characteristics. *Cell Biol Toxicol* 21:1–26.
123. Sandri G, Rossi S, Ferrari F, Bonferoni MC, Zerrouk N, Caramella C (2004) Mucoadhesive and penetration enhancement properties of three different grades of hyaluronic acid using porcine buccal and vaginal tissue, Caco-2 cell lines and rat jejunum. *J Pharm Pharmacol* 56:1083–1090.
124. Sawada GA, Barsuhn CL, Lutzke BS, Houghton ME, Padbury GE, Ho NFH, Raub TJ (1999) Increased lipophilicity and subsequent cell partitioning decrease passive transcellular diffusion of novel, highly lipophilic antioxidants. *J Pharmacol Exp Ther* 288:1317–1326.
125. Schmiedlin-Ren P, Thummel KE, Fisher JM, Paine MF, Lown KS, Watkins PB (1997) Expression of enzymatically active CYP3A4 by Caco-2 cells grown on extracellular matrix-coated permeable supports in the presence of 1α -25-dihydroxyvitamin D₃. *Mol Pharmacol* 51:741–754.
126. Schrickx J, Lektarau Y, Fink-Gremmels J (2006) Ochratoxin A secretion by ATP-dependent membrane transporters in Caco-2 cells. *Arch Toxicol* 80:243–249.
127. Schuetz EG, Schuetz JD, Strom SC, Thompson MT, Fisher RA, Molowa DT, Li D, Guzelian PS (1993) Regulation of human liver cytochromes P-450 in family 3A in primary and continuous culture of human hepatocytes. *Hepatology* 18:1254–1262.
128. Seithel A, Karlsson J, Hilgendorf C, Bjorquist A, Ungell AL (2006) Variability in mRNA expression of ABC- and SLC-transporters in human intestinal cells: Comparison between human segments and Caco-2 cells. *Eur J Pharm Sci* 28:291–9.
129. Seo PR, Teksin ZS, Kao JP, Polli JE (2006) Lipid composition effect on permeability across PAMPA. *Eur J Pharm Sci* 29:259–68.
130. Shen Q, Lin Y, Handa T, Doi M, Sugie M, Wakayama K, Okada N, Fujita T, Yamamoto A (2006) Modulation of intestinal P-glycoprotein function by polyethylene glycols and their derivatives by in vitro transport and in situ absorption studies. *Int J Pharm* 313:49–56.
131. Smith P, Mirabelli C, Fondacaro J, Ryan F, Dent J (1988) Intestinal 5-fluorouracil absorption: Use of Ussing chambers to assess transport and metabolism. *Pharm Res* 5:598–603.

132. Söderholm JD, Hedman L, Artursson P, Larsson J, Pantzar N, Permert J, Olaison G (1998) Integrity and metabolism of human ileal mucosa in vitro in the Ussing chamber. *Acta Physiol Scand* 162:47–56.
133. Söderholm JD, Holmgren Petersson K, Olaison G, Franzén LE, Weström B, Magnusson KE, Sjödal R (1999) Epithelial permeability to proteins in the non-inflamed ileum of Crohn's disease? *Gastroenterology* 117:65–72.
134. Stipanuk MH (2000) Digestion and absorption of macronutrients. In: Stipanuk MH (Ed) *Biochemical and Physiological Aspects of Human Nutrition*. WB Saunders Company, Philadelphia, pp 75–152.
135. Stockmann M, Gitter AH, Sorgenfrei D, Fromm M, Schulzke JD (1999) Low edge damage container insert that adjusts intestinal forceps biopsies into Ussing chamber systems. *Eur J Physiol* 438:107–112.
136. Sugano K, Hamada H, Machida M, Ushio H (2001a) High-throughput prediction of oral drug absorption: Improvement of the composition of the lipid solution used in parallel artificial membrane permeation assay. *J Biomol Screen* 6:189–196.
137. Sugano K, Hamada H, Machida M, Ushio H, Saitoh K, Terada K (2001b) Optimized conditions of bio-mimetic artificial membrane permeability assay. *Int J Pharm* 228:181–188.
138. Sugano K, Takata N, Machida M, Saitoh K, Terada K (2002) Prediction of passive intestinal absorption using bio-mimetic artificial membrane permeation assay and the paracellular pathway model. *Int J Pharm* 241:241–251.
139. Sugawara M, Kadamura S, He X, Takekuma Y, Kohri N, Miyazaki K (2005) The use of an in vitro dissolution and absorption system to evaluate oral absorption of two weak bases in pH-independent controlled-release formulations. *Eur J Pharm Sci* 26:1–8.
140. Sun D, Lennernas H, Welage LS, Barnett JL, Landowski CP, Foster D, Fleisher D, Lee KD, Amidon GL (2002) Comparison of human duodenum and Caco-2 gene expression profiles for 12,000 gene sequences tags and correlation with permeability of 26 drugs. *Pharm Res* 19:1400–1416.
141. Taipalensuu J, Tornblom H, Lindberg G, Einarsson C, Sjöqvist F, Melhus H, Garberg P, Sjöström B, Lundgren B, Artursson P (2001) Correlation of gene expression of ten drug efflux proteins of the ATP-binding cassette transporter family in normal human jejunum and in human intestinal epithelial Caco-2 cell monolayers. *J Pharmacol Exp Ther* 299:164–170.
142. Taipalensuu J, Tavelin S, Lazorova L, Svensson AC, Artursson P (2004) Exploring the quantitative relationship between the level of MDR1 transcript, protein and function using digoxin as a marker of MDR1-dependent drug efflux activity. *Eur J Pharm Sci* 21:69–75.
143. Takahashi Y, Kondo H, Yasuda T, Watanabe T, Kobayashi S, Yokohama S (2002) Common solubilizers to estimate the Caco-2 transport of poorly water-soluble drugs. *Int J Pharm* 246:85–94.
144. Tang F, Horie K, Borchardt RT (2002) Are MDCK cells transfected with the human MDR1 gene a good model of the human intestinal mucosa? *Pharm Res* 19:765–772.
145. Tavelin S, Milovic V, Ocklind G, Olsson S, Artursson P (1999) A conditionally immortalized epithelial cell line for studies of intestinal drug transport. *J Pharmacol Exp Ther* 290:1212–1221.
146. Tavelin S, Taipalensuu J, Hallbook F, Vellonen KS, Moore V, Artursson P (2003a) An improved cell culture model based on 2/4/A1 cell monolayers for studies of intestinal drug transport: Characterization of transport routes. *Pharm Res* 20:373–381.
147. Tavelin S, Taipalensuu J, Soderberg L, Morrison R, Chong S, Artursson P (2003b) Prediction of the oral absorption of low-permeability drugs using small intestine-like 2/4/A1 cell monolayers. *Pharm Res* 20:397–405.

148. Teodori E, Dei S, Martelli C, Scapecchi S, Gualtieri F (2006) The functions and structure of ABC transporters: Implications for the design of new inhibitors of P-gp and MRP1 to control multidrug resistance (MDR). *Curr Drug Targets* 7: 893–909.
149. Thompson M, Krull UJ, Worsfold PJ (1980) The structure and electrochemical properties of a polymer-supported lipid biosensor. *Anal Chim Acta* 117:133–145.
150. Thummel KE, Brimer C, Yasuda K, Thottassery J, Senn T, Lin Y, Ishizuka H, Kharasch E, Schuetz J, Schuetz E (2001) Transcriptional control of intestinal cytochrome P-4503A by 1- α , 25-dihydroxy vitamin D₃. *Mol Pharmacol* 60:1399–1406.
151. Tso P, Crissinger K (2000) Chapter 4: Overview of digestion and absorption. In: Stipanuk M (Ed) *Biochemical and Physiological Aspects of Human Nutrition*. W.B. Saunders Publisher, Philadelphia PA, USA, pp. 79–81.
152. Tsutsumi K, Li SK, Ghanem AH, Ho NFH, Higuchi WI (2003) A systematic examination of the in vitro Ussing chamber and the in situ single-pass perfusion model systems in rat ileum permeation of model solutes. *J Pharm Sci* 92: 344–359.
153. Thwaites DT, Hirst BH, Simmons NL (1993) Passive transepithelial absorption of thyrotropin-releasing hormone (TRH) via a paracellular route in cultured intestinal and renal epithelial cell lines. *Pharm Res* 10:674–681.
154. Tukker JJ (2000) In vitro methods for the assessment of permeability. In: Dresmann JB, Lennernäs H (Eds) *Oral Drug Absorption. Prediction and Assessment*. Marcel Dekker, New York, pp 51–72.
155. Tukker JJ (2002) Characterization of transport over epithelial barriers. In: Lehr CM (Ed) *Cell Culture Models of Biological Barriers. In-vitro Test Systems for Drug Absorption and Delivery*. Taylor and Francis, London, pp 52–61.
156. Ungell AL, Andreasson A, Lundin K, Utter L (1992) Effects of enzymatic inhibition and increased paracellular shunting on transport of vasopressin analogues in the rat. *J Pharm Sci* 81:640–645.
157. Ungell AL (1997) In vitro absorption studies and their relevance to absorption from the GI tract. *Drug Dev Ind Pharm* 23:879–892.
158. Ungell AL, Nylander S, Bergstrand S, Sjönerg A, Lennernäs H (1998) Membrane transport of drugs in different regions of the intestinal tract of the rat. *J Pharm Sci* 87:360–366.
159. Ungell AL (2002) Transport studies using intestinal tissue ex vivo. In: Lehr CM (Ed) *Cell Culture Models of Biological Barriers*. Taylor and Francis, London, pp 164–188.
160. Ussing HH, Zerahn K (1951) Active transport of sodium as the source of electric current in the short-circuited isolated frog skin. *Acta Physiol Scand* 23:110–127.
161. Van de Kerkhof EG, Ungell AL, Sjöberg AK, de Jager MH, Hilgendorf C, de Graaf IA, Groothuis GG (2006) Innovative methods to study human intestinal drug metabolism: Precision-cut slices compared with Ussing chamber preparations. *Drug Metab Dispos* 34:1893–902.
162. Van Gelder J, Annaert P, Naesens L, de Clercq E, Van den Mooter G, Kinget R, Augustijns P (1999) Inhibition of intestinal metabolism of the antiviral ester prodrug bis(POC)-PMPA by nature-identical fruit extracts as a strategy to enhance its oral absorption: An in vitro study. *Pharm Res* 16:1035–1040.
163. Van Gelder J, Deferme S, Annaert P, Naesens L, De Clercq E, Van den Mooter G, Kinget R, Augustijns P (2000a) Increased absorption of the antiviral ester prodrug tenofovir disoproxil in rat ileum by inhibiting its intestinal metabolism. *Drug Metab Dispos* 28:1394–1396.
164. Van Gelder J, Shafiee M, de Clercq E, Penninckx F, Van den Mooter G, Kinget R, Augustijns P (2000b) Species-dependent and site-specific intestinal metabolism of ester prodrugs. *Int J Pharm* 205:93–100.

165. Veber DF, Johnson SR, Cheng HY, Smith BR, Ward KW, Kopple KD (2002) Molecular properties that influence the oral bioavailability of drug candidates. *J Med Chem* 45:2615–2623.
166. Wachter VJ, Salphati L, Benet LZ (2001) Active secretion and enterocytic drug metabolism barriers to drug absorption. *Adv Drug Deliv Rev* 46:89–102.
167. Wagner D, Spahn-Langguth H, Hanafy A, Koggel A, Langguth P (2001) Intestinal drug efflux: Formulation and food effects. *Adv Drug Deliv Rev* 50:S13–S31.
168. Walter E, Kissel T (1995) Heterogeneity in the human intestinal cell line Caco-2 leads to differences in transepithelial transport. *Eur J Pharm Sci* 3:215–230.
169. Watanabe E, Takahashi M, Hayashi M (2004) A possibility to predict the absorbability of poorly water-soluble drugs in humans based on rat intestinal permeability assessed by an in vitro chamber method. *Eur J Pharm Biopharm* 58:659–665.
170. Watkins PB, Wrighton SA, Schuetz EG, Guzelian PS (1987) Identification of the glucocorticoid-inducible cytochromes P-450 in the intestinal mucosa of rats and man. *J Clin Invest* 80:1029–1036.
171. Weinstein K, Kardos P, Strab R, Hidalgo IJ (2004) Cultured epithelial cell assays used to estimate intestinal absorption potential. In: Borchardt RT, Kerns EH, Lipinski CA, Thakker DR, Wang B (Eds) *Biotechnology: Pharmaceutical Aspects Vol I: Pharmaceutical Profiling in Drug Discovery for Lead Selection*. AAPS Press, Arlington, pp 197–216.
172. Wikman-Larhed A, Artursson P (1995) Co-cultures of human intestinal goblet (HT29-H) and absorptive (Caco-2) cells for studies of drug and peptide absorption. *Eur J Pharm Sci* 3:171–193.
173. Wils P, Warnery A, Phung-Ba V, Legrain S, Scherman D (1994) High lipophilicity decreases drug transport across intestinal epithelial cells. *J Pharmacol Exp Ther* 269:654–658.
174. Wire MB, Shelton MJ, Studenberg S (2006) Fosamprenavir: Clinical pharmacokinetics and drug interactions of the amprenavir prodrug. *Clin Pharmacokinet* 45:137–168.
175. Wohnsland F, Faller B (2001) High-throughput permeability pH profile and high-throughput alkane/water log P with artificial membranes. *J Med Chem* 44:923–930.
176. Yamashita S, Tanaka Y, Endoh Y, Taki Y, Sakane T, Nadai T, Sezaki H (1997) Analysis of drug permeation across Caco-2 monolayer: Implication for predicting in vivo drug absorption. *Pharm Res* 14:486–491.
177. Youdim KA, Avdeef A, Abbott NJ (2003) In vitro trans-monolayer permeability calculations: Often forgotten assumptions. *DDT* 8:997–1003.
178. Zakej S, Sturm K, Kristl A (2006) Ciprofloxacin permeability and its active secretion through rat small intestine in vitro. *Int J Pharm* 313:175–180.
179. Zhu C, Jiang L, Chen TM, Hwng KK (2002) A comparative study of artificial membrane permeability assay for high-throughput profiling of drug absorption potential. *Eur J Med Chem* 37:399–407.
180. Zhu HJ, Wang JS, Markowitz JS, Donovan JL, Gibson BB, Gefroh HA, Devane CL (2006) Characterization of P-glycoprotein inhibition by major cannabinoids from marijuana. *J Pharmacol Exp Ther* 317:850–857.

9

In Vitro Cellular Models for Nasal Drug Absorption Studies

Dae-Duk Kim

Abstract Nasal drug delivery has emerged as a noninvasive alternative for labile drugs including peptides and proteins. In order to evaluate these novel formulations, reliable *in vivo* and/or *in vitro* models are needed. *In vivo* animal models or *in vitro* excised animal tissue models are frequently used for nasal drug absorption studies due to various methodological and ethical limitations associated with the use of human nasal specimens. However, there are several disadvantages in the use of animal models including species differences and peculiarities in anatomical features of animal nasal cavities compared to those of human counterparts. Although still in their infancy, *in vitro* cell culture models of human nasal epithelium based on primary culture technologies have proven to be extremely useful for nasal epithelial permeability and drug absorption studies. Nevertheless, difficulty in obtaining a reliable human tissue source is a major limiting factor that hinders the usefulness of the *in vitro* nasal cell culture model. Therefore, to overcome the apparent shortage of human nasal tissues, passage cultures of nasal epithelial cells could be an efficient alternative to primary cultures of nasal epithelial cells. In this chapter, *in vivo* and *in vitro* models currently available for nasal drug transport studies are presented, following a brief review of biological barrier properties of the human nasal mucosa. Implications of *in vitro* human primary cell culture models are further discussed.

Keywords: Nasal absorption; Air-interfaced culture; Absorption enhancer; Liquid-covered culture; Mucociliary clearance; Nasal epithelial cell monolayer; Paracellular absorption; Tight junction; Transcellular absorption; Drug transport

Abbreviations

AIC	Air-interfaced culture
BEGM	Bronchial epithelial cell growth medium
DMEM	Dulbecco's modified Eagle's medium
DMEM/F12	Dulbecco's modified Eagle's medium/F12 Ham's (1:1)
JAM	Junctional adhesion molecule
LCC	Liquid-covered culture

log <i>P</i>	Partition coefficient (octanol–water)
<i>P</i> _{app}	Apparent permeability coefficient
RPMI	Roswell Park Memorial Institute
SEM	Scanning electron microscopy
TEER	Transepithelial electrical resistance
TJM	Tight junction modulating

9.1. Introduction

Nasal drug delivery has emerged as a noninvasive alternative route for drugs that are susceptible to enzymatic or acidic degradation [1]. The sizable surface area of the nasal cavity, avoidance of the hepatic first-pass effect, and relatively high blood flow promoting rapid absorption are some of attractive features of nasal drug delivery [2–4]. Conventionally, the nasal route has been used for local delivery of drugs for treating nasal allergy, nasal congestion, or nasal infections. However, systemic delivery through the nasal route has recently begun to explore possibilities for those requiring a rapid onset of action or necessitating avoidance of severe proteolysis involved in oral administration (e.g., most peptide and protein drugs). Successful attempts to deliver corticosteroid hormones through the nasal route for systemic absorption [2, 5] have triggered further studies in this area.

Today, drugs ranging from small chemicals to large macromolecules, including peptide/protein therapeutics, hormones, and vaccines, are being delivered through the nasal cavity [6]. Marketed products include a range of antimigraine drugs (e.g., sumatriptan from GlaxoSmithKline, zolmitriptan from AstraZeneca, ergotamine from Novartis, and butorphanol from BristolMyersSquibb) as well as some peptides (e.g., calcitonin marketed by Novartis, desmopressin from Ferring, and buserelin from Aventis) [7]. Lately, the use of the nasal route for delivery of vaccines, especially against respiratory infections such as influenza, is attracting interest from vaccine delivery scientists [8].

For successful formulation of a nasal delivery system, testing with reliably established *in vivo* and *in vitro* models are crucial. Because of methodological and ethical limitations inherent in the use of human nasal specimens, *in vivo* animal models or *in vitro* excised animal tissue models are frequently utilized for nasal drug absorption studies. Several *in vivo* models of rat, rabbit, dog, sheep, and monkey were reported for delivering hormones (e.g., testosterone) and peptide/proteins (e.g., growth hormones and insulin) via nasal routes [9–11]. Using rat and rabbit *ex vivo* (*in situ*) nasal perfusion models, pharmacokinetics of drugs were studied following nasal instillation [9]. *In vitro* models of the excised nasal mucosae of rabbit, sheep, and dog mounted on diffusion chambers are frequently used for nasal transport and metabolism studies [12]. However, there are several disadvantages in *in vivo* animal and *in vitro* tissue/cell models, including species differences and peculiarities in many anatomical features in various animal nasal cavities, compared with those of the human.

In vitro cell culture models of human nasal epithelium based on primary culture technologies have proven to be extremely useful for mechanistic studies of nasal epithelial permeability and drug absorption [13]. However, efforts

to develop and characterize various nasal culture systems are still in their infancy. Moreover, difficulty in obtaining reliable tissue sources, especially if human tissue is preferred, is a limiting factor that hinders the widespread usage and usefulness of an *in vitro* primary nasal cell culture model. The apparent shortage of human nasal tissue has prompted researchers to seek an alternative to primary cultures of nasal epithelial cells, that is, the passage culture of nasal epithelial cells. The importance of these types of *in vitro* cell culture model is introduced in this chapter by briefly reviewing the biological barrier of the nasal mucosa, followed by a summary of the currently available *in vitro* cell culture models for nasal drug transport studies.

9.2. Structure and Physiology of the Nasal Cavity

In both humans and animals, primary functions of the nasal cavity are breathing and olfaction. In addition, resonance of produced sounds, cleaning the air as it is inhaled, mucociliary clearance, immunological activities, and heating and humidification of the inspired air before it reaches the lungs are also important functions of the nasal cavity [14]. Hairs in the nasal vestibule or mucus layer covering the surface of nasal cavities trap inhaled particles or microorganisms. Moreover, the nasal mucosa has the capacity to aid in the metabolism of endogenous materials into compounds that can easily be eliminated from the body.

9.2.1. Anatomy and Function

The human nose is divided by the median septum and each symmetrical half opens to the face through nostrils, while extending posterior to the nasopharynx [15]. The most anterior part of the nasal cavity is the nasal vestibule, adjacent to the intermediate region called the atrium. Turbinates or conchae of the nasal cavity considerably increase the surface area. The nasal cavity consists of three regions, which are the vestibule, olfactory region, and respiratory region. The human vestibule is the region just inside nostrils with an area of about 0.6 cm². The olfactory region in humans is situated on the roof of nasal cavities and covers only about 10% of the total nasal area of 150 cm², of which the respiratory region covers about 85%. The respiratory region contains three nasal turbinates: the superior, middle, and inferior turbinates, which project from the lateral wall of each half of the nasal cavity. The human nasal cavity has a total volume of 15–20 ml. The presence of turbinates in the respiratory region creates a turbulent airflow through nasal passages ensuring better contact between the inhaled air and mucosal surface [16]. The anterior nasal cavity is lined with a stratified, squamous, and transitional epithelium.

The highly vascularized respiratory epithelium is composed of five major cell types: ciliated cells, nonciliated cells, columnar cells, goblet cells, and basal cells. Low numbers of neurosecretory cells are present in the basement membrane [17]. Approximately 20% of the total number of cells in the lower turbinate area is ciliated with fine projections (~100 per cell) on the apical cell surface. Cilia are used to transport the mucus toward the nasopharynx. These long (4–6 μm) and thin projections are mobile and beat with a frequency of 1,000 strokes per min. Ciliated and nonciliated columnar cells are populated with about 300 microvilli per cell, which help in enlarging the surface area.

Around 60–70% of the respiratory mucosa is lined with nonciliated cells that are thought to be responsible for high metabolic activity and fluid transport into and out of mucosal cells [17].

9.2.2. Physiology of Nasal Mucosa

Mucus gel covers the nasal epithelium, as in many other epithelia in contact with the external environment. The mucus plays a number of important physiological roles, including (a) entrapment of substances entering the nasal cavity and participation in the removal of particulates via mucociliary clearance and (b) humidification of inspired air to aid in heat transfer by holding water. Goblet cells, which cover ~10% of the mucosa in the turbinate area, contain numerous secretory granules. The flow rate of human nasal mucus is in the order of 5 mm/min, renewing the mucus layer every 15–20 min. However, basal cells (thought to be precursors of columnar and goblet cells) are poorly differentiated and reside at the serosal aspect of the mucosa. It is believed that basal cells have the ability to replace other cell types after differentiation [17]. The olfactory mucosa is a pseudostratified, columnar epithelium which covers the superior region of the human nasal cavity and composed of supporting cells, basal cells, microvillar cells, and the typical receptor cells or olfactory cells [16, 18]. The basal lamina or basement membrane is situated between the epithelium and *lamina propria*. It is situated adjacent to underlying skeletal structures and is composed of a loose type of connective tissue containing glands, subepithelial cells, and vascular and nervous tissue [19].

9.3. Factors Affecting the Nasal Absorption

Drug transport across the nasal epithelium is assumed to occur by one or more of the following mechanisms: transcellular passive diffusion, paracellular passive diffusion, carrier-mediated transport, and transcytosis. The factors influencing nasal drug absorption are related to nasal physiology, physicochemical characteristics of the drug, and formulation approaches used for specific drugs. As with most sites of drug absorption, the bioavailability of nasally delivered drug is affected by several factors, including the surface area available for absorption, contact time between the drug and absorption site(s), metabolism of the drug, and pathology of absorbing tissue(s) [20].

9.3.1. Physiological Factors

9.3.1.1. Mucociliary Clearance

Combined actions of the mucus layer and cilia dictate the mucociliary clearance, which is an important factor in the physiological defense of the respiratory tract against inhaled hazardous substances including pathogens and particles [21]. Although the speed of mucociliary clearance in healthy humans is assumed to be about 5 mm/min [22], this is easily altered by pharmaceutical excipients, airborne irritants, or nasal diseases. Generally, the length of time that the drug is in contact with absorbing tissues influences the amount of drug that crosses the mucosa. In the nasal cavity, this is influenced by the rate at which the drug is cleared from the absorption site(s) by mucociliary clearance as well as metabolism.

9.3.1.2. Enzymes

Even though nasally administered drugs are thought to avoid first-pass hepatic metabolism, bioavailability of nasally administered peptide or protein drugs can be limited because of the broad range of metabolic enzymes localized in the nasal mucosal cavity and epithelial cells lining the cavity [23, 24]. However, the enzymatic degradation of peptide/protein drugs is generally smaller in magnitude than that found in the gastrointestinal tract, although it has been reported that nasally administered peptides resulted in low bioavailability due to degradation by peptidases in the nasal cavity/epithelial cells. Nevertheless, it is of note that up to 100% of relative bioavailability for nasal administration of insulin was reported in a rat study [9]. Therefore, the nasal route is a better alternative to oral delivery for some enzymatically labile drugs such as insulin whose bioavailability via oral routes may be close to nil. It is of importance to note that various pathophysiological conditions, including the common cold, seasonal rhinitis, nasal polyps, and cancer, may alter absorption from the nasal cavity by affecting the rate of mucociliary clearance, thereby altering the rate of clearance of nasally administered drugs. However, a more thorough investigation on this topic is still necessary.

9.3.2. Physicochemical Characteristics of the Drugs

Physicochemical characteristics of nasally administered drugs can influence nasal absorption. These include molecular weight, solubility, dissolution rate, charge, partition coefficient, pK_a , particle size, and the presence of polymorphism [25]. Nasal absorption is known to be sharply decreased for a compound with a molecular weight of greater than 1,000 Da [26]. Nasal absorption of water-soluble, ionizable compounds (e.g., benzoic acid) is dependent on the pH of the solution where the drug is dissolved. Nasal absorption of drugs decreases as their ionized fractions increase. However, the role of lipophilicity of compounds in their nasal absorption rates is controversial. Although the lipophilicity measured as a simple octanol–water partition coefficient ($\log P$) may not be the best way to predict the nasal absorption, it is generally accepted that permeability of lipophilic solutes increases as the $\log P$ value of the solute increases. However, some studies report that the correlation between solute lipophilicity and nasal absorption rate of the solute is not very significant. As reported for the case of progesterone and its derivatives, systemic bioavailability seems to correlate well with the partition coefficient determined using the rabbit nasal mucosa-buffer system, where isotonic phosphate buffer (pH 8.0) was used to mimic mucosal liquid [9].

9.3.3. Effect of Formulation

Formulation-related factors that should be taken into consideration to obtain successful nasal absorption of drugs include the concentration of drugs, dose and volume of administration, and pH, viscosity, and osmolarity of the solution in which the drug is dissolved. Moreover, excipients (e.g., preservatives and absorption enhancers) in general affect the bioavailability. In addition, dosage forms (e.g., drops, spray, and powder), administration techniques (e.g., inhalation, mechanically assisted and others), and devices used to administer the drug will also affect the level of absorption. An important factor for low drug absorption via the nasal cavity is the general rapid clearance of

administered formulations due to the mucociliary clearance mechanism. This has led to the development of a bioadhesive powder dosage form and mucoadhesive powder spray formulation for the nasal delivery [27].

For the nasal delivery of polar drugs, addition of absorption-promoting agents called enhancers can be very helpful. Enhancers described in the literature include surfactants (e.g., lauric acid), bile salts and bile salt derivatives (e.g., sodium taurodihydrofusidate), fatty acids or fatty acid derivatives, phospholipids, and various cyclodextrins [28]. These enhancer systems help increase absorption via a variety of mechanisms but generally lead to changes in the permeability of epithelial cell layers by modifying phospholipid bilayers, leaching out proteins through the cell membrane, or even stripping off the outer layer of the mucosa. Some of these enhancers also have an effect on tight junctions and/or act as enzymatic inhibitors. In animal studies with various enhancing agents, a direct correlation between absorption-enhancing effect and damage caused to the nasal epithelial barrier have been observed [29]. This is particularly true for surfactants and bile salts. However, for other enhancers (e.g., some of the cyclodextrins, chitosan, and selected phospholipids) the absorption-enhancing effect outweighed any damage caused to the mucosa. Moreover, in a Caco-2 cell culture study, chitosan has been shown to increase the paracellular transport of polar drugs by transiently opening the tight junctions between the adjacent epithelial cells [30]. As described above for surfactant-type enhancers, a major limiting factor associated with the addition of enhancers to a nasal formulation is the potential toxicity to the nasal mucosa. Thus, nasal absorption enhancers should be chosen carefully, making sure that they are nonirritating, nontoxic, and nonallergenic or at least able to demonstrate reversible effects in a short time period. Needless to say, they should be potent and compatible with the drug and other excipients in the formulation.

9.4. Transport Routes of Nasal Epithelial Barrier

There are two routes potentially involved in drug absorption across the nasal epithelial barrier: the transcellular and paracellular routes [20]. Several experimental evidences dealing with the mechanism of transnasal permeation support the existence of both lipoidal pathway (i.e., transcellular route) and an aqueous pore pathway (i.e., paracellular route).

9.4.1. Transcellular Route

This refers to the transport across the epithelial cells, which can occur by passive diffusion, carrier-mediated transport, and/or endocytic processes (e.g., transcytosis). Traditionally, the transcellular route of nasal mucosa has been simply viewed as primarily crossing the “lipoidal barrier,” in which the absorption of a drug is determined by the magnitude of its partition coefficient and molecular size. However, several investigators have reported the lack of linear correlation between penetrant lipophilicity and permeability [9], which implies that cell membranes of nasal epithelium cannot be regarded as a simple lipoidal barrier. Recently, compounds whose transport could not be fully explained by passive simple diffusion have been investigated to test if they could be utilized as specific substrates for various transporters which have been identified in the

nasal mucosa [31–33]. The transcellular route can be categorized into three different processes as described below.

9.4.1.1. Transcellular Passive Diffusion

For most conventional, small, and lipophilic drug molecules, absorption occurs by transcellular passive diffusion across the epithelial cell. Molecular size of drugs is known to be one of the important factors in determining the passive diffusion. It was reported that nasal absorption sharply decreased for a drug with molecular weight higher than 1,000 Da [9]. Because the degree of ionization of a given drug is also an important property for absorption via this route, transport is dependent on the pK_a of the drug and pH of the environment (e.g., the pH of nasal secretions is normally in the region 5.5–6.5).

9.4.1.2. Carrier-Mediated Processes

The existence of a carrier-mediated transport in nasal mucosa was first suggested by Kimura et al. [34]. P-glycoprotein, organic cation transporter, dopamine transporter, and amino acid transporters have all been identified in the nasal mucosa, especially in the olfactory mucosa [31, 32, 35, 36]. These transporters determine the polarized absorption and excretion of their substrates including amino acids, amines, and cations.

9.4.1.3. Endocytic Processes

Since the uptake of particles in nasal epithelial tissue is known to be mostly mediated by M cells, nasal administration has been investigated as a noninvasive delivery of vaccines [37]. However, since the uptake of naked DNA by endocytosis is limited, use of either nanoparticles as mucosal delivery systems [37] or hypotonic shock [38] is reported for the efficient transfection of gene and vaccine into the nasal epithelium. It was also reported that polypeptides and polypeptide-coated nanospheres (diameter: about 500 nm) are transported through endocytic process in rat M cells [39].

9.4.2. Paracellular Route

This refers to the transport taking place between adjacent epithelial cells by passive diffusion or solvent drag mechanisms. Paracellular permeability profile of the nasal epithelium is similar to that of the intestinal epithelial barriers. Thus, small hydrophilic molecules can passively diffuse through paracellular routes between adjacent nasal epithelial cells. Passive diffusion of hydrophilic solutes via paracellular routes is driven by a concentration gradient across the epithelium with the rate of absorption governed by the Fick's first law of diffusion. Polar and charged drugs with molecular weights below 1,000 Da are thought to permeate the nasal epithelium via this paracellular route. A major limiting site of paracellular pathways is known to be the tight junctional region, which is characterized as the joining of contiguous cells via various tight junctional proteins. There are many molecular components of the tight junction such as occludin, various claudin isoforms, junctional adhesion molecule (JAM), zonula occludens, and actin. Among these components, the perijunctional actin is known to play a major role in controlling the paracellular permeability [40]. Although tight junctions are dynamic structures and can open and close to a certain degree when appropriate signaling mechanisms are activated [41], the average diameter of the equivalent pores becomes less than 1 nm, considerably limiting the transport of larger molecules

including peptide and proteins [26]. However, recent discoveries on the molecular identity of various tight junctional proteins initiated new approaches for enhancing nasal drug delivery, thereby improving the bioavailability of small, polar molecules as well as biopharmaceutical products (e.g., peptide/protein therapeutics, vaccines, and genes) [41]. It is reported that the modulation of tight junctional routes is possible by using a toxin (e.g., cholera toxin) as an adjuvant in mucosal vaccines [42], or using a tight junction modulating (TJM) peptide (e.g., PN159) [43], or encapsulating drugs of interest in polymer-based microspheres [44]. For example, when insulin was encapsulated in aminated gelatin microspheres as a nasal delivery system, the hydrogel nature of the microsphere resulted in temporary dehydration of the epithelial cells and as a result loosening up the tight junctions, leading to an increase in insulin absorption [45].

9.5. Models for Nasal Drug Transport and Absorption Studies

Ethical issues as well as difficulty in obtaining enough human nasal tissue specimens have called for the need to use alternative in vitro and in vivo methods. Various in vivo animal models and in vitro excised tissue models have been described in the literature for nasal drug transport studies. However, due to the difficulty in both controlling the experimental conditions in in vivo animal models and obtaining intact excised tissue samples, in vitro cell culture models are also being actively developed.

Cultured nasal cells are reliable models for drug transport and metabolism studies, since they are known to express important biological features (e.g. tight junctions, mucin secretion, cilia, and various transporters), resembling those found in vivo systems. Moreover, easy control of experimental conditions as well as separation of the permeation step from the subsequent absorption cascade is also possible. A relatively simple primary culture condition using human nasal epithelial cells for in vitro drug transport studies has been established and applied in transport and metabolism studies of drugs. It is known that the culture condition and/or selection of culture media are critical in the recapitulation of well-differentiation features of in vivo nasal mucosal epithelium [46].

9.5.1. In Vivo Animal Models

There are two types of animal models which can be used for nasal absorption studies: the whole animal model and isolated organ perfusion model. The rat model used for studying the nasal delivery of drugs was first presented in the late 1970s [47]. The animal models using rat [2, 45], rabbit [43, 48], dog [49], sheep [50], and monkey [51] have been reported for evaluation of nasal absorption studies. Ex vivo nasal perfusion models using sheep [52] and rat [9] are also reported. Although the rat model is easy to perform because of the small animal size and low in overall cost (e.g., maintenance of the animal and setup of the preparation), the small animal size is also a disadvantage (e.g., limiting the number of blood samplings) and hence it is useful only for preliminary studies of nasal drug absorption. The primate model would be very useful, even though it is very expensive. Scientists are, however,

hesitant to use this particular model due to the increasing pressure from animal rights groups. Alternatively, rabbit, dog, and sheep models are excellent for evaluating formulation and pharmacokinetic studies, although anatomical and physiological differences in nasal mucosae of the human versus these animals are very important issues that should be taken into account.

9.5.2. In Vitro Excised Models

Excised nasal mucosae obtained from various animal species are tools frequently used to study nasal transport and metabolism ([53], Chap. 4). Maintaining the viability of the excised nasal tissues during the experimental period is crucial. Most studies were performed with epithelia excised from rabbits, bovine, sheep, and dogs tissues [54–57]. This excised nasal tissue model has been shown to be well suited for studies on nasal permeation and metabolism of drugs. However, species differences in the activity of various enzymes found in human versus these animal nasal mucosae have become an important issue.

9.5.3. Cell Line Models

RPMI 2650 is the only human nasal epithelial cell line derived from a spontaneously formed tumor. This particular cell line has been mostly used for nasal metabolism studies, since it grows into a multilayer and does not form confluent monolayers (although perijunctional actin rings are present). Thus, RPMI 2650 cell monolayer is rarely used for nasal transport studies [44, 58].

9.5.4. In Vitro Primary and Passaged Cell Culture Models

In vitro cell culture models offer many advantages, including (a) a controlled environment for the study of epithelial cell growth and differentiation, (b) the elucidation of drug transport pathways and mechanisms, (c) rapid and convenient means of evaluating drug permeability, and (d) opportunity to minimize the expensive and limited controversial use of animals [12]. Although recent advances in human nasal primary cell culture techniques appear to be very promising, some hurdles remain to be resolved, including the relatively small amount of obtainable cells and epithelial cell differentiation issues. Primary culture of human nasal epithelial cells using tissue culture plates shows some natural cell differentiation. The presence of tight junctions is confirmed by actin staining. Using such primary culture systems, basic functional and biochemical characteristics of the tissue have been demonstrated [59]. Primary culture of cells and tissues obtained from differentiated human nasal epithelium is an established tool for many studies, including fibrosis, electrolyte transport, ciliogenesis, and ciliary movement [60, 61] as well as peptide transport and metabolism [62, 63]. Primary cultures of human nasal epithelial cells on Transwell[®] insert as in vitro models are very promising for the study of nasal drug absorption, especially for peptide transport studies [58, 64, 65]. Recently, primary culture of nasal epithelial from a variety of animal species, including human [62], bovine [59], rat, and rabbit [66], has provided valuable information on nasal physiology in health and disease. Several research groups are actively developing and validating human nasal cell culture systems as an alternative to animal models.

9.5.4.1. Liquid-Covered Culture Method

Human primary nasal epithelial cell culture on Transwell[®] insert for in vitro drug transport studies was first reported by Werner et al. [58, 64]. This culture method has been applied in transport and metabolism studies of insulin and other peptides [62, 63, 67]. Despite its advantages, it is difficult to obtain adequate amounts of human nasal cells since most of the biopsies are used for diagnostic examinations and yield only very limited amount of usable nasal epithelial cells. The limited resources for in vitro primary cell culture have been a serious obstacle for conducting diverse experiments, and thus, high-throughput screening studies have not been possible. Other restrictions of primary cell culture include contamination with pathogens and large donor-to-donor variability [68]. To overcome these limitations of primary cell culture of human nasal epithelial cells, a serially passaged culture system was considered as an alternative. Although studies on the development of a passaged culture of primary human respiratory epithelial cells yielded information on some physiological characteristics (e.g., mucin secretion) [68–72], there are not many reports on serially passaged cells being cultured on a permeable support for in vitro drug transport studies. The formation of functional tight junctions would be the most essential factor to be considered for studies of drug transport across the nasal epithelial cell layer derived from serially passaged cells. Yoo et al. [40] reported that passage-cultured (e.g., up to passage number 4) human nasal epithelial cells can be grown as a confluent cell monolayer on the Transwell[®] insert utilizing the liquid-covered culture (LCC) method. Each passaged culture formed a tight epithelial cell monolayer with high transepithelial electrical resistance (TEER) value (up to 3,000 ohm cm²), enabling drug transport studies. However, differentiation of cilia and mucin-secreting cells was not deemed to be complete in these cultures. Of important note is that the feasibility of the passage-cultured human nasal epithelial cell layer for in vitro drug transport studies was confirmed by transport experiments with ¹⁴C-mannitol and budesonide. Apparent permeability coefficient (P_{app}) values of ¹⁴C-mannitol and budesonide at each passage (Figure 9.1) suggest that the culture model would be suitable for reliable drug transport studies up to passage-4 culture. Contrary to mannitol transport, budesonide showed rather constant P_{app} values regardless of TEER values, suggesting that rather high lipophilicity of budesonide may be the predominant factor governing the permeation. In other words, the contribution of paracellular permeation via tight junctions of the cultured cell layer does not seem to significantly influence P_{app} of lipophilic solute(s), since the transcellular route is the major transport route of such lipophilic drugs. When the TEER value was higher than 500 ohm cm², constant P_{app} values were obtained regardless of the budesonide concentration (10 and 20 μg/ml) and passage number. These data suggest that the passage-cultured human nasal epithelial cell monolayer could be utilized reliably for in vitro drug transport studies.

In order to verify the utility of this passaged culture model for actual nasal transepithelial drug delivery, a series of antiallergic drugs were selected for transport studies and evaluated for the influence of lipophilicity of these drugs on their permeabilities observed across the cultured cell layer [73]. Permeability characteristics of model drugs across the cell layer were then compared with those reported for excised porcine nasal mucosa to demonstrate the feasibility of the passage-cultured nasal epithelial culture model for drug

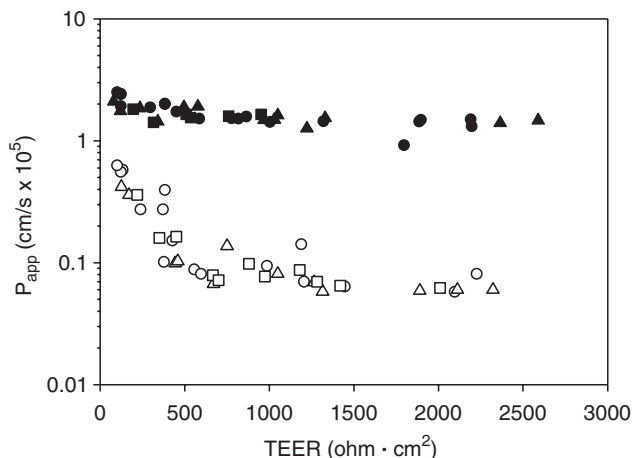


Figure 9.1 Relationship between the transepithelial electrical resistance (TEER) value of the passage-cultured human nasal epithelial cell layer and permeability of ^{14}C -mannitol (\circ , passage-2; Δ , passage-3; \square , passage-4) and budesonide (\bullet , passage-2; \blacktriangle , passage-3; \blacksquare , passage-4). (Data from Ref. [40]).

transport studies [73]. As shown in Figure 9.2, a similar log-linear relationship was reported for transport of various compounds across the excised porcine nasal mucosa ($r^2 = 0.81$, when lidocaine was ignored as an outlier) [55, 74]. P_{app} values of antiallergic drugs across the passage-cultured human nasal epithelial cell layer were significantly lower than those estimated across the excised porcine nasal mucosa. For example, mannitol P_{app} across the passage-cultured human nasal epithelial cell layer was $0.90 \pm 0.30 (\times 10^{-6} \text{ cm/s})$ [40], while the excised porcine nasal mucosa showed mannitol P_{app} of $3.9 \pm 2.2 (\times 10^{-6} \text{ cm/s})$ [55]. This discrepancy could be due to the species differences between human versus porcine tissues/cells and/or to differences in tight junctional properties of the two nasal models. TEER values of 40–120 ohm cm^2 reported for the nasal mucosa excised from various animals (e.g., sheep, rabbit, and cow/ox) and human [12] are considerably lower than that obtained in passage-cultured human nasal epithelial cell layer studies ($>1,000 \text{ ohm cm}^2$). However, a good log-linear relationship between lipophilicity index and P_{app} found in both nasal models indicates that lipophilicity index (i.e., $\log P$) of compounds is the most important factor that determine the nasal permeability and that the passage-cultured human nasal epithelial cell layer model is indeed quite useful for predicting the nasal permeability of small molecular drugs.

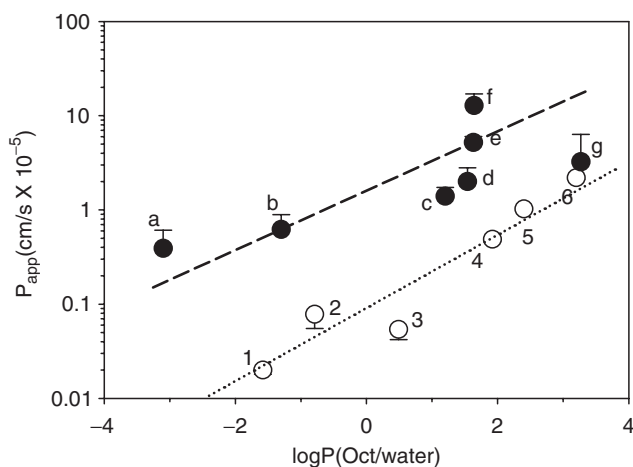


Figure 9.2 Relationship between $\log P$ values of various drugs and P_{app} across the passage-cultured human nasal epithelial cell monolayer using LCC method. 1 = albuterol hemisulfate, 2 = albuterol, 3 = fexofenadineHCl, 4 = dexamethasone, 5 = triamcinolone acetonide, 6 = budesonide, a = mannitol, b = melagatran, c = sumatriptan, d = propranolol, e = nicotine, f = lidocaine, g = testosterone. \circ : transport across the human nasal epithelial cell monolayer passage-cultured on Transwell, \bullet : data observed using excised porcine nasal mucosa mounted in Ussing chambers (Data from Ref. [73]).

9.5.4.2. Air-Interfaced Culture Method

In nasal epithelium, important properties of cultured epithelial cells include the formation of confluent cell layers functionally interconnected by tight junctional proteins, expression of apical cilia, and mucin production and secretion. Among them, ciliated cells of nasal epithelium play an important role in physiological function (e.g., mucociliary clearance), which may also be relevant to nasal drug delivery [21]. Additionally, the expression of various transporters and presence of enzymatic systems in in vitro cell culture models will increase the predictive potential of such models. However, compared to the in vivo nasal epithelium, the passaged nasal culture model has been reported to exhibit relatively undifferentiated epithelial cells with few ciliated cells when cultured with LCC method [40]. The attainment of differentiated phenotype as well as morphological and functional features of cells akin to those found in in vivo setting may be greatly affected by specific culture conditions. These conditions are the substratum on to which cells are cultivated, culture media including appropriate additives for induction of cell differentiation (e.g., retinoic acid), and liquid-covered versus air-interfaced (AIC) culture conditions. Moreover, the development of serum-free (but hormone-supplemented) culture medium has made it possible to induce the differentiation of airway epithelial cells with morphologically resembling the epithelium in vivo [69, 75]. Thus, AIC culture condition coupled with defined, serum-free medium is commonly used for epithelial cell cultures [65, 76, 77], resulting in more ciliated cells and/or enhanced mucin secretion.

For AIC conditions, the apical surface of the epithelial cell layer is exposed to air after the nasal cells reached confluence on the Transwell® insert, while the basolateral side is fed with culture fluid. Figure 9.3 shows TEER changes in epithelial cell layers cultured up to 20 days in LCC versus AIC methods [46]. In AIC condition (initiated from day 3 after seeding), TEER peaked on day 5 and maintained above the TEER values observed for LCC counterparts. By contrast, TEER observed for LCC conditions peaked on day 2 and declined toward zero by day 15. These data indicate that human nasal epithelial cells at an air interface culture exhibit better electrophysiological characteristics than those cultured by the conventional liquid-covered conditions.

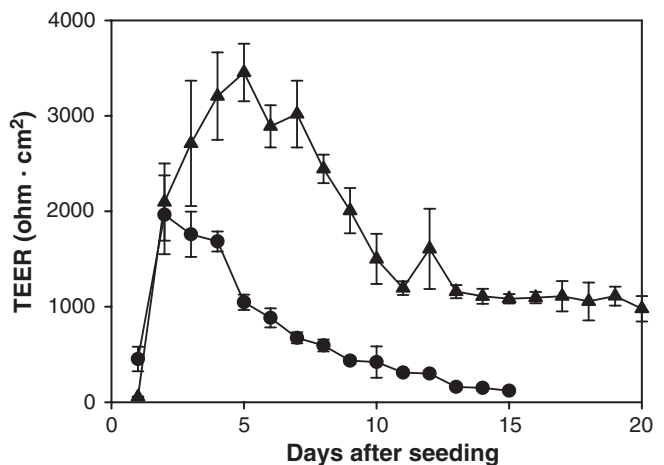


Figure 9.3 Changes in transepithelial electrical resistance (TEER) of human nasal epithelial cell layers grown under LCC (●) versus AIC (▲) conditions. Each data point represents the mean \pm SD of three determinations. (Data from Ref. [46]).

Morphological characteristics of nasal epithelial cells, especially the development of cilia, were observed by scanning electron microscopy (SEM) studies [46]. The most prominent morphological difference between LCC versus AIC cultures was the development of ciliated cells. The presence of cilia on the apical surface of AIC culture was evident on day 7 in culture. The number of ciliated cells increased on the 14th day. Markedly increased numbers of ciliated cells matured with long and beating healthy cilia were observed after 3 weeks of AIC culture. In short, AIC conditions allow growth of epithelial cells in a configuration resembling that in *in vivo* conditions. It has also shown that cells grown in AIC conditions not only mimic the morphological features of the epithelium but also exhibit many of the physiological and biochemical activities observed *in vivo* [68]. In LCC conditions, by contrast, flattened ciliated cells and numerous microvilli were observed after 3 weeks. It can be stressed that the selection of culture medium used in AIC cultures may also have played an important role. The bronchial epithelial cell growth medium (BEGM), which is commonly used for AIC cultures, is reported to be suitable for obtaining more homogeneous cell morphology than Dulbecco's modified Eagle's medium (DMEM), which was used in the LCC method [77]. DMEM with 10% FBS seems to be critical to stimulate cell proliferation in the early stage of the culture [40], while retinoic acid in BEGM seems to be an important factor for the growth and differentiation of airway epithelial cells [78, 79]. Therefore, the mixture of BEGM and DMEM/F12 (Dulbecco's modified Eagle's medium/F12 Ham's) (1:1) with all supplements may be suitable for AIC cultures of human nasal epithelial cells, as greater and prolonged TEER values of AIC cultures are found (Figure 9.3).

It can be noted that airway mucin gene expression was more significant in AIC culture on 21 days than LCC on 7 days, perhaps confirming the importance of retinoic acid in BEGM and AIC conditions on the growth and differentiation of airway epithelial cells [78, 79]. We surmise that AIC cultures probably can deliver oxygen much more efficiently across the thin film of liquid to the cells, subsequently changing cellular respiration to a more aerobic nature in AIC conditions [76] and improving the differentiation of nasal epithelial cells than LCC conditions. These factors may have led to higher TEER values for up to 21 days of human nasal epithelial cell culture in AIC conditions.

Because mucin and/or cilia systems of AIC cultured epithelial cells may work as a barrier for drug transport, lower P_{app} values are expected in cell layers cultured in AIC than in LCC methods. However, it was interesting to note that no significant differences in P_{app} values were observed between the cell layers cultured with the two methods (Table 9.1). This is in contrast to solute permeabilities reported previously for cell layers cultured with LCC versus AIC methods [76, 80]. For example, Yang et al. reported that P_{app} of lipophilic solutes (e.g., various β -blockers) across the primary cultured conjunctival epithelial cell layer are about threefold lower when cultured under AIC than LCC conditions, suggesting that the permeability of AIC cultured cell layers generally better reflects that of the excised tissue than LCC counterparts. Mathias et al. [76] also reported that the permeability of hydrophilic solutes across the primary rabbit tracheal epithelial cell layer cultured under AIC conditions was only half of that observed for cell layers cultured under

Table 9.1 Apparent permeability coefficients (P_{app}) of ^{14}C -mannitol and budesonide across the passage-cultured human nasal epithelial cell layer grown under AIC or LCC conditions for 7 days.

Culture method	$P_{app} (\times 10^{-6} \text{ cm/s})$	
	^{14}C -Mannitol	Budesonide
LCC	0.90 ± 0.30	15.34 ± 0.66
AIC	0.86 ± 0.04	16.53 ± 1.58

Source: Data from Ref. [46].

AIC, Air-interfaced culture.

LCC, Liquid-covered culture.

LCC conditions, whereas the permeability of lipophilic solutes was similar to each other for cell layers grown in either AIC or LCC method. These investigators suggested that the tight junctional arrangement (e.g. number of strands, junctional length, presence of pores or channels within the junction, or length of lateral intercellular space) might be widely different, depending on specific culture conditions. The higher than expected P_{app} of mannitol found in the human nasal epithelial cell layer cultured using AIC method may be due to factors related to characteristics of the human nasal cells which differs from the conjunctival cells used by Yang et al. [80] or tracheal cells used by Mathias et al. [76]. However, the exact nature of factor(s) that would have caused these disparate results would require further investigations. Nevertheless, these data imply that the intact tight junction was well developed in both AIC and LCC methods of culturing human nasal epithelial cell layers, enabling useful mechanistic studies using both hydrophilic and lipophilic drugs. In a recent study, the enhancing effect of various surfactants on the nasal permeability of fexofenadine-HCl was evaluated using AIC-cultured human nasal epithelial cell monolayer model [81]. It was demonstrated that this model is a useful tool not only for evaluating the in vitro nasal drug transport but also for studying the mechanism and toxicity of enhancers.

9.6. Conclusions

Recent development of an in vitro model of human nasal epithelial cells cultured on permeable supports may be useful for various mechanistic studies of nasal transport/physiology in health and disease. Although the model is promising and important, problems including the limited amount of available cells and issues pertaining to epithelial cell differentiation in culture remain to be resolved further. Cultures of human nasal epithelial cell layers on Transwell[®] insert under AIC or LCC conditions may be particularly useful for in vitro drug transport studies. Serially passaged culture under AIC conditions allows the preparation of a comparably larger number of highly differentiated epithelial cell layers with cilia on the apical surface and mucin gene expression, compared to cells cultured in LCC conditions. Higher TEER value observed in AIC conditions was maintained for a longer duration than that in LCC. Thus, the AIC culture of passaged human nasal epithelial cell layers seems to be

an appropriate and more reliable in vitro model for nasal epithelial studies of mucin secretion and cell differentiation, in addition to nasal drug transport studies.

References

1. S. E. Chang and Y. W. Chien. Intranasal drug administration for systemic medication. *Pharm Int* 5:287–288 (1984).
2. A. Hussain, S. Hirai, and R. Bawarshi. Nasal absorption of natural contraceptive steroids in rats-progesterone absorption. *J Pharm Sci* 70:466–467 (1981).
3. J. A. Faraj, A. A. Hussain, Y. Aramaki, K. Iseki, M. Kagoshima, and L. W. Dittert. Mechanism of nasal absorption of drugs, III. Nasal absorption of leucine enkephalin. *J Pharm Sci* 79:698–702 (1990).
4. F. W. Merkus, N. G. Schipper, and J. C. Verhoef. The influence of absorption enhancers on intranasal insulin absorption in normal and diabetic subjects. *J Control Release* 41:69–75 (1996).
5. B. J. Lipworth and C. M. Jackson. Safety of inhaled and intranasal corticosteroids: Lessons for the new millennium. *Drug Saf* 23:11–33 (2000).
6. M. Hinchcliffe and L. Illum. Intranasal insulin delivery and therapy. *Adv Drug Deliv Rev* 35:199–234 (1999).
7. L. Illum. Nasal drug delivery-possibilities, problems and solutions. *J Control Release* 87:87–198 (2003).
8. M. Singh, M. Briones, and D. T. O'Hagan. A novel bioadhesive intranasal delivery system for inactivated influenza vaccines. *J Control Release* 70:267–276 (2001).
9. Y. W. Chien. Nasal drug delivery and delivery systems. In Y. W. Chien (ed.), *Novel Drug Delivery Systems* (2nd ed.), Marcel Dekker, Inc., New York, 1992, pp. 229–268.
10. Z. Shao, R. Krishnamoorthy, and A. K. Mitra. Cyclodextrins as nasal absorption promoters of insulin: Mechanistic evaluations. *Pharm Res* 9:1157–1163 (1992).
11. A. H. Krauland, V. M. Leitner, V. Grabovac, and A. Bernkop-Schnurch. In vivo evaluation of a nasal insulin delivery system based on thiolated chitosan. *J Pharm Sci* 95:2463–2472 (2006).
12. H. P. Merkle, G. Ditzinger, S. R. Lang, H. Peter, and M. C. Schmidt. In vitro cell models to study nasal mucosal permeability and metabolism. *Adv Drug Deliv Rev* 29:51–79 (1998).
13. N. R. Mathias, F. Yamashita, and V. H. Lee. Respiratory epithelial cell culture models for evaluation of ion and drug transport. *Adv Drug Deliv Rev* 22:215–249 (1996).
14. Y. W. Chien and S. F. Chang. Intranasal drug delivery for systemic medications. *Crit Rev Ther Drug Carrier Syst* 4:67–194 (1987).
15. Y. W. Chien, K. S. Su, and S. F. Chang. Anatomy and physiology of the nose. In Y.W. Chen, K.S. Su, and S.F. Chang (eds.), *Nasal Systemic Drug Delivery: Drugs and the Pharmaceutical Sciences*, Marcel Dekker, Inc., New York, 1989, pp. 1–26.
16. E. E. Morrison and R. M. Constanzo. Morphology of the human olfactory epithelium. *J Comp Neurol* 297:1–13 (1990).
17. F. M. Baroody. Nasal and paranasal sinus anatomy and physiology. *Clin Allergy Immunol* 19:1–21 (2007).
18. S. Mathison, R. Nagilla, and U. B. Kompella. Nasal route for direct delivery of solutes to the central nervous system: Fact or fiction? *J Drug Target* 5:415–441 (1998).
19. B. Petruson, H. A. Hansson, and G. Karlsson. Structural and functional aspects of cells in the nasal mucociliary system. *Arch Otolaryngol* 110:576–581 (1984).

20. B. L. Alison and P. M. Gary. Nasal drug delivery. In M. H. Anya, W. L. Andrew, and S. James (eds.), *Drug Delivery and Targeting*, Taylor & Francis, London, 2001, pp. 237–268.
21. N. G. Schipper, J. C. Verhoef, and F. W. Merkus. The nasal mucociliary clearance: Relevance to nasal drug delivery. *Pharm Res* 8:807–814 (1991).
22. D. F. Proctor. The mucociliary system. In D. F. Proctor and I. Andersen (eds.), *The Nose: Upper Airway Physiology and the Atmospheric Environment*, Elsevier Biomedical Press, Amsterdam, 1982, pp. 245–305.
23. F. Y. Chung and M. D. Donovan. Nasal pre-systemic metabolism of peptide drugs: Substance P metabolism in the sheep nasal cavity. *Int J Pharm* 128:229–237 (1996).
24. M. A. Hussain and B. J. Aungst. Nasal mucosal metabolism of an LH-RH fragment and inhibition with boroleucine. *Int J Pharm* 105:7–10 (1994).
25. V. D. Romeo, J. deMeireles, A. P. Sileno, H. K. Pimplaskar, and C. R. Behl. Effects of physicochemical properties and other factors on systemic nasal drug delivery. *Adv Drug Deliv Rev* 29:89–116 (1998).
26. C. McMartin, L. E. Hutchinson, R. Hyde, and G. E. Peters. Analysis of structural requirements for the absorption of drugs and macromolecules from the nasal cavity. *J Pharm Sci* 76:535–540 (1987).
27. M. I. Ugwoke, R. U. Agu, N. Verbeke, and R. Kinget. Nasal mucoadhesive drug delivery: Background, applications, trends and future perspectives. *Adv Drug Deliv Rev* 57:1640–1665 (2005).
28. K. Abe, T. Irie, and K. Uekama. Enhanced nasal delivery of luteinizing hormone releasing hormone agonist buserelin by oleic acid solubilized and stabilized in hydroxypropyl- β -cyclodextrin. *Chem Pharm Bull* 43:2232–2237 (1995).
29. S. S. Davis and L. Illum. Absorption enhancers for nasal drug delivery. *Clin Pharmacokinet* 42:1107–1128 (2003).
30. V. Dodane, M. A. Khan, and J. R. Merwin. Effect of chitosan on epithelial permeability and structure. *Int J Pharm* 182:21–32 (1999).
31. K. K. Kandimalla and M. D. Donovan. Localization and differential activity of P-glycoprotein in the bovine olfactory and nasal respiratory mucosae. *Pharm Res* 22:1121–1128 (2005).
32. K. K. Kandimalla and M. D. Donovan. Carrier mediated transport of chlorpheniramine and chlorcyclizine across bovine olfactory mucosa: Implications on nose-to-brain transport. *J Pharm Sci* 94:613–624 (2005).
33. N. V. Chemuturi, J. E. Haraldsson, T. Prisinzano, and M. Donovan. Role of dopamine transporter (DAT) in dopamine transport across the nasal mucosa. *Life Sci* 79:1391–1398 (2006).
34. R. Kimura, M. Miwa, Y. Kato, S. Yamada, and M. Sato. Nasal absorption of tetraethylammonium in rats. *Arch Int Pharmacodyn Ther* 302:7–17 (1989).
35. R. Agu, H. V. Dang, M. Jorissen, T. Willems, S. Vandoninck, J. Van Lint, J. V. Vandenheede, R. Kinget, and N. Verbeke. In vitro polarized transport of L-phenylalanine in human nasal epithelium and partial characterization of the amino acid transporters involved. *Pharm Res* 20:1125–1132 (2003).
36. N. V. Chemuturi, P. Hayden, M. Klausner, and M. D. Donovan. Comparison of human tracheal/bronchial cell culture and bovine nasal respiratory explants for nasal drug transport studies. *J Pharm Sci* 94:1976–1985 (2005).
37. J. Singh, S. Pandit, V. W. Bramwell, and H. O. Alpar. Diphtheria toxoid loaded poly-(ϵ -caprolactone) nanoparticles as mucosal vaccine delivery systems. *Methods* 38:96–105 (2006).
38. J. L. Lemoine, R. Farley, and L. Huang. Mechanism of efficient transfection on the nasal airway epithelium by hypotonic shock. *Gene Ther* 12:1275–1282 (2005).
39. C. Porta, S. Dossena, V. Rossi, M. Pinza, and D. Cremaschi. Rabbit nasal mucosa: Nanosphere coated polypeptides bound to specific anti-polypeptide IgG are better

- transported than nanospheres coated with polypeptides or IgG alone. *Biochim Biophys Acta* 1466:115–124 (2000).
40. J. W. Yoo, Y. S. Kim, S. H. Lee, M. K. Lee, H. J. Roh, B. H. Jhun, C. H. Lee, and D. D. Kim. Serially passaged human nasal epithelial cell monolayer for *in vitro* drug transport studies. *Pharm Res* 20:1690–1696 (2003).
 41. P. H. Johnson and S. C. Quay. Advances in nasal drug delivery through tight junction technology. *Expert Opin Drug Deliv* 2:281–298 (2005).
 42. M. T. De Maqistris. Zonula occludens toxin as a new promising adjuvant for mucosal vaccines. *Vaccine* 24:S60–S61 (2006).
 43. S. C. Chen, K. Eiting, K. Cui, A. K. Leonard, D. Morris, C. Y. Li, K. Farber, A. P. Sileno, M. E. Houston Jr., P. H. Johnson, S. C. Quay, and H. R. Costantino. Therapeutic utility of a novel tight junction modulating peptide for enhancing intranasal drug delivery. *J Pharm Sci* 95:1364–1371 (2006).
 44. S. Harikarnpakdee, V. Lipipun, N. Sutanthavibul, and G. C. Ritthidei. Spray-dried mucoadhesive microspheres: Preparation and transport through nasal cell monolayer. *AAPS PharmSciTech* 7:E12 (2006).
 45. J. Wang, Y. Tabata, and K. Morimoto. Aminated gelatin microspheres as a nasal delivery system for peptide drugs: Evaluation of *in vitro* release and *in vivo* insulin absorption in rats. *J Control Release* 113:31–37 (2006).
 46. M. K. Lee, J. W. Yoo, H. Lin, Y. S. Kim, D. D. Kim, Y. M. Choi, S. K. Park, C. H. Lee, and H. J. Roh. Air-liquid interface culture of serially passaged human nasal epithelial cell monolayer for *in vitro* drug transport studies. *Drug Deliv* 12: 305–311 (2005).
 47. S. Hirai, T. Yashiki, and H. Mima. Effect of surfactants on the nasal absorption of insulin in rats. *Int J Pharm* 9:165–172 (1981).
 48. P. Russo, C. Sacchetti, I. Pasquali, R. Bettini, G. Massimo, P. Colombo, and A. Rossi. Primary microparticles and agglomerates of morphine for nasal insufflation. *J Pharm Sci* 95:2553–2561 (2006).
 49. R. J. Henry, N. Ruano, D. Casto, and R. H. Wolf. A pharmacokinetic study of midazolam in dogs: Nasal drop vs. atomizer administration. *Pediatr Dent* 20:321–326 (1998).
 50. E. Gavini, A. B. Heqqe, G. Rassu, V. Sanna, C. Testa, G. Pirisino, J. Karlsen, and P. Giunchedi. Nasal administration of carbamazepine using chitosan microspheres; *in vitro/in vivo* studies. *Int J Pharm* 307:9–15 (2006).
 51. J. T. Kelly, B. Asgharian, and B. A. Wong. Inertial particle deposition in a monkey nasal mold compared with that in human nasal replicas. *Inhal Toxicol* 17:823–830 (2005).
 52. C. Tas, C. K. Ozkan, A. Savaser, Y. Ozkan, U. Tasdemir, and H. Altunav. Nasal absorption of metoclopramide from different Carbopol 981 based formulations: *In vitro*, *ex vivo* and *in vivo* evaluation. *Eur J Pharm Biopharm* 64:246–254 (2006).
 53. M. C. Schmidt, D. Simmen, M. Hilbe, P. Boderke, G. Ditzinger, J. Sandow, S. Lang, W. Rubas, and H. P. Merkle. Validation of excised bovine nasal mucosa as *in vitro* model to study drug transport and metabolic pathways in nasal epithelium. *J Pharm Sci* 89:396–407 (2000).
 54. K. Hosoya, H. Kubo, H. Natsume, K. Sugibayashi, and Y. Morimoto. Evaluation of enhancers to increase nasal absorption using Ussing chamber technique. *Biol Pharm Bull* 17:316–322 (1994).
 55. C. Wadell, E. Bjork, and O. Camber. Permeability of porcine nasal mucosa correlated with human nasal absorption. *Eur J Pharm Sci* 18:47–53 (2003).
 56. S. Lang, P. Langguth, R. Oschmann, B. Traving, and H. P. Merkle. Transport and metabolic pathway of thymocartin (TP4) in excised bovine nasal mucosa. *J Pharm Pharmacol* 48:1190–1196 (1996).

57. M. A. Wheatley, J. Dent, E. B. Wheeldon, and P. Smith. Nasal drug delivery: An *in vitro* characterization of transepithelial electrical properties and fluxes in the presence or absence of enhancers. *J Control Release* 8:167–177 (1988).
58. U. Werner and T. Kissel. In-vitro cell culture models of the nasal epithelium: A comparative histochemical investigation of their suitability for drug transport studies. *Pharm Res* 13:978–988 (1996).
59. K. L. Audus, R. L. Bartel, I. J. Hidalgo, and R. T. Borchardt. The use of cultured epithelial and endothelial cells for drug transport and metabolism studies. *Pharm Res* 7:435–451 (1990).
60. C. Ruckes, U. Blank, K. Moller, J. Rieboldt, H. Lindemann, G. Munker, W. Clauss, and W. M. Weber. Amiloride-sensitive Na⁺ channels in human nasal epithelium are different from classical epithelial Na⁺ channels. *Biochem Biophys Res Commun* 237:488–491 (1997).
61. M. Jorissen and A. Bessems. Influence of culture duration and ciliogenesis on the relationship between ciliary beat frequency and temperature in nasal epithelial cells. *Eur Arch Otorhinolaryngol* 252:451–454 (1995).
62. T. Kissel and U. Werner. Nasal delivery of peptides: An *in vitro* cell culture model for the investigation of transport and metabolism in human nasal epithelium. *J Control Release* 53:195–203 (1998).
63. H. V. Dang, R. U. Agu, M. Jorissen, R. Kinget, and N. Verbeke. Characterization of human nasal primary culture systems to investigate peptide metabolism. *Int J Pharm* 238:247–256 (2002).
64. U. Werner and T. Kissel. Development of a human nasal cell culture model and its suitability for transport and metabolism studies under in vitro conditions. *Pharm Res* 12:565–571 (1995).
65. R. U. Agu, M. Jorissen, T. Willems, P. Augustijns, R. Kinget, and N. Verbeke. In-vitro nasal drug delivery studies: Comparison of derivatised, fibrillar and polymerised collagen matrix-based human nasal primary culture systems for nasal drug delivery studies. *J Pharm Pharmacol* 53:1447–1456 (2001).
66. V. E. Steele and J. T. Arnold. Isolation and long-term culture of rat, rabbit and human nasal turbinate epithelial cells. *In Vitro Cell Dev Biol* 21:671–687 (1985).
67. R. U. Agu, H. Vu Dang, M. Jorissen, T. Willems, R. Kinget, and N. Verbeke. Nasal absorption enhancement strategies for therapeutic peptides: An *in vitro* study using cultured human nasal epithelium. *Int J Pharm* 237:179–191 (2002).
68. T. E. Gray, K. Guzman, C. W. Davis, L. H. Abdullah, and P. Nettesheim. Mucociliary differentiation of serially passaged normal human tracheobronchial epithelial cells. *Am J Respir Cell Mol Biol* 14:104–112 (1996).
69. R. Wu, J. Yankaskas, E. Cheng, M. R. Knowles, and R. Boucher. Growth and differentiation of human nasal epithelial cells in culture. Serum-free, hormone-supplemented medium and proteoglycan synthesis. *Am Rev Respir Dis* 132:311–320 (1985).
70. D. P. Chopra, J. Sullivan, J. J. Wille, and K. M. Siddiqui. Propagation of differentiating normal human tracheobronchial epithelial cells in serum-free medium. *J Cell Physiol* 130:173–181 (1987).
71. H. J. Roh, E. K. Goh, S. G. Wang, K. M. Chon, J. H. Yoon, and Y. S. Kim. Serially passaged normal human nasal epithelial cells: Morphology and mucous secretory differentiation. *Kor J Rhinol* 6:107–112 (1999).
72. D. J. Thornton, T. Gray, P. Nettesheim, M. Howard, J. S. Koo, and J. K. Sheehan. Characterization of mucins from cultured normal human tracheobronchial epithelial cells. *Am J Physiol* 278:L1118–L1128 (2000).
73. H. Lin, J. W. Yoo, H. J. Roh, M. K. Lee, S. J. Chung, C. K. Shim, and D. D. Kim. Transport of anti-allergic drugs across the passage cultured human nasal epithelial cell monolayer. *Eur J Pharm Sci* 26:203–210 (2005).

74. K. Osth, J. Grasjo, and E. Bjork. A new method for drug transport studies on pig nasal mucosa using a horizontal Ussing chamber. *J Pharm Sci* 91:1259–1273 (2002).
75. D. C. Gruenert, C. B. Basbaum, and J. H. Widdicombe. Long-term culture of normal and cystic fibrosis epithelial cells grown under serum-free condition. *In Vitro Cell Dev Biol* 26:411–418 (1990).
76. N. R. Mathias, K. J. Kim, T. W. Robison, and V. H. Lee. Development and characterization of rabbit tracheal epithelial cell monolayer models for drug transport studies. *Pharm Res* 12:1499–1505 (1995).
77. C. Mattinger, T. Nyugen, D. Schafer, and K. Hormann. Evaluation of serum-free culture conditions for primary human nasal epithelial cells. *Int J Hyg Environ Health* 205:235–238 (2002).
78. J. H. Yoon, H. J. Moon, J. K. Seong, C. H. Kim, J. J. Lee, L. Y. Choi, M. S. Song, and S. H. Kim. Mucociliary differentiation according to time in human nasal epithelial cell culture. *Differentiation* 70:77–83 (2000).
79. L. Kaartinen, P. Nettesheim, K. B. Adler, and S. H. Randell. Rat tracheal epithelial cell differentiation in vitro. *In Vitro Cell Dev Biol* 29A: 481–492 (1993).
80. J. J. Yang, H. Ueda, K. Kim, and V. H. Lee. Meeting future challenges in topical ocular drug delivery: Development of an air-interfaced primary culture of rabbit conjunctival epithelial cells on a permeable support for drug transport studies. *J Control Release* 65:1–11 (2000).
81. H. Lin, M. Gebhardt, S. Bian, K. A. Kwon, C. K. Shim, S. J. Chung, and D. D. Kim. Enhancing effect of surfactants on fexofenadine-HCl transport across the human nasal epithelial cell monolayer. *Int J Pharm* 330:23–31 (2007).

In Vitro Models of the Tracheo-Bronchial Epithelium

Carsten Ehrhardt, Ben Forbes, and Kwang-Jin Kim

Abstract The lung is composed of two major anatomically distinct regions: the conducting airways (tracheo-bronchial region) and the gas-exchanging airspaces (alveolar region). The conducting airways can be further subdivided into the trachea plus larger bronchi and the distal bronchiolar airways. Each of these regions consists of distinct types of epithelial cells with unique phenotypes, morphologies and associated physiological functions. This chapter focuses on various model systems that have been utilised to study drug transport and metabolism in the adult tracheo-bronchial epithelium. This includes primary cell cultures, airway cell lines and culture systems with or without the cystic fibrosis gene deletion. The permeability of increasing numbers of compounds in these drug absorption models has been reported. Cell culture systems are particularly amenable to the study of transport mechanisms and the expression of a variety of active transport mechanisms in airway cell culture systems is summarised. Another application of epithelial cell models is to predict drug absorption in vivo. The drug metabolising capacity of electrically tight and non-barrier forming airway cell models is also summarised in terms of the P450, phase II enzymes plus peptidase and protease activity.

Keywords: Bronchial epithelium; Pulmonary drug absorption; Pulmonary metabolism; Drug transport; Permeability

Abbreviations

ABC	ATP-binding cassette
ACE	Angiotensin-converting enzyme
AIC	Air-interfaced culture
AP	Aminopeptidase
ATB	Broad-spectrum amino acid transporter
ATCC	American type culture collection
ATP	Adenosine triphosphate
BCRP	Breast cancer-related protein
CAT	Cationic amino acid transporter
CD	Cluster of differentiation
CF	Cystic fibrosis

CFTR	Cystic fibrosis transmembrane conductance regulator
COPD	Chronic obstructive pulmonary disease
CP	Carboxypeptidase
CYP	Cytochrome P450
DPP	Dipeptidyl peptidase
FMO	Flavin monooxygenase
GSH	Glutathione
GST	Glutathione S-transferase
GTP	Glutamyltranspeptidase
HBE	Human bronchial epithelium
HIV	Human immunodeficiency virus
I_{sc}	Short-circuit current
LAT	L-amino acid transporter
LCC	Liquid-covered culture
LRP	Lung resistance protein
MRP	Multidrug resistance-associated protein
MT	Methyltransferase
NAT	<i>N</i> -acetyl transferase
NEP	Neutral endopeptidase
NHBE	Normal human bronchial epithelial cells
OCT	Organic cation transporter
OCTN	Novel organic cation transporter
P_{app}	Apparent permeability coefficient
PEPT	Di/Tri-peptide transporter
P-gp	P-glycoprotein
Rh123	Rhodamine 123
RT-PCR	Reverse transcription-polymerase chain reaction
SLC	Solute carrier protein
SULT	Sulfotransferase
TEER	Transepithelial electrical resistance
UGT	UDP-glucuronosyl transferase

10.1. Introduction

10.1.1. Anatomy of the Lung Airways

The respiratory system can be separated anatomically into the conducting and respiratory regions. The conducting airways consist of the air-transmitting passages of the nose, nasopharynx, larynx, trachea, bronchi and bronchioles [1, 2], where the latter three entities form the tracheo-bronchial region of the lung (generations 1–16 in the bifurcating airway model; Figure 6.1, Chap.6). The actual exchange of gases (i.e., fresh oxygen into and carbon dioxide out of the body) occurs across the distal lung respiratory epithelium, comprising the alveolar ducts and saccules (i.e., the alveoli, generations 17–23 in the bifurcating airway model; Figure 6.1, Chap. 6). The main function of the conducting airways is to act as conduit for air movement and in addition to provide filtration, warming and humidification of inhaled air. Specialised extra-pulmonary parts of the conducting system also serve other functions, for example the nose with the sense of smell, the pharynx in alimentation and the larynx in phonation [3].

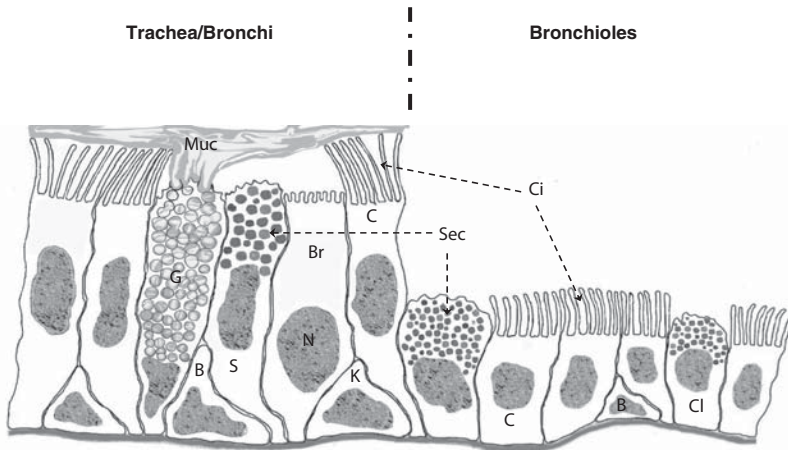


Figure 10.1 Typical tracheo-bronchial and bronchiolar epithelia showing the major cell types. The tracheo-bronchial epithelium showing the pseudostratified nature of the columnar epithelium, principally composed of ciliated cells (C), interspersed with goblet cells (G), brush cells (Br), serous cells (S), Kulchitsky's cells (K) and basal cells (B). The bronchiolar epithelium showing the cuboidal nature of the epithelium, principally composed of ciliated cells (C), Clara cells (Cl) and infrequent basal cells. Muc = mucus; Ci = cilia; N = nucleus; Sec = secretory granules.

Gradual changes in the structure of the conducting airways occur as the diameter of the respiratory tubes becomes smaller [4]. The epithelium gradually changes from being pseudostratified and ciliated with goblet cells and submucosal glands interspersed to becoming a flattened squamous epithelium devoid of goblet cells or glands (Figure 10.1). The *lamina propria* also decreases in thickness and elastic fibres become more numerous, as the airways bifurcate. A smooth muscle layer forms a conspicuous component of the subepithelial wall of the higher generation conducting airways but becomes less prominent in the alveolar ducts and is absent in alveolar walls. The cartilage around the bronchi is also gradually reduced and finally disappears when the airway diameter decreases to about 1 mm in size. At this point, the tube is termed a bronchiole and the lack of cartilage enables bronchioles to constrict to the point of closure in asthmatic patients [5].

The tracheo-bronchial epithelium forms the interface between the conducting airways and inspired air. As described above, the epithelium is layered upon a connective tissue substratum consisting of a basement membrane, *lamina propria*, and submucosa [6]. The submucosa contains elastic fibres, a *muscularis mucosa*, connective tissues and seromucous glands. Lymphatics are also located in the bronchial walls [2].

In the trachea and bronchi, the pseudostratified, ciliated, columnar epithelium changes to a ciliated simple columnar one in smaller airway branches and seromucous glands decrease in number. Goblet cells are present in the tracheo-bronchial epithelium at all levels. The bronchioles (1 mm or less in diameter) possess a ciliated epithelium of columnar to cuboidal shape (Figure 10.1). The number of goblet cells in the bronchioles is reduced further compared to the proximal bronchi, and Clara cells are present [2]. The sheathing spirals of smooth muscles in this region are thicker than those found elsewhere in the lung, and are thought to stabilise the tissue in absence of cartilage. In the

smaller bronchioles, which represent a transitional zone from the airway to the respiratory region, the epithelium is cuboidal with less ciliated cells and more Clara cells are present while goblet cells are absent. Thin connective tissues and an incomplete layer of smooth muscles form the supporting wall of the distal bronchioles.

10.1.1.1. Cell Types of Tracheo-Bronchial Epithelia

Several morphologically distinct cell types comprise the human tracheo-bronchial epithelium. Ciliated cells are terminally differentiated columnar cells that are thought to originate from basal or secretory cells. As a component of the mucociliary escalator system, their main function is to remove inhaled particulate matters, including viruses and bacteria, which have been trapped in the mucus [7]. There are also ciliated-secretory cells which bear fully developed cilia and contain mucus granules, albeit these are seen only occasionally. In general, secretory cells bear microvilli, but not cilia, on their apical surface. Secretory cells comprise 15–25% of the bronchial epithelium and are present in several forms. Mucous cells (also known as goblet cells) are the main producers of airway mucus and the predominant secretory cell type in the larger airways; neuroendocrine cells (Kulchitsky's cells, K-cells or small granule cells) contain amines and peptide hormones and rarely reach the lumen. Clara cells are the predominant cell type in the bronchioles and produce the surfactant apoproteins A and B and secretory leukoprotease inhibitors [3, 8–13]. The Clara cells may also participate in the clearance of noxious agents via the metabolic detoxification of inhaled agents. The contribution of Clara cells to the generation of normal human bronchiolar epithelium is substantial, demonstrating a role of the Clara cell in maintaining the normal epithelium of the distal airway [14].

While all the aforementioned cell types form the epithelial surface of the airways, basal cells reside deep in the tracheo-bronchial epithelium and are not directly in contact with the airway lumen. Basal cells are considered as the stem cell or progenitor cell of the bronchial epithelium and are pyramidal in shape with a low cytoplasmic/nuclear volume ratio [8, 15–17].

10.1.1.2. Barrier Function of the Airways

Bronchial epithelial cells are part of the non-specific immune system and they not only defend against the noxious substances gaining access into the body across the airway epithelial barriers but also impede the absorption of therapeutically useful agents [18]. This defence is mediated via the integrity of the airway epithelium that incorporates the physical barrier and secretory as well as ciliary functions. This provides the effective mucociliary clearance and secretion of mediators, protecting against a wide range of potentially injurious agents. Thus, the integrity of airway epithelial function is important for host defence.

10.1.1.2.1. Integrity of tracheo-bronchial epithelia: The bronchial epithelium forms a continuous layer, its integrity maintained by several cell–cell adhesion mechanisms [19]. The desmosomes (macula adherens) and the intermediate junctions (adherence junctions or zonula adherens) are involved in cell–cell adhesions. The tight junctions (zonula occludens) are narrow, belt-like structures surrounding each cell at the apical pole. These tight junctions provide a physical barrier, thereby preventing 'leakage' of water, ions and other

molecules (e.g., serum proteins). The epithelial cells are all anchored to the basement membrane by hemidesmosomes and other focal adhesion molecules (e.g., integrins, vinculin and radixin).

10.1.1.2.2. Mucociliary clearance: Inhaled particles are cleared from the airways through trapping of the particles in mucus upon deposition and subsequent clearance of the mucus (with trapped particles) which is propelled by the coordinated beating of cilia towards the throat. This is termed the mucociliary escalator system. The mucociliary function is regulated by a variety of factors, such as bradykinin, histamine and cytokines [20–24].

10.1.1.2.3. Secretion of protective mediators: To provide protection against potentially injurious agents which enter the respiratory tract from the environment during inspiration, the bronchial epithelium secretes a number of mediators, including antibacterial substances (e.g., lactoferrin and lysozyme), anti-proteases (e.g., alpha₁-protease inhibitor, secretory leuko-protease inhibitor, alpha₁-anti-chymotrypsin, alpha₂-macroglobulin and tissue inhibitors of metalloproteinases) and anti-oxidant molecules plus other molecules involved in redox regulation (e.g., glutathione, GSH, enzymes involved in GSH redox cycle, superoxide dismutase, ceruloplasmin, transferrin and catalase) [25–28]. The bronchial epithelium also produces components of the complement system, which act as opsonins, facilitating efficient phagocytosis by macrophages and eventual clearance [29]. In addition, bronchial epithelial cells transport secretory immunoglobulin A into the bronchial lumen [30].

10.1.2. Drug Delivery to the Tracheo-Bronchial Region

Aerosolised medicines have been used for centuries to treat respiratory diseases, with inhalation therapy for the airways focused primarily on the treatment of asthma and chronic obstructive pulmonary disease (COPD). The development of new products for delivery to the lungs for these respiratory diseases includes new steroids and beta agonists plus combination products featuring both agents. New classes of anti-asthma medication are also being developed for inhalation with the aim of delivering them directly to the inflamed airways.

With the recent advances in biotechnology, many companies have been formed with the goal of finding ways to deliver new drugs to the lung, with the target being the systemic circulation and not the lung itself [31, 32]. In particular, biopharmaceutical therapeutics based on proteins and peptides are expensive to produce and often have narrow therapeutic windows, requiring them to be delivered efficiently and reproducibly. The alveolar epithelium is obviously a more attractive target as a portal for drug entry into the systemic circulation from the standpoints of vast surface area coupled with an extremely thin barrier thickness. However, tracheo-bronchial targeting of biopharmaceuticals might benefit from delivery to the airways where the epithelium is leakier compared to the tighter alveolar epithelium and relatively free from macrophage surveillance.

Two specialised delivery strategies which target inhaled therapies to the lung are gene delivery and vaccination. These have been investigated widely with some degree of success [33]. The goal of aerosolised gene therapy in treating cystic fibrosis (CF) patients is to reconstitute the cystic fibrosis transmembrane conductance regulator (CFTR) function and normal chloride channel function

in the lung and in the airways in particular. Over 20 clinical trials have been carried out since the cloning of the CFTR gene in 1989 using three gene-transfer platforms: adenovirus, adeno-associated virus 2 and cationic liposomes. All three vectors have demonstrated proof-of-principle for gene transfer to airway epithelia and efforts to develop the first gene delivery product for inhalation are progressing. [33].

Another disease that has been targeted for treatment via aerosolised gene therapy is lung cancer [34]. Studies have demonstrated that inhaled delivery of polyethyleneimine DNA complexes results in a substantial gene expression level in mice lungs, with polyethylenimine-p53 and polyethyleneimine-interleukin 12 therapy both significantly reducing the number and size of osteosarcoma lung metastases in mice. Studies are underway to clarify the response to long-term repeated exposures of these aerosol gene therapies in lung cancer models [35].

The rationale for the inhaled delivery of vaccines is based on a number of advantages over injection therapy [36]. First, vaccination via inhalation avoids the need for disposal strategies for the large number of needles that would be used in mass vaccination campaigns in developing countries. Second, it prevents the spread of blood-borne diseases such as human immunodeficiency virus (HIV), which can be transmitted by improper use and handling of used sharps that may have been contaminated with the virus. Third, protection can be induced by exposing the airway mucosa to a variety of viruses, as the airways are the natural route of infection for many diseases. Finally, inhaled vaccination may work better than subcutaneous vaccination with young children, in whom the persistence of maternal antibodies does not appear to interfere with inhaled mucosal immunisation but does interfere with subcutaneous immunisation. Vaccination by inhalation was pioneered in the 1980s by Albert Sabin and his colleagues who were vaccinating children in Mexico against measles using an aerosolised vaccine [37]. By the mid-1990s, it was clear that this is an effective means of measles vaccination and accordingly several investigators began to consider the possibility of mass vaccination campaigns with an aerosolised measles vaccine in other developing countries [38, 39].

10.2. In Vitro Models of the Tracheo-Bronchial Epithelium

10.2.1. Primary Cell Cultures

Protocols for the isolation and culture of primary tracheo-bronchial epithelial cells obtained from the lungs of many species have been developed over the last 30 years. These include primary cultures of airway epithelial cells of the mouse [40], hamster [41], guinea pig [42], rat [43], ferret [44], rabbit [45, 46], dog [47], pig [48], cow [49], horse [50] and human [51–53]. Most of the protocols result in well-differentiated epithelial cells with mixed phenotypes and these primary cell cultures are generally good for drug absorption studies for the first couple of subcultures after which they lose their ability to form tight junctions and to generate high transepithelial electrical resistance (TEER). A linear drop in short-circuit current (I_{sc}) was observed over successive passages in human tracheal epithelial cells in primary culture [54]. These subcultures exhibited minimal rates of active Na^+ and Cl^- transport by passage 3 and beyond passage 4, the cells failed to generate any active ion transport when studied

using Ussing chamber techniques. These data suggest that it is important to develop airway epithelial cell lines that retain the ability to differentiate, form tight junctions and maintain ion channel/pump physiology when grown in vitro [54].

Ready-to-use culture systems of human tracheo-bronchial cell layers exhibiting well-differentiated ciliated and goblet cell phenotypes are commercially available (EpiAirway™ system, Mattek Corporation, Ashland, MA, USA) [55]. Although the EpiAirway™ is marketed for use in drug delivery studies, little data has been reported to date, perhaps reflecting low uptake or due to cost or usage in industry that is subject to confidentiality. In general, primary culture is less convenient and economical than the use of cell lines. Hence, primary cultured tracheo-bronchial cell layers have not been widely utilised for biopharmaceutical purposes [56].

10.2.2. Tracheo-Bronchial Epithelial Cell Lines

In addition to the significantly reduced costs, a major advantage of using immortalised airway epithelial cell models over primary lung airway epithelial cells is the ability to reduce the variability in cultures that arises from donor to donor differences. In contrast to gastrointestinal in vitro testing where Caco-2 cells have emerged as the gold standard, there is no such consensus to date on the preferred cell line(s) for modelling the bronchial epithelium in vitro. Several detailed protocols for culture, maintenance, growth and permeability assessment of tracheo-bronchial epithelial cell lines have been published in recent years [56], with the most commonly used systems being the Calu-3 and 16HBE14o- cell lines. Additionally, BEAS-2B are frequently used for studies of metabolism and the interaction of cells with xenobiotics, and the use of the NuLi-1 cell line has recently been explored [57, 58].

Calu-3 (American type culture collection; ATCC HTB-55) is a human bronchial epithelial cell line derived from an adenocarcinoma of the lung [59]. This cell line has been shown to exhibit serous cell properties and form confluent monolayers of mixed cell phenotypes, including ciliated and secretory cell types [60], but the cilia are formed very irregularly and seem to disappear with increasing passage number (unpublished observations, C.E. and B.F.). Calu-3 cells have shown utility as a model to examine transport [61–63] and metabolism in human bronchial epithelial cells for many therapeutic compounds [64]. Furthermore, they have been used in a number of particle–cell interaction studies [65–67]. The interactions between respiratory epithelial cells and particulates are discussed more in detail in Chap. 19.

Another continuous bronchial epithelial cell line, 16HBE14o-, was generated by transformation of normal bronchial epithelial cells obtained from a 1-year-old male heart-lung transplant patient. Transformation was accomplished with SV40 large T antigen using the replication defective pSVori-plasmid [68]. 16HBE14o- cells can be obtained from Dieter C. Gruenert, Ph.D., at the California Pacific Medical Center (see also Chap. 26 for more details of the immortalisation procedures). The non-commercial availability of the cell line might be one of the reasons they have been less widely used than Calu-3. 16HBE14o- cells have a non-serous, non-ciliated phenotype and are generally rounder in shape and smaller in size than Calu-3. When grown under liquid-covered culture (LCC) conditions, 16HBE14o- form confluent, polarised cell

layers with functional tight junctions and the expression of several drug transport proteins [69, 70]. In contrast, air-interfaced culture (AIC) conditions lead to cell layers of less desirable phenotypic and morphological traits. Since most epithelial cells, which are normally located at an air interface, *in vivo*, function optimally under AIC conditions for cultivation, the superior performance of the 16HBE14o- cell line under LCC conditions is an exception for which the exact reasons or mechanism are currently unknown. Like Calu-3, the 16HBE14o- cell line has been utilised for drug absorption and particle–cell interaction studies [71, 72].

The BEAS-2B cell line was derived from normal human epithelial cells that were immortalised using the hybrid virus of adenovirus 12 and simian virus 40 [73]. BEAS-2B is available from the ATCC (CRL-9609) and has been popular in studies of airway epithelial cell structure and function, including phenotyping and mechanistic investigation of cytokine regulation [74]. BEAS-2B cells have also been used to evaluate responses to challenges such as tobacco smoke [75], environmental particles [76, 77] and hyperoxia [78]. However, as it is challenging to generate TEER values higher than 100 ohm cm² using BEAS-2B cells [79], they have not been used much in drug permeability studies, but have frequently been utilised to investigate the expression and activity of drug metabolising enzymes [80, 81].

A relatively new cell line that has not to date been characterised for its use in biopharmaceutics is based on primary airway epithelial cells infected with retroviruses expressing hTERT and HPV-16 E6/E7 (NuLi-1) [54]. NuLi-1 cells were cultured on plastic up to passage 30. When grown on collagen-coated, semi-permeable membranes (Millicell-PCF), NuLi-1 TEER decreased only slightly over the 30 passages from 685 ± 31 to 389 ± 21 ohm.cm². The TEER of NuLi-1 is similar to that observed with the primary bronchial cultures of 532 ± 147 ohm.cm². Thus, NuLi-1 cells can form an electrically tight airway epithelial barrier that mimics active and passive ion transport properties of primary human bronchial epithelial cells [54].

10.2.3. In Vitro Models of CF Airway Epithelium

Cystic fibrosis (CF) is an autosomal recessive disease and is the most common lethal genetic disease. There are ~30,000 patients in the USA and Europe [33, 82]. CF is caused by mutation in the CFTR gene located at chromosome 7 and is associated mostly with defective chloride transport in airway epithelial cells. Lung pathology in CF includes abnormally low to nil chloride transport, increased mucus viscosity, reduced mucociliary clearance rates, recurrent infections, chronic inflammations and airway damage. Because of the significance of the disease, the most visible gene therapy schemes in development are inhalable regimens (containing complementary DNA of CFTR) to treat CF by restoration of CFTR function in the airways of the lung.

In vitro models based on CF airway epithelium have been used widely in order to better understand the CF pathophysiology, to have a tool to study alterations in airway permeability and to assess the efficiency of gene vectors. Utilising approaches similar to those for cultivation of cells from healthy tissues, several protocols have been developed to culture airway epithelial cells harvested from CF patients [83, 84]. The development of immortalised cell lines with a CF phenotype has been a significant benefit for investigators in

the CF field, alleviating the major limitation inherent in primary cell culture models, that is the very limited availability of suitable CF tissues [85, 86]. A number of these CF cell lines have been reported to show the ability to form polarised cell layers with the necessary bioelectrical tightness that makes them potentially useful for drug permeability studies. Examples of human immortalised CF airway epithelial cell lines are NCF3 [87], CFT1 [88], CFBE41o- [89] and CuFi-3 and -4 [54]. It should be noted that only the CFBE41o- and CuFi cell lines have been characterised and validated regarding their long-term stability as reliable in vitro models.

10.3. Use of In Vitro Models of Tracheo-Bronchial Epithelial Barriers in Biopharmaceutical Research

10.3.1. Drug Absorption Studies

Despite the fact that the alveolar epithelium with its extremely thin barrier ($<0.5 \mu\text{m}$) and vast surface area ($>100 \text{m}^2$) is regarded as the most favourable site for achieving delivery of therapeutic molecules into the systemic circulation following inhalation, several cell lines of the tracheo-bronchial origin have been employed to gain mechanistic information on drug transport and metabolism in the lung. This can be explained, in part, by the relative ease and low costs by which continuously growing tracheo-bronchial cell lines can be maintained, compared to primary cultures of alveolar epithelial cells. The airways also constitute the target for therapeutic compounds for asthma and COPD and, depending upon the site of deposition and physicochemical properties of an inhaled compound, may contribute significantly to the pulmonary absorption of inhaled therapeutics.

10.3.1.1. Drug Permeability

The permeability of a large number of compounds has been measured in airway epithelial cell culture models and the results of these studies have been reviewed [56], with dependence on molecular size and lipophilicity being seen in the Calu-3 and 16HBE14o- cell lines. Observations in these cell lines were similar to those made in primary rabbit tracheo-bronchial cell cultures. The use of airway epithelial cell models in pulmonary biopharmaceutical research in general appears to be well justified, since permeability (P_{app}) values observed in such in vitro cell culture models appear to be predictive of absorption from intact lungs [58]. Drug delivery applications such as absorption enhancement and the effects of inhaled formulation excipients on drug permeability have also been investigated using these two cell lines [56].

10.3.1.2. Active Transport Mechanisms in Tracheo-Bronchial Epithelial Cells

10.3.1.2.1. ATP-binding cassette Transporters: P-glycoprotein (P-gp) expression and functionality have been determined in several lung cell culture models. In freshly isolated primary human bronchial epithelial cells, P-gp was present and efflux of the P-gp substrate, rhodamine 123 (Rh123), was measured, confirming functional activity of P-gp, albeit whether the transporter is localised to the apical or basolateral membrane is not investigated [90]. In 16HBE14o- cells, P-gp was expressed at the apical membrane. Functional activity was

measured with Rh123 and the transport was inhibited by the P-gp inhibitor, verapamil [70]. For Calu-3 cells, published data are somewhat conflicting in that some groups observed net secretion of the P-gp substrate [91, 92], others observed P-gp-mediated absorption [93], while another could not detect P-gp expression at all [94]. Net secretion of Rh123 across Calu-3 cells may be explained further by multidrug resistance-associated protein 1 (MRP1) activity in these cells (most likely with a basolateral orientation), because Rh123 is also an MRP1 substrate [95]. However, it appears that different Calu-3 clones may have been utilised in the various studies, whereby the cell line may yield different phenotypes, dependent upon the culture conditions used by investigators. In CFBE41o- cells, P-gp was expressed at both message and protein levels, although it lacked functionality in the efflux or secretion of Rh123 [89]. Whether this is a result of the CF phenotype or a finding specific to the cell line is unclear.

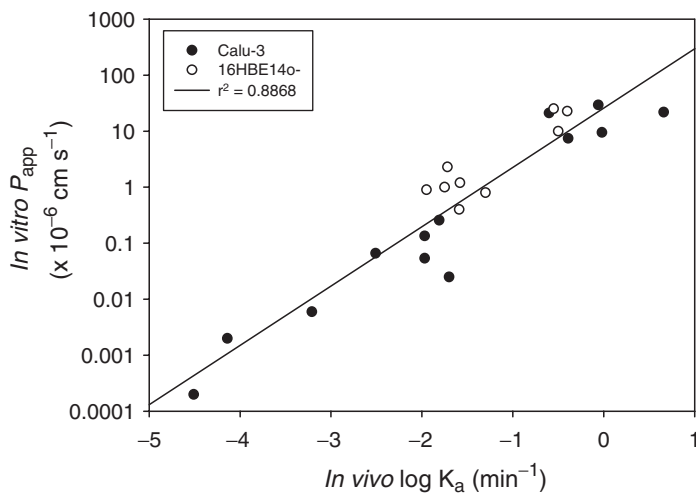
MRP1 protein has been shown to be expressed in freshly isolated human bronchial epithelial cells, where the efflux of carboxy-dichlorofluorescein (an MRP1 substrate) was inhibited by MK571, a specific MRP inhibitor [90]. Both 16HBE14o- and Calu-3 cell lines have also been reported to express MRP1 basolaterally, which is thought to contribute to the net absorption of certain substrates, for example monochlorobimane GSH conjugate [95, 96]. Real-time PCR analysis of Calu-3 cells for ATP-binding cassette (ABC) transporters confirmed the presence of transcripts for MRP1 and MRP2, although the expression of P-gp, MRP3 or breast cancer-related protein (BCRP) was not found [94].

10.3.1.2.2. SLC-Transporters: OCT1 and OCT2 may mediate acetylcholine release and re-absorption from epithelial cells [97] and involvement of OCTN1 and OCTN2-mediated drug absorption from the airways in a pH-dependent manner has been demonstrated [98]. With respect to carrier-mediated cationic drug absorption in functional (i.e. electrically tight) cell layer cultures, however, only limited information on transporter expression and drug absorption profiles is available. Net absorption of salbutamol (albuterol) across both Calu-3 and 16HBE14o- cell layers has recently been shown and at the same time, expression of OCT1 and OCT2 as well as OCTN1 and OCTN2 mRNA transcripts in both cell types were confirmed [99, 100].

The presence of a high-affinity peptide transporter PEPT2 in bronchial epithelium was demonstrated by measuring the uptake of peptides into bronchial cells following intra-tracheal instillation [101]. The functional expression of PEPT2 in primary cultured human lung cells from multiple donor subjects has also been demonstrated [102]. Reverse transcription-polymerase chain reaction (RT-PCR) analysis of the gene for cationic amino acid transporters (CATs) expressed in Calu-3 cells detected amplicons of the expected size for *SLC7A1* (coding for hCAT1 transporter), *SLC7A2* (for transcripts hCAT2B and hCAT2A), *SLC7A4*, *SLC7A6* (for y^+ LAT2), *SLC7A7* (for y^+ LAT1), *SLC3A2* (for 4F2hc/CD98) and *SLC6A14* (for ATB⁰⁺) [103].

10.3.1.2.3. Lung resistance protein: Lung resistance protein (LRP) is expressed in normal human bronchial epithelium (NHBE) as well as in other tissues potentially exposed to toxins [104]. LRP was reported to be expressed in both Calu-3 cells [105] and 16HBE14o- model [70]. However, the role of LRP in different cellular locations is not clear to date.

Figure 10.2 Apparent permeability coefficients (P_{app}) observed in vitro across Calu-3 (●) [62] and 16HBE14o- (○) [72] cell layers vs. in vivo rate constants (K_a) determined for absorption from the rat lung after intratracheal delivery of various molecules.



10.3.1.3. In Vitro–In Vivo Correlation Using Tracheo-Bronchial Epithelial Cells

Data are emerging slowly on the use of in vitro respiratory epithelial models as predictive screens for drugs administered via pulmonary routes [62, 72]. Although excellent predictive power has been achieved (Figure 10.2), the experimental conditions are far from the reality where a patient would be administered with the drug as an aerosol cloud and a significant proportion of absorption from the lung is likely to occur from the alveolar region.

10.3.2. Drug Metabolism Studies Using Tracheo-Bronchial Epithelial Cells

The human lung and the lining fluid in its lumen are frequently exposed to all sorts of aerosolised compounds (among them drug molecules). Therefore, the lung has a significant capability to biotransform such compounds to reduce their potential toxicity. Biotransformation of lipophilic xenobiotics enables the elimination of substances that might accumulate otherwise in tissues and cause (cyto)toxic effects. Chemical modification of the compounds results in the appearance of more polar and reactive functional groups in the molecule (phase I reactions). These are followed by conjugation with endogenous molecules such as glucuronic acid, GSH, sulphate and amino acids (phase II reactions). Most phase I reactions consist of oxidation reactions catalysed by two groups of monooxygenases, that is cytochrome P450 (CYP)-dependent monooxygenases and flavin monooxygenases (FMO).

In general, biotransformation reactions are beneficial in that they facilitate the elimination of xenobiotics from pulmonary tissues. Sometimes, however, the enzymes convert a harmless substance into a reactive form. For example, CYP-mediated oxidation often results in the generation of more reactive intermediates. Thus, many compounds that elicit toxic injury to the lung are not intrinsically pneumotoxic but cause damage to target cells following metabolic activation. A classic example of this is the activation of benzo(*a*)pyrene, which is a constituent of tobacco smoke and combustion products, and is

transformed into reactive forms capable of binding to DNA with neoplastic consequences.

Lung metabolism studies would greatly benefit from the availability of reliable *in vitro* experimental models that are able to reproduce biochemical and toxicological processes that occur in the human lung. Because of differences in the expression profiles of biotransformation enzymes between animal species, conclusions drawn from experimental animals may not be representative of what occurs in the human lung.

The bioactivation and biological effects of a xenobiotic can be investigated in metabolically competent cells (i.e., cells expressing the xenobiotic biotransformation enzymes), but not reliably using subcellular fractions (microsomes containing the enzyme activities). The spectrum of effects elicited by xenobiotics interacting with cells (bioactivation of toxins, effects on cellular metabolism, regulation of CYP expression) can be properly observed only in a biological system fully capable of transcribing and translating genes in response to the action of toxins. Human cells isolated from pulmonary tissues meet such requirements, although the feasibility of establishing a physiologically faithful *in vitro* model is hampered by the difficulties in isolating and culturing functional cells from human lungs [106]. Even when human bronchial epithelial cells are obtained from biopsy specimens, a major drawback is their limited lifespan [107]. Although attempts have been made to immortalise human bronchial epithelial cells, the phenotype of transformed cells inevitably differs from that of normal cells in a variety of ways [107–109].

10.3.2.1. Expression of P450 Enzymes in Tracheo-Bronchial Mucosa and Cell Cultures

The proteins encoded by the CYP superfamily (P450 monooxygenases) are responsible for the oxidative metabolism of the vast majority of xenobiotics (including drugs, environmental pollutants, carcinogens) as well as endogenous compounds. The human P450 system consists of ~50 isoforms that exhibit major differences with respect to their catalytic specificities and tissue patterns of expression. P450 enzymes act as monooxygenases, that is, they use one atom of molecular oxygen to oxidise xenobiotics and require the aid of NADPH-CYP reductase to provide the electrons required for the reduction of the second oxygen atom to H₂O. CYP enzymes are grouped in families and subfamilies according to their amino acid sequence homology. The families CYP1, CYP2 and CYP3 are the main players in the oxidative metabolism of xenobiotics [110]. Although the liver is the organ with the highest expression of most CYP isoforms, other tissues have their own particular profiles of CYP enzyme expression, which ultimately determines their capability for biotransformation (and bioactivation).

The limited availability of suitable human tissue for experimental studies and the rather low CYP expression level in the human lung, compared to that found in rodents [111], have notably limited identification of the lung CYP isoforms. By means of RT-PCR, it has been possible to qualitatively demonstrate the presence of several CYP mRNAs in the human bronchial mucosa, namely CYP1A1, 2A6, 2B6, 2C, 2E1 and 3A5, whereas the expression of CYP1A2, 2D6, 3A4 and 3A7 could be detected only in some samples (Table 10.1) [109, 111, 112]. Immunohistochemical analysis has shown the significant expression of CYP enzymes in different pulmonary cells including

Table 10.1 Expression profiles of CYP P450 mRNA and protein in human lung tissue and cell culture models.

Enzyme	Bronchial mucosa	NHBE	Calu-3	BEAS-2B
CYP1A1	+ ^{a,b}	+ ^b / ^{#d}	^{#d,d}	^{#d}
CYP1A2	+ ^{b,c}	+ ^b		
CYP1B1	+ ^a			
CYP2A6	+ ^b	+ ^{b,e}		
CYP2B6/7	+ ^{a,b}	+ ^b	^{#f}	
CYP2C	+ ^b	+ ^b / ^{###d}	^{###d}	^{#d}
CYP2D6	+ ^{b,c}	- ^b		
CYP2E1	+ ^{a,b}	+ ^{b,e}	^{#f}	
CYP3A4	+ ^{b,c}	+ ^b / ^{####d}	^{#f,d} / ^{-g}	^{#d}
CYP3A5	+ ^b	+ ^b	^{#g}	
CYP3A7	+ ^{b,c}		- ^g	
CYP4B1	+ ^a			

- not detectable; + detectable (not quantified); # low intensity; ## medium intensity; ### high intensity.

^aRef. [112] (RT-PCR); ^bRef. [109] (RT-PCR); ^cNot in all samples;

^dRef. [116] (RT-PCR); ^eRef. [115] (RT-PCR);

^fRef. [61] (Western blot and EROD/PROD assays); ^gRef. [117] (RT-PCR).

alveolar type I and type II cells, Clara cells, ciliated columnar epithelial cells and macrophages [113]. Nevertheless, the vast majority of data published on CYP expression in human lung is of a qualitative nature. Real-time PCR methods can now be used for a precise quantitative assessment of CYP mRNA levels. The analysis of the various CYP mRNA in pooled human lung tissues revealed that the most abundant transcripts were CYP1A1, 1B1, 2A6, 2B6, 2E1 and 3A5. Other minor, but measurable, CYP mRNA were CYP2C, 2D6 and 3A4 [114].

When the CYP expression in normal human bronchial epithelial cells (NHBE cells) at passages 1 and 2 was compared with the expression previously observed in the bronchial mucosa, a general reduction in CYP levels was observed in the cultured cells [109, 115, 116]. Moreover, the BEAS-2B cell line displayed limited CYP expression, since only low levels of CYP1A1, 2C and 4A4 mRNAs were detected [116]. In the case of Calu-3 cells, the presence of CYP1A1, CYP2B6, CYP2E1 and CYP3A5 was confirmed, while conflicting data were reported for CYP3A4 (Table 10.1) [61, 117]. However, all enzymes were detected with low to moderate activities [61].

10.3.2.2. Expression of Phase II Enzymes in Tracheo-Bronchial Mucosa and Cell Cultures

In phase II metabolism, conjugation reactions of phase I metabolites with endogenous substance occur, increasing the hydrophilicity of the compound and/or eliminating its biological activity. Phase II metabolism is energy- and/or energy equivalent-requiring and can be attributed to the families of UDP-glucuronosyl transferases (UGT, conjugation with glucuronic acid), glutathione S-transferases (GST, conjugation with GSH), *N*-acetyl transferases

Table 10.2 Expression profiles of phase II metabolic enzymes in human bronchial mucosa and in vitro cell culture models.

Enzyme	Bronchial mucosa ^{a,b}	NHBE	Calu-3	BEAS-2B
GSTM1	## ^a	## ^c		# ^c
GSTM3	### ^a			
NAT1	### ^a /# ^b			
NAT2	– ^a /# ^b			
UGT1A		#### ^d	#### ^d	# ^d
UGT2B4		# ^d	# ^d	### ^d
UGT2B10		– ^d	– ^d	– ^d
UGT2B11		# ^d	## ^d	### ^d
UGT2B17		### ^d	### ^d	#### ^d

– not detectable; # low intensity; ## medium intensity; ### high intensity; #### very high intensity.

^aRef. [109]; ^bRef. [120]; ^cRef. [122]; ^dRef. [116].

(NAT, acetylation of nitrogen), sulfotransferases (SULT, formation of sulfate esters) and methyltransferases (MT, addition of methyl group).

In the human lung cytosol, SULT1A1 and SULT1A3 proteins are detectable and histological studies have shown that these proteins are present in the epithelial cells of respiratory bronchioles [118]. Immunohistochemical localisation of SULT2B1b in human tissues indicated expression in the cytoplasm of ciliated columnar or cuboidal epithelial cells in terminal bronchioles [119]. NAT1 and NAT2 have also been found in the bronchial mucosa; however, there is some inconsistency in the data reported. One report describes abundant NAT1 expression and no trace of NAT2 [109], while another paper reports the absence of NAT1 and a low activity of NAT2 (Table 10.2) [120].

The BEAS-2B cell line has been described previously as retaining the expression of most of the phase II enzymes (i.e., epoxide hydrolase, GST pi, GSH peroxidase and catalase) [121]. However, when Kuzuya and co-workers quantitatively compared UGT levels amongst NHBE, Calu-3 and BEAS-2B cells, the Calu-3 cell line showed expression levels most comparable to NHBE, while results from BEAS-2B cells were significantly different from others (Table 10.2) [116].

10.3.2.3. Expression of Peptidases and Proteinases in Tracheo-Bronchial Mucosa and Cell Cultures

Proteolytic enzymes in the respiratory mucosa play important role(s) in the regulation of lung inflammation and remodelling [123, 124]. Pulmonary proteolytic enzymes, however, also comprise one of the barriers which pulmonary-administered protein/peptide drugs have to overcome in order to achieve adequate bioavailability [125]. Intriguingly, the pulmonary enzymatic barrier is an aspect that has been little investigated and is poorly understood. Inconsistencies in the data available to date are most likely a result of the use of different techniques (e.g., PCR, immunotechniques and enzyme activity assays), different species and different cell (pheno)types, for example primary cells vs. cell lines.

By PCR and immunohistochemistry, neutral endopeptidase 24.11 (NEP 24.11) expression was detectable in both alveolar and airway epithelial tissues [126, 127]. These findings were replicated using BEAS-2B cells [81, 128]. Aminopeptidases M (APM) and N (APN) are functionally expressed in BEAS-2B cells, while no signal was obtained for aminopeptidase P (APP), carboxypeptidase M (CPM), angiotensin-converting enzyme (ACE) or dipeptidyl peptidase IV (DPP IV) [81, 128]. The presence of APN and the absence of ACE in BEAS-2B were confirmed by Juillerat-Jeanneret and co-workers [129], who additionally reported DPP IV and γ -glutamyltranspeptidase (γ -GTP) activities. DPP IV was also positively identified in NHBE cells at both mRNA and protein levels [130]. Proteolytic activity of Calu-3 cells towards cell-penetrating peptides has also been reported recently [131].

10.3.2.4. Other Metabolic Activities in Tracheo-Bronchial Mucosa and Cell Cultures

Calu-3 cells have shown the ability to perform fatty acid esterification of budesonide [132]. In pre-clinical studies, this esterification results in a prolonged local tissue binding and efficacy, which is not found when the esterification is inhibited [133]. The precise mechanism remains undefined in that the identity of specific enzyme(s) responsible for this metabolic reaction is unclear [134]. Assessment of the potential toxicity and metabolism of pharmaceuticals and other xenobiotics using in vitro respiratory models is still at its infancy. The development of robust in vitro human models (i.e., cell lines from human pulmonary origin) has the potential to contribute significantly to better understanding the role of biotransformation enzymes in the bioactivation/detoxication processes in the lung.

10.4. Concluding Remarks

A variety of cell culture systems for the modelling of the tracheo-bronchial epithelium are available. These include primary cultures and cell lines of human and animal origins, plus airway cells with characteristics of lung disease such as CF. The advantages and limitations of using a simple culture system compared to one that recreates to a greater extent the epithelial structure and function in vitro should be considered according to the pre-clinical application required. However, this choice is complicated by the lack of comparative data, both between the different cell systems and for in vitro–in vivo correlation, upon which to base such decisions.

For permeability screening, the barrier function of the cells in vitro is essential and only cell lines and primary culture systems that form tight junctions in culture are suitable. For passively transported compounds, it appears that in vitro–in vivo correlation with absorption from the rat lung can be obtained with cell lines (16HBE14o- and Calu-3 cells) as well as primary cultures. However, predictive relationships are not exclusively obtained by airway cell cultures and may be obtained using non-respiratory epithelial cells (e.g., Caco-2). The extent to which cell lines or indeed primary cultures can model the absorption of actively transported compounds remains to be shown. For metabolic or toxicological studies, the requirement for an organ-specific cell system that is of human origin is paramount. Existing data in

this area is diverse, but more systematic studies are underway. The evaluation of cell systems in critical *in vitro*–*in vivo* and other benchmarking studies will permit the rational selection of tracheo-bronchial epithelial cell cultures for pre-clinical applications. Accordingly, the use of such well-characterised epithelial cell systems with validated protocols for studying drug disposition will enhance our understanding of drug transport and metabolism in the lung.

Acknowledgments: The authors thank Sibylle Endter (Trinity College, Dublin) for the drawing of Figure 10.1. K.J.K. was supported in part by research grants from the National Institutes of Health (HL38658 and HL64365) and the Hastings Foundation.

References

1. Gray H (1918, 2000) *Anatomy of the Human Body*. Lea & Febiger, Philadelphia, Bartleby.com, www.bartleby.com/107/
2. Itoh H, Nishino M, Hatabu H (2004) Architecture of the lung: Morphology and function. *J Thorac Imaging* 19(4):221–227.
3. McDowell EM, Barrett LA, Glavin F, Harris CC, Trump BF (1978) The respiratory epithelium. I. Human bronchus. *J Natl Cancer Inst* 61(2):539–549.
4. Weibel ER, Gomez DM (1962) Architecture of the human lung. Use of quantitative methods establishes fundamental relations between size and number of lung structures. *Science* 137(3530):577–585.
5. van der Velden VH, Versnel HF (1998) Bronchial epithelium: Morphology, function and pathophysiology in asthma. *Eur Cytokine Netw* 9(4):585–597.
6. Bai A, Eidelman DH, Hogg JC, James AL, Lambert RK, Ludwig MS, Martin J, McDonald DM, Mitzner WA, Okazawa M, Pack RJ, Pare PD, Schellenberg RR, Tiddens HA, Wagner EM, Yager D (1994) Proposed nomenclature for quantifying subdivisions of the bronchial wall. *J Appl Physiol* 77(2):1011–1014.
7. Harkema JR (1991) Comparative aspects of nasal airway anatomy: Relevance to inhalation toxicology. *Toxicol Pathol* 19(4 Pt 1):321–336.
8. Ayers MM, Jeffery PK (1988) Proliferation and differentiation in mammalian airway epithelium. *Eur Respir J* 1(1):58–80.
9. Franken C, Meijer CJ, Dijkman JH (1989) Tissue distribution of anti-leukoprotease and lysozyme in humans. *J Histochem Cytochem* 37(4):493–498.
10. Beckmann JD, Spurzem JR, Rennard SI (1993) Phenol sulfotransferase expression in the airways: Enzymological and immunohistochemical demonstration. *Cell Tissue Res* 274(3):475–485.
11. de Water R, Willems LN, van Muijen GN, Franken C, Fransen JA, Dijkman JH, Kramps JA (1986) Ultrastructural localization of bronchial anti-leukoprotease in central and peripheral human airways by a gold-labeling technique using monoclonal antibodies. *Am Rev Respir Dis* 133(5):882–890.
12. Jeffery PK (1983) Morphologic features of airway surface epithelial cells and glands. *Am Rev Respir Dis* 128(2 Pt 2):S14–S20.
13. Widdicombe JG, Pack RJ (1982) The Clara cell. *Eur J Respir Dis* 63(3):202–220.
14. Boers JE, Ambergen AW, Thunnissen FB (1999) Number and proliferation of Clara cells in normal human airway epithelium. *Am J Respir Crit Care Med* 159(5 Pt 1):1585–1591.
15. Inayama Y, Hook GE, Brody AR, Jetten AM, Gray T, Mahler J, Nettesheim P (1989) *In vitro* and *in vivo* growth and differentiation of clones of tracheal basal cells. *Am J Pathol* 134(3):539–549.

16. Thompson AB, Robbins RA, Romberger DJ, Sisson JH, Spurzem JR, Teschler H, Rennard SI (1995) Immunological functions of the pulmonary epithelium. *Eur Respir J* 8(1):127–149.
17. Breuer R, Zajicek G, Christensen TG, Lucey EC, Snider GL (1990) Cell kinetics of normal adult hamster bronchial epithelium in the steady state. *Am J Respir Cell Mol Biol* 2(1):51–58.
18. Rennard SI, Romberger DJ, Sisson JH, Von Essen SG, Rubinstein I, Robbins RA, Spurzem JR (1994) Airway epithelial cells: Functional roles in airway disease. *Am J Respir Crit Care Med* 150(5 Pt 2):S27–S30.
19. Roche WR, Montefort S, Baker J, Holgate ST (1993) Cell adhesion molecules and the bronchial epithelium. *Am Rev Respir Dis* 148(6 Pt 2):S79–S82.
20. Jain B, Rubinstein I, Robbins RA, Sisson JH (1995) TNF-alpha and IL-1 beta upregulate nitric oxide-dependent ciliary motility in bovine airway epithelium. *Am J Physiol* 268(6 Pt 1):L911–L917.
21. Burman WJ, Martin WJ 2d (1986) Oxidant-mediated ciliary dysfunction. Possible role in airway disease. *Chest* 89(3):410–413.
22. Sanderson MJ, Dirksen ER (1989) Mechanosensitive and beta-adrenergic control of the ciliary beat frequency of mammalian respiratory tract cells in culture. *Am Rev Respir Dis* 139(2):432–440.
23. Khan AR, Bengtsson B, Lindberg S (1986) Influence of substance P on ciliary beat frequency in airway isolated preparations. *Eur J Pharmacol* 130(1–2): 91–96.
24. Mussatto DJ, Garrard CS, Lourenco RV (1988) The effect of inhaled histamine on human tracheal mucus velocity and bronchial mucociliary clearance. *Am Rev Respir Dis* 138(4):775–779.
25. Coonrod JD (1986) The role of extracellular bactericidal factors in pulmonary host defense. *Semin Respir Infect* 1(2):118–129.
26. Ellison RT 3rd, Giehl TJ (1991) Killing of gram-negative bacteria by lactoferrin and lysozyme. *J Clin Invest* 88(4):1080–1091.
27. Heffner JE, Repine JE (1989) Pulmonary strategies of anti-oxidant defense. *Am Rev Respir Dis* 140(2):531–554.
28. Arnold RR, Cole MF, McGhee JR (1977) A bactericidal effect for human lactoferrin. *Science* 197(4300):263–265.
29. Rothman BL, Merrow M, Bamba M, Kennedy T, Kreutzer DL (1989) Biosynthesis of the third and fifth complement components by isolated human lung cells. *Am Rev Respir Dis* 139(1):212–220.
30. Goodman MR, Link DW, Brown WR, Nakane PK (1981) Ultrastructural evidence of transport of secretory IgA across bronchial epithelium. *Am Rev Respir Dis* 123(1):115–119.
31. Patton JS, Byron PR (2007) Inhaling medicines: Delivering drugs to the body through the lungs. *Nat Rev Drug Discov* 6(1):67–74.
32. Gonda I (2006) Systemic delivery of drugs to humans via inhalation. *J Aerosol Med* 19(1):47–53.
33. Laube BL (2005) The expanding role of aerosols in systemic drug delivery, gene therapy, and vaccination. *Respir Care* 50(9):1161–1176.
34. Rao RD, Markovic SN, Anderson PM (2003) Aerosol therapy for malignancy involving the lungs. *Curr Cancer Drug Targets* 3(4):239–250.
35. Densmore CL (2006) Advances in noninvasive pulmonary gene therapy. *Curr Drug Deliv* 3(1):55–63.
36. Bivas-Benita M, Ottenhoff TH, Junginger HE, Borchard G (2005) Pulmonary DNA vaccination: Concepts, possibilities and perspectives. *J Control Release* 107(1):1–29.
37. Sabin AB (1983) Immunization against measles by aerosol. *Rev Infect Dis* 5(3):514–523.

38. LiCalsi C, Christensen T, Bennett JV, Phillips E, Witham C (1999) Dry powder inhalation as a potential delivery method for vaccines. *Vaccine* 17(13–14):1796–1803.
39. Roth Y, Chapnik JS, Cole P (2003) Feasibility of aerosol vaccination in humans. *Ann Otol Rhinol Laryngol* 112(3):264–270.
40. Oreffo VI, Morgan A, Richards RJ (1990) Isolation of Clara cells from the mouse lung. *Environ Health Perspect* 85:51–64.
41. Kaufman DG (1976) Biochemical studies of isolated hamster tracheal epithelium. *Environ Health Perspect* 16:99–110.
42. Robison TW, Dorio RJ, Kim KJ (1993) Formation of tight monolayers of guinea pig airway epithelial cells cultured in an air-interface: Bioelectric properties. *Biotechniques* 15(3):468–473.
43. Suda T, Sato A, Sugiura W, Chida K (1995) Induction of MHC class II antigens on rat bronchial epithelial cells by interferon-gamma and its effect on antigen presentation. *Lung* 173(2):127–137.
44. Chung Y, Kerckmar CM, Davis PB (1991) Ferret tracheal epithelial cells grown *in vitro* are resistant to lethal injury by activated neutrophils. *Am J Respir Cell Mol Biol* 5(2):125–132.
45. Liedtke CM (1988) Differentiated properties of rabbit tracheal epithelial cells in primary culture. *Am J Physiol* 255(6 Pt 1):C760–C770.
46. Mathias NR, Kim KJ, Robison TW, Lee VH (1995) Development and characterization of rabbit tracheal epithelial cell monolayer models for drug transport studies. *Pharm Res* 12(10):1499–1505.
47. Welsh MJ (1985) Ion transport by primary cultures of canine tracheal epithelium: Methodology, morphology, and electrophysiology. *J Membr Biol* 88(2):149–163.
48. Black PN, Ghatei MA, Takahashi K, Bretherton-Watt D, Krausz T, Dollery CT, Bloom SR (1989) Formation of endothelin by cultured airway epithelial cells. *FEBS Lett* 255(1):129–132.
49. Sisson JH, Tuma DJ, Rennard SI (1991) Acetaldehyde-mediated cilia dysfunction in bovine bronchial epithelial cells. *Am J Physiol* 260(2 Pt 1):L29–L36.
50. Sime A, McKellar Q, Nolan A (1997) Method for the growth of equine airway epithelial cells in culture. *Res Vet Sci* 62(1):30–33.
51. Masui T, Wakefield LM, Lechner JF, LaVeck MA, Sporn MB, Harris CC (1986) Type beta transforming growth factor is the primary differentiation-inducing serum factor for normal human bronchial epithelial cells. *Proc Natl Acad Sci USA* 83(8):2438–2442.
52. de Jong PM, van Sterkenburg MA, Kempenaar JA, Dijkman JH, Ponc M (1993) Serial culturing of human bronchial epithelial cells derived from biopsies. *In Vitro Cell Dev Biol* 29A(5):379–387.
53. Galiotta LJ, Lantero S, Gazzolo A, Sacco O, Romano L, Rossi GA, Zegarra-Moran O (1998) An improved method to obtain highly differentiated monolayers of human bronchial epithelial cells. *In Vitro Cell Dev Biol Anim* 34(6):478–481.
54. Zabner J, Karp P, Seiler M, Phillips SL, Mitchell CJ, Saavedra M, Welsh M, Klingelutz AJ (2003) Development of cystic fibrosis and noncystic fibrosis airway cell lines. *Am J Physiol* 284(5):L844–L854.
55. Chemuturi NV, Hayden P, Klausner M, Donovan MD (2005) Comparison of human tracheal/bronchial epithelial cell culture and bovine nasal respiratory explants for nasal drug transport studies. *J Pharm Sci* 94(9):1976–1985.
56. Forbes B, Ehrhardt C (2005) Human respiratory epithelial cell culture for drug delivery applications. *Eur J Pharm Biopharm* 60(2):193–205.
57. Forbes B (2000) Human airway epithelial cell lines for *in vitro* drug transport and metabolism studies. *Pharm Sci Technol Today* 3(1):18–27.

58. Sakagami M (2006) In vivo, in vitro and ex vivo models to assess pulmonary absorption and disposition of inhaled therapeutics for systemic delivery. *Adv Drug Deliv Rev* 58(9–10):1030–1060.
59. Fogh J and Trempe G (1975) New human tumor cell lines. In: Fogh J (ed.) *Human Tumor Cells In Vitro*. Plenum Press, New York, pp.115–159.
60. Shen BQ, Finkbeiner WE, Wine JJ, Mrsny RJ, Widdicombe JH (1994) Calu-3: A human airway epithelial cell line that shows cAMP-dependent Cl⁻ secretion. *Am J Physiol* 266(5 Pt 1):L493–L501.
61. Foster KA, Avery ML, Yazdanian M, Audus KL (2000) Characterization of the Calu-3 cell line as a tool to screen pulmonary drug delivery. *Int J Pharm* 208(1–2):1–11.
62. Mathias NR, Timoszyk J, Stetsko PI, Megill JR, Smith RL, Wall DA (2002) Permeability characteristics of calu-3 human bronchial epithelial cells: In vitro-in vivo correlation to predict lung absorption in rats. *J Drug Target* 10(1):31–40.
63. Grainger CI, Greenwell LL, Lockley DJ, Martin GP, Forbes B (2006) Culture of Calu-3 cells at the air interface provides a representative model of the airway epithelial barrier. *Pharm Res* 23(7):1482–1490.
64. Florea BI, Cassara ML, Junginger HE, Borchard G (2003) Drug transport and metabolism characteristics of the human airway epithelial cell line Calu-3. *J Control Release* 87(1–3):131–138.
65. Fiegel J, Ehrhardt C, Schaefer UF, Lehr CM, Hanes J (2003) Large porous particle impingement on lung epithelial cell monolayers—toward improved particle characterization in the lung. *Pharm Res* 20(5):788–796.
66. Cooney D, Kazantseva M, Hickey AJ (2004) Development of a size-dependent aerosol deposition model utilising human airway epithelial cells for evaluating aerosol drug delivery. *Altern Lab Anim* 32(6):581–590.
67. Amidi M, Romeijn SG, Borchard G, Junginger HE, Hennink WE, Jiskoot W (2006) Preparation and characterization of protein-loaded N-trimethyl chitosan nanoparticles as nasal delivery system. *J Control Release* 111(1–2):107–116.
68. Cozens AL, Yezzi MJ, Kunzelmann K, Ohru T, Chin L, Eng K, Finkbeiner KE, Widdicombe JH, Gruenert DC (1994) CFTR expression and chloride secretion in polarized immortal human bronchial epithelial cells. *Am J Respir Cell Mol Biol* 10(1):38–47.
69. Ehrhardt C, Kneuer C, Fiegel J, Hanes J, Schaefer UF, Kim KJ, Lehr CM (2002) Influence of apical fluid volume on the development of functional intercellular junctions in the human epithelial cell line 16HBE14o-: Implications for the use of this cell line as an in vitro model for bronchial drug absorption studies. *Cell Tissue Res* 308(3):391–400.
70. Ehrhardt C, Kneuer C, Laue M, Schaefer UF, Kim KJ, Lehr CM (2003) 16HBE14o- human bronchial epithelial cell layers express P-glycoprotein, lung resistance-related protein, and caveolin-1. *Pharm Res* 20(4):545–551.
71. Forbes B, Lim S, Martin GP, Brown MB (2002) An in vitro technique for evaluating inhaled nasal delivery systems. *STP Pharma Sci* 12:75–79.
72. Manford F, Tronde A, Jeppsson AB, Patel N, Johansson F, Forbes B (2005) Drug permeability in 16HBE14o- airway cell layers correlates with absorption from the isolated perfused rat lung. *Eur J Pharm Sci* 26(5):414–420.
73. Reddel RR, Ke Y, Gerwin BI, McMenamin MG, Lechner JF, Su RT, Brash DE, Park JB, Rhim JS, Harris CC (1988) Transformation of human bronchial epithelial cells by infection with SV40 or adenovirus-12 SV40 hybrid virus, or transfection via strontium phosphate coprecipitation with a plasmid containing SV40 early region genes. *Cancer Res* 48(7):1904–1909.
74. Atsuta J, Sterbinsky SA, Plitt J, Schwiebert LM, Bochner BS, Schleimer RP (1997) Phenotyping and cytokine regulation of the BEAS-2B human bronchial

- epithelial cell: Demonstration of inducible expression of the adhesion molecules VCAM-1 and ICAM-1. *Am J Respir Cell Mol Biol* 17(5):571–582.
75. Sun W, Wu R, Last JA (1995) Effects of exposure to environmental tobacco smoke on a human tracheobronchial epithelial cell line. *Toxicology* 100(1–3):163–174.
 76. Steerenberg PA, Zonnenberg JA, Dormans JA, Joon PN, Wouters IM, van Bree L, Scheepers PT, Van Loveren H (1998) Diesel exhaust particles induced release of interleukin 6 and 8 by (primed) human bronchial epithelial cells (BEAS 2B) in vitro. *Exp Lung Res* 24(1):85–100.
 77. Veranth JM, Kaser EG, Veranth MM, Koch M, Yost GS (2007) Cytokine responses of human lung cells (BEAS-2B) treated with micron-sized and nanoparticles of metal oxides compared to soil dusts. *Part Fibre Toxicol* 4(1):2.
 78. Odoms K, Shanley TP, Wong HR (2004) Short-term modulation of interleukin-1beta signaling by hyperoxia: uncoupling of IkappaB kinase activation and NF-kappaB-dependent gene expression. *Am J Physiol* 286(3):L554–L562.
 79. Noah TL, Yankaskas JR, Carson JL, Gambling TM, Cazares LH, McKinnon KP, Devlin RB (1995) Tight junctions and mucin mRNA in BEAS-2B cells. *In Vitro Cell Dev Biol Anim* 31(10):738–740.
 80. Eaton EA, Walle UK, Wilson HM, Aberg G, Walle T (1996) Stereoselective sulphate conjugation of salbutamol by human lung and bronchial epithelial cells. *Br J Clin Pharmacol* 41(3):201–206.
 81. Proud D, Subauste MC, Ward PE (1994) Glucocorticoids do not alter peptidase expression on a human bronchial epithelial cell line. *Am J Respir Cell Mol Biol* 11(1):57–65.
 82. Boucher RC (2004) New concepts of the pathogenesis of cystic fibrosis lung. *Eur Respir J* 23(1):146–158.
 83. Stutts MJ, Cotton CU, Yankaskas JR, Cheng E, Knowles MR, Gatzky JT, Boucher RC (1985) Chloride uptake into cultured airway epithelial cells from cystic fibrosis patients and normal individuals. *Proc Natl Acad Sci USA* 82(19):6677–6681.
 84. Gruenert DC, Basbaum CB, Widdicombe JH (1990) Long-term culture of normal and cystic fibrosis epithelial cells grown under serum-free conditions. *In Vitro Cell Dev Biol* 26(4):411–418.
 85. Gruenert DC, Finkbeiner WE, Widdicombe JH (1995) Culture and transformation of human airway epithelial cells. *Am J Physiol* 268(3 Pt 1):L347–L360.
 86. Gruenert DC, Willems M, Cassiman JJ, Frizzell RA (2004) Established cell lines used in cystic fibrosis research. *J Cyst Fibros* 3 (Suppl 2):191–196.
 87. Scholte BJ, Kansen M, Hoogeveen AT, Willemsse R, Rhim JS, van der Kamp AW, Bijman J (1989) immortalization of nasal polyp epithelial cells from cystic fibrosis patients. *Exp Cell Res* 182(2):559–571.
 88. Olsen JC, Johnson LG, Stutts MJ, Sarkadi B, Yankaskas JR, Swanstrom R, Boucher RC (1992) Correction of the apical membrane chloride permeability defect in polarized cystic fibrosis airway epithelia following retroviral-mediated gene transfer. *Hum Gene Ther* 3(3):253–266.
 89. Ehrhardt C, Collnot EM, Baldes C, Becker U, Laue M, Kim KJ, Lehr CM (2006) Towards an in vitro model of cystic fibrosis small airway epithelium: Characterisation of the human bronchial epithelial cell line CFBE41o-. *Cell Tissue Res* 323(3):405–415.
 90. Lehmann T, Kohler C, Weidauer E, Taege C, Foth H (2001) Expression of MRP1 and related transporters in human lung cells in culture. *Toxicology* 167(1):59–72.
 91. Hamilton KO, Backstrom G, Yazdanian MA, Audus KL (2001) P-glycoprotein efflux pump expression and activity in Calu-3 cells. *J Pharm Sci* 90(5):647–658.
 92. Patel J, Pal D, Vangal V, Gandhi M, Mitra AL (2002) Transport of HIV-protease inhibitors across 1 alpha,25 di-hydroxy vitamin D3-treated Calu-3 cell monolayers: Modulation of P-glycoprotein activity. *Pharm Res* 19(11):1696–1703.

93. Florea BI, van der Sandt IC, Schrier SM, Kooiman K, Deryckere K, de Boer AG, Junginger HE, Borchard G (2001) Evidence of P-glycoprotein mediated apical to basolateral transport of flunisolide in human broncho-tracheal epithelial cells (Calu-3). *Br J Pharmacol* 134(7):1555–1563.
94. Yen WC, Corpuz MR, Prudente RY, Cooke TA, Bissonnette RP, Negro-Vilar A, Lamph WW (2004) A selective retinoid X receptor agonist bexarotene (Targretin) prevents and overcomes acquired paclitaxel (Taxol) resistance in human non-small cell lung cancer. *Clin Cancer Res* 10(24):8656–8664.
95. Hamilton KO, Topp E, Makagiansar I, Siahaan T, Yazdanian M, Audus KL (2001) Multidrug resistance-associated protein-1 functional activity in Calu-3 cells. *J Pharmacol Exp Ther* 298(3):1199–1205.
96. van der Deen M, Timmer-Bosscha H, Timens W, Postma DS, de Vries EG (2004) Effect of cigarette smoke extract on MRP1 function in bronchial epithelial cells. *Proc Am Assoc Cancer Res* 45:A508.
97. Lips KS, Volk C, Schmitt BM, Pfeil U, Arndt P, Miska D, Ermert L, Kummer W, Koepsell H (2005) Polyspecific cation transporters mediate luminal release of acetylcholine from bronchial epithelium. *Am J Respir Cell Mol Biol* 33(1):79–88.
98. Horvath G, Schmid N, Fragoso MA, Schmid A, Conner GE, Salathe M, Wanner A (2007) Epithelial organic cation transporters ensure pH-dependent drug absorption in the airway. *Am J Respir Cell Mol Biol* 36(1):53–60.
99. Ehrhardt C, Kneuer C, Bies C, Lehr CM, Kim KJ, Bakowsky U (2005) Salbutamol is actively absorbed across human bronchial epithelial cell layers. *Pulm Pharmacol Ther* 18(3):165–170.
100. Rytting E and Audus KL (2005) Novel organic cation transporter 2-mediated carnitine uptake in placental choriocarcinoma (BeWo) cells. *J Pharmacol Exp Ther* 312(1):192–198.
101. Groneberg DA, Fischer A, Chung KF, Daniel H (2004) Molecular mechanisms of pulmonary peptidomimetic drug and peptide transport. *Am J Respir Cell Mol Biol* 30(3):251–260.
102. Bahadduri PM, D'Souza VM, Pinsonneault JK, Sadee W, Bao S, Knoell DL, Swaan PW (2005) Functional characterization of the peptide transporter PEPT2 in primary cultures of human upper airway epithelium. *Am J Respir Cell Mol Biol* 32(4):319–325.
103. Rotoli BM, Bussolati O, Sala R, Gazzola GC, Dall'Asta V (2005) The transport of cationic amino acids in human airway cells: Expression of system y + L activity and transepithelial delivery of NOS inhibitors. *FASEB J* 19(7):810–812.
104. Izquierdo MA, Scheffer GL, Flens MJ, Giaccone G, Broxterman HJ, Meijer CJ, van der Valk P, Scheper RJ (1996) Broad distribution of the multidrug resistance-related vault lung resistance protein in normal human tissues and tumors. *Am J Pathol* 148(3):877–887.
105. Berger W, Elbling L, Micksche M (2000) Expression of the major vault protein LRP in human non-small-cell lung cancer cells: Activation by short-term exposure to antineoplastic drugs. *Int J Cancer* 88(2):293–300.
106. Schwarze PE, Johnsen NM, Samuelsen JT, Thrane EV, Lund K, Lag M, Refsnes M, Kongerud J, Becher R, Boe J, Holme JA, Wiger R (1996) The use of isolated lung cells in in vitro pulmonary toxicology: Studies of DNA damage, apoptosis and alteration of gene expression. *Cent Eur J Public Health* 4 Suppl: 6–10.
107. Ramirez RD, Sheridan S, Girard L, Sato M, Kim Y, Pollack J, Peyton M, Zou Y, Kurie JM, Dimaio JM, Milchgrub S, Smith AL, Souza RF, Gilbey L, Zhang X, Gandia K, Vaughan MB, Wright WE, Gazdar AF, Shay JW, Minna JD (2004) Immortalization of human bronchial epithelial cells in the absence of viral oncoproteins. *Cancer Res* 64(24):9027–9034.

108. Reddel RR, Salghetti SE, Willey JC, Ohnuki Y, Ke Y, Gerwin BI, Lechner JF, Harris CC (1993) Development of tumorigenicity in simian virus 40-immortalized human bronchial epithelial cell lines. *Cancer Res* 53(5):985–991.
109. Mace K, Bowman ED, Vautravers P, Shields PG, Harris CC, Pfeifer AM (1998) Characterisation of xenobiotic-metabolising enzyme expression in human bronchial mucosa and peripheral lung tissues. *Eur J Cancer* 34(6):914–920.
110. Hall SD, Thummel KE, Watkins PB, Lown KS, Benet LZ, Paine MF, Mayo RR, Turgeon DK, Bailey DG, Fontana RJ, Wrighton SA (1999) Molecular and physical mechanisms of first-pass extraction. *Drug Metab Dispos* 27(2):161–166.
111. Wheeler CW, Park SS, Guenther TM (1990) Immunochemical analysis of a cytochrome P-450IA1 homologue in human lung microsomes. *Mol Pharmacol* 38(5):634–643.
112. Willey JC, Coy E, Broly C, Utell MJ, Frampton MW, Hammersley J, Thilly WG, Olson D, Cairns K (1996) Xenobiotic metabolism enzyme gene expression in human bronchial epithelial and alveolar macrophage cells. *Am J Respir Cell Mol Biol* 14(3):262–271.
113. Kim JH, Sherman ME, Curriero FC, Guengerich FP, Strickland PT, Sutter TR (2004) Expression of cytochromes P450 1A1 and 1B1 in human lung from smokers, non-smokers, and ex-smokers. *Toxicol Appl Pharmacol* 199(3):210–219.
114. Nishimura M, Yaguti H, Yoshitsugu H, Naito S, Satoh T (2003) Tissue distribution of mRNA expression of human cytochrome P450 isoforms assessed by high-sensitivity real-time reverse transcription PCR. *Yakugaku Zasshi* 123(5):369–375.
115. Crawford EL, Weaver DA, DeMuth JP, Jackson CM, Khuder SA, Frampton MW, Utell MJ, Thilly WG, Willey JC (1998) Measurement of cytochrome P450 2A6 and 2E1 gene expression in primary human bronchial epithelial cells. *Carcinogenesis* 19(10):1867–1871.
116. Kuzuya Y, Adachi T, Hara H, Anan A, Izuhara K, Nagai H (2004) Induction of drug-metabolizing enzymes and transporters in human bronchial epithelial cells by beclomethasone dipropionate. *IUBMB Life* 56(6):355–359.
117. Medina PP, Carretero J, Ballestar E, Angulo B, Lopez-Rios F, Esteller M, Sanchez-Cespedes M (2005) Transcriptional targets of the chromatin-remodelling factor SMARCA4/BRG1 in lung cancer cells. *Hum Mol Genet* 14(7):973–982.
118. Hempel N, Barnett A, Gamage N, Duggleby RG, Windmill KF, Martin JM, McManus ME (2005) Human SULT1A SULTs. In: Pacifici GM and Coughtrie MW (eds.) *Human Cytosolic Sulfotransferases*. CRC Press, Boca Raton, FL, pp. 43–61.
119. He D, Frost AR, Falany CN (2005) Identification and immunohistochemical localization of Sulfotransferase 2B1b (SULT2B1b) in human lung. *Biochim Biophys Acta* 1724(1–2):119–126.
120. Windmill KF, Gaedigk A, Hall PM, Samaratinga H, Grant DM, McManus ME (2000) Localization of N-acetyltransferases NAT1 and NAT2 in human tissues. *Toxicol Sci* 54(1):19–29.
121. Mace K, Gonzalez FJ, McConnell IR, Garner RC, Avanti O, Harris CC, Pfeifer AM (1994) Activation of promutagens in a human bronchial epithelial cell line stably expressing human cytochrome P450 1A2. *Mol Carcinog* 11(2):65–73.
122. Ritz SA, Wan J, Diaz-Sanchez D (2007) Sulforaphane-stimulated phase II enzyme induction inhibits cytokine production by airway epithelial cells stimulated with diesel extract. *Am J Physiol* 292(1):L33–L39.
123. Ohbayashi H (2002) Matrix metalloproteinases in lung diseases. *Curr Protein Pept Sci* 3(4):409–421.
124. Reed CE, Kita H (2004) The role of protease activation of inflammation in allergic respiratory diseases. *J Allergy Clin Immunol* 114(5):997–1008.

125. Yang X, Rojanasakul Y, Wang L, Ma JY, Ma JK (1998) Enzymatic degradation of luteinizing hormone releasing hormone (LHRH)/[D-Ala6]-LHRH in lung pneumocytes. *Pharm Res* 15(9):1480–1484.
126. Cohen AJ, Bunn PA, Franklin W, Magill-Solc C, Hartmann C, Helfrich B, Gilman L, Folkvord J, Helm K, Miller YE (1996) Neutral endopeptidase: Variable expression in human lung, inactivation in lung cancer, and modulation of peptide-induced calcium flux. *Cancer Res* 56(4):831–839.
127. Baraniuk JN, Ohkubo K, Kwon OJ, Mak J, Ali M, Davies R, Twort C, Kaliner M, Letarte M, Barnes PJ (1995) Localization of neutral endopeptidase (NEP) mRNA in human bronchi. *Eur Respir J* 8(9):1458–1464.
128. van der Velden VH, Naber BA, van der Spoel P, Hoogsteden HC, Versnel MA (1998) Cytokines and glucocorticoids modulate human bronchial epithelial cell peptidases. *Cytokine* 10(1):55–65.
129. Juillerat-Jeanneret L, Aubert JD, Leuenberger P (1997) Peptidases in human bronchoalveolar lining fluid, macrophages, and epithelial cells: Dipeptidyl (amino)peptidase IV, aminopeptidase N, and dipeptidyl (carboxy)peptidase (angiotensin-converting enzyme). *J Lab Clin Med* 130(6):603–614.
130. Wesley UV, Tiwari S, Houghton AN (2004) Role for dipeptidyl peptidase IV in tumor suppression of human non small cell lung carcinoma cells. *Int J Cancer* 109(6):855–866.
131. Trehin R, Nielsen HM, Jahnke HG, Krauss U, Beck-Sickinger AG, Merkle HP (2004) Metabolic cleavage of cell-penetrating peptides in contact with epithelial models: human calcitonin (hCT)-derived peptides, Tat(47–57) and penetratin(43–58). *Biochem J* 382(Pt 3):945–956.
132. Borchard G, Cassara ML, Roemele PE, Florea BI, Junginger HE (2002) Transport and local metabolism of budesonide and fluticasone propionate in a human bronchial epithelial cell line (Calu-3). *J Pharm Sci* 91(6):1561–1567.
133. Miller-Larsson A, Mattsson H, Hjertberg E, Dahlback M, Tunek A, Brattsand R (1998) Reversible fatty acid conjugation of budesonide. Novel mechanism for prolonged retention of topically applied steroid in airway tissue. *Drug Metab Dispos* 26(7):623–630.
134. Sudsakorn S, Liu H, LeDuc B, Williams D (2005) In vitro oleate esterification of budesonide. *AAPS J* 7(S2):R6244.

11

In Vitro Models of the Alveolar Epithelial Barrier

Carsten Ehrhardt, Michael Laue, and Kwang-Jin Kim

Abstract Aerosol administration of therapeutics to the respiratory system represents a significant opportunity for many classes of drugs, both small molecules and macromolecules, including recently engineered peptide and protein therapeutics. Advantages of aerosol administration include a more rapid absorption into the systemic circulation (this may be particularly important for drugs where fast onset of action is critical), a higher bioavailability than with other non-invasive modes of administration and avoidance of the first-pass metabolism or intestinal efflux transporters that may limit oral bioavailability. The main portal of entry for therapeutic molecules into the systemic circulation via pulmonary routes is very likely the alveolar epithelium, with its extremely thin barrier ($<0.5 \mu\text{m}$) and vast surface area ($>100 \text{m}^2$). Assessment of mechanistic information from *in situ/in vivo* lungs is not feasible, if not impossible, because the complex lung architecture prevents the study of isolated organs or minimally invasive *in vivo* approaches. Thus, *in vitro* models of the alveolar barrier have been widely used to help us in understanding how these inhaled molecules gain access to the systemic circulation of the body. With the overview of constituent cell types in mammalian lung blood–air barrier, we provide information on various *in vitro* models of alveolar epithelium, emphasising pros and cons of each model. Some examples of *in vitro* transport and metabolism studies using some of the reliable models are presented as well.

Keywords: Pneumocytes; Pulmonary drug delivery; Pulmonary metabolism, Alveolar epithelium

Abbreviations

ABC	ATP-binding cassette
ACE	Angiotensin-converting enzyme
AEC	Alveolar epithelial cell
AQP	Aquaporin
ATCC	American Type Culture Collection
ATI	Alveolar epithelial type I (cell)
ATII	Alveolar epithelial type II (cell)
ATP	Adenosine triphosphate

CAT	Cationic amino acid transporter
CPM	Carboxypeptidase M
CYP	Cytochrome P450
DC	Dendritic cells
ENaC	Epithelial sodium channel
FITC	Fluorescein isothiocyanate
GABRP	Gamma-aminobutyric acid receptor pi subunit
GLUT	Glucose transporter
GST	Glutathione S-transferases
hAEpC	Human alveolar epithelial cell
ICAM-1	Intercellular adhesion molecule-1
IVIVC	In vitro/in vivo correlation
LRP	Lung resistance protein
MLE	Mouse lung epithelium
MRP	Multidrug resistance-associated protein
NAT	<i>N</i> -acetyl transferases
OCT	Organic cation transporter
P_{app}	Apparent permeability coefficient
PEPT2	peptide transporter
P-gp	P-glycoprotein
RAGE	Receptor for advanced glycation end products
RT-PCR	Reverse transcription-polymerase chain reaction
SLC	Solute carrier protein
SP	Surfactant protein
SVCT	Sodium-dependent vitamin C transporter
TEER	Transepithelial electrical resistance
UGT	UDP-glucuronosyl transferases
VC	Vitamin C
ZO	Zonula occludens

11.1. Introduction

11.1.1. The Alveolar Epithelium

The respiratory system consists of the nasopharynx, trachea, bronchial tree and terminal air saccules. The nasopharynx, trachea and bronchi conduct air into respiratory parts of the lung, that is the alveoli [1]. The human alveoli are small, round or polyhedral chambers with an average diameter of about 250 μm , which form connected groups at the end of bronchoalveolar ductules. The wall of an alveolus is lined by the alveolar epithelium with underlying connective tissues and capillary networks. Two neighbouring alveoli form a common septum with the alveolar epithelium on each side, with connective tissues and capillaries in between. The average surface area covered by the alveolar epithelium is reported to be about 102 m^2 in humans [2]. Because of their smaller body sizes, rodents have much smaller alveolar epithelial surface areas than larger mammals (e.g., mice: 0.05 m^2 ; rats: 0.4 m^2 ; and dogs: 52 m^2). However, there is a very good correlation between the lung size and cell numbers when analysed using data from various mammalian species [2].

The human alveolar epithelium consists of two cell types: type I (alveolar epithelial type I [ATI], pneumocyte I) and type II (alveolar epithelial type II

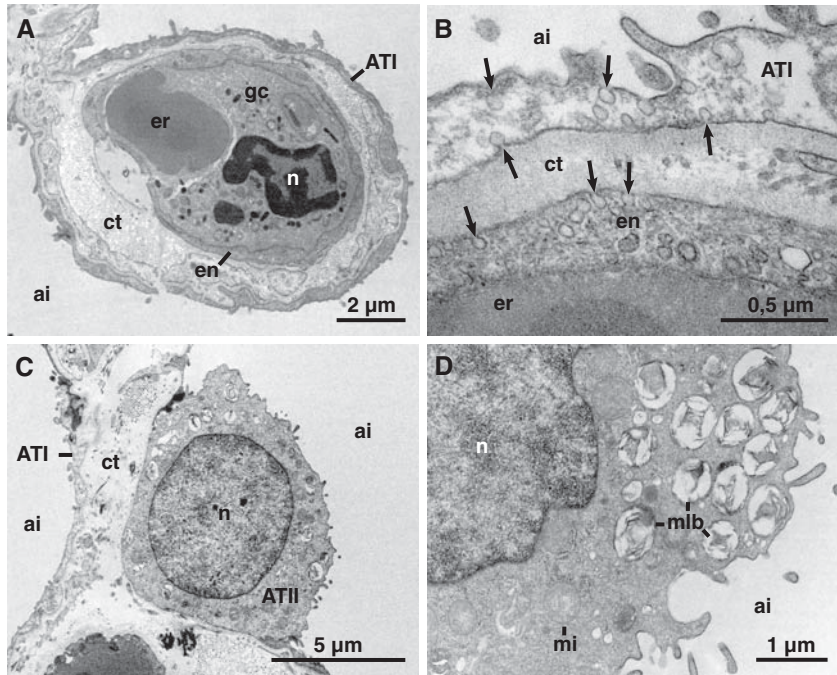


Figure 11.1 Ultrastructure of the human lung alveolar barrier. The tissue specimen is obtained via lung resection surgery. (A) Section through a septal wall of an alveolus. The wall is lined by a thin cellular layer formed by alveolar epithelial type I cells (ATI). Connective tissues (ct) separate ATI cells from the capillary endothelium (en) within which an erythrocyte (er) and granulocyte (gc) can be seen. The minimal distance between the alveolar airspace (ai) and erythrocyte is about 800–900 nm. The endothelial nucleus is denoted as n. (B) Details of the lung alveolar epithelial and endothelial barriers. Numerous caveolae (arrows) are seen in the apical and basal plasma membranes of an ATI cell as well as endothelial cell (en) membranes. Caveolae may partake transport of some solutes (e.g., albumin). (C) ATII cells (ATII) are often localised in the corners of alveoli where septal walls branch off. (D) ATII cells are characterised by numerous multilamellar bodies (mlb) which contain components of surfactant. A mitochondrion is denoted as mi.

[ATII], pneumocyte II) (Figure 11.1). ATI cells are very flat, spread out and cover >93% of the alveolar surface [3], while ATII cells are cuboidal and cover the remainder of the alveolar airspace. Although ATII cells are much more numerous than ATI cells (67% vs. 33%; [4]), ATI cells provide most of the surface area in alveoli, due to their larger cell surface of $\sim 7,000 \mu\text{m}^2$ versus $\sim 250 \mu\text{m}^2$ for ATII cells [2]. The height of ATI cells varies from about $2 \mu\text{m}$ to $3 \mu\text{m}$ in the nuclear region to about $0.2 \mu\text{m}$ in the cytoplasmic extensions. In many regions of the ATI cell, the apical and basal plasma membranes form caveolae, omega-shaped invaginations, which further decrease the distance between the apical and basal plasma membranes to a few tens of nanometres [5]. Caveolae are also a characteristic feature of the microcapillary endothelial cells which, in many parts of the alveolar wall, are localised close to the alveolar epithelium, separated from each other only by a thin layer of basement membrane. Thus, alveoli form an extremely thin barrier, allowing efficient gas exchange between the air and blood compartments (Figure 11.1). This thin barrier may also be utilised for fast absorption of therapeutics.

ATII cells are taller and cuboidal, with a height of $\sim 10 \mu\text{m}$ [4, 6]. The cells often reside at positions in the alveolar wall where three alveoli are connecting each other. Occasionally, ATII cells can be found in groups, which may represent daughter cells from a preceding cell division of an ATII mother cell. Characteristic structural features of ATII cells are the (multi)lamellar bodies. These structures are membrane-bound, intracellular compartments (up to $1 \mu\text{m}$ in size [7]) which contain densely packed membrane materials appearing as *lamellae* in cross sections. The membrane content of lamellar bodies is secreted onto the surface of the alveolar wall where it forms a mostly single layer of surfactant. The surfactant consists of a mixture of phospholipids ($\sim 90\%$) and surfactant-associated proteins (SP, $\sim 10\%$): SP-A, SP-B, SP-C and SP-D. The main function of the surfactant layer is to reduce the surface tension and thereby preventing the alveoli from collapsing and help expand them with inspiration of air. Moreover, the surfactant contains molecules (e.g., immunoglobulins, proteases and ceruloplasmin) for the defence against microorganisms and antioxidants (e.g., catalase) which prevent the oxidation (= inactivation) of proteins [8]. The surfactant proteins, SP-A and SP-D, belong to the family of collectins which bind with broad specificities to a variety of microorganisms and possess antimicrobial properties [9]. These proteins also exhibit both inflammatory and anti-inflammatory functions, which occur through interactions with pattern recognition receptors, including toll-like receptors and CD14, signal inhibitory regulatory protein alpha and a receptor complex of calreticulin and CD91 [10]. While the composition of the surfactant is well known, the structural organisation of the surfactant and the aqueous hypophase is still under debate. Major points of the discussion are whether or not the alveolar epithelium is lined by a continuous fluid layer and to what extent the surfactant covers the alveolar epithelium [11, 12].

Alveolar epithelial cells (AECs) are connected with each other by various epithelial cell–cell contacts (i.e., tight junctions, adherens junctions and others). These contacts comprise several groups of proteins, such as occludin, zonula occludens (ZO-1, -2, -3), claudins, tricellulin, E-cadherin and intercellular adhesion molecule-1 (ICAM-1) [13–15]. Their regulation and interplay, which has influence on epithelial barrier properties, however, is largely unknown to date.

11.1.1.1. Molecular Markers of Alveolar Epithelial Cells

While morphological features of AECs are well characterised, only few molecules have been identified which can be used as clear signatures for the respective cell type. These markers are summarised in the following paragraphs. The best marker for AT II cells is SP-C, which is exclusively expressed in this cell type. All other SP, such as SP-D, are also expressed in cells of the bronchial epithelium or even other epithelial cells of the body [16].

There is still some discordance about markers for ATI cells [17, 18]. Varieties of glycocalyx appear to be expressed in ATI versus ATII cells, which can be distinguished by the binding of specific lectins. *Lycopersicon esculentum* lectin, for example, appears to adhere specifically to the apical plasma membrane of ATI cells [19, 20]. Other lectin markers that have been reported in AEC typing are *Ricinus communis* agglutinin, *Erythrina cristagalli* lectin, soybean lectin and *Bauhinia purpurea* agglutinin (all for the ATI phenotype),

and *Maclura pomifera* agglutinin, *Helix pomatia* lectin and *Sambucus nigra* agglutinin (for the ATII phenotype) [21].

T1 α was the first protein marker observed to have a high specificity for mammalian ATI cells [22]. Based on its DNA sequence, T1 α is projected to be an integral membrane protein of ~ 18 kDa which is also expressed in cells of the choroid plexus of the central nervous system and the ciliary epithelium of the eye in both fetuses and adults. However, physiological function of T1 α remains largely unknown to date [23]. Very recently, mice lacking the T1 α gene [T1 α (-/-)] were reported to fail formation of expanded alveolar sacs, resulting in respiratory failure at birth [24]. It might be of interest to note that an attempt to generate antibodies recognising homologous structures in human tissue against T1 α has not been successful (personal communication with Dr. Michael Kasper). The expression of caveolin-1, the main structural protein of caveolae, has also been used to distinguish ATI from ATII cells, since ATI (but not ATII) cells contain numerous caveolae [25]. Caveolin-1, however, has only a limited potential as a differentiation marker in the alveolus, as it is highly expressed in lung microcapillary endothelial cells as well [26].

Furthermore, aquaporin-5 (AQP-5) has received some attention as an ATI cell marker. Of all mammalian cells studied to date, ATI cells reveal the highest water permeability in in vitro isolated cell studies [27], perhaps reflecting the expression of various water channels in alveolar epithelium, such as AQP-5, in addition to the active ion transport proteins, including epithelial sodium channels (e.g., ENaC) and Na⁺/K⁺-ATPase [28]. AQP-5 belongs to the aquaporin family of transmembrane proteins, which form water permeable channels and is also expressed in several other tissues (e.g., salivary and lacrimal glands, cornea and parts of the upper airway). In the human and rat alveolar epithelium, AQP-5 is localised specifically in the apical plasma membrane of ATI cells [29, 30]. Recent studies also indicate the expression of other members of the aquaporin family, such as AQP-3 and AQP-4, in the alveolar epithelium of the human lung. Although initially attributed to upper airway epithelia, immunolabelling of aquaporins in human lung tissue sections suggest that AQP-3 is expressed in ATII cells, whereas AQP-4, like AQP-5, is localised in ATI cells [31].

The transmembrane receptor for advanced glycation end products (RAGE) is a member of the immunoglobulin superfamily and highly expressed not only in the lung but also in other organs, including blood vessels. RAGE interacts with a broad spectrum of molecules, such as advanced glycation end products, amyloid beta fibrils, amphoterin and members of S100/calgranulin family, by recognising pattern of the tertiary protein structure. RAGE is involved in inflammatory processes, diabetic vascular disease and Alzheimer's disease [32]. Different reports from in situ studies as well as in vitro data have shown that RAGE is expressed in the alveolar epithelium. Although initial reports were controversial regarding the exact cellular localisation, a growing amount of experimental data supports the localisation of RAGE to the basolateral plasma membrane of ATI cells [33, 34]. Very recent studies suggest that RAGE expressed in the alveolar epithelium might play a role in inflammation and cell-matrix interactions [30, 35].

In the healthy lung, ICAM-1, an adhesion molecule that is involved in migration and activation of T-cells and macrophages, is highly expressed in the ATI cell [36]. In comparison, the expression of ICAM-1 in ATII and other cells in

Table 11.1 Constituents/Compartments of the Distal Blood–Air Barrier of the Lung.

Air
Surfactant
Hypophase
Epithelium (cells and basement membrane)
Connective tissue (collagen and elastic fibres)
Free (unattached to basement membranes) cells: fibroblasts, macrophages, granulocytes and lymphocytes
Endothelium (cells and basement membrane)
Blood plasma
Blood cells

the lung, such as endothelial cells, usually is low. In response to inflammatory stimulation and hyperoxia, expression levels of ICAM-1 increase in these other cell types, rendering distinction between cell types based on ICAM-1 levels rather difficult [37]. Expression of this immunologically important adhesion molecule also involves complex spatial interactions of the cells with the basal lamina and other epithelial cells [38].

Another protein which has been suggested as a differentiation marker between the ATI and ATII phenotypes is HTI56, a membrane protein which seems to be expressed exclusively in ATI cells [39]. In addition, Chen and co-workers confirmed four new ATI genes and one ATII gene by quantitative real-time PCR and immunostaining of both cultured alveolar cells and rat lung tissue: fibroblast growth factor receptor-activating protein 1, P2 purinergic receptor 7 (P2X7), interferon-induced protein and Bcl2-associated protein were found in ATI cells, while the gamma-aminobutyric acid receptor pi subunit (GABRP) was associated with ATII cells [40].

11.1.1.2. Functions of the Blood–Air Barrier of the Alveolus

In the alveolus, gases, liquids and solutes (e.g., metabolites) are exchanged or transported between the blood and air compartments. Moreover, the surfactant and exogenously presented material is taken up for degradation or inactivation into various cells. The trafficking molecules have to travel through different extracellular and cellular compartments by passive and sometimes also active processes. Table 11.1 gives a list of the components which molecules translocating from the blood to air and vice versa may encounter.

While gases and other small molecules dissolved in the extracellular fluid in the airspace of the alveolus or the blood are predominantly transported by passive diffusion, larger molecules in some cases traverse the distal blood–air barrier of the lung using active processes, for example cell-energy requiring transcytosis [41, 42]. Translocation of molecules can involve passive paracellular and/or transcellular pathways. Receptor-mediated endocytosis (via clathrin-coated pits or caveolae), adsorptive endocytosis and pinocytosis (non-specific fluid-phase endocytosis) of various molecules across the alveolar epithelium are expected. For larger particles/molecules, phagocytosis may also occur. Barrier properties of the alveolar epithelium are mainly determined by the tightness of alveolar epithelium and endothelium for passively transported molecules.

This tightness depends on the quality of cell–cell contacts (and apical and basolateral plasma membranes, in part). In particular, cell–cell contacts can be regulated, allowing certain molecules or even cells (e.g., macrophages, lymphocytes and/or granulocytes) to cross the blood–air barrier in the lung [43, 44].

Almost all transport studies for the alveolar epithelial barrier have been performed in animal models or cell lines, making the relevance of observed results in relation with the human situation somewhat questionable [45]. Observations on the clearance of lung oedema, which involves the removal of liquid and macromolecules from alveoli, revealed significant species differences in the regulation of the process, indicating that transport pathways might be different among the mammalian lungs and/or that the experimental parameters (e.g., concentrations and administration modality for molecules) studied may need further refinement for each species studied [46]. Our current understanding is that many molecules are transported across the alveolar epithelial barrier into the interstitial space or blood [41, 42]. Paracellular transport seems to be predominant for most small hydrophilic molecules (≤ 6 nm Stokes-Einstein radius for hydrophilic molecules ≤ 40 kDa) under normal physiological conditions. Larger molecules are usually transported by transcytosis, albeit their transport rates may vary significantly. Proteolytic degradation in alveolar airspaces and/or epithelial/endothelial cells seems to contribute to the observed variable fractions of intact peptides/proteins appearing in the systemic circulation following pulmonary delivery.

Caveolae might serve as a main transport conduit across alveolar epithelial and endothelial barriers, since they are abundant in both ATI and microvascular endothelial cells in the lung. Although the function and *modus operandi* of caveolae are still under debate, they seem to be involved in various transport processes (e.g., endocytosis and transcytosis of various molecules [e.g., folates and albumin]). A growing body of evidence suggests that caveolae are more stable structures than coated pits, but also pinch off from the plasma membrane and form small vesicles in the cytoplasm. Furthermore, caveolae are the site where several receptors are expressed/congregated, which might act as the centre controlling the activity of receptors and molecules involved in cell signalling (see Chap. 22 for a detailed description of caveolae function). Insights into the importance of caveolin-1 for the function of the distal lung blood–air barrier have mainly emerged from knockout mice studies, where the loss of caveolin-1 resulted in severe lung abnormalities and thickened alveolar septa [47]. Under pathophysiological conditions, AEC damage is associated with lower levels of caveolin-1, which is probably mainly due to the high vulnerability of ATI cells and consequently the significant loss of ATI cells in response to several sources of injury [26].

Regulation of the intra- and extracellular fluid homeostasis is an important challenge. Several ion and water channels are involved in this regulation. However, the significance of a few individual molecules playing the field has been reported to date. In ATII and ATI cells, Na^+ channels are localised at apical cell membranes, while Na^+/K^+ -ATPases are found at the basolateral cell membranes [28, 48]. Na^+/K^+ -ATPases extrude sodium ions out of the cell into the interstitium, thereby building up a sodium ion gradient across the apical cell membranes, setting up an electrical gradient across the epithelium as a result. This electrochemical gradient drives transport of the counter ion, Cl^- , from

the alveolar airspace across the alveolar epithelium into interstitium, creating an osmotic gradient which in turn drags water into the interstitium as well. The importance of aquaporins for this water transport has been elucidated in AQP-5 knockout mice, where a markedly reduced water flow was observed in response to an artificially imposed osmotic pressure in the lung. Interestingly, however, the near iso-osmolar water flux (secondary to active Na^+ absorption in AQP-5 knockout mice) was not affected at all [49]. Elucidation of transport mechanisms in the human alveolus is crucial, since pathophysiological conditions (e.g., lung oedema and acute respiratory distress syndrome) are demonstrated in part to be associated with abnormal and severely impaired transport across the alveolar epithelial barrier.

In addition to movement of water, solutes and proteins across alveolar epithelium, intact cells are known to cross the blood–air barrier of the lung. Interstitial and/or vascular macrophages are able to travel to the alveolar lumen where they may take up exogenously instilled molecules, for example microorganisms. After an initial contact with a potential pathogen, macrophages then migrate back into the connective tissue (or stay in the airspace) and recruit lymphocytes via cytokine release [50]. The alveolar epithelium might also be an important source of chemokines, such as CCL20. ATII cells may play a critical role in controlling the movement of dendritic cells (DC) through the distal lung blood–air barrier under both normal and inflammatory conditions. In vitro studies showed that cultured DC start migrating in response to conditioned media from human ATII cell cultures (but not those from alveolar macrophages) [51].

11.1.1.3. Developmental Biology and Wound Repair of the Alveolus

During human embryogenesis, the lung bud is formed by a diverticulum of the foregut. In the initial phase, development of the lung bud resembles that of sub-epithelial tubulo-acinar gland. Epithelial stalks grow and branch into the embryonic mesenchyme and finally widen to form tubes. The period between weeks 17 and 26 of gestation is characterised by a further growth of the system, the formation of terminal saccules and thinning of the mesenchymal structure. In addition, epithelial cells differentiate into type I and type II cells and surfactant production (by ATII cells) starts at the end of this period. Groups of alveoli first appear from about week 29 of gestation as indentations of the saccules reaching full functional development by 34 weeks of gestation. At birth, about one third to one half of the alveoli are present, steadily increasing in number during the first 2–3 years with their size and surface area continuing to increase until after adolescence. [52, 53]

In the mature, that is, adult alveolar epithelium, ATII cells serve as a progenitor with the ability to restore AEC populations by proliferation, especially when injury occurs. Daughter cells may proliferate and/or some may differentiate into ATI cells [54]. This process, under the control of still largely unknown regulatory mechanisms, is the basis for the normal cell turnover in the alveolar epithelium under physiological conditions. In case of an injured alveolar epithelium, the ability of ATII cells to proliferate and differentiate into ATI cells is thought to be a key factor in alveolar epithelial repair following injury. Nevertheless, recent findings also imply a possible role of bone marrow derived stem cells in the repair process or cell turnover in alveolar epithelium, although the relative contribution of bone marrow derived stem cells to these

processes, especially under normal physiological conditions, is unknown at best [55, 56].

The differentiation process of ATII daughter cells or progenitor cells towards the ATI cell phenotype has only been characterised largely in cell culture setting. In a human cell culture model, the morphology of isolated ATII cells shifts towards ATI cell morphology within 5–10 days [30, 57, 58]. The molecular signatures also change concomitantly, for example SP-C expression declines while levels for caveolin-1, RAGE and AQP-5 expression increase with time in culture. In parallel, typical epithelial cell–cell contacts are formed, accompanying the expression of typical cell–cell adhesion molecules (e.g., occludin, ZO-1 and ICAM-1). These molecules may be used as indicators/markers for the epithelial development/injury/repair. For a general overview on alveolar cell biology, various articles by Fehrenbach [59], Williams [17] and Mason [60] may be consulted.

11.2. In Vitro Models of the Alveolar Epithelial Barrier for Drug Absorption Studies

Although there is consensus about the crucial role of the distal lung epithelial tract in systemic drug absorption, not many useful in vitro model systems exist to date [61]. Because of the intricate and delicate network of the alveoli, an ex vivo approach (e.g., mounting excised mammalian lung alveolar epithelium in a diffusion chamber set-up) is impossible, although amphibian alveolar epithelial tissues have been studied as such to provide some useful information on transport properties in the past [62]. Furthermore, neither in vivo nor in situ studies (as discussed in Chap. 6) allow for precise assessment/prediction of the actual absorption sites involved. Therefore, cellular models based on primary or cell line cultures or co-culture of epithelial cells with either alveolar macrophages, capillary endothelial cells or DC are the only tools available to investigate drug absorption mechanisms in the alveolar epithelial barrier [63].

11.2.1. In Vitro Models of the Alveolar Epithelial Barrier

11.2.1.1. Alveolar Epithelial Cell Lines

While a number of immortalised cell lines emanating from different cell types of the airway (i.e., tracheo-bronchial) epithelium of lungs from various mammalian species are available (see Chap. 10), reliable and continuously growing cell lines that possess AEC morphology and phenotype are not reported to date. Most studies use cell lines of alveolar epithelial origin for drug absorption studies, while the observations are hard or meaningless to extend to in vivo human situation.

Probably the most frequently used alveolar epithelial model is the A549 cell line (American Type Culture Collection, ATCC CL-185), continuously growing cells derived from a human pulmonary adenocarcinoma that have some morphologic and biochemical features of the human pulmonary alveolar type II cell in situ [64]. A549 cells contain multilamellar cytoplasmic inclusion bodies, like those typically found in human lung ATII cells, although these hallmarks disappear as culture time increases. At early and late passage levels, the cells synthesise lecithin with a high percentage of disaturated fatty acids utilising

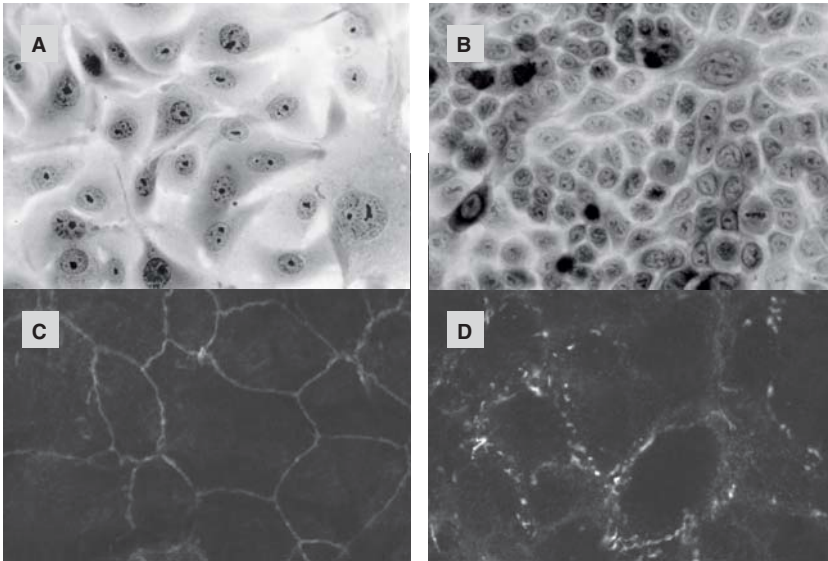


Figure 11.2 Morphological differences between human alveolar epithelial cells in primary culture (A and C) and the A549 cell line (B and D). Cells are visualised by light microscopy (A and B) and immunofluorescence microscopy (C and D) using an antibody against a tight junctional protein, occludin.

the cytidine diphosphocholine pathway [64]. The cell line has been utilised for many biopharmaceutical studies, albeit A549 cells lack the ability to form tight monolayers of polarised cells, due to the inability to form functional tight junctions [61, 63, 65, 66].

Figure 11.2 shows marked differences in morphology between primary human alveolar epithelial cells (hAEPs) that started as ATII cells and differentiated into ATI-like morphology on day 8 in primary culture (Panel A) and A549 cells on day 5 in culture (Panel B) by light microscopy. In addition, Figures 11.1C and 11.1D show results of immunofluorescence microscopy using an antibody against occludin (a tight junctional protein) for the hAEPc monolayer and A549 cells, respectively. Despite their obvious unsuitability, due to their lack of good transepithelial electrical resistance (TEER), some investigators still employed A549 cell layers in drug absorption studies [67, 68]. The absorption data reported by these groups were not able to clearly show differences in transport rates between proteins and peptides of various sizes where the published permeability values were 2–4 orders of magnitude higher than those obtained in tight monolayer systems (e.g., hAEPc monolayers) using identical compounds [63]. Moreover, the reported A549 TEER of $\sim 600 \text{ ohm}\cdot\text{cm}^2$ by one group [67] may be in gross error. Their data indicate that large hydrophilic molecules are translocated across A549 cell layers at rates approaching near-free diffusion limits. In other words, such large fluxes probably took place via large gaps between A549 cells, contradicting to the very large TEER they reported. It should be noted that TEER of A549 cells is usually in the range of 20–60 $\text{ohm}\cdot\text{cm}^2$, which makes much more sense, as it is known that no functional tight junctions are present in A549 cell layers. Notwithstanding, A549 cells might be a useful model in other areas

of biopharmaceutical research, including metabolism studies or cytotoxicity studies for various substances [65, 69, 70].

Other cell lines of an alveolar epithelial origin that can be found in the literature include R3/1 and L-2 (rat), mouse lung epithelium (MLE-12 and 15) (mouse) and H441 (human). Of these, NCI-H441 cell line (ATCC HTB-174), which emanated from a human lung adenocarcinoma, has been described to have characteristics of both ATII [71, 72] and bronchiolar (i.e., Clara) epithelial cells [73, 74]. Studies can thus be designed to characterise metabolism and transport properties of these two particular cell types. There is an emerging evidence that H441 cells are capable to form monolayers of polarised cells, exhibiting a significant TEER [75, 76], although the cell line has not been used for drug absorption experiments so far.

Wikenheiser and co-workers generated a series of continuous AEC lines [MLE-7, -12 and -15] from transgenic mice harbouring the SV40 large T antigen under the control of the human SP-C promoter region. These MLE cell lines show morphological and functional characteristics of distal respiratory epithelial cells normally lost after isolation and primary culture [77], which are consistent with those seen in non-ciliated bronchiolar and ATII cells. However, morphological and functional characteristics associated with an individual cell type do not appear to always coexist in a clonal cell line. For example, MLE-12 cells express SP-C mRNA (i.e., indicative of ATII cells in the adult mouse), but other characteristics (e.g., SP-A mRNA expression or presence of lamellar bodies) are missing in MLE-12 cells. The heterogeneity of cellular markers thought to be characteristic of ATII cells may be related to the immortalisation of cells at various stages of lung development. Alternatively, MLE cell lines may represent distinct subtypes of distal respiratory epithelial cells. MLE-12 can be obtained from the American Type Culture Collection (ATCC CRL-2110).

L-2 cells (ATCC HTB-149) have been isolated by clonal culture techniques from the adult rat lung. These cells appear to retain differentiated functions that are present in ATII cells of intact rat lungs. L-2 cells are diploid, epithelial cells. They contain osmiophilic lamellar bodies in their cytoplasm and synthesise lecithin by the same *de novo* pathways as in a whole lung [78]. It is not known if L-2 cells are capable to form confluent and electrically tight monolayers. L-2 cells have not been systematically investigated regarding their suitability as a model for absorption studies.

The rat cell line R3/1 was established from cells obtained from broncho-alveolar tissues of foetal Wistar rats at 20 days of gestation. This cell line displays a phenotype with several characteristic features of ATI cells. R3/1 cells were analysed to show a positive expression for mRNA and protein content of markers related to the ATI cell type (e.g., T1 α , ICAM-1, connexin-43 and caveolin-1 and -2) [79]. Whether or not this cell line can form functional tight junctions is currently under investigation in our laboratories.

11.2.1.2. Primary Alveolar Epithelial Cell Culture Models

Because of the paucity of appropriate AEC lines that form functional tight junctions, primary cultures of AEC are used for most *in vitro* studies of alveolar epithelial function (e.g., solute transport and metabolism). Primary mammalian AEC techniques involve isolation, purification and culture of ATII cells from tissues obtained either after lung resections or isolated perfused lungs. These

ATII cells, when plated on permeable supports or plastics under appropriate culture conditions, acquire features of type I cell-like phenotype and morphology [30, 57, 80]. Although isolation of ATI pneumocytes from rat lungs has recently been reported with some success [28, 48, 81], development of confluent ATI cell monolayer with electrically tight characteristics has not been reported yet. It should be noted that unlike many other cells in primary culture, AEC exhibits generally a very limited proliferation profile and is therefore not suitable for passaging. Thus, a new preparation of cells has to be used for each data set, which drives the costs up tremendously, and a reliable normalisation scheme of data observed from each set of cell preparations is needed.

Because of the limited availability of human lung tissues and some ethical issues pertaining to use of human tissues, most studies were based on isolation and culture of cells from the lungs of animals, including mouse [82], rat [83], rabbit [84] and pig [85]. In the Appendix, a universal protocol has been developed by us for the isolation and purification of mammalian ATII cells, followed by monolayer cultures of ATII or ATI cell-like phenotype and morphology. However, since evidence for species differences between human and rodents might be more significant than once assumed [45], confirmation using human pneumocyte cultures has been performed for various aspects [58, 86, 87].

11.2.2. The Use of Alveolar Epithelial Cells in Biopharmaceutical Research

With the lung emerging as an attractive non-invasive delivery routes for systemic absorption of biopharmaceuticals and fast-acting conventional drugs, it appears pivotal to gather knowledge about modes of transport and the fate of these compounds at the alveolar epithelial barrier. Although an in vitro/in vivo correlation (IVIVC) using AEC monolayers could not be established definitively currently, various in vitro models can help elucidate underlying transport mechanisms of drug molecules, as well as their metabolic stability in the lung. Therefore, the available in vitro systems need to be carefully characterised and validated prior to using them in the context of biopharmaceutical research.

11.2.2.1. Drug Absorption Studies

Absorptive processes have first been studied in the context of ion and fluid clearance from the lung in health and disease (e.g., oedema), which were conducted largely using monolayers of rat pneumocytes [e.g., 88]. Following studies of active and passive ion movement across alveolar epithelium using the in vitro model, translocation of plasma proteins (which are commonly found in the alveolar lumen, e.g., albumin, immunoglobulin G and transferrin) was investigated [41]. Since rat-based monolayers have been considered the gold standard in elucidation of AEC physiology/biology for several decades, it is not surprising that the same well-established primary rat pneumocyte monolayer model was also employed for drug delivery studies [89–91]. However, as stated above, newer models based on different animal species (which might more closely resemble human, e.g., derived from porcine lung [85]) were developed and a number of laboratories also started to use hAEPc monolayers for drug absorption studies [66, 92].

Effros and Mason showed an apparent inverse relationship between molecular weights and rates of in vivo lung clearance of molecules of different sizes, both in log scales [93]. A similar relationship has also been found in

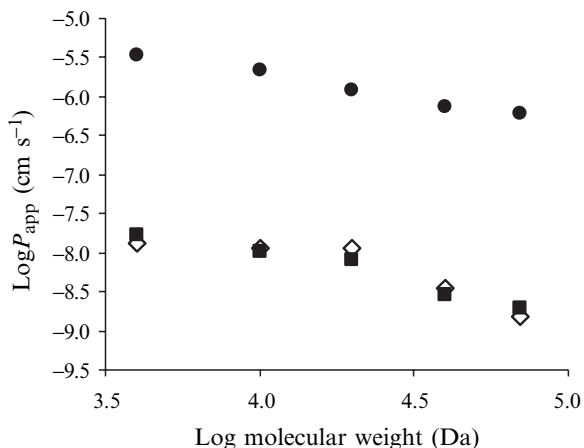


Figure 11.3 Permeability to FITC-labelled dextrans across rat (◇, [94]) and human (■, [66]) alveolar type I (ATI) cell-like monolayers compared with the permeability across A549 cell layers (●, [67]).

two in vitro alveolar epithelial models of primary rat [94] and human [66] monolayers (Figure 11.3). By comparison, Fluorescein isothiocyanate (FITC)-dextran permeabilities observed with A549 cells [67] are over two orders of magnitude greater [63] (Figure 11.3).

Active transport mechanisms by which some compounds traverse the distal lung blood–air barrier are more likely to provide new insights and improved strategies for pulmonary delivery of drugs into the systemic circulation and/or targeting drugs to lung parenchymal cells. The expression pattern of ATP-binding cassette (ABC)-transporters in both the healthy and pathological lung has recently been reviewed by van der Deen et al. [95]. Several transporters have been identified in AEC, which might have an impact on pulmonary bioavailability of drugs, especially lipophilic drugs (e.g., cytostatics). P-glycoprotein (P-gp, MDR1) is probably the best characterised efflux pump in the body. In 2001, Lehmann and co-workers reported the presence of P-gp and multidrug resistance-associated protein 1 (MRP1) in rat ATII cells in primary culture [96]. These findings were later confirmed using both human and rat lung tissue sections as well as ATI cell-like monolayers by immunohistochemistry and efflux studies using vinblastine and rhodamine 123 as respective substrates for P-gp and MRP1 [97, 98]. MRP1 and lung resistance protein (LRP) were also identified in cultures of human peripheral lung epithelial cells [99].

ABCA1 and *ABCA3* gene transcripts were found in cell lines (e.g., A549) of human lung origin, in ATII cells of human, rat, and mouse, as well as different tissues of rat, but the highest expression of *ABCA1* and *ABCA3* was observed in murine ATII cells [100, 101]. Molecular and biochemical studies show that *ABCA1* mediates basolateral surfactant efflux, while *ABCA3* is found in the limiting membrane of lamellar bodies. Because both transporters are members of a subfamily of ABC-transporters that are predominantly known to be involved in the regulation of lipid transport and membrane trafficking, it can be speculated that these transporter proteins may play a key role in lipid organisation during the formation of lamellar bodies. It should also be noted that there are some conflicting reports regarding the activity and localisation of ABC-transporters in mammalian AEC [95].

Other solute transporters (solute carrier protein [SLC]) are also expressed in the alveolus. The mRNA transcripts of glucose transporters, GLUT1, GLUT4, GLUT5 and SGLT1, have been detected in freshly isolated rat ATII cells by

reverse transcription-polymerase chain reaction (RT-PCR) and Western blot analyses. However, a gradual loss of sodium-glucose co-transport activity and transcription during transdifferentiation of ATII cells towards the type I-like cell phenotype in culture has been reported [102].

Efficient gas exchange and other functions (e.g., active Na^+ absorption) in alveoli are thought to be tied to transepithelial clearance of luminal proteins, albeit little is known about alveolar epithelial mechanisms of protein transport. Protein degradation followed by transport of resultant peptides and amino acids may play an important role in this process. Groneberg reported the expression and activity of the high-affinity proton-coupled peptide transporter, PEPT2, in rat and murine ATII cells [103]. The neutral and cationic amino acid transporter (CAT), ATB^{0+} , is expressed in mouse ATI cells in situ [104]. The important role of peptide and amino acid removal was further supported by the recent finding of Rothenberg et al. that the arginine transport protein, CAT2, has a critical role in regulating lung inflammatory responses, in that CAT2-deficient mice revealed spontaneous inflammation in the lung [105].

Vitamin C (VC, L-ascorbic acid) is known to be essential for many enzymatic reactions. Sodium-dependent VC transporters (SVCT), SVCT1 and SVCT2, were recently identified and reported to be localised in the apical cell membrane of AECs in the lung of adult rats. These results suggest that SVCT proteins could transport the reduced form of VC from the airway/alveolar surface liquid into respiratory epithelial cells [106].

Primary rat and mouse ATII cells exhibit pH-sensitive, reversible transport of choline, a process blocked pharmacologically with phenoxybenzamine, an inhibitor of organic cation transporters (OCT). RT-PCR products for choline transporters, OCT1 and OCT2, were detected in AEC, with only OCT2 protein being robustly expressed [107]. In 1999, Shen and co-workers published evidence that rabbit AEC in primary culture shows a concentration-dependent net absorption of organic cations [84], although the molecular identity of the OCT involved was lacking. Our laboratories recently published data on net absorption of salbutamol across hAEPc monolayers [108]. Since salbutamol carries a positive charge at physiological pH, involvement of OCT family member(s) in the alveolar epithelial absorption of salbutamol can be surmised.

Investigations utilising tight monolayers of either rat or human AEC showed that clearance of a number of endogenous proteins (e.g., immunoglobulin G, albumin and transferrin) occurs in a cell energy-dependent manner [92, 109–111]. These observations strongly suggest that transcytotic processes (e.g., caveolae-mediated or via clathrin-coated pits) may be responsible for removal of these endogenous proteins from alveolar lining fluid. Intriguingly, these proteins were net absorbed as intact molecules with variable degrees of degradation [41]. Table 11.2 summarises the current literature data on absorption of various peptides and proteins across tight monolayers of primary human and rat AEC.

Although there appears to be no significant species differences in absorption rates for small lipophilic drugs, some interspecies differences are noted with water-soluble drugs absorbed from distal airspaces of in vivo mammalian lungs [112]. These species differences have not been systematically studied yet. However, some marked differences were reported for protein absorption rates

Table 11.2 Molecular Weights and Apparent Permeability Coefficients (P_{app}) of Various Proteins and Peptides Across Primary Human Versus Rat AEC Monolayers.

	Molecular weight (Da)	P_{app} a-to-b (human)	P_{app} b-to-a (human)	P_{app} a-to-b (rat)	P_{app} b-to-a (rat)	References
Gly-L-Phe	222	na	na	3.29/1.38 ^a	1.58/1.29 ^a	[89]
Gly-D-Phe	222	na	na	1.55	1.60	[89]
TRH ^b	362	na	na	3.27	3.80	[113]
acXASNH ₂	491	na	na	1.19	Na	[114]
Vasopressin	1,056	na	na	0.45	0.45	[115]
acXAS(GAS) ₇ NH ₂	1,998	na	na	0.25	Na	[114]
GLP-1(7-37)	3,355	6.13	1.91	na	Na	[92]
PTH(1-38)	4,458	2.20	1.80	na	Na	[92]
Insulin	5,800	0.77	0.72	0.21	0.12	[92, 116]
Cytochrome c	12,300	na	na	0.48	0.44	[109]
G-CSF	20,000	na	na	0.029	0.034	[109]
Growth hormone	22,125	8.33	9.02	0.041	0.074	[92, 117]
HRP	40,000	na	na	0.069	0.073	[90]
Ovalbumin	43,000	na	na	1.09	0.58	[109]
Albumin	65,000	2.45	0.21	0.77	0.39	[92, 109]
Transferrin	76,500	0.88	0.30	1.10	0.47	[91, 92, 109]
IgG	150,000	0.36	0.15	0.91	0.17	[92, 109, 111]

Notes: All P_{app} values are expressed as mean ($\times 10^{-7}$ cm/s). The abbreviations of a-to-b and b-to-a denote the apical-to-basolateral and basolateral-to-apical directions, respectively.

^a Concentrations were 1 mM/10 mM. ^b Based on ³H-labelled TRH. The entry 'na' denotes 'not available'.

found in primary human versus rat AEC monolayers [92]. Absorption rates for most peptides and proteins in primary rat versus human AEC monolayers, however, remain largely unknown.

11.2.2.2. Drug Metabolism Studies

While most textbooks and review articles on pulmonary drug delivery appear to assume that lungs have a low metabolic activity and consider this as one of the major advantages for pulmonary drug delivery (of peptide and protein therapeutics), little is known about the pulmonary metabolism of endogenous compounds and exogenously administered xenobiotics. As Chap. 10 contains a general introduction to pulmonary metabolism, only a concise overview of the metabolic activity in the alveolus is given here.

Some features, such as morphology and functionality of A549 cells, are consistent with those of ATII cells in vivo, for example surfactant synthesis and oxidative metabolism [65, 118]. Qualitative RT-PCR analysis revealed the presence of several transcripts of cytochrome P450 (CYP) 1A1, CYP1B1, CYP2B6, CYP2C, CYP2E1, CYP3A5 and CYP3A7 mRNA in A549 cells [119]. More recently, quantitative RT-PCR studies revealed the presence of CYP1A1, CYP1B1, CYP2B6, CYP2C, CYP3A4 and CYP3A5 messages in A549 cells, whereas no detectable CYP1A2, CYP2A6, CYP2A13 and CYP2F1 transcripts were found [120]. Compared to the profile found in human distal lung tissues, CYP1B1 mRNA was the most abundantly expressed transcript in

Table 11.3 Summary of the Expression Pattern and Activities of Phase I and Phase II Metabolic Enzymes and Various Peptidases/Proteases in Human Peripheral Lung Tissues, Primary Rat AEC Culture and Human Alveolar Epithelial Cell Line, A549.

Enzyme	Lung mRNA ^a	Lung protein ^{a,e}	Peripheral tissue ^{g,h}	Rat AEC ^{l,e} ATII/ATI	A549 ^{j,k,l,h,e}
CYP1A1	? (***) ^b	– (***) ^b	+	+	+
CYP1A2	?	?	+		–
CYP1B1	** ^c	? ^c	+	+	+
CYP2A6	**	?	–		+/-
CYP2A7					–
CYP2A13			+		–
CYP2B1/2				+	
CYP2B6/7	***	***	+		+ ^m /–
CYP2C	? ^d	? ^d	–/+		+
CYP2D6	?	?	–		+
CYP2E1	***	***	+	+	+/-
CYP2F1	***				–
CYP2J3				+	
CYP3A2				–	
CYP3A4	?	* ^f	+		–
CYP3A5	***	**	+		+
CYP3A7	?				+
CYP4B1	***				–
GST			+		+
UGT			+		+
NAT1			+		
NAT2			+		
APN		24.77 ^e		16.16/23.99 ^e	47.74 ^e /8.8 ^k
DPP IV		69.26 ^e		36.65/16.29 ^e	24.24 ^e /4.6 ^k
NEP 24.11		0.99 ^e		1.81/0.96 ^e	2.41 ^e
ACE		10.80 ^e		4.29/nd ^e	–
CPM		4.63 ^e		nd/5.20 ^e	4.28 ^e

*: weak evidence; **: moderate evidence; ***: strong evidence; ?: conflicting evidence; –: no evidence/undetectable; +: detectable (but not quantified); nd: not detected.

^a [123]; ^b Strong evidence in smokers; ^c In alveolar macrophages; ^d In bronchial cells; ^e [69]; ^f In ~20% of samples; ^g [122]; ^h [120]; ⁱ [125]; ^j [65]; ^k [124]; ^l [119]; ^m not inducible.

A549 cell line, followed by CYP3A5. Although the amount of specific CYP transcripts in A549 cells is markedly lower than that found using lung lysates, the profile of CYP expression shows a similar trend in overall profiles in both systems. These results show that the A549 lung adenocarcinoma cell line expresses limited numbers of phase I enzymes and responds to P450 inducers, but at much lower levels than those observed in lung lysates.

The phase II metabolising step of conjugation reactions can be attributed to the families of UDP-glucuronosyl transferases (UGT), glutathione S-transferases (GST) and *N*-acetyl transferases (NAT) [121]. Using specific primers for the detection of GST and NAT isoenzymes, it was reported that GSTM1 is expressed in 25% of the peripheral lung tissues, whereas GSTM3 and NAT1 and NAT2 mRNAs are found in all samples [122]. Castell et al. found very similar results in samples of human lung tissues versus A549 cells for UGT and GST activities [120].

It has been suggested that the lung may possess relatively low proteolytic activities, but the inaccessibility of the peripheral lung for experimental manoeuvres and/or manipulations may have confounded the correct assessment of such data regarding the extent of metabolism in the deep lung for exogenously inhaled peptides/protein therapeutics. Nevertheless, only 60% of insulin was still intact after transport across rat AEC monolayers *in vitro* [116]. This might be an indication of an underestimated protease activity in the alveolar epithelium and lining fluid/surfactant, which could account for low systemic bioavailabilities of some protein drugs after inhalation. The activity of individual peptidases in A549 cells and primary rat ATII or ATI-like pneumocytes has been studied by Forbes and co-workers [69]. The pattern of peptidase expression appears to change over time in primary rat AEC culture. Interestingly, A549 cells revealed levels of activity closest to those of primary ATI-like cells, further complicating the pulmonary metabolic research (Table 11.3).

11.3. Concluding Remarks

As seen above, the lung alveolar epithelium serves an essential and efficient function of providing fresh oxygen in exchange for the waste product of carbon dioxide across its very thin and wide expanse of epithelial barrier. This latter arrangement of thinness and enormous surface area of the alveolar epithelium has been considered by many as the advantage for systemic delivery via pulmonary routes of therapeutic drugs, especially peptides and protein molecules that show very poor bioavailability via oral routes because of extensive degradation at stomach and intestines. However, currently we have to rely on primary cell culture models, as many cell lines developed to date for alveolar epithelium failed to recapitulate what has been shown for *in vivo* properties of AECs. Most formidable may be the lack of genuine type II cell models, although some success using keratinocyte growth factor to keep the ATII cell morphology and phenotype has been documented for generating monolayer cultures with functional tight junctions. For non-transport studies (e.g., metabolism of certain classes of xenobiotics) may be performed using cell line culture models (e.g., A549) for alveolar epithelium. Major hurdles, however, still remain for successful development of passageable alveolar type I and type II cell (lines), either as separate or mixed cell types of ATI and ATII coexisting in one monolayer setting, thus mimicking the *in vivo* setting. Moreover, the co-culture models of alveolar epithelium and capillary endothelium of the mammalian lung are in their infancy at best. With further refinement of such co-culture systems, additional cell types (e.g., macrophages, lymphocytes, DC and/or polymorphonuclear cells) can be added to the culture to study various cell biology-related questions in the lung field (including drug

metabolism and modulation of properties of lung air–blood barrier). Moreover, no meaningful IVIVC has been established to date for lung alveolar epithelial drug transport/metabolism, asking us in the field to interpret with extreme caution the observed data using various *in situ* to *in vitro* models over the years. Notwithstanding these difficulties and challenges in various aspects of the *in vitro* alveolar epithelial models, mechanistic studies of pulmonary drug delivery using the alveolar epithelium as the main portal of entry into the systemic circulation from the lung airspaces are expected to provide us a wealth of information in coming years and enable us to devise newer and more efficient ways of treating lung-specific diseases using targeting approaches as well as improved bioavailability of those therapeutics that yield very poor absorption via other routes.

Acknowledgments: KJK was supported in part by research grants from the National Institutes of Health (HL38658 & HL64365) and the Hastings Foundation.

References

1. Gray H (1918, 2000) *Anatomy of the Human Body*. Lea & Febiger, Philadelphia, Bartleby.com www.bartleby.com/107/
2. Stone KC, Mercer RR, Gehr P, Stockstill B, Crapo JD (1992) Allometric relationships of cell numbers and size in the mammalian lung. *Am J Respir Cell Mol Biol* 6:235–243
3. Crapo JD, Barry BE, Gehr P, Bachofen M, Weibel ER (1982) Cell number and cell characteristics of the normal human lung. *Am Rev Respir Dis* 126:332–337
4. Crapo JD, Young SL, Fram EK, Pinkerton KE, Barry BE, Crapo RO (1983) Morphometric characteristics of cells in the alveolar region of mammalian lungs. *Am Rev Respir Dis* 128(2 Pt 2):S42–S46
5. Dormans JA (1983) The ultrastructure of various cell types in the lung of the rat: a survey. *Exp Pathol* 24:15–33
6. Fehrenbach H, Schmiedl A, Wahlers T, Hirt SW, Brasch F, Riemann D, Richter J (1995) Morphometric characterisation of the fine structure of human type II pneumocytes. *Anat Rec* 243(1):49–62
7. Ryan US, Ryan JW, Smith DS (1975) Alveolar type II cells: studies on the mode of release of lamellar bodies. *Tissue Cell* 7(3):587–599
8. Veldhuizen R, Possmayer F (2004) Phospholipid metabolism in lung surfactant. *Subcell Biochem* 37:359–388
9. Floros J, Hoover RR (1998) Genetics of the hydrophilic surfactant proteins A and D. *Biochim Biophys Acta* 1408(2–3):312–322
10. Takahashi H, Sano H, Chiba H, Kuroki Y (2006) Pulmonary surfactant proteins A and D: innate immune functions and biomarkers for lung diseases. *Curr Pharm Des* 12(5):589–598
11. Dorrington KL, Young JD (2001) Development of the concept of a liquid pulmonary alveolar lining layer. *Br J Anaesth* 86(5):614–617
12. Hills BA (2002) The alveolar lining. *Br J Anaesth* 88(4):607–608
13. Chen SP, Zhou B, Willis BC, Sandoval AJ, Liebler JM, Kim KJ, Ann DK, Crandall ED, Borok Z (2005) Effects of transdifferentiation and EGF on claudin isoform expression in alveolar epithelial cells. *J Appl Physiol* 98(1):322–328
14. Madjdpour C, Oertli B, Ziegler U, Bonvini JM, Pasch T, Beck-Schimmer B (2000) Lipopolysaccharide induces functional ICAM-1 expression in rat alveolar epithelial cells *in vitro*. *Am J Physiol* 278(3):L572–L579

15. Cavanaugh KJ Jr, Oswari J, Margulies SS (2001) Role of stretch on tight junction structure in alveolar epithelial cells. *Am J Respir Cell Mol Biol* 25(5):584–591
16. Bernhard W, Haslam PL, Floros J (2004) From birds to humans: new concepts on airways relative to alveolar surfactant. *Am J Respir Cell Mol Biol* 30(1):6–11
17. Williams MC (2003) Alveolar type I cells: molecular phenotype and development. *Annu Rev Physiol* 65:669–695
18. Dahlin K, Mager EM, Allen L, Tigue Z, Goodglick L, Wadehra M, Dobbs L (2004) Identification of genes differentially expressed in rat alveolar type I cells. *Am J Respir Cell Mol Biol* 31(3):309–316
19. Bankston PW, Porter GA, Milici AJ, Palade GE (1991) Differential and specific labeling of epithelial and vascular endothelial cells of the rat lung by *Lycopersicon esculentum* and *Griffonia simplicifolia* I lectins. *Eur J Cell Biol* 54(2):187–195
20. Barkhordari A, Stoddart RW, McClure SF, McClure J (2004) Lectin histochemistry of normal human lung. *J Mol Histol* 35(2):147–156
21. Kasper M, Singh G (1995) Epithelial lung marker: current tools for cell typing. *Histol Histopathol* 10:155–169
22. Rishi AK, Joyce-Brady M, Fisher J, Dobbs LG, Floros J, VanderSpek J, Brody JS, Williams MC (1995) Cloning, characterization, and development expression of a rat lung alveolar type I cell gene in embryonic endodermal and neural derivatives. *Dev Biol* 167(1):294–306
23. Williams MC, Cao Y, Hinds A, Rishi AK, Wetterwald A (1996) T1 alpha protein is developmentally regulated and expressed by alveolar type I cells, choroid plexus, and ciliary epithelia of adult rats. *Am J Respir Cell Mol Biol* 14(6):577–585
24. Millien G, Spira A, Hinds A, Wang J, Williams MC, Ramirez MI (2006) Alterations in gene expression in T1 alpha null lung: a model of deficient alveolar sac development. *BMC Dev Biol* 6:35
25. Newman GR, Campbell L, von Ruhland C, Jasani B, Gumbleton M (1999) Caveolin and its cellular and subcellular immunolocalisation in lung alveolar epithelium: implications for alveolar epithelial type I cell function. *Cell Tissue Res* 295(1):111–120
26. Kasper M, Reimann T, Hempel U, Wenzel KW, Bierhaus A, Schuh D, Dimmer V, Haroske G, Muller M (1998) Loss of caveolin expression in type I pneumocytes as an indicator of subcellular alterations during lung fibrogenesis. *Histochem Cell Biol* 109(1):41–48
27. Dobbs LG, Gonzalez R, Matthay MA, Carter EP, Allen L, Verkman AS (1998) Highly water-permeable type I alveolar epithelial cells confer high water permeability between the airspace and vasculature in rat lung. *Proc Natl Acad Sci USA* 95(6):2991–2996
28. Borok Z, Liebler JM, Lubman RL, Foster MJ, Zhou B, Li X, Zabski SM, Kim KJ, Crandall ED (2002) Na transport proteins are expressed by rat alveolar epithelial type I cells. *Am J Physiol* 282(4):L599–L608
29. Nielsen S, King LS, Christensen BM, Agre P (1997) Aquaporins in complex tissues. II. Subcellular distribution in respiratory and glandular tissues of rat. *Am J Physiol* 273(5 Pt 1):C1549–C1561
30. Demling N, Ehrhardt C, Kasper M, Laue M, Knels L, Rieber EP (2006) Promotion of cell adherence and spreading: a novel function of RAGE, the highly selective differentiation marker of human alveolar epithelial type I cells. *Cell Tissue Res* 323(3):475–488
31. Kreda SM, Gynn MC, Fenstermacher DA, Boucher RC, Gabriel SE (2001) Expression and localization of epithelial aquaporins in the adult human lung. *Am J Respir Cell Mol Biol* 24(3):224–234
32. Bierhaus A, Stern DM, Nawroth PP (2006) RAGE in inflammation: a new therapeutic target? *Curr Opin Investig Drugs* 7(11):985–991

33. Fehrenbach H, Kasper M, Tschernig T, Shearman MS, Schuh D, Muller M (1998) Receptor for advanced glycation endproducts (RAGE) exhibits highly differential cellular and subcellular localisation in rat and human lung. *Cell Mol Biol (Noisy-le-grand)* 44(7):1147–1157
34. Shirasawa M, Fujiwara N, Hirabayashi S, Ohno H, Iida J, Makita K, Hata Y (2004) Receptor for advanced glycation end-products is a marker of type I lung alveolar cells. *Genes Cells* 9(2):165–174
35. Uchida T, Shirasawa M, Ware LB, Kojima K, Hata Y, Makita K, Mednick G, Matthay ZA, Matthay MA (2006) Receptor for advanced glycation end-products is a marker of type I cell injury in acute lung injury. *Am J Respir Crit Care Med* 173(9):1008–1015
36. Christensen PJ, Kim S, Simon RH, Toews GB, Paine R 3rd (1993) Differentiation-related expression of ICAM-1 by rat alveolar epithelial cells. *Am J Respir Cell Mol Biol* 8(1):9–15
37. Kang BH, Crapo JD, Wegner CD, Letts LG, Chang LY (1993) Intercellular adhesion molecule-1 expression on the alveolar epithelium and its modification by hyperoxia. *Am J Respir Cell Mol Biol* 9(4):350–355
38. Paine R 3rd, Christensen P, Toews GB, Simon RH (1994) Regulation of alveolar epithelial cell ICAM-1 expression by cell shape and cell-cell interactions. *Am J Physiol* 266(4 Pt 1):L476–L484
39. Dobbs LG, Gonzalez RF, Allen L, Froh DK (1999) HTI56, an integral membrane protein specific to human alveolar type I cells. *J Histochem Cytochem* 47:129–137
40. Chen Z, Jin N, Narasaraju T, Chen J, McFarland LR, Scott M, Liu L (2004) Identification of two novel markers for alveolar epithelial type I and II cells. *Biochem Biophys Res Commun* 319(3):774–780
41. Kim KJ, Malik AB (2003) Protein transport across the lung epithelial barrier. *Am J Physiol* 284(2):L247–L259
42. Hastings RH, Folkesson HG, Matthay MA (2004) Mechanisms of alveolar protein clearance in the intact lung. *Am J Physiol* 286(4):L679–L689
43. Evans SM, Blyth DI, Wong T, Sanjar S, West MR (2002) Decreased distribution of lung epithelial junction proteins after intratracheal antigen or lipopolysaccharide challenge: correlation with neutrophil influx and levels of BALF sE-cadherin. *Am J Respir Cell Mol Biol* 27(4):446–454
44. Herold S, von Wulffen W, Steinmueller M, Pleschka S, Kuziel WA, Mack M, Srivastava M, Seeger W, Maus UA, Lohmeyer J (2006) Alveolar epithelial cells direct monocyte transepithelial migration upon influenza virus infection: impact of chemokines and adhesion molecules. *J Immunol* 177(3):1817–1824
45. King LS, Agre P (2001) Man Is not a rodent: aquaporins in the airways. *Am J Respir Cell Mol Biol* 24(3):221–223
46. Matthay MA, Folkesson HG, Clerici C (2002) Lung epithelial fluid transport and the resolution of pulmonary edema. *Physiol Rev* 82(3):569–600
47. Razani B, Engelman JA, Wang XB, Schubert W, Zhang XL, Marks CB, Macaluso F, Russell RG, Li M, Pestell RG, Di Vizio D, Hou H Jr, Kneitz B, Lagaud G, Christ GJ, Edelmann W, Lisanti MP (2001) Caveolin-1 null mice are viable but show evidence of hyperproliferative and vascular abnormalities. *J Biol Chem* 276(41):38121–38138
48. Johnson MD, Widdicombe JH, Allen L, Barbry P, Dobbs LG (2002) Alveolar epithelial type I cells contain transport proteins and transport sodium, supporting an active role for type I cells in regulation of lung liquid homeostasis. *Proc Natl Acad Sci USA* 99(4):1966–1971
49. Ma T, Fukuda N, Song Y, Matthay MA, Verkman AS (2000) Lung fluid transport in aquaporin-5 knockout mice. *J Clin Invest* 105(1):93–100

50. Center DM (2000) A role for the alveolar epithelium in recruitment of mononuclear cells into the lung. *J Clin Invest* 106(6):741–743
51. Thorley AJ, Goldstraw P, Young A, Tetley TD (2005) Primary human alveolar type II epithelial cell CCL20 (macrophage inflammatory protein-3 α)-induced dendritic cell migration. *Am J Respir Cell Mol Biol* 32(4):262–267
52. Burri PH (1984) Fetal and postnatal development of the lung. *Annu Rev Physiol* 46:617–628
53. Burri PH (2006) Structural aspects of postnatal lung development—alveolar formation and growth. *Biol Neonate* 89(4):313–322
54. Adamson IY, Bowden DH (1974) The type 2 cell as progenitor of alveolar epithelial regeneration. A cytodynamic study in mice after exposure to oxygen. *Lab Invest* 30(1):35–42
55. Kotton DN, Summer R, Fine A (2004) Lung stem cells: new paradigms. *Exp Hematol* 32(4):340–343
56. Neuringer IP, Randell SH (2006) Lung stem cell update: promise and controversy. *Monaldi Arch Chest Dis* 65(1):47–51
57. Fuchs S, Hollins AJ, Laue M, Schaefer UF, Roemer K, Gumbleton M, Lehr CM (2003) Differentiation of human alveolar epithelial cells in primary culture—Morphological characterisation and expression of caveolin-1 and surfactant protein-C. *Cell Tissue Res* 311:31–45
58. Wang J, Edeen K, Manzer R, Chang Y, Wang S, Chen X, Funk CJ, Cosgrove GP, Fang X, Mason RJ (2007) Differentiated human alveolar epithelial cells and reversibility of their phenotype in vitro. *Am J Respir Cell Mol Biol* [Epub ahead of print] doi:10.1165/rcmb.2006-0410OC
59. Fehrenbach H (2001) Alveolar epithelial type II cell: defender of the alveolus revisited. *Respir Res* 2(1):33–46
60. Mason RJ (2006) Biology of alveolar type II cells. *Respirology* 11 Suppl:S12–S15
61. Kim KJ, Borok Z, Crandall ED (2001) A useful in vitro model for transport studies of alveolar epithelial barrier. *Pharm Res* 18:253–255
62. Crandall ED, Kim KJ (1982) Transport of water and solutes across bullfrog alveolar epithelium. *J Appl Physiol* 52(4):902–909
63. Forbes B, Ehrhardt C (2005) Human respiratory epithelial cell culture for drug delivery applications. *Eur J Pharm Biopharm* 60(2):193–205
64. Lieber M, Smith B, Szakal A, Nelson-Rees W, Todaro G (1976) A continuous tumor-cell line from a human lung carcinoma with properties of type II alveolar epithelial cells. *Int J Cancer* 17(1):62–70
65. Foster KA, Oster CG, Mayer MM, Avery ML, Audus KL (1998) Characterization of the A549 cell line as a type II pulmonary epithelial cell model for drug metabolism. *Exp Cell Res* 243(2):359–366
66. Elbert KJ, Schäfer UF, Schäfers HJ, Kim KJ, Lee VHL, Lehr CM (1999) Monolayers of human alveolar epithelial cells in primary culture for pulmonary absorption and transport studies. *Pharm Res* 16(5):601–608
67. Kobayashi S, Kondo S, Juni K (1995) Permeability of peptides and proteins in human cultured alveolar A549 cell monolayer. *Pharm Res* 12(8):1115–1119
68. Wang Z, Zhang Q (2004) Transport of proteins and peptides across human cultured alveolar A549 cell monolayer. *Int J Pharm* 269(2):451–456
69. Forbes B, Wilson CG, Gumbleton M (1999) Temporal dependence of ectopeptidase expression in alveolar epithelial cell culture: implications for study of peptide absorption. *Int J Pharm* 180(2):225–234
70. Anabousi S, Bakowsky U, Schneider M, Huwer H, Lehr CM, Ehrhardt C (2006) In vitro assessment of transferrin-conjugated liposomes as drug delivery systems for inhalation therapy of lung cancer. *Eur J Pharm Sci* 29(5):367–374

71. Duncan JE, Whitsett JA, Horowitz AD (1997) Pulmonary surfactant inhibits cationic liposome-mediated gene delivery to respiratory epithelial cells in vitro. *Hum Gene Ther* 8(4):431–438
72. Rehan VK, Torday JS, Peleg S, Gennaro L, Vouros P, Padbury J, Rao DS, Reddy GS (2002) 1 α ,25-dihydroxy-3- ϵ -vitamin D₃, a natural metabolite of 1 α ,25-dihydroxy vitamin D₃: production and biological activity studies in pulmonary alveolar type II cells. *Mol Genet Metab* 76(1):46–56
73. Newton DA, Rao KM, Dluhy RA, Baatz JE (2006) Hemoglobin is expressed by alveolar epithelial cells. *J Biol Chem* 281(9):5668–5676
74. Zhang L, Whitsett JA, Stripp BR (1997) Regulation of Clara cell secretory protein gene transcription by thyroid transcription factor-1. *Biochim Biophys Acta* 1350(3):359–367
75. Shlyonsky V, Goolaerts A, van Beneden R, Sariban-Sohraby S (2005) Differentiation of epithelial Na⁺ channel function. An in vitro model. *J Biol Chem* 280(25):24181–24187
76. Woolthead AM, Baines DL (2006) Forskolin-induced cell shrinkage and apical translocation of functional enhanced green fluorescent protein-human α ENaC in H441 lung epithelial cell monolayers. *J Biol Chem* 281(8):5158–5168
77. Wikenheiser KA, Vorbroker DK, Rice WR, Clark JC, Bachurski CJ, Oie HK, Whitsett JA (1993) Production of immortalized distal respiratory epithelial cell lines from surfactant protein C/simian virus 40 large tumor antigen transgenic mice. *Proc Natl Acad Sci USA* 90(23):11029–11033
78. Douglas WH, Kaighn ME (1974) Clonal isolation of differentiated rat lung cells. *In Vitro* 10(3–4):230–237
79. Koslowski R, Barth K, Augstein A, Tschernig T, Bargsten G, Aufderheide M, Kasper M (2004) A new rat type I-like alveolar epithelial cell line R3/1: bleomycin effects on caveolin expression. *Histochem Cell Biol* 121(6):509–519
80. Danto SI, Shannon JM, Borok Z, Zabski SM, Crandall ED (1995) Reversible transdifferentiation of alveolar epithelial cells. *Am J Respir Cell Mol Biol* 12(5):497–502
81. Chen J, Chen Z, Narasaraju T, Jin N, Liu L (2004) Isolation of highly pure alveolar epithelial type I and type II cells from rat lungs. *Lab Invest* 84(6):727–735
Erratum in: *Lab Invest* 85(9):1181 (2005)
82. Corti M, Brody AR, Harrison JH (1996) Isolation and primary culture of murine alveolar type II cells. *Am J Respir Cell Mol Biol* 14:309–315
83. Goodman BE, Crandall ED (1982) Dome formation in primary cultured monolayers of alveolar epithelial cells. *Am J Physiol* 243:C96–C100
84. Shen J, Elbert KJ, Yamashita F, Lehr CM, Kim KJ, Lee VH (1999) Organic cation transport in rabbit alveolar epithelial cell monolayers. *Pharm Res* 16(8):1280–1287
85. Steimer A, Franke H, Haltner-Ukomado E, Laue M, Ehrhardt C, Lehr CM (2007) Monolayers of porcine alveolar epithelial cells in primary culture as an in vitro model for drug absorption studies. *Eur J Pharm Biopharm* [Epub ahead of print] doi:10.1016/j.ejpb.2006.11.006
86. Bingle L, Bull TB, Fox B, Guz A, Richards RJ, Tetley TD (1990) Type II pneumocytes in mixed cell culture of human lung: a light and electron microscopic study. *Environ Health Perspect* 85:71–80
87. Ehrhardt C, Kim KJ, Lehr CM (2005) Isolation and culture of human alveolar epithelial cells. *Methods Mol Med* 107:207–216
88. Cheek JM, Kim KJ, Crandall ED (1989) Tight monolayers of rat alveolar epithelial cells: bioelectric properties and active sodium transport. *Am J Physiol* 256 (3 Pt 1):C688–C693
89. Morimoto K, Yamahara H, Lee VH, Kim KJ (1993) Dipeptide transport across rat alveolar epithelial cell monolayers. *Pharm Res* 10(11):1668–1674

90. Matsukawa Y, Yamahara H, Lee VH, Crandall ED, Kim KJ (1996) Horseradish peroxidase transport across rat alveolar epithelial cell monolayers. *Pharm Res* 13(9):1331–1335
91. Widera A, Kim KJ, Crandall ED, Shen WC (2003) Transcytosis of GCSF-transferrin across rat alveolar epithelial cell monolayers. *Pharm Res* 20(8):1231–1238
92. Bur M, Huwer H, Lehr CM, Hagen N, Guldbandt M, Kim KJ, Ehrhardt C (2006) Assessment of transport rates of proteins and peptides across primary human alveolar epithelial cell monolayers. *Eur J Pharm Sci* 28(3):196–203
93. Effros RM, Mason GR (1983) Measurements of pulmonary epithelial permeability in vivo. *Am Rev Respir Dis* 127(5 Pt 2):S59–S65
94. Matsukawa Y, Lee VH, Crandall ED, Kim KJ (1997) Size-dependent dextran transport across rat alveolar epithelial cell monolayers. *J Pharm Sci* 86(3):305–309
95. Van der Deen M, de Vries EG, Timens W, Scheper RJ, Timmer-Bosscha H, Postma DS (2005) ATP-binding cassette (ABC) transporters in normal and pathological lung. *Respir Res* 6:59
96. Lehmann T, Kohler C, Weidauer E, Taege C, Foth H (2001) Expression of MRP1 and related transporters in human lung cells in culture. *Toxicology* 167(1):59–72
97. Campbell L, Abulrob AN, Kandalaf LE, Plummer S, Hollins AJ, Gibbs A, Gumbleton M (2003) Constitutive expression of p-glycoprotein in normal lung alveolar epithelium and functionality in primary alveolar epithelial cultures. *J Pharmacol Exp Ther* 304(1):441–452
98. Endter S, Becker U, Daum N, Huwer H, Lehr CM, Gumbleton M, Ehrhardt C (2007) P-glycoprotein (MDR1) functional activity in human alveolar epithelial cell monolayers. *Cell Tissue Res* [Epub ahead of print] doi:10.1007/s00441-006-0346-6
99. Lehmann T, Torky AR, Stehfest E, Hofmann S, Foth H (2005) Expression of lung resistance-related protein, LRP, and multidrug resistance-related protein, MRP1, in normal human lung cells in long-term cultures. *Arch Toxicol* 79(10):600–609
100. Mulugeta S, Gray JM, Notarfrancesco KL, Gonzales LW, Koval M, Feinstein SI, Ballard PL, Fisher AB, Shuman H (2002) Identification of LBM180, a lamellar body limiting membrane protein of alveolar type II cells, as the ABC transporter protein ABCA3. *J Biol Chem* 277(25):22147–22155
101. Agassandian M, Mathur SN, Zhou J, Field FJ, Mallampalli RK (2004) Oxysterols trigger ABCA1-mediated basolateral surfactant efflux. *Am J Respir Cell Mol Biol* 31(2):227–233
102. Mamchaoui K, Makhloufi Y, Saumon G (2002) Glucose transporter gene expression in freshly isolated and cultured rat pneumocytes. *Acta Physiol Scand* 175(1):19–24
103. Groneberg DA, Paul H, Welte T (2006) Novel strategies of aerosolic pharmacotherapy. *Exp Toxicol Pathol* 57 Suppl 2:49–53
104. Sloan JL, Grubb BR, Mager S (2003) Expression of the amino acid transporter ATB 0 + in lung: possible role in luminal protein removal. *Am J Physiol* 284(1):L39–L49
105. Rothenberg ME, Doepker MP, Lewkowich IP, Chiamonte MG, Stringer KF, Finkelman FD, MacLeod CL, Ellies LG, Zimmermann N (2006) Cationic amino acid transporter 2 regulates inflammatory homeostasis in the lung. *Proc Natl Acad Sci USA* 103(40):14895–14900
106. Jin SN, Mun GH, Lee JH, Oh CS, Kim J, Chung YH, Kang JS, Kim JG, Hwang DH, Hwang YI, Shin DH, Lee WJ (2005) Immunohistochemical study on the distribution of sodium-dependent vitamin C transporters in the respiratory system of adult rat. *Microsc Res Tech* 68(6):360–367

107. Miakotina OL, Agassandian M, Shi L, Look DC, Mallampalli RK (2005) Adenovirus stimulates choline efflux by increasing expression of organic cation transporter-2. *Am J Physiol* 288(1):L93–L102
108. Ehrhardt C, Kneuer C, Baldes C, Kim KJ, Lehr CM (2006) Albuterol is net absorbed across human alveolar epithelial cell monolayers. *Proc Am Thor Soc* 3:A761
109. Matsukawa Y, Yamahara H, Yamashita F, Lee VH, Crandall ED, Kim KJ (2000) Rates of protein transport across rat alveolar epithelial cell monolayers. *J Drug Target* 7(5):335–342
110. Kim KJ, Matsukawa Y, Yamahara H, Kalra VK, Lee VH, Crandall ED (2003) Absorption of intact albumin across rat alveolar epithelial cell monolayers. *Am J Physiol* 284(3):L458–L465
111. Kim KJ, Fandy TE, Lee VH, Ann DK, Borok Z, Crandall ED (2004) Net absorption of IgG via FcRn-mediated transcytosis across rat alveolar epithelial cell monolayers. *Am J Physiol* 287(3):L616–L622
112. Schanker LS (1978) Drug absorption from the lung. *Biochem Pharmacol* 27(4):381–385
113. Morimoto K, Yamahara H, Lee VH, Kim KJ (1994) Transport of thyrotropin-releasing hormone across rat alveolar epithelial cell monolayers. *Life Sci* 154(26):2083–2092
114. Dodoo AN, Bansal SS, Barlow DJ, Bennet F, Hider RC, Lansley AB, Lawrence MJ, Marriott C (2000) Use of alveolar cell monolayers of varying electrical resistance to measure pulmonary peptide transport. *J Pharm Sci* 89(2):223–231
115. Yamahara H, Morimoto K, Lee VH, Kim KJ (1994) Effects of protease inhibitors on vasopressin transport across rat alveolar epithelial cell monolayers. *Pharm Res* 11(11):1617–1622
116. Yamahara H, Lehr CM, Lee VH, Kim KJ (1994) Fate of insulin during transit across rat alveolar epithelial cell monolayers. *Eur J Pharm Biopharm* 40(5):294–298
117. Bosquillon C, Kim KJ, Crandall ED, Borok Z, Hoet PH, Preat V, Vanbever R (2004) Transport of human growth hormone across monolayers of rat alveolar epithelial cells. *Proc Intern Symp Control Rel Bioact Mat* 31:475
118. Balis JU, Bumgarner SD, Paciga JE, Paterson JF, Shelley SA (1984) Synthesis of lung surfactant-associated glycoproteins by A549 cells: description of an in vitro model for human type II cell dysfunction. *Exp Lung Res* 6(3–4):197–213
119. Hukkanen J, Lassila A, Paivarinta K, Valanne S, Sarpo S, Hakkola J, Pelkonen O, Raunio H (2000) Induction and regulation of xenobiotic-metabolizing cytochrome P450s in the human A549 lung adenocarcinoma cell line. *Am J Respir Cell Mol Biol* 22(3):360–366
120. Castell JV, Donato MT, Gomez-Lechon MJ (2005) Metabolism and bioactivation of toxicants in the lung. The in vitro cellular approach. *Exp Toxicol Pathol* 57 Suppl 1:189–204
121. Collier AC, Tingle MD, Keelan JA, Paxton JW, Mitchell MD (2000) A highly sensitive fluorescent microplate method for the determination of UDP-glucuronosyl transferase activity in tissues and placental cell lines. *Drug Metab Dispos* 28(10):1184–1186
122. Mace K, Bowman ED, Vautravers P, Shields PG, Harris CC, Pfeifer AM (1998) Characterisation of xenobiotic-metabolising enzyme expression in human bronchial mucosa and peripheral lung tissues. *Eur J Cancer* 34(6):914–920
123. Hukkanen J, Pelkonen O, Raunio H (2001) Expression of xenobiotic-metabolizing enzymes in human pulmonary tissue: possible role in susceptibility for ILD. *Eur Respir J Suppl* 32:122s–126s

124. Juillerat-Jeanneret L, Aubert JD, Leuenberger P (1997) Peptidases in human bronchoalveolar lining fluid, macrophages, and epithelial cells: dipeptidyl (amino)peptidase IV, aminopeptidase N, and dipeptidyl (carboxy)peptidase (angiotensin-converting enzyme). *J Lab Clin Med* 130(6):603–614
125. Borlak J, Blickwede M, Hansen T, Koch W, Walles M, Levsen K (2005) Metabolism of verapamil in cultures of rat alveolar epithelial cells and pharmacokinetics after administration by intravenous and inhalation routes. *Drug Metab Dispos* 33(8):1108–1114

Cell Culture Models of the Corneal Epithelium and Reconstructed Cornea Equivalents for In Vitro Drug Absorption Studies

Stephan Reichl and Ulrich Becker

Abstract For the development of new ophthalmic drugs and ocular medications, it is indispensable to perform drug permeation studies. Generally, the main barrier for topically applied drugs is represented by the cornea. Therefore, examining the corneal tissue is an important subject in ocular research. In vitro examinations on transcorneal permeation are often performed with excised corneal tissues from laboratory animals or killed livestock. But the use of such tissues has disadvantages, for example, sacrifice of animals for experimental purposes is deemed as inappropriate by some sectors of the society and has high cost of animal maintenance and man-hours involved. Moreover, procurement of homogeneous materials from slaughtered animals is very difficult and variances of observed data from nonhomogeneous animal tissue specimens are unavoidable. Extension of such animal data to human setting would also be a formidable issue. In order to alleviate these disadvantages inherent in *ex vivo* studies using animal tissues, cell culture models derived from corneal tissues have been established in the last two decades. These models are designed to replace excised tissues in toxicity tests and drug permeation studies. This chapter will give an overview on available in vitro models of mammalian/human corneal epithelium, human corneal constructs, and their use to mimic in vivo corneal drug absorption. Moreover, the reader will be introduced to simple protocols for the setup of corneal epithelial cell cultures and organotypic cornea constructs.

Keywords: Transcorneal drug absorption; Corneal epithelium; Corneal cell lines; Primary culture of rabbit corneal epithelium; Cornea equivalents; Human cornea construct

Abbreviations

3-D	Three-dimensional
AIC	Air-interfaced culture
HCC	Human cornea construct
HPV	Human papilloma virus

LCC	Liquid-covered culture
MTT	3-(4,5-Dimethylthiazol-2-yl)-2,5-diphenyltetrazolium bromide
P_{app}	Apparent permeability
P-gp	P-glycoprotein
PHCl	Pilocarpine hydrochloride
RCE	Rabbit corneal epithelium
SIRC	Statens Seruminstitut rabbit cornea
SV40	<i>Simian virus 40</i>
TEER	Transepithelial electrical resistance

12.1. Introduction

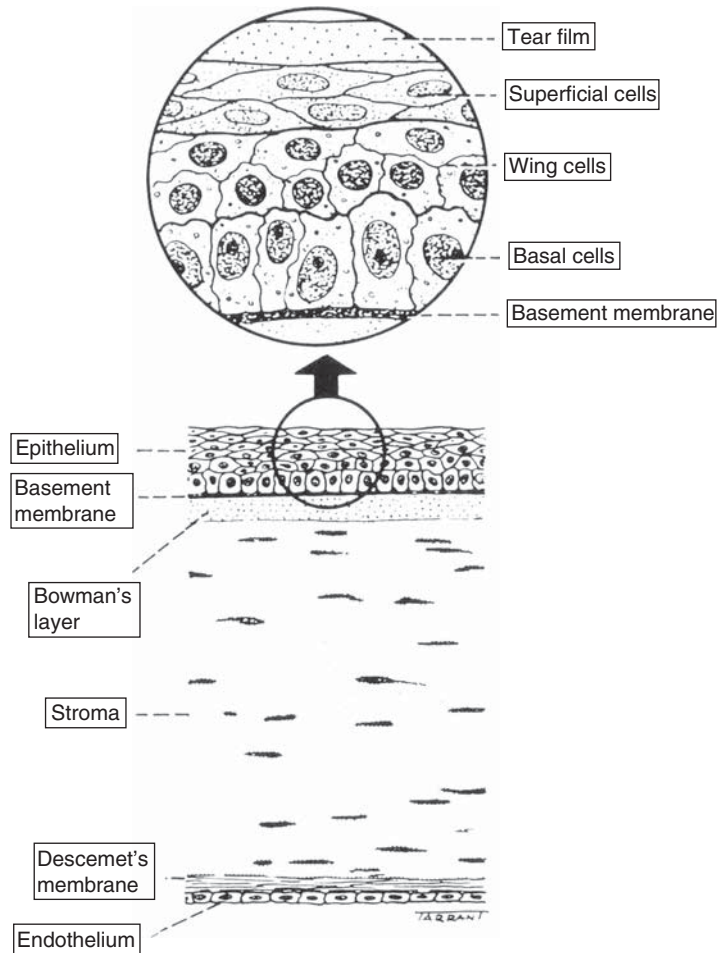
Dosing substances to the eye is a technique performed since the start of civilization. First eye cosmetics have been described around 1550 BC by the ancient Egyptians. Later, eye preparations for women (e.g., containing belladonna extracts) have been described during the Baroque period of Europe. Major importance for eye medications was gained through the discovery of alkaloids in the nineteenth century. Since then, eye medications always played a major role in therapeutics.

Targeting drugs to the mammalian eye via topical application is a formidable task and of major interest for ophthalmic research. A major advantage is the easy application for the patient and considerably low systemic availability, which might alleviate unwanted side effects. In addition, to opt for the ocular route of drug delivery might avoid drug degradation caused by the first-pass effect occurring in the liver. It is also possible to target drugs to several ocular sites or tissues of interest [1], a technique that is generally applied in many pharmaceutical applications.

Potential disadvantages of ocular drug delivery may include the rather low applicable volume and rapid drainage of the drug solution through nasolacrimal ducts, resulting in a low ocular bioavailability. Moreover, all pharmacopoeias require a low irritant potential for eye medications. To assess the irritancy of drugs and vehicles as well as acceptable transcorneal drug delivery, test systems suitable for prescreening are needed.

For a long time, drugs have been tested using animals or animal tissues as means to determine ocular delivery, toxicity, and eye irritation. But since such animal-based testing is controversial and often met with resistance from some sectors of the society, great efforts have been made into establishing other more accepted and easier methods. One such effort resulted in the introduction of cell culture techniques in the early part of the twentieth century [2, 3]. Major drawbacks for animal-based testing are high maintenance costs and efforts. Scientifically, complexity of the “test” system and high variation of the outcome are major points for criticism. Last, but not least, animal testing does have a bad reputation and low acceptance in the modern society. Therefore, lots of efforts have been put into the development of cell culture systems that replace laboratory animals in scientific studies. This chapter provides a thorough review about the efforts made on the rewarding field of in vitro models suitable for studies of transcorneal drug delivery and metabolism.

Figure 12.1 Schematic cross section of a human cornea (adapted, with permission from the publisher, from Kanski and Spitznas (1987) *Lehrbuch der klinischen Ophthalmologie*, Thieme-Verlag, Stuttgart, New York).



12.2. Anatomy and Physiology of Human Cornea

The cornea is the transparent frontal part of the eye that covers the iris, pupil, and anterior chamber and acts as a part of our visualization system by being the gateway for the external images into back of the eye (Figure 12.1). Furthermore, the cornea provides a refractive function and forms a mechanically tough and chemically impermeable barrier between the eye and environment. Additionally, the cornea also is a part of the ocular biodefense system.

However, an intrinsic physiological requirement for the cornea is the maintenance of its transparency, ensuring proper vision. This clarity as well as maintenance of the corneal shape (surface smoothness and total thickness) is critical to refraction. The unique transparency of corneal tissues is strongly dependent on their avascularity and a functionally intact endothelium, which are crucial for the maintenance of both stromal clarity and thickness by regulating corneal hydration. Macroscopically, the cornea is a transparent and avascular tissue

that is exposed to the external environment, joining the opaque sclera at the corneoscleral limbus. The anterior corneal surface is covered by the tear film while the posterior surface is directly bathed in the aqueous humor. Average horizontal and vertical diameters of the human cornea are 12.6 and 11.7 mm, respectively. The central cornea of the human eye is $\sim 520 \mu\text{m}$ thick, whereas in the periphery a thickness of about $700 \mu\text{m}$ is found. The shape of the anterior corneal surface is convex and nonspherical. Its average radius of curvature is 7.8 mm, providing ~ 48 diopters for the human eye [4].

Microscopically, the cornea shows a rather simple and multilayered structure that can be divided into six layers: the epithelium, basement membrane, Bowman's layer, stroma, Descemet's membrane, and endothelium. The corneal tissue consists of three different cell types: epithelial cells, keratocytes (corneal fibroblasts), and endothelial cells. The outermost corneal surface is covered with the preocular tear film, which is functionally associated with the cornea. The epithelial surface must be kept moist and smooth, a role played by the tear film in conjunction with a spreading function of the eyelids during blinking motions. Furthermore, the tear film provides a protection against infectious agents that may gain access into the eye.

The human tear film is $\sim 7 \mu\text{m}$ thick and consists of three layers: the most superficial lipid layer ($\sim 0.1 \mu\text{m}$), the underlying aqueous layer ($\sim 7 \mu\text{m}$), which forms the bulk of the tear film, and the innermost mucous layer, which is intimately attached to the corneal epithelium ($0.02\text{--}0.05 \mu\text{m}$). These three different layers of the tear film are produced by various cells and glands in the eye. The lipid layer is primarily secreted by the Meibomian glands located in a row near the edge of upper and lower eyelids, while the aqueous layer is produced by main and accessory lacrimal glands. The mucus is excreted by conjunctival goblet cells. The normal tear volume is about $7 \mu\text{l}$ with an average aqueous tear flow rate of about $1.2 \mu\text{l}/\text{min}$ (ranges from 0.5 to $2.2 \mu\text{l}/\text{min}$) in humans. The osmolarity of normal human tear film averages to be 302 mOsm/l . The aqueous layer of the tear film contains many biologically important factors, including electrolytes, glucose, immunoglobulins, lysozyme, albumin, and oxygen [5].

The corneal epithelium ($\sim 50 \mu\text{m}$) represents about 10% of the thickness of corneal tissue and is a nonkeratinized, noncornified, stratified, and squamous epithelium. None of the other multilayered human epithelia show a more regular structure than the corneal epithelium, which is composed of five to six cell layers in total and three cell types: basal, wing, and superficial cells. Only basal cells show a mitotic activity, in that during a differentiation process (taking 7–14 days) the cells continue to move anteriorly and become superficial cells before they disintegrate and desquamate into the tear film. Thus, corneal epithelium continuously renews its surface. The presence of a centripetal movement of corneal epithelial cells (the "XYZ" hypothesis) has been demonstrated [6]. Furthermore, in this context, localization of epithelial stem cells at the limbus (the region where the corneal epithelium graduates into transitional epithelium and then into conjunctival epithelium) has been described [7–9].

At the corneal surface, two to four layers of polygonal, extremely flat, and terminally differentiated superficial cells can be found. The cell diameters are $40\text{--}60 \mu\text{m}$ with about $2\text{--}6 \mu\text{m}$ thickness. The corneal surface is populated with microvilli and microplicae, resulting in surface area enlargement. These structures are associated with the tear film. Superficial corneal epithelial cells are

joined by desmosomes and ribbon-like tight junctional complexes, surrounding the entire cell at the most apical region [10]. Desmosomal attachments provide lateral mechanical stability. However, presence of tight junctional complexes (zonula occludens) prevents the movement of substances from the tear film into intercellular spaces of the epithelium as well as the deeper layers of corneal tissues. Tight junctions are designed to resist the flow of fluid (and other molecular substances, e.g., pharmaceutical compounds) through the epithelial barrier. Hence the epithelium is the main barrier for topically applied hydrophilic drugs (see Sect. 12.3). It has been shown that the removal of corneal epithelium *per se* results in a significant increase in transcorneal drug permeability [11].

The wing cells, possessing a characteristic wing-like shape, are arranged in two to three layers. They are located between the basal and superficial cells, exhibiting an intermediate state of differentiation. These cells have an extensive cytoskeletal network consisting of intermediate filaments. The 64-kDa keratin (K3) is specific to corneal epithelial cells [12]. Furthermore, numerous desmosomes and gap junctions are present between wing cells, but functional tight junctional proteins have not yet been established in this state of differentiation.

The columnar, cuboidal basal cells are 18–20 μm in height and 8–10 μm in diameter. They form a monolayer adhered to a basement membrane by hemidesmosomes which are linked to anchoring fibrils of collagen type VII. At the lateral borders, basal cells are extensively interdigitated and joined together in places only by junctional complexes (zonula adherens), desmosomes, and gap junctions.

The basement membrane, 40–60 nm in thickness, is produced by basal epithelial cells and composed of the lamina lucida (adjacent to the cell membrane of basal cells) and lamina densa where the main components include collagen type IV, laminin, and fibronectin. As in other epithelial and endothelial barriers, the basement membrane in the corneal epithelium seems to be important for the maintenance of a multilayered, well structured epithelium and its adhesion to the corneal stroma. The basement membrane may also play a significant role in epithelial wound healing and re-epithelialization. Using the rat cornea, Suzuki et al. [13] found that the presence of a basement membrane may be required for the re-formation of intercellular junctions during wound repair. This matches with findings made in the clinic during laser treatment [14]. It was noticed that patients with basement membrane dystrophy show a higher tendency for postsurgical sloughing of the corneal epithelium than do patients with intact basement membrane. Furthermore, a careful literature review done by Saika et al. [15] also supports the hypothesis of the importance of the extracellular matrix and its metabolism in the repair process of the corneal epithelium.

As another extracellular component in the cornea, the Bowman's layer is an acellular and amorphous band between the corneal epithelium and stroma. The layer is about 8–12 μm thick and consists of randomly arranged collagen fibers (types I and III) and proteoglycans. The physiological function of Bowman's layer is not yet completely understood, since not all animal species exhibit this membrane in the corneal structures, but an important role in the maintenance of the corneal epithelial structure is expected or probable, since a damaged Bowman's membrane usually results in scarring during wound repair [16].

Stacked lamellae of collagen fibrils are the most obvious morphological characteristics of the stroma, which comprises more than 90% of the whole cornea. The stroma consists of about 78% water, an extracellular matrix, and about 3 to 5% cellular components (keratocytes). Keratocytes, also known as stromal or corneal fibroblasts, are spindle-shaped cells that are embedded network-like in the stromal matrix. They produce the extracellular matrix that mainly consists of collagen (predominantly type I and a minor content of type V) and glycosaminoglycans (predominantly keratan sulfate, followed by smaller fractions of dermatan sulfate and chondroitin sulfate proteoglycans). Collagen constitutes about 71% of the corneal dry weight, contributing to the corneal transparency and mechanical resistance against the intraocular pressure. Stromal collagen fibers are remarkably uniform in their diameter. The distance between collagen fibers is also remarkably constant. These regular arrangements of collagen fibers as well as the “relatively” constant water content in the stroma are essential requirements for corneal transparency. Any disturbance in the uniformity of the fixed interfiber distance may cause a loss of corneal transparency.

The Descemet’s membrane, which is also termed as “basement membrane of corneal endothelium,” is a 7 μm thick assembly of collagen fibrils secreted by endothelial cells. It is an acellular layer like the Bowman’s layer and mainly consists of collagen type IV and laminin. Beneath the Descemet’s membrane, corneal endothelial cells form a single layer of $\sim 400,000$ cells with a total thickness of about 5 μm . The endothelium represents the innermost surface of cornea and acts as a barrier to the aqueous humor. Endothelial cells exhibit predominantly a hexagonal shape and are $\sim 20 \mu\text{m}$ wide. The most important physiological functions of the corneal endothelium are formation of an effective barrier against the penetration of the aqueous humor into the cornea and a pump function, therefore preserving the corneal transparency. Barrier properties of the endothelial cell layer are mainly of the physiological aspect and not considered critical for drug permeation. Because of the less pronounced formation of tight cell–cell connections and also its low total thickness, the corneal endothelium exhibits less resistance to substance diffusion than the corneal epithelium. The basis for corneal clarity is an intact endothelial layer with a cell density of 2,000–3,000 cells/ mm^2 in adults, ensuring the formation of numerous cell–cell contacts (i.e., via tight junctions and gap junctions). The presence of a pump mechanism afforded by $\text{Na}^+ - \text{K}^+ - \text{ATPase}$ is also important for the maintenance of the corneal clarity. Na^+ -pumps (about 3,000,000 per cell [17]) are mainly localized at the lateral part of endothelial cell membranes (i.e., facing intercellular spaces [18]). Damage or dysfunction of the endothelium (e.g., by cell loss; so-called “endothelial decompensation” occurs at a critical cell density below 500 cells/ mm^2), traumatic disease, reduction of pump function or tight junctions, or both, will all lead to corneal edema (i.e., resulting in opacity of stroma). Thus, destruction of the corneal endothelium is one of the major causes for corneal transplantation. Several studies focusing on transplantation of cultured endothelial cells have been recently performed [19, 20]. Current results in the field of corneal equivalents for transplantation will be described in Sect. 12.4.3. More details about the anatomy and function of the cornea are available in articles written by Nishida [21] and Klyce and Beuerman [22]. A review on the ultrastructure of the human cornea written by Beuerman and Pedroza [23] can also be consulted for details.

12.3. Transcorneal Drug Absorption into the Eye

Since most eye medications need to enter the eye for a pharmacological effect, ocular drug delivery is a major issue in ocular research. Generally, three routes into the eye have been described in the literature [24]:

1. *Drug distribution in the eye through the blood vessels, either by systemic dosing or by local treatment.* Because the blood route always involves a distribution of the drug in the whole human body, the ocular level of drugs achieved by this way of application is much less than that achievable by ocular topical treatment. Thus, this way of drug distribution is not preferred for ocular dosing.
2. *Drug entry into the eye region utilizing the conjunctival-scleral pathway, with topical dosing.* Even though this pathway can be of high efficiency for intraocular drug delivery and does bypass cornea and local vasculature, only a few (high molecular) substances were delivered using this route.
3. *The transcorneal route.* This is still the major pathway for ocular drug delivery, representing the direct pathway into the eye and is applicable for most of drug substances.

If the medical drug is applied topically to the eye, another important factor for ocular drug delivery and penetration has to be taken in account: that is, the precorneal clearance which rapidly reduces the drug amount available for penetration. Thus, it is a major factor to take into consideration while evaluating (transcorneal) absorption. So far, due to experimental limitations, not much thought has been given to precorneal clearance in cell-based *in vitro* models.

For absorption through the cornea, which is the major pathway for drug absorption into the eye, certain physicochemical properties are required for the substance to cross the corneal barrier. Since the cornea, as described in Sect. 12.2, is divided into three parts with different characteristics, only amphiphilic substances can easily penetrate all corneal layers. Purely lipophilic substances, in contrast, will not face much hindrance in the epithelial and endothelial cell layers but will be unable to cross the aqueous stroma. The same considerations also apply for purely hydrophilic drugs that are not withheld from penetration by the stroma but are unable to cross the lipid bilayers of cells (i.e., cell plasma membranes) and tight junctions in the epithelium and endothelium. Thus, the ability to switch between the lipophilic and hydrophilic states is indispensable for ocular absorption. Other factors can also influence ocular penetration, for example, charge and molecular weight, which have to be taken into consideration when opting for the ocular route of drug delivery. Generally, the main barrier in the cornea is represented by the corneal epithelium. It is a multilayered epithelium with progressive states of differentiation from basal to superficial cells. The superficial cells adhere to each other through desmosomes and are surrounded by tight junctions [25], creating a tight cellular barrier against xenobiotics and limiting permeation of hydrophilic substances. Stroma and endothelium, on the other hand, do not represent a critical barrier for transcorneal permeation, compared to the corneal epithelium. Only highly lipophilic substances show limited diffusion due to the hydrophilic characteristics of the stroma.

12.4. Corneal Cell Culture Models

For *in vitro* toxicity studies and assessment of the barrier function, drug transport, cell physiology, and metabolism as well as the development of delivery systems, cell culture models provide powerful systems for scientific research. As the corneal epithelium is the main barrier for ocular penetration, various corneal epithelial cell cultures were established besides the corneal constructs that mimic the whole cornea and serve as reductionist models for the ocular barrier. In general, two types of cell culture models are available: primary cell cultures and immortalized, continuous cell lines.

12.4.1. Primary Corneal Cell Cultures

Since the cell culture technique was introduced in the early twentieth century, many attempts have been undertaken to mimic the human organism in simplified *in vitro* cell systems. First approaches were performed with tissue explants, which later led to more refined cell culture systems. Among the first tissues to be examined and applied in cell culture was the cornea. With the development of enzymatic isolation protocols in the 1960s [26, 27], cultivation of corneal cells (covering epithelial, stroma, and endothelial cells) started in a greater extent. Since the establishment of the 3R principle (**R**eplace, **R**educe, **R**efine) in 1959 by Russell and Burch [28] and guidelines setup banning animal-based drug tests by the cosmetics industry in the European Union in 2003, immense efforts have been made to improve these cell cultures and substitute animal experiments by suitable *in vitro* methods. A variety of corneal epithelial cell cultures have therefore been established in recent years. These models were developed in most part to serve as a tool for toxicity and eye irritation testing, but in recent years some models for drug transport and permeation studies have been made available as well. Besides the immortalized cell culture models that have an extended life span and improved cell growth characteristics with easy handling [29], various attempts have been made to establish primary corneal epithelial cell cultures that better resemble the *in vivo* situation and have features of original cell properties [30]. Different techniques have been applied to generate primary cell culture models, including explantation techniques [31, 32], enzymatic treatments [33, 34], and mechanical processing [35, 36]. Successful primary cultures of the corneal epithelium have been generated for following species: rabbit [31, 33], cow [37], guinea pig [38], rat [39], mouse [40], and pig [41]. Even though several attempts have been undertaken, a successful setup of a human corneal epithelial cell model in a bigger scale for permeation studies has not been achieved yet.

The main aspect of the primary cell cultures was to authentically mimic the ocular surface in eye irritation and toxicity testing. In addition, issues of fundamental research were addressed with these models as well, for example, investigating cell proliferation in the cornea and location of the corneal stem cells [42]. Two cell culture models of rabbit origin have mainly influenced ocular research and cell culture efforts. For example, Kawazu et al. [43] were among the first to introduce a primary corneal epithelial model that could be grown in a larger scale. This cell culture system has been widely used to examine permeation, drug absorption, and P-glycoprotein (P-gp) activity [43–45]. The cultured cells morphologically resemble those found in intact

rabbit cornea, but a major drawback of the model is the lack of reasonable electrical resistance of the cultured corneal barrier. In other words, a measure for the tightness of the cell–cell connections or tight connections between cells (thought to be established mainly by tight junctions) is very low. In an ideal model, electrical resistance of cultured cell layers should be comparable to excised corneal tissues. These primary cultured corneal cell layers do form multiple cell layers, but only a maximum transepithelial electrical resistance (TEER) of about 150 ohmcm^2 has been reported. This value is generally considered insufficient for a tight cell layer, which usually exceeds 400 ohmcm^2 in tight cell culture models [46]. Another primary corneal epithelial cell culture model is described by Chang and coworkers [33]. This latter corneal cell culture model of rabbit origin was designed for in vitro drug permeation studies and exhibits tight cell layers ($\text{TEER} > 1,000 \text{ ohmcm}^2$). The nature of the cultured tight cell layer is also reflected from the apparent permeability coefficients (P_{app}) reported by Chang et al. [33] and Scholz et al. [47], using the same cell culture model. For hydrophilic mannitol and fluorescein, P_{app} was 0.044 and $0.32 (\times 10^{-6} \text{ cm/s})$, respectively [33], while the more lipophilic pilocarpine-HCl showed a higher P_{app} of $2.19 (\times 10^{-6} \text{ cm/s})$ [47], as expected. The model was also used to study ion fluxes across corneal epithelium, where Chang-Lin et al. [48] reported that the cultured rabbit corneal epithelial cell layers exhibit active ion transport properties similar to those of excised rabbit corneal tissues (focusing on Na^+ absorption, Cl^- secretion, and K^+ exchange). This model has thus been widely used and proved to be useful in scientific research and pharmaceutical applications. An isolation and culture protocol for rabbit primary corneal epithelial cells is described in the appendix (available online) for this chapter. Isolation and culture of these cells are rather easy even for novices in cell culture techniques.

12.4.2. Immortalized Continuous Cell Lines for Corneal Epithelial Cells

Since Gey et al. successfully established a human cell line derived from tumor tissues (HeLa cells) in 1952 [49], the interest in human tissues as basis for continuous cell lines was intense. Today, imitating the human organism as closely as possible by means of human cell culture is still a major task. After the hybridoma technique for fusing functional cells (e.g., B cells) with tumor (e.g., myeloma) was discovered [50] and later refined by the development of viral vectors for transfection and immortalization, the field of continuous cell lines exploded in scope and usage. The extended life span and the improved growth characteristics are considered major advantages of continuous immortalized cell lines. In the last decade, several continuous cell lines representing the corneal epithelium have been reported. Application topics of these models include drug permeation, eye irritation testing, basic research, and characterization.

12.4.2.1. Rabbit Corneal Epithelial Cell Line

The first immortalized cell line to gain major impact in the development of corneal epithelial cell clones was the rabbit corneal epithelial cell line (RCE, also known as K'RCE) introduced by Araki et al. in 1993 [51]. Corneal epithelial cells from a New Zealand albino rabbit were transfected with an SV40-vector. After transfection, the cells grew with cobblestone-like appearance and showed stratification, desmosomes, microvilli, and some typical types of

keratin. The cell line has recently been used for drug transport studies [52]. These studies revealed that the cell line exhibits only low TEER values of about 150 ohmcm^2 , suggesting that RCE may not be suitable for drug permeation studies due to lack of functionally tight barrier properties. This cell line also has the disadvantage of being nonhuman and being derived from an albino rabbit. The albino origin and thus the absence of pigments in the eye are sometimes considered a blemish by investigators in the field. Still, this model paved the way for the important human corneal epithelium (HCE-T) cell line. The RCE cell line can be obtained from the European Cell Culture Collection (ECACC, Cat. No. 95081046).

12.4.2.2. Statens Seruminstitut Rabbit Cornea

The Statens Seruminstitut rabbit cornea (SIRC) cell line was derived by M. Volkert of the Statens Seruminstitut, Copenhagen, Denmark, from the cornea of a normal rabbit in 1957. Little is recorded relating to the history of this cell line for approximately the first 400 passages. It was originally used for the cultivation of rubella viruses. In 1990, the cells were morphologically characterized by Niederkorn and coworkers [53]. The SIRC cells do not exhibit an epithelial, cobblestone-like morphology but do have a fibroblast phenotype, which is rated as a major drawback of this particular culture system. In the early 1990s, the cells were utilized for examination of their suitability for drug transport studies by Hutak and coworkers [54]. Even though the reported TEER values in this study were very promising (about $2,233 \text{ ohmcm}^2$ on day 8 in culture), recent attempts failed to reproduce these results [55; Becker et al., in press]. Notwithstanding, the cell line has been used for uptake experiments in some studies [55], in which no tight cell–cell connections may be absolutely required. This cell line can be obtained from American Type Culture Collection (ATCC, Cat. No. CCL-60).

There are many immortalized human corneal epithelial cell models that gained high acceptance for various ocular studies (e.g., toxicity testing and corneal epithelial transport; Table 12.1).

12.4.2.3. HCE-T Cells

The HCE-T model was established in 1995 by Araki-Sasaki and coworkers [56]. It was formed by transfection of human corneal epithelial cells from a 47-year-old female donor with a recombinant SV40-adenovirus, which lacked the origin of viral replication (i.e., not able to produce viral particles). The cell line has good growth characteristics and shows a cobblestone-like appearance. The cell line is intensively used by Urtti and coworkers and represents a standard

Table 12.1 Immortalized human corneal epithelial cell culture models.

Cell model	Supplier (or introduced by)
HCE-T (human corneal epithelium, SV 40)	Araki-Sasaki [56]
Reconstituted human corneal epithelium	Skinethic
EpiOcular-Model	MatTek
Clonetics Human Corneal Epithelium	Cambrex
HCE-T (10.014 pRSV-T)	Gillette Medical Evaluation Laboratories
CEPI-17-CL 4 cell line	Nestec
tet HPV16-E6/E7 transduced HCE	Mohan [64]

tool for drug permeation, bioavailability prescreening, and toxicity assessment [57–59]. The cell culture model exhibits tight cell layers under air-interface conditions with TEER >400 ohm cm^2 . These findings were verified by drug transport studies with mannitol (low-permeability marker) and rhodamine B (high-permeability marker). The respective P_{app} values were 1.42 and 16.3 ($\times 10^{-6}$ cm/s) [57]. This confirms that HCE-T cell layers discriminate well between the hydrophilic and lipophilic substances (that are thought to cross the epithelial barrier via passive diffusion) and do indeed form a tight barrier. It should, however, be noted that some drawbacks of HCE-T system regarding ABC-transporters have recently been reported [60].

12.4.2.4. Reconstituted HCE

Reconstituted HCE (order no. RHC/S/5) is available from Skinethic, Nice, France. It consists of transformed human corneal epithelial cells immortalized by Roger Beuerman from the Louisiana State University–Eye Center, New Orleans, USA. This reconstituted human corneal epithelium forms a multi-layered cell culture model that does not exhibit tight junctions and is therefore unsuitable for in vitro drug transport studies. Main focus of the model is eye irritation and toxicity testing and it is commonly used in this area with good prediction qualities. Major advantage of this model is the high reproducibility and uniform appearance. The commercial availability provides a ready-to-use model that is easy to handle.

12.4.2.5. EpiOcular Cell Culture System

The corneal model provided by MatTek (order no. OCL-200) consists of normal, human-derived epidermal keratinocytes which have been cultured to form a stratified, squamous epithelium similar to that found in the cornea. Thus, this cell model does not provide “real” corneal epithelial cells, but cells derived from skin, which resemble corneal epithelial cell-like structures. Certain cell culture conditions allow these cells to turn into a multilayered structure which is corneal epithelium-like. In histological staining, clear differences in cell structure and arrangement of the cell layers to corneal epithelium can be seen. These differences can be construed as serious drawbacks for the model. Similar to the Skinethic system discussed above, the EpiOcular system provides a well-defined model whose main applications may include toxicity testing and (partly) substitution of the Draize test. Even though the model does not feature the signs of redness and tear flow, the number of Draize test runs can be reduced. Using a corneal epithelial cell culture as prescreening tool for drug substances, one can screen various eye-irritant substances in an early development stage, thus reducing the number of animal preparations (e.g., rabbit eye test).

12.4.2.6. Clonetics Corneal Epithelial Cell Line

The “Clonetics” cell line from Cambrex Bio Science represents a cultured human corneal epithelial model (order no. CMS-2015; Cambrex Bio Science, Walkersville, MD). The culture model was generated by isolation of cells from normal human corneal tissues. The cells were then infected with an amphotropic recombinant retrovirus containing HPV-16 E6/E7 genes to extend the useful cell life span. The Clonetics cell model is a very recent entry into the immortalized corneal cell line field, but it has been proved to be useful for toxicity testing as well as in vitro drug permeation studies so far. Because of its very recent introduction, further examinations have to be undertaken to

fully evaluate the benefits of this particular model for in vitro corneal drug delivery research.

12.4.2.7. HCE-T (10.014 pRSV-T)

This human-derived cell line was established by Kahn and coworkers at the Gillette Medical Evaluation Laboratories [61]. Further evaluation of the cell line was performed by Kruszewski et al. [62]. This corneal cell culture was generated through transfection with plasmid pRSV-T that contains the SV40 early region genes and the *Rous sarcoma virus* long terminal repeat. The cell line has been found to exhibit a typical cobblestone morphology and optimal growth characteristics. It was designated to serve as a model for toxicity testing and tool to investigate corneal epithelial cell biology. The cell line is available via ATCC (Cat. No. CRL-11515).

12.4.2.8. CEPI-17-CL 4

This cell line was developed by Nestec (Nestlé Research Center, Lausanne, Switzerland) and described by Offord et al. [63]. Originally, this cell model was used for testing toxicity and ocular irritation. The cell line also is intensively used in organotypic cornea constructs (*vide infra* for details).

12.4.2.9. tet HPV16-E6/E7 Transduced HCE

This cell line was recently established by Mohan et al. [64]. Intensive testing of this cell line regarding its suitability for pharmaceutical purposes has not been performed yet. The cell line is highly interesting, however, because of its controlled cell growth and differentiation capabilities. An integrated DNA section allows cell growth to be “switched” on or off. Therefore, further examination of this cell line should be of major interest and importance for various pharmaceutical researches.

Thus far, a wide array of useful cell culture models of the corneal epithelium has been established. Many of these cell culture models focus on toxicity testing and ocular irritation, but some cell layer models for drug permeation studies are also available. Indispensable for successful drug penetration testing is a cell layer that exhibits a tight epithelial barrier. This latter requirement of tight barrier properties disqualifies some of the models that were established as substitutes for the Draize test. At least two cell lines are available for pharmaceutical studies and some newer models may qualify as a useful tool, once they are characterized for their barrier properties.

12.5. Organotypic Equivalents

During the cultivation of differentiating cells, including corneal cells, an approximation or recapitulation of the in vivo situation such as expression of typical histological parameters was attempted by variation of culture conditions at an early stage. With this approach, it has been shown that an improvement of growth behavior and cell differentiation can be achieved by using extracellular matrices that resemble the basement membrane, especially type I collagen, or attachment factors, for example, laminin and fibronectin, as growth substrates [33, 65]. A further adaptation or mimicking of in vivo conditions was attempted by coculture of corneal epithelial cells with keratocytes or endothelial cells [66]. Corneal epithelial cells were cocultivated

with primary cultures of keratocytes as well as cell growth on 3T3 feeder layers [67, 68]. Typical characteristics of cells were found more frequently by coculturing schemes. Furthermore, these systems as well as the use of keratocyte-conditioned media allowed mechanistic investigations of cell–cell interactions [69]. An improvement of barrier properties by coculturing with keratocytes could be shown for permeation models of epithelial cells as well [57]. Toropainen and coworkers showed that the TEER value was increased, while the permeation rate of mannitol reduced in the keratocyte coculturing schemes, suggesting an increased tightness of the cultured corneal epithelial barrier. With air-interfaced culture (AIC) of several cells (e.g., dermal, nasal, lung, and other epithelial cells) which are normally in contact with the air in an *in vivo* setting, a stronger expression of *in vivo* phenotypic features was also found in cultured cells. This has also been found to be applicable to the *in vitro* cultivation of corneal epithelium, establishing AIC as a standard condition for corneal epithelial cell cultures. Especially, certain histological markers for the multilayered corneal epithelium, for example, K3 expression [70], and in particular the formation of a tight barrier of corneal epithelial cells [33] could be promoted. For example, Chang and coworkers [33] showed the necessity of AIC conditions in their primary cultures of rabbit corneal epithelial cells for developing tight epithelial cell layers. Toropainen et al. [57] also demonstrated an increase in TEER values, when immortalized human corneal epithelial cells were grown under AIC conditions in comparison to the liquid-covered culture (LCC) method. It is now well accepted by the scientific community that the formation of functional multilayered epithelial barriers for both corneal epithelial cell models and organotypic constructs requires AIC conditions.

At the beginning of the 1990s, due to the more rapid expansion of tissue-engineering methods, first important steps were laid down for development of a three-dimensional (3-D) model of the cornea. Models composed of both epithelial cells and stroma were established, which later led to more elaborate constructs composed of all three cell types (i.e., epithelial cells, keratocytes, and endothelial cells). The usage of such corneal equivalents is quite varied in scope. The 3-D constructs can be applied in various ways: (a) investigations regarding cell–cell interactions, (b) a replacement for the Draize test for toxicological studies, (c) *in vitro* permeation studies, and (d) transplantation (profoundly challenging but envisioned to be a possibility in the near future). The aims of studies were very different and the used cells (animal or human, primary or immortalized cells) and methods are widely different. In the following section, some of the models that gained major importance in the development of organotypic constructs are described.

The first 3-D cornea equivalent was characterized in 1993 by Minami and coworkers [35]. This *in vitro* corneal construct model, containing bovine primary cells, was developed by a stepwise reconstruction and final cultivation of the whole construct under AIC conditions. This design was further modified and used by many other groups in subsequent studies. First, pure primary cultures of the different corneal cell types were established. The cultivation was performed in permeable membrane inserts (e.g., made from nitrocellulose). A stroma-biomatrix containing incorporated keratocytes was formed from gelled type I collagen. Endothelial and epithelial cells were seeded and cultivated on the top and bottom side, respectively, of the collagen gel matrix. After reaching confluence, the levels of culture medium was adjusted in such a way

that the epithelial cell layers were further cultivated under AIC conditions. The resulting construct possessed a three-layered structure with a multilayered epithelium comparable to the *in vivo* situation. In addition, the 55/64-kDa keratin pair was detected in the epithelium, indicating corneal epithelial cell differentiation. However, no further pharmaceutical/bioelectrical investigations were performed utilizing this bovine corneal equivalent. Thus, it remains unclear to what extent the construct could be used (e.g., as permeation model).

Another 3-D cornea model, comprising rabbit primary cultures of epithelial and stromal cells as well as mouse immortalized endothelial cells, was described in 1994 by Zieske and coworkers [70]. They showed the influence of endothelial cells on the formation of a tightly packed, multilayered epithelium as well as the expression of laminin, type VII collagen, α_6 integrin, keratin K3, and α -enolase. Furthermore, their findings suggested that the formation of an *in vivo*-like epithelium requires the cultivation of the 3-D corneal construct under AIC conditions. By contrast, LCC methods of cultivating corneal equivalents in the absence of endothelial cells failed to promote the expression of differentiation markers and basement membrane components.

With the objective of creating an *in vitro* corneal model for an alternative to the Draize test, Schneider and coworkers developed a 3-D cornea construct, which also comprised all three cell types from fetal porcine primary cultures [71]. In contrast to other studies, they cultivated this cell culture model under LCC methods. They validated the cornea equivalent regarding cell materials and culture conditions (especially the growth media). They found an *in vivo*-like cell morphology as well as the expression of basement membrane components like laminin and fibronectin. In addition, the formation of glycosaminoglycans was detected in the artificial stroma. In another study, they reported, using a modified MTT cytotoxicity test, that the data of five chemical test compounds observed with this *in vitro* corneal model correlate well with the Draize test classification [72]. This model was the first 3-D organotypic cornea construct for *in vitro* toxicity studies and therefore seems to be an interesting and useful approach for an alternative to the Draize test. Unfortunately, no further investigations on this model are reported and thus its usefulness as an *in vitro* corneal model for drug absorption studies remains to be confirmed.

In another approach, Parnigotto and coworkers reconstructed corneal structures *in vitro* by using corneal stroma containing keratocytes to which corneal epithelial cells from bovine primary cultures were overlaid [73]. However, this particular corneal model did not contain an endothelial layer. This model was histochemically characterized and the toxicity of different surfactants was tested using MTT methods. This stroma-epithelium model has been reported to show a cornea-like morphology, where a multilayered epithelial barrier composed of basal cells (of a cuboidal shape) and superficial cells (of a flattened shape) is noted. Furthermore, the formation of a basement membrane equivalent and expression of the 64-kDa keratin were reported, indicating the presence of differentiated epithelial cells. The toxicity data for various surfactants obtained with this model correlate well with those seen by the Draize test [73]. However, this corneal equivalent was not further validated or used as a model for permeation studies.

In 1999, Germain and coworkers developed a corneal stroma-epithelium equivalent without endothelial cell coculture, using human primary cultures

[34]. They isolated human epithelial cells from the limbus of human donor corneas and cultivated them on a collagen gel containing keratocytes under AIC conditions. This *in vitro* corneal model was investigated to exhibit an *in vivo*-like morphology as well as expression of basement membrane components when studied using histological and immunohistochemical methods. Germain's corneal equivalent possesses epithelial cell layers (four to five layers), including cuboidal and basal cells. In addition, laminin, type VII collagen, fibronectin, and $\beta_1\alpha_{3,5,6}$ integrin subunits were detectable. Germain and coworkers described their *in vitro* corneal model as a promising tool for further physiological, toxicological, and pharmacological investigations as well as a useful model for gene expression studies. Although Germain's group is known for its wide expertise in the field of tissue engineering (in particular, corneal tissue engineering) [74, 75], toxicity or permeation data using their model of stroma-corneal epithelium equivalent were lacking to date.

The first 3-D corneal construct composed of all three cell types of human cells has been described by Griffith and coworkers [76]. Each cellular layer was fabricated from immortalized human cells that were screened for use on the basis of morphological, biochemical, and electrophysiological similarity to their *in vivo* counterparts. This *in vitro* human corneal model exhibits similarities with respect to biophysical and physiological functions, morphology, biochemical marker expression, transparency, ion and fluid transport as well as gene expression profiles observed *in vivo*. In addition to the fact that a whole human cornea was reconstructed *in vitro* for the first time, this human corneal equivalent was entirely formed from several immortalized cell lines, using HPV E6/E7. This maneuver allows the production of a great number of cornea equivalents with much decreased variability due to the extended life span of cells showing the same properties over many population doublings. However, as is well known, immortalized cells may represent features of a less differentiated state compared to primary cells in culture. Nonetheless, the human corneal equivalent showed morphology similar to the *in vivo* features, including well-defined epithelial, stromal, and endothelial cell layers. The transparency of the artificial stroma should be pointed out as a big advantage, as the transparency of corneal models is an absolute requirement for possible transplantation. In contrast to previously developed corneal equivalents, the stroma-biomatrix was formed from a collagen-chondroitin sulfate substrate that was cross-linked by treatment with glutaraldehyde. The *in vitro* human corneal model was cultivated under AIC conditions, similar to those corneal equivalents mentioned above. Besides morphology, this particular construct possesses a similar degree of stromal swelling as well as a physiologically active endothelium, mimicking those observed in an *in vivo* setting. After exposure to sodium dodecylsulfate, the construct showed a wound-healing progress that was comparable to healing found in eye bank donor corneas in the same experimental setup. Furthermore, this construct exhibits the same opacification after treatment with different surfactants, as found in rabbit and human corneas. Thus, Griffith and coworkers described their model as a promising tool for irritancy testing, wound healing, and other biomedical research (e.g., cell-matrix interactions), and as basis for the development of temporary or permanent cornea replacements. Unfortunately, this human corneal construct has not been tested further as an *in vitro* model for both toxicity and drug

absorption studies yet. However, Griffith's group has acquired a strong expertise in the field of corneal tissue engineering, particularly in the development of stroma-biomatrices (e.g., collagen-based polymers) for both transplantation and keratoprotheses [77–80]. Subsequent studies from Griffith and coworkers have also been published, dealing with innervated human corneal equivalents as *in vitro* models for studying interactions between nerve cells and their target, that is, corneal epithelial cells [81, 82].

In the last decade, several investigations were performed with regard to *in vitro* reconstruction of corneal epithelium for transplantation. Meanwhile, many studies have also been reported, dealing with the cultivation and transplantation of corneal epithelium grown on amniotic membranes (i.e., the innermost membrane of the placenta), fibrin gels, or temperature-responsive culture dishes [83–85]. However, none of these models has been examined for suitability as a model for drug absorption studies.

Following the report by Griffith et al. [76–79] on the human 3-D cornea model, two more human models were reported. One model was described as an alternative to the Draize test [86, 87] while the other as an *in vitro* model for permeation studies [88]. Both will be presented in more details in this section due to their major impacts. Engelke and coworkers [86] developed an *in vitro* corneal model that was also reconstructed using immortalized cells (in this case, using SV-40). The cultivation was performed according to the methods established by Minami et al. [35], using a type I collagen stroma-matrix and AIC methods. This construct comprised the well-characterized epithelial cell line HCE-T [56] (see Sect. 12.4.2), endothelial cell line HENC (established by Bednarz and coworkers [89]), and keratocyte cell line HCK (generated in-house from primary cultures by pSV40-dN-Plasmid DNA-transfection [86]). This cornea equivalent exhibited an *in vivo*-like morphology, including multilayered epithelial cells. Engelke et al. [87] further investigated the usefulness of their *in vitro* cornea model in toxicological studies. The quantification of cell damage caused by different detergents was carried out via confocal laser scanning microscopy using simultaneous vital dye staining by calcein AM and ethidium homodimer-1. This human cornea equivalent is still under investigation, regarding its suitability as an alternative to the Draize test.

Three-dimensional cornea constructs, comprising all three cell types present in corneal tissues *in vivo* and possessing an *in vivo*-like structure, were described specifically as a model for *in vitro* permeation studies for the first time by Müller-Goymann's group [90]. First, a cornea construct from bovine primary cultures in the style of that reported by Minami et al. [35] was established and characterized. Similar techniques were then applied to develop a porcine primary construct. The current construct is composed of a combination of immortalized and native human cells. The bovine cornea construct exhibited an *in vivo*-like morphology including a multilayered epithelium as well. In addition to the typical corneal epithelial morphology, exhibiting basal cells of cuboidal shapes and superficial cells of flattened architectures, the expression of the 64-kDa keratin K3 was demonstrated [91]. The permeation through this corneal construct of pilocarpine hydrochloride (PHCl) from either an array of commercially available aqueous and oily eye drop solutions or an inverse micellar solution (i.e., an oily solution containing an emulsifier that forms inverted micelles with drugs trapped inside) was compared with permeation

coefficients from experiments using excised bovine corneas. Comparison of permeation rates through the excised bovine cornea versus this *in vitro* cornea construct model showed the same rank order for the different formulations. Permeation coefficients obtained with this cornea construct were about twofold to fourfold higher than those observed in the excised bovine cornea. Similar results were also described for permeation studies including timolol maleate, a frequently applied antiglaucoma drug [91]. The porcine cornea construct appears to exhibit similar results on permeation of PHCl from different ophthalmic formulations in comparison to excised porcine cornea [92]. About twofold to fourfold greater permeability indices for the porcine cornea construct than those found in the excised porcine cornea were demonstrated for different formulations of befunolol hydrochloride, another standard drug in glaucoma therapy. Furthermore, a keratin pattern (mimicking the *in vivo* cornea), basement membrane components (such as laminin and fibronectin) as well as surface structures (microvilli and microplicae) like those found in the *in vivo* setting were also observed in the porcine cornea construct [41, 93]. In order to avoid species-specific differences and get a more precise prediction of transcorneal drug absorption into human eye, Müller-Goymann and coworkers additionally developed a human cornea construct (HCC). The HCC was reconstructed from native keratocytes and immortalized cells of corneal epithelium and endothelium. The poor availability of human corneal materials for isolating primary cells and a better standardization of the equivalent through the use of immortalized cell lines both influenced the choice of the cellular components. The corneal epithelial cell line, CEPI-17-CL 4, consists of SV-40 transfected human corneal epithelial cells and was established by Sharif and coworkers [94]. This cell line is well characterized with respect to expression of keratins, cytokines, growth factors, and cytochrome P450 enzymes and used for ocular toxicity and inflammation studies [63]. The endothelial cell line HENC established by Bednarz et al., already mentioned above, was used to form the endothelial barrier in this HCC model. An *in vivo*-like morphology was found in this HCC model. About 1.6-fold to 1.8-fold higher permeabilities were found in this HCC model, compared to those observed in the excised porcine cornea, when aqueous formulations of three model drugs with various physicochemical properties ($\log P_{\text{octanol/water}}$ ranged between 1.6 and -1.3) were studied [88]. In another study, the permeation of six different ophthalmic drugs through the HCC model and human donor corneas was evaluated [95]. The HCC model showed a similar permeation behavior comparable to that found in the human donor corneas for all substances studied and permeation coefficients varied by a factor of 0.8 to 1.4, when compared to native human cornea. These data indicate that P_{app} values correlate well with those of human corneas, even though some substances did not match their P_{app} with that of the human cornea exactly. In a follow-up permeation study using hydrocortisone acetate and *p*-nitrophenyl acetate, the HCC was demonstrated to have esterase enzyme activities similar to those observed in both the excised porcine cornea and human donor cornea. Hence the HCC model could be used for permeation studies, including ester prodrugs [96].

As can be seen above, it has been shown that cultivation of 3-D *in vitro* models of animal and human cornea is possible and the model resembles the *in vivo* cornea of the animal and human. In order to use these cornea constructs as models for *in vitro* drug absorption studies and alternative to the Draize test, further

validation studies are needed. With regard to the use as permeation models, additional investigations are required for the assessment of epithelial tightness (e.g., TEER measurement), expression of transport proteins, and enzyme patterns, to name a few. Also needed is a further refinement/development of artificial stroma-biomatrices with respect to the use of such cornea constructs for *in vitro* toxicity studies as well as investigations addressing wound healing. In view of the creation of a 3-D cornea construct for transplantation, enormous efforts will be needed in particular for the cultivation of autologous cells on a biocompatible transparent biomatrix. First steps in this direction are performed within a project supported by the European Union (Sixth Framework Program, FP6-NMP, Project Reference: 504017, Three-dimensional reconstruction of human corneas by tissue engineering, <http://www.cornea-engineering.org/>).

12.6. Concluding Remarks

For the examination of transcorneal drug permeation, generally two *in vitro* tools are available: (a) corneal epithelial cell cultures and (b) organotypic constructs. For corneal epithelial cell cultures, a much broader variety of primary or immortalized cells are available. Corneal constructs resemble the *in vivo* situation more truthfully, as the construct is comprised with all three cell types in the *in vivo* cornea. Primary corneal cell cultures still require the sacrifice of animals, but these primary cultures can form uncontaminated and tight corneal epithelial barriers in the *in vitro* setting and are convenient to work with as well as to study mechanisms for transport and metabolism, all under controlled experimental conditions. Immortalized corneal cell lines also provide easy handling, although some may fail to form confluent functional barriers (i.e., no tight barrier properties) and are not very useful for permeation studies.

Organotypic corneal constructs do resemble the *in vivo* cornea in many aspects, but they have the drawback of a complex isolation/setup procedure and longer cultivation periods. Additionally, in contrast to the well-established corneal cell lines that have been used for several years, these constructs are relatively new and further validation of the barrier characteristics and transporter expression/function are needed. Nonetheless, we surmise that both *in vitro* models are promising tools for evaluating transcorneal drug delivery.

We envision that future research will involve a further examination of specific transporters and underlying mechanisms in both corneal epithelial cell culture models and corneal constructs. For pharmaceutical applications, these systems will be tested and evaluated for modern drug delivery systems, gene delivery, and oligonucleotide and peptide delivery. The models will also provide good prescreening tools for penetration enhancement afforded by either chemical or physical means. Besides transcorneal drug delivery, a rewarding field in research remains to be eye irritation and toxicity testing in the quest for a replacement for the Draize test. Major applications for the commercially available corneal epithelial models, therefore, will include toxicity testing and drug transport studies (e.g., the Clonetics system appears to be promising for this latter investigations). For the complex task of providing an organotypic

transplant, only a few first steps have been undertaken while the future perspectives are still unclear at best.

Reference

1. Newsome A, Stern R. Pilocarpine adsorption by serum and ocular tissues. *Am J Ophthalmol* 77:918–922 (1974).
2. Harrison RG. Observations on the living developing nerve fiber. *Proc Soc Exp Biol Med* 4:140–143 (1907).
3. Carrel A. On the permanent life of tissues outside the organism. *J Exp Med* 15:516–528 (1912).
4. Mutschler E, Geisslinger G, Kroemer HK, Schäfer-Korting M (eds). *Arzneimittelwirkungen*, 8th ed. Wissenschaftliche Verlagsgesellschaft mbH, Stuttgart (2001).
5. Chow CYC, Gilbard JP. Tear film. In: Krachmer JH (ed.) *Cornea: Fundamentals of Cornea and External Disease*, Vol 1. Mosby, St. Louis, pp 49–60 (1997).
6. Thoft RA, Friend J. The X, Y, Z hypothesis of corneal epithelial maintenance. *Invest Ophthalmol Vis Sci* 24:1442–1443 (1983).
7. Ebato B, Friend J, Thoft RA. Comparison of limbal and peripheral human corneal epithelium in tissue culture. *Invest Ophthalmol Vis Sci* 29:1533–1537 (1988).
8. Tseng SCG. Concept and application of limbal stem cells. *Eye* 3:141–157 (1989).
9. Thoft RA, Wiley LA, Sundarraj N. The multipotential cells of the limbus. *Eye* 3:109–113 (1989).
10. McLaughlin BJ, Caldwell RB, Sasaki Y, Wood TO. Freeze-fracture quantitative comparison of rabbit corneal epithelial and endothelial membranes. *Curr Eye Res* 4:951–961 (1985).
11. Scholz M, Schrunder S, Gartner S, Keipert S, Hartmann C, Pleyer U. Ocular drug permeation following experimental excimer laser treatment on the isolated pig eye. *J Ocul Pharmacol Ther* 18:177–183 (2002).
12. Schermer A, Galvin S, Sun TT. Differentiation-related expression of a major 64K corneal keratin in vivo and in culture suggests limbal location of corneal epithelial stem cells. *J Cell Biol* 103:49–62 (1986).
13. Suzuki K, Tanaka T, Enoki M, Nishida T. Coordinated reassembly of the basement membrane and junctional proteins during cornea epithelial wound healing. *Invest Ophthalmol Vis Sci* 41:2495–2500 (2000).
14. Dastgheib KA, Clinch TE, Manche EE, Hersh P, Ramsey J. Sloughing of corneal epithelium and wound healing complications associated with laser in situ keratomileusis in patients with epithelial basement membrane dystrophy. *Am J Ophthalmol* 130:297–303 (2000).
15. Saika S, Ohnishi Y, Ooshima A, Liu CY, Kao WW. Epithelial repair: Roles of extracellular matrix. *Cornea* 21:S23–S29 (2002).
16. Merindano MD, Costa J, Canals M, Potau JM, Ruano D. A comparative study of Bowman's layer in some mammals: Relationships with other constituent corneal structures. *Eur J Anat* 6:133–139 (2002).
17. Geroski DH, Edelhauser HF. Quantitation of Na/K ATPase pump sites in the rabbit corneal endothelium. *Invest Ophthalmol Vis Sci* 25:1056–1060 (1984).
18. Kaye GI, Tice LW. Studies on the cornea. V. Electron microscopic localization of adenosine triphosphatase activity in the rabbit cornea in relation to transport. *Invest Ophthalmol Vis Sci* 5:22–32 (1966).
19. Engelmann K, Bednarz J, Valtink M. Prospects for endothelial transplantation. *Exp Eye Res* 78:573–578 (2004).
20. Sumide T, Nishida K, Yamato M, Ide T, Hayashida Y, Watanabe K, Yang J, Kohno C, Kikuchi A, Maeda N, Watanabe H, Okano T, Tano Y. Functional human corneal

- endothelial cell sheets harvested from temperature-responsive culture surfaces. *FASEB J* 20:392–394 (2006).
21. Nishida T. Cornea. In: Krachmer JH (ed.) *Cornea: Fundamentals of Cornea and External Disease*, Vol 1. Mosby, St. Louis, pp 3–27 (1997).
 22. Klyce SD, Beuerman RW. Structure and function of the cornea. In: Kaufman HE, McDonald MB, Barron BA (eds.) *The Cornea*, 2nd ed. Butterworth–Heinemann, London, pp 3–50 (1997).
 23. Beuerman RW, Pedroza L. Ultrastructure of the human cornea. *Microsc Res Tech* 33:320–335 (1996).
 24. Järvinen K, Järvinen T, Urtti A. Ocular absorption following topical delivery. *Adv Drug Deliv Rev* 16:3–19 (1995).
 25. Klyce SD, Crosson CE. Transport processes across the rabbit corneal epithelium: A review. *Curr Eye Res* 4:323–331 (1985).
 26. Slick WC, Mannagh J, Yuhasz Z. Enzymatic removal and pure culture of rabbit corneal endothelial cells. *Arch Ophthalmol* 73:229–232 (1965).
 27. Mannagh J, Irvine AR. Human corneal endothelium: Growth in tissue cultures. *Arch Ophthalmol* 74:847–849 (1965).
 28. Russell WM, Burch RL. *The Principles of Humane Experimental Technique*, Charles Thomas Publishers, (online issue available at: http://altweb.jhsph.edu/publications/humane_exp/het-toc.htm) (1959).
 29. Daniele N, Halse R, Grinyo E, Yeaman SJ, Shepherd PR. Conditionally immortalized cell lines as model systems for high-throughput biology in drug discovery. *Biochem Soc Trans* 30:800–802 (2002).
 30. Tian J, Ishibashi K, Handa JT. The expression of native and cultured RPE grown on different matrices. *Physiol Genomics* 17:170–182 (2004).
 31. Stocker FW, Eiring A, Georgiade R, Georgiade N. A tissue culture technique for growing corneal epithelial, stromal and endothelial tissues separately. *Am J Ophthalmol* 46:294–298 (1958).
 32. Ebato B, Friend J, Thoft RA. Comparison of central and peripheral human corneal epithelium in tissue culture. *Invest Ophthalmol Vis Sci* 28:1450–1456 (1987).
 33. Chang JE, Basu SK, Lee VHL. Air-interface condition promotes the formation of tight corneal epithelial cell layers for drug transport studies. *Pharm Res* 17:670–676 (2000).
 34. Germain L, Auger FA, Grandbois E, Guignard R, Giasson M, Boisjoly H, Guerin SL. Reconstructed human cornea produced in vitro by tissue engineering. *Pathobiology* 67:140–147 (1999).
 35. Minami Y, Sugihara H, Oono S. Reconstruction of cornea in three-dimensional collagen matrix culture. *Invest Ophthalmol Vis Sci* 34:2316–2324 (1993).
 36. Chialbi RG. Primär- und Subkultur humaner zentraler Corneaepithelzellen. PhD-Thesis, Rheinisch-Westfälische Technische Hochschule Aachen, Aachen, Germany (1996).
 37. Sarkar P, Basu PK, Carré F. Bovine corneal epithelium in tissue culture. Chromosomal stability in a serially subcultured line. *Am J Ophthalmol* 61:553–557 (1966).
 38. Favata BV. Growth and behavior of guinea pig iris, retina and cornea in vitro. *Am J Ophthalmol* 58:651–663 (1964).
 39. Ellingson DJ, Yao KT. Separation and in vitro growth of mammalian corneal epithelial and endothelial cells. *Exp Cell Res* 66:478–482 (1971).
 40. Kawakita T, Espana EM, He H, Yeh LK, Liu CY, Tseng SC. Calcium-induced abnormal epidermal-like differentiation in cultures of mouse corneal-limbal epithelial cells. *Invest Ophthalmol Vis Sci* 45:3507–3512 (2004).
 41. Reichl S, Muller-Goymann CC. The use of a porcine organotypic cornea construct for permeation studies from formulations containing befunolol hydrochloride. *Int J Pharm* 250:191–201 (2003).

42. Tungsiripat T, Sarayba MA, Taban M, Sweet PM, Osann KE, Chuck RS. Viability of limbal epithelium after anterior lamellar harvesting using a microkeratome. *Ophthalmology* 111:469–475 (2004).
43. Kawazu K, Shiono H, Tanioka H, Ota A, Ikuse T, Takashina H, Kawashima Y. Beta-adrenergic antagonist permeation across cultured rabbit corneal epithelial cells grown on permeable supports. *Curr Eye Res* 17:125–131 (1998).
44. Kawazu K, Midori Y, Ota A. Cultured rabbit corneal epithelium elicits levofloxacin absorption and secretion. *J Pharm Pharmacol* 51:791–796 (1999).
45. Kawazu K, Yamada K, Nakamura M, Ota A. Characterization of cyclosporin a transport in cultured rabbit corneal epithelial cells: P-glycoprotein transport activity and binding to cyclophilin. *Invest Ophthalmol Vis Sci* 40:1738–1744 (1999).
46. Ehrhardt C, Kneuer C, Fiegel J, Hanes J, Schaefer UF, Kim KJ, Lehr CM. Influence of apical fluid volume on the development of functional intercellular junctions in the human epithelial cell line 16HBE14o-: Implications for the use of this cell line as an in vitro model for bronchial drug absorption studies. *Cell Tissue Res* 308:391–400 (2002).
47. Scholz M, Lin JE, Lee VH, Keipert S. Pilocarpine permeability across ocular tissues and cell cultures: Influence of formulation parameters. *J Ocul Pharmacol Ther* 18:455–468 (2002).
48. Chang-Lin JE, Kim KJ, Lee VH. Characterization of active ion transport across primary rabbit corneal epithelial cell layers (RCrECL) cultured at an air-interface. *Exp Eye Res* 80:827–836 (2005).
49. Gey GO, Coffman WD, Kubicek MT. Tissue culture studies of the proliferative capacity of cervical carcinoma and normal epithelium. *Cancer Res* 12:364–365 (1952).
50. Kohler G, Milstein C. Continuous cultures of fused cells secreting antibody of predefined specificity. *Nature* 256:496–497 (1975).
51. Araki K, Ohashi Y, Sasabe T, Kinoshita S, Hayashi K, Yang XZ, Hosaka Y, Aizawa S, Handa H. Immortalization of rabbit corneal epithelial cells by a recombinant SV40-adenovirus vector. *Invest Ophthalmol Vis Sci* 34:2665–2671 (1993).
52. Buralassi S, Monti D, Brignoccoli A, Fabiani O, Lenzi C, Pirone A, Chetoni P. Development of cultured rabbit corneal epithelium for drug permeation studies: A comparison with excised rabbit cornea. *J Ocul Pharmacol Ther* 20:518–532 (2004).
53. Niederkorn JY, Meyer DR, Ubelaker JE, Martin JH. Ultrastructural and immunohistological characterization of the SIRC corneal cell line. *In Vitro Cell Dev Biol* 26:923–930 (1990).
54. Goskonda VR, Khan MA, Hutak CM, Reddy IK. Permeability characteristics of novel mydriatic agents using an in vitro cell culture model that utilizes SIRC rabbit corneal cells. *J Pharm Sci* 88:180–184 (1999).
55. Tak RV, Pal D, Gao H, Dey S, Mitra AK. Transport of acyclovir ester prodrugs through rabbit cornea and SIRC-rabbit corneal epithelial cell line. *J Pharm Sci* 90:1505–1515 (2001).
56. Araki-Sasaki K, Ohashi Y, Sasabe T, Hayashi K, Watanabe H, Tano Y, Handa H. An SV40-immortalized human corneal epithelial cell line and its characterization. *Invest Ophthalmol Vis Sci* 36:614–621 (1995).
57. Toropainen E, Ranta VP, Talvitie A, Suhonen P, Urtti A. Culture model of human corneal epithelium for prediction of ocular absorption. *Invest Ophthalmol Vis Sci* 42:2942–2948 (2001).
58. Hämäläinen KM, Kontturi K, Auriola S, Murtomäki L, Urtti A. Estimation of pore size and pore density of biomembranes from permeability measurements of polyethylene glycols using an effusion-like approach. *J Control Release* 49:97–104 (1997).

59. Saarinen-Savolainen P, Jarvinen T, Araki-Sasaki K, Watanabe H, Urtti A. Evaluation of cytotoxicity of various drugs, eye drop excipients and cyclodextrins in an immortalized human corneal epithelial cell line. *Pharm Res* 15:1275–1280 (1998).
60. Becker U, Ehrhardt C, Daum N, Baldes C, Schaefer UF, Ruprecht KW, Kim KJ, Lehr CM. Expression of ABC-transporters in human corneal tissue and the transformed cell line HCE-T. *J Ocul Pharmacol Ther* 23(2): 172–181 (2007).
61. Kahn CR, Young E, Lee IH, Rhim JS. Human corneal epithelial primary cultures and cell lines with extended life span: In vitro model for ocular studies. *Invest Ophthalmol Vis Sci* 34:3429–3441 (1993).
62. Kruszewski FH, Walker TL, DiPasquale LC. Evaluation of a human corneal epithelial cell line as an in vitro model for assessing ocular irritation. *Fundam Appl Toxicol* 36:130–140 (1997).
63. Offord EA, Sharif NA, Mace K, Tromvoukis Y, Spillare EA, Avanti O, Howe WE, Pfeifer AM. Immortalized human corneal epithelial cells for ocular toxicity and inflammation studies. *Invest Ophthalmol Vis Sci* 40:1091–1101 (1999).
64. Mohan RR, Possin DE, Mohan RR, Sinha S, Wilson SE. Development of genetically engineered tet HPV16-E6/E7 transduced human corneal epithelial clones having tight regulation of proliferation and normal differentiation. *Exp Eye Res* 77:395–407 (2003).
65. Taliana L, Evans MD, Dimitrijevic SD, Steele JG. The influence of stromal contraction in a wound model system on corneal epithelial stratification. *Invest Ophthalmol Vis Sci* 42:81–89 (2001).
66. Orwin EJ, Hubel A. In vitro culture characteristics of corneal epithelial, endothelial and keratocyte cells in a native collagen matrix. *Tissue Eng* 6:307–319 (2000).
67. Tseng SC, Kruse FE, Merritt J, Li DQ. Comparison between serum-free and fibroblast-cocultured single-cell clonal culture systems: Evidence showing that epithelial anti-apoptotic activity is present in 3T3 fibroblast-conditioned media. *Curr Eye Res* 15:973–984 (1996).
68. Ohji M, SundarRaj N, Hassell JR, Thoft RA. Basement membrane synthesis by human corneal epithelial cells in vitro. *Invest Ophthalmol Vis Sci* 35:479–485 (1994).
69. Chan KY, Haschke RH. Epithelial-stromal interactions: Specific stimulation of corneal epithelial cell growth in vitro by a factor(s) from cultured stromal fibroblasts. *Exp Eye Res* 36:231–246 (1983).
70. Zieske JD, Mason VS, Wasson ME, Meunier SF, Nolte CJ, Fukai N, Olsen BR, Parenteau NL. Basement membrane assembly and differentiation of cultured corneal cells: Importance of culture environment and endothelial cell interaction. *Exp Cell Res* 214:621–633 (1994).
71. Schneider AI, Maier-Reif K, Graeve T. Constructing an in vitro cornea from cultures of the three specific corneal cell types. *In Vitro Cell Dev Biol Anim* 35:515–526 (1999).
72. Schneider AI, Maier-Reif K, Graeve T. The use of an in vitro cornea for predicting ocular toxicity. *In Vitro Toxicol* 10:309–318 (1997).
73. Parnigotto PP, Bassani V, Montesi F, Conconi MT. Bovine corneal stroma and epithelium reconstructed in vitro: Characterisation and response to surfactants. *Eye* 12:304–310 (1998).
74. Germain L, Carrier P, Auger FA, Salesse C, Guerin SL. Can we produce a human corneal equivalent by tissue engineering? *Prog Retin Eye Res* 19:497–527 (2000).
75. Gaudreault M, Carrier P, Larouche K, Leclerc S, Giasson M, Germain L, Guerin SL. Influence of sp1/sp3 expression on corneal epithelial cells proliferation and differentiation properties in reconstructed tissues. *Invest Ophthalmol Vis Sci* 44:1447–1457 (2003).

76. Griffith M, Osborne R, Munger R, Xiong X, Doillon CJ, Laycock NL, Hakim M, Song Y, Watsky MA. Functional human corneal equivalents constructed from cell lines. *Science* 286:2169–2172 (1999).
77. Griffith M, Hakim M, Shimmura S, Watsky MA, Li F, Carlsson D, Doillon CJ, Nakamura M, Suuronen E, Shinozaki N, Nakata K, Sheardown H. Artificial human corneas: Scaffolds for transplantation and host regeneration. *Cornea* 21:S54–S61 (2002).
78. Carlsson DJ, Li F, Shimmura S, Griffith M. Bioengineered corneas: How close are we? *Curr Opin Ophthalmol* 14:192–197 (2003).
79. Li F, Griffith M, Li Z, Tanodekaew S, Sheardown H, Hakim M, Carlsson DJ. Recruitment of multiple cell lines by collagen-synthetic copolymer matrices in corneal regeneration. *Biomaterials* 26:3093–3104 (2005).
80. Liu Y, Gan L, Carlsson DJ, Fagerholm P, Lagali N, Watsky MA, Munger R, Hodge WG, Priest D, Griffith M. A simple, cross-linked collagen tissue substitute for corneal implantation. *Invest Ophthalmol Vis Sci* 47:1869–1875 (2006).
81. Suuronen EJ, Nakamura M, Watsky MA, Stys PK, Muller LJ, Munger R, Shinozaki N, Griffith M. Innervated human corneal equivalents as in vitro models for nerve-target cell interactions. *FASEB J* 18:170–172 (2004).
82. Suuronen EJ, McLaughlin CR, Stys PK, Nakamura M, Munger R, Griffith M. Functional innervation in tissue engineered models for in vitro study and testing purposes. *Toxicol Sci* 82:525–533 (2004).
83. Han B, Schwab IR, Madsen TK, Isseroff RR. A fibrin-based bioengineered ocular surface with human corneal epithelial stem cells. *Cornea* 21:505–510 (2002).
84. Nishida K. Tissue engineering of the cornea. *Cornea* 22:S28–S34 (2003).
85. Kinoshita S, Koizumi N, Nakamura T. Transplantable cultivated mucosal epithelial sheet for ocular surface reconstruction. *Exp Eye Res* 78:483–491 (2004).
86. Zorn-Kruppa M, Tykhonova S, Belge G, Diehl HA, Engelke M. Comparison of human corneal cell cultures in cytotoxicity testing. *ALTEX* 21:129–134 (2004).
87. Engelke M, Patzke J, Tykhonova S, Zorn-Kruppa M. Assessment of ocular irritation by image processed quantification of cell injury in human corneal cell cultures and in corneal constructs. *Altern Lab Anim* 32:345–353 (2004).
88. Reichl S, Bednarz J, Müller-Goymann CC. Human corneal equivalent as cell culture model for in vitro drug permeation studies. *Br J Ophthalmol* 88:560–565 (2004).
89. Bednarz J, Teifel M, Friedl P, Engelmann K. Immortalization of human corneal endothelial cells using electroporation protocol optimized for human corneal endothelial and human retinal pigment epithelial cells. *Acta Ophthalmol Scand* 78:130–136 (2000).
90. Tegtmeier S, Papantoniou I, Müller-Goymann CC. Reconstruction of an in vitro cornea and its use for drug permeation studies from different formulations containing pilocarpine hydrochloride. *Eur J Pharm Biopharm* 51:119–125 (2001).
91. Tegtmeier S, Reichl S, Müller-Goymann CC. Cultivation and characterization of a bovine in vitro model of the cornea. *Pharmazie* 59:464–471 (2004).
92. Reichl S, Müller-Goymann CC. Development of an organotypic corneal construction as an in vitro model for permeability studies. *Ophthalmologe* 98:853–858 (2001).
93. Reichl S. Entwicklung porciner und humaner organotypischer cornealer Zellkulturmodelle für in vitro Permeationsuntersuchungen. PhD Thesis, TU Braunschweig, Germany (2003).
94. Sharif NA, Wiernas TK, Howe WE, Griffin BW, Offord EA, Pfeifer AM. Human corneal epithelial cell functional responses to inflammatory agents and their antagonists. *Invest Ophthalmol Vis Sci* 39:2562–2571 (1998).

95. Reichl S, Döhring S, Bednarz J, Müller-Goymann CC. Human cornea construct HCC-an alternative for in vitro permeation studies? A comparison with human donor corneas. *Eur J Pharm Biopharm* 60:305–308 (2005).
96. Meyer L, Bednarz J, Müller-Goymann CC, Reichl S. Esterase activity of human organotypic cornea construct (HCC) as in vitro model for permeation studies. *Ophthalmologe* 102:971–980 (2005).

The Conjunctival Barrier in Ocular Drug Delivery

Hovhannes J. Gukasyan, Kwang-Jin Kim, and Vincent H.L. Lee

Abstract Within the context of topical and local drug delivery to the eye, the mammalian conjunctiva functions as a unique biological barrier. Various model systems as *in vitro* tools have been refined and validated over the years to assess drug absorption across the conjunctiva. Passive and active drug transport as well as endocytic routes of transconjunctival drug permeation have been extensively characterized. The subconjunctival space offers the possibility of delivering multiple types of sustained release formulations to the eye. Additionally, the concept of transscleral/conjunctival iontophoresis has been proven as a viable option for topical, relatively noninvasive delivery of select categories of molecules. Furthermore, a number of ocular surface disorders have been associated with conjunctival phenotypes, making this tissue a potential drug target. The aim of this chapter is to facilitate the understanding of conjunctival (transport) physiology and establishment of *in vitro* models of conjunctiva validated for predicting drug delivery to the eye in health and disease. The models are evaluated in terms of assessing their electrical, morphological, and permeability properties as well as expression profiles of endogenous active transporter(s) and marker enzyme(s). Finally, we provide protocols and methods, as an appendix to this chapter, to be used for *in vitro* studies of the conjunctiva for testing preclinical biopharmaceutics.

Keywords: Ocular drug delivery; Noncorneal route; Transporters; Iontophoresis; Endocytosis; Dry eye; Inflammation; Subconjunctival injections

Abbreviations

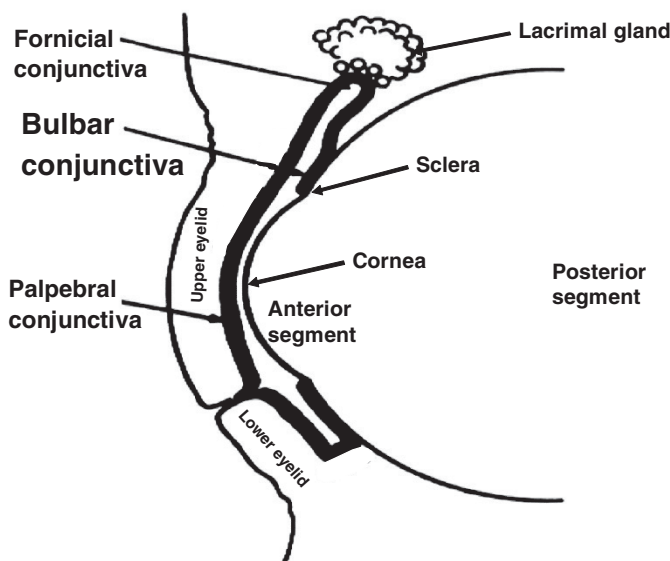
Ad5	Adenovirus type 5
AIC	Air-interfaced culture
ATB	Na ⁺ /Cl ⁻ -coupled broad specificity amino acid transporter B ^{0,+}
ATP	Adenosine triphosphate
cAMP	Cyclic adenosine monophosphate
CFTR	Cystic fibrosis transmembrane conductance regulator
GSH	Glutathione
<i>I</i> _{sc}	Short-circuit current

L-NA	N ^G -nitro-L-arginine
NO	Nitric oxide
NOS	Nitric oxide synthase
PD	Potential difference
P-gp	P-glycoprotein
RCEC	Rabbit conjunctival epithelial cells
TEER	Trans epithelial electrical resistance

13.1. Introduction to the Ocular Surface and the Relative Contribution of the Conjunctiva

The conjunctiva is a thin, mucus-secreting, relatively well vascularized (compared to avascular cornea) tissue that covers ~80% of the ocular surface. It comprises the inner surface of the eyelids and is part of the anterior sclera ending where the cornea begins. While the conjunctiva has been long thought to play a simple protective role in the eye by functioning as a passive physical barrier, it is an intricate and heterogeneous tissue which participates in the maintenance of tear film stability due to the mucus secreted by its resident goblet cells [1, 2]. Studies performed in recent years have characterized additional functional and practical features of the conjunctiva, that is, contributing to the regulation of electrolyte and fluid balance in the microenvironment of its mucosal surface as well as providing a unique conduit for drug delivery to the anterior and posterior segments of the eye when drugs are applied topically to ocular surfaces [3, 4]. The dynamic nature of conjunctiva was demonstrated from the identification of several transport mechanisms for Na⁺ absorption from the conjunctival mucosa: Na⁺-glucose, Na⁺-amino acid, and Na⁺-nucleoside cotransporters, in addition to the predominant and active Cl⁻ secretion. Permeability of the conjunctiva to a wide variety of hydrophilic and lipophilic molecules and drugs was also characterized in the recent past, which is detailed in a recent review [5]. Furthermore, multiple reports substantiate mechanisms of conjunctival ion transport, a key defining property of this tissue. Pharmacological fingerprints of conjunctival ion transport include significant reduction by the serosal application of bumetanide, an inhibitor of Na⁺/K⁺/2Cl⁻ cotransporter, the only known serosal entry pathway for Cl⁻ into conjunctival cells to date [6–8]. Net conjunctival Cl⁻ secretion is modulated by cyclic adenosine monophosphate (cAMP), protein kinase C, and Ca²⁺, suggesting the presence of at least three mucosal Cl⁻ exit pathways [8]. Moreover, the existence and apical localization of CFTR (cystic fibrosis transmembrane conductance regulator) was confirmed by electrophysiological, molecular, biological, and immunocytochemical methods in the pigmented rabbit conjunctival epithelium [9, 10]. By contrast, metabolic enzymes or biochemical elimination mechanisms in the conjunctiva remain largely unknown. In addition to acting as a highly specialized secretory epithelium within the context of biochemical and metabolic capabilities, the conjunctiva also displays esterase activity [11], and is likely to express isoforms of drug efflux pumps (e.g., P-glycoprotein, P-gp) [12]. Lastly, the vectorial secretion of glutathione (GSH, an abundant and ubiquitous antioxidant tripeptide) from conjunctival epithelial cells has been functionally characterized in both the primary

Figure 13.1 A cross-sectional representation of the ocular surface, highlighting the conjunctival tissue as a thick black contour. Three distinct areas of the conjunctiva are labeled along with adjacent ocular tissues.



culture model and excised tissues of conjunctivas obtained from the pigmented rabbit [13].

The ocular epithelium, obtained from other mammalian epithelial tissues that serve as primary barriers from the outside environment, is atypical in structure and function. Comprising relatively and proportionally a small area of the total body surface, the ocular surface includes two continuous but very different tissues of the conjunctiva and cornea. While the conjunctiva covers most of the ocular surface area, only a small fraction (called the bulbar region) covers the anterior sclera, which has an air interface exposed to the environment during “open-eye” intervals (Figure 13.1). It continues through the fornicial and palpebral regions as highly vascularized, thin/semitransparent, elastic, and heterogeneous tissue (Figure 13.1). The cornea is a hydrophobic barrier continuous with the bulbar conjunctiva (Figure 13.1), has a smaller relative surface area, shows a clear transparency to light, exhibits a characteristic high resistance to passive diffusion of ions and molecules, and withstands against the intraocular pressure. Both the corneal and conjunctival epithelial tissues are constantly subjected to light irradiation, atmospheric oxygen, environmental chemicals, and physical abrasion. Each of these factors poses stress of primarily oxidative nature that can ultimately contribute to ocular surface damage and disease, if left unchecked. Natural protective components like water-soluble antioxidants (e.g., vitamin C, L-cyst(e)ine, GSH, uric acid, pyruvate, and tyrosine), lipid-soluble antioxidants (e.g., tocopherols and retinols), and highly specialized enzymes (e.g., superoxide dismutase, catalase, and GSH peroxidase) have all been identified in human tear fluid collected at normal and stimulated secretion rates and are thought to serve as a frontline defense for the ocular surface tear film and underlying tissues. While mechanisms or glandular sources of these antioxidants have not been identified definitively, the conjunctiva may be a possible source due to its dynamic properties of biochemical, electrophysiological, and secretory functions.

13.2. Trans- and Sub-Conjunctival Ocular Drug Delivery

Although the cornea is the primary route of drug entry into the eye following topical administration, applied drugs also reach intraocular tissues by conjunctiva–scleral pathway. About 1–5% of a topically applied drug dose often reaches the anterior segment of the eye. Therefore, subsequent diffusion of absorbed drugs to the posterior segment of the eye will often be relatively insignificant. Eye drops are eliminated from the precorneal area within 90 s and absorbed systemically by way of the highly vascular conjunctival stroma and nasolachrymal ducts. Despite several anatomical hurdles for intraocular drug delivery by the conjunctival pathway, a number of critical discoveries have been reported which highlight the importance of this route. Nipradilol, a β -blocker, and iganidipine, a Ca^{2+} antagonist, are good examples that have been reported to reach the posterior segment of the eye in preclinical species, respectively [5].

Improving the conjunctival drug permeability is one of the major challenges in ocular drug delivery. Enhancing transcellular drug penetration by increasing drug lipophilicity through the use of prodrugs or analogs or improving paracellular penetration by using enhancers to open tight junctions was reported with some success. The transcellular route significantly contributes toward the absorption of lipophilic drugs, but is less significant for hydrophilic species. Propranolol, with a log partition coefficient between octanol and water (log PC) of 3.21, is absorbed through cornea and conjunctiva up to tenfold greater than a hydrophilic drug of similar size, for example, sotalol with a log PC of -0.62 . A sigmoidal relationship, reported in various other tissues and in vitro epithelial cell culture systems, describes penetration of compounds through the conjunctiva and cornea, in a manner that an increase in lipophilicity is seen with a rise in permeation, followed by apparent saturation at high lipophilicity. Since hydrophilic drugs penetrate primarily via the paracellular pathway between epithelial cells through the tight junctions, their penetration area is extremely small compared to the surface area offered by transcellular route for absorption of lipophilic species. However, most lipophilic drugs are prone to efflux mechanisms afforded by pumps (e.g., P-gp) localized on the apical side of conjunctiva [5].

Delivery of biologic pharmaceuticals via the conjunctival route has been studied as an alternative to injections. Because of their hydrophilic nature, peptide and protein drugs permeate across ocular epithelia predominantly via the paracellular route. In conjunctival tissues, penetration through tight junctions comprising the paracellular pathway is the rate-limiting step for diffusion of macromolecule drugs. When this pathway is modeled to be populated with equivalent pores having a cylindrical shape, analysis suggests that conjunctiva may allow the passive restricted diffusion via such pores of hydrophilic substances $<20,000$ Da. The theoretical radius of such equivalent pores is predicted to be ~ 5.5 nm [14]. In addition, an external enzymatic barrier also restricts the penetration of peptide drugs across the conjunctiva, where enkephalins, substance P, and insulin have been shown to significantly degrade during penetration across the tissue when instilled to the mucosal fluid of conjunctivas mounted in modified Ussing chambers [15–17]. Within this context, the coapplication of protease inhibitors (e.g., camostat mesylate and leupeptin) in the mucosal fluid afforded the absorption of an increased

fraction of intact vasopressin across the excised pigmented rabbit conjunctiva [18]. Recent reports indicate that the conjunctival tissue may also be endowed with endocytic vesicular routes for absorption of macromolecules [19, 20]. It is important to note that the roles and their respective contributions of caveolae, clathrin-coated pits, and other subcellular vesicle-associated elements in absorption/secretion of protein drugs remain ambiguous at best [5].

Most of the prominent carrier-mediated transport systems, which have been extensively characterized in the gastrointestinal tract, have been reported for ocular absorption of amino acids, small peptides, sugars, monocarboxylates, organic cations, phosphates, bile acids, and several water-soluble vitamins [5]. These carrier-mediated transport systems can contribute toward the ocular absorption of mimetic drugs. Since paracellular transport of drugs in ocular epithelia, especially the cornea and conjunctiva, is relatively limited in its capacity, carrier-mediated drug transport systems endowed in the conjunctival epithelium (which has a larger surface area than the cornea) offer great advantages. Na^+ -coupled cotransport of D-glucose, L-arginine, nucleosides, and monocarboxylates as well as proton-dependent dipeptide cotransport have all been reported in the conjunctival mucosa [5]. Utilizing these transporters for absorption of (pro)-drugs has been proven conceptually feasible in local, ocular drug delivery. Nitric oxide synthase (NOS) inhibitors (e.g., N^{G} -nitro-L-arginine methyl ester, N^{G} -monomethyl-L-arginine, and N^{G} -nitro-L-arginine, L-NA) are absorbed by the same active mechanism of the $\text{B}^{0,+}$ ($\text{ATB}^{0,+}$) which utilizes the essential amino acid L-arginine in the excised pigmented rabbit conjunctiva [21, 22]. As nitric oxide (NO) plays a cytostatic or cytotoxic role in the conjunctiva and anterior uveal tract, transconjunctival delivery of NOS inhibitors is a practical strategy to alleviate symptoms associated with NO overproduction. Since $\text{ATB}^{0,+}$ is abundantly expressed in the mucosal aspect of conjunctiva and recognizes almost all of naturally occurring neutral and cationic amino acids as substrates, it may be a major drug delivery facilitator to target by rational design approaches. Therefore, there are a wide range of options for chemical modification of drugs through the application of prodrug approaches. For example, herpes simplex virus inhibitor, valacyclovir, is transported as a substrate through mouse and human $\text{ATB}^{0,+}$, in various tissues including the eye. By virtue of analogous or similar amino acid structures, $\text{ATB}^{0,+}$ also affords the transport of acyclovir glutamic acid γ -ester [23]. Dipeptide transporters known to play a key role in the oral absorption of certain β -lactam antibiotics and angiotensin-converting enzyme inhibitors are also present in the mucosal aspect of the conjunctiva (albeit with relatively lower expression levels) [24–26]. Nucleoside transporters are reported to be expressed in the conjunctival mucosa [27], offering the potential for the targeting of nucleoside mimetic antiviral drugs. However, this class of transporter proteins exhibit narrow specificity for substrates, which may entail a comparatively narrow option for chemical design in targeted drug delivery [5].

The use of polymeric nanoparticles in the eye has gained considerable interests in recent years. Ocular disposition, safety, efficacy, and pharmacokinetic profiles of various nanoparticles offer a wide range of application for the delivery of many drugs used to treat common ocular disorders. Polymeric nanoparticles have been utilized to enhance the performance of ibuprofen and cyclosporine, while reducing systemic side effect of carteolol compared with

commercial aqueous eye drops [28]. Poly-D,L-lactide-co-glycolide nanoparticles have been shown to be internalized (albeit direct proof of endocytosis is lacking) in primary cultures of pigmented rabbit conjunctival epithelial cells (RCEC) [19]. As alluded above, although endocytic mechanisms of nanoparticles in the conjunctiva have not been fully characterized, this drug delivery strategy may be a useful tool to apply in ocular delivery of novel therapeutics through this tissue. The use of polymeric nano- and microparticles in subconjunctival route of ocular drug delivery offers a unique method for enhancing local exposure level of drugs by maximizing and maintaining intraocular concentrations with minimal frequency of dosing. Compared to direct intravitreal injection, this approach is less invasive, although it requires the rational formulation design/small-scale engineering of both dimension and surface properties of the drug. Subconjunctival injection of polylactide microparticles (3.6 μm) led to a much higher budesonide concentration in retina and vitreous humor over 14 days, compared to solutions of dosing nanoparticles of smaller (345 nm) size [29]. Collagen matrix and fibrin-based sealants provided a better controlled release of cisplatin and carboplatin, compared to a simple drug solutions, attaining higher drug concentrations after subconjunctival administration of rabbits in several intraocular tissues [30]. Since the sclera, an immediate underlying tissue, is significantly more permeable than the conjunctiva, physical and biological barriers of both cornea and conjunctiva are circumvented in subconjunctival injections [5].

Iontophoresis is a relatively noninvasive technique that uses electric currents to drive introduction of ionized drug substances into tissues or across the tissue barriers. Transcorneal or transscleral/conjunctival iontophoresis has been utilized in ocular drug delivery. Transcorneal iontophoresis effectively enhances aqueous humor concentrations of drugs including gentamicin, tobramycin, and vidarabine monophosphate, but falls short of delivering these therapeutics in high enough concentrations to the posterior segment of the eye due to the presence of the iris-lens barrier [31–35]. In contrast, transscleral/conjunctival iontophoresis affords higher concentrations of ticarcillin, cefazolin, and gentamicin in the vitreous humor as a function of applied current density and duration [36]. Iontophoretic drug penetration heavily depends on the intensity and duration of applied currents, perhaps two of the major limitations of this technique from practical and commercial points of view. Recently, this technique was successfully applied for intraocular gene delivery of fluorescein-labeled anti-NOS oligonucleotides to the retina with an efficacy in the rat model of endotoxin-induced uveitis, suggesting that transscleral/conjunctival iontophoresis facilitates the topical penetration of intact oligonucleotides into intraocular tissues [5].

13.3. An Overview of Conjunctival Disorders

Conjunctivitis, or “pink eye,” is an inflammation of the conjunctiva and probably the most widespread form of ailment in this tissue. If left untreated, it can have serious consequences on vision and overall health. There are many forms of conjunctivitis, and symptoms can range from itchy, burning, or teary eyes (allergic conjunctivitis) to more severe cases of bacterial and viral conjunctivitis (commonly known as “pink eye”). Each type requires

different treatment regimen and is highly contagious except for allergic conjunctivitis. Because of the similarity of the symptoms, only medical doctors trained well in ophthalmology can definitively distinguish between various types of conjunctivitis and could determine the appropriate course of therapy [37].

A number of ocular surface disorders collectively termed as “Dry Eye Syndromes” have also been associated with the conjunctiva. For example, a deficiency and/or imbalance in compositions of the tear film is often found on the ocular surface during *keratoconjunctivitis sicca*. Since the conjunctiva plays a direct role in the maintenance of the tear fluid stability via secretion of mucin [1] by its resident goblet cells [4] and basal fluid secretion driven by electro-osmotic gradients across the tissue [3], the conjunctiva is a well deserved, but not intensively studied, target of interest in research efforts aimed against combating Dry Eye Syndromes.

Anatomical characteristics of disease in conjunctival inflammatory conditions have been reported. In contrast to the bacterial form of conjunctivitis, viral conjunctivitis shows a clear, watery discharge. The affected eye is irritated and red with a swollen eyelid. This condition is also highly contagious and while onset is in one eye it can quickly infect the other eye. There are a number of viruses that can trigger this form of conjunctivitis. Some viral infection is a relatively mild form that clears up on its own, while other viruses produce a more severe form of the infection, such as herpes simplex conjunctivitis frequently seen in children or herpes zoster conjunctivitis which can lead to serious eye damage. Adenovirus (Ad) is the most frequent viral cause of epidemic ocular infections. Ocular Ad infection may lead to disseminated disease, which can be fatal in children or in individuals with acquired immunodeficiencies. A wealth of knowledge about the relationship (that can be applied to improve treatment) between Ad and human ocular tissues is made possible with the development of cotton rat and rabbit models, Ad-induced pulmonary and ocular infections, together with the availability of human Ad mutants [38–40]. The adenovirus type 5 (Ad5) rabbit ocular infection model has been established for evaluation of various antiviral and anti-inflammatory agents in Ad5-induced ocular disease treatment [38].

13.4. Models for Studying Conjunctival Transport Properties

13.4.1. Excised Conjunctival Tissues

The Ussing chamber technique, originally engineered to study transepithelial ion transport, has been optimized to study drug transport and electrophysiology of excised mammalian conjunctivas. This technique utilizes small tissue sheets that are mounted between two compartments of mucosal and serosal aspects of the isolated conjunctival tissue, which are bathed with a physiological buffer that is continuously bubbled with a stream of gas (compressed air or air balanced with 5% CO₂). In addition to providing sufficient oxygen tension for maintaining tissue viability, this configuration creates essential fluid circulation in each reservoir. A schematic diagram of Ussing chamber approaches is shown in Figure 13.2. Compounds of interest are added to either the mucosal or serosal

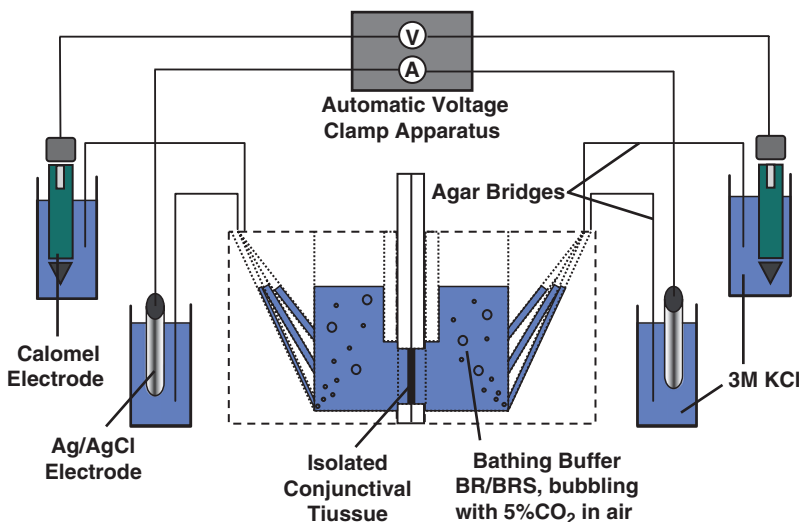


Figure 13.2 A schematic diagram of excised conjunctival tissues (shown) or Transwell-grown, primary cultured rabbit conjunctival epithelial cell layers mounted in a modified Ussing-type chamber. Two calomel electrodes for measurements of transepithelial voltages and two Ag/AgCl electrodes for passing electrical currents across the conjunctival epithelial barrier are shown. This represents a four-electrode setup where one set of voltage and current electrodes connect via agar (containing 1–3 M KCl) bridges to mucosal (or apical) fluid and the other to serosal (or basolateral) fluid (See also color insert).

side of the excised conjunctiva (mounted in the chamber) to estimate fluxes in the absorptive or secretory directions, respectively. Viability of isolated conjunctival tissues mounted in the Ussing chambers can be monitored continuously throughout transport studies, enabling the measurement of subtle changes due to experimental agents (e.g., certain drugs under test) over those afforded by the vehicle alone in control tissues. Validation studies have demonstrated measurements of active transport properties of excised conjunctivas for at least 4 h. Concurrent studies of paracellular transport markers (e.g., D-mannitol) are usually carried out to ascertain the integrity of the excised conjunctiva under investigation. A separate study using morphological investigation of tissue ultrastructure for duration of experiments may provide some useful information. Monitoring tissue viability and integrity during the transport experiments is achieved by measuring transepithelial potential difference (PD) and resistance using the automatic voltage clamp unit. Other advantages of using Ussing chamber techniques for conjunctival tissue transport studies include the added feasibility of looking at largely unknown mechanisms underlying ocular drug metabolism, regional absorption differences (i.e., bulbar, fornicial, or palpebral conjunctiva segments), and relatively small amounts of drug needed to perform flux estimates, with analytically cleaner samples being collectible. While dissection of the tissue requires some practices that may be technically taxing at first, the conjunctival Ussing chamber model of excised tissues and primary cultured conjunctival models (*vide infra*) are critical and rewarding tools for studies classifying compounds used in ophthalmic drug delivery. In this subsection, we provide a brief synopsis of Ussing chamber techniques.

Conjunctival short-circuit current, termed I_{sc} , describes the cumulative sum of all active, energy-driven, and electrogenic transport processes occurring across the conjunctiva. The Ussing chamber apparatus can impose an experimental condition called “zero voltage clamp”, where the electrical PD developed across the conjunctival tissue is forced to zero (i.e., offset to zero) by imposing an electrical PD of the same magnitude but opposite sign. The resultant current flowing across the tissue is termed “short-circuit current” (I_{sc}), bringing down the spontaneously developed PD to zero (thus the name short-circuiting is used to describe the procedure). Under short-circuited conditions, there are no electrical gradient across the tissue and by using the same Ringer’s solution or culture medium on both sides of the barrier, the chemical gradients are also zero. Thus, asymmetric fluxes of ions or solutes measured under such zero gradient conditions across the barrier have to be energized by the barrier itself (e.g., via utilization of cell energy in the form of ATP consumption; e.g., sodium pumps and/or vesicular transport dependent on cytoskeletal network-based movements of cell organelles and so forth). Surgically excised pigmented rabbit conjunctival tissues display a tear side negative PD of 15.5 ± 1.5 mV (mean \pm S.E.M. of 70–80 determinations) when mounted in a modified Ussing-type chamber [6–8, 41]. The voltage detection apparatus is composed of two matched calomel electrodes positioned very closely to the tissue surfaces. A pair of Ag/AgCl electrodes is used to send and receive electrical currents (that are generated by imposing an electrical PD of the same magnitude with opposite sign of the observed PD), which are positioned away from the tissue surfaces in order to ensure uniform current density across the tissue and short the bath-tissue-bath circuit (Figure 13.2). Overall tissue resistance (transepithelial electrical resistance, TEER) can then be estimated by taking the ratio between the observed PD and I_{sc} , or $TEER = PD/I_{sc}$ (which describes the Ohm’s law). Conjunctival TEER ranges from 0.75 to 1.5 $k\Omega \cdot cm^2$ [6, 7].

A variety of automatic voltage clamp devices with special modifications have been extensively utilized in electrophysiological studies of I_{sc} in several ocular tissues including the amphibian corneal epithelium [42] and human fetal retinal pigment epithelium [43, 44], as well as non-ocular tissues like the rat tracheal epithelium [45]. A strong temperature dependency and inhibitory effect of serosally instilled ouabain on the rabbit conjunctival I_{sc} are characteristic of active ion transport driven by Na^+/K^+ -ATPases in the conjunctiva [6, 7].

Utilizing healthy conjunctival tissues under various *ex vivo* configurations has allowed for mechanistic studies of potential drug transport routes. Moreover, it is just as feasible to surgically isolate conjunctivas from ocular disease models for transport studies under pathological conditions with some limitations. Ocular infection models have been established using competent human Ad and thoroughly characterized in pigmented and albino rabbits [38, 39]. As compared to excised conjunctival tissues in health or disease, *in vitro* cultivations of respective epithelial cells on permeable matrices under primary culture conditions allow further investigative control on many additional dimensions. Studies of the conjunctival epithelial barrier alone, i.e., excluding the participation of systemic and lymphatic routes, provide a unique opportunity for a greater throughput in simultaneous transport investigations that consume minimal animal resources with lowest data variability [26].

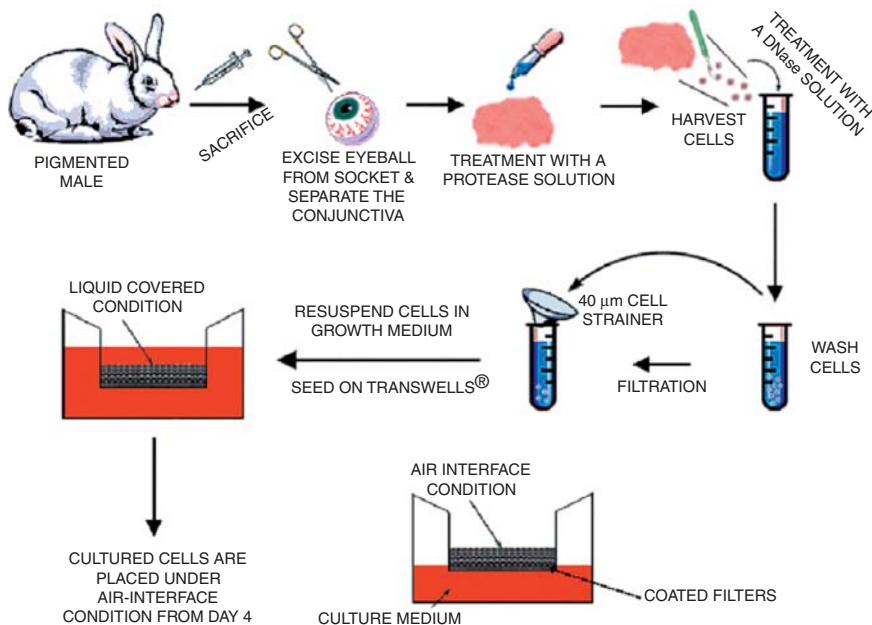


Figure 13.3 A flowchart illustrating various steps for the preparation and maintenance of primary rabbit conjunctival epithelial cell layers, cultured under liquid-covered and air-interfaced conditions (See also color insert).

13.4.2. Primary Culture Models of Conjunctival Epithelial Cell Layers

Cell cultures are a useful, high throughput means for evaluating drug transport mechanisms, impact of formulations, and physiological factors influencing absorption across biological barriers (e.g., epithelia). Functional primary cultures of RCEC under conventional liquid-covered or advanced air-interfaced culture (AIC) conditions are available (Figure 13.3) [26, 46]. Conjunctival epithelial cell cultures exhibit morphological as well as functional similarities to the tissue *in vitro* or *in vivo*. Cultured cells form functional tight junctions and express various enzymes (e.g., esterases, phosphodiesterases, and GSH metabolizing enzymes) and transporters (for amino acids, dipeptides, and nucleosides), similarly to those found in tissues *in vitro* or *in vivo*. Primary isolates of conjunctival epithelial cells achieve differentiated phenotypes and form multilayer of cells, displaying epithelial characteristics with isles of mucin-secreting goblet cell populations. Culture time-dependent organization of tight junctions, development of cell polarity, and expression of various transport mechanisms have been reported [26, 46]. Test compounds are typically added to the apical side of the multilayer of cultured cells, while the cumulative appearance in the basolateral compartment is measured using appropriate measurement schemes (e.g., radioactivity assays or fluorescence determinations depending on the tags on the drugs of interest). Evaluation of *in vitro* system integrity is performed through measuring electrical resistance across the multilayered cells cultured on permeable supports (e.g., Transwell™ systems) using specially engineered voltage-sensing and current-passing electrodes, attached to a portable voltohmmeter (e.g., MilliCell device, Millipore Corp., Billerica, MA, or EVOM device, World Precision Instruments, Sarasota, FL).

An alternative method for assessing cell layer integrity is through the use of hydrophilic paracellular transport markers (e.g., radiolabeled D-mannitol or fluorescein- Na^+), which passively traverse cells by the paracellular route. Small amounts of compound required for in vitro conjunctival cell culture transport experiments make this approach well suited for screening purposes. Relative absorption index of a series of pharmacologically active molecules can be ranked against known markers for the identification of candidates with potential absorption problems, which is a reliable tool to select drug candidates with optimal characteristics.

13.4.3. Conjunctival Disease Models

Understanding differences in drug transport and metabolism in diseased conjunctival tissue is also important. A number of critical and physiological characteristics of conjunctival epithelial cells are altered in inflammatory states. An Ad5 infection model of the conjunctiva has been developed for utility in studying modulations of transport mechanisms in health and disease [38]. This virus-inoculated model has been adapted for tissue studies in the Ussing chamber configuration, as well as for primary cultures of conjunctival epithelial cells. The Ad5 infection model is a pertinent and critical tool for understanding the ophthalmic drug delivery paradigm across the conjunctival tissue in (health and) disease. Detailed protocols for this and other related subjects described above are included as appendix to this chapter.

13.5. Summary and Conclusions

The conjunctival tissue covers ~80% of the ocular surface in higher mammalian species and offers a unique route of delivering drugs locally to the eye. Paracellular, transcellular, active, and endocytic routes of drug absorption play a key role in topical ocular delivery via the conjunctiva. Transscleral/conjunctival iontophoresis offers an alternative noninvasive topical delivery strategy for charged drugs including macromolecular biologics. Lastly, the subconjunctival route of drug delivery provides critical space and capacity for minimally invasive, safe, and sustained exposure of therapeutics to intraocular compartments. The conjunctiva plays an important role in the etiology of a number of ocular surface disorders as potential drug targets and an absorption conduit. Multiple methods (see details in appendix) are available to study the preclinical biopharmaceutics of the conjunctiva, facilitating physiological traits of the conjunctiva, and improving the design of ocular drug delivery strategies to the eye in health and disease.

Acknowledgments: Supported by grants HL38658 (KJK), HL64365 (KJK and VHLL), EY12356 (VHLL), and the Hastings Foundation. HJG thanks the AFPE, PhRMA, and USC Town and Gown. The authors appreciate contributions by scientists who have worked on conjunctival transport in collaboration or directly in our laboratories (in the alphabetical order of last names): Drs P. Ashton, S. K. Basu, E. Hayakawa, Y. Horibe, K. I. Hosoya, S. D. Kashi, U. B. Kompella, A.A. Kulkarni, M. A. Narawane, M. G. Qaddoumi, J. R. Robinson, P. Saha, M. H. Shiue, R. E. Stratford Jr., L. Sun, H. Ueda, W. Wang, and J. J. Yang.

References

1. V. H. Lee and J. R. Robinson. Preliminary examination of rabbit conjunctival mucins. *J Pharm Sci* 69:430–438 (1980)
2. B. D. Srinivasan, F. A. Jakobiec, and T. Iwamoto. Conjunctiva. In Jakobiec F. A. (ed.), *Ocular Anatomy, Embryology, and Teratology*, Harper and Row, Philadelphia, 1982, pp. 733–760
3. M. H. Shiue, A. A. Kulkarni, H. J. Gukasyan, J. B. Swisher, K. J. Kim, and V. H. Lee. Pharmacological modulation of fluid secretion in the pigmented rabbit conjunctiva. *Life Sci* 66:L105–L111 (2000)
4. M. A. Shatos, J. D. Rios, V. Tepavcevic, H. Kano, R. Hodges, and D. A. Dartt. Isolation, characterization, and propagation of rat conjunctival goblet cells in vitro. *Invest Ophthalmol Vis Sci* 42:1455–1464 (2001)
5. K. Hosoya, V. H. Lee, and K. J. Kim. Roles of the conjunctiva in ocular drug delivery: a review of conjunctival transport mechanisms and their regulation. *Eur J Pharm Biopharm* 60:227–240 (2005)
6. U. B. Kompella, K. J. Kim, and V. H. Lee. Active chloride transport in the pigmented rabbit conjunctiva. *Curr Eye Res* 12:1041–1048 (1993)
7. X. P. Shi and O. A. Candia. Active sodium and chloride transport across the isolated rabbit conjunctiva. *Curr Eye Res* 14:927–935 (1995)
8. M. H. Shiue, K. J. Kim, and V. H. Lee. Modulation of chloride secretion across the pigmented rabbit conjunctiva. *Exp Eye Res* 66:275–282 (1998)
9. M. H. Shiue, H. J. Gukasyan, K. J. Kim, D. D. Loo, and V. H. Lee. Characterization of cyclic AMP-regulated chloride conductance in the pigmented rabbit conjunctival epithelial cells. *Can J Physiol Pharmacol* 80:533–540 (2002)
10. H. C. Turner, A. Bernstein, and O. A. Candia. Presence of CFTR in the conjunctival epithelium. *Curr Eye Res* 24:182–187 (2002)
11. H. J. Gukasyan, B. R. Yerxa, W. Pendergast, and V. H. Lee. Metabolism and transport of purinergic receptor agonists in rabbit conjunctival epithelial cells. *Adv Exp Med Biol* 506:255–259 (2002)
12. J. J. Yang, K. J. Kim, and V. H. Lee. Role of P-glycoprotein in restricting propranolol transport in cultured rabbit conjunctival epithelial cell layers. *Pharm Res* 17:533–538 (2000)
13. H. J. Gukasyan, V. H. Lee, K. J. Kim, and R. Kannan. Net glutathione secretion across primary cultured rabbit conjunctival epithelial cell layers. *Invest Ophthalmol Vis Sci* 43:1154–1161 (2002)
14. Y. Horibe, K. Hosoya, K. J. Kim, T. Ogiso, and V. H. Lee. Polar solute transport across the pigmented rabbit conjunctiva: size dependence and the influence of 8-bromo cyclic adenosine monophosphate. *Pharm Res* 14:1246–1251 (1997)
15. E. Hayakawa, D. S. Chien, K. Inagaki, A. Yamamoto, W. Wang, and V. H. Lee. Conjunctival penetration of insulin and peptide drugs in the albino rabbit. *Pharm Res* 9:769–775 (1992)
16. R. E. Stratford, Jr. and V. H. Lee. Ocular aminopeptidase activity and distribution in the albino rabbit. *Curr Eye Res* 4:995–999 (1985)
17. R. E. Stratford, Jr., L. W. Carson, S. Dodda-Kashi, and V. H. Lee. Systemic absorption of ocularly administered enkephalinamide and inulin in the albino rabbit: extent, pathways, and vehicle effects. *J Pharm Sci* 77:838–842 (1988)
18. L. Sun, S. K. Basu, K. J. Kim, and V. H. Lee. Arginine vasopressin transport and metabolism in the pigmented rabbit conjunctiva. *Eur J Pharm Sci* 6:47–52 (1998)
19. M. G. Qaddoumi, H. J. Gukasyan, J. Davda, V. Labhasetwar, K. J. Kim, and V. H. Lee. Clathrin and caveolin-1 expression in primary pigmented rabbit conjunctival epithelial cells: role in PLGA nanoparticle endocytosis. *Mol Vis* 9:559–568 (2003)

20. M. G. Qaddoumi, H. Ueda, J. Yang, J. Davda, V. Labhasetwar, and V. H. Lee. The characteristics and mechanisms of uptake of PLGA nanoparticles in rabbit conjunctival epithelial cell layers. *Pharm Res* 21:641–648 (2004)
21. K. Hosoya, Y. Horibe, K. J. Kim, and V. H. Lee. Na⁺-dependent L-arginine transport in the pigmented rabbit conjunctiva. *Exp Eye Res* 65:547–553 (1997)
22. K. I. Hosoya, Y. Horibe, K. J. Kim, and V. H. Lee. Carrier-mediated transport of NG-nitro-L-arginine, a nitric oxide synthase inhibitor, in the pigmented rabbit conjunctiva. *J Pharmacol Exp Ther* 285:223–227 (1998)
23. T. Hatanaka, M. Haramura, Y. J. Fei, S. Miyauchi, C. C. Bridges, P. S. Ganapathy, S. B. Smith, V. Ganapathy, and M. E. Ganapathy. Transport of amino acid-based prodrugs by the Na⁺- and Cl⁻-coupled amino acid transporter ATB^{0,+} and expression of the transporter in tissues amenable for drug delivery. *J Pharmacol Exp Ther* 308:1138–1147 (2004)
24. B. S. Anand and A. K. Mitra. Mechanism of corneal permeation of L-valyl ester of acyclovir: targeting the oligopeptide transporter on the rabbit cornea. *Pharm Res* 19:1194–1202 (2002)
25. S. K. Basu, I. S. Haworth, M. B. Bolger, and V. H. Lee. Proton-driven dipeptide uptake in primary cultured rabbit conjunctival epithelial cells. *Invest Ophthalmol Vis Sci* 39:2365–2373 (1998)
26. J. J. Yang, H. Ueda, K. Kim, and V. H. Lee. Meeting future challenges in topical ocular drug delivery: development of an air-interfaced primary culture of rabbit conjunctival epithelial cells on a permeable support for drug transport studies. *J Control Release* 65:1–11 (2000)
27. K. Hosoya, Y. Horibe, K. J. Kim, and V. H. Lee. Nucleoside transport mechanisms in the pigmented rabbit conjunctiva. *Invest Ophthalmol Vis Sci* 39:372–377 (1998)
28. H. Z. Bu, H. J. Gukasyan, L. Goulet, X. J. Lou, C. Xiang, and T. Koudriakova. Ocular disposition, pharmacokinetics, efficacy and safety of nanoparticle-formulated ophthalmic drugs. *Curr Drug Metab* 8:91–107 (2007)
29. U. B. Kompella, N. Bandi, and S. P. Ayalasonmayajula. Subconjunctival nano- and microparticles sustain retinal delivery of budesonide, a corticosteroid capable of inhibiting VEGF expression. *Invest Ophthalmol Vis Sci* 44:1192–1201 (2003)
30. J. A. Gilbert, A. E. Simpson, D. E. Rudnick, D. H. Geroski, T. M. Aaberg, Jr., and H. F. Edelhauser. Transscleral permeability and intraocular concentrations of cisplatin from a collagen matrix. *J Control Release* 89:409–417 (2003)
31. R. E. Grossman, D. F. Chu, and D. A. Lee. Regional ocular gentamicin levels after transcorneal and transscleral iontophoresis. *Invest Ophthalmol Vis Sci* 31:909–916 (1990)
32. D. Maurice. Iontophoresis and transcorneal penetration of tobramycin. *Invest Ophthalmol Vis Sci* 30:1181–1182 (1989)
33. D. S. Rootman, J. A. Jantzen, J. R. Gonzalez, M. J. Fischer, R. Beuerman, and J. M. Hill. Pharmacokinetics and safety of transcorneal iontophoresis of tobramycin in the rabbit. *Invest Ophthalmol Vis Sci* 29:1397–1401 (1988)
34. B. S. Kwon, L. P. Gangarosa, N. H. Park, D. S. Hull, E. Fineberg, C. Wiggins, and J. M. Hill. Effect of iontophoretic and topical application of antiviral agents in treatment of experimental HSV-1 keratitis in rabbits. *Invest Ophthalmol Vis Sci* 18:984–988 (1979)
35. J. M. Hill, N. H. Park, L. P. Gangarosa, D. S. Hull, C. L. Tuggle, K. Bowman, and K. Green. Iontophoresis of vidarabine monophosphate into rabbit eyes. *Invest Ophthalmol Vis Sci* 17:473–476 (1978)
36. M. Barza, C. Peckman, and J. Baum. Transscleral iontophoresis of cefazolin, ticarcillin, and gentamicin in the rabbit. *Ophthalmology* 93:133–139 (1986)
37. C. G. Begley, B. Caffery, R. L. Chalmers, and G. L. Mitchell. Use of the dry eye questionnaire to measure symptoms of ocular irritation in patients with aqueous tear deficient dry eye. *Cornea* 21:664–670 (2002)

38. Y. J. Gordon, E. Romanowski, and T. Araullo-Cruz. An ocular model of adenovirus type 5 infection in the NZ rabbit. *Invest Ophthalmol Vis Sci* 33:574–580 (1992)
39. M. D. Trousdale, R. Nobrega, D. Stevenson, T. Nakamura, P. M. dos Santos, L. LaBree, and P. J. McDonnell. Role of adenovirus type 5 early region 3 in the pathogenesis of ocular disease and cell culture infection. *Cornea* 14:280–289 (1995)
40. J. C. Tsai, G. Garlinghouse, P. J. McDonnell, and M. D. Trousdale. An experimental animal model of adenovirus-induced ocular disease. The cotton rat. *Arch Ophthalmol* 110:1167–1170 (1992)
41. K. Hosoya, U. B. Kompella, K. J. Kim, and V. H. Lee. Contribution of Na⁺-glucose cotransport to the short-circuit current in the pigmented rabbit conjunctiva. *Curr Eye Res* 15:447–451 (1996)
42. O. A. Candia and P. S. Reinach. Thermodynamic analysis of active sodium and potassium transport in the frog corneal epithelium. *Am J Physiol* 242:F690-F698 (1982)
43. R. H. Quinn and S. S. Miller. Ion transport mechanisms in native human retinal pigment epithelium. *Invest Ophthalmol Vis Sci* 33:3513–3527 (1992)
44. R. H. Quinn, J. N. Quong, and S. S. Miller. Adrenergic receptor activated ion transport in human fetal retinal pigment epithelium. *Invest Ophthalmol Vis Sci* 42:255–264 (2001)
45. J. S. Jung, J. Y. Lee, S. O. Oh, P. G. Jang, H. R. Bae, Y. K. Kim, and S. H. Lee. Effect of t-butylhydroperoxide on chloride secretion in rat tracheal epithelia. *Pharmacol Toxicol* 82:236–242 (1998)
46. P. Saha, K. J. Kim, and V. H. Lee. A primary culture model of rabbit conjunctival epithelial cells exhibiting tight barrier properties. *Curr Eye Res* 15:1163–1169 (1996)

Inner Blood–Retinal Barrier: Transport Biology and Methodology

Ken-ichi Hosoya and Masatoshi Tomi

Abstract Inner blood–retinal barrier (inner BRB) contains complex tight junctions of retinal capillary endothelial cells, limiting nonspecific transport between the circulating blood and the neural retina. Thus, understanding of inner BRB transport mechanisms is an important step toward drug targeting of the retina. Nevertheless, information of inner BRB transport is very limited due in part to the difficulty in precise determination of inner BRB transport properties. Although *in vivo* transport studies (e.g., retinal uptake index, RUI, method) have been performed to investigate solute transport into the retina, it is difficult to identify which substrates are taken up by the inner BRB versus other side of the retinal barrier (i.e., outer BRB which consists of retinal pigment epithelial cells). We recently developed various analytical methods that can be applied to *in vitro*, *ex vivo*, and *in vivo* settings, enabling to study mechanistically the influx and efflux via transporters and assess transporter gene levels at the inner BRB. Using a combination of newly developed and other conventional methods, we have elucidated various mechanisms as to how vitamin C, amino acids, creatine, and nucleosides are supplied to the retina and how organic anions are effluxed from the retina.

Keywords: Inner blood–retinal barrier; Transporter; Influx transport; Efflux transport; Microdialysis; Cell line; Drug delivery

Abbreviations

AUC	Area under curve
BBB	Blood–brain barrier
BRB	Blood–retinal barrier
C_p	Plasma concentration
CRT	Creatine transporter
CsA	Cyclosporine A
ECF	Extracellular fluid
ENT	Equilibrative nucleoside transporter
E17 β G	Estradiol 17- β glucuronide
4F2hc	Heavy chain of 4F2 cell surface antigen
GLUT	Facilitative glucose transporter

GSH	Gluthathione
HBSS	Hank's balanced salt solution
$K_{in,retina}$	Apparent retinal influx clearance
LAT	L-type amino acid transporter
MCT	Monocarboxylate transporter
MRP	Multidrug resistance-associated protein
OAT	Organic anion transporter
Oatp	Organic anion-transporting polypeptide
PAH	<i>p</i> -aminohippuric acid
RPE	Retinal pigment epithelial cells
RUI	Retinal uptake index
RVEC	Retinal vascular endothelial cells
TAUT	Taurine transporter
tsA58 SV 40	Temperature-sensitive Simian virus 40
V_d	Apparent retina-to-plasma concentration ratio
V_i	Vascular volume of the retina

14.1. Introduction

This chapter will describe the inner blood–retinal barrier (BRB) transport methodology used for *in vitro*, *ex vivo*, and *in vivo* studies. Transporters expressed in the inner BRB and drug delivery to the retina will also be discussed. The retina is a thin tissue (~0.5 mm in thickness) which lines the interior of the posterior globe of the eye, is highly organized as about ten layers, and plays an important role in vision. Retinal diseases (e.g., age-related macular degeneration, diabetic retinopathy, glaucoma, and retinitis pigmentosa) accompany severe vision loss and pose a serious socioeconomic burden. The treatment of these retinal diseases is challenging, since the ocular barriers that effectively protect the eye from foreign materials also hinders efficient absorption of pharmaceuticals.

In addition, the BRB maintains a constant milieu and provides shields for the neural retina from the circulating blood. The BRB forms complex tight junctions of retinal capillary endothelial cells (inner BRB) and retinal pigment epithelial cells (RPE; outer BRB) (Figure 14.1) [1, 2]. The inner two thirds of the human retina is nourished by retinal capillaries and the remainder is covered by choriocapillaris via the outer BRB [3]. The BRB is thought to play an essential role in supplying nutrients to the neural retina to maintain visual functions. It must be responsible for the efflux of neurotransmitter metabolites from the retina; otherwise, metabolites are accumulated in the retina. Most of current understanding of BRB functions is primarily based on *in vivo* data obtained using the retinal uptake index (RUI) method, where a rapid intracarotid injection of test substrates followed by sampling from the retina was used extensively to assess the permeability properties of the rat BRB [4–7]. For example, Törnquist and Alm reported that transport of D-glucose, amino acids, and L-lactate from the blood to the retina across the BRB takes place via carrier-mediated processes [5–7]. In relation to this maneuver, we recently developed an *in vivo* microdialysis method to evaluate the efflux transport of test substrates across the rat BRB by monitoring the vitreous concentration of a test substrate and bulk flow marker in rat vitreous humor [8].

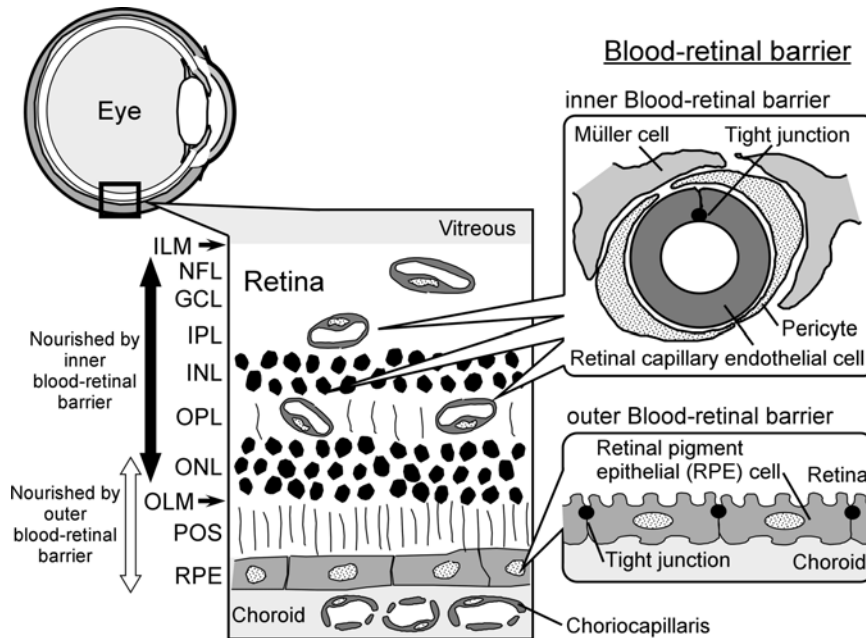


Figure 14.1 Schematic diagram of the blood–retinal barrier (BRB). The retinal cell layers seen histologically consist of retinal pigment epithelium (RPE); photoreceptor outer segments (POS); outer limiting “membrane” (OLM); outer nuclear layer (ONL); outer plexiform layer (OPL); inner nuclear layer (INL); inner plexiform layer (IPL); ganglion cell layer (GCL); nerve fiber layer (NFL); inner limiting “membrane” (ILM).

Unfortunately, information specific to each barrier (i.e., the inner BRB and outer BRB) and details of the transport mechanisms are difficult to obtain using the *in vivo* approaches described above. Therefore, *in vitro* models of retinal endothelial cells (i.e., the inner BRB) and RPE (i.e., the outer BRB) have been developed by us and others. Although many RPE models for the primary culture of different species [9–11] and the human RPE cell line (ARPE-19) [12] have been used to investigate ion and solute transport properties, the use of primary cultures of retinal capillaries is not so easy due to the very small amount of cells/tissues that can be obtained from a single eye of the experimental animal. For example, only 170–250 μg protein (capillary) can be obtained from a single bovine eye [13]. In order to circumvent such paucity of cells/tissues that can be obtainable from the eye of the experimental animal(s), conditionally immortalized cell lines for rat retinal capillary endothelial cells, pericytes, and Müller cells have been successfully developed and used for the acquisition of information involving transport, metabolism, and other cellular functions (transporter gene regulation and cell-to-cell interaction) [14–18]. In addition, for the purpose of measuring reliably the expression levels of various transporter genes in the inner BRB *in vivo*, we have used magnetic beads coated with anti-rat CD31 antibodies to isolate rat retinal vascular endothelial cells and quantify transporter gene levels in the inner BRB using real-time quantitative polymerase chain reaction (PCR) analysis [19]. This latter *ex vivo* approach provides specific information on expression levels for transporter genes in the inner BRB.

14.2. Conditionally Immortalized Cell Lines as a Novel in Vitro Inner Blood–Retinal Barrier Model (Uptake Studies)

A transgenic rat harboring the temperature-sensitive Simian virus 40 (tsA58 SV 40) large T-antigen (tsA58 Tg rat) has been developed as a source of conditionally immortalized cell lines [20]. Several conditionally immortalized cell lines with differentiated functions, such as brain capillary endothelial cells (TR-BBB), brain pericytes (TR-PCT), astrocytes (TR-AST), choroid plexus epithelial cells (TR-CSFB), syncytiotrophoblasts (TR-TBT), small intestine epithelial cells (TR-SIE), and lymphatic endothelial cells (TR-LE) have all been derived from tsA58 Tg rats [21–23]. The tsA58 Tg rats have several advantages as far as establishing immortalized cell lines are concerned (see other reviews [1, 24]). The tsA58 SV 40 large T-antigen gene is stably expressed in all tissues, and cultured cells can be easily immortalized by activation of the SV 40 large T-antigen at 33°C. The activated large T-antigen is thought to induce cell proliferation by interacting with the retinoblastoma gene products and p53, which normally regulate cell proliferation and inactivate the growth-suppressive function of these two proteins [24].

The retinal capillary endothelium is surrounded by pericytes and Müller cell foot processes as shown in Figure 14.1. The overall retinal microvascular biology is thought to be governed, if not entirely, by paracrine interaction between endothelial cells, pericytes, and Müller cells. In order to provide mechanistic information on how the transporters function as well as paracrine cell-to-cell interactions take place, we have established conditionally immortalized cell lines for rat retinal capillary endothelial cells (TR-iBRB), retinal pericytes (TR-rPCT), and Müller cells (TR-MUL) from tsA58 Tg rats (Figure 14.2A) [14–16, 18]. TR-iBRB, TR-rPCT, and TR-MUL cells express typical markers for endothelial, pericyte, and Müller cells, respectively [14–16]. TR-iBRB cells were shown to express facilitative glucose transporter 1 (GLUT1, Slc2A1), P-glycoprotein (ABCB1), creatine transporter (CRT, Slc6A8), and L-type amino acid transporter 1 (LAT1, Slc7A5), which are expressed in the inner BRB in vivo. Accordingly, TR-iBRB cells maintain certain in vivo functions and are considered to be a suitable and useful in vitro model for the inner BRB [1, 14, 25, 26].

For uptake studies, TR-iBRB cells are seeded on rat tail collagen type I-coated 24-well plates at a cell density of 1×10^5 cells/cm². Typically, cells are cultured at 33°C for 48 h to reach confluence for uptake studies. Upon confirming confluence using an inverted microscope under phase-contrast optics, cells are washed with 1 mL extracellular fluid (ECF) buffer consisting of 122 mM NaCl, 25 mM NaHCO₃, 3 mM KCl, 1.4 mM CaCl₂, 1.2 mM MgSO₄, 0.4 mM K₂HPO₄, 10 mM D-glucose, and 10 mM HEPES (pH 7.4) at 37 °C. After washing, uptake is initiated by incubating cells with a suitable ECF buffer containing an appropriate concentration of the test substrate (e.g., [³H]- or [¹⁴C]-labeled compounds). In order to test if the test substrate is taken up into the cells via transporter(s), uptake studies are carried out in the presence of various concentrations of unlabeled substrates and/or potential competitors/inhibitors/stimulators. Uptake studies are also carried out at 4°C, in the presence of metabolic inhibitors, or in the presence or absence (or substitutions) of any particular ion(s) that are required for ion-coupled

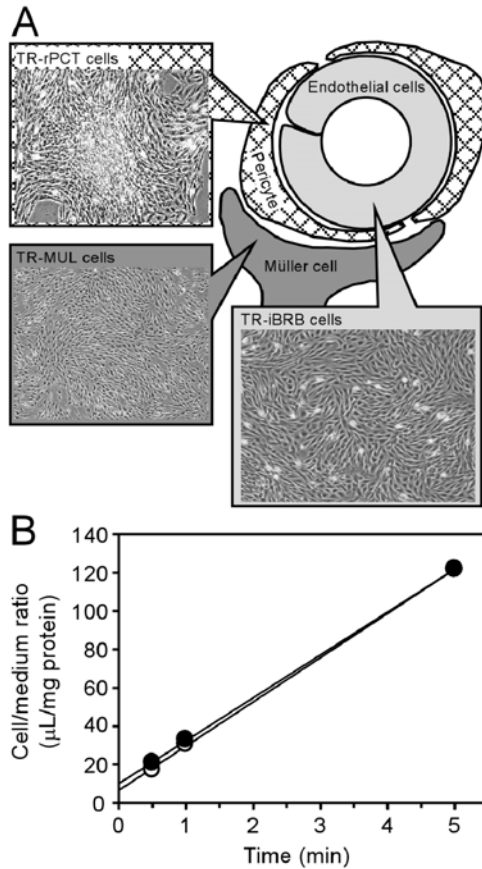


Figure 14.2 Phase contrast microscopic images of conditionally immortalized cells forming the inner blood–retinal barrier (A) and time-course of $[^3\text{H}]$ adenosine uptake by TR-iBRB cells (B). A: Conditionally immortalized rat retinal capillary endothelial cell line; TR-iBRB, retinal pericyte cell line; TR-rPCT and Müller cell line; TR-MUL. B: The $[^3\text{H}]$ adenosine (14 nM) uptake was performed at 37°C in the presence (closed circle) or absence (open circle) of Na^+ .

transport process(es) in the ECF buffer. Uptake is usually measured for the range of 10 s–10 min at 37°C (Figure 14.2B), in order to ensure the kinetics of uptake is within a linear range, which makes the determinations of the kinetic parameters for uptake meaningful. After a predetermined period, uptake is terminated by removing the solution, followed by immersing cells in ice-cold ECF buffer to stop uptake process(es). The cells are then solubilized in 1 N NaOH and subsequently neutralized with 1 N HCl. Cell-associated radioactivity and protein content are assayed by liquid scintillation spectrometry and detergent compatible protein assay (a DC protein assay kit, Bio-rad, Hercules, CA) with bovine serum albumin used as a standard, respectively.

An example of this analysis method is shown in Figure 14.2B for $[^3\text{H}]$ adenosine, which is taken up into TR-iBRB cells. $[^3\text{H}]$ Adenosine uptake increases linearly for at least 5 min in the presence or absence of Na^+ . Concentration-dependent adenosine uptake is known to take place with

a Michaelis-Menten (K_m) constant of $28.5 \mu\text{M}$ in a nitrobenzylmercaptopurine riboside-insensitive manner, suggesting that ENT2 is involved in [^3H]adenosine uptake by TR-iBRB cells. Quantitative real-time PCR data indicate that ENT2 mRNA is predominantly expressed in TR-iBRB cells [27].

14.3. In Vivo Blood-to-Retina Influx Transport

14.3.1. Integration Plot Analysis

The primary objective of integration plot analysis is to analyze the data on influx of the test substrate from the circulating blood to the retina (i.e., blood-to-retina direction) across the BRB after intravenous administration of the test substrate. The advantage of this approach is that it allows reliable determination of the retinal uptake (i.e., clearance) of the test substrate which has a slow permeability across the BRB [28]. On the other hand, due to the intravenous injection, interference by endogenous substrates and plasma-protein binding of the test substrate can produce an unseemingly low estimate of the retinal uptake.

The apparent retinal influx clearance, $K_{\text{in,retina}}$, expressed as $\text{mL}/(\text{min} \cdot \text{g retina})$, of the test substrate labeled with either [^3H] or [^{14}C] from the circulating blood to the retina is determined by integration plot analysis. In brief, rats are anesthetized, followed by injection of the test substrate (e.g., an [^3H]-labeled compound, about $10 \mu\text{Ci}/\text{head}$) into the femoral vein. After collection of plasma samples, rats are decapitated and the retinas removed. The retinas are dissolved in 2 N NaOH and subsequently neutralized with 2 N HCl. The radioactivity of retinal cell lysates is measured by liquid scintillation spectrometry. As an index of the retinal distribution characteristics of the radiolabeled test substrate, the apparent retina-to-plasma concentration ratio (V_d) as a function of time is used. This ratio [$V_d(t)$] ($\text{mL}/\text{g retina}$) is defined as the amount of [^3H] per gram retina divided by that per milliliter plasma, calculated over the time-period of the experiment. The $K_{\text{in,retina}}$ can be described by the following relationship:

$$V_d(t) = K_{\text{in,retina}} \times \frac{\text{AUC}(t)}{C_p(t)} + V_i \quad (14.1)$$

where $\text{AUC}(t)$ ($\text{dpm} \cdot \text{min}/\text{mL}$), $C_p(t)$ (dpm/mL), and V_i ($\text{mL}/\text{g retina}$) represent the area under curve showing time course of the plasma concentration of the [^3H] test substrate from time 0 to t , the concentration of plasma [^3H] test substrate at time t , and the rapidly equilibrated distribution volume of the [^3H] test substrate in the retina, respectively. V_i is usually comparable with the vascular volume of the retina, while $K_{\text{in,retina}}$ can be obtained from the initial slope of a plot of $V_d(t)$ versus $\text{AUC}(t)/C_p(t)$, as an integration plot.

An example of this integration plot analysis using [^3H]adenosine is shown in Figure 14.3A. The estimated $K_{\text{in,retina}}$ of [^3H]adenosine is $2.58 \times 10^{-2} \pm 0.07 \times 10^{-2} \text{ mL}/(\text{min} \cdot \text{g retina})$ (mean \pm S.D.) from the slope of Figure 14.3A (27), which is far greater than that for nonpermeable paracellular markers (e.g., [^{14}C]sucrose [$2.6 \times 10^{-4} \text{ mL}/(\text{min} \cdot \text{g retina})$] and [^3H]D-mannitol [$7.5 \times 10^{-4} \text{ mL}/(\text{min} \cdot \text{g retina})$]) [28].

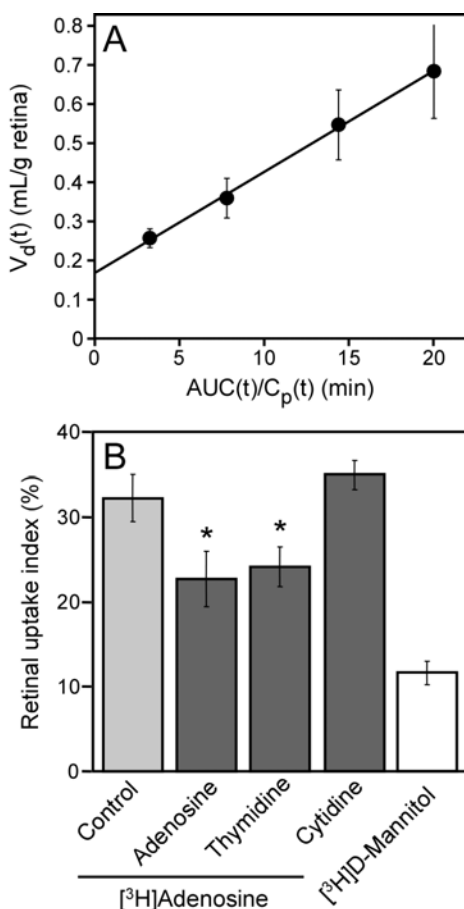


Figure 14.3 Integration plot of the initial uptake of [3 H]adenosine by the retina after intravenous administration (A) and retinal uptake index (RUI) of [3 H]adenosine and [3 H]D-mannitol (B). A: [3 H]Adenosine (10 μ Ci/head) was injected into the femoral vein. B: A test compound, [3 H]adenosine or [3 H]D-mannitol (10 μ Ci/head), and a reference compound, [14 C]n-butanol (0.1 μ Ci/head), were injected into the common carotid artery in the presence or absence of 2 mM inhibitors. * $p < 0.05$, significantly different from the control. Data from *Biochimica et Biophysica Acta*, 1758, Nagase et al., Functional and molecular characterization of adenosine transport at the rat inner blood–retinal barrier. 13–19, 2006, with permission from Elsevier.

14.3.2. Retinal Uptake Index Method

The RUI method is a modification of the brain uptake index method [29] which was first described by Alm and Törnquist [4]. The RUI approach consists of a single-arterial (e.g., intracarotid) injection technique, where the primary objective is to analyze the influx of the test substrate from the circulating blood to the retina through the BRB (i.e., blood-to-retina direction). This approach, for example, has been used to determine the retinal uptake of the test substrate which has a relatively high permeability across the BRB. The advantage of this approach is that it avoids the effect of plasma–protein binding of the test substrate and allows the retinal uptake of the test substrate

to be investigated in the presence of unlabeled competitor, since there is less than 5% mixing of the injected bolus (e.g., around 0.2 mL) with the plasma [29].

In brief, the rats are anesthetized, followed by an injection of 0.2 mL of the test solution into the common carotid artery. The injection solution consists of a HEPES buffered Ringer's solution (containing 141 mM NaCl, 4 mM KCl, 2.8 mM CaCl₂, and 10 mM HEPES, pH 7.4) which contains both the test substrate (e.g., a [³H]-labeled compound, about 10 μCi) and a reference compound, which is highly extracted by the tissue (e.g., 0.1 μCi [¹⁴C]n-butanol) in the presence or absence of transport inhibitors. If a [¹⁴C]-labeled compound is used as a test substrate, [³H]H₂O can be selected as a reference compound. Rats are decapitated at 15 s after injection and the retina is removed. The retina is dissolved in 2 N NaOH and subsequently neutralized with 2 N HCl. The radioactivity is measured by liquid scintillation spectrometry. The RUI value, an index of the retinal distribution characteristics of the [³H] test substrate, is estimated using the following relationship:

$$\text{RUI} = \frac{([\text{}^3\text{H}]/[\text{}^{14}\text{C}] \text{ (dpm in the retina)})}{([\text{}^3\text{H}]/[\text{}^{14}\text{C}] \text{ (dpm in the injection solution)})} \times 100 \quad (14.2)$$

An example of RUI analysis method using [³H]adenosine is shown in Figure 14.3B. The RUI value of [³H]adenosine is greater than that of [³H]D-mannitol (used as a paracellular transport marker) and significantly reduced by ~30% in the presence of 2 mM unlabeled adenosine and thymidine, while 2 mM cytidine has no effect. Thus, the nature of the inhibition shown by this approach confirms the carrier-mediated transport of adenosine from the blood to the retina across the BRB in vivo [27].

14.4. In Vivo Vitreous/Retina-to-Blood Efflux Transport (Microdialysis Study)

Vitreous fluorophotometry has been used to determine the transport of fluorescein across the BRB in the blood-to-vitreous humor direction as well as in the opposite direction [30, 31]. Although this method is very useful for monitoring the integrity of the BRB, it is of limited value for studying the efflux mechanisms for other test substrates due to the required use of a fluorescent probe. In order to circumvent such limitations, microdialysis has been used for sampling the vitreous fluid in the rabbit and monitoring drug concentrations in the vitreous humor [32], as well as estimation of neurotransmitter concentrations in the vitreous/retina tissue [33]. It is of importance to note that experimental animal species should be chosen carefully for these experiments. For example, although rabbits are generally used to evaluate the ocular kinetics of drugs due in part to the fact that rabbits have eyes whose size is similar to that of human eyes [32], the anatomy of the rabbit eye is unusual among mammals in that the retina in rabbits is almost avascular [34]. In contrast, the retinas in rats are well vascularized, similar to humans [34]. Therefore, microdialysis applied to the rat eye is preferable to evaluate the vitreous/retina-to-blood efflux mechanisms for the test substrate taking place via the BRB.

We insert a vertical probe (O.D. 0.5 mm, the length of the tubing, which consists of cellulose membrane, is 2.0 mm, and the molecular cutoff for the dialysis tubing is 50 kDa., TEP-50, Eicom, Kyoto, Japan), which is designed specifically to accommodate experiments intended for the rat eye, into the vitreous humor [8] to assess the efflux rates of the test substrate (e.g., a [^3H]-labeled compound) from the vitreous humor/retina to the blood across the BRB. We monitor the concentrations of both [^3H] test substrate and [^{14}C]-labeled bulk flow marker (e.g., [^{14}C]D-mannitol) in the vitreous humor after vitreous bolus injection using the labeled compounds (Figure 14.4A). The rats are anesthetized and their heads are immobilized using a stereotaxic frame. A 25-gauge needle is then inserted about 1 mm below the corneal scleral limbus through the pars plana at a depth of 3 mm (Figure 14.4A(a)). The needle is removed and [^3H] test substrate (5 μCi) and [^{14}C]D-mannitol (1 μCi) dissolved in 1.0×10^{-3} mL HEPES-buffered Ringer's solution is administered using a microsyringe at a depth of 3.0 mm from the surface of the eye, Figure 14.4A(b). The microdialysis probe is implanted immediately into the vitreous chamber and fixed with surgical glue on the surface of the eye. HEPES-buffered Ringer's solution at 37°C is delivered to the probe continuously at 2.0×10^{-3} mL/min via a polyethylene tubing (inner diameter 0.35 mm, outer diameter 1.05 mm) connected to an infusion pump. The dialysate is collected at 10-min intervals in vials over a period of 5 h and the radioactivity in each fraction is determined by liquid scintillation spectrometry, Figure 14.4A(c) [8].

An example of this analysis method is shown in Figure 14.4B for [^3H]estradiol 17- β glucuronide ([^3H]E17 β G) used as a model compound for amphipathic organic anions. After bolus injection of [^3H]E17 β G and [^{14}C]D-mannitol, both compounds are biexponentially eliminated from the vitreous humor. Although the initial rapid decline is almost the same for both compounds, the second decline in [^3H]E17 β G is significantly greater than that of [^{14}C]D-mannitol, which is a bulk flow marker. The elimination rate constant of [^3H]E17 β G during the terminal phase is twofold greater than that of [^{14}C]D-mannitol, supporting the hypothesis that [^3H]E17 β G undergoes efflux transport from the vitreous humor across the BRB in addition to elimination by bulk flow.

In order to discover whether an organic anion transport process is involved in the efflux transport of E17 β G at the BRB, a microdialysis study is performed in the presence of several organic anions. In the presence of 0.3 mM E17 β G in the retina, the elimination rate constant of [^3H]E17 β G during the terminal phase is significantly reduced and almost the same as that of [^{14}C]D-mannitol, suggesting that E17 β G is transported via a carrier-mediated efflux transport process across the BRB. The [^3H]E17 β G efflux transport from rat vitreous humor/retina is significantly inhibited by probenecid, sulfobromophthalein, and dehydroepiandrosterone sulfate, but not by *p*-aminohippuric acid (PAH). This inhibition pattern agrees well with that of the organic anion-transporting polypeptide (Oatp) family rather than the organic anion transporter (OAT) family [35, 36]. Moreover, [^3H]E17 β G efflux transport is significantly inhibited by 0.35 μM digoxin, which is a specific substrate for Oatp1a4 (Slc21a5; Oatp 2) with a K_m of 0.24 μM [37]. A functional *in vivo* inhibition study suggests that the BRB is involved in the efflux transport of E17 β G, insofar as Oatp1a4 is concerned [8].

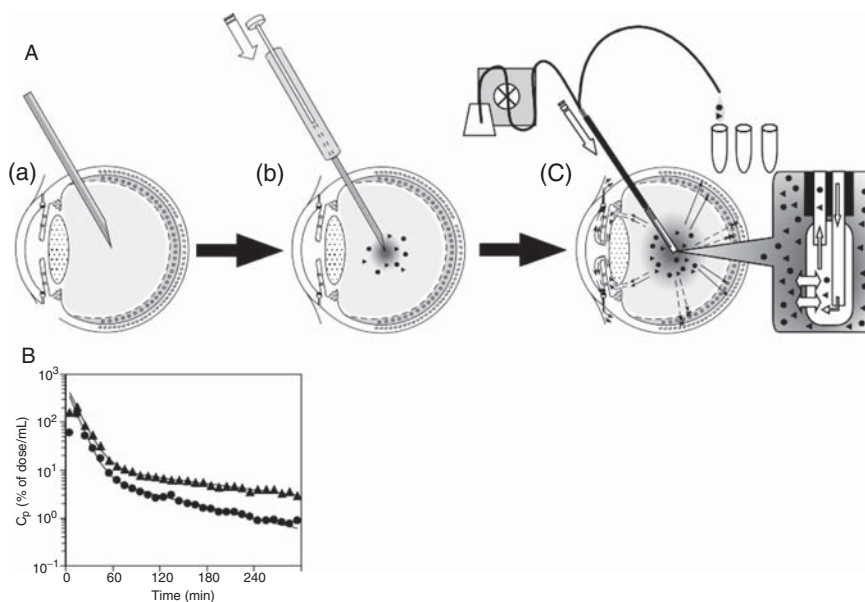


Figure 14.4 Schematic diagram of microdialysis monitoring of the test substrate and a bulk flow marker after vitreous bolus injection (A) and typical outflow pattern of [³H]E17βG and [¹⁴C]D-mannitol from the microdialysis probe (B). A: Closed circles and triangles denote a test substrate and a bulk flow marker, respectively. Bold and dashed lines represent the tight epithelial barrier and porous tissue boundary, respectively. Bold and dashed circles represent tight and fenestrated blood vessels, respectively. (a): A 25-gauge needle is inserted to make a hole on the sclera. (b): HEPES-buffered Ringer's solution (1.0×10^{-3} mL) containing [³H]test compound (5 μCi) and [¹⁴C]D-mannitol (1 μCi, a bulk flow marker) is administered via a microsyringe. (c): Microdialysis probe is implanted into the vitreous chamber. B: Closed triangles and circles represent the concentrations of [¹⁴C]D-mannitol and [³H]E17βG, respectively, in the dialysate. Data taken from *Journal of Neuroscience Methods*, 156, Katayama et al., Application of microdialysis to evaluate the efflux transport of estradiol 17-β glucuronide across the rat blood–retinal barrier. 249–256, 2006, with permission from Elsevier.

14.5. Ex Vivo Transporter Gene Expression Levels at the Inner Blood–Retinal Barrier (Magnetic Isolation of Retinal Vascular Endothelial Cells)

Primary cultured and immortalized RVEC have been used to study transporter expression and transport functions as an *in vitro* model of the inner BRB [14, 38]. Although it is easy to carry out transport studies and measure the mRNA expression of transporters by RT-PCR analysis, there is no way of knowing whether transporter expression levels are changed by passages and conditions of cell culture. In order to determine transporter gene levels at the *in vivo* inner BRB, an *ex vivo* approach has been devised to isolate rat retinal vascular endothelial cells using magnetic beads coated with rat-CD31 (platelet-endothelial cell adhesion molecule-1) antibody (which is generated for a marker exclusively and extensively expressed on the membrane of endothelial cells). The transcript levels of transporters

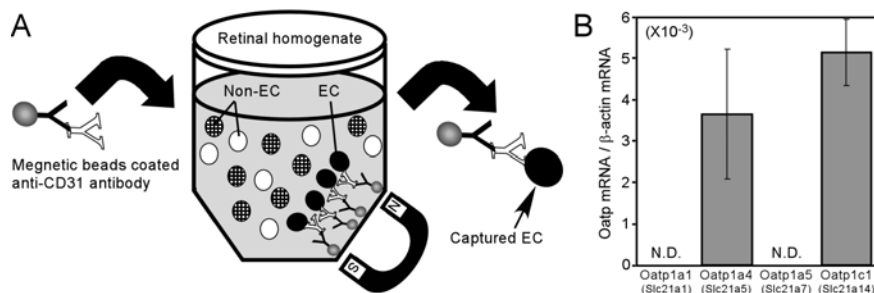


Figure 14.5 Schematic diagram of the magnetic isolation method for rat retinal vascular endothelial cells (RVEC) (A) and the transcript level of organic anion-transporting polypeptides (Oatps) in RVEC (B). A: Endothelial cells (RVEC); EC, Nonendothelial cells (Non-RVEC); Non-EC. B: Not detected; N.D. Data taken from *Journal of Neurochemistry*, 91, Tomi and Hosoya, Application of magnetically isolated rat retinal vascular endothelial cells for the determination of transporter gene expression levels at the inner blood–retinal barrier. 1244–1248, 2004, with permission from Blackwell Publishing.

in the RVEC fraction are measured using real-time quantitative PCR analysis.

The RVEC isolation method is a modification of the procedure described by Su et al. [39] involving affinity purification using magnetic beads coated with anti-rat CD31 antibodies. Mouse anti-rat CD31 antibodies are incubated with Dynabeads pan mouse IgG (DynaL Biotech, Lake Success, NY) overnight at 4°C to prepare magnetic beads coated with anti-rat CD31 antibodies. Rat retinas are minced and digested in 0.1% collagenase type I and 0.01% DNase I in Ca²⁺- and Mg²⁺-free Hank's balanced salt solution (HBSS) for 30 min at 37°C with agitation. Digests are filtered through a 30 μ M nylon mesh and then centrifuged at 200 g for 10 min. The pellets are resuspended in Dulbecco's modified Eagle's medium containing 10% fetal bovine serum and incubated with magnetic beads coated with anti-rat CD31 antibodies for 1 h at room temperature. The RVEC labeled with the magnetic beads are positively selected by immobilizing magnetic beads through the use of a magnet, followed by decanting the fluid (Figure 14.5A). The transcript levels of endothelial markers (e.g., CD31, Tie-2, claudin-5, occludin, Jam-1) in the RVEC fraction are more than 100-fold greater than those in the non-RVEC fraction, supporting the hypothesis that using this method the RVEC fraction of the rat retina can be enriched more than 100-fold compared to the non-RVEC fraction [19].

In vivo microdialysis studies using [³H]E17 β G as a substrate suggest that Oatp 1a4 is involved in the retina-to-blood efflux transport of E17 β G. The identification of the transporter responsible is essential for designing and selecting optimal drug candidates. The transcript levels of Oatp family, including Oatp1a1 (Slc21a1), Oatp1a4, Oatp1a5 (Slc21a7) and Oatp1c1 (Slc21a14; Oatp14), are examined in the RVEC fraction (Figure 14.5B). Oatp1a4 and 1c1 are detected, whereas Oatp1a1 and 1a5 are not. Oatp1a4 and 1c1 are predominantly expressed at the inner BRB. In the case of Oatp1a4, this result supports the in vivo transport function of E17 β G at the BRB as described above and is consistent with a previous immunohistochemical study [40]. Oatp1c1 has been

identified as a blood–brain barrier (BBB)-specific organic anion transporter which uses E17 β G as a substrate [41, 42]. However, Oatp1c1 does not have a high affinity for digoxin (50% inhibition observed at a concentration >0.5 mM) [42]. The role of Oatp1c1 and the involvement of other organic anion transporters, such as the multidrug resistance-associated protein (MRP, ABCC) family and OAT family, at the inner BRB are unclear and remain the subject of ongoing investigations.

14.6. Mechanism of Drug Transport at the Inner Blood–Retinal Barrier

When designing neural retina-active drugs, it is important to consider the pharmacokinetics of these drugs after administration. The pharmacological effect of drugs in the retina reflects their retinal interstitial fluid concentration. If we consider systemic administration, little drug actually reaches the retina, since drugs need to cross either the inner or outer BRB into the retina. One approach is to increase the blood-to-retina influx transport of the drug and the other is to reduce the retina-to-blood efflux transport or total body clearance. Although making drugs more hydrophobic may lead to an increased BRB permeability, this benefit may be offset by an increase in the total body clearance and binding to plasma proteins. Therefore, it is important to design and select optimal drug candidates by taking into account that drugs should be recognized by influx transport systems as well as the efflux transport systems at the BRB be avoided. Until 1999, only three transporters, GLUT1 [43], monocarboxylate transporter 1 (MCT1) [44], and P-glycoprotein [45], had been identified immunohistochemically at the inner BRB, but now several influx and efflux transporters have been identified using novel *in vitro*, *ex vivo*, and *in vivo* techniques as shown in Table 14.1.

14.6.1. Blood-to-Retina Influx Transport

The blood-to-retina influx transporters at the inner BRB act as a support system for the retina, since the inner BRB supplies nutrients and other essential molecules to the retina (Table 14.1). The GLUT1 and MCT1 transport D-glucose and L-lactate, respectively, as an energy source in the retina [43, 44], while CRT transports creatine to support ATP homeostasis in the retina [25]. Creatine plays an essential role in the storage and transmission of phosphate-bound energy via the conversion of creatine to phosphocreatine. ATP is generated from D-glucose and L-lactate, which converts pyruvate, by glycolysis and the tricarboxylic acid cycle, respectively. Therefore, these transporters act in conjunction to maintain energy homeostasis in the retina.

Both LAT1 and xCT require an additional subunit protein of the heavy chain of 4F2 cell surface antigen (4F2hc) in order to transport amino acids [26, 46]. The LAT1 transports branched-chain and aromatic amino acids, which are essential amino acids, as a precursor for neurotransmitters and protein synthesis. To protect the retina against light-induced oxidative stress and maintain intracellular antioxidants, such as glutathione (GSH) and vitamin C at an appropriate level, translocation of L-cyst(e)ine (one of the constituent amino acids for GSH) and vitamin C into retina is critical for the health of the retina. xCT transports L-cystine, which is also one of the rate-limiting precursors of

Table 14.1 Representative transporters and transport processes at the inner BRB.

Transporters and transport processes	Expression and functions			References
	Substrates	In vivo	In vitro	
Blood-to-retina influx transport				
GLUT1	D-Glucose/Dehydroascorbic acid	+	TR-iBRB Isolated retinal capillary	[5, 13, 14, 43, 47]
MCT1	L-Lactic acid	+	TR-iBRB	[6, 44, 55]
CRT	Creatine	+	TR-iBRB	[25]
LAT1/4F2hc (system L)	Large neutral amino acids	+	TR-iBRB	[7, 26]
xCT/4F2hc (system X _c ⁻)	L-Cystine	ND	TR-iBRB	[46]
TAUT	Taurine	RUI	TR-iBRB	[7, 56]
ENT2	Nucleosides	RUI	TR-iBRB	[27]
Retina-to-blood efflux transport				
P-Glycoprotein (mdr 1a)	Cyclosporin A and others	+	TR-iBRB	[14, 19, 45, 53, 54]
Oatp1a4	E17βG and organic anions	+	ND	[8, 19, 40]
Oatp1c1	Organic anions	ex vivo	ND	[19]
PAH efflux transport	<i>p</i> -Aminohippuric acid	ND	Isolated retinal capillary	[13]

+: Immunohistochemical study; ND: not determined; GLUT1: facilitative glucose transporter; MCT1: monocarboxylate transporter; CRT: creatine transporter; LAT1: L-type amino acid transporter; TAUT: taurine transporter; ENT: equilibrative nucleoside transporter; Oatp: organic anion-transporting polypeptide; PAH: *p*-aminohippuric acid; RUI: retinal uptake index; TR-iBRB: rat retinal capillary endothelial cells.

GSH synthesis. GLUT1 transports dehydroascorbic acid, an oxidized form of vitamin C, to supply the retina with ascorbic acid [47].

LAT1 at the inner BRB could be useful for drug delivery into the retina. L-Dopa is the most widely used drug for Parkinson's disease, since L-Dopa and its metabolite, 3-O-methyldopa, are able to be transported via LAT1 at the BBB [48]. Many patients with Parkinson's disease have blurred vision or other visual disturbances, which are reflected in the reduced retinal dopamine concentration and the delay of visual evoked potentials [49]. L-Dopa administration reduces the delay of visual evoked potentials in Parkinson's disease [50]. In addition to L-Dopa, amino acid mimetic-drugs, such as melphalan, gabapentin, and baclofen, are substrates of LAT1 and are transported to the brain via LAT1 at the BBB [51]. Therefore, it appears that LAT1 at the inner BRB plays a key role in transporting amino acid mimetic-drugs from the circulating blood to the retina and contributes to their pharmacological actions in the retina.

14.6.2. Retina-to-Blood Efflux Transport

The inner BRB plays a role in acting not only as a structural barrier to regulate the passive diffusion of hydrophilic compounds but also as an efflux pump involved in the retina-to-blood efflux transport of hydrophobic xenobiotics and neurotransmitter metabolites in the retina as a detoxifying system. P-Glycoprotein, which is an ATP-dependent 170 kDa membrane glycoprotein, exhibits a protective role by restricting the entry of a wide variety of chemotherapeutic agents and hydrophobic compounds in tumor cells as well as normal tissues [52]. When cyclosporine A (CsA) is orally administered to the rabbit at a dose of 20 mg/kg per day, no CsA is detected in the intraocular tissues, although the blood level of CsA achieved is within the therapeutic window of 400–600 ng/mL [53]. This suggests that P-glycoprotein at the blood–ocular barrier acts as an efflux pump for hydrophobic drugs (e.g., CsA and quinidine) [53, 54]. In support of this functional evidence, immunofluorescence studies have shown that P-glycoprotein is present in rat retinal capillary endothelial cells [1, 45].

Betz and Goldstein demonstrated that PAH uptake by isolated retinal capillaries was slightly greater than that of the extracellular marker sucrose and inhibited by fluorescein and penicillin [13]. These results suggest that the OAT family or other organic anion transport process (e.g., MRP) are present at the inner BRB in addition to Oatp1a4, since PAH is not a substrate of the Oatp family [35, 36]. The expression and functions of the OAT and MRP families at the inner BRB remain largely unknown at present and there is a need to investigate the efflux transport mechanisms of these substrates, since drugs, hormones, and neurotransmitters are mostly metabolized in the form of organic anions (which are substrates of the OAT and MRP families).

14.7. Conclusions

The experimental methods for evaluating the BRB transport *in vivo* and the ocular pharmacokinetics of systemic drug administration are relatively straightforward and have been in use for over two decades. Overall, they are useful as a guide for the selection of drug candidates for the treatment of retinal diseases. With the combined use of conventional *in vivo* methods and newly developed

in vitro and ex vivo methods, we can identify the transport mechanisms in operation and the responsible transporters. As more information becomes available regarding inner BRB transport, we may be able to design simpler and more effective routes for drug delivery to the retina and, consequently, improve the treatment of retinal diseases.

Acknowledgments: This work was supported, in part, by a Grant-in-Aid for Scientific Research from the Japan Society for the Promotion of Science and a grant for Research on Sensory and Communicative Disorders by the Ministry of Health, Labor and Welfare, Japan. The authors thank Drs. T. Terasaki, S. Ohtsuki, M. Obinata, M. Ueda, K. Katayama, T. Kondo, and M. Tachikawa and Messrs. T. Funaki, H. Abukawa, A. Minamizono, T. Nakashima, M. Mori, K. Nagase, and Y. Ohshima for their insights and contributions to ongoing research in the authors' laboratory.

References

1. K. Hosoya and M. Tomi. Advances in the cell biology of transport via the inner blood-retinal barrier: Establishment of cell lines and transport functions. *Biol. Pharm. Bull.* **28**:1–8 (2005).
2. J. G. Cunha-Vaz. The blood-retinal barriers system. Basic concepts and clinical evaluation. *Exp. Eye Res.* **78**:715–721 (2004).
3. A. Harris, D. P. Bingaman, T. A. Ciulla, and B. J. Martin. Retina and choroidal blood flow in health and disease. In S. J. Ryan (ed.), *Retina 3rd Edition*, Mosby, St. Louis, 2001, pp. 68–88.
4. A. Alm and P. Törnquist. The uptake index method applied to studies on the blood-retinal barrier. I. A methodological study. *Acta Physiol. Scand.* **113**:73–79 (1981).
5. A. Alm, P. Törnquist, and O. Mäepea. The uptake index method applied to studies on the blood-retinal barrier. II. Transport of several hexoses by a common carrier. *Acta Physiol. Scand.* **113**:81–84 (1981).
6. A. Alm and P. Törnquist. Lactate transport through the blood-retinal and the blood-brain barrier in rats. *Ophthalmic. Res.* **17**:181–184 (1985).
7. P. Törnquist and A. Alm. Carrier-mediated transport of amino acids through the blood-retinal and the blood-brain barriers. *Graefes Arch. Clin. Exp. Ophthalmol.* **224**:21–25 (1986).
8. K. Katayama, Y. Ohshima, M. Tomi, and K. Hosoya. Application of microdialysis to evaluate the efflux transport of estradiol 17- β glucuronide across the rat blood-retinal barrier. *J. Neurosci. Methods* **156**:249–256 (2006).
9. J. C. Zech, I. Pouvreau, A. Cotinet, O. Goureau, B. Le Varlet, and Y. de Kozak. Effect of cytokines and nitric oxide on tight junctions in cultured rat retinal pigment epithelium. *Invest. Ophthalmol. Vis. Sci.* **39**:1600–1608 (1998).
10. S. Peng, C. Rahner, and L. J. Rizzolo. Apical and basal regulation of the permeability of the retinal pigment epithelium. *Invest. Ophthalmol. Vis. Sci.* **44**:808–817 (2003).
11. T. Nakanishi, T. Hatanaka, W. Huang, P. D. Prasad, F. H. Leibach, M. E. Ganapathy, and V. Ganapathy. Na⁺- and Cl⁻-coupled active transport of carnitine by the amino acid transporter ATB(0,+)₁ from mouse colon expressed in HRPE cells and Xenopus oocytes. *J. Physiol.* **532**:297–304 (2001).
12. K. C. Dunn, A. E. Aotaki-Keen, F. R. Putkey, and L. M. Hjelmeland. ARPE-19, a human retinal pigment epithelial cell line with differentiated properties. *Exp. Eye Res.* **62**:155–169 (1996).
13. A. L. Betz and G. W. Goldstein. Transport of hexoses, potassium and neutral amino acids into capillaries isolated from bovine retina. *Exp. Eye Res.* **30**:593–605 (1980).

14. K. Hosoya, M. Tomi, S. Ohtsuki, H. Takanaga, M. Ueda, N. Yanai, M. Obinata, and T. Terasaki. Conditionally immortalized retinal capillary endothelial cell lines (TR-iBRB) expressing differentiated endothelial cell functions derived from a transgenic rat. *Exp. Eye Res.* **72**:163–172 (2001).
15. M. Tomi, T. Funaki, H. Abukawa, K. Katayama, T. Kondo, S. Ohtsuki, M. Ueda, M. Obinata, T. Terasaki, and K. Hosoya. Expression and regulation of L-cystine transporter, system X_c^- , in the newly developed rat retinal Müller cell line (TR-MUL). *Glia* **43**:208–217 (2003).
16. T. Kondo, K. Hosoya, S. Hori, M. Tomi, S. Ohtsuki, H. Takanaga, E. Nakashima, H. Iizasa, T. Asashima, M. Ueda, M. Obinata, and T. Terasaki. Establishment of conditionally immortalized rat retinal pericyte cell lines (TR-rPCT) and their application in a co-culture system using retinal capillary endothelial cell line (TR-iBRB2). *Cell Struct. Funct.* **28**:145–153 (2003).
17. T. Nakashima, M. Tomi, M. Tachikawa, M. Watanabe, T. Terasaki, and K. Hosoya. Evidence for creatine biosynthesis in Müller glia. *Glia* **52**:47–52 (2005).
18. T. Kondo, K. Hosoya, S. Hori, M. Tomi, S. Ohtsuki, and T. Terasaki. PKC/MAPK signaling suppression by retinal pericyte conditioned medium prevents retinal endothelial cell proliferation. *J. Cell. Physiol.* **203**:378–386 (2005).
19. M. Tomi and K. Hosoya. Application of magnetically isolated rat retinal vascular endothelial cells for the determination of transporter gene expression levels at the inner blood-retinal barrier. *J. Neurochem.* **91**:1244–1248 (2004).
20. R. Takahashi, M. Hirabayashi, N. Yanai, M. Obinata, and M. Ueda. Establishment of SV40-tsA58 transgenic rats as a source of conditionally immortalized cell lines. *Exp. Anim.* **48**:255–261 (1999).
21. T. Terasaki, S. Ohtsuki, S. Hori, H. Takanaga, E. Nakashima, and K. Hosoya. New approaches to in vitro models of the blood-brain barrier drug transport. *Drug Discov. Today* **8**:944–954 (2003).
22. K. Hosoya, M. Tomi, M. Takayama, Y. Komokata, D. Nakai, T. Tokui, K. Nishimura, M. Ueda, M. Obinata, S. Hori, S. Ohtsuki, G. L. Amidon, and T. Terasaki. Transporter mRNA expression in a conditionally immortalized rat small intestine epithelial cell line (TR-SIE). *Drug Metabol. Pharmacokinet.* **19**:264–269 (2004).
23. M. Matsuo, K. Koizumi, S. Yamada, M. Tomi, R. Takahashi, M. Ueda, T. Terasaki, M. Obinata, K. Hosoya, O. Ohtani, and I. Saiki. Establishment and characterization of conditionally immortalized endothelial cell lines from the thoracic duct and inferior vena cava of tsA58/EGFP double-transgenic rats. *Cell Tissue Res.* **326**:749–758 (2006).
24. M. Obinata. Possible applications of conditionally immortalized tissue cell lines with differentiation functions. *Biochem. Biophys. Res. Commun.* **286**:667–672 (2001).
25. T. Nakashima, M. Tomi, K. Katayama, M. Tachikawa, M. Watanabe, T. Terasaki, and K. Hosoya. Blood-to-retina transport of creatine via creatine transporter (CRT) at the rat inner blood-retinal barrier. *J. Neurochem.* **89**:1454–1461 (2004).
26. M. Tomi, M. Mori, M. Tachikawa, K. Katayama, T. Terasaki, and K. Hosoya. L-Type amino acid transporter 1 (LAT1)-mediated L-leucine transport at the inner blood-retinal barrier. *Invest. Ophthalmol. Vis. Sci.* **46**:2522–2530 (2005).
27. K. Nagase, M. Tomi, M. Tachikawa, and K. Hosoya. Functional and molecular characterization of adenosine transport at the rat inner blood-retinal barrier. *Biochim. Biophys. Acta* **1758**:13–19 (2006).
28. S. L. Lightman, A. G. Palestine, S. I. Rapoport, and E. Rechthand. Quantitative assessment of the permeability of the rat blood-retinal barrier to small water-soluble non-electrolytes. *J. Physiol.* **389**:483–490 (1987).

29. W. M. Pardridge, E. M. Landaw, L. P. Miller, L. D. Braun, and W. H. Oldendorf. Carotid artery injection technique: Bounds for bolus mixing by plasma and by brain. *J. Cereb. Blood Flow Metab.* **5**:576–583 (1985).
30. J. G. Cunha-Vaz and D. Maurice. Fluorescein dynamics in the eye. *Doc. Ophthalmol.* **26**:61–72 (1969).
31. C. B. Engler, B. Sander, M. Larsen, P. Koefoed, H. H. Parving, and H. Lund-Andersen. Probenecid inhibition of the outward transport of fluorescein across the human blood-retina barrier. *Acta Ophthalmol.* **72**:663–667 (1994).
32. S. Macha and A. K. Mitra. Ocular pharmacokinetics in rabbits using a novel dual probe microdialysis technique. *Exp. Eye Res.* **72**:289–299 (2001).
33. P. Louzada-Junior, J. J. Dias, W. F. Santos, J. J. Lachat, H. F. Bradford, and J. Coutinho-Netto. Glutamate release in experimental ischaemia of the retina: An approach using microdialysis. *J. Neurochem.* **59**:358–363 (1992).
34. D. V. Pow. Amino acids and their transporters in the retina. *Neurochem. Int.* **38**:463–484 (2001).
35. C. Reichel, B. Gao, J. Van Montfoort, V. Cattori, C. Rahner, B. Hagenbuch, B. Stieger, T. Kamisako, and P. J. Meier. Localization and function of the organic anion-transporting polypeptide Oatp2 in rat liver. *Gastroenterology* **117**:688–695 (1999).
36. T. Sekine, S. H. Cha, and H. Endou. The multispecific organic anion transporter (OAT) family. *Pflügers Arch.* **440**:337–350 (2000).
37. B. Noé, B. Hagenbuch, B. Stieger, and P. J. Meier. Isolation of a multispecific organic anion and cardiac glycoside transporter from rat brain. *Proc. Natl. Acad. Sci. USA* **94**:10346–10350 (1997).
38. P. D. Bowman, A. L. Betz, and G. W. Goldstein. Primary culture of microvascular endothelial cells from bovine retina: Selective growth using fibronectin coated substrate and plasma derived serum. *In Vitro* **18**:626–632 (1982).
39. X. Su, C. M. Sorenson, and N. Sheibani. Isolation and characterization of murine retinal endothelial cells. *Mol. Vis.* **9**:171–178 (2003).
40. B. Gao, A. Wenzel, C. Grimm, S. R. Vavricka, D. Benke, P. J. Meier, and C. E. Reme. Localization of organic anion transport protein 2 in the apical region of rat retinal pigment epithelium. *Invest. Ophthalmol. Vis. Sci.* **43**:510–514 (2002).
41. J. Y. Li, R. J. Boado, and W. M. Pardridge. Blood-brain barrier genomics. *J. Cereb. Blood Flow Metab.* **21**:61–68 (2001).
42. D. Sugiyama, H. Kusuhara, H. Taniguchi, S. Ishikawa, Y. Nozaki, H. Aburatani, and Y. Sugiyama. Functional characterization of rat brain-specific organic anion transporter (Oatp14) at the blood-brain barrier: High affinity transporter for thyroxine. *J. Biol. Chem.* **278**:43489–43495 (2003).
43. K. Takata, T. Kasahara, M. Kasahara, O. Ezaki, and H. Hirano. Ultracytochemical localization of the erythrocyte/HepG2-type glucose transporter (GLUT1) in cells of the blood-retinal barrier in the rat. *Invest. Ophthalmol. Vis. Sci.* **33**:377–383 (1992).
44. D. Z. Gerhart, R. L. Leino, and L. R. Drewes. Distribution of monocarboxylate transporters MCT1 and MCT2 in rat retina. *Neuroscience* **92**:367–375 (1999).
45. J. A. Holash and P. A. Stewart. The relationship of astrocyte-like cells to the vessels that contribute to the blood-ocular barriers. *Brain Res.* **629**:218–224 (1993).
46. M. Tomi, K. Hosoya, H. Takanaga, S. Ohtsuki, and T. Terasaki. Induction of the xCT gene expression and L-cystine transport activity by diethyl maleate at the inner blood-retinal barrier. *Invest. Ophthalmol. Vis. Sci.* **43**:774–779 (2002).
47. K. Hosoya, A. Minamizono, K. Katayama, T. Terasaki, and M. Tomi. Vitamin C transport in oxidized form across the rat blood-retinal barrier. *Invest. Ophthalmol. Vis. Sci.* **45**:1232–1239 (2004).

48. T. Kageyama, M. Nakamura, A. Matsuo, Y. Yamasaki, Y. Takakura, M. Hashida, Y. Kanai, M. Naito, T. Tsuruo, N. Minato, and S. Shimohama. The 4F2hc/LAT1 complex transports L-DOPA across the blood-brain barrier. *Brain Res.* **879**:115–121 (2000).
49. I. Bodis-Wollner. Visual electrophysiology in Parkinson's disease: PERG, VEP and visual P300. *Clin. Electroencephalogr.* **28**:143–147 (1997).
50. P. A. Bhaskar, S. Vanchilingam, E. A. Bhaskar, A. Devaprabhu, and R. A. Ganesan. Effect of L-dopa on visual evoked potential in patients with Parkinson's disease. *Neurology* **36**:1119–1121 (1986).
51. H. Uchino, Y. Kanai, K. Kim do, M. F. Wempe, A. Chairoungdua, E. Morimoto, M. W. Anders, and H. Endou. Transport of amino acid-related compounds mediated by L-type amino acid transporter 1 (LAT1): Insights into the mechanisms of substrate recognition. *Mol. Pharmacol.* **61**:729–737 (2002).
52. S. V. Ambudkar, C. Kimchi-Sarfaty, Z. E. Sauna, and M. M. Gottesman. P-glycoprotein: From genomics to mechanism. *Oncogene* **22**:7468–7485 (2003).
53. D. BenEzra and G. Maftzir. Ocular penetration of cyclosporin A. The rabbit eye. *Invest. Ophthalmol. Vis. Sci.* **31**:1362–1366 (1990).
54. S. Duvvuri, M. D. Gandhi, and A. K. Mitra. Effect of P-glycoprotein on the ocular disposition of a model substrate, quinidine. *Curr. Eye Res.* **27**:345–353 (2003).
55. K. Hosoya, T. Kondo, M. Tomi, H. Takanaga, S. Ohtsuki, and T. Terasaki. MCT1-mediated transport of L-lactic acid at the inner blood-retinal barrier: A possible route for delivery of monocarboxylic acid drugs to the retina. *Pharm. Res.* **18**:1669–1676 (2001).
56. M. Tomi, T. Terayama, T. Isobe, F. Egami, A. Morito, M. Kurachi, S. Ohtsuki, Y. S. Kang, T. Terasaki, and K. Hosoya. Function and regulation of taurine transport at the inner blood-retinal barrier. *Microvasc. Res.* **73**:100–106 (2007).

Regulation of Paracellular Permeability in Low-Resistance Human Vaginal-Cervical Epithelia

George I. Gorodeski

Abstract The paracellular (intercellular) route is the main transepithelial transport pathway in low-resistance secretory (and absorptive) epithelia, and is composed of the tight junctional resistance (R_{TJ}) and the resistance of the lateral intercellular space (R_{LIS}). Recent studies in human vaginal-cervical epithelia revealed novel mechanisms of regulation of the paracellular resistance (R_{PCR}), including both the R_{TJ} and the R_{LIS} . Steroid hormones and particularly estrogens have been shown to regulate assembled tight junctions as well as the cortical acto-myosin ring, which determine epithelial cell deformability and the R_{LIS} . The knowledge gained from these studies on the molecular mechanisms involved may improve the understanding of dysregulation of water and solutes, and related diseases. The data may be also used in future clinical trials to improve topical drug delivery via the vaginal route in women.

Keywords: Transepithelial; Transport; Tight junction; Lateral intercellular space; Estrogen; ATP; Calcium

Abbreviations

ADP	Adenosine diphosphate
AE	Acid ($\text{Cl}^-/\text{HCO}_3^-$) exchanger
ATP	Adenosine triphosphate
ATPase	Adenosine triphosphatase
ATP _o	Extracellular ATP level
Ca _o	Extracellular calcium level
cGMP	Cyclic guanosine monophosphate
CK2	Casein kinase II
diC8	sn-1,2-Dioctanoyl diglyceride
EGF	Epidermal growth factor
EGFR	Epidermal growth factor receptor
eNOS	Endothelium-type nitric oxide
ER α	Estrogen receptor α
ERK	Extracellular signal-regulated kinase
JAM	Junctional adherence molecules
MAPK	Mitogen-activated protein kinase

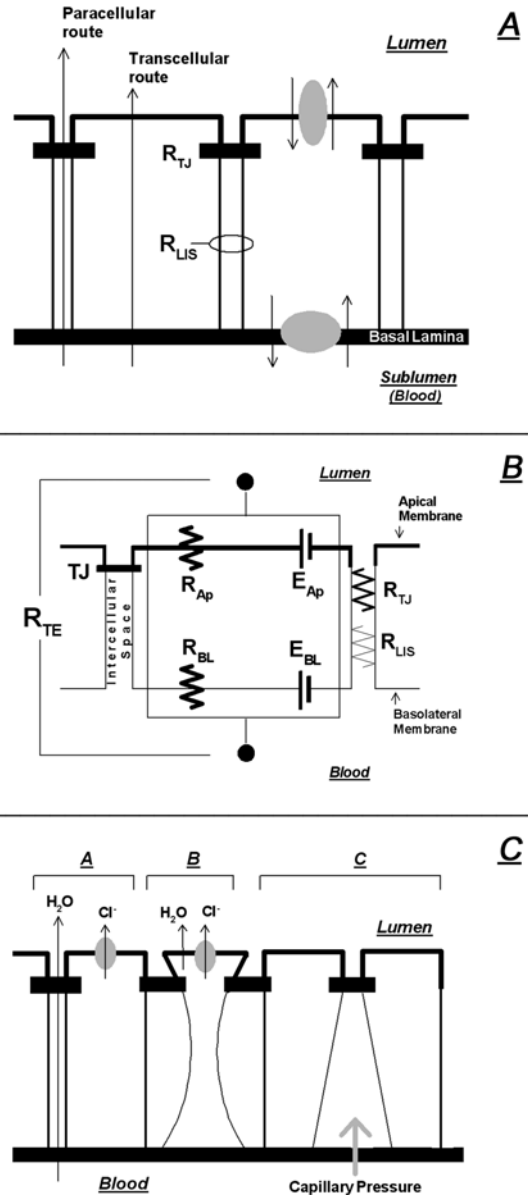
MCT	Monocarboxylate transporter
MgATPase	Magnesium ATPase
MMP-7	Matrix metalloproteinase 7
mRNA	Messenger ribonucleic acid
Na ⁺ /K ⁺ -ATPase	Sodium/Potassium ATPase
NBC	Na ⁺ /HCO ₃ ⁻ co-transporter
NHE	Na ⁺ /H ⁺ exchangers
NMM-IIB	Non-muscle myosin IIB
NO	Nitric oxide
PKC	Protein kinase C
PKG	cGMP-dependent protein kinase
RhoA-p160	ROCK Rho-associated coiled coil-forming protein kinase
<i>R</i> _{LIS}	Resistance of the lateral intercellular space
<i>R</i> _{PCR}	Paracellular resistance
<i>R</i> _{PM}	Resistance of the plasma membranes
<i>R</i> _{TE}	Transepithelial resistance
<i>R</i> _{TJ}	Tight junctional resistance
TJ	Tight junctions
V-ATPase	Vesicular ATPase
ZO-1	Zonula occludens protein 1

15.1. Introduction

One of the main functions of epithelia is to control water and solutes, compartmentalized by the regulation of transport across the epithelium from body interior to exterior (or vice versa). Deviations from the meticulously regulated movement of water and solutes across the epithelial barrier can lead to states of disease and can be detrimental to life. Fluids can traverse epithelia by one of two routes: through the cells (transcellular transport) or between cells (intercellular or paracellular transport) (Figure 15.1A).

Most of previous studies investigated regulation of transport in high-resistance epithelia. This chapter provides an overview of mechanisms that control and regulate the paracellular permeability in low-resistance (“leaky”) secretory epithelia. Until recently this topic was relatively unexplored, because experimental systems displaying high-baseline permeability were considered artifactual. Based on publications from the author’s lab using the model of cultured human vaginal-cervical epithelia [1–45], which were confirmed independently by others [46–56], it is now realized that some epithelia form low-resistance barriers naturally. These leaky epithelia do control free movement of water and solutes, but they differ from high-resistance epithelia in that they exhibit specialized mechanisms that regulate the paracellular permeability. Studies using low-resistance epithelia have shown that the cells can respond to stimuli that induce acute and reversible changes in the gating properties of the epithelium. These novel data refute the dogma that epithelia form rigid fenced-like structures, and highlight mechanisms and signaling pathways that may be important in vivo for hormonal regulation of water and ion transport.

Figure 15.1 (A) Schema of cross section of a secretory epithelium (shown are four cells). Tight junctions (TJ), part of the apical junctional complex are shown as solid bars. Transepithelial transport from the subluminal compartment (blood or exterior) into the luminal compartment (lumen or exterior) occurs either through the cells (transcellular transport) or between cells (intercellular [paracellular] transport). Paracellular transport is controlled by the resistance of the tight junctions (R_{TJ}) and the resistance of the lateral intercellular space (R_{LIS}). The tight junctions also sort membrane proteins, including ion transporters (shown in grey) into basolateral and apical (thicker lines) domains of the plasma membrane. (B) The Ussing-Zerahn model of transepithelial transport. R_{TE} —transepithelial resistance. R_A and R_B are resistances of the apical and basolateral membranes, which face the respective luminal and subluminal compartments. R_{TJ} is the tight junctional (TJ) resistance. R_{LIS} is the resistance of the lateral intercellular space. E_A and E_B represent electromotive forces across apical and basolateral membranes, respectively, of ion transport mechanisms that utilize energy to secrete (or absorb) ions against electrochemical gradients. The R_{TE} is modeled by two parallel groups of resistors, so that $1/R_{TE} = 1/(R_A + R_B) + 1/(R_{TJ} + R_{LIS})$. Since the resistance across the plasma membrane is high ($\sim 2 \text{ G}\Omega$), in leaky epithelia $1/R_{TE} \approx 1/(R_{TJ} + R_{LIS})$, indicating that the paracellular pathway becomes the higher conductive route. (C) Regulation of paracellular transport in secretory epithelia. *Panel A*: Apical ion secretion by the cells (e.g., Cl^-) draws movement of water (and Na^+ [not shown], to compensate for charge and resultant local osmotic imbalance) from the blood through the paracellular route and into the lumen. *Panel B*: Apical ion plus water secretion results in temporary cell shrinkage. *Panel C*: Transepithelial hydrostatic gradients dilate the lateral intercellular space near its basolateral end.



15.2. The Ussing-Zerahn Model of Transepithelial Fluid Transport

The theoretical model that best describes regulation of transepithelial transport is derived from the Ussing-Zerahn equivalent electrical circuit model of ion transport theory [57] (Figure 15.1B). The model predicts that epithelia are organized as a layer(s) of confluent cells, where plasma membranes of neighboring cells come into close contact and functionally occlude the intercellular space. Accordingly, molecules can move across epithelia either through the cells

(transcellular route) or between cells via the intercellular space (paracellular route) (Figures 15.1A, B). The Ussing-Zerah model describes total transepithelial resistance (R_{TE}) in terms of the resistance of the plasma membranes (R_{PM}) and the paracellular resistance (R_{PCR}), in parallel, so that $1/R_{TE} = 1/R_{PM} + 1/R_{PCR}$ (Figure 15.1B). Usually, R_{PM} is larger than R_{PCR} (by about 10^5 [58]), and $R_{TE} \approx R_{PCR}$. The Ussing-Zerah model predicts that the total R_{TE} is reflected in most part by R_{PCR} . This probably applies to most types of epithelia, and in particular leaky types of epithelia. However, exceptions exist such as the salivary epithelium which exhibits low-transcellular resistance compared to R_{PCR} [58a], and the toad urinary bladder where the measured overall resistance is lower than the tight junctional resistance (R_{TJ}), suggesting that the overall resistance probably is governed more by the transcellular resistance [58b].

R_{PCR} is determined by R_{TJ} and by the resistance of the lateral intercellular space (R_{LIS}) in series, that is, $R_{PCR} = R_{TJ} + R_{LIS}$, and therefore in most types of epithelia $R_{TE} \approx R_{TJ} + R_{LIS}$. Tight epithelia are characterized by a commensurably large R_{TJ} , while R_{LIS} plays a relatively small role in R_{PCR} . In contrast, in leaky types of epithelia, such as the cervical epithelium [1], R_{LIS} may contribute significantly to the total R_{PCR} . R_{TJ} is determined by the tight junctional complexes that are usually located at apical regions of the cells (facing the lumen) above the zonula adherence and desmosomes. The tight junctions extend in a belt-like manner around the perimeter of each epithelial cell and connect neighboring cells, and they include domains where plasma membranes of neighboring cells come into direct contact.

Tight junctions serve as a fence, contributing to the polarized organization of the epithelium. Apical and basolateral cell membranes are segregated at the tight junctions which function as a fence between the apical and basolateral cell membranes and prevent the intermixing of apical and basolateral lipid bilayers that are endowed with different ion transport processes (including channels and pumps). As a result, appropriate sorting/targeting of various proteins at each cell membrane can be achieved (Figure 15.1C). Another important function of tight junctions is the segregation or gating of movement (transport) of cations and anions (and water as well to a certain extent). This function depends, in part, on the selective localization of ion transporters in the apical or basolateral aspects of the plasma membrane (Figures 15.1C and 15.2).

The complex arrangement of ion transporters in human vaginal-ectocervical epithelial cells (modified from references [1, 21] and Gorodeski, unpublished data) is shown in Figure 15.2. The basolateral Na^+/K^+ -adenosine triphosphatase (ATPase), K^+ channel, and $\text{Na}^+/\text{K}^+/2\text{Cl}^-$ co-transporter as well as apical Cl^- channel control plasma membrane potential and regulate intracellular Na^+ , Cl^- , and H_2O homeostasis. The cells acidify the lumen through active H^+ secretion via an apical vesicular ATPase (V-ATPase) where the accompanying anions are lactate⁻ (a majority) and Cl^- . The mechanism of lactate⁻ secretion is not well understood. Lactate⁻ secretion can be driven by an apical electroneutral lactate⁻/ Cl^- exchanger [59, 60], where extrusion of Cl^- via the apical Cl^- channels will suffice to maintain the steady-state level of intracellular Cl^- . Lactate⁻ secretion may also be driven by an apical electroneutral $\text{H}^+/\text{lactate}^-$ co-transporter or by an apical electrogenic lactate⁻ transporter (not shown in the figure). Cl^- secretion is probably both electrogenic (via apical Cl^- channels) and passive Cl^- diffusion via the paracellular pathway.

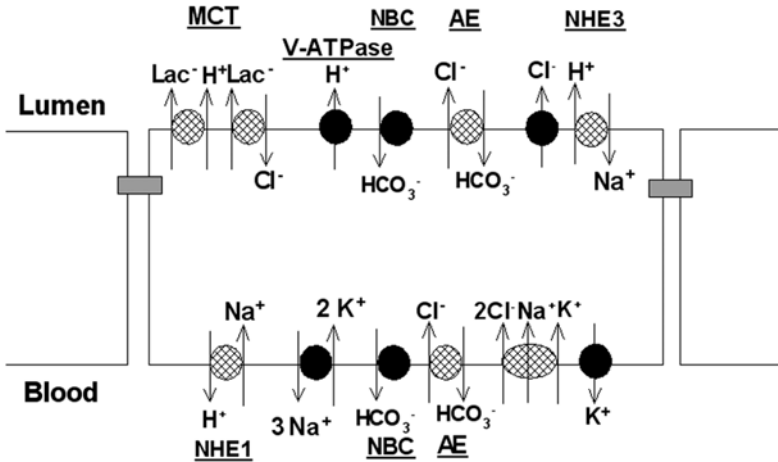


Figure 15.2 Ion transporters in human vaginal-ectocervical epithelial cells, sorted into the apical and basolateral domains of the plasma membrane. Black solid symbols depict electrogenic transporters; hatched symbols depict electroneutral transporters. Squares are tight junctions. MCT— monocarboxylate transporter; NBC— $\text{Na}^+/\text{HCO}_3^-$ co-transporter; AE—acid ($\text{Cl}^-/\text{HCO}_3^-$) exchanger; NHE (types 1 or 3)— Na^+/H^+ exchangers.

Cellular Cl^- replenishment is maintained by a basolateral anion-exchanger (Cl^-/OH^- or $\text{Cl}^-/\text{HCO}_3^-$) or via the $\text{Na}^+/\text{K}^+/2\text{Cl}^-$ co-transporter, whose activities are closely tied synergistically through action of Na^+/K^+ -ATPase, K^+ channels, and the $\text{HCO}_3^-/\text{Na}^+$ co-transporter (with a 3:1 stoichiometry) that extrudes HCO_3^- [61]. Passive Cl^- diffusion through the paracellular pathway can occur because of the greater mobility of Cl^- than Na^+ in the paracellular space (≈ 1.3) [13]. Electroneutrality is maintained by transcellular Na^+ transport in the luminal to subluminal direction, accomplished by both the apical Na^+/H^+ exchanger (NHE-3) and a basolateral $\text{HCO}_3^-/\text{Na}^+$ co-transporter (with a 3:1 stoichiometry).

The main function of the tight junctions, however, is to occlude the intercellular space and restrict free movement of water, ions, and hydrophilic molecules. The microscopic structure of tight junctions was elaborated by the electron-microscopy freeze-fracture technique. The technique employs chemically fixed cells in liquid nitrogen in the presence of a cryoprotectant. The frozen specimen is then cracked, and the fracture plane which usually passes through the hydrophobic center of lipid bilayers produces two fracture surfaces: one on the exterior leaflet (exoplasmic fracture face, or E-face) and the other on the interior leaflet (the protoplasmic fracture face, P-face). Electron microscopy of epithelia subjected to freeze-fracture procedures showed that regions of the tight junction are those where plasma membranes of neighboring cells come into direct contact. At those sites, the tight junctions appear as continuous anastomosing intramembranous strands on the P-face, with complementary grooves on the E-face [62–70]. The studies also showed that the intramembranous particles interact with or extend to particles that reside in the extracellular space, and the latter form long branching fibrils that circumscribe the cell. These were defined in terms of functionality as the tight junction elements (or units).

Biochemical studies have shown that tight junctions are composed of an array of tight junctional proteins, which include cytoplasmic and transmembrane proteins [21]. Cytoplasmic tight junctional proteins couple the transmembrane tight junctional proteins to the cortical actin, mediating signal-dependent modifications of R_{TJ} [71]. Transmembrane tight junctional proteins, including the junctional adherence molecules (JAM, present mainly in endothelial cells [72, 73]), claudins [74–79], and occludins [80, 81] are thought to represent linear polymers of transmembrane proteins with extracellular stretches. It is believed that the latter groups of proteins associate laterally with members of the same protein family in the apposing membrane of adjacent cells to “seal” the intercellular space. Recent reviews described in detail the structure of tight junctional proteins [82–87].

While the regions of the tight junction are considered to be a highly resistive element, R_{LIS} is considered to have a low resistance. The *lateral intercellular space* can be modeled as an element governed by Poiseuille law, consisting of a series of narrow tubes. In this model, the resistance of each tube depends on the length of the intercellular space from the tight junction to basal lamina (i.e., the height of epithelial cells) as well as is inversely proportional to the fourth power of the intercellular width (i.e., the radius of the tube). The latter parameter is determined by the proximity of plasma membranes of neighboring cells and intercellular digitations [88], indicating that even minor perturbations of the cell membrane at the lateral intercellular border can markedly affect the R_{LIS} .

15.3. Regulation of Paracellular Transport Across Secretory Epithelia

Secretory epithelia control transport of water and solutes from the subluminal compartment (blood) into the lumen or body exterior. At present, there is no single unifying model for transepithelial fluid or water transport. In some epithelia, transcellular routes of fluid transport via water channels may predominate [88a]. However, in other types of epithelia, such as the cervical-vaginal epithelia, transport of fluids usually occurs via the paracellular route [1, 14]. In the latter, movement of fluid can be driven by three main mechanisms (Figure 15.1C):

- A. Ion or osmotic gradients that are created by active transcellular ion secretion [89], which drive water and other solutes (e.g., counter-ions) from the subluminal compartment (blood) into the lumen to compensate for the electrochemical gradients (Figure 15.1C, panel A). This mechanism may play a role in the vaginal-cervical epithelia, thereby contributing to lubrication of the vaginal-cervical canal. In the woman, the vaginal-cervical fluid is a mixture of water, water-insoluble components (mucins), and water-soluble components (vaginal-cervical plasma). The water-soluble components constitute 80–99% of the total weight of the vaginal-cervical plasma, and originate by transudation of fluid and solutes from the blood into the vaginal-cervical canal. In contrast, the mucins are secreted by exocytosis through the apical membrane [90]. Accumulation of mucins in the lumen

may generate an osmotic gradient in the luminal to subluminal direction that will draw water in the subluminal to luminal direction.

- B. Ion gradients can be created by active transcellular ion secretion followed by efflux of intracellular water, resulting in net cellular water loss and temporary cell shrinkage that is restored by ions and water influx (Figure 15.1C, panel B). This mechanism is activated primarily in response to acute stimuli. For instance, in human vaginal-cervical epithelia, agonists such as histamine, serotonin, or extracellular adenosine triphosphate (ATP) induce acute Cl^- secretion via apical Cl^- channels, followed by water loss and temporary cell shrinkage. The result would be an acute decrease in cell width which would reciprocally increase the volume of the lateral intercellular space and therefore decrease the R_{LIS} . The net effect would be decreased total R_{PCR} and increased transepithelial permeability. In the case of the vagina and cervix, this mechanism can be important for regulation of vaginal-cervical epithelial permeability by sperm cells during sperm migration [21].
- C. Transepithelial hydrostatic gradients in the subluminal to luminal direction are generated by the pressure of blood in the capillary bed (Figure 15.1C, panel C). Our understanding of this mechanism stems from the pioneering research of Spring and Hope [91] who showed that hydrostatic gradients in the subluminal to luminal direction induce fluid accumulation in the intercellular space at basolateral regions of the epithelium and dilate the intercellular space. The effect is limited to basolateral regions of the intercellular space, that is, those in proximity to the subluminal (the “blood” compartment) because of the near-apical location of the tight and adherence junctions, and the desmosomes, which prevent expansion of the intercellular space at near-apical domains. This mechanism explains how surface epithelia maintain lubrication of the lumen: blood pressure in the capillary bed generates a subluminal to luminal hydrostatic gradient that expands the basolateral intercellular space and decreases the R_{LIS} , allowing plasma transudation from the blood into lumen through the paracellular route. Similar to the mechanism described in Figure 15.1C, panel B, this mechanism also entails a change in the shape of epithelial cells and reciprocally an increase in the width of the intercellular space.

15.4. Regulation of Paracellular Permeability

Until recently, a commonly held view was that epithelial cells form rigid fence-like sheets, and that paracellular transport can be regulated only secondary to changes in the transport driving forces described above. An alternative hypothesis was that paracellular transport could be regulated through changes in paracellular permeability. However, most previous data were obtained using non-physiological perturbations or pathological conditions that resulted in disintegration of the epithelium [92]. Studies in cultured human vaginal-cervical epithelia used experimental conditions and drug concentrations in the physiological range for the woman, providing data of acute and chronic reversible changes in paracellular permeability that did not produce toxic effects to the cells. *Based on these data, it was suggested that regulation of paracellular*

permeability is a physiological mechanism in vivo for regulation of paracellular transport. Summarized below are novel data about regulation of the paracellular permeability, including effects on R_{TJ} and R_{LIS} .

15.5. Regulation of R_{TJ}

In the past, changes in R_{TJ} were viewed in terms of assembly/disassembly of the tight junctional complex (reviewed in 93). Recent studies in human vaginal-cervical epithelia have shown acute and reversible modulation of R_{TJ} that are the result of conformational changes in assembled tight junctions [13]. The examples presented below relate to effects of modulation of extracellular calcium level (Ca_o) and treatments with ATP.

15.5.1. Role of Ca_o

The dependence of R_{TJ} on Ca^{2+} is well established [13, 15, 19, 94–105]. Past studies looked at the effect of Ca^{2+} on R_{PCR} within hours after lowering Ca_o or after shifting cells back to normal Ca_o . Studies described the “calcium-switch,” whereby lowering Ca_o abrogates the R_{PCR} , and shifting cells back to normal Ca_o restores the resistance. These studies provided important information on (i) modulation of R_{PCR} secondary to changes in cytosolic calcium; (ii) modulation of the cytoskeleton and adherence junctions, leading to changes in cell configuration and intercellular adherence; and (iii) metabolic effects of calcium that affect synthesis, folding, and insertion of tight junctional proteins into the plasma membrane. However, the results of these studies cannot be explained in terms of direct modulation by calcium of tight junctional proteins at extracellular domains.

Studies in the low-resistance vaginal-cervical epithelia, in contrast, can be interpreted as direct regulation of R_{TJ} by calcium [13, 15, 19]. In these latter epithelia, lowering Ca_o decreases R_{TJ} acutely (half-time [$t_{1/2}$] of 2.5 min), and reversibly; the effect is dose-dependent and saturable with an EC_{50} of 0.3 mM for Ca_o ; the effects of Ca_o on R_{TJ} are not associated with changes in intracellular calcium [19]; lowering Ca_o does not affect messenger ribonucleic acid (mRNA) or protein levels of occludin and cellular distribution of occludin; within the time frame of calcium effects on R_{TJ} , lowering Ca_o has no effect on the tight junctional proteins (e.g., claudin-4 and zonula occludens protein 1 [ZO-1]) or adherence protein (e.g., E-Cadherin) [13, 15, 19]; and among tested di- and trivalent cations, only Mn^{2+} is found to have partial agonist characteristics of Ca_o , restoring R_{TJ} to near baseline levels [19]. Thus, the short time frame required for reversal of Ca_o effects rules out modulation of protein synthesis or assembly of tight junctional proteins as candidates for calcium action [97]. It is likely that Ca^{2+} interacts with extracellular sites of tight junctional protein(s) directly and induces conformational change that results in tighter occlusion of the intercellular space at the region of the tight junction.

These data on Ca_o effects observed in the low-resistance epithelia raised a question related to their physiological relevance, in light of the tight regulation of extracellular Ca^{2+} level at 1.2–1.5 mM range. The extracellular Ca^{2+} level at the cell surface is likely to vary because of the presence of cell surface or cell secreted Ca^{2+} -binding proteins [106, 107]. Therefore, the experimental EC_{50}

(0.3 mM) for Ca_o for changes in R_{TJ} in vaginal-cervical epithelia would be in the predicted Ca_o range at the cell surface.

The molecular mechanism of Ca_o effects on R_{TJ} of low-resistance epithelia is unknown, but it may involve direct modulation of extracellular domains of tight junctional proteins. In epithelial cells, including vaginal-cervical cells, the main transmembrane tight junctional proteins are the claudins and occludin. Claudins are four-transmembrane domain proteins exhibiting two short hydrophobic extracellular loops that possibly form homotypic or heterotypic interactions to connect adjacent cells and occludin also is similarly organized [71]. Human occludin is a 65-kDa protein with a predicted 65-amino acid N-terminus, two extracellular loops of 56 and 48 amino acids separated by an 11-amino acid cytosolic segment; four transmembrane stretches of 11–24 amino acids; and a C-terminus tail of 256 amino acids that interacts with the cytoplasmic tight junctional proteins (e.g., ZO-1) [81].

The claudins and occludin appear to have different biological roles. Claudins are the main building units of the tight junction, and confer the baseline gating properties of the intercellular space. Claudins regulate the R_{TJ} , in a manner mainly dependent on the density of the proteins, since cells expressing a greater density of claudins may generate high-resistance epithelia [107a]. The role of occludin as a tight junctional protein was until recently unclear, following publications that in some types of cells occludin is not sufficient to form an effective barrier [108, 109]. These latter studies stood in contrast to earlier studies showing that occludin is a necessary component of tight junctions [71, 110–117]. More recent studies in occludin-deficient mice suggest additional, previously unknown roles of occludin in the gastric epithelium and other types of epithelial tissues. Thus, in occludin-null mice, the tight junctions did not appear to be affected morphologically, and the barrier function of intestinal epithelium was normal as far as examined electrophysiologically. However, histological abnormalities were found in several tissues, that is, chronic inflammation and hyperplasia of the gastric epithelium, calcification in the brain, testicular atrophy, loss of cytoplasmic granules in striated duct cells of the salivary gland, and thinning of the compact bone [117a]. An additional study suggested a specific role for occludin in gastric epithelial differentiation [117b].

In human vaginal-cervical epithelia, occludin appears to play a significant role in the regulation of R_{TJ} . In the vaginal-cervical epithelia, occludin is present in two forms: the full length 65-kDa isoform and a truncated 50-kDa isoform [35, 43]. A shift from 65 kDa to 50 kDa dominance is associated with abrogation of R_{TJ} [35, 43], suggesting that in low-resistance epithelia, occludin plays an important role in R_{TJ} .

The prevailing theory of underlying mechanisms afforded by claudin and occludin for modulating properties of solute transport (including water, ions, and hydrophilic non-electrolytes) via the intercellular space is best illustrated by the organization of tight junctions. According to this model, the extracellular loops of transmembrane tight junctional proteins (e.g., claudins and occludin) of neighboring cells are predicted to come into direct contact and form either homotypic (i.e., occludin/occludin or interactions between same isoforms of claudins such as claudin-1/claudin-1) or heterotypic (e.g., claudin-1/claudin-5) contacts (Figure 15.3). These contacts made by the hydrophobic segments of the extracellular loops form intercellular bridges that impede the free movement of water through the paracellular space.

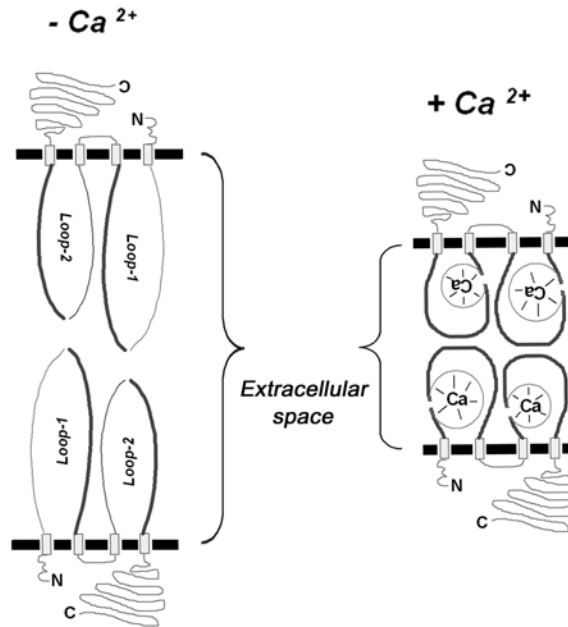


Figure 15.3 A novel Ca^{2+} -mediated regulation model of occludin-based occlusion of the tight junction [118]. The figure shows homotypic occludin–occludin contacts made by four extracellular loops of two occludin molecules shared by two neighboring cells (one in the top of the figure and the other at the bottom part of the figure). The horizontal thick lines are the plasma membranes of the two cells, and the space delineated by the plasma membranes is the extracellular space. Occludin is a tetra-span transmembrane protein that is found in the regions of tight junctions. Occludin extracellular loops (loops 1 and 2) are each composed of a proximal Ca^{2+} -binding segment (thin lines in Figure 15.3), and a distal segment (thick lines in Figure 15.3) composed of a hydrophobic stretch [118]. In the absence of Ca^{2+} the loops are in a relaxed stretched mode (left panel, Figure 15.3) that results in low degree of occlusion of the extracellular space. In the presence of Ca^{2+} , the Ca^{2+} -binding domains transform into calcium-pockets that pack as a core and cause the hydrophobic segments of the residual, remaining part of the loop to swing outwardly and face the extracellular space (right panel, Figure 15.3). The approximation of hydrophobic segments of the occludin extracellular loops originating from neighboring cells results in formation of hydrophobic intercellular bridges that narrow the extracellular space at the level of the tight junction and result in higher degree of occlusion of the intercellular space. N–N-terminus; C–C-terminus.

More recently, a novel hypothesis has been advanced, suggesting that extracellular loops of occludin are composed each of two functional domains: the proximal part (containing Ca^{2+} -binding sites) that is anchored via an α -helix to the plasma membrane and a distal part (composed of a hydrophobic loop segment) that attaches to the proximal segment via a short communicating α -helix [118]. The residual loop segment of occludin extracellular loop 1 also contains a glycine-rich sequence $(GY)_n$, which predicts a sequence that can be readily folded. This predicted structure supports a model of conformational change of the loops following binding of Ca^{2+} . In the presence of Ca^{2+} , the Ca^{2+} -binding domains transform into calcium-pockets that pack as a core and cause the communicating α -helices and residual loop segments to swing outwardly and face the extracellular space. Accordingly, binding of Ca^{2+} induces conformational change [119] so that the hydrophobic residues swing

out to form globular structures with a core containing the Ca^{2+} -pocket, and a hydrophobic shell [120]. The approximation of hydrophobic segments of the occludin extracellular loops results in formation of hydrophobic intercellular bridges that narrow the extracellular space at the level of the tight junction and result in higher degree of occlusion of the intercellular space.

The extracellular loops of claudins, in contrast to those of occludin (*vide supra*), do not exhibit potential Ca^{2+} -sensitive mechanisms. Therefore, R_{TJ} regulation in epithelia containing tight junctions composed predominantly of claudins is predicted to be less sensitive to Ca_o regulation. Since tight junctional regions of most epithelia are composed both of occludin and various isoforms of claudins, it appears likely that Ca_o regulation of R_{TJ} will be more apparent in epithelia expressing higher relative densities of occludin than claudins. An additional mode of Ca_o regulation of R_{TJ} is through Ca_o modulation of cytosolic Ca^{2+} levels, in that tight junctional proteins are in turn modulated by cytosolic Ca^{2+} signaling [94–103].

15.5.2. Regulation of Assembled Tight Junctions by Extracellular ATP

ATP, which is present in extracellular fluids at nanomolar to low-micromolar concentrations, is an important regulator of cellular functions. ATP has been shown to operate through activation of purinergic P2 receptors [121]. Human vaginal-cervical epithelial cells express different types of P2 receptors [32, 33, 44] and one of the observed effects following treatment with ATP is changes in R_{TJ} [13]. Treatment with micromolar concentrations of ATP (an EC_{50} of 3 μM) induces an acute and reversible increase in R_{TJ} . The effect involves activation of calcium channels operated by P2X₄ receptor, that is, pertussis toxin-sensitive, G protein-coupled, dihydropyridine-sensitive, and voltage-dependent. Enhanced calcium influx stimulates activation of phospholipase D, upregulation of diacylglycerol and activation of protein kinase C (PKC) [13, 14, 16, 20, 22, 32, 33]. One of the consequences of activation of PKC is acute threonine dephosphorylation of the 65-kDa (full length) isoform of occludin [43]. The acute and reversible effect on increases in R_{TJ} by extracellular ATP level (ATP_o) suggest an involvement of conformational change(s) in occludin that leads to increased occlusion of the intercellular space [43]. These novel data were the first to show the estrogen receptor-mediated modulation of assembled tight junctions and refute the previously held opinion that the tight junctions, once assembled, form a rigid unmodifiable fence-like structure.

15.5.3. Estrogen Regulation of R_{TJ}

The cultured vaginal-cervical epithelia provide useful experimental systems to determine the regulation of paracellular permeability by estrogen, since the cells are estrogen responsive [23, 24, 26, 30, 31]. These data, which until recently were lacking, may be physiologically and clinically important because in vivo estrogen controls lubrication of the lower genital canal and dysregulation of vaginal-cervical transport can be associated with infertility and states of disease. Experiments using cultured vaginal-cervical epithelia showed that depletion of estrogen increases, while treatment with physiological concentrations of the naturally occurring 17β -estradiol decreases the R_{TJ} [23, 24, 26, 30, 31, 35, 38, 43]. The effect of estrogen involves proximally the nuclear estrogen receptor (ER) mechanism, $\text{ER}\alpha$, whereas it also modulates

distally occludin. At low concentrations, estrogen enhances synthesis of the full length 65-kDa occludin isoform, while at higher concentrations (but still within the physiological range for the woman) estrogen augments turnover and downregulation of the 65-kDa occludin isoform (concomitantly with upregulation of the 50-kDa occludin isoform [35]) by a calpain-mediated process [43]. A biphasic effect of estrogen was previously described in modulation of transendothelial paracellular permeability [122] and occludin mRNA level in human endothelial cells [123]. Protease digestion analysis suggests that estrogen induces degradation of occludin at the middle portion of the extracellular loop 2, resulting in formation of a truncated 50-kDa isoform [35]. Since occludin extracellular loops are important for occlusion of the intercellular space, estrogen effect on occludin 65-kDa and 50-kDa isoforms can explain the decrease in R_{TJ} elicited by high concentrations of estrogen (Figure 15.3).

15.5.4. Early Stages of Tight Junctional Disassembly

Disassembly of tight junctions is a well-studied mechanism of abrogation of the R_{TJ} . One aspect of tight junctional disassembly that remains relatively little understood is events that precede to induce the effect, particularly in pathological conditions. It is important to note that early stages of tight junctional disassembly are reversible phenomena. For instance, prolonged exposure of cervical cells to high concentrations of ATP is toxic to cells, leading to abrogation of the R_{TJ} [43], whereas removal of the nucleotide from the bathing medium even as late as 45 min reverses the outcome [43].

In some types of cells, disassembly of tight junctions is preceded by and associated with augmented phosphorylation of tight junctional proteins. One such example is the phosphorylation of occludin. Occludin is a phosphoprotein that is constitutively phosphorylated on threonine and tyrosine residues by PKC [93, 122–128], as well as by Rho-associated coiled coil-forming protein kinase (RhoA-p160ROCK) [129] and extracellular signal-regulated kinase (ERK)1/2 cascades [130]. Continued exposure to activated PKC has been associated with decreased R_{TJ} , secondary to disassembly of tight junctions [93].

An additional mechanism of tight junctional disassembly is tyrosine phosphorylation of occludin. For example, shear stress-induced phosphorylation of occludin and the disassembly of tight junctions in the bovine aortic endothelium are mediated by tyrosine kinase [129]. Likewise, acetaldehyde-induced disruption of epithelial tight junctions in Caco-2 cells involves tyrosine phosphorylation of junctional proteins by inhibition of tyrosine phosphatase [130]. In cervical cells (CaSki), treatment with the cell-permeable diacylglyceride, sn-1,2-dioctanoyl diglyceride (diC8), augments tyrosine phosphorylation of the occludin 65-kDa isoform [43], suggesting the involvement of PKC. Although prolonged activation of PKC α does induce disassembly of tight junctions and abrogation of the R_{TJ} in CaSki cells, the effect is not mediated through tyrosine phosphorylation of occludin, since pre-treatment with staurosporine does not affect tyrosine phosphorylation in occludin [43].

Recent studies using vaginal-cervical cells suggest yet another mechanism for the early stage of tight junctional disassembly, namely, the breakdown of occludin 65-kDa isoform to the lesser functional 50-kDa isoform. Occludin appears to constitutively undergo calpain-mediated proteolysis, increasing the amount of non-functional 50-kDa isoform [35, 43]. As described above,

estrogen also stimulates conversion of occludin 65-kDa isoform to the 50-kDa isoform, albeit the effect of estrogen does not appear to involve activation of calpain. The lack of calpain involvement is supported by the observation that estrogen abrogation of the R_{TJ} is only partial and that treatment with estrogen does not abolish the R_{TJ} regardless of dose and duration [23, 24, 26, 30, 31, 35, 43]. The estrogen signaling and molecular regulation of estrogen modulation of occludin were recently described. The 65-kDa to 50-kDa occludin turnover is associated with increased extracellular activity of the matrix metalloproteinase 7 (MMP-7). Estrogen, acting via the estrogen receptor α ($ER\alpha$) mechanism, upregulates activation of the MMP-7 intracellularly at the level of Golgi, and augments secretion of activated MMP-7 through SNARE-dependent exocytosis [130a]. These data indicate that the functional occludin 65-kDa isoform is constitutively phosphorylated on threonine and tyrosine residues and constitutively undergoes calpain-mediated conversion to a non-functional 50-kDa isoform, where the effect can be augmented by estrogen. These processes predict occludin breakdown and abrogation of the R_{TJ} , consistent with the thesis that occludin must be continuously produced and transported to the tight junctional complex in order to maintain the steady-state level of junctional occlusion.

15.5.5. Claudin/Occludin Model of Regulation of the R_{TJ}

The current theory of junctional gating of the intercellular space predicts that functional tight junction elements are composed of extracellular loops of occludin and claudins. One strand of tight junctional proteins associate laterally with the other strand in the apposing membrane of adjacent cells, forming “paired” tight junction strands to “seal” the intercellular space (Figure 15.3). The extracellular loops may form hydrophobic occludin intercellular bridges [71] or claudin–claudin bisulfide bonds [83] that occlude intercellular space to the movement of charged molecules. Claudins are the main building units of the tight junction that confer the baseline gating properties of the tight junction, where different claudin isoforms are predicted to confer variable and widely different ion permselectivities. Regulation of the R_{TJ} by claudins is likely to depend on the density of the proteins localizing at the tight junctional region: cells expressing greater density of claudins at the tight junctional region will tend to exhibit a higher resistance. Similar to the claudins, regulation of the R_{TJ} by occludin will also depend on its expression and density at the tight junctional region [35, 43]. However, in contrast to the claudins, occludin occlusion of the intercellular space can be acutely and reversibly regulated irrespective of its density and expression by at least two known mechanisms, threonine dephosphorylation at intracellular domains (N- or C-termini) of occludin [43] and Ca^{2+} binding to extracellular loops of occludin [15]. Therefore, the combined expression of claudins and occludin provides tight junctions with stability (claudins and occludin) and regulability (occludin). The importance of occludin is apparent in low-resistance epithelia, while in high-resistance epithelia the role of occludin is probably masked by the predominance of claudins.

Tight junction elements are modeled as pores that flicker between open and closed states [131], such that each small segment can be at one of two states, sealed (r_{closed}) or open (r_{open}) (r being referred to as the “microscopic

resistance”). According to this model, the net junctional permeability depends on both the density of the pores and probability of the open state of the pore. This model predicts regulation of the junctional permeability by modulating the number of pores, probability of the open state of pores, or both [15]. The first mode of regulation will most often require protein synthesis and subsequent expression at the tight junction requiring a longer time period, while the second involves conformational change(s) of existing tight junction proteins requiring a relatively shorter time period (e.g., seconds to minutes) for action.

Using calcium-mediated regulation of R_{TJ} for functional analysis [15], the experimental results in low-resistance epithelia can be modeled to predict that each tight junctional element with a microscopic resistance r_i contributes to the macroscopic R_{TJ} , such that $R_{TJ} \approx \sum r_i$. In the case of occludin, the model predicts two Ca^{2+} -binding sites per tight junction element, where binding of Ca^{2+} in one site is independent of the other. By extrapolation, low-resistance epithelia could be best described in terms of a cooperative parallel model where the macroscopic permeability of the epithelium is determined by the cooperative opening or closing of the complete set of cell-associated resistive elements where these sets are arranged in parallel. The parallel model predicts low density of resistive elements, composed predominantly of occludin, that reside at one planar level of the epithelium. In contrast, high-resistance epithelia are best modeled by a cooperative serial model, where the resistive elements are composed predominantly of claudins and arranged serially within the intercellular space [15].

15.6. Regulation of the R_{LIS}

An important contribution to the understanding of regulation of paracellular permeability is recent data obtained in the low-resistance vaginal-cervical epithelia. In this model, changes in R_{PCR} are the result of modulation of both the R_{TJ} and the R_{LIS} [14], in that uncoupling modulation of R_{TJ} and R_{LIS} makes it possible to study the mechanisms that mediate the changes in R_{LIS} . R_{LIS} is determined primarily by the width of the intercellular space, that is, reciprocally by the proximity of the lateral plasma membranes of neighboring epithelial cells that establish this space (Figure 15.1A). Therefore, R_{LIS} is determined by the ability of epithelial cells to change their shape (width) in response to stimuli, for example, hydrostatic gradients in the subluminal to luminal direction (Figure 15.1C, panel C). Since changes in cell shape depend on the cytoskeletal organization, cells expressing a dynamic, flexible cytoskeleton will tend to change their shape more readily in response to stimuli than would cells expressing a rigid cytoskeleton.

R_{LIS} is considered to be an element with low resistance, but its contribution to the total resistance can be significant in low-resistance epithelia. Comparative analysis in human-cultured skin versus vaginal-cervical epithelia showed total R_{PCR} of $200 \Omega \cdot \text{cm}^2$ and $25 \Omega \cdot \text{cm}^2$, respectively [7]. R_{LIS} was about $2\text{--}5 \Omega \cdot \text{cm}^2$ in both of these two epithelia, thereby contributing very little to the total resistance in the cultured skin epithelium, but contributing significantly to the overall resistance of the vaginal-cervical epithelium. Additional analyses in the vaginal-cervical epithelium found that R_{LIS} contributes 5–25% to the total R_{PCR} [14] and that it depended on the estrogen status of the cells [23, 24, 26,

30, 31]. The vaginal-cervical epithelium system was therefore used to probe R_{PCR} in order to understand mechanisms that control and regulate R_{LIS} . Data summarized below suggest that both estrogen status and aging may critically affect the R_{LIS} of vaginal-cervical cells in women.

15.6.1. Estrogen Regulation of the R_{LIS}

Evidence that estrogen increases permeability of vaginal-cervical epithelia by decreasing the R_{LIS} stemmed from experiments showing an early increase in permeability after estrogen treatment, which preceded the decrease in R_{TJ} [23–27]. Treatment with estrogen shortened the response time relative to decreases in cell size and augmented the decrease in cell size in response to both hypertonicity [23] (which stimulates loss of cellular water and induces cell shrinkage [14]) and hydrostatic gradients in the subluminal to luminal direction (Figure 15.1C, panel C, and [45]), suggesting that the estrogen-induced increase in R_{LIS} is associated with increased deformability of the cells.

Possible mechanisms by which estrogens could modulate the deformability of vaginal-cervical cells are changes in permeability [132]; modulation of transcellular movement of water [133]; regulation of ion transport mechanisms such as the sodium/potassium ATPase (Na^+/K^+ -ATPase) [134], K^+ [135] and Ca^{2+} channels [136]; and proton transport [137]. Estrogen could also modulate calcium mobilization [100] and cell volume changes [138]. Experiments in vaginal-cervical cells ruled out estrogen modulation of Cl^- secretion [23], the main regulatory mechanism for ion secretion in vaginal-cervical cells [21]. In contrast, estrogen does upregulate apical V-ATPase activity and luminal H^+ secretion [40, 42], whereas it blocks Ca^{2+} influx [15]. However, these effects cannot sufficiently explain the estrogen decrease in R_{LIS} .

More likely, the estrogen-caused decrease in R_{LIS} relates to modulation of the cytoskeletal organization [139–141]. The structure and shape of attached epithelial cells depends mainly on the stability of the cortical submembranous acto-myosin ring. The actin component of the cortical acto-myosin ring is composed of actin filaments (F-actin) that are made of oriented globular monomeric G-actin molecules. Actins are maintained in a dynamic state of remodeling and allow cells to change their shape in response to environmental and intrinsic stimuli [138, 142]. Actin filaments are in a steady-state equilibrium between polymerization of monomeric G-actin and depolymerization of filamentous F-actin [138, 142]. Actin filaments are polar molecules with two different ends: a slow growing “pointed end” and a faster growing “barbed end”. During actin polymerization, the growth of the barbed end is balanced at steady state by loss of actin molecules at the pointed end. Thermodynamically, actin polymerization is preferred to actin depolymerization, but most cells possess at least two mechanisms to inhibit filament formation: filament nucleation sites might be blocked so that the monomers have nothing to grow off or actin monomer might be sequestered in a non-polymerizable form so that filaments have nothing to grow with [138, 143–148]. Enhanced polymerization of G-actin to form F-actin leads to a more dense and rigid cytoskeleton, while depolymerization of F-actin is associated with a more dynamic cytoskeleton.

In epithelial cells, including vaginal-cervical cells, cortical actin associates with myosin filaments, and the actin-myosin interaction facilitates stabilization of the cytoskeleton. Myosins are protein molecular motors that bind to actin in an ATP-dependent manner. Upon ATP binding, the myosin head (containing the magnesium ATPase [MgATPase]) detaches from actin and hydrolyzes ATP [149]. In muscle cells, the main function of myosin is generation of force for contractility and movement. In non-muscle cells, interactions of myosin with cytoskeletal actin involve regulation of cytokinesis, cell motility, and cell polarity [150]. In epithelial cells, interactions of non-muscle myosin II with actin regulate exocytosis [151] and control the rigidity of the cytoskeleton [45]. Of the three known types of non-muscle myosin II isoforms [152–154], non-muscle myosin IIB (NMM-IIB) is the most abundant cortical myosin in epithelial vaginal-cervical cells [45, 45a]. NMM-IIB has adapted for maintaining tension in a static manner and displays a low-steady-state MgATPase activity and a positive thermodynamic coupling between actin and adenosine diphosphate (ADP) binding [155, 156]. These characteristics confer an advantage of energetic economy within the cell and make its working cycle more suited for sustained maintenance of tension, as opposed to generation of short duration force that occurs with muscle myosins [156] and other non-muscle myosins [149].

In human vaginal-cervical cells, the estrogen-induced increase in permeability is mediated in part by decreases in R_{LIS} that involve fragmentation of the cytoskeleton [23]. The effects of estrogen on cytoskeletal organization involve modulation of both cortical actin [29] and myosin [45] (Figure 15.4A, C, D).

15.6.2. Estrogen Regulation of Actin Polymerization

One of the mechanisms by which estrogen decreases R_{LIS} is modulation of actin polymerization [23]. Estrogen shifts the steady-state equilibrium of actins in vaginal-cervical cells toward G-actins (Figure 15.4A, C). The effect is relatively fast (1–6 h); it involves proximally the $ER\alpha$, nitric oxide (NO) and cyclic guanosine monophosphate (cGMP) as essential mediators, and distally the cGMP-dependent protein kinase (PKG) [23–25, 27–29]. NO, in a direct action, or operating through activation of guanylate cyclase, upregulates cGMP activity and activation of PKG, resulting in depolymerization of actin by ADP-ribosylation of monomeric G-actin [29]. The net effect is shift in actin steady state toward G-actin, which results in fragmentation of the cytoskeleton. This novel signaling cascade was one of the first to show an effect of estrogen that involves upregulation by transcription of a necessary mediator, as has been shown by $ER\alpha$ -dependent increase in NO activity through upregulation of the NO synthase, endothelium-type nitric oxide (eNOS) [28, 29].

15.6.3. Modulation of Actin Polymerization: Estrogen vis-à-vis Aging Effects

Vaginal dryness is a common symptom of postmenopausal women, and traditionally it was attributed to decline in plasma estrogen activity after menopause and atrophy of the vaginal-cervical epithelia. The results of a recent study aimed at better understanding the age-related contributions of R_{TJ} and R_{LIS} to the transcervical–transvaginal permeability showed an apparent lack of aging effect on R_{TJ} , but a significant aging-related increase in R_{LIS} [38]. The results also showed diminished capacity of cells obtained from older women

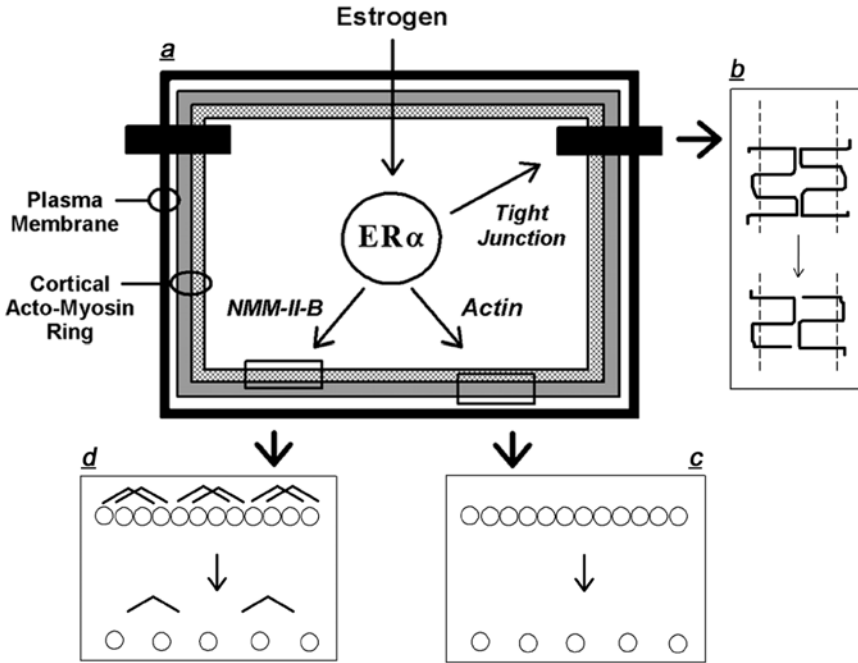


Figure 15.4 Model of estrogen modulation of paracellular permeability. (A) Cell cross section showing the permeability-related functional components targeted by estrogen. ER α —estrogen receptor- α . Wide-filled bars are tight junctions. (B) Occludin extracellular loops of neighboring cells approximate and occlude the intercellular space. The upper set is occludin 65-kDa molecules while the lower set is occludin 50-kDa molecules. Estrogen upregulates expression of the occludin truncated 50-kDa isoform, which is deficient in occlusion of the intercellular space, compared to the functional 65-kDa form. (C) Estrogen shifts the cortical acto-myosin ring from a structure dominated by polymerized F-actins (stretch of circles) into that dominated by depolymerized G-actins (single circles). This effect induces fragmentation of the cytoskeleton into a less rigid, more flexible structure. (D) Estrogen augments disassociation of non-muscle myosin IIB (NMM-IIB, pointed lines) from cortical actin (circles), thereby furthering fragmentation of the cytoskeleton. Estrogen effects on NMM-IIB involve two independent mechanisms: phosphorylation of NMM-IIB filaments on serine and threonine residues inhibits NMM-IIB filamentation; and increased NMM-IIB MgATPase activity which may accelerate disassociation of the myosin from actin. All four effects of estrogen are mediated by the ER α .

to remodel cellular actin from polymerized actin toward monomeric G-actin in response to NO stimulation [38]. Therefore, aging appears to confer diminished deformability of the cytoskeleton of vaginal-cervical epithelial cells, which could be aggravated by estrogen deficiency.

15.6.4. Estrogen Regulation of Cortical Myosin

An additional mechanism by which estrogen decreases R_{LIS} is modulation of the cortical acto-myosin, and the effect of estrogen involves at least two molecular mechanisms: modulation of phosphorylation and oligomerization of NMM-IIB filaments [45] and modulation of NMM-IIB MgATPase activity [157] (Figure 15.4A, D). Estrogen augments phosphorylation of NMM-IIB filaments on serine and threonine residues. Estrogen thus decreases

NMM-IIB filamentation, abrogates interactions between NMM-IIB and actins, and induces redistribution of the myosin from submembranous regions into cytoplasmic and peri-nuclear domains [45]. The effect of estrogen is mediated via the ER α . The epidermal growth factor receptor (EGFR) and ERK/MAPK (mitogen-activated protein kinase) cascades are involved in ER α signaling as proximal mediators, while modulation of myosin heavy-chain phosphatase (dependent on both casein kinase II [CK2] and Rho-associated kinase) is involved as distal mediators [45]. Thus, enhanced phosphorylation inhibits oligomerization of the myosin filaments and may lead to decreased interaction of the NMM-IIB filaments with cortical actin. Disassociation of the myosin from the cortical actin could in turn disrupt the acto-myosin ring and contribute to fragmentation of the cytoskeleton (Figure 15.4A, C, D). The signaling cascade of estrogen modulation of NMM-IIB phosphorylation also involves the upregulation of intermediary steps and activation of kinase-initiated signaling cascades that participate in the signal cascade through ER α transcription [45]. Estrogen modulation of NMM-IIB filamentation depended on epidermal growth factor (EGF) and the EGFR. Since the EGFR is transcriptionally upregulated by estrogen [8], it is possibly a rate-limiting mediator involved in activation of the CK2. Estrogen, in an effect mediated by the ER α /EGFR/ERK-MAPK and CK2, also increases NMM-IIB MgATPase activity independent of NMM-IIB filamentation status [157]. The NMM-IIB filamentation and effects of estrogen on MgATPase may act in concert to augment dissociation between NMM-IIB and actin, inducing fragmentation of the cortical cytoskeletal acto-myosin ring [45, 157].

15.6.5. Composite Effects of Estrogen on Paracellular Permeability

Figure 15.4 presents a mechanistic model of estrogen regulation of the paracellular permeability in human vaginal-cervical cells. Estrogen decrease in R_{TJ} is believed to involve modulation of occludin and formation of tight junctions composed of the defective 50-kDa isoform (Figure 15.4B). Estrogen decrease in R_{LIS} is believed to be the result of formation of a fragmented cytoskeleton, which involves at least three reported mechanisms: a shift in the cortical acto-myosin ring from a polymerized F-actin structure into that dominated by depolymerized G-actins (Figure 15.4C); augmented disassociation of NMM-IIB from cortical actin due to inhibition of NMM-IIB filamentation; and augmented disassociation of NMM-IIB from cortical actin due to increased NMM-IIB MgATPase activity (Figure 15.4D). The effects of estrogen on myosin are unrelated to estrogen modulation of actin, but they may work in concert with the effects of estrogen on actin and augment defragmentation of the cytoskeleton.

Since all three groups of effects of estrogen on the vaginal-cervical epithelium lead to decreased R_{PCR} , the question of specific function versus redundancy was raised. Although for all three effects the dose requirements of 17 β -estradiol as well as the specificity and agonist profile were similar (EC_{50} of 1–3 nM), the time courses were different [23, 24, 26, 30, 31, 45a, 157]. Estrogen modulation of actin is relatively fast (1–6 h); modulation of NMM-IIB phosphorylation is slower (12–24 h); and modulation of occludin and R_{TJ} is the slowest (24–48 h). Clinically, there is evidence that estrogen modulation of vaginal-cervical permeability depends on the length of exposure to

estrogen. Thus, during the pre-ovulatory phase of the menstrual cycle, the estrogen surge (which lasts 6–12 h) suffices to induce massive secretion of fluid, but the effect is limited in duration to about 12–24 h [90]. It is possible that this effect, interpreted as increased water transudation secondary to decreased R_{PCR} , is mediated by estrogen modulation of cortical actin. In contrast, treatment of estrogen-deficient postmenopausal women requires prolonged administration of estrogen to induce appropriate lubrication of the lumen [90]. It is possible that the latter effect requires the concerted actions of estrogen modulation of occludin (decreased R_{TJ}) and estrogen modulation of the cortical acto-myosin ring (decreased R_{LIS} through the effects of estrogen on actin as well as NMM-IIB). Therefore, the author of this chapter puts forward the hypothesis that short-term increases in paracellular permeability operate through estrogen modulation of actin polymerization, while long-lasting effects require the estrogen-mediated modulation of occludin and actin polymerization, along with modulation of interactions between actin and NMM-IIB.

15.7. Implications of the Data for Topical Drug Delivery

Modulation of paracellular permeability in secretory epithelial may affect not only transport from the blood into the exterior (or lumen) but also the transport of drugs in the reverse direction from the exterior into the blood. Under such conditions, the driving force is the chemical gradient of the drug in the luminal to subluminal direction, and the main determinant for drug delivery through the paracellular route is R_{PCR} . By modulating the paracellular permeability, it may be possible to more efficiently regulate delivery of topically applied drugs. The vaginal route has been recognized as a useful mode of drug delivery in females. The advances in understanding conditions and mechanisms that control R_{PCR} may be used in future clinical studies to improve pharmacological treatments utilizing the vaginal route.

15.8. Concluding Remarks

The main difference between tight and leaky epithelia is the relative greater contribution in the latter of the R_{LIS} to the total paracellular permeability. The paracellular permeability of leaky epithelia can be hormone-regulated through modulation of R_{TJ} and R_{LIS} . In cervical-vaginal epithelia, the estrogen-induced decrease in R_{TJ} is associated with modulation of occludin and formation of tight junctions composed of the defective 50-kDa isoform. The estrogen-mediated decrease in R_{LIS} is believed to be the result of formation of a fragmented cytoskeleton, involving formation of cytoskeletal organization dominated by depolymerized G-actins, leading to augmented disassociation of NMM-IIB from cortical actin due to inhibition of NMM-IIB filamentation and increased NMM-IIB MgATPase activity.

Acknowledgments: The paper was supported by NIH grants HD29924 and AG15955.

References

1. Gorodeski GI, Romero MF, Hopfer U, Rorke E, Utian WH, and Eckert RL [1994] Human uterine cervical epithelial cells grown on permeable support—a new model for the study of differentiation and transepithelial transport. *Differentiation* 56:107–118
2. Gorodeski GI, Eckert RL, Utian WH, Sheean L, and Rorke EA [1989] Retinoids, sex steroids and glucocorticoids regulate ectocervical cell envelope formation but not the level of the envelope precursor, involucrin. *Differentiation* 42: 75–80
3. Gorodeski GI, Eckert RL, Utian WH, and Rorke EA [1990] Maintenance of in vivo-like keratin expression, sex steroid responsiveness and estrogen receptor expression in cultured human ectocervical epithelial cells. *Endocrinology* 126:399–406
4. Gorodeski GI, Eckert RL, Utian WH, Sheean L, and Rorke EA [1990] Cultured human ectocervical epithelial cell differentiation is regulated by the combined direct actions of sex steroids, glucocorticoids and retinoids. *J Clin Endocrinol Metab* 70:1624–1630
5. Sizemore N, Kasturi L, Gorodeski G, Eckert RL, Jetten AM, and Rorke EA [1993] Retinoid regulation of human ectocervical epithelial cell transglutaminase activity and keratin gene expression. *Differentiation* 54: 219–225
6. Gorodeski GI, Hopfer U, Eckert RL, Utian WH, De-Santis BJ, Rorke ER, and Romero MF [1994] ATP decreases acutely and reversibly transport through the paracellular pathway in human uterine cervical cells. *Am J Physiol* 266:C1692–C1698
7. Gorodeski GI, Merlin D, De Santis BJ, Frieden KA, Hopfer U, Eckert RL, and Romero MF [1994] Characterization of paracellular permeability in cultured human cervical epithelium: Regulation by extracellular ATP. *J Soc Gynecol Investig* 1:225–233
8. Jacobberger JW, Sizemore N, Gorodeski GI, and Rorke EA [1995] Transforming growth factor β regulation of epidermal growth factor receptor in ectocervical epithelial cells. *Exp Cell Res* 220:390–396
9. Gorodeski GI, Hopfer U, De Santis BJ, Eckert RL, Rorke ER, and Utian WH [1995] Biphasic regulation of paracellular permeability in human cervical cells by two distinct nucleotide receptors. *Am J Physiol* 268:C1215–C1226
10. Gorodeski GI and Hopfer U [1995] Regulation of the paracellular permeability of cultured human cervical epithelium by a purinergic P_2 -receptor. *J Soc Gynecol Investig* 2:716–720
11. Gorodeski GI, De Santis BJ, Goldfarb J, Utian WH, and Hopfer H [1995] Osmolar changes regulate the paracellular permeability of cultured human cervical epithelium. *Am J Physiol* 269:C870–C877
12. Macinga D, Jain V, Sizemore N, Gorodeski GI, Eckert RL, and Rorke EA [1995] Tamoxifen regulation of ectocervical cell differentiation. *J Soc Gynecol Investig* 2:754–761
13. Gorodeski GI, Peterson D, De Santis BJ, and Hopfer U [1996] Nucleotide-receptor mediated decrease of tight-junctional permeability in cultured human cervical epithelium. *Am J Physiol* 270:C1715–C1725
14. Gorodeski GI [1996] The cultured human cervical epithelium: A new model for studying transepithelial paracellular transport. *J Soc Gynecol Investig* 3: 267–280
15. Gorodeski GI, Wenwu J, and Hopfer U [1997] Extracellular Ca^{2+} directly regulates tight junctional permeability in the human cervical cell line CaSki. *Am J Physiol* 272:C511–C524

16. Gorodeski GI and Goldfarb J [1997] Extracellular ATP regulates transcervical permeability by modulating two distinct paracellular pathways. *Am J Physiol* 272:C1602–C1610
17. Gorodeski GI, Eckert RL, Pal D, Utian WH, and Rorke EA [1997] Retinoids regulate tight junctional resistance of cultured human cervical cells. *Am J Physiol* 273:C1707–C1713
18. Gorodeski GI and Goldfarb J [1998] Seminal fluid factor increases the resistance of the tight junctional complex of the cultured human cervical epithelium CaSki. *Fertil Steril* 69:309–317
19. Gorodeski GI, Pal D, Rorke EA, Eckert RL, and Burfeind P [1998] Retinoids modulate P_{2U} purinergic receptor-mediated changes in transcervical paracellular permeability. *Am J Physiol* 274:C1108–C1116
20. Gorodeski GI, Hopfer U, and Wenwu J [1998] Purinergic receptor induced changes in paracellular resistance across cultures of human cervical cells are mediated by two distinct cytosolic calcium related mechanisms. *Cell Biochem Biophys* 29:281–306
21. Gorodeski GI and Whittembury J [1998] A novel fluorescence chamber for the determination of volume changes in human CaSki cell cultures attached on filters. *Cell Biochem Biophys* 29:307–332
22. Gorodeski GI, Burfeind F, Uin Gan S, Pal D, and Abdul-Karim F [1998] Regulation by retinoids of P2Y₂ nucleotide receptor mRNA in human uterine cervical cells. *Am J Physiol* 275:C758–C765
23. Gorodeski GI [1998] Estrogen increases the permeability of the cultured human cervical epithelium by modulating cell deformability. *Am J Physiol* 275: C888–C899
24. Gorodeski GI and Pal D [2000] Involvement of estrogen receptors α and β in the regulation of cervical permeability. *Am J Physiol* 278:C689–C696
25. Gorodeski GI [2000] Role of nitric oxide and cGMP in the estrogen regulation of cervical epithelial permeability. *Endocrinology* 141:1658–1666
26. Gorodeski GI [2000] Effects of menopause and estrogen on cervical epithelial permeability. *J Clin Endocrinol Metab* 85:2584–2595
27. Gorodeski GI [2000] NO increases permeability of cultured human cervical epithelia by cGMP-mediated increase in G-actin. *Am J Physiol* 278:C942–C952
28. Gorodeski GI [2000] Calcium regulates estrogen increase in permeability of cultured CaSki epithelium by eNOS dependent mechanism. *Am J Physiol* 279:C1495–C1505
29. Gorodeski GI [2000] cGMP-dependent ADP-depolymerization of actin mediates estrogen increase in human cervical epithelia permeability. *Am J Physiol* 279:C2028–C2036
30. Gorodeski GI [2000] Vaginal—Cervical epithelial permeability decreases after menopause. *Fertil Steril* 76:753–761
31. Gorodeski GI [2001] Estrogen biphasic regulation of paracellular permeability of cultured human vaginal—cervical epithelia. *J Clin Endocrinol Metab* 86: 4233–4243
32. Gorodeski GI [2002] Regulation of transcervical permeability by two distinct P₂-purinergic receptor mechanisms. *Am J Physiol* 282:C75–C83
33. Gorodeski GI [2002] Expression regulation and function of P2X₄ receptor in human cervical epithelial cells. *Am J Physiol* 282:C84–C93
34. Gorodeski GI [2004] Estrogen attenuates P2X₇-R—mediated apoptosis of uterine cervical cells by blocking calcium influx. *Nucleosides Nucleotides and Nucleic Acids* 23:209–215
35. Zeng R, Li X, and Gorodeski GI [2004] Estrogen abrogates transcervical tight junctional resistance by acceleration of Occludin modulation. *J Clin Endocrinol Metab* 89:5145–5155

36. Wang Q, Wang L, Feng YH, Li X, Zeng R, and Gorodeski GI [2004] P2X₇-receptor mediated apoptosis of human cervical epithelial cells. *Am J Physiol* 287:C1349–C1358
37. Wang Q, Li X, Wang L, Feng YH, Zeng R, and Gorodeski GI [2004] Anti-apoptotic effects of estrogen in normal and in cancer human cervical epithelial cells. *Endocrinology* 145:5568–5579
38. Gorodeski GI [2005] Aging and estrogen effects on transcervical—transvaginal epithelial permeability. *J Clin Endocrinol Metab* 90:345–351
39. Wang L, Feng YH, and Gorodeski GI [2005] EGF facilitates epinephrine inhibition of P2X₇-receptor mediated pore formation and apoptosis: a novel signaling network. *Endocrinology* 146:164–174
40. Gorodeski GI, Hopfer U, Liu CC, and Margles E [2005] Estrogen acidifies vaginal pH by upregulation of proton secretion via the apical membrane of vaginal-ectocervical epithelial cells. *Endocrinology* 146:816–824
41. Feng YH, Wang L, Wang Q, Li X, Zeng R, and Gorodeski GI [2005] ATP ligation stimulates GRK-3—mediated phosphorylation and β -arrestin-2- and dynamin-dependent internalization of the P2X₇-receptor. *Am J Physiol* 288: C1342–C1356
42. Gorodeski GI [2005] Effects of estrogen on proton secretion via the apical membrane in vaginal-ectocervical epithelial cells of postmenopausal women. *Menopause* 12:679–684
43. Zhu L, Li X, Zeng R, and Gorodeski GI [2006] Changes in tight junctional resistance of the cervical epithelium are associated with modulation of content and phosphorylation of occludin 65 kDa and 50 kDa forms. *Endocrinology* 147:977–989
44. Feng YH, Li X, Wang L, Zhou L, and Gorodeski GI [2006] A truncated P2X₇ receptor variant (P2X_{7-j}) endogenously expressed in cervical cancer cells antagonizes the full-length P2X₇ receptor through hetero-oligomerization. *J Biol Chem* 281:17228–17237
45. Li X, Zhou L, and Gorodeski GI [2006] Estrogen regulates epithelial cell deformability by modulation of cortical acto-myosin through phosphorylation of non-muscle myosin-heavy-chain II-B filaments. *Endocrinology* 147: 5236–5248
- 45a. Li X, and Gorodeski GI [2006] Non-muscle myosin-II-B filament regulation of paracellular resistance in cervical epithelial cells is associated with modulation of the cortical acto-myosin. *J Soc Gynecol Investig* 13:579–591
46. Kasturi L, Sizemore N, Eckert RL, Martin K, and Rorke EA [1993] Calcium modulates cornified envelope formation, involucrin content, and transglutaminase activity in cultured human ectocervical epithelial cells. *Exp Cell Res* 205: 84–90
47. Hembree JR, Agarwal C, Beard RL, Chandraratna RA, and Eckert R [1996] Retinoid X receptor-specific retinoids inhibit the ability of retinoic acid receptor-specific retinoids to increase the level of insulin-like growth factor binding protein-3 in human ectocervical epithelial cells. *Cancer Res* 56: 1794–1799
48. Agarwal C, Chandraratna RA, Johnson AT, Rorke EA, and Eckert RL [1996] AGN193109 is a highly effective antagonist of retinoid action in human ectocervical epithelial cells. *J Biol Chem* 271:12209–12212
49. Agarwal C, Chandraratna RAS, Teng M, Nagpal S, Rorke EA, and Eckert RL [1996] Differential regulation of human ectocervical epithelial cell line proliferation and differentiation by retinoid x receptor- and retinoic acid receptor-specific retinoids. *Cell Growth Differentiation* 7:521–530
50. Hembree JR, Lambert A, Agarwal C, Efimova T, and Eckert RL [1999] Insulin-like growth factor binding protein-3 does not mediate the interferon-dependent

- suppression of human ectocervical epithelial cell proliferation. *Int J Oncol* 14:1163–1168
51. Agarwal C, Rorke EA, Irwin JC, and Eckert RL [1991] Immortalization by human papillomavirus type 16 alters retinoid regulation of human ectocervical epithelial cell differentiation. *Cancer Res* 51:3982–3989
 52. Choo CK, Rorke EA, and Eckert RL [1993] Calcium regulates the differentiation of human papillomavirus type 16 (HPV16) immortalized ectocervical epithelial cells, but not the expression of the papillomavirus E6 and E7 oncogenes. *Exp Cell Res* 208:161–169
 53. Sizemore N and Rorke EA [1993] Human papillomavirus 16 immortalization of normal human ectocervical epithelial cells alters retinoic acid regulation of cell growth and epidermal growth factor receptor expression. *Cancer Res* 53:4511–4517
 54. Rorke EA and Jacobberger JW [1995] Transforming growth factor-beta 1 (TGF beta 1) enhances apoptosis in human papillomavirus type 16-immortalized human ectocervical epithelial cells. *Exp Cell Res* 216:65–72
 55. Sizemore N, Choo CK, Eckert RL, and Rorke EA [1998] Transcriptional regulation of the EGF receptor promoter by HPV16 and retinoic acid in human ectocervical epithelial cells. *Exp Cell Res* 244:349–356
 56. Baltes S, Nau H, and Lampen A [2004] All-trans retinoic acid enhances differentiation and influences permeability of intestinal Caco-2 cells under serum-free conditions. *Dev Growth Differentiation* 46:503–514
 57. Ussing HH and Zerahn K [1951] Active transport of sodium as the source of electric current in the short-circuited isolated frog skin. *Acta Physiol Scand* 23:110–127
 58. Reuss L [1991] Tight junction permeability to ions and water. In: Cereijido M (ed.), *Tight-Junctions*. CRC Press, Boca Raton, Ann Arbor, London, pp. 49–66
 - 58a. Garty H, and Palmer LG [1997] Epithelial sodium channels: function, structure, and regulation. *Physiol Rev* 77:359–396
 - 58b. Verkman AS [1989] Mechanisms and regulation of water permeability in renal epithelia. *Am J Physiol* 257:C837–C850
 59. Enerson BE and Drewes LR [2003] Molecular features, regulation, and function of monocarboxylate transporters: implications for drug delivery. *J Pharm Sci* 92:1531–1544
 60. Halestrap AP and Meredith D [2004] The SLC16 gene family—from monocarboxylate transporters (MCTs) to aromatic amino acid transporters and beyond. *Pflugers Arch* 447:619–628
 61. Gross E, Hawkins K, Pushkin A, Sassani P, Dukkupati R, Abuladze N, Hopfer U, and Kurtz I [2001] Phosphorylation of Ser982 in the sodium bicarbonate cotransporter kNBC1 shifts the $\text{HCO}_3^-:\text{Na}^+$ stoichiometry from 3:1 to 2:1 in murine proximal tubule cells. *J Physiol* 537:659–665
 62. Farquhar MG and Palade GE [1963] Junctional complexes in various epithelia. *J Cell Biol* 17:375–412
 63. Claude P and Goodenough DA [1973] Fracture faces of zonulae occludentes from “tight” and “leaky” epithelia. *J Cell Biol* 58:390–400
 64. Staehelin LA [1973] Further observations on the fine structure of freeze-cleaved tight junctions. *J Cell Sci* 13:763–786
 65. Martinez-Palomo A and Erljij D [1975] Structure of tight junctions in epithelia with different permeability. *Proc Natl Acad Sci USA* 72:4487–4491
 66. Claude P [1978] Morphological factors influencing transepithelial permeability: a model for the resistance of the zonula occludens. *J Membr Biol* 39:219–232
 67. Kachar B and Pinto da Silva P [1981] Rapid massive assembly of tight junction strands. *Science* 213:541–544

68. Madara JL and Dharmasathaphorn K [1985] Occluding junction structure function relationships in a cultured epithelial monolayer. *J Cell Biol* 101: 2124–2133
69. Marcial MA, Carlson SL, and Madara JL [1987] Partitioning of paracellular conductance along the ileal crypt-villus axis: a hypothesis based on structural analysis with detailed consideration of tight junction-structure function relationships. *J Membr Biol* 80:59–70
70. Lane NJ, Reese TS, and Kachar B [1992] Structural domains of the tight junctional intramembrane fibrils. *Tissue Cell* 24:291–300
71. Tsukita S, Furuse M, and Itoh M [2001] Multifunctional strands in tight junctions. *Nat Rev (Mol Cell Biol)* 2:285–293
72. Martin-Padura I, Lostaglio S, Schneemann M, Williams L, Romano M, Fruscella P, Panzeri C, Stoppacciaro A, Ruco L, Villa A, Simmons D, and Dejana E [1998] Junctional adhesion molecule, a novel member of the immunoglobulin superfamily that distributes at intercellular junctions and modulates monocyte transmigration. *J Cell Biol* 142:117–127
73. Aurrand-Lons MA, Duncan L, Du Pasquiere L, and Imhof BA [2000] Cloning of JAM-2 and JAM-3; an emerging junctional adhesion molecular family? *Curr Top Microbiol Immunol* 251:91–98
74. Furuse M, Fujita K, Hiiragi T, Fujimoto K, and Tsukita S [1998] Claudin-1 and -2: Novel integral membrane proteins localizing at tight junctions with no sequence similarity to occludin. *J Cell Biol* 141:1539–1550
75. Furuse M, Sasaki H, Fujimoto K, and Tsukita S [1998] A single gene product, claudin-1 or -2, reconstitutes tight junction strands and recruits occludin in fibroblasts. *J Cell Biol* 143:391–401
76. Morita K, Furuse M, Fujimoto K, and Tsukita S [1999] Claudin multigene family encoding four-transmembrane domain protein components of tight junction strands. *Proc Natl Acad Sci USA* 96:511–516
77. Tsukita S and Furuse M [2000] Pores in the wall: claudins constitute tight junction strands containing aqueous pores. *J Cell Biol* 149:13–16
78. Heiskal M, Peterson PA, and Yang Y [2000] The roles of claudin superfamily proteins in paracellular transport. *Traffic* 2:92–98
79. Van Itallie CM and Anderson JM [2006] Claudins and epithelial paracellular transport. *Annu Rev Physiol* 68:403–429
80. Furuse M, Hirase T, Itoh M, Nagafuchi A, Yonemura S, Tsukita S, and Tsukita S [1993] Occludin: a novel integral membrane protein localizing at tight junctions. *J Cell Biol* 123:1777–1788
81. Ando-Akatsuka Y, Saitou M, Hirase T, Kishi M, Sakakibara A, Itoh M, Yonemura S, Furuse M, and Tsukita S [1996] Interspecies diversity of the occludin sequence: cDNA cloning of human, mouse, dog and rat kangaroo homologues. *J Cell Biol* 133:43–47
82. Gonzalez-Mariscal L, Betanzos A, Nava P, and Jaramillo BE [2003] Tight junction proteins. *Prog Biophys Mol Biol* 81:1–44
83. Van Itallie CM and Anderson JM [2004] The Molecular Physiology of Tight Junction Pores. *Physiology* 19:331–338
84. Miyoshi J and Takai Y [2005] Molecular perspective on tight-junction assembly and epithelial polarity. *Adv Drug Deliv Rev* 57: 815–855
85. Salama NN, Eddington ND, and Fasano A [2006] Tight junction modulation and its relationship to drug delivery. *Adv Drug Deliv Rev* 58:15–28
86. Van Itallie CM and Anderson JM [2006] Claudins and epithelial paracellular transport. *Annu Rev Physiol* 68:403–429
87. Nusrat A, Brown GT, Tom J, Drake A, Bui TTT, Quan C, and Mrsny RJ [2005] Multiple protein interactions involving proposed extracellular loop domains of the tight junction protein occludin. *Mol Biol Cell* 16:1725–1734

88. Stevenson RS, Siliciano JD, Mooseker MS, and Goodenough DA [1986] Identification of ZO-1: A high molecular weight polypeptide associated with the tight junction (Zonula Occludens) in a variety of epithelia. *J Cell Biol* 103: 755–766
- 88a. Zeuthen T [2002] General models for water transport across leaky epithelia. *Int Rev Cytol* 215:285–317
89. Hopfer U [1992] Digestion and absorption of basic nutritional constituents. In: Devlin TM (ed.), *Textbook of Biochemistry*, 3rd ed. Wiley-Lise, New York, Chichester, Brisbane, Toronto, Singapore, pp. 1059–1092
90. Gorodeski GI [1996] The Cervical Cycle. In: Adashi EY, Rock JA and Rosenwaks Z (eds.), *Reproductive Endocrinology, Surgery, and Technology*. Lippincott-Raven Publishers, Philadelphia New York, pp. 301–324
91. Spring KR and Hope A [1978] Size and shape of the lateral intercellular spaces in a living epithelium. *Science* 200:54–58
92. Kondo M, Finkbeiner WE, and Widdicombe JH [1992] Changes in permeability of dog tracheal epithelium in response to hydrostatic pressure. *Am J Physiol* 262:L176–L182
93. Clarke H, Marano CW, Soler AP, and Mullin JM [2000] Modification of tight junction function by protein kinase-C isoforms. *Adv Drug Deliv Rev* 41: 283–301
94. Balda MS, Gonzales-Mariscal L, Macias-Silva M, Torres-Marquez ME, Garcia Sainz JA, and Cereijido M [1991] Assembly and sealing of tight junctions: possible participation of G- proteins, phospholipase C, protein kinase C and calmodulin. *J Membr Biol* 122:193–202
95. Cereijido M, Robbins ES, Dolan WJ, Rotunno CA, and Sabatini DD [1978] Polarized monolayers formed by epithelial cells on a permeable and translucent support. *J Cell Biol* 77:853–880
96. Martinez-Palomo A, Meza I, Beaty G, and Cereijido M [1980] Experimental modulation of occluding junctions in a cultured transporting epithelium. *J Cell Biol* 87:736–745
97. Gonzalez-Mariscal L, Contreras RG, Bolivar JJ, Ponce A, Chavez de Ramirez B, and Cereijido M [1990] Role of calcium in tight junction formation between epithelial cells. *Am J Physiol* 259:C978–C986
98. Nigam SK, Rodriguez-Boulan E, and Silver RB [1992] Changes in intracellular calcium during the development of epithelial polarity and junctions. *Proc Natl Acad Sci USA* 89:6162–6166
99. Contreras RG, Miller JH, Zamora M, Gonzalez-Mariscal L, and Cereijido M [1992] Interaction of calcium with the plasma membrane of epithelial (MDCK) cells during junction formation. *Am J Physiol* 263:C313–C318
100. Jovov B, Lewis SA, Crowe WE, Berg JR, and Wills NK [1994] Role of intracellular Ca^{2+} in modulation of tight junction resistance in A6 cells. *Am J Physiol* 266:F775–F784
101. Stuart RO, Sun A, Panichas M, Hebert SC, Brenner BM, and Nigam SK [1994] Critical role for intracellular calcium in tight junction biogenesis. *J Cell Physiol* 159:423–433
102. Sigurdson SL and Lwebuga-Mukasa JS [1994] Divalent cation dependent regulation of rat alveolar epithelial cell adhesion and spreading. *Exp Cell Res* 213:719–727
103. Stuart RO, Sun A, Bush KT, and Nigam SK [1996] Dependence of epithelial intercellular junction biogenesis on thapsigargin-sensitive intracellular calcium stores. *J Biol Chem* 271:13636–13641
104. Ye J, Tsukamoto T, Sun A, and Nigam SK [1999] A role for intracellular calcium in tight junction reassembly after ATP depletion-repletion. *Am J Physiol* 277:F524–F532

105. Ma TY, Tran D, Nguyen D, Merryfield M, and Tarnawski A [2000] Mechanism of extracellular calcium regulation of intestinal epithelial tight junction permeability role of cytoskeletal involvement. *Microsc Res Tech* 51:156–168
106. Munshi HG, Wu YI, Ariztia EV, and Stack MS [2002] Calcium regulation of matrix metalloproteinase-mediated migration in oral squamous cell carcinoma cells. *J Biol Chem* 277:41480–41488
107. Hwang M, Kalinin A, and Morasso MI [2005] The temporal and spatial expression of the novel Ca⁺⁺-binding proteins, Scarf and Scarf2, during development and epidermal differentiation. *Gene Expr Patterns* 5:801–808
- 107a. Koval M [2006] Claudins—key pieces in the tight junction puzzle. *Cell Commun Adhes* 13:127–138
108. Saitou M, Fujimoto K, Doi Y, Itoh M, Fujimoto T, Furuse M, Takano H, Noda T, and Tsukita S [1998] Occludin-deficient embryonic stem cells can differentiate into polarized epithelial cells bearing tight junctions. *J Cell Biol* 141:397–408
109. Kubota K, Furuse M, Sasaki H, Sonoda N, Fujita K, Nagafuchi A, and Tsukita S [1999] Ca²⁺-independent cell-adhesion activity of claudins, a family of integral membrane proteins localized at tight junctions. *Curr Biol* 9:1035–1038
110. Balda MS, Whitney JA, Flores C, Gonzalez-Mariscal L, Cerejido M, and Matter K [1996] Functional dissociation of paracellular permeability and transepithelial electrical resistance and disruption of the apical-basolateral intramembrane diffusion barrier by the expression of a mutant tight junction membrane protein. *J Cell Biol* 134:1031–1049
111. Balda MS, Flores-Maldonado C, Cerejido M, and Matter K [2000] Multiple domains of occludin are involved in the regulation of paracellular permeability. *J Cell Biochem* 78:85–96
112. Huber D, Balda MS, and Matter K [2000] Occludin modulates transepithelial migration of neutrophils. *J Biol Chem* 275:5773–5778
113. Saitou M, ando-Akatsuka Y, Itoh M, Furuse M, Inazawa J, Fujimoto K, and Tsukita, S [1997] Mammalian occludin in epithelial cells: its expression and subcellular distribution. *Eur J Cell Biol* 73:222–231
114. Furuse M, Fujimoto K, Sato N, Hirase T, Tsukita S, and Tsukita S [1996] Overexpression of occludin, a tight junction-associated integral membrane protein, induces the formation of intracellular multilamellar bodies bearing tight junction-like structures. *J Cell Sci* 109: 429–435
115. McCarthy KM, Skare IB, Stankewich MC, Furuse M, Tsukita S, Rogers RA, Lynch RD, and Schneeberger EE [1996] Occludin is a functional component of the tight junction. *J Cell Sci* 109:2287–2298
116. Medina R, Rahner C, Mitic LL, anderson JM, and Van Itallie CM [2000] Occludin localization at the tight junction requires the second extracellular loop. *J Membr Biol* 178:235–247
117. Wong V and Gumbiner BM [1997] A synthetic peptide corresponding to the extracellular domain of occludin perturbs the tight junction permeability barrier. *J Cell Biol* 136:399–409
- 117a. Saitou M, Furuse M, Sasaki H, Schulzke JD, Fromm M, Takano H, Noda T, and Tsukita S [2000] Complex phenotype of mice lacking occludin, a component of tight junction strands. *Mol Biol Cell* 11:4131–4142
- 117b. Schulzke JD, Gitter AH, Mankertz J, Spiegel S, Seidler U, Amasheh S, Saitou M, Tsukita S, and Fromm M [2005] Epithelial transport and barrier function in occludin-deficient mice. *Biochim Biophys Acta* 1669:34–42
118. Gorodeski GI [2006] A new model of occludin regulation of tight-junctional resistance in low resistance epithelia. *Medical Hypotheses and Research* 3:769–784

119. Zhang M, Tanaka T, and Ikura M [1995] Calcium-induced conformational transition revealed by the solution structure of apo calmodulin. *Nat Struct Biol* 2:758–767
120. Jurado LA, Chockalingam PS, and Jarrett HW [1999] Apocalmodulin. *Physiol Rev* 79:661–682
121. Ralevic V and Burnstock G [1998] Receptors for purines and pyrimidines. *Pharmacol Rev* 50:413–492
122. Cho MM, Ziats NP, Pal D, Utian WH, and Gorodeski GI [1999] Estrogen modulates paracellular permeability of human umbilical vein endothelial cells by eNOS and iNOS related mechanisms. *Am J Physiol* 276:C337–C349
123. Ye L, Martin TA, Parr C, Harrison GM, Mansel RE, and Jiang WG [2003] Biphasic effects of 17- β -estradiol on expression of occludin and transendothelial resistance and paracellular permeability in human vascular endothelial cells. *J Cell Physiol* 196:362–369
124. Banan A, Zhang LJ, Shaikh M, Fields JZ, Farhadi A, and Keshavarzian A [2004] Theta-isoform of PKC is required for alterations in cytoskeletal dynamics and barrier permeability in intestinal epithelium: a novel function for PKC-theta. *Am J Physiol* 287:C218–C234
125. Ohtake K, Maeno T, Ueda H, Ogihara M, Natsume H, and Morimoto Y [2003] Poly-L-arginine enhances paracellular permeability via serine/threonine phosphorylation of ZO-1 and tyrosine dephosphorylation of occludin in rabbit nasal epithelium. *Pharm Res* 20:1838–1845
126. Yoo J, Nichols A, Mammen J, Calvo I, Song JC, Worrell RT, Matlin K, and Matthews JB [2003] Bryostatin-1 enhances barrier function in T84 epithelia through PKC-dependent regulation of tight junction proteins. *Am J Physiol* 285:C300–C309
127. Hirase T, Kawashima S, Wong EYM, Ueyama T, Rikitake Y, Tsukitai S, Yokoyama M, and Staddon JM [2001] Regulation of tight junction permeability and Occludin phosphorylation by RhoA-p160ROCK-dependent and -independent mechanisms. *J Biol Chem* 276:10423–10431
128. Wang Y, Zhang J, Yi XJ, and Yu FS [2004] Activation of ERK1/2 MAP kinase pathway induces tight junction disruption in human corneal epithelial cells. *Exp Eye Res* 78:125–136
129. DeMaio L, Chang YS, Gardner TW, Tarbell JM, and Antonetti DA [2001] Shear stress regulates Occludin content and phosphorylation. *Am J Physiol* 281:H105–H113
130. Atkinson KJ and Rao RK [2001] Role of protein tyrosine phosphorylation in acetaldehyde-induced disruption of epithelial tight junctions. *Am J Physiol* 280:G1280–G1288
- 130a. Gorodeski GI [2007] Estrogen decrease in tight junctional resistance involves matrix-metalloproteinase-7-mediated remodeling of occludin. *Endocrinology* 148:218–231
131. Cereijido M [1991] Evolution of ideas on the tight junction. In: Cereijido M (ed.), *Tight-Junctions*. CRC Press, Boca Raton, Ann Arbor, London, pp. 1–14
132. Widmark A, Grankvist K, Bergh A, Henriksson R, and Damber JE [1995] Effects of estrogen and progestogens on the membrane permeability and growth of human prostatic carcinoma cells (PC-3) in vitro. *Prostate* 26:5–11
133. Calamita G, Le Guevel Y, and Bourguet J [1991] ADH-induced water permeability and particle aggregates: alteration by a synthetic estrogen. *Am J Physiol* 261:F144–152
134. Davis RA, Kern F Jr, Showalter R, Sutherland E, Sinensky M, and Simon FR [1978] Alterations of hepatic Na⁺, K⁺-ATPase and bile flow by estrogen: effects

- on liver surface membrane lipid structure and function. *Proc Natl Acad Sci USA* 75:4130–4134
135. Pragnell M, Snay KJ, Trimmer JS, MacLusky NJ, Naftolin F, Kaczmarek LK, and Boyle MB [1990] Estrogen induction of a small, putative K⁺ channel mRNA in rat uterus. *Neuron* 4:807–812
 136. Yamamoto T [1995] Effects of estrogens on Ca²⁺ channels in myometrial cells isolated from pregnant rats. *Am J Physiol* 268:C64–C69
 137. Van Dyke RW and Root KV [1993] Ethynylestradiol decreases acidification of rat liver endocytic vesicles. *Hepatology* 18:604–613
 138. De la Cruz EM and Pollard TD [1996] Kinetics and thermodynamics of phalloidin binding to actin filaments from three divergent species. *Biochemistry* 35:14054–14061
 139. Gaulin-Glaser T, Watson CA, Pardi R, and Bender JR [1996] Effects of 17 β -estradiol on cytokine-induced endothelial cell adhesion molecule expression. *J Clin Invest* 98:36–42
 140. Sapino A, Pietribiasi F, Bussolati G, and Marchisio PC [1986] Estrogen- and tamoxifen-induced rearrangement of cytoskeletal and adhesion structures in breast cancer MCF-7 cells. *Cancer Res* 46:2526–2531
 141. Tabibzadeh S, Babaknia A, Kong QF, Zupi E, Marconi D, Romanini C, and Satyaswaroop PG [1995] Menstruation is associated with disordered expression of desmoplakin I/II and cadherin/catenins and conversion of F- to G-actin in endometrial epithelium. *Hum Reprod* 10:776–784
 142. Sheterline P, Clayton J, and Sparrow J [1995] Actin. *Protein Profile* 2:1–103
 143. Wang YL [1985] Exchange of actin subunits at the leading edge of living fibroblasts: possible role of treadmilling. *J Cell Biol* 101:597–602
 144. Forscher P and Smith SJ [1988] Actions of cytochalasins on the organization of actin filaments and microtubules in a neuronal growth cone. *J Cell Biol* 107:1505–1516
 145. Sampath P and Pollard TD [1991] Effects of cytochalasin, phalloidin and pH on the elongation of actin. *Biochemistry* 30:1973–1980
 146. Pollard TD, Goldberg I, and Schwarz WH [1992] Nucleotide exchange, structure, and mechanical properties of filaments assembled from ATP-actin and ADP-actin. *J Biol Chem* 267:20339–20345
 147. Brock MA and Chrest F [1993] Differential regulation of actin polymerization following activation of resting T lymphocytes from young and aged mice. *J Cellular Phys* 157:367–378
 148. Dufort PA and Lumsden CJ [1996] How profilin/barbed-end synergy controls actin polymerization: a kinetic model of the ATP hydrolysis circuit. *Cell Motil Cytoskeleton* 35:309–330
 149. Kovacs M, Wang F, Hu A, Zhang Y, and Sellers JR [2003] Functional divergence of human cytoplasmic myosin II: Kinetic characterization of the non-muscle IIA isoform. *J Biol Chem* 278:38132–38140
 150. Sellers JR [2000] Myosins: a diverse superfamily. *Biochim Biophys Acta* 1496:3–22
 151. Jerdeva GV, Wu K, Yarber FA, Rhodes CJ, Kalman D, Schechter JE, and Hamm-Alvarez SF [2005] Actin and non-muscle myosin II facilitate apical exocytosis of tear proteins in rabbit lacrimal acinar epithelial cells. *J Cell Sci* 118:4797–4812
 152. Golomb E, Ma X, Jana SS, Preston YA, Kawamoto S, Shoham NG, Goldin E, Conti MA, Sellers JR, and Adelstein RS [2004] Identification and characterization of non-muscle myosin II-C, a new member of the myosin II family. *J Biol Chem* 279:2800–2808
 153. Itoh K and Adelstein RS [1995] Neuronal cell expression of inserted isoforms of vertebrate nonmuscle myosin heavy chain II-B. *J Biol Chem* 270:14533–14540

154. Shohet RV, Conti MA, Kawamoto S, Preston YA, Brill DA, and Adelstein RS [1989] Cloning of the cDNA encoding the myosin heavy chain of a vertebrate cellular myosin. *Proc Natl Acad Sci USA* 86:7726–7730
155. Rosenfeld SS, Xing J, Chen LQ, and Sweeney HL [2003] Myosin IIb is unconventionally conventional. *J Biol Chem* 278:27449–27455
156. Wang F, Kovacs M, Hu A, Limouze J, Harvey EV, and Sellers JR [2003] Kinetic mechanism of non-muscle myosin IIB: functional adaptations for tension generation and maintenance. *J Biol Chem* 278:27439–27448
157. Gorodeski GI [2006] Estrogen modulation of MgATPase activity of non-muscle myosin-II-B filaments. *Endocrinology* 148:279–292

16

In Vitro Models and Multidrug Resistance Mechanisms of the Placental Barrier

Pallabi Mitra and Kenneth L. Audus

Abstract The placenta barrier comprises a dynamic fetal:maternal interface for controlling the exchange of essential nutrients, gases, metabolic wastes, toxins, and drugs. Long considered a “leaky” filter, the characterization of several prominent efflux transporters in the placenta suggests a more active role for the tissue in regulating exposure of the fetus to substances circulating in the maternal circulation. Understanding the role of the placenta in regulating drug distribution is key to the future of design of therapeutic agents that are safe for use in pregnancy. Reviewed herein are in vitro model systems for studying placental transport as well as consideration of some of the well-represented multidrug resistance transporters naturally expressed in this unique tissue.

Keywords: Placenta; Trophoblast; Multidrug resistance; Transport; Cell culture

Abbreviations

ABC	ATP-binding cassette
BCRP	Breast cancer resistant protein
cAMP	Cyclic adenosine monophosphate
CAR	Constitutive androstane receptor
cDNA	Complementary deoxyribonucleic acid
CF-1	Carworth Farms inbred type 1
cGMP	Cyclic guanosine monophosphate
CYP	Cytochrome P450
DHEAS	Dehydroepiandrosterone sulfate
E1	Estrone
E2	17 β -estradiol
EE	Ethinyl estradiol
EGF	Epidermal growth factor
ELISA	Enzyme-linked immunosorbent assay
ER α	Estrogen receptor α
ER β	Estrogen receptor β
FDA	Food and Drug Administration

FXR	Farnesoid-X-receptor
GSH	Glutathione
hCG	Human chorionic gonadotropin
HIV	Human immunodeficiency virus
MDCKII	Madin-Darby canine kidney strain II
MDR	Multidrug resistant protein
MRP	Multidrug resistance-associated protein
OCT	Organic cation transporter
OCTN2	Organic cation transporter novel
P-gp	P-glycoprotein
PPAR α	Peroxisome proliferators-activated receptor type alpha
PR _B	Progesterone receptor B
PXR	Pregnane X receptor
RXR	Retinoid X receptor
SAR	Structure–activity relationship
T3	Tri-iodothyronine
T4	Thyroxine
WBC	White blood cells

16.1. Introduction

During pregnancy, the placenta is responsible for the transfer of essential nutrients and respiratory gases from the maternal circulation to the fetus and also for clearing out fetal metabolic wastes. It is also the site of synthesis of many hormones and regulatory factors required to support a healthy pregnancy. While earlier on it was believed that the placenta prevents the passage of toxic substances from the maternal circulation to the fetus, the thalidomide disaster in the 1960s called into question the characterization of the placenta as a protective “barrier.” Since then, many studies have indicated that most chemical substances and drugs have the ability to cross the placenta [1–4]. However, drugs are often necessary during pregnancy either to treat ongoing chronic conditions, such as asthma, diabetes, and psychiatric disorders, or for complications that develop during pregnancy. Recent studies indicate that ~50% of pregnant women take prescription drugs [5, 6] and around 4% use drugs for which fetal risk has been demonstrated in animals or humans. Moreover, these studies did not take into account exposure to over-the-counter medications. It is possible that some of these drugs may accumulate in the placenta and interfere with normal placental functions; or they may be transformed in the placenta to a toxic metabolite; or after transplacental passage, they may accumulate in the fetus in concentrations high enough to produce abnormalities. Therefore, a way to reduce the potential toxicity posed by these drugs upon the embryo/fetus would be to modulate the extent to which they undergo transplacental transfer or modification.

The human placenta expresses a number of nutrient and efflux transporters, as well as metabolic enzymes. Information about the placental function and regulation of these systems, and how they interact with the administered drug, can help to target them appropriately so as to limit fetal exposure to harmful substances.

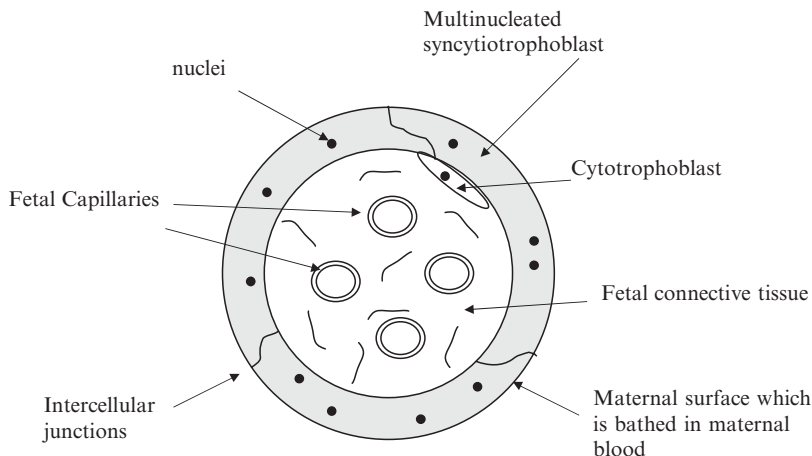


Figure 16.1 Illustration of the anatomical arrangement of the syncytiotrophoblast (placental barrier) and the fetal capillaries as would appear in a cross section of a human placental villus. Reprinted from Audus [10] with permission from Elsevier B.V.

16.2. Structure of the Placenta

The anatomical units of the human placenta are the placental lobes or cotyledons and at term the placenta has 20–30 such lobes [7]. Cotyledons have villous trees containing the fetal blood vessels. Maternal blood enters and leaves through the basal plate on the maternal side of the cotyledon and circulates in the intervillous space [8]. There are essentially three layers separating the maternal and fetal circulations—a single layer of multinucleated syncytiotrophoblast (also containing some precursor cytotrophoblasts), a connective tissue layer, and a layer of endothelial cells of the fetal capillaries. As illustrated in Figure 16.1, the syncytiotrophoblast layer is in direct contact with maternal blood and constitutes the rate-limiting barrier for transfer of substances between mother and fetus [9]. During the embryonic period of pregnancy, when the placenta is not completely structured, components of the maternal circulation have much easier access to the embryo [7]. Also, with the progress of gestation, the placenta undergoes some structural alterations, such as an increase in surface area and thinning of the syncytiotrophoblast layer [10].

16.3. Placental Transport Mechanisms

Passive diffusion is considered to be the major pathway by which xenobiotics cross the placenta. Paracellular diffusion was shown to be the predominant pathway for transfer of hydrophilic solutes, such as chloride ions across perfused placental lobes and opioid peptides and dextrans across BeWo cells [11–13]. It has been proposed that denudations in the syncytiotrophoblasts-containing fibrinoid deposits provide a possible paracellular route across the placenta [14]. Transtrophoblast channels in the syncytiotrophoblasts could also be responsible for this mode of diffusion [15]. For more lipophilic solutes, the transplacental route appears to be the preferred mode of passage

[16–18]. As observed with other physiological barriers, compounds having a low degree of ionization and experiencing low protein binding in the placenta permeate well. The molecular weight cutoff appears to be around 600 Da although larger compounds also seem to experience adequate permeation [10]. A number of carrier-mediated transport mechanisms exist at the placental barrier for transport of endogenous substances, such as amino acids, neurotransmitters, and glucose [19–21]. Their pharmaceutical importance is underscored by the fact that drugs/drugs of abuse can restrict endogenous substances for uptake via these transporters [22]. Several phase I and phase II metabolic enzymes are also expressed in placenta, indicating the possibility of production of inactive or toxic metabolites. Efflux transporters are present in many tissues, such as intestine, liver, and kidney, where they limit xenobiotic exposure by extruding them out of the cells. This process also confers tumor cells with the property of multidrug resistance. The human placenta is known to express several multidrug resistance transporters, such as P-glycoprotein (P-gp/MDR1), multidrug resistance-associated protein (MRP), and breast cancer resistance protein (BCRP). Although all of these processes together (i.e., nutrient transporters, metabolic enzymes, and efflux transporters) contribute to the amount of drug/xenobiotic that the fetus is exposed to, it is beyond the scope of this chapter to review all of them and hence the focus will be on in vitro models of the human placenta, specifically models focusing on efflux transporters, as well as placental multidrug resistance proteins and their regulation. Knowledge about the mechanisms of interactions of drugs with placental efflux transporters, as well as transporter regulation, can provide different ways of controlling the amount of drug reaching the fetus. To this effect, Sect. 16.4 will focus on the available placental model systems and Sect. 16.5 on the major efflux transporters detected in human placenta and their regulatory mechanisms.

16.4. Available Model Systems

The degree of exposure of the fetus to a particular substance can be best assessed in human subjects, but concerns of fetal safety have restricted the use of this approach. Moreover, clinical studies cannot elucidate the various mechanisms that contribute to transplacental transport of a particular compound. There are many structural differences between the human placenta and the placenta of other mammalian species, which complicates extrapolation of data obtained from in vivo animal models to humans [7]. Thus, several ex vivo and in vitro techniques have been developed to study the placental role in drug transfer and metabolism during pregnancy and there are some excellent articles that discuss these systems in detail [7]. Both isolated tissues and various cell culture techniques are currently in use and these have been summarized below.

16.4.1. Perfused Placental Model

Of all the models, the ex vivo perfused placenta most closely resembles the in vivo situation, because it retains the placental organization. It has been used to estimate drug transport across the placenta [23, 24]. The cotyledon is the anatomical unit of the placenta and at term, the human placenta contains about 20–30 cotyledons. In the perfused placenta technique, term placentas are

collected immediately after delivery and a cotyledon without leaks is selected. The fetal artery and vein of a single cotyledon are cannulated to establish the fetal circulation and flushed with a heparinized solution to remove fetal blood. The maternal circulation is established via cannulation through the maternal decidual basal plate into the intervillous space. The entire system along with the maternal and fetal perfusion reservoirs is housed at 37°C. Either an open or a closed mode can be utilized, with the perfusates recycling in the latter but not in the former [7]. The system is allowed to equilibrate for 20–30 min with a drug-free perfusate to achieve stabilization and determine viability. To assess maternal to fetal transfer, perfusate containing drug is added to the maternal chamber, while the fetal chamber is drug free. Samples are then collected from maternal inflow perfusate and fetal outflow perfusate and analyzed for drug. For estimating fetal to maternal transfer, initially drug is added to fetal chamber, but not to the maternal. Samples are collected from fetal inflow and maternal outflow perfusate. If an open system is used then maternal and fetal clearance values can be calculated at steady state [23]. To correct for experimental variables, such as flow rates and perfused area, antipyrine is often used as a reference molecule (it exhibits rapid diffusion, minimal metabolism, and low protein binding) [25]. In closed systems, the percentage drug transferred is calculated instead of clearance. The physical integrity of the system is assessed by monitoring the fetal volume loss, stability of fetal perfusion pressure, etc. while metabolic stability is assessed by consumption of glucose and oxygen and production of lactate and human placental lactogen [26, 27]. The model can also be used to determine the effects of endogenous and exogenous substances on transport. It can provide information on placental metabolism, as well as release of endogenous substances into the maternal and fetal circulation [28, 29]. Transfer of a wide variety of drugs, such as anti-hyperglycemics, HIV protease inhibitors, and antibiotics, has been assessed with the placental perfusion model [3, 30, 31] and some studies have reported very good correlations between results obtained from *in vivo* situations and the perfusion experiments [32, 33].

The placental expression of many transporters and metabolic enzymes vary with advancing gestation and hence, it is worthwhile to assess drug transfer at different stages of pregnancy. One of the drawbacks of the perfused placental system is that it cannot be used to study processes occurring during the first trimester. It also does not take into account the effects that metabolites (maternal or fetal) may have on drug transfer. Further, because of a lack of pregnant body mass it underestimates the volume of distribution [7]. These make it difficult to extrapolate the results to *in vivo* situations, but the model still provides a lot of relevant information.

16.4.2. Trophoblast Tissue Preparations

It has been mentioned before that the syncytiotrophoblast cells form the outermost layer of the placental villi and constitute the rate-limiting barrier for the transfer of drugs, nutrients, etc. They are a result of the fusion of blastocyst-derived precursor cytotrophoblast stem cells. This syncytium is polarized both with respect to membrane morphology and expression of transporters, enzymes, and hormones. Throughout gestation, the maternal-facing apical membrane contains a microvillous border that is lacking in the basal membrane. Similarly some efflux and nutrient transporters are expressed

predominantly in the apical membrane (e.g., P-gp, BCRP, OCTN2), while others are localized to the basolateral membrane (e.g., MRP1, OCT3) [34–36]. Because of their obvious importance in pregnancy with relation to transplacental transfer of drugs and nutrients, various types of trophoblast preparations have been isolated from placenta and studied extensively.

16.4.2.1. Villous Preparations

In this technique villous tissue obtained from placenta are further dissected into fragments about 2 mm in size and incubated in media containing the drug/nutrient (often radioactively labeled) whose uptake is being evaluated. After an appropriate time period, the fragment is removed, washed, and lysed in distilled water to release the radioactive substrate, which is analyzed by scintillation counting. The fragments are then denatured in sodium hydroxide to obtain the uptake in terms of amount/mass of protein [19, 37]. To name a few of the applications, the system has been utilized to study placental uptake of amino acid and glucose, hormonal regulation of placental glucose and amino acid transporters, and determination of P-gp expression and activity [20, 37, 38]. Since syncytiotrophoblast cells form the outermost layer of the placental villi, it can be assumed that the results reflect uptake into the syncytiotrophoblast layer. This *ex vivo* model maintains its structural integrity up to at least 3 h, as evidenced by an intact microvillous border membrane, thick syncytium, intact plasma membrane, cell organelle frequency, distribution similar to the beginning of the incubation period, etc. Parameters such as similar rates of production of human placental lactogen and 17β -estradiol for the entire length of the experiment, as well as lactate dehydrogenase release, have been used to assess the functional integrity of the system [20, 37, 39]. Since in this technique the syncytiotrophoblast cells do not require extensive culture, one advantage over cell cultures of trophoblasts is that transporter expressions is unlikely to change during the course of the study. Furthermore, polarization and cell–cell contacts are more likely to resemble the *in vivo* situation than either cultured trophoblast cell lines or isolated cytotrophoblast cells. The villous preparation technique has been successfully applied to comparisons of amino acid uptake between first trimester and term placenta, suggesting that it can be utilized throughout gestation [39].

It should be mentioned that the placental villous fragments can be used to measure uptake into the syncytiotrophoblast layer but they cannot be used for trans-cellular transport studies. If the transporter is expressed in the microvillous border membrane, the effects of various factors on transporter function can be determined. Another disadvantage is that the villous fragments may be heterogenous in composition and hence, uptake experiments may not be reflective of syncytiotrophoblast uptake alone.

16.4.2.2. Microvillous Border Membrane and Basal Membrane Vesicles

Primarily to elucidate transporter localization and function, vesicles enriched in trophoblast apical or basolateral membranes have frequently been utilized. To give a few instances, they have been used to investigate P-gp-mediated transport, mechanisms of transport of cationic compounds, drug interactions with nutrient transport, and differences in amino acid transport in pathological conditions of the placenta [36, 40–42]. Briefly, for preparation of microvillus membrane vesicles the cord, amniochorion and decidua are removed from placenta, and the tissue cut on the maternal side. The mince is stirred to loosen

the microvillus membrane and filtered through two layers of woven cotton gauze. The filtrate is then subjected to a series of centrifugation steps to obtain the microvillar membrane preparation. To prepare the basal membrane vesicles, again placental tissue is excised off cord, amnion, and deciduas, and cut on the maternal side and sliced. The tissue is washed, sonicated, and strained through a nylon mesh a few times. The supernatant is collected, centrifuged a couple of times, and the pellet is recovered. This is resuspended to obtain the crude basal membrane fraction which is further purified by centrifugation on a Ficoll gradient [36, 43]. Membrane preparations are then tested for their integrity and orientation by monitoring marker enzyme activity. The apical membrane vesicles are characterized by enrichment of the activity of several marker enzymes, such as alkaline phosphatase and γ -glutamyl transpeptidase. The orientation or sidedness of the vesicles is detected by measuring the nucleotide pyrophosphatase activity in the presence or absence of detergent [44, 45]. P-gp is also sometimes used as a marker, due to its enrichment in the microvillous border membrane of the syncytiotrophoblast. Basolateral membrane vesicle enrichment is measured by the binding of the β -adrenergic antagonist dihydroalprenolol and the orientation by binding of ouabain in the presence or absence of detergent [43, 46].

This system has been widely used in uptake experiments to study transporter function. As Glazier et al. [47] have pointed out, an advantage of the system is that transporter function can be assessed independently of the contributions of metabolic systems. A disadvantage, however, is that all transporter regulatory mechanisms (many of which may be intracellular) are not preserved in this system, thus making the extrapolation of the results to *in vivo* situations somewhat difficult.

16.4.3. Trophoblast Cultures

Advances in cell culture techniques have allowed the use of trophoblast cell cultures to evaluate the various transporter and metabolic systems of the placenta. Many studies have used primary cultures of undifferentiated cytotrophoblasts isolated from placentas, whereas others have used trophoblast cell lines as a model. Trophoblast cell lines can be generated from normal tissues or malignant tissues and also from embryonal carcinomas exhibiting trophoblast differentiation [48].

Since transport across the syncytiotrophoblast layer is the rate-limiting step in the absorption of substances from the maternal circulation to the fetal, these cells can provide information on uptake processes which are subject to intracellular regulatory mechanisms or affected by intracellular metabolism. However, it is very difficult to isolate this layer because of its syncytial nature. As a result, the undifferentiated precursor cytotrophoblast cells have been isolated and cultured. These cells do not proliferate in culture, but aggregate and spontaneously differentiate into syncytiotrophoblasts [49].

Morphologically, this is demonstrated by the development of a multinuclear syncytium with apical microvilli [49], while functional differentiation is associated with induction and synthesis of hormones, such as human chorionic gonadotropin (hCG) and human placental lactogen (hPL) [50, 51]. Cultures of primary cytotrophoblasts have been used to study functional expression of P-gp, amino acid uptake, and hormonal stimulation of amino acid uptake and

cytochrome P450 activity, demonstrating that they provide a very good in vitro model for studying uptake, efflux, metabolism, and hormone secretion [52–55]. These cells have been widely used to evaluate variations in transporter expression as they differentiate into syncytiotrophoblasts. Evseenko et al., for example, found that as the cytotrophoblasts differentiated into syncytiotrophoblasts there was a significant decrease in P-gp levels, but a significant increase in BCRP protein and mRNA levels [56]. Similarly, the expression of MRP5 increased as the cytotrophoblasts differentiated into syncytiotrophoblasts, as observed by immunohistochemistry and correlation with hCG production [44]. MRP2 mRNA increased up till day 2 in culture, but decreased from day 2 to day 5 [57]. In culture, however, as the cytotrophoblasts spontaneously differentiate into syncytiotrophoblasts, they tend to aggregate, producing large intercellular spaces, and do not form a confluent monolayer with tight junctions. This renders them unsuitable for transtrophoblast transport studies. Hemmings et al. have proposed a system that consists of multiple seedings of highly purified cytotrophoblasts grown in the presence of the epidermal growth factor (EGF), which has been reported to promote differentiation [58]. The resulting cell cultures were confluent, demonstrated tight junctions, and limited passive diffusion of high and low molecular weight markers. The culture, however, consisted of multiple layers of syncytial units instead of a single monolayer and may thus be more representative of first trimester pregnancy, where there are multiple layers of trophoblast cells.

Trophoblast-like cell lines isolated from malignant choriocarcinoma (e.g., BeWo, Jar, and JEG-3) provide alternative in vitro models for studying transtrophoblast transport and placental metabolism. The choriocarcinoma derived cell line, BeWo, has proven to be very useful for studying the transcellular distribution of drugs and nutrients across trophoblast cells, as they form polarized, confluent monolayers. The BeWo cell cultures, though somewhat heterogeneous in nature, consist predominantly of cytotrophoblasts and secrete hormones like typical trophoblast cells [59, 60]. They are easy to maintain and grow to a confluent monolayer within a short period of time. Liu et al. utilized the b30 subclone of BeWo cells and reported that a confluent monolayer is formed between 4 and 6 days in culture [13]. Transmission electron micrographs of the cells grown on Transwell® inserts indicated the presence of a single layer of cells with close cell apposition. The presence of apical microvilli reflected morphological characteristics similar to placental trophoblasts. That the cells form an effective physical barrier was shown by the decreased permeation of hydrophilic marker molecules as a function of increasing molecular weight. The cells exhibit placental differentiation markers, such as placental alkaline phosphatase and hCG, and display many of the characteristics of third-trimester trophoblasts [60, 61]. On treatment with forskolin, an activator of adenylate cyclase, the cells fuse, their nuclei cluster, no intercellular spaces are visible and there is development of an apical microvillus border, a process morphologically resembling the differentiation of cytotrophoblasts into syncytiotrophoblasts [62]. Unlike primary cytotrophoblasts, however, this differentiation process is not spontaneous. In addition, when grown on Transwell® inserts, the cells are polarized with respect to the expression of transporters specific to the apical and basolateral membranes, and marker enzymes similar to trophoblasts [60]. Vardhana et al. have hypothesized that since glucose transporters are expressed predominantly in the microvillous membrane of the

syncytiotrophoblast layer, the basal membrane may be rate limiting for the transepithelial transport of glucose. They used BeWo cells as a placental model, because these exhibit the same asymmetric distribution of glucose transporters as the syncytiotrophoblast layer. With the help of the basal membrane glucose transport inhibitors, it was shown that transepithelial glucose transport is rate limited by the basal membrane [63]. Utoguchi et al. demonstrated functional P-gp activity (using calcein-AM and vinblastine uptake studies in the presence of specific P-gp inhibitors) in both primary cytotrophoblast cells and BeWo cells [53]. Cerneus et al. noted the similarity of transferrin receptor expression in BeWo cells and trophoblasts [64]. The BeWo cell line has been successfully utilized in the transtrophoblast transport and uptake of several nutrients, such as carnitine, cholesterol, amino acids, and folic acid [54, 65–68], as well as drugs, including diphenhydramine and salicylic acid [69, 70]. It has also been shown that the BeWo cells are a good model for studying placental metabolism. For example, they express the major cytochrome P450 isoforms (CYP1A1 and 1A2) present in placenta, and the inducibility of these isoforms makes the cell line a suitable model for studying enzyme induction in the human placenta [52].

Either Transwell[®] inserts or side-by-side diffusion chambers can be used for transport studies. Bode et al. have provided an excellent review on this subject [60]. Briefly, cells are incubated for 30–60 min with a buffer solution. To initiate the transport study, a transport buffer containing the drug under investigation is added to either the apical or the basal chamber depending on the transport direction of interest. At predetermined time points, the respective receiver chamber is sampled and the withdrawn volume is replaced with the same volume of fresh buffer. The permeability coefficient (P_{app}) is calculated and the ratio of P_{app} in the basolateral-to-apical direction versus that in the apical-to-basolateral direction gives the efflux ratio. These sort of transport experiments are well suited to determine if drugs/xenobiotics are substrates of the placental efflux proteins.

A study by Evseenko et al. has shown that in some cases the choriocarcinoma cell lines, including BeWo cells, may have limited application in demonstration of transtrophoblast transport. They showed that the expression of P-gp/MDR1 varied widely among cytotrophoblasts and the choriocarcinoma cell lines, BeWo and JAr, though the activity did not vary so much [56]. P-gp/MDR1 protein expression was very high in the trophoblast cells, but was barely expressed in BeWo cells. Utoguchi, et al., however, have successfully demonstrated P-gp functional activity in the b30 subclone of BeWo cells [53], demonstrating difference in transporter expression between subclones. In the same study, Evseenko et al. showed that BCRP expression varied between BeWo and primary trophoblast cells though activity levels were similar among all cell types studied. The overall expression pattern of the different transporters in this study revealed that the BeWo cells are more similar to syncytiotrophoblasts than to cytotrophoblasts though previously it has been shown that morphologically BeWo bears closer resemblance to cytotrophoblasts than to syncytiotrophoblasts [61].

The choriocarcinoma cell line JAr bears close resemblance to early trophoblast, as their secretion pattern of hCG and steroids is similar, and the cells can differentiate into syncytiotrophoblasts in vitro [71]. In a study comparing efflux transporter expression and activity in trophoblast cell lines and choriocarcinoma cells, the expression profiles indicated that while BeWo are more

similar to syncytiotrophoblasts, JAr cells are more similar to cytotrophoblasts [56]. JAr cells have been used as a suitable in vitro model to study the uptake of serotonin, cholesteryl esters, tri-iodothyronine (T3), and thyroxine (T4) [72, 73]. However, they are not suitable for transepithelial transport experiments, as they do not form confluent monolayers in culture. Freshly isolated JAr cells form monolayers, but fail to display cell surface polarization. The monolayers were also unstable, as with prolonged proliferation there was observed formation of multilayer aggregates and a further loss of tight junction-associated proteins [74].

The JEG-3 cells were originally derived from the BeWo cells [71]. In culture they form large multinucleated syncytial aggregates. At high densities, the cells form multilayers and express large quantities of the trophoblast markers, hCG and placental lactogen [71, 75]. Like JAr cells, they are suitable for uptake experiments [69, 75], but not for transepithelial transport, due to their inability to form electrically tight polarized monolayers.

Xu et al. [76] have showed that human embryonic stem cells by treatment with bone morphogenetic protein-4 can be driven to differentiate into trophoblasts which have the ability to syncytialize and form confluent monolayers. The differentiated cells express a number of trophoblast markers and secrete placental hormones and thus may provide an alternative placental model. Under the culture conditions used, however, the cells propagated poorly.

16.5. Multidrug Resistant Transporters of the Placenta

16.5.1. MDR1/P-Glycoprotein (ABCB1)

The efflux pump P-glycoprotein (P-gp/MDR1) is a member of the ATP-binding cassette (ABC) superfamily of transporter proteins. Members of this family are usually located in the plasma membrane where they extrude a wide variety of substrates out of cells. This process depends on ATP hydrolysis and can take place against a concentration gradient. In humans, P-gp is the product of the MDR1 gene and is a 170-kDa protein. Structurally, it consists of two homologous halves, each half containing one transmembrane domain (that consists of six transmembrane segments) and another hydrophilic nucleotide-binding domain [77].

P-gp is expressed in many different tissues, such as intestine, kidney, liver, and brain, and is associated with limiting oral absorption, brain uptake, facilitating elimination, etc. A variety of clinically relevant compounds are P-gp substrates or interact with P-gp, including anticancer drugs (e.g., paclitaxel, vincristine), HIV protease inhibitors (e.g., saquinavir, zidovudine), calcium channel blockers (e.g., verapamil), immunosuppressive agents (e.g., cyclosporine A), and antibiotics (e.g., telithromycin) [78–80]. P-gp recognizes substrates that are structurally very diverse and this can lead to drug–drug interactions on coadministration of substrates and/or inhibitors. Thus, there is a lot of interest in elucidating the characteristic structural features of P-gp substrates and inhibitors beforehand. Literature abounds with studies dedicated to understanding the SAR (structure–activity relationships) of P-gp substrates [81]. To summarize briefly, P-gp substrates are mostly lipophilic. They are generally amphiphilic although weakly cationic substrates are also transported. Acidic compounds, such as methotrexate and phenytoin, are also transported, though

to a much lesser extent. Substrates generally contain groups capable of forming H-bonds and electronegative groups that confer dipole moment [81]. Some studies have shown that an increase in the number of H-bonding groups can increase P-gp-mediated efflux while conformational restraints, such as cyclization, produce the opposite effect. Computational modeling approaches have also recently shown that a difference in the capability to form H-bonds is what separates substrates from inhibitors [82]. Passive permeability of the substrate also appears to be a critical factor, since too high or too low a passive permeability decreases local concentrations of the substrate, ultimately reducing P-gp-mediated transport.

Cordon-Cardo et al. used immunohistochemistry to show that P-gp is expressed in trophoblasts, and similar studies since then have shown P-gp to be localized to the microvillous (maternal-facing) membrane of syncytiotrophoblast, although there also seems to be some expression in the placental macrophages (Hofbauer cells) [83–85]. It has been shown in mice that placental P-gp can play a role in limiting the fetal exposure to chemicals. In mice there are two P-gp isoforms encoded by the *Mdr1a* and *Mdr1b* genes. A fraction of the CF1 mice strain naturally lacks the *Mdr1a* gene, leading to a loss of placental P-gp. During pregnancy, mice from this strain were exposed to an isomer of the pesticide avermectin that can produce cleft palate [86]. It was seen that fetuses with the genotype *Mdr1a*($-/-$) were most susceptible and fetuses with the genotype *Mdr1a*($+/+$) were least susceptible to cleft palate. Smit et al. used the *Mdr1a/Mdr1b* mice knockout model where they mated mice of the genotype *Mdr1a* $+/-$ *Mdr1b* $+/-$ so as to obtain the fetal genotypes *Mdr1a* $+/+$ *Mdr1b* $+/+$, *Mdr1a* $+/-$ *Mdr1b* $+/-$, and *Mdr1a* $-/-$ *Mdr1b* $-/-$ in a single mother [87]. Pregnant dams were exposed to three P-gp substrates and in each case, fetuses with the genotype *Mdr1a* $-/-$ *Mdr1b* $-/-$ had the greatest substrate exposure. Both these studies illustrate that placental P-gp in mice can reduce fetal exposure to chemicals. Uptake studies and immunoblotting experiments have shown P-gp to be functional in both cytotrophoblast cells isolated from human placenta and trophoblast-like cell lines [53, 56]. Furthermore, human and mouse P-gp, particularly MDR1 and MDR1a, have similar substrate specificities. The activity of P-gp in human placenta, as well as its similarity to the mouse isoform, indicates that in humans also placental P-gp may play a similar role of reducing fetal exposure to teratogens.

Some P-gp inhibitors have been tested in clinical trials (e.g., GF120918, PSC 833) [88, 89]. Shortly before birth, it is often desirable to expose the fetus to anti-HIV medications to prevent HIV transmission from the mother to the fetus during delivery. Preperfusion with P-gp inhibitors increased fetal penetration of the protease inhibitor saquinavir in *in vitro* placental models, and it has been hypothesized that P-gp may be responsible for limiting fetal exposure to HIV protease inhibitors, methadone, anthracyclines, and taxanes [90–93].

It needs to be mentioned here that there remains some controversy over the placental expression of P-gp as a function of gestational age. An immunohistochemical study done by Macfarland et al. showed that P-gp was localized to the microvillous border of trophoblasts in first trimester placenta, but not in term placenta [85]. Subsequent studies refuted this to show that MDR1 mRNA is present throughout pregnancy [94]. More recently, enzyme-linked immunosorbent assay (ELISA) performed in syncytial microvillous membrane showed that P-gp protein expression in early gestational age placenta is about

fivefold higher than at term. P-gp mRNA expression followed a similar pattern with respect to increasing gestational age, indicating transcriptional regulation at least in part [34]. This pattern of expression has been corroborated by other authors though the degree of variation differs between the studies [95, 96]. In another study, Evseenko et al. observed the expression of P-gp as term cytotrophoblasts spontaneously differentiated into syncytiotrophoblasts in vitro [56]. Cells at 120 h had significantly less MDR1 mRNA than cells at 24 h. Taken together, this seems to indicate that P-gp expression is under developmental control. During the early period of pregnancy, when precursor cytotrophoblast cells have not fully differentiated into syncytiotrophoblasts, the expression of P-gp is maximal, possibly to protect the fetus from potential teratogens present in the maternal circulation. In addition to the gestational-age-related variation in P-gp, apical membrane preparations from 81 placentas showed a big interindividual difference in P-gp expression. Hence, when targeting placental P-gp for modulating transplacental drug passage, these variations should be taken into account, as they may affect the efficacy of individual drug treatments.

Information about the regulation of efflux transporter can provide more pathways of targeting the transporter protein for the purpose of drug delivery. Progesterone is one of the major hormones produced during pregnancy and it is produced by the trophoblast cells themselves. Young et al. have demonstrated that progesterone has the ability to modulate placental P-gp expression and activity [97]. At term, the placenta produces about 1 mmol progesterone/day and local concentrations may be much higher than the observed maternal plasma concentrations of 400–500 nM [97]. Progesterone is not transported by P-gp, but does bind at a non-transporting, allosteric site and reverses multidrug resistance [98–100]. In fact, there appear to be as many as four different binding sites on MDR1 for progesterone [101]. In many instances it has been demonstrated that progesterone is an acute inhibitor of P-gp. It has been shown that progesterone inhibits P-gp-mediated efflux of [³H]-vinblastine and rhodamine 123 [99, 102]. In a murine monocytic leukemia cell line over-expressing *mdr1a/1b*, progesterone and its derivatives inhibited calcein-AM accumulation, although progesterone did so at a tenfold higher concentration than the potent P-gp inhibitor quinidine [103]. In L-MDR1 cells it inhibited P-gp with approximately equal potency as quinidine. A common feature among these studies has been that steroid hydrophobicity is most effective for P-gp inhibition [99, 103, 104]. C-7 analogs of progesterone with bulky aromatic substituents were found to be the most potent P-gp inhibitors [104]. Kim et al. took a different approach and observed P-gp expression as a function of chronic exposure (48–72 h) to progesterone in a human colon carcinoma cell line [105]. At 5 and 50 μ M, progesterone produced a two- and threefold increase in MDR1 mRNA, respectively. The induction was also time dependent and progesterone also stimulated P-gp ATPase activity in a concentration-dependent manner. Although none of the above studies have actually looked into the effects of progesterone and its derivatives on P-gp in placental tissue, the possible interactions should be carefully considered, especially since local placental concentrations of progesterone can be high as mentioned previously and could affect the P-gp-mediated transfer of drugs/xenobiotics across the placenta. Young et al. observed that progesterone inhibited P-gp at 1 h incubations, but long-term exposures produced a decrease in calcein accumulation in BeWo

cells and this difference was eliminated in the presence of the P-gp inhibitor cyclosporine A [97]. This indicated that progesterone produced an increase either in P-gp activity or in expression. Western blots indicated that under chronic exposure progesterone induced P-gp expression. The authors suggested that the long-term effects of progesterone could be mediated by pregnane X receptor (PXR) as long-term exposure also increased PXR protein expression. It seems that acute and chronic exposures to progesterone produce the opposite effects on P-gp expression in placenta but since progesterone is one of the major hormones produced during pregnancy, its long-term effects on P-gp are more likely. Estrogenic compounds also exercise some regulation over P-gp expression. Although estrogen levels are low early in pregnancy, at term maternal estrogen concentrations parallel those of progesterone. Along with progesterone, estrogens are also produced by the placenta during pregnancy [106]. The xenobiotic bisphenol A, which mimics the actions of endogenous estrogens, stimulated P-gp in the placental cell line BeWo in a dose-dependent manner as evidenced by calcein accumulation [107]. The effect was observed only with acute exposures to bisphenol A and was reversed in the presence of the P-gp inhibitor cyclosporine A. In the same study it was also reported that 17- β -estradiol also significantly decreased calcein accumulation. Together they produced an additive effect. Since neither produced any marked changes in P-gp protein expression, it was assumed that the effect of bisphenol A on P-gp was due to a direct effect on P-gp. Seventy-two hour incubations with estrone and estriol upregulated expression of MDR1 mRNA and protein but beta-estradiol had no effect on MDR1 mRNA [105]. 17 β -Estradiol seems to stimulate P-gp expression of MDR1 mRNA and protein but only in cells expressing the estrogen receptor ER- α [108]. In BeWo subclone b30, which expresses ER- β but not ER- α , it produced no such effect [107].

MDR1 expression mediated by drugs/xenobiotics in other human tissues is in many cases modified by activation of the PXR pathway [109]. Forming a heterodimer with the retinoid X receptor (RXR), it binds to specific DNA sequences and modulates transcription of genes, such as CYP3A4 and MDR1. To evaluate, if placental P-gp is under PXR control, Mathias et al. [34] examined the expression of PXR and MDR1 transcripts in placenta as a function of gestational age. While P-gp expression was inversely correlated to gestational age, PXR expression did not depend on it, suggesting a P-gp regulation mechanism independent of PXR. In contrast, Young et al. have suggested a possibility of upregulation of P-gp protein by chronic progesterone exposure to be mediated by PXR [97]. Mathias et al., [34] however, did find a good correlation between the expression of the pregnancy-specific hormone hCG- β and P-gp, and indicated that this could mean either that hCG- β regulates P-gp or that both are regulated by a common mechanism. Another nuclear receptor, constitutive androstane receptor (CAR), also activates MDR1 expression by binding to a hormone-responsive element in the MDR1 gene [110]. However, Mathias et al. have demonstrated that the CAR mRNA was gestational age independent, indicating that the placental P-gp regulation is independent of CAR [34]. Several excellent reviews have focused on other regulators of P-gp, such as the tumor suppressor protein, DNA methylation, inflammation, hypoxia, and exposure to carcinogens [111].

More information about the placental regulation of MDR1 will provide more options to choose from, when the intention is to modify its placental expression levels to either treat or protect the fetus. The various regulatory mechanisms of

P-gp outlined above are potential pathways that can be exploited to improve or prevent the transplacental passage of drugs. It should be noted that most of these pathways involve a complex interplay of several factors that may vary in a cell- or tissue-specific manner and hence their contribution to placental P-gp should be explored.

16.5.2. Multidrug Resistance-Associated Proteins

The MRPs also belong to the ABC family. To date, nine MRPs have been discovered and the structures of six of these (MRP 1–6) have been characterized. Like P-gp, MRP4 and MRP5 have 12 transmembrane domains, while MRP1, MRP2, MRP3, MRP6, and MRP7 have five additional transmembrane domains at the N terminus [111, 112]. Among these the MRP1 protein has been studied most extensively.

16.5.2.1. MRP1/ABCC1

MRP1 is a 190-kDa protein which is expressed in many tissues in the human body, such as lung, testis, kidney, and peripheral blood mononuclear cells. Like P-gp, MRP1 is overexpressed in many tumor cell lines and is responsible for tumor resistance to anticancer agents. Anticancer agents transported by MRP1 include the vinca alkaloids, anthracyclines, epipodophyllines, mitoxantrone, and methotrexate. MRP1 can transport anionic molecules, as well as neutral drugs conjugated with glutathione, glucuronide, or sulfate. It also exports substrates by cotransport with glutathione [113]. Unlike P-gp, MRP1 seems to be more prevalently localized to the basolateral membranes of epithelial cells. In spite of the localization, the protein seems to have cytoprotective effects. In MRP1 knockout mice, vincristine produced bone marrow toxicity (as assessed by loss of WBCs or white blood cells) compared with wild-type mice [114]. Moreover, intravenous administration of etoposide produced toxicity in the mucosa of tongue and cheek of MRP1^{-/-} knockout mice [115]. Mouse embryonic fibroblasts isolated from MRP1^{-/-} knockout mice accumulated twice as much unconjugated bilirubin as opposed to MRP1^{+/+} mice. The enhanced accumulation was associated with increased toxicity [116]. There seems to be some controversy about the placental localization of MRP1. St-Pierre et al. used immunofluorescence and immunoblotting to demonstrate localization primarily to the endothelium of fetal blood vessels and somewhat to the apical membrane of syncytiotrophoblasts, but more recent studies performed in trophoblasts from term placenta show MRP1 localization in the basal membrane of syncytiotrophoblasts [46, 84, 117]. Immunohistochemical staining revealed a much more diffuse distribution throughout the syncytiotrophoblast as well as the fetal capillary endothelium. Functional expression of MRP1 was determined by the efflux activity of calcein-AM in trophoblast cells using the specific MRP inhibitor MK 571 [56]. Interestingly, MRP1 activity was much lower in trophoblast cells than in the choriocarcinoma cells BeWo and JAr and hence care should be exercised when extrapolating information obtained in these models to in vivo situations. The polarized localization of P-gp and MRP1 to the apical and basolateral membranes, respectively, in the trophoblast could be indicative of very different functions in vivo. P-gp being localized on the microvillous border membrane would be ideal to protect the fetus from potential teratogens, but MRP1 would likely mediate the transport of substances toward the fetus.

In the case where xenobiotics have already gained fetal access, MRP1 would prevent their transfer back into the maternal circulation, thereby enhancing fetal susceptibility to side effects. Its placental function remains unclear to date. In an estrogen-responsive tissue in chick (the oviduct), mRNA of MRP1 (72% identity with the human isoform) was downregulated by estrogen. To the best of our knowledge the effects of estrogen on MRP1 in human placenta has not been tested so far.

16.5.2.2. MRP2/ABCC2

MRP2 facilitates transport of anticancer substances, such as cisplatin, vinblastine, and camptothecin derivatives and various glutathione, glucuronate, and sulfate conjugates. In placenta, MRP2 is localized to the apical membrane of syncytiotrophoblasts [46, 57] and like P-gp may contribute to fetal protection. In cases of perinatal HIV infection it is desirable to deliver drugs to the fetus. It has been seen that many antiretroviral drugs administered during pregnancy do not reach the fetus in therapeutic concentrations [91]. HIV protease inhibitors, such as saquinavir and indinavir, are MRP2 substrates and coadministration of MRP2 inhibitors could be a way of improved HIV medication delivery to the fetus. Like P-gp, MRP2 appears to be under developmental control, as it has been observed that there was an increase in mRNA and protein levels with advanced gestation, as was with differentiation of cytotrophoblasts into syncytiotrophoblasts [57]. Some steroid hormones regulate MRP2—in rats, for example, the protein is regulated by a combination of thyroxine and growth hormone [118]. The synthetic glucocorticoid dexamethasone induces MRP2 expression and function in rat hepatocytes [119]. The synthetic estrogen ethinylestradiol induces mRNA expression but decreases protein levels, suggesting posttranscriptional regulation [120]. The dexamethasone induction of MRP2 is probably mediated through PXR [121]. Protein expression is downregulated by PPAR α ligands [121], while mRNA expression seems to be induced also by farnesoid-X-receptor (FXR) and constitutive androstane receptor (CAR) [122]. While drug distribution across the placenta could benefit from more information about MRP2, some controversy still remains regarding its placental expression. Evseenko et al. found very low and undetectable levels of protein expression in primary trophoblasts and choriocarcinoma cell lines (BeWo and Jar), in spite of high levels of mRNA expression in all three cell types [56]. Meyer zu Schwabedissen et al. observed that in preterm placenta one of the single nucleotide polymorphisms in MRP2 was associated with low mRNA and protein expression, which could be a probable reason for the discrepancies observed in MRP2 expressions across different studies [57]. These interindividual variations in expression may affect the efficacy of drug treatments in cases where this transporter is targeted.

16.5.2.3. MRP3/ABCC3

Among the MRP transporters, MRP3 is the one most similar to MRP1 (58% homology) and like MRP1 is expressed predominantly in the basal membrane of epithelial cells [112, 123, 124]. It is an organic anion transporter, extruding glucuronate, sulfate, and glutathione conjugates, as well as bile salts [125, 126]. St. Pierre et al. have used immunoblotting to demonstrate MRP3 localization primarily not only in fetal blood vessels but also in the apical membrane of syncytiotrophoblast [46]. A later study found abundant mRNA expression both

in first trimester and term trophoblasts, but no detectable protein in Western blotting experiments which the authors concluded could be due to antibody issues [127]. MRP3-transfected cells exhibit a low degree of resistance to anticancer drugs and provide resistance to very few of them [128]. This and its controversial expression in placenta may indicate that it would play a limited role in relevant fetal drug delivery.

16.5.2.4. MRP5/ABCC5

MRP5 is expressed in tissues, such as the gut and kidney, and like the other MRP transporters, it transports organic anions. Additionally, it can transport the cyclic nucleotides cGMP and cAMP, indicative of its possible role in the signal transduction pathways of these molecules. In polarized MDCKII cells it was found to be localized to the basolateral membrane [129]. Along with MRP4, it confers resistance to anticancer agents, such as 6-mercaptopurine and 6-thioguanine, by extrusion of their thiopurine monophosphate metabolites out of cells [130]. However, it confers resistance to much fewer anticancer agents than do MRP1 or MRP2 [131]. MRP5 mRNA and protein have been detected in placenta, as well as in polarized BeWo cells [44, 127]. It has been shown in a recent study by immunolocalization techniques that in preterm placenta MRP5 is localized to the basal membrane of syncytiotrophoblasts, as well as fetal blood vessels [44]. In term placenta in addition to the basolateral membrane, MRP5 is also present in the apical membrane, but at a much lower amount. Significantly higher levels of cGMP transport in vesicles prepared from the basal membrane, as opposed to apical membrane vesicles, supported this. Like P-gp, MRP5 levels change as a function of gestation. Immunoblots showed that the total MRP5 protein was significantly less in term placenta compared with preterm placenta. As cytotrophoblasts differentiated in culture to syncytiotrophoblasts, the amount of MRP5 protein also increased, indicating its expression to be under developmental control. As of yet, its role in clinically relevant drug delivery during pregnancy has not been elucidated. In pituitary cells two different processes exist for transport of cGMP and cAMP, and MRP5 most likely mediates transport of cGMP [132]. In the same cells progesterone inhibited cGMP efflux, indicating that it may be a MRP5 inhibitor. The increasing levels of progesterone during pregnancy should be considered if targeting MRP5 for drug delivery. Cytotrophoblasts in culture differentiate to syncytiotrophoblasts in the presence of 8-Br-cAMP and 8-Br-cGMP. A possible role of MRP5 could be modulation of the intracellular levels of cGMP [44].

16.5.3. Breast Cancer Resistance Protein (BCRP/ABCG2)

In contrast to P-gp and the MRP proteins, the breast cancer resistance protein (BCRP) contains six transmembrane domains and only one ATP-binding domain. It was first cloned from the breast cancer cell line MCF-7 selected in doxorubicin, in the presence of the P-gp inhibitor verapamil. It is found in many human tissues, such as the placenta, small intestine, colon, and liver [133]. It is localized to the apical membrane of epithelial cells of the small intestine and colon and to the bile canalicular membrane in the liver and is involved in reducing intestinal uptake, increasing hepatobiliary excretion, etc., leading to diminished oral bioavailability. cDNA sequences identical to BCRP and named MXR and ABCP, respectively, were independently isolated from human colon carcinoma cells and human placenta [134]. BCRP requires

homo- or hetero-dimerization for its transport properties and is hence known as a half transporter [9]. Like P-gp and MRP1, it confers resistance against many drugs—mitoxantrone, topotecan, HIV-1 nucleoside reverse transcriptase inhibitors, to name just a few [135, 136]. Immunohistochemistry and immunofluorescence studies have confirmed BCRP expression in syncytiotrophoblast, as well as in the apical membrane of BeWo cells, and endothelium of small blood vessels in stem villi [133, 137]. In *mdr1a/1b(-/-)* knockout pregnant dams treated with GF120918 (inhibitor of both P-gp and BCRP), levels of the BCRP substrate topotecan in fetus were 3.2-fold higher than in control subjects that were vehicle treated only [138]. The location of the human homolog in the apical membrane of trophoblast indicates the possibility of a similar role of fetal protection in humans. In fact, in a recent study, siRNAs were synthesized for knocking down BCRP and transfected into BeWo cells, which normally express high levels of BCRP. Transfection decreased both BCRP mRNA and protein levels by 50%. Transfection increased the intracellular accumulation of the BCRP substrate topotecan and increased the sensitivity of the cells to mitoxantrone and topotecan by 10.5- and 8.2-fold [139].

To elucidate the placental function of BCRP, several in vitro models have been utilized. Evseenko et al. did a comparative study of BCRP expression and function across placenta, primary trophoblasts, and the choriocarcinoma cell lines BeWo and JAr [56]. Protein and mRNA levels were highest in BeWo and lowest in placenta. That BCRP is functional in placenta was proven by the significantly enhanced accumulation of the BCRP substrate Hoechst 33342 in the presence of the selective BCRP inhibitor, fumitremorgin C. It was also observed that BCRP expression increased almost threefold upon trophoblast differentiation. The authors proposed that this could either indicate BCRP participation in trophoblast differentiation or simply reflect a phenotypic difference between the differentiated and undifferentiated cells. Mathias et al. tested the effects of gestational age on BCRP expression and function [34]. Unlike P-gp, BCRP mRNA and protein expression did not change with advancing pregnancy, suggesting that they are regulated through different pathways. In a more recent study, Ceckova et al. [137] have shown that the mRNA levels of BCRP are almost tenfold higher than MDR1 in placenta, which is paralleled by data in BeWo cells where BCRP levels were also much higher than those of MDR1. In BeWo cells increased accumulation of mitoxantrone (both a P-gp and BCRP substrate) occurred in the presence of the BCRP-specific inhibitor, Ko143, with respect to control. Increased accumulation was also observed in the presence of the P-gp-specific inhibitor, PSC 833, though it was lower than what was observed with Ko143. The increased expression of BCRP compared to MDR1 suggests that it is as important as P-gp, if not more in extruding substances from the fetal to the maternal direction.

Substrates of BCRP include large hydrophobic, both positively and negatively charged molecules. Substrates include chemotherapeutic agents, such as camptothecin derivatives (topotecan, irinotecan, and the active metabolite of irinotecan SN-38), sulfate/glucuronate/glutathione conjugates of endogenous compounds, fluorescent dyes (e.g., Hoechst 33342), and chemical toxicants (2-amino-1-methyl-6-phenylimidazo [4,5-b] pyridine or PhIP and pheophorbide a) [140, 141]. SAR studies have shown that transport of the camptothecin derivatives seem to be dependent on polarity with the highly polar

camptothecin analogs being better substrates than the ones having a lower polarity [142]. Also, presence of a hydroxyl group at specific positions of the camptothecin A ring enhances recognition by BCRP [143]. Sulfated steroids such as estrone-3-sulfate and dehydroepiandrosterone sulfate (DHEAS), which are also synthesized and secreted in the syncytiotrophoblasts, are BCRP substrates [140]. Mutations in BCRP have been associated with different substrate specificities [140, 141]. A large number of structurally diverse BCRP inhibitors have been identified, such as tyrosine kinase inhibitors (imatinib and gefitinib), flavonoids (chrysin and biochanin A), HIV protease inhibitors (ritonavir, saquinavir, and nelfinavir), and novobiocin [144–146], but only a few of these have been tested for their possible clinical use in reversing BCRP-mediated efflux. In mice, gefitinib coadministration significantly increased the oral bioavailability of irinotecan [147]. The authors suggested that this was likely due to inhibition of BCRP as in *in vitro* studies gefitinib inhibited BCRP and BCRP is expressed on the apical membrane of the intestinal epithelium. While these inhibitors may be utilized to modulate placental BCRP and affect drug distribution across the placenta, caution should be exercised as it could affect the efflux of physiologic BCRP substrates, such as estrone sulfate and DHEAS.

A few studies have looked into the effects of the major pregnancy hormones, progesterone and 17β -estradiol, on BCRP function and expression. Human BCRP was functionally expressed in the bacterium *Lactococcus lactis*. In this system both estradiol and progesterone alone stimulated BCRP-associated ATPase activity fourfold, and the initial stimulation period was followed by inhibition [148]. Generally stimulation of P-gp ATPase activity by a substance is believed to be an indication of it being a P-gp substrate. If this is extended to BCRP, then both estradiol and progesterone can be assumed to be substrates of BCRP. However, as Mao et al have pointed out, many known BCRP substrates inhibit BCRP-associated ATPase activity [140]. Thus conclusions drawn from the BCRP ATPase as to whether substances are BCRP substrates or not should be carefully considered. Janvilisri et al showed in a bacterial system that 17β -estradiol is a BCRP substrate as evidenced by its reduced uptake in BCRP expressing cells as well as its competitive inhibition of the transport of the BCRP substrate Hoechst 33342 [148]. Imai et al. however reported that in mammalian cells neither estradiol nor estrone is a BCRP substrate [149], even though their sulfated forms are. Estrogenic substances appear to be acute inhibitors of BCRP. In BCRP-transfected K562 cells both estrone (E1) and 17β -estradiol (E2) increased topotecan accumulation compared with control K562 cells. In membrane vesicles prepared from BCRP-transfected K562 cells, free E1 and E2 blocked uptake of sulfated E1. In BCRP-transfected MDCKII cells the BCRP-mediated transepithelial transport of both topotecan and PhIP was abrogated by $100\ \mu\text{M}$ estradiol [149–151]. Majority of the literature indicates that BCRP is downregulated on chronic exposure to estrogens though there are some contradictions. Imai et al. observed the long-term effects of estrogen exposure on BCRP expression. Incubations for 4 days with E1 or E2 produced a dose-dependent decrease in both endogenous and exogenously transfected BCRP protein. This was also observed at the functional level where the cellular accumulation of topotecan increased with E2 treatment. This effect was observed only in cells functionally expressing the estrogen receptor $\text{ER}\alpha$, suggesting interactions between E2 and $\text{ER}\alpha$ are required for BCRP downregulation. Additionally, after siRNA knockout of $\text{ER}\alpha$, E2 failed to produce the

same effect. The lack of any effect of E2 on BCRP mRNA expression indicates that the regulation mechanism is posttranscriptional [152].

In the placental choriocarcinoma cells BeWo 72-h incubations with E2 produced a dose-dependent increase in BCRP mRNA and protein levels. The upregulation observed with estradiol was abolished in the presence of progesterone [153]. Wang et al. observed contradictory effects when assessing the effects of chronic exposure to estradiol and progesterone on BCRP function and expression in BeWo cells [154]. E2 downregulated BCRP protein and mRNA, whereas progesterone had the opposite effect. A combination of the two increased BCRP protein and mRNA expression even more than what was observed in the presence of progesterone alone. Similar effects were observed in fumitremorgin C inhibitable mitoxantrone efflux activity, although the effects on activity were lower than the effects observed on expression. E2 also significantly downregulated ER β expression, but did not have any effect on ER α mRNA. This effect on ER β was completely abolished by the estrogen receptor antagonist ICI-182,780. A combination of E2 and progesterone did not downregulate ER β mRNA, but significantly increased progesterone receptor B (PR $_B$) mRNA. Progesterone alone did not have any effect on the expression of estrogen or the progesterone receptors. This indicates that E2 alone downregulates BCRP expression, probably via ER β , but in combination with progesterone the regulation is through the PR $_B$ in BeWo cells. It should be mentioned that there are some differences observed between primary trophoblasts and BeWo cells with respect to ABC transporter expression and caution should be exercised when extrapolating the results to the in vivo situation.

16.6. Conclusions

To summarize, the human placenta expresses several efflux transporters, nutrient transporters, and metabolic enzymes that can control the amount of drug or xenobiotic that the fetus is exposed to. An improved understanding of their placental localization, function, and regulation will allow exploiting them to either prevent or promote drug delivery to the fetus as demanded by the situation. Since drug testing in pregnant women is not encouraged for obvious reasons of safety, in vitro placental models can be utilized for this purpose. Although there are disadvantages associated with each model that prevent direct extrapolation of the obtained information to the in vivo situation, they still provide important means of studying the transplacental transfer and metabolism of drugs, thus establishing the safety and efficacy of drug treatment during pregnancy.

Acknowledgments: Support for this work was received from an NICHD grant (HD39878-03).

References

1. S.S. Siu, M.T. Chan, and T.K. Lau. Placental transfer of ondansetron during early human pregnancy. *Clin Pharmacokinet.* 45:419–423 (2006).
2. G.M. Pacifici. Placental transfer of antibiotics administered to the mother: A review. *Int J Clin Pharmacol Ther.* 44:57–63 (2006).

3. L. Gavard, S. Gil, G. Peytavin, P.F. Ceccaldi, C. Ferreira, R. Farinotti, and L. Mandelbrot. Placental transfer of lopinavir/ritonavir in the ex vivo human cotyledon perfusion model. *Am J Obstet Gynecol.* 195:296–301 (2006).
4. E.C. Moises, L. de Barros Duarte, R. de Carvalho Cavalli, V.L. Lanchote, G. Duarte, and S.P. da Cunha. Pharmacokinetics and transplacental distribution of fentanyl in epidural anesthesia for normal pregnant women. *Eur J Clin Pharmacol.* 61:517–522 (2005).
5. E.H. Riley, E. Fuentes-Afflick, R.A. Jackson, G.J. Escobar, P. Brawarsky, M. Schreiber, and J.S. Haas. Correlates of prescription drug use during pregnancy. *J Womens Health (Larchmt).* 14:401–409 (2005).
6. S.E. Andrade, J.H. Gurwitz, R.L. Davis, K.A. Chan, J.A. Finkelstein, K. Fortman, H. McPhillips, M.A. Raebel, D. Roblin, D.H. Smith, M.U. Yood, A.N. Morse, and R. Platt. Prescription drug use in pregnancy. *Am J Obstet Gynecol.* 191:398–407 (2004).
7. B.V. Sastry. Techniques to study human placental transport. *Adv Drug Deliv Rev.* 38:17–39 (1999).
8. A.C. Enders and T.N. Blankenship. Comparative placental structure. *Adv Drug Deliv Rev.* 38:3–15 (1999).
9. A.M. Young, C.E. Allen, and K.L. Audus. Efflux transporters of the human placenta. *Adv Drug Deliv Rev.* 55:125–132 (2003).
10. K.L. Audus. Controlling drug delivery across the placenta. *Eur J Pharm Sci.* 8:161–165 (1999).
11. I.M. Doughty, J.D. Glazier, S.L. Greenwood, R.D. Boyd, and C.P. Sibley. Mechanisms of maternofetal chloride transfer across the human placenta perfused in vitro. *Am J Physiol.* 271:R1701–R1706 (1996).
12. C. Ampasavate, G.A. Chandorkar, D.G. Vande Velde, J.F. Stobaugh, and K.L. Audus. Transport and metabolism of opioid peptides across BeWo cells, an in vitro model of the placental barrier. *Int J Pharm.* 233:85–98 (2002).
13. F. Liu, M.J. Soares, and K.L. Audus. Permeability properties of monolayers of the human trophoblast cell line BeWo. *Am J Physiol.* 273:C1596–C1604 (1997).
14. P. Brownbill, D. Mahendran, D. Owen, P. Swanson, K.L. Thornburg, D.M. Nelson, and C.P. Sibley. Denudations as paracellular routes for alphafetoprotein and creatinine across the human syncytiotrophoblast. *Am J Physiol Regul Integr Comp Physiol.* 278:R677–R683 (2000).
15. S. Kertschanska, G. Kosanke, and P. Kaufmann. Pressure dependence of so-called transtrophoblastic channels during fetal perfusion of human placental villi. *Microsc Res Tech.* 38:52–62 (1997).
16. T. Heikkinen, U. Ekblad, and K. Laine. Transplacental transfer of amitriptyline and nortriptyline in isolated perfused human placenta. *Psychopharmacology (Berl).* 153:450–454 (2001).
17. R.G. Dickinson, D.W. Fowler, and R.M. Kluck. Maternofetal transfer of phenytoin, p-hydroxy-phenytoin and p-hydroxy-phenytoin-glucuronide in the perfused human placenta. *Clin Exp Pharmacol Physiol.* 16:789–797 (1989).
18. D.W. Fowler, M.J. Eadie, and R.G. Dickinson. Transplacental transfer and bio-transformation studies of valproic acid and its glucuronide(s) in the perfused human placenta. *J Pharmacol Exp Ther.* 249:318–323 (1989).
19. A. Ericsson, B. Hamark, T.L. Powell, and T. Jansson. Glucose transporter isoform 4 is expressed in the syncytiotrophoblast of first trimester human placenta. *Hum Reprod.* 20:521–530 (2005).
20. N. Jansson, S.L. Greenwood, B.R. Johansson, T.L. Powell, and T. Jansson. Leptin stimulates the activity of the system A amino acid transporter in human placental villous fragments. *J Clin Endocrinol Metab.* 88:1205–1211 (2003).
21. P.D. Prasad, B.J. Hoffmans, A.J. Moe, C.H. Smith, F.H. Leibach, and V. Ganapathy. Functional expression of the plasma membrane serotonin transporter

- but not the vesicular monoamine transporter in human placental trophoblasts and choriocarcinoma cells. *Placenta*. 17:201–207 (1996).
22. A. Pastrakuljic, L.O. Derewlany, B. Knie, and G. Koren. The effects of cocaine and nicotine on amino acid transport across the human placental cotyledon perfused in vitro. *J Pharmacol Exp Ther*. 294:141–146 (2000).
 23. S. Sudhakaran, H. Ghabrial, R.L. Nation, D.C.M. Kong, N.M. Gude, P.W. Angus, and C.R. Rayner. Differential bidirectional transfer of indinavir in the isolated perfused human placenta. *Antimicrob Agents and Chemother*. 49:1023–1028 (2005).
 24. J. Kraemer, J. Klein, A. Lubetsky, and G. Koren. Perfusion studies of glyburide transfer across the human placenta: Implications for fetal safety. *Am J Obstet Gynecol*. 195:270–274 (2006).
 25. J.C. Challier. Criteria for evaluating perfusion experiments and presentation of results. *Contributions to gynecology and obstetrics*. 13:32–39 (1985).
 26. G.R. Cannell, R.M. Kluck, S.E. Hamilton, R.H. Mortimer, W.D. Hooper, and R.G. Dickinson. Markers of physical integrity and metabolic viability of the perfused human placental lobule. *Clin Exp Pharmacol Physiol*. 15:837–844 (1988).
 27. R. Boskovic, D.S. Feig, L. Derewlany, B. Knie, G. Portnoi, and G. Koren. Transfer of insulin lispro across the human placenta: In vitro perfusion studies. *Diabetes Care*. 26:1390–1394 (2003).
 28. K. Linnemann, A. Malek, R. Sager, W.F. Blum, H. Schneider, and C. Fusch. Leptin production and release in the dually in vitro perfused human placenta. *J Clin Endocrinol Metab*. 85:4298–4301 (2000).
 29. F. Staud, K. Mazancova, I. Miksik, P. Pavek, Z. Fendrich, and J. Pacha. Corticosterone transfer and metabolism in the dually perfused rat placenta: Effect of 11beta-hydroxysteroid dehydrogenase type 2. *Placenta*. 27:171–180 (2006).
 30. H.J. Holmes, B.M. Casey, and R.E. Bawdon. Placental transfer of rosiglitazone in the ex vivo human perfusion model. *Am J Obstet Gynecol*. 195:1715–1719 (2006).
 31. H. Polachek, G. Holcberg, G. Sapir, M. Tsadkin-Tamir, J. Polachek, M. Katz, and Z. Ben-Zvi. Transfer of ciprofloxacin, ofloxacin and levofloxacin across the perfused human placenta in vitro. *Eur J Obstet Gynecol Reprod Biol*. 122:61–65 (2005).
 32. T. Tuntland, A. Odinecs, C.M. Pereira, C. Nosbisch, and J.D. Unadkat. In vitro models to predict the in vivo mechanism, rate, and extent of placental transfer of dideoxynucleoside drugs against human immunodeficiency virus. *Am J Obstet Gynecol*. 180:198–206 (1999).
 33. M. Nandakumaran and A.S. Eldeen. Transfer of cyclosporine in the perfused human placenta. *Dev Pharmacol Ther*. 15:101–105 (1990).
 34. A.A. Mathias, J. Hitti, and J.D. Unadkat. P-glycoprotein and breast cancer resistance protein expression in human placentae of various gestational ages. *Am J Physiol Regul Integr Comp Physiol*. 289:R963–R969 (2005).
 35. M. Grube, H. Meyer zu Schwabedissen, K. Draber, D. Praeger, K.-U. Moeritz, K. Linnemann, C. Fusch, G. Jedlitschky, and H.K. Kroemer. Expression, localization, and function of the carnitine transporter OCTN2 (SLC22A5) in human placenta. *Drug Metab Dispos*. 33:31–37 (2005).
 36. R. Sata, H. Ohtani, M. Tsujimoto, H. Murakami, N. Koyabu, T. Nakamura, T. Uchiumi, M. Kuwano, H. Nagata, K. Tsukimori, H. Nakano, and Y. Sawada. Functional analysis of organic cation transporter 3 expressed in human placenta. *J Pharmacol Exp Ther*. 315:888–895 (2005).
 37. A. Ericsson, B. Hamark, N. Jansson, R. Johansson Bengt, L. Powell Theresa, and T. Jansson. Hormonal regulation of glucose and system A amino acid transport in first trimester placental villous fragments. *Am J Physiol Regul, Integr Comp Physiol*. 288:R656–R662 (2005).

38. D.E. Atkinson, C.P. Sibley, L.J. Fairbairn, and S.L. Greenwood. MDR1 P-gp expression and activity in intact human placental tissue; upregulation by retroviral transduction. *Placenta*. 27:707–714 (2006).
39. S.R. Sooranna, E. Oteng-Ntim, R. Meah, T.A. Ryder, and R. Bajoria. Characterization of human placental explants: Morphological, biochemical and physiological studies using first and third trimester placenta. *Hum Reprod (Oxford, England)*. 14:536–541 (1999).
40. F. Ushigome, N. Koyabu, S. Satoh, K. Tsukimori, H. Nakano, T. Nakamura, T. Uchiyumi, M. Kuwano, H. Ohtani, and Y. Sawada. Kinetic analysis of P-glycoprotein-mediated transport by using normal human placental brush-border membrane vesicles. *Pharm Res*. 20:38–44 (2003).
41. S.-P. Wu, M.-K. Shyu, H.-H. Liou, C.-S. Gau, and C.-J. Lin. Interaction between anticonvulsants and human placental carnitine transporter. *Epilepsia*. 45:204–210 (2004).
42. P.F. Speake, J.D. Glazier, P.T.Y. Ayuk, M. Reade, C.P. Sibley, and S.W. D'Souza. L-Arginine transport across the basal plasma membrane of the syncytiotrophoblast of the human placenta from normal and preeclamptic pregnancies. *J Clin Endocrinol Metab*. 88:4287–4292 (2003).
43. M. Inuyama, F. Ushigome, A. Emoto, N. Koyabu, S. Satoh, K. Tsukimori, H. Nakano, H. Ohtani, and Y. Sawada. Characteristics of L-lactic acid transport in basal membrane vesicles of human placental syncytiotrophoblast. *Am J Physiol*. 283:C822–C830 (2002).
44. H.E. Meyer Zu Schwabedissen, M. Grube, B. Heydrich, K. Linnemann, C. Fusch, H.K. Kroemer, and G. Jedlitschky. Expression, localization, and function of MRP5 (ABCC5), a transporter for cyclic nucleotides, in human placenta and cultured human trophoblasts: Effects of gestational age and cellular differentiation. *Am J Pathol*. 166:39–48 (2005).
45. H. Nakamura, F. Ushigome, N. Koyabu, S. Satoh, K. Tsukimori, H. Nakano, H. Ohtani, and Y. Sawada. Proton gradient-dependent transport of valproic acid in human placental brush-border membrane vesicles. *Pharm Res*. 19:154–161 (2002).
46. M.V. St-Pierre, M.A. Serrano, R.I. Macias, U. Dubs, M. Hoechli, U. Lauper, P.J. Meier, and J.J. Marin. Expression of members of the multidrug resistance protein family in human term placenta. *Am J Physiol Regul Integr Comp Physiol*. 279:R1495–R1503 (2000).
47. J.D. Glazier and C.P. Sibley. In vitro methods for studying human placental amino acid transport: Placental plasma membrane vesicles. *Methods Mol Med*. 122:241–252 (2006).
48. A. King, L. Thomas, and P. Bischof. Cell culture models of trophoblast II: Trophoblast cell lines—a workshop report. *Placenta*. 21 Suppl A:S113–S119 (2000).
49. H.J. Kliman, J.E. Nestler, E. Sermasi, J.M. Sanger, and J.F. Strauss, III. Purification, characterization, and in vitro differentiation of cytotrophoblasts from human term placentae. *Endocrinology*. 118:1567–1582 (1986).
50. R.G. Richards, S.M. Hartman, and S. Handwerger. Human cytotrophoblast cells cultured in maternal serum progress to a differentiated syncytial phenotype expressing both human chorionic gonadotropin and human placental lactogen. *Endocrinology*. 135:321–329 (1994).
51. Y. Kato and G.D. Braunstein. Discordant secretion of placental protein hormones in differentiating trophoblasts in vitro. *J Clin Endocrinol Metab*. 68:814–820 (1989).
52. M.L. Avery, C.E. Meek, and K.L. Audus. The presence of inducible cytochrome P450 types 1A1 and 1A2 in the BeWo cell line. *Placenta*. 24:45–52 (2003).

53. N. Utoguchi, G.A. Chandorkar, M. Avery, and K.L. Audus. Functional expression of P-glycoprotein in primary cultures of human cytotrophoblasts and BeWo cells. *Reprod Toxicol.* 14:217–224 (2000).
54. T.C. Furesz, C.H. Smith, and A.J. Moe. ASC system activity is altered by development of cell polarity in trophoblast from human placenta. *Am J Physiol.* 265:C212–C217 (1993).
55. P.I. Karl, K.L. Alpy, and S.E. Fisher. Amino acid transport by the cultured human placental trophoblast: Effect of insulin on AIB transport. *Am J Physiol.* 262:C834–C839 (1992).
56. D.A. Evseenko, J.W. Paxton, and J.A. Keelan. ABC drug transporter expression and functional activity in trophoblast-like cell lines and differentiating primary trophoblast. *Am J Physiol Regul Integr Comp Physiol.* 290:R1357–R1365 (2006).
57. H.E. Meyer zu Schwabedissen, G. Jedlitschky, M. Gratz, S. Haenisch, K. Linnemann, C. Fusch, I. Cascorbi, and H.K. Kroemer. Variable expression of MRP2 (ABCC2) in human placenta: Influence of gestational age and cellular differentiation. *Drug Metab Dispos.* 33:896–904 (2005).
58. D.G. Hemmings, B. Lowen, R. Sherburne, G. Sawicki, and L.J. Guilbert. Villous trophoblasts cultured on semi-permeable membranes form an effective barrier to the passage of high and low molecular weight particles. *Placenta.* 22:70–79 (2001).
59. J.D. Aplin, A. Sattar, and A.P. Mould. Variant choriocarcinoma (BeWo) cells that differ in adhesion and migration on fibronectin display conserved patterns of integrin expression. *J Cell Sci.* 103 (Pt 2):435–444 (1992).
60. C.J. Bode, H. Jin, E. Rytting, P.S. Silverstein, A.M. Young, and K.L. Audus. In vitro models for studying trophoblast transcellular transport. *Methods Mol Med.* 122:225–239 (2006).
61. S.J. Friedman and P. Skehan. Morphological differentiation of human choriocarcinoma cells induced by methotrexate. *Cancer Res.* 39:1960–1967 (1979).
62. B. Wice, D. Menton, H. Geuze, and A.L. Schwartz. Modulators of cyclic AMP metabolism induce syncytiotrophoblast formation in vitro. *Exp Cell Res.* 186:306–316 (1990).
63. P.A. Vardhana and N.P. Illsley. Transepithelial glucose transport and metabolism in BeWo choriocarcinoma cells. *Placenta.* 23:653–660 (2002).
64. D.P. Cerneus and A. Van der Ende. Apical and basolateral transferrin receptors in polarized BEWO cells recycle through separate endosomes. *J Cell Biol.* 114:1149–1158 (1991).
65. K.E. Schmid, W.S. Davidson, L. Myatt, and L.A. Woollett. Transport of cholesterol across a BeWo cell monolayer: Implications for net transport of sterol from maternal to fetal circulation. *J Lipid Res.* 44:1909–1918 (2003).
66. E. Rytting and K.L. Audus. Novel organic cation transporter 2-mediated carnitine uptake in placental choriocarcinoma (BeWo) cells. *J Pharmacol Exp Ther.* 312:192–198 (2005).
67. B.A. Way, T.C. Furesz, K. Schwarz, A.J. Moe, and C.H. Smith. Sodium-independent lysine uptake by the BeWo choriocarcinoma cell line. *Placenta.* 19:323–328 (1998).
68. T. Takahashi, N. Utoguchi, A. Takara, N. Yamamoto, T. Nakanishi, K. Tanaka, K.L. Audus, and Y. Watanabe. Carrier-mediated transport of folic acid in BeWo cell monolayers as a model of the human trophoblast. *Placenta.* 22:863–869 (2001).
69. J. Mueller, I. Born, R.H. Neubert, and M. Brandsch. Apical uptake of choline and cationic drugs in epithelial cell lines derived from human placenta. *Placenta.* 26:183–189 (2005).
70. A. Emoto, F. Ushigome, N. Koyabu, H. Kajiya, K. Okabe, S. Satoh, K. Tsukimori, H. Nakano, H. Ohtani, and Y. Sawada. H⁺-linked transport of salicylic acid, an

- NSAID, in the human trophoblast cell line BeWo. *Am J Physiol.* 282:C1064–C1075 (2002).
71. D.N. Karunaratne, P.S. Silverstein, V. Vasandani, A.M. Young, E. Rytting, B. Yops, and K.L. Audus. *Cell Culture Models for Drug Transport Studies. Drug Delivery: Principles and Applications* (Wang, B, Siahaan, T.J, and Soltero, RA, Eds), John Wiley & Sons, Inc, New York:103–125 (2005).
 72. F. Martel and E. Keating. Uptake of 1-methyl-4-phenylpyridinium (MPP+) by the JAR human placental choriocarcinoma cell line: Comparison with 5-hydroxytryptamine. *Placenta.* 24:361–369 (2003).
 73. C. Wadsack, A. Hrzenjak, A. Hammer, B. Hirschmugl, S. Levak-Frank, G. Desoye, W. Sattler, and E. Malle. Trophoblast-like human choriocarcinoma cells serve as a suitable in vitro model for selective cholesteryl ester uptake from high density lipoproteins. *Eur J Biochem.* 270:451–462 (2003).
 74. A.M. Mitchell, A.S. Yap, E.J. Payne, S.W. Manley, and R.H. Mortimer. Characterization of cell polarity and epithelial junctions in the choriocarcinoma cell line, JAR. *Placenta.* 16:31–39 (1995).
 75. R.S. Tuan, C.J. Moore, J.W. Brittingham, J.J. Kirwin, R.E. Akins, and M. Wong. In vitro study of placental trophoblast calcium uptake using JEG-3 human choriocarcinoma cells. *J Cell Sci.* 98 (Pt 3):333–342 (1991).
 76. R.-H. Xu, X. Chen, D.S. Li, R. Li, G.C. Addicks, C. Glennon, T.P. Zwaka, and J.A. Thomson. BMP4 initiates human embryonic stem cell differentiation to trophoblast. *Nat Biotechnol.* 20:1261–1264 (2002).
 77. T.W. Loo and D.M. Clarke. Recent progress in understanding the mechanism of P-glycoprotein-mediated drug efflux. *J Membr Biol.* 206:173–185 (2005).
 78. M.D. Chavanpatil, Y. Patil, and J. Panyam. Susceptibility of nanoparticle-encapsulated paclitaxel to P-glycoprotein-mediated drug efflux. *Int J Pharm.* 320:150–156 (2006).
 79. C.J. Bachmeier, T.J. Spitzenberger, W.F. Elmquist, and D.W. Miller. Quantitative assessment of HIV-1 protease inhibitor interactions with drug efflux transporters in the blood-brain barrier. *Pharm Res.* 22:1259–1268 (2005).
 80. S. Yamaguchi, Y.L. Zhao, M. Nadai, H. Yoshizumi, X. Cen, S. Torita, K. Takagi, K. Takagi, and T. Hasegawa. Involvement of the drug transporters p glycoprotein and multidrug resistance-associated protein Mrp2 in telithromycin transport. *Antimicrob Agents Chemother.* 50:80–87 (2006).
 81. T.J. Raub. P-glycoprotein recognition of substrates and circumvention through rational drug design. *Mol Pharm.* 3:3–25 (2006).
 82. P. Crivori, B. Reinach, D. Pezzetta, and I. Poggesi. Computational models for identifying potential P-glycoprotein substrates and inhibitors. *Mol Pharm.* 3:33–44 (2006).
 83. C. Cordon-Cardo, J.P. O'Brien, J. Boccia, D. Casals, J.R. Bertino, and M.R. Melamed. Expression of the multidrug resistance gene product (P-glycoprotein) in human normal and tumor tissues. *J Histochem Cytochem.* 38:1277–1287 (1990).
 84. D.E. Atkinson, S.L. Greenwood, C.P. Sibley, J.D. Glazier, and L.J. Fairbairn. Role of MDR1 and MRP1 in trophoblast cells, elucidated using retroviral gene transfer. *Am J Physiol Cell Physiol.* 285:C584–C591 (2003).
 85. A. MacFarland, D.R. Abramovich, S.W. Ewen, and C.K. Pearson. Stage-specific distribution of P-glycoprotein in first-trimester and full-term human placenta. *Histochem J.* 26:417–423 (1994).
 86. G.R. Lankas, L.D. Wise, M.E. Cartwright, T. Pippert, and D.R. Umbenhauer. Placental P-glycoprotein deficiency enhances susceptibility to chemically induced birth defects in mice. *Reprod Toxicol.* 12:457–463 (1998).
 87. J.W. Smit, M.T. Huisman, O. van Tellingen, H.R. Wiltshire, and A.H. Schinkel. Absence or pharmacological blocking of placental P-glycoprotein profoundly increases fetal drug exposure. *J Clin Invest.* 104:1441–1447 (1999).

88. A.S.T. Planting, P. Sonneveld, A. van der Gaast, A. Sparreboom, M.E.L. van der Burg, G.P.M. Luyten, K. de Leeuw, M. de Boer-Dennert, P.S. Wissel, R.C. Jewell, E.M. Paul, N.B. Purvis, and J. Verweij. A phase I and pharmacologic study of the MDR converter GF120918 in combination with doxorubicin in patients with advanced solid tumors. *Cancer Chemother. Pharmacol.* 55:91–99 (2005).
89. P.M. Fracasso, K.A. Blum, M.K. Ma, B.R. Tan, L.P. Wright, S.A. Goodner, C.L. Fears, W. Hou, M.A. Arquette, J. Picus, A. Denes, J.E. Mortimer, L. Ratner, S.P. Ivy, and H.L. McLeod. Phase I study of pegylated liposomal doxorubicin and the multidrug-resistance modulator, valspodar. *Br J Cancer.* 93:46–53 (2005).
90. M. Molsa, T. Heikkinen, J. Hakkola, K. Hakala, O. Wallerman, M. Wadelius, C. Wadelius, and K. Laine. Functional role of P-glycoprotein in the human blood-placental barrier. *Clin Pharmacol Ther.* 78:123–131 (2005).
91. C. Marzolini, C. Rudin, L.A. Decosterd, A. Telenti, A. Schreyer, J. Biollaz, and T. Buclin. Transplacental passage of protease inhibitors at delivery. *Aids.* 16:889–893 (2002).
92. I.A. Nekhayeva, T.N. Nanovskaya, S.V. Deshmukh, O.L. Zharikova, G.D. Hankins, and M.S. Ahmed. Bidirectional transfer of methadone across human placenta. *Biochem Pharmacol.* 69:187–197 (2005).
93. A. Gadducci, S. Cosio, A. Fanucchi, V. Nardini, M. Roncella, P.F. Conte, and A.R. Genazzani. Chemotherapy with epirubicin and paclitaxel for breast cancer during pregnancy: Case report and review of the literature. *Anticancer Res.* 23:5225–5229 (2003).
94. P. Mylona, J.D. Glazier, S.L. Greenwood, M.K. Sides, and C.P. Sibley. Expression of the cystic fibrosis (CF) and multidrug resistance (MDR1) genes during development and differentiation in the human placenta. *Mol Hum Reprod.* 2:693–698 (1996).
95. S. Gil, R. Saura, F. Forestier, and R. Farinotti. P-glycoprotein expression of the human placenta during pregnancy. *Placenta.* 26:268–270 (2005).
96. M. Sun, J. Kingdom, D. Baczyk, S.J. Lye, S.G. Matthews, and W. Gibb. Expression of the multidrug resistance P-glycoprotein, (ABCB1 glycoprotein) in the human placenta decreases with advancing gestation. *Placenta.* 27:602–609 (2006).
97. A.M. Young. Characterization of efflux transporters of the human trophoblast using BeWo as a model. PhD Thesis, University of Kansas, Lawrence, Kansas, USA (2005).
98. A.B. Shapiro, K. Fox, P. Lam, and V. Ling. Stimulation of P-glycoprotein-mediated drug transport by prazosin and progesterone. Evidence for a third drug-binding site. *Eur J Biochem.* 259:841–850 (1999).
99. K.M. Barnes, B. Dickstein, G.B. Cutler, Jr., T. Fojo, and S.E. Bates. Steroid treatment, accumulation, and antagonism of P-glycoprotein in multidrug-resistant cells. *Biochemistry.* 35:4820–4827 (1996).
100. C.P. Yang, S.G. DePinho, L.M. Greenberger, R.J. Arceci, and S.B. Horwitz. Progesterone interacts with P-glycoprotein in multidrug-resistant cells and in the endometrium of gravid uterus. *J Biol Chem.* 264:782–788 (1989).
101. E. Buxbaum. Co-operative binding sites for transported substrates in the multiple drug resistance transporter Mdr1. *Eur J Biochem.* 265:64–70 (1999).
102. K.O. Hamilton, M.A. Yazdanian, and K.L. Audus. Modulation of P-glycoprotein activity in Calu-3 cells using steroids and beta-ligands. *Int J Pharm.* 228:171–179 (2001).
103. M. Frohlich, N. Albermann, A. Sauer, I. Walter-Sack, W.E. Haefeli, and J. Weiss. In vitro and ex vivo evidence for modulation of P-glycoprotein activity by progestins. *Biochem Pharmacol.* 68:2409–2416 (2004).

104. F. Leonessa, J.H. Kim, A. Ghiorghis, R.J. Kulawiec, C. Hammer, A. Talebian, and R. Clarke. C-7 analogues of progesterone as potent inhibitors of the P-glycoprotein efflux pump. *J Med Chem.* 45:390–398 (2002).
105. W.Y. Kim and L.Z. Benet. P-glycoprotein (P-gp/MDR1)-mediated efflux of sex-steroid hormones and modulation of P-gp expression in vitro. *Pharm Res.* 21:1284–1293 (2004).
106. J.F. Strauss, 3rd, F. Martinez, and M. Kiriakidou. Placental steroid hormone synthesis: Unique features and unanswered questions. *Biol Reprod.* 54:303–311 (1996).
107. H. Jin and K.L. Audus. Effect of bisphenol A on drug efflux in BeWo, a human trophoblast-like cell line. *Placenta.* 26:S96–S103 (2005).
108. L. Zampieri, P. Bianchi, P. Ruff, and P. Arbutnot. Differential modulation by estradiol of P-glycoprotein drug resistance protein expression in cultured MCF7 and T47D breast cancer cells. *Anticancer Res.* 22:2253–2259 (2002).
109. H. Masuyama, N. Suwaki, Y. Tateishi, H. Nakatsukasa, T. Segawa, and Y. Hiramatsu. The pregnane X receptor regulates gene expression in a ligand- and promoter-selective fashion. *Mol Endocrinol.* 19:1170–1180 (2005).
110. O. Burk, K.A. Arnold, A. Geick, H. Tegude, and M. Eichelbaum. A role for constitutive androstane receptor in the regulation of human intestinal MDR1 expression. *Biol Chem.* 386:503–513 (2005).
111. K.W. Scotto. Transcriptional regulation of ABC drug transporters. *Oncogene.* 22:7496–7511 (2003).
112. H.M. Prime-Chapman, R.A. Fearn, A.E. Cooper, V. Moore, and B.H. Hirst. Differential multidrug resistance-associated protein 1 through 6 isoform expression and function in human intestinal epithelial Caco-2 cells. *J Pharmacol Exp Ther.* 311:476–484 (2004).
113. C.S. Morrow, C. Peklak-Scott, B. Bishwokarma, T.E. Kute, P.K. Smitherman, and A.J. Townsend. Multidrug resistance protein 1 (MRP1, ABCC1) mediates resistance to mitoxantrone via glutathione-dependent drug efflux. *Mol Pharmacol.* 69:1499–1505 (2006).
114. O. van Tellingen, T. Buckle, J.W. Jonker, M.A. van der Valk, and J.H. Beijnen. P-glycoprotein and Mrp1 collectively protect the bone marrow from vincristine-induced toxicity in vivo. *Br J Cancer.* 89:1776–1782 (2003).
115. J. Wijnholds, G.L. Scheffer, M. van der Valk, P. van der Valk, J.H. Beijnen, R.J. Scheper, and P. Borst. Multidrug resistance protein 1 protects the oropharyngeal mucosal layer and the testicular tubules against drug-induced damage. *J Exp Med.* 188:797–808 (1998).
116. S. Calligaris, D. Cekic, L. Roca-Burgos, F. Gerin, G. Mazzone, J.D. Ostrow, and C. Tiribelli. Multidrug resistance associated protein 1 protects against bilirubin-induced cytotoxicity. *FEBS Lett.* 580:1355–1359 (2006).
117. M. Nagashige, F. Ushigome, N. Koyabu, K. Hirata, M. Kawabuchi, T. Hirakawa, S. Satoh, K. Tsukimori, H. Nakano, T. Uchiumi, M. Kuwano, H. Ohtani, and Y. Sawada. Basal membrane localization of MRP1 in human placental trophoblast. *Placenta.* 24:951–958 (2003).
118. F.R. Simon, M. Iwahashi, L.J. Hu, I. Qadri, I.M. Arias, D. Ortiz, R. Dahl, and E. Sutherland. Hormonal regulation of hepatic multidrug resistance-associated protein 2 (Abcc2) primarily involves the pattern of growth hormone secretion. *Am J Physiol Gastrointest Liver Physiol.* 290:G595–G608 (2006).
119. R.Z. Turncliff, P.J. Meier, and K.L. Brouwer. Effect of dexamethasone treatment on the expression and function of transport proteins in sandwich-cultured rat hepatocytes. *Drug Metab Dispos.* 32:834–839 (2004).
120. H.M. Kauffmann and D. Schrenk. Sequence analysis and functional characterization of the 5'-flanking region of the rat multidrug resistance protein 2 (mrp2) gene. *Biochem Biophys Res Commun.* 245:325–331 (1998).

121. D.R. Johnson and C.D. Klaassen. Regulation of rat multidrug resistance protein 2 by classes of prototypical microsomal enzyme inducers that activate distinct transcription pathways. *Toxicol Sci.* 67:182–189 (2002).
122. H.R. Kast, B. Goodwin, P.T. Tarr, S.A. Jones, A.M. Anisfeld, C.M. Stoltz, P. Tontonoz, S. Kliewer, T.M. Willson, and P.A. Edwards. Regulation of multidrug resistance-associated protein 2 (ABCC2) by the nuclear receptors pregnane X receptor, farnesoid X-activated receptor, and constitutive androstane receptor. *J Biol Chem.* 277:2908–2915 (2002).
123. V. Keitel, M. Burdelski, U. Warskulat, T. Kuhlkamp, D. Keppler, D. Haussinger, and R. Kubitz. Expression and localization of hepatobiliary transport proteins in progressive familial intrahepatic cholestasis. *Hepatology.* 41:1160–1172 (2005).
124. D. Rost, J. Konig, G. Weiss, E. Klar, W. Stremmel, and D. Keppler. Expression and localization of the multidrug resistance proteins MRP2 and MRP3 in human gallbladder epithelia. *Gastroenterology.* 121:1203–1208 (2001).
125. N. Zelcer, K. van de Wetering, R. de Waart, G.L. Scheffer, H.U. Marschall, P.R. Wielinga, A. Kuil, C. Kunne, A. Smith, M. van der Valk, J. Wijnholds, R.O. Elferink, and P. Borst. Mice lacking *Mrp3* (*Abcc3*) have normal bile salt transport, but altered hepatic transport of endogenous glucuronides. *J Hepatol.* 44:768–775 (2006).
126. H. Zeng, G. Liu, P.A. Rea, and G.D. Kruh. Transport of amphipathic anions by human multidrug resistance protein 3. *Cancer Res.* 60:4779–4784 (2000).
127. L. Pascolo, C. Ferneti, D. Pirulli, S. Crovella, A. Amoroso, and C. Tiribelli. Effects of maturation on RNA transcription and protein expression of four MRP genes in human placenta and in BeWo cells. *Biochem Biophys Res Commun.* 303:259–265 (2003).
128. P. Borst, C. de Wolf, and K. van de Wetering. Multidrug resistance-associated proteins 3, 4, and 5. *Pflugers Arch.* 453:661–673 (2006).
129. J. Wijnholds, C.A. Mol, L. van Deemter, M. de Haas, G.L. Scheffer, F. Baas, J.H. Beijnen, R.J. Scheper, S. Hatse, E. De Clercq, J. Balzarini, and P. Borst. Multidrug-resistance protein 5 is a multispecific organic anion transporter able to transport nucleotide analogs. *Proc Natl Acad Sci USA.* 97:7476–7481 (2000).
130. P.R. Wielinga, G. Reid, E.E. Challa, I. van der Heijden, L. van Deemter, M. de Haas, C. Mol, A.J. Kuil, E. Groeneveld, J.D. Schuetz, C. Brouwer, R.A. De Abreu, J. Wijnholds, J.H. Beijnen, and P. Borst. Thiopurine metabolism and identification of the thiopurine metabolites transported by MRP4 and MRP5 overexpressed in human embryonic kidney cells. *Mol Pharmacol.* 62:1321–1331 (2002).
131. G.D. Kruh, H. Zeng, P.A. Rea, G. Liu, Z.S. Chen, K. Lee, and M.G. Belinsky. MRP subfamily transporters and resistance to anticancer agents. *J Bioenerg Biomembr.* 33:493–501 (2001).
132. S.A. Andric, T.S. Kostic, and S.S. Stojilkovic. Contribution of Multidrug Resistance Protein MRP5 in Control of Cyclic Guanosine 5'-Monophosphate Intracellular Signaling in Anterior Pituitary Cells. *Endocrinology.* 147:3435–3445 (2006).
133. M. Maliepaard, G.L. Scheffer, I.F. Faneyte, M.A. Van Gastelen, A.C.L.M. Pijnenborg, A.H. Schinkel, M.J. Van de Vijver, R.J. Scheper, and J.H.M. Schellens. Subcellular localization and distribution of the breast cancer resistance protein transporter in normal human tissues. *Cancer Res.* 61:3458–3464 (2001).
134. P. Krishnamurthy and J.D. Schuetz. Role of ABCG2/BCRP in biology and medicine. *Annu. Rev Pharmacol Toxicol.* 46:381–410, 381 plate (2006).
135. P. Jia, S. Wu, F. Li, Q. Xu, M. Wu, G. Chen, G. Liao, S. Wang, J. Zhou, Y. Lu, and D. Ma. Breast cancer resistance protein-mediated topotecan resistance in ovarian cancer cells. *Int J Gynecol Cancer: Official J Int Gynecol Cancer Soc.* 15:1042–1048 (2005).
136. X. Wang and M. Baba. The role of breast cancer resistance protein (BCRP/ABCG2) in cellular resistance to HIV-1 nucleoside reverse transcriptase inhibitors. *Antivir Chem Chemother.* 16:213–216 (2005).

137. M. Ceckova, A. Libra, P. Pavek, P. Nachtigal, M. Brabec, R. Fuchs, and F. Staud. Expression and functional activity of breast cancer resistance protein (BCRP, ABCG2) transporter in the human choriocarcinoma cell line BeWo. *Clin Exp Pharmacol Physiol*. 33:58–65 (2006).
138. J.W. Jonker, J.W. Smit, R.F. Brinkhuis, M. Maliepaard, J.H. Beijnen, J.H.M. Schellens, and A.H. Schinkel. Role of breast cancer resistance protein in the bioavailability and fetal penetration of topotecan. *J Natl Cancer Inst*. 92:1651–1656 (2000).
139. P.L.R. Ee, X. He, D.D. Ross, and W.T. Beck. Modulation of breast cancer resistance protein (BCRP/ABCG2) gene expression using RNA interference. *Mol Cancer Ther*. 3:1577–1584 (2004).
140. Q. Mao and J.D. Unadkat. Role of the breast cancer resistance protein (ABCG2) in drug transport. *AAPS J*. 7:E118–E133 (2005).
141. B. Sarkadi, C. Ozvegy-Laczka, K. Nemet, and A. Varadi. ABCG2—a transporter for all seasons. *FEBS Lett*. 567:116–120 (2004).
142. R. Rajendra, M.K. Gounder, A. Saleem, J.H.M. Schellens, D.D. Ross, S.E. Bates, P. Sinko, and E.H. Rubin. Differential effects of the breast cancer resistance protein on the cellular accumulation and cytotoxicity of 9-aminocamptothecin and 9-nitrocamptothecin. *Cancer Res*. 63:3228–3233 (2003).
143. T. Ishikawa, Y. Ikegami, K. Sano, H. Nakagawa, and S. Sawada. Transport mechanism-based drug molecular design: Novel camptothecin analogues to circumvent ABCG2-associated drug resistance of human tumor cells. *Curr Pharm Des*. 12:313–325 (2006).
144. A. Gupta, Y. Zhang, J.D. Unadkat, and Q. Mao. HIV protease inhibitors are inhibitors but not substrates of the human breast cancer resistance protein (BCRP/ABCG2). *J Pharmacol Exp Ther*. 310:334–341 (2004).
145. K. Shiozawa, M. Oka, H. Soda, M. Yoshikawa, Y. Ikegami, J. Tsurutani, K. Nakatomi, Y. Nakamura, S. Doi, T. Kitazaki, Y. Mizuta, K. Murase, H. Yoshida, D.D. Ross, and S. Kohno. Reversal of breast cancer resistance protein (BCRP/ABCG2)-mediated drug resistance by novobiocin, a coumermycin antibiotic. *Int J Cancer*. 108:146–151 (2003).
146. S. Zhang, X. Yang, and M.E. Morris. Flavonoids are inhibitors of breast cancer resistance protein (ABCG2)-mediated transport. *Mol Pharmacol*. 65:1208–1216 (2004).
147. C.F. Stewart, M. Leggas, J.D. Schuetz, J.C. Panetta, P.J. Cheshire, J. Peterson, N. Daw, J.J. Jenkins, III, R. Gilbertson, G.S. Germain, F.C. Harwood, and P.J. Houghton. Gefitinib enhances the antitumor activity and oral bioavailability of irinotecan in mice. *Cancer Res*. 64:7491–7499 (2004).
148. T. Janvilisri, H. Venter, S. Shahi, G. Reuter, L. Balakrishnan, and H.W. Van Veen. Sterol transport by the human breast cancer resistance protein (ABCG2) expressed in *Lactococcus lactis*. *J Biol Chem*. 278:20645–20651 (2003).
149. Y. Imai, S. Asada, S. Tsukahara, E. Ishikawa, T. Tsuruo, and Y. Sugimoto. Breast cancer resistance protein exports sulfated estrogens but not free estrogens. *Mol Pharmacol*. 64:610–618 (2003).
150. Y. Imai, S. Tsukahara, E. Ishikawa, T. Tsuruo, and Y. Sugimoto. Estrone and 17beta-estradiol reverse breast cancer resistance protein-mediated multidrug resistance. *Jpn J Cancer Res: Gann*. 93:231–235 (2002).
151. P. Pavek, G. Merino, E. Wagenaar, E. Bolscher, M. Novotna, J.W. Jonker, and A.H. Schinkel. Human breast cancer resistance protein: Interactions with steroid drugs, hormones, the dietary carcinogen 2-amino-1-methyl-6-phenylimidazo(4,5-b)pyridine, and transport of cimetidine. *J Pharmacol Exp Ther*. 312:144–152 (2005).
152. Y. Imai, E. Ishikawa, S. Asada, and Y. Sugimoto. Estrogen-mediated post-transcriptional down-regulation of breast cancer resistance protein/ABCG2. *Cancer Res*. 65:596–604 (2005).

153. S. Yasuda, S. Itagaki, T. Hirano, and K. Iseki. Effects of sex hormones on regulation of ABCG2 expression in the placental cell line BeWo. *J Pharm Pharm Sci.* 9:133–139 (2006).
154. H. Wang, L. Zhou, A. Gupta, R.R. Vethanayagam, Y. Zhang, D. Unadkat Jashvant, and Q. Mao. Regulation of BCRP/ABCG2 expression by progesterone and 17beta-estradiol in human placental BeWo cells. *American journal of physiology Endocrinol Metab.* 290:E798–E807 (2006).

In Vitro Models to Study Blood–Brain Barrier Function

Gert Fricker

Abstract The blood–brain barrier is formed by endothelial cells of brain capillaries. It protects the central nervous system from xenobiotics, dangerous metabolites, and toxins. This chapter gives a short overview about the history of blood–brain barrier research and the morphological and functional features of the barrier with special emphasis on the impact of ABC-transport proteins on drug permeability, as well as some examples to overcome or bypass export proteins, such as P-glycoprotein. Regulatory mechanisms underlying P-glycoprotein expression and function will be discussed. Ex vivo and in vitro models are introduced and methods to study drug permeation across the endothelial cell barrier will be described.

Keywords: Blood–brain barrier; P-glycoprotein; Multidrug resistance-associated protein; Capillaries; Endothelial cells; Pregnane X receptor

Abbreviations

ABC	ATP-binding cassette
BCRP	Breast cancer resistance protein
CNS	Central nervous system
DMSO	Dimethyl sulfoxide
ENT	Equilibrative nucleoside transporter
ET	Endothelin
FITC	Fluorescein isothiocyanate
GFAP	Glial fibrillary acidic protein
GLUT	Glucose transporter
i.v.	Intravenous
LPS	Lipopolysaccharide
MBEC	Mouse brain endothelial cells
MDR	Multidrug resistance
MRP	Multidrug resistance-associated protein
NOS	Nitric oxide synthase
OAT	Organic anion transporter
OATP	Organic anion transporting polypeptide
OCT	Organic cation transporter

PBEC	Porcine brain microvessel endothelial cells
PCN	Pregnenolone 16 α -carbonitrile
K	Protein kinase
PXR	Pregnane X receptor
RT-PCR	Reverse transcriptase-polymerase chain reaction
RXR	Retinoid X receptor
SNP	Sodium nitroprusside
TNF	Tumor necrosis factor
ZO	Zonula occludens

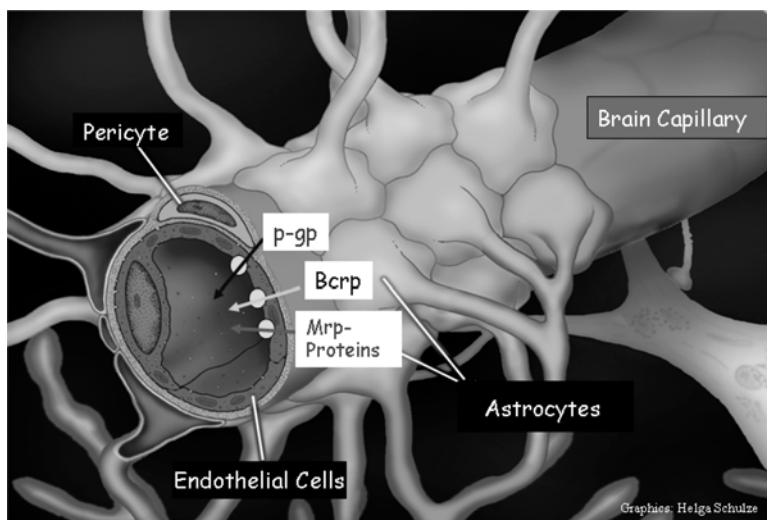
17.1. Introduction

The blood–brain barrier forms the interface between the bloodstream and the brain parenchyma and thus controls the passage of endogenous substances and xenobiotics into and out of the central nervous system. Brain microvessels exhibit a variety of unique structural features, such as an extremely tight endothelium without fenestration, a very low rate of pinocytosis, tight junctions between endothelial cells excluding paracellular permeability, and a series of polarized transport proteins. The following chapter describes the structural and functional characteristics of the blood–brain barrier with emphasis on transport proteins, as well as in vitro techniques, which allow studying this complex barrier in the brain.

17.1.1. Discovery of the Blood–Brain Barrier

The current knowledge about the blood–brain barrier, which is formed by brain capillaries, is the result of intensive research over decades starting in the late nineteenth century. In 1885, the German physician Paul Ehrlich observed that after intravenous injection of a dye all organs became colored except for the brain [1]. When Edwin Goldmann, a student of Ehrlich, repeated the experiment in 1909, he saw a clear staining of the choroid plexus, whereas the surrounding brain tissue remained colorless [2], thus confirming observations of other scientists from the years before [3–6]. Goldmann further found that after subarachnoidal injection, the brain was stained, but not the choroid plexus and concluded that the plexus epithelium was the barrier preventing the transfer of dye into the brain [7]. The physiologist Lina Stern recognized that after intravenous (i.v.) administration some test compounds were found in brain and cerebrospinal fluid but others were not and named this phenomenon “barrière hématoencéphalique” [8]. A couple of years later, Spatz and colleagues suggested a separation of the two terms blood–brain barrier and blood–liquor barrier [9–12]. In 1929, H. Foertig wrote the first scientific paper entitled “Die Bluthirnschranke” or “the blood–brain barrier,” which was rather provocative at that time. In 1946, August Krogh asked the question, how the nutrient supply should occur, if the blood–brain barrier is an impermeable obstacle, and he speculated about active transport mechanisms within the barrier [13]. The localization of the barrier function within brain capillaries was finally demonstrated by electron microscopic studies with brain slices [14, 15].

Hence, an organ had been discovered, which is still the subject of intensive studies and is yet far away from a complete understanding.



From: K. Ladage, Bochum

Figure 17.1 Schematic cross section of a brain capillary formed by endothelial cells which are surrounded by pericytes and foot processes of astrocytes. Endothelial cells express various ABC-transport proteins at their luminal surface which significantly contribute to the barrier function.

17.2. Structure and Function of the Blood–Brain Barrier

The blood–brain barrier is markedly different from peripheral capillaries: Peripheral capillaries are fenestrated with openings up to 50 nm wide. In contrast, cerebral endothelial cells are closely connected by tight junctions and zonulae occludentes, resulting in extremely high transendothelial resistances of up to 1500–2000 $\Omega \text{ cm}^2$ [16] (Figure 17.1). The capillaries are surrounded by a basal membrane enclosing intermittently pericytes, which have been postulated to be involved in host defense. The outer surface of the basement membrane is covered by astrocytic foot processes. Most likely, secretion of soluble growth factors by astrocytes plays an important role in endothelial cell differentiation.

The cerebral endothelial cells of the blood–brain barrier originate from the middle germinal sheet of the embryo, the mesoderm [17]. Concomitant with migration and proliferation of capillary endothelial cells during formation of the cerebral vascular network occurs the imprinting of the cells. Thereby, induction by the cellular surrounding plays an important role [18–21]. The relevance of the cellular environment for the development of the barrier function of cerebral microvessels was first demonstrated by Stewart and Wiley [22], who transplanted embryonic brain tissue of a quail into embryonic gut tissue of chicken and vice versa. The cerebral transplant was vascularized by intestinal vessels, in which properties of the blood–brain barrier had been induced. In transplanted brain vessels, however, no characteristics of a barrier could be demonstrated, due to the lack of a neuronal environment. These results indicated that the cerebral microvessels are of extraneuronal origin, with properties that are induced by the cellular environment. In addition, brain tissue has the capability to induce blood–brain barrier characteristics also in noncerebral vascular tissue [23].

Proper functioning of the blood–brain barrier is extremely important for the maintenance of the cerebral homeostasis. The human brain (1200–1400 g or 2% of the total body weight) has a blood flow of 650–750 ml/min and needs ~20% of the total energy generated by the body. This corresponds to 75 mg glucose and 50 ml oxygen per minute [24–27]. The interneuronal communication is a very complex process, which is only possible in a constant extracellular milieu. Changes in pH value, as they occur under pressure in the blood, must not be forwarded into the brain. Furthermore, alterations in ion concentrations would have fatal consequences for the membrane potential of neurons. Peripheral neurotransmitters must not invade the cerebral tissue. On the other hand, central neurotransmitters and neurohormones, which are released at very low concentrations to exert local effects, have to be restricted to the brain tissue. In addition, neurons have to be protected against irreversible damages by xenobiotics [23–25, 28–32]. In summary, the brain is to be protected by a dynamic barrier which guarantees sufficient supply with energy and nutrients, as well as a wide-ranging defense.

The density of cerebral capillaries, especially in the cortical grey matter, is very high with mean distances of ~40 μm . The capillary network has a total length of 600–650 km, the mean velocity of the blood flow is below 0.1 cm/s, and the luminal surface extends to ~15–30 m^2 . Thus the blood–brain barrier represents an important surface for potential drug delivery besides gut (300–400 m^2), lung (70–120 m^2), or skin (1.8 m^2) [24–26, 33–37].

17.3. Relevance of the Barrier for Drug Delivery

With respect to drug transport, the central nervous system (CNS) gains more and more interest from academic research, as well as from pharmaceutical industry, since the demand for effective treatment of CNS-related disorders is greater than ever. For example, more than 24 million people worldwide suffer from schizophrenia and ~37 million people suffer from different kinds of dementia, the majority of them diagnosed with Alzheimer's disease. In addition, tens of thousands of patients suffer from various kinds of brain tumors. However, the number of drugs for the treatment of CNS diseases is relatively small, as compared to those for other indications. One major reason is the fact that there is only very restricted access of xenobiotics to the brain. Indeed, more than 98% of small molecule drugs and almost all larger drug molecules, including recombinant proteins, monoclonal antibodies, and gene therapeutics, do not cross the blood–brain barrier [38]. Enormous efforts are ongoing to overcome this barrier without causing permanent damage to brain tissue.

Regarding drug transport, the blood–brain barrier has two primary elements. The first one identified was a diffusional or passive element. It reflects the physical properties of both the tight junctions between brain capillary endothelial cells, which form a seal to intercellular diffusion, and the cells themselves, which display a low rate of endocytosis. Diffusion through paracellular spaces is almost negligible at the blood–brain barrier, due to the restriction by tight junctions. The junctions effectively close off diffusion through intercellular pores; as a result, most solutes cross the blood–brain barrier either by diffusing across the lipid endothelial cell membranes or by carrier-mediated specific transport. However, with regard to passive diffusion, several studies indicate

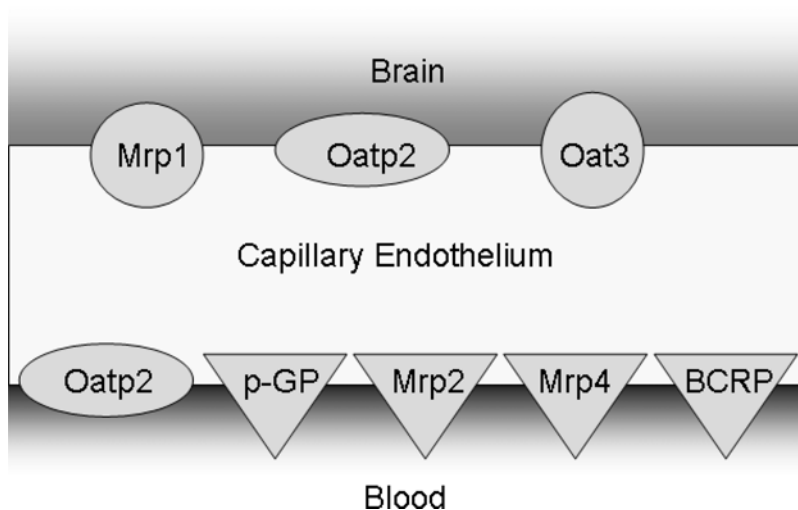


Figure 17.2 Transport proteins expressed at the blood–brain barrier.

that a correlation between lipophilicity and permeation can only be made for compounds with a molecular weight between 400 and 600 Da [39, 40].

More recently, a second element has been identified, which reflects the transport properties of solute carrier proteins (transporters) embedded in the plasma membranes of the endothelial cells (Figure 17.2). For hydrophilic nutrients, active transport is essential to satisfy the metabolic needs of the CNS. For example, the transport of amino acids through the endothelial wall is an important control point for the overall regulation of cerebral metabolism, including protein synthesis and neurotransmitter production [41, 42]. Glucose uptake is predominantly mediated by the glucose transporter Glut-1, which is expressed in high levels at the blood–brain barrier [43].

The transport proteins at the blood–brain barrier play an outstanding role in the barrier function. At present, mRNAs encoding for 15 different drug transporters have been detected in brain capillaries or brain capillary endothelial cell lines [44–46], including organic anion transporting polypeptides (OATP), organic anion transporters (OAT), organic cation transporters (OCT), concentrative nucleoside transporters (CNT), equilibrative nucleoside transporters (ENT), and members from the multidrug resistance-associated protein (MRP) and multidrug resistance protein (MDR) subfamilies. It is likely that this list is incomplete and additional transport proteins remain to be detected.

Several of these transporters have been immunolocalized within brain capillary endothelial cells. Four ATP-driven drug export pumps, P-glycoprotein (Mdr1 gene product; Abcb1), breast cancer resistance protein (BCRP, Abcg2), MRP2 (Abcc2), and MRP4 (Abcc4), are located on the luminal (blood-side) plasma membrane, where they transport their substrates back into the blood circulation. Together, these transporters handle a very wide range of anionic (MRP2 and MRP4), cationic (P-glycoprotein and BCRP), and uncharged (all four) xenobiotics. The presence of MRP2 in the blood–brain barrier is considered controversial. It was not detected by Western blotting in whole brain homogenates [47]; however, it could be found at the luminal membrane of freshly isolated functionally intact brain capillaries [48]. Recent studies

indicate that it may be involved in the efflux of anticonvulsant drugs at the blood–brain barrier of rats [49].

Also localized at the luminal membrane is OATP2 (Slc21a5), an organic anion transporter that handles steroid and drug conjugates, certain opioid peptides, and the cardiac glycoside, digoxin [50]. OATP2 could drive concentrative efflux from the cells, if energetically coupled to the electrical potential difference across the luminal membrane. Additional transport proteins are located in the basolateral plasma membrane (brain-side) of the brain capillary endothelial cells. These include OATP2 [51], OAT3 [52], and MRP1 [53]. When coupled to the appropriate ion gradients, both OATP2 and OAT3 are capable of driving organic anions into the endothelial cells. Thus, basolateral OATP2 and OAT3 may be able to pair with luminal MRP2 and OATP2 to drive anionic xenobiotics across the endothelium, from the CNS into the blood.

Among all these transporters, the primary active ATP-dependent export pump, P-glycoprotein, has received the highest attention. This protein, which is also overexpressed in various tumor types, has generally been recognized to be the most important selective element of the blood–brain barrier, because the remarkably wide specificity limits of the protein ensure that it handles a large number of commonly prescribed drugs. This became particularly evident by *in vivo* studies using P-glycoprotein knockout mice. Dosing studies in such animals showed that brain-to-plasma ratios for a large number of drugs that are P-glycoprotein substrates are increased 5- to 50-fold [54]. In addition, treatment of the knockout animals with ivermectin, a widely used anthelmintic drug, caused significantly elevated drug concentrations in the brain and dramatic neurotoxicity [39].

For some other drugs, the relevance of P-glycoprotein at the blood–brain barrier has also impressingly been demonstrated. A number of studies have shown that indinavir, ritonavir, and saquinavir are substrates of P-glycoprotein in brain capillary endothelial cells [55, 56]. Other clinically relevant drugs, which have been shown to be actively transported by P-glycoprotein, include anticancer drugs, such as vinca alkaloids or doxorubicin. Similarly to the HIV protease inhibitors, the presence of P-glycoprotein results in a reduced drug permeation and hence a diminished therapeutic efficacy in the chemotherapy of brain tumors [57].

One possibility to enhance, in a controlled manner, entry of drugs into the CNS would be to alter P-glycoprotein function at the blood–brain barrier. Such an enhancement could result from (1) direct modification of export pump function by inhibitors and intracellular signals or (2) bypassing the export pump by delivery systems not being recognized as substrates (e.g., nanoparticles or vector-coupled liposomes, which are taken up by endocytotic mechanisms) [58–65].

Recently, several relatively specific P-glycoprotein inhibitors have been developed and tested [66, 67]. The first generation of compounds used as P-glycoprotein inhibitors *in vitro* and *in vivo* included drugs, such as verapamil or cyclosporine A. These compounds were rather unspecific inhibitors and/or highly susceptible to metabolism. A second generation of inhibitors included valsopodar (PSC-833), a non-immunosuppressive cyclosporine analog, elacridar (GF 120918), biricodar (VX-710), or dextriguldipine (B8509–035). Unfortunately, the clinical outcome of these compounds as co-medication in various cancer indications has not been convincing so far. The third generation

of P-glycoprotein blockers [ONT-093; zosuquidar (LY335–979), tariquidar (XR9576), or laniquidar (R101–9333)] exhibit more favorable transporter specificities, as well as metabolic profiles.

Interestingly, our own recent experiments with nude mice bearing a human glioblastoma indicate that valsopodar is highly effective at the blood–brain barrier [68]. Malignant brain tumors, such as higher-grade gliomas, are rarely cured by surgery or radiotherapy, and chemotherapy has been of limited value, as long as the blood–brain barrier remains intact. In addition, the brain is a sanctuary for metastases in cancer patients otherwise responding to cytostatic drugs [69]. Taxol and derivatives are active against various tumors; however, for brain tumors the therapeutic benefit of taxol has been low and variable, primarily because of its limited entry into the CNS. Using a combined *in vitro/in vivo* approach, we identified the mechanism that limits taxol access to the CNS. We first showed in isolated brain capillaries that luminal accumulation of taxol is concentrative, specific, and blocked by the specific P-glycoprotein inhibitor valsopodar. We then demonstrated that valsopodar pretreatment not only increased brain levels of taxol (following *i.v.* dosing) but also produced a dramatic therapeutic effect on a paclitaxel-sensitive transplanted human glioblastoma. Taxol by itself did not affect the volume of intracerebrally implanted U-118 MG tumors. In contrast, a combined valsopodar/taxol therapy decreased tumor volume by 90% (animals dosed twice over a 5-week period). In contrast, neither taxol nor PSC833-taxol therapy affected the volume of implanted U-87 MG tumors, derived from a cell line that is not taxol-sensitive. Neither glioblastoma cell line exhibited a multidrug-resistance phenotype. These findings suggest that coadministration of PSC833 or other P-glycoprotein inhibitors can be of clinical benefit for chemotherapy of brain tumors sensitive to cytostatics, which are substrates of P-glycoprotein [66–68]. A recent review [70] gives an excellent overview about the use of P-glycoprotein inhibitors to improve CNS penetration of anticancer drugs. Whether this turns out to be a general strategy to increase brain permeation of P-glycoprotein substrates remains yet to be determined.

17.3.1. Rapid Transport Protein Modulation

An interesting approach to modulate the general permeability of the blood–brain barrier would be the possibility to modulate P-glycoprotein activity over a short period of time, but to retain protection of the CNS over the longer-term. Unfortunately, the regulatory mechanisms we know work over hours to days rather than minutes [71, 72]. However, in other barrier and excretory tissues regulatory pathways have been detected that signal rapid changes in P-glycoprotein function. For example, in renal proximal tubule, recent data showed that the polypeptide hormone endothelin-1 (ET-1), through signaling via ET_B receptors, nitric oxide synthase (NOS), guanylyl cyclase, protein kinase G (PKG), and protein kinase C (PKC), rapidly reduces transport mediated by P-glycoprotein and MRP2 [73, 74]. At the blood–brain barrier, we could also show that ET-1 regulates P-glycoprotein function via the ET_B receptor, which is localized at the luminal and abluminal side of brain capillaries [75]. In intact rat brain microvessels, subnanomolar to nanomolar concentrations of ET-1 rapidly and reversibly decreased P-glycoprotein-mediated luminal accumulation of a fluorescent cyclosporine

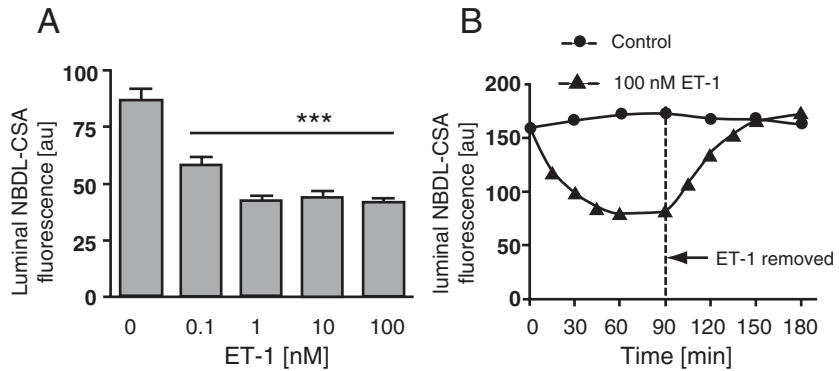


Figure 17.3 Effects of endothelin-1 (ET-1) on NBDL-CSA (P-glycoprotein substrate) transport in isolated capillaries. (A) Concentration-dependent decrease in steady-state luminal NBDL-CSA accumulation caused by ET-1. (B) Effect of ET-1 on steady-state luminal NBDL-CSA accumulation. Capillaries were loaded to steady state in medium with 2 μ M NBDL-CSA. Then, 100 nM ET-1 was added to the medium (time 0 on graph); 90 min later, ET-1 was removed. Each point represents the value for 7–15 isolated capillaries from a single preparation (tissue from 3 to 10 rats). Variability is given by S.E. bars. Units are arbitrary fluorescence units. Statistical comparison: ***, significantly smaller than control, $P < 0.0001$ (with permission from 75).

analog, nitrobenzoxadiazol-cyclosporine (NBD-CSA) (Figure 17.3). A concomitant opening of tight junctions, resulting in a general increase in microvessel permeability was not observed, which is in clear contrast to findings with sucrose and 1-*O*-pentylglycerol, compounds known to open tight junctions rapidly [76, 77]. The effects of ET-1 could be blocked by an ET_B receptor antagonist, but not by an ET_A receptor antagonist [75]. Sodium nitroprusside (SNP), an NO generator, also reduced P-glycoprotein-mediated transport, presumably mimicking the effects of NOS activation. Inhibition of PKC blocked the effects of ET-1 and of SNP. Inhibition of NOS blocked the effects of ET-1, but not of PKC activation. In summary, a linear signaling pathway exists, going from the ET_B receptor via NOS to PKC.

Direct use of endothelin is not practical for clinical purposes. However, this signaling pathway shows a way that might be useful to manipulate P-glycoprotein and to help in the short term to treat patients with P-glycoprotein substrates that do not cross the blood–brain barrier.

Recent studies show a link between the brain's innate immune response and functional regulation of P-glycoprotein [78]. Exposing brain capillaries to the inflammatory cytokine tumor necrosis factor- α (TNF- α), activates a TNF-R1 receptor, releases ET-1, activates ET_B receptor signaling, and essentially abolishes P-glycoprotein-mediated transport. Bacterial lipopolysaccharide (LPS), an activator of the brain's innate immune response, reduces P-glycoprotein activity through TNF- α release, ET-1 release, and ET_B receptor signaling. TNF- α and LPS effects have a rapid onset (minutes), are reversible, and do not involve changes in tight junctional permeability.

17.3.2. Modulation of P-glycoprotein Transcription

Recently, Geick et al. [79] discovered a complex regulatory cluster of several binding sites for the ligand-activated nuclear receptor, pregnane X receptor

(PXR), in the 5'-upstream region of hMDR1. Electrophoretic mobility shift assays revealed that PXR binds as a heterodimer with the retinoid X receptor α (RXR α). In addition, reporter gene assays confirmed that this cluster of response elements is responsible for PXR-mediated hMDR1 induction. The PXR (NR1I2) was first discovered by Kliewer et al. [80, 81] as a new member of a superfamily of ligand-activated transcription factors, the so-called orphan nuclear receptors. PXR is activated by naturally occurring steroids, such as pregnenolone and progesterone, as well as by synthetic glucocorticoids and antiglucocorticoids. Most interestingly, PXR can also be activated by a wide variety of xenobiotics including dietary compounds, toxicants, and also commonly prescribed drugs [82, 83]. It is considered to be a “master regulator” of xenobiotic removal, since it regulates a number of target genes, mainly in liver and intestine, that are involved in xenobiotic metabolism (Phase I and Phase II) and efflux [84]. In addition to P-glycoprotein, several other efflux transporters are regulated by PXR, including MRP isoforms 2 and 3, MRP2 and MRP3 (ABCC2, ABCC3), OATP2, SLCO1A4, and the bile salt export pump (ABCB11) [79–81]. At present, PXR is the only known ligand-activated nuclear receptor controlling transcription of MDR1, and thus expression of P-glycoprotein.

Recently, our group detected PXR mRNA and protein expression in isolated rat brain capillaries by reverse transcriptase-polymerase chain reaction (RT-PCR) and immunostaining, respectively [72]. When we treated rat brain capillaries with pregnenolone 16 α -carbonitrile (PCN) and dexamethasone, both PXR ligands, increased mRNA (quantitative RT-PCR) and protein (Western blots and quantitative immunostaining) levels for P-glycoprotein, as well as P-glycoprotein-mediated transport of fluorescent drug derivatives into the capillary lumen, could be detected [72]. Dosing rats with PCN and dexamethasone increased P-glycoprotein expression in brain capillaries and upregulated specific transport in the capillaries. Initial experiments also indicated an upregulation of MRP2 at the blood–brain barrier. These *in vitro* and *in vivo* dosing experiments gave the first evidence for PXR expression in brain and for regulation of a xenobiotic export pump by nuclear receptors at the blood–brain barrier, and suggested a selective tightening of the blood–brain barrier in patients exposed to the wide range of xenobiotics that are PXR ligands. The data may also explain other findings of an increased expression of P-glycoprotein after exposure of brain endothelial cells to ritonavir, dexamethasone, or puromycin [85, 86]. Since P-glycoprotein is responsible for the efflux of neurotoxins and metabolites out of the CNS, increased pump expression in response to PXR ligands should result in an improved neuroprotection. However, since many P-glycoprotein substrates are used to treat CNS disorders, increased pump expression also implies reduced access of those drugs to sites of action within the CNS and an elevated drug resistance after chronic exposure to these compounds.

17.4. Models to Study Blood–Brain Barrier Function

In vitro models mimicking the characteristics of the blood–brain barrier in a realistic manner provide a broad field of application in experimental, pharmaceutical, and clinical studies. In contrast to *in vivo* studies, which are mainly

based on effect models or models requiring surgical procedures (e.g., microdialysis), they offer direct access to brain capillary endothelial cells without interference with other structures of the brain. At present, two experimental approaches gain broader attention: freshly isolated, functionally intact brain capillaries, and isolated brain capillary endothelial cells, kept in monolayer cultures, either on permeable filter supports or grown on plastic supports.

17.4.1. Isolated Cerebral Capillaries

Isolated capillaries have been used for a long time to study transport and metabolic function of the blood–brain barrier [61, 72, 75, 76, 78, 87–91]. In contrast to monolayer cell cultures, which are susceptible to induction or inhibition of carrier protein expression, experiments with freshly isolated capillaries directly reflect the situation at the luminal side of brain capillaries.

Capillaries can easily be isolated from whole brain, cutting brain tissue into little pieces, suspending them in buffer solution in a petri dish, and dissecting them with fine forceps. Capillary fragments can be found adhering to the glass bottom of the dish.

To obtain larger quantities of capillary fragments, pieces of grey matter can be homogenized by means of razor blades and Teflon homogenizers in appropriate buffers with subsequent dextran gradient centrifugation. After filtration of the homogenate through 200 μm nylon mesh, the filtrate is passed over a column filled with little glass beads. The beads are carefully removed from the column and the adhering capillaries can be washed off the beads by gentle agitation. Then, the capillary suspension is centrifuged and the resulting pellet is resuspended in ice-cold medium. Floating capillary fragments are kept in carbogen (95% O_2 /5% CO_2) pre-gassed buffer until use.

However, one inconvenience in using isolated capillaries for studying of transport processes is that tested substrates approach the capillaries from the abluminal side, which is exactly opposite to the *in vivo* situation. Therefore, isolated capillaries are of special value when the influence of ATP-binding cassette (ABC)-transporters has to be investigated. A series of studies applying confocal laser scanning microscopy and fluorescent-labeled substrates of ABC-transport proteins showed the active extrusion of substrates of P-glycoprotein and MRP-proteins into the capillary lumen (Figure 17.4) of freshly isolated porcine, rat, and fish brain capillaries [48, 68, 90–92].

Such studies are not limited to studying the interaction of potential substrates with ABC-transport proteins at the luminal membrane of brain capillaries but can also be used to investigate the regulatory mechanisms underlying the expression and function of these proteins as discussed above [72, 75, 78].

17.4.2. Brain Capillary Endothelial Cell Culture

Freshly isolated or subcultured brain microvascular endothelial cells offer a notable *in vitro* tool to study drug transport across the blood–brain barrier. Cells can be grown to monolayers on culture plates or permeable membrane supports. The cells retain the major characteristics of brain endothelial cells *in vivo*, such as the morphology, specific biochemical markers of the blood–brain barrier, and the intercellular tight junctional network. Examples of these markers are γ -glutamyl transpeptidase, alkaline phosphatase, von-Willebrandt factor-related antigen, and ZO-1 tight junctional protein. The methods of

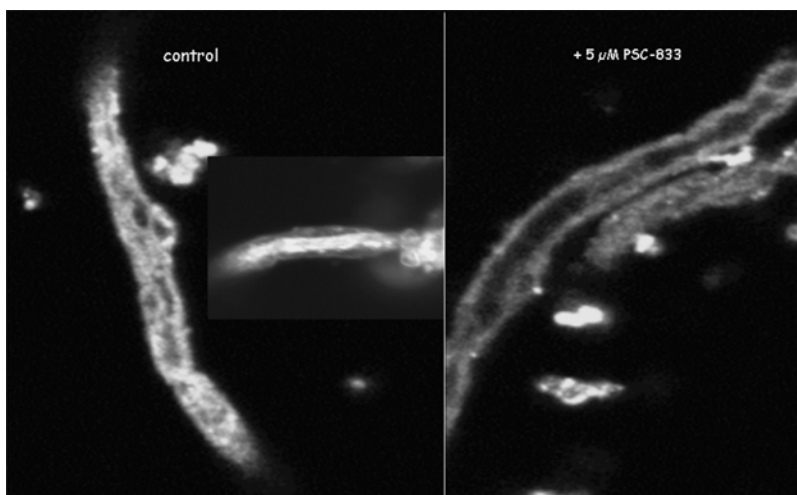


Figure 17.4 Extrusion of a P-glycoprotein substrate (BODIPY-ivermectin) into the lumen of freshly isolated brain capillaries from porcine brain in the absence and in the presence of the P-glycoprotein blocker, PSC-833. PSC-833 abolishes BODIPY-ivermectin excretion completely (with permission from 90).

isolation of brain capillary endothelial cells are similar for most mammalian species [93–98] including human brain microvessel endothelial cells [99–102]. Therefore, the isolation procedure of porcine brain capillary endothelial cells is exemplary described.

17.4.2.1. Preparation of Porcine Brain Microvessel Endothelial Cells

Porcine brain microvessel endothelial cells (PBEC) can be prepared by several methods, for example, following a procedure of Bowman et al. [93] modified by Franke et al. [94]. The latter reference provides a detailed protocol, troubleshooting, and further discussion. In brief, meninges and secretory areas of the brains of freshly slaughtered animals are removed and cerebral matter is homogenized mechanically with fine scissors or razor blades. The homogenate is subjected to digestion in 1% dispase followed by a dextran density gradient centrifugation to obtain capillary fragments as a pellet. These are further treated in a trituration step and a second digestion in 0.1% collagenase/dispase solution. Released endothelial cells are collected from the interface of a density gradient centrifugation. Then, the isolated cells are plated on collagen-coated culture flasks and cultivated in M199 medium containing 10% oxen serum, 0.7 mM L-glutamine, 10,000 U/ml penicillin/streptomycin, and 10 mg/ml gentamicin. Twenty-four hours after initial plating, cells are washed with phosphate-buffered saline containing Ca^{2+} and Mg^{2+} and supplied with fresh culture medium.

For further purification, primary cultures of PBEC are passaged at the third day of culture by gentle trypsinization at room temperature. This enzymatic treatment selectively releases endothelial cells, leaving behind contaminating cells, such as pericytes and smooth muscle cells. Usually, contamination by nonendothelial cells should be below 1–3%. Endothelial cells are then seeded at a density of 30,000–50,000 cells/cm² on rat-tail collagen-coated cell culture inserts (Figure 17.5).

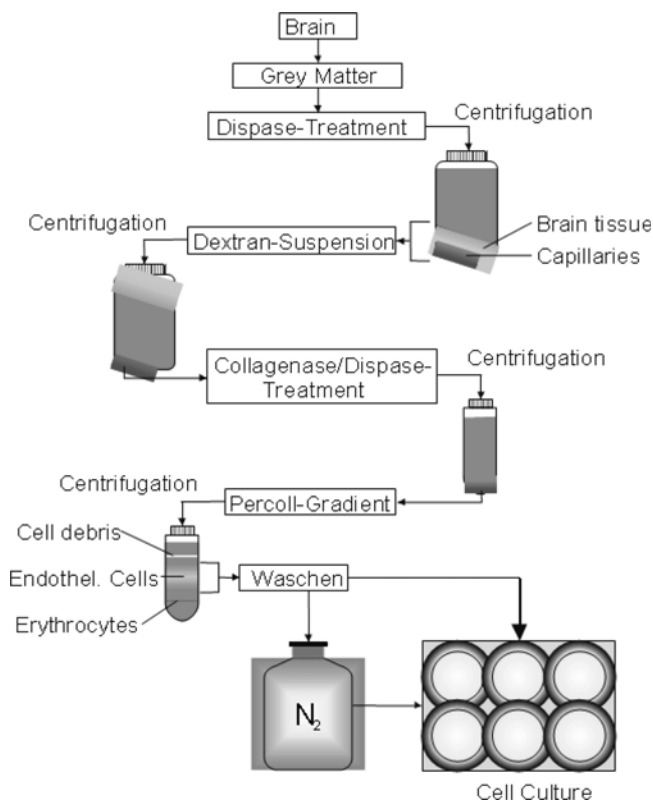


Figure 17.5 Schematic describing the isolation of porcine brain capillary endothelial cells.

17.4.2.2. Uptake Studies

Uptake assays are usually performed at 37°C using confluent monolayers of endothelial cells, ~7–10 days after cell isolation. Cells are incubated with serum-free Krebs–Ringer solution, unless binding studies with serum proteins are to be performed. The substance of interest is added to the respective donor side. In the case of a water-insoluble compound, dimethyl sulfoxide (DMSO) with a final concentration not exceeding 1% in the incubation medium can be used as a cosolvent. After a designated time interval, the supernatant is carefully removed and following two washings with ice-cold (4°C) Krebs–Ringer solution, the cell monolayers can be solubilized with 1% Triton X-100 and subjected to further analysis by high-performance liquid chromatography (HPLC), fluorescence quantification, or other appropriate analytical methods.

17.4.2.3. Permeation Experiments

Isolated cerebral endothelial cells can be grown on permeable filter supports, such as polycarbonate or polyester filters. The commonly used filter pore size is ~0.4 μm. Larger pore sizes can also be used; however, cells may then grow through filter pores, thus forming irregular monolayers. For permeation experiments, 6-well or 12-well filter dishes are recommended. Cells usually grow for 7–10 days, before forming confluent monolayers. Prior to permeation experiments, the monolayer integrity should be assessed either by determining the transendothelial electrical resistance or by running control experiments with paracellular markers, such as radiolabeled mannitol, sucrose, and inulin, respectively, or fluorescence-labeled compounds, such as FITC-dextran.

17.4.2.4. Problems During Cell Culturing and Assaying

Several problems may occur during the cultivation of brain capillary cells on filter membranes, one example being that the cell monolayers may not grow to sufficient confluence. The integrity of the cell monolayer can easily be damaged while replacing the cell culture media with pipettes. Care has to be taken not to harm the monolayer when aspirating medium from the filter insert. Furthermore, pipetting fresh medium into the culture well has to be carried out applying minimal force to the cells. Another reason for nonconfluent monolayers may be an irregular collagen coating of the incubation well or the filter support. Coating conditions have to be optimized for filter inserts from different manufacturers. As long as primary cell cultures are involved, the contamination of cultures by pericytes, smooth muscle, and other cell types remains problematic. Therefore, brain microvessel endothelial cell cultures have to be carefully characterized with respect to cross-contamination by pericytes and astrocytes and smooth muscle cells to ensure their purity.

Horse serum in the culture medium results in a growth inhibition of pericytes [103] and using the respective culture conditions, the number of contaminating pericytes is normally low (<3%). By adding puromycin to the cell culture medium, the number of pericytes can be reduced to almost zero. Astrocytes can be detected by immunostaining of the astrocytes-specific glial fibrillary acidic protein (GFAP) [104]. In good preparations, <1% of all cells show a positive immunostaining and thus astrocyte contamination can be neglected during the assays.

A sufficient plating density has also to be chosen in order to obtain confluent monolayers within the limited time of viability of primary cell cultures.

An also frequently occurring problem may be the low solubility of test compounds in aqueous solvents. Organic cosolvents, such as DMSO or ethanol can be used; however, due to limited cell viability, final concentrations above 1% have to be avoided.

17.4.2.5. Coculture

Monocultures form the base of most cerebral endothelial cell culture models [105–107]. In the case of filter-grown cells, some authors recommend coculture with astrocytes or the use of astrocyte-conditioned media [108–110]. The necessity of this approach is presently under discussion, as cells which had been cultured without supplementation with conditioned media show similar features [94, 111].

Considering the spatial geometry of cerebral capillaries and capillary blood flow, a number of dynamic models of the blood–brain barrier have been developed, in which endothelial cells are cultured inside a permeable tube, the outer surface of which is coated with astrocytes. Supply of the cells with nutrients and artificial blood flow are maintained by using a peristaltic pump system [112, 113].

17.4.2.6. Endothelial Cells Lines

A cell line is a continuously growing cell population, which is derived from tumor cells or from primary cells, which have been immortalized using appropriate vectors. There are several lines of blood–brain barrier endothelial cells available, for example, MBECs (mouse brain endothelial cells), RBE4 cells (rat brain endothelial cells, clone 4), PBMECs (porcine brain microvessel

endothelial cells), and others [106, 114]. An advantage of cerebral microvessel cell lines is their unproblematic culture and easy passage. However, with increasing number of passage, several typical features of brain microvessels may get lost and therefore, the usefulness of these cell lines as a representative model of the blood–brain barrier is under debate [105, 115, 116].

17.4.3. In Silico Methods

The rather time- and cost-expensive preparation of primary brain microvessel endothelial cells, as well as the limited number of experiments which can be performed with intact brain capillaries, has led to an attempt to predict the blood–brain barrier permeability of new chemical entities *in silico*. Artificial neural networks have been developed to predict the ratios of the steady-state concentrations of drugs in the brain to those of the blood from their structural parameters [117, 118]. A summary of the current efforts is given in Chap. 25. Quantitative structure–property relationship models based on *in vivo* blood–brain permeation data and systematic variable selection methods led to success rates of prediction of over 80% for barrier permeant and nonpermeant compounds, thus offering a tool for virtual screening of substances of interest [119].

17.5. Perspectives

Our knowledge about the structure and function of the blood–brain barrier has made tremendous progress in the past decade. It has become increasingly clear that the brain capillary endothelium forms a dynamic barrier, with the properties of the passive elements (tight junctions) and active/selective elements, including transport proteins capable of changing dramatically as a result of hormonal signaling, injury, disease, and therapy. Thirty years after its first identification, P-glycoprotein and other ABC-export pumps have been recognized to be key players in the protective machinery of the blood–brain barrier. Devising strategies to deliver therapeutics into the CNS, while limiting entry of toxic chemicals and preserving an optimal extracellular environment, is a substantial challenge. Certainly, understanding of how the different components of the barrier function are modulated is an important first step to meet this challenge.

Therefore, studying how the activity of these efflux transporters is modulated may provide practical strategies for selectively manipulating barrier permeability for a large number of drugs. Although we are making rapid progress in identifying the multiple mechanisms that modulate ABC-transporter function, much still remains to be discovered. Areas to be investigated further include (1) practical aspects of the use of specific ABC-transport protein inhibitors (e.g., targeting, optimal dosing protocols, reversibility, and safety), (2) dietary and pharmacological treatments to modify nuclear receptor actions, and (3) possible use of inflammatory and stress pathways to lower ABC-transporter expression at the blood–brain barrier.

With the use of isolated cells and functionally intact isolated brain capillaries, we certainly have the appropriate tools to study and to better understand the regulation and function of this important endothelial barrier.

References

1. Ehrlich P (1885) Das Sauerstoffbedürfniss des Organismus. Eine farbenanalytische Studie. August Hirschwald, Berlin
2. Goldmann EE (1909) Die äussere und innere Sekretion des gesunden und kranken Organismus im Lichte der, vitalen Färbung“. *Beitr Klin Chir* 64:192–265
3. Loewit M (1881) Ueber den Einfluss der Gallensauerer Salze auf die Herzthätigkeit sowie auf einige Funktionen der peripheren und centralen Nervensubstanzen. *Zeitschr Heilkunde* 2:459–495
4. Biedl A, Kraus R (1898) Über eine bisher unbekannte toxische Wirkung der Gallensäuren auf das Zentralnervensystem. *Centralblatt Inn Med* 47:1185–1200
5. Roux MME, Borrel A (1898) Tétanos cerebral et immunité contre le tétanos. *Annales de l’Institut Pasteur* 4:225–238
6. Lewandowsky M (1900) Zur Lehre von der Cerebrospinalflüssigkeit. *Zeitschr Klin Med* 40:480–494
7. Goldmann EE (1913) Vitalfärbung am Zentralnervensystem. Beitrag zur Physiopathologie des Plexus Choroideus und der Hirnhäute. Verlag der königlichen Akademie der Wissenschaften Berlin, 1–60
8. Stern L (1921) Le liquide céphalorachidien au point de vue de ses rapports avec la circulation sanguine et avec les éléments nerveux de l’axe cérébrospinal. *Schweiz Arch Neurol* 8:215–232
9. Behnsen G (1926) Über die Farbstoffspeicherung im Zentralnervensystem der weissen Maus in verschiedenen Alterszuständen. *Zeitschr Zellforsch* 4: 515–572
10. Spatz H (1933) Die Bedeutung der vitalen Färbung für die Lehre vom Stoffaustausch zwischen dem Zentralnervensystem und dem übrigen Körper. *Arch Psych* 101:267–358
11. Walter FK (1929) Die Blut-Liquorschranke—eine physiologische und klinische Studie. Georg Thieme Verlag. Stuttgart, Germany
12. Walter FK (1933) Die allgemeinen Grundlagen des Stoffaustausches zwischen dem Zentralnervensystem und dem übrigen Körper. *Arch Psych* 101:195–230
13. Krogh A (1946) The active and passive exchanges of inorganic ions through the surfaces of living cells and through living membranes generally. *Proc Royal Soc London* 133:140–200
14. Reese TS, Karnowsky MJ (1967) Fine structural localization of a blood-brain barrier to exogenous peroxidase. *J Cell Biol* 32:207–217
15. Brightman MW, Reese TS (1969) Junctions between intimately apposed cell membranes in the vertebrate brain. *J Cell Biol* 40:648–677
16. Crone C, Olesen SP (1982) Electrical resistance of brain microvascular endothelium *Brain Res* 241:49–55
17. Van Bree JB, de Boer AG Danhof M, Breimer DD (1992) Drug transport across the blood-brain barrier. I. Anatomical and physiological aspects. *Pharm Weekblad Sci Ed* 14:305–310
18. Risau W, Wolburg H (1990) Development of the blood-brain barrier. *Trends Neurosci* 13:174–178
19. Saunders NR, Dziegielewska KM, Mollgard K, Risau W, Wolburg H (1991) The importance of the blood-brain barrier in fetuses and embryos. *Trends Neurosci* 14:14–15
20. Nico B, Cantino D, Sasso’e’Pogentto M, Bertossi M, Ribatti D, Roncalli L (1994) Orthogonal arrays of particles (OAPs) in perivascular astrocytes and tight junctions in endothelial cells. A comparative study in developing and adult brain microvessels. *J Submicroscop Cytol Pathol* 26:103–109
21. Kniesel U, Risau W, Wolburg H (1996) Development of blood-brain barrier tight junctions in the rat cortex. *Develop Brain Res* 96:229–240

22. Stewart PA, Wiley MJ (1981) Developing nervous tissue induces formation of blood-brain barrier characteristics in invading endothelial cells: A study using quail-chick transplantation chimeras. *Develop Biol* 84:183–192
23. Schlosshauer B (1993) The blood-brain barrier: Morphology. Molecules and neuroendothelin. *BioEssays* 15:341–346
24. Abbott NJ, Romero IA (1996) Transporting therapeutics across the blood-brain barrier. *Mol Med Today* 3:103–113
25. Wolf S, Seehaus B, Minol K, GaAssen HG (1996) Die Blut-Hirn Schranke: Eine Besonderheit des cerebralen Mikrozeirlulationssystems. *Naturwiss* 83:302–311
26. Drewes LR (1999) What is the blood brain barrier? A molecular perspective. *Adv Exp Med Biol* 474:1147–1152
27. Thews G, Mutschler E, Vaupel P (1999) *Anatomie, Physiologie und Pathophysiologie des Menschen*, 5. Edition, Wissenschaftl Verlagsges mbH, Stuttgart
28. Goldstein GW, Betz AL (1986) The blood-brain barrier. *Sci Am* 255:70–79
29. Ghersi-Egea JF, Minn A, Siest G (1988) A new aspect of the protective functions of the blood-brain barrier: Activities of four drug-metabolizing enzymes in isolated brain microvessels. *Life Sci* 42:2515–2523
30. Minn A, Ghersi-Egea JF, Perrin R, Leininger B, Siest G (1991) Drug metabolizing enzymes in the brain and cerebral microvessels. *Brain Res Rev* 16:65–82
31. Abbott NJ (1992) Comparative physiology of the blood-brain barrier. In: *Handbook of Experimental Pharmacology* 103:371–396
32. Bradbury MWB (1993) The blood-brain barrier. *Exp Physiol* 78:453–472
33. Crone C (1963) The permeability of capillaries in various organs as determined by use of the indicator dilution method. *Acta Physiol Scand* 58:292–305
34. Lierse W, Horstmann E (1965) Quantitative anatomy of the cerebral vascular bed with especial emphasis on homogeneity and inhomogeneity in small parts of the grey and white matter. *Acta Neurol Scand* 14:15–19
35. Steinhausen M (1993) *Medizinische Physiologie*, 3. Aufl., Gustav Fischer Verlag
36. De Boer, Breimer (1996) Reconstitution of the blood-brain barrier in cell culture studies of drug transport and metabolism. *NIDA Res Monograph* 22: 251–264
37. Zlokovic BV, Apuzzo MLJ (1998) Strategies to circumvent vascular barriers of the central nervous system. *Neurosurgery* 43:877–878
38. Pardridge W (2003) Blood-brain barrier drug targeting: The future of brain drug development. *Molec Intervent* 3:90–105
39. Schinkel AH, Smit JJ, van Tellingen O, Beijnen JH, Wagenaar E, van Deemter L, Mol CA, van der Valk MA, Robanus-Maandag EC, te Riele HP, Berns AJ, Borst P (1994) Disruption of the mouse *mdr1a* P-glycoprotein gene leads to a deficiency in the blood-brain barrier and to increased sensitivity to drugs. *Cell* 77:491–502
40. Schinkel AH, Mayer U, Wagenaar E, Mol CA, van Deemter L, Smit JJ, van der Valk MA, Voordouw AC, Spits H, van Tellingen O, Zijlmans JM, Fibbe WE, Borst P (1997) Normal viability and altered pharmacokinetics in mice lacking *mdr1*-type (drug-transporting) P-glycoproteins. *Proc Natl Acad Sci USA* 94:4028–4033
41. Pardridge W (1999) Blood-brain barrier biology and methodology. *J Neurovirol* 5:556–569
42. Smith QR (2000) Transport of glutamate and other amino acids at the blood-brain barrier. *J Nutr* 130:1016S–1022S
43. Maher F, Vannucci SJ, Simpson IA (1994) Glucose transporter proteins in brain. *FASEB Journal* 8:1003–1011

44. Zhang, Y, Han, H, Elmquist, WF, Miller, DW (2000) Expression of various multidrug resistance-associated protein (MRP) homologues in brain microvessel endothelial cells. *Brain Res* 876:148–153.
45. Zhang Y, Schuetz JD, Elmquist WF, Miller DW (2004) Plasma membrane localization of multidrug resistance-associated protein (MRP) homologues in brain capillary endothelial cells. *J Pharmacol Exp Ther* 311:449–55
46. Omidi Y, Campbell L, Barar J, Connell D, Akhtar S, Gumbleton M (2003) Evaluation of the immortalised mouse brain capillary endothelial cell line, b.End3, as an in vitro blood-brain barrier model for drug uptake and transport studies. *Brain Res* 990:95–112
47. Johnson BM, Zhang P, Schuetz J, Brouwer KL (2006) Characterization of transport protein expression in multidrug resistance-associated protein (MRP)2-deficient rats. *Drug Metab Dispos* 34:556–62
48. Miller DS, Nobmann S, Gutmann H, Drewe J, Fricker G (2000) Xenobiotic transport in isolated brain microvessels studied by confocal microscopy. *Mol Pharmacol* 58:1357–1367
49. Potschka H, Fedrowitz M, Löscher W (2003) Brain access and anticonvulsant efficacy of carbamazepine, lamotrigine and flebamate in ABCC2/MRP2-deficient TR- rats. *Epilepsia* 44:1479–1486
50. Meier PJ, Stieger B (2002) Bile salt transporters. *Annu Rev Physiol* 64:635–661
51. Gao B, Stieger B, Noe B, Fritschy JM, Meier PJ (1999) Localization of the organic anion transporting polypeptide 2 (Oatp2) in capillary endothelium and choroid plexus epithelium of rat brain. *J Histochem Cytochem* 47:1255–1264
52. Ohtsuki S, Asaba H, Takanaga H, Deguchi T, Hosoya K, Otagiri M, Terasaki T (2002) Role of blood-brain barrier organic anion transporter 3 (OAT3) in the efflux of indoxyl sulfate, a uremic toxin: Its involvement in neurotransmitter metabolite clearance from the brain. *J Neurochem* 83:57–66
53. Wijnholds J, deLange EC, Scheffer GL, van den Berg DJ, Mol CA, van der Valk M, Schinkel AH, Scheper RJ, Breimer DD, Borst P (2000) Multidrug resistance protein 1 protects the choroid plexus epithelium and contributes to the blood-cerebrospinal fluid barrier. *J Clin Invest* 105:279–285
54. Schinkel AH, Wagenaar E, Mol CA, van Deemter L (1996) P-glycoprotein in the blood-brain barrier of mice influences the brain penetration and pharmacological activity of many drugs. *J Clin Invest* 97:2517–2524
55. Kim RB, Fromm MF, Wandel C, Leake B, Wood AJJ, Roden DM, Wilkinson GR (1998) The drug transporter P-glycoprotein limits oral absorption and brain entry of HIV protease inhibitors. *J Clin Invest* 101:289–294
56. Gutmann H, Fricker G, Drewe J, Török M, Miller DS (1999) Interactions of HIV protease inhibitors with multiple ATP-dependent drug export proteins. *Mol Pharmacol* 56:383–389
57. Tsuji A (1998) P-glycoprotein-mediated efflux transport of anticancer drugs at the blood-brain barrier. *Therap Drug Monitor* 20:588–590
58. Huwyler J, Cerletti A, Fricker G, Eberle AN, Drewe J (2002) By-Passing of P-glycoprotein effect on digoxin uptake by immunoliposomes. *J Drug Target* 10:73–79
59. Huwyler J, Wu D, Pardridge WM (1996) Brain drug delivery of small molecules using immunoliposomes. *Proc Natl Acad Sci USA* 93:14164–14169
60. Cerletti A, Drewe J, Fricker G, Eberle AN, Huwyler J (2000) Endocytosis and trans cytotaxis of an immunoliposome-based brain drug delivery system. *J Drug Target* 8:435–47
61. Thöle M, Nobmann S, Huwyler J, Bartmann A, Fricker G (2002) Uptake of cationized albumin-coupled liposomes by cultured porcine brain

- microvessel endothelial cells and intact brain capillaries *J Drug Target* 10:337–44
62. Kreuter J (2001) Nanoparticulate systems for brain delivery of drugs. *Adv Drug Deliv Rev* 47:65–81
 63. Kreuter J, Shamenkov D, Petrov V, Ränge P, Cychutek K, Koch-Brandt C, Alyautdin R (2002) Apolipoprotein-mediated transport of nanoparticle-bound drugs across the blood-brain barrier. *J Drug Target* 10:317–325
 64. Kreuter J, Ränge P, Petrov V, Hamm S, Gelperina SE, Engelhardt B, Alyautdin R, von Briesen H, Begley DJ (2003) Direct evidence that polysorbate-80-coated poly(butylcyanoacrylate) nanoparticles deliver drugs to the CNS via specific mechanisms requiring prior binding of drug to the nanoparticles. *Pharm Res* 20:409–416
 65. Steiniger SC, Kreuter J, Khalansky AS, Skidan IN, Bobruskin AI, Smirnova ZS, Severin SE, Uhl R, Kock M, Geiger KD, Gelperina SE (2004) Chemotherapy of glioblastoma in rats using doxorubicin-loaded nanoparticles. *Int J Cancer* 109:759–767
 66. Kemper EM, van Zandbergen AE, Cleypool C, Mos HA, Boogerd W, Beijnen JH, van Tellingen, O (2003) Increased penetration of paclitaxel into the brain by inhibition of P-glycoprotein. *Clin Cancer Res* 9:2849–2855
 67. Kemper EM, Verheij M, Boogerd W, Beijnen JH, van Tellingen O (2004) Improved penetration of docetaxel into the brain by co-administration of inhibitors of P-glycoprotein. *Eur J Cancer* 40:1269–1274
 68. Fellner S, Bauer B, Miller DS, Schaffrik M, Fankhanel M, Spruss T, Bernhardt G, Graeff C, Farber L, Gschaidmeier H, Buschauer A, Fricker G (2002) Transport of paclitaxel (Taxol) across the blood-brain barrier in vitro and in vivo. *J Clin Invest* 110:1309–1318
 69. Arnold SM, Patchell RA (2001) Diagnosis and management of brain metastases. *Hematol Oncol Clin North Am* 15:1085–1107
 70. Breedveld P, Beijnen JH, Schellens JHM (2006) Use of P-glycoprotein and BCRP inhibitors to improve oral bioavailability and CNS penetration of anticancer drugs. *Trends Pharmacol Sci* 27:17–24
 71. Nwaozuzu OM, Sellers LA, Barrand MA (2003) Signalling pathways influencing basal and H(2)O(2)-induced P-glycoprotein expression in endothelial cells derived from the blood-brain barrier. *J Neurochem* 87:1043–1051
 72. Bauer B, Hartz AMS, Fricker G, Miller DS (2004) Pregnane X receptor upregulation of P-glycoprotein expression and transport function at the blood-brain barrier. *Mol Pharmacol* 66:413–419
 73. Masereeuw R, Terlouw SA, van Aubel RA, Russel FG, Miller DS (2000) Endothelin B receptor-mediated regulation of ATP-driven drug secretion in renal proximal tubule. *Mol Pharmacol* 57:59–67
 74. Terlouw SA, Masereeuw R, Russel FG, Miller DS (2001) Nephrotoxicants induce endothelin release and signaling in renal proximal tubules: Effect on drug efflux. *Mol Pharmacol* 59:1433–1440
 75. Hartz AM, Bauer B, Fricker G, Miller DS (2004) Rapid regulation of P-glycoprotein at the blood-brain barrier by endothelin-1. *Mol Pharmacol* 66:387–394
 76. Erdlenbruch B, Alipour M, Fricker G, Miller DS, Kugler W, Eibl H, Lakomek M (2003) Alkylglycerol opening of the blood-brain barrier to small and large fluorescence markers in normal and C6 glioma-bearing rats and isolated rat brain capillaries. *Br J Pharmacol* 140:1201–1210
 77. Kroll RA, Neuwelt EA (1998) Outwitting the blood-brain barrier for therapeutic purposes: Osmotic opening and other means. *Neurosurgery* 42:1083–1099

78. Hartz AM, Bauer B, Fricker G, Miller DS (2006) Rapid modulation of P-glycoprotein-mediated transport at the blood-brain barrier by tumor necrosis factor- α and lipopolysaccharide. *Mol Pharmacol* 69:462–470
79. Geick A, Eichelbaum M, Burk O (2001) Nuclear receptor response elements mediate induction of intestinal MDR1 by rifampin. *J Biol Chem* 276:14581–14587
80. Kliewer SA, Moore JT, Wade L, Staudinger JL, Watson MA, Jones SA, McKee DD, Oliver BB, Willson TM, Zetterstrom RH, Perlmann T, Lehmann JM (1998) An orphan nuclear receptor activated by pregnanes defines a novel steroid signaling pathway. *Cell* 92:73–82
81. Lehmann JM, McKee DD, Watson MA, Willson TM, Moore JT, Kliewer SA (1998) The human orphan nuclear receptor PXR is activated by compounds that regulate CYP3A4 gene expression and cause drug interactions. *J Clin Invest* 102:1016–1023
82. Schuetz E, Strom S (2001) Promiscuous regulator of xenobiotic removal. *Nat Med* 7:536–537
83. Watkins RE, Noble SM, Redinbo MR (2002) Structural insights into the promiscuity and function of the human pregnane X receptor. *Curr Opin Drug Discov Devel* 5:150–158
84. Dussault I, Forman BM (2002) The nuclear receptor PXR: A master regulator of “homeland” defense. *Crit Rev Eukaryot Gene Expr* 12:53–64
85. Perloff MD, von Molke LL, Greenblatt DJ (2004) Ritonavir and dexamethasone induce expression of CYP3A and P-glycoprotein in rats. *Xenobiotica* 34:133–150
86. Demeuse P, Fragner P, Leroy-Noury C, Mercier C, Payen L, Fardel O, Couraud PO, Roux F (2004) Puromycin selectively increases *mdr1a* expression in immortalized rat brain endothelial cell lines. *J Neurochem* 88:23–31
87. Mrsulja BB, Mrsulja BJ, Fujimoto T, Klatzo I, Spatz M (1976) Isolation of brain capillaries: A simplified technique. *Brain Res* 110:361–365
88. Williams H, Neuhaus J, Kniessel U, Krauß B, Schmid E-M, Öcalan M, Farell C, Risau W (1980) Modulation of tight junction structure in blood-brain barrier endothelial cells. *J Cell Sci* 107:1347–1357
89. Goldstein GW, Betz AL, Bowman PD (1984) Use of isolated brain capillaries and cultured endothelial cells to study the blood-brain barrier. *Fed Proc* 43:191–195
90. Nobmann S, Bauer B, Fricker G (2001) Ivermectin excretion by isolated functionally intact brain endothelial capillaries. *Brit J Pharmacol* 132:722–728
91. Miller DS, Graeff C, Droulle L, Fricker S, Fricker G (2002) Xenobiotic efflux pumps in isolated fish brain capillaries. *Am J Physiol* 282:R191–R198
92. Fricker G, Nobmann S, Miller DS (2002) Permeability of porcine blood-brain barrier to somatostatin analogs. *Brit J Pharmacol* 135:1308–1314
93. Bowman PD, Betz AL, Ar D, Wolinsky JS, Penney JB, Shivers RR, Goldstein GW (1981) Primary culture of capillary endothelium from rat brain. *In Vitro* 17:353–362
94. Franke H, Gallah HJ, Beuckmann CT (2000) Primary cultures of brain microvessel endothelial cells: A valid and flexible method to study drug transport through the blood-brain barrier in vitro. *Brain Res Prot* 5:248–256
95. Spatz M, Bembry J, Dodson RF, Hervonen H, Murray MR (1980) Endothelial cells culture derived from isolated brain microvessels. *Brain Res* 191:577–582
96. Tontsch U, Bauer HC (1989) Isolation, characterization and long-term cultivation of porcine and murine capillary endothelial cells. *Microvasc Res* 37:148–161
97. Shi F, Audus KL (1994) Biochemical characteristics of primary and passaged cultures of primate brain microvessel endothelial cells. *Neurochem Res* 19:427–433
98. Faso L, Trowbridge RS, Quan W, Yao XL, Jenkins EC, Maciulis A, Bunch TD, Wisniewski HM (1994) Characterization of a strain of cerebral endothelial cells

- derived from goat brain which retain their differentiated traits after long-term passage. *In Vitro Cell Dev Biol Anim* 30A:226–235
99. Dorovini-Zis K, Pramey R, Bowman PD (1991) Culture and characterization of microvascular endothelial cells derived from human brain. *Lab Invest* 64:425–436
 100. Rubin LL, Hall DE, Porter S, Barbu K, Cannon C, Horner HC, Janatpour M, Liaw CW, Manning K, Morales J, Tanner LI, Tomaselli KJ, Bard F (1991) A cell culture model of the blood-brain barrier. *J Cell Biol* 115:1725–1735
 101. Biegel D, Spencer DD, Pachter JS (1994) Isolation and culture of human brain microvessel endothelial cells for the study of blood-brain barrier properties in vitro. *Brain Res* 692:183–189
 102. Seetharaman S, Barrand MA, Maskell L, Scheper RJ (1998) Multidrug resistance-related transport proteins in isolated human brain microvessels and in cells cultured from these isolates. *J Neurochem* 70:1151–1159
 103. Krause D, Mischek U, Galla HJ, Dermietzel R (1991) Correlation of zonula occludens ZO-1 antigen expression and transendothelial resistance in porcine and rat cultured cerebral endothelial cells. *Neurosci Letters* 128:301–304
 104. White FP, Dutton GR, Norenberg MD (1981) Microvessels isolated from rat brain: Localization of astrocyte processes by immunohistochemical techniques. *J Neurochem* 36:328–332
 105. Garberg P (1998) In vitro models of the blood-brain barrier. *Altern Lab Animals* 26:821–847
 106. Gumbleton M, Audus KL (2001) Progress and limitation in the use of in vitro cell cultures to serve as a permeability screen for the blood-brain barrier. *J Pharm Sci* 90:1681–1698
 107. Bauer B, Miller DS, Fricker G (2003) Compound profiling for P-glycoprotein at the blood-brain barrier using a microplate screening system. *Pharm Res* 20:1170–1176
 108. Dehouck MP, Jolliet-Riant P, Bree F, Fruchart J-C, Cecchelli R, Tillement JP (1992) Drug transfer across the blood-brain barrier: Correlation between in vitro and in vivo models. *J Neurochem* 58:1790–1797
 109. Ghazanfari FA, Stewart RR (2001) Characteristics of endothelial cells derived from the blood-brain barrier and of astrocytes in culture. *Brain Res* 890:49–65
 110. Cecchelli R, Dehouck B, Descamps L, Fenart L, Buee-Scherrer VV, Duhem C, Lundquist S, Rentfel M, Torpier G, Dehouck MP (1999) In vitro model for evaluating drug transport across the blood-brain barrier. *Adv Drug Deliv Rev* 36:165–178
 111. Galla H-J (2000) Zellkulturmodelle für die Pharmaforschung. *Bioforum* 3:123–125
 112. Stanness KA, Neumaier JF, Sexton TJ, Grant GA, Emmi A, Maris DO, Janigro D (1999) A new model of the blood-brain barrier: Co-culture of neuronal, endothelial and glial cells under dynamic conditions. *Neuroreport* 10:3725–3731
 113. Stanness KA, Westrum LE, Fornaciari E, Mascagni P, Nelson JA, Stenglein SG, Myers T, Janigro D (1997) Morphological and functional characterization of an in vitro blood-brain barrier model. *Brain Res* 771:329–342
 114. Morgan SJ, Darling DC (1994) Kultur tierischer Zellen. Spektrum Akademischer Verlag, Heidelberg
 115. Mitsunaga Y, Taganaka H, Matsuo H, Naito M, Tsuruo T, Ohtani H, Sawada Y (2000) Effects of bioflavonoids on vincristine transport across blood-brain barrier. *Europ J Pharmacol* 395:193–201
 116. Fischer D, Kissel T (2001) Histochemical characterization of primary capillary endothelial cells from porcine brains using monoclonal antibodies and fluorescein isothiocyanate-labelled lectins: Implications for drug delivery. *Europ J Pharm Biopharm* 52:1–11

117. Engkvist O, Wrede P, Rester U (2003) Prediction of CNS activity of compound libraries using substructure analysis. *J Chem Inf Comput Sci* 43:155–160
118. Garg P, Verma J (2006) In silico prediction of blood-brain barrier permeability: An artificial neural network model. *J Chem Inf Model* 46:289–297
119. Narayanan R, Gunturi SB (2005) In silico ADME modelling: Prediction models for blood-brain barrier permeation using a systematic variable selection method. *Bioorg Med Chem* 15:3017–3028

18

High-Throughput Screening Using Caco-2 Cell and PAMPA Systems

Cheng Li, Sam Wainhaus, Annette S. Uss, and Kuo-Chi Cheng

Abstract This chapter will focus on the two most commonly used high-throughput screening methods detecting cellular/bio-membrane permeability in the pharmaceutical industry: Caco-2 cells and the parallel artificial membrane permeability assay (PAMPA). Both assays have advantages and disadvantages, and it is essential to understand these limitations. Since it is well recognized that human intestinal absorption cannot be precisely predicted by a single screening assay, it is important to utilize various *in vitro* and *in vivo* preclinical studies during lead optimization in drug discovery.

Keywords: High-throughput screening; Caco-2 monolayer; PAMPA; *In vitro* absorption models

Abbreviations

BCRP	Breast cancer resistance protein
NCEs	New chemical entities
PAMPA	Parallel artificial membrane permeability assay
P-gp	P-glycoprotein
TEER	Trans epithelial electrical resistance

18.1. Introduction

Lead optimization of new chemical entities (NCEs) based on pharmacokinetic behavior plays a major role in modern drug discovery. Despite advancement of drug delivery methods, the oral route remains the most frequent route of administration for approved new drugs. Therefore, during lead optimization it is essential to identify NCEs with sufficient oral absorption predicted using a variety of *in vitro* and *in vivo* assays. It is well recognized that in order for a NCE to achieve reasonable oral absorption, it will need to have adequate aqueous solubility, as well as intestinal permeability [1]. Recent advancements in chemistry, such as parallel and combinatorial synthesis, have resulted in a multifold increase in the number of compounds that are available for evaluation in new drug discovery. Furthermore, a variety of improved structural chemistry

tools, such as X-ray crystallography, structural modeling and ligand/substrate docking algorithms, and improved molecular biology tools, such as high-throughput binding targets and cell-based activity assays, provides new drug discovery scientists with an unprecedented level of structure-based designs to further guide the synthesis of new chemotypes as potential drug leads. Along with the advancement of chemistry and biology, new automated screening tools have become commercially available that can carry out complex, programmable, and adaptable robotic operations to test hundred of thousands of compounds in a speedy and precise manner. As a result, these new forces have worked together to increase our ability to create NCEs that exhibit targeted pharmacological activity. Hence, the task of screening compounds for their biopharmaceutical properties, such as solubility, permeability, and metabolic stability, has become a major challenge in drug discovery. This change, in turn, has compelled the invention and implementation of high-throughput screening methods that predict *in vivo* oral absorption.

Drug absorption through the gastrointestinal (GI) tract following oral administration is a rather complex and dynamic process. Passive diffusion can occur through the cell membranes of enterocytes (transcellular) or the tight junctions between the enterocytes (paracellular) [2–4]. Influx and efflux through various drug transporters also play roles in dictating drug absorption. Since many processes are occurring simultaneously, it is often impossible for a single *in vitro* model to simulate the entire *in vivo* process. However, two *in vitro* screening models, Caco-2 cell and parallel artificial membrane permeability assay (PAMPA), have been developed over the last decade and are currently used by most major pharmaceutical companies in their drug discovery efforts. In the following pages, we will describe these two assays, their pros and cons, and how to use them for lead optimization in the discovery process.

18.2. Caco-2 Cell Monolayer System

There are several cell monolayer models that are frequently used for the evaluation of drug permeability and absorption potential (Table 18.1). For a more detailed discussion, please refer to Chap. 8. Caco-2 cells (adenocarcinoma cells derived from colon) are the most extensively characterized and frequently used of the available cell lines [5–9]. A unique feature of Caco-2 cells is that they undergo spontaneous enterocyte differentiation in cell culture. Unlike intestinal enterocytes, Caco-2 cells are immortalized and replicate rapidly into confluent monolayers. When the cells reach confluency during culture on a semi-porous membrane, they start to polarize and form tight junctions, creating an ideal system for permeability and transport studies. During the past decade, use of

Table 18.1 Commonly used monolayer cell models for estimating permeability and transcellular flux.

Cells	Species/tissue origin	Cell type
Caco-2	Human/colon	Epithelial
2/4/A1	Rat/intestine	Epithelial
MDCK	Canine/kidney	Epithelial
LLC-PK1	Porcine/kidney	Epithelial

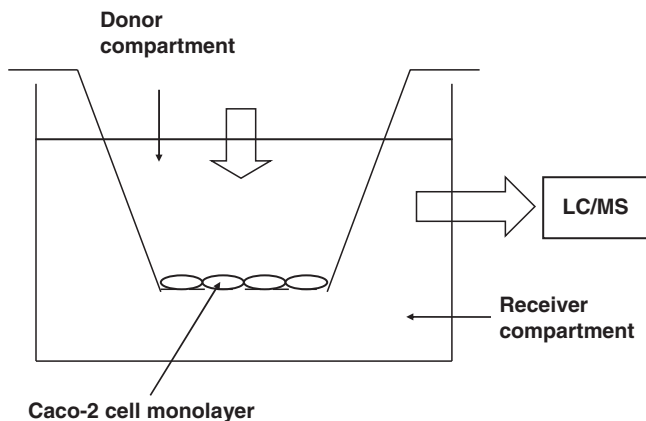


Figure 18.1 Schematic of Caco-2 monolayers grown on a Transwell[®] filter insert.

Caco-2 cells in high-throughput screening for NCEs in the pharmaceutical industry has increased tremendously. The utility of this monolayer model to either rank order or filter out compounds has been exemplified by many previous studies [10, 11].

The Caco-2 permeability assay is usually performed in a Transwell[®] device (Figure 18.1). The Transwell[®] contains two compartments: a donor and a receiver compartment. The apical donor compartment contains a porous membrane that supports the growth of the Caco-2 monolayer. Caco-2 cells are seeded on the porous membrane. Upon confluency of the cell culture, the compound is added into the donor compartment at a concentration range from one to several hundred micromolar. Samples are collected from the receiver compartment for up to 2 h, then LC-UV or LC-MS methods are used to quantify compound in each sample. The permeability coefficient of the compound is calculated based on the following equation:

$$P_{\text{app}} = \frac{dM/dt}{C_0 S}$$

C_0 is the initial compound concentration, S is the surface area of Caco-2 cell membrane on the insert, and M is the compound amount transported to the receiver side at time point t .

In order to assure tight junction formation, the electrical resistance of the cell monolayer is often tested. A transepithelial electrical resistance (TEER) value above 300–500 Ωcm^2 usually indicates reasonably tight junctions that prevent leakage and, thus, high-background basal concentration in the receiver compartment. Additionally, impermeable standard compounds, such as Lucifer yellow and mannitol, are also used to test for leakage of the cell monolayer. The resulting permeability coefficients are compared to those reported in the literature. Reported permeability coefficients, however, may vary significantly from lab to lab, particularly for compounds that pass through the Caco-2 monolayer via the paracellular route. According to Walter and Kissel [12], permeability coefficients of mannitol in the literature range from 2 to 221 nm/s. Even within the same laboratory, several factors, such as cell source, age of cell culture, and culturing conditions, may affect the reproducibility of permeability results. The cell passage number may specifically affect the tight junctions and the expression level of drug transporters such as P-glycoprotein

Table 18.2 Caco-2 permeability and human absorption of 28 marketed drugs and excipients.

Compound	Human absorption (%)	Caco-2 permeability (nm/s)
PEG-4000	0	2
Doxorubicin	5	3
Mannitol	16	7
Acyclovir	30	13
Nadolol	34	6
Terbutaline	44	8
Ranitidine	50	21
Furosemide	55	13
Atenolol	56	16
Cimetidine	60	27
Etoposide	60	15
Metolazone	64	38
Sulfasalazine	65	46
Hydrochlorothiazide	67	15
Methylprednisolone	82	146
Propranolol	90	394
Hydrocortisone	91	207
Alprenolol HCl	93	366
Metoprolol	95	332
Antipyrine	97	357
Caffeine	100	345
Carbamazepine	100	425
Ketoprofen	100	347
Naproxen	100	338
Theophylline	100	226
Verapamil	100	457
Corticosterone	100	414
Dexamethasone	100	125

(P-gp). Nevertheless, it is not difficult to differentiate a highly permeable drug from a poorly permeable drug if the conditions of the assay are carefully maintained. This is particularly true for compounds that are absorbed transcellularly.

Table 18.2 shows the Caco-2 permeability and human absorption for 28 marketed compounds. Figure 18.2 shows the correlation between permeability coefficients and the oral absorption of 30 marketed compounds. As reported by many other laboratories, sigmoidal relationships were observed between the fraction absorbed and the permeability coefficients in the Caco-2 model [13, 14]. Based on this sigmoidal relationship, one may design cutoff values for low, medium, and high groups. The dynamic range of permeability values for highly absorbed compounds versus poorly absorbed compounds is usually

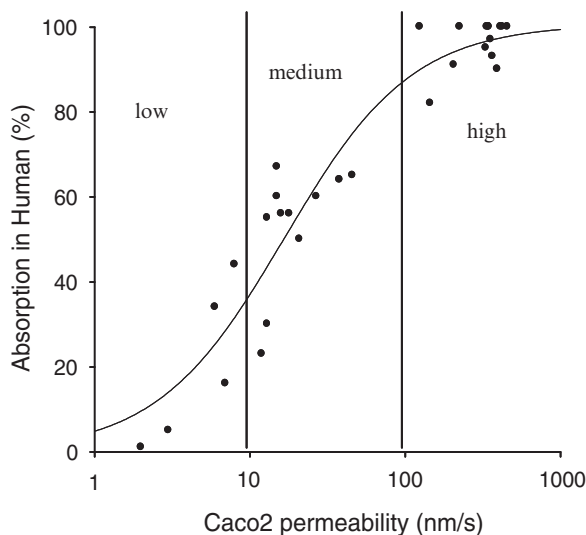


Figure 18.2 Flux of 30 commonly prescribed drugs across Caco-2 monolayers versus absorption in humans.

close to two orders of magnitude in the Caco-2 model. The steepness of the slope may reflect the predictability of the model for compounds that are moderately absorbed. Figure 18.2 also demonstrates the difficulty in differentiating compounds in the mid range due to large variability in this range of the curve. During routine screening, a few compounds may be used repeatedly as benchmarks for calibration of day-to-day and batch-to-batch variations. For example, pindolol may be used for medium- to high-permeability cutoffs, whereas lovastatin may be used for medium- to low-permeability cutoffs. Metoprolol is a favored compound for the benchmarking of high-permeability compounds. Using these benchmarks, one may normalize permeability coefficients to allow comparison of a large number of compounds over a long period of time.

It is generally accepted that the Caco-2 model would be most helpful during early lead optimization in the pharmaceutical setting. This type of early screening would provide medicinal chemists with guidance in choosing the more favorable chemotypes. Hence, in order to accommodate a large volume of screening, the trend over the last decade has been to fully or semi-automate the entire Caco-2 screening. A fully automated Caco-2 system allows higher throughput and increases productivity without a proportional increase of resources. The components for a fully automated robotic system include an automated cell seeding and feeding system. This system is often housed in a clean room to prevent potential contamination of the cells. The second component comprises a robot that doses and aliquots samples from the Caco-2 plate. When the Caco-2 system is teamed up with high-throughput LC/MS, a group of two to three scientists could screen 500–2000 compounds per month. In addition, using 24-well or even 96-well plate systems coupled with LC/MS, significantly reduces the amount of compound required to perform permeability experiments with this model. This is a remarkable feature that is useful when combinatorial chemistry generates a large array of structurally related compounds. Recently, the Food and Drug Administration (FDA) issued

guidelines for the Biopharmaceutical Classification System (BCS), which utilizes permeability and solubility for the classification of compounds [15]. A class 1 compound with excellent Caco-2 permeability and aqueous solubility may obtain a waiver for modification of formulation in clinical trials, whereas, a class 4 compound with low Caco-2 permeability and aqueous solubility may have difficulty in obtaining such a waiver.

During the differentiation process in cell culture that leads to formation of tight junctions and development of cell polarity, various drug transporters may also be expressed in Caco-2 cells in a polarized manner. It is well documented that the major efflux pumps, such as P-gp and breast cancer resistant protein (BCRP), are highly expressed in Caco-2 cells [16, 17]. Both drug transporters are located on the apical membrane when the Caco-2 cells establish cell polarity. In addition, other transporters, such as multidrug resistance-associated proteins (MRPs), may also play a significant role in Caco-2 efflux. Hence, the Caco-2 model has also been used for evaluation of efflux and identification of efflux substrates. Following separate dosing of the test compound in either the apical compartment or the basolateral compartment, the apical-to-basal and basal-to-apical permeability coefficients are calculated and compared in order to generate an efflux ratio ($=P_{app} B$ to $A/P_{app} A$ to B). When the efflux ratio is larger than two, the test compound is flagged as a potential efflux substrate. It is usually feasible to use specific inhibitors to identify the transporter that is responsible for the efflux. For example, the efflux ratio for digoxin ranges from 10 to 40 [18]. When co-dosed with cyclosporine (a P-gp inhibitor), the efflux ratio of digoxin decreases to about one. Other P-gp inhibitors commonly used for such experiments are cyclosporine A [19] and ketoconazole, while probenecid and indomethacin are commonly used to inhibit MRP2 [20].

There are several potential issues that may restrict use of the Caco-2 model as the sole screening tool for evaluation of absorption potential. First, despite the fact that Caco-2 cells show sufficient levels of expression of P-gp, BCRP, and MRPs, many other transporters involved in the influx of substrates are under-expressed. These transporters include organic anion transporting polypeptides (OATPs), organic cation transporter (OCT), and PepT1. For example, PepT1 substrates, such as beta-lactam antibiotics (cefadroxil and amoxicillin), are well absorbed, but show poor Caco-2 permeability [21]. The Caco-2 model is likely to generate false negatives with NCEs actively transported by under-expressed transporters. When Caco-2 permeability data differ greatly from animal absorption data, it may require additional studies to understand if the drug candidate is the substrate of active transporters.

A second issue limits use of the Caco-2 model for compounds that diffuse paracellularly. Many small hydrophobic compounds, such as atenolol and furosemide, show poor Caco-2 cell permeability despite adequate absorption (>50%) in humans [22]. The plausible explanation for this discrepancy is that these small molecules which translocate through a paracellular absorption mechanism are not adequately solubilized and cannot diffuse across the Caco-2 less-permeable tight junctions. Perturbation of the tight junctions by treatment with calcium-chelating chemicals, such as ethylenediaminetetraacetic acid (EDTA), may be helpful in evaluating such compounds; however, the use of organic solvents is contraindicated. The integrity of tight junctions in the

Caco-2 model is easily affected by commonly used organic solvents or co-solvents [e.g., methanol, ethanol, polyethylene glycol (PEG), dimethyl sulfoxide (DMSO)] at relatively low concentrations (<1% v/v). Therefore, NCEs with poor aqueous solubility may not be adequately evaluated by this model. It has become a common practice in the pharmaceutical industry to test solubility of compounds before performing any other *in vitro* screens and eliminate NCEs with poor aqueous solubility, thus preventing false negatives due to this issue.

A third issue arises with NCEs that bind to plastic surfaces due to the hydrophobic physical nature of the molecule. A significant loss due to this type of non-specific binding to the Caco-2 device may lead to underestimation of permeability. Addition of protein (e.g., bovine serum albumin) in the receiver compartment appears to be capable of preventing some non-specific binding [23].

Lastly, the preparation of fully differentiated Caco-2 cells generally requires a 3-week cell culture period with eight to ten cell feedings. A fully automated system for cell seeding and feeding can be used for industrial high-throughput screening purposes; however, for more limited use, this labor intensive cell culture process could become a rate-limiting factor. The cell preparation time can be substantially reduced by using an available coating material and supplemented growth medium. Generation of a functional monolayer in a shorter cell culturing period not only increases the productivity but also decreases the chance of having contamination.

Other potential cell models are Madin-Darby canine kidney cells (MDCK), 2/4/A1 cells, HT-29, and LLC-PK1 cells. The 2/4/A1 cell line originates from fetal rat intestine and mimics the permeability of human small intestine with regards to both paracellular and transcellular drug transport [24]. The permeability of some poorly permeable compounds, such as mannitol and creatine, across a 2/4/A1 cell monolayer appears to be comparable to that in human jejunum suggesting that this cell line could be a better model for compounds that are absorbed via the paracellular route. MDCK cells differentiate into columnar epithelial cells and form tight junctions when cultured on semi-permeable membranes. Irving et al. [25] compared the permeability values of 55 compounds in an MDCK model with human absorption values and found a good correlation between these two values. The major concern with using MDCK cells for permeability screening is that the cell line is derived from dog kidney cells, and it is very likely that the expression levels and substrate specificity of various transporters may be different from the *in vivo* situation in humans. In contrast, the major advantage of MDCK cells is that they require only a 3-day culture period.

Despite the availability of other cell lines, Caco-2 cells remain the most widely used intestinal cell culture model at present. This model has provided valuable information necessary for lead optimization in the drug discovery process. However, it is important to understand that compounds with high permeability in this model are typically well absorbed, whereas compounds with low solubility and low permeability in this model may not necessarily be poorly absorbed *in vivo*. Although this type of positive selection limits the usefulness in providing a structure-permeability relationship, the Caco-2 model has the most effect in drug discovery when the screen is implemented early and in conjunction with other types of *in vitro* and *in vivo* permeability/absorption screens.

18.3. Parallel Artificial Membrane Permeability Assays

PAMPA was first demonstrated by Kansy et al. [26] as a high-throughput screening tool for predicting absorption. This model utilizes an artificial lipid membrane created by coating a hydrophobic filter with a mixture of lecithin/phospholipids dissolved in an inert organic solvent such as dodecane. Since then, several variants of PAMPA have been developed using different types of lipid barriers. The first commercially available lipid barrier was based on 2% w/v dioleoylphosphatidylcholine (DOPC) dissolved in n-dodecane [27]. An improved preparation was subsequently introduced [28] based on a 20% w/v mixture of negatively charged phospholipids also dissolved in n-dodecane in a variant called Double-Sink PAMPA (DS-PAMPA). Table 18.3 shows the PAMPA permeability and human absorption of 19 marketed compounds. As shown in Figure 18.3, there is a good correlation between the flux rate across the PAMPA membrane using DS-PAMPA and the absorption of these 19 structurally diverse compounds in humans. These results appear to be consistent with recent findings that show DS-PAMPA may yield the best correlation in comparison with other variant PAMPA systems [29].

The use of 96-well microtiter plates coupled with the rapid quantification by a spectrophotometric plate reader allows this system to screen a large array of compounds in a relatively short period of time. Alternatively, the compound analysis can be performed with fast and sensitive LC/MS by pooling the samples together. Both the spectrophotometric and mass spectrometric methods

Table 18.3 Parallel artificial membrane permeability assay (PAMPA) permeability and human absorption for 19 drug compounds.

Compounds	Human absorption (%)	PAMPA permeability (nm/s)
Ganciclovir	5	0
Bretylum Tosylate	18	0
Acyclovir	20	0
Nadolol	34	0
Terbutaline	44	1.9
Etoposide	60	26
Metolazone	64	60
Ketoconazole	80	1000
Methylprednisolone	82	286
Pindolol	90	378
Propranolol	90	371
Hydrocortisone	91	101
Alprenolol	93	840
Metoprolol	95	1000
Caffeine	100	9.6
Carbamazepine	100	498
Corticosterone	100	223
Dexamethasone	100	354
Verapamil	100	1000

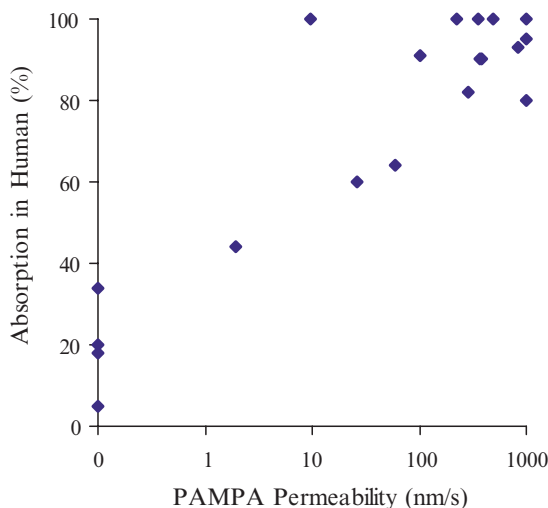


Figure 18.3 Correlation between flux across parallel artificial membrane permeability assay (PAMPA) and absorption in humans.

can be used for low-solubility compounds since the limit of quantitation can reach nanomolar concentrations. The major advantage of PAMPA is that it is much less labor intensive than cell culture or *in vivo* studies that have similar predictive power.

There are several limitations, however, in using this model for prediction of human absorption. First, as mentioned previously, the composition of the phospholipid bilayers in different variants of PAMPA systems may cause some major variation in permeability coefficients. Second, PAMPA can significantly underestimate the absorption of compounds that are actively transported by influx drug transporters, such as PepT1 and OATPs, or hydrophobic small molecules that may be transported through the paracellular route. Despite these limitations, PAMPA has become a popular permeability screen during the early drug discovery process because of its high-throughput capability.

18.4. Combining Use of Caco-2 and PAMPA

PAMPA and the Caco-2 cell model are often used in combination to evaluate permeability potential. While the Caco-2 cell model has been the *in vitro* gold standard for permeability screening, PAMPA has recently become a more efficient, economical, and higher-throughput screen. Both models show approximately two orders of magnitude in their dynamic range of permeability values. Both work well in categorizing compound permeability (high, medium, and low), but lack predictive accuracy. In order to efficiently combine these two models in drug discovery, one will need to understand the pros and cons. The sole purpose of using PAMPA for screening is to identify compounds that have good transcellular passive permeability across a lipid barrier. This type of evaluation of “intrinsic” passive permeability may provide a positive selection of compounds that will demonstrate good *in vivo* absorption. Since PAMPA is often placed as a tier-1 screen, compounds with good permeability may obtain

a higher priority for subsequent screening. Obviously, a simple lipid barrier such as the PAMPA system lacks other biological characteristics of intestinal enterocyte membranes. Hence, PAMPA may not predict compounds that are transported by influx and efflux drug transporters, permeate through the tight junctions, or are absorbed by other types of cellular mechanisms. Similar to PAMPA, the Caco-2 cell model can also identify compounds with good passive permeability via the transcellular route. It is also possible to identify compounds such as small hydrophobic molecules that may permeate via the tight junctions (paracellular) with proper perturbation of the tight junctions. The high levels of expression of certain drug transporters, such as P-gp, BCRP, and MRPs, certainly allow Caco-2 cells to retain many pharmacological characteristics of enterocytes. However, many influx transporters, such as PepT1 and OATPs, are not well expressed in Caco-2 cells. Understanding these capacities and limitations, PAMPA and Caco-2 models can both be used to better predict absorption during the early stages of drug discovery.

18.5. Concluding Remarks

Drug absorption across the intestinal membrane is a complex process. Absorption due to passive diffusion occurs most commonly via the cell membrane of enterocytes (transcellular) or the tight junctions between enterocytes (paracellular). Carrier-mediated absorption may occur via the active transport process, while efflux transporters may limit the absorption. Because of the multivariate processes involved in intestinal absorption of drugs, it is impossible to rely on a single in vivo or in vitro model to accurately predict the absorption potential. A large variety of in vivo and in vitro models are available for the prediction of intestinal permeability of compounds at varying stages of the drug discovery process. PAMPA and Caco-2 cell models are the most frequently used high-throughput systems for the screening of compounds in the early stages of drug discovery. In combination as first tier (or primary) screens, these two assays offer the right balance and synergies. Furthermore, they have proven to be valuable in modern drug discovery.

References

1. Chiou WL (2001) The rate and extent of oral bioavailability versus the rate and extent of oral absorption: Clarification and recommendation of terminology. *J Pharmacokinet Biopharm* 28:3–6.
2. Balimane PV, Chong S, Morrison RA (2000) Current methodologies used for evaluation of intestinal permeability and absorption. *J Pharmacol Toxicol Methods* 44:301–312.
3. Balimane PV, Han YH, Chong S (2006) Current industrial practices of assessing permeability and P-glycoprotein interaction. *AAPS J* 8:E1–E13.
4. Bergstrom CAS (2005) In silico predictions of drug solubility and permeability: two rate-limiting barriers to oral drug absorption. *Basic Clin Pharmacol Toxicol* 96:156–161.
5. Artursson P (1991) Cell cultures as models for drug absorption across the intestinal mucosa. *Crit Rev Ther Drug Carrier Syst* 8:305–330.
6. Artursson P, Palm K, Luthman K (2001) Effect of molecular charge on intestinal epithelial drug transport: pH-dependent transport of cationic drugs. *Adv Drug Deliv Rev* 46:27–43.

7. Borchardt R (1995) Application of cell culture systems in drug discovery and development. *J Drug Target* 3:179–182.
8. Hidalgo I, Raub T, Borchardt R (1989) Characterization of the human colon carcinoma cell line (Caco-2) as a model system for intestinal epithelial permeability. *Gastroenterology* 96:736–749.
9. Rubas W, Jezyk N, Grass GM (1993) Comparison of the permeability characteristics of a human colonic epithelial (Caco-2) cell line to colon of rabbit, monkey, and dog intestine and human drug absorption. *Pharm Res* 10:113–118.
10. Artursson P, Karlsson J (1991) Correlation between oral drug absorption in humans and apparent drug permeability coefficients in human intestinal epithelial (Caco-2) cells. *Biochem Biophys Res Comm* 175:880–885.
11. Chong S, Dando S, Morrison RA (1997) Evaluation of Biocoat intestinal epithelium differentiation environment (3-day cultured Caco-2 cells) as an absorption screening model with improved productivity. *Pharm Res* 14:1835–1837.
12. Walter E, Kissel T (1995) Transport of peptidomimetic renin inhibitors across monolayers of a human intestinal cell line (Caco-2): Evidence for self-enhancement of paracellular transport route. *J Pharm Sci* 3:215–230.
13. Artursson P, Borchardt RT (1997) Intestinal drug absorption and metabolism in cell cultures: Caco-2 and beyond. *Pharm Res* 14:1655–1658.
14. Artursson P, Lindmark T, Davis SS, Illum L (1994) Effect of chitosan on the permeability of monolayers of intestinal epithelial cells (Caco-2). *Pharm Res* 11:1358–1361.
15. Brouwers J, Ingels F, Tack J, Augustijns P (2005) Determination of intraluminal theophylline concentrations after oral intake of an immediate- and a slow-release dosage form. *J Pharm Pharmacol* 57:987–996.
16. Adachi Y, Suzuki H, Sugiyama Y (2001) Comparative studies on in vitro methods for evaluating in vivo function of MDR1 P-glycoprotein. *Pharm Res* 18:1660–1668.
17. Breedveld P, Beijnen JH, Schellens JH (2006) Use of P-glycoprotein and BCRP inhibitors to improve oral bioavailability and CNS penetration of anticancer drugs. *Trends Pharmacol Sci* 27:17–24.
18. Yao HM, Chiou WL (2006) The complexity of intestinal absorption and exsorption of digoxin in rats. *Int J Pharm* 322:79–86.
19. Loor F, Tiberghien F, Wenandy T, Didier A, Traber R (2002) Cyclosporins: Structure-activity relationships for the inhibition of the human FPR1 formylpeptide receptor. *J Med Chem* 45:4598–4612.
20. Mallants R, Van Oosterwyck K, Van Vaeck L, Mols R, De Clercq E, Augustijns P (2005) Multidrug resistance-associated protein 2 (MRP2) affects hepatobiliary elimination but not the intestinal disposition of tenofovir disoproxil fumarate and its metabolites. *Xenobiotica* 35:1055–1066.
21. Chong S, Dando S, Soucek K, Morrison RA (1996) In vitro permeability through caco-2 cells is not quantitatively predictive of in vivo absorption for peptide-like drugs absorbed via the dipeptide transporter system. *Pharm. Res* 13:120–123.
22. Bourdet DL, Pollack GM, Thakker DR (2006) Intestinal absorptive transport of the hydrophilic cation ranitidine: A kinetic modeling approach to elucidate the role of uptake and efflux transporters and paracellular vs. transcellular transport in Caco-2 cells. *Pharm Res* 23:1178–87.
23. Saha P, Kou J (2002) Effect of bovine serum albumin on drug permeability estimation across Caco-2 monolayers. *Eur J Pharm Biopharm* 54:319–324.
24. Tavelin S, Milovic V, Oecklind G, Olsson S, Artursson P (1999) A conditionally immortalized epithelial cell line for studies of intestinal drug transport. *J Pharmacol Exper Ther* 290:1212–1221.

25. Cho M, Thompson D, Cramer C, Vidmar T, Scieszka J (1989) The Madin Darby canine kidney (MDCK) epithelial cell monolayer as a model cellular transport barrier. *Pharm Res* 6:71–77.
26. Kansy M, Senner F, Gubernator K (1998) Physicochemical high throughput screening: Parallel artificial membrane permeation assay in the description of passive absorption processes. *J Med Chem* 41:1007–1010.
27. Avdeef A, Strafford M, Block E, Balogh MP, Chabliiss W, Khan I (2001) Drug absorption in vitro model: Filter-immobilized artificial membranes. 2. Studies of the permeability properties of lactones in Piper methysticum Forst. *Eur J Pharm Sci* 14:271–280.
28. Avdeef A (2003) Absorption and drug development. Wiley-Interscience, New York, NY, pp. 116–246.
29. Avdeef A, Tsinman A (2006) PAMPA—a drug absorption in vitro model 13. Chemical selectivity due to membrane hydrogen bonding: in combo comparisons of HDM-, DOPC-, and DS-PAMPA models. *Eur J Pharm Sci* 28:43–50.

19

Instrumented In Vitro Approaches to Assess Epithelial Permeability of Drugs from Pharmaceutical Formulations

Stephan A. Motz, Michael Bur, Ulrich F. Schaefer, and Claus-Michael Lehr

Abstract The following chapter gives an overview of instrumented approaches to investigate the interactions of orally or pulmonary administered formulations with epithelial cell cultures in vitro. The first section is focused on the combined assessment of drug release/dissolution and subsequent absorption/permeation for solid oral dosage forms. Experimental approaches to mimic the complex physiologically surroundings in the gastrointestinal tract are presented as well as combinations of dissolution and permeation apparatus.

The second part describes different experimental approaches to simultaneously assess deposition and subsequent absorption of pharmaceutical aerosol formulations, typically by adapting some existing impactor/impinger devices to accommodate pulmonary epithelial cell culture systems. Differences between longtime and low-dose aerosol deposition in environmental toxicology and short time bolus inhalation of pharmaceutical aerosols are elucidated.

Keywords: Dissolution; Permeability; Dosage forms; Bioavailability; Blood-air barrier; Cascade impactor

Abbreviations

AIC	Air-interfaced culture
API	Active pharmaceutical ingredient
ASL	Alveolar surface liquid
AUC	Area under the curve
BCS	Biopharmaceutical classification system
BML	Bronchial mucus layer
CLSM	Confocal laser scanning microscope
CMC	Critical micellar concentration
FaSSIF	Fasted state-simulating intestinal fluid
FeSSIF	Fed state-simulating intestinal fluid
GI	Gastrointestinal
hAEPc	Human alveolar epithelial cells
HBSS	Hanks balanced salt solution
HEPES	4-(2-Hydroxyethyl)piperazine-1-ethanesulfonic acid
IVIVC	in vivo/in vitro correlation

KBR	Krebs bicarbonate ringer buffer
KRB	Krebs ringer buffer
LCC	Liquid-covered condition
LID	Liquid-interfaced deposition
MES/HEPES	Morpholineethanesulfonic acid/HEPES
MSLI	Multistage liquid impinger
MTT	3-(4,5-Dimethylthiazol-2-yl)-2,5-diphenyl-2H-tetrazoliumbromid
P_{app}	Apparent permeability coefficient
PEPT1	Di/Tri-peptide transporter 1
P-gp	P-glycoprotein
SEM	Scanning electron microscopy
SIA	Sequential injection analysis
TEER	Transepithelial electrical resistance
USP	United States Pharmacopoeia

19.1. Introduction

For most drugs, extravasal administration of the pure active pharmaceutical ingredient (API) to patients is not feasible mainly due to low dose/mass. Hence, drugs are formulated in order to facilitate dosing and to improve patient compliance. Furthermore, for various routes of drug delivery, the dosage form is a key factor determining in vivo bioavailability. However, only little is known about interaction formulated drugs and the several mucosal barriers in vivo. The following chapter comprises an overview of instrumented approaches which are assessing the interactions between formulated drugs and epithelial cells in vitro, with the aim of elucidating effects occurring in vivo.

The first section is focused on orally administered solid dosage forms, whereas within the second section, approaches for pulmonary administered aerosols are highlighted.

19.2. Intestinal Permeability of Drugs Delivered as Solid Dosage Forms

19.2.1. Rationale for Connecting Dissolution and Permeation Measurements

Release from the dosage form and subsequent permeation through intestinal epithelia are the two dominant processes in oral drug delivery, whereby each of both may be rate limiting. Unnumbered parameters affect these processes, such as subsequent wetting, swelling, and disintegration of the dosage form and dissolution of the active compound within the intestinal transit time, depending on the surrounding microclimate pH, osmolarity, and surface tension. While sufficient disintegration and dissolution are prerequisite for oral absorption, critical parameters can also be seen in the pH value of the gastrointestinal (GI) lumen and the cell covering, rather acidic mucus. Further factors include the apical concentration of drug, affinity to active cellular uptake or efflux systems, sink conditions in the trans-mucosal receptor fluid, concomitant administration of food, and disposability of active excipients, just to mention the most important ones. Summarized as L(iberation) and A(bsorption) of the LADME model,

both processes are influenced by and therefore relevant to the design of solid oral dosage forms.

Regarding dissolution testing, many successful efforts have been made to imitate the physiological surroundings in the GI lumen more and more closely. Variables such as temperature, osmolarity, pH, surface tension, and presence of bile salts were altered. As a result of the effort, two *in vitro* dissolution buffers coming most closely to *in vivo* conditions were reported as fasted state simulated intestinal fluid (FaSSIF) and fed state simulated intestinal fluid (FeSSIF) by the group of Dressman [1]. Dissolution testing is routinely carried out using complete dosage forms, except for the assessment of intrinsic solubility at very early stages in the drug development process. In contrast, permeability testing is typically performed with nonformulated compounds, because it is considered as an intrinsic property of a given API. Hence permeability testing does usually address the role of formulation factors and excipients. A number of issues underpin this statement: (i) the dissimilarity between a normal dose of a solid dosage form and the permeation area of Caco-2 monolayers in a Transwell[®] system, potentially resulting in enormous osmotic pressure differences between apical and basolateral compartment; (ii) the sheer impossibility to insert a complete dosage form into a standard Transwell[®] device; (iii) nonappropriate dissolution features of the apical compartment (volume, pH, hydrodynamics, etc.). In conclusion, researchers tend to determine two related and connected issues—solubility and permeability—separately. Of course, when dissolution and permeation assays are to be connected, experimental and technical efforts will increase dramatically. Thus, the question raise for the benefits of the concomitant determination of dissolution and permeation that might justify such efforts. However, significant progress in the development of solid dosage forms by combined dissolution and permeation testing may be expected under the following aspects:

- 1 Improved *in vivo/in vitro* correlation for bioavailability screening of new APIs.
- 2 Improved screening of innovative formulation approaches.
- 3 Investigation of potential food effects on drug absorption.

19.2.1.1. Improved In Vivo/In Vitro Correlation for Bioavailability Screening of New APIs

As described by Artursson et al. [2], *in vitro* permeability of drugs through Caco-2 cell monolayers is correlating well with absorption in humans. However, pure permeation experiments disregard possible solubility issues of a compound that might potentially limit absorption from the gut. By combining dissolution and permeation assay, a deeper insight into the processes happening *in vivo* in the intestine may be given, especially, if one considers the clinical dose to be dissolved in the limited liquid volume of the intestinal fluid. Furthermore, dissolution testing is generally accepted as a validated tool for generating valid *in vivo/in vitro* correlations (IVIVC), but this works only for drugs where absorption is not limited by poor permeability, that is, classes I and II of the biopharmaceutical classification system (BCS).

However, for BCS class III (and IV), an *in vitro/in vivo* correlation of the dissolution result is often not possible, since dissolution is not rate limiting and other parameters cannot be detected in a dissolution setup. The latter therefore

appears possible only when both the dissolution process and the absorption process are considered.

19.2.1.2. Improved Screening of Innovative Formulation Approaches

Considering the LADME model, liberation and absorption of drugs pose crucial parameters for bioavailability after oral administration and are the only factors accessible for manipulation by designing adequate dosage forms. Evidently, detection of formulation parameters affecting dissolution processes is easier accessible, than effects of the formulation on absorption processes. Dissolution studies have been shown to be a good predictor for in vivo performance of solid dosage forms, for example, Refs. [1, 3, 4], under the assumption that the more compound gets into solution within an acceptable time in a more or less physiological surrounding, the higher the bioavailability and the better the in vivo performance. This central paradigm of predictive dissolution testing relies on the assumption that intestinal permeation is not rate limiting and that excipients administered along with the drug do not alter the permeability of intestinal epithelia. In contrast, during the past decades, more and more drugs have been recognized as absorbed by active cellular uptake mechanisms or hindered from absorption by active cellular efflux systems. Simultaneously, several excipients have been detected to interact with intestinal epithelia and have been discussed as intestinal absorption enhancers. The mini-review of Aungst [5] and the review of Swenson et al. [6] may serve as an overview on that particular topic. Terao et al. [7], for example, reported an increased AUC of furosemide in rats by decreasing intraluminal pH at distal portions of the GI by means of Eudragit L100-55, a proton-releasing polymer. For the influx transporter di/tri-peptide transporter 1 (PEPT1), a proton gradient coupled oligopeptide transporter, it has been reported that lower luminal pH values increase the driving force for the uptake, due to a secondary uptake coupled with a proton gradient. Accordingly, Nozawa et al. [8] found that by decreasing the pH in the lumen of rats' small intestines by means of proton-releasing polymers, the bioavailability of PEPT1 substrates, such as cefadroxil and cefixime, increases. Although the authors use remarkably high amounts of excipient (500 mg excipient per kg rat weight), a proof of principle that excipients can affect the active uptake of drugs in vivo was given. In addition to improving uptake, other excipients enhance oral absorption by means of interaction with the tight junctions of intestinal epithelia. Lindmark et al. [9] reported an increased oral absorption after addition of medium-chain fatty acids in the Caco-2 model. Medium-chain fatty acids affect membrane fluidity or interact with tight junction proteins such as occludin and increase in vitro permeability of the hydrophilic marker compound fluorescein-sodium. Sakai et al. [10] supported this theory by means of confocal laser scanning microscopy (CLSM) and by increasing permeability of hydrophilic, passively permeating compounds after coadministration of sodium caprate and sodium deoxycholate. Borchard et al. [11] reported that mucoadhesive polymers, such as chitosan-glutamate and carbomer, widen tight junctions following CLSM studies. However, only coadministration of carbomer together with chitosan-glutamate leads to significant increase in permeability. Ranaldi et al. [12] found that chitosan and other polycationic polymers decrease the transepithelial electrical resistance (TEER) reversibly and thus increase permeability of inulin across Caco-2 monolayers (for a review on that particular topic, see [13]).

On the other hand, several publications are suggesting that commonly used surface active excipients affect cellular efflux systems, namely, P-glycoprotein (P-gp) or other efflux pumps, for example, Refs. [5, 14–20]. Many authors report increased drug fluxes from apical to basolateral and decreased fluxes in the adverse direction in presence of polyethoxylated surface active excipients such as Tween 80, vitamin E TPGS, pluronic block polymers, and Cremophor EL. While the mechanisms of action are still under discussion, there is increasing evidence that the inhibition of apical efflux pumps by this class of excipients is determined by an interaction with the energy-providing ATPase rather than by effects on membrane fluidity or competitive interactions of substrate binding ([21]). The application of these excipients in oral solid dosage forms affects the absorption process from the GI lumen in two ways. First, they can enhance the dissolution rate by decreasing surface tension and improving wetting and hence increase the solubility by means of micellar entrapment. Second, they can increase permeability through intestinal epithelia by inhibiting P-gp-mediated efflux. However, these excipients can also decrease permeability, since micellar entrapped active compound may no longer be thermodynamically as active and lower fluxes may result. However, the findings reported in literature remain contradictory. Although statistically significant results in permeability assays have been found when adding these excipients in solution to the transport media, in vivo relevance remains questionable. Brouwers et al. [22] reported for amprenavir, being marketed as a dosage form (Agenerase®) with the P-gp inferring excipient vitamin E TPGS, a much more complicated behavior than generally anticipated. The authors showed that increasing concentrations of vitamin E TPGS lead to higher dissolution rates and solubility of amprenavir in vivo. The in vitro permeation experiment showed initially increasing and subsequently decreasing apparent permeability (P_{app}) values for increasing vitamin E TPGS concentrations, which can be due to micellar entrapment above the critical micellar concentration (CMC). However, at concentrations of vitamin E TPGS and amprenavir which are relevant in vivo, a P-gp-inhibiting action of vitamin E TPGS might be made irrelevant by the enormous luminal concentration of amprenavir as a result of the solubilizing effect of vitamin E TPGS. Ramsay-Olocco [23] published data on a clinical evaluation of a P-gp substrate formulated in soft capsules along with vitamin E TPGS. Although increase of flux in presence of vitamin E TPGS was observed in the absorptive direction in vitro, no significant difference was detectable in clinical studies, performed in mini pigs and humans. In contrast, Bogman et al. [24] reported for talinolol perfused intraduodenally along with vitamin E TPGS, a statistically increased AUC, compared to talinolol administered alone or with Poloxamer 188, a non-P-gp-interfering surfactant. To conclude, for formulation development, it is crucial to know the actual luminal concentration not only of the API but also of the active excipients. Beside the increase in bioavailability, researchers hope to use these excipients to lower the intersubject variability of bioavailability, normally associated with low-permeability and low-solubility compounds. Although being potent absorption enhancer in vitro, the in vivo relevance of these findings remains unclear. From a clinical point of view, the relative contribution of intestinal P-gp to overall drug absorption has been questioned, unless only a small amount of API is administered or dissolution and permeation rate is rather low [25]. Additionally, it remains unclear, whether cell culture-derived in vitro data can be directly scaled up

to the human situation [25]. Obviously, the in vivo relevance of P-gp is not depending exclusively on the affinity of the API to cellular efflux systems, but also on the actual luminal concentration of the API and excipient.

In this context, a combination of dissolution and permeation assessment may be very valuable, especially when excipients interfere at different stages in a concentration-dependent manner. As shown above, a combined setup yielding physiological relevant concentrations may reveal these phenomena before testing the dosage form in animal and human studies. Moreover, a concept of combined dissolution/permeation might also be imagined to serve as a quality assurance tool for dosage forms containing active excipients.

19.2.1.3. Investigation of Potential Food Effects on Drug Absorption

Effects of concomitant intake of food with drugs on disintegration [26] and dissolution [14, 27–31] of oral solid dosage forms have been extensively described in the literature. For dissolution testing, the development of biorelevant dissolution media by Galia et al. [1], simulating intestinal fluid in fed (FeSSIF) and fasted state (FaSSIF), led to a generally accepted in vitro method to forecast food effects on dissolution. Nevertheless, effects of food components on absorption processes are getting more and more into the focus of research [14, 32]. Wu et al. [33] suspected that concomitant intake of high-fat meals with drugs is inhibiting intestinal influx and efflux drug transporters and thus may lead to decreased bioavailability of BCS class III compounds; however, due to increased solubility in the intestinal lumen after fatty meals, BCS class II compounds may show an increased postprandial bioavailability. Inhibition of intestinal efflux transporters may also be mediated by flavonols in grapefruit and orange juice, as stated in a review by Wagner et al. [14]. Ingels et al. [34] reported that the application of FaSSIF in Caco-2 permeability assessment does not affect the permeability of passively permeating compounds. However, actively secreted compounds show a significant lower permeability in basolateral to apical direction, whereas apical to basolateral transport is not affected and thus polarity in transports diminishes. Ingels et al. suggested that the bile salts present in FaSSIF may inhibit P-gp and other efflux transporters and concluded that the interferences between efflux pumps and food components which have been detected in vitro might be generally overestimated.

Consequently, the interplay between solubility and permeability with too many free variables is hindering the researcher or developer from clear statements. Interactions of food with oral absorption may happen at different stages, which again can be titled as dissolution and permeation, and a combined dissolution and permeation assessment might give a deeper insight into possible interaction and food effects.

To summarize, there are several rationales to justify the approach for permeation and dissolution testing. Nevertheless, it has to be pointed out that for the rather “uncomplicated” BCS class I and some BCS class II compounds, where it can be anticipated that increased luminal concentrations will lead to increased transepithelial fluxes, no significant additional information should be expected to the conventional dissolution testing. However, for “difficult” compounds, mainly belonging to BCS classes III and IV, important information about the drug in the dosage form can be obtained.

19.2.2. Connecting Dissolution and Permeation Measurement in One Instrumented Setup

19.2.2.1. Limitations/Specifications Concerning Dissolution/Permeation Media

The choice of dissolution/permeation media is limited, mostly due to the need to maintain viability and integrity of Caco-2 cell monolayers. Main requirements of the media to be in contact with Caco-2 cells are (i) isotonic conditions (Caco-2 cell monolayers are basolaterally more sensitive to osmotic pressure than apically); (ii) appropriate pH, which may be in a range from 5 to 8 [35], again this should be handled more restrictive basolaterally; (iii) presence of calcium and magnesium ions in order to maintain monolayer integrity by stabilizing adherens junctions; and (iv) physiological ratio between extracellular sodium and potassium, in order to warrant an appropriate potential difference across the epithelia. To circumvent these limitations, rendering dissolution media before getting into contact with Caco-2 cells may be appropriate. However, it has to be kept in mind that the original dissolution concentrations are diluted by doing so, and that the system is getting more and more complicated. Therefore, one has to find some compromise concerning the dissolution/permeation media between simplicity, in vivo relevance, and analytical requirements. For dissolution testing, numerous media as described in current pharmacopoeiae are generally accepted and mimic to some extent the physiological surroundings of disintegration and dissolution processes. For permeation assessment, however, it still remains unclear which transport media generates best results. Permeability assessment through Caco-2 monolayers is routinely carried out using Krebs Ringer buffer (KRB), Krebs bicarbonate Ringer buffer (KBR), or Hank's balanced salt solution (HBSS), though those might pose too restrictive conditions for low-soluble compounds, due to the lack of lipids and surface active ingredients and their excessive amount of counter-ions. A shortcoming for low-solubility compounds can generally be seen in the addition of either Dimethylsulfoxide or other cosolvents (a comprehensive review of applied substance together with concentrations is comprised in [36]). For more comparable in vivo permeation conditions in Caco-2 assays, Ingels et al. [37] recommend to use FaSSIF on the apical side, while basolaterally an analytical-friendly buffer, such as HBSS, may be the best choice. Table 19.1 summarizes the composition of the previously mentioned buffer systems. Differences among KRB, KBR, and HBSS are not that distinct and the most important difference may be seen in the absence of carbonate in KRB. Degassing procedures prior to dissolution testing may affect the carbonate concentration and thus alter the pH. Therefore, KRB appears to be most suitable for combined dissolution/permeation measurement.

Ingels et al. tested FaSSIF and FeSSIF for compatibility with Caco-2 monolayer integrity, a prerequisite for valid permeation experiments [37]. Only FaSSIF turns out to maintain Caco-2 monolayer integrity throughout a 3-h experiment, as indicated by TEER measurements and flux studies using fluorescein-sodium. These data were confirmed by means of a 3-(4,5-Dimethylthiazol-2-yl)-2,5-diphenyl-2H-tetrazoliumbromid (MTT) cytotoxicity assay. FeSSIF is immediately toxic to the cell monolayer; Ingels et al [37] attribute this to the high osmolarity (≈ 600 mOsm), low pH (5.0), and the high content of Na-taurocholate (15 mM). In addition, the lack of glucose, and especially calcium

Table 19.1 Composition of various buffer systems possibly eligible for combined dissolution and permeation testing. Concentrations may vary from reference to reference. Composition of FaSSIF and FeSSIF is shown as reported by Galia et al. [3]; in the meantime, several publications denoted a change from potassium to sodium as the main cation [91] or others changes. Abbreviations are given in the text.

Compound [mM]	HBSS [36]	KRB [56]	KBR [38]	FaSSIF [3]	FeSSIF [3]	FaSSIF modified by [38]	FeSSIF modified by [38]
CaCl ₂	1.26	1.41	1.20	—	—	1.67	1.67
Fumaric acid	—	—	5.40	—	—	—	—
KCl	5.36	3.00	4.69	103.27	203.86	5.37	5.37
MgCl ₂	0.49	2.56	—	—	—	—	—
MgSO ₄	0.41	—	1.20	—	—	0.81	0.81
NaCl	136.89	142.03	108.01	—	—	136.89	136.89
NaHCO ₃	4.26	—	16.0	—	—	0.42	0.42
K ₂ HPO ₄	—	—	0.47	—	—	—	—
KH ₂ PO ₄	0.44	—	—	28.66	—	0.44	0.44
Na ₂ HPO ₄	0.34	0.44	—	—	—	0.34	0.34
NaH ₂ PO ₄	—	—	5.38	—	—	—	—
Na-pyruvate	—	—	4.90	—	—	—	—
D-Glu	25.00	4.00	11.50	—	—	5.55	5.55
L-Glutamine	—	—	5.67	—	—	2.00	2.00
MES/HEPES ^a	10.0/20.0	10.0/20.0	—	—	—	—	—
Acetic acid	—	—	—	—	144.17	—	—
Na-taurocholate	—	—	—	3.00	15.00	3.00	15.00
Lecithin	—	—	—	0.75	3.75	0.75	7.50
NaOH	ad 7.4/6.5	ad 7.4/6.5	ad 7.4	ad 6.5	ad 5.0	ad 6.5	ad 6.0
Osmolarity [mOsm/kg H ₂ O]	~ 300	~ 300	~ 300	~ 300	~ 630	~ 343	~ 336

^a For resulting pH of 6.5: MES; for 7.4: HEPES; HBSS; Hanks balanced salt solution; KRB: Krebs ringer buffer; KBR: Krebs bicarbonate ringer buffer; FaSSIF: Fasted state-simulating intestinal fluid; FeSSIF: Fed state-simulating intestinal fluid.

and magnesium, may increase damage to the monolayers. Recently, Patel et al. [38] modified FaSSIF and FeSSIF in order to obtain Caco-2 compatible *in vivo* relevant transport media. Changes of the composition are outlined in Table 19.1. Briefly, magnesium and calcium salts are added, osmolality of FeSSIF is reduced to 330 mOsmol/kg H₂O, sodium and potassium ions are present in a physiological ratio, lecithin concentration in FeSSIF is doubled, in order to mitigate toxicity of taurocholic acid and buffering phosphate, and carbonate salts are added. Caco-2 monolayers retain their integrity throughout 2 h indicated by mannitol flux and TEER. By means of scanning electron microscopy (SEM), no severe damage to the cells is detectable, except a minor microvilli loss and shortening. Apparent permeability of metoprolol is significantly reduced in the presence of FaSSIF/FeSSIF; the authors attribute that to micellar entrapment into the bile salt lecithin mixed micelles. Nevertheless, the influence of the modification of FaSSIF/FeSSIF on dissolution and solubilization properties of the media is not tested yet.

19.2.2.2. Historical Evolution of Combined Dissolution and Permeation Testing

First attempts to combine both dissolution and permeation in one device have been made in the mid 1970s. Typical devices from that era employed distribution between three phases, each of different polarity, that is, the distribution between the aqueous and lipoid phases and subsequently between the lipoid and the aqueous phases was measured. Both aqueous phases were kept apart by baffles. Some inevitable compromise resulted from the fact that the “membrane” (i.e., the lipoid phase) was much thicker than the *in vivo* membranes, and transport rates found *in vitro* appeared to be too strongly controlled by that. In 1969, Dibbern et al. [39, 40] circumvent this drawback by separating aqueous acceptor and donor phase by lipid-treated polymeric membranes and thus were able to improve prediction of *in vivo* behavior of dosage forms containing passively permeating compounds (the apparatus became commercially available under the name “Resomat” of the company Desaga). However, the validity of the obtained data was limited due to the employment of artificial lipid membranes and thus omitted conclusions concerning actively secreted or absorbed drugs and metabolism. In 1980, Koch et al. [41] reported a simplified experimental tool (“Resotest Apparatus”), again reviving the experimental determination of the partition between organic and aqueous phases. However, the apparatus was reduced to a rotating two-neck pear-shaped flask containing two aqueous phases conjointly covered with a layer of suitable organic solvent. Although being a crude simplification and exhibiting a nonphysiologic lipid membrane, the model made it into the textbooks may be just because it was very easy to handle, due to its simplicity. However, none of these early dissolution-permeation devices were listed in the pharmacopoeiae. As computing power started to increase tremendously from the early 1980s, and computational modeling sciences emerged, those simplified models for dissolving and passively permeating substances became obsolete.

In the meantime, dissolution testing was more and more standardized and gained enormous impact on the fields of quality assurance and drug development in pharmaceutical industry. Several dissolution apparatus made their way into the pharmacopoeiae, such as the rotating paddle, rotating bas-

ket, reciprocation cylinder, and the flow through cell, just to mention the most important ones. For comprehensive discussion on dissolution equipment, the reader is referred to previously published books, a good example being Ref. [42].

At the beginning of the 1990s, the general acceptance of Caco-2 cell monolayers as a model of the small intestinal mucosa caused a significant push toward the field of permeability testing [2, 43]. For detailed information about the Caco-2 cell line, the reader is referred to Chap. 8. As a consequence, the pharmaceutical community became more aware that permeation through intestinal epithelia is oftentimes more sophisticated than mere diffusion through a lipophilic membrane.

In 1995, Amidon et al. [44] initiated the theoretical base for a biopharmaceutical drug classification, which was also addressed in several food and drug administration (FDA) guidelines [45, 46]. The BCS assigns drugs into classes I–IV according to their solubility and permeability properties, thus highlighting the importance of both fundamental parameters—dissolution and permeation. Nowadays, the BCS has gained tremendous impact on drug development process.

19.2.2.3. Published Approaches for Combined Dissolution and Permeation Assessment

Recently, an approach mimicking the GI tract and feasible for pharmaceutical dissolution studies has been published [47]. Coming from the area of nutritional research, this approach reflects some promising aspects, such as relevant luminal pH values, peristalsis, luminal bacterial colonization, and relevant fluid volumes. However, permeation is only reflected by diffusion through hollow fiber membranes and thus is not in the scope of this chapter. Nevertheless, it will be interesting to see whether it will be possible to expand such a perfect in vitro device toward a more realistic intestinal epithelium.

Several approaches combining Caco-2 permeation assessment with dissolution testing have been published in the past. In the following, these systems are described in chronological order of their publication.

Approach of Ginski and Polli [48]: In 1999, Ginski et al. [48] published a continuous dissolution/Caco-2 system. Dissolution takes place in a paddle apparatus (apparatus I, United States Pharmacopoeia, USP) and Caco-2 monolayers are mounted in a side-by side diffusion cell, whereas a peristaltic pump transfers media from the dissolution vessel to the permeation chambers. Dissolution and permeation media is HBSS (pH 6.8). The system (Figure 19.1a) can be seen as a closed model, since no drug was allowed to leave the experimental setup. The study had several objectives. The main objective was to test whether the experimental data fit to the previously described mathematical model determining the dissolution/absorption relationship [48, 49]. Another objective was to detect possible effects of the formulation (disintegrating agent, solubilizers, such as Tween 80 and cyclodextrins) on the dissolution/absorption relationship. Although being a rather simple experimental setup, the results were promising. Ginski et al. [48] were able to confirm the validity of their setup with in vivo data using piroxicam and ranitidine oral solid dosage forms with varying release kinetics. The addition of croscarmellose-Na as an in vitro permeation enhancing agent led to an increased permeated amount across Caco-2 cell monolayers, although in vivo no absorption

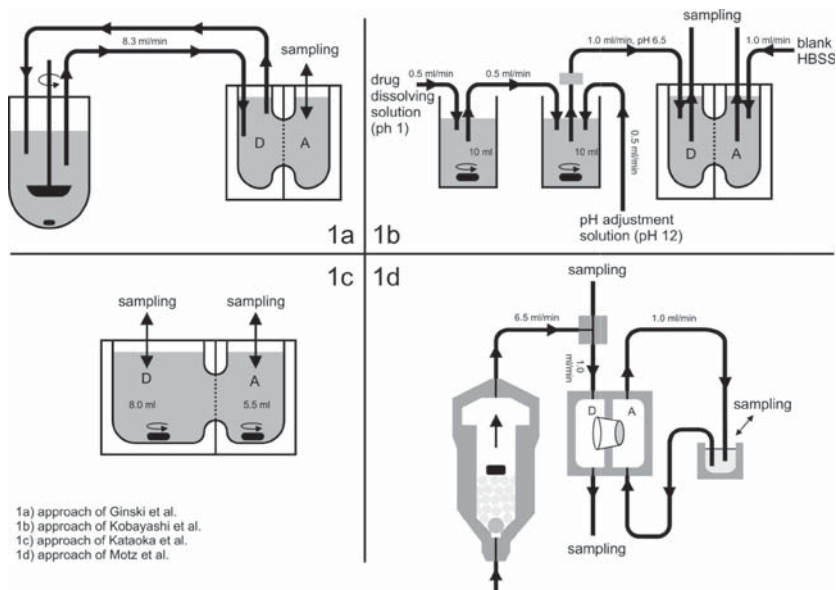


Figure 19.1 Schematic depiction of the published approaches for concomitant assessment of dissolution and permeation. Figure 19.1a adopted from Ref. [48], Figure 19.1b from Ref. [51], and Figure 19.1c from Ref. [54], respectively. Donor compartments are denoted as “D,” acceptor compartments as “A.” Dotted lines between “D” and “A” represent Caco-2 monolayers. Flow rates are given where necessary.

enhancing effect of croscarmellose-Na was detected. This phenomenon was hence attributed to the calcium sequestering properties of croscarmellose-Na and was identified as a false positive in vitro finding, since complete sequestering of all extracellular calcium may not happen in vivo. For the variation of solubilizers the authors prove that only dissolution is altered, not permeation. Finally, the authors concluded that this continuous dissolution/Caco-2 may be a tool to forecasting formulation effects on in vivo dissolution and in vivo permeation.

Approach of Miyazaki et al. [50–53]: Shortly after Ginski et al. [48], Kobayashi and coworkers [50] published an open dissolution/permeation approach in 2001. A stirred glass vessel serves as a flow through dissolution device, from where the eluted solution is pumped into a second glass vessel for pH adjustment to a pH of 6.0. The solution is then transferred into a flow through diffusion chamber with a Caco-2 monolayer between the acceptor and donor compartments. A schematic drawing of the most recently published setup is shown in Figure 19.1b. The authors routinely carry out their experiment with an HBSS-like buffer, which is generated prior to contact of the buffer with the Caco-2 monolayers. The system is able to mimic effects of pH on the drug; however, the device is not capable of changing the pH acting on the drug in one experiment and thus one might argue that in vitro, the undissolved drug appears to stay in the gastric compartment rather than being transferred to the small intestine with its increasing pH values. This issue is almost circumvented in later publications by employing several gastric acid models [52]. Nevertheless, the authors are able to mimic precipitation of weak bases in the “pH adjustment vessel,” such as for albendazol [53]. Furthermore, the

apparatus of Kobayashi et al. [50] and He et al. [51] shows a good linear relationship between the amount cumulatively permeated into the acceptor compartment and the fraction absorbed in humans, although clinical doses of the drugs are disregarded. Interestingly, the authors used this system also for assessing the metabolism of prodrugs to be cleaved in intestinal cells, for instance, ampicillin/pivampicillin. The experiments with either rat intestine or Caco-2 monolayers indicate that pivampicillin is undergoing cleavage during the permeation through the intestinal barriers and again the obtained values correlated well with in vivo data.

In comparison to the approach of Ginski et al. [48], the Miyazaki's method appears to be more elaborate and complex and is thus coming closer to the in vivo situation. The device can simulate various effects of pH on dissolution and is, as an open system, closer to in vivo conditions compared to a closed one. However, it exhibits the drawback of not freely "adjustable" pH values acting on the drug. Low flow rate in the dissolution vessel may limit applications of complete dosage forms and allows predominantly only the use of granules, pellets, or grinded tablets. Furthermore, the application of compendial dissolution devices appears to be a more robust approach.

Approach of Kataoka et al. [54]: In 2003, Kataoka et al. [54] published an in vitro system for simultaneous evaluation of dissolution and permeation of poorly water soluble drugs. In contrast to Ginski et al. [48], this system assesses dissolution and permeation in a downsized dissolution vessel (1% of the volume estimated in vivo, 8 ml) with a Caco-2 monolayer mounted between acceptor (5.5 ml) and donor compartments with 8 ml (Figure 19.1c). When reducing the volumes by a factor of ~ 100 compared to concentration of dissolution testing, the dose of the drug is also to be reduced by the same scale, which may raise some balancing and handling issues when adding 0.1 mg drug or even less to the dissolution compartment. In comparison to previously published papers, the authors highlight the importance of clinical doses of the compounds tested, as compounds are assigned into the four BCS classes according to their solubility of the highest dose in 250 ml [44]. The authors find a good correlation between the amount permeated after 120 min and the fraction absorbed in humans, whereas the 120-min time point was chosen with regard to the mean small intestinal transit time. The setup was also able to assign correctly all compounds into BCS classes I–III; however, the study was lacking any BCS class IV compound. Furthermore, experiments with apically added taurocholate (at 5 mM, thus, between FaSSIF and FeSSIF concentration) in the dissolution compartment showed increased permeated amount for griseofulvin, mainly due to higher dissolution rate and solubility. Moreover, the addition of 4.5% bovine serum albumine (BSA) in the acceptor compartment increased the permeation rate of griseofulvin, which may be attributed to increased sink conditions.

The approach of Kataoka et al. [54] shows some desirable features, such as downsized, in vivo relevant volumes, and low complexity of the device and thus low error proneness. However, the device lacks the possibility to add complete dosage forms and the use of compendial dissolution devices would be a more robust approach.

Approach of Motz et al. [55, 56]: In 2006, Motz and coworkers published a dissolution permeation device combining a compendial flow through dissolution

cell (apparatus 4, USP) with a flow through permeation cell. In order to connect both, a stream splitter providing appropriate low flow rates for the shear stress sensitive Caco-2 monolayer was installed. The dissolution module was designed open, whereas the transmucosal receptor compartment was closed. Nevertheless, sink conditions were given for the published experiments. Several sampling ports were implemented, in order to monitor dissolution and permeation thoroughly: sampling port D (dissolution), shortly after apparatus 4; sampling port A (apical), after the stream splitter and after passage through the flow through permeation cell; and finally sampling port B (basolateral) in the acceptor compartment. As the apparatus is intended to assess permeability across Caco-2 monolayers after drugs being released from solid dosage forms, several propranolol HCl immediate release tablets with increasing dosage strength, and two different propranolol HCl extended release tablets, were manufactured and subsequently tested. Mean time approach for the different sampling ports D, A, and B yielded plausible and conclusive results for this setup. In addition, the stream splitter was found to work reliable. The permeated amount is linearly dependent on the dosage strength, expected for a passively permeating compound. For the extended release tablets, a delay in release of propranolol from the solid dosage form was observed in the permeation profile. Nevertheless, the cumulatively permeated amount was not statistically different for all the differently releasing tablets. Advantage of such a setup can be seen in the hydrodynamically separated modular setup providing the possibility to employ the dissolution module with compendial, sinusoidal flow profile generating pumps. A further advantage may be seen in the possibility to use complete solid dosage forms together with physiological flow rates and volumes in the dissolution module and thus facilitating the application of relevant concentrations. In addition, the three sampling ports allow thorough monitoring of both dissolution and permeation. After this preliminary testing of the apparatus, the time for quantification was found to be suboptimal. Therefore, the system got automated using sequential injection analysis (SIA) [55], the throughput is increased, and comparison of the results obtained with the automated setup reveal results similar to those from the nonautomated version. The automated setup allows online measurement at the three different sampling ports D, A, and B or partially online analysis in combination with high performance liquid chromatography (HPLC). The automation facilitates in the future more and faster experiments, as well as higher reproducibility of the measurement due to the less error sources.

The approach of Motz et al. [55, 56] can be seen as a combination of the approach of Ginski et al. [48] (compendial dissolution equipment) and the approach of Kobayashi et al. [50] (open dissolution module). The most dominant advantage may be seen in the application of complete dosage forms and the application flow rates resulting in physiologically relevant concentrations. Furthermore, the apparatus appears to be robust being equipped with compendial dissolution equipment. However, the apparatus is still lacking a pH simulation unit.

19.2.3. Critical Evaluation of the State of the Art and Further Needs

To connect two *in vitro* assays displaying fundamental processes occurring during oral absorption *in vivo* appears to be a promising approach. Such setups, as

they are already published, allow the researcher intense comprehension of the interplay of dissolution and permeation with surrounding media and excipients. Application of complete dosage forms bears the advantage to detect possible interactions of excipients with intestinal epithelia and might help to better understand and select promising formulation approaches in drug development. However, the mentioned apparatus still need improvements. Simulation of the pH profile in the human intestine has to be improved in order to be able to freely adjust the pH acting on the dosage form. In addition, devices have to be improved and tested, as well as media feasible for detecting possible food–drug interaction. Also, studies focusing on the detection of formulations effects as already started by Ginski et al. [48] have to be continued in order to finally disclose the value of the obtained data. For the future, assessment of permeation of solid oral dosage forms may lead to more realistic and more relevant devices, improving drugability of difficult drugs.

19.3. Permeability Assessment of Pulmonary Aerosol Formulations

The inhalation route is of general interest for the application of drugs, in order to treat systemic and local diseases [57–59]. Recent advances in the development of inhalation devices and particle technology allow to deliver small molecules as well as proteins and peptides with sufficient efficacy to the lung [60]. However, this approach is often limited by missing data regarding safety and efficacy of aerosol formulations. In particular, the lack of safety data is one reason that to date only few drugs and excipients are approved for pulmonary application by the regulatory authorities, and this situation decelerates the development of modern inhalable medicines. Innovative development tools must therefore acknowledge the complexity of the interplay between the lung, the inhalation maneuver [61], and pulmonary deposition, which is difficult to simulate *in vitro*.

Depending on particle characteristics and breathing pattern, aerosols are deposited in various regions of the lung. In the bronchial as well as in the alveolar region, the particles are settling on an epithelium, in both cases the main barrier for pulmonary drug absorption. Already back in the 1980s, attempts have been made to simulate the respiratory epithelia using isolated organs or organ slices [62]. However, these approaches have been limited by functional breakdown of the tissue [63], lacking reproducibility, and high costs involved [64]. Finally, progress in cell culture overcame these issues and led to standardized and validated models of the blood–air barrier. The continuously growing bronchial epithelial cell lines, Calu-3 [65] and 16HBE14o- [66], develop tight and polarized monolayers suitable for transport studies, when grown on filter inserts. For the alveolar region, up to now, no immortalized cell line with sufficient barrier properties is available. However, primary cell cultures isolated from different species [67], including human alveolar epithelial cells (hAEPc), are reported in literature [68–71].

Inspired by the successful implementation of the intestinal cell line, Caco-2, as a model to predict oral drug absorption, pulmonary-based models are used in a similar manner. The use of pulmonary cells which are covered by a comparatively thick fluid layer (liquid-interfaced deposition, LID) is probably

not adequate to model the blood–air barrier [72]. Structure and surface properties of the pulmonary surface liquid are locally different in the human lung. Because of difficulties of its preservation, only few facts are known about composition and especially thickness. The bronchial tree is comprised by a columnar epithelial cell lining. The airway epithelium consists in its majority of ciliated cells and interspaced goblet cells for the production of mucus. Mucus consists primarily of mucin, a highly glycosylated peptide. A bilayer structure with an aqueous sol phase of mucus adjacent to the epithelial cells that includes the beating cilia and an overlying more viscous gel phase of mucus covers all conducting airways. Particle embedding and subsequent particle clearance to the pharynx, wetting of the inhaled air, and temperature control are the three main functions of the bronchial mucus layer (BML). Its thickness has been reported to vary between 20 and 60 μm [73]. This means that particles in a size between 2 and 5 μm could be completely submersed in and would need to travel distances between 4 and 12 times of their diameter before reaching the actual epithelial cell membrane.

The situation is, however, different in the alveolar region of the lung where the respiratory gas exchange takes place. Its thin squamous epithelium is covered by the so-called alveolar surface liquid (ASL). Its outermost surface is covered by a mixture of phospholipids and proteins with a low surface tension, also often referred to as lung surfactant. For this surfactant layer only, Scarpelli et al. [74] reported a thickness between 7 and 70 nm in the human lung. For the thickness of an additional water layer in between the apical surface of alveolar epithelial cells and the surfactant film no conclusive data are available. Hence, the total thickness of the complete ASL layer is actually unknown, but is certainly thinner than 1 μm .

Particles in the typical size range of pharmaceutical aerosols (2–5 μm), when deposited in the bronchial region of the central lung, can be completely submersed in the BML where they either dissolve, are cleared by the mucociliary escalator, or eventually reach the apical membrane of the bronchial epithelial cells. On the other hand, when deposited in the alveolar region of the peripheral lung, particles of the same size will be wetted by the ASL, but the amount of liquid to dissolve them is much smaller than in the bronchial region. If particles deposited in the alveolar region dissolve in this limited volume of the ASL, the concentration gradient driving transepithelial absorption is much steeper than after bronchial deposition. In absence of the mucociliary clearance escalator in the distal region of the lung, nondissolved particles will interact with and perhaps penetrate the alveolar epithelial cells, if they are not rapidly cleared by alveolar macrophages.

Application of a given drug to an *in vitro* model should aim to mimic the physiological situation of drug delivery *in vivo* as closely as possible. Limitations, however, may be imposed either by biological demands of the cell culture systems or by technological challenges to realistically mimic the process of drug administration. This is particularly true in pulmonary drug delivery where the drug is administered as an aerosol and deposition and subsequent absorption occurs across epithelial cells which are covered by an aqueous film of perhaps less than 1 μm and not exceeding 100 μm on their surface. Therefore, it appears logical that an *in vitro* model should represent humid rather than submersed conditions.

19.3.1. Measuring Drug Transport Across Epithelial Barriers in Submersed Conditions: Ussing Chamber and Transwell®-Like Systems

The concept of characterizing epithelial barrier properties and transport processes was originally developed using tissues that are exposed to an aqueous environment at both the apical and the basolateral side. This is the physiologically normal situation for, for example, gall or urine bladder epithelium, intestinal epithelium, and the skin of amphibians. Because these tissues grow as sheets or tubes, it was relatively easy to isolate them from animals and mount such biopsies into appropriate apparatus to perform diffusion experiments. Typically, the epithelium acts as a diffusing barrier, its apical and basolateral side facing different compartments, which can be filled with buffer and will act as donor or receptor, when transport of a solute is measured from one compartment to the other. As reference to the pioneering work of Hans Ussing, who introduced the concept of bioelectrical measurements and transport experiments at epithelial tissues, such setups are often referred to as Ussing chambers, although their design might be quite different to the original [75].

The intention to study transport processes at pulmonary epithelia, however, raised two particular problems: (i) the apical side of these epithelia is typically in contact with air rather than with a liquid and (ii) in order to maximize the surface area, the lungs have a complex treelike structure, ending in millions of tiny alveolar bubbles. The total surface area of the human alveolar epithelium is almost half of that of the intestines (100–120 m²), with its macroscopic appearance resembling a sponge, and it is virtually impossible to use such a tissue for transport experiments in a diffusion-chamber setup.

As a first compromise, scientists started to work with the lungs of amphibians, such as the bull frog, which consist of only one single alveolus that can be isolated and mounted between the compartments of an Ussing chamber. Experiments of that type provided important first information about physiological transport processes at the alveolar epithelium [76] and were also adopted by some pharmaceutical scientists to study pulmonary drug absorption. Yamamoto et al. [92], for example, investigated the permeability of insulin across *Xenopus* pulmonary membrane, using a modified Ussing chamber. Simultaneously, they measured the effects of various absorption enhancers, such as sodium caprate, on the membrane's integrity. While the cumbersome work with amphibian lung tissue was more and more abandoned, once methods became available to grow bronchial or alveolar epithelial cells on permeable filter inserts (such as Corning's Transwell® system or analogues of it), the Ussing chamber technique is still used by quite a few researchers to study drug transport processes at pulmonary epithelial barriers. In the same way as it is established working with Caco-2 cells, it is relatively straightforward to determine P_{app} coefficients of drugs or to evaluate effects of various additives and excipients on permeation processes and tissue integrity using epithelial cells of the lung (see Chaps. 10 and 11). Control of the membrane integrity by TEER measurements during the transport experiments is a clear advantage of the Ussing chamber technique. Nevertheless, the submersion of the epithelial barrier is necessary for doing so. Direct administration of aerosols to the epithelium is thus not possible. Another disadvantage of the system is that in vertical diffusion chambers, which comprise the vast majority of commercially

available systems, particle sedimentation within the transport medium will make it impossible to interpret the data.

19.3.2. Setups Allowing to Measure Drug Transport Across Pulmonary Epithelia Interfacing Air

As addressed earlier, application of drug particles in a physiologically relevant manner can solely be conducted as aerosol deposition on air-interfaced growing cell cultures. Typically used submerged cell culture monolayers are covered with liquid layers of several millimeters. For several respiratory epithelial cell types, such as Calu-3, 16HBE14o-, and hAEPc, the possibility of air-interfaced culture (AIC) was confirmed [77]. Under AIC conditions the cells are cultivated without a fluid-filled apical compartment, and fluid homeostasis across the epithelial barrier is maintained by a complex network of ion, protein, and water movement. The resulting liquid layer is thin enough to enable interaction between cells, particles, and/or gas. Moreover, coculture approaches with endothelial cells [78], dendritic cells [79], or macrophages [80] were conducted, in order to increase the complexity and the explanatory power of these models. In conclusion, suitable cell culture systems representing an air rather than liquid interface of pulmonary epithelia are available [81–83].

When studying deposition and subsequent absorption of aerosolized drugs using pulmonary cell culture models, pharmaceutical scientists may take advantage of the experience gathered in environmental toxicology. However, it must be kept in mind that those studies are typically focused on the exposure of xenobiotics/particles over a prolonged period of time, while the focus of pharmaceutically motivated studies is to evaluate efficacy and safety of medicines, that is, to administer single and relatively high doses of drugs and excipients.

19.3.2.1. Longtime, Low-Dose Deposition in Environmental Toxicology

Cultex system [84]: The recently published aerosol deposition system CULTEX [84] allows continuous exposure of lung cell monolayers to complex atmospheres. The device was developed as a research tool in environmental lung toxicology. CULTEX enables treatment of epithelial cells, cultivated on permeable filter inserts, with aerosols. Subsequent to the impingement, in vitro assays and permeability measurement can be carried out [85]. By controlling pO_2 , pCO_2 , and humidity, cells and lung slices stay viable for at least 48 h. The apparatus setup is shown in Figure 19.2a: pulmonary cell monolayers are placed on membranes inside a deposition chamber. The CULTEX system is entirely made of glass, facilitating the housing of three vessels with cell culture inserts, and the temperature of these vessels is controlled. Nutrient medium is directed to the cell culture insert vessels via a tubing system. The device allows sampling of medium for biological analysis in the course of the experiment, for example, for assessment of transported drug amount. The test aerosol is drawn into the deposition chamber using negative pressure (ΔP). The analysis of several aerosol parameters, including particle concentrations, can be performed online, parallel to the cell exposure.

Aufderheide et al. [84] performed experiments with human lung cells that were directly exposed to diesel exhaust. In contrast to other exposure concepts for complex mixtures, this experimental setup facilitates a direct and reproducible contact between the cell monolayer and the test atmosphere. This could be achieved by following improvements: (i) a strict separation of the medium

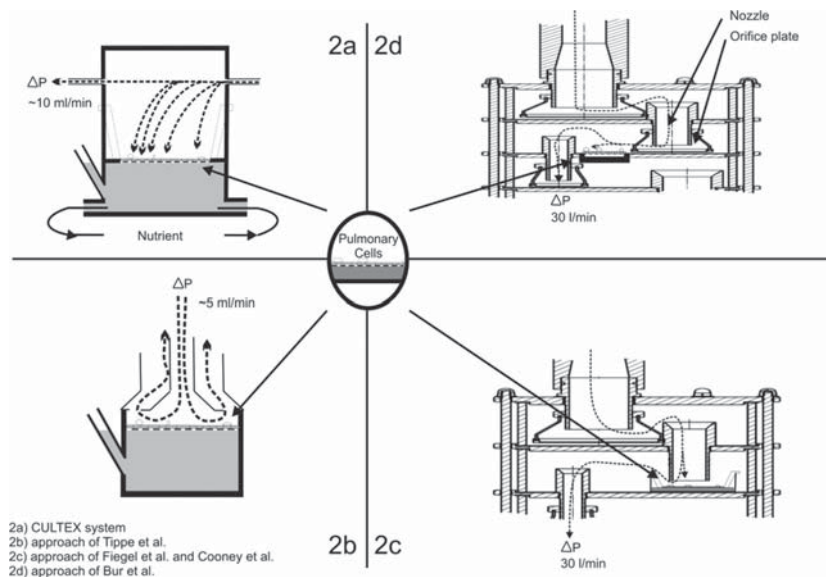


Figure 19.2 Schematic depiction of the described approaches for deposition and subsequent cell–aerosol interaction measurement. Figure 19.2a based on Ref. [84], Figure 19.2b on Ref. [86], and Figure 19.2c on Refs. [54, 89, 90], respectively. Dotted lines represent airflow.

and gas supply; (ii) the application of cell culture membranes with small pore size ($0.4 \mu\text{m}$), thus preventing accidental donor fluid contact with the aerosol during the exposure; and (iii) a transport of the test atmosphere directly to the apical side of the cells.

Results clearly indicated effects of diesel exhausts from different engine operating conditions on the cells already after 1 h of exposure. However, a 1-h continuous exposure to a therapeutic aerosol is probably of limited clinical relevance. To study the effect of drugs administered by typical pharmaceutical single-dose inhalers (MDI, DPI) effective deposition of one “puff” within the time of one breathing maneuver (~ 5 s) is probably more relevant.

Approach of Tippe et al. [86]: Another setup developed for environmental toxicology-related questions was described by Tippe et al. [86]. A commercially available perfusion unit (MINUCCELL, Bad Abbach, Germany) was adapted to study the biological effects of fine and ultrafine particles on cells [87]. The radially symmetric stagnation point flow arrangement deposits particles uniformly and quantifiable onto a cell layer. Because of the low flow velocity over the membrane (~ 5 ml/min), mechanisms of particle deposition are mostly convective transport and diffusion. For cell exposure, Anodisc[®] membranes (Whatman, Maidstone, UK) with 47 mm diameter and a pore size of $0.2 \mu\text{m}$ were used. These membranes remain completely plane after humidification, which is important for homogeneous supply with nutrient medium from the basolateral compartment and for homogeneous particle deposition during exposure. Confluent A549 alveolar epithelial cells were used in the chamber system. Ultrafine carbonaceous model particles with a count median mobility diameter of about 95 ± 5 nm were delivered. After 6 h, 87 ± 23 ng/cm² of particles were deposited homogeneously on the cell surface with

a deposition efficiency of 2%. Compared to pharmaceutical aerosols, where typically doses up to 500 μg are deposited at rates between 10% and 70% within 5 s, this approach is probably of limited value. Nevertheless, after appropriate modifications the aerosol deposition system of Tippe et al. may possibly be adopted to address pharmaceutical questions.

19.3.2.2. High-Dose, Short Time Application of Aerosols on Models of the Blood–Air Barrier

The pharmacopoeiae describe different aerosol classification devices for metered bolus inhalation. Particularly, the multistage liquid impinger (MSLI) shows good correlation to the in vivo deposition and is the most used impingement system in pharmaceutical research. Because of the high air flow rate in the device (30 l/min), only impaction and sedimentation as deposition mechanism are simulated sufficiently; however, diffusion, the major deposition process in the deep lung in vivo, is not reflected correctly. A thin liquid layer on the stages mimics the fluid layer in the lung and avoids rebound of particles after initial impaction. In addition, an Anderson cascade impactor can be used for deposition studies, but the missing water layer can make particle rebound an issue.

Approach of Schreier et al. [88] and Cooney [90]: Schreier et al. [88] used an Anderson cascade impactor to generate a simulation aerosol system for quasi-realistic gene transfection. The system consisted of a PARI nebulizer, a controller for temperature and humidity, and an Andersen cascade impactor, in which the stages were seeded with pulmonary cells (2CFSMEo-). Cell viability retains over 95% subsequent to the deposition experiments. A fluorescent dye was used to visualize aerosol distribution and to monitor cellular uptake. Additionally, the majority of a gene product was delivered to stages 1 through 5, which are corresponding to the in vivo area from the pharynx down to the terminal bronchi. A corresponding, although very low, transfection of cells was found, with the majority of transfected cells on stages 4 and 5. This system was the first example for a modification of an Anderson cascade impactor to facilitate deposition of pharmaceutical aerosols on pulmonary epithelial cell cultures and has inspired further experimental approaches in this direction.

A further “proof of principle” was conducted by Cooney et al. who demonstrated the feasibility of the Andersen cascade impactor as a cell compatible deposition device [90]. Permeability coefficients of fluorescent isothiocyanate-labeled dextrans after impaction as aerosols on Calu-3 cells were calculated. Deposition did not negatively affect the cell monolayer integrity.

Approach of Fiegel et al. [89]: A crucial question for pulmonary drug delivery is the effect of aerosol impaction on cell viability. In contrast with the slow air streams applied in environmental toxicology setups (only a few milliliter per minute), pharmaceutical setups are working with high air velocities between 30 and 60 l/min. At such high air velocities even small particles have high impaction forces and hence might induce cell-damaging effects. In a study from Fiegel et al., the integrity of Calu-3 cell monolayers impinged with polymeric large porous particles was investigated by means of measurement of the TEER and transport of the paracellularly transported marker, fluorescein-sodium. Filter inserts containing cell monolayers were placed directly under the second

stage nozzle of an Astra-type MSLI, as shown in Figure 19.2c. Microparticles were aerosolized onto the monolayers for 30 s at 30 l/min via a Spinhaler device. The filter insert was then returned to a cell culture plate and returned to an incubator. Light microscopy images of the monolayers confirmed that particles were not aggregated when deposited on the monolayers, which showed homogeneously dispersed particles across the entire surface of the monolayer. In addition, SEM images of both AIC and liquid-covered condition (LCC) grown monolayers impinged with microparticles revealed no apparent damage. Although there was no detectable effect on TEER values, monolayers grown under LCC conditions showed an increased flux of fluorescein-sodium, when compared to the AIC monolayers. Mucus staining of the cell monolayers exhibited positive staining only for Calu-3 cells grown under AIC conditions. This adherent mucus gel layer may protect cells against microparticle impingement like a protective coating, thus cushioning the landing of the particles. In contrast, mucus produced by cells grown under LCC conditions easily dissolves into the apical fluid as it is removed by aspiration of the supernatant prior to particle impinging. Therefore, microparticles landing directly on the surface of cells grown under LCC conditions may cause damage to the barrier properties.

In all three described setups, deposition on the inserts was ~50% or less of the amount usually anticipated on an equal sized area without cell culture inserts. This difference may be explained by the changed distance between orifice plate and impaction surface in the cell culture insert. The collection efficacy of an impactor/impinger decreases with an increase in the ratio of the orifice plate to impaction plate distance over jet width. Observations indicate that although the inserts are not at an optimal distance from the orifice plate and are not exactly at the same position compared to the original collection stage, the cell culture inserts do function as an impaction surface for particles in a relevant size range.

Approach of Bur et al.: A serious disadvantage of the previously described approaches may be seen in the changed aerodynamics and deposition patterns of the originally “cell free” impactors/impingers following modifications with cell culture inserts. In order to overcome this issue, the adaptation of an MSLI to fit filter grown epithelial cell monolayers is currently being further improved. It appears pivotal that the cell culture inserts do not disturb the air stream in the stage, and as a consequence deposition efficacy and deposition pattern is not altered compared to a nonmodified MSLI. To achieve this, two holes per stage were drilled into the bottom of the stages 2 and 3, housing the inverted cell culture inserts. Consequently, cultivation of pulmonary cells on the bottom side of a cell culture insert was necessary. In this “upside down” cell culture, no significant differences have been found concerning barrier properties. The inner diameter of the drilled wholes exactly matches the external diameter of commercially available Transwell[®] filter inserts, as can be seen in Figure 19.2d. Since the cell culture insert extends into the lower stage, and thus might affect aerodynamic properties in this particular stage, the filter was encapsulated with stainless steel. The MSLI was operated with a vacuum pump with an air flow rate of 30 or 60 l/min. Time of inhalation was managed by a testing unit for dry powder inhalations allowing adjustment of the duration of inhalation and therefore controlling the cumulative amount of air. First

experiments with the model substance sodium-fluorescein suggest successful deposition of aerosols on cell monolayers.

19.3.3. Critical Evaluation of the State of the Art and Further Needs

In order to characterize pharmaceutical aerosols *in vitro*, particularly with regard to the cellular response on the deposition, various experimental setups are reported in literature. Devices having their roots in environmental toxicology provide promising starting points for further development of *in vitro* devices, which must allow application of single high-dose aerosols. Attempts have been made combining commercial impinger and impactor systems with pulmonary cell culture models. However, the high deposition rate used in these systems can only be achieved by applying high flow rates, hence allowing impaction and sedimentation as impingement mechanism and excluding diffusion. Thus, these devices are mainly suitable for modeling deposition in the upper airways. The currently most effective experimental approach is based upon the principle of the air-liquid exposure technique in the MSLI during deposition.

An ideal *in vitro* model for the characterization of aerosol formulations would incorporate cell types from various regions of the lung (tracheal, bronchial, and alveolar) and would facilitate simulation of deposition mechanisms by impaction, sedimentation, and diffusion of a high-metered single-bolus inhalation. In the future, such systems may reduce the need for animal studies and may offer to correlate in a predictive way the results from such *in vitro* tests to clinical bioavailability data after pulmonary drug delivery *in vivo*.

References

1. Galia E, Nicolaides E, Horter D, Löbenberg R, Reppas C, Dressman JB (1998) Evaluation of various dissolution media for predicting *in vivo* performance of class I and II drugs. *Pharm Res* 15: 698–705
2. Artursson P, Karlsson J (1991) Correlation between oral drug absorption in humans and apparent drug permeability coefficients in human intestinal epithelial (Caco-2) cells. *Biochem Biophys Res Commun* 175: 880–885
3. Nicolaides E, Galia E, Efthymiopoulos C, Dressman JB, Reppas C (1999) Forecasting the *in vivo* performance of four low solubility drugs from their *in vitro* dissolution data. *Pharm Res* 16: 1876–1882
4. Löbenberg R, Krämer J, Shah VP, Amidon GL, Dressman JB (2000) Dissolution testing as a prognostic tool for oral drug absorption: Dissolution behavior of glibenclamide. *Pharm. Res.* 17: 439–444
5. Aungst BJ (2000) Intestinal permeation enhancers. *J Pharm Sci* 89: 429–442
6. Swenson EC, Curatolo WJ (1992) Intestinal permeability enhancement for proteins, peptides and other polar drugs: Mechanisms and potential toxicity. *Advanced Drug Delivery Reviews* 8: 39–92
7. Terao T, Matsuda K, Shouji H (2001) Improvement in site-specific intestinal absorption of furosemide by Eudragit L100–55. *J Pharm Pharmacol* 53: 433–440
8. Nozawa T, Toyobuku H, Kobayashi D, Kuruma K, Tsuji A, Tamai I (2003) Enhanced intestinal Absorption of drugs by activation of peptide transporter PEPT1 using proton releasing polymer. *J Pharm Sci* 92: 2208–2216
9. Lindmark T, Kimura Y, Artursson P (1998) Absorption enhancement through intracellular regulation of tight junction permeability by medium chain fatty acids in Caco-2 cells. *J Pharmacol Exp Ther* 284: 362–369

10. Sakai M, Imai T, Ohtake H, Azuma H, Otagiri M (1997) Effects of absorption enhancers on the transport of model compounds in Caco-2 cell monolayers: Assessment by confocal laser scanning microscopy. *J Pharm Sciences* 86: 779–785
11. Borchard G, Lueßen HL, De Boer AG, Verhoef JC, Lehr C-M, Junginger HE (1996) The potential of mucoadhesive polymers in enhancing intestinal peptide drug absorption. III: Effects of chito and carbomer on epithelial tight junctions in vitro. *J Control Release* 39: 131–138
12. Ranaldi G, Marigliano I, Vespignani I, Perozzi G, Sambuy Y (2002) The effect of chitosan and other polycations on tight junction permeability in the human intestinal Caco-2 cell line. *J Nutr Biochem* 13: 157–167
13. Thanou M, Verhoef JC, Junginger HE (2001) Oral drug absorption enhancement by chitosan and its derivatives. *Adv Drug Del Rev* 52: 117–126
14. Wagner D, Spahn-Langguth H, Hanafy A, Koggel A, Langguth P (2001) Intestinal drug efflux: Formulation and food effects. *Adv Drug Del Rev* 50 (Suppl 1): S13–S31 *Pflügers Archiv European Journal of Physiology*
15. Shen Q, Lin Y, Handa T, Doi M, Sugie M, Wakayama K, Okada N, Fujita T, Yamamoto A (2006) Modulation of intestinal P-glycoprotein function by polyethylene glycols and their derivatives by in vitro transport and in situ absorption studies. *Int J Pharm* 313: 49–56
16. Collnot E-M, Baldes C, Wempe MF, Hyatt J, Navarro L, Edgar KJ, Schaefer UF, Lehr C-M (2006) Influence of vitamin E TPGS poly(ethylene glycol) chain length on apical efflux transporters in Caco-2 cell monolayers. *J Control Release* 111: 35–40
17. Seeballuck F, Ashford MB, O’Driscoll CM (2003) The effects of Pluronic® block copolymers and Cremophor® EL on intestinal lipoprotein processing and the potential link with P-glycoprotein in Caco-2 cells. *Pharm Res* 20: 1085–1092
18. Lo Y-L (2003) Relationships between the hydrophilic-lipophilic balance values of pharmaceutical excipients and their multidrug resistance modulating effect in Caco-2 cells and rat intestines. *J Control Release* 90: 37–48
19. Shah P, Jogani V, Bagchi T, Misra A (2006) Role of Caco-2 cell monolayers in prediction of intestinal drug absorption. *Biotechnol Prog* 22: 186–198
20. Nerurkar MM, Burton PS, Borchardt RT (1996) The use of surfactants to enhance the permeability of peptides through caco-2 cells by inhibition of an apically polarized efflux system. *Pharm Res* 13: 528–534
21. Collnot EM, Wempe C, Kappl M, Huettermann R, Hyatt J, Edgar KJ, Schaefer UF, Lehr CM (2007) Mechanism of inhibition of P-glycoprotein mediated efflux by Vitamin E TPGS: Influence on ATPase activity and membrane fluidity. *Mol Pharm* 4 (3) 465–474
22. Brouwers J, Tack J, Lammert F, Augustijns P (2006) Intraluminal drug and formulation behavior and integration in vitro permeability estimation: A case study with amprenavir. *J Pharm Sci* 95: 372–383
23. Ramsay-Olococo K, Alexandrova L, Nellore R, Killion R, Li L, Coen P, Ho Q, Jung D, Rocha C (2004) Pre-clinical and clinical evaluation of solution and soft gelatin capsule formulations for a BCS class 3 compound with atypical physicochemical properties. *J Pharm Sci* 93: 2214–2221
24. Bogman K, Zysset Y, Degen L, Hopfgartner G, Gutmann H, Alsenz J, Drewe J (2005) P-glycoprotein and surfactants: Effect on intestinal talinolol absorption. *Clin Pharmacol Ther* 77: 24–32
25. Lin JH, Yamazaki M (2003) Role of P-glycoprotein in pharmacokinetics: Clinical Implications. *Clin Pharmacokinet* 42: 59–98
26. Abrahamsson B, Albery T, Eriksson A, Gustafsson I, Sjöberg M (2004) Food effects on tablet disintegration. *Eur J Pharm Sci* 22: 165–172
27. Wonnemann M, Schug B, Schmücker K, Brendel E, van Zwieten PA, Blume H (2006) Significant food interactions observed with a nifedipine modified-release

- formulation marketed in the European Union. *Int J Clin Pharmacol Ther* 44: 38–48
28. Welling PG (1996) Effects of food on drug absorption. *Annu Rev Nutr* 16: 383–415
 29. Singh BN, Malhotra BK (2004) Effects of food on the clinical pharmacokinetics of anticancer agents: Underlying mechanisms and implications for oral chemotherapy. *Clin Pharmacokinet* 43: 1127–1156
 30. Persson EM, Gustafsson A-S, Carlsson AS, Nilsson RG, Knutson L, Forsell P, Hanisch G, Lennernäs H, Abrahamsson B (2005) The effects of food on the dissolution of poorly soluble drugs in human and in model small intestinal fluids. *Pharmaceut Res* 22: 2141–2151
 31. Charman WN, Porter CJ, Mithani S, Dressman JB (1997) Physicochemical and physiological mechanisms for the effects of food on drug absorption: The role of lipids and pH. *J Pharm Sci* 86: 269–282
 32. Fleisher D, Li C, Zhou Y, Pao LH, Karim A (1999) Drug, meal and formulation interactions influencing drug absorption after oral administration. Clinical implications. *Clin Pharmacokinet* 36: 233–254
 33. Wu C-Y, Benet LZ (2005) Predicting Drug Disposition via Application of BCS: Transport/Absorption/Elimination Interplay and Development of a Biopharmaceutics Drug Disposition Classification System. *Pharm. Res.* 22: 11–23
 34. Ingels F, Oth M, Beck B, Augustijns P (2004) Effect of simulated intestinal fluid on drug permeability estimation across Caco-2 monolayers. *Int J Pharm* 274: 221–232
 35. Neuhoff S, Ungell AL, Zamora I, Artursson P (2003) pH-dependent bidirectional transport of weakly basic drugs across Caco-2 monolayers: Implications for drug-drug interactions. *Pharm Res* 20: 1141–1148
 36. Ingels FM, Augustijns PF (2003) Biological, pharmaceutical, and analytical considerations with respect to the transport media used in the absorption screening system, Caco-2. *J Pharm Sci* 92: 1545–1558
 37. Ingels F, Deferme S, Destexhe E, Oth M, Van den Mooter G, Augustijns P (2002) Simulated intestinal fluid as transport medium in the Caco-2 cell culture model. *Int J Pharm* 232: 183–192
 38. Patel N, Forbes B, Eskola S, Murray J (2006) Use of simulated intestinal fluids with Caco-2 cells and rat ileum. *Drug Dev Ind Pharm* 32: 151–161
 39. Dibbern HW (1966) On the resorption profile of drugs. 2. On studies with the resorption model. *Arzneimittelforschung* 16: 1304–1306
 40. Dibbern HW, Scholz GH (1969) Resorption model experiments with artificial lipid membranes. 3. Model experiments for gastrointestinal resorption. *Arzneimittelforschung* 19: 1140–1145
 41. Koch HP (1980) The Resotest Apparatus. A universally applicable biopharmaceutical experimental tool. *Methods Find Exp Clin Pharmacol* 2: 97–102
 42. Dressman J, Krämer J (2005) *Pharmaceutical Dissolution Testing*. Taylor & Francis Group
 43. Artursson P, Palm K, Luthman K (1996) Caco-2 monolayers in experimental and theoretical predictions of drug transport. *Adv Drug Del Rev* 22: 67–84
 44. Amidon GL, Lennernas H, Shah VP, Crison JR (1995) A theoretical basis for a biopharmaceutic drug classification: The correlation of in vitro drug product dissolution and in vivo bioavailability. *Pharm Res* 12: 413–420
 45. FDA (August 2000) Guidance for industry: Waiver of In Vivo Bioavailability and Bioequivalence Studies for Immediate-Release Solid Oral Dosage Forms Based on a Biopharmaceutics Classification System. <http://www.fda.gov/cder/guidance/index.htm#Biopharmaceutics>
 46. FDA (August 1997) Guidance for industry: Dissolution Testing of Immediate Release Solid Oral Dosage Forms. <http://www.fda.gov/cder/guidance/index.htm#Biopharmaceutics>

47. Souliman S, Blanquet S, Beyssac E, Cardot J-M (2006) A level a in vitro/in vivo correlation in fasted and fed states using different methods: Applied to solid immediate release oral dosage form. *Eur J Pharm Sci* 27: 72–79
48. Ginski MJ, Taneja R, Polli JE (1999) Prediction of dissolution-absorption relationships from a continuous dissolution/Caco-2 system. *AAPS PharmSci* 1: E3
49. Polli JE, Crison JR, Amidon GL (1996) Novel approach to the analysis of in vitro-in vivo relationships. *J Pharm Sci* 85: 753–760
50. Kobayashi M, Sada N, Sugawara M, Iseki K, Miyazaki K (2001) Development of a new system for prediction of drug absorption that takes into account drug dissolution and pH change in the gastro-intestinal tract. *Int J Pharm* 221: 87–94
51. He X, Sugawara M, Kobayashi M, Takekuma Y, Miyazaki K (2003) An in vitro system for prediction of oral absorption of relatively water-soluble drugs and ester prodrugs. *Int J Pharm* 263: 35–44
52. He X, Kadomura S, Takekuma Y, Sugawara M, Miyazaki K (2004) A new system for the prediction of drug absorption using a pH-controlled Caco-2 model: Evaluation of pH-dependent soluble drug absorption and pH-related changes in absorption. *J Pharm Sci* 93: 71–77
53. Sugawara M, Takekuma Y, Miyazaki K, Kadomura S, He X, Kohri N (2005) The use of an in vitro dissolution and absorption system to evaluate oral absorption of two weak bases in pH-independent controlled-release formulations. *Eur J Pharm Sci* 26: 1–8
54. Kataoka M, Masaoka Y, Yamazaki Y, Sakane T, Sezaki H, Yamashita S (2003) In vitro system to evaluate oral absorption of poorly water-soluble drugs: Simultaneous analysis on dissolution and permeation of drugs. *Pharm Res* 20: 1674–1680
55. Motz SA, Klimundová J, Schaefer UF, Balbach S, Eichinger T, Solich P, Lehr C-M (2007) Automated measurement of permeation and dissolution of propranolol HCl tablets using sequential injection analysis. *Anal Chim Acta* 581: 174–180
56. Motz SA, Schaefer UF, Balbach S, Eichinger T, Lehr CM (2006) Permeability assessment for solid oral drug formulations based on Caco-2 monolayer in combination with a flow through dissolution cell. *Eur J Pharm Biopharm* 66 (2) 286–295
57. Patton JS, Fishburn CS, Weers JG (2004) The lungs as a portal of entry for systemic drug delivery. *Proc Am Thorac Soc* 1: 338–344
58. Laube BL (2005) The expanding role of aerosols in systemic drug delivery, gene therapy, and vaccination. *Respir Care* 50: 1161–1176
59. Gonda I (2006) Systemic delivery of drugs to humans via inhalation. *J Aerosol Med* 19: 47–53
60. Patton JS, Bukar J, Nagarajan S (1999) Inhaled insulin. *Adv Drug Deliv Rev* 35: 235–247
61. Luo XY, Hinton JS, Liew TT, Tan KK (2004) LES modelling of flow in a simple airway model. *Med Eng Phys* 26: 403–413
62. Niemeier RW (1984) The isolated perfused lung. *Environ Health Perspect* 56: 35–41
63. Saldias FJ, Comellas A, Guerrero C, Ridge KM, Rutschman DH, Sznajder JI (1998) Time course of active and passive liquid and solute movement in the isolated perfused rat lung model. *J Appl Physiol* 85: 1572–1577
64. Tronde A, Norden B, Jeppsson AB, Brunmark P, Nilsson E, Lennernas H, Bengtsson UH (2003) Drug absorption from the isolated perfused rat lung—correlations with drug physicochemical properties and epithelial permeability. *J Drug Target* 11: 61–74
65. Mathias NR, Timoszyk J, Stetsko PI, Megill JR, Smith RL, Wall DA (2002) Permeability characteristics of calu-3 human bronchial epithelial cells: In vitro–in vivo correlation to predict lung absorption in rats. *J Drug Target* 10: 31–40

66. Manford F, Tronde A, Jeppsson AB, Patel N, Johansson F, Forbes B (2005) Drug permeability in 16HBE14o- airway cell layers correlates with absorption from the isolated perfused rat lung. *Eur J Pharm Sci* 26: 414–420
67. Kim KJ, Malik AB (2003) Protein transport across the lung epithelial barrier. *Am J Physiol Lung Cell Mol Physiol* 284: L247–L259
68. Lehr CM (2001) In vitro models of intestinal and alveolar epithelium cultures in pharmaceutical research. *Altex* 18: 59–63
69. Elbert KJ, Schafer UF, Schafers HJ, Kim KJ, Lee VH, Lehr CM (1999) Monolayers of human alveolar epithelial cells in primary culture for pulmonary absorption and transport studies. *Pharm Res* 16: 601–608
70. Ehrhardt C, Kim KJ, Lehr CM (2005) Isolation and culture of human alveolar epithelial cells. *Methods Mol Med* 107: 207–216
71. Fuchs S, Hollins AJ, Laue M, Schaefer UF, Roemer K, Gumbleton M, Lehr CM (2003) Differentiation of human alveolar epithelial cells in primary culture: Morphological characterization and synthesis of caveolin-1 and surfactant protein-C. *Cell Tissue Res* 311: 31–45
72. Steimer A, Haltner E, Lehr CM (2005) Cell culture models of the respiratory tract relevant to pulmonary drug delivery. *J Aerosol Med* 18: 137–182
73. Widdicombe J (1997) Airway and alveolar permeability and surface liquid thickness: Theory. *J Appl Physiol* 82: 3–12
74. Scarpelli EM (2003) Physiology of the alveolar surface network. *Comp Biochem Physiol A Mol Integr Physiol* 135: 39–104
75. Ussing HH (1965) Transport of electrolytes and water across epithelia. *Harvey Lect* 59: 1–30
76. Kim KJ, Crandall ED (1983) Heteropore populations of bullfrog alveolar epithelium. *J Appl Physiol* 54: 140–146
77. Ehrhardt C, Kneuer C, Fiegel J, Hanes J, Schaefer UF, Kim KJ, Lehr CM (2002) Influence of apical fluid volume on the development of functional intercellular junctions in the human epithelial cell line 16HBE14o-: Implications for the use of this cell line as an in vitro model for bronchial drug absorption studies. *Cell Tissue Res* 308: 391–400
78. Gueven N, Glatthaar B, Manke HG, Haemmerle H (1996) Co-cultivation of rat pneumocytes and bovine endothelial cells on a liquid-air interface. *Eur Respir J* 9: 968–975
79. Rothen-Rutishauser BM, Kiama SG, Gehr P (2005) A three-dimensional cellular model of the human respiratory tract to study the interaction with particles. *Am J Respir Cell Mol Biol* 32: 281–289
80. Wottrich R, Diabate S, Krug HF (2004) Biological effects of ultrafine model particles in human macrophages and epithelial cells in mono- and co-culture. *Int J Hyg Environ Health* 207: 353–361
81. Ehrhardt C, Fiegel J, Fuchs S, Abu-Dahab R, Schaefer UF, Hanes J, Lehr CM (2002) Drug absorption by the respiratory mucosa: Cell culture models and particulate drug carriers. *J Aerosol Med* 15: 131–139
82. Florea BI, Cassara ML, Junginger HE, Borchard G (2003) Drug transport and metabolism characteristics of the human airway epithelial cell line Calu-3. *J Control Release* 87: 131–138
83. Forbes B, Ehrhardt C (2005) Human respiratory epithelial cell culture for drug delivery applications. *Eur J Pharm Biopharm* 60: 193–205
84. Aufderheide M, Mohr U (1999) CULTEX—a new system and technique for the cultivation and exposure of cells at the air/liquid interface. *Exp Toxicol Pathol* 51: 489–490
85. Aufderheide M, Mohr U (2000) CULTEX—an alternative technique for cultivation and exposure of cells of the respiratory tract to airborne pollutants at the air/liquid interface. *Exp Toxicol Pathol* 52: 265–270

86. Tippe AH, U. Roth, C. (2002) Deposition of fine and ultrafine aerosol particles during exposure at the air/cell interface. *J Aerosol Sci* 207–218
87. Bitterle E, Karg E, Schroepfel A, Kreyling WG, Tippe A, Ferron GA, Schmid O, Heyder J, Maier KL, Hofer T (2006) Dose-controlled exposure of A549 epithelial cells at the air-liquid interface to airborne ultrafine carbonaceous particles. *Chemosphere* 65: 1784–1790
88. Schreier H, Gagne L, Conary JT, Laurian G (1998) Simulated lung transfection by nebulization of liposome cDNA complexes using a cascade impactor seeded with 2-CFSME0-cells. *J Aerosol Med* 11: 1–13
89. Fiegel J, Ehrhardt C, Schaefer UF, Lehr CM, Hanes J (2003) Large porous particle impingement on lung epithelial cell monolayers—toward improved particle characterization in the lung. *Pharm Res* 20: 788–796
90. Cooney D, Kazantseva M, Hickey AJ (2004) Development of a size-dependent aerosol deposition model utilising human airway epithelial cells for evaluating aerosol drug delivery. *Altern Lab Anim* 32: 581–590
91. Vertzoni M, Fotaki N, Kostewicz E, Stippler E, Leuner C, Nicolaidis E, Dressman J, Reppas C (2004) Dissolution media simulating the intraluminal composition of the small intestine: Physiological issues and practical aspects. *J Pharm Pharmacol* 56: 453–462
92. Yamamoto A, Tanaka H, Okumura S, Shinsako K, Ito M, Yamashita M, Okada N, Fujita T, Muranishi S (2001) Evaluation of insulin permeability and effects of absorption enhancers on its permeability by an in vivo epithelial system using *Xenopus* pulmonary membrane. *Biol Pharm Bull*: 385–389

Modeling Transdermal Absorption

Dirk Neumann

Abstract The human skin has long since been realized as a possible pathway for drug molecules to enter the human body. The skin, however, impedes drug absorption quite effectively, since one of its main purposes, like in all epithelial tissues, is the protection of the organism by sealing off the body from the environment. While several laboratory techniques exist to assess the migration of drug molecules into and through the skin, computational models able to predict such experimental results in a reliable manner hold obvious advantages. The interest in such models has given rise to numerous and quite different approaches, which makes it virtually impossible to list all of them. Here, a selection of computational models—divided into different classes according to their underlying concept—is presented. The chapter starts with the fundamentals outlining the properties of the skin barrier and the experimental assessment of permeability. In the next sections, the theoretical framework for each class is presented followed by a description of representative models. The chapter concludes with an outlook illustrating current and possible future trends.

Keywords: Skin permeability; Percutaneous absorption; Skin penetration; Mathematical model; Quantitative structure-activity relationships; Permeability coefficient; Human skin

Abbreviations

AIC	Akaike information criterion
ANN	Artificial neural network
COSMO	Conductor-like screening model
<i>k</i> NN	<i>k</i> -nearest-neighbor
LSE	Linear solvation energy relationship
PCA	Principal component analysis
QSPR	Quantitative structure permeability relationship
RC	Retardation coefficient
RMS	Root-mean-square

20.1. Introduction

Despite its physical properties like softness and thinness, the skin forms a formidable and surprisingly effective barrier keeping harmful substances from entering the body while at the same time reducing water loss from the inside. For systemic administration of drugs, however, pharmaceutical companies strive to find means for overcoming this barrier in a predictive manner. Here, computational models for estimating the rate and extent of drug permeation into the human body allow for increased productivity. On the other hand, prediction of transdermal drug absorption may help in risk assessment in cosmetic and agrochemical fields. Consequently, many different predictive models have been developed—which might lead to the premature presumption that the problem of predicting transdermal permeation has been fully solved. When it comes to skin diseases the skin is also a site of topical administration. Strangely enough, the number of models for predicting time-dependent concentration changes within skin layers (skin penetration) is quite small.

This chapter starts with a short introduction on the skin barrier's properties and the methods employed for analyzing experimental data. This is followed by an overview of several selected approaches to predict steady-state diffusion through the skin. Then a few approaches that approximate the structural complexity of the skin by predicting drug diffusion in biphasic or even multiphasic two-dimensional models will be presented. Finally, the chapter concludes with a short summary of the many variables possibly influencing drug permeation and penetration.

20.2. The Skin Barrier

It is beyond the scope of this chapter to point out all the different aspects of the skin structure as only a few of these features are actually taken into account in predictive models. For a more in-depth description of the skin structure, see Chap. 1 or [1]. The mammalian skin is made up of two distinct layers, the dermis and the epidermis. The dermis which forms the bulk of the skin is highly vascular and contains—among others—pilosebaceous units and sweat glands. The epidermis features a thickness of 100–150 μm and may be subdivided into two different layers: the viable epidermis (stratum basale, stratum spinosum, and stratum granulosum) and the stratum corneum. Although the outermost layer, the stratum corneum, is only $\sim 15 \mu\text{m}$ thick, it has long been identified as the primary resistance for many molecules trying to overcome the skin barrier. It is a composite of several layers of corneocytes embedded in a lipid rich phase which gives it a brick-and-mortar organization. Molecules may cover the stratum corneum by either staying within the lipid phase or by repeatedly partitioning between the protein-enriched corneocytes and the lipids. The first transport mechanism leads to a longer path length due to the tortuosity of this route. The second pathway appears shorter and equal to the thickness of the stratum corneum at first glance. Having reached the bottom of the stratum corneum, the permeant has now to cover the viable epidermis from where it is taken up in the bloodstream. The influence of the viable epidermis on transdermal drug absorption is usually negligible in comparison to that of the stratum corneum, so many experimental and theoretical studies focused on

the transport through the outermost layer. In some cases, however, the viable epidermis was shown to be the decisive resistance to the drug transport [2]. In addition to these two afore-mentioned pathways through the stratum corneum, a permeant may also bypass this layer entirely by following a shunt pathway, for example, the follicular route. Again, these shunt pathways are often ignored because the orifices of shunts occupy only 0.1% of the surface area [3].

20.3. The Diffusion Equation

The transport of single molecules through the skin barrier is usually assumed to occur by diffusion alone until the permeant reaches the bloodstream, that is, there are no active transport processes involved like in other barriers, for example, P-glycoprotein in the blood–brain barrier. The process of diffusion itself can be explained from a macroscopic or a microscopic point of view. In the first case, the driving force is the concentration gradient, while in the second case the driving force is the thermal heat—which for solutes larger than the solvent molecules results in the so-called Brownian motion. The macroscopic description for mass transfer in one dimension due to differences in concentration is given by Fick’s second law of diffusion (Eq. 1):

$$\frac{\partial c}{\partial t} = \frac{\partial}{\partial x} \left(D \frac{\partial c}{\partial x} \right) \quad (1)$$

which simplifies to Eq. 2 if the diffusion coefficient D is constant:

$$\frac{\partial c}{\partial t} = D \frac{\partial^2 c}{\partial x^2} \quad (2)$$

Analytical solutions for these partial differential equations are found by assuming certain initial conditions (e.g., starting concentrations in the different compartments) and boundary conditions (e.g., finite or infinite media). These initial and boundary conditions are often simplifications and therefore apply only for certain experimental settings. For example, a diffusant permeating from a donor compartment through a biological barrier into an acceptor compartment has to overcome a series of diffusion barriers like the unstirred solvent layers at the liquid–membrane interface in the case of liquid donor and acceptor and the interfacial resistances between solvent and membrane [4]. If the major contribution to the overall resistance is attributed to the membrane itself like in the case of human skin, such additional barriers may be neglected and the resulting solutions for Eq. 1 or Eq. 2 allow for estimating values for the diffusion coefficient and hence for interpreting the experimental results. Numerous analytical solutions for the diffusion equations have been compiled by Crank in [5].

20.4. Data Analysis

In many cases, transdermal drug absorption is investigated using a Franz-diffusion cell. The concentrations both in the membrane and the acceptor compartment are assumed to be zero at the start of the experiment. At different time points, the cumulative drug amount per unit area in the receptor $q(t)$ is determined and plotted versus time t (Figure 20.1). After some time, the flux

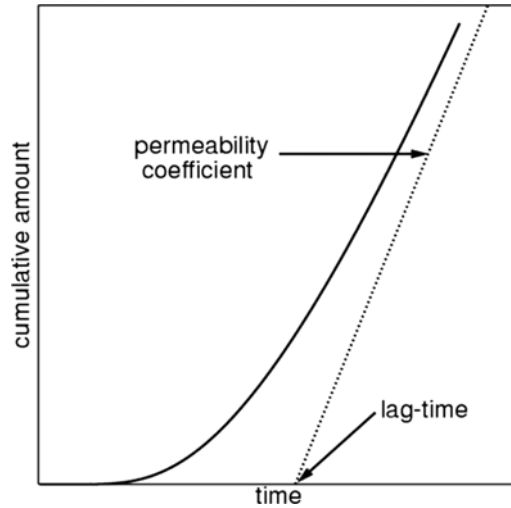


Figure 20.1 Plotting cumulative amount *versus* time in a Franz-diffusion cell experiment results in a curve approaching a straight line.

through the barrier is nearly constant: the system has reached a quasi-steady state which is sustained until a considerable amount of drug has permeated through the barrier.

With $t \rightarrow \infty$, the linear part of the curve approaches the straight line

$$q(t) = \frac{DK}{l} c_D \left(t - \frac{l^2}{6D} \right) \quad (3)$$

Dividing the slope by the drug concentration in the donor compartment c_D allows for determining the permeability coefficient

$$k_p = \frac{DK}{l} \quad (4)$$

which depends only on the effective diffusion coefficient of the permeant in the barrier D and the concentration gradient in the membrane, which, in turn, is given by the ratio of the partition coefficient K between the membrane and the donor compartment and the membrane thickness l . The intersection of the straight line with the time-axis, the so-called lag time, is given by

$$t_{\text{lag}} = \frac{l^2}{6D} \quad (5)$$

and may be used to estimate the effective diffusion coefficient through the barrier. However, under certain experimental conditions, for example, when using full-thickness skin or slowly diffusing substances, the experiment may be stopped well before the steady state has been reached resulting in erroneous data for the permeability coefficient and the lag time. A way to circumvent this problem and to determine the permeability coefficient more precisely is to fit all available data points to an appropriate solution of the diffusion equation:

$$q(t) = P_1 c_D \left[P_2 t - \frac{1}{6} - \frac{2}{\pi^2} \sum_{n=1}^{\infty} \frac{(-1)^n}{n^2} \exp(-P_2 n^2 \pi^2 t) \right] \quad (6)$$

where $P_1 = K \cdot l$ and $P_2 = D/l^2$. When evaluating the experimental data, it should be kept in mind that both Eq. 3 and Eq. 6 are valid solutions to Eq. 1 under certain conditions only. For example, they neglect drug accumulation in the membrane itself. A possible swelling of the biological membrane during the experiment—as observed for, for example, full-thickness skin—is not taken into account, too. Often, the path length of diffusion is assumed to be equal to the thickness of the membrane, which is only true for homogeneous membranes.

Despite these simplifications, data analysis using Eq. 3¹ and Eq. 6 allows to compare results for different substances with reasonable accuracy and to obtain reliable values for the permeability coefficient k_p .

20.4.1. QSPR Models

20.4.1.1. Developing QSPR Models

Quantitative structure permeability relationship (QSPR) models try to find a relationship between the logarithm of the permeability coefficient k_p and molecular features (descriptors). The general approach for developing a QSPR model—irrespective of the barrier for which permeability is to be predicted—can be described as follows: (a) generate a data set, (b) calculate possible descriptors, (c) reduce the number of descriptors, (d) train your model using a training set, and (e) predict permeabilities for a validation set to verify the model. Many data sets for skin permeability models employ the collection of the logarithms of permeability coefficients by Flynn [6] or subsets thereof. The reliability of some data of the Flynn data set has repeatedly been questioned: Some $\log k_p$ values in the Flynn data set show large variations, possibly due to the experimental conditions, while some simply are not permeability coefficients at all, but rather describe the disappearance of the drug molecule from a solution [7]. Still, the Flynn data set has been one of the most important resources for developing QSPR models. Another, partially overlapping compilation of 123 measured permeation coefficients for 99 different chemicals was published by Wilschut et al. in 1995 [8]. Data were included only if the studies met five criteria defined by the authors. Using this procedure, Wilschut et al. aimed at setting up a reliable database for comparing QSPR models. In some cases [9, 10], the $\log k_p$ values are probably not experimentally determined but artificial data generated employing a previously established QSPR model [11, 12].

For some compounds in the Wilschut database more than one permeability coefficient was gathered from literature. In some cases, the differences in k_p were greater than one log unit underlining the interlaboratory variations of such measurements. For the development of a new QSPR model one may now either choose one representative data point for each molecule or combine the multiple data points in a reasonable way. In some cases authors even employed all the available data for a single compound. Apart from the permeability data, the data on the partition coefficient and even on the molecular weight may vary from one report to another. Differences in the partition coefficient are easily explained: Some collections list experimentally determined values which depend on the experimental procedure employed

¹ Eq. 3 is a good approximation of Eq. 6 when $t > 2.4 t_{\text{lag}}$.

and *per se* show some variation. In some cases, both calculated and experimental data were mixed. And of course even calculated data may differ because they depend on the computational method employed (e.g., AlogP, ClogP [13]), too. Differences in molecular weight are most probably based on employing the weight of the corresponding sodium salt instead of the free acid (see diclofenac in [14]) or additional crystal water instead of the drug molecule alone. Finally, a problem common for all values are transcription errors from one publication to another. Although numerous experimental investigations were performed since the publication of the Flynn data set, similar and especially well-documented collections of $\log k_p$ values are hard to find.

While at first only a few descriptors were employed in QSPR models, today programs used to calculate molecular features allow for computing a vast number of descriptors. Despite the large number of readily available descriptors, new descriptors are still emerging. Intriguingly, the number of different descriptors in the various successful skin QSPR models is quite small when compared to models for other barriers (e.g., blood–brain barrier). Reduction of the number of descriptors during the development of the QSPR model is certainly one of the main reasons for this seemingly strange phenomenon. The rationale for reducing the number of descriptors is to find a subset of possibly orthogonal descriptors, that is, from two (or more) highly correlated descriptors such as molecular weight and surface area only one descriptor should be employed in developing the QSPR model. Of two such descriptors many investigators select the one which has either been established before or whose importance can be explained from a mechanistically point of view. However, seemingly linear relationships between descriptors may be the result of the data set under investigation: data sets cover by nature only a small fraction of chemical space. Substances that are investigated have somehow attracted the interest of researchers and are usually not being tested to enlarge the chemical space of the data set.

The first QSPR models for skin tried to establish linear relationships between the descriptors and the permeability coefficient. In many cases validation of these models using, for example, external data sets was not performed. Authors of more recent models took advantage of the progress in statistical methods and used nonlinear relationships between descriptors and predicted permeability and often tried to assess their predictive quality using some validation method.

20.4.1.2. Early QSPR Models

Although Eq. 4 allows for describing diffusion in homogeneous membranes only and therefore seems unsuited for modeling passive transport processes in biological membranes, Eq. 4 was successfully employed to describe diffusion across synthetic membranes first. Assuming a similarity between such well-characterized synthetic polymers and biological membranes Lieb and Stein demonstrated the usefulness of Eq. 4 for describing diffusion of nonelectrolytes across biological membranes [15]. While the thickness l of a given membrane may be easily measured, the values of the two unknown variables D and K have to be determined somehow. When a sphere of radius r diffuses in a continuous fluid, the diffusion coefficient D is given by the well-known

Stokes-Einstein equation:

$$D = \frac{k_B T}{(6\pi\eta r)} \quad (7)$$

where k_B is the Boltzmann constant, T the absolute temperature, and η the viscosity of the solvent. When diffusion occurs in polymers, however, it was found empirically that instead by Eq. 7 the diffusion coefficient for a small molecule is better approximated by

$$D = D^0 MW_{\text{rel}}^{-c} \quad (8)$$

where MW_{rel} is the molecular weight of the diffusant relative to a reference molecule (e.g., methanol) and D^0 and c are constants characteristic of the polymer at a given temperature. By introducing a permeability constant $k_p^0 = D^0/l$ for the membrane being considered, Eq. 4 may be written as

$$k_p = k_p^0 K MW_{\text{rel}}^{-c} \quad (9)$$

or in logarithmic form

$$\log k_p = \log k_p^0 + \log K - c \log MW_{\text{rel}} \quad (10)$$

Assuming that for a solute the properties of the biological membrane resemble those of olive oil on an atomistic level, the membrane/donor partition coefficient K may be estimated from the olive oil-water partition coefficient $K_{\text{oo/w}}$ according to the general relationship [16–18]:

$$K = a^* K_{\text{oo/w}}^b \quad (11)$$

Replacing the membrane/donor partition coefficient K in Eq. 10 by Eq. 11, Lieb and Stein obtained

$$\log k_p = \log k_p^0 + b \log K_{\text{oo/w}} - c \log MW_{\text{rel}} \quad (12)$$

A linear fit of Eq. 12 to experimental permeability data for cell membranes gave a good correlation. Lieb and Stein determined also the value of c for several different cell membranes and found c to be equal or greater than one in all cases, which suggests that diffusion in cell membranes resembles diffusion in synthetic polymers.

Starting from Eq. 12 several similar models were developed for predicting skin permeability. Probably the most popular such model was presented by Potts and Guy in 1992 [19]. Instead of using Eq. 8, Potts and Guy estimated the diffusion coefficient in human skin using the relationship

$$D = D^0 \exp(-b MV) \quad (13)$$

where the constant b is inversely proportional to the average free-volume available for diffusion, MV is the molecular volume of the diffusant, and D^0 is the diffusivity of a molecule with vanishingly small MV . Eq. 13 was derived from a statistical analysis of the diffusion process [20]: The diffusing molecule of given volume MV was assumed to have to wait for the formation of a hole adjacent to it with a volume equal to or larger than MV (free-volume diffusion). Only after this hole had occurred the diffusant could move to its new position. This non-Stokesian diffusion process was later used to describe the transverse diffusion of small molecules in membranes of human red blood cells [21].

Since molecular weight and molecular volume are highly correlated, the diffusion coefficient may also be estimated by using molecular weight MW in Eq. 13. Furthermore, Potts and Guy did not use the olive oil–water partition coefficient but the octanol–water partition coefficient $K_{o/w}$. Employing experimental data for k_p from different sources the authors fitted the coefficients for several models which either used molecular volume or molecular weight by multiple linear regression analysis. The model for data of 93 compounds from the Flynn data set featured an r^2 of 0.67 and had been built using Eq. 14.

$$\log k_p = -6.3 + 0.71 \log K_{o/w} - 0.0061 \text{ MW} \quad (14)$$

In accordance with the underlying model, the regression coefficient for $\log K_{o/w}$ was positive while the coefficient for MW was negative, which is consistent with D being inversely related to this descriptor. Potts and Guy underlined the general applicability of their model for predicting skin permeability by pointing out that since 30% variation in experimental data is not uncommon their model completely describes the data. They also concluded that the path length for diffusion across the stratum corneum is $h = 500 \mu\text{m}$ and that the stratum corneum lipids are more polar than octanol. The Potts–Guy equation has several advantages over other models: First of all, being a linear model, the influence of the two descriptors on the permeability coefficient can be readily estimated. Second, the good performance of the equation appears to confirm the assumption that skin resembles a homogeneous membrane during steady-state conditions when only the diffusion coefficient and the concentration gradient in the membrane influence permeation. Therefore, it seemed unnecessary to assume that molecules of differing polarity follow different (e.g., aqueous or lipophilic) pathways through the skin. Similarly, in 1969 Lieb and Stein had concluded that it is unnecessary to postulate alternative pathways for the diffusion of small molecules or the existence of pores to explain the permeability behavior of cell membranes [15]. Later, the Potts–Guy model was slightly modified such that it used $\sqrt{\text{MW}}$ instead of MW [8]. The importance of the two descriptors $K_{o/w}$ and MW was shown repeatedly in later studies [22, 23].

In 1994 Pugh and Hadgraft published two linear models which employed a strikingly simple and fundamental empirical approach [24]. Instead of using molecular weight and $K_{o/w}$ values, the models assigned additive numerical values to a molecule's functional groups. The number of groups was 11 and 17 for the two models. Although the number of descriptors may appear large, it has to be kept in mind that these descriptors have to encode information similar to that of the molecular weight and octanol–water partition coefficients. Computational models for predicting the latter usually employ a considerably larger number of descriptors [13]. Although the two models perform better on the training set than the previously established Potts–Guy model as shown by the comparison of the adjusted r^2 values², leave-one-out crossvalidation³ employing the same data set showed that the best model is comparable but

² Adjusted r^2 is given by $r_{\text{adj}}^2 = 1 - (1 - r^2)(n - 1)/(n - p)$, where p is the number of parameters and n is the number of data points.

³ In a leave-one-out crossvalidation the experimental value for each compound is omitted in turn from the data set and predicted by the model trained on the remaining data.

not superior in predictive quality to the Potts–Guy model. A major advantage of this 11 descriptor model over the Potts–Guy model has to be pointed out: Except for the permeability coefficients, no additional experimental data were necessary to train the models—a fact which is of high interest when performing predictions for large data sets or even for new chemical entities.

In 1976, Kamlet and Taft introduced their solvatochromic comparison method [25, 26]. The hydrogen-bond donor acidity α and basicity β together with the solvent polarity and polarizability π^* were employed to correlate the solvent effects on reaction rates, equilibria, and spectroscopic properties XYZ according to equations of the form

$$\log XYZ = c + s\pi^* + a\alpha + b\beta \quad (15)$$

where c is a constant. While at first the solvatochromic methods were employed to account for the influences of the different solvents [27] on a given solute property, a similar approach was used later to describe the properties of solutes in a given solvent in terms of a general linear solvation energy relationship (LSER [28]):

$$\log XYZ = c + rR + s\pi^* + a \sum \alpha + b \sum \beta + vV_x \quad (16)$$

where R is an excess molar refractivity, $\sum \alpha$ and $\sum \beta$ are the effective hydrogen-bond acidity and basicity, respectively, π^* is the solute dipolarity-polarizability, and V_x is McGowan's characteristic volume [29]. Such LSERs have been applied to predict the solubility of simple organic molecules in water [30], the octanol–water partition coefficient [31, 32], cell permeation [33], and blood–brain distribution [34]. Abraham and coworkers used Eq. 16 also to predict $\log k_p$ values for a set of 46 compounds [35]. Since the excess molar refractivity R was statistically not significant, it was discarded. The resulting equation showed a good correlation between predicted and observed permeabilities ($r^2 = 0.958$):

$$\log k_p = -5.05 - 0.59\pi^* - 0.63 \sum \alpha - 3.48 \sum \beta + 1.79V_x \quad (17)$$

In two subsequent studies by Abraham and coworkers, the use of Eq. 16 was reinvestigated. In 1997, a slightly larger data set of 53 compounds encompassing some steroids was used. Including the excess molar refractivity term R again in the equation gave an equally good correlation ($r^2 = 0.958$) [36]. In a more recent study, values of $\log k_p$ for 119 compounds were correlated with Eq. 16 [37] and yielded an equation with $r^2 = 0.832$. From the coefficients in Eq. 17 Abraham et al. concluded that a molecule's permeability is only slightly reduced if the molecule is dipolar or a hydrogen-bond acid, while the value of $\log k_p$ is considerably reduced if the solute is a hydrogen-bond base. Molecules with higher volumes seem to permeate more readily through the barrier, which is at first sight hard to explain though.

Confining their study to monofunctional molecules, Roberts et al. [38] compared seven different models for predicting human stratum corneum permeability coefficients. The performance of the models was assessed by the adjusted coefficient of determination r_{adj}^2 and the Akaike Information Criterion (AIC) [39]. Both r_{adj}^2 and AIC allow for comparing models with different numbers of variables (degrees of freedom). Exclusion of polyfunctional molecules led to a comparatively small set of only 24 molecules. The previously reported

solvatochromic approach employing parameters for hydrogen-bond acidity (α) and basicity (β) [28] and a volume term V_I performed very well ($r_{\text{adj}}^2 = 0.933$, AIC = 4.6):

$$\log k_p = -1.35 + 2.05V_I - 1.37\alpha - 4.53\beta \quad (18)$$

In accordance with the results by Abraham and coworkers, the coefficients for both α and β were negative, indicating that a molecule's ability for hydrogen bonding reduces its permeability. The coefficient of the volume term on the other hand is positive which would suggest that permeability for larger molecules is enhanced. Roberts et al. argued that the molecular volume represents the hydrophobic nature of the penetrant. This is based on the observation that the partition coefficient increases with mass for organic molecules. This is certainly true for many substances, but this assumption does not hold for all molecules. A fragmental approach based on the work by Pugh and Hadgraft [24] using a reduced set of fragments performed similarly well on the data set ($r_{\text{adj}}^2 = 0.935$, AIC = 5.0). Consistent with the original method, halides and aliphatic carbons seem to increase the permeability, while aromaticity, "O," and hydroxyl groups have a negative influence on $\log k_p$. The authors also attempted to model the process of penetration through the epidermis by employing partition coefficients for various solvent–water systems. A promising equation ($r_{\text{adj}}^2 = 0.928$, AIC = 2.9) was found for the first two-phase model:

$$\begin{aligned} \log k_p = & -2.66 + 0.316 \log K_{\text{ether}} + 0.237 \log K_{\text{hexane}} \\ & + 0.237 \log K_{\text{chloroform}} \end{aligned} \quad (19)$$

Quite intriguingly, the model lacked a volume term. Although this new model outperformed the previously reported models on the small data set, its serious drawback was the use of experimental values for the various partition coefficients.

Roberts et al. criticized the attempts to predict permeabilities since permeability is the result of two processes, partitioning and diffusion [40]. Therefore, instead of following the approach of Potts and Guy, Roberts et al. tried to find a predictive model for each of these processes separately. For the partitioning step they found a Collander-type linear relationship (Eq. 11) between the logarithms of the stratum corneum–water and the octanol–water partition coefficients with a high correlation coefficient ($r^2 = 0.839$):

$$\log K_{\text{sc/w}} = -0.024 + 0.590 \log K_{\text{o/w}} \quad (20)$$

To determine the molecular properties influencing the diffusion process they investigated the relationship between experimental stratum corneum–water partition coefficients and permeability data for 45 compounds. Rearrangement of the logarithmic form of Eq. 4 led to

$$\log \left(\frac{D}{l} \right) = \log k_p - \log K_{\text{sc/w}} \quad (21)$$

Using experimental data for $\log k_p$ and $\log K_{\text{sc/w}}$, the values of $\log (D/l)$ were calculated. A fit of $\log (D/l)$ versus the number of hydrogen-bonding groups

$\sum H$ resulted in a rather low correlation ($r_{\text{adj}}^2 = 0.624$, AIC = 137):

$$\log\left(\frac{D}{l}\right) = -2.80 - 0.500 \sum H \quad (22)$$

This indicated that the hydrogen bonding ability is an important feature of the diffusion process. Plotting D/l against the number of H-bonding groups shows that while the existence of a single H-bonding group in a molecule reduces its diffusivity considerably, the effect of additional H-bonding groups decreases quickly. The curve shape resembled that of Langmuir adsorption isotherms. Using solvatochromic parameters instead of an arbitrary number of hydrogen bonding groups resulted in an excellent regression ($r_{\text{adj}}^2 = 0.904$, AIC = 58.5) underlining once more the usefulness of this approach. Based on these observations Pugh et al. [41] defined a retardation coefficient (RC) which was related to the α and β values of the penetrant according to

$$\text{RC} = 0.0024 + 1.36(\alpha - \beta) + 3.18\beta \quad (23)$$

Combining the RC with the approach by Potts and Guy resulted in a good correlation ($r_{\text{adj}}^2 = 0.929$, AIC = 85.6):

$$\log\left(\frac{D}{l}\right) = -1.97 - 2.01 \log \text{RC} - 0.00708 \text{MW} \quad (24)$$

In contrast to Eq. 18 the molecular weight now reduces the diffusivity which is well in accordance with the result expected for the underlying theoretical model. In summary, having split the processes involved in permeation into two different equations allowed for establishing two separate relationships and to identify the molecular features which best describe each single process. A principal components analysis (PCA) of the various data performed in 2000 [42] confirmed the composite nature of the term $\log k_p$.⁴ In order to predict $\log(D/l)$ with higher accuracy, Pugh et al. introduced the new descriptor "Charge," which is simply the sum of the modulus of the atomic charges of the atoms constituting a molecule. From the results of the PCA it was found that $\log(D/l)$ is inversely related to the equally important descriptors MW and Charge. Since both descriptors seemed correlated ($r^2 = 0.61$), they were combined to the term $\text{MW} \times \text{Charge}$ for predicting $\log(D/l)$:

$$\log\left(\frac{D}{l}\right) = -2.70 - 0.00264 \text{MW} \times \text{Charge} \quad (25)$$

While the regression coefficient ($r^2 = 0.78$) was lower than the one in previous models (e.g., Eq. 18), the new model was satisfying from a mechanistic point of view.

The success of the Potts–Guy equation led many authors to advocate a single mechanism as the rate determining step for permeation through the skin barrier for all or at least a wide range of solutes: diffusion was assumed to occur primarily via the interkeratinocyte lipids of the stratum corneum, a mixture of ceramides, fatty acids, and sterols. While from a macroscopic point of view these lipids may be modeled as a bulk solvent, on a microscopic scale they

⁴ A principal components analysis detects relationships between variables that account for the data variation.

exist in the form of multibilayers [43–45]. This structural arrangement gives rise to different processes that may occur one after another during diffusion of a permeant through the lipid domains of the stratum corneum [46]. The solute molecule must first enter the topmost lipid bilayer from the donor. After its passage through the stratum corneum lipids it exits the bottommost layer and enters the acceptor. Assuming aqueous donor and acceptor phases the resistances for these two steps are equal. Within the interkeratinocyte space the solute may diffuse along the plane of a bilayer without diffusing between different phases (lateral diffusion). At some point the molecule diffuses from the current bilayer to a neighboring one (intramembrane bilayer transport). Since diffusion occurs presumably at the tail region of a bilayer, in this process a molecule has to cross the tail-group region of the current bilayer, two ordered head-group regions, and into the tail-group region of the adjacent bilayer. If all the transport processes just outlined contribute to the diffusion through the lipid domains of the stratum corneum, its total resistance is given by

$$R(\text{sc, lip}) = \frac{2}{k_1} + \frac{l\tau^*}{K_{\text{lip/w}}D_{\text{lat}}} + \frac{n}{k'K_{\text{lip/w}}} \quad (26)$$

where k_1 is the mass transfer coefficient for entering the bilayer from the aqueous phase, l and τ^* are the stratum corneum thickness and effective tortuosity, respectively, D_{lat} the diffusion coefficient for the lateral diffusion, $K_{\text{lip/w}}$ the partition coefficient between the lipid bilayer and the aqueous phase, k' the mass transfer coefficient for intramembrane transbilayer transport, and n the number of bilayers to be crossed internally. The effective tortuosity τ^* accounts for the reduction of the flux by the impermeable keratinocytes and is defined as the ratio of the diffusive flux through a homogeneous membrane to that of a membrane with impediments. Employing typical values Johnson et al. constructed a two-dimensional model of the stratum corneum of which the properties were consistent with previous studies and analyzed the relative importance of each term to the overall stratum corneum resistance by assuming each resistance in turn to be the largest in Eq. 26. For the lateral diffusion this reduced Eq. 26 to

$$R(\text{sc, lip}) = \frac{l\tau^*}{K_{\text{lip/w}}D_{\text{lat}}} \quad (27)$$

which was rearranged to

$$D_{\text{lat}} = k_p(\text{sc, lip}) \frac{l\tau^*}{K_{\text{lip/w}}} \quad (28)$$

Substituting $h\tau^* = 3.6$ cm and $K_{\text{lip/w}} = K_{\text{o/w}}^{0.76}$ into Eq. 28 Johnson et al. calculated solute lateral diffusion coefficients in stratum corneum bilayers from macroscopic permeability coefficients. Measurements with highly ionized or very hydrophilic compounds were not performed because of the possible transport along a nonlipoidal pathway. Comparison of the computed D_{lat} values with experimentally determined data for fluorescent probes in extracted stratum corneum lipids [47] showed a highly similar curve shape. The diffusion coefficient for the lateral transport showed a bifunctional size dependence with a weaker size dependence for larger, lipophilic compounds (> 350 Da), than

for smaller molecules and was given by

$$D_{\text{lat}} = aMW^{-b} + \frac{k_{\text{B}}T}{4\pi\eta_0h} \ln\left(\frac{\eta_0H}{\eta r_{\text{c}}} - \gamma_{\text{e}}\right) \quad (29)$$

where k_{B} is Boltzmann's constant, T the absolute temperature, η_0 the effective viscosity of the bilayer, η the viscosity of the aqueous phase, h the bilayer thickness, r_{c} the radius of the permeant, and γ_{e} Euler's constant. On the basis of their results, Johnson et al. suggested that the transport by lateral diffusion is the rate-limiting resistance to skin permeation except for very hydrophilic substances. The importance of the lateral diffusion was later confirmed by Mitragotri who derived equations for the solute partition coefficient into and the diffusion coefficient in lipid bilayers based on the Scaled Particle Theory [48]. The solute was assumed to rattle in a free-volume pocket until it jumped into another adjacent hole large enough to accommodate the molecule. The average direction of diffusion was found to depend on the solute size and was mainly parallel to the plane of lipid head groups for solutes relevant to transdermal drug delivery which confirmed Johnson et al. assuming lateral diffusion to be very important. The Scaled Particle Theory approach allowed also predicting the free-volume stratum corneum diffusion coefficients for solutes with a molecular weight in the range of 50–400 Da according to

$$D^{\text{fv}} = 2 \times 10^{-5} \exp(-0.46r_{\text{c}}) \quad (30)$$

Combining the equation for the diffusion coefficient with a Collander-type expression for the lipid–water partition coefficient resulted in an expression for calculating the permeability across the stratum corneum:

$$k_{\text{p}}^{\text{fv}} = 5.6 \times 10^{-6} K_{\text{o/w}}^{0.7} \exp(-0.46r_{\text{c}}) \quad (31)$$

Eq. 31 offered an easy method for predicting transdermal transport of small solutes ($MW < 400$ Da) but may not be used for larger molecules. The size of these larger molecules becomes comparable that of the lipid molecules and thus violates the underlying mechanistic model.

20.4.1.3. Multiple Barriers and Pathways

Despite the success of the comparatively simple models presented so far, they implicitly assume that the skin barrier may be modeled by a homogeneous membrane—which implies that the properties of the barrier do not change with depth and that there exists only a single pathway through the barrier. Obviously, skin is not a homogeneous membrane and therefore in several studies the simple model was extended to include several subsequent skin layers. In addition, possible transport along hair follicles and sweat ducts, for example, was sometimes included.

It has been established that in analogy to Ohm's law the overall resistance to diffusion of a multilayer laminate is given simply by the sum of the separate resistances of the layers (Figure 20.2). For example, the total resistance of skin being composed of stratum corneum, viable epidermis, and dermis may be expressed as

$$R_{\text{total}} = R_{\text{sc}} + R_{\text{ve}} + R_{\text{dermis}} \quad (32)$$

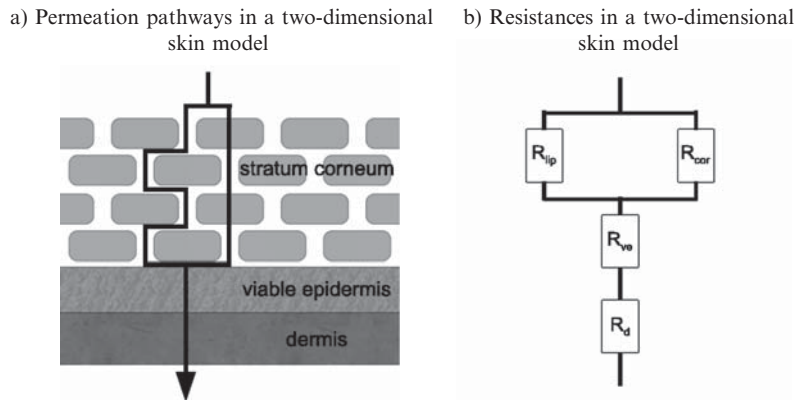


Figure 20.2 A skin model showing possible diffusion pathways and its equivalent circuit diagram. (a) Permeation pathways in a two-dimensional skin model. (b) Resistances in a two-dimensional skin model.

Since permeability is the inverse of resistance, the total permeability through the laminate is given by

$$\frac{1}{k_p} = \frac{1}{k_p(\text{sc})} + \frac{1}{k_p(\text{ve})} + \frac{1}{k_p(\text{dermis})} \quad (33)$$

For parallel permeation pathways within a single layer of such a laminate, the total permeability may be calculated as the sum of the permeabilities [49]. For example, when assuming that permeation may occur through both a lipid fraction and a protein fraction of the stratum corneum, the total permeability is calculated according to Eq. 34:

$$k_p(\text{sc}) = k_p(\text{sc}, \text{lip}) + k_p(\text{sc}, \text{prot}) \quad (34)$$

In an early, quite elaborate model for the diffusion through the stratum corneum, Michaels et al. derived an equation for diffusion through a two-dimensional brick-and-mortar structure [50]. In this model, stratum corneum permeability for a given compound depended only on two parameters: one was the product of the partition coefficient between the protein and the donor phase $K_{\text{prot}/\text{donor}}$ and the diffusion coefficient in the protein phase D_{prot} ; the other was the product of the partition coefficient between the lipid and protein phases $K_{\text{lip}/\text{prot}}$ and the ratio of the diffusion coefficients in the two phases $D_{\text{lip}}/D_{\text{prot}}$.

Estimating the geometric parameters for the model from micrographs and experimental data on the lipid content of the stratum corneum, the equation for the permeability through the stratum corneum reduced to Eq. 35:

$$k_p(\text{sc}) = K_{\text{prot}/\text{donor}} D_{\text{prot}} \left(\frac{1.16}{0.16 \frac{D_{\text{prot}}}{K_{\text{lip}/\text{prot}} D_{\text{lip}}} + 1} + 0.0017 \frac{K_{\text{lip}/\text{prot}} D_{\text{lip}}}{D_{\text{prot}}} \right) \quad (35)$$

Using the mineral oil–water partition coefficient to estimate the partition coefficient between the stratum corneum lipid and protein phases, and using a fixed value of $D_{\text{prot}} = 2 \times 10^{-7} \text{ cm}^2/\text{s}$, Eq. 35 showed a remarkable agreement with experimental data for a value of $D_{\text{lip}}/D_{\text{prot}}$ of 2×10^{-3} . Unfortunately, data

for only 10 different compounds were employed for verifying this theoretical model.

In the revised Robinson model, the skin was modeled as a two-layer laminate consisting of stratum corneum and a watery epidermal layer. Permeation through the stratum corneum was assumed to occur through two different pathways [8]:

$$\frac{1}{k_p} = \frac{1}{k_p(\text{sc, lip}) + k_p(\text{sc, prot})} + \frac{1}{k_p(\text{aq})} \quad (36)$$

with

$$\begin{aligned} \log k_p(\text{sc, lip}) &= b1 + b2 + \log K_{o/w} + b3\sqrt{MW} \\ k_p(\text{sc, prot}) &= \frac{b4}{\sqrt{MW}} \\ k_p(\text{aq}) &= \frac{b5}{\sqrt{MW}} \end{aligned}$$

Obviously, the model for permeation through the lipid fraction of the stratum corneum is the same as the Potts–Guy equation (Eq. 14). Although the Robinson model (Eq. 36) extended the underlying Potts–Guy model, only the three coefficients $b1$, $b2$, $b3$ were found to be statistically significantly different from zero. The coefficient $b5$ for permeation through the aqueous layer could not be determined by regression and was assigned a value of 2.5 on theoretical grounds. In summary, the Robinson model showed only a slight improvement over the previously established Potts–Guy equation while lacking its simplicity.

In 2003, Mitragotri developed a model for predicting stratum corneum permeability which included four different pathways. The overall skin permeability was described by the following equation:

$$k_p = k_p^{\text{fv}} + k_p^{\text{lateral}} + k_p^{\text{pore}} + k_p^{\text{shunt}} \quad (37)$$

where k_p^{fv} corresponds to permeability associated with free-volume diffusion through lipid bilayers, k_p^{lateral} corresponds to permeability due to lateral diffusion of lipids, and k_p^{pore} and k_p^{shunt} correspond to permeability through pores and shunts, respectively. Transport by free-volume diffusion happens for molecules smaller than the lipids constituting the bilayers. Larger lipophilic molecules were assumed to move with the lipids themselves and thus with a similar diffusion coefficient. Transport through pores was important for large hydrophilic solutes like sucrose. This aqueous or polar pathway was assumed to arise from imperfections in the stratum corneum bilayers. Very large molecules ($MW < 100,000$ Da) were assumed to cross the skin by diffusion through shunts. The model showed a very good correlation between calculated and experimental data for both hydrophobic and hydrophilic solutes. The predominant pathway for a given molecule was dependent on both its molecular weight and lipophilicity. A major drawback of the model was its complexity: The values of several parameters must be determined a priori and the large number of equations made its practical use difficult.

20.4.1.4. Recent Empirical QSPR Models

Many QSPR models rely on some sort of idealized theoretical model for the transport of a molecule through the skin barrier. The descriptors necessary for predicting skin permeability—usually molecular weight and the octanol–water

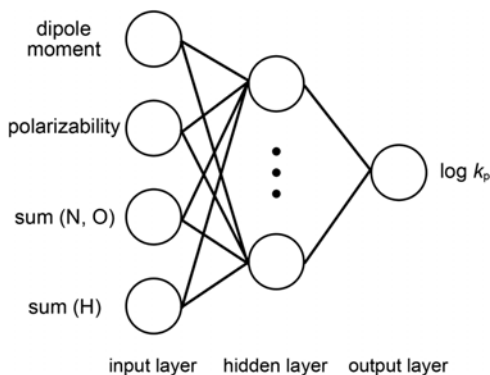


Figure 20.3 Schematic representation of a three-layered artificial neural network.

partition coefficient—and the type of relationship between these input data and the observed permeability coefficients is given by the mechanistic understanding of the diffusion process itself. In such models the permeability coefficients were usually determined by linear regression analysis which provides an interpretable description of how the inputs affect the output. Ultimately, these idealized models do neglect the possible interactions of the diffusant with the barrier and the resulting influences on the diffusion process. For example, protein binding might hinder diffusion whereas fluidization of the lipids in the barrier would increase the permeability. Such effects may be responsible for the varying outliers often reported for simple mechanistic models employing linear regression analysis [24].

In contrast to the mechanistic models, empirical models make no a priori assumptions about the importance of single descriptors and the type of relationship (e.g., linear or nonlinear) between the input and the observed data. Still, many empirical models either employed descriptors that had been previously found to be important or the descriptors in the final model were replaced by such that could be easily interpreted from a mechanistic point of view.

Among the fancier nonlinear models that have been employed in predicting skin permeability are the artificial neural networks (ANN) and the k -nearest-neighbor (k NN) models. ANNs try to model the target values as a nonlinear function of the input data. Topologically, the most widely used neural net consists of an input layer, a single hidden layer, and an output layer (Figure 20.3). Typically the number of units in the input layer equals to the number of descriptors to be used in the model and there exists only one output unit in the output layer. Each unit in the layers is influenced by all units in the adjacent layers with the degree of influence of those units being given by the value of the connection, the so-called weight. When training the neural network to the experimental data, the unknown parameters—the weights between the units—are fitted. If an ANN has too many weights, for example, by employing many units in the hidden layer or several hidden layers, it may overfit the data. However, to avoid overfitting there exist several methods. For a more detailed description of this type of statistical learning method please refer to [51, 52].

ANNs have been applied to model many different processes. They have been used in cardiology [53] and cancer research [54]. ANNs were also employed to

predict pharmacokinetic parameters [55], to optimize pharmaceutical formulations [56], or design controlled release drug delivery systems [57].

Despite the huge success of ANNs, the first study applying an ANN in the field of drug permeation across skin appeared not until 2001. Instead of using skin permeability data, Agatonovic–Kustrin et al. modeled data for the maximum flux across polydimethylsiloxane membrane, which supposedly is a model for skin permeation [58]. Data for 254 structurally diverse compounds were collected from literature [59, 60] and 42 descriptors were calculated for each substance. The authors started with an ANN featuring an input layer of 42 units and two hidden layers. Using a genetic algorithm, they subsequently reduced the number of units. For the training of the ANN, 200 compounds were employed and randomly split into a training set and a validation set containing 160 and 40 compounds, respectively. An external test set (54 compounds) was used to estimate the generalization error of the final model. The final chosen model featured a considerably reduced topology using only 12 molecular features and thus only 12 input units and 5 hidden units. The goodness-of-fit was evaluated by the root-mean-square (RMS) error defined as follows:

$$\text{RMS error} = \frac{\sqrt{(\log k_p^{\text{obs}} - \log k_p^{\text{calc}})^2}}{n} \quad (38)$$

where $\log k_p^{\text{obs}}$ and $\log k_p^{\text{calc}}$ are the experimental and predicted permeabilities and n is the number of data points. The RMS error for the training set was 0.36 and the RMS errors for the validation and the test set were 0.59 and 0.60, respectively. The most important of the 12 remaining descriptors was found to be the dielectric energy which is connected to hydrogen bond strength. Two other important descriptors were the number of hydroxyl and amine groups which are capable of hydrogen bonding. While MW appeared also in the final set of descriptors, the calculated octanol–water partition coefficient was not included.

Using descriptors obtained from semiempirical molecular orbital calculations and experimental data for 92 compounds [6] Lim et al. [61] developed a 3-layered ANN for predicting skin permeability. The authors tested several topologies with varying numbers of units in the hidden layer and calculated their predictive RMS errors in leave-one-out prediction analysis. A 4-4-1 configuration with an RMS error of 0.669 was found to be optimal. In comparison, a multiple linear regression model using the same data and descriptors achieved an RMS error of only 0.930 ($r^2 = 0.418$). The descriptors employed were dipole moment, polarizability, the sum of charges of nitrogen and oxygen atoms, and the sum of charges of hydrogen atoms bound to nitrogen or oxygen atoms. Polarizability was found to be highly correlated to molecular weight and hence to molecular volume. The sum of charges is similar to earlier descriptors used in this field but reflects here mainly the ability of a substance to act as a hydrogen bond acceptor or donor. On the basis of differences in the RMS error, Lim et al. concluded that in contrast to the linear model the nonlinear ANN is able to capture the different processes that contribute to passive diffusion through skin: some units in the hidden layer may account mainly for the permeation of hydrophilic compounds whereas other units are responsible for the transport of lipophilic substances.

In the same year Fu et al. presented their ANN model for predicting permeability across skin [62]. The authors employed five descriptors of which three were equal to descriptors used by Lim et al.: molecular volume (which is related to the polarizability), the sum of the absolute values of the net atomic charges of oxygen and nitrogen atoms, and the sum of net atomic charges of hydrogen atoms attached to oxygen or nitrogen atoms. In addition Fu et al. employed the energies of the highest occupied and the energy of lowest unoccupied molecular orbital. Their ANN had two hidden layers consisting of four units each. The ANN was trained on data for 45 substances and tested by predicting permeabilities of eight compounds. A linear model trained on the same set as the ANN produced a mean prediction error of 32.1% whereas the ANN had a prediction error of only 2.6%. The more accurate prediction by the ANN indicates that there exists a complex nonlinear relationship between the chosen descriptors and the permeability coefficients.

Another of the few studies using ANNs for predicting skin permeability was published by Degim et al. in 2003 [14]. Using $\log k_p$ values for 40 compounds [8, 63] as a training set and three descriptors ($\log K_{o/w}$, MW, and sum of the modulus of the partial charges of the atoms constituting the molecules) the authors tested ANNs of differing topologies for their performance. The best model was then selected for predicting permeability data for an external test set of 11 compounds. While the ANN gave a good correlation coefficient both for the training ($r^2 = 0.997$) and the test set ($r^2 = 0.946$), the RMS error of the test set (0.43) was considerably higher than the error for the training set (0.04). Still, the good performance of the ANN model indicates the possibility of successfully applying such nonlinear statistical models for predicting k_p .

More recently, another nonlinear model was employed to calculate skin permeability from molecular descriptors [64]. Here, the authors employed a combination of k NN model and ridge regression. Although it is beyond the scope of this chapter to give a detailed description a short outline of the method is presented: Similar to stepwise linear regression, ridge regression constructs a linear model by selecting a subset from a large number of descriptors. The k NN routine calculates the activity (i.e., the permeability) of each compound as the weighted average of the k most similar compounds in the data set. The similarity between two substances is determined by the distance in multidimensional descriptor space. Both statistical methods, ridge regression and k NN, were combined to find a predictive model with as few descriptors as possible. Starting from 190 descriptors for the 110 compounds in the data set, the number of descriptors was reduced to three in the final model. These descriptors were the molecular weight, the calculated octanol–water partition coefficient, and the solvation free energy in water computed using the COSMO (Conductor-like screening model) continuum solvation model [65]. This latter descriptor accounts for the interaction of the solute with the solvent and thus encodes similar information like the acidity and basicity descriptors of the solvatochromic method when used for predicting solubility [30]. The robustness of the model was assessed using both a leave-one-out and a threefold crossvalidation. The values for the crossvalidated correlation coefficients, and the relative mean square errors were found to be nearly equal which was taken to confirm the robustness of the model. Using a smaller dataset the new model's performance was then compared to that of earlier linear models and found to outperform

the linear models. As before with the ANNs, this result underlines again the usefulness of such nonlinear statistical methods in predicting complex processes.

20.4.2. Non Steady-State Solutions and Morphological Models

Most models of the permeation of drugs through skin consider only steady-state conditions: the drug amount in the donor is infinite and the concentration of accumulated drug in the acceptor is comparatively small and therefore negligible. Under these conditions the concentration-depth profile for a homogeneous membrane at time t is given by

$$c(x, t) = K c_D \left[\left(1 - \frac{x}{l} \right) - \frac{2}{\pi} \sum_{n=1}^{\infty} \frac{1}{n} \sin \left(\frac{n\pi x}{l} \right) \exp \left(-\frac{Dn^2\pi^2 t}{l^2} \right) \right] \quad (39)$$

where x is the position in the membrane with $0 < x < l$. Under clinical or 'use' conditions, the amounts of material applied are limited and thus the donor is depleted with time. Under such finite dose conditions, steady-state is not reached [66]. Moreover, the stratum corneum is no homogeneous membrane but a structurally complex barrier for which analytical solutions to the diffusion equation are impossible. Therefore, in some models, where transport is supposed to happen via parallel pathways, interchange between these pathways (e.g., dynamic partitioning between corneocytes and lipids in the stratum corneum) is neglected [67] to obtain an analytical solution.

Non steady-state models that try to account for the structural heterogeneity of the barrier may help to understand the importance of the various routes through the skin. One of the first two-dimensional non steady-state models was presented by Heisig et al. in 1996 [68]. The stratum corneum was modeled as biphasic membrane having a brick-and-mortar structure the bricks and mortar respectively corresponding to the corneocytes and the surrounding intercellular bilayers. Diffusion was assumed to occur in both phases and the concentrations at the phase boundaries of the two phases were controlled by a corneocyte–lipid partition coefficient. While the model was not trained to reproduce experimental permeability coefficients, valuable insight into the behavior of such a biphasic membrane was gained. Irrespective of the permeability of the corneocytes, in the steady-state phase the stratum corneum behaves as a homogeneous membrane. The alignment of the corneocytes was shown to have little influence once the offset was 1/8 of the corneocyte width. The permeability of the stratum corneum depends strongly on the ratio between the diffusion coefficients in the two phases $D_{\text{cor}}/D_{\text{lip}}$ and the partition coefficient between these two phases $K_{\text{cor/lip}}$. Increasing drug lipophilicity was found to reduce the uptake into the corneocytes thus decreasing both lag time and permeability.

While Heisig et al. solved the diffusion equation numerically using a finite volume method and thus from a macroscopic point of view, Frasch took a mesoscopic approach: the diffusion of single molecules was simulated using a random walk [69]. A limited number of molecules were allowed moving in a two-dimensional biphasic representation of the stratum corneum. The positions of the molecules were changed with each time step by adding a random number to each of the molecule's coordinates. The displacement was related

to the molecular weight according to Eq. 8 and dependent on the phase the molecule was currently located in. Crossing of phase boundaries was governed by the partition coefficient between the two phases and a random integer number. By varying the ratio $D_{\text{cor}}/D_{\text{lip}}$ and $K_{\text{cor}/\text{lip}}$ Frasch obtained values for the corresponding effective diffusivities and path lengths. These were then approximated by algebraic expression as functions of the molecular weight and octanol–water partition coefficient. Regression of the four-parameter model against the Flynn data base gave very good results ($r^2 = 0.84$). In contrast to many previous models, the random walk-based model predicted more favorable corneocyte partitioning over lipids. Non steady-state predictions were not made with the model.

Using a finite element package Barbero and Frasch compared the steady-state flux for a two-dimensional mouse stratum corneum model with that of a brick-and-mortar model having identical averaged dimensions [70]. The regular geometry was found to give a good approximation of the more realistic but complicated irregular geometry.

Probably the currently most sophisticated morphological model is that published by Wang et al. [71]: the structure of the lipid phase surrounding the corneocytes was further subdivided and transport in this phase was assumed to occur both by diffusion within the bilayer plane and by transfer between bilayers. In addition, keratin binding was included although not using a saturable-binding isotherm but as a partitioning step which slows down the diffusion process irrespective of the drug concentration. At the time of writing, however, the model has not been applied to predict permeability coefficients.

20.5. Pharmacokinetic Models

In some cases not only the uptake of a chemical into and/or through the skin is of interest, but its pharmacokinetics also. Finding analytical functions for describing the diffusion processes in skin quickly becomes arduous or even impossible with increasing numbers of the barrier properties to be included in the model or clinical boundary conditions, for example, repeated exposures or varying drug concentration on the skin (see [72, 73]). This is especially true if the diffusion model is combined with a pharmacokinetic model of the body. To alleviate the difficulties in combining the diffusion models with pharmacokinetic models, the skin is often modeled as a one or two, well-stirred compartment(s) [74, 75]. Such skin-pharmacokinetic models gave acceptable results except for short exposure times [76]. In 2004, Kretsos et al. presented a model which took into account the diffusion through the skin and the uptake into the bloodstream [77]. Diffusion in the donor phase was not modeled, but depletion of the donor was possible. Non steady-state solutions were obtained by numerically approximating the diffusion equations. Transient subsurface concentration profiles levels after application from a finite dose were predicted for salicylic acid. Although the model was limited in its predictivity, it shows the potential of combining diffusion models with pharmacokinetic models. Additional experimental data are necessary to take advantage of the increase in computational speed which allows for performing such calculations.

20.6. Outlook

Today, a comparatively large number of models for predicting steady-state permeation exist. Applying modern statistical learning methods will probably increase the number further. With the increase in computational speed more and more models for predicting non steady-state are being developed. The success of many of these models may suggest that predicting skin permeation has come to a dead end—which is certainly not the case as there is much room for improvement.

Usually, a drug is not applied in an aqueous solution but in some sort of formulation (e.g., ointment, powder). The drug interacts with both the formulation and the skin barrier. Similarly, the formulation's ingredients and its manner of application influence the skin's properties (Figure 20.4).

New models for the drug interacting with the skin may only be developed if our understanding of the skin's structure is improved. For example only a few studies so far have aimed at explicitly taking into account additional effects like protein binding. Protein binding (or a similar process) may lead to drug accumulation in the skin possibly influencing the speed of permeation of drugs from subsequently applied formulations. One reason for neglecting protein binding is certainly the absence of a sufficiently large dataset or a reliable method to estimate the extent of protein binding. In addition, many studies determined only permeability coefficients which are independent of protein binding [79] while reports on non steady-state concentration-skin depth profiles are scarce. Similarly, while the existence of a water and pH gradient in the stratum corneum [80, 81] as well as the change in lipid composition [82, 83] have been shown experimentally, their possible influences on drug permeation have not been investigated in detail in predictive models. Skin metabolism has been shown to influence the percutaneous absorption [84], too, and was modeled for single drugs [85], but a general model is still missing.

The properties of a formulation and its composition affect skin permeability. For example, the pH of formulations was shown to have an effect on skin permeability. Using experimental data a predictive model could be established [86]. A mechanistic understanding of this effect is still missing—as well as a purely computational model. Various substances are known to enhance

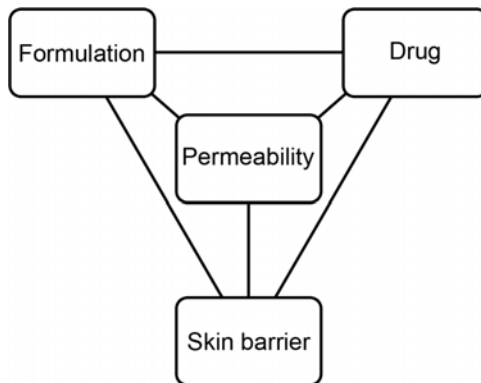


Figure 20.4 Permeability arises from a complex interplay of different variables. Adapted from [78].

transdermal drug uptake and most probably their effect arises from different types of interaction with the stratum corneum constituents: enhancers can act on the lipid domains by, for example, increasing the lipid fluidity [87] or influence the conformation of keratin in the corneocytes or of the proteins in the desmosomes. Another possible mechanism is the alteration of the solvent nature of the stratum corneum leading to an increased stratum corneum/donor partition coefficient [88]. Despite the use of enhancers in many formulations, the number of predictive models that include the effect of enhancers is small although already in 1998 Manitz presented a mathematical basis for this purpose [89]. Recently, Riviere and Brooks presented a model for predicting skin permeability from chemical mixtures [90]. The model employed a mixture factor which encoded properties of the mixture components. For the data set of 16 penetrants in 24 mixtures the predictivity of the model ($r^2 = 0.78$) was higher than that without the mixture factor ($r^2 = 0.62$).

Extraction of lipids in the upper layers by the formulation or swelling of the skin during the application due to, for example, occlusion will also influence the drug diffusion process. Using a set of 48 data points, Hostynek and Magee developed a relationship between varying degrees of occlusion and a permeability coefficient calculated from the maximum flux observed (k_p^{\max}) [91]:

$$\log k_p^{\max} = -3.76 + 0.13 \log K_{o/w} - 0.0168 \text{MR} - 0.28 \text{HBD} - 0.26 \text{OCCL} \quad (40)$$

where MR is the molar refractivity, HBD the number of hydrogen bond donors, and OCCL an indicator variable encoding the extent of occlusion (i.e., a value of one for open, two for protected, and three for occluded). The correlation of this model with experimental data was good ($r^2 = 0.66$), but more experimental data are necessary to validate this approach.

Finally, the skin itself affects the permeation of molecules. The barrier function depends on a variety of aspects such as the body region and the age of the patient.

For non steady-state prediction, skin is increasingly modeled as a two-dimensional biphasic or even multiphasic barrier. These models certainly offer new insights into the barrier properties of the skin, but so far predictions using these models for steady-state or non steady-state are limited to a few compounds. Diffusion through follicles and sweat ducts is neglected, although calculations have shown the importance of transport during the first few minutes after the application of a substance through these skin appendages [92, 93].

References

1. Menon GK (2002) New insights into skin structure: scratching the surface. *Adv Drug Deliv Rev* 54(Suppl 1):S3–S17.
2. Wenkers BP, Lippold BC (1999) Skin penetration of nonsteroidal antiinflammatory drugs out of a lipophilic vehicle: influence of the viable epidermis. *J Pharm Sci* 88:1326–1331.
3. Barry BW (2002) Drug delivery routes in skin: a novel approach. *Adv Drug Deliv Rev* 54(Suppl 1):S31–S40.

4. Scheuplein RJ (1968) On the application of rate theory to complex multibarrier flow co-ordinates: membrane permeability. *J Theoret Biol* 18:72–89.
5. Crank J (2001) *The mathematics of diffusion*—2nd ed. Oxford Science Publications New York 2001.
6. Flynn GL (1990) Physicochemical determinants of skin absorption. In: Gerrity, TR, Henry, CJ (eds.) *Principle of route-to-route extrapolation for risk assessment*. Elsevier, New York, pp 93–127.
7. Dutkiewicz T, Tyras H (1967) A study of skin absorption of ethylbenzene in man. *Brit J Industr Med* 24:330–332.
8. Wilschut A, Ten Berge WF, Robinson PJ, McKone TE (1995) Estimating skin permeation. The validation of five mathematical skin permeation models. *Chemosphere* 30:1275–1296.
9. Kirchner LA, Moody RP, Doyle E, Bose B, Jeffry J, Chu I (1997) The prediction of skin permeability by using physicochemical data. *ATLA* 25:359–370.
10. Cronin MTD, Dearden JC, Moss GP, Murray-Dickson G (1999) Investigation of the mechanism of flux across human skin in vitro by quantitative structure-permeability relationships. *Eur J Pharm Sci* 7:325–330.
11. Poda GI, Landsittel DP, Brumbaugh K, Sharp DS, Frasch HF, Demchuk E (2001) Random sampling or 'random' model in skin flux measurements? *Eur J Pharm Sci* 14:197–220.
12. Frasch HF, Landsittel DP (2002) Regarding the sources of data analyzed with quantitative structure-skin permeability relationship methods. *Eur J Pharm Sci* 15:399–403.
13. Ghose AK, Viswanadhan VN, Wendoloski JJ (1998) Prediction of hydrophobic (lipophilic) properties of small organic molecules using fragmental methods: an analysis of ALOGP and CLOGP methods *J Phys Chem A* 102:3762–3772.
14. Degim T, Hadgraft J, Ilbasmis S, Özkan Y (2003) Prediction of skin penetration using artificial neural network (ANN) modeling. *J Pharm Sci* 92:656–664.
15. Lieb WR, Stein WD (1969) Biological membranes behave as non-porous polymeric sheets with respect to the diffusion of non-electrolytes. *Nature* 224:240–243.
16. Collander R (1947) On "lipid solubility". *Acta Physiol Scand* 13:363–381.
17. Collander R (1950) The distribution of organic compounds between isobutanol and water. *Acta Chem Scand* 4:1085–1098.
18. Collander R (1951) The partition of organic compounds between higher alcohols and water. *Acta Chem Scand* 5:774–780.
19. Potts RO, Guy RH (1992) Predicting skin permeability. *Pharm Res* 9:663–669.
20. Cohen MH, Turnbull D (1959) Molecular transport in liquids and gases. *J Chem Phys* 31:1164–1169.
21. Lieb WR, Stein WD (1986) Non-stokesian nature of transverse diffusion within human red blood cells. *J Membrane Biol* 92:111–119.
22. Patel H, ten Berge W, Cronin MTD (2002) Quantitative structure-permeability relationships (QSPRs) for percutaneous absorption. *Toxicol. In Vitro* 16:299–317.
23. Moody RP, MacPherson H (2003) Determination of dermal absorption QSAR/QSPRs by brute force regression: multiparameter model development with Molsuite 2000. *J Toxicol Env Health A* 66:1927–1942.
24. Pugh WJ, Hadgraft J (1994) Ab initio prediction of human skin permeability coefficients. *Int J Pharm* 103:163–178.
25. Kamlet MJ, Taft RW (1976) The solvatochromic comparison method. 1. The β -scale of solvent hydrogen-bond acceptor (HBA) basicities. *J Am Chem Soc* 98:377–383.
26. Taft RW, Kamlet MJ (1976) The solvatochromic comparison method. 2. The α -scale of solvent hydrogen-bond donor (HBD) acidities. *J Am Chem Soc* 98:2886–2894.

27. Kamlet MJ, Abboud JLM, Abraham MH, Taft RW (1983) Linear solvation energy relationships. 23. A comprehensive collection of the solvatochromic parameters, π^* , α , and β , and some methods for simplifying the generalized solvatochromic equation. *J Org Chem* 48:2877–2887.
28. Abraham MH (1993) Scales of solute hydrogen-bonding: their construction and application to physicochemical and biochemical processes. *Chem Soc Rev* 22:73–83.
29. Abraham MH, McGowan JC (1987) The use of characteristic volumes to measure cavity terms in reversed phase liquid chromatography. *Chromatographia* 23:243–246.
30. Taft RW, Abraham MW, Doherty RM, Kamlet MJ (1985) The molecular properties governing solubilities of organic molecules in water. *Nature* 315:384–386.
31. Kamlet MJ, Abraham MH, Doherty RM, Taft RW (1984) Solubility properties in polymers and biological media. 4. Correlation of octanol/water partition coefficients with solvatochromic parameters. *J Am Chem Soc* 106:464–466.
32. Kamlet MJ, Doherty RM, Abraham MH, Marcus Y, Taft RW (1988) Linear solvation energy relationships. 46. An improved equation for correlation and prediction of octanol/water partition coefficients of organic nonelectrolytes (including strong hydrogen bond donor solutes). *J Phys Chem* 92:5244–5255.
33. Platts JA, Abraham MH, Hersey A, Butina D (2000) Estimation of molecular linear free energy relationship descriptors. 4. Correlation and prediction of cell permeation. *Pharm Res* 17:1013–1018.
34. Abraham MH, Chadha HS, Mitchel RC (1994) Hydrogen bonding 33. Factors that influence the distribution of solutes between blood and brain. *J Pharm Sci* 83:1257–1268.
35. Abraham MH, Chadha HS, Mitchell RC (1995) The factors that influence skin penetration of solutes. *J Pharm Pharmacol* 47:8–16.
36. Abraham MH, Martins F, Mitchell RC (1997) Algorithms for skin permeability using hydrogen-bond descriptors: the problem of steroids. *J Pharm Pharmacol* 49:858–865.
37. Abraham MH, Martins F (2004) Human skin permeability and partition: general linear free-energy relationship analysis. *J Pharm Sci* 93:1508–1523.
38. Roberts MS, Pugh WJ, Hadgraft J, Watkinson AC (1995) Epidermal permeability-penetrant structure relationships: 1. An analysis of methods of predicting penetration of monofunctional solutes from aqueous solutions. *Int J Pharm* 126:219–233.
39. Yamaoka K, Nakagawa T, Uno T (1978) Application of Akaike's Information criterion (AIC) in the evaluation of linear pharmacokinetic equations. *J Pharmacokinet Biopharm* 6:165–175.
40. Roberts MS, Pugh WJ, Hadgraft J (1996) Epidermal permeability-penetrant structure relationships: 2. The effect of H-bonding groups in penetrants on their diffusion through the stratum corneum. *Int J Pharm* 132:23–32.
41. Pugh WJ, Roberts MS, Hadgraft J. (1996) Epidermal permeability-penetrant structure relationships: 3. The effect of hydrogen bonding interactions and molecular size on diffusion across the stratum corneum. *Int J Pharm* 138:149–165.
42. Pugh WJ, Degim IT, Hadgraft J (1996) Epidermal permeability-penetrant structure relationships: 4. QSAR of permeant diffusion across human stratum corneum in terms of molecular weight, H-bonding and electronic charge. *Int J Pharm* 197:203–211.
43. Bouwstra JA, Gooris GS, vd Spek JA, Bras W (1991) Structural investigations of human stratum corneum by small-angle X-ray scattering. *J Invest Dermatol* 97:1005–1012.
44. Schreiner V, Gooris GS, Pfeiffer S, Lanzendorfer G, Wenck H, Diembeck W, Proksch E, Bouwstra J (2000) Barrier characteristics of different human skin

- types investigated with X-ray diffraction, lipid analysis, and electron microscopy imaging. *J Invest Dermatol* 114:654–660.
45. Swartzendruber DC (1992) Studies of epidermal lipids using electron microscopy. *Semin Dermatol* 11:157–161.
 46. Johnson ME, Blankschtein D, Langer R (1997) Evaluation of solute permeation through the stratum corneum: lateral bilayer diffusion as the primary transport mechanism. *J Pharm Sci* 86:1162–1172.
 47. Johnson ME, Berk DA, Blankschtein D, Golan DE, Jain RK, Langer RS (1996) Lateral diffusion of small compounds in human stratum corneum and model lipid bilayer systems. *Biophys J* 71:2656–2668.
 48. Mitragotri S (2002) A theoretical analysis of permeation of small hydrophobic solutes across the stratum corneum based on scaled particle theory. *J Pharm Sci* 91:744–752.
 49. Scheuplein RJ (1966) Analysis of permeability data for the case of parallel diffusion pathways. *Biophys J* 6:1–17.
 50. Michaels AS, Chandrasekaran SK, Shaw JE (1975) Drug permeation through human skin: theory and in vitro experimental measurement. *AIChE Journal* 21:985–996.
 51. Mitragotri S (2003) Modeling skin permeability to hydrophilic and hydrophobic solutes based on four permeation pathways. *J Contr Rel* 86:69–92.
 52. Hastie T, Tibshirani R, Friedman J (2001) *The elements of statistical learning*. Springer, New York.
 53. Itchhaporia D, Snow PB, Akmassy RJ, Oetgen WJ (1996) Artificial neural networks: current status in cardiovascular medicine. *J Am Coll Cardiol* 28:515–521.
 54. Naguib RN, Sherbet GV (1997) Artificial neural networks in cancer research. *Pathobiology* 65:129–139.
 55. Yamamura S (2003) Clinical application of artificial neural network (ANN) modeling to predict pharmacokinetic parameters of severely ill patients. *Adv Drug Deliv Rev* 5:1233–1251.
 56. Takayama K, Fujikawa M, Nagai T (1999) Artificial neural networks as a novel method to optimize pharmaceutical formulations. *Pharm Res* 16:1–6.
 57. Sun Y, Peng Y, Chen Y, Shukla AJ (2003) Application of artificial neural networks in the design of controlled release drug delivery systems. *Adv Drug Deliv Rev* 55:1201–1215.
 58. Agantonovic-Kastrin S, Beresford R, Yusof AP (2001) ANN modeling of the penetration across a polydimethylsiloxane membrane from theoretically derived molecular descriptors. *J Pharm Biomed Anal* 26:241–254.
 59. Chen Y, Vayuhauwan P, Matheson LE (1996) Prediction of flux through polydimethylsiloxane membranes using atomic charge calculations: application to an extended data set. *Int J Pharm* 137:149–158.
 60. Cronin MTD, Dearden JC, Gupta R, Moss GP (1998) An investigation of flux across polydimethylsiloxane membranes by use of quantitative structure-permeability relationship. *J Pharm Pharmacol* 50:143–152.
 61. Lim CW, Fujiwara S, Yamashita F, Hashida M (2002) Prediction of human skin permeability using a combination of molecular orbital calculations and artificial neural network. *Biol Pharm Bull* 25:361–366.
 62. Fu XC, Ma XW, Liang WQ (2002) Prediction of skin permeability using an artificial neural network. *Pharmazie* 57:655–656.
 63. Deigm IT, Pugh WJ, Hadgraft J (1998) Skin permeability: anomalous results. *Int J Pharm* 170:129–133.
 64. Neumann D, Kohlbacher O, Merkwirth C, Lengauer T (2006) A fully computational model for predicting percutaneous drug absorption. *J Chem Inf Model* 46:424–429.

65. Klamt A, Schüürmann G (1993) COSMO: a new approach to dielectric screening in solvents with explicit expressions for the screening. *J Chem Soc, Perkin Trans 2*:799–805.
66. Franz TJ (1978) The finite dose technique as a valid *in vitro* model for the study of percutaneous absorption in man. *Curr Probl Dermatol* 7:58–68.
67. Lee AJ, King JR, Rogers TG (1996) A multiple-pathway model for the diffusion of drugs in skin. *IMA J Math Appl Med Biol* 13:127–150.
68. Heisig M, Lieckfeldt R, Wittum G, Mazurkevich G, Lee G (1996) Non steady-state descriptions of drug permeation through stratum corneum. I. The biphasic brick-and-mortar model. *Pharm Res* 13:421–426.
69. Frasch HF (2002) A random walk model of skin permeation. *Risk Anal* 22:265–276.
70. Barbero AM, Frasch HF (2005) Modeling of diffusion with partitioning in stratum corneum using a finite element model. *Ann Biomed Eng* 33:1281–1292.
71. Wang TF, Kasting GB, Nitsche JM (2006) A multiphase microscopic diffusion model for stratum corneum permeability. 1. Formulation, solution, and illustrative results for representative compounds. *J Pharm Sci* 95:620–647.
72. Kubota K, Dey F, Matar SA, Twizell EH (2002) A repeated-dose model of percutaneous drug absorption. *Appl Math Model* 26:529–544.
73. Simon L, Loney NW (2005) An analytical solution for percutaneous drug absorption: application and removal of the vehicle. *Math Biosci* 197:119–139.
74. McCarley K, Bunge AL (1998) Physiologically relevant one-compartment pharmacokinetic models for skin. 1. Development of models. *J Pharm Sci* 87:470–481.
75. McCarley KD, Bunge AL (2000) Physiologically relevant two-compartment pharmacokinetic models for skin. *J Pharm Sci* 89:1212–1235.
76. Reddy MC, McCarley K, Bunge AL (1998) Physiologically relevant one-compartment pharmacokinetic models for skin. 2. Comparison of models when combined with a systemic pharmacokinetic model. *J Pharm Sci* 87:482–490.
77. Kretsos K, Kasting GB, Nitsche JM (2004) Distributed diffusion-clearance model for transient drug distribution within the skin. *J Pharm Sci* 93:2820–2835.
78. Lippold GC (1992) How to optimize drug penetration through the skin. *Pharm Acta Helv* 67:294–300.
79. Kubota K, Twizell EH (1992) A nonlinear numerical model of percutaneous drug absorption. *Math Biosci* 108:157–178.
80. Wagner H, Kostka KH, Lehr CM, Schaefer UF (2003) pH profiles in human skin: influence of two *in vitro* test systems for drug delivery testing. *Eur J Pharm Biopharm* 55:57–65.
81. Hanson KM, Behne MJ, Barry NP, Mauro TM, Gratton E, Clegg RM (2002) Two-photon fluorescence lifetime imaging of the skin stratum corneum pH gradient. *Biophys J* 83:1682–1690.
82. Bonté F, Saunois A, Pinguet P, Meybeck A (1997) Existence of a lipid gradient in the upper stratum corneum and its possible biological significance. *Arch Dermatol Res* 289:78–92.
83. Weerheim A, Ponc M (2001) Determination of stratum corneum lipid profile by tape-stripping in combination with high-performance thin-layer chromatography. *Arch Dermatol Res* 293:191–199.
84. Bando H, Mohri S, Yamashita F, Takakura Y, Hashida M (1997) Effects of skin metabolism on percutaneous penetration of lipophilic drugs. *J Pharm Sci* 86:759–761.
85. Bando H, Sahashi M, Yamashita F, Takakura Y, Hashida M (1997) *In vivo* evaluation of acyclovir prodrug penetration and metabolism through rat skin using a diffusion/bioconversion model. *Pharm Res* 14:56–62.
86. Martínez-Pla JJ, Martín-Biosca Y, Sagrado S, Villanueva-Camañas RM, Medina-Hernández MJ (2004) Evaluation of the pH effect of formulations on the skin

- permeability of drugs by biopartitioning micellar chromatography. *J Chromatogr A* 1047:255–262.
87. Golden GM, MvKie JE, Potss RO (1987) Role of stratum corneum lipid fluidity in transdermal drug flux. *J Pharm Sci* 76:25–28.
 88. Williams AC, Barry BW (2004) Penetration enhancers. *Adv Drug Deliv Rev* 56:603–618.
 89. Manitz R, Lucht W, Strehmel K, Weiner R, Neubert R (1998) On mathematical modeling of dermal and transdermal drug delivery. *J Pharm Sci* 97:873–879.
 90. Riviere JE, Brooks JD (2005) Predicting skin permeability from complex chemical mixtures. *Toxicol Appl Pharmacol* 208:99–110.
 91. Hostynek JJ, Nagee PS (1997) Modelling in vivo human skin absorption. *Quant Struc Act Relat* 16:473–479.
 92. Scheuplein RJ, Blank IH (1971) Permeability of the skin. *Physiol Rev* 51:702–747.
 93. Ho CK (2004) Probabilistic modeling of percutaneous absorption for risk-based exposure assessments and transdermal drug delivery. *Statistical Methodology* 1:47–69

21

Physiologically Based in Silico Models for the Prediction of Oral Drug Absorption

Fredrik Johansson and Ronnie Paterson

Abstract The ability to accurately predict the oral absorption of drugs based solely on in vitro data provides an opportunity to assess the developability, from an absorption point of view, of new chemical entities before any preclinical or clinical in vivo studies are performed. There have been several reports on physiologically based mathematical models that are capable of producing such predictions, and there are a few commercially available software packages (e.g., GastroPlusTM, iDEATM, Intellipharm[®]PK, and PK-Sim[®]) that have been shown to predict the human absorption properties with a fairly high degree of accuracy. As these models use the interplay between the drug characteristics and the human physiology to simulate the processes involved in the oral absorption of drugs, they also give information about the underlying mechanisms for absorption limitations and as such they are well suited to be used in progressing new chemistry and to support formulation development. The aim of this chapter is to briefly summarize the underlying principles for some of the physiologically based in silico models for the prediction of human absorption and to discuss their relative performance as well as limitations in their use.

Keywords: Absorption; In silico; Mixing tank; Maximum absorbable dose; Mass balance approach; Compartmental absorption; Transit models

Abbreviations

ACAT	Advanced compartmental absorption and transit
An	Absorption number
AP	Absorption potential
ASF	Absorption scale factors
CAT	Compartmental absorption and transit
Dn	Dissolution number
Do	Dose number
F_{abs}	Fraction dose absorbed
FaSSIF	Fasted state simulated intestinal fluid
GI	Gastrointestinal
GITA	Gastrointestinal transit absorption
HTS	High throughput

K_a	Absorption constant
MAD	Maximum absorbable dose
P_{app}	Apparent permeability coefficient
P_{eff}	Effective permeability coefficient
QSA(P)R	Quantitative structure activity (property) relation

21.1. Introduction

The number of compounds produced in early drug discovery has been constantly increasing since the introduction of techniques such as High Throughput Screening (HTS) and combinatorial chemistry. This means that the pressure to develop screening methods for the assessment of different compound characteristics is also increasing. Although the above techniques are very useful in identifying structural elements that are important for the activity of the compound in terms of its ability to bind or interact with the desired target, there is still a challenge to go from such “hits” to potent, selective compounds with the pharmacokinetic properties needed for an effective in vivo performance. Several studies have shown that poor pharmacokinetic properties are one major reason for attrition in the development of drugs (e.g., [15,42]), and it is therefore very important to have the knowledge and tools to be able to identify compounds with potential pharmacokinetic problems early in the drug selection process. As a result of this it is important to be able to identify, at an early stage, compounds that are likely to show absorption limitations in humans and animals.

Historically, different animal models have been the common approach for assessing drug absorption properties. Running valid animal experiments often requires more compound than is normally available in an early phase and testing all compounds in animals would also be both time consuming and ethically debatable. However, in the later discovery phase animal models are normally used to predict human pharmacokinetic properties including absorption properties. Attempts have been made to correlate absorption between different animal species and humans, for example, dogs [9], rats [7, 66], and monkeys [8]. These studies have shown that oral drug absorption in dogs often exceeds the one obtained in humans due to a more “leaky” intestine. On the other hand, good correlations were shown for rats and monkeys. As most of the compounds were dosed to the animals as solutions or suspensions, few compounds showing dose-dependent absorption were included and as compounds showing particle size dependent absorption were excluded, solubility and dissolution rate-limited absorption was not fully investigated. From this it can be concluded that rat could be a reasonable model for predicting the human fraction dose absorbed (F_{abs}) for permeability limited compounds; however, this is not as obvious for solubility or dissolution rate-limited absorption. In one study, Chiou et al. [10] suggested that rat was a good model for predicting dose-dependent absorption in man, if the doses given were corrected for body surface area or body weight. A good correlation was shown for four compounds but again, none of them showed solubility or dissolution rate-limited absorption.

As described elsewhere in this book, there are several single parameter in vitro models that are often used to predict human absorption properties. Caco-2 cell monolayers have widespread use within the pharmaceutical industry

as a means to study drug permeability and to predict human F_{abs} , and several reports exist where good correlations have been demonstrated (e.g., [2, 56]). Although the Caco-2 cell model is a very useful tool for prediction of in vivo permeability and to assess transport mechanisms across the intestinal epithelium, it does not take into account all factors affecting intestinal drug absorption. This was obvious when a large set of structurally diverse compounds (the iDEA database) was used to investigate different types of single parameter models and poor correlations with human absorption were obtained [20].

The use of multiparameter mathematical models to predict the human F_{abs} of orally administered drugs is also widespread within the industry. There are two main types of models used, physiologically based and nonphysiologically based models. The later category involves models that use quantitative structure activity/property relations (QSA(P)R, for example, [31, 50, 64, 65]). These models use the interplay between different molecular descriptors that are important for drug absorption, in order to calculate human intestinal absorption. Although these structure-based algorithms can be very useful early in the drug discovery phase, as they only require a compound structure to predict the human absorption, they do not give any information about the underlying mechanisms for absorption limitations and are of limited use in supporting the progression of new chemistry or formulation development. Physiologically based models, on the contrary, are mathematical models that use the interplay between the drug characteristics and the human physiology to simulate the processes involved in the oral absorption of a drug and as a result the human F_{abs} of orally administered drugs can be predicted based merely on in vitro data [1, 20, 28, 62, 63]. In this review the focus is on physiologically based models described in the literature. The aim is to briefly describe how the models work, the input data required and to assess the relative performance of the models as well as limitations in their use.

21.2. Absorption Process

21.2.1. Overall Absorption Process

The absorption of drugs from the gastrointestinal (GI) tract involves several different processes including release of the drug from the dosage form, dissolution of the drug in the GI fluids, possible degradation, adsorption or complex binding in the GI fluids as well as the absorptive flux across the epithelial cells lining the intestinal wall (e.g., [19, 38]; see Figure 21.1). If a drug is administered as a solid dosage form, the first step in the absorption process is the release and dispersion of the solid material in the GI fluids. This process involves the physical disintegration of the dosage form as well as wetting of the drug powder. These processes are not easily simulated and when using mathematical models to predict absorption, the release from the dosage form and the wetting of the compound is normally assumed to be fast. Moreover, the processes of release and wetting of the solid drug on one hand and dissolution on the other hand are taking place within the same time scale and are therefore not easy to differentiate from each other. As the drug is dissolved in the GI fluids, the free concentration of drug can be affected by processes such as degradation and adsorption or complex binding to contents in the intestinal

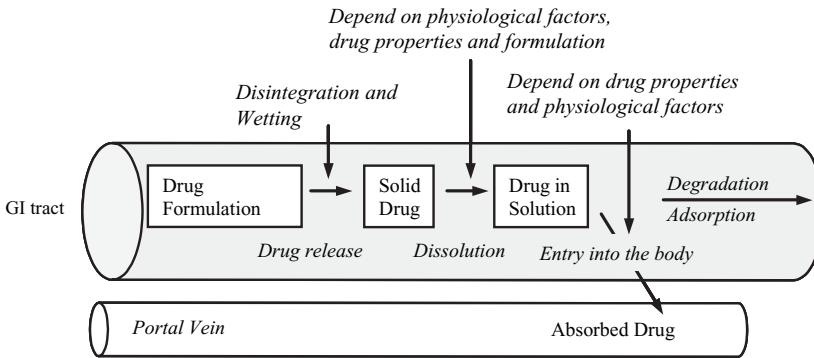


Figure 21.1 Schematic representation of the main processes involved in oral drug absorption.

fluids. The concentration gradient across the intestinal epithelium together with the compound's inherent permeability properties governs the absorption of the drug from the intestinal lumen to the portal vein. In this chapter we will consider compounds absorbed when they have entered the enterocytes lining the intestinal wall, as the models discussed are generally not taking gut wall metabolism into consideration.

21.2.2. Drug Dissolution

The dissolution of a solid drug can be described by a modified Noyes-Whitney equation (Eq. 1; e.g., [13])

$$\text{Dissolution rate} = \frac{dX}{dt} = \frac{AD}{h} \left(C_s - \frac{X_d}{V} \right) \quad (1)$$

where A is the drug surface area available for dissolution, D is the diffusion coefficient of the drug in the dissolution medium, h is the diffusion layer thickness, C_s is the saturation solubility of the drug, X_d is the amount of dissolved drug, and V is the volume of dissolution medium. The main factors affecting the dissolution of a drug in the GI tract are the saturation solubility of the solid drug in the GI fluids, the surface area of the solid drug and the concentration of the drug in solution.

The solubility of the drug is affected by several physiological and physicochemical factors [26]. Drug properties are defined not only by the chemical structure but also by the solid material, and a drug can potentially exist in many different solid state forms which may differ in solubility. Amorphous materials tend to show much higher aqueous solubility than crystalline forms of the same compound and different crystal modifications of the same compound may also have different solubility (e.g., [25]).

The solubility of a compound may also be affected by physiological factors such as pH, lipid, and bile acid concentrations (e.g., [13, 26]). Basic or acidic drugs often have very different solubility in the gastric and intestinal fluids resulting in differences in dissolution rate in the stomach and the small intestine. For compounds with highly pH-dependent solubility, changes in GI pH due to, for example, food intake, can have a large impact on the dissolution and hence absorption of the drug. Poorly soluble compounds often show an increased solubility in the presence of surfactants, for example, bile acids,

and the concentration of bile acids is also different in the fasted versus fed states [13, 26].

The total drug surface area available for dissolution is important and can sometimes limit the dissolution rate and absorption of poorly soluble drugs given at low doses [29]. The surface area available depends on several things such as the wettability of the solid drug, the size of the primary drug particles and simply by the amount drug dosed [26]. Again, bile acids can affect the wetting of the solid drug and the particle size can be influenced by different milling techniques. The diffusion of the dissolved compound through the boundary layer surrounding the dissolving particles is affected by the diffusion coefficient of the drug in the dissolution media and the thickness of the boundary layer. The diffusion coefficient is inversely proportional to the viscosity of the dissolution media and the size of the drug molecule (e.g., [38]). The sizes of most drug molecules are similar but the viscosity of the intestinal fluids can be increased by food intake [26]. The thickness of the boundary layer is affected by the in vivo hydrodynamics and as such it is also affected by food intake [26].

All in all, the dissolution rate of a drug in the GI tract is dependent on several physiological and physicochemical factors that need to be considered when trying to simulate drug dissolution as a part of the absorption process.

21.2.3. Drug Absorption

When a drug has dissolved in the GI fluids and is present in solution at the site of absorption it has to pass a biological barrier, that is, the enterocytes lining the gut wall, in order to be absorbed into the body. The absorptive flux (J) can be described as a function of the permeability of the intestinal mucosa to the drug (P_{eff}), the surface area available for absorption (SA), and the concentration gradient (ΔC) across the mucosa (e.g., [6], Eq. 2)

$$J = P_{\text{eff}} \times SA \times \Delta C \quad (2)$$

There are several physicochemical and physiological factors that affect the permeability of a compound. The size, shape, and charge of the drug molecule affect its inherent potential to pass lipophilic membranes or to pass through the tight junctions between adjacent epithelial cells. Molecules can also use active transport mechanisms to facilitate passage through the mucosa and several drug-like compounds are substrates to efflux mechanisms and hence their absorption can be hindered (e.g., [51]). The regional intestinal pH, leakiness of the mucosa, as well as the expression of active influx or efflux proteins are physiological factors that can affect the extent of absorption across the intestinal mucosa. Permeability is most often described as apparent permeability coefficients that can be determined using different in vitro (e.g., the Caco-2 cell model; [2]) or in situ (e.g., perfused rat intestine; [16]) methods, and human permeability coefficients can be measured in vivo using perfusion techniques [32]. It is not possible to perform these human in vivo permeability measurements early in the drug development process but there are reports showing that correlations can be established with other models, for example, Caco-2 cell monolayers [47], rat intestinal segments in Ussing chambers [48], and perfused rat intestine [16].

The concentration gradient across the intestinal mucosa, being the driving force for passive absorption, is affected by the thermodynamic solubility and dissolution rate of the drug in the intestinal fluids as described earlier.

21.3. Physiologically-Based Absorption Models

21.3.1. General Considerations

There are several different physiologically based approaches for the prediction of human oral absorption described in the literature. Yu et al. [62, 63] divided the different approaches into (i) qualitative methods such as the pH-partitioning hypothesis and the absorption potential (AP) concept and (ii) quantitative methods including dispersion models, mass balance models, and compartmental absorption and transit models. The qualitative models aim to correlate physico-chemical and physiological properties to the oral absorption of drugs in a simple way. On the basis of the fact that the F_{abs} of a drug is dependent on factors such as permeability of the gut wall to the drug, aqueous solubility of the drug, the dose administered, the fraction of the drug in nonionized form, and the volume of the intestinal fluids, Dressman et al. [12] defined a dimensionless parameter, the absorption potential, that was shown to correlate with human F_{abs} for orally administered drugs. However, bearing in mind the simplicity of such qualitative models, they are not likely to work in all cases. The quantitative models are designed to predict the actual F_{abs} after oral administration and as such they are well suited, not only to predict the extent of absorption but also to assess the underlying mechanisms. Yu et al. [62] further categorized the quantitative models into two groups, steady-state models and dynamic models, to emphasize that the steady-state models depend on a spatial variable whereas the dynamic models depend on a temporal variable. As a result of this the steady-state models can only predict the extent of absorption whereas the dynamic models can also predict the rate of absorption. The steady-state models include mass balance models [40, 45] and the dynamic models include mixing tank models (e.g., [14, 24]) and compartmental absorption and transit models ([19, 60], [1], [30]). The background and mathematical principles behind the different approaches have been extensively reviewed elsewhere (e.g., [61–63]). This chapter will provide some basic background information on the different approaches and the main focus will be on models, described in the literature, whose performance has been assessed for the prediction of human F_{abs} .

Common to all the physiologically based prediction models is that they describe the key physical processes, such as drug dissolution and mass transport across the gut membrane, as a series of interrelated differential equations. Due to their nature, it is normally not possible to derive simple analytical solutions to these equations, and numerical integration techniques are generally needed in order to generate numerical solutions. During the course of a simulation, they calculate the predicted rate of drug absorption at all time points (or in the case of spatial methods, the amount absorbed as a function of distance) and are therefore able to estimate the net amount of the drug absorbed with time. The predicted F_{abs} is simply the net amount absorbed at the end of the simulation divided by the total amount of drug in the dose. In the case of dynamic models, other processes, for example, drug distribution and

elimination, are often coupled to the absorption process and then the resulting plasma concentrations after oral administration of drugs can be predicted (e.g., [1, 28]).

21.3.2. Mixing Tank Models

21.3.2.1. Overview of Mixing Tank Models

The main feature of a mixing tank model is that it describes the intestine as one or more tanks that are well mixed and have a uniform concentration of dissolved and solid drug. Furthermore, if more than one compartment is used, both dissolved and solid drug is transferred between the mixing tanks in series by first-order transit kinetics [14, 62, 63]. In the mixing tank models described in the literature, modified Noyes-Whitney equations are used to account for drug dissolution and first-order absorption constants (K_a) are used to account for mass transport of drug across the intestinal mucosa [14, 24, 28]. In 1986, Dressman and Fleicher presented a one-tank mixing-tank model that accounted for nonsink dissolution behavior. In their work, assumptions were made that solid drug is composed of spherical particles of uniform size, that solid and dissolved drug is moving at the same rate in the intestine and that both absorption and transit are first-order processes. Using this model they predicted the absorption of both griseofulvin and digoxin (two poorly soluble compounds) to be dependent on dose and particle size respectively in accordance with what had been reported from clinical studies [14].

Hintz and Johnson [24] reproduced the model presented by Dressman and Fleicher [14] but extended the model to account for polydisperse powders. In both models, all drug particles were assumed to be spherical, and this might introduce an error in the calculations of the total drug surface area if the particles of interest are truly nonspherical. As spheres will give the smallest area to volume ratios and surface area is the parameter of interest, the surface areas and hence dissolution rates might be underestimated if spherical morphology is assumed. To account for this problem, Lu et al. [37] refined the mixing-tank model so that the surface area could be described using cylindrical geometry. In their study, they showed that this significantly improved the accuracy of dissolution predictions for both fine and coarse hydrocortisone, indicating the importance of particle morphology on the surface area and hence dissolution. Lu et al. [37] also investigated the effect of hydrodynamics on the dissolution of dispersed drug particles. The hydrodynamic diffusion layer (h) surrounding the drug particles is also important for the dissolution rate. The diffusion layer is normally assumed to be equal to the particle radius until a plateau value is reached at larger particle radii after which it is held constant [37]. Normally, the diffusion layer is kept constant throughout a simulation but this is of course not the case in real life. As dissolution proceeds, particles will get smaller and so will the diffusion layer. Lu et al. [37] included a time dependency on the diffusion layer but the results did not support any significant improvements in accuracy of predictions.

21.3.2.2. *Intellipharm*[®]PK

Intellipharm[®]PK (*Intellipharm*, LCC, Niantic, CT, USA) is a commercially available computer program that is based on a mixing tank model ([28]; www.intellipharm.com). *Intellipharm*[®]PK utilizes Noyes-Whitney dissolution

equations to account for drug dissolution and absorption rate constants (K_a) to account for permeation across the intestinal wall. The coupled differential equations that are used in Intellipharm[®]PK to simulate drug dissolution and absorption are summarized in Eqs. 3–5 ([28]; www.intellipharm.com).

$$\text{Solid drug : } \frac{dX_s}{dt} = - \frac{3DX_0^{\frac{1}{3}}X_s^{\frac{2}{3}}}{\rho hr_0} \left(C_s - \frac{X_d}{V} \right) \quad (3)$$

$$\text{Dissolved drug : } \frac{dX_d}{dt} = + \frac{3DX_0^{\frac{1}{3}}X_s^{\frac{2}{3}}}{\rho hr_0} \left(C_s - \frac{X_d}{V} \right) - K_a X_d \quad (4)$$

$$\text{Absorbed drug : } \frac{dX_a}{dt} = K_a X_d \quad (5)$$

where X_s is the mass of solid drug, X_d is the mass of dissolved drug, X_a is the mass of absorbed drug, D is the diffusivity, C_s is the saturation solubility in the intestine, V is the volume of intestinal fluids present for the drug to dissolve in, K_a is the absorption rate constant, r_0 is the initial drug particle radius, and h is the diffusion layer thickness. In Intellipharm[®]PK the equations are modified to account for polydisperse powders. Although the model only uses one compartment, the solubility, absorption constant and volume available for dissolution can be varied with time and therefore, by altering these parameters, the changing physiology along the GI tract can be accounted for ([28], see Figure 21.2). By changing the solubility with time, the regional solubility of acidic or basic drugs can be described. If, for instance, the solubility decreases when going from low pH (stomach) to higher pH (small intestine), the Noyes-Whitney dissolution equation will be reversed resulting in precipitation of solid drug on existing particles. It is well known that the permeability of drugs often differ in different parts of the intestine [48] and by changing the absorption constant (K_a) with time, this can be accounted for. An important feature of Intellipharm[®]PK compared to other commercially available software (e.g., GastroPlus[™], version 5.0) is that Intellipharm[®]PK can handle particle size distributions and hence offers a more realistic approach to drug particle dissolution (this feature was included in version 5.1.0 of GastroPlus[™]). In Intellipharm[®]PK the hydrodynamic diffusion layer (h) can be assumed to be either time dependent or not [37], and the initial h is assumed to be equal to the particle radius until a defined radius is reached, thereafter it will be kept constant. The resulting differential equations in Intellipharm[®]PK are solved

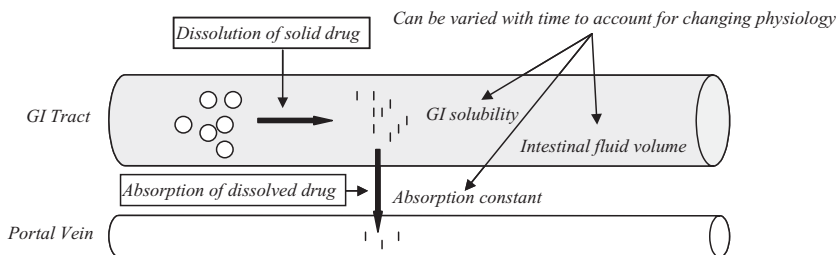


Figure 21.2 Schematic representation of the absorption processes modelled in Intellipharm[®]PK.

numerically using a fourth-order Runge-Kutta method and the step sizes in the calculations can be defined in order to optimize the relationship between accuracy and run time. In Intellipharm[®]PK the absorption modeling is coupled to a standard pharmacokinetic model and this makes it possible to simulate plasma concentration versus time profiles and to assess the effect of absorption rate on the drug exposure (www.intellipharm.com).

21.3.2.3. Maximum Absorbable Dose

The maximum absorbable dose (MAD) can be derived from the mixing tank model as shown by Johnson and Swindell [29]. The amount of drug absorbed (X_a) at any time is a function of a first-order absorption constant (K_a) and the amount of dissolved drug (X_d) as described in Eq. 6.

$$\frac{dX_a}{dt} = K_a X_d \quad (6)$$

By integrating Eq. 6, the cumulative amount absorbed can be calculated. If the dose is hypothetically increased to extreme doses, a constant concentration (equal to the thermodynamic solubility of the drug in the intestinal fluids, C_s) could be maintained over the integrated time period. In this case the amount in solution would equal the thermodynamic solubility of the drug multiplied by the volume present in the intestine ($X_d = C_s V$) and the maximum absorbable dose (MAD) would be given by Eq. 7 [11, 29].

$$\text{MAD} = K_a \times C_s \times V \times t \quad (7)$$

where K_a is the absorption constant (min^{-1}), C_s is the solubility in any relevant media (mg/mL), t is the small intestinal transit time (min), and V is the small intestinal water volume (mL).

21.3.3. Mass Balance Models

21.3.3.1. Macroscopic Mass Balance Models

A macroscopic mass balance model for the prediction of F_{abs} was developed by Sinko et al. [45], and has been thoroughly reviewed by Yu et al. [62, 63]. In the model, the intestine is assumed to be a cylindrical tube with a surface area of $2\pi RL$ where R and L are the radius and length of the tube, respectively. The rate of mass entering the intestine is the product of the inlet concentration (C_0) and the volumetric flow rate (Q), and the mass leaving the intestine is the product of the outlet concentration (C_{out}) and volumetric flow rate. The difference between the mass flow in and out of the intestine represents the mass absorbed per unit of time (i.e. the flux), and this is proportional to the permeability (P_{eff}) of the drug and the concentration of the drug in the intestine. The total mass of drug absorbed per unit time ($-dM/dt$) can be described as the integral of the absorption flux over the surface area of the intestine (Eq. 8; [45])

$$-\frac{dM}{dt} = Q(C_0 - C_{\text{out}}) = 2\pi RP_{\text{eff}} \int_0^L C dz \quad (8)$$

where z is the axial coordinate along the intestine. Assuming steady-state conditions, F_{abs} is equal to $1 - C_{\text{out}}/C_0$ and hence:

$$F_{\text{abs}} = 1 - \frac{C_{\text{out}}}{C_0} = \frac{2\pi RP_{\text{eff}}}{QC_0} \int_0^L C dz = 2An \int_0^L C^* dz^* \quad (9)$$

where C^* and z^* are dimensionless variables, $C^* = C/C_0$, $z^* = z/L$, and An is the dimensionless absorption number defined as the ratio between the mean small intestinal transit time and the absorption time.

To be able to calculate the F_{abs} using Eq. 9, the concentration profile in the intestine has to be understood. Sinko et al. [45] considered three different cases covering conditions where the inlet and outlet drug concentrations are below the saturation solubility (C_s) of the drug in the intestinal fluids, where the drug inlet and outlet concentrations are above C_s (i.e., solid drug exists throughout the intestine), and the intermediate situation where the inlet concentration is above but the outlet concentration below C_s .

21.3.3.2. Microscopic Mass Balance Models

In 1993, Oh et al. [40] presented a microscopic mass balance approach developed to predict the F_{abs} of poorly soluble compounds administered as suspensions. Different from the macroscopic mass balance model discussed before, the microscopic mass balance model includes the dissolution resistance as a function of solid drug surface area or particle size. The model assumes that all particles are spheres of the same size and that the solubility is constant throughout the intestine. In the model, a mass balance approach is applied for both the solid phase and the solution phase in order to derive a set of differential equations. Applying the mass balance approach for the solid phase, assuming that the diffusion layer surrounding all particles is equal to the particle radius, gives the rate of change for the particle radius of the solid drug (Eq. 10; [40])

$$\frac{dr_p}{dz} = -\frac{D\pi R^2}{Q\rho} \times \frac{C_s - C_L}{r_p} \quad (10)$$

where z is the axial coordinate along the intestine, D is diffusivity of the drug molecule in the GI fluids, R is the radius of the intestine, Q is the flow rate, ρ is the particle density, C_s is the saturation solubility of the drug in the intestinal fluids, C_L is the luminal concentration of the drug, and r_p is the radius of the solid drug particles. Applying the same mass balance approach for drug in solution yields the rate of change of drug concentration in the lumen (Eq. 11; [40])

$$\frac{dC_L}{dz} = \frac{D \cdot (N_0/V_0) \cdot 4\pi^2 R^2}{Q} \cdot r_p(C_s - C_L) - \frac{P_{\text{eff}} \cdot 2\pi R}{Q} \cdot C_L \quad (11)$$

where N_0 is the number of particles in a dose, V_0 is the volume in the intestine present for dissolution, and P_{eff} is the effective permeability across the intestinal mucosa. Oh et al. [40] made the variables dimensionless by letting $z^* = z/L$, $r^* = r_p/r_0$ and $C^* = C_L/C_s$. By doing so the microscopic mass balance model can be summarized in a system of two differential equations with the unknowns r^* and C^* , where r^* is the current radius of the drug particles relative to the radius of the ingested particles and C^* is the current luminal concentration relative to the saturation solubility of the drug in the

intestinal fluids. The system can be described as a system of nonlinear ordinary differential equations with constant coefficients (An, Do, and Dn; [40]).

$$\frac{dr^*}{dz^*} = -\frac{Dn}{3} \left(\frac{1 - C^*}{r^*} \right) \quad (12)$$

$$\frac{dC^*}{dz^*} = DnDor^*(1 - C^*) - 2AnC^* \quad (13)$$

where

$$An = \text{absorption number} = \frac{P_{\text{eff}}\pi RL}{Q} \quad (14)$$

$$Do = \text{dose number} = \frac{M_0/V_0}{C_s} \quad (15)$$

$$Dn = \text{dissolution number} = \frac{(D/r_0)C_s(4\pi r_0^2)/(\frac{4}{3}\pi r_0^3\rho)}{Q/(\pi R^2L)} \quad (16)$$

In this model there is no stomach compartment but possible dissolution in the stomach can be partly accounted for by defining the boundary conditions (C^* and r^*) in the beginning of the intestine. If fast dissolution is expected in the stomach, the boundary conditions for C^* can be set to 1, that is, the luminal concentration when entering the intestine equals the saturation solubility in the intestine. If no dissolution is expected in the stomach, the starting value for C^* will be 0. C^* can then have all values between 0 and 1 as the boundary condition and this results in the restriction that super-saturation in the intestine due to fast dissolution and high solubility in the stomach can not be accounted for. Assuming that the difference between the mass into and out of the intestine is equal to the mass absorbed at steady state, the F_{abs} can be calculated from Eq. 17 [40]

$$F_{\text{abs}} = 1 - \left\{ r^*(l)^3 \right\} - \frac{C^*(l)}{Do} \quad (17)$$

where $r^*(l)$ is the dimensionless particle radius at the end of the intestine and $C^*(l)$ is the dimensionless drug concentration at the end of the intestine.

21.3.4. Compartmental Absorption and Transit (CAT) Models

21.3.4.1. Overview of CAT Models

The basis for all CAT models is the fundamental understanding of the transit flow of drugs in the gastrointestinal tract. Yu et al. [61] compiled published human intestinal transit flow data from more than 400 subjects, and their work showed the human mean small intestinal transit time to be 199 min. and that seven compartments were optimal in describing the small intestinal transit process using a compartmental approach. In a later work, Yu et al. [58] showed that between 1 and 14 compartments were needed to optimally describe the individual small intestine transit times in six subjects but in agreement with the earlier study, the mean number of compartments was found to be seven. This compartmental transit model was further developed into a compartmental absorption and transit (CAT) model ([60], [63]). The assumptions made for this CAT model was that no absorption occurs in the stomach or in the colon and that dissolution is instantaneous. Yu et al. [59] extended the CAT model

to include the estimation of saturable intestinal absorption. This model also accounted for degradation in the intestine but similarly to the earlier published CAT model it did not account for drug dissolution. Yu [57] presented a version of the CAT model, modified to account for drug dissolution, suitable for investigating the causes for poor oral drug absorption. This model used a version of the Noyes-Whitney equation to account for dissolution and the earlier compartmental transit model to account for small intestinal drug transit. Several other versions of CAT models have been presented in the literature (see Sects. 21.3.4.2–21.3.4.4).

21.3.4.2. The ACAT Model—GastroPlus™

The commercially available absorption simulation software package, GastroPlus™ (Simulationsplus, Inc. Lancaster, CA, USA), is based on an Advanced Compartmental Absorption and Transit (ACAT, [1]) model that is a further development of the CAT model presented by Yu et al. ([60], [63]). The ACAT model is based on the transit model describing the small intestine as a series of seven compartments but in this model stomach and colon compartments are added. The ACAT model in GastroPlus™, models the rate of change of drug in solution in a compartment as a function of transit of dissolved drug into the compartment from the previous compartment, dissolution of solid particles, precipitation of dissolved drug, degradation of drug in solution, absorption of drug, and flow of drug out from the compartment. In a controlled release mode, the release of drug from the dosage form can also be simulated (see Figure 21.3).

The transit between the compartments is described by a transfer rate constant that is determined from the mean transit time within each compartment. The dissolution of solid drug particles is described by a modified version of the Noyes-Whitney equation (the option to account for particle size distributions was included in version 5.1.0), and the absorption from the intestinal lumen is described by an absorption constant. In GastroPlus™, the absorption constant is calculated as a function of the human effective permeability (P_{eff}) and an absorption scale factor (ASF) that corrects the absorption constant for regional differences in permeability along the intestine due to differences in pH (affecting the ionization and hence permeability of some drug molecules), absorption surface area, and epithelial integrity. In the default mode, the ASF's are automatically computed as a function of input P_{eff} values, pH in the different compartments, and log D ([1]; GastroPlus™ 5.0 user manual). In GastroPlus™, every compartment is assigned a certain mean transit time, pH, and volume available for dissolution. The software suggests default values for

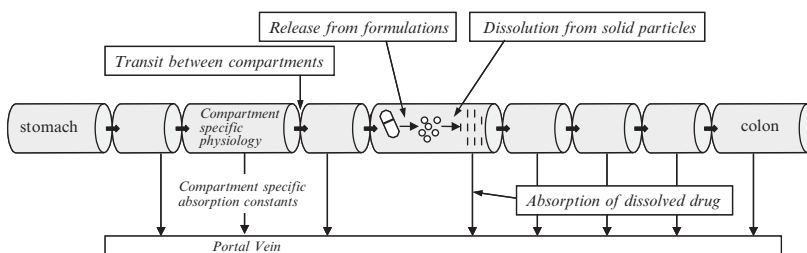


Figure 21.3 Schematic representation of the absorption processes modelled in GastroPlus™.

several species but the user can also define the values. In the default modes, the models in GastroPlus™ include one (Human-Equal Transit Time model) or two (Human-Physiological model) colonic compartments with large fluid volumes present for drug dissolution and long mean transit times available for absorption. As the physiology (pH, fluid volume, etc) is changing when going from the proximal to the distal colon, the use of only one or two colon compartments is a limitation when simulating drug absorption from the colon. This will mostly provide an issue when predicting the absorption from controlled release formulations or when predicting the absorption of poorly soluble drugs given at a high dose.

21.3.4.3. The iDEA™ Model

The iDEA™ model is a physiologically based model developed at Lion Biosciences (LION Biosciences, Heidelberg, Germany). The model is based on the work of Grass [19] but many of the model features are not published in detail. Grass [19] used the simulation software tool STELLA® (Structural Thinking Experimental Learning Laboratory with Animation) to build a simulation model that combines a model for the drug transit through the GI tract with a model for the flux of drug from the GI tract to the portal vein. The GI tract is divided into different compartments with different tissue areas, as depicted from literature, and different pH. The drug flux from the different compartments is described as a function of permeability, solubility, and intestinal surface area. The model mimics drug transit (intestinal fluid flow) by allowing fluid to reside in more than one compartment at a given time and hence the drug molecules will be spread over the intestine during its transit through the GI tract. The amount of drug absorbed is calculated by summing the drug flux in each compartment to give a total absorption rate that is divided with the total time of the simulation. From the work that has been published (e.g., [19, 39, 46]) it is not obvious how iDEA™ handles drug dissolution but it seems as if dissolution rate is not considered as a limiting factor as no input on particle size, particle density, or diffusivity is required in the model [41, 46].

21.3.4.4. The GI-Transit Absorption (GITA) Model

Another compartmental transit and absorption model, the GITA model, has been described by Sawamoto et al. [44] and reviewed by Kimura and Higaki [30]. In this model the GI tract is divided into eight different well-stirred compartments and similarly to the CAT model presented by Yu et al. ([60], [63]), the transit of drug is described by a first-order transit rate constant (K_i for the intestine and K_s for the stomach). The absorption in each segment is assumed to be a first-order process described by an absorption rate constant (K_a). The amounts of compound in the different compartments are described by Eq. 18 for the stomach (X_s) and Eq. 19 for the intestinal compartments (X_{i+1}) [44].

$$\frac{dX_s}{dt} = -(K_s + K_{a_s})X_s \quad (18)$$

$$\frac{dX_{i+1}}{dt} = X_i K_i - (K_{i+1} + K_{a_{i+1}})X_{i+1} \quad (19)$$

where K is the transit rate constant and K_a is the absorption rate constant (subscript s for stomach and i for intestine). The transit rate constants for rat was estimated from in vivo studies using phenol red as an unabsorbable marker and

the absorption rate constants for the different segments were measured using an in situ closed-loop method. Using this model, coupled to a pharmacokinetic model, Sawamoto et al. [44] could predict the plasma concentration profiles of several drugs administered as oral solutions. A four compartment model was later used to describe the GI transit in humans and using that model the human plasma concentrations of theophylline after oral administration of aminophylline could be reasonably well simulated [21].

21.3.5. Other Models (PK-MapTM/PK-Sim[®])

Willman et al. [53, 54] developed a physiological model simulating the GI flow and absorption of drugs. Different to the compartmental models, the GI tract is modeled as a single tube with changing properties along the length of the tube. The drug flow is described as a continuous plug flow with a longitudinal spreading around the median location. Based on rat physiological parameters collected from the literature, Willman et al. [53] described the intestine as a tube with changing radius and effective surface area. A transit function (T_{SI}) was used to describe the gastric emptying from the stomach and the subsequent movement of drug through the intestine. The transit function was derived on the basis of the experimentally determined transit in rat [44]. Using the transit function, the concentration in the intestinal lumen is calculated by Eq. 20 [53]

$$C_{\text{lumen}}(z, t) = \frac{\text{total dose}(1 - F_{\text{abs}}(t))}{\pi r^2(z)L} T_{SI}(z, t) \quad (20)$$

where, F_{abs} denotes the fraction of dose that has already been absorbed, $r(z)$ denotes the intestinal radius in the intestine at distance z from the stomach, and L is the length of the intestine. In the model it is assumed that dissolution occurs instantaneously but the solubility in the intestinal fluids can limit the luminal concentration of drug, and it is assumed that if the calculated luminal concentration is above the saturation solubility of the compound then the luminal concentration is set to equal the saturation solubility of the drug. The amount of drug that is absorbed (M) will depend on the permeability of the compound, the concentration in the lumen (assuming sink conditions), and the effective surface area present for absorption. This can be expressed for a region (z to $z + 1$) in a given time interval (t to $t + 1$) as given by Eq. 21 [53]

$$\frac{d^2 M(z, t)}{dz dt} = P_{\text{eff}} C_{\text{lumen}}(z, t) \frac{dA_{\text{eff}}(z)}{dz} \quad (21)$$

where P_{eff} is the effective permeability coefficient and $A_{\text{eff}}(z)$ is the effective intestinal area at position z . Integrating this expression with respect to time or position in the intestine will give the F_{abs} as a function of either time or position in the intestine as shown in Eq. 22 [53].

$$F_{\text{abs}} = \int_{t=0}^{\infty} \int_{z=0}^L \frac{d^2 M(z, t)}{dz dt} dz dt / \text{total dose} \quad (22)$$

Using literature data on human physiology and transit patterns, Willman et al. [54] adjusted the described model to account for human physiology. There are two commercially available in silico simulation software packages,

PK-Map™ and PK-Sim® (Bayer Technology Services, Wuppertal, Germany), that are based on the models described by Willman et al. [54]. In these software packages, the intestinal permeability coefficient can be calculated using a compound's lipophilicity and molecular weight [52,54] and hence, no experimental permeability data is needed. Different to the model described by Willman et al. [54], the commercial prediction tools model the dissolution rate taking the particle size distribution of the solid particles into account (www.pk-sim.com).

21.4. The Use and Validation of Physiologically Based Simulation Models

21.4.1. How Predictive are the Models?

As described earlier, absorption from the GI tract is a complex process that depends on several physiological and physicochemical properties. In the early drug discovery process it is very valuable to be able to identify a potential risk for poor absorption based only on a limited set of in vitro data. Based on the work of Johnson and Swindell [29], Curatolo [11] suggested the use of the MAD approach as a means to combine the aspects of permeability, solubility, and GI transit time in order to evaluate absorption properties of drugs. The concept is used widely within the industry and is often used as a way to confirm that the physicochemical properties of a drug candidate are within an acceptable range [34]. Hilgers et al. [23] used the MAD concept to predict the F_{abs} of 27 oxazolindiones in rat and compared the results with estimated F_{abs} data obtained after oral administration of the drugs. In their work, they showed that the predicted F_{abs} using this approach correlated better with the in vivo data compared to only using measured Caco-2 permeabilities. Hilgers et al. [23] noted a tendency for the MAD concept to underpredict the absorption of poorly soluble compounds and this was supported by results presented by Sun et al. [47] and Willman et al. [54] who showed that the MAD approach, suggested by Curatolo [11], gives lower predicted MAD values compared to other models. All in all, the MAD approach can be an effective tool to rank compounds based on their potential absorption properties early in the drug discovery process, before therapeutic doses are known. The model is, however, simple and does not consider dissolution rate as a limiting factor for absorption. For more thorough absorption evaluations, more complex multiparameter models are needed.

Although several physiologically based mathematical models designed to predict absorption properties have been available for several years (see Sect. 21.3), there is still only a limited number of studies describing their evaluation with respect to their ability to predict human F_{abs} and the relevance of how the input data (e.g., solubility and permeability) is generated in the drug discovery process.

The commercially available CAT model, iDEA™ (see Sect. 21.3.4.3) has been evaluated in a few studies. In one study [20], Roche Ltd. Supplied eight compounds without any supplemented data. In vitro permeability (using Caco-2 cell monolayers) and solubility values were generated and the human F_{abs} were predicted and compared to clinical data. In this study, the predicted

F_{abs} values compared very well with the observed F_{abs} data. In another study, Norris et al. [39] tested iDEATM for its ability to correctly predict the F_{abs} for 12 different compounds. A good correlation factor was found ($r^2 = 0.92$), but the compounds were gathered in two clusters, one with high absorption and one with poor absorption. In their study, Norris et al. [39] also showed evidence that iDEATM could predict the dose-dependent absorption of gancliclovir in both dogs and humans. Stoner et al. [46], used iDEATM in combination with in vitro data on metabolic clearance to predict the rat bioavailability of 140 drugs with wide distribution in physicochemical properties (solubility and permeability). Using this approach, they showed that they could differentiate between good (>30%) and bad (<30%) bioavailability with a reasonable degree of confidence. However, as the bioavailability was predicted from a combination of predicted F_{abs} using iDEATM and estimated first pass metabolism from in vitro clearance measurements, it is not straightforward to evaluate the performance of the F_{abs} predictions.

Parrott and Lavé [41] compared the performances of two different commercially available software packages, that is, iDEATM and GastroPlusTM (see Sect. 21.3.4), with the respect to their ability to predict the human F_{abs} for a set of 28 drugs. The drugs were selected to cover a large range of physicochemical properties (solubility 5 to $> 1 \times 10^6 \mu\text{g/mL}$, Caco-2 permeability, 0.2 to $> 60 \times 10^{-6} \text{ cm/s}$). They used three different approaches for inputting solubility and permeability data, that is i) pure in silico input for solubility and permeability, ii) measured solubility but in silico calculated permeability, iii) measured solubility and measured permeability using Caco-2 cell monolayers. The two models require slightly different input data but to make a fair comparison between the two models, efforts were made to ensure that identical input data was used as far as possible. The results were evaluated by both comparative plots between predicted and observed human F_{abs} and by categorizing the compounds as highly (>66%), medium ($33\% < F_{\text{abs}} < 66\%$), or poorly (<33%) absorbed. When basing the simulations on purely in silico calculated input values or on in silico calculated permeability but measured solubility, the performances were similar for the two models. Both models could categorize about 70% of the compounds in the right absorption category although the predicted F_{abs} versus observed F_{abs} plots appeared quite scattered. If permeability as determined using Caco-2 cell monolayers were used, the picture was slightly different. iDEATM then categorized 78% in the right class but the result using GastroPlusTM was unaffected. This difference can possibly be explained by the fact that for GastroPlusTM, the Caco-2 permeabilities had to be translated to human effective permeabilities using an established correlation, whereas iDEATM is trained to use Caco-2 permeabilities directly as input data. The extra step of translating the permeabilities when using GastroPlusTM introduces an additional source of error [41]. In the study, none of the compounds assessed seemed to show dissolution rate-limited absorption. As no drug surface area input is required for the iDEATM simulations, such limitations would not be possible to evaluate. On the contrary, GastroPlusTM uses the dose and particle size input to calculate dissolution and hence dissolution rate-limited absorption would be possible to evaluate using GastroPlusTM.

In a limited independent evaluation of GastroPlusTM, Hendriksen et al. [22] used literature data on solubility together with calculated human permeability values to predict the human F_{abs} for 21 drugs for which observed human F_{abs}

values could be found in the literature. The over all correlation between predicted and observed F_{abs} was low ($r^2 = 0.44$) but if only passively transported compounds were assessed, the correlation was much better ($r^2 = 0.8$). As the permeability was predicted using an in silico approach, active transport was not accounted for and compounds that are substrates to an efflux mechanism were underpredicted.

In a recent study, Johansson et al. [27] assessed three different in silico models for the prediction of human F_{abs} that is GastroPlusTM, Intellipharm[®]PK and the microscopic mass balance model described by Oh et al. ([40]). In this study, 46 drugs with a large range of observed human F_{abs} as well as a large range of permeability (Caco-2 P_{app} , 0.04 to 42×10^{-6} cm/s) and solubility values (1 to > 5000 $\mu\text{g/mL}$) were selected from the literature. The Caco-2 permeabilities were measured for all compounds and human effective permeability values were estimated using a preestablished correlation between Caco-2 permeability and human jejunum permeability. In order to assess the importance of the media used for the solubility measurements, Johansson et al. [27] used buffers, simulated GI fluid (FaSSIF), and real human GI fluids for the solubility experiments. The human F_{abs} were predicted using all models with the solubility in buffer, simulated GI media, or true GI fluids as solubility input. The study showed that the use of all models resulted in reasonable correlations between predicted and observed human F_{abs} for passively transported drugs ($r^2 \approx 0.7\text{--}0.8$) but that slightly poorer correlations were observed when drugs with significant levels of active transport (efflux or influx) were introduced. As the Caco-2 permeability was measured at a low drug concentration (10 μM) and active transport mechanisms might be saturated at higher concentrations, it is not surprising that some of the substrates to efflux mechanisms were underpredicted whereas other substrates to active influx mechanisms were overpredicted. Johansson et al. [27] could not detect any significant differences in the F_{abs} predictions associated with the use of different media for the generation of solubility inputs. However, the use of simulated GI fluids (FaSSIF) showed a tendency to result in higher solubility values compared to human intestinal fluids and the use of buffers resulted in the opposite situation.

The physiologically based model developed by Willman et al. [53, 54], for the prediction of both rat and human F_{abs} , was shown to be predictive for the human situation if passively transported compounds were studied. In their study, they used a semiempirical formula for the prediction of human permeability trained with a set of 119 passively transported drugs that did not show solubility or dissolution rate-limited absorption.

Moreover, several studies are published where the absorption properties of occasional compounds have been correctly predicted. However, such studies will not be discussed here as they do not act as independent evaluations of the performances of the different models.

21.4.2. Situations Where Less Accurate Predictions Can Be Encountered

Irrespective of the model used to predict the human F_{abs} , there are situations where less accurate predictions can be expected. This could be due to either variability or error in the input data or due to more fundamental problems in the understanding of drug behavior.

For all models described in this chapter, an input on permeability is needed to calculate the flux across the intestinal epithelium. In iDEA™ a Caco-2 permeability is required, but for most of the models a human effective permeability coefficient (P_{eff}) or a human absorption constant (K_a) is needed. The iDEA™ software package is trained with Caco-2 permeability data generated at one single lab and as it is well-known that the interlab variability is high [3], a correlation might need to be established with the Caco-2 cell batch used, which can introduce an additional source of error. As described above, most other models (e.g., GastroPlus™ and the mass balance models) require a human effective permeability (P_{eff}). Human P_{eff} values can be generated using perfusion techniques [32] but this is not practically possible early in the drug discovery process. A way around this problem is to use in vitro (e.g., Caco-2 cell monolayers) or in situ techniques (e.g., perfused rat intestine) to obtain permeability values and then convert them into human P_{eff} values via preestablished correlations. There are a few reports on correlations between human P_{eff} values and Caco-2 permeability coefficients (P_{app}) (e.g., [47]), rat effective permeabilities (e.g., [16]), and permeability coefficients obtained using intestinal rat tissue mounted in Ussing chambers [33]. However, as the variability on reported human P_{eff} is large (e.g., [55]), this will introduce uncertainties in the conversions between the different permeability coefficients. Intellipharm®PK uses human absorption constants as permeability inputs and these can be obtained from the estimated P_{eff} (via the expression: $k_a = 2P_{\text{eff}}/\text{intestinal radius}$, [47]).

An alternative way of using some in silico models (e.g., GastroPlus™) is to fit or optimize a permeability value using a plasma concentration versus time profile obtained after dosing a solution or a suspension (in the case of a highly soluble compound). If all other pharmacokinetic inputs are available, in order to describe the distribution and elimination phases, the only remaining unknown needed to fit the profile is the P_{eff} value. The operator can choose a random permeability value in the first instance and then change the value accordingly to fit the slope of the absorption phase of the profile. This optimized P_{eff} value can then be used in subsequent predictions, for example, if predicting what happens when a suspension (at a different dose) or a solid dosage form is dosed.

The in vivo permeability for a compound that is a substrate to an active efflux or influx mechanism can be expected to vary with the drug concentration in the intestine, and using an in vitro determined permeability value measured at one drug concentration might give a misleading result. It is also possible that the expression of the active transport mechanisms might vary between different models making it difficult to predict the in vivo relevance of obtained in vitro data. All in all, these uncertainties have to be considered when predicting the human F_{abs} for drugs with a low permeability or where active transport mechanisms are suspected.

The main input parameter used to define the highest possible drug concentration in the intestine and to calculate the dissolution rate in the GI tract is the solubility of the drug in the GI fluids. As described earlier (Sect. 21.2) there are several, both physiological and physicochemical, factors that can affect the solubility in the GI tract and it is therefore important to consider the relevance of the solubility data generated in the early drug discovery phase. A common approach is to use in silico models to predict the solubility of drugs (e.g., [5]). The advantage of this approach is that only the chemical

structure of the drug molecule is needed and the main disadvantage is that the effect of the solid state on the solubility is most often neglected in these models [5]. If using solubility data obtained from in vitro experiments, the influence of the dissolution media used has to be considered. Water and simple buffers often underpredict the GI solubility of poorly soluble compounds due to the lack of surfactants (bile acids and lipids) present in the human intestinal fluids. As true human GI fluids are not easily collected there is a drive to develop simulated GI fluids that mimic the important features of true human GI fluids, and hence could be used to generate relevant drug solubility data. As a result of this, several different simulated GI media have been suggested in the literature (e.g., [17, 35, 36,49]). Johansson et al. [27] suggested that the fasted state simulated small intestinal fluids (FaSSIF), described by Galia et al. [17], could potentially overpredict the GI solubility of poorly soluble compound and that simple buffers could potentially underpredict the GI solubility of the same drugs. Johansson et al. [27] could, however, not show an effect on the predicted human F_{abs} (using GastroPlusTM, Intellipharm[®]PK, and a microscopic mass balance model) in the compound set studied. Moreover, the solubility in GI fluids of many poorly soluble drugs will also often be different in the fed compared to the fasted states (e.g., [43]).

As described earlier, most of the physiologically based absorption simulation models use versions of the Noyes-Whitney equation to calculate the in vivo dissolution rate of compounds dosed as suspensions or solid dosage forms. This will result in a linear relationship between the measured saturation solubility and the calculated dissolution rate (assuming sink conditions). As several poorly soluble compounds show significantly higher solubility in GI fluids compared to buffers due to the presence of bile acids and lipids, the use of solubility values generated in real GI fluids will also result in proportionally faster calculated dissolution rates. However, studies, using both simulated and true GI fluids, have shown that the increased solubility seen in the presence of bile acids and lipids is not always reflected in a concomitant increase in dissolution rate [43]. Furthermore, it has been shown that the addition of surfactants to dissolution media may increase the solubility more than the dissolution rate [4,18]. This was attributed to the fact that the lower diffusivity of drug-loaded surfactant micelles compared to free drug counteract the effect of increased solubility on the over all dissolution rate. As the increased solubility seen for poorly soluble compounds in GI fluids is due to solubilization by mixed micelles containing bile acids and lipids, an effect of lowered diffusivity on the in vivo dissolution rate could be expected. This suggests that the Noyes-Whitney equation might overpredict the dissolution rate for poorly soluble compounds if the saturation solubility in real GI fluids is used as simulation input. As stated by Persson et al. [43], the Noyes-Whitney equation might need to be modified when more complex, surfactant containing, media is used.

All in all, it is important to understand the relevance of how solubility data has been generated and care should be taken when predicting the human F_{abs} of drugs with a low aqueous solubility.

In silico models should also be used with care when it comes to predicting the absorption properties of salts and bases with low solubility in the intestinal fluids. All models use the thermodynamic solubility to calculate the dissolution rate and the saturation solubility in the different parts in the GI tract. However,

salts are often not stable in the full physiological pH range and hence, the intestinal concentration of a compound administered as a salt might vary with time, with high transient concentrations, followed by lower concentrations due to precipitation of the free acid or base form. Precipitation is not easily predicted in vitro and might vary with experimental conditions such as agitation rate, particle size, and volume of the dissolution media. Weak bases might have a high solubility in the gastric environment but a much lower solubility in the more neutral pH found in the intestines. As a result, bases can be supersaturated in the upper intestines for a period of time before precipitating out, resulting in lower concentrations. The extent and time for such a supersaturation is not easily predicted and using the intestinal solubility as simulation input data might represent the worst-case scenario. In some cases the precipitation rate can vary between subjects due to physiological differences (e.g., transit time, pH, and volume) and this can cause variability in absorption. Prediction of variability in absorption across a population has received little attention but can cause development hurdles such as low absorption in population subgroups and risk for bioequivalence failure.

Some, but not all models described attempt to model colon absorption (e.g., GastroPlusTM). Colon absorption can have a large impact on the MAD and F_{abs} for poorly soluble compounds with a high permeability in the colon. For drugs with a low intestinal permeability, colon absorption is probably less important as such drugs have been suggested to have even lower permeability in the colon [48]. More work is needed to increase the understanding of the factors affecting colon absorption and to update existing physiologically based absorption models accordingly. This will be especially important for the prediction of the absorption behavior of poorly soluble drugs, and drugs delivered as modified release formulations.

21.5. Summary

Physiologically based in silico models for the prediction of human absorption properties of orally administered drugs can be most useful, both in the early drug discovery process and in the development of drug candidates. There are literature data to support that several of the published models, for example, GastroPlusTM, Intellipharm[®]PK, iDEATM, the mass balance models etc, can be used to predict the human fraction dose absorbed of orally administered drugs with a reasonable degree of confidence (e.g., [20]; [22]; [27, 41]). Although good correlations have been shown between predicted and observed human F_{abs} for passively transported compounds, slightly poorer correlations are normally obtained when drugs with significant levels of efflux or active transport are introduced ([22]; [27]).

The results obtained when using these in silico models depend to a large extent on the quality and relevance of the input data used. Both permeability and solubility data needs to be generated in such a way that the data reflects the in vivo situation as much as possible.

From the above we conclude that in silico absorption models are very useful tools in assessing the development potential of compounds in the drug discovery process, and their use in discovery projects could help to reduce the attrition rate due to poor pharmacokinetic properties in later phases. The

models are also useful for highlighting the potential need for solubilized drug delivery approaches during the development phase. Also in many cases there is the potential to reduce the prescriptive use of animal models in the assessment of drug absorption.

References

1. Agoram B, Woltosz WS, Bolger MB (2001) Predicting the impact of physiological and biochemical processes on oral drug bioavailability. *Adv. Drug Deliv. Rev.* 50:41–67.
2. Artursson P, Karlsson J (1991) Correlation between oral drug absorption in humans and apparent drug permeability coefficients in human intestinal epithelial (Caco-2) cells. *J. Biochem. Biophys. Res. Commun.* 175:880–885.
3. Artursson P, Palm K, Luthman K (1996) Caco-2 monolayers in experimental and theoretical predictions of drug transport. *Adv. Drug Deliv. Rev.* 22:67–84.
4. Balakrishnan A, Rege BG, Amidon GL, Polli JE (2004) Surfactant-mediated dissolution: Contribution of solubility enhancement and relatively low micelle diffusivity. *J. Pharm. Sci.* 93:2064–2075.
5. Bergström CSA (2004) In silico predictions of drug solubility and permeability: Two rate-limiting barriers to oral drug absorption. *Basic Clin. Pharmacol. Toxicol.* 96:156–161.
6. Burton PS, Goodwin JT, Vidar TJ, Amore BM (2002) Predicting drug absorption: How nature made it a difficult problem. *J. Pharm. Exp. Ther.* 303:889–895.
7. Chiou WL, Barve A (1998) Linear correlation of the fraction of oral dose absorbed of 64 drugs between humans and rats. *Pharm. Res.* 15:1792–1795.
8. Chiou WL, Buehler PW (2002) Comparison of oral absorption and bioavailability of drugs between monkey and human. *Pharm. Res.* 19:868–874.
9. Chiou WL, Jeong HY, Chung SM, Wu TC (2000) Evaluation of using dog as animal model to study the fraction of oral dose absorbed of 43 drugs in humans. *Pharm. Res.* 17:135–140.
10. Chiou WL, Ma C, Chung SM, Wu TC, Jeong HY (2000) Similarity in the linear and non-linear oral absorption of drugs between human and rat. *Int. J. Clin. Pharmacol. Therap.* 38:532–539.
11. Curatolo W (1998) Physical chemical properties of oral drug candidates in the discovery and exploratory development settings. *Pharm. Sci. Tech. Today* 1:387–393.
12. Dressman JB, Amidon GL, Fleicher D (1985) Absorption potential: Estimating the fraction absorbed for orally administered compounds. *J. Pharm. Sci.* 74:588–589.
13. Dressman JB, Amidon GL, Reppas C, Shah VP (1998) Dissolution testing as a prognostic tool for oral drug absorption: Immediate release dosage form. *Pharm. Res.* 15:11–21.
14. Dressman JB, Fleicher D (1986) Mixing-tank model for predicting dissolution rate control of oral absorption. *J. Pharm. Sci.* 75:109–116.
15. Eddershaw PJ, Beresford AP, Bayliss MK (2000) ADME/PK as part of a rational approach to drug discovery. *Drug Discov. Today* 5:409–414.
16. Fagerholm U, Johansson M, Lennernäs H (1996) Comparison between permeability coefficients in rat and human jejunum. *Pharm. Res.* 13:1336–1342.
17. Galia E, Nicolaidis E, Hörter D, Löbenberg R, Reppas C, Dressman JB (1998) Evaluation of various dissolution media for predicting in vivo performance of class I and II drugs. *Pharm. Res.* 15:698–705.

18. Granero GE, Ramachandran C, Amidon GL (2005) Dissolution and solubility behavior of fenofibrate in sodium lauryl sulfate solutions. *Drug Dev. Ind. Pharm.* 31:917–922.
19. Grass GM (1997) Simulation models to predict oral drug absorption from in vitro data. *Adv. Drug Deliv. Rev.* 23:199–219.
20. Grass GM, Sinko PJ (2002) Physiologically-based pharmacokinetic simulation modelling. *Adv. Drug Deliv. Rev.* 54:433–451.
21. Haruta S, Kawai K, Nishii R, Jinnouchi S, Ogawara K-I, Higaki K, Tamura S, Arimori K, Kimura T (2002) Prediction of plasma concentration-time curve of orally administered theophylline based on scintigraphic monitoring of gastrointestinal transit in human volunteers. *Int. J. Pharm.* 233:179–190.
22. Hendriksen BA, Sanchez Felix MV, Bolger MB (2003) The composite solubility versus pH profile and its role in intestinal absorption prediction. *AAPS PharmSci.* 5:35–49.
23. Hilgers AR, Smith DP, Biermacher JJ, Day JS, Jensen JL, Sims SM, Adams WJ, Friis JM, Palandra J, Hosley JD, Shobe EM, Burton PS (2003) Predicting oral absorption of drugs: A case study with a novel class of antimicrobial agents. *Pharm. Res.* 20:1149–1155.
24. Hintz RJ, Johnson KC (1989) The effect of particle size distribution on dissolution rate and oral absorption. *Int. J. Pharm.* 51:9–17.
25. Huang L-F, Tong W-Q (2004) Impact of solid state properties on developability assessment of drug candidates. *Adv. Drug Deliv. Rev.* 56:321–334.
26. Hörter D, Dressman JB (1997) Influence of physiological properties on dissolution of drugs in the gastrointestinal tract. *Adv. Drug Deliv. Rev.* 25:3–14.
27. Johansson F, Patterson R, Arvidsson PO, Moore V, Grant I, Bäckman P (2005) Prediction of human oral absorption using multi-parameter *in silico* models. *AAPS J.* 17: Abstract M1158.
28. Johnson KC (2003) Dissolution and absorption modeling: Model expansion to simulate the effect of precipitation, water absorption, longitudinally changing intestinal permeability, and controlled release on drug absorption. *Drug Dev. Ind. Pharm.* 29:833–842.
29. Johnson KC, Swindell AC (1996) Guidance in the setting of drug particle size specifications to minimize variability in absorption. *Pharm. Res.* 13:1795–1798.
30. Kimura T, Higaki K (2002) Gastrointestinal transit and drug absorption. *Biol. Pharm. Bull.* 25:149–164.
31. Klopman G, Stefan LR, Saiakhov RD (2002) ADME evaluation 2. A computer model for the prediction of intestinal absorption in humans. *Eur. J. Pharm. Sci.* 17:253–263.
32. Lennernäs H (1997) Human intestinal permeability. *J. Pharm. Sci.* 87:403–410.
33. Lennernäs H, Nylander S, Ungell A-L (1997) Jejunal permeability: A comparison between the Ussing chamber technique and the single perfusion in humans. *Pharm. Res.* 14:667–671.
34. Lipinski CA (2000) Drug-like properties and the causes of poor solubility and poor permeability. *J. Pharmacol. Toxicol. Methods* 44:235–249.
35. Lomstein Pedersen B, Brondstedt H, Lennernäs H, Norring Christensen F, Mullertz A, Gjelstrup Kristensen H (2000) Dissolution of Hydrocortisone in human and simulated intestinal fluids. *Pharm. Res.* 17:183–189.
36. Lomstein Pedersen B, Mullertz A, Brondstedt H, Gjelstrup Kristensen H (2000) A comparison of the solubility of danazol in human and simulated gastrointestinal fluids. *Pharm. Res.* 17:891–894.
37. Lu ATK, Frisella ME, Johnson KC (1993) Dissolution modeling: Factors affecting the dissolution rates of polydisperse powders. *Pharm. Res.* 10:1308–1314.

38. Martinez MN, Amidon GL (2002) A mechanistic approach to understanding the factors affecting drug absorption: A review of fundamentals. *J. Clin. Pharmacol.* 42:620–643.
39. Norris DA, Leesman GD, Sinko PJ, Grass GM (2000) Development of predictive pharmacokinetic simulation models for drug discovery. *J. Control. Release* 65:55–62.
40. Oh DM, Curl RL, Amidon GL (1993) Estimating the fraction dose absorbed from suspensions of poorly soluble compounds in humans: A mathematical model. *Pharm. Res.* 10:264–270.
41. Parrot N, Lavé T (2002) Prediction of intestinal absorption: comparative assessment of GastroplusTM and iDEATM. *Eur. J. Pharm. Sci.* 17:51–61.
42. Prentis RA, Lis Y, Walker SR (1988) Pharmaceutical innovation by seven U.K.-owned pharmaceutical companies (1964–1985). *J. Pharm. Sci.* 25:387–396.
43. Persson EM, Gustafsson A-S, Carlsson AS, Nilsson RG, Knutson L, Forsell P, Hanisch G, Lennernäs H, Abrahamsson B (2005) The effect of food on the dissolution of poorly soluble drugs in human and model small intestinal fluids. *Pharm. Res.* 22:2141–2151.
44. Sawamoto T, Haruta S, Kurosaki Y, Higaki K, Kimura T (1997) Prediction of the plasma concentration profiles of orally administered drugs in rat on the basis of gastrointestinal transit kinetics and absorbability. *J. Pharm. Pharmacol.* 49:450–457.
45. Sinko PJ, Leesman GD, Amidon GL (1991) Predicting fraction dose absorbed in humans using a macroscopic mass balance approach. *Pharm. Res.* 8:979–998.
46. Stoner CL, Cleton A, Johnson K, Oh D-M, Hallak H, Brodfuehrer J, Surendran N, Han H-K (2004) Integrated oral bioavailability projection using in vitro screening data as a selection tool in drug discovery. *Int. J. Pharm.* 269:241–249.
47. Sun D, Lawrence XY, Hussain MA, Wall DA, Smith RL, Amidon GL (2004) In vitro testing of drug absorption for drug developability assessment: Forming an interface between in vitro preclinical data and clinical outcome. *Curr. Opin. Drug Discov. Dev.* 7:75–85.
48. Ungell A-L, Nylander S, Bergstrand S, Sjöberg Å, Lennernäs H (1997) Membrane transport of drugs in different regions of the intestinal tract of the rat. *J. Pharm. Sci.* 87:360–366.
49. Vertzoni M, Fotaki N, Kostewicz E, Stippler E, Leuner C, Nicolaidis E, Dressman J, Reppas C (2004) Dissolution media simulating the intraluminal composition of the small intestine: Physiological issues and practical aspects. *J. Pharm. Pharmacol.* 56:453–462.
50. Votano JR (2005) Recent uses of topological indices in the development of *in silico* ADMET models. *Curr. Opin. Drug Discovery Dev.* 8:32–37.
51. Wagner D, Spahn-Langguth H, Hanafly A, Koggel A, Langguth P (2001) Intestinal drug efflux: Formulation and food effects. *Adv. Drug. Deliv. Rev.* 50:13–31.
52. Willman S, Lippert J, Schmitt W (2005) From physicochemistry to absorption and distribution: Predictive mechanistic modelling and computational tools. *Expert Opin. Drug Metab. Toxicol.* 1:159–168.
53. Willman S, Schmitt W, Keldenich J, Dressman JB (2003) A physiologic model for simulating gastrointestinal flow and drug absorption in rats. *Pharm. Res.* 20:1766–1771.
54. Willman S, Schmitt W, Keldenich J, Lippert J, Dressman JB (2004) A Physiological model for the estimation of the fraction dose absorbed in humans. *J. Med. Chem.* 47:4022–4031.
55. Winiwarter S, Bonham NM, Ax F, Hallberg A, Lennernäs H, Karlén A (1998) Correlation of human jejunal permeability (in vivo) of drugs with experimentally and theoretically derived parameters. A multivariate data approach. *J. Med. Chem.* 41:4939–4949.

56. Yazdanian M, Glynn SL, Wright JL, Hawi A (1998) Correlating partitioning and Caco-2 cell permeability of structurally diverse small molecular weight compounds. *Pharm. Res.* 15:1490–1494.
57. Yu LX (1999) An integrated model for determining causes of poor oral drug absorption. *Pharm. Res.* 16:1883–1887.
58. Yu LX, Amidon GL (1998) Characterization of small intestinal transit time distribution in humans. *Int. J. Pharm.* 171:157–163.
59. Yu LX, Amidon GL (1998) Saturable small intestinal drug absorption in humans: Modeling and interpretation of cefatrizine data. *Eur. J. Pharm. Sci.* 45:199–203.
60. Yu LX, Amidon GL (1999) A compartmental absorption and transit model for estimating oral drug absorption. *Int. J. Pharm.* 186:119–125.
61. Yu LX, Crison JR, Amidon GL (1996) Compartmental transit and dispersion model analysis of small intestinal transit flow in humans. *Int. J. Pharm.* 140:111–118.
62. Yu LX, Gatlin L, Amidon G (2000) Predicting oral drug absorption in humans. In Amidon GL, Lee PI, Topp EM (ed.) *Transport processes in pharmaceutical systems*. Marcel Dekker, New York, pp 377–409.
63. Yu LX, Lipka E, Crison JR, Amidon GL (1996) Transport approaches to the biopharmaceutical design of oral drug delivery systems. Prediction of intestinal absorption. *Adv. Drug Deliv. Rev.* 19:359–376.
64. Zhao YH, Abraham MH, Le J, Hersey A, Eddershaw PJ, Luscombe CN, Boutina D, Beck G, Sherborne B, Cooper I (2001) Evaluation of human intestinal absorption data and subsequent derivation of quantitative structure activity relationship (QSAR) with the Abraham descriptors. *J. Pharm. Sci.* 90:749–784.
65. Zhao YH, Abraham MH, Le J, Hersey A, Luscombe CN, Beck G, Sherborne B, Cooper I (2002) Rate-limited steps of human oral absorption and QSAR studies. *Pharm. Res.* 19:1446–1457.
66. Zhao YH, Abraham MH, Le J, Hersey A, Luscombe CN, Beck G, Sherborne B, Cooper I (2003) Evaluation of rat intestinal absorption data and correlation with human intestinal absorption. *Eur. J. Med. Chem.* 38:233–243.

22

In Silico Modeling for Blood–Brain Barrier Permeability Predictions

Prabha Garg, Jitender Verma, and Nilanjan Roy

Abstract The blood–brain barrier (BBB) is the single most important factor hindering the development of neurotherapeutics. Experimental methods of BBB permeation determination are cumbersome and expensive; thus, *in silico* methods for BBB permeation prediction gained momentum in recent past. Most of the approaches seem to achieve >80% accuracy in prediction as well as gained insights into the molecular determinants of passive BBB permeation. However, none of the methods account for the role of active transport and efflux systems, predominantly because of lack of experimental data. Accuracy and predictability of *in silico* modeling can be increased further by incorporating the data emerging from the noninvasive methods of measuring the distribution of compounds within the brain.

Keywords: Blood–brain permeability prediction; Artificial neural network; QSAR

Abbreviations

BBB	Blood–brain barrier
BNN	Bayesian neural nets
DFA	Discriminant function analysis
DPLS	Discriminant partial least square
GA	Genetic algorithm
G/PLS	Genetic partial least square
GRNN	General regression neural network
LR	Linear regression
MFNN	Multilayer feedforward neural network
MLR	Multiple linear regression
PCA	Principal component analysis
PLS	Partial least square
VSMP	Variable selection and modeling method based on the prediction

22.1. Introduction

The blood–brain barrier (BBB) is a physiological barrier in the circulatory system which is responsible for maintaining the homeostasis of the central nervous system (CNS) by separating the brain from the systemic blood circulation, and thus stopping many substances from entering into the CNS. Thus the BBB is often the rate-limiting factor in determining permeation of therapeutic drugs into the brain. It is a critical yet underdeveloped part of neurotherapeutics development and is the single most important factor limiting the future growth of neurotherapeutics. The BBB bottleneck can be illustrated by the fact that more than 98% of all small-molecule drugs and ~100% of large-molecule drugs or genes do not cross the BBB [36, 37].

There are at least two distinguishing features of the BBB that makes it a formidable barrier to the candidate CNS drug. First, in terms of its morphology, the endothelial cells of which the BBB is composed are interlinked by highly complex tight junctions, which severely limit any paracellular drug transport. Moreover, a minimal level of pinocytosis and lack of significant membrane fenestrae affords an additional obstruction to the transport of hydrophilic molecules. Second, the BBB includes a range of metabolic enzyme systems and efflux transporters that constitutes a biochemical barrier to the majority of xenobiotics [13]. This combination of physical and biochemical barriers establishes the BBB endothelium as quite distinct from the other endothelia.

The smallest molecules like oxygen, carbon dioxide, and sugars pass the barrier with no difficulty, but most of the drugs are too large to pass the barrier. Low lipid (fat) soluble as well as highly charged molecules also do not penetrate into the brain. Hypertension, hyperosmolality, exposure to radiations, microwaves, infections, and injury to the brain in the form of trauma, ischemia, inflammation, and pressure are some of the conditions or factors which increase the BBB permeability. There are several areas in the brain where the BBB is weak. These weak areas allow substances to cross into the brain somewhat freely. These areas are known as “Circumventricular Organs.” Through these organs, the brain is able to monitor the makeup of the blood. They include pineal body, posterior pituitary, area postrema, subfornical organ, median eminence, and the vascular organ of the lamina terminalis [9].

One of the biopharmaceutical properties that is of utmost significance in drug design is the ability of a molecule to penetrate the BBB. The drugs which are intended to interact with their molecular targets in the CNS must cross the BBB in order to be used as therapeutic agents. At the same time, the peripherally acting agents should not cross the BBB so as to avoid the CNS-related side effects. In both the cases the BBB permeability of the molecules must be known. The experimental determination of BBB permeability is often very difficult, time consuming, and expensive and requires a sufficient quantity of the pure compounds and hence not suitable for providing results in a high-throughput manner. Therefore, there is an increasing demand for good, reliable, and easily applicable computational tools that can rapidly predict the BBB penetration capability of molecules. Such predictive models could be of immense use in enhancing the pace of the drug discovery process particularly in the area of CNS.

22.2. In Silico Methods Published for Prediction of BBB Permeability

In silico modeling of BBB permeability started with the assumption that the majority of drugs are transported across the BBB by passive diffusion. Absence of the data regarding P-glycoprotein (P-gp)-mediated active transport as well as the limited understanding of the behavior of drugs as substrates or inhibitors of these P-gp transporters has restricted the people from generating BBB models based on active transport [42].

Various methods that have been commonly used by the researchers for model generation include the traditional statistical approaches like multiple linear regression (MLR), partial least square (PLS), linear discriminant analysis, and grid-based approaches like Volsurf [12]. BBB models have also been generated using modern artificial intelligence techniques like genetic algorithm (GA) [22] and artificial neural network (ANN) [18]. The advantage of these newer methods over the traditional ones is that they can efficiently handle the nonlinearity in the data. But sometimes they may also act as “Black Boxes” and fail to explain their decisions or results. Despite all the limiting factors, a number of attempts have been made in the last two decades to generate improved computational models for predicting the BBB permeability of molecules.

The in silico modeling of BBB permeability predictions started in 1988 when Young et al. [49] investigated the importance of lipophilicity for brain penetration using linear regression (LR) method on centrally acting histamine H₂ antagonists. They developed a model initially based upon a small data set of six compounds including three typical histamine H₂ receptor antagonists, which do not readily cross the BBB, and three brain-penetrating drugs clonidine, mepyramine, and imipramine. A good correlation was obtained between the log BB in rat and $\Delta \log P$ [defined as $\log P$ (octanol/water) – $\log P$ (cyclohexane/water)] as well as for $\log P$ in chloroform/water solution systems and $\log P_{\text{cyh}}$ but no correlation was found with $\log P$ in octanol (Eqs. 1–4).

$$\log \text{BB} = -0.604(\pm 0.169)\Delta \log P + 1.23 (\pm 0.56) \quad (1)$$

$$n = 6, r = 0.98, s = 0.249, F = 98.0$$

$$\log \text{BB} = 0.679(\pm 0.877) \log P_{\text{chl}} - 3.12(\pm 3.73) \quad (2)$$

$$n = 4, r = 0.92, s = 0.636, F = 11.08$$

$$\log \text{BB} = 0.385(\pm 0.369) \log P_{\text{cyh}} - 0.598(\pm 0.815) \quad (3)$$

$$n = 6, r = 0.824, s = 0.713, F = 8.43$$

$$\log \text{BB} = 0.15(\pm 1.295) \log P_{\text{oct}} - 0.96(\pm 4.29) \quad (4)$$

$$n = 6, r = 0.16, s = 1.241$$

The authors concluded that the BBB permeability can be increased by lowering the overall hydrogen-bonding ability of a compound, for example, facilitating intramolecular hydrogen bonding, protecting with nonpolar groups, and by making less polar prodrugs.

In the same article data set was expanded to include some 20 potent histamine H₂ antagonists. Analysis of these compounds indicated the significance of lipophilicity and hydrogen bonding for penetration of BBB, since a good

correlation was established with $\Delta \log P$ variable (Eq. 5). For the same 20 compounds, a rather less significant correlation was found with the $\log P_{\text{cyh}}$ variable (Eq. 6), while that with $\log P_{\text{oct}}$ (Eq. 7) was not significant.

$$\begin{aligned} \log \text{BB} &= -0.485(\pm 0.16) \Delta \log P + 0.889(\pm 0.5) \\ n &= 20, r = 0.831, s = 0.439, F = 40.23 \end{aligned} \quad (5)$$

$$\begin{aligned} \log \text{BB} &= 0.250(\pm 0.115) \log P_{\text{cyh}} - 0.471(\pm 0.253) \\ n &= 20, r = 0.732, s = 0.538, F = 20.74 \end{aligned} \quad (6)$$

$$\begin{aligned} \log \text{BB} &= 0.266(\pm 0.272) \log P_{\text{oct}} - 1.22(\pm 0.83) \\ n &= 20, r = 0.436, s = 0.711, F = 4.23 \end{aligned} \quad (7)$$

Authors interpreted that $\log P_{\text{cyh}}$ and $\log P_{\text{oct}}$ (both of which contribute to $\Delta \log P$) represent two different processes involved in the distribution of a compound between the blood and the brain. The former parameter reflects the partitioning process into the nonpolar regions of the brain, while the latter variable accounts for the protein binding in blood, which could limit the amount of free drug available for passage into the brain. They used this model as a reference in the design of novel brain-penetrating H_2 antagonists by the systematic structural modification of representatives of different structural types of H_2 antagonists. Although they achieved noticeable increases in brain penetration among congeners of cimetidine, ranitidine, and tiotidine, no compound was found with a satisfactory combination of H_2 antagonist activity ($-\log \text{KB}$ in the guinea pig atrium greater than 7.0) and brain penetration (steady-state brain–blood concentration ratio greater than 1.0). On the contrary, structural modification of N-[(piperidinyl-methyl) phenoxy] propyl acetamide led to several potent, novel compounds which readily cross the BBB [49].

van de Waterbeemd and Kansy [46] used the same data set of compounds used by Young et al. to further investigate the importance of hydrogen bonding to $\log \text{BB}$, and obtained a good relationship (Eq. 8) with $\log \text{BB}$ using the polarity Λ :

$$\begin{aligned} \log \text{BB} &= -0.22\Lambda_{\text{alk}} + 2.66 \\ n &= 56, r = 0.939, s = 0.431, F = 30 \end{aligned} \quad (8)$$

Where Λ was derived from experimental $\log P$ measurements in an alkane–water system (i.e., cyclohexane/water) and the computed molar volumes (Eq. 9):

$$\log P = aV_{\text{m}} + \Lambda \quad (9)$$

The authors also computed the polar parts of the van der Waals surface (Eq. 10) and the water-accessible surface (Eq. 11) using a Roche in-house program, MOLOC, and achieved relationships of similar quality to Young's model (Eq. 1):

$$\begin{aligned} \log \text{BB} &= -0.037\text{PSA} + 1.156 \\ n &= 56, r = 0.972, s = 0.294, F = 69.3 \end{aligned} \quad (10)$$

$$\begin{aligned} \log \text{BB} &= -0.025\text{PSA}_{\text{w}} + 0.945 \\ n &= 56, r = 0.952, s = 0.387, F = 38.3 \end{aligned} \quad (11)$$

where PSA is the polar van der Waals surface and PSA_w denotes the polar water-accessible surface calculated for a water molecule with a radius of 1.45 Å. On the basis of these findings, the authors concluded that the brain–blood partition coefficient, log BB, can be predicted using only calculated descriptors. This statement was supported by the close correlation between Δ_{alk} and PSA ($r = 0.97$). The correlation with PSA gave a poorer result ($r = 0.781$) for 20 compound data set. Introducing the calculated molar volume in the model gave a slightly improved equation (Eq. 12). The authors reported that replacing the molar volume with the nonpolar surface area would give an equation with similar statistics ($r = 0.845$).

$$\begin{aligned} \log BB &= -0.021 PSA - 0.003 V_m + 1.643 \\ n &= 20, r = 0.835, s = 0.448, F = 19.5 \end{aligned} \quad (12)$$

Calder and Ganellin [8] also investigated Young's data set employing the approach of Young et al. using both experimental $\Delta \log P$ values and theoretically computed parameters. To establish the latter model they used the approach originally developed by van de Waterbeemd and Kansy. Two parameters related to size (molar volume, V_m) and hydrogen bonding (hydrophilic part of van der Waals surface, SP) were computed using the Macromodel software and correlated against the blood–brain partitioning. A fair statistical model was obtained (Eq. 13):

$$\begin{aligned} \log BB &= -0.002 V_m - 0.024 SP + 1.51 \\ n &= 20, r = 0.85 \end{aligned} \quad (13)$$

However, when the authors tried to predict six new compounds that acted on the histamine H_1 or H_3 receptors, they were all overestimated by the derived models. This tendency was especially noticeable for the model based on molar volume and van der Waals surface (Eq. 13). Incorporation of the new histamine H_1 agonists into the models resulted in rather degraded statistics (Eq. 14–15):

$$\begin{aligned} \log BB &= -0.42 \Delta \log P + 0.60 \\ n &= 25, r = 0.73 \end{aligned} \quad (14)$$

$$\begin{aligned} \log BB &= 0.00075 V_m - 0.019 SP + 0.29 \\ n &= 25, r = 0.68 \end{aligned} \quad (15)$$

The authors concluded that empirical models must be used with caution when applied to other chemical structures, but that the models gave an approximate indication of likely brain penetration. It is important to note, however, that the training set was small and not diverse.

Abraham et al. [2] published a number of papers in which they analyzed Young's data set using MLR and gave a general solvation equation in which various solvent–solute interactions were described by solute descriptors and equation coefficients (Eq. 16)

$$\log SP = c + rR_2 + s\pi_2^H + a \sum \alpha_2^H + b \sum \beta_2^H + vV_x \quad (16)$$

where SP is a solubility-related property for a series of solutes in a given system, R_2 is the excess molar refraction, π_2^H the new solute dipolarity/polarizability parameter, $\sum \alpha_2^H$ the summation solute hydrogen-bond acidity, $\sum \beta_2^H$ the summation hydrogen-bond basicity, and V_x the characteristic

volume of McGowan. The parameters π_2^H , $\sum \alpha_2^H$, and $\sum \beta_2^H$ were determined from the partition coefficients $\log P_{\text{oct}}$, $\log P_{\text{cyh}}$, and $\log P_{\text{chl}}$.

Later on the authors found this approach disappointing since the resulting parameter values were many times numerically irrational [3]. Also it involves the procurement of the compounds in question and their $\log P$ determination in three different systems. To overcome this issue, they used a fragment-based approach to calculate the necessary parameters but found problems in that also since it is important to ensure the absence of specific intramolecular interactions between the fragments, which may become a serious problem in case of molecules with many functional groups or substructural moieties. After adding 10 more compounds to Young's data set and removing 8 outliers, they developed the following model with the remaining 22 compounds (Eq. 17):

$$\begin{aligned} \log \text{BB} &= 0.088 + 0.264R_2 - 0.966\pi_2^H - 0.705 \sum \alpha_2^H - 0.756 \sum \beta_2^H \\ &\quad + 1.189V_x \\ n &= 22, \quad r = 0.941, \quad s = 0.27, \quad F = 25.0 \end{aligned} \quad (17)$$

They accounted the eight strong outliers to conformational change or change in intramolecular hydrogen bonding between blood and brain phases, experimental difficulties in measuring the $\log \text{BB}$ values, and the possibility of a compound being metabolized in either phase.

The authors then extended Young's data set with 35 small organic compounds including gases also, to form Abraham's data set of 57 compounds, consisting of both drugs and nondrugs [4]. These were from the data set of Abraham and Weathersby. The analysis of the data set of Abraham and Weathersby by Eq. 18 and that of the full data set (Eq. 19) resulted in the following relationships:

$$\begin{aligned} \log \text{BB} &= -0.079 + 0.236R_2 - 0.548\pi_2^H - 0.362 \sum \alpha_2^H - 0.736 \sum \beta_2^H \\ &\quad + 0.961V_x \\ n &= 35, \quad r = 0.945, \quad s = 0.134, \quad F = 48.1 \end{aligned} \quad (18)$$

$$\begin{aligned} \log \text{BB} &= -0.038 + 0.198R_2 - 0.687\pi_2^H - 0.715 \sum \alpha_2^H - 0.698 \sum \beta_2^H \\ &\quad + 0.995V_x \\ n &= 57, \quad r = 0.952, \quad s = 0.197, \quad F = 99.2 \end{aligned} \quad (19)$$

Addition of the eight outlier molecules mentioned earlier into this model resulted in an inferior model (Eq. 20):

$$\begin{aligned} \log \text{BB} &= -0.044 + 0.223R_2 - 0.613\pi_2^H - 0.486 \sum \alpha_2^H - 0.986 \sum \beta_2^H \\ &\quad + 0.909V_x \\ n &= 65, \quad r = 0.866, \quad s = 0.397, \quad F = 36.2 \end{aligned} \quad (20)$$

Later on, the authors tested the models (17) and (19) using an external data set including five molecules from the test set of Calder and Ganellin and two SKF compounds from SmithKline Beecham. With the exception of two molecules, both the models displayed good overall predictivity. Finally, they predicted seven additional compounds from the model (19) and obtained good statistics again.

On the basis of these results, they concluded that $\log P_{\text{oct}}$ cannot be used to predict the blood–brain distribution rectilinearly, but could be combined with

Abraham's solute descriptors to yield a predictive regression equation. Further, the solute dipolarity/polarizability, hydrogen bond acidity, and hydrogen bond basicity were found to favor blood and solute size favor brain.

Realizing the significance of the fact that the partition coefficient of a solute in two immiscible phases is related to the solvation free energies of the solute in the two phases, Lombardo et al. [29] analyzed Abraham's data set with a different approach based on the calculations of solvation free energy in water (G_{W}^0) using AMSOL methodology incorporating the AM1-SM2.1 solvation model. After removing two outlier molecules (which were also among the eight compounds removed by Abraham and workers to arrive at their relationship), they developed the following model (Eq. 21):

$$\log \text{BB} = 0.054(\pm 0.005)\Delta G_{\text{W}}^0 + 0.43(\pm 0.07) \quad (21)$$

$$n = 55, r = 0.82, s = 0.41, F = 108.3$$

They considered a variety of additional parameters in determining Eq. 21 through the multivariate analysis, such as molecular weight, molecular volume, or surface area of each compound. But later these additional terms were not found to be statistically significant for the experimental data considered, and were subsequently dropped from further consideration. This was not astonishing since the computed ΔG_{W}^0 encompasses terms for the creation of a molecular-shaped cavity, solvent-accessible surface area, and polarization effects. Additionally, ΔG_{W}^0 was also expected to reflect many of the properties contained within the parameters Abraham used, such as dipolarity/polarizability, hydrogen bond acidity and basicity, and a molecular volume descriptor. They also determined the solvation free energy in hexadecane expecting it to be more representative of the environment that the molecule might face while crossing the membrane. But unfortunately this did not lead to any significant improvement in the correlation. They predicted an external test set of six compounds using this model but the results were not found to be satisfactory.

From the model, the authors interpreted that a polar compound, well solvated in water, would have a relatively large negative value for ΔG_{W}^0 , resulting in low partitioning into the brain. On the contrary, a relatively nonpolar compound would yield a more positive value for ΔG_{W}^0 , which is consistent with higher brain partitioning. This was in agreement with the positive sign for the coefficient of $\log P_{\text{cyh}}$ in Young's models, the negative coefficients for the hydrogen bond donor and acceptor and dipolarity/polarizability term in Abraham's models, and the generally accepted concept that lipophilic compounds partition well into the brain, suggesting that solute hydrogen-bonding ability has a large negative effect on brain partitioning.

Basak et al. [5] used discriminant function analysis (DFA) to determine the efficacy of using nonempirical parameters ($\log P$, hydrogen-bonding parameter, and topological indices) in the estimation of blood-brain transport, inferred from CNS activity, for a set of 28 compounds from the work of Seelig and colleagues [43]. Three distinct models based on topological indices, a hydrogen-bonding parameter, and $\log P$ were built. Model 1 was constructed from 94 topological indices and hydrogen-bonding parameter. Models 2 and 3 used hydrogen-bonding parameter along with the subsets of topological indices, selected after principal component analysis (PCA). Interestingly, the $\log P$

parameter was not included in any of the models, though it was available for selection during model construction. Analysis of the stepwise discrimination procedure, used to select features for model inclusion, revealed that $\log P$ was not statistically significant in any step of the model construction. This observation further confirmed the conclusion of Seelig et al. that lipophilicity is not a reliable parameter for classifying the CNS activity of this particular set of 28 compounds. All the three models correctly classified the CNS+ and CNS– compounds with an accuracy of 100% and 91.75%, respectively. Only one compound, mequitazine, was misclassified by all the three models as a CNS+ agent instead of CNS– agent.

Kaliszan and Markuszewski [23] used the 20-compound Young's data set with slightly different parameters and reported several equations. In Eq. 22, they used the measured $\log P$ values given by Young and workers together with the molecular weight:

$$\begin{aligned} \log \text{BB} = & -0.00794(\pm 0.00172)\text{MW} + 0.541(\pm 0.106) \log P_{\text{oct}} \\ & + 0.476(\pm 0.454) \\ n = 20, r = & 0.801, s = 0.486, F = 15.2 \end{aligned} \quad (22)$$

Replacement of $\log P_{\text{oct}}$ with $\log P_{\text{cyh}}$ gave a better regression (Eq. 23):

$$\begin{aligned} \log \text{BB} = & -0.00570(\pm 0.00098)\text{MW} + 0.309(\pm 0.034) \log P_{\text{cyh}} \\ & + 1.296(\pm 0.313) \\ n = 20, r = & 0.919, s = 0.321, F = 46.0 \end{aligned} \quad (23)$$

The authors increased the quality of their correlation by replacing the molecular weight with the water-accessible volume, which gave a slightly higher correlation coefficient than did Eq. 23:

$$\begin{aligned} \log \text{BB} = & -0.00275(\pm 0.00037)V_{\text{wav}} + 0.373(\pm 0.032) \log P_{\text{cyh}} \\ & + 1.979(\pm 0.339) \\ n = 20, r = & 0.943, s = 0.271, F = 67.9 \end{aligned} \quad (24)$$

Taking 33 of the 35 gases, hydrocarbons, and other volatile compounds assembled by Abraham and workers and using the same descriptors as in Eq. 22 resulted in the following relationship (Eq. 25):

$$\begin{aligned} \log \text{BB} = & -0.00116(\pm 0.00049)\text{MW} + 0.272(\pm 0.017) \log P \\ & - 0.088(\pm 0.051) \\ n = 33, r = & 0.947, s = 0.126, F = 131.1 \end{aligned} \quad (25)$$

Salminen et al. [41] presented a new data set which contained 29 diverse drug-like molecules. In the data set, only four compounds were taken from Young's data set. One compound, imipramine, was present in both data sets but had different experimental values: $\log \text{BB}$ was 1.30 and 0.83 in the Salminen's and Young's data sets, respectively. The authors developed models where they used the measured retention from immobilized artificial membrane ($\log k_{\text{IAM}}$) chromatography together with the molecular volume and an indicator variable of ionization, I_3 . The indicator variable, I_3 , was assigned a value of 1 for compounds with an amino nitrogen and -1 for compounds with a carboxyl group. Otherwise, it was equal to zero. The authors showed a close correlation

between $\log k_{IAM}$ and calculated $\log P_{oct}$, presenting two equations with only calculated parameters (Eqs. 26, 27):

$$\log BB = -0.01V_m + 0.62 \log k_{IAM} + 1.00I_3 + 1.18$$

$$n = 26, r = 0.762, s = 0.56, F = 10.2 \quad (26)$$

$$\log BB = -0.01V_m + 0.32 \log P_{oct} + 0.96I_3 + 1.06$$

$$n = 26, r = 0.839, s = 0.47, F = 17.5 \quad (27)$$

After removing the outliers, the model statistics were significantly improved (Eqs. 28, 29):

$$\log BB = -0.01V_m + 0.58 \log k_{IAM} + 0.89I_3 + 1.28$$

$$n = 21, r = 0.921, s = 0.27, F = 31.5 \quad (28)$$

$$\log BB = -0.01V_m + 0.35 \log P_{oct} + 0.99I_3 + 1.25$$

$$n = 23, r = 0.921, s = 0.32, F = 35.2 \quad (29)$$

The cross-validated r^2 values for these improved models were 0.627 and 0.776, respectively. The models implied that the brain favors cationic compounds over phospholipids membranes. Although $\log k_{IAM}$ offered no advantage in these models over $\log P_{oct}$ in predicting $\log BB$ ratios of the drugs (in particular because $\log P_{oct}$ can be calculated with sufficient accuracy), it appeared to provide a better model than $\log P_{oct}$ for the membrane distribution of the ionized compounds.

Norinder et al. [33] also analyzed the 63 compounds previously studied by Lombardo et al. using theoretically computed molecular descriptors and multivariate PLS method. The authors used a strategy involving both semi-empirical and quantum mechanical ab initio calculations followed by the final computation of molecular descriptors by MolSurf technology. They selected a training set consisting of 28 molecules from the 57 compounds studied by both Abraham et al. and Lombardo et al. using the maximin approach of Marengo and Todeschini in the development of model 1. The remaining 28 structures (compound no. 12 excluded) were used as an external test set (test set 1) to assess the predictive ability of the derived model 1. Model 2 was derived from the data set of 56 structures. A second test set (test set 2) consisting of six compounds, identical to the test set used by Lombardo et al., was also used for the assessment of the derived PLS statistical models. The PLS models predicted the brain–blood partitioning of the second test set with greater precision (RMSE 0.473 and 0.508, respectively) than did the model reported by Lombardo (RMSE 1.244). The results from the PLS analyses are summarized as follows:

$$n = 28, r^2 = 0.862, s = 0.311, F = 49.93, q^2 = 0.782,$$

$$\text{RMSE (training set)} = 0.288, \text{ RMSE (test set2)} = 0.473$$

Model 2 based on all 56 compounds resulted in the following statistics:

$$n = 56, r^2 = 0.834, s = 0.312, F = 86.95, q^2 = 0.775,$$

$$\text{RMSE (training set)} = 0.301, \text{ RMSE (test set2)} = 0.508$$

A number of compounds with the lowest $\log BB$ values were overestimated by model 2. These entities were all drug-like compounds with a variety of structures and functional groups. Compounds at the other end of the scale, that is, compounds that exhibit high $\log BB$ values, are somewhat better predicted. These latter compounds were all hydrocarbons, for example, butanes, pentanes,

and heptanes, and not as complex with respect to structure and chemical functionality compared with the former class of compounds. The hydrocarbons are much easier to characterize with physicochemical parameters of MolSurf type and to correlate with the respective brain–blood partitioning data. This probably accounts for the somewhat less accurate prediction of the compounds with the lowest log BB values compared to those compounds with the highest log BB values.

The most important factors influencing the models were found to be associated with polarity and Lewis base strength. Properties related to the hydrogen-bonding potential were also found to be important and should be kept to the bare minimum to assist high brain–blood partitioning. High lipophilicity (log P) was also identified to be complementary for high partitioning. Additionally, the presence of polarizable electrons, e.g., conjugated and aromatic substructures as well as the larger halogens, is also advantageous for the compound to penetrate the brain effectively. A part of the informational content of the polarizable variable may also be related to the charge-transfer interactions. This is supported by the fact that the charge-transfer term was one of the most important variables and has a positive PLS coefficient, that is, such interactions promote high brain–blood partitioning, possibly by the interaction of the compound with the surrounding membrane phospholipids.

Clark [10] used the same data set of Lombardo et al. and obtained a good regression by using only the polar surface area (PSA) (Eq. 30):

$$\begin{aligned} \log \text{BB} &= -0.016(\pm 0.0001)\text{PSA} + 0.547(\pm 0.05) \\ n &= 57, r = 0.819, s = 0.455, F = 112.4 \end{aligned} \quad (30)$$

Comparing this model with the one-parameter equation given by Lombardo et al. led the authors to correlate the computed ΔG_{W}^0 values with PSA. Indeed, there was a very strong relationship between these two parameters ($r = 0.962$). However, this purely PSA-based model failed to distinguish between compounds which lack a PSA (i.e., nonpolar compounds, e.g., benzene and 3-methylpentane which have zero PSA but their log BB values are -0.69 and 2.01 , respectively). Therefore, to search for an additional descriptor that would differentiate between the nonpolar compounds in the set, molecular weight, molecular volume, and nonpolar surface area were tried, but none led to a significant improvement in the model. Finally, the most successful addition was the calculated log P , Clog P , which gives the following equation after removing nitrogen and one more compound found as outlier by other groups also (Eq. 31):

$$\begin{aligned} \log \text{BB} &= -0.0148(\pm 0.001)\text{PSA} + 0.152(\pm 0.036)\text{C log } P + 0.139(\pm 0.073) \\ n &= 55, r = 0.887, s = 0.354, F = 95.8 \end{aligned} \quad (31)$$

Because of the difficulty in calculating the accurate values of Clog P for some compounds, another model was developed using Mlog P instead of Clog P , which gave a slight change in the coefficients (Eq. 32):

$$\begin{aligned} \log \text{BB} &= -0.0145(\pm 0.001)\text{PSA} + 0.172(\pm 0.022)\text{M log } P + 0.131(\pm 0.033) \\ n &= 55, r = 0.876, s = 0.369, F = 86.0 \end{aligned} \quad (32)$$

In order to allow a direct comparison of Eqs. 31 and 32 with a purely PSA-based model, Eq. 30 was rederived based on the same 55 compounds as were used in the derivation of Eqs. 31 and 32 resulting in the following Eq. 33:

$$\begin{aligned} \log \text{BB} &= -0.0156(\pm 0.001)\text{PSA} + 0.548(\pm 0.048) \\ n &= 55, r = 0.841, s = 0.410, F = 128.4 \end{aligned} \quad (33)$$

To test Eqs. 31 and 32, Clark used two test sets; test set 1 consisted of seven compounds used by Abraham et al. and test set 2 consisted of six compounds used by Lombardo et al. as well as Norinder et al. The performance of models 31 and 32 on both test sets measured by the mean absolute error (MAE) was found to be better than Lombardo, which underpredicts log BB, and Norinder, which predicts too high a value. The authors concluded that BBB permeability would be better for compounds with high Clog *P* and low PSA.

Kelder et al. [25] also explored the role of PSA as a determinant for the transport of drugs through the BBB. Initially, they calculated and correlated the PSA of 45 drug molecules with their known brain-penetration data. A linear relationship was obtained between brain penetration and dynamic polar surface area (DPSA) as shown in Eq. 34:

$$\begin{aligned} \log \text{BB} &= -0.0322\text{DPSA} + 1.33 \\ n &= 45, r = 0.917, F = 229 \end{aligned} \quad (34)$$

The authors deduced that the brain penetration decreases with increasing PSA. For independent validation, they selected a set of 776 orally administered CNS active agents, analyzed their polar surfaces, and made a comparison with a set of 1590 orally administered non-CNS active drugs. They obtained an apparent difference between the distribution of the PSA of the CNS-active and CNS-inactive agents. They interpreted that the orally active drugs that are transported passively by the transcellular route should not exceed the PSA of 120 Å². They can be customized to brain permeation by decreasing the PSA <60–70 Å². Apparently, the BBB forms an extra limitation for orally administered compounds reaching the brain, diminishing the maximal PSA of the CNS-active compounds by ~50%.

The authors have also used the static polar surface and found a similar relationship with log BB ($r = 0.883$). Comparing this model (Eq. 34) with Clark's model (Eq. 30) shows a prominent difference in the statistics. The main reason is that the data set used by Kelder and workers does not contain any molecules without PSAs, while Clark's training set contains 16 molecules which lack a PSA. Inclusion of Clog *P* in the relationship describes those molecules (Eq. 31). It is noteworthy that Kelder and workers tested a number of parameters together with PSA, such as molecular weight, molecular volume, log *P*, and dipole moment, by multiple regression analysis, without achieving any significant improvement of Eq. 34.

Luco [30] employed the multivariate partial least squares projections to latent structures technique for modeling the brain–blood concentration ratio of 61 structurally diverse compounds. He used a training set of 61 compounds including 30 compounds from Young's data set and 36 compounds from Abraham's data set together with 5 acids from Salminen's and Greig's data sets. The descriptors used were mainly topological and constitutional in nature, like the Wiener index, the valence and connectivity molecular indexes, the kappa shape indexes, the differential molecular connectivity indexes, the charge and geometrical indexes, molecular volume, molecular weight, hydrogen bond

acceptors and donors, and several other constitutional descriptors. It is notable that $\log P$ and PSA were not among the descriptors. Because of the large number of structural descriptors considered, the VIP (variable importance for the projection) parameter was used to unravel which descriptor variables were the most relevant to explain $\log BB$. Preliminary analysis of the obtained models showed that different combinations of descriptor variables yielded PLS models of similar statistical relevance. Thus, the selection of the definitive model was carried out on the basis of predictions for the compounds comprising the validation sets. After omitting three outliers, a significant 3-component model was developed with the following statistics:

$$n = 58, r = 0.922, s = 0.318, q = 0.867, F = 102$$

The model accounted for 85% (49.8%, 26.5%, and 8.7%, respectively) of the variance in $\log BB$. Analyzing the PLS components showed some interesting results. The first component was mainly related to the polarity (HBA, HBD, etc.) and the second component was mainly related to molecular size even if the hydrogen-bond-donating ability has a strong weight. The third component gave a small contribution from the molecular shape.

The predictive ability of the model was assessed by means of cross-validation and also by using BB partitioning data, BBB permeability data, and one set of qualitative brain-penetration data, resulting in blood–brain distribution data for 97 compounds. Test set 1 (for brain–blood partitioning) consisted of 14 compounds from the test sets of Calder and Ganellin and Lombardo. For this set, the predictions using the Luco model were generally better than those made by most of the earlier relationships. Test set 2 contained blood–brain distribution values for 25 drug-like compounds compiled from various sources. The $\log BB$ values for this set were predicted with an RMSE of 0.541. After removing three outliers, the RMSE value was improved to 0.408.

The author also evaluated the model by PLS modeling of two representative sets of BBB permeability data but using only 18 selected descriptors. For the first data set, which consisted of the rat brain capillary permeabilities for 27 miscellaneous drugs, the statistical parameters were found to be $n = 27$, $r = 0.945$, $s = 0.356$, $q = 0.773$, and $F = 47.29$. The second data set included the permeabilities of 10 miscellaneous drugs reported by Lombardo and coworkers. Its statistical parameters were $n = 10$, $r = 0.976$, $s = 9.30$, $q = 0.90$, and $F = 69.41$. Finally, the author validated the model by predicting the BB ratios for compounds to which only discrete and unambiguous data of brain penetration have been established. For this, 22 compounds were selected from the data set of Seelig and workers falling into two categories according to CNS availability: high or low CNS penetration. To give a larger selection of compounds, an additional five compounds were selected from different sources. Compounds with predicted $\log BB$ values of < -1 were classified as poor brain penetrators (CNS–), whereas compounds with values of > -1 were classified as easy brain penetrators (CNS+). The PLS model was successful in achieving 100% accuracy for classifying CNS+ compounds and 84.6% accuracy for classifying CNS– compounds.

Osterberg and Norinder [35] analyzed the improvement in the prediction of drug transport processes by the combination of the hydrogen-bonding descriptors and calculated $\log P$. Two data sets were used. The calculated static PSA and the experimental $\log BB$ values for 70 compounds (data set 1) were taken from the work of Clark. The calculated dynamic PSA and the experimental \log

BB values for 45 compounds (data set 2) were taken from the work of Kelder et al. The compounds were arranged in increasing order of the response variable (log BB), and every second compound was selected as the training set, the remaining compounds being used as the test set. The number of nitrogen and oxygen atoms in the chemical formula was taken as the number of acceptor nitrogen (#HBAn) and oxygen atoms (#HBAo), respectively. The number of hydrogen bond donor atoms was the sum of hydrogen atoms bound to oxygen and to nitrogen atoms (#HBD). The relationships between the response variables and the calculated descriptors were determined using the PLS method. The statistical modeling of the brain–blood partitioning with the hydrogen-bonding parameters only showed fair results, with $r^2 = 0.65$ and $q^2 = 0.64$ for data set 1 and $r^2 = 0.76$ and $q^2 = 0.75$ for data set 2. The combination of the hydrogen-bonding parameters and log P improved the statistics of BB data set 1 ($r^2 = 0.76$ and $q^2 = 0.75$), but not of BB data set 2 ($r^2 = 0.72$ and $q^2 = 0.71$). This was probably explained by the fact that data set 1 contained many small organic solutes, which generally show very strong linear relationships with log P . To estimate the external predictive ability of the model, data sets 1 and 2 were divided into training set and test set. The results of the statistical analyses gave RMSEP values of 0.37 and 0.50, respectively.

Ertl et al. [14] devised a new fragment-based approach for computing PSA from the summation of tabulated surface contributions of the polar fragments. They called it as topological polar surface area (TPSA). It is practically identical to 3D-PSA but faster and easy to compute and that also from the 2D representation of the molecule. The new TPSA methodology was validated by using published data of various types of drug transport properties, including intestinal absorption, BBB penetration, and Caco-2 cell permeability. For modeling BBB permeability, the authors used two data sets: the data set of Kelder and workers and that of Clark. By employing the TPSA method, they generated two models with the statistics $n = 45$, $r = 0.883$ for Kelder's data set and $n = 57$, $r = 0.812$ for the Clark's data set. They thus suggested the use of this new fragment-based TPSA methodology for fast bioavailability screening of virtual libraries having millions of molecules.

Feher et al. [15] used the data set of Luco and found the following relationship (Eq. 35):

$$\log \text{BB} = 0.4275 - 0.3873n_{\text{acc.solv}} + 0.1092 \log P - 0.0017\text{PSA} \quad (35)$$

$$n = 61, r^2 = 0.730, q^2 = 0.688, \text{RMSE} = 0.424, F = 0.51$$

where $n_{\text{acc.solv}}$ is the number of hydrogen-bond acceptors in aqueous medium using the Patty rules. However, the PSA calculated by Feher et al. was somewhat different from the PSA computed by Clark or Kelder. The authors compared their predictions on the two test sets ($n = 14$, $r^2 = 0.576$, $\text{RMSE} = 0.628$ and $n = 25$, $r^2 = 0.616$, $\text{RMSE} = 0.789$) with the predictions of Luco and found the three-parameter equation to be only slightly worse compared with Luco's PLS model. They showed that, of the three above parameters, $n_{\text{acc.solv}}$ and PSA were the most correlated, but with a correlation coefficient of only 0.30. The substitution of PSA with water-accessible surface area or even the total no. of single bonds in the molecules led to a moderate (<10%) increase in RMSE in the fit and predictions. The replacement of log P with log D left the fit largely unchanged, presumably because log D is highly correlated with log P and $n_{\text{acc.solv}}$ ($r^2 = 0.70$). No replacement descriptor could be found

for the number of solvated hydrogen bond acceptors and hence this term was both essential and unique to the model. However, the number of hydrogen bond donors was found to have a little impact on the model statistics. This was clearly not the result of under representation of the molecules with hydrogen bond donors groups in the data set. It might be partly because a large proportion of the donor groups were already accounted for in $n_{\text{acc.solv}}$, namely, those that can be simultaneously acceptors and donors such as OH, those that can tautomerize to act as either, such as the nitrogen in imidazole, or have $\text{p}K_a$ values near neutrality, such as the nitrogen in aromatic sulphonamides. The diversity of the 100 molecule data set (i.e., training + test sets) was assessed by comparing the distribution of the Tanimoto similarity index within the data set to the distribution of 18,222 compounds from the *Dictionary of Drugs*. They concluded that the molecules in the data set of 100 compounds were at least as diverse as marketed drug molecules.

Crivori et al. [12] generated discriminant PLS-based models for estimating the BBB permeability of the molecules using 3D-molecular fields-derived descriptors from the Volsurf program. The various molecular descriptors obtained from Volsurf were related to the molecular size and shape, to the size and shape of hydrophilic and hydrophobic regions, and to the balance between them. Hydrogen bonding, amphiphilic moments, and critical packing parameters were other useful descriptors. The experimental data for the training and test sets which consisted of 110 and 120 compounds respectively with well-characterized BBB behavior were collected from the literature. In both training and test sets, the racemic drugs were modeled as separate enantiomers. On the basis of the assumption of passive permeation, the data set contained a number of related, but chemically diverse, compounds which were either brain-penetrating (BBB+), have a moderate permeation (BBB±), or have little if any ability to cross the BBB-. Initially, the authors searched for a relationship between the 3D structure and BBB permeation of the 110 compounds of the training set and 72 descriptors using PCA. No biological input was given to the model. Three significant principal components (PCs) were found by the cross-validation technique, which explained about 65% of the total variance of the data set. While the second and third PCs described the chemical variability and spatial geometry, the first PC was able to discriminate between the BBB-, the BBB±, and the BBB+ compounds. These results were considered to be of high significance since neither classification of compounds nor any training information was given to the PCA model. In other words, the first PC in the model was found to be potential enough, without any external information or training, to qualitatively and correctly predict the BBB permeation of the compounds. The model was validated with an external test set of 120 drugs, of which 49 compounds were BBB+ and the remaining 71 BBB-. Although the model failed to correctly predict the BBB profile of a few compounds, the predictive ability of the model was found to be quite satisfactory, with a correct classification of 90% of the BBB+ compounds (40 out of 44) and about 65% accuracy for the BBB- compounds (46 out of 71). The prediction of the BBB- compounds appeared to be more difficult than that of BBB+ compounds. This was supported by the fact that CNS- drugs can be stopped by the BBB, metabolized before producing their effects, and/or readily expelled back by active efflux processes. Since the model was able to predict only passive diffusion, it was not surprising that

predictions for BBB– compounds were apparently less reliable than for BBB+ compounds.

Model 35 was further refined by performing PLS discriminant analysis on the combined data set of 229 compounds (the major outlier mequitazine was removed) and using 72 descriptors. For this, the BBB+ compounds were assigned a categorical (not thermodynamic) score of 1, and the BBB– and BBB± compounds a score of –1. Based on the two significant latent variables from the PLS and cross-validation, the model distinguished well between the BBB+ and BBB– compounds, better than the unbiased PCA model. For evaluating the model, a BBB+ behavior was assigned to a compound having a score >0 and a BBB– behavior to a compound having a score <0. The model correctly assigned the BBB profile to more than 90% of the compounds.

On the basis of the results, the authors interpreted that the descriptors of polarity, such as hydrophilic regions, capacity factors, and Hydrogen-bonding, are inversely correlated with BBB permeability. The BBB permeation was found to decrease with an increase in polar surface, indicating that besides Hydrogen-bonding potential other factors, for example, charge distribution and electron lone pairs, also influence BBB permeation. While the diffuse polar regions are acceptable for BBB permeation, dense and localized polar regions are clearly unfavorable. An increase in hydrogen-bonding capacity is already known to be damaging for permeation. In addition, the contribution of the integy moment parameter demonstrated that besides the number of hydrogen bonds, their 3D distribution also influences the BBB permeation. Further, the descriptors of hydrophobic interactions are directly correlated with BBB permeation, but their role appeared smaller than that of the polar descriptors. The size and shape descriptors have no marked impact on BBB permeation. In contrast, critical packing and the hydrophilic–lipophilic balance were found to be the important descriptors.

Keseru and Molnar [26] chose an approach similar to that previously employed by Lombardo et al. by computing solvation free energies. The authors used a thermodynamic approach based on the generalized Born/ surface area (GB/SA) continuum solvation model. The main difference between similar approaches used previously and the variant used by Keseru and Molnar is the speed of the latter achievement. The GB/SA method employed by the authors calculated ~10 compounds/min, which was considerably faster than with previous methods. The method permits virtual screening at a medium throughput level, which is adequate considering the trend in combinatorial chemistry and high throughput screening of moving toward smaller and more focused libraries. The experimental log BB data for the 60 compounds used in the training set was taken from the data set of Young, van Belle, Lin, and Abraham and workers. The test set consisted of 8700 CNS-active compounds extracted from the CIPSLINE database. After removing five outliers, they developed the following model correlating the free energy of solvation G_{solv} with the experimental log BB (Eq. 36):

$$\begin{aligned} \log \text{BB} &= 0.035G_{\text{solv}} + 0.2592 \\ n &= 55, r = 0.85, s = 0.37 \end{aligned} \quad (36)$$

This equation is remarkably similar to the corresponding equation of Lombardo et al. (Eq. 21). Furthermore, the statistics of both equations are also similar. On the basis of experimental log BB values, it was concluded

that compounds with log BB greater than 0.3 cross the barrier readily, while compounds with log BB less than -1.0 are only poorly distributed to the brain. The linear relationship between brain penetration and the solvation free energy of the compounds suggested that considering only passive diffusion orally administered CNS-active drugs should have a solvation free energy higher than -40 kJ/mol. This was confirmed by calculating G_{solv} for 8700 CNS-active compounds available from the CIPSLINE database. The results showed that 96% of the CNS-active molecules have G_{solv} higher than -50 kJ/mol, and this, the authors suggested, can be used as a suitable criterion for the rapid identification of molecules that might penetrate to the brain via passive transport.

Kaznessis et al. [24] used Monte Carlo simulations on a data set of 85 molecules collected from various sources, to calculate physically significant descriptors such as solvent accessible surface area (SASA), solute dipole, number of hydrogen-bond acceptors (HBAC) and donors (HBDN), molecular volume (MVOL), and the hydrophilic, hydrophobic, and amphiphilic components of SASA and related them with BBB permeability using the MLR method. After removing nine strong outliers, the following relationship was developed (Eq. 37):

$$\begin{aligned} \log \text{BB} = & -0.2339(\pm 0.013)\text{HBAC} + 0.00147(\pm 0.00011)\text{MVOL} - 31.6099 \\ & \times (\pm 4.0837)\text{HBAC} \times \text{HBDN}^{1/2}/\text{SASA} - 0.04579(\pm 0.05808) \\ n = 76, r = 0.97, s = 0.173, F = 311.307 \end{aligned} \quad (37)$$

The model indicated that hydrophilicity negatively impacts the BBB permeation. Further, the most important descriptors were found to be HBAC and MVOL. The third term could be replaced with HBDN with only a minor deterioration in the predictive quality of the model (Eq. 38):

$$\begin{aligned} \log \text{BB} = & -0.28902(\pm 0.012)\text{HBAC} + 0.0017(\pm 0.00011)\text{MVOL} \\ & - 0.07464(\pm 0.01543)\text{HBDN} - 0.13956(\pm 0.06618) \\ n = 76, r = 0.958, s = 0.203, F = 270.46 \end{aligned} \quad (38)$$

The authors also generated a model similar to that of Feher et al. but with better predictivity, employing the hydrophilic surface area (FISA) along with HBAC and log P (Eq. 39):

$$\begin{aligned} \log \text{BB} = & -0.1096(\pm 0.0107)\text{HBAC} - 0.00241(\pm 0.00046)\text{FISA} \\ & + 0.20229(\pm 0.02408) \log P + 0.27961(\pm 0.08252) \\ n = 79, r = 0.932, s = 0.256, F = 104.37 \end{aligned} \quad (39)$$

Another model developed using log P and MWEI indices resulted in following statistics (Eq. 40):

$$\begin{aligned} \log \text{BB} = & -0.00329(\pm 0.00038)\text{MWEI} + 0.41267(\pm 0.03071) \log P \\ & - 0.03688(\pm 0.01521) \\ n = 77, r = 0.862, s = 0.363, F = 180.59 \end{aligned} \quad (40)$$

Finally, the use of PSA (instead of FISA) and MVOL led to rather poor results with $n = 76$, $r = 0.688$, $s = 0.52$, and $F = 38.138$.

Liu et al. [27] introduced a new lipoaffinity descriptor to account for the effect of molecular hydrophobicity on BBB penetration. The descriptor was defined based on Kier and Hall's atom-type electrotopological state indices and therefore its evaluation is fast, requires no molecular 3D information, and

is also not bundled with hydroaffinity. The authors described the lipoaffinity descriptor (LA) as follows:

$$LA = \sum (a_i S_i), \text{ where } i \neq N \text{ and } O$$

where a_i is the LR coefficient and S_i is the E-state index. Thus, LA refers to the contribution to $\log P_{\text{oct}}$ from atoms other than nitrogen and oxygen. It includes contributions mainly from carbon atoms and atoms of low hydrogen-bonding capacity such as Cl and F as well as atoms of high polarizability such as P, S, Br, and I. The LR coefficients, a_i , can be considered as scaling factors or weights that make the contributions to LA from different atom types compatible.

For modeling the BBB penetration, authors used Abraham's data set of 57 compounds as the training set. The test set consisted of 13 compounds, 7 of which were taken from Abraham's data set and 6 from the data set of Lombardo and workers. In addition to the lipoaffinity descriptor, the other descriptors used by them include molecular weight and TPSA. Two models were developed: one based on stepwise MLR and the other one based on ANN. To test the performance of different descriptors, they first carried out a simple LR of the 55 training set compounds (two outliers were removed) using TPSA as the only descriptor (Eq. 41). The equation was comparable to Clark's model (Eq. 33).

$$\begin{aligned} \log \text{BB} &= 0.524(0.081) - 0.0153(0.0014)\text{TPSA} \\ n &= 55, r^2 = 0.694, r_{\text{loo}}^2 = 0.670, s = 0.42, F = 120.3 \end{aligned} \quad (41)$$

Next, they applied the stepwise MLR to the training set providing TPSA, LA, and MW as the descriptors so as to take into account hydroaffinity, lipoaffinity, and molecular size effects. However, the calculation failed to generate a statistically sound linear equation using all three descriptors. Instead the following linear model was generated (Eq. 42) which was comparable to Clark's Eq. 31:

$$\begin{aligned} \log \text{BB} &= 0.138(0.104) - 0.0112(0.0008)\text{MW} + 0.364(0.033)\text{LA} \\ n &= 55, r^2 = 0.790, r_{\text{loo}}^2 = 0.763, s = 0.35, F = 97.7 \end{aligned} \quad (42)$$

Incorporation of all three descriptors—TPSA, MW, and LA—into one linear equation by MLR resulted in the following equation (Eq. 43):

$$\begin{aligned} \log \text{BB} &= 0.181(0.109) - 0.00876(0.00205)\text{MW} + 0.296(0.061)\text{LA} \\ &\quad - 0.00412(0.00315)\text{TPSA} \\ n &= 55, r^2 = 0.797, r_{\text{loo}}^2 = 0.760, s = 0.35, F = 66.6 \end{aligned} \quad (43)$$

Since MW correlates with molecular size, the negative sign of its coefficient indicated indeed that larger molecules have lower permeation rates. The positive coefficient of LA indicated that lipoaffinity enhances the permeation rate, and the negative coefficient of TPSA was in agreement with the perception that hydrophilicity reduces the permeation rate.

Authors also performed MLR with MW and $\text{Hlog } P_{\text{oct}}$, the 1-octanol/water partition coefficient calculated by Huuskonen's simple $\log P_{\text{oct}}$ model, to examine whether the hypothesis that bundling hydroaffinity and lipoaffinity into a single $\log P_{\text{oct}}$ parameter is inferior to separating them. The results obtained were as follows (Eq. 44):

$$\begin{aligned} \log \text{BB} &= -0.0454(0.1261) - 0.00673(0.00056)\text{MW} \\ &\quad + 0.470(0.050)\text{Hlog } P_{\text{oct}} \\ n &= 55, r^2 = 0.741, r_{\text{loo}}^2 = 0.710, s = 0.39, F = 74.3 \end{aligned} \quad (44)$$

They compared the performance of Eqs. 44 and 42, it is clear that $H\log P_{\text{oct}}$ is indeed inferior to LA as a descriptor of BBB permeation. They also tried the combination of MW and TPSA using MLR (Eq. 45), but the results failed to show any significant improvement over the earlier model (Eq. 41).

$$\log \text{BB} = 0.423(0.116) - 0.0171(0.0020)\text{TPSA} + 0.000822(0.000679)\text{MW}$$

$$n = 55, r^2 = 0.703, r_{\text{loo}}^2 = 0.663, s = 0.42, F = 61.4 \quad (45)$$

From the best model, that is, Eq. (42), the r^2 and standard deviation between the predicted and experimental log BB for the 55 training set compounds were 0.790 and 0.35, respectively. However for the 13 test set compounds, the corresponding values were 0.419 and 0.60. Excluding two outliers, the r^2 and standard deviation were improved to 0.838 and 0.30, respectively.

The authors also performed ANN analysis on the same data set in order to explore nonlinear dependencies of log BB on the descriptors and try to bring all three descriptors (TPSA, LA, and MW) into one model. A three-layered, fully connected neural network was trained with a logistic $f(x) = 1/(1 + e^{-x})$ activation function for both the hidden and output nodes. All three descriptors, TPSA, LA, and MW, were used as input nodes. Two hidden neurons were used, resulting in a 3–2–1 network architecture. The network was trained with the 55 training set compounds, and predictions were made for the 13 test set compounds. For the training set compounds, the r^2 and standard deviation between the predicted and experimental log BB were 0.808 and 0.30, respectively. After removing two outliers, the corresponding values for the remaining 11 test set molecules were 0.806 and 0.35, respectively. Thus the ANN results showed a slight improvement over the corresponding MLR results.

Platts et al. [39] reported linear free energy relation (LFER) models of the equilibrium distribution of molecules between blood and brain, relating log BB values to fundamental molecular properties, such as hydrogen-bonding capability, polarity/polarizability, and size. They used the following modified form of Abraham's general Eq. 46:

$$\text{SP} = c + e.E + s.S + a.A + b.B + v.V \quad (46)$$

where SP is a set of solute properties in a given system, for example, a set of log BB values, E is an excess molar refraction, S is the dipolarity/polarizability, A and B are the hydrogen-bond acidity and basicity, respectively, and V is the solute McGowan volume in units of ($\text{cm}^3 \text{mol}^{-1}/100$). A total of 157 values of log BB were collected from a number of sources including directly measured and indirectly determined values. Coefficients e , s , a , b , and v in Eq. 46 were determined by multivariate LR analysis. Only those parameters were included in the regression analyses for which a standard t -test indicated more than 95% probability of significance. An initial regression of all 157 log BB values against LFER descriptors showed a reasonably accurate fit, but nine molecules had to be omitted as outliers. The remaining set of 148 values yielded the Eq. 47:

$$\log \text{BB} = 0.044 + 0.511E - 0.886S - 0.724A - 0.666B + 0.861V \quad (47)$$

$$n = 148, R^2 = 0.710, R_{\text{CV}}^2 = 0.682, s = 0.367, F = 71$$

Unfortunately, several large discrepancies were observed in Eq. 47 for carboxylic acid-containing molecules, such as salicylic acid and indomethacin. Later an improvement over Eq. 47 was achieved by the inclusion of I_1 , an

indicator variable that was set to 1 for a compound containing a carboxylic acid fragment and 0 otherwise, giving Eq. 48:

$$\log \text{BB} = 0.021 + 0.463E - 0.864S - 0.564A - 0.731B + 0.933V - 0.567I_1$$

$$n = 148, r^2 = 0.745, r_{\text{CV}}^2 = 0.711, s = 0.343, F = 69 \quad (48)$$

In order to remove large intercorrelations between the descriptors, the authors performed PCR analysis in which log BB data were linearly regressed against orthogonal PCs formed from the original descriptors. Five PCs were found to be significant on regression against log BB, and after transforming back into the original descriptors yielded Eq. 49:

$$\log \text{BB} = 0.062 + 0.469E - 0.864S - 0.586A - 0.713B + 0.895V - 0.564I_1$$

$$n = 148, r^2 = 0.744, r_{\text{CV}}^2 = 0.715, s = 0.342, F = 83 \quad (49)$$

Since Eqs. 48 and 49 were found to be identical within the standard errors on coefficients, it indicated that the coefficients in Eq. 48 were not greatly affected by the intercorrelation of descriptors. On this basis they conclude that Eq. 48 is as good as, or better than, the models based on subsets of the data used in the study.

To examine the predictive ability of the model, the full set of 148 compounds was divided into two sets of 74. The first set was used to construct an equation similar to Eq. 48, which was then used to predict log BB values for the second set, and vice versa. The two regressions yielded $r^2 = 0.767$, $s = 0.331$ and $r^2 = 0.763$, $s = 0.344$, with coefficients identical within regression standard errors to Eq. 48. These regressions were then used to predict log BB values for the 74 molecules not used in training sets with $r^2 = 0.735$, $s = 0.376$ and $r^2 = 0.701$, $s = 0.385$. The authors have also taken five randomly selected test sets, each of 30 compounds (20% of the full set) and regenerated models analogous to Eq. 48 using the remaining 118 compounds as training sets. These models, each of which was statistically identical to Eq. 48, were then used to predict log BB for the 30 test compounds. The accuracy of prediction showed considerable variation among the five test sets, with estimated standard deviation (ESD) ranging from 0.32 to 0.42, but the average ESD was 0.36, almost identical to that found in Eq. 48, which could be taken as an estimate of the likely predictive ability of Eq. 48.

The positive e - and v -coefficients in Eq. 48 indicated that increasing molecular size and (less importantly) the presence of n - and π -electron pairs tend to push compounds out of blood and into brain. In this respect, equation (48) was found to be similar to many water-solvent partition ($\log P$) equations, where also large e - and v -coefficients were reported. The coefficients of the polar descriptors S, A, and B were all very negative, indicating that polarity and hydrogen-bond donor and acceptor ability act to keep compounds in blood and out of the brain. In turn, this indicated that the brain is less polar/polarizable, acidic and basic than is blood, but is more able to accommodate bulky solutes and interact with them via dispersive forces than blood. Again this was similar to many previously published $\log P$ equations, where the aqueous phase attracts polar, hydrogen-bonding molecules and the organic phase favors solution of bulky solutes. The large negative coefficient of the indicator variable, I_1 , in equation (48) and its low correlation with other descriptors indicated a previously unknown factor affecting the transfer of solutes between blood and brain. It is apparent that the presence of $-\text{COOH}$ group hinders brain

penetration further than would simply be due to the intrinsic hydrogen bonding and polarity properties of neutral acids. Since it is known that acidic drugs, in general, are bound to albumin present in plasma and blood, this may account for at least some of the negative contribution of I_1 . It may also be that ionization to $-\text{CO}_2^-$ is the cause of this, as one can certainly imagine such groups increasing E and B over those for $-\text{COOH}$. Finally, such $-\text{COOH}$ groups may be removed from the brain by some efflux mechanism. It is worth mentioning that similar indicator variables for strong bases, such as amines, were not found to be significant in their models, or indeed in previous analyses of log BB.

The model has been claimed to predict the log BB values at a rate of 700 molecules per min, some two orders of magnitude faster than the calculations of Keserü and Molnar. To test the likely accuracy of such predictions, the authors took 105 compounds for which experimental descriptors were used in constructing equation (48) and calculated their log BB values using same with descriptors calculated by the method of Platts and workers. The observed and calculated values agreed with $\text{ESD} = 0.294$, thus indicating that Platts' calculation method can be used in conjunction with equation (48) to predict further log BB values faster with an estimated accuracy of around 0.30 to 0.35 log units.

Fu et al. [16] analyzed a set of 57 compounds previously used by Lombardo and other workers also. Their molecular geometries were optimized using the semiempirical self-consistent field molecular orbital calculation AM1 method. Polar molecular surface areas and molecular volumes were calculated by the Monte Carlo method. The stepwise multiple regression analysis was used to obtain the correlation equations between the log BB values of the training set compounds and their structural parameters. The following model was generated after removing one outlier (Eq. 50):

$$\log \text{BB} = -1.03 \times 10^{-5} V^2 + 6.735 \times 10^{-3} V - 0.01808 \text{PSA} - 0.1581 \quad (50)$$

$$n = 56, r = 0.8732, s = 0.3733, F = 53.62$$

By replacing PSA in Eq. (50) with other parameters relevant to the polar molecular surface areas, two more significant regression equations were obtained (Eqs. 51, 52):

$$\log \text{BB} = -1.390 \times 10^{-5} V^2 + 9.181 \times 10^{-3} V - 0.01996 \text{SA} - 0.4274 \quad (51)$$

$$n = 56, r = 0.8951, s = 0.3415, F = 69.85$$

$$\log \text{BB} = -1.331 \times 10^{-5} V^2 + 9.228 \times 10^{-3} V - 0.02439 S_{\text{O,N}} - 0.4318 \quad (52)$$

$$n = 56, r = 0.9043, s = 0.3269, F = 77.78$$

where SA is PSA minus surface areas of the nitrogen atoms in nitrogen molecule or in nitro and $S_{\text{O,N}}$ is the sum of the surface areas of oxygen atoms and nitrogen atoms except those in nitrogen molecule or in nitro.

The authors concluded that BBB permeability of a compound is favored by weak hydrogen-bonding potential, high lipophilicity, and small size. Since the nitrogen atoms in nitrogen molecule or in nitro are difficult to form hydrogen bonds with hydrogen bond donors, SA might be a more appropriate parameter indicating the capacity of a molecule to form hydrogen bonds than PSA and better correlated with log BB. Among the atoms involved in SA, hydrogen atom is hydrogen bond donor whereas oxygen and nitrogen atoms are hydrogen

bond acceptors. Upon dividing SA into $S_{O,N}$ and S_H (which is the sum of the surface areas of hydrogen atoms attached to oxygen or nitrogen atoms) and relating them to $\log BB$ along with V , they obtained the equation (52) in which there was no S_H term. This showed that oxygen and nitrogen atoms are more important than the hydrogen atoms in $\log BB$ prediction.

Rose et al. [40] collected the experimental BBB data of 106 neutral compounds from the data sets of Young, Abraham, Salminen, Clark, Luco, Yazdaniyan, Grieg, Lin, Lombardo, Van Belle, and Calder. For QSAR analysis, they selected atom-type E-State and hydrogen E-State indices, along with molecular connectivity chi and difference chi indices, and kappa shape indices. The pairwise correlation matrix was examined for correlation coefficients greater than 0.80. For each such occurrence, one of the pair of correlated variables was eliminated. After data matrix reduction, 41 variables remained for statistical analysis in the model development. The data matrix was submitted for statistical analysis using the SAS system. The RSQUARE selection method in proc REG was used to examine every QSAR equation from one to five variables, listing the top 10 most statistically significant. The number of variables in a model was limited to five. The three most prominent descriptors were E-State indices that emphasize hydrogen bond donating ability, $HS^T(\text{HBd})$, along with certain nonpolar structure features, $HS^T(\text{arom})$, and skeletal architecture, in the difference chi index, $d^2\chi^v$. The authors further introduced squares of the prominent variables to simulate a possible nonlinear relation between structure and $\log BB$. Significant improvement was obtained in the regression statistics. Only the squares of the $HS^T(\text{arom})$ and $d^2\chi^v$ variables were found to be statistically significant. In four- and five-variable equations, only the linear term in $d^2\chi^v$ was observed to be statistically significant when the squares were also present. Based on these preliminary investigations, three structure descriptors were selected for further modeling and validation: $HS^T(\text{HBd})$, $[HS^T(\text{arom})]^2$, and $[d^2\chi^v]^2$.

The final model for prediction of compounds not in the current data set was developed for the whole set of 106 compounds. To optimize the predictive ability, the authors removed observations with large residuals, that is, residuals greater than 2.5 standard deviations. Four observations with residuals greater than ± 1.2 were found and finally deleted. The q^2 value improved from 0.52 to 0.62 upon removal of these four observations. The final model is as follows (Eq. 53):

$$\begin{aligned} \log BB = & -0.202(\pm 0.026)HS^T(\text{HBd}) + 0.00627(\pm 0.00095)[HS^T(\text{arom})]^2 \\ & - 0.105(\pm 0.016)[d^2\chi^v]^2 - 0.425(\pm 0.069) \\ r^2 = & 0.66, \quad s = 0.45, \quad F = 62.4, \quad n = 102, \quad q^2 = 0.62, \quad s_{\text{press}} = 0.48 \end{aligned} \quad (53)$$

The model was claimed to compute 5000–6000 molecules per min. The predictive ability of the model was validated by four approaches. In the first approach, a set of 20 compounds was randomly selected as an initial validation test set. A model was developed from the remaining 86 compounds with an MAE of 0.33, from which the test set values were then predicted. The results of this test prediction were very good and provided momentum for support of the three structure descriptors. In the second approach, a full cross-validation test of the model was investigated. The data set of 102 compounds was divided

randomly into five groups of almost the same size. Each group was left out (Leave-Group-Out, LGO) and that group predicted by model developed from the remaining observations. In this way, every observation was left out once, in groups of 20, and its value predicted. The overall MAE of predictions was found to be 0.38. In the third approach, the experimental data for 108 compounds was examined and the compounds were assigned as “+” if their log BB value > 0 and “-” if log BB < 0.1 . From this data set, the authors selected 28 compounds whose BB values were obtained by methods similar to those for their data set and that are not already included in their data. Twenty-seven of these compounds were predicted correctly by Eq. 53 for their + or - values. Finally, the model was used to predict log BB values for 20039 drug and drug-like compounds taken from a modified form of the Pomona MedChem database. Organometallic compounds and salts were removed. The compounds were selected from a somewhat larger data set by selecting only those whose structure descriptor values fall within the parameter values of data set. The results indicated that the predicted values fall in a range consistent with drug-like molecule properties.

On the basis of the results, the variable with the single best correlation to log BB was found to be $HS^T(\text{HBd})$, a representation of hydrogen bond donation ability. The negative coefficient on $HS^T(\text{HBd})$ indicated that hydrogen bond donor groups lead to negative or low values of log BB. This effect arises from increased water solubility and decreased membrane affinity of compounds with hydrogen bond donor groups. The $HS^T(\text{HBd})$ variable contributed 32.7% on average to the calculated log BB value and ranged from 0.0% to 100.0% across the data set. The second variable in the model is the square of the atom-type hydrogen E-State descriptor for aromatic CH groups, $HS^T(\text{arom})$. This descriptor of nonpolar aromatic CHs is the sum of the hydrogen atom-level E-State indices for all aromatic hydrogen atoms in the molecule. The $HS^T(\text{arom})$ descriptor contributed 21.6% on average to the calculated log BB values and ranged from 0.0% to 99.8%. Because of the positive coefficient on this descriptor, larger values are related to larger log BB values. The third variable in the model is the square of the second-order valence molecular connectivity difference chi index, $d^2\chi^v$. This variable increases with increased branching in the structure and it is a measure of overall skeletal structure variation. The $d^2\chi^v$ index is derived from the ${}^2\chi^v$ descriptor, an index that increases with molecular size. The $d^2\chi^v$ index contributed 45.6% on an average to the calculated log BB and ranged from 0.0% to 100.0% across the data set. Because of the negative coefficient on $[d^2\chi^v]^2$, larger values are related to more negative log BB values. In summary, equation (53) indicated that BBB penetration is increased for compounds with aromatic CH groups, less skeletal branching, and fewer or weaker hydrogen bond donor groups.

Iyer et al. [22] developed the membrane-interaction quantitative structure–activity relationship (MI-QSAR) approach (where structure-based design methodology was combined with classic intramolecular QSAR analysis to model chemically and structurally diverse compounds interacting with cellular membranes) to generate predictive models of BBB partitioning of organic compounds by, in part, simulating the interaction of an organic compound with the phospholipid-rich regions of cellular membranes. This method was based on the assumption that the phospholipids regions of a cellular membrane constitute the receptor required in structure-based design that permits

the incorporation of structural and chemical diversity into a training set. A training set of 56 structurally diverse compounds whose BBB partition coefficients were measured was used to construct the MI-QSAR models. Molecular dynamics simulations were used to determine the interaction of each test compound with a model DMPC (dimyristoylphosphatidylcholine) monolayer membrane model. An additional set of intramolecular solute descriptors was computed and considered in the trial pool of descriptors for building MI-QSAR models. The QSAR models were optimized using multidimensional LR fitting and GA. A test set of seven compounds was evaluated using the MI-QSAR models as part of a validation process. Significant MI-QSAR models of the blood–brain partitioning process were constructed using a combination of general intramolecular solute, intermolecular solute–solvation, and intermolecular membrane–solute descriptors. The best model was found to have the following statistics (Eq. 54):

$$\begin{aligned} \log \text{BB} = & 70.0156 - 0.0231\text{PSA} + 0.1591\text{C} \log P - 0.0071E_{\text{MS}}(\text{chg} + \text{hbd}) \\ & + 0.0346E_{\text{ss}}(\text{tor}) + 0.0075\Delta E_{\text{TT}}(1-4) \\ n = & 56, r^2 = 0.845, q^2 = 0.795 \end{aligned} \quad (54)$$

where $E_{\text{MS}}(\text{chg} + \text{hbd})$ is the total intermolecular electrostatic and hydrogen-bonding interaction energy between the solute and DMPC monolayer, $0.0346E_{\text{ss}}(\text{tor})$ is the torsion energy of the solute, and $\Delta E_{\text{TT}}(1-4)$ is the change in 1, 4 nonbonded interaction energy of the system. The authors concluded that the BBB partitioning process can be reliably described for structurally diverse molecules provided interactions of the molecule with the phospholipids-rich regions of cellular membranes are explicitly considered.

Hutter [21] analyzed a data set of 174 compounds for which either the experimental log BB or the observed CNS activity were known. Out of these, 90 compounds were used as the training set to derive the log BB prediction equations and 23 compounds were used as an external validation set. Another 61 compounds were employed as the test set for the qualitative brain-penetration data. Initially, a large number of descriptors were computed for each molecule. Later the author identified the most relevant descriptors by careful inspection of the data set and the intercorrelation matrix. Strongly correlated and insignificant descriptors were then dropped from further statistical analysis. A best combination regression analysis was performed to elucidate how the remaining variables correlate with the observed log BB. The regression equation between log BB and the employed descriptors describing the ESP found was (Eq. 55)

$$\begin{aligned} \log \text{BB} = & 0.669 - 0.012(\pm 0.004)\text{ESPMIN} + 0.038(\pm 0.014)\text{M} - \text{ESP} \\ & - 0.010(\pm 0.002)\text{VXBAL} + 0.093(\pm 0.077)\text{QSUMH} \\ & + 0.292(\pm 0.044)\text{QSUMN} + 0.673(\pm 0.115)\text{QSUMO} \\ n = & 90, r = 0.873, r^2 = 0.762, \text{adj.}r^2 = 0.745, F = 44.228, \\ s = & 0.395 \end{aligned} \quad (55)$$

After further reduction in the number of variables by grouping them into categories, a total of 12 variables were retained for the final model. They were divided into five blocks each representing specific properties and the block-wise multiple regressions showed that all of these five groups contributed significantly to the correlation, giving rise to the final regression equation (56). Compared to the training set (values given in parentheses), the MAE in the test

set ($n = 23$) was 0.566 (0.217), the variance of the error was 0.450 (0.082), and the standard deviation of the error was 0.671 (0.287).

$$\begin{aligned} \log \text{BB} = & 3.5075 + 0.0449(\pm 0.0089)\text{M} - \text{ESP} - 0.0096(\pm 0.0027)\text{VXBAL} \\ & - 0.3723(\pm 0.0516)\text{HBDON} + 0.0181(\pm 0.0074)\text{CHBBA} \\ & + 0.0948(\pm 0.0287)\text{HALO} + 0.4456(\pm 0.1623)\text{NO} 2 \\ & + 0.2148(\pm 0.1215)\text{SU} - 0.0927(\pm 0.0626)\text{AR} 6 \\ & - 0.2457(\pm 0.0552)\text{IP} + 0.1170(\pm 0.0253)\text{PCGA} \\ & - 0.0205(\pm 0.0066)\text{PCGC} - 0.0395(\pm 0.0182)\text{ROTB} \\ n = & 90, r = 0.930, r^2 = 0.865, \text{adj.}r^2 = 0.844, F = 41.125, \\ \text{se} = & 0.309 \end{aligned} \quad (56)$$

Further, the resulting principal components of the variables were used to assign the CNS activity of compounds in the test set: low penetration (BBB−), medium permeability (BBB±), or ready absorbance (BBB+). Although some of the molecules were found to exhibit problems throughout all prediction approaches, the prediction was very good for the group of quinolones (difloxacin and related compounds), similar to the results of Crivori et al. and Rose et al. The CNS activity of the steroids also showed a clear differentiation between those that are readily absorbed and CNS-inactive compounds.

Hou and Xu [20] used a data set of 115 diverse organic compounds collected from different sources. The data set was divided into a training set of 78 compounds and two test sets of 14 compounds (from several literature sources) and 23 drug molecules (from the data set of Salminen and workers), respectively. They employed a new method, Slog P , for calculating log P of organic molecules by summing the contribution of atom-weighted solvent accessible surface areas and correction factors. Apart from log P , the other descriptor used were PSA, high-charged PSA (HCPSA, the PSA surrounding polar atoms with absolute partial charges larger than 0.1|e|), number of hydrogen-bond acceptors (HBA) and donors (HBD), molecular weight (MW), and molecular solvent-accessible surface area (SASA). Log P was found to be an important factor although it correlated with log BB poorly. A direct fitting of log P values with log BB of the compounds in the training set produced an r of ~ 0.5 (Eq. 57):

$$\begin{aligned} \log \text{BB} = & -0.552 + 0.236 \log P \\ n = & 72, r = 0.499, s = 0.659, F = 23.1 \end{aligned} \quad (57)$$

A simple LR of the 78 compounds in the training set using TPSA as the only descriptor resulted in the following equation and statistics (Eq. 58):

$$\begin{aligned} \log \text{BB} = & 0.571 - 0.0156\text{TPSA} \\ n = & 72, r = 0.755, s = 0.499, F = 92.8 \end{aligned} \quad (58)$$

Considering the effect of partial charges, a correlation between HCPSA and log BB led to the equation (59)

$$\begin{aligned} \log \text{BB} = & 0.589 - 0.0177\text{HCPSA} \\ n = & 72, r = 0.782, s = 0.474, F = 110.0 \end{aligned} \quad (59)$$

Then, they considered both log P and HCPSA in MLR. It was interesting to find that the partitioning of compounds between the blood and

brain compartments was effectively described by a combination of $\log P$ and HCPSA (Eq. 60):

$$\log BB = 0.219 + 0.139 \log P - 0.0158\text{HCPSA} \quad (60)$$

$$n = 72, r = 0.835, s = 0.421, F = 79.4$$

Incorporation of the number of hydrogen-bond donors and acceptors in Eq. 60 resulted in Eqs. 61 and 62. But HCPSA was found to be significantly correlated with HBD and HBA, indicating that it can be used to replace the descriptors related to hydrogen bonds.

$$\log BB = 0.221 + 0.139 \log P - 0.0156\text{HCPSA} - 0.00463n_{\text{HBA}} \quad (61)$$

$$n = 78, r = 0.827, s = 0.422, F = 53.3$$

$$\log BB = 0.212 + 0.139 \log P - 0.013\text{HCPSA} - 0.150n_{\text{HBD}} \quad (62)$$

$$n = 78, r = 0.830, s = 0.422, F = 54.6$$

Addition of molecular bulkiness properties, such as molecular weight, into the equation (60) led to the equation (63)

$$\log BB = 0.225 + 0.174 \log P - 0.0138\text{HCPSA} - 0.000709\text{MW} \quad (63)$$

$$n = 78, r = 0.829, s = 0.423, F = 54.2$$

To discover the effective range of MW, they applied a spline model for MW. The spline model was denoted with angled brackets. For example, $\langle \text{MW} - a \rangle$ was equal to zero if the value of $\text{MW} - a$ was negative; otherwise, it was equal to $\text{MW} - a$. The regression with splines allowed the incorporation of features that do not have a linear effect over their entire range. The best regression equation was as follows (Eq. 64):

$$\log BB = 0.00845 + 0.197 \log P - 0.0135\text{HCPSA} - 0.0140 \langle \text{MW} - 360 \rangle \quad (64)$$

$$n = 72, r = 0.886, s = 0.358, F = 82.6$$

The threshold value of 360 in Eq. 64 demonstrated that larger molecular weight produces lower permeation rates, but the effect takes effect only when the molecular weight is larger than 360. Since MW correlates well with molecular sizes, other similar descriptors such as molecular volume or molecular surface were also tried to be correlated with $\log BB$ but out of these the best model remained Eq. 64.

Subramanian and Kitchen [44] modeled the BBB permeability of a structurally diverse set of 281 compounds using LR and a multivariate genetic partial least squares (G/PLS) approach. They used $\log P$, PSA, and a variety of electrotopological indices for generating the models for predicting BBB permeability of the molecules. The best models revealed a good correlation ($r > 0.9$) for a training set of 58 compounds. Likewise, the comparison of the average $\log BB$ values obtained from an ensemble of QSAR models with experimental values also validated the statistical quality of the models ($r > 0.9$). The models provided good agreement ($r \sim 0.7$) between the predicted $\log BB$ values for 34 molecules in the external validation set and the experimental values. To further validate the models for use during the drug discovery process, a prediction set of 181 drugs with reported CNS penetration data was used. A $>70\%$ success rate was obtained by using any of the QSAR models in the qualitative prediction for CNS permeable (active) drugs. A lower success rate ($\sim 60\%$) was obtained for the best model for CNS impermeable (inactive)

drugs. Combining the predictions obtained from all the models (consensus) did not significantly improve the discrimination of CNS-active and CNS-inactive molecules. Finally, using the therapeutic classification as a guiding tool, the CNS penetration capability of over 2000 compounds in the Synthline database was estimated. The results were found to be very similar to the smaller set of 181 compounds.

Fu et al. [17] developed and compared MLR- and ANN-based models to predict log BB from their molecular structural parameters. The descriptors used include molecular volume (V), the sum of the absolute values of the net atomic charges of oxygen and nitrogen atoms which are hydrogen-bond acceptors ($Q_{O,N}$), and the sum of the net atomic charges of hydrogen atoms attached to oxygen or nitrogen atoms (Q_H). These parameters were calculated with the semiempirical self-consistent field molecular orbital calculation CNDO/2 method, using the minimum energy conformation obtained from the optimization of the standard molecular geometry with the molecular mechanics MM+ method. The atomic radii used to calculate molecular volumes (V , nm³) were similar those used by Clark.

A training set of 57 compounds studied by Lombardo et al., Norinder et al., and Clark was used to develop the following model using stepwise multiple regression analysis, after removing one outlier (Eq. 65):

$$\log \text{BB} = -0.5088 - 10.98V^2 + 9.991V + 1.554Q_H^2 - 2.037Q_{O,N} \quad (65)$$

$n = 56, r = 0.9044, s = 0.33, F = 57.28$

Again, a parabolic correlation between log BB and V indicated the twofold effects of molecular size on BBB penetration. Increasing molecular volume on one hand decreases the log BB value by decreasing the molecular diffusion through a lipid membrane. On the other hand, bigger molecular volume also increases lipophilicity, which, in turn, facilitates BBB penetration when $Q_{O,N}$ and Q_H remain unchanged.

In addition of the MLR-based model 65, the authors also generated an ANN model to predict log BB. The back-propagation algorithm with a modified learning rule, normalized cumulative delta was used to train the network. A “tanh” transfer function was used with a four-layered network that included an input layer, two hidden layers, and an output layer. Three descriptors V , $Q_{O,N}$, and Q_H were supplied as inputs to the neural network. The hidden layers consisted of three neurons and four neurons, respectively, whereas the output layer contained a single neuron. For the training set of 56 compounds, root mean squared errors (RMSE) between experimental log BB values and calculated log BB values from Eq. 65 (i.e., using MLR) and from the trained neural network were 0.368 and 0.236, respectively. The calculated results obtained from the neural network model were found to be better than those obtained from the MLR-based equation (65), thereby indicating that there are more complicated nonlinear relationships between log BB of a compound and its V , $Q_{O,N}$, and Q_H . To further assess the predictive abilities of Eq. 65 and the neural network model, the authors predicted the log BB values of six compounds outside the training set and compared them with other models developed by earlier workers. Although a very small test set was used, the neural network model performed better than these models.

Abraham [1] modeled the BBB penetration in terms of the permeability-surface area product, PS (in units of cm³ s⁻¹ g⁻¹), using the linear free energy

relationship approach based on the following general solvation equation given in Eq. 46: The data set consisted of experimental log PS values for perfusion from saline at pH 7.4, of 30 neutral compounds collected from the works of Gratton et al., Hider et al., Chikhale et al., and Pardridge and Mietus. Application of the above general equation of solvation to the 30 log PS values for neutral compounds led to Eq. 66. Leaving the insignificant term $e.E$ in Eq. 66 resulted in Eq. 67:

$$\begin{aligned} \log PS = & -0.639(0.408) + 0.312(0.515)E - 1.009(0.158)S \\ & - 1.895(0.385)A - 1.636(0.410)B + 1.709(0.392)V \\ n = 30, r^2 = & 0.870, = 0.52, F = 32.2 \end{aligned} \quad (66)$$

$$\begin{aligned} \log PS = & -0.716(0.383) - 0.974(0.146)S - 1.802(0.349)A \\ & - 1.603(0.401)B + 1.893(0.245)V \\ n = 30, r^2 = & 0.868, S = 0.52, F = 41.2 \end{aligned} \quad (67)$$

Because of the absence of enough data points, the predictive power of the model was not validated through division into a training set and a test set. Although the statistics of Eqs. 66 and 67 appeared to be quite good, some of the descriptors were significantly cross-correlated. However, a PLS analysis with five components yielded exactly the same coefficients as those in Eq. 66. Analyses with four components or three components also yielded coefficients in reasonable agreement with those in Eq. 66, which suggested that Eqs. 66 and 67 were quite soundly based. On the basis of model 65, the author concluded that compound polarity of any sort, that is, dipolarity/polarizability, hydrogen bond acidity, and hydrogen bond basicity, leads to a decrease in the rate of permeation, and compound size as measured by the McGowan volume, V , leads to an increase in permeation rate.

Liu et al. [28] determined the BBB permeability (in terms of log permeability-surface area product, log PS) for 28 drug-like compounds with a range of physicochemical properties, using a brain perfusion method. Compound structures were sketched into MOE package and charged and optimized by MMFF94 force field. Initially, 106 two-dimensional and internal three-dimensional descriptors were calculated in MOE but finally, only 50 most interpretable descriptors were used for statistical analysis. Two uptake substrates, phenylalanine and levodopa, and three P-gp substrates, CP-141938, digoxin, and quinidine, were excluded from the 28 compounds log PS data set. The remaining 23 compounds (training set) were considered as compounds with passive diffusion as the primary mechanism for BBB permeability for the purpose of modeling.

Two observations were made by the authors from their log PS data. First, disregarding the physical properties of compounds, the order of BBB permeability was active uptake compounds > passive diffusion compounds > efflux compounds. The average log PS of the two active uptake substrates was approximately one log unit greater than that of passive diffusion substrates; the average of log PS of diffusion substrates was approximately one log unit greater than that of efflux substrates. Second, basic compounds appeared to have higher BBB permeability than neutral and acidic compounds in this data set. The rank order of the average log PS values for the passive diffusion compounds by

ionization charge status was basic compounds > neutral compounds > acidic compounds.

A stepwise multivariate LR analysis of the log PS values of the 23 diffusion compounds and 50 descriptors yielded a linear equation that consisted of 10 descriptors. After considering the relevance in physical meaning of each descriptor and statistical significance, the 10-descriptor model was reduced to a 3-descriptor model (Eq. 68):

$$\begin{aligned} \log \text{PS} &= -2.19 + 0.262 \log D + 0.0583 \text{vas_base} - 0.00897 \text{TPSA} \\ n &= 23, \quad r^2 = 0.74, \quad s = 0.50, \quad F = 18.2 \end{aligned} \quad (68)$$

where log D is the partition coefficient in octanol/water at pH 7.4, TPSA is the topological van der Waals PSA, and vsa_base is the van der Waals surface area of the basic atoms. The F values for descriptors log D , vas_base , and TPSA were 24.3, 10.6, and 16.9, respectively. As per this model, log D and vas_base were found to have positive contributions to the log PS value, whereas TPSA had a negative contribution to the log PS value. Excluding one outlier from the model, the r^2 and s values were improved to 0.80 and 0.44, respectively. However, the log PS values of uptake substrates were underpredicted whereas those of the efflux substrates were overpredicted by the model.

The proposed model was tested against two literature data sets. The first data set contained 12 compounds reported by Gratton et al. [19], and the second data set included 13 compounds reported by Murakami et al. [31]. The two data sets led to Eqs. 69 and 70, respectively.

$$\begin{aligned} \log \text{PS}_{\text{Observed}} &= 1.17 + 0.639 \log \text{PS}_{\text{Predicted}} \\ n &= 12, \quad r^2 = 0.94, \quad s = 0.38, \quad F = 159 \end{aligned} \quad (69)$$

$$\begin{aligned} \log \text{PS}_{\text{Observed}} &= -0.161 + 0.950 \log \text{PS}_{\text{Predicted}} \\ n &= 12, \quad r^2 = 0.77, \quad s = 0.51, \quad F = 40 \end{aligned} \quad (70)$$

The model was also tested with the other literature models: log P , log D , log ($D \cdot \text{MW}^{-0.5}$), and LFER, resulting in Eqs. 71, 72, and 73. Log PS was found to have a better correlation with log D (Eq. 72) than log P (Eq. 71). Using log ($D \cdot \text{MW}^{-0.5}$) (Eq. 73) instead of log D was not found to improve the correlation significantly.

$$\begin{aligned} \log \text{PS} &= -3.02 + 0.269 \log P \\ n &= 23, \quad r^2 = 0.33, \quad s = 0.76, \quad F = 9.3 \end{aligned} \quad (71)$$

$$\begin{aligned} \log \text{PS} &= -2.71 + 0.312 \log D \\ n &= 23, \quad r^2 = 0.44, \quad s = 0.69, \quad F = 14.8 \end{aligned} \quad (72)$$

$$\begin{aligned} \log \text{PS} &= -2.32 + 0.322 \log(D \times \text{MW}^{-0.5}) \\ n &= 23, \quad r^2 = 0.45, \quad s = 0.69, \quad F = 15.7 \end{aligned} \quad (73)$$

On the basis of their results, the authors made the following interpretations. Consistent with literature reports, log D , a measure of lipophilicity, had positive contribution to BBB permeability. TPSA measures a compound's polarity and hydrogen-bonding potential and had negative contribution to log PS. A larger TPSA value usually deters a compound from entering the brain.

Descriptor *vsa_base* represents van der Waals surface area of basic atoms and indicates the basicity of a compound. Under physiological conditions, a compound with a high *vsa_base* value tends to be protonated and carries positive charges. The positive contribution to log PS indicated that basicity facilitates the compound's permeability across the BBB. This was consistent with their observation that basic compounds have higher log PS values than neutral and acidic compounds.

Winkler and Burden [47] used the same data set of 106 compounds as was used by Rose and workers. These were *in vivo* measurements in rats of the partition coefficient of the compound between the brain and the blood. The diversity of the data set was very high, with structures ranging from low molecular weight simple gases such as nitrogen and nitrous oxide to complex drug molecules such as codeine and imipramine. Three families of descriptors were investigated: feature based (number of hydrogen bond donors, acceptors, rotatable bonds, hydrophobes, log *P*, molecular weight, PSA), topological indices (Randic, electrotopological, atomistic, and functional group), and finally those based on eigenvalues of modified adjacency matrices (CIMI) and atomic charges binned into fingerprints. In order to determine the relative importance of the molecular descriptors, the authors employed an automatic relevance determination (ARD) approach which uses multiple regularization constants, one associated with each input. By applying Bayes theorem, the regularization constants for noninformative inputs are automatically inferred to be large, preventing those inputs from causing overfitting. Descriptors were mean autoscaled (mean centered and divided by the standard deviation), and biological data scaled to between zero and one. Bayesian regularized neural nets implemented in MATLAB were used, which are known to be independent of the network architecture (provided that a minimum number of hidden layer nodes were used), and are very resistant to overtraining and overfitting. The network architecture consisted of a single hidden layer, with a variable number of nodes, depending on the number descriptors chosen. The Bayesian net were trained using a gradient descent method until the log of the evidence was a maximum. The training was repeated several times but models were essentially identical, due to the robustness introduced into the training process by the Bayesian regularization.

The property-based descriptors resulted in the best training set statistics, with the topological indices and CIMI/binning charges descriptors producing models with inferior training statistics. With the property-based descriptors, it was necessary to use at least three hidden layer nodes to obtain good models. Increasing the number of hidden layer nodes beyond this minimum resulted in very similar models. This robustness was even more apparent with the other two descriptors classes that had 37 and 21 descriptors compared with 7 for the property-based descriptor class. The topological and CIMI/bc descriptor families produced essentially identical models with as few as one hidden layer node. This was suggestive of a fairly linear model when these descriptors were employed. Analysis of the test set regression statistics showed that all three descriptor families generated models with essentially the same predictive power.

The results suggested that the property-based descriptors are the most efficient, as they predicted new molecules as well or better than the other two families, and involve fewer descriptors than the topological descriptor family.

However, the CIMI/bc descriptors are relatively simplistic as they did not recognize differences between some important atom types (e.g., halogens). Based on the results of ARD approach, the octanol–water partition coefficient ($\log P$), the molecular flexibility (number of rotatable bonds), the PSA, and the number of hydrogen bond donors were the most important descriptors in the model. None of the descriptors were significantly correlated with each other except $\log P$ and PSA for which the correlation was not high (~ 0.5). The molecular weight was found to be the least significant descriptor in the model.

Cabrera et al. [7] predicted the BBB permeability of the molecules using a topological substructural molecular design approach (TOPS-MODE) and descriptors such as hydrophobicity and PSA. An LR model was developed to predict the *in vivo* blood–brain partitioning coefficient on a data set of 119 compounds, treated as the logarithm of the blood–brain concentration ratio. The final model explained 70% of the variance and it was validated through the use of an external validation set (33 compounds of the 119, MAE = 0.33), a leave-one-out cross-validation ($q^2 = 0.65$, $S_{\text{press}} = 0.43$), fivefold full cross-validation (removing 28 compounds in each cycle, MAE = 33, RMSE = 0.43), and the prediction of $+/-$ values for an external test set (85.7% of correct prediction). The methodology indicated that the hydrophobicity increases the BBB permeation, while the polar surface and its interaction with the atomic mass of compounds decrease it. Finally, by this approach, positive and negative substructural contributions to the brain permeation were identified, and their possibilities in the lead generation and optimization processes were evaluated.

Sun [45] generated predictive models for octanol/water partition coefficient ($\log P$), aqueous solubility ($\log S$), BBB ($\log \text{BB}$), and human intestinal absorption (HIA) from a universal, generic molecular descriptor system, designed on the basis of atom type classification. The advantage of using the atom types as generic molecular descriptors was to avoid preselecting the properties presumably related to the target property, thus reducing the opportunity of introducing bias at the beginning of model establishment. The emphasis of atom type classification was placed on maximizing the difference among the molecules by using as few atom types as possible. The contributions of different atom types to different target properties were automatically computed by PLS analysis. In total, 218 atom types were identified, including 88 types of C, 7 types of H, 55 types of N, 31 types of O, 8 types of halides, 23 types of S, and 6 types of P, together with 26 correction factors. The models to predict aqueous solubility, BBB, and HIA were built from the same atom types and correction factors identified from the trained atom classification tree. PLS regression was utilized to derive the models for $\log S$ and $\log \text{BB}$ with sevenfold cross-validations.

Abraham's data set of 57 compounds was selected as training set for $\log \text{BB}$ prediction. The test set contained the 13 compounds used by Clark and Liu et al. A three-component model was built from the atom type descriptors, and it estimated the data set of 57 compounds with an $r^2 = 0.897$, $q^2 = 0.504$, and RMSEE = 0.259. The relatively lower q^2 resulted from the small size of the data set. Totally, 94 different atom types were identified for the 57 compounds, and half of these atom types occurred only once or twice through the whole data set. When the compounds containing these atom types were left out in cross-validation, the contribution of these atom types could not be predicted accurately, since they did not appear in the training set. After

changing the cross-validation scheme from seven rounds to leave-one-out, the q^2 value increased to 0.552.

When the model built from Abraham's data set was used to predict the 13-compound test set, the RMSEP was 0.671, worse than Clark's or Abraham's models. The major reason was that the 13 compounds in the test set were not well covered by the chemical space defined by the training set. The 57-compound Abraham's data set contained 22 compounds from Young's data set and 35 of their own compounds. Young's data set is mostly composed of three structural analogues, cimetidines, guanidinotiazoles, and ranitidines, while the other compounds were largely small organic compounds. So, Abraham's data set is not structurally diverse. Abraham's descriptors and PSA used by Clark were less sensitive to the slight structural variation; thus, their models performed very well in this case. After exchanging four pairs of compounds in the training and test data sets to improve the chemical space coverage of the training set, r^2 and RMSEE of the new model improved to 0.910 and 0.502, and RMSEP of the new test set of 13 compounds was significantly reduced to 0.326.

Burns and Weaver [6] developed an MLR-based BBB permeability model using two experimental measures of BBB penetrability (brain/plasma ratio and the brain-uptake index) and 14 theoretically derived biophysical predictors based on Stein's hydrogen-bonding number and Randic's topological properties of the molecules. The final model accurately predicted the ability of test molecules to cross the BBB.

Yap and Chen [48] realized the significance of the nonlinear nature of relationship between the pharmacokinetic property of interest and the structural and physicochemical properties of the studied compounds. They developed a relatively new kind of nonlinear method, general regression neural network (GRNN), for modeling three drug distribution properties based on diverse sets of drugs. The three properties were BBB penetration, binding to human serum albumin, and milk-plasma distribution. The prediction capability of GRNN-developed models was compared to those developed using MLR and a nonlinear multilayer feedforward neural network (MLFN) method. For BBB penetration, the computed r^2 and MSE values of the GRNN-, MLR-, and MLFN-developed models were found to be 0.701 and 0.130, 0.649 and 0.154, and 0.662 and 0.147, respectively, by using an independent validation set. The corresponding values for human serum albumin binding are 0.851 and 0.041, 0.770 and 0.079, and 0.749 and 0.089, respectively, and that for milk-plasma distribution are 0.677 and 0.206, 0.224 and 0.647, and 0.201 and 0.587, respectively.

Ma et al. [31] developed BB penetration models using a training set of 37 organic compounds and a test set of 8 organic compounds (from Abraham's data set). The molecules were built and minimized, dissolved in liquid, and optimized by Monte Carlo method and molecular mechanics. Finally, the dominant conformations of these compounds were obtained. The intramolecular solute descriptors included molecular mechanism (MM) parameters, quantum chemistry parameters, hydrophobic parameters (such as Clog P), stereo parameters (such as Es and Balaban Index), and so on. The MM parameters comprised bending energy, stretch-bend energy, torsion energy, total energy, van der Waals energy, and others. The quantum chemistry parameters consisted of electronic energy, HOMO energy, LUMO energy, total energy, and so on. The data of molecular PSA were taken from the work of Iyer and colleagues. The

Membrane-Interaction (MI)-QSAR approach developed by Iyer et al. was used to develop predictive models of some organic compounds through BBB, and to simulate the interaction of a solute with the phospholipide-rich regions of cellular membranes surrounded by a layer of water. Molecular dynamics simulations were used to determine the explicit interaction of each test compound with the DMPC-water model (a model of dimyristoylphosphatidylcholine membrane monolayer, constructed using the software Material Studio according to the work done by van der Ploeg and Berendsen). Six MI-QSAR equations were constructed (Eqs. 74–79):

$$\log BB = 0.552 - 1.73 \times 10^{-2} \text{PSA}$$

$$n = 37, r = 0.835, s = 0.398 \quad (74)$$

$$\log BB = 0.229 - 1.70 \times 10^{-2} \text{PSA} + 0.131C \log P$$

$$n = 37, r = 0.878, s = 0.352 \quad (75)$$

$$\log BB = 4.965 \times 10^{-2} - 1.28 \times 10^{-2} \text{PSA} + 0.211C \log P$$

$$- 6.40 \times 10^{-7} B_{\text{Idx}} \quad (76)$$

$$n = 37, r = 0.924, s = 0.285$$

$$\log BB = 6.262 \times 10^{-2} - 1.36 \times 10^{-2} \text{PSA} + 0.205C \log P$$

$$- 7.11 \times 10^{-7} B_{\text{Idx}} - 0.185 E_{\text{sb}}$$

$$n = 37, r = 0.938, s = 0.264 \quad (77)$$

$$\log BB = 6.580 \times 10^{-2} - 1.21 \times 10^{-2} \text{PSA} + 0.206C \log P$$

$$- 7.77 \times 10^{-7} B_{\text{Idx}} - 0.197 E_{\text{sb}} + 1.330 \times 10^{-3} \text{DE}_{\text{total}}$$

$$n = 37, r = 0.947, s = 0.248 \quad (78)$$

$$\log BB = 8.730 \times 10^{-2} - 1.04 \times 10^{-2} \text{PSA} + 0.222C \log P$$

$$- 9.60 \times 10^{-7} \times B_{\text{Idx}} - 0.183 E_{\text{sb}} + 1.364 \times 10^{-3} \text{DE}_{\text{total}}$$

$$- 2.68 \times 10^{-3} \text{DE}_{\text{torsion}}$$

$$n = 37, r = 0.955, s = 0.232 \quad (79)$$

where B_{Idx} is the Balaban Index, namely, connective index of molecular average total distance (relative covalent radius), and E_{sb} is the stretch-bend energy of a molecule. In addition, intermolecular descriptors DE_{total} and $\text{DE}_{\text{torsion}}$ calculated from the molecular dynamics simulation were related to interactions between a solute and the DMPC-water model. They represented the change in the total potential energy and the dihedral torsion energy of the solute–membrane–water complex comparing with that of the DMPC-water model, respectively. With the increase in the number of variable from one to six, the relativity of MI-QSAR equations was also improved, and the predictive ability of the models was enhanced. Equation 79 was found to be the most significant, which indicated that the potential of an organic compound through BBB is directly proportional to $\text{Clog } P$ and DE_{total} , but inversely proportional to PSA , B_{Idx} , E_{sb} , and $\text{DE}_{\text{torsion}}$.

Narayanan and Gunturi [33] developed QSPR models based on *in vivo* blood–brain permeation data of 88 diverse compounds, 324 descriptors, and a systematic variable selection method called “Variable Selection and Modeling method based on the Prediction” (VSMP). VSMP efficiently explored all

possible combinations of descriptors and provided the best possible descriptor combination within the given pool of input descriptors. The VSMP methodology selected the descriptor combinations based on two parameters, namely, the intercorrelation coefficient between pairs of descriptors, r_{int} , and the correlation coefficient of prediction, q^2 .

The data containing 324 descriptor values of 88 molecules was given as an input to VSMP program, to build models based on three and four descriptors, keeping the interdescriptor correlation below 0.75. The best three-descriptors model, Eq. 80, was based on descriptors 254 (atomic type E-state index), 311 (AlogP98), and 320 (2D Van der Waals surface area) with a correlation coefficient, r , of 0.8425, and the cross-validated correlation coefficient, q , of 0.8239. The correlation coefficients of the other two VSMP models, Eqs. 81 and 82 were 0.8411 and 0.8329, respectively. Significantly, the descriptors 254 and 311 were selected in all the best three-descriptors models of VSMP. The three descriptors, in the models 80, 81, and 82 were 320, 144 (Kappa shape index of order 1), and 30 (topological Xu index), respectively.

$$\begin{aligned} \log \text{BB} = & (0.378578 + 0.230139) \text{ Desc 254} + 0.367865 \text{ Desc 311} \\ & - 0.00652 \text{ Desc 320} \end{aligned} \quad (80)$$

$$\begin{aligned} \log \text{BB} = & 0.273546 - 0.10856 \text{ Desc 144} + 0.192249 \text{ Desc 254} \\ & + 0.358259 \text{ Desc 311} \end{aligned} \quad (81)$$

$$\begin{aligned} \log \text{BB} = & 0.165811 - 0.19247 \text{ Desc 30} + 0.209871 \text{ Desc 254} \\ & + 0.347238 \text{ Desc 311} \end{aligned} \quad (82)$$

The best four-descriptors model, Eq. 83, was based on the descriptors 144, 254, 291 (atomic level-based AI topological descriptor), and 311 with $r = 0.8638$ and $q = 0.8472$. Descriptors 254 and 311 were again selected in all the best four-descriptors models of VSMP, 83, 84, and 85; descriptor 291 was common in 83 and 84, and 320 was common in 84 and 85.

$$\begin{aligned} \log \text{BB} = & 0.320182 - 0.11313 \text{ Desc 144} + 0.17469 \text{ Desc 254} \\ & + 0.046464 \text{ Desc 291} + 0.347461 \text{ Desc 311} \end{aligned} \quad (83)$$

$$\begin{aligned} \log \text{BB} = & 0.413638 + 0.214969 \text{ Desc 254} + 0.039116 \text{ Desc 291} \\ & + 0.357370 \text{ Desc 311} - 0.006690 \text{ Desc 320} \end{aligned} \quad (84)$$

$$\begin{aligned} \log \text{BB} = & 0.355632 + 0.286818 \text{ Desc 201} + 0.235403 \text{ Desc 254} \\ & + 0.334636 \text{ Desc 311} - 0.006140 \text{ Desc 320} \end{aligned} \quad (85)$$

The models 80 to 85 were validated using Leave-One-Out (LOO) method. The confidence level of prediction of these models was 100% for BBB- compounds with experimental log BB values in the range of -2.15 to -0.50 and 66% for compounds in the range of -0.50 to 0 . Similarly, the confidence level of prediction was 76% in the case of BBB+ compounds with experimental log BB in the range $+0.01$ to $+1.0$ and 100% for compounds in the range of $+1$ to $+1.5$. Based on these analyses, models 80 and 83 were found to be the best three- and four-descriptors models, generated by VSMP. The qualities of models were also tested using compounds that were not used in the training set. Of the 28 compounds used for external validation, models 80 and 83 were able to predict the correct log BB sign in 82% of the cases and 93% of the cases,

respectively. Further, model 83 was used to screen a test set of 92 drugs and drug-like compounds from the data set of Crivori and workers. The prediction of BBB using model 83 was found to be very good, with a correct classification of 80% of the BBB+ compounds (32 out of 40) and about 81% accuracy for the BBB– compounds (42 out of 52).

Garg and Verma [18] developed the ANN model for predicting BBB permeability of the molecules. A large data set of 191 experimental log BB values was collected from various published papers and online sources. Initially, 18 descriptors were selected for model development but many of them were found to be strongly correlated with each other. After removing such variables, finally seven descriptors were used for model building. They include molecular weight, TPSA, Clog P , number of hydrogen-bond acceptors and donors, number of rotatable bonds and P-gp substrate probability. In contrast to the earlier works, the authors have taken into consideration active transport of the molecules in the form of their probability of becoming a substrate to P-gp (P-gp is a transporter protein involved in extruding a variety of structurally unrelated compounds and preventing their accumulation within the brain) so as to generate accurate and reliable BBB models that can more closely mimic the *in vivo* situation.

The data set ($n = 191$) was divided into training ($n = 141$) and test sets ($n = 50$). A four-layered 7-5-2-1 neural network architecture was used with log-sigmoid transfer function in the hidden layers and linear transfer function in the output layer. Training of the neural network model was initially started with 141 molecules using MATLAB. But nine molecules were found to be the outliers. After removing these outliers, the remaining set of 132 molecules was used to train the neural network model. The trained model was then validated with a test set of 50 molecules. Results were found to be very good with the following model statistics:

For training set, $n = 132$, $r = 0.90$, adjusted $r^2 = 0.81$, and $s = 0.30$

For test set, $n = 50$, $r = 0.89$, adjusted $r^2 = 0.80$, and $s = 0.32$

During training, nine molecules were found to be the outliers. Interestingly, except one molecule, all other outlier molecules belonged to the class of neuromuscular blockers, and the experimental log BB values of all of them were extremely low. From their descriptor values, the most probable reasons for these molecules to act as outliers were found to be high molecular weight followed by high P-gp substrate probability and low Clog P .

The authors further validated their model by comparing the results with other computational models for predicting log BB values. The log BB values of the training and test sets molecules were also predicted using the online ADMET prediction tools such as PreADME, CSBBB, and commonly used commercial software Cerius2. The predicted values from these software were then compared with those predicted using the ANN model developed. The ANN model clearly outperformed the other models with $r^2 = 0.81$ followed by PreADME ($r^2 = 0.58$), CSBBB ($r^2 = 0.57$), and then Cerius2 ($r^2 = 0.44$).

The authors also determined the significance of each descriptor by setting its value to zero (leave-one-parameter approach). Out of the various descriptors used, molecular weight appeared to be the most significant parameter for predicting the BBB permeability, followed by TPSA, Clog P , number of hydrogen-bond acceptors, number of hydrogen-bond donors, P-gp substrate probability,

and finally the number of rotatable bonds. Although from these results it appears that P-gp substrate probability does not appear to be significantly contributing toward log BB, but after carefully examining the descriptor values of the molecules, it was found that P-gp substrate probability do play a role in determining the BBB permeability of the molecules. For example, the log BB value of icotidine was very low (-2.0) despite its acceptable molecular weight (379.47) and Clog P (1.99) values. This might be because its P-gp substrate probability was sufficiently high (0.78). Similarly a high P-gp substrate probability (0.81) of quinidine was responsible for its low log BB value (-0.46) despite having molecular weight (324.43) and Clog P (2.79) values within the acceptable range. Out of 182 molecules analyzed, only 18 molecules were having the value of P-gp substrate probability ≥ 0.5 . The coefficient of determination (r^2) between observed and predicted values of log BB for these molecules was also found to be good enough (0.81); hence the model appeared to be a robust and accurate BBB permeability predictor for most of the drug-like molecules.

The predictive performance of majority of the log BB models developed so far is ~ 0.4 log units, despite the great diversity of molecular descriptors employed and the variations in the composition of the training sets. This seems like a large error in comparison to the range of log BB determined by experiment (~ -2 to $+1.5$, i.e. ~ 3.5 log units). However, it should be remembered that the experimental error in log BB measurements can be around 0.3 log units, and so this value provides a limit to the accuracy of in silico methods.

22.3. Summary

Over recent years, there has been a great deal of work done to generate predictive models for brain permeation. Available data sets were studied using a variety of molecular descriptors and computational methods. Most of the approaches seem to achieve $>80\%$ correct classifications based on CNS+/CNS- data and predictions on small log BB test sets. Helpful insights into the molecular determinants of passive BBB permeation have also been gained. In particular, the crucial role of hydrogen-bonding/polarity has been brought to light. Gained knowledge can be applied in ongoing drug discovery programmes, perhaps in a qualitative manner [11]. Looking to the future, the most fundamental need is for more data, both in vitro and in vivo, upon which the next generation of predictive models can be built. As highlighted earlier, the largest log BB dataset consists of only ~ 190 compounds, of which some are not at all “drug-like.” Clearly, the small size of these training sets limits the general applicability of any model that is derived from them. Also, for increased effectiveness, brain permeation models will need to account for the role of active transport and efflux systems, as more data on these become available. Finally, in silico modeling will need to embrace the more information-rich data emerging from the noninvasive methods (e.g., positron emission tomography) of measuring the distribution of compounds within the brain.

Various models for BBB permeability prediction are summarized in terms of their data sets, methods employed, statistical parameters and descriptors, important outcomes in Tables 22.1 and 22.2, respectively.

Table 22.1 Data sets, methods and statistical parameters of the models

Working Group and References	Data Set	n	R^2	S	F	Q^2	Method		
Young et al. [49]	Histamine H ₂ -receptor antagonists (cimetidines, guanidinothiazoles, ranitidines, and other small organic compounds)	6	0.635	0.760	6.950		LR		
		6	0.025	1.241			LR		
		4	0.846	0.636	11.080		LR		
		6	0.678	0.713	8.430		LR		
		6	0.960	0.249	98.000		LR		
		20	0.690	0.439	40.230		LR		
		20	0.535	0.538	20.740		LR		
		20	0.190	0.711	4.230		LR		
		Waterbeemd and Kansy [46]	Young's data set	6	0.882	0.431	30.000		MLR
				6	0.945	0.294	69.300		MLR
6	0.906			0.387	38.300		MLR		
20	0.697			0.448	19.500		MLR		
20	0.720						MLR		
25	0.530						MLR		
Calder and Ganellin [8]	Young's data set	25	0.460				MLR		
		22	0.890	0.270	25.000		MLR		
		49	0.900	0.201	136.100		MLR		
Abraham et al. [2], [3], [4]	Young's data set + new compounds (hydrocarbons, gases, and other volatile molecules)	57	0.910	0.197	99.200		MLR		
		65	0.750	0.397	36.200		MLR		
		55	0.672	0.410	108.300		MLR		
Lombardo et al. [29]	Young's data set + Abraham's data set	28					DFA		
Basak et al. [5]	New compounds	20	0.642	0.486	15.200		MLR		
Kaliszan and Markuszewski [23]	Young's data set + Abraham's data set	20	0.845	0.321	46.000		MLR		
		20	0.889	0.271	67.900		MLR		
		33	0.897	0.126	131.100		MLR		

(cont.)

Table 22.1 (Continued)

Working Group and References	Data Set	<i>n</i>	<i>R</i> ²	<i>S</i>	<i>F</i>	<i>Q</i> ²	Method
Salminen et al. [41]	New data set (diverse drug-like molecules)	23	0.848	0.320	35.200		MLR
		26	0.581	0.560	10.200		MLR
Norinder et al. [34]	Data set assembled by Lombardo	28	0.862	0.311	49.930	0.782	PLS
		56	0.834	0.312	86.950	0.775	PLS
Clark [10]	Data set assembled by Lombardo	55	0.787	0.354	95.800		MLR
		55	0.767	0.369	86.000		MLR
		55	0.707	0.410	128.400		MLR
		57	0.670	0.455	112.400		MLR
Kelder et al. [25]	Data set assembled by Lombardo + new compounds	45	0.841		229.000		MLR
Luco [30]	Young's data set + Abraham's data set + new compounds	58	0.850	0.318	102.000	0.752	PLS
Osterberg and Norinder [35]	Data sets assembled by Clark and Kelder	45	0.758			0.747	PLS
		45	0.720			0.707	PLS
		69	0.649			0.640	PLS
		69	0.756			0.746	PLS
Ertl et al. [14]	Data sets assembled by Clark and Kelder	45	0.780				MLR
		55	0.660				MLR
Fehér [15]	Data set assembled by Luco	61	0.730		0.510		MLR
Crivori et al. [12]	New qualitative data set	110					PCA, DPLS
Keseru and Molnar [26]	Young's data set + Abraham's data set + new compounds	55	0.720	0.370			LR
Kaznessis et al. [24]	Young's data set + Abraham's data set + new compounds	76	0.941	0.173	311.307		MLR

Liu et al. [27]	Abraham's data set + Young's data set	55	0.790	0.350	97.700	MLR
		55	0.694	0.420	120.300	MLR
		55	0.797	0.350	66.600	MLR
		55	0.741	0.390	74.300	MLR
		55	0.703	0.420	61.400	MLR
		55	0.808	0.300		ANN
		11	0.806	0.350		ANN
Platts [39]	Data sets of Young, Abraham, Salminen, Kelder, Norinder + new compounds	148	0.745	0.343	69.000	MLR
		148	0.710	0.367	71.000	MLR
		148	0.744	0.342	83.000	MLR
		74	0.767	0.331		MLR
		74	0.763	0.344		MLR
		74	0.735	0.376		MLR
		74	0.701	0.385		MLR
Fu et al. [16]	Data set assembled by Lombardo	56	0.818	0.327	77.780	MLR
		56	0.762	0.373	53.620	MLR
		56	0.801	0.341	69.850	MLR
Rose et al. [40]	Data sets of Young, Abraham, Salminen, Clark, Luco, Lombardo, Calder + new compounds	102	0.660	0.450	62.400	MLR
Iyer et al. [22]	New data set	56	0.845			MLR, GA
Hutter [21]	Data sets of Young, Abraham, Salminen, Clark, Luco, Kelder, Crivori, Rose, Lombardo, Calder + new compounds	90	0.865	0.309	41.125	MLR, PCA
		90	0.762	0.395	44.228	MLR, PCA
		90	0.825	0.347	37.237	MLR, PCA
Hou and Xu [20]	Data set assembled by Rose + new compounds	78	0.774	0.360	81.500	MLR
		78	0.242	0.649	24.300	MLR
		78	0.567	0.490	100.400	MLR
		78	0.606	0.468	117.400	MLR
		78	0.683	0.422	81.100	MLR

(cont.)

Table 22.1 (Continued)

Working Group and References	Data Set	n	R^2	S	F	Q^2	Method
Subramanian and Kitchen [44]	Young's data set + Abraham's data set + new compounds	78	0.683	0.422	53.300		MLR
		78	0.688	0.422	54.600		MLR
		78	0.687	0.423	54.200		MLR
		78	0.767	0.364	81.500		MLR
		78	0.760	0.370	78.400		MLR
		78	0.751	0.377	74.400		MLR
		78	0.743	0.375	66.900		MLR
		58	0.810				
Abraham [1]	New data set	30	0.870	0.520	32.200		PLS
		30	0.868	0.520	41.200		PLS
Fu et al. [17]	Data sets of Lombardo, Norinder, and Clark	56	0.818	0.330	57.280		ANN
		5					ANN
Liu et al. [28]	New data set	23	0.800	0.440			MLR
		23	0.740	0.500	18.200		MLR
		12	0.940	0.380	159.000		MLR
		12	0.770	0.510	40.000		MLR
		23	0.330	0.760	9.300		MLR
		23	0.440	0.690	14.800		MLR
23	0.450	0.690	15.700		MLR		
10	0.610	0.590	12.400		MLR		

Winkler and Burden [47]	Data set assembled by Rose	85	0.760	0.390	0.650	BNN										
		86	0.630	0.500	0.590	BNN										
		115	0.690	0.430	0.610	BNN										
		94	0.790	0.370	0.590	BNN										
		86	0.810	0.370	0.650	BNN										
		92	0.800	0.370	0.650	BNN										
		86	0.800	0.370	0.640	BNN										
		85	0.790	0.370	0.650	BNN										
		81	0.740	0.390	0.650	BNN										
		88	0.780	0.370	0.650	BNN										
		86	0.620	0.500	0.650	BNN										
Cabrera et al. [7]	Data set assembled by Rose + new molecules	86	0.610	0.500	0.650	BNN										
		86	0.550	0.540	0.650	BNN										
		86	0.540	0.540	0.640	BNN										
		119			0.650	MLR										
		Sun [45]	Data sets assembled by Abraham, Clark, and Liu	57	0.900			PLS								
				Burns and Weaver [6]	Data set assembled from earlier works + new compounds					MLR						
						Yap and Chen [48]	Data set assembled from earlier works + new compounds	0.701			GRNN					
								0.662			MFNN					
								0.649			MLR					
								Ma et al. [31]	Abraham's data set	37	0.912	0.232		MLR		
										Narayanan and Gunturi [32]	Data sets of Young, Abraham, Clark, Kelder, Crivori, Rose, Ertl, Lombardo, Keseru, Liu, Hou, Norinder, and Hutter	88	0.746	0.391	60.982	VSMP,MLR
88	0.709											0.416	68.490	VSMP,MLR		
Garg and Verma [18]	Data sets assembled by Platts, Rose + new molecules											146	0.965	0.263	181.622	ANN
												49	0.786	0.921	1.356	ANN
												132	0.810	0.333	76.559	ANN
		50	0.815									0.292	32.380	ANN		

Table 22.2 Descriptors employed and important outcomes of the models

Working Group and References	Descriptors Used	Important Conclusions
Young et al. [49]	Lipophilicity and hydrogen-bonding	BBB permeability increases with decreasing overall hydrogen-bonding ability of a compound (for e.g., by facilitating intramolecular hydrogen bonding, protecting with nonpolar groups, and by making less polar prodrugs).
Waterbeemd and Kansy [46]	Hydrogen-bonding	Predicted log BB with calculated molecular descriptors and concluded that BBB permeability can be increased by reducing the hydrogen-bonding ability of a compound.
Calder and Ganellin [8]	Size and hydrogen-bonding	BBB permeability decreases with increasing overall size and hydrogen-bonding ability of a compound.
Abraham et al. [2], [3], [4]	Solubility, excess molar refraction, polarizability, hydrogen-bond acidity/basicity, and McGowan volume	Log P should only be used in conjunction with solute descriptors. Solute dipolarity/polarizability, hydrogen-bond acidity, and hydrogen-bond basicity favors blood and solute size favors brain.
Lombardo et al. [29]	Solvation free energy in water	Nonpolar/lipophilic compounds partition well into the brain as compared to the polar/hydrophilic compounds.
Basak et al. [5]	Log P, hydrogen-bonding parameter, and topological indices	Lipophilicity is not a reliable parameter for classifying the CNS activity of the particular set of compounds used in the study.
Kaliszan and Markuszewski [23]	Lipophilicity, size, and water-accessible volume	BBB permeability increases with increasing lipophilicity and reducing size and water-accessible volume.
Salminen et al. [41]	log k_{IAM} , molecular volume, and an ionization variable	Provided a better model for membrane distribution of ionized compounds and concluded that brain favors cationic compounds over phospholipid membranes.
Norinder et al. [34]	Polarity, Lewis base strength, and hydrogen-bonding	High lipophilicity, low hydrogen-bonding potential, presence of polarizable electrons, and charge-transfer interactions enhances BBB permeability.
Clark [10]	Lipophilicity and PSA	Compounds with high lipophilicity and low PSA tend to penetrate the brain better.
Kelder et al. [25]	PSA	Orally active drugs that are transported passively by the transcellular route can be tailored to brain permeation by decreasing the PSA to less than 60–70 Å ² .

Luco [30]	Topological and constitutional descriptors	Molecular size, shape, polarity, and hydrogen-bonding potential are the primary factors governing a compound's ability to penetrate BBB.
Osterberg and Norinder [35]	Lipophilicity and hydrogen-bonding	BBB permeability can be increased by increasing lipophilicity and decreasing hydrogen-bonding ability.
Ertl et al. [14]	TPSA	Low PSA increases BBB permeability of compounds. Fragment-based TPSA methodology is also fast and easy to compute for large number of compounds.
Feher (2000) [15]	Lipophilicity and hydrogen-bonding	A highly diverse set of molecules was used to show some conclusions regarding lipophilicity and hydrogen-bonding, as interpreted by other workers.
Crivori et al. [12]	Molecular size, shape, polarity, hydrogen-bonding, and other Volsurf-generated variables	Descriptors of polarity such as hydrophilic regions, capacity factors, and hydrogen-bonding are inversely correlated with BBB permeability. Diffuse polar regions are acceptable for BBB permeation as compared to dense and localized polar regions.
Keseru and Molnar [26]	Solvation free energy in water	Compounds with log BB greater than 0.3 cross the barrier readily, while compounds with log BB less than -1.0 are only poorly distributed to the brain. Orally administered CNS-active drugs should have a solvation free energy higher than -40 kJ/mol.
Kaznessis et al. [24]	Solvent accessible surface area, hydrogen-bonding, solute dipole, molecular volume, etc.	BBB penetration can be increased by reducing the hydrophilicity of the compounds. hydrogen-bond acceptors and molecular volume are the important parameters influencing BBB permeability of the compounds.
Liu et al. [27]	Lipoaffinity, molecular weight, and TPSA	Larger molecular size and hydrophilicity reduces the permeation rate, whereas lipoaffinity (molecular hydrophobicity) enhances the BBB permeability of the molecules.
Platts [39]	Hydrogen-bonding, polarity/polarizability, and size	Increasing molecular size and the presence of n - and π -electron pairs tend to push compounds out of blood and into brain. Polarity and hydrogen-bonding ability act to keep compounds in blood and out of the brain.
Fu et al. [16]	PSA and molecular volume	BBB permeability of a compound is favored by weak hydrogen-bonding potential, high lipophilicity, and small size.

(cont.)

Table 22.2 (Continued)

Working Group and References	Descriptors Used	Important Conclusions
Rose et al. [40]	E-State indices, chi indices, and kappa shape indices	BBB permeability of the compounds increases with increasing number of aromatic CH groups, less skeletal branching, and fewer or weaker H-bond donor groups.
Iyer et al. [22]	Intramolecular solute, intermolecular solute-solvation and intermolecular membrane-solute descriptors	For describing BBB permeability of the compounds, interactions of the molecule with the phospholipids-rich regions of cellular membranes should be considered explicitly.
Hutter [21]	Molecular size, polarizability, hydrogen-bonding, and many quantum-chemically derived descriptors	Descriptors related to PSA, ionization potential, and hydrogen-bonding are significant in influencing the BBB permeability of compounds.
Hou and Xu [20]	Lipophilicity, size, and hydrogen-bonding	Compounds with molecular weight more than 360 tend to have lower BBB permeability. High lipophilicity and low hydrogen-bonding ability of compounds favors BBB permeation.
Subramanian and Kitchen [44]	Lipophilicity, hydrogen-bonding, and electrotopological indices	BBB permeability can be enhanced by increasing the lipophilicity and decreasing the hydrogen-bonding potential of the compounds.
Abraham [1]	Solubility, excess molar refraction, polarizability, hydrogen-bond acidity/basicity, and McGowan volume	Increase in polarity, polarizability, and hydrogen-bonding ability leads to a decrease in BBB permeation rate. Compound size as measured by the McGowan volume leads to an increase in the permeation rate.
Fu et al. [17]	Molecular volume, hydrogen-bond donors, and hydrogen-bond acceptors	Increasing molecular volume decreases the log BB value by decreasing the molecular diffusion through a lipid membrane. But at the same time, bigger molecular volume also increases lipophilicity, which, in turn, facilitates BBB penetration.
Liu et al. [28]	Lipophilicity, total PSA, and van der Waals surface area	High lipophilicity and van der Waals surface area of basic atoms facilitates a compound's BBB permeability, whereas high polarity and hydrogen-bonding potential have a negative impact on the BBB permeability.
Winkler and Burden [47]	Topological, constitutional, hydrogen-bonding, and descriptors based on adjacency matrices	Property-based descriptors, lipophilicity, molecular flexibility, PSA, and number of hydrogen-bond donors are the main parameters influencing the BBB permeability of compounds.

Cabrera et al. [7]	Hydrophobicity, PSA, and topological descriptors	Hydrophobicity increases the BBB permeability of compounds, whereas the polar surface and its interaction with the atomic mass of compounds decrease the BBB permeation rate.
Sun [45]	Descriptors based on atom-types and correction factors	By analyzing the atomic contributions to different target properties like BBB permeability, specific atom-types affecting these properties can be identified.
Burns and Weaver [6]	Stein's hydrogen-bonding number and Randić's topological properties	Reducing the hydrogen-bonding potential of the compounds can enhance their ability to penetrate BBB.
Yap and Chen [48]	Structural and physicochemical properties	General regression neural network methodology is potentially more useful for predicting the QSPR relationships as compared to multiple linear regressions.
Ma et al. [31]	Hydrophobicity, stereo parameters, and descriptors based on molecular and quantum mechanics	BBB permeability increases with an increase in lipophilicity and solute–membrane interactions. PSA, Balaban index, and stretching-bending energy of the molecules have negative contributions toward their BBB permeability.
Narayanan and Gunturi [33]	Lipophilicity, E-state indices, Van der Waals surface area, etc.	Molecular lipophilicity, topological indices, and Van der Waals surface area are the important parameters governing BBB permeability of the compounds.
Garg and Verma [18]	Lipophilicity, hydrogen-bonding, size, and P-gp substrate probability	Molecular weight is the most significant parameter for predicting the BBB permeability, followed by TPSA, log <i>P</i> , number of hydrogen-bond acceptors, number of hydrogen-bond donors, P-gp substrate probability, and finally the number of rotatable bonds.

References

1. Abraham MH (2004) The factors that influence permeation across the blood-brain barrier. *Eur J Med Chem* 39:235–240.
2. Abraham MH, Chadha HS, Mitchell RC (1994) Hydrogen bonding. 33. Factors that influence the distribution of solutes between blood and brain. *J Pharm Sci* 83:1257–1268.
3. Abraham MH, Chadha HS, Mitchell RC (1995) Hydrogen-bonding. Part 36. Determination of blood brain distribution using octanol-water partition coefficients. *Drug Des Discov* 13:123–131.
4. Abraham MH, Takacs-Novak K, Mitchell RC (1997) On the partition of ampholytes: application to blood-brain distribution. *J Pharm Sci* 86:310–315.
5. Basak SC, Gute BD, Drewes LR (1996) Predicting blood-brain transport of drugs: a computational approach. *Pharm Res* 13:775–778.
6. Burns J, Weaver DF (2004) A mathematical model for prediction of drug molecule diffusion across the blood-brain barrier. *Can J Neurol Sci* 31:520–527.
7. Cabrera MA, Bermejo M, Perez M, Ramos R (2004) TOPS-MODE approach for the prediction of blood-brain barrier permeation. *J Pharm Sci* 93:1701–1717.
8. Calder JA, Ganellin CR (1994) Predicting the brain-penetrating capability of histaminergic compounds. *Drug Des Discov* 11:259–268.
9. Chudler E (1996) Neuroscience for Kids - Blood-Brain-Barrier, available at <http://faculty.washington.edu/chudler/bbb.html>.
10. Clark DE (1999) Rapid calculation of polar molecular surface area and its application to the prediction of transport phenomena. 2. Prediction of blood-brain barrier penetration. *J Pharm Sci* 88:815–821.
11. Clark DE (2003) In silico prediction of blood-brain barrier permeation. *Drug Discov Today* 8:927–933.
12. Crivori P, Cruciani G, Carrupt PA, Testa B (2000) Predicting blood-brain barrier permeation from three-dimensional molecular structure. *J Med Chem* 43:2204–2216.
13. de Boer AG, van der Sandt IC, Gaillard PJ (2003) The role of drug transporters at the blood-brain barrier. *Annu Rev Pharmacol Toxicol* 43:629–656.
14. Ertl P, Rohde B, Selzer P (2000) Fast calculation of molecular polar surface area as a sum of fragment-based contributions and its application to the prediction of drug transport properties. *J Med Chem* 43:3714–3717.
15. Feher M, Sourial E, Schmidt JM (2000) A simple model for the prediction of blood-brain partitioning. *Int J Pharm* 201:239–247.
16. Fu XC, Chen CX, Liang WQ, Yu QS (2001) Predicting blood-brain barrier penetration of drugs by polar molecular surface area and molecular volume. *Acta Pharmacol Sin* 22:663–668.
17. Fu XC, Wang GP, Liang WQ, Yu QS (2004) Predicting blood-brain barrier penetration of drugs using an artificial neural network. *Pharmazie* 59:126–130.
18. Garg P, Verma J (2006) In silico prediction of blood brain barrier permeability: an artificial neural network model. *J Chem Inf Model* 46:289–297.
19. Gratton JA, Abraham MH, Bradbury MW, Chadha HS (1997) Molecular factors influencing drug transfer across the blood-brain barrier. *J Pharm Pharmacol* 49:1211–1216.
20. Hou TJ, Xu XJ (2003) ADME Evaluation in Drug Discovery. 3. Modeling Blood-Brain Barrier Partitioning Using Simple Molecular Descriptors. Erratum in: *J Chem Inf Comput Sci*. 2004 Mar-Apr;44(2):766–70. *J Chem Inf Comput Sci* 43:2137–2152.
21. Hutter MC (2003) Prediction of blood-brain barrier permeation using quantum chemically derived information. *J Comput Aided Mol Des* 17:415–433.

22. Iyer M, Mishru R, Han Y, Hopfinger AJ (2002) Predicting blood-brain barrier partitioning of organic molecules using membrane-interaction QSAR analysis. *Pharm Res* 19:1611–1621.
23. Kaliszán R, Markuszewski M (1996) Brain/blood distribution described by a combination of partition coefficient and molecular mass. *Int J Pharm* 145:9–16.
24. Kaznessis YN, Snow ME, Blankley CJ (2001) Prediction of blood-brain partitioning using Monte Carlo simulations of molecules in water. *J Comput Aided Mol Des* 15:697–708.
25. Kelder J, Grootenhuís PD, Bayada DM, Delbressine LP, Ploemen JP (1999) Polar molecular surface as a dominating determinant for oral absorption and brain penetration of drugs. *Pharm Res* 16:1514–1519.
26. Keseru GM, Molnar L (2001) High-throughput prediction of blood-brain partitioning: a thermodynamic approach. *J Chem Inf Comput Sci* 41:120–128.
27. Liu R, Sun H, So SS (2001) Development of quantitative structure-property relationship models for early ADME evaluation in drug discovery. 2. Blood-brain barrier penetration. *J Chem Inf Comput Sci* 41:1623–1632.
28. Liu X, Tu M, Kelly RS, Chen C, Smith BJ (2004) Development of a computational approach to predict blood-brain barrier permeability. *Drug Metab Dispos* 32:132–139.
29. Lombardo F, Blake JF, Curatolo WJ (1996) Computation of brain-blood partitioning of organic solutes via free energy calculations. *J Med Chem* 39:4750–4755.
30. Luco JM (1999) Prediction of the brain-blood distribution of a large set of drugs from structurally derived descriptors using partial least-squares (PLS) modeling. *J Chem Inf Comput Sci* 39:396–404.
31. Ma XL, Chen C, Yang J (2005) Predictive model of blood-brain barrier penetration of organic compounds. *Acta Pharmacol Sin* 26:500–512.
32. Murakami H, Takanaga H, Matsuo H, Ohtani H, Sawada Y (2000) Comparison of blood-brain barrier permeability in mice and rats using in situ brain perfusion technique. *Am J Physiol* 279:H1022–H1028.
33. Narayanan R, Gunturi SB (2005) In silico ADME modelling: prediction models for blood-brain barrier permeation using a systematic variable selection method. *Bioorg Med Chem* 13:3017–3028.
34. Norinder U, Sjöberg P, Osterberg T (1998) Theoretical calculation and prediction of brain-blood partitioning of organic solutes using MolSurf parametrization and PLS statistics. *J Pharm Sci* 87:952–959.
35. Osterberg T, Norinder U (2000) Prediction of polar surface area and drug transport processes using simple parameters and PLS statistics. *J Chem Inf Comput Sci* 40:1408–1411.
36. Pardridge WM (2003) Blood-brain barrier drug targeting: the future of brain drug development. *Mol Interv*, 3: 90–105.
37. Pardridge WM (2001) Drug targeting, drug discovery, and brain drug development. In: *Brain Drug Targeting: The Future of Brain Drug Development*, 1 ed., Cambridge University Press, pp. 1–12 (ISBN 0521800773).
38. Pardridge WM (2004) Log(BB), PS products and in silico models of drug brain penetration. *Drug Discov Today* 9:392–393.
39. Platts JA, Abraham MH, Zhao YH, Hersey A, Ijaz L, Butina D (2001) Correlation and prediction of a large blood-brain distribution data set—an LFER study. *Eur J Med Chem* 36:719–730.
40. Rose K, Hall LH, Kier LB (2002) Modeling blood-brain barrier partitioning using the electrotopological state. *J Chem Inf Comput Sci* 42:651–666.
41. Salminen T, Pulli A, Taskinen J (1997) Relationship between immobilised artificial membrane chromatographic retention and the brain penetration of structurally diverse drugs. *J Pharm Biomed Anal* 15:469–477.

42. Scala S, Akhmed N, Rao US, Paull K, Lan LB, Dickstein B, Lee JS, Elgemeie GH, Stein WD, Bates SE (1997) P-glycoprotein substrates and antagonists cluster into two distinct groups. *Mol Pharmacol* 51:1024–1033.
43. Seelig A, Gottschlich R, Devant RM (1994) A method to determine the ability of drugs to diffuse through the blood-brain barrier. *Proc Natl Acad Sci USA* 91:68–72.
44. Subramanian G, Kitchen DB (2003) Computational models to predict blood-brain barrier permeation and CNS activity. *J Comput Aided Mol Des* 17:643–664.
45. Sun H (2004) A Universal Molecular Descriptor System for Prediction of LogP, LogS, LogBB, and Absorption. *J Chem Inf Comput Sci* 44:748–757.
46. van de Waterbeemd H, Kansy M (1992) Hydrogen-bonding capacity and brain penetration. *Chimia* 46:299–303.
47. Winkler DA, Burden FR (2004) Modelling blood-brain barrier partitioning using Bayesian neural nets. *J Mol Graph Model* 22:499–505.
48. Yap CW, Chen YZ (2005) Quantitative Structure-Pharmacokinetic Relationships for drug distribution properties by using general regression neural network. *J Pharm Sci* 94:153–168.
49. Young RC, Mitchell RC, Brown TH, Ganellin CR, Griffiths R, Jones M, Rana KK, Saunders D, Smith IR, Sore NE, et al. (1988) Development of a new physicochemical model for brain penetration and its application to the design of centrally acting H2 receptor histamine antagonists. *J Med Chem* 31:656–671.

Impact of Drug Transport Proteins

Tomohiro Terada and Ken-ichi Inui

Abstract Drug transporters play critical roles in the absorption, distribution, and excretion of drugs and have been classified into five major families, peptide transporters (PEPT, SLC15), organic anion-transporting polypeptides (OATP, SLCO), organic ion transporters (OCT/OCTN/OAT/URAT, SLC22), H⁺/organic cation antiporters (MATE, SLC47), and ABC drug transporters, such as P-glycoprotein (P-gp/MDR1, ABCB1). Their structures, tissue distribution, functions, and pharmacokinetic roles vary. The roles of drug transporters can be assessed in vitro and in vivo, using techniques spanning from cellular expression systems to gene knockout animals. Research outcomes from such studies have been applied to clinical science and drug development. In this chapter, the basic characteristics of drug transporters were reviewed with an emphasis on their impact on clinical/preclinical research.

Abbreviations

ABC	ATP-binding cassette
ACR	Acute cellular rejection
BCRP	Breast cancer resistance protein
BSEP	Bile salt export pump
CYP	Cytochrome P450
GFR	Glomerular filtration rate
HGNC	Human Gene Nomenclature Committee
HMG-CoA	3-Hydroxy-3-methylglutaryl coenzyme A
LDLT	Living-donor liver transplantation
MATE	Multidrug and toxin extrusion
MDR	Multidrug resistance protein
MRP	Multidrug resistance-associated protein
NBD	Nucleotide-binding domain
OAT	Organic anion transporter
OATP	Organic anion-transporting polypeptide
OCT	Organic cation transporter
OCTN	Novel organic cation transporter
PAH	P-aminohippurate
PCR	Polymerase chain reaction

PEPT	H ⁺ /peptide cotransporter
P-gp	P-glycoprotein
SLC	Solute carrier
SNP	Single nucleotide polymorphism
SUR	Sulfonylurea receptor
TEA	Tetraethylammonium
TM	Transmembrane
URAT	Urate transporter

Keywords: Drug transporter; SLC-transporter; ABC transporter; Drug delivery; Intestinal absorption barrier

23.1. Introduction

Drug efficacy and safety are determined by the interplay of multiple processes that regulate pharmacokinetics (e.g., absorption, distribution, metabolism, and excretion) and pharmacodynamics (e.g., drug action). For orally administered drugs, pharmacologic action is dependent on an adequate intestinal absorption and distribution before elimination via metabolic and excretory pathways. Drug-metabolizing enzymes have been believed to be the key determinants of pharmacokinetics. The membrane transport processes are also recognized as important to pharmacokinetic properties, but classical analyses were mainly performed *in vivo* or in excised tissues, mostly lacking *in vitro* methodologies to precisely evaluate the membrane transport characteristics of drugs.

In the early 1980s, studies of membrane vesicles and cultured epithelial cell lines were introduced into the research field of drug transport and the biochemical characterization of drug transport advanced remarkably. For example, the driving force and substrate specificity of a drug transporter were clearly demonstrated using membrane vesicles, and transepithelial transport and regulatory aspects were characterized by using cultured cell lines. At the end of 1980s, the molecular nature of drug transporters was unveiled by cDNA cloning and the first clinically important drug transporter, the P-glycoprotein (P-gp), was identified. Subsequently, various primary and secondary active drug transporters were isolated by expression cloning, polymerase chain reaction (PCR) cloning, and *in silico* homology screening strategies. The most recently identified drug transporters are the renal H⁺/organic cation antiporters reported in 2005–2006. Although numerous drug transporters have been characterized so far, many others remain unidentified. For example, the molecular nature of the facilitative peptide transporters, which are located at the basolateral membranes of intestinal epithelial cells and are quite important for the transepithelial transport of peptide-like drugs, has not been elucidated.

Many drugs have been recognized to cross the intestinal epithelial cells via passive diffusion, thus their lipophilicity has been considered important. However, as described above, recent studies have demonstrated that a number of drug transporters including uptake and efflux systems determine the membrane transport process. In this chapter, we provide an overview of the basic characteristics of major drug transporters responsible not only for absorption but also for disposition and excretion in order to delineate the impact of drug transport proteins on pharmacokinetics.

23.2. Determination and Classification of Drug Transporters

Transporters have been functionally classified as primary and secondary active transporters. Primary active transporters include ATP-binding cassette (ABC) transporters that utilize the hydrolysis of ATP as a driving force. Secondary active transporters utilize various driving forces such as ion concentration gradients and electrical potential differences across cell membranes, according to the physicochemical properties of substrates and membrane localization of transporters. The Human Gene Nomenclature Committee (HGNC) has classified drug transporters based on sequence similarity as solute carriers (SLCs) and ABC transporters.

Although many members of the ABC and SLC families are categorized as drug transporters, because of their pharmacokinetic relevance and detailed characterization, only the following transporters are discussed in this chapter: peptide transporters (PEPT, SLC15), organic anion-transporting polypeptides (OATP, SLCO), organic ion transporters (OCT/OCTN/OAT/URAT, SLC22) and H⁺/organic cation antiporters (MATE, SLC47), P-glycoprotein (P-gp/MDR1, ABCB1), multidrug resistance-associated proteins (MRP2 and MRP3, ABCC), and breast cancer-resistance protein (BCRP, ABCG2). Secondary structures of these transporters are shown in Figure 23.1.

23.3. Characteristics of Major Drug Transporters

23.3.1. PEPT (SLC15)

23.3.1.1. Structure and Tissue Distribution

A cDNA encoding the H⁺/peptide cotransporter (PEPT1) was initially identified by expression cloning using a rabbit small intestinal cDNA library [1]. cDNA for the renal peptide transporter PEPT2 cDNA, an isoform of the intestinal PEPT1 has also been isolated [2]. PEPT1 and PEPT2 consist of 707–710 and 729 amino acid residues, respectively, and possess 12 transmembrane (TM) domains. The overall amino acid identity between them is ~50% [1–4]. PEPT1 is localized to brush-border membranes of intestinal and renal epithelial cells [5], whereas PEPT2 is preferentially expressed in the kidney and located at brush-border membranes of renal epithelial cells.

23.3.1.2. Function and Pharmacokinetic Roles

PEPT1 and PEPT2 can transport di- and tripeptides with different molecular sizes and charges, but not free amino acids and peptides composed of four or more peptide bonds [6]. Pharmacologically active peptide-like drugs such as β -lactam antibiotics, bestatin, and angiotensin-converting enzyme (ACE) inhibitors have been also reported to be transported by PEPT1 and PEPT2 [7]. It has been believed that the presence of peptide bonds is the most important factor in the recognition of substrates by peptide transporters. However, the structural requirements of PEPT1 and PEPT2 were reevaluated (most studies were performed with PEPT1), and it was demonstrated that even compounds without peptide bonds can be accepted as substrates (e.g., δ -amino levulinic acid [8], ω -amino fatty acid [9], and amino acid ester compounds [10–12]). Recently, a mathematical model of H⁺-coupled transport phenomena via PEPT1 was proposed [13, 14].

Over the last decade, PEPT1 has been utilized as a target for improving the intestinal absorption of poorly absorbed drugs through amino acid-based modifications. For example, the enhanced oral bioavailability of valacyclovir and valganciclovir, L-valine ester prodrugs of acyclovir and ganciclovir,

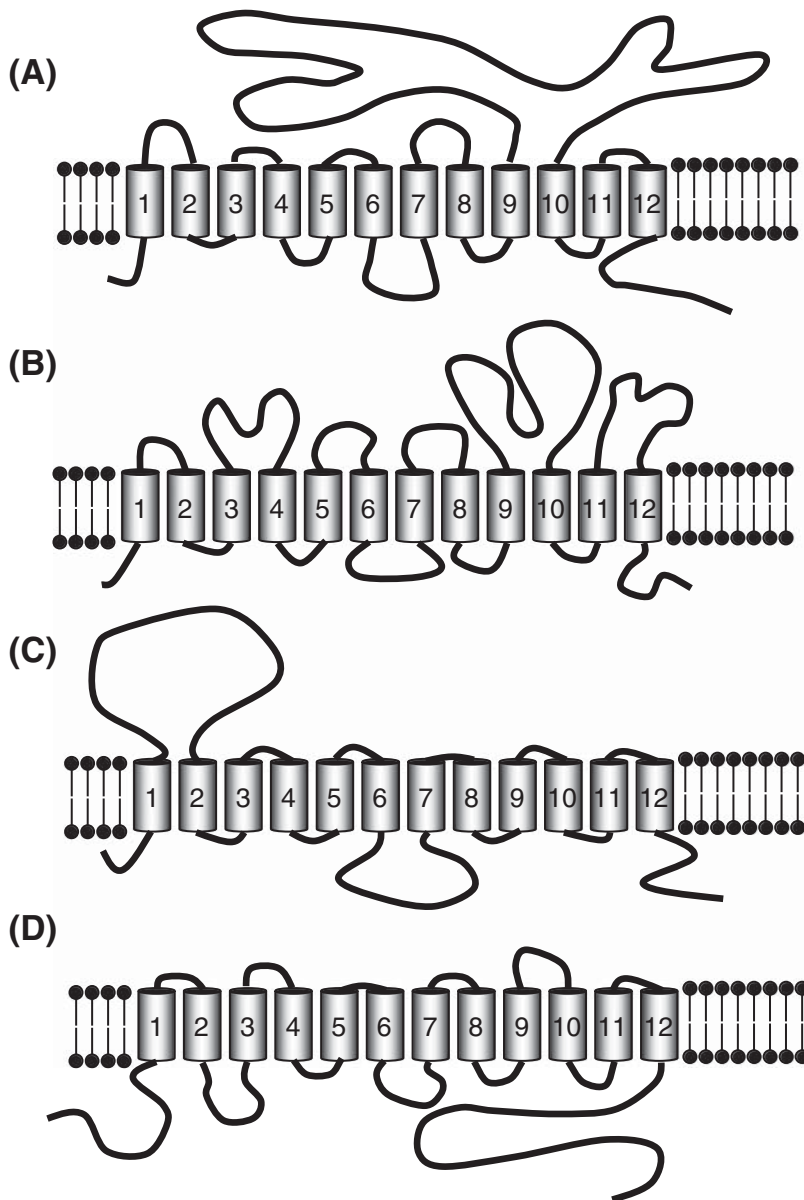


Figure 23.1 Putative secondary structures of various drug transporters. (A–D) Putative secondary structures of SLC drug transporters: (A) Peptide transporters (PEPT, SLC15), (B) Organic anion transporting polypeptides (OATP, SLCO), (C) Organic ion transporters (OCT/OCTN/OAT/URAT, SLC22), and (D) H⁺/organic cation antiporter (MATE). (E–G) Putative secondary structures of ABC drug transporters: (E) P-glycoprotein (P-gp/MDR1, ABCB1), (F) Multidrug resistance-associated proteins (MRP, ABCC), and (G) Breast cancer-resistance protein (BCRP, ABCG2).

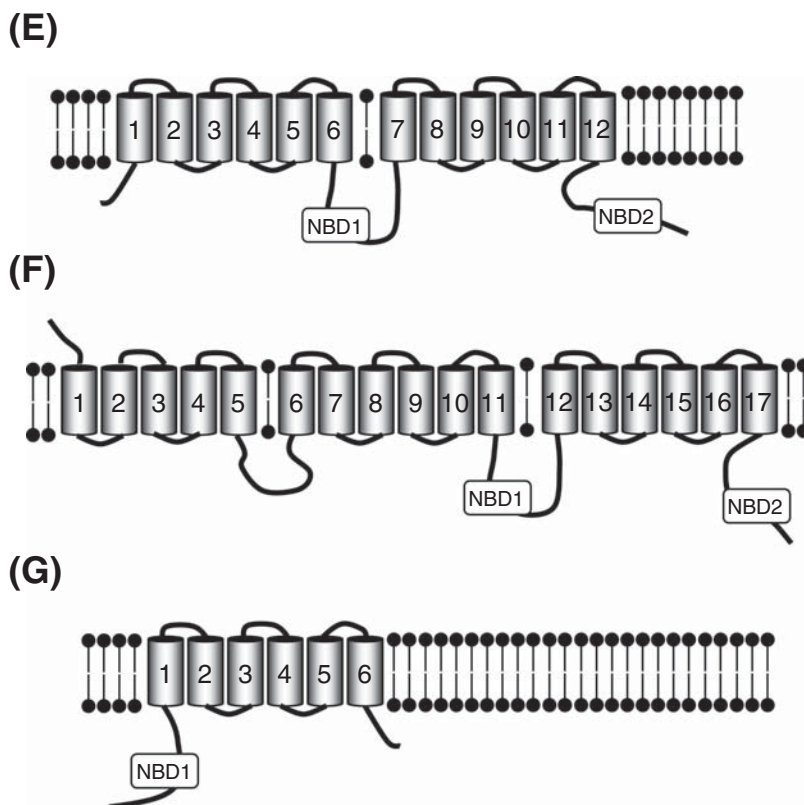


Figure 23.1 (Continued.)

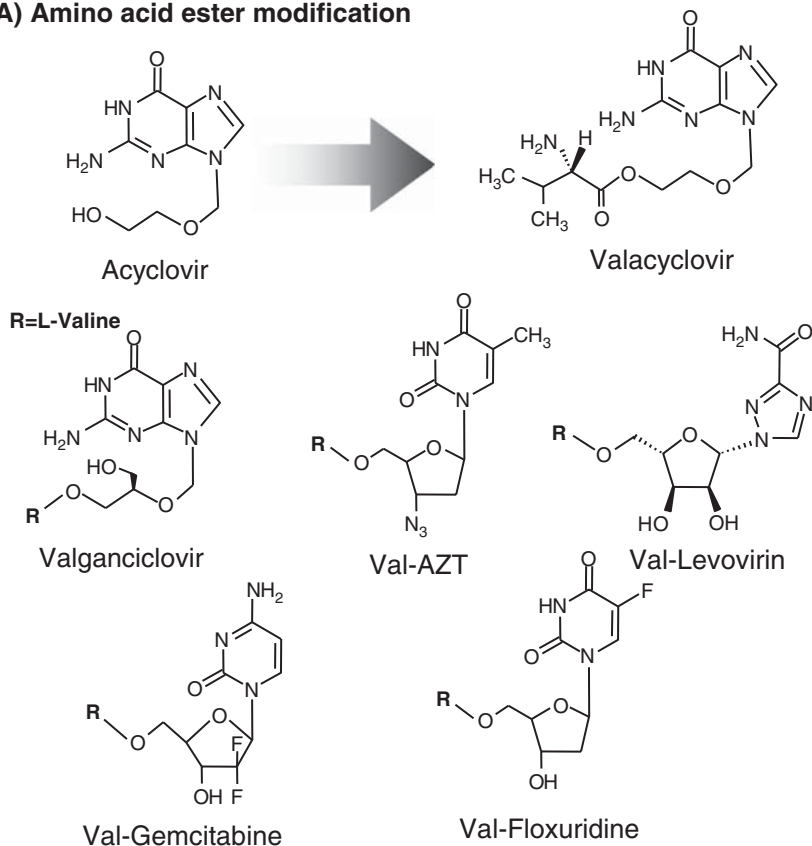
respectively, has been attributed to their enhanced intestinal transport via PEPT1 [10, 12], and these drugs have been used in the clinical setting. The anticancer agents (e.g., gemcitabine [15] and floxuridine [16]) and antiviral drugs (e.g., azidothymidine [10] and levovirin [17]) were also converted to PEPT1 substrates by modifying the L-valine ester (Figure 23.2A). Another strategy for converting PEPT1 substrates is an amino acid peptide modification. For example, midodrine, an antihypotension prodrug for combining glycine via a peptide bond with an active drug, was recently demonstrated to be a substrate for PEPT1 [18] (Figure 23.2B). Thus, conversion of poorly absorbed drugs to PEPT1 substrates should be useful for improving oral bioavailability.

23.3.2. OATP (SLCO)

23.3.2.1. Structure and Tissue Distribution

In 1994, a Na^+ -independent organic anion-transporting polypeptide (Oatp1) was originally cloned from a rat liver cDNA library [19]. Thereafter, many isoforms of Oatp (rodents)/OATP (human) were identified, but unlike other transporters, this family exhibits large interspecies differences [20]. HGNC designated the OATP family as the SLC21 family early on, but since the traditional *SLC21* gene classification does not permit an unequivocal and species-independent identification of genes and gene products, thereafter, all

A) Amino acid ester modification



B) Amino acid peptide modification

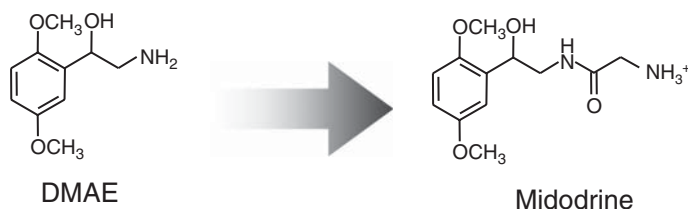


Figure 23.2 Improvement of poorly absorbed drugs using the broad substrate specificity of intestinal PEPT1. (A) Amino acid ester modification of various drugs (e.g., antiviral and anticancer drugs). Among amino acids, L-valine has been suggested to be suitable for this modification. (B) Amino acid peptide modification of the antihypertensive drug midodrine. Among amino acids, glycine has been suggested to be suitable for this modification.

Oatps/OATPs were newly classified within the OATP (protein)/*SLCO* (*gene*) (human) and Oatp (protein)/*Slco* (*gene*) (rodents) superfamily according to their phylogenetic relationships and chronology of identification. The methods of classification and the nomenclature were described in detail in a recent review [21].

All members of OATP/Oatp family contain 12 TM domains. Certain transporters show a more restricted tissue expression pattern (i.e., OATP1B1 [old name: OATP-C]/liver), while others such as OATP2B1 (old name: OATP-B) can be detected in almost every tissue that has been investigated [22]. This indicates that some OATPs/Oatps have organ-specific functions, while others might be involved in housekeeping functions.

23.3.2.2. *Function and Pharmacokinetic Roles*

OATP/Oatp families mediate the Na⁺-independent transport of a wide range of amphipathic organic compounds, including bile salts, organic dyes, steroid conjugates, thyroid hormones, anionic oligopeptides, numerous drugs, and other xenobiotic substances [20]. Among the human OATP families, OATP1B1 (old name: OATP-C) has been well characterized. This transporter is exclusively expressed in the liver and located at sinusoidal membranes. Thus, the major pharmacokinetic role of OATP1B1 is hepatic uptake of various clinically important drugs such as pravastatin (3-Hydroxy-3-methylglutaryl coenzyme A [HMG-CoA] reductase inhibitor) [23], enalapril (ACE inhibitor) [24], and valsartan (an angiotensin II receptor antagonist) [25]. Recently, the clinical implications of single nucleotide polymorphisms (SNPs) for the *SLCO1B1* gene were reported first by Nishizato et al. [26], in that the 521T>C (Val174Ala) polymorphism in *SLCO1B1* is associated with increased systemic exposures to pravastatin in Japanese subjects. Thereafter, it was also reported that genetic polymorphisms in *SLCO1B1* are a major determinant of interindividual variability in the pharmacokinetics of pravastatin [27–29], the antidiabetic drug repaglinide [30], and atrasentan, a selective endothelin A receptor antagonist [31]. As described above, the OATP/Oatp family exhibits large interspecies differences and this feature may be responsible for the frequency with which SNPs in *SLCO* genes induce functional changes.

OATP2B1 (old name: OATP-B) is expressed at brush-border membranes of intestinal epithelial cells [32]. OATP2B1 exhibited pH-sensitive transport activities for various organic anions such as estrone-3-sulfate, dehydroepiandrosterone sulfate, taurocholic acid, pravastatin, and fexofenadine [33]. However, further studies are needed to determine the specific physiological and pharmacokinetic contribution of OATP2B1 for intestinal absorption of these compounds.

23.3.3. OCT/OCTN/OAT/URAT (SLC22)

23.3.3.1. *Structure and Tissue Distribution*

The organic ion transporter superfamily is composed of various isoforms differing in the mode of transport (uniporters, symporters, and antiporters) and selectivity of substrate charges, although all isoforms have a similar secondary structure of 12 TM domains. In 1994, the first member of the SLC22 family, organic cation transporter 1 (OCT1), was identified from a rat kidney cDNA library by expression cloning [34]. Rat OCT2 was identified in 1996 [35], and the human zwitterion/cation transporter OCTN1 was discovered in 1997 [36]. In the same year, the first organic anion transporter (OAT1) was cloned from rats [37]. In 1998, OCT3 was identified in rats and humans [38, 39], and the human Na⁺-carnitine cotransporter OCTN2 was cloned [40, 41]. Thereafter, various human OAT isoforms (OAT2–OAT4 and urate transporter [URAT1]) were identified [42–45].

In humans, the major expression sites of the SLC22 transporter family are as follows: OCT1/liver (sinusoidal membranes of hepatocytes), OCT2/kidney (basolateral membranes of renal proximal tubules), OCT3/skeletal muscle, placenta, heart, OCTN1/widely distributed, OCTN2/kidney and intestine (brush-border membranes), OAT1/kidney (basolateral membranes of renal proximal tubules), OAT2/liver (sinusoidal membranes of hepatocytes), OAT3/kidney (basolateral membranes of renal proximal tubules), OAT4/kidney (brush-border membranes of renal proximal tubules), and URAT1/kidney (brush-border membranes of renal proximal tubules) [46].

23.3.3.2. Function and Pharmacokinetic Roles

The SLC22 family plays important roles for renal secretion of various compounds (e.g., drugs, toxins, and endogenous metabolites via OCTs and OATs) [47–49], the reabsorption of urate (via URAT1) [50], and the intestinal and renal absorption of carnitine (via OCTN2) [51]. OCTs mediate the membrane potential-dependent uptake of organic cations such as tetraethylammonium (TEA, a typical substrate of OCTs), cimetidine (H₂ blocker), and metformin (antidiabetic agent). Previously, it was believed that the substrate recognition of OCT1, OCT2, and OCT3 is not very different, but a recent study revealed that creatinine is a specific substrate for OCT2 [52]. This finding is clinically relevant, because creatinine clearance is widely used to estimate the glomerular filtration rate (GFR). In other words, creatinine clearance may not reflect the true GFR. Moreover, if cationic drugs (OCT2 substrates) are coadministered, creatinine clearance may be decreased by inhibition of OCT2-mediated creatinine secretion, leading to an underestimation of the renal function. Cisplatin (anticancer agent) is a preferred substrate for OCT2 [53, 54], suggesting that the renal toxicity of cisplatin may be triggered by its uptake via OCT2 into renal proximal tubular cells.

OATs can transport various organic anions and the substrate specificity of each isoform has been characterized. P-aminohippurate (PAH) has been widely used as a typical substrate for renal organic anion transport systems. PAH uptake by OAT1 was stimulated by an outwardly directed gradient of α -ketoglutarate, which is consistent with experimental results from studies using renal basolateral membrane vesicles [55]. Antiviral drugs such as adefovir are preferably recognized by OAT1, suggesting that OAT1 may be responsible for the renal toxicity of antiviral agents [56]. Although OAT3 also recognizes PAH, its substrate specificity is different from that of OAT1. For example, estrone sulfate [43], cimetidine [43], and famotidine [57] are preferentially transported by OAT3, but not by OAT1. In addition, OAT3 exhibits a greater activity to transport cephalosporin antibiotics including cefazolin, as compared with OAT1 [58]. This is supported by clinical findings that the mRNA level of OAT3 is significantly correlated with the rate of elimination of cefazolin [59, 60].

OCTN2 is highly expressed in the human intestine from the jejunum to colon [61]. It was recently demonstrated that OCTN2 is predominantly responsible for the uptake of carnitine from the apical surface of mouse small intestinal epithelial cells, suggesting that OCTN2 could be a promising target for the oral delivery of therapeutic agents [62]. Mutations of transporters for the SLC22 family are responsible for specific diseases such as “primary systemic carnitine deficiency” (OCTN2) [63] or “idiopathic renal hypouricemia” (URAT1) [45],

and also thought to be linked with rheumatoid arthritis (OCTN1) [64] and Crohn's disease (OCTN2) [65].

23.3.4. MATE (SLC47)

23.3.4.1. Structure and Tissue Distribution

Organic cations are excreted by the H⁺/organic cation antiporter in the brush-border membranes. As described above, the membrane potential-dependent organic cation transporters located to the basolateral membranes (OCT1–3, SLC22A1–3) have been identified and well characterized [47, 48], but the molecular nature of the H⁺/organic cation antiporter has not been elucidated. Recently, based on *in silico* homology screening, human and mouse orthologs of the multidrug and toxin extrusion (MATE) family, which confers multidrug resistance to bacteria, have been identified [66, 67]. Rat MATE1 [68] and the kidney-specific human MATE2 (MATE2-K) [69] were identified next. This particular drug transporter family recently designated as SLC47 family.

MATE1 and MATE2-K consist of 566–570 amino acid residues with 12 TM domains and show about 50% amino acid identity. Human MATE1 is mostly expressed in luminal membranes of renal proximal tubules and liver canalicular membranes. Mouse MATE1 is also predominantly expressed in the kidney and liver, but it is also expressed in brain glia-like cells and capillaries, pancreatic duct cells, urinary bladder epithelium, and adrenal gland cortex [67]. Rat MATE1 mRNA is highly expressed in the kidney, especially in proximal tubules and placenta, but not in the liver [68]. These findings suggest a clear species difference in the distribution of MATE1 among human, mouse, and rat. Human MATE2-K as well as human MATE1 was located at brush-border membranes of renal proximal tubules [69].

23.3.4.2. Function and Pharmacokinetic Roles

MATE1 can transport not only organic cations such as cimetidine and metformin but also the zwitterionic compound cephalexin [68]. MATE2-K also transports various organic cations, but not cephalexin [69]. The substrate recognition characteristics of MATEs are quite similar, but not identical to those of OCTs. For example, cephalexin is a substrate for MATE1, but not for OCTs, while creatinine is a substrate for OCT2, but not for MATEs. MATE1 exhibits pH-dependent transport properties for cellular uptake and efflux studies using TEA as a substrate, while intracellular acidification by NH₄Cl pretreatment stimulates TEA transport [66–69]. Direct evidence that a proton gradient is the driving force for MATE1 activity was reported recently, utilizing membrane vesicles prepared from cells stably expressing MATE1. TEA transport exhibited the overshoot phenomenon only when there was an outwardly directed H⁺ gradient across the vesicles [70], which has been also observed in rat renal brush-border membrane vesicles [71]. These findings indicate that an oppositely directed H⁺ gradient serves as a driving force for MATE1.

23.3.5. ABC Transporters

23.3.5.1. Structure and Tissue Distribution

P-glycoprotein (P-gp, MDR1) was first isolated from cancer cells where it extrudes chemotherapeutic agents out of the cell thereby conferring multidrug resistance [72]. Subsequent analyses have demonstrated that P-gp is expressed

in various normal tissues and involved in the pharmacokinetics of a wide range of drugs, mediating the efflux of drugs from the intracellular to the extracellular space [73]. Many isoforms of ABC drug transporters have been isolated and characterized. Currently, the ABC superfamily is designated based on the sequence and organization of their ATP-binding domains, representing the largest family of TM proteins (e.g., transporters, ion channels, and receptors). This family is subdivided based on similarities in domain structure, nucleotide-binding folds, and TM domains [74]. Of the 48 members identified to date, several members are well characterized as drug transporters. P-gp/MDR1 is now designated as ABCB1. MDR3 (ABCB4) and BSEP (bile salt export pump or sister P-gp, ABCB11) are included in the ABCB subfamily. The MRP subfamily includes MRP1 (ABCC1), MRP2 (ABCC2), MRP3 (ABCC3), MRP4 (ABCC4), and other MRP isoforms [75]. Other members of the ABCC subfamily include CFTR (cystic fibrosis transmembrane conductance regulator, a Cl⁻ channel) and SUR1 and SUR2 (sulfonylurea receptors). BCRP (ABCG2) belongs to a different subfamily known as the White subfamily [76]. The clinical relevance of P-gp has been demonstrated in terms of drug interaction, gene polymorphisms, and expression levels.

The general structure of ABC transporters comprises 12 TM regions, split into two halves, each with a nucleotide-binding domain (NBD) [77]. However, there are a number of exceptions to this arrangement. For example, MRP1–3 have an additional five TM regions at the N terminus. BCRP has only six TM regions and one NBD and is known as a half transporter. In general, ABC transporters are expressed in blood–tissue barriers such as the blood–brain barrier and at the luminal surface of epithelial cells such as intestinal epithelial cells to protect the cells from toxic substances.

23.3.5.2. Function and Pharmacokinetic Roles

23.3.5.2.1. MDR1 (P-GP and ABCB1): P-gp has an extremely broad substrate specificity, with a tendency towards lipophilic, cationic compounds. The list of its substrates/inhibitors is continually growing and includes anticancer agents, antibiotics, antivirals, calcium channel blockers, and immunosuppressive agents. Its physiological function was clearly demonstrated by creating an *Mdr1a/1b*^{-/-} mouse [78]. Studies in vivo using this mouse model revealed that MDR1 functions as a gatekeeper of the blood–brain barrier, blood–placental barrier, blood–testis barrier, and gut [79, 80]. P-gp is expressed at brush-border membranes of enterocytes, where it functions as the efflux pump for xenobiotics in the intestinal lumen before they can access the portal circulation.

The antituberculosis drug rifampicin (rifampin) is known to affect a number of drug-metabolizing enzymes such as cytochrome P450 (CYP) 3A4 in the liver and in the small intestine, causing a loss of efficacy of drugs metabolized by CYP3A4. In addition, rifampicin induces the intestinal expression of P-gp, decreasing the oral bioavailability of P-gp substrates such as digoxin [81] and talinorol [82]. Not only drugs but also herbal products, that is, St. John's wort, administered for a long term have been shown to induce the intestinal expression of CYP3A and P-gp, consistent with the loss of efficacy of various drug therapies in earlier case reports and specific clinical studies [83].

The expression level of intestinal MDR1 mRNA has been utilized to the personalized immunosuppressant therapy with tacrolimus in cases of living-donor liver transplantation (LDLT) [84]. Tacrolimus shows wide

intra- and interindividual pharmacokinetic variability, especially in bioavailability after oral administration. P-gp and CYP3A4 are suggested to cooperate in the intestinal absorption of tacrolimus. Our laboratories reported an inverse correlation between the tacrolimus concentration/dose (C/D) ratio and the intestinal mRNA level of MDR1 ($r = -0.776$), but not of CYP3A4 ($r = -0.096$), in 46 cases [85] which was confirmed in studies with a larger population ($r = -0.645$, $n = 104$) [86]. Furthermore, a higher level of intestinal MDR1 expression was strongly associated with the probability of acute cellular rejection (ACR), but there was no significant association between the intestinal CYP3A4 mRNA level and ACR. These results indicate that the expression level of intestinal MDR1 mRNA found with LDLT is not only a pharmacokinetic factor, but also a significant biomarker for ACR [87].

23.3.5.2.2. MRP2 (ABCC2): MRP2 was first functionally characterized as a canalicular multispecific organic anion transporter in canalicular membranes of hepatocytes [88]. This transporter can accept a diverse range of substrates, including glutathione, glucuronide, and sulfate conjugates of many endo- and xenobiotics and expressed at the apical domain of hepatocytes, enterocytes of the proximal small intestine and proximal renal tubular cells, as well as in the brain and placenta. Mutation of MRP2 causes the Dubin-Johnson syndrome [89].

23.3.5.2.3. MRP3 (ABCC3): In contrast to other ABC drug transporters, MRP3 is mainly expressed at basolateral membranes of epithelial cells in the liver and intestine [90]. Substrates for MRP3 include glucuronosyl and sulfated conjugates, whereas glutathione conjugates are relatively poor substrates for MRP3 compared with MRP1 and MRP2 [91]. As MRP3 also transports some bile salts [92], this transporter has been believed to play important roles in the enterohepatic circulation of bile salts by transporting them from enterocytes into the circulating blood to prevent the accumulation of intracellular bile acids. Mice lacking *Mrp3* were recently developed which are viable and fertile, exhibiting no apparent phenotype [93].

23.3.5.2.4. BCRP (ABCG2): Unlike P-gp and MRPs, BCRP has only one ABC and six putative TM domains, and therefore, is referred to as a half-ABC transporter, most likely functioning as a homodimer [76]. Among human tissues, the placenta showed the highest level of BCRP mRNA, followed by the liver and small intestine [94]. Unlike humans, mice exhibited high levels of mRNA in the kidney and only moderate levels in the placenta [95]. BCRP is capable of transporting a diverse array of substrates, which overlap those of P-gp and MRP1 to a certain extent [76]. Using mice lacking *Bcrp*, it was demonstrated that this transporter protects against the gastrointestinal absorption of a potent phototoxic agent, pheophorbide [96]. BCRP also mediates the intestinal efflux of an antibiotic, nitrofurantoin [97].

23.4. Conclusions and Perspectives

In this chapter, basic characteristics of major drug transporters and their pre-clinical/clinical implications are discussed. During the past 10 years, molecular information on each transporter has been organized. Novel technologies and various useful public databases such as SNP have improved our understanding

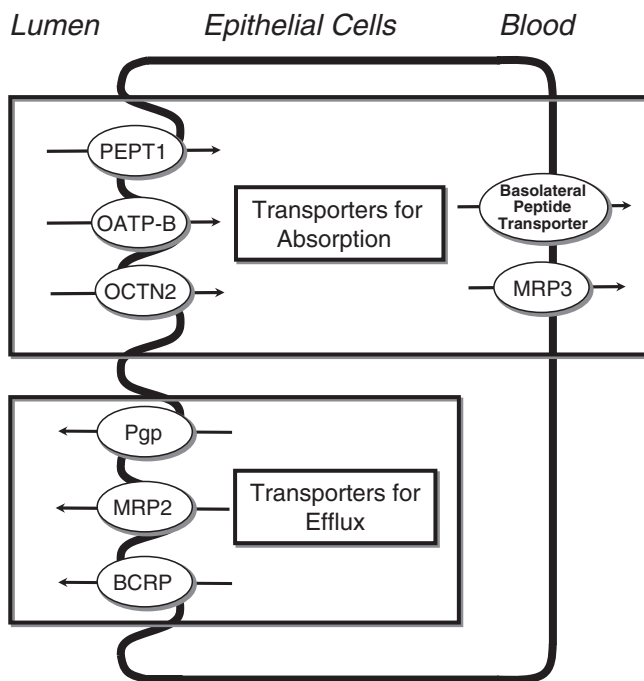


Figure 23.3 Drug transporters in the intestinal epithelial cells. PEPT1 is the most characterized transporter for intestinal drug absorption. The basolateral peptide transporter, which is not identified at the molecular level, also plays important roles. OATP-B, OCTN2 and MRP3 may be responsible for the intestinal absorption of some drugs. On the contrary, ABC transporters such as P-gp located at brush-border membranes mediated the efflux of drugs from intestinal epithelial cells, contributing to the low bioavailability of drugs such as the immunosuppressive agent, tacrolimus.

of the physiological, pharmacokinetic, and pharmacotherapeutic roles of these drug transporters. Drug transporter research can be actually applied to clinical science and drug development; that is, applications of drug delivery, the clarification of drug/drug interactions, application of personalized pharmacotherapy, and clarification of the relationship of each transporter to particular disease(s).

Various drug transporters are responsible for determining the oral bioavailability of drugs (Figure 23.3), although the extent of their contribution to the overall intestinal absorption process *in vivo* is not clear in some cases. Among them, peptide transporters, P-gp, MRP2, and BCRP unequivocally function as important factors regulating the oral bioavailability of drugs. Molecular determination of absorption by peptide transporters or secretion/excretion by ABC drug transporters will contribute to help the oral bioavailability of drugs under study.

Acknowledgments: This work was supported by the 21st Century COE Program “Knowledge Information Infrastructure for Genome Science”, a Grant-in-Aid from the Japan Health Sciences Foundation and a Grant-in-Aid for Research on Advanced Medical Technology from the Ministry of Health, Labor and Welfare of Japan.

References

1. Y. J. Fei, Y. Kanai, S. Nussberger, V. Ganapathy, F. H. Leibach, M. F. Romero, S. K. Singh, W. F. Boron, and M. A. Hediger. Expression cloning of a mammalian proton-coupled oligopeptide transporter. *Nature* **368**: 563–566 (1994).
2. S. Ramamoorthy, W. Liu, Y. Y. Ma, T. L. Yang-Feng, V. Ganapathy, and F. H. Leibach. Proton/peptide cotransporter (PEPT 2) from human kidney: functional characterization and chromosomal localization. *Biochim Biophys Acta* **1240**: 1–4 (1995).

3. H. Saito, M. Okuda, T. Terada, S. Sasaki, and K. Inui. Cloning and characterization of a rat H⁺/peptide cotransporter mediating absorption of beta-lactam antibiotics in the intestine and kidney. *J Pharmacol Exp Ther* **275**: 1631–1637 (1995).
4. H. Saito, T. Terada, M. Okuda, S. Sasaki, and K. Inui. Molecular cloning and tissue distribution of rat peptide transporter PEPT2. *Biochim Biophys Acta* **1280**: 173–177 (1996).
5. H. Ogihara, H. Saito, B. C. Shin, T. Terado, S. Takenoshita, Y. Nagamachi, K. Inui, and K. Takata. Immuno-localization of H⁺/peptide cotransporter in rat digestive tract. *Biochem Biophys Res Commun* **220**: 848–852 (1996).
6. H. Daniel. Molecular and integrative physiology of intestinal peptide transport. *Annu Rev Physiol* **66**: 361–384 (2004).
7. T. Terada, and K. Inui. Peptide transporters: structure, function, regulation and application for drug delivery. *Curr Drug Metab* **5**: 85–94 (2004).
8. F. Doring, J. Walter, J. Will, M. Focking, M. Boll, S. Amasheh, W. Clauss, and H. Daniel. Delta-aminolevulinic acid transport by intestinal and renal peptide transporters and its physiological and clinical implications. *J Clin Invest* **101**: 2761–2767 (1998).
9. F. Doring, J. Will, S. Amasheh, W. Clauss, H. Ahlbrecht, and H. Daniel. Minimal molecular determinants of substrates for recognition by the intestinal peptide transporter. *J Biol Chem* **273**: 23211–23218 (1998).
10. H. Han, R. L. de Vruet, J. K. Rhie, K. M. Covitz, P. L. Smith, C. P. Lee, D. M. Oh, W. Sadee, and G. L. Amidon. 5'-Amino acid esters of antiviral nucleosides, acyclovir, and AZT are absorbed by the intestinal PEPT1 peptide transporter. *Pharm Res* **15**: 1154–1159 (1998).
11. K. Sawada, T. Terada, H. Saito, Y. Hashimoto, and K. Inui. Recognition of L-amino acid ester compounds by rat peptide transporters PEPT1 and PEPT2. *J Pharmacol Exp Ther* **291**: 705–709 (1999).
12. M. Sugawara, W. Huang, Y. J. Fei, F. H. Leibach, V. Ganapathy, and M. E. Ganapathy. Transport of valganciclovir, a ganciclovir prodrug, via peptide transporters PEPT1 and PEPT2. *J Pharm Sci* **89**: 781–789 (2000).
13. M. Irie, T. Terada, T. Katsura, S. Matsuoka, and K. Inui. Computational modelling of H⁺-coupled peptide transport via human PEPT1. *J Physiol* **565**: 429–439 (2005).
14. M. Sala-Rabanal, D. D. Loo, B. A. Hirayama, E. Turk, and E. M. Wright. Molecular interactions between dipeptides, drugs and the human intestinal H⁺-oligopeptide cotransporter hPEPT1. *J Physiol* **574**: 149–166 (2006).
15. X. Song, P. L. Lorenzi, C. P. Landowski, B. S. Vig, J. M. Hilfinger, and G. L. Amidon. Amino acid ester prodrugs of the anticancer agent gemcitabine: synthesis, bioconversion, metabolic bioevasion, and hPEPT1-mediated transport. *Mol Pharm* **2**: 157–167 (2005).
16. C. P. Landowski, X. Song, P. L. Lorenzi, J. M. Hilfinger, and G. L. Amidon. Floxuridine amino acid ester prodrugs: enhancing Caco-2 permeability and resistance to glycosidic bond metabolism. *Pharm Res* **22**: 1510–1518 (2005).
17. F. Li, L. Hong, C. I. Mau, R. Chan, T. Hendricks, C. Dvorak, C. Yee, J. Harris, and T. Alfredson. Transport of levovirin prodrugs in the human intestinal Caco-2 cell line. *J Pharm Sci* **95**: 1318–1325 (2006).
18. M. Tsuda, T. Terada, M. Irie, T. Katsura, A. Niida, K. Tomita, N. Fujii, and K. Inui. Transport characteristics of a novel peptide transporter 1 substrate, antihypotensive drug midodrine, and its amino acid derivatives. *J Pharmacol Exp Ther* **318**: 455–460 (2006).
19. E. Jacquemin, B. Hagenbuch, B. Stieger, A. W. Wolkoff, and P. J. Meier. Expression cloning of a rat liver Na⁺-independent organic anion transporter. *Proc Natl Acad Sci U S A* **91**: 133–137 (1994).
20. B. Hagenbuch, and P. J. Meier. The superfamily of organic anion transporting polypeptides. *Biochim Biophys Acta* **1609**: 1–18 (2003).

21. B. Hagenbuch, and P. J. Meier. Organic anion transporting polypeptides of the OATP/SLC21 family: phylogenetic classification as OATP/SLCO superfamily, new nomenclature and molecular/functional properties. *Pflugers Arch* **447**: 653–665 (2004).
22. I. Tamai, J. Nezu, H. Uchino, Y. Sai, A. Oku, M. Shimane, and A. Tsuji. Molecular identification and characterization of novel members of the human organic anion transporter (OATP) family. *Biochem Biophys Res Commun* **273**: 251–260 (2000).
23. M. Iwai, H. Suzuki, I. Ieiri, K. Otsubo, and Y. Sugiyama. Functional analysis of single nucleotide polymorphisms of hepatic organic anion transporter OATP1B1 (OATP-C). *Pharmacogenetics* **14**: 749–757 (2004).
24. L. Liu, Y. Cui, A. Y. Chung, Y. Shitara, Y. Sugiyama, D. Keppler, and K. S. Pang. Vectorial transport of enalapril by Oatp1a1/Mrp2 and OATP1B1 and OATP1B3/MRP2 in rat and human livers. *J Pharmacol Exp Ther* **318**: 395–402 (2006).
25. W. Yamashiro, K. Maeda, M. Hirouchi, Y. Adachi, Z. Hu, and Y. Sugiyama. Involvement of transporters in the hepatic uptake and biliary excretion of valsartan, a selective antagonist of the angiotensin II AT1-receptor, in humans. *Drug Metab Dispos* **34**: 1247–1254 (2006).
26. Y. Nishizato, I. Ieiri, H. Suzuki, M. Kimura, K. Kawabata, T. Hirota, H. Takane, S. Irie, H. Kusuhara, Y. Urasaki, A. Urae, S. Higuchi, K. Otsubo, and Y. Sugiyama. Polymorphisms of OATP-C (SLC21A6) and OAT3 (SLC22A8) genes: consequences for pravastatin pharmacokinetics. *Clin Pharmacol Ther* **73**: 554–565 (2003).
27. M. Niemi, E. Schaeffeler, T. Lang, M. F. Fromm, M. Neuvonen, C. Kyrklund, J. T. Backman, R. Kerb, M. Schwab, P. J. Neuvonen, M. Eichelbaum, and K. T. Kivisto. High plasma pravastatin concentrations are associated with single nucleotide polymorphisms and haplotypes of organic anion transporting polypeptide-C (OATP-C, SLCO1B1). *Pharmacogenetics* **14**: 429–440 (2004).
28. M. Niemi, P. J. Neuvonen, U. Hofmann, J. T. Backman, M. Schwab, D. Lutjohann, K. von Bergmann, M. Eichelbaum, and K. T. Kivisto. Acute effects of pravastatin on cholesterol synthesis are associated with SLCO1B1 (encoding OATP1B1) haplotype *17. *Pharmacogenet Genomics* **15**: 303–309 (2005).
29. K. Maeda, I. Ieiri, K. Yasuda, A. Fujino, H. Fujiwara, K. Otsubo, M. Hirano, T. Watanabe, Y. Kitamura, H. Kusuhara, and Y. Sugiyama. Effects of organic anion transporting polypeptide 1B1 haplotype on pharmacokinetics of pravastatin, valsartan, and temocapril. *Clin Pharmacol Ther* **79**: 427–439 (2006).
30. M. Niemi, J. T. Backman, L. I. Kajosaari, J. B. Leathart, M. Neuvonen, A. K. Daly, M. Eichelbaum, K. T. Kivisto, and P. J. Neuvonen. Polymorphic organic anion transporting polypeptide 1B1 is a major determinant of repaglinide pharmacokinetics. *Clin Pharmacol Ther* **77**: 468–478 (2005).
31. D. A. Katz, R. Carr, D. R. Grimm, H. Xiong, R. Holley-Shanks, T. Mueller, B. Leake, Q. Wang, L. Han, P. G. Wang, T. Edeki, L. Sahelijo, T. Doan, A. Allen, B. B. Spear, and R. B. Kim. Organic anion transporting polypeptide 1B1 activity classified by SLCO1B1 genotype influences atrasentan pharmacokinetics. *Clin Pharmacol Ther* **79**: 186–196 (2006).
32. D. Kobayashi, T. Nozawa, K. Imai, J. Nezu, A. Tsuji, and I. Tamai. Involvement of human organic anion transporting polypeptide OATP-B (SLC21A9) in pH-dependent transport across intestinal apical membrane. *J Pharmacol Exp Ther* **306**: 703–708 (2003).
33. T. Nozawa, K. Imai, J. Nezu, A. Tsuji, and I. Tamai. Functional characterization of pH-sensitive organic anion transporting polypeptide OATP-B in human. *J Pharmacol Exp Ther* **308**: 438–445 (2004).

34. D. Gründemann, V. Gorboulev, S. Gambaryan, M. Veyhl, and H. Koepsell. Drug excretion mediated by a new prototype of polyspecific transporter. *Nature* **372**: 549–552 (1994).
35. M. Okuda, H. Saito, Y. Urakami, M. Takano, and K. Inui. cDNA cloning and functional expression of a novel rat kidney organic cation transporter, OCT2. *Biochem Biophys Res Commun* **224**: 500–507 (1996).
36. I. Tamai, H. Yabuuchi, J. Nezu, Y. Sai, A. Oku, M. Shimane, and A. Tsuji. Cloning and characterization of a novel human pH-dependent organic cation transporter, OCTN1. *FEBS Lett* **419**: 107–111 (1997).
37. T. Sekine, N. Watanabe, M. Hosoyamada, Y. Kanai, and H. Endou. Expression cloning and characterization of a novel multispecific organic anion transporter. *J Biol Chem* **272**: 18526–18529 (1997).
38. D. Gründemann, B. Schechinger, G. A. Rappold, and E. Schomig. Molecular identification of the corticosterone-sensitive extraneuronal catecholamine transporter. *Nat Neurosci* **1**: 349–351 (1998).
39. R. Kekuda, P. D. Prasad, X. Wu, H. Wang, Y. J. Fei, F. H. Leibach, and V. Ganapathy. Cloning and functional characterization of a potential-sensitive, polyspecific organic cation transporter (OCT3) most abundantly expressed in placenta. *J Biol Chem* **273**: 15971–15979 (1998).
40. I. Tamai, R. Ohashi, J. Nezu, H. Yabuuchi, A. Oku, M. Shimane, Y. Sai, and A. Tsuji. Molecular and functional identification of sodium ion-dependent, high affinity human carnitine transporter OCTN2. *J Biol Chem* **273**: 20378–20382 (1998).
41. X. Wu, P. D. Prasad, F. H. Leibach, and V. Ganapathy. cDNA sequence, transport function, and genomic organization of human OCTN2, a new member of the organic cation transporter family. *Biochem Biophys Res Commun* **246**: 589–595 (1998).
42. T. Sekine, S. H. Cha, M. Tsuda, N. Apiwattanakul, N. Nakajima, Y. Kanai, and H. Endou. Identification of multispecific organic anion transporter 2 expressed predominantly in the liver. *FEBS Lett* **429**: 179–182 (1998).
43. H. Kusuhara, T. Sekine, N. Utsunomiya-Tate, M. Tsuda, R. Kojima, S. H. Cha, Y. Sugiyama, Y. Kanai, and H. Endou. Molecular cloning and characterization of a new multispecific organic anion transporter from rat brain. *J Biol Chem* **274**: 13675–13680 (1999).
44. S. H. Cha, T. Sekine, H. Kusuhara, E. Yu, J. Y. Kim, D. K. Kim, Y. Sugiyama, Y. Kanai, and H. Endou. Molecular cloning and characterization of multispecific organic anion transporter 4 expressed in the placenta. *J Biol Chem* **275**: 4507–4512 (2000).
45. A. Enomoto, H. Kimura, A. Chairoungdua, Y. Shigeta, P. Jutabha, S. H. Cha, M. Hosoyamada, M. Takeda, T. Sekine, T. Igarashi, H. Matsuo, Y. Kikuchi, T. Oda, K. Ichida, T. Hosoya, K. Shimokata, T. Niwa, Y. Kanai, and H. Endou. Molecular identification of a renal urate anion exchanger that regulates blood urate levels. *Nature* **417**: 447–452 (2002).
46. H. Koepsell, and H. Endou. The SLC22 drug transporter family. *Pflugers Arch* **447**: 666–676 (2004).
47. K. Inui, S. Masuda, and H. Saito. Cellular and molecular aspects of drug transport in the kidney. *Kidney Int* **58**: 944–958 (2000).
48. S. H. Wright, and W. H. Dantzler. Molecular and cellular physiology of renal organic cation and anion transport. *Physiol Rev* **84**: 987–1049 (2004).
49. B. C. Burckhardt, and G. Burckhardt. Transport of organic anions across the basolateral membrane of proximal tubule cells. *Rev Physiol Biochem Pharmacol* **146**: 95–158 (2003).
50. M. A. Hediger, R. J. Johnson, H. Miyazaki, and H. Endou. Molecular physiology of urate transport. *Physiology (Bethesda)* **20**: 125–133 (2005).

51. R. R. Ramsay, R. D. Gandour, and F. R. van der Leij. Molecular enzymology of carnitine transfer and transport. *Biochim Biophys Acta* **1546**: 21–43 (2001).
52. Y. Urakami, N. Kimura, M. Okuda, and K. Inui. Creatinine transport by basolateral organic cation transporter hOCT2 in the human kidney. *Pharm Res* **21**: 976–981 (2004).
53. G. Ciarimboli, T. Ludwig, D. Lang, H. Pavenstadt, H. Koepsell, H. J. Piechota, J. Haier, U. Jaehde, J. Zisowsky, and E. Schlatter. Cisplatin nephrotoxicity is critically mediated via the human organic cation transporter 2. *Am J Pathol* **167**: 1477–1484 (2005).
54. A. Yonezawa, S. Masuda, K. Nishihara, I. Yano, T. Katsura, and K. Inui. Association between tubular toxicity of cisplatin and expression of organic cation transporter rOCT2 (Slc22a2) in the rat. *Biochem Pharmacol* **70**: 1823–1831 (2005).
55. H. Shimada, B. Moewes, and G. Burckhardt. Indirect coupling to Na⁺ of p-aminohippuric acid uptake into rat renal basolateral membrane vesicles. *Am J Physiol* **253**: F795–F801 (1987).
56. T. Cihlar, D. C. Lin, J. B. Pritchard, M. D. Fuller, D. B. Mendel, and D. H. Sweet. The antiviral nucleotide analogs cidofovir and adefovir are novel substrates for human and rat renal organic anion transporter 1. *Mol Pharmacol* **56**: 570–580 (1999).
57. H. Motohashi, Y. Uwai, K. Hiramoto, M. Okuda, and K. Inui. Different transport properties between famotidine and cimetidine by human renal organic ion transporters (SLC22A). *Eur J Pharmacol* **503**: 25–30 (2004).
58. H. Ueo, H. Motohashi, T. Katsura, and K. Inui. Human organic anion transporter hOAT3 is a potent transporter of cephalosporin antibiotics, in comparison with hOAT1. *Biochem Pharmacol* **70**: 1104–1113 (2005).
59. Y. Sakurai, H. Motohashi, K. Ogasawara, T. Terada, S. Masuda, T. Katsura, N. Mori, M. Matsuura, T. Doi, A. Fukatsu, and K. Inui. Pharmacokinetic significance of renal OAT3 (SLC22A8) for anionic drug elimination in patients with mesangial proliferative glomerulonephritis. *Pharm Res* **22**: 2016–2022 (2005).
60. Y. Sakurai, H. Motohashi, H. Ueo, S. Masuda, H. Saito, M. Okuda, N. Mori, M. Matsuura, T. Doi, A. Fukatsu, O. Ogawa, and K. Inui. Expression levels of renal organic anion transporters (OATs) and their correlation with anionic drug excretion in patients with renal diseases. *Pharm Res* **21**: 61–67 (2004).
61. T. Terada, Y. Shimada, X. Pan, K. Kishimoto, T. Sakurai, R. Doi, H. Onodera, T. Katsura, M. Imamura, and K. Inui. Expression profiles of various transporters for oligopeptides, amino acids and organic ions along the human digestive tract. *Biochem Pharmacol* **70**: 1756–1763 (2005).
62. Y. Kato, M. Sugiura, T. Sugiura, T. Wakayama, Y. Kubo, D. Kobayashi, Y. Sai, I. Tamai, S. Iseki, and A. Tsuji. Organic cation/carnitine transporter octn2 (slc22a5) is responsible for carnitine transport across apical membranes of small intestinal epithelial cells in mouse. *Mol Pharmacol* **70**: 829–837 (2006).
63. J. Nezu, I. Tamai, A. Oku, R. Ohashi, H. Yabuuchi, N. Hashimoto, H. Nikaido, Y. Sai, A. Koizumi, Y. Shoji, G. Takada, T. Matsuishi, M. Yoshino, H. Kato, T. Ohura, G. Tsujimoto, J. Hayakawa, M. Shimane, and A. Tsuji. Primary systemic carnitine deficiency is caused by mutations in a gene encoding sodium ion-dependent carnitine transporter. *Nat Genet* **21**: 91–94 (1999).
64. S. Tokuhira, R. Yamada, X. Chang, A. Suzuki, Y. Kochi, T. Sawada, M. Suzuki, M. Nagasaki, M. Ohtsuki, M. Ono, H. Furukawa, M. Nagashima, S. Yoshino, A. Mabuchi, A. Sekine, S. Saito, A. Takahashi, T. Tsunoda, Y. Nakamura, and K. Yamamoto. An intronic SNP in a RUNX1 binding site of SLC22A4, encoding an organic cation transporter, is associated with rheumatoid arthritis. *Nat Genet* **35**: 341–348 (2003).
65. V. D. Peltekova, R. F. Wintle, L. A. Rubin, C. I. Amos, Q. Huang, X. Gu, B. Newman, M. Van Oene, D. Cescon, G. Greenberg, A. M. Griffiths, P. H. St

- George-Hyslop, and K. A. Siminovitch. Functional variants of OCTN cation transporter genes are associated with Crohn disease. *Nat Genet* **36**: 471–475 (2004).
66. M. Otsuka, T. Matsumoto, R. Morimoto, S. Arioka, H. Omote, and Y. Moriyama. A human transporter protein that mediates the final excretion step for toxic organic cations. *Proc Natl Acad Sci U S A* **102**: 17923–17928 (2005).
 67. M. Hiasa, T. Matsumoto, T. Komatsu, and Y. Moriyama. Wide variety of locations for rodent MATE1, a transporter protein that mediates the final excretion step for toxic organic cations. *Am J Physiol Cell Physiol* **291**: C678–G686 (2006).
 68. T. Terada, S. Masuda, J. Asaka, M. Tsuda, T. Katsura, and K. Inui. Molecular cloning, functional characterization and tissue distribution of rat H⁺/organic cation antiporter MATE1. *Pharm Res* **23**: 1696–1701 (2006).
 69. S. Masuda, T. Terada, A. Yonezawa, Y. Tanihara, K. Kishimoto, T. Katsura, O. Ogawa, and K. Inui. Identification and functional characterization of a new human kidney-specific H⁺/organic cation antiporter, kidney-specific multidrug and toxin extrusion 2. *J Am Soc Nephrol* **17**: 2127–2135 (2006).
 70. M. Tsuda, T. Terada, J. Asaka, M. Ueba, T. Katsura, and K. Inui. Oppositely-directed H⁺ gradient functions as a driving force of rat H⁺/organic cation antiporter MATE1. *Am J Physiol Renal Physiol* **292**: F593–F598 (2007).
 71. M. Takano, K. Inui, T. Okano, H. Satio, and R. Hori. Carrier-mediated transport systems of tetraethylammonium in rat renal brush-border and basolateral membrane vesicles. *Biochim Biophys Acta* **773**: 113–124 (1984).
 72. I. B. Roninson, J. E. Chin, K. G. Choi, P. Gros, D. E. Housman, A. Fojo, D. W. Shen, M. M. Gottesman, and I. Pastan. Isolation of human mdr DNA sequences amplified in multidrug-resistant KB carcinoma cells. *Proc Natl Acad Sci U S A* **83**: 4538–4542 (1986).
 73. A. T. Fojo, K. Ueda, D. J. Slamon, D. G. Poplack, M. M. Gottesman, and I. Pastan. Expression of a multidrug-resistance gene in human tumors and tissues. *Proc Natl Acad Sci U S A* **84**: 265–269 (1987).
 74. M. Dean, A. Rzhetsky, and R. Allikmets. The human ATP-binding cassette (ABC) transporter superfamily. *Genome Res* **11**: 1156–1166 (2001).
 75. R. G. Deeley, C. Westlake, and S. P. Cole. Transmembrane transport of endo- and xenobiotics by mammalian ATP-binding cassette multidrug resistance proteins. *Physiol Rev* **86**: 849–899 (2006).
 76. P. Krishnamurthy, and J. D. Schuetz. Role of ABCG2/BCRP in biology and medicine. *Annu Rev Pharmacol Toxicol* **46**: 381–410 (2006).
 77. G. A. Altenberg. Structure of multidrug-resistance proteins of the ATP-binding cassette (ABC) superfamily. *Curr Med Chem Anticancer Agents* **4**: 53–62 (2004).
 78. A. H. Schinkel, U. Mayer, E. Wagenaar, C. A. Mol, L. van Deemter, J. J. Smit, M. A. van der Valk, A. C. Voordouw, H. Spits, O. van Tellingen, J. M. Zijlmans, W. E. Fibbe, and P. Borst. Normal viability and altered pharmacokinetics in mice lacking mdr1-type (drug-transporting) P-glycoproteins. *Proc Natl Acad Sci U S A* **94**: 4028–4033 (1997).
 79. M. F. Fromm. Importance of P-glycoprotein at blood-tissue barriers. *Trends Pharmacol Sci* **25**: 423–429 (2004).
 80. C. G. Dietrich, A. Geier, and R. P. Oude Elferink. ABC of oral bioavailability: transporters as gatekeepers in the gut. *Gut* **52**: 1788–1795 (2003).
 81. B. Greiner, M. Eichelbaum, P. Fritz, H. P. Kreichgauer, O. von Richter, J. Zundler, and H. K. Kroemer. The role of intestinal P-glycoprotein in the interaction of digoxin and rifampin. *J Clin Invest* **104**: 147–153 (1999).
 82. K. Westphal, A. Weinbrenner, M. Zschiesche, G. Franke, M. Knoke, R. Oertel, P. Fritz, O. von Richter, R. Warzok, T. Hachenberg, H. M. Kauffmann, D. Schrenk, B. Terhaag, H. K. Kroemer, and W. Siegmund. Induction of P-glycoprotein by rifampin increases intestinal secretion of talinolol in human beings: a new type of drug/drug interaction. *Clin Pharmacol Ther* **68**: 345–355 (2000).

83. D. Durr, B. Stieger, G. A. Kullak-Ublick, K. M. Rentsch, H. C. Steinert, P. J. Meier, and K. Fattinger. St John's Wort induces intestinal P-glycoprotein/MDR1 and intestinal and hepatic CYP3A4. *Clin Pharmacol Ther* **68**: 598–604 (2000).
84. S. Masuda, and K. Inui. An up-date review on individualized dosage adjustment of calcineurin inhibitors in organ transplant patients. *Pharmacol Ther* **112**: 184–198 (2006).
85. T. Hashida, S. Masuda, S. Uemoto, H. Saito, K. Tanaka, and K. Inui. Pharmacokinetic and prognostic significance of intestinal MDR1 expression in recipients of living-donor liver transplantation. *Clin Pharmacol Ther* **69**: 308–316 (2001).
86. S. Masuda, M. Goto, M. Okuda, Y. Ogura, F. Oike, T. Kiuchi, K. Tanaka, and K. Inui. Initial dosage adjustment for oral administration of tacrolimus using the intestinal MDR1 level in living-donor liver transplant recipients. *Transplant Proc* **37**: 1728–1729 (2005).
87. S. Masuda, M. Goto, S. Fukatsu, M. Uesugi, Y. Ogura, F. Oike, T. Kiuchi, Y. Takada, K. Tanaka, and K. Inui. Intestinal MDR1/ABCB1 level at surgery as a risk factor of acute cellular rejection in living-donor liver transplant patients. *Clin Pharmacol Ther* **79**: 90–102 (2006).
88. H. Suzuki, and Y. Sugiyama. Excretion of GSSG and glutathione conjugates mediated by MRP1 and cMOAT/MRP2. *Semin Liver Dis* **18**: 359–376 (1998).
89. R. O. Elferink, and A. K. Groen. Genetic defects in hepatobiliary transport. *Biochim Biophys Acta* **1586**: 129–145 (2002).
90. G. L. Scheffer, M. Kool, M. de Haas, J. M. de Vree, A. C. Pijnenborg, D. K. Bosman, R. P. Elferink, P. van der Valk, P. Borst, and R. J. Scheper. Tissue distribution and induction of human multidrug resistant protein 3. *Lab Invest* **82**: 193–201 (2002).
91. T. Hirohashi, H. Suzuki, and Y. Sugiyama. Characterization of the transport properties of cloned rat multidrug resistance-associated protein 3 (MRP3). *J Biol Chem* **274**: 15181–15185 (1999).
92. T. Hirohashi, H. Suzuki, H. Takikawa, and Y. Sugiyama. ATP-dependent transport of bile salts by rat multidrug resistance-associated protein 3 (Mrp3). *J Biol Chem* **275**: 2905–2910 (2000).
93. N. Zelcer, K. van de Wetering, R. de Waart, G. L. Scheffer, H. U. Marschall, P. R. Wielinga, A. Kuil, C. Kunne, A. Smith, M. van der Valk, J. Wijnholds, R. O. Elferink, and P. Borst. Mice lacking Mrp3 (Abcc3) have normal bile salt transport, but altered hepatic transport of endogenous glucuronides. *J Hepatol* **44**: 768–775 (2006).
94. L. A. Doyle, and D. D. Ross. Multidrug resistance mediated by the breast cancer resistance protein BCRP (ABCG2). *Oncogene* **22**: 7340–7358 (2003).
95. J. D. Allen, S. C. Van Dort, M. Buitelaar, O. van Tellingen, and A. H. Schinkel. Mouse breast cancer resistance protein (Bcrp1/Abcg2) mediates etoposide resistance and transport, but etoposide oral availability is limited primarily by P-glycoprotein. *Cancer Res* **63**: 1339–1344 (2003).
96. J. W. Jonker, M. Buitelaar, E. Wagenaar, M. A. Van Der Valk, G. L. Scheffer, R. J. Scheper, T. Plosch, F. Kuipers, R. P. Elferink, H. Rosing, J. H. Beijnen, and A. H. Schinkel. The breast cancer resistance protein protects against a major chlorophyll-derived dietary phototoxin and protoporphyria. *Proc Natl Acad Sci U S A* **99**: 15649–15654 (2002).
97. G. Merino, J. W. Jonker, E. Wagenaar, A. E. van Herwaarden, and A. H. Schinkel. The breast cancer resistance protein (BCRP/ABCG2) affects pharmacokinetics, hepatobiliary excretion, and milk secretion of the antibiotic nitrofurantoin. *Mol Pharmacol* **67**: 1758–1764 (2005).

Cloning and Functional Heterologous Expression of Transporters

Carsten Kneuer and Walther Honscha

Abstract Progress in molecular biology and advanced cell culture techniques has allowed identifying, isolating and expressing genes encoding membrane proteins which affect the transmembrane passage of drugs and drug candidates. Such membrane proteins, also called drug transporters or carriers, are not only involved in multi-drug resistance but also play a major role in intestinal absorption, passage of the blood–brain or blood–placenta barrier, as well as hepatic and renal elimination. Here, an overview of techniques suitable for the isolation of coding sequences of such drug transporters will be given. This is followed by a section dedicated to the in vitro expression of these sequences as it is required to study their function.

Keywords: Carrier; cDNA; Cloning; Expression; RACE; Transporter

Abbreviations

ABC	ATP-binding cassette
ADME	Absorption, distribution, metabolism and elimination
EST	Expressed sequence tag
GTP	guanosine triphosphate
IPTG	Isopropyl-beta-D-thiogalactopyranoside
MDR	Multi-drug resistance
MRP	Multi-drug resistance-associated protein
MW	Molecular weight
OAT/oat	Organic anion transporter (protein / nucleic acid)
OATP/oatp	Organic anion transporting polypeptide (protein / nucleic acid)
OCT/oct	Organic cation transporter (protein / nucleic acid)
PCR	Polymerase chain reaction
pIRES	Plasmid with internal ribosome entry site
RACE	Rapid amplification of cDNA ends
SLC/slc	Solute carrier (protein / nucleic acid)
TE	Tris/EDTA
T_m	Melting temperature

24.1. Introduction

Overwhelming evidence has been accumulated during the last two decades that the pharmacokinetic behaviour of drugs and xenobiotics, often described as absorption, distribution, metabolism and elimination (ADME), is also influenced by active transmembrane transport processes. For example, export pumps of the ATP-binding cassette (ABC) family of transporters, such as multi-drug resistance protein 1 (MDR1, P-glycoprotein) are expressed at the apical face of enterocytes and have been shown to limit the oral bioavailability of their substrates by rapid extrusion from the intestinal lining back into the lumen. By the same mechanism, ABC-transporters localised in the vascular side of the blood–brain barrier limit the distribution into the cerebrospinal fluid and the brain. Transport proteins of the families of the organic anion transporters (OAT) and organic anion transporting polypeptides (OATP), which are found in the basolateral membrane of hepatocytes, represent the gate through which various hydrophilic molecules can gain access to their metabolic liver enzymes. Finally, numerous renal transport proteins including OATs, OATPs, ABC-transporters and others participate in the secretion of drugs into the urine, or their re-absorption from urine and are hence integral part of the elimination process [16].

Similar processes with impact on the ADME behaviour of a substance as those described above occur in virtually all organs of the human and animal body. Consequently, a wealth of models has been developed to study such processes *ex vivo* or *in vitro*, including organ preparations (e.g. intestinal loops), tissue slices and isolated cells. With these tools, a detailed characterisation of the transport processes and the proteins involved was achieved at the cellular level. For a molecular characterisation such as determination of substrate/inhibitor spectrum, kinetic variables or identification of protein structure and binding sites, however, these complex models are rarely ideal. The existence of further carriers, receptors and/or metabolic enzymes with overlapping substrate specificity complicates the generation and interpretation of suitable data. Isolation of transport proteins in sufficient amount and purity as required for structural analysis is a major challenge, and modifications to the proteins, such as targeted mutations and attachment of affinity tags is practically impossible [18]. Therefore, techniques for cloning of the cDNA encoding carrier proteins, as well as expression these cDNAs in a foreign but suitable environment have been developed.

24.2. Cloning Techniques

24.2.1. Historical Overview and General Considerations

At the beginning of the 1980s, cloning of transporters for physiological substances or xenobiotics was hampered by the fact that no sequence information about the corresponding cDNA or the protein was available. Therefore, the application of classical molecular cloning methods by homology screening of cDNA libraries was not possible. In order to identify the genes for drug carriers, two different strategies were used. One approach was based on the isolation of the involved carrier protein by biochemical methods for subsequent amino

acid sequencing. With this sequence information the generation of primers for cDNA library screening should be possible. The other strategy represented the generation of antibodies for screening of bacterial expression libraries. However, both approaches required the purification of integral plasma membrane proteins which are very lipophilic, often of low abundance and difficult to handle. Whereas the progress of the purification of a cytosolic enzyme can easily be followed by measuring the enzymatic activity in solution, the determination of the activity of a carrier requires the insertion of the protein fraction under investigation into an artificial membrane. Such reconstitution is very laborious and extremely difficult. Hence, alternative methods, such as photoaffinity labelling were pursued. Here, the carrier protein is labelled by cross-linking with a radioactive substrate and subsequently separated from the crude plasma membrane preparation by gel electrophoresis. The labelled protein band(s) were excised from one-dimensional (1D) sodium dodecyl sulphate (SDS) gels and used for the immunisation of rabbits to raise specific antisera against the carrier protein under investigation. Unfortunately, analysis of these protein bands by 2D gel electrophoresis revealed that they often consisted of 20 or more different proteins. Therefore, the preparative 2D gel electrophoresis of integral membrane proteins was developed to obtain pure preparations. Because of the hydrophobicity of the proteins, they had the tendency to aggregate on top of the gels prior to isoelectric focussing and the amount of protein which could be loaded on the gels was limited. Hundred or more preparative 2D gels were required for isolation of a few micrograms of the putative transporter protein. Other methods for isolation of these proteins were developed. One of these was the free-flow isoelectric focussing, which was very expensive, due to the great amount of ampholytes needed, but it avoided aggregation of the membrane proteins. Nevertheless, the results of the amino acid analysis of these purified proteins were, in most cases, very disappointing. A high degree of homology to structural cell proteins and intracellular enzymes was found. Similarly disappointing results were obtained by the groups using antisera generated from crudely purified plasma membrane fractions.

To solve this dilemma, a new method which allowed the separation of the transmembrane transporter not as the protein, but as the nucleic acid, followed by subsequent expression of the isolated nucleic acid and a screening of the functional activity of the encoded polypeptide was suggested.

The tools for this method had to be carefully selected, as biosynthesis of functional membrane proteins requires at least partial translocation of the nascent polypeptide chain into the endoplasmic reticulum, post-translational modifications in the Golgi apparatus, and transport to, as well as proper insertion/folding into the membrane. Because of this complexity, it was difficult to achieve the synthesis of functional eukaryotic membrane proteins *in vitro* or in prokaryotic cells. Thus, functional expression of these proteins requires the utilisation of eukaryotic cells which are able not only to express the nascent polypeptide, but also to produce a functional protein. Although different methods to express heterologous DNA-sequences in eukaryotic cell lines were published at the beginning of the 1990s, the transfection of a whole cDNA library or parts thereof into cell lines was difficult to achieve. The small size of the individual cells, the low amount of protein expressed per cell and the endogenous expression of carrier proteins resulting in a considerable

background made eukaryotic cell cultures inappropriate for cloning projects unless a selection method was available to enrich the desired cDNA clone.

24.2.2. *Xenopus Laevis* Oocytes for Cloning of Drug Carrier

The expression cloning strategy using *Xenopus laevis* oocytes, first reported by Hediger and Wright [8] to clone the sodium/glucose co-transporter from rabbit intestinal brush border, can be regarded as the major breakthrough in the molecular cloning of drug carriers.

Its principle can be described as follows: First, total polyA⁺-RNA prepared from the tissue of interest expressing the carrier is injected into *Xenopus laevis* oocytes. After 3–7 days, functional uptake studies with radioactively labelled transporter substrates are performed and the typical characteristics of the carrier are tested. In the next step, the same mRNA is fractionated according to size and aliquots of the fractions are injected. Ideally, only one mRNA-fraction will show transport of the test substrate. Then, this mRNA-fraction is used to construct a cDNA library using a vector which contains an upstream *Salmonella typhimurium* (SP6), T3 or T7 promoter, allowing in vitro transcription of the cloned cDNA. Pools of cDNA clones—depending on the signal strength, usually 500–1,000 clones are pooled—are transcribed in vitro and the resulting cRNAs (copy RNAs) are injected into oocytes. These oocytes are then individually tested for acquisition of the desired activity and positive pools are subdivided and reanalysed until the functional activity can be attributed to one single cDNA clone.

The ability of *Xenopus laevis* oocytes to express large quantities of foreign protein from injected mRNA represents the major advantage of this method [6]. Although this cloning strategy has its limitations, it is also extremely attractive, as it allows clonal selection not on the basis of protein structure, but on the basis of transport activity. Direct measurement of the transport activity mediated by the expressed carrier protein is used to identify the mRNA coding for this protein. With this procedure, a large number of carrier proteins—usually the first representative of the different drug carrier families—were cloned in the following years. This included, for example, the organic anion transporting polypeptide (oatp1) [9], the organic cation transporter (oct1) [5] and the organic anion transporter (oat1) from flounder [27] and rat [23, 20].

With the sequence information of these carriers, further members of the different families and their orthologues from various species were isolated using less laborious cloning techniques. Until now, about 360 transporters and their orthologues for endogenous and exogenous substances of the solute carrier (SLC) family from various species were cloned [7] and at least 49 human ABC-transporters, including members of the multi-drug resistance protein family and the multi-drug resistance associated protein (MRP) family are identified. Nevertheless, the *Xenopus laevis* system is still popular for the characterisation of substrate specificities, kinetic parameters and IC₅₀ values of many of these carriers (see Sect. 24.3.4).

In the following, a short overview of the expression cloning method with *Xenopus laevis* oocytes is given. Protocols for standard procedures are provided in the Appendix, while those methods that are subject to frequent modification are described in general and the reader is referred to the corresponding hand-books for further details.

24.2.2.1. Maintenance of *Xenopus laevis* and Preparation of Oocytes

Mature, oocyte positive, female *Xenopus laevis* are kept in (mesh) covered grey plastic tanks in tap water (depth 15–20 cm, 3–4 L per animal) at 16–19°C under constant light regime (12-h day/night cycle). The quality of the tap water should be tested at the beginning and care should be taken on the chlorine and heavy metal content. A simple way to eliminate excessive chlorine from the water is storage of the water for 24 h. Clay tubes in the tanks allow the frogs to cover themselves. The animals are fed a commercially available pellet diet twice a week, and occasionally they receive small pieces of bovine heart. The tanks have to be cleaned after each meal.

As mature *Xenopus laevis* females carry ~30,000 oocytes and a typical experiment consumes not more than 1,000 oocytes, it is not necessary to kill a frog for each experiment. Instead, pieces of the ovary are removed by laparotomy and the incision is sutured. The same animal can serve as a donor of fresh oocytes after a convalescence of 2–3 weeks, and 10–15 oocyte preparations can be made from each frog without affecting its health. Hence, not more than 20–30 animals, in most cases 10–15, are maintained at the same time. For details see also Protocol 1 in the Appendix.

24.2.2.2. Preparation of mRNA, Size Fractionation

A tissue in which the transporter of interest is expressed in high abundance is used as starting material for functional expression cloning, supposing that a high copy number of the corresponding mRNA is present in the organ. Cloning of low abundance mRNAs for transporter proteins is often not successful with this strategy.

Total RNA can be prepared using commercially available kits according to the protocols of the manufacturer or by the guanidinium isothiocyanate method, followed by caesium chloride centrifugation (CsCl). Details are published in handbooks of molecular biology techniques. In our hands, both methods are equivalent, but if budgets are limited, the CsCl method may be more suitable for the preparation of large amounts of RNA.

Next, poly A⁺-RNA is isolated from total RNA. Again, various kits from known suppliers can be used. In recent years, an increasing number of kits for the direct preparation of poly A⁺-RNA from tissue and cells have become available. Although the integrity of directly isolated mRNA seems to be given, the expression of the protein of interest was lower in our hands. Therefore, we still favour the classical two-step procedure. Fractionation of the mRNA, cDNA library construction, quality controls and the potential need to repeat experiments require substantial amounts of starting material. We usually begin with at least 500 µg of high-quality mRNA, which is then dissolved in Tris/EDTA (TE) buffer, heated for 10 min to 65°C to destroy any secondary structures, and then chilled on ice. The quality of the mRNA is best checked by denaturing agarose gel electrophoresis and functional expression in oocytes. For long-term storage, the mRNA should be precipitated with ethanol and kept at –80°C. For microinjection, the RNA is also precipitated, washed with cold ethanol (70%) and resuspended in RNase-free water. After expression of the total mRNA in *Xenopus oocytes*, a clear induction of transport activity in comparison with water-injected oocytes should be detectable (see also Protocols 2 and 3 in the Appendix). It is important to verify that the signal reflects the characteristics of the carrier searched for in terms of specificity, substrate spectrum and inhibition by related substrates.

If the expression of the mRNA results in a clear signal, a linear sucrose gradient (6–20% sucrose, 5 mM EDTA, 0.25% (w/v) sarcosyl, 15 mM PIPES-NaOH, pH 6.4) is prepared in SW27 tubes or equivalent and the mRNA is carefully loaded on top. After centrifugation (19 h, 80,000×g), about 33 fractions of 1 ml each are collected, and the mRNA is precipitated using sodium acetate and ethanol. Prior to injection, the RNA of each fraction is pelleted, washed and dissolved in RNase-free water as described above. Upon injection of 50 ng fractionated mRNA, a two- to fivefold increase in transport activity is expected for the positive mRNA-fraction compared with unfractionated mRNA. All other fractions should not show any specific functional activity. In cases where two neighbouring fractions induce transport activity, pooling of these should be considered.

24.2.2.3. cDNA Synthesis

The mRNA-fraction selected as described above is used for directional cloning of a cDNA library. It is important that the fractionation is as narrow as possible to limit the number of cDNA clones to be tested by time-consuming functional expression in oocytes to a minimum. In addition, a cDNA cloning kit which enables the generation of a directional library should be used as a random library containing 50% clones in antisense orientation which are not functional in oocytes. Antisense transcripts will also compete with the sense transcript and reduce putative positive signals in the library. Directional cloning systems introduce two different restriction sites at the 5'- and the 3'-end of the cDNA. Usually, the oligo dT primer employed for reverse transcription contains a rare cutter restriction site (e.g. NotI, XbaI and SalI) at its 5'-end, whereby a definite 3'-end is introduced during first strand synthesis. After second strand synthesis, the blunt-end cDNA is used for adaptor ligation. This adaptor contains a second, but different restriction site. Hence, a cDNA with two different ends is generated by digestion with the corresponding restriction enzymes, allowing positional cloning into a suitable vector. Before cloning into the plasmid vector, however, a size fractionation via gel chromatography with a cut off <500 bp should be performed to exclude degraded fragments. The cloning vector must contain a bacteriophage (T7, T3) or an SP6 promoter upstream of the insert, enabling the *in vitro* transcription of the cloned sequences. Library construction itself is achieved by standard procedures and can be expected to yield 6,000–8,000 independent cDNA clones, when starting from a size-selected mRNA-fraction. Amplification of the primary library by growing in liquid culture is not recommended as clones with small inserts can suppress the growth of low-abundance recombinants carrying large fragments.

For unknown reasons, some proteins are difficult to express in *Xenopus laevis* oocytes. In these cases, subcloning into specialised vectors which contain 5'- and 3'-untranslated regions of genes from *Xenopus laevis*, which show an enhanced transcriptional activity, may be helpful [15]. The vector pSP64T, for example, carries untranslated sequences of the β -globin gene. The cDNA-sequence of interest is cloned in between these flanking regions.

24.2.2.4. *In Vitro* Transcription

In vitro transcription from cloned cDNA sequences is required to produce mRNA that can be injected into *Xenopus oocytes* for expression of the encoded protein and is achieved by standard procedures. While oocyte isolation and injection generally follows the protocols provided below, *in vitro* transcription into mRNA may be modified in accordance to the instructions provided with

the enzyme kit. In brief, plasmid DNA of a single cDNA clone (or a pool of clones if desired) is linearised by a single cutter at the 3'-end of the cDNA. After proteinase K digestion, phenol/chloroform extraction and ethanol precipitation, the DNA is transcribed in the presence of a capping analogue, yielding up to 20–30 µg of cRNA from 1 µg of DNA. With its 7-methyl guanosine structure at the 5'-end, capped RNA mimics most eukaryotic mRNAs found in vivo. Various in vitro transcription kits are available from numerous suppliers. In our laboratory we prefer the mMMESSAGE mMACHINE kit from Ambion (Austin, TX, USA) which introduces the cap analogue G(5')ppp(5')G only at the 5' terminal G of the transcript as its structure precludes incorporation at any other position. A cap analogue:GTP ratio of 4:1 and a reaction time of 2 h was chosen to maximise transcript yield and the proportion of capped transcripts. Following transcription, the plasmid DNA is degraded by addition of an amount of RNase-free DNase which should be as small as possible to protect the transcript from contaminating RNase. Extensive purification of the synthesised mRNA, particularly removal of free nucleotides, is important for successful expression in oocytes. This can be achieved either by column chromatography or by proteinase K digestion and two rounds of phenol/chloroform extraction. Afterwards, the nucleic acid is precipitated with lithium chloride (or ammonium acetate) and ethanol (or isopropanol) to remove the excess of free nucleotides. It is recommendable to check the quality of the cRNA at this stage, which should appear as a single band of RNA of the expected molecular weight (MW) in the agarose gel without any sign of degradation. Faint bands with a lower MW are an indication of premature termination of transcription. Contamination of the plasmid DNA with substances which inhibit the polymerase may be the reason. If a pool of cDNAs is transcribed, a smear corresponding to the total mRNA is detected in the gel, but the smallest cRNA should be larger than the cut-off of the column used for cDNA cloning. Repeated freezing and thawing of the RNA leads to a gradual loss of activity and should be avoided.

24.2.2.5. Screening of a cDNA Library for a Drug Carrier

Definition of the background activity of microinjected oocytes is a clear prerequisite for any functional cloning procedure, as a positive signal needs to be distinguished from the endogenous transport activities. Key characteristics of the carrier, such as a dependency on sodium ions or a specific inhibitor are very helpful. In addition, unspecific binding of the radioactive transporter substrate to the oocyte membrane needs to be examined carefully.

Once the functional activity of the total cRNA prepared from all cDNA clones of the library is confirmed, as described in Protocol 3 in the Appendix, aliquots of the primary library consisting of 300–1,000 clones are plated separately on agar plates, and duplicates of the master plates are produced by laying a nitrocellulose sheet on top of the agar plate and inoculating fresh agar plates. After overnight culture, the colonies from each filter are pooled, plasmid DNA is isolated, linearised and transcribed in vitro to be microinjected as pooled cRNAs. The pool of cDNA clones which induced transport activity now needs to be identified which may be difficult, as the signal to noise ratio with a mix of clones is usually rather poor. The number of cDNAs per pool may be reduced to improve the signal. However, the number of cDNA pools cannot be increased freely, as comparability of the results requires that all pools of a library are tested at once with one charge of oocytes.

After identification of a pool which contained a clone conferring transport activity to the injected oocyte, this pool is further subdivided. If the starting material consisted of, for example, 1,000 colonies, it is subdivided into 5 pools with 200 colonies each and the procedure is repeated with these, as well as with a positive control including all cDNAs of the 5 pools. When 100 or less colonies are left to select from, we recommend growing the individual colonies in a microtiter plate. Now, pools are generated using all colonies of each row and also all colonies of each column. After functional testing, only one row and one column should be positive, identifying the final cDNA clone encoding the carrier protein.

24.2.2.6. Controls

On the basis of the assumption that *Xenopus oocytes* synthesise a minimal amount of endogenous proteins at this stage of development, most researchers only use water-injected oocytes as a control for background activity of endogenous carriers, and unspecific binding of the radiolabelled tracer for the transport studies. However, we consider it important to carry along positive controls during the functional screening of mRNA-fractions and cDNA libraries. These consist of the starting material for fractionation and also allow assessing the degree of enrichment of the signal. An incremental increase of the transport activity should be seen during the whole screening procedure. Water-injected oocytes may be replaced by non-injected ones if their background activity is the same for a number of independent preparations. In addition to these standard controls, it is worthwhile to exclude the possibility that the radioactively labelled substrate of the carrier is metabolised by the oocyte, although their metabolic capacity is generally regarded as very low.

To ensure the specificity of the signal, it will always be very helpful to test a unique feature of the carrier under investigation, such as specific inhibition, dependence on anions/cations/protons or trans-activation by another substrate. Sodium dependency, for example, can be tested by replacement with *N*-methyl-D-glucamine, whereas choline chloride as substitute of sodium is not recommended, since it may influence the membrane potential. In light of the recent finding that many transport proteins display an overlapping substrate spectrum, such specificity controls should receive adequate appreciation.

24.2.3. Complementation Cloning Strategies

Another cloning strategy is based on the phenotypic complementation of mutant cell lines by transfection of cloned DNA sequences (cosmid libraries, phage λ). This procedure enabled, for example, the identification of a reduced folate carrier [26] which is also able to transport the cytotoxic drug methotrexate. A Chinese hamster ovary (CHO) cell line carrying an inactive mutant transporter was chosen for screening cosmid and cDNA libraries, as this cell line was both dependent on supplementation of the medium with higher concentrations of folates and insensitive to methotrexate. Growth in medium with only 2 nM folates allowed selective enrichment of CHO clones transfected with the desired cDNA, and the function of the protein encoded by the selected cDNAs was confirmed by its ability to restore the sensitivity towards methotrexate.

The first cloned sequences of the multi-drug resistance transporter (P-glycoprotein, MDR1, ABCB1) were isolated from multi-resistant cell lines in which the gene was strongly amplified. By in-gel renaturation analysis these

amplified genes were identified and subsequently cloned [4]. Afterwards, it was demonstrated that transfection of these genes into sensitive cell lines altered the phenotype of the parental cell line.

24.2.4. Homology Cloning

When the first member of a new carrier family is cloned, the cDNAs of highly homologous family members can be isolated by screening cDNA libraries with primers or probes deduced from the original cDNA clone. In fact, most members of many carrier families, as well as the corresponding orthologues from other species were identified using this strategy. To facilitate this process, information from expressed sequence tags (EST) was used to identify cDNAs with a high degree of homology which may represent further members of a carrier family.

In addition, the differential hybridisation technique allows comparing mRNA pools from two cell lines exhibiting different transport characteristics. Such hybridisation removes the mRNAs which are common to both sources and enriches those that cause the phenotypic difference, including (hopefully) the mRNA encoding the transport protein under investigation.

24.2.4.1. RACE-PCR

A very elegant method for cloning low-abundancy mRNAs was provided by the rapid amplification of cDNA ends (RACE) technique [1]. Nearly at the same time, the method of RNA ligase-mediated RACE and oligo-capping RACE was developed [19]. One problem of cDNA cloning is that the reverse transcriptase stops before the end of the mRNA is reached, resulting in truncations of the 5'-region. These prematurely terminated cDNA clones are not functional and originally the RACE method was developed for synthesis of the missing cDNA ends. Soon afterwards, it was recognised that this method allowed the generation of full-length cDNA clones by long-distance polymerase chain reaction (PCR). The multiple amplification by PCR allows the cloning of mRNAs of low-abundancy (frequently the case for transporter RNAs), which represents a major advantage. As the method only requires gene-specific primers with a length of 23–28 nucleotides, it is also possible to clone cDNAs of which only EST are known. RACE-PCR is also possible using degenerated primers.

In principle, the method involves two separate PCR-reactions for the 5'- and the 3'-end, respectively, using a double-stranded adaptor-ligated cDNA as template and the corresponding gene-specific primers (Marathon[®] cDNA amplification kit, Clontech, Mountain View, CA, USA). Both RACE-products containing the 5'- and the 3'-end of the cDNA, respectively, are at first cloned individually before the final full-length clone is generated, utilising a region of overlap either by end-to-end PCR or by conventional subcloning (Figure 24.1). The procedure is critically dependent on the quality of the gene-specific primers, which should have an annealing temperature of at least 70°C, corresponding to the melting temperature (T_m) of the adaptor primers. Theoretically, the complete cloning procedure starting from the cDNA synthesis to the final recombination of the 5'- and 3'-RACE fragments can be done in 2 days. In practice, the complete cloning procedure will consume several weeks as up to 50 different PCRs for RACE-fragments have to be performed, before the protocol is sufficiently optimised and the identity of the products is verified either by hybridisation with gene-specific primers or sequencing.

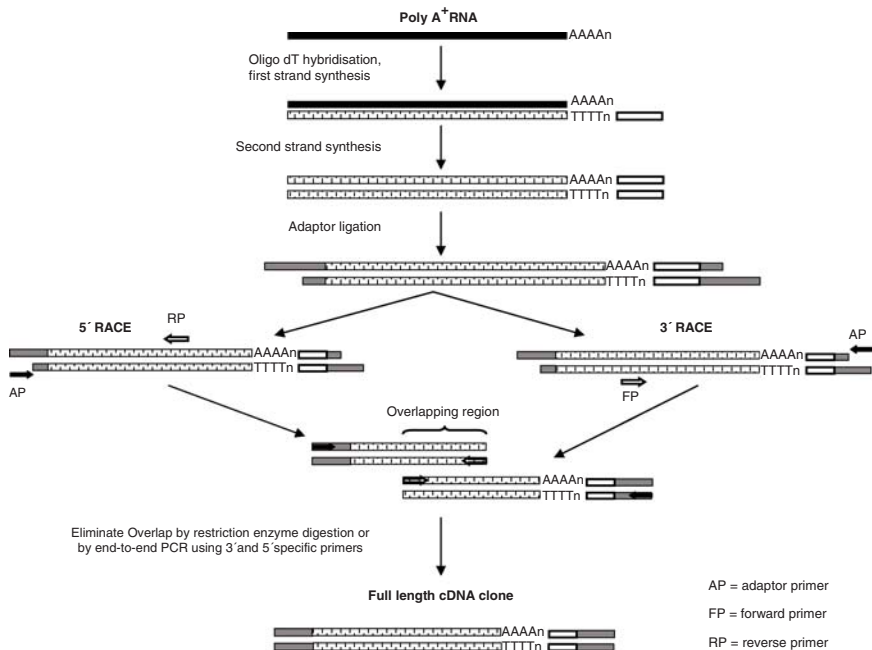


Figure 24.1 Flow chart of RACE-PCR protocol adopted with slight modifications from the instruction manual of the Marathon[®] cDNA amplification kit. Poly A⁺ RNA is used for the generation of an adaptor-ligated cDNA library. Fragments containing the 5'- and the 3'-end of the cDNA coding for the carrier are amplified from the uncloned library with adaptor primers and gene-specific primers. Afterwards, a full-length clone is generated from the individual RACE products by subcloning or end-to-end PCR.

In general, isolation of the poly A⁺-RNA and synthesis of the double-stranded cDNA should not present major problems and can be performed using standard techniques. Commercially available kits (e.g. Marathon[®] cDNA-amplification kit, Clontech) worked well in our hands, but it was found crucial that the mRNA is of high purity and undegraded. All glass, plastic ware and buffers not supplied by the manufacturer should be absolutely RNase free. If the reverse transcription reaction works suboptimal, the amount of the specific gene is reduced and the amplification of the corresponding cDNA is difficult. It should be realised that during the cloning procedure one specific gene from about 40,000 genes is later amplified in a single PCR reaction.

Reverse transcription is followed by second-strand cDNA synthesis, the efficiency of which we recommend to check on an agarose gel. A smear between 0.5 and ~10 kb with some stronger bands (abundant mRNAs) should be observed. If [α -³²P]dCTP is used as a tracer during cDNA synthesis, Czerenkov counts may be measured as indication about the yield of the reaction. In the next step, the partially double-stranded cDNA-adaptors are ligated to the ds cDNA. This step is greatly enhanced by using phosphorylated adaptors. The efficiency of ligation is important, as unligated double-stranded cDNA molecules do not provide the site for adaptor primer binding during the first PCR cycle. A simple method to check the uncloned cDNA library is to perform an internal PCR reaction with gene-specific primers.

Now, the specific cDNA fragments are amplified by PCR to amounts which are sufficient for subsequent cloning into plasmid vectors. Particularly, if the mRNA of interest is of low abundance, the amplification of the corresponding cDNA is critical. In this case, robust primers and the use of touchdown PCR is strongly recommended. As an alternative, the primary RACE-PCR reaction can be diluted and a second PCR is performed with nested primers. It is important that all PCRs are performed in one type of thermal cycler as ramping temperatures of different cyclers may vary. Use of a high-fidelity long-distance polymerase, as well as some form of hot start (TaqStart antibody, wax beads or manual hot start) is recommendable. Touchdown PCR protocols usually include 5 initial cycles at a temperature 2°C above the T_m of the primer, 5 cycles at the T_m -value and about 25 cycles 2°C below the T_m . Frequently, a primer pair results in an unacceptably high background fails to yield the desired product or produces only a very faint band. It is therefore helpful to design and test a set of different primers for each RACE-PCR. In our hands, the initial PCR often produced a smear after separation in the agarose gels. Sometimes, a faint band of the expected MW and some other unrelated bands were seen. At this stage, it is important to characterise these initial PCR fragments. We recommend confirming the identity of the RACE-products by Southern blot analysis. This control experiment gives an indication about the presence of the desired PCR product, the MW and whether multiple bands with sequence homology (members of multigene families) or unrelated bands exist. A careful optimisation of the amplification conditions is necessary after identification of the target PCR product, in order to reduce background and truncated PCR fragments, as well as to improve yield. Increasing the number of the initial cycles (e.g. 10 cycles at high, 5 cycles at medium and 25 cycles at low temperature) enhances the specific product, while additional cycles at the low temperature usually result in higher background. If there is no product, the number of cycles can be increased and the annealing temperature lowered. If the PCR product of interest is visible after agarose gel electrophoresis, but the background is high, then a serial dilution of the cDNA used for RACE-PCR is helpful. This additional dilution of cDNA reduces the background while the specificity for the desired product persists.

Another possibility to enhance the specific DNA-fragment is to perform a nested PCR. With this PCR method, sequences of very low abundance can be amplified, but the risk to enhance the background at the same time is very high. For a nested PCR, a small aliquot of the first PCR reaction is used together with gene-specific primers which bind within the initial PCR product.

After optimisation of the reaction conditions, the final RACE-PCRs for the 3'- and the 5'-end are performed, the corresponding DNA-fragments are then gel purified, extracted and cloned in an appropriate vector by standard techniques. By using a restriction enzyme in the overlapping region of both fragments or by an end-to-end PCR the full-length cDNA clone is generated.

Another method for direct full-length cDNA cloning, called GeneRacer™ (Invitrogen, Carlsbad, CA, USA) is based on the fact that RNA ligase cannot link dephosphorylated polyA⁻ mRNA, as well as truncated mRNA lacking the cap structure to the oligoribonucleotide that contains the binding site for the GeneRacer™ 5'-primer. In contrast dephosphorylated but capped full-length mRNAs which are treated with tobacco acid pyrophosphatase which cleaves within the triphosphate of the capping structure (removing the cap and

exposing a terminal 5'-phosphate) will be ligated. This technique guarantees that only full-length mRNAs can be amplified during RACE-PCR after converting the mRNA into single-stranded cDNA with an oligo dT primer that contains the binding site for the 3'-GeneRacerTM primer. RACE reactions and the final cloning are performed in analogy to the Marathon[®] kit.

24.3. Heterologous Expression Systems

Once the cDNA encoding a (new) drug transport protein is cloned and sequenced, there are various reasons for which this sequence may need to be expressed and translated. Objectives are manifold and may include investigations of the protein structure (crystal structure, glycosylation, phosphorylation, membrane topology), expression of larger amounts of the protein for immunisation and production of specific antisera, or a functional characterisation including substrate and inhibitor spectrum as well as the kinetic parameters of the protein–ligand interaction. Hence, the ideal system would at least provide (1) ease of transfection with the cDNA, (2) its efficient transcription and translation, (3) correct processing and sufficient stability of the polypeptide, (4) the possibility to easily assess protein structure as well as function and (5) stability and reproducibility of this model. Obviously, no single expression system can possess all these properties and the biopharmaceutical questions to be addressed must determine the choice of the model.

Today, there are a wide variety of laboratory protein expression systems available, ranging from cell-free systems over bacterial and yeast cultures to eukaryotic models including the *Xenopus oocytes* or insect and mammalian cell cultures, some of which even form polarised epithelial-like cells layers. In Table 24.1, an overview of the most important systems, as well as their particular strength and weaknesses in the expression of transmembrane transport proteins is provided.

24.3.1. Cell-Free Expression Systems

In principle, heterologous expression of a protein does require only four components: (1) a nucleic acid encoding the protein, preceded by transcription and translation signals; (2) a RNA polymerase and co-factors enabling DNA binding of the polymerase as well as mRNA synthesis; (3) ribosomes as well as tRNA for mRNA translation and finally (4) protein modifying enzymes, such as glycosyltransferases as well as their co-factors. Early systems were based simply on crude cell extracts depleted of endogenous DNA and mRNA or—a little more sophisticated—the depleted S100 fraction supplemented with isolated ribosomes and tRNA. The more sophisticated cell-free expression systems are instead composed of the pure components only [21].

Most frequently, extracts of either prokaryotic or eukaryotic origin as such from *Escherichia coli*, wheat germ or rabbit reticulocytes are employed for cost reasons and availability. While those based on *E. coli* are unable of post-translational protein modification, eukaryotic extracts do allow synthesis of glycosylated or phosphorylated proteins to some extent when additional components, such as microsomes for glycosylation are added. Care needs to be taken with cell-free systems recombined from the individual components when a native protein is to be produced that does not fold spontaneously

Table 24.1 Overview of Expression Systems, Advantages and Disadvantages in the Expression of Drug Transport Proteins.

Expression system	Advantages	Disadvantages	Suitable for
Cell-free in vitro transcription and translation	Commercially available, no transfection (-duction) required, expression of toxic products possible	Low-yield, missing introduction into membranes, modification dependent on additives	Structural studies, reconstitution in artificial membranes
Bacterial cultures (<i>E. coli</i>)	Rapidly installed, easy, fast, cheap, high protein yield (potentially)	Misfolding (inclusion bodies), very limited post-translational modification, different membrane composition	Large scale expression, especially for antigen production
Yeast cultures	Similar to bacterial cultures	Often misfolding, limited modification, different membrane composition	Like bacteria, functional studies may be possible but rarely described
Insect cell cultures	High protein yield, correct folding, some post-translational protein modification	Different culture temperature, endogenous transport activity	Preparation of membrane vesicles
<i>Xenopus laevis</i> oocytes	Large size of individual cells for easy and sensitive functional evaluation	Different culture temperature, different membrane composition endogenous transport activity depending on stage	Screening of cDNAs, identification of substrates and inhibitors, transport kinetics
Simple mammalian cell cultures	Mostly correct folding and post-translational modification, correct membrane composition, direct uptake assays possible	More expensive and time-consuming, variable levels of protein expression, only indirect efflux studies	(screening of cDNAs), identification of substrates and inhibitors, transport kinetics and co-factors, intracellular localisation
Mammalian cell cultures with polarised, differentiated phenotype	Mostly correct folding, modification and localisation; correct membrane composition, transport assays possible, (regulatory) co-factors may be present	More expensive, labour- and time-consuming, transfection partly complicated, variable levels of protein expression	Identification of substrates and inhibitors, transport kinetics and co-factors, vectorial transport, intracellular trafficking, regulation

during translation. This is the case with most transmembrane proteins, and addition of chaperones to the reaction has shown only limited success. Another challenge remains in the correct formation of disulphide bonds, but iodoacetamide treatment may successfully remove any endogenous reducing activity. Finally, any transmembrane protein will suffer from severe solubility problems when synthesised in an unmodified cell-free transcription and translation system. Simple approaches overcome this problem by subsequent detergent

solubilisation. Addition of either compatible detergents as proposed by Klammt et al. [10] or inverted membrane vesicles serving as matrix for the newly synthesised protein [14] are certainly more elegant but requires case-by-case optimisation. For these reasons, the cell-free expression remains currently used only for expression of transmembrane protein fragments for structural studies, for example nuclear magnetic resonance spectroscopy, toxic proteins that are hard to produce in living cells, or complete transmembrane proteins of special interest which will then be subjected to detergent solubilisation and reconstitution in artificial membranes.

Technically, *in vitro* transcription is achieved from standard expression plasmids typically carrying SP6 or T7 promoters using marketed kits. Translation into the polypeptide may be either coupled directly to the transcription (*in vitro* TnT) or require isolation of the RNA. Again, a large number of suitable prokaryotic and eukaryotic cell extracts as well as complementation factors are freely available.

24.3.2. Bacterial Expression Systems

Bacterial expression systems based on laboratory strains of *E. coli* or, less frequently, other bacterial species remain the most widely used means for production of recombinant proteins to date. Although easy to use, there are severe limitations when the synthesis of functional transmembrane proteins is intended. Recombinant transmembrane proteins are rarely folded correctly after expression in bacteria, resulting in the storage in inclusion bodies or even partial or full degradation. Post-translational modifications, such as glycosylation often found on transmembrane proteins are also unlikely to occur in bacteria, although such modification is usually not essential for protein function. If the heterologously expressed transmembrane protein should nevertheless be folded into its native form and have received all essential modifications, it will still be embedded into a vastly artificial microenvironment. Major differences in lipid composition of the surrounding membrane, electrochemical gradients across this membrane and presence of a cell wall are only the most important factors.

For these reasons, bacterial expression systems are not suitable to study the functional aspects of mammalian transport proteins. However, they are very useful to produce large amounts of such proteins or their fragments for immunisation of mice and rabbits as well as for studies of protein structure. In this case, protein misfolding and inclusion body formation can be very helpful to purify the recombinant protein after cell lysis from the bacterial biomass by fractionated dissolution with detergents of increasing strength (e.g. TE buffer–Triton X-100–SDS–guanidinium chloride). Measures to ensure maximum yield include the use of strong but inducible bacterial promoters in the plasmid vector or an auxiliary sequence present in the *E. coli* strain. Most frequently, this element is activated by addition of the inducer IPTG (isopropyl-beta-D-thiogalactopyranoside) causing either transcription of the transgene or a co-factor, such as T7 polymerase, which will then initiate transgene expression. This method of inducible expression of the recombinant protein has found widespread use as it allows rapid expansion of the producer strain without negative selective pressure from over-expression of a foreign protein and equally rapid production of large amounts of the protein over a period of usually

0.5–2 h after induction. A further element of an effective bacterial expression plasmid comprises a ribosomal binding site 5–9 nucleotides upstream of the translation initiation codon (ATG).

Finally, a frequent problem encountered in recombinant protein expression is the difference in codon usage between mammalian and bacterial cells. The nucleotide triplets preferentially encoding a particular amino acid of the mammalian product may be only rarely found in the bacterial genome, and the respective tRNA will only be present in the bacterium at low levels. Translation of the mammalian gene will quickly deplete the tRNA pool, resulting in aberrant polypeptide chains and limited yield. Special high-capacity expression strains of *E. coli* have been engineered to overcome this problem without modifications to the transgene sequence. For further particulars on this issue as well as the aspects of expression plasmid design and function, reference is made to [22].

24.3.3. Yeast Expression Systems

The baker's yeast *Saccharomyces cerevisiae* represents probably the currently best researched and understood eukaryotic organism. Most of its genes have been knocked out for functional studies, and hence a vast variety of mutant strains as well as tools for their manipulation are available. This in concordance with short generation times and a growth medium that is comparable in cost and complexity to bacterial media has made the yeast system a frequent choice for the evaluation of transmembrane carriers.

Using high-activity promoters (PMA1, PDR5), a yield of recombinant protein of up to 10% of the plasma protein content can be achieved. This is often sufficient to purify the protein for subsequent structural or functional studies. Bacterial expression systems clearly provide higher yields, but a protein expressed in *S. cerevisiae* is more likely to be folded correctly and to carry some of its post-translational modifications, although these are not fully identical with those in the parent cell type. If not folded correctly, however, the quality control of *Saccharomyces* will retain the protein within the endoplasmic reticulum and subsequently degrade it, making expression of larger amounts of the protein virtually impossible.

Functional characterisation of transport proteins in *S. cerevisiae* is simplified by the availability of a large number of mutant strains. Selection of the right host may reduce the background activity or possible interference from endogenous proteins with similar activity. Nevertheless, some caution should be used when extrapolating the quantitative and qualitative results of functional characteristics of one transport protein expressed in yeast to the same protein in another host. Particularly, differences in membrane lipid composition (e.g. ergosterol vs. cholesterol) have been demonstrated to influence substrate binding constants as well as substrate/inhibitor properties of selected molecules. For example, MDR1 expressed in *Schizosaccharomyces pombe* did not accept adriamycin (doxorubicin) as substrate.

Technically, cDNAs are cloned into plasmids carrying an antibiotic selection marker for propagation in bacteria, a nutritional selection marker for selection of transfected yeast as well as the respective origins of replication. After amplification in bacteria, the plasmids are transfected into the corresponding auxotrophic yeast strain using similar methods as for bacteria and stably

maintained in selection medium. Expression of the transport protein can be achieved either from strong constitutive or inducible promoters. An overview of suitable elements as well as potential host strains is provided in Ton and Rao [24].

24.3.4. *Xenopus Oocytes*

The South African clawed frog, *Xenopus laevis*, has been previously used in laboratory medicine for many years as diagnostic tool for pregnancy tests, as a laboratory animal for muscle and renal physiology, developmental biology and more recently for the use of its oocytes. *Xenopus laevis* is easily kept and bred in captivity and therefore, available from commercial suppliers at low costs. The oocytes are easily prepared, as described above and easy to handle with their large diameter of 1.1–1.3 mm. As animals are living in ponds or dead river arms, the oocytes are adapted to unfavourable environments. They are also fully equipped with all required organelles, nutrients, enzymes and substrates and hence provide autonomous protein manufacturing machinery. As there is no need to resorb nutrients from the growth medium, the endogenous activity of transmembrane transporters is probably low—a property which makes them very attractive for evaluation of heterologously expressed carriers. The oocyte expression system is therefore used not only for expression cloning of cDNAs but also for characterisation of the expressed protein or its mutants regarding transport activity (import and export), electrophysiology or protein localisation and modification (glycosylation).

However, some limitations of the system must be taken into consideration. Injection of foreign genetic material can result in induction of endogenous proteins or the heterologously expressed polypeptide may interact with endogenous proteins. In this case, not the function of the foreign protein, but instead an unusual endogenous process may be mistakenly investigated. Furthermore, altered protein behaviour may result from differences in membrane composition and the lower temperature. Frogs are poikilothermic and oocyte culture, as well as expression experiments are performed at room temperature or below. This will affect above all the kinetic transport parameters such as K_m/K_i , k_{on} and k_{off} . In fact, differences in substrate specificities and affinities have been reported when cloned drug carriers were characterised in several different expression systems. The OATP8, for example, was reported to transport different bile salts when expressed in oocytes than when expressed in the Madin-Darby canine kidney (MDCK) cells [13, 11]. Another disadvantage of *Xenopus laevis* is the seasonal variability of the oocytes, as reported by some groups. From spring to autumn, the quality of the oocytes is sometimes reduced or healthy frogs may have low amounts of stage-VI oocytes which are preferred for heterologous expression. In some cases multiple surgeries of the same animal may induce the production of more high-quality oocytes [25].

Transport studies for characterisation of import or export proteins are easily performed according to the protocol provided below. In addition, mechanistic properties of electrogenic carriers (transport of charged substrates or co-transport of ions) can be characterised using standard electrophysiological techniques. Finally, trans-accelerating and trans-inhibition studies can also be performed. Such detailed studies are mostly done during later stages of the characterisation of a cloned transporter, while inhibition studies are already

highly relevant earlier to specify that the transport activity is specific for the cloned carrier and not due to background. In this context, it should be noted that an inhibitor of the transport is not automatically a substrate of the carrier. Various examples in the literature show that a direct transport assay with the labelled substrate is necessary for unequivocal identification of a carrier substrate.

24.3.5. Insect Cell Lines

Expression in insect cell lines has become popular when membrane vesicles containing high amounts of the carrier protein are to be prepared. Such vesicles are particularly suitable for mechanistic studies of, for example, the driving forces of transport, as electrochemical gradients can be easily controlled. Typically, the infection of insect cell cultures with recombinant baculoviruses encoding the transporter gene under control of a strong viral promoter yields 3–10 times the amounts which are obtained after stable transfection of mammalian cells. Common host cell lines, such as Sf9, Sf21 (*Spodoptera frugiperda*) and engineered HighFive are maintained in media and using equipment similar, but not identical to those used for mammalian cell culture. A convenient system for generation of recombinant baculoviruses (bac-to-bac) requires sub-cloning of the transporter gene into a transfer vector, which is then transformed into bacteria carrying a replicating circular baculovirus genome. Transfer of the gene of interest into the virus genome is realised by the site-specific transposition. Bacterial clones carrying the desired recombinants can be selected, and transfection of the isolated virus genome into insect cell cultures generates an infectious cell culture supernatant. This, in turn, can be used for insect cell infection at a high m.o.i. (multiplicity of infection) to produce the protein which is mostly folded correctly and can carry post-translational modifications, often similar to those in the parent cell or tissue. Although insect cells do also present a background of transport activities, these do usually interfere much less with functional evaluation than in mammalian cells as the relative expression level of the transgene is considerably higher. Nevertheless, substrate spectra and kinetic characteristics can be different between transporters expressed in insect and mammalian cells, probably as a result of major difference in membrane lipid composition (low cholesterol, no phosphatidylserine and sphingolipids), culture temperature and co-factor availability. For example, the activity of various well-known transporters including P-glycoprotein, the glutamic acid transporter or Na^+/K^+ -ATPase are stimulated by cholesterol in the membrane [17].

24.3.6. Mammalian Cell Lines

With the widespread availability of cell culture facilities, the reduced costs of media and reagents and above all, the commercialisation of a variety of transfection and expression kits, mammalian cells have now become probably the standard for functional studies of transmembrane transporters. Unsurpassed predictivity of the mammalian models may outweigh the higher costs and the lengthiness of the process, compared with bacterial cultures or *Xenopus oocytes*. Nevertheless, structural studies may require larger amounts than those easily produced in mammalian cells and the appeal of insect cell cultures for

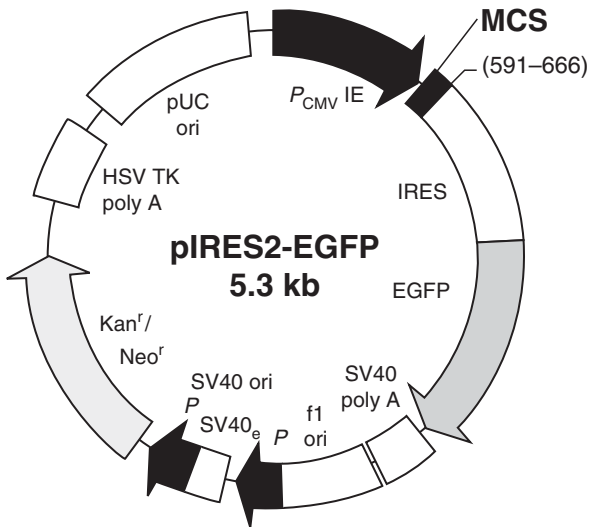


Figure 24.2 Typical dual expression plasmid with internal ribosome entry site for heterologous expression of proteins in mammalian cell cultures. Elements for prokaryotic replication and selection: pUC ori, Kan^r; elements for eukaryotic replication and selection: SV40 ori, Neo^r; promoter for translation of transgene mRNA and polyadenylation signal for RNA stability: P_{CMV}-IE, SV40 polyA, HSV TK polyA; site for insertion cloning of the transgene: MCS; gene encoding fluorescent expression marker and internal ribosome entry site for translation of the corresponding mRNA: EGFP, IRES.

the production of membrane vesicles carrying the functional transporter protein of interest has been discussed above.

24.3.6.1. Expression Vectors

A variety of commercial vectors has simplified the attachment of affinity tags to the protein that allow its detection when no specific antiserum is available (Flag, HA, GFP, etc.). This is particularly helpful, as antibiotic selection is usually not sufficient for generation of stably transfected mammalian cell clones. However, presence or activity of the carrier always needs to be assessed to exclude lines with absent or low expression (see also Protocol 4 in the Appendix). Dual expression vectors carrying an internal ribosome entry site (pIRES) couple the transcription of the transgene to that of a marker, usually GFP, and provide an elegant alternative solution of the problem. Irrespective of these helpful features, a suitable mammalian expression plasmid will always contain some basic features: prokaryotic origin of replication and resistance marker (ampicillin, kanamycin or chloramphenicol) (see Figure 24.2).

24.3.6.2. Non-Polarised and Polarised Cell Lines

Of the hundreds of available mammalian cell lines, only a comprehensive list is frequently used for the functional heterologous expression of transmembrane transport proteins. A further subdivision can be made as follows: (1) non-polarising cells that are easier to maintain and to manipulate with low background activity of xenobiotic transporters and (2) more sophisticated, polarising cells permitting studies of subcellular sorting that often express tissue-specific co-factors and substantial background of other transport activities. The latter ones are generally more complicated in maintenance and manipulation, but offer the possibility to study the contribution of the transfected carrier protein to transepithelial transport when grown on Transwell[®] filter systems. Non-polarising cell lines are often, but not always, of mesenchymal instead of epithelial origin. This is possibly the reason why they generally proliferate faster, are easier to transfect and have lower transporter background, but may be unable to correctly glycosylate the individual protein. However, as correct glycosylation is usually irrelevant for carrier protein function, non-polarising cells remain the first choice for studies of properties, such as

Table 24.2 Mammalian Cell Lines Frequently Used for Expression and Study of Carrier Proteins.

Cell line	Origin
Non-polarising	
BHK	(Baby) Syrian hamster kidney, fibroblast-like
CHO	Chinese hamster ovary, fibroblast-like
Cos-1, Cos-7	African green monkey kidney, fibroblast-like
HEK-293	Human embryonic kidney, epithelial
Polarising	
Caco-2	Human colon adenocarcinoma, epithelial, enterocyte-like
LLC-PK1	Porcine kidney, epithelial, proximal tubule cell-like
MDCK	Canine kidney, epithelial, distal tubule cell-like

substrate and inhibitor spectrum, affinity constants (K_m , K_i) and transport capacity (V_{max}), or simple structural details including MW and membrane topology (orientation of the transmembrane domains). Nevertheless, it remains highly recommendable to test the background activity of a selected cell line for transport of the anticipated substrates before investing time and money into the generation of stable transfectants. An overview of popular mammalian cell lines and their origin can be found in Table 24.2.

Most polarised immortal cell lines which are often used for expression of foreign proteins endogenously express a number of import and export carriers [3]. For example, mRNA of the canine homologue of human OATP-A and OATP-C has been demonstrated in MDCK cells, but not in MDCKII and LLC-PK1 cells. Both MDCK cell lines show MDR1 and MRP1 activity, and MDCKII cells express MRP2 in contrast to MDCK cells. Similar results were obtained in a study of the expression profiles of porcine kidney cells. Such endogenous activity may considerably complicate the determination of substrate/inhibitor profiles, particularly, if the substrate spectrum is overlapping. However, it may be desired when the contribution of a carrier to transepithelial flux is investigated as such involves not only import but also export. Conversely, inhibition of an export carrier may require access of the potential inhibitor to the cytoplasmic face. This can be facilitated by an endogenous background of transport activity. Ideally, however, this interplay of import and export should not be left to chance.

24.3.6.3. Expression of Multiple Transport Proteins

Double- and quadruple-transfected cells, expressing typically import as well as export carriers have recently been introduced [2,12] to demonstrate their interplay in the vectorial transport of drugs. With such systems, it could be demonstrated that the biliary excretion of enalapril, for example, is achieved by uptake via OATP1B1 and OATP1B3 at the basolateral membrane, and extrusion into the bile by MRP2. A quadruple-transfected cell line expressing the major hepatic OATP family members 1B1, 1B3 and 2B1 along with MRPs was claimed to be a suitable model to identify substrates and inhibitors that undergo this typical liver transport pathway. Isolated and mixed expression of the transporters allows elucidating their individual contribution and an estimation of the overall flux. Technically, the generation of double transfectants is simply achieved by subsequent transfection of a suitable cell line with one cDNA cloned into an expression vector containing a selection marker, isolation of a stable clone and transfection with the second cDNA cloned into another

vector, carrying a non-interfering selection marker (compare also Protocol 4 in the Appendix). The generation of more than quadruple transfectants will, if ever desired, require a new strategy, as the number of available selection markers is limited. To obtain the model cited above, resistance genes for G418, hygromycin, zeocin and blasticidin were used simultaneously.

24.4. Concluding Remarks

For structural and functional characterisation, high levels of expression of drug transport proteins are best achieved from cloned cDNA which represents reverse-transcribed mRNA lacking undesired genomic structures, such as introns and many upstream regulatory elements. Depending on the amount of sequence information available, this cDNA can be obtained by more laborious expression and complementation cloning or, more efficiently, by homology cloning and direct (full-length) RT-PCR amplification. Considerable attention must be paid to the selection of a suitable combination of expression vector and host, as this choice will determine, for example, yield, extent of post-translational protein modification and protein functionality. This choice can only be made in a case-by-case manner and often, expression in more than one system is necessary for cross-validation or to address different aspects of one particular transport protein.

References

1. Chenchik, A., Moqadam, F. and Siebert, P. A new method for full-length cDNA cloning by PCR. In: *A Laboratory Guide to RNA: Isolation, Analysis and Synthesis*. P.A. Krieg, (ed.) Wiley Liss, Inc. pp. 273–321, 1996.
2. Cui, Y., König, J. and Keppler, D. Vectorial transport by double-transfected cells expressing the human uptake transporter SLC21A8 and the apical export pump ABCC2. *Mol Pharmacol* 60: 934–943, 2001.
3. Goh, L.-B., Spears, K.J., Yao, D., Ayrton, A., Morgan, P., Wolf, D.R. and Friedberg, T. Endogenous drug transporters in in vitro and in vivo models for the prediction of drug disposition in man. *Biochem Pharmacol* 64: 1569–1578, 2002.
4. Gros, P., Croop, J., Roninson, I., Varshavsky, A. and Housman, D. Isolation and characterization of DNA sequences amplified in multidrug-resistant hamster cells. *Proc Natl Acad Sci USA* 83: 337–341, 1986.
5. Gründemann, D., Gorboulev, V., Gambaryan, S., Veyhl, M. and Koepsell, H. Drug excretion mediated by a new prototype of polyspecific transporter. *Nature* 372: 549–552, 1994.
6. Gurdon, J.B., Lane, C.D., Woodland, H.R. and Marbaix, G. Use of frog eggs and oocytes for the study of messenger RNA and its translation in living cells. *Nature* 233: 177–182, 1971.
7. Hediger, M.A., Romero, M.F., Peng, J.B., Rolfs, A., Takanaga, H. and Bruford, E.A. The ABCs of solute carriers: Physiological, pathological and therapeutic implications of human membrane transport proteins. Introduction. *Pflügers Arch* 447: 465–468, 2004.
8. Hediger, M.A., Coady, M., Ikeda, T.S. and Wright, E.M. Expression cloning and cDNA sequencing of the Na⁺/glucose co-transporter. *Nature* 330: 379–381, 1987.
9. Jacquemin, E., Hagenbuch, B., Stieger, B., Wolkoff, A.W. and Meier, P.J. Expression cloning of a rat liver Na⁽⁺⁾-independent organic anion transporter. *Proc Natl Acad Sci USA* 91: 133–137, 1994.

10. Klammt, C., Schwarz, D., Fendler, K., Haase, W., Dötsch, V. and Bernhard, F. Evaluation of detergents for the soluble expression of α -helical and β -barrel-type integral membrane proteins by a preparative scale individual cell-free expression system. *FEBS J* 272: 6024–6038, 2005.
11. König, J., Cui, Y., Nies, A. and Keppler, D. Localization and genomic organization of a new hepatocellular organic anion transporting polypeptide. *J Biol Chem* 275: 23161–23168, 2000.
12. Kopplow, K., Letschert, K., König, J., Walter, B. and Keppler, D. Human hepatobiliary transport of organic anions analyzed by quadruple-transfected cells. *Mol Pharmacol* 68: 1031–1038, 2005.
13. Kullak-Ublick, G.A., Ismail, M.G., Stieger, B., Landmann, L., Huber, R., Pizzagalli, F., Fattinger, K., Meier, P.J. and Hagenbuch, B. Organic anion-transporting polypeptide B (OATP-B) and its functional comparison with three other OATPs of human liver. *Gastroenterologia* 120: 525–533, 2001.
14. Kuruma, Y., Nishiyama, K., Shimizu, Y., Müller, M. and Ueda, T. Development of a minimal cell-free translation system for the synthesis of presecretory and integral membrane proteins. *Biotechnol Prog* 21: 1243–1251, 2005.
15. Mager, S., Cao, Y. and Lester, H.A. Measurement of transient currents from neurotransmitter transporters expressed in *Xenopus* oocytes In: *Methods in Enzymology*. 296, S.G. Amara, (ed.) p.551, Academic Press London, 1998.
16. Mizuno, N., Niwa, T., Yotsumoto, Y. and Sugiyama, Y. Impact of drug transporter studies on drug discovery and development. *Pharmacol Rev* 55: 425–461, 2003.
17. Opekarova, M. and Tanner, W. Specific lipid requirements of membrane proteins—a putative bottleneck in heterologous expression. *Biochim Biophys Acta* 1610: 11–22, 2003.
18. Pritchard, J.B. and Miller, D.S. Expression systems for cloned xenobiotic transporters. *Toxicol Appl Pharmacol* 204: 256–262, 2005.
19. Schaefer, B.C. Revolutions in rapid amplification of cDNA ends: New strategies for polymerase chain reaction cloning of full-length cDNA ends. *Anal Biochem* 227: 255–273, 1995.
20. Sekine, T., Watanabe, N., Hosoyamada, M., Kanai, N. and Endou, H. Expression cloning and characterization of a novel multispecific organic anion transporter. *J Biol Chem* 272: 18526–18529, 1997.
21. Spirin, A.S. High-throughput cell-free systems for synthesis of functionally active proteins. *Trends Biotechnol* 22: 538–545, 2004.
22. Sorensen, H.P. and Mortensen, K.K. Advanced genetic strategies for recombinant protein expression in *Escherichia coli*. *J Biotechnol* 115: 113–128, 2005.
23. Sweet, D.H., Wolff, N.A. and Pritchard, J.B. Expression cloning and characterization of ROAT1. *J Biol Chem* 272: 30088–30095, 1997.
24. Ton, V.K. and Rao, R. Functional expression of heterologous proteins in yeast: Insights into Ca^{2+} signalling and Ca^{2+} -transporting ATPases. *Am J Physiol* 287: C580–C589, 2004.
25. Wagner, C.A., Friedrich, B., Setiawan, I., Lang, F. and Broer, S. The use of *Xenopus laevis* oocytes for the functional characterization of heterologously expressed membrane proteins. *Cell Physiol Biochem* 10: 1–12, 2000.
26. Williams, F.M.R., Murray, R.C., Underhill, T.M. and Flintoff, W.F. Isolation of a hamster cDNA clone coding for a function involved in methotrexate uptake. *J Biol Chem* 269: 5810–5816, 1994.
27. Wolff, N.A., Werner, A., Burkhardt, S. and Burkhardt, G. Expression cloning and characterization of a renal organic anion transporter from winter flounder. *FEBS Lett* 417: 287–291, 1997.

25

The Pharmacology of Caveolae

Stuart A. Ross, William V. Everson, and Eric J. Smart

Abstract Based on work in the last 15 years, caveolae are now recognized as rather complex and dynamic plasma membrane domains with important roles in cellular uptake of molecules, signal transduction, lipid homeostasis, and tumorigenesis. Functionally, caveolae orchestrate very specific events in distinct cell types, thereby making these organelles one of the most interesting compartments in cells. In this chapter, we will discuss the salient features of these active cellular domains. We begin with a general introduction to the biochemistry and cell biology of caveolae, describe some of the myriad signaling events that initiate in caveolae (or traffic through caveolae) and how they can go awry in cancer, describe how caveolar proteins can be exploited for novel drug discovery, and finally provide commentary over a growing body of evidence that suggests how molecules are presented to caveolae makes a difference in the pharmacological effects that ensue.

Keywords: Automotility factor; Caveolae; Caveolin; CD36; Cholera toxin; Cholesterol; Drug targeting; Endocytosis; Estradiol; Folate conjugates; Folate receptor; Lipid raft; Macrophages; Multidrug resistance; Neutrophils; Potocytosis; Vesicular drug trafficking

Abbreviations

AMF	Automotility factor
AMF-R	Automotility factor receptor
AMPK	AMP-kinase
CD36	Cluster of differentiation 36, a receptor for high-density lipoprotein
CD59	Cluster of differentiation 59, a complement regulatory protein
CT-B	Cholera toxin B
E ₂	Estradiol
EGF	Epidermal growth factor receptor
EM	Electron microscopy
eNOS	Endothelial nitric oxide synthase
ER	Endoplasmic reticulum
GIC	Golgi intermediate compartment
GM1	Ganglioside M1

GPI	Glycosyl phosphatidylinositol
HDL	High-density lipoprotein
MDCK	Manine-Darby Canine Kidney cell line
MDR	Multidrug resistance
PDGFR	Platelet derived growth factor receptor
PEG	Polyethylene glycol
P-gp	P-glycoprotein
SDS-PAGE	SDS (lauryl-sulfate)-PAGE (polyacrylamide gel electrophoresis)
SER	Smooth endoplasmic reticulum
SR-B1	Scavenger receptor B1, a receptor for HDL

25.1. Introduction

Caveolae (Latin for “small caves”), first identified in the 1950s by Palade [1] and Yamada [2], are small, 50–100 nm Erlenmeyer flask-shaped, detachable plasma membrane invaginations enriched in cholesterol and sphingolipids (see Figure 25.1). For several decades following their initial discovery, these organelles remained largely a cell biological enigma, likely due to the absence of a bona fide marker protein. Interest in caveolae intensified in the early 1990s with the cloning of caveolin (formerly known as VIP21) from these organelles [3–6]. Indeed 4,300-plus citations in the caveolae field emanate from the description of caveolin as the coat/marker protein of caveolae. Research into caveolae has exploded with the findings that they function as dynamic centers of small molecule transport including non-clathrin endocytic and transcytotic movement of macromolecules and vesicular internalization of small molecules via a process termed potocytosis. Furthermore, caveolae coordinate a myriad of signal transduction events.

The distinguishing structural and functional protein for caveolae is caveolin. Caveolin proteins display properties that are likely involved in the distinguishing morphology of caveolae. Caveolins have a high affinity for both cholesterol and sphingolipids coupled with 3 carboxy-terminal palmitoylated cysteine residues. Three isoforms of caveolin exist and show distinct tissue distribution. Likely because it was discovered first and is perhaps most abundant, caveolin-1 has garnered the lion’s share of research attention.

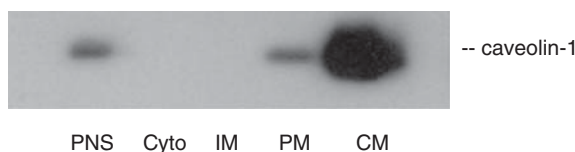


Figure 25.1 Enrichment of caveolin in the caveolae fraction by a two-stage non-detergent subcellular fractionation method. Caveolae were isolated by the two-stage method [96]. Ten micrograms of protein was loaded into each lane from the post-nuclear supernatant (PNS), cytosol (Cyto), intracellular membrane (IM), plasma membrane (PM), and caveola membrane (CM) fractions. After resolution by SDS (lauryl-sulfate)-PAGE (polyacrylamide gel electrophoresis), proteins were transferred to membrane and subjected to western immunoblotting using polyclonal antibody against caveolin-1 (BD Biosciences, San Jose, CA). Bands were visualized using Pierce SuperSignal chemiluminescence reagents (Pierce, Rockford, IL). The intensity of the band reflects the enrichment of caveolin in the highly purified caveolae membrane fraction.

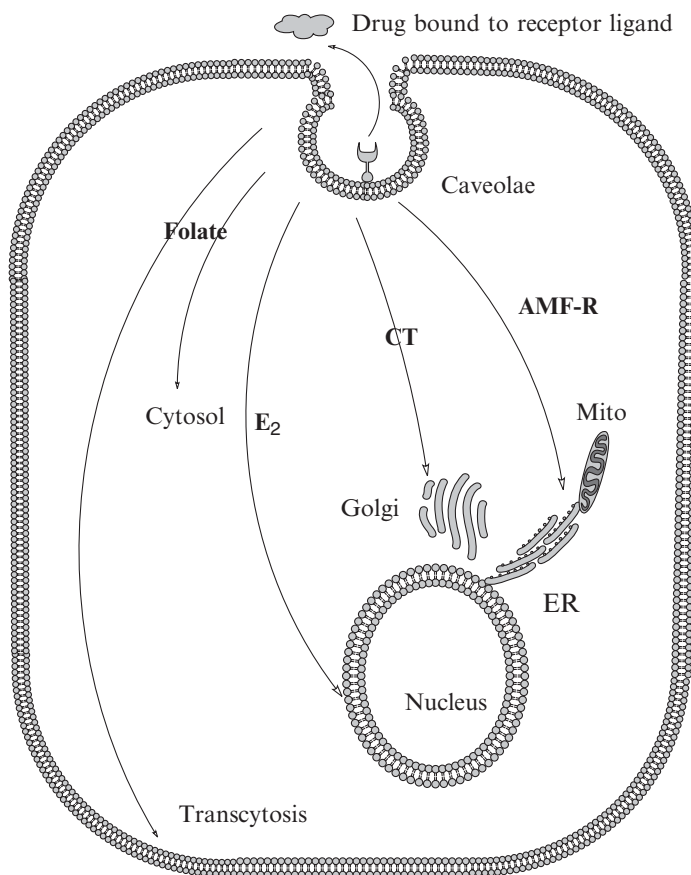
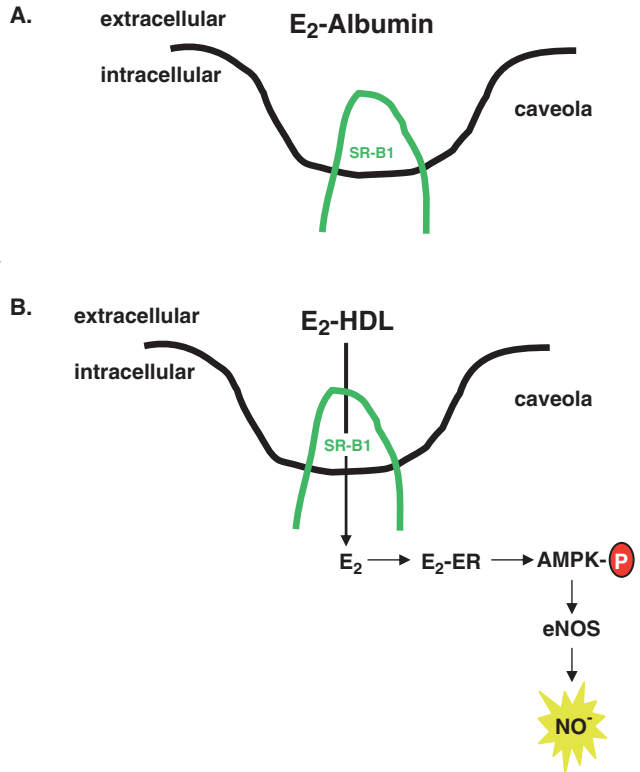


Figure 25.2 Drug delivery by caveolae-mediated endocytosis to distinct intracellular sites. Caveolae provide potential targeting of drugs to distinct intracellular sites as discussed in the text. Drugs bound to ligands for different receptors that are localized to caveolae link to pathways connecting distinct intracellular sites. For example, folate conjugates are linked to delivery of drugs to the cytosol (and to transcytosis); automotility factor bound to its receptor (AMFR) links to the endoplasmic reticulum (ER) at a region adjacent to mitochondria (mito); cholera toxin B chain (CT-B) bound to the ganglioside GM1 in caveolae endocytoses to the Golgi; high-density lipoprotein (HDL) bound to scavenger receptors links to delivery to caveolae of estradiol (E₂); and vesicular and non-vesicular pathways connecting caveolae to the ER and nucleus.

The advent of caveolin-specific reagents made it possible to identify both flask-shaped and flattened morphologies of caveolin-containing caveolar plasma membrane sections, physically isolate the organelles, and to study their components and functions [7]. The terms caveolae and lipid rafts have been used somewhat interchangeably in the literature. However, the origins of the two terms reflect a major distinction between them. Lipid rafts were identified as buoyant fractions of membranes resistant to Triton X-100 extraction at low temperatures, which have been shown to originate from multiple membrane sites within cells and addition of components due to detergent mixing [8, 9]. Caveolae, on the contrary, were identified morphologically as domains within the plasma membrane (Figure 25.2). A method for isolation of caveolae was developed based on a two-stage fractionation procedure in which the first

Figure 25.3 Presentation of estradiol to endothelial cells affects signaling. (A) Physiological levels of estradiol (E_2) complexed with albumin do not elicit the production of nitric oxide when presented to cultured endothelial cells although E_2 -albumin binds to caveolar SR-B1. (B) Physiological levels of estradiol complexed with HDL elicit the production of nitric oxide by activating AMPK and then eNOS. Although it is depicted in this figure that AMPK is activated by binding of estradiol to the estrogen receptor, this mechanism has not been experimentally demonstrated. Other mechanisms of E_2 -HDL activation of AMPK and eNOS are thus possible (See also color insert).



step was isolation of the plasma membrane, from which caveolae were then isolated, initially by fragmentation of the plasma membrane by using Triton X-100 at 4°C followed by isolation of the buoyant membranes. Subsequently, a cleaner method of fragmentation was developed that avoided detergent-induced mixing, by use of sonication to fragment the isolated plasma membranes to yield a highly purified fraction of caveolae. A representative western blot of caveolin from several of the fractions obtained during a typical caveolae preparation is shown in Figure 25.3. The fractions were matched for protein content, thus the intensity of the caveolin band shows the enrichment of caveolin-1 in the highly purified caveolae membrane (CM) fraction. Lipid rafts differ from caveolae in that they do not originate solely from the plasma membrane, may not contain caveolin, and may contain both lipid and protein components that originate from other sources and associate through detergent mixing. Thus, for the purpose of this chapter we define caveolae as caveolin-containing regions of the plasma membrane. Indeed in cells lacking caveolin, no flask-shaped, morphologically identifiable caveolae exist. Furthermore, as discussed below, the presence of caveolin likely affects the function of the entire caveolae population and the cell surface.

Caveolae are particularly abundant, accounting for 30–70% of the plasma membrane in differentiated epithelial (e.g., pneumocytes) and endothelial cells, fibroblasts, smooth muscle cells, and adipocytes. Indeed there is a general trend for caveolin induction in differentiated cell types. Adipose tissue is replete with caveolae, and caveolin mRNA and protein are strongly induced during differentiation of 3T3-L1 preadipocytes (fibroblasts) to adipocytes [10]. While

initial reports showed little or no caveolin in neuronal cells, recent data demonstrated an upregulation of both caveolin-1 and caveolin-2 in both differentiating pheochromocytoma (PC-12) cells and neurons of the dorsal root ganglion [11]. Similarly, caveolin-1 expression is high in differentiated Schwann cells and diminishes when the cells revert to a non-myelinated phenotype [12]. Also, caveolin-1 expression increases when lung cells acquire an alveolar epithelial type I phenotype. Thus, a general phenomenon of caveolin expression is increased expression during the transition to differentiated cellular phenotypes.

25.2. Action at Caveolae

Shortly after the cloning of caveolin, subcellular fractionation studies revealed that a large number of signaling molecules and receptors are clustered in caveolae [13, 14]. In these early studies, proteins associated with signaling, including members of the small guanosine triphosphate (GTP) binding protein family, tyrosine kinases including several members of the Src family, growth factor receptors, oncogenes, and other signal transducers such as protein kinase C (PKC) α were all localized to caveolae. An increasing number of signaling molecules, receptors, and signal transducers have been reported to be localized to caveolae in the last decade (some more comprehensive listings are found in reviews by Anderson [7] and Smart et al. [15]). In addition, enzymes involved in second messenger activation have been localized to caveolae and are regulated in complexes within caveolae, including endothelial nitric oxide synthase (eNOS) [16–22], nicotinamide adenine dinucleotide phosphate (NADPH) oxidases [23], and enzymes associated with prostaglandin production [24, 25].

25.3. Caveolae and Vesicular Drug Transport

25.3.1. Exploiting Caveolae for Drug Delivery

Exploitation of caveolae may provide a way to specifically deliver drugs, gene therapy vectors, and imaging reagents to targeted tissues. Given their relative abundance, caveolae may also provide a means to cross the relatively impermeant endothelial cell barrier. This could potentially increase therapeutic efficacy via rapid delivery to the intended action locale of most therapies, the cells deep inside tissues. Burgeoning evidence indicates that various molecules gain access to cells via docking to receptor sites on the external side of caveolae and enter cells after docking and prior to caveolae vesicularization/internalization. Internalization is initiated upon ligand binding as exemplified by caveolar uptake of folate, cholesterol, sex hormones, and specific lipid components of serum lipoproteins. A distinguishing feature of caveolae internalization is that caveolae can transit intracellularly through pathways that are distinct from the lysosomal compartment that is the destination in classical clathrin-mediated endocytosis. Importantly, and of potential benefit for drug development, caveolae internalization can proceed without a fusion step to lysosomes, thereby circumventing an acidic compartment which may attenuate the efficacy of a therapeutic small molecule or protein. Since caveolae are

restricted in tissue distribution (e.g., pneumocytes, adipocytes, and fibroblasts) and to certain therapeutically significant cells (e.g., endothelial cells), targeting of caveolae for pharmaceutical interventions may add a degree of selectivity to the molecules. Pharmaceuticals in the form of small molecules, proteins, or antibodies may selectively gain access to cells if appropriately positioned on a protein, peptide, or small molecule that adheres to a caveolar protein. Therefore, a thorough comprehension of caveolar transport may assist in the rational design of more selective drug carriers and more efficacious drugs.

25.3.2. Caveolae-Linked Endocytosis and Non-Caveolae, Clathrin-Independent Endocytosis Offer Delivery of Drugs to Novel Intracellular Targets

When interest in caveolae flared in the 1990s, a major question of investigation was whether the flask-shaped caveolar structure could vesiculate and internalize in a fashion akin to clathrin-mediated endocytosis. Several early studies showed that caveolin can be rapidly internalized, within as little as 30 sec, after addition of hormone [26] or by other manipulations such as addition of cholesterol oxidase [27]. Caveolin-1 disappeared from the surface and was found localized in clusters of endocytic vesicles near the microtubule organizing center of either A431 or Manine-Darby Canine Kidney cell line (MDCK) cells, by immunogold electron microscopy (EM) labeling of caveolin-1 in response to clustering of alkaline phosphatase in caveolae (A431 cells), okadaic acid treatment, or addition of hypertonic media [28]. The use of gold-labeled cholera toxin B subunits, which specifically label ganglioside M1 (GM1) in caveolae, revealed caveolae and a network of tubulovesicular structures which penetrate extensively into A431 or MDCK cells. The morphology of these tubulovesicular structures is strikingly similar to a set of very dynamic structures in neutrophils and macrophages which have been characterized by use of cytochemical staining for alkaline phosphatase and superoxide production [29–31]. Alkaline phosphatase was initially identified within tubular vesicles, which upon activation rapidly (1 min) fused into clusters of tubulovesicular structures in the center of cells. These clusters then extend and connect to the surface, allowing alkaline phosphatase to gather on the surface in a pattern similar to the clustering of the 5-methyltetrahydrofolate receptor, another glycosyl phosphatidylinositol (GPI)-anchored protein associated with cholesterol domains [32]. The complex forms a network that remains connected to the surface. Localized clusters of intracellular vesicles appear during the following 15 min [29]. Similarly, cytochemical staining for superoxide production revealed activity within this same network, though the activity first appeared within intracellular tubular structures, then migrated to either regions of the plasma membrane where vesicles fuse or the larger aggregates of tubules and vesicles that elongate and enlarge [30, 31]. Studies on caveolae-mediated transport in the endothelium have shown that caveolae are linked to transcytosis of bulk macromolecules such as albumin, specific transcytosis of peptide hormones such as insulin, and endocytosis of scavenged macromolecules such as oxidized albumin which are delivered to the lysosome for degradation [33]. These elegant, early studies on non-clathrin vesicular transport, using cytochemical, immunogold, and EM methods reveal a very dynamic, complex set of

intracellular vesicles and tubules involved in both activation of cells and bulk transport processes.

In addition to the localization of specific receptors within caveolae/lipid rafts that can be exploited for therapeutic drug delivery to specific cell types, caveolae and lipid rafts provide endocytic pathways that could be manipulated to target drug delivery to novel intracellular sites. Early studies on caveolae endocytosis showed that caveolin-1 rapidly translocated in bulk from the surface to a site close to the nucleus identified as the ER-GIC, and then subsequently trafficked to the Golgi and ER [27]. The GPI-anchored folate receptor accumulates in the endosomal compartment that is marked by transferrin [34] and then proceeds through acidifying endosomes, allowing release of the conjugated drug or compound [35]. Automotility factor receptor (AMFR), a receptor that is highly expressed in tumor cells, initially was found to endocytose to a specific subdomain of the smooth endoplasmic reticulum (SER) which is a region of the ER that is in close apposition to mitochondria [36] without acidification of vesicles. A follow-up study showed that in contrast to AMFR, cholera toxin (which binds to GM1, a lipid component of caveolae) translocated from caveolae to the Golgi [37]. Cholera toxin uptake and translocation to the site where it can be activated is dependent on caveolae structure [38] and the localization of GM1 to caveolae [39], although cholera toxin can be taken up by other pathways [40, 41]. Thus, from caveolae, automotility factor (AMF) or cholera toxin can be used to deliver agents to a region of the ER in close association to mitochondria, or to the Golgi, respectively. Similarly, in lipid rafts, different GPI-anchored receptors have been shown to traffic to distinct sites. In contrast to folate receptors which are endocytosed to the transferrin-positive compartment, CD59 translocates directly to the Golgi [34]. These intriguing studies have revealed the presence of a novel set of non-clathrin trafficking pathways which are still being characterized. A recent review of the clathrin-independent pathways has summarized the current state of characterization and identified at least four distinct, clathrin-independent uptake pathways in cells and some of the characteristics that are unique to each pathway [41]. As these non-clathrin pathways become more rigorously characterized, they too, like caveolae, offer the potential of selective targeting of distinct cells, tissues, or intracellular organelles for therapeutic drug delivery.

25.4. Caveolae and Cancer

Carcinogenesis involves a complex series of genetic and biochemical events that enable transformed cells to proliferate, metastasize, migrate to secondary sites, and, sometimes, acquire resistance to chemotherapy. In Sect. 25.4.1, we will discuss how caveolin-1 expression correlates with cancerous growth, a potential mechanism of chemotherapy drug resistance, and how caveolae may be particularly exploited for cancer therapeutic strategies.

25.4.1. Caveolin Expression

Several lines of experimental evidence provide *prima facie* evidence for a role of caveolin in oncogenesis. Consistent with a role in cancer, the caveolin-1 gene is localized to a putative tumor suppressor locus on chromosome 7 (7q31.11 D7S522) that is known to be missing in some types of cancers [42,

43]. Caveolin-1 was initially identified as a substrate of the Src kinase oncogene in v-Src Rous sarcoma transformed cells [44]. A relatively large list of growth factor receptors appear to be regulated by caveolin. Caveolin contains ~20 amino acid stretch called the scaffolding domain that has been shown to interact with a large number of receptor tyrosine kinases and dampen signaling [45]. Altered interactions of this domain with various caveolin-interacting proteins may lead to aberrant signaling and the development of cancer.

In contrast to the general phenomenon of increased caveolin expression in differentiated cell phenotypes, many oncogenically transformed cells exhibit decreased caveolin-1 expression. For example, caveolin-1 expression in human mammary carcinoma cells was shown to be strongly decreased relative to controls [46]. Consistent with this finding, caveolin-1 mRNA and protein levels are decreased or not detectable in many oncogenically transformed cells [47–49]. Similarly, antisense-mediated inhibition of caveolin-1 expression in NIH3T3 fibroblasts was sufficient to induce oncogenic transformation [50]. Strikingly, caveolin expression has been demonstrated to track with both oncogenic transformation and its reversal. Reintroduction of caveolin-1 into the metastatic breast cancer line 4T1.2 cells was sufficient to reduce primary tumor growth when the cells were injected into the mammary gland [51]. These data are consistent with caveolin-1 being a tumor suppressor, whereby diminished levels elicit oncogenesis and normal expression levels keep oncogenic transformation in check.

However, as with many stories in science, caveolin expression and oncogenic transformation are a complex and controversial tale. Indeed, numerous other types of cancer cells display increased caveolin-1 expression. For example, caveolin-1 expression has been reported to be overexpressed in several cancers including prostate and breast [52], lung [53], and bladder [54], to name a few. What to make of the dizzying array of caveolin expression data in the context of cancer from a diagnostic or therapeutic standpoint at this time is unclear.

25.4.2. A Caveolar Mechanism of Multidrug Resistance

Multidrug resistance (MDR) is the name ascribed to the phenomenon whereby cancer cells and tumors develop resistance to chemotherapeutic agents. Conceptually, this can be viewed as a survival response whereby cancer cells endeavor to ward off cytotoxic compounds. Mechanistically, MDR is typically mediated by overexpression of P-glycoprotein (P-gp aka ABCB1) or other plasma membrane ATPases that export cytotoxic drugs used in chemotherapy, thereby reducing their efficacy.

In MDR cells, a significant fraction of P-gp is found associated with caveolin-rich membranes, and there is a substantial increase in the number of caveolae and caveolin-1 protein level. For example, both multidrug resistant human colon adenocarcinoma HT-29 cells and adriamycin-resistant breast adenocarcinoma MCF-7 cells display about a 12-fold increase in caveolin expression, which correlates with an approximate fivefold increase in morphologically identifiable caveolae [55]. In addition, these cells exhibit increased amounts of phospholipase D and lipids such as cholesterol, glucosylceramide, and sphingomyelin [56, 57]. Similarly, taxol-resistant A549 cells display both increased caveolin expression and caveolae numbers [58]. While these correlations track with MDR, they do not suggest a simple mechanism for the role of

caveolin in MDR. Perhaps caveolin interacts with P-gp to modulate function. Evidence for this is scant, although one report in rat astrocytes documented a physical association by co-immunoprecipitation of the two proteins using a caveolin-specific antibody [59]. The upregulation of caveolin may track with MDR by affecting cholesterol homeostasis, possibly by increased cholesterol efflux activity, which could facilitate drug transport to the plasma membrane and removal by P-gp.

As with caveolin expression in oncogenic cells and tissues, the Adriamycin studies described above cannot simply be extrapolated to a general, all-inclusive, one size fits all mechanism of MDR. Unlike the situation with MCF-7 cells whereby increased caveolin/caveolae promotes drug resistance, doxorubicin-resistant Hs578T cells, which contain low levels of caveolin-1 and relatively high levels of P-gp, become drug sensitive with the overexpression of caveolin-1 [60]. Overexpressed caveolin-1 appears to increase plasma membrane fluidity with a concomitant decrease in P-gp function. Here too a possible caveolin-1-P-gp interaction is also observed by co-immunoprecipitation. Thus in this example upregulation of caveolin-1 is not essential for the development of drug resistance, but instead confers drug sensitivity possibly through interaction and inhibition of P-gp.

So what emerges from this? At the present time, a simple explanation of the effect of alterations in caveolin expression in the context of both oncogenesis and MDR cannot be easily derived. It appears to be a case-by-case scenario. However, caveolar localization of P-gp and alterations in P-gp activity in response to changes in caveolae number and lipid structure are beginning to reveal a more complex model of growth signal perturbations that has parallels to a complex model of regulation of MDR. Indeed experiments that perturbed cell surface cholesterol either by depleting with cyclodextrin followed by approximate stoichiometric repletion or saturation showed the importance of caveolae structure in MDR function. Depletion of cholesterol elicited a redistribution of P-gp from caveolar membranes which manifested as increased intracellular retention of labeled verapamil. Stoichiometric or saturated repletion of cholesterol showed caveolar localization of P-gp and reduced or even enhanced verapamil efflux [61]. More careful investigations of caveolae structure, lipid composition, and function of caveolae-associated proteins such as P-gp will likely lead to new models that offers novel opportunities for development of therapeutic interventions.

25.4.3. A Gateway to Targeted Cancer Cell Ablation

Targeted cancer cell ablation without affecting healthy cells is the holy grail of cancer treatment. Efforts in this regard have focused on the clinical administration of tumor-specific immunotoxins. Mechanistically, these drugs work by targeting epitopes specifically expressed on cancer cells. In vitro studies reveal impressive specificity in killing cancer cells while sparing normal cells. Cultured cells typically form monolayers that symmetrically present themselves to therapeutics. While efficacious with cultured cells, clinically these approaches have been disappointing. Internal cells within solid tumors may simply be inaccessible to the therapeutic antibodies and/or shielded by relatively impervious endothelial cells.

The concept of exploiting caveolae (e.g., in endothelial cells) in the development of drugs that gain entry into cells through caveolae-specific portals is one

that holds promise particularly in the treatment of cancer. As most chemotherapeutic treatments are broadly cytotoxic, they amount to global thermonuclear destruction by analogy. Caveolae may represent sites for deployment of tactical nukes. It is quite feasible that pharmaceutical warheads could be delivered specifically to tumor sites through caveolae, leaving noncancerous cells functioning normally in their wake. This approach would perhaps have the added benefits of concentrating drugs at their desired locales and potentially reducing dosages. In the near future, this idea may be progress from science fiction to science fact.

One example of this approach is the development of a compound that specifically targets caveolae in lung endothelial cells. Lung endothelial caveolae were isolated and utilized to generate a monoclonal antibody called TX3.833 that specifically recognizes lung caveolae. This reagent was shown to selectively target caveolae and be transcytosed to alveolar tissue. Interestingly, the antibody was able to rapidly and specifically shuttle several drugs linked to the TX3.833 antibody to the lungs after intravenous injection [62].

Suramin, a urea derivative, was initially used to treat parasitic diseases such as African sleeping sickness (trypanosomiasis) and river blindness (oceriasis), but may have expanded utility in the treatment of cancer. Suramin has been shown to dose dependently inhibit angiogenesis in a chick chorioallantoic membrane assay [63], inhibit human microvascular endothelial cell growth *in vitro* [64], and may interfere in the interaction of many growth factors with their receptors [65] or with growth factor signaling via modulation of regulatory tyrosine phosphatases [66]. Interestingly, suramin appears to gain specific access to endothelial cells through caveolae [67]. Thus, suramin itself represents an example of a tactical nuke. Conceptually, one can envision utilizing the caveolae-specific nature of suramin, or dissecting the portion of the molecule that directs caveolae targeting as a molecular Trojan horse, to perhaps selectively ferry other anticancer agents to endothelial cells.

Ferrying of molecules into cells via entry through caveolae may represent a way to traffic specifically cytotoxic molecules to specific action sites. For example, elevating the intracellular level of the sphingolipid ceramide is known to exert antimitogenic and proapoptotic effects. While ceramide is cell-permeable and displays antiapoptotic properties *in vitro*, systemic *in vivo* use of ceramide is hampered by its hydrophobicity. Using a C6-ceramide formulation in pegylated liposomes was shown to elicit a sixfold reduction in solid phase tumors, when compared to unloaded liposomes in a mouse model of breast adenocarcinoma [68].

25.4.4. Caveolae, Folate Receptor, Receptor Clustering, and Potocytosis

Potocytosis of folate is one of the first functions attributed to caveolae after the cloning of caveolin-1 [69]. The uptake and internalization of folate involved binding to a receptor which is clustered in caveolae, allowing folate to be internalized [70, 71]. This pathway could be blocked by removal of cholesterol from these cell surface caveolae [72], by PKC activators [73], or a variety of inhibitors including several anti-inflammatory compounds [74]. Folate receptors are upregulated in several pathological conditions, including cancer [35, 75, 76]. In some cells and systems, folate receptors can be isolated in lipid rafts that are distinct from caveolae [8, 77–79], although it is clear that folate receptors are present in caveolae in other systems. In ovarian tumors and some

cell lines derived from ovarian tumors, the expression of caveolin-1 shows a reverse correlation to the cell surface expression of folate receptor. Expressing caveolin-1 in tumor cells which lack it caused a downregulation of the surface expression of folate receptor. This reciprocal change in the surface expression of folate receptor and caveolae in these ovarian derived cells is intriguing. It suggests either that caveolin expression alters folate receptor uptake and recycling or that some reciprocal relationship exists that regulates the net surface area of the plasma membrane that is taken up by caveolae versus non-caveolae lipid rafts marked by folate receptor [80].

25.4.5. Folate Conjugates and Therapeutics

Folate receptor, whether localized in caveolae or in lipid rafts, has been exploited as a possible target for drug delivery in several therapeutic applications. The expression of folate receptor is high in many tumors, including brain, breast, colon, lung, leukemia, ovary, prostate, and throat [81–88] and comparatively low in normal tissues. This observation may allow for the selective delivery of folate-containing drugs to cancerous tissues. Indeed folate conjugates have been developed that allow the folate receptor to be targeted for delivery of a wide range of agents to cells for use in imaging tumors and targeting tumors with therapeutic agents [35, 75, 89]. Even DNA particles have been delivered to tumor cells by packaging them with poly-L-lysine conjugated to folate [90] or within a polyethylene glycol (PEG)-folate coat [91]. Some folate conjugates are progressing from bench to bedside, as phase I human clinical testing is currently underway. In addition, folate receptors are highly expressed in activated, nonresting macrophages and thus folate conjugates have been used therapeutically to target arthritis [76, 92], macrophages within atherosclerotic lesions [93], and macrophages associated with ovarian cancer [94].

25.5. Pharmacology at Caveolae: Presentation, Presentation, Presentation

An emerging trend with pharmacological action at caveolae is how the presentation of molecules to cells influences interactions with caveolae. A dramatic example of this is the effects of estrogen. Supraphysiological levels of estrogen presented to endothelial cells affect many cellular processes by nonspecific mechanisms such as acting as an antioxidant [95]. However, if physiological levels of estrogen are added to endothelial cells in association with albumin, so that the estrogen remains soluble, nitric oxide is not generated [17]. Importantly, estrogen associated with albumin does not affect the activity of eNOS and generation of nitric oxide. In contrast, physiological levels of estrogen associated with high-density lipoproteins (HDLs) stimulate the production of nitric oxide and subsequent vasodilation of blood vessels. The effects of HDL-associated estrogen require the presence of the HDL receptor, scavenger receptor B1 (SR-B1), which is localized to caveolae [17]. Although not formally demonstrated, it is thought that the interaction of estrogen-containing HDL with SR-B1 facilitates the delivery of the estrogen directly to caveolae, where it affects nitric oxide synthesis. In contrast to estrogen, the free fatty

acid myristic acid stimulates nitric oxide production when added to cells in association with albumin [22], but not when associated with HDL (Smart and Ross, unpublished observations). At present, it is unclear if the nature of the presentation is restricted to hydrophobic molecules or if specificity also exists for hydrophilic molecules.

Altering caveolae function has the potential to modify numerous signaling and metabolic pathways which makes caveolae an important pharmacological target. A critical consideration when designing future pharmacological reagents is the method whereby the reagent will be delivered to caveolae. The method of presentation is important for two reasons. First, not all caveolae contain the same protein components, a fact which can be exploited to target reagents to a subset of cells. For example, a reagent that interacts with CD36, a protein known to be associated with caveolae, would be expected to affect heart function because CD36 is highly expressed in cardiac myocytes. However, since CD36 is not expressed in neurons, liver, epithelial cells, and so forth, the reagent should not affect these tissues/cells. Second, as discussed above, different molecules give different responses or no responses, depending on how they are presented to caveolae. Consideration must also be given if the pharmacological reagent is being presented with a carrier that can affect caveolae, such as cyclodextrin. Cyclodextrin and other cholesterol-binding carriers can alter caveolae function independent of the pharmacological reagent. In summary, advancements with generating specific pharmacological reagents for caveolae show promise, although extensive consideration of how the reagents are to be presented to caveolae will definitely be needed.

Acknowledgments: The authors thank the members of the Kentucky Pediatric Research Institute working group for valuable advice and assistance. This work was supported, in part, by the National Heart, Lung, and Blood Institute (HL68509 and HL78976: EJS).

References

1. G. E. Palade. Fine structure of blood capillaries. *J. Appl. Phys.* **24**: 1424–1436 (1953).
2. E. Yamada. The fine structure of the gall bladder epithelium of the mouse. *J. Biophys. Biochem. Cytol.* **1**: 445–448 (1955).
3. J. R. Glenney Jr. and D. Soppet. Sequence and expression of caveolin, a protein component of caveolae plasma membrane domains phosphorylated on tyrosine in Rous sarcoma virus-transformed fibroblasts. *Proc. Natl. Acad. Sci. USA* **89**: 10517–10521 (1992).
4. J. R. Glenney Jr. The sequence of human caveolin reveals identity with VIP21, a component of transport vesicles. *FEBS Lett.* **314**: 45–48 (1992).
5. T. V. Kurzchalia, P. Dupree, R. G. Parton, R. Kellner, H. Virta, M. Lehnert, and K. Simons. VIP21, a 21-kD membrane protein is an integral component of trans-Golgi-network-derived transport vesicles. *J. Cell Biol.* **118**: 1003–1014 (1992).
6. K. G. Rothberg, J. E. Heuser, W. C. Donzell, Y. S. Ying, J. R. Glenney, and R. G. Anderson. Caveolin, a protein component of caveolae membrane coats. *Cell* **68**: 673–682 (1992).
7. R. G. Anderson. The caveolae membrane system. *Annu. Rev. Biochem.* **67**: 199–225 (1998).

8. P. Oh and J. E. Schnitzer. Segregation of heterotrimeric G proteins in cell surface microdomains. Gq binds caveolin to concentrate in caveolae, whereas Gi and Gs target lipid rafts by default. *Mol. Biol. Cell* **12**: 685–698 (2001).
9. K. Gaus, M. Rodriguez, K. R. Ruberu, I. Gelissen, T. M. Sloane, L. Kritharides, and W. Jessup. Domain-specific lipid distribution in macrophage plasma membranes. *J. Lipid Res.* **46**: 1526–1538 (2005).
10. P. E. Scherer, M. P. Lisanti, G. Baldini, M. Sargiacomo, C. C. Mastick, and H. F. Lodish. Induction of caveolin during adipogenesis and association of GLUT4 with caveolin-rich vesicles. *J. Cell Biol.* **127**: 1233–1243 (1994).
11. F. Galbiati, D. Volonte, O. Gil, G. Zanazzi, J. L. Salzer, M. Sargiacomo, P. E. Scherer, J. A. Engelman, S. A. T. Parenti, T. Okamoto, and M. P. Lisanti. Expression of caveolin- and -2 in differentiating PC12 cells and dorsal root ganglion. *Proc. Natl. Acad. Sci. USA* **95**: 10257–10262 (1998).
12. D. D. Mikol, H. L. Hong, H. L. Cheng, and E. L. Feldman. Caveolin-1 expression in Schwann cells. *Glia* **27**: 39–52 (1999).
13. W.-J. Chang, Y.-S. Ying, K. G. Rothberg, N. M. Hooper, A. J. Turner, H. A. Gambliel, J. De Gunzburg, S. M. Mumby, A. G. Gilman, and R. G. W. Anderson. Purification and characterization of smooth muscle caveolae. *J. Cell Biol.* **126**: 127–138 (1994).
14. M. P. Lisanti, P. E. Scherer, J. Vidugiriene, Z. tang, A. Hermanoski-Vosatka, Y.-H. Tu, R. F. Cook, and M. Sargiacomo. Characterization of caveolin-rich membrane domains isolated from an endothelial-rich source: implications for human disease. *J. Cell Biol.* **126**: 111–126 (1994).
15. E. J. Smart, G. A. Graf, M. A. McNiven, W. C. Sessa, J. A. Engelman, P. E. Scherer, T. Okamoto, and M. P. Lisanti. Caveolins, liquid-ordered domains, and signal transduction. *Mol Cell Biol.* **19**: 7289–7304 (1999).
16. A. Blair, P. W. Shaul, I. S. Yuhanna, P. A. Conrad, and E. J. Smart. Oxidized low density lipoprotein displaces endothelial nitric-oxide synthase (eNOS) from plasmalemmal caveolae and impairs eNOS activation. *J. Biol. Chem.* **274**: 32512–32519 (1999).
17. M. Gong, M. Wilson, T. Kelly, W. Su, J. Dressman, J. Kincer, S. V. Matveev, L. Guo, T. Guerin, X.-A. Li, W. Zhu, A. Uittenbogaard, and E. J. Smart. HDL-associated estradiol stimulates endothelial NO synthase and vasodilation in an SR-BI-dependent manner. *J. Clin. Invest.* **111**: 1579–1587 (2003).
18. X.-A. Li, W. B. Titlow, B. A. Jackson, N. Giltiay, M. Nikolova-Karakashian, A. Uittenbogaard, and E. J. Smart. High Density Lipoprotein Binding to Scavenger Receptor, Class B, Type I Activates Endothelial Nitric-oxide Synthase in a Ceramide-dependent Manner. *J. Biol. Chem.* **277**: 11058–11063 (2002).
19. P. W. Shaul, E. J. Smart, L. J. Robinson, Z. German, I. S. Yuhanna, Y. Ying, R. G. W. Anderson, and T. Michel. Acylation Targets Endothelial Nitric-oxide Synthase to Plasmalemmal Caveolae. *J. Biol. Chem.* **271**: 6518–6522 (1996).
20. A. Uittenbogaard, P. W. Shaul, I. S. Yuhanna, A. Blair, and E. J. Smart. High density lipoprotein prevents oxidized low density lipoprotein-induced inhibition of endothelial nitric-oxide synthase localization and activation in caveolae. *J. Biol. Chem.* **275**: 11278–11283 (2000).
21. W. Zhu and E. J. Smart. Caveolae, estrogen and nitric oxide. *Trends Endocrinol. Metab.* **14**: 114–117 (2003).
22. W. Zhu and E. J. Smart. Myristic Acid Stimulates Endothelial Nitric-oxide Synthase in a CD36- and an AMP Kinase-dependent Manner. *J. Biol. Chem.* **280**: 29543–29550 (2005).
23. L. L. Hilenski, R. E. Clempus, M. T. Quinn, J. D. Lambeth, and K. K. Griendling. Distinct subcellular localizations of Nox1 and Nox4 in vascular smooth muscle cells. *Arterioscler. Thromb. Vasc. Biol.* **24**: 677–683 (2004).

24. J. Y. Liou, W. G. Deng, D. W. Gilroy, S. K. Shyue, and K. K. Wu. Colocalization and interaction of cyclooxygenase-2 with caveolin-1 in human fibroblasts. *J. Biol. Chem.* **276**: 34975–34982 (2001).
25. E. Spisni, C. Griffoni, S. Santi, M. Riccio, R. Maulli, G. Bartolini, M. Toni, V. Ullrich, and V. Tomasi. Colocalization prostacycline (PGI₂) synthase - caveolin-1 in endothelial cells and new roles for PGI₂ in angiogenesis. *Exp. Cell Res.* **266**: 31–43 (2001).
26. E. J. Smart, Y. S. Ying, and R. G. Anderson. Hormonal regulation of caveolae internalization. *J. Cell Biol.* **131**: 929–938 (1995).
27. E. J. Smart, Y. S. Ying, P. A. Conrad, and R. G. Anderson. Caveolin moves from caveolae to the Golgi apparatus in response to cholesterol oxidation. *J. Cell Biol.* **127**: 1185–1197 (1994).
28. R. G. Parton, B. Joggerst, and K. Simons. Regulated internalization of caveolae. *J. Cell Biol.* **127**: 1199–1215 (1994).
29. T. Kobayashi and J. M. Robinson. A novel intracellular compartment with unusual secretory properties in human neutrophils. *J. Cell Biol.* **113**: 743–756 (1991).
30. T. Kobayashi, J. M. Robinson, and H. Seguchi. Identification of intracellular sites of superoxide production in stimulated neutrophils. *J. Cell Sci.* **111**: 81–91 (1998).
31. J. M. Robinson, T. Kobayashi, H. Seguchi, and T. Takizawa. Evaluation of neutrophil structure and function by electron microscopy: cytochemical studies. *J. Immunol. Methods* **232**: 169–178 (1999).
32. K. G. Rothberg, Y.-S. Yin, B. A. Kamen, and R. G. W. Anderson. Cholesterol controls the clustering of the glycopospholipid-anchored membrane receptor for 5-methyltetrahydrofolate. *J. Cell Biol.* **111**: 2931–2938 (1990).
33. J. E. Schnitzer, P. Oh, E. Pinney, and J. Allard. Filipin-sensitive caveolae-mediated transport in endothelium: reduced transcytosis, scavenger endocytosis, and capillary permeability of select macromolecules. *J. Cell Biol.* **127**: 1217–1232 (1994).
34. B. J. Nichols, A. K. Kenworthy, R. S. Polishchuk, R. Lodge, T. H. Roberts, K. Hirschberg, R. D. Phair, and J. Lippincott-Schwartz. Rapid cycling of lipid raft markers between the cell surface and Golgi complex. *J. Cell Biol.* **153**: 529–541 (2001).
35. A. R. Hilgenbrink and P. S. Low. Folate receptor-mediated drug targeting: from therapeutics to diagnostics. *J. Pharm. Sci.* **94**: 2135–2146 (2005).
36. N. Benlimame, P. U. Le, and I. R. Nabi. Localization of autocrine motility factor receptor to caveolae and clathrin-independent internalization of its ligand to smooth endoplasmic reticulum. *Mol. Biol. Cell* **9**: 1773–1786 (1998).
37. P. U. Le and I. Nabi. Distinct caveolae-mediated endocytic pathways target the Golgi apparatus and the endoplasmic reticulum. *J. Cell Sci.* **116**: 1059–1071 (2003).
38. P. A. Orlandi and P. H. Fishman. Filipin-dependent inhibition of cholera toxin: evidence for toxin internalization and activation through caveolae-like domains. *J. Cell Biol.* **141**: 905–915 (1998).
39. A. A. Wolf, M. G. Jobling, S. Wimer-Mackin, M. Ferguson-Maltzman, J. L. Madara, R. K. Holmes, and W. I. Lencer. Ganglioside structure dictates signal transduction by cholera toxin and association with caveolae-like membrane domains in polarized epithelia. *J. Cell Biol.* **141**: 917–927 (1998).
40. M. Kirkham, A. Fujita, R. Chadda, S. J. Nixon, T. V. Kurzchalia, D. K. Sharma, R. E. Pagaon, J. F. Hancock, S. Mayor, and R. G. Parton. Ultrastructural identification of uncoated caveolin-independent early endocytic vesicles. *J. Cell Biol.* **168**: 465–476 (2005).
41. M. Kirkham and R. G. Parton. Clathrin-independent endocytosis: New insights into caveolae and non-caveolar lipid raft carriers. *Biochim. Biophys. Acta* **1745**: 273–286 (2005).

42. J. A. Engelman, X. L. Zhang, and M. P. Lisanti. Genes encoding human caveolin-1 and caveolin-2 are co-localized to the D7S522 locus (7q31.1), a known fragile site (FRA7G) that is frequently deleted in human cancers. *FEBS Lett.* **436**: 403–410 (1998).
43. J. A. Engelman, X. L. Zhang, and M. P. Lisanti. Methylation of a CpG island in the 5' promoter region of the caveolin-1 gene in human breast cancer cell lines. *FEBS Lett.* **448**: 221–230 (1999).
44. J. R. Glenney Jr. Tyrosine phosphorylation of a 22-kDa protein is correlated with transformation by Rous sarcoma virus. *J. Biol. Chem.* **264**: 20163–20166 (1989).
45. J. Couet, S. Li, T. Okamoto, T. Izeku, and M. P. Lisanti. Identification of peptide and protein ligands for the caveolin-scaffolding domain. Implications for the interaction of caveolin with caveolae-associated proteins. *J. Biol. Chem.* **272**: 6525–6533 (1997).
46. R. Sager, S. Sheng, A. Anisowicz, G. Sotiropoulou, Z. Zou, G. Stenman, K. Swishelm, Z. Chen, M. J. Hendrix, P. R. Pemberton, and K. Ryan. RNA genetics of breast cancer: maspin as paradigm. *Cold Spring Harb. Symp. Quant. Biol.* **59**: 537–547 (1994).
47. J. A. Engelman, R. J. Lee, A. Karnezis, D. J. Bearss, M. Webster, P. Siegel, W. J. Muller, J. J. Windle, R. G. Pestell, and M. P. Lisanti. Reciprocal regulation of neu tyrosine kinase activity and caveolin-1 protein expression in vitro and in vivo. Implications for human breast cancer. *J. Biol. Chem.* **273**: 20448–20455 (1998).
48. A. J. Koleske, D. Baltimore, and M. P. Lisanti. Reduction of caveolin and caveolae in oncogenically transformed cells. *Proc. Natl. Acad. Sci. USA* **92**: 1381–1385 (1995).
49. S. W. Lee, C. L. Reimer, P. Oh, D. B. Campbell, and J. E. Schnitzer. Tumor cell growth inhibition by caveolin re-expression in human breast cancer cells. *Oncogene* **16**: 1391–1397 (1998).
50. F. Galbiati, D. Volonte, J. A. Engelman, G. Watanabe, R. Burke, R. G. Pestell, and M. P. Lisanti. Targeted downregulation of caveolin-1 is sufficient to drive cell transformation hyperactivate the p42/44 MAP kinase cascades. *EMBO J.* **17**: 6633–6648 (1998).
51. E. K. Sloan, K. L. Stanley, and R. L. Anderson. Caveolin-1 inhibits breast cancer growth and metastasis. *Oncogene* **23**: 7893–7897 (2004).
52. G. Yang, L. D. Truong, T. L. Timme, C. Ren, T. M. Wheeler, S. H. Park, Y. Nasu, C. H. Bangma, M. W. Kattan, P. T. Scardino, and T. C. Thompson. Elevated expression of caveolin is associated with prostate and breast cancer. *Clin. Cancer Res.* **4**: 1873–1880 (1998).
53. C. C. Ho, P. H. Huang, H. Y. Huang, Y. H. Chen, P. C. Yang, and S. M. and Hsu. Up-regulated caveolin-1 accentuates the metastasis capability of lung adenocarcinoma by inducing filopodia formation. *Am. J. Pathol.* **161**: 1647–1656 (2002).
54. P. H. Rajjayabun, S. Garg, G. C. Durkham, R. Charlton, M. C. Robinson, and J. K. Mellon. Caveolin-1 expression is associated with high-grade bladder cancer. *Urology* **58**: 811–814 (2001).
55. Y. Lavie, G. Fiucci, and M. Liscovitch. Up-regulation of caveolae and caveolar constituents in multidrug-resistant cancer cells. *J. Biol. Chem.* **273**: 32380–32383 (1998).
56. Y. Lavie, G. Fiucci, M. Czarny, and M. Liscovitch. Changes in membrane microdomains and caveolae constituents in multidrug-resistance cancer cells. *Lipids* **34 Suppl**: S57–63 (1999).
57. Y. Lavie and M. Liscovitch. Changes in lipid and protein constituents of rafts and caveolae in multidrug resistant cancer cells and their functional consequences. *Glycoconj. J.* **17**: 253–259 (2000).

58. C. P. Yang, F. Galbiati, D. Volonte, S. B. Horwitz, and M. P. Lisanti. Upregulation of caveolin-1 and caveolae organelles in Taxol-resistant A549 cells. *FEBS Lett.* **439**: 368–372 (1998).
59. P. T. Ronaldson, M. Bendayan, D. Gingras, M. Piquette-Miller, and R. Bendayan. Cellular localization and functional expression of P-glycoprotein in rat astrocyte cultures. *J. Neurochem.* **89**: 788–800 (2004).
60. C. Cai and J. Chen. Overexpression of caveolin-1 induces alteration of multidrug resistance in Hs578T breast adenocarcinoma cells. *Int. J. Cancer* **111**: 317–323 (2004).
61. J. Troost, H. Lindenmaier, W. E. Haefeli, and J. Weiss. Modulation of cellular cholesterol alters P-glycoprotein activity in multidrug-resistant cells. *Mol. Pharmacol.* **66**: 1332–1339 (2004).
62. D. P. McIntosh, X.-Y. Tan, P. Oh, and J. E. Schnitzer. Targeting endothelium and its dynamic caveolae for tissue-specific transcytosis in vivo: A pathway to overcome cell barriers to drug and gene delivery. *Proc. Natl. Acad. Sci. USA* **99**: 1996–2001 (2002).
63. A. R. Gagliardi, H. Hadd, and D. C. Collins. Inhibition of angiogenesis by suramin. *Cancer Res.* **52**: 5073–5075 (1992).
64. A. R. Gagliardi, M. Kassack, A. Kremeyer, G. Muller, P. Nickel, and D. C. Collins. Antiangiogenic and antiproliferative activity of suramin analogues. *Cancer Chemother. Pharmacol.* **41**: 117–124 (1998).
65. C. R. Middaugh, H. Mach, C. J. Burke, D. B. Volkin, J. M. Dabora, P. K. Tsai, M. W. Bruner, J. A. Ryan, and K. E. Marfia. Nature of the interaction of growth factors with suramin. *Biochemistry* **31**: 9016–9024 (1992).
66. D. F. McCain, L. Wu, P. Nickel, M. U. Kassack, A. Kreimeyer, A. Gagliardi, D. C. Collins, and Z.-Y. Zhang. Suramin derivatives as inhibitors and activators of protein-tyrosine phosphatases. *J. Biol. Chem.* **279**: 14713–14725 (2004).
67. A. R. Gagliardi, M. F. Taylor, and D. C. Collins. Uptake of suramin by human microvascular endothelial cells. *Cancer Lett.* **125**: 97–102 (1998).
68. T. C. Stover, A. Sharma, G. P. Robertson, and M. Kester. Systemic delivery of liposomal short-chain ceramide limits solid tumor growth in murine models of breast adenocarcinoma. *Clin. Cancer Res.* **11**: 3465–3474 (2005).
69. R. G. Anderson, B. A. Kamen, K. G. Rothberg, and S. W. Lacey. Potocytosis: sequestration and transport of small molecules by caveolae. *Science* **255**: 410–411 (1992).
70. S. Mayor, K. G. Rothberg, and F. R. Maxfield. Sequestration of GPI-anchored proteins in caveolae triggered by cross-linking. *Science* **264**: 1948–1951 (1994).
71. E. J. Smart, C. Mineo, and R. G. Anderson. Clustered folate receptors deliver 5-methyltetrahydrofolate to cytoplasm of MA104 cells. *J. Cell Biol.* **134**: 1169–1177 (1996).
72. W. J. Chang, K. G. Rothberg, B. A. Kamen, and R. G. Anderson. Lowering the cholesterol content of MA104 cells inhibits receptor-mediated transport of folate. *J. Cell Biol.* **118**: 63–69 (1992).
73. E. J. Smart, D. C. Foster, Y. S. Ying, B. A. Kamen, and R. G. Anderson. Protein kinase C activators inhibit receptor-mediated potocytosis by preventing internalization of caveolae. *J. Cell Biol.* **124**: 307–313 (1994).
74. E. J. Smart, K. Estes, and R. G. Anderson. Inhibitors that block both the internalization of caveolae and the return of plasmalemmal vesicles. *Cold Spring Harb. Symp. Quant. Biol.* **60**: 243–248 (1995).
75. Y. Lu, E. Segal, C. P. Leamon, and P. S. Low. Folate receptor-targeted immunotherapy of cancer: mechanism and therapeutic potential. *Adv. Drug Deliv. Rev.* **56**: 1161–1176 (2004).

76. C. M. Paulos, M. J. Turk, G. J. Breur, and P. S. Low. Folate receptor-mediated targeting of therapeutic and imaging agents to activated macrophages in rheumatoid arthritis. *Adv. Drug Deliv. Rev.* **56**: 1205–1217 (2004).
77. C. H. Kim, Y. S. Park, K. N. Chung, and P. C. Elwood. Sorting and function of the human folate receptor is independent of the caveolin expression in Fisher rat thyroid epithelial cells. *J. Biochem. Mol. Biol.* **35**: 395–402 (2002).
78. J. Wang, W. Gunning, K. M. Kelley, and M. Ratnam. Evidence for segregation of heterologous GPI-anchored proteins into separate lipid rafts within the plasma membrane. *J. Membr. Biol.* **189**: 35–43 (2002).
79. M. Wu, J. Fan, W. Gunning, and M. Ratnam. Clustering of GPI-anchored folate receptor independent of both cross-linking and association with caveolin. *J. Membr. Biol.* **159**: 137–147 (1997).
80. M. Bagnoli, A. Tomassetti, M. Figini, S. Flati, V. Dolo, S. Canevari, and S. Miotti. Downmodulation of caveolin-1 expression in human ovarian carcinoma is directly related to alpha-folate receptor overexpression. *Oncogene* **19**: 4754–4763 (2000).
81. R. Corrocher, L. M. Bambara, M. L. Pachor, A. M. Stanzial, C. Lunardi, and G. De Sandre. Breast cancer and serum folate binding capacity. *Eur. J. Cancer* **16**: 1233–1236 (1980).
82. J. Holm, S. I. Hansen, M. Hoier-Madsen, K. Sondergaard, and M. Bzorek. The high-affinity folate receptor of normal and malignant human colonic mucosa. *APMIS* **102**: 828–836 (1994).
83. J. Holm, S. I. Hansen, and J. Lyngbye. High affinity folate binding in chronic myelogenous leukaemia serum, relationship of binding characteristics to activity of disease and binder concentration. *Scand. J. Haematol.* **26**: 153–155 (1981).
84. J. Holm, S. I. Hansen, K. Sondergaard, and M. Hoier-Madsen. The high-affinity folate binding protein in normal and malignant mammary gland tissue. *Adv. Exp. Med. Biol.* **338**: 757–760 (1993).
85. J. F. Ross, P. K. Chaudhuri, and M. Ratnam. Differential regulation of folate receptor isoforms in normal and malignant tissues in vivo and in established cell lines. Physiologic and clinical implications. *Cancer* **73**: 2432–2443 (1994).
86. A. Tomassetti, L. R. Coney, S. Canevari, S. Miotti, P. Facheris, V. R. J. Zurawski, and M. I. Colnaghi. Isolation and biochemical characterization of the soluble and membrane forms of folate binding protein expressed in the ovarian carcinoma cell line IGROV1. *FEBS Lett.* **317**: 143–146 (1993).
87. S. D. Weitman, K. M. Frazier, and B. A. Kamen. The folate receptor in central nervous system malignancies of childhood. *J. Neurooncol.* **21**: 107–112 (1994).
88. S. D. Weitman, R. H. Lark, L. R. Coney, D. W. fort, V. Frasca, V. R. J. Zurawski, and B. A. Kamen. Distribution of the folate receptor GP38 in normal and malignant cell lines and tissues. *Cancer Res.* **52**: 3396–3401 (1992).
89. S. M. Stephenson, P. S. Low, and R. J. Lee. Folate receptor-mediated targeting of liposomal drugs to cancer cells. *Methods Enzymol.* **387**: 33–50 (2004).
90. S. Gottschalk, R. J. Cristiano, L. C. Smith, and S. L. Woo. Folate receptor mediated DNA delivery into tumor cells: potosomal disruption results in enhanced gene expression. *Gene Ther.* **1**: 185–191 (1994).
91. E. Dauty, J.-S. Remy, G. Zuber, and J.-P. Behr. Intracellular delivery of nanometric DNA particles via the folate receptor. *Bioconjug. Chem.* **13**: 831–839 (2002).
92. C. M. Paulos, B. Varghese, W. R. Widmer, G. J. Breur, E. Vlashi, and P. S. Low. Folate-targeted immunotherapy effectively treats established adjuvant and collagen-induced arthritis. *Arthritis Res. Ther.* **28**: R77 Epub ahead of print (2006).

93. F. Antohe, L. Radulescu, E. Puchianu, M. D. Kennedy, P. S. Low, and M. Simionescu. Increased uptake of folate conjugates by activated macrophages in experimental hyperlipemia. *Cell Tissue Res.* **320**: 277–285 (2005).
94. M. J. Turk, D. J. Waters, and P. S. Low. Folate-conjugated liposomes preferentially target macrophages associated with ovarian carcinoma. *Cancer Lett.* **213**: 165–172 (2004).
95. M. T. Subbiah. Mechanisms of cardioprotection by estrogens. *Proc. Soc. Exp. Biol. Med.* **217**: 23–29 (1998).
96. E. J. Smart, Y. S. Ying, C. Mineo, and R. G. Anderson. A detergent-free method for purifying caveolae membrane from tissue culture cells. *Proc. Natl. Acad. Sci. USA* **92**: 10104–10108 (1995).

26

Immortalization Strategies for Epithelial Cells in Primary Culture

David de Semir Frappart, Rosalie Maurisse, Esther H. Vock, and Dieter C. Gruenert

Abstract The development of immortalized cell culture systems has been a tremendous asset to basic research as well as to the pharmaceutical and biotechnology industries. These cell culture systems have facilitated advances in our knowledge of the biochemical and metabolic mechanisms underlying cell function and disease pathology. The immortalization of epithelial cells has been particularly important for elucidating specialized cell function and/or neoplastic progression. The strategies required for the generation of epithelial cell systems, in particular, human airway epithelial cells, can serve a paradigm for other specialized cell systems such as endothelial cells. Numerous airway epithelial cell systems have been generated from tumor tissue and primary cells. The methodologies for establishing these transformed and immortalized cultures have relied primarily on oncogenic viruses and expression vectors carrying oncogenes and/or telomerase. Because of the extensive work that has already been carried out over the last two decades, these human epithelial cell systems provide an ideal model for defining the parameters that lead to cell transformation and immortalization as well as those that result in cells with differentiated functions similar to those of primary epithelial cells. With this in mind, the strategies and techniques employed to develop transformed and immortalized cells that can be used to study neoplastic progression or differentiated function can be readily extrapolated to other cell systems.

Keywords: Immortalization; Transformation; Cell lines; Primary culture; Oncogenes

Abbreviations

BSA	Bovine serum albumin
DMEM	Dulbecco's modified Eagle's medium
DTT	Dithiothreitol
EBV	Epstein-Barr virus
ECM	Extracellular matrix
HPV	Human papilloma virus
hTERT	Human telomerase reverse transcriptase
PBS	Phosphate buffered saline

PD	Population doublings
Rb	Retinoblastoma protein
SV40	Simian virus 40
TGF- β	Transforming growth factor- β

26.1. Introduction

The limited lifespan of cultured cells has been an impediment in the long-term characterization of the cellular and molecular mechanisms regulating cell metabolism and neoplastic progression. A finite number of cell divisions lead to cell senescence and ultimately to cell death (Figure 26.1) [1–4]. As opposed to apoptosis that eliminates unwanted cells through a series of pathways that lead to cell death [5–12], senescence is a state in which cells are growth arrested and cannot be stimulated to reenter the cell cycle by physiological mitogens. Senescent cells are resistant to apoptosis and generally acquire altered differentiated functions.

One approach to overcome limitations associated with the culture of primary cells has been the transformed and/or immortalized cell systems. These cell systems have played a critical role in advancing the understanding of the biochemical and genetic mechanisms underlying cell function and disease pathology. The development of transformed and immortalized cell lines has been instrumental for studying inherited and infectious diseases, carcinogenesis, and regulation of gene expression leading to differentiated function [13–15]. The primary focus of this overview will be a discussion of the strategies underlying in vitro transformation and immortalization of human airway epithelial cells, although cells from other mammalian species and organ systems will also be discussed. The airway epithelial cell systems provide an excellent paradigm for the development of immortalized cell systems and can be used for studying the mechanisms underlying cell function and disease pathology as well as for the development of therapies.

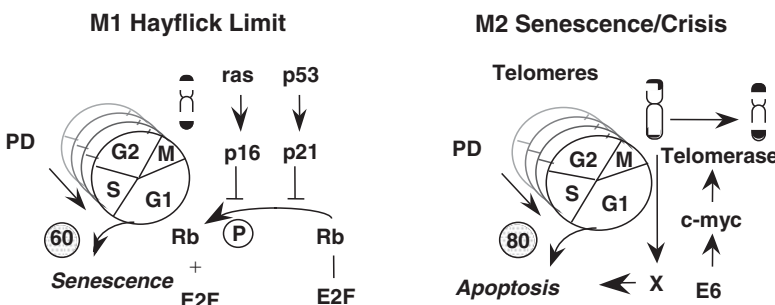


Figure 26.1 Immortalization of human cells: Cells enter replicative senescence at mortality stage 1 (M1 Hayflick limit) after about 60 population doublings (PD). The protein p16 accumulates in senescent cells. The simian virus 40 (SV40) large T antigen as well as the human papilloma virus (HPV) type 16-E6 and E7 proteins sequester the retinoblastoma protein (Rb) and/or p53 constitutively releases the transcription factor E2F. E2F induces expression proteins required for progression through G1/S transition, thus the cells escape cell cycle arrest. At mortality stage 2 (M2), transformed cells must overcome senescence and crisis before they are immortalized. This is likely to involve the activation of telomerase either by the introduction of hTERT cDNA or by a genetic change that activates telomerase.

26.2. Cell Transformation and Immortalization Strategies

26.2.1. Transformation Versus Immortalization

In vitro transformation and immortalization is a multistep process that can be viewed as mimicking the stages of neoplastic progression in vivo [13, 16–18]. In addition to generating cells that can be used to model carcinogenesis and neoplastic progression, cell transformation can be used to generate long-lived and immortalized cells that express differentiated features characteristic of primary cell cultures [13, 16, 19]. It is therefore important to distinguish a transformed cell with enhanced growth characteristics from one that is transformed and immortalized. In terms of in vitro neoplastic progression, these are two early steps, that is, transformation and immortalization, which can result in cells that are tumorigenic or are non-tumorigenic and have defined differentiated features [13, 16].

Segregating between long-lived or immortalized cell systems requires the long-term culture of a cell line and attention to the behavior of the cells as they go through multiple subcultures. Since not all transformed cells become immortalized even though their proliferative potential exceeds that of primary cultures, it is critical to evaluate a cell line over both multiple generations and multiple subcultures [20]. The difference between the number of generations (population doublings, PD) that a culture undergoes and the number of subcultures is dependent on the plating efficiency. A 10% plating efficiency generally translates into 6–8 PD before reaching confluence [21]. Therefore, a claim of 100–200 generations may not yield an immortalized cell line with indefinite growth potential. This is particularly relevant to studies that require long-term culture of cells with a consistency of phenotype.

26.2.2. Selecting the Appropriate Cell Line

When determining which transformed cell system is the most appropriate for a particular study, there are a number of points that must be considered to identify those cell systems that might be appropriate. One needs to consider whether the studies will be evaluating differentiated or neoplastic growth endpoints. Cells in different organs, even if they are from the same developmental lineage, are generally a conglomeration of different cell subtypes that are similar but phenotypically distinct. It is, therefore, possible to generate clones of cells representing not only the mesodermal, ectodermal, or endodermal lineage but also the individual differentiated subtypes. Cells that display differentiated features such as tight junctions or cell type-specific ion transport or secretory properties are generally not the same in cell lines that would be used to evaluate anchorage independent growth or tumor production. Another consideration is the number of cells required for a given study. If the cells have a limited lifespan, albeit enhanced relative to primary cells, they may not be adequate for long-term studies or for large-scale production of cellular components (e.g., proteins). Finally, one needs to consider the retention of specific phenotypic endpoints as a function of time in culture or exposure to different extracellular regulatory factors (e.g., cytokines, growth factors, and/or extracellular matrices). While this is not an exhaustive list for choosing a given cell line, it encompasses the most significant points to be considered in the choice of an established cell line.

26.2.3. Human Epithelial Cells as a Model for Transformation and Immortalization

The usefulness of a given cell line will depend on which differentiated or neoplastic endpoints the cells express and/or whether the cell line is long-lived or immortal. Assessment of whether a cell line expresses specific metabolic or functional endpoints generally requires empirical analysis. The development of transformed/immortalized epithelial cell systems has been particularly significant, since these cells are responsible for 85–90% of all cancers and they often manifest a broad range of specialized functions in addition to their neoplastic phenotype [13, 16, 22–34].

Because transformed and/or immortalized cells can be defined in terms of their growth characteristics relative to primary cultures, epithelial cells are ideal for the study of neoplastic progression and cell-specific function. Primary epithelial cells have very limited growth potential and readily senesce, while transformed epithelial cells can be selected by their ability to continue proliferating [16, 21]. Allowing the cells to grow and remain at confluence after exposure to a given transforming agent can generally accelerate selection of transformants. The primary cells will undergo squamous differentiation and eventually detach from the dish, and the successfully transformed cells will continue to proliferate as “clonal islands” within the sea of dead cells. Isolation of transformants from other cell types, such as fibroblasts, often takes longer and the cells are not as readily distinguished from the population of cells that have not been successfully transformed [16, 18, 35–43]. However, some of the same strategies used to generate transformed and/or immortalized human epithelial cells can be applied to other cell types to generate established cell lines [13, 14, 16, 19, 40].

26.2.4. Strategies to Generate Transformed and/or Immortalized Epithelial Cells

Cells with enhanced or unlimited growth potential can be generated by a number of mechanisms. The vast majority of established cell lines have been generated through the exposure of primary or tumor-derived cultures to a transforming agent that is either chemical, physical, viral, and/or genetic in origin [13, 16, 19]. Since the primary purpose of this overview is the generation of immortalized cell lines that can be used to evaluate the biochemical and genetic pathways that underlie differentiated function, the strategies discussed will concentrate on the use of viral oncogenes and telomerase. Even though chemical and physical insult to mammalian cells has produced transformed cells [13, 16, 44, 45], human cells are more recalcitrant to such insult and generally require the introduction of oncogenes to effectively achieve cell transformation.

26.2.4.1. Spontaneous Transformation

Unlike rodent cells that readily undergo spontaneous transformation [46–50], human cells tend to be very refractory to this process [51, 52] and will undergo spontaneous transformation only on rare occasions [53, 54]. The biochemical and molecular mechanisms that underlie such an event are not yet clearly elucidated; however, it is likely that there have been preneoplastic insults that have occurred to initiate spontaneous transformation. Of the few reports

describing spontaneous transformation of human cells, most describe the transformation of fibroblasts [17, 52, 55, 56], which appears to be associated with specific chromosomal deletions [53, 54, 56–58] and cell cycle genes (e.g., p53 and other genes) [17, 18, 57–66]. Such events are often the underlying cause of the ability to establish cell lines from tumor samples without exposure to additional chemical or physical insult or to oncogenic viruses or genes.

26.2.4.2. Viral and Oncogene Transformation

For human cells, human airway epithelial cells in particular, exposure to viral oncogenes, either alone or in combination with other genes and/or chemical or physical agents, has been most effective for generating long-lived or immortalized cell lines. Most human airway epithelial cell lines have been developed using simian virus 40 (SV40) polyoma virus or oncogenes derived from the SV40 genome [14], while a few have been generated using human papilloma virus (HPV) [67, 68] and adeno-SV40 hybrid virus [69, 70]. The advantage of using these transforming viruses stems from the effectiveness of virus transduction, that is, their ability to infect the human cells. However, a drawback of these viral transformation systems is the potential for subsequent viral replication and viral-induced cell lysis. Even in the case of SV40 where the human cells are semi-permissive hosts, a lytic viral replicative cycle can occur and result in the death of the transformed cells.

To circumvent the potential for viral replication, cells have been transfected with plasmids containing replicatively inactivated viruses such as the pSVori-, which contains the entire SV40 genome deleted by 6-bp in the SV40 origin of replication [71]. Some of the first human airway epithelial cell lines were generated with this plasmid [21, 72–77]. Numerous cell lines have been transformed and immortalized human airway epithelial cell lines in different stages of neoplastic progression and with defined differentiated features have been generated with the pSVori- plasmid [14]. These cell lines have been utilized for numerous studies designed to elucidate the mechanisms underlying airway disease in general, and cystic fibrosis in particular.

As with the virally transduced epithelial cells, cells transfected with a plasmid containing a replication defective virus or a cellular oncogene will first show properties of enhanced growth that can eventually lead to immortalization. However, not all transformations lead to cells that have unlimited growth potential and are immortalized. Often a viral oncogene in and of itself is not sufficient to result in an immortalized cell and will require additional oncogenes or genetic events altering the expression of endogenous proto-oncogenes or suppressor genes.

Beyond the Hayflick limit, cells that have escaped senescence and/or crisis must progress beyond mortality stage 2 (Figure 26.1). Recent studies have shown that human telomerase reverse transcriptase cDNA (hTERT) in combination with viral oncogenes also has the potential to immortalize human airway epithelial cells [15, 78–82]. However, even though hTERT alone will cause enhanced growth potential of a cell line, with the exception of one study [81],

hTERT appears to require the presence of an additional exogenous oncogene or the activation of an endogenous oncogene to have actual immortalization of human epithelial cells [83–87].

26.3. Protocols

The generation of transformed and immortalized cell systems from primary cells or tumor cells with limited lifespan is a multistep process (Figure 26.2). The development of immortalized cell systems from tumor tissue can either involve the long-term growth in culture or the augmentation of growth potential with an oncogene (viral or cellular) and/or telomerase, and the subsequent emergence of cells that continue to proliferate. Primary cells, on the contrary, will generally require the introduction of oncogenes and/or telomerase to generate cells that have enhanced growth potential or are immortal. To develop cell lines from individuals with specific inherited disorders, with exception of inherited diseases with a predisposition for cancer, it is usually necessary to begin with primary cells from the organ of interest, for example, the organ that manifests a prominent disease pathology.

26.3.1. Generation, Isolation, and Characterization

26.3.1.1. Primary Cultures

Since the human airway epithelial cells will be used as a paradigm for the transformation of different cell lines, the following descriptions will focus on primary airway epithelial cells. The generation and isolation of an immortalized cell line is relatively straightforward, but requires attention to detail. Generally, primary cultures of cells are isolated from tissue using mechanical and/or enzymatic cellular dissociation protocols [21, 88–90] (Appendix 1).

TRANSFORMATION PROTOCOL

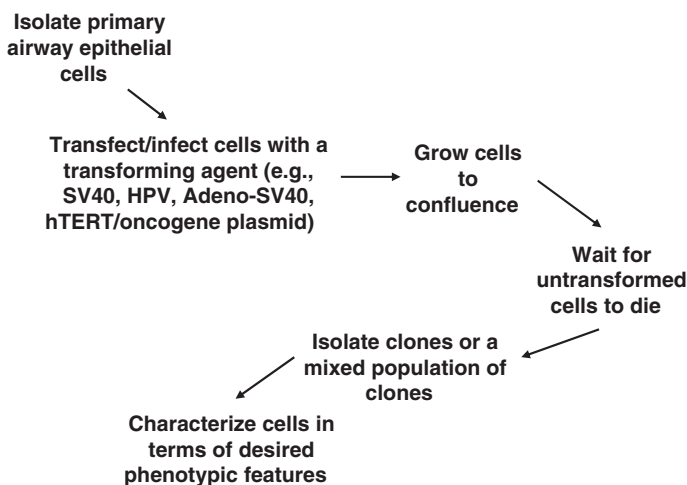


Figure 26.2 Transformation protocol algorithm. The steps required to generate transformed/immortalized cells and ensure that the cells have the appropriate phenotypic characteristics for the studies intended.

All airway tissue is washed several times in phosphate buffered saline (PBS) containing antibiotics and dithiothreitol (DTT) to remove microorganisms and mucus. Tracheal and bronchial epithelial cultures can then be initiated either from tissue explants or by an overnight enzymatic dissociation of epithelial strips [88, 89]. If the tissue samples are small, it is necessary to initiate the cultures from tissue explants. However, initiating cultures by enzymatic dissociation is generally preferable both in terms of time and yield. It is important that exposure to serum-containing medium is minimized and that the cells are grown in serum-free medium, since the presence of transforming growth factor- β (TGF- β) from blood-derived serum in the growth medium enhances the growth of contaminating fibroblasts and stimulates squamous differentiation of the epithelial cells [91]. Therefore, primary cultures are grown in serum-free LHC-8 medium that has been slightly modified (MLHC-8e) [92]. Not only is this medium serum free, but it also has low calcium levels that will mitigate squamous or terminal differentiation. This medium has also been successfully used to grow airway epithelial cells from other species. The growth medium used for primary cultures of epithelial cells or for cells of other lineages will vary and needs to be determined either empirically or by surveying the literature.

Another key element in the generation of primary cultures is the extracellular matrix (ECM) upon which the cells are grown. While many cells will grow on tissue culture plastic, the composition of the ECM is a critical element in the activation of second messenger pathways that influence the expression of differentiated characteristics and/or the expression of cell type-specific genes. A standard ECM used for the routine culture of airway epithelial cells that maintains many airway epithelial ion transport and cell polarity features is a liquid coating that contains human fibronectin/Vitrogen/bovine serum albumin (BSA, Fraction V) (FN/V/BSA) [88, 93]. While the cells can be grown on plastic or using other matrices, it will be important to verify that the desired differentiated endpoints are maintained over time. Clearly, the culture conditions, including the growth medium, will help define the characteristics that a cell expresses.

When subculturing the cells, a trypsin/versine solution containing ethylene glycol tetraacetic acid (EGTA) and polyvinylpyrrolidone (PET) is used to detach the cells. The PET helps stabilize the plasma membrane after trypsin damage and will enhance cell viability. Cells should not be allowed to remain at confluence for more than 24 h, since this will trigger terminal differentiation and lead to poor viability following trypsinization. In general, cultures that are 70–90% confluent will yield the highest number of viable proliferating cells following trypsinization. Because the growth medium is serum free, it is important to neutralize the trypsin-containing cell suspension with serum-containing growth medium. The cells can then be pelleted by centrifugation and resuspended for plating.

A critical feature for the generating transformed and immortalized cells from primary culture is the ability of the primary cell to proliferate. Whether the transforming agent is an infectious virus, a viral vector, or an expression vector containing an oncogene, the cells' ability to undergo at least one cell division appears to be a prerequisite for subsequent transformation and immortalization. Therefore, primary cells that have limited or reduced proliferative potential are generally not ideal for initiating transformed and immortalized cells. Cultures

that have been subcultured numerous times will be more recalcitrant to being transformed or immortalized. In addition, using confluent cultures of cells is generally minimally (if at all) effective at generating cell lines. Transfecting the cells at 70–80% confluence will usually give a sufficient yield of clones that are transformed and have enhanced growth properties.

26.3.1.2. *Transfection and Isolation of Transformants*

After pure cultures of epithelial cells are established, the cells are generally grown to 70–90% confluence before the introduction of the transforming gene(s). These genes can be introduced either through a viral transduction/infection process or by a physical or chemical transfection protocol [94]. While there are advantages of using viral systems (either naturally occurring or recombinant) to deliver a transforming gene, there are also limitations inherent virus preparation and recombinant viral vector construction that make transfection of expression plasmids by chemical or physical means an attractive alternative approach for gene delivery.

The various transfection methods that have been employed to deliver plasmid-based transformation systems into cells include, but are not limited to, physical methods such as electroporation [95] and microinjection [96] as well as the chemically based transfection systems such as calcium phosphate [21, 72, 75] (Appendices 2 and 3), strontium phosphate [69, 97] (Appendix 4), cationic lipids [98] (e.g., Lipofectin [99], Lipofectamine [100], polyamidoamine dendrimers [101, 102], polyethylenimine [103–106], and poly-L-lysine conjugates [107–109]). Although there are a number of chemical transfection reagents that have been developed, the classical calcium phosphate precipitation (CaPO_4 ppt) transfection protocol has been highly effective for stable transfection of primary cells and generating colonies of transformed/immortalized airway epithelial cells [16, 21, 72, 74–77, 94]. Ultimately, the best transfection system for any given cell type will need to be determined empirically, keeping in mind that an agent that is effective for transient transfection may not be the most appropriate for the stable transfections required in cell transformation.

Primary epithelial cells should be grown on 100 mm Petri dishes (Falcon) in MLHC-8e medium to ~70–80% confluence and then transfected (Figure 26.3). They are grown on dishes to facilitate the isolation of individual clones. Because the efficiency of transformation decreases with passage number [110, 111] (unpublished observations), cells up to passage 4 can be routinely used for transfection. Growth medium is replaced with 5 ml hypotonic Dulbecco's modified Eagle's medium (DMEM) diluted 6:5.5 with sterile H_2O [21] to facilitate cell swelling and increase the plasma membrane area. Calcium phosphate (CaPO_4)/DNA precipitate is prepared by initially making a DNA/ CaCl_2 solution (Appendix 2). The dropwise addition of 250 μl of a 2 \times HEPES buffered saline (HBS) solution (280 mM NaCl, 50 mM HEPES, 1.5 mM $\text{Na}_2\text{HPO}_4 \cdot 7\text{H}_2\text{O}$, pH 7.1) into the CaCl_2 /DNA solution while concurrently bubbling sterile air through the solution generates a small particulate precipitate. The CaPO_4 /DNA precipitate forms within 10–15 min at room temperature. The solution containing the precipitate can then be added dropwise (0.5 ml per 100 mm culture dish) to the hypotonic medium and evenly dispersed throughout the dish. Cultures are incubated at 37°C under 5% CO_2 in air for 3–4 h. The transfection solution is removed and the cultures washed three

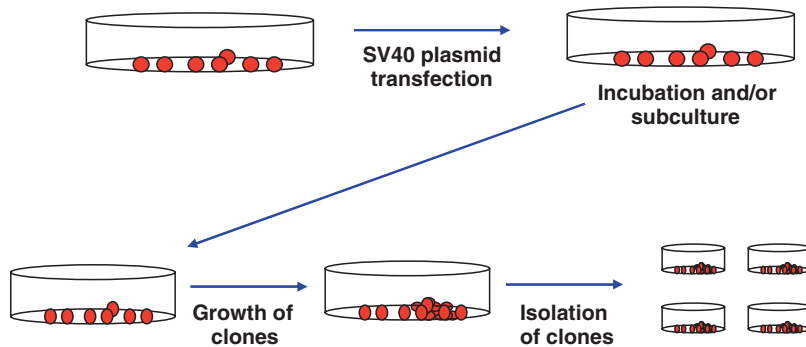


Figure 26.3 Schematic representation of the steps involved in generating clonal isolates of transformed cells. Cells that are not transformed will terminally differentiate and die, while clonal growths of transformed cells will continue to proliferate and expand on the dish. Individual clones are isolated using “cloning rings” (glass cylinders that are ~1 cm in diameter). Clones can also be pooled if it is desirable to have a population of transformed cells with a mixed origin (*See also* color insert).

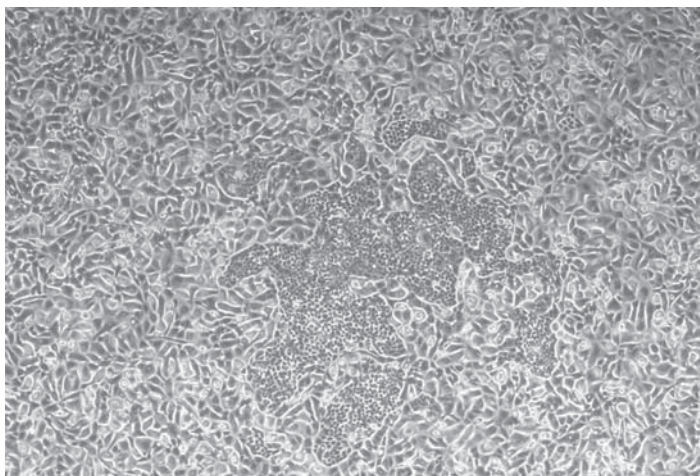


Figure 26.4 Typical colony of transformed airway epithelial cells. The formation of a high density colony growing in a monolayer of non-transformed cells 1 week after transfection ([21], Figure 26.1A). After several weeks, the non-transformed cells die and come off the dish.

to five times with LHC basal medium until no precipitate is microscopically detectable. Washed cultures are then grown in MLHC-8e medium until cells with altered growth characteristics appear [13, 16, 21] (Figure 26.4).

As an alternative to the chemical transfection systems, the primary cells can be effectively transfected by electroporation (Appendix 5). Amaxa has developed a “nucleofection” (electroporation) system that is very effective for delivering expression vectors into cells at high efficiency and low cellular mortality. The step-by-step conditions for the transfection of numerous primary cell types, including human airway epithelial cells, can be found at <http://www.amaxa.com/primary-cells.html>.

Colonies of transformants are most effectively isolated enzymatically with “cloning rings.” Cloning rings are sterile glass cylinders ~1 cm in diameter.

The glass circle at one opening of the cloning ring is coated with sterile vacuum grease so that the glass will form a liquid impermeable seal when it is placed on the Petri dish around a clone of cells. Prior to placing the cloning ring on the dish, the growth medium is removed and the cells are washed with HBS [92, 93] or PBS. A cloning ring is placed around individual colonies and the cylinder is filled with trypsinization solution. When the cells in the colony “round up,” they can be removed by a few cycles of aspiration and expulsion of the trypsin solution with a Pasteur pipette. It is important to grow the cultures on Petri dishes for easy access to individual clones unless the clones are pooled and grown as a mixed population. Individual clones can then be expanded for further characterization and cryopreservation [88] (Figure 26.2).

26.3.1.3. Characterization of Transformed/Immortalized Cells

The characterization of the cells isolated after transformation with a gene that alters the proliferative properties of the primary cells is approached at several different levels. The first stage is the verification that the cells are transformed and have altered growth properties when compared with primary cells. The next stage is the verification that the transformed cells are epithelial in origin. Finally, the cells can be characterized for specific genotypic and/or phenotypic endpoints that are of interest.

With epithelial cells it is relatively straightforward to verify that the cells are transformed and have altered growth properties [13, 15, 16, 19], since the primary cells will die and come off the dish after being maintained at confluence for an extended period. The transformed cells will continue to proliferate and have a small punctate morphology distinct from the residual larger terminally differentiated primary cells (Figure 26.4). The other marker that can be used for verifying that the cells are transformed is the expression of the transforming transgene. In the case of SV40 or the pSVori- plasmid, the SV40 large T antigen can be assayed by immunocytochemical staining, western-blot hybridization, and/or by measuring mRNA [13, 16, 112].

The determination of whether a transformed cell is immortalized is not as straightforward as determining whether a cell has enhanced growth properties. The process of immortalization is often accompanied by a “crisis” event [13, 113]. When the cells go into crisis, the majority of the cells will die and a subpopulation of cells will emerge that continues to proliferate. These proliferating cells will generally be immortal.

The next stage in the characterization of the transformed cells is the verification of their origin, for example, whether they are epithelial in origin. The hallmarks of epithelial origin such as cytokeratin filaments, tight junction formation, and cell polarity can be assessed immunocytochemically (e.g., Appendix 4), by electron microscopy, and/or electrophysiologically. Cells are generally fixed on well slides and assayed for epithelial-specific cytokeratin (keratin-18) and junctional complex (ZO-1 or E-cadherin) antigens [21, 72, 74, 76, 77, 114–117] (Figure 26.5). The presence of these features will confirm epithelial origin. Other cell type-specific markers can be assayed if the transformed cells are not of epithelial origin.

The final stage in the characterization of a transformed cell line is an extension of the verification of epithelial origin and likely the most relevant in assessing the usefulness of a given cell line for the study of features and pathways associated with differentiated functions. The cells can be evaluated

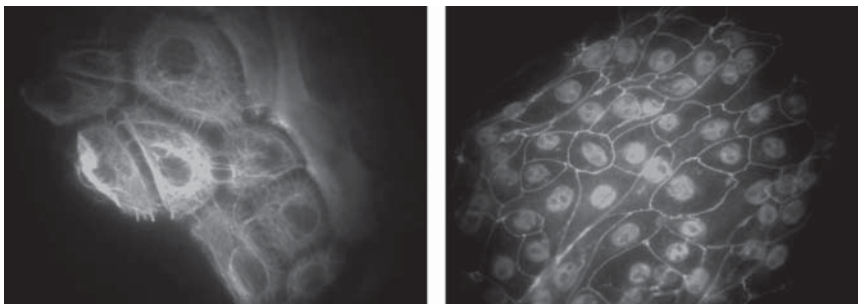


Figure 26.5 Immunofluorescent staining for transformed airway epithelial cells with antibodies specific for (A) keratin 18 (a marker of epithelial cells) and (B) ZO-1 (marker of tight junction formation). Both markers indicate that the cells have retained epithelial characteristics after transformation. The staining for the presence of ZO-1 at the periphery of the cells indicates that the cells have not lost their polarity and can form “tight” monolayers that will generate a transepithelial resistance. This is a particularly attractive feature for the analysis of ion transport and transcellular transport of macromolecules. ZO-1 is also found in the nucleus and can also be detected by the anti-ZO-1 antibody.

in terms of gene expression, secretory properties, intracellular organelles and trafficking, cell surface proteins, and ion transport characteristics [13, 15, 16, 21, 72, 74–77, 79, 114, 116–128].

Another important feature of the transformed/immortalized cells is their karyotype. While in the early stages of transformation, most of the cells will retain a near diploid karyotype. However, once the cells have gone through a crisis event or are growing well beyond the typical crisis period (~15–30 subcultures), they are aneuploid with a characteristic distribution of individual chromosomes, that is, there are likely to be multiple copies of specific chromosomes while others are not cytogenetically detectable.

26.4. Summary

The *in vitro* transformation of human epithelial cells has important implications for both epithelial cell and cancer biology. Numerous approaches have been tried for the induction of epithelial cell transformation, but the most effective schemes rely on the transfer of viral oncogenes into the host epithelial cell [13, 14, 18, 38, 39, 41, 43, 84, 129–139]. Since the use of an infectious virus can lead to complications such as background viral replication, other delivery systems have been developed that introduce viral oncogenes in expression plasmid or as recombinant non-replication viruses [94]. There have been a number of chemical and physical methods developed to deliver DNA into cells, although not all of them have proven efficacious for generation of stably transfected epithelial cell lines. Furthermore, there are subtle nuances that can be manipulated to facilitate transfection efficacy and cell viability using a specific technique. While CaPO_4 ppt has been shown to cause lysis and squamous differentiation of epithelial cells if specific protocols are not adhered to [97], this technique can be successfully used without adverse effects [21, 72, 74–77, 140].

Transformation/immortalization of epithelial cells is correlated with the neoplastic process [16]. The change in the growth properties of the transformed/immortalized cells as they progress neoplastically can indicate how neoplasia is regulated in the context of the expression of specific genes. These cell systems can also facilitate an understanding of the role that oncogenes play in the regulation of differentiated functions [141–149]. Numerous oncogenes including *myc*, *fos*, and TGF- β have been implicated in differentiation [141, 150–154], and *ras* has been associated with the degranulation of mast cells [155, 156], indicating a possible role in secretion. There is also a strong correlation between SV40 large T antigen transformation and the maintenance of differentiated functions in epithelial cells [13, 16, 21, 40, 42, 53, 69, 74, 76, 77, 85, 112, 142, 143, 157–163] that can be further manipulated using a temperature-sensitive mutant of the SV40 large T antigen [19, 43, 92, 131, 144, 164–172].

There appears to be no difference in the frequency of transformation/immortalization of epithelial cells from different organs using a specific transforming gene and the sample DNA delivery system [13, 16, 19]. However, factors such as cell type, the DNA delivery system, plasmid concentration, genetic background, and/or the transforming gene(s) can influence the frequency of obtaining colonies of transformed/immortalized cells.

As outlined above, there are multiple steps that will result in transformed or immortalized cells, and although many of these steps seem trivial, they must be carefully adhered to or addressed if the goal of a transformed/immortalized cell line with specific phenotypic characteristics is to be achieved. In brief, the choice of the transformation system and its compatibility with the cells to be transformed is critical. In general, the SV40 systems, whether live virus, replication defective virus, or individual oncogenes, has proven to be one of the most versatile having a broad cell type host range. There are some cell systems, such as the hematopoietic cells, that tend to be refractory to SV40 transformation, and must rely on other virus systems, such as the Epstein-Barr virus (EBV) [14]. Another key factor is the primary cells and the state that those cells are in before the transforming agent is introduced. The degree of confluence of the cells is important to ensure that there are cells within the population that are still proliferating [88, 173]. Cells that are at 60–80% confluence are generally the best. Passage number is also an important element, since cells that are close to senescence or terminal differentiation are also more refractory to transformation. With epithelial cells, in particular, this is very important, because the cells readily undergo squamous differentiation at later passages and if they are either too confluent or too sparse. With respect to the maintenance of phenotypic characteristics, specific phenotypes can be maintained by exposing the cells to serum-containing medium containing high (1 mM) Ca^{2+} and/or various cytokines, hormones, or growth factors (e.g., retinoic acid, dexamethasone or hydrocortisone, epidermal growth factor, and fibronectin). Finally, the ECM will play a role throughout the growth of epithelial cells from primary [88, 173] to immortalized cells [13, 16, 143]. Primary epithelial cells require ECM to prevent squamous differentiation [88, 93, 173, 174], while transformed and immortalized cells require the ECM to minimize the loss of differentiated features [13, 16, 143]. The specific ECM required for a given cell type and for the maintenance of specific phenotypic characteristics has either already

been determined and can be found by reviewing the literature, or needs to be determined empirically.

Most transformed cells will undergo crisis before they become immortalized [21, 36, 41, 113, 175–182]. This event has to some extent been mitigated, albeit not completely eliminated, by the use of hTERT as a cotransforming gene [137, 183–186]. Because there are numerous genetic changes that need to occur to result in immortalization [41, 66, 183, 187–190], it is important that the cells are grown for extended periods (generally >150–200 generations) to ascertain whether they are in fact immortalized. Once the cells have gone through a crisis event, it will be important to reevaluate them in the context of the desired phenotypic endpoints. The phenotype can vary after the cells go through crisis because of changes in karyotype and/or the concomitant loss of genes associated with regulating immortalization or phenotype.

The maintenance of desired phenotypic features over multiple generations will need to be periodically evaluated. If a feature is unstable over the experimental period, it will be necessary to evaluate other clones or generate new clones. If the phenotype changes as a result of multiple subcultures, earlier passages can be thawed (if they have been appropriately generated and stored) and utilized appropriately. Once the immortalized clones have been established and characterized for desired phenotypic features, they can then be used for numerous biochemical, molecular biological, and pharmacological studies.

Acknowledgments: The authors acknowledge all those researchers who over the years have contributed to the wealth of data that has made it possible to develop immortalized human cells from a myriad of tissues. These cell systems have been and are still the underpinnings of in vitro research on human systems, and continue to be an important factor in our understanding of cell function, neoplastic progression and cancer, genetic diseases, and biological systems as well as in the development of novel therapies. This manuscript would not be possible without their efforts. Our regret is that we could not survey and reference everyone's work.

References

1. Hayflick, L. 1974. The strategy of senescence. *Gerontologist* 14(1):37–45.
2. Hayflick, L. 1974. The longevity of cultured human cells. *J Am Geriatr Soc* 22(1):1–12.
3. Hayflick, L. 1979. Cell biology of aging. *Fed Proc* 38(5):1847–50.
4. Hayflick, L. 1998. A brief history of the mortality and immortality of cultured cells. *Keio J Med* 47(3):174–82.
5. Chaudhari, B. R., R. F. Murphy, and D. K. Agrawal. 2006. Following the TRAIL to apoptosis. *Immunol Res* 35(3):249–62.
6. Romer, L., C. Klein, A. Dehner, H. Kessler, and J. Buchner. 2006. p53—a natural cancer killer: Structural insights and therapeutic concepts. *Angew Chem Int Ed Engl* 45(39):6440–60.
7. Szegezdi, E., S. Cahill, M. Meyer, M. O'Dwyer, and A. Samali. 2006. TRAIL sensitisation by arsenic trioxide is caspase-8 dependent and involves modulation of death receptor components and Akt. *Br J Cancer* 94(3):398–406.
8. Du, G. J., H. H. Lin, Q. T. Xu, and M. W. Wang. 2006. Bcl-2 switches the type of demise from apoptosis to necrosis via cyclooxygenase-2 upregulation in HeLa cell induced by hydrogen peroxide. *Cancer Lett* 232(2):179–88.

9. Du, W., and J. Pogoriler. 2006. Retinoblastoma family genes. *Oncogene* 25(38):5190–200.
10. Henson, P. M., and D. A. Hume. 2006. Apoptotic cell removal in development and tissue homeostasis. *Trends Immunol* 27(5):244–50.
11. Festjens, N., T. Vanden Berghe, and P. Vandenabeele. 2006. Necrosis, a well-orchestrated form of cell demise: Signalling cascades, important mediators and concomitant immune response. *Biochim Biophys Acta* 1757(9–10):1371–87.
12. Festjens, N., S. Cornelis, M. Lamkanfi, and P. Vandenabeele. 2006. Caspase-containing complexes in the regulation of cell death and inflammation. *Biol Chem* 387(8):1005–16.
13. Gruenert, D. C., W. E. Finkbeiner, and J. H. Widdicombe. 1995. Culture and transformation of human airway epithelial cells. *Am J Physiol* 268(3 Pt 1):L347–60.
14. Gruenert, D. C., M. Willems, J. J. Cassiman, and R. A. Frizzell. 2004. Established cell lines used in cystic fibrosis research. *J Cyst Fibros* 3 Suppl 2:191–6.
15. Zabner, J., P. Karp, M. Seiler, S. L. Phillips, C. J. Mitchell, M. Saavedra, M. Welsh, and A. J. Klingelutz. 2003. Development of cystic fibrosis and non-cystic fibrosis airway cell lines. *Am J Physiol Lung Cell Mol Physiol* 284(5):L844–54.
16. Gruenert, D. C. 1987. Differentiated properties of human epithelial cells transformed *in vitro*. *BioTechniques* 5:740–50.
17. Fusenig, N. E., and P. Boukamp. 1998. Multiple stages and genetic alterations in immortalization, malignant transformation, and tumor progression of human skin keratinocytes. *Mol Carcinog* 23(3):144–58.
18. Namba, M., K. Mihara, and K. Fushimi. 1996. Immortalization of human cells and its mechanisms. *Crit Rev Oncog* 7(1–2):19–31.
19. Hopfer, U., J. W. Jacobberger, D. C. Gruenert, R. L. Eckert, P. S. Jat, and J. A. Whitsett. 1996. Immortalization of epithelial cells. *Am J Physiol* 270(1 Pt 1):C1–11.
20. Small, M. B., K. Hubbard, J. R. Pardinas, A. M. Marcus, S. N. Dhanaraj, and K. A. Sethi. 1996. Maintenance of telomeres in SV40-transformed pre-immortal and immortal human fibroblasts. *J Cell Physiol* 168(3):727–36.
21. Gruenert, D. C., C. B. Basbaum, M. J. Welsh, M. Li, W. E. Finkbeiner, and J. A. Nadel. 1988. Characterization of human tracheal epithelial cells transformed by an origin-defective simian virus 40. *Proc Natl Acad Sci USA* 85(16):5951–5.
22. Abraham, G., C. Kneuer, C. Ehrhardt, W. Honscha, and F. R. Ungemach. 2004. Expression of functional beta2-adrenergic receptors in the lung epithelial cell lines 16HBE14o-, Calu-3 and A549. *Biochim Biophys Acta* 1691(2–3):169–79.
23. Shen, B.-Q., W. E. Finkbeiner, J. J. Wine, R. J. Mrsny, and J. H. Widdicombe. 1994. Calu-3: A human airway epithelial cell line which shows cAMP-dependent Cl secretion. *Am J Physiol* 266:L493–501.
24. Stark, J. M., E. A. van, J. J. Zimmerman, S. K. Carabell, and M. F. Tosi. 1992. Detection of enhanced neutrophil adhesion to parainfluenza-infected airway epithelial cells using a modified myeloperoxidase assay in a microtiter format. *J Virol Methods* 40:225–42.
25. Gougat, C., D. Jaffuel, R. Gagliardo, C. Henriquet, J. Bousquet, P. Demoly, and M. Mathieu. 2002. Overexpression of the human glucocorticoid receptor alpha and beta isoforms inhibits AP-1 and NF-kappaB activities hormone independently. *J Mol Med* 80(5):309–18.
26. Blaine, S. A., M. Wick, C. Dessev, and R. A. Nemenoff. 2001. Induction of cPLA2 in lung epithelial cells and non-small cell lung cancer is mediated by Sp1 and c-Jun. *J Biol Chem* 276(46):42737–43.

27. Ogretmen, B., J. M. Kravaka, D. Schady, J. Usta, Y. A. Hannun, and L. M. Obeid. 2001. Molecular mechanisms of ceramide-mediated telomerase inhibition in the A549 human lung adenocarcinoma cell line. *J Biol Chem* 276(35):32506–14.
28. Lin, D. L., M. C. Whitney, Z. Yao, and E. T. Keller. 2001. Interleukin-6 induces androgen responsiveness in prostate cancer cells through up-regulation of androgen receptor expression. *Clin Cancer Res* 7(6):1773–81.
29. Tanaka, M., N. Inase, S. Miyake, and Y. Yoshizawa. 2001. Neuron specific enolase promoter for suicide gene therapy in small cell lung carcinoma. *Anticancer Res* 21(1A):291–4.
30. Winton, H. L., H. Wan, M. B. Cannell, D. C. Gruenert, P. J. Thompson, D. R. Garrod, G. A. Stewart, and C. Robinson. 1998. Cell lines of pulmonary and non-pulmonary origin as tools to study the effects of house dust mite proteinases on the regulation of epithelial permeability. *Clin Exp Allergy* 28(10):1273–85.
31. Rasola, A., L. J. Galletta, D. C. Gruenert, and G. Romeo. 1992. Ionic selectivity of volume-sensitive currents in human epithelial cells. *Biochim Biophys Acta* 1139(4):319–23.
32. Wagner, J. A., T. V. McDonald, P. T. Nghiem, A. W. Lowe, H. Schulman, D. C. Gruenert, L. Stryer, and P. Gardner. 1992. Antisense oligodeoxynucleotides to the cystic fibrosis transmembrane conductance regulator inhibit cAMP-activated but not calcium-activated chloride currents. *Proc Natl Acad Sci U S A* 89(15):6785–9.
33. Merlin, D., S. Sitaraman, X. Liu, K. Eastburn, J. Sun, T. Kucharzik, B. Lewis, and J. L. Madara. 2001. CD98-mediated links between amino acid transport and beta 1 integrin distribution in polarized columnar epithelia. *J Biol Chem* 276(42):39282–9.
34. Burrus, V., C. Bontemps, B. Decaris, and G. Guedon. 2001. Characterization of a novel type II restriction-modification system, Sth368I, encoded by the integrative element ICES_{St1} of *Streptococcus thermophilus* CNRZ368. *Appl Environ Microbiol* 67(4):1522–8.
35. Weinberg, R. A. 1982. Oncogenes of spontaneous and chemically induced tumors. *Adv Cancer Res* 36:149–63.
36. Steinberg, M. L., and V. Defendi. 1983. Transformation and immortalization of human keratinocytes by SV40. *J Invest Dermatol* 81(1 Suppl):131s–6s.
37. Gattoni-Celli, S., W. L. Hsiao, M. Lambert, P. Kirschmeier, and I. B. Weinstein. 1985. Genetic targets in multistage carcinogenesis. *Carcinog Compr Surv* 9:29–40.
38. DiPaolo, J. A., N. C. Popescu, L. Alvarez, and C. D. Woodworth. 1993. Cellular and molecular alterations in human epithelial cells transformed by recombinant human papillomavirus DNA. *Crit Rev Oncog* 4(4):337–60.
39. Rhim, J. S. 1993. Neoplastic transformation of human cells in vitro. *Crit Rev Oncog* 4(3):313–35.
40. Reddel, R. R., R. De Silva, E. L. Duncan, E. M. Rogan, N. J. Whitaker, D. G. Zahra, Y. Ke, M. G. McMenamin, B. I. Gerwin, and C. C. Harris. 1995. SV40-induced immortalization and ras-transformation of human bronchial epithelial cells. *Int J Cancer* 61(2):199–205.
41. Duncan, E. L., and R. R. Reddel. 1997. Genetic changes associated with immortalization. A review. *Biochemistry (Mosc)* 62(11):1263–74.
42. Kim, S. H., S. Banga, K. K. Jha, and H. L. Ozer. 1998. SV40-mediated transformation and immortalization of human cells. *Dev Biol Stand* 94:297–302.
43. Jha, K. K., S. Banga, V. Palejwala, and H. L. Ozer. 1998. SV40-Mediated immortalization. *Exp Cell Res* 245(1):1–7.
44. Chang, F., S. Syrjanen, K. Kurvinen, and K. Syrjanen. 1993. The p53 tumor suppressor gene as a common cellular target in human carcinogenesis. *Am J Gastroenterol* 88(2):174–86.

45. Emura, M., U. Mohr, T. Kakunaga, and J. Hilfrich. 1985. Growth inhibition and transformation of a human fetal tracheal epithelial cell line by long-term exposure of diethylnitrosamine. *Carcinogenesis* 6:1955–61.
46. Kraemer, P. M., F. A. Ray, A. R. Brothman, M. F. Bartholdi, and L. S. Cram. 1986. Spontaneous immortalization rate of cultured Chinese hamster cells. *J Natl Cancer Inst* 76(4):703–9.
47. Rong, S., S. Segal, M. Anver, J. H. Resau, and G. F. Vande Woude. 1994. Invasiveness and metastasis of NIH 3T3 cells induced by Met-hepatocyte growth factor/scatter factor autocrine stimulation. *Proc Natl Acad Sci USA* 91(11):4731–5.
48. Rong, S., and G. F. Vande Woude. 1994. Autocrine mechanism for met proto-oncogene tumorigenicity. *Cold Spring Harb Symp Quant Biol* 59:629–36.
49. Santos, E., E. P. Reddy, S. Pulciani, R. J. Feldmann, and M. Barbacid. 1983. Spontaneous activation of a human proto-oncogene. *Proc Natl Acad Sci USA* 80(15):4679–83.
50. Tavassoli, M., and S. Shall. 1988. Transcription of the c-myc oncogene is altered in spontaneously immortalized rodent fibroblasts. *Oncogene* 2(4):337–45.
51. Greenberg, R. A., R. C. Allsopp, L. Chin, G. B. Morin, and R. A. DePinho. 1998. Expression of mouse telomerase reverse transcriptase during development, differentiation and proliferation. *Oncogene* 16(13):1723–30.
52. Kuroki, T., and N. H. Huh. 1993. Why are human cells resistant to malignant cell transformation in vitro? *Jpn J Cancer Res* 84(11):1091–100.
53. Boukamp, P., R. T. Petrussevska, D. Breitkreutz, J. Hornung, A. Markham, and N. E. Fusenig. 1988. Normal keratinization in a spontaneously immortalized aneuploid human keratinocyte cell line. *J Cell Biol* 106(3):761–71.
54. Takahashi, K., Y. Sawasaki, J. Hata, K. Mukai, and T. Goto. 1990. Spontaneous transformation and immortalization of human endothelial cells. *In Vitro Cell Dev Biol* 26(3 Pt 1):265–74.
55. Noble, J. R., E. M. Rogan, A. A. Neumann, K. Maclean, T. M. Bryan, and R. R. Reddel. 1996. Association of extended in vitro proliferative potential with loss of p16INK4 expression. *Oncogene* 13(6):1259–68.
56. Hubbard-Smith, K., P. Patsalis, J. R. Pardinias, K. K. Jha, A. S. Henderson, and H. L. Ozer. 1992. Altered chromosome 6 in immortal human fibroblasts. *Mol Cell Biol* 12(5):2273–81.
57. Rice, R. H., K. E. Steinmann, L. A. deGraffenried, Q. Qin, N. Taylor, and R. Schlegel. 1993. Elevation of cell cycle control proteins during spontaneous immortalization of human keratinocytes. *Mol Biol Cell* 4(2):185–94.
58. Shay, J. W., G. Tomlinson, M. A. Piatyszek, and L. S. Gollahon. 1995. Spontaneous in vitro immortalization of breast epithelial cells from a patient with Li-Fraumeni syndrome. *Mol Cell Biol* 15(1):425–32.
59. Jones, S. N., A. T. Sands, A. R. Hancock, H. Vogel, L. A. Donehower, S. P. Linke, G. M. Wahl, and A. Bradley. 1996. The tumorigenic potential and cell growth characteristics of p53- deficient cells are equivalent in the presence or absence of Mdm2. *Proc Natl Acad Sci USA* 93(24):14106–11.
60. Kiyono, T., S. A. Foster, J. I. Koop, J. K. McDougall, D. A. Galloway, and A. J. Klingelutz. 1998. Both Rb/p16INK4a inactivation and telomerase activity are required to immortalize human epithelial cells [see comments]. *Nature* 396(6706):84–8.
61. Kaufmann, W. K., E. N. Levedakou, H. L. Grady, R. S. Paules, and G. H. Stein. 1995. Attenuation of G2 checkpoint function precedes human cell immortalization. *Cancer Res* 55(1):7–11.
62. Agiostratidou, G., A. Derventzi, and E. S. Gonos. 2001. Over-expression of CDKIs p15INK4b, p16INK4a and p21CIP1/WAF1 genes mediate growth arrest in human osteosarcoma cell lines. *In Vivo* 15(5):443–6.

63. De Luca, A., A. Baldi, V. Esposito, C. M. Howard, L. Bagella, P. Rizzo, M. Caputi, H. I. Pass, G. G. Giordano, F. Baldi, M. Carbone, and A. Giordano. 1997. The retinoblastoma gene family pRb/p105, p107, pRb2/p130 and simian virus-40 large T-antigen in human mesotheliomas. *Nat Med* 3(8):913–6.
64. Hara, E., R. Smith, D. Parry, H. Tahara, S. Stone, and G. Peters. 1996. Regulation of p16CDKN2 expression and its implications for cell immortalization and senescence. *Mol Cell Biol* 16(3):859–67.
65. Xiong, Y., H. Zhang, and D. Beach. 1993. Subunit rearrangement of the cyclin-dependent kinases is associated with cellular transformation. *Genes Dev* 7(8):1572–83.
66. Rogan, E. M., T. M. Bryan, B. Hukku, K. Maclean, A. C. Chang, E. L. Moy, A. Englezou, S. G. Warneford, L. Dalla-Pozza, and R. R. Reddel. 1995. Alterations in p53 and p16INK4 expression and telomere length during spontaneous immortalization of Li-Fraumeni syndrome fibroblasts. *Mol Cell Biol* 15(9):4745–53.
67. Willey, J. C., A. Broussoud, A. Sleemi, W. P. Bennett, P. Cerutti, and C. C. Harris. 1991. Immortalization of normal human bronchial epithelial cells by human papillomaviruses 16 or 18. *Cancer Res* 51(19):5370–7.
68. Yankaskas, J. R., J. E. Haizlip, M. Conrad, D. Koval, E. Lazarowski, A. M. Paradiso, C. J. Rinehart, B. Sarkadi, R. Schlegel, and R. C. Boucher. 1993. Papilloma virus immortalized tracheal epithelial cells retain a well-differentiated phenotype. *Am J Physiol* 264:C1219–30.
69. Reddel, R. R., Y. Ke, B. I. Gerwin, M. G. McMenamin, J. F. Lechner, R. T. Su, D. E. Brash, J. B. Park, J. S. Rhim, and C. C. Harris. 1988. Transformation of human bronchial epithelial cells by infection with SV40 or adenovirus-12 SV40 hybrid virus, or transfection via strontium phosphate coprecipitation with a plasmid containing SV40 early region genes. *Cancer Res* 48:1904–09.
70. Zeitlin, P. L., L. Lu, J. Rhim, G. Cutting, G. Stetten, K. A. Kieffer, R. Craig, and W. B. Guggino. 1991. A cystic fibrosis bronchial epithelial cell line: Immortalization by adeno-12-SV40 infection. *Am J Respir Cell Mol Biol* 4:313–9.
71. Small, M. B., Y. Gluzman, and H. L. Ozer. 1982. Enhanced transformation of human fibroblasts by origin-defective simian virus 40. *Nature* 296(5858):671–2.
72. Cozens, A. L., M. J. Yezzi, L. Chin, E. M. Simon, W. E. Finkbeiner, J. A. Wagner, and D. C. Gruenert. 1992. Characterization of immortal cystic fibrosis tracheobronchial gland epithelial cells. *Proc Natl Acad Sci USA* 89(11):5171–5.
73. Cozens, A. L., M. J. Yezzi, L. Chin, E. M. Simon, D. S. Friend, and D. C. Gruenert. 1991. Chloride ion transport in transformed normal and cystic fibrosis epithelial cells. *Adv Exp Med Biol* 290:187–94; discussion 194–6.
74. Cozens, A. L., M. J. Yezzi, K. Kunzelmann, T. Ohri, L. Chin, K. Eng, W. E. Finkbeiner, J. H. Widdicombe, and D. C. Gruenert. 1994. CFTR expression and chloride secretion in polarized immortal human bronchial epithelial cells. *Am J Respir Cell Mol Biol* 10(1):38–47.
75. Cozens, A. L., M. J. Yezzi, M. Yamaya, D. Steiger, J. A. Wagner, S. S. Garber, L. Chin, E. M. Simon, G. R. Cutting, P. Gardner, and et al. 1992. A transformed human epithelial cell line that retains tight junctions post crisis. *In Vitro Cell Dev Biol* 28A (11–12):735–44.
76. Kunzelmann, K., D. C. Lei, K. Eng, L. C. Escobar, T. Koslowsky, and D. C. Gruenert. 1995. Epithelial cell specific properties and genetic complementation in a delta F508 cystic fibrosis nasal polyp cell line. *In Vitro Cell Dev Biol Anim* 31(8):617–24.
77. Kunzelmann, K., E. M. Schwiebert, P. L. Zeitlin, W. L. Kuo, B. A. Stanton, and D. C. Gruenert. 1993. An immortalized cystic fibrosis tracheal epithelial cell line homozygous for the delta F508 CFTR mutation. *Am J Respir Cell Mol Biol* 8(5):522–9.

78. Hahn, W. C., S. K. Dessain, M. W. Brooks, J. E. King, B. Elenbaas, D. M. Sabatini, J. A. DeCaprio, and R. A. Weinberg. 2002. Enumeration of the simian virus 40 early region elements necessary for human cell transformation. *Mol Cell Biol* 22(7):2111–23.
79. Lundberg, A. S., S. H. Randell, S. A. Stewart, B. Elenbaas, K. A. Hartwell, M. W. Brooks, M. D. Fleming, J. C. Olsen, S. W. Miller, R. A. Weinberg, and W. C. Hahn. 2002. Immortalization and transformation of primary human airway epithelial cells by gene transfer. *Oncogene* 21(29):4577–86.
80. James, M. A., J. H. Lee, and A. J. Klingelutz. 2006. Human papillomavirus type 16 E6 activates NF-kappaB, induces cIAP-2 expression, and protects against apoptosis in a PDZ binding motif-dependent manner. *J Virol* 80(11):5301–7.
81. Piao, C. Q., L. Liu, Y. L. Zhao, A. S. Balajee, M. Suzuki, and T. K. Hei. 2005. Immortalization of human small airway epithelial cells by ectopic expression of telomerase. *Carcinogenesis* 26(4):725–31.
82. Vaughan, M. B., R. D. Ramirez, W. E. Wright, J. D. Minna, and J. W. Shay. 2006. A three-dimensional model of differentiation of immortalized human bronchial epithelial cells. *Differentiation* 74(4):141–8.
83. Cerni, C. 2000. Telomeres, telomerase, and myc. An update. *Mutat Res* 462(1):31–47.
84. Harley, C. B. 2002. Telomerase is not an oncogene. *Oncogene* 21(4):494–502.
85. Toouli, C. D., L. I. Huschtscha, A. A. Neumann, J. R. Noble, L. M. Colgin, B. Hukku, and R. R. Reddel. 2002. Comparison of human mammary epithelial cells immortalized by simian virus 40 T-Antigen or by the telomerase catalytic subunit. *Oncogene* 21(1):128–39.
86. Yang, J., E. Chang, A. M. Cherry, C. D. Bangs, Y. Oei, A. Bodnar, A. Bronstein, C. P. Chiu, and G. S. Herron. 1999. Human endothelial cell life extension by telomerase expression. *J Biol Chem* 274(37):26141–8.
87. Zhang, A., C. Zheng, M. Hou, C. Lindvall, K. L. Wallin, T. Angstrom, X. Yang, A. C. Hellstrom, E. Blennow, M. Bjorkholm, A. Zetterberg, A. Gruber, and D. Xu. 2002. Amplification of the telomerase reverse transcriptase (hTERT) gene in cervical carcinomas. *Genes Chromosomes Cancer* 34(3):269–75.
88. Gruenert, D. C., C. B. Basbaum, and J. H. Widdicombe. 1990. Long-term culture of normal and cystic fibrosis epithelial cells grown under serum-free conditions. *In Vitro Cell Dev Biol* 26(4):411–8.
89. Widdicombe, J. H. 1990. Use of cultured airway epithelial cells in studies of ion transport. *Am J Physiol* 258:L13–8.
90. Widdicombe, J. H., D. L. Coleman, W. E. Finkbeiner, and I. Tuet. 1985. Electrical properties of monolayers cultured from cells of human tracheal mucosa. *J Appl Physiol* 58:1729–35.
91. Masui, T., L. M. Wakefield, J. F. Lechner, M. A. LaVeck, M. B. Sporn, and C. C. Harris. 1986. Type β transforming growth factor is the primary differentiation-inducing serum factor for normal human bronchial epithelial cells. *Proc Natl Acad Sci USA* 83:2438–42.
92. Gruenert, D. C., L. Chin, E. M. Simon, and A. L. Cozens. 1990. Transformation of human airway epithelial cells with a plasmid containing a temperature-sensitive SV40 T antigen. *Ped Pulmonol Suppl* 5:146.
93. Lechner, J. F., and M. A. LaVeck. 1985. A serum-free method for culturing normal human bronchial epithelial cells at clonal density. *J Tissue Culture Methods* 9:43–8.
94. Colosimo, A., K. K. Goncz, A. R. Holmes, K. Kunzelmann, G. Novelli, R. W. Malone, M. J. Bennett, and D. C. Gruenert. 2000. Transfer and expression of foreign genes in mammalian cells. *Biotechniques* 29(2):314–8, 320–2, 324 passim.

95. Bednarz, J., M. Teifel, P. Friedl, and K. Engelmann. 2000. Immortalization of human corneal endothelial cells using electroporation protocol optimized for human corneal endothelial and human retinal pigment epithelial cells. *Acta Ophthalmol Scand* 78(2):130–6.
96. Pantel, K., A. Dickmanns, A. Zippelius, C. Klein, J. Shi, W. Hoechtlen-Vollmar, G. Schlimok, D. Weckermann, R. Oberneder, E. Fanning, and et al. 1995. Establishment of micrometastatic carcinoma cell lines: A novel source of tumor cell vaccines. *J Natl Cancer Inst* 87(15):1162–8.
97. Brash, D. E., R. R. Reddel, M. Quanrud, K. Yang, M. P. Farrell, and C. C. Harris. 1987. Strontium phosphate transfection of human cells in primary culture: Stable expression of the simian virus 40 large-T-antigen gene in primary human bronchial epithelial cells. *Mol Cell Biol* 7(5):2031–4.
98. Felgner, P. L., Y. J. Tsai, L. Sukhu, C. J. Wheeler, M. Manthorpe, J. Marshall, and S. H. Cheng. 1995. Improved cationic lipid formulations for in vivo gene therapy. *Ann N Y Acad Sci* 772:126–39.
99. Duan, D., Z. Yan, Y. Yue, W. Ding, and J. F. Engelhardt. 2001. Enhancement of muscle gene delivery with pseudotyped adeno-associated virus type 5 correlates with myoblast differentiation. *J Virol* 75(16):7662–71.
100. Takenouchi, T., Y. Iwamaru, M. Sato, T. Yokoyama, M. Shinagawa, and H. Kitani. 2007. Establishment and characterization of SV40 large T antigen-immortalized cell lines derived from fetal bovine brain tissues after prolonged cryopreservation. *Cell Biol Int* 31(1):57–64.
101. Dufes, C., J. M. Muller, W. Couet, J. C. Olivier, I. F. Uchegbu, and A. G. Schatzlein. 2004. Anticancer drug delivery with transferrin targeted polymeric chitosan vesicles. *Pharm Res* 21(1):101–7.
102. Arima, H., F. Kihara, F. Hirayama, and K. Uekama. 2001. Enhancement of gene expression by polyamidoamine dendrimer conjugates with alpha-, beta-, and gamma-cyclodextrins. *Bioconjug Chem* 12(4):476–84.
103. Kircheis, R., L. Wightman, and E. Wagner. 2001. Design and gene delivery activity of modified polyethylenimines. *Adv Drug Deliv Rev* 53(3):341–58.
104. Lemkine, G. F., and B. A. Demeneix. 2001. Polyethylenimines for in vivo gene delivery. *Curr Opin Mol Ther* 3(2):178–82.
105. Godbey, W. T., K. K. Wu, and A. G. Mikos. 1999. Poly(ethylenimine) and its role in gene delivery. *J Control Release* 60(2–3):149–60.
106. Pichon, C., C. Goncalves, and P. Midoux. 2001. Histidine-rich peptides and polymers for nucleic acids delivery. *Adv Drug Deliv Rev* 53(1):75–94.
107. Ravi Kumar, M., G. Hellenmann, R. F. Lockey, and S. S. Mohapatra. 2004. Nanoparticle-mediated gene delivery: State of the art. *Expert Opin Biol Ther* 4(8):1213–24.
108. Garnett, M. C. 1999. Gene-delivery systems using cationic polymers. *Crit Rev Ther Drug Carrier Syst* 16(2):147–207.
109. Liu, G., M. Molas, G. A. Grossmann, M. Pasumarthy, J. C. Perales, M. J. Cooper, and R. W. Hanson. 2001. Biological properties of poly-L-lysine-DNA complexes generated by cooperative binding of the polycation. *J Biol Chem* 276(37):34379–87.
110. Milo, G. E., I. Noyes, J. Donahoe, and S. Weisbrode. 1981. Neoplastic transformation of human epithelial cells in vitro after exposure to chemical carcinogens. *Cancer Res* 41(12 Pt 1):5096–102.
111. Milo, G. E., J. W. Oldham, R. Zimmerman, G. G. Hatch, and S. A. Weisbrode. 1981. Characterization of human cells transformed by chemical and physical carcinogens in vitro. *In Vitro* 17(8):719–29.

112. Yankaskas, J. R., and R. C. Boucher. 1990. Transformation of airway epithelial cells with persistence of cystic fibrosis or normal ion transport phenotypes. *Methods Enzymol* 192:565–71.
113. Girardi, A. J., F. C. Jensen, and H. Koprowski. 1965. Sv40-Induced transformation of human diploid cells: Crisis and recovery. *J Cell Physiol* 65: 69–83.
114. Ehrhardt, C., E. M. Collnot, C. Baldes, U. Becker, M. Laue, K. J. Kim, and C. M. Lehr. 2006. Towards an in vitro model of cystic fibrosis small airway epithelium: Characterisation of the human bronchial epithelial cell line CFBE41o. *Cell Tissue Res* 323(3):405–15.
115. Jetten, A. M. 1989. Multistep process of squamous differentiation in tracheo-bronchial epithelial cells in vitro: Analogy with epidermal differentiation. *Environ Health Perspect* 80:149–160.
116. Kammouni, W., B. Moreau, F. Becq, A. Saleh, A. Pavirani, C. Figarella, and M. D. Merten. 1999. A cystic fibrosis tracheal gland cell line, CF-KM4. Correction by adenovirus-mediated CFTR gene transfer. *Am J Respir Cell Mol Biol* 20(4):684–91.
117. Merten, M. D., W. Kammouni, W. Renaud, F. Birg, M. G. Mattei, and C. Figarella. 1996. A transformed human tracheal gland cell line, MM-39, that retains serous secretory functions. *Am J Respir Cell Mol Biol* 15(4):520–8.
118. Becq, F., M. D. Merten, M. A. Voelckel, M. Gola, and C. Figarella. 1993. Characterization of cAMP dependent CFTR-chloride channels in human tracheal gland cells. *FEBS Lett* 321:73–8.
119. Jefferson, D. M., J. D. Valentich, F. C. Marini, S. A. Grubman, M. C. Iannuzzi, H. L. Dorkin, M. Li, K. W. Klinger, and M. J. Welsh. 1990. Expression of normal and cystic fibrosis phenotypes by continuous airway epithelial cell lines. *Am J Physiol* 259:L496–505.
120. Jetten, A. M., J. R. Yankaskas, M. J. Stutts, N. J. Willumsen, and R. C. Boucher. 1989. Persistence of abnormal chloride conductance regulation in transformed cystic fibrosis epithelia. *Science* 244:1472–5.
121. Kunzelmann, K., S. Kathofer, A. Hipper, D. C. Gruenert, and R. Gregner. 1996. Culture-dependent expression of Na⁺ conductances in airway epithelial cells. *Pflugers Arch* 431(4):578–86.
122. Lo-Guidice, J. M., M. D. Merten, G. Lamblin, N. Porchet, M. C. Houvenaghel, C. Figarella, P. Roussel, and J. M. Perini. 1997. Mucins secreted by a transformed cell line derived from human tracheal gland cells. *Biochem J* 326(Pt 2): 431–7.
123. Scholte, B. J., M. Kansen, A. T. Hoogeveen, R. Willemse, J.-S. Rhim, A. W. M. Vander Kamp, and J. Bijman. 1989. Immortalization of nasal polyp epithelial cells from cystic fibrosis patients. *Exp Cell Res* 182:559–71.
124. Schoumacher, R. A., J. Ram, M. C. Iannuzzi, N. A. Bradbury, R. W. Wallace, C. T. Hon, D. R. Kelley, S. M. Schnid, F. B. Gelder, T. A. Rado, and R. A. Frizzell. 1990. A cystic fibrosis pancreatic adenocarcinoma cell line. *Proc Natl Acad Sci USA* 87:4012–6.
125. Schwiebert, E. M., F. Gesek, L. Ercolani, C. Wjasow, D. C. Gruenert, K. Karlson, and B. A. Stanton. 1994. Heterotrimeric G proteins, vesicle trafficking, and CFTR Cl⁻ channels. *Am J Physiol* 267(1 Pt 1):C272–81.
126. Schwiebert, E. M., D. C. Gruenert, W. B. Guggino, and B. A. Stanton. 1995. G protein G alpha i-2 inhibits outwardly rectifying chloride channels in human airway epithelial cells. *Am J Physiol* 269(2 Pt 1):C451–6.
127. Schwiebert, E. M., N. Kizer, D. C. Gruenert, and B. A. Stanton. 1992. GTP-binding proteins inhibit cAMP activation of chloride channels in cystic fibrosis airway epithelial cells. *Proc Natl Acad Sci USA* 89(22):10623–7.

128. Shen, B. Q., R. A. Barthelson, W. Skach, D. C. Gruenert, E. Sigal, R. J. Mrsny, and J. H. Widdicombe. 1993. Mechanism of inhibition of cAMP-dependent epithelial chloride secretion by phorbol esters. *J Biol Chem* 268(25):19070–5.
129. Baserga, R., C. Sell, P. Porcu, and M. Rubini. 1994. The role of the IGF-I receptor in the growth and transformation of mammalian cells. *Cell Prolif* 27(2): 63–71.
130. Bocchetta, M., I. Di Resta, A. Powers, R. Fresco, A. Tosolini, J. R. Testa, H. I. Pass, P. Rizzo, and M. Carbone. 2000. Human mesothelial cells are unusually susceptible to simian virus 40-mediated transformation and asbestos cocarcinogenicity. *Proc Natl Acad Sci USA* 97(18):10214–9.
131. Bryan, T. M., and R. R. Reddel. 1994. SV40-induced immortalization of human cells. *Crit Rev Oncog* 5(4):331–57.
132. Cheng, R. Z., M. A. Shammass, J. Li, and R. J. Shmookler Reis. 1997. Expression of SV40 large T antigen stimulates reversion of a chromosomal gene duplication in human cells. *Exp Cell Res* 234(2):300–12.
133. Colgin, L. M., and R. R. Reddel. 1999. Telomere maintenance mechanisms and cellular immortalization. *Curr Opin Genet Dev* 9(1):97–103.
134. Cooper, G. M., and M. A. Lane. 1984. Cellular transforming genes and oncogenesis. *Biochim Biophys Acta* 738(1–2):9–20.
135. Coursen, J. D., W. P. Bennett, L. Gollahon, J. W. Shay, and C. C. Harris. 1997. Genomic instability and telomerase activity in human bronchial epithelial cells during immortalization by human papillomavirus-16 E6 and E7 genes. *Exp Cell Res* 235(1):245–53.
136. Galy, B., A. Maret, A. C. Prats, and H. Prats. 1999. Cell transformation results in the loss of the density-dependent translational regulation of the expression of fibroblast growth factor 2 isoforms. *Cancer Res* 59(1):165–71.
137. Halvorsen, T. L., G. Leibowitz, and F. Levine. 1999. Telomerase activity is sufficient to allow transformed cells to escape from crisis. *Mol Cell Biol* 19(3):1864–70.
138. Hayflick, L. 1997. Mortality and immortality at the cellular level. A review. *Biochemistry (Mosc)* 62(11):1180–90.
139. Rundell, K., and R. Parakati. 2001. The role of the SV40 ST antigen in cell growth promotion and transformation. *Semin Cancer Biol* 11(1):5–13.
140. Bruscia, E., F. Sangiuolo, P. Sinibaldi, K. K. Goncz, G. Novelli, and D. C. Gruenert. 2002. Isolation of CF cell lines corrected at DeltaF508-CFTR locus by SFHR-mediated targeting. *Gene Ther* 9(11):683–5.
141. Prins, J., E. G. De Vries, and N. H. Mulder. 1993. The myc family of oncogenes and their presence and importance in small-cell lung carcinoma and other tumour types. *Anticancer Res* 13(5A):1373–85.
142. Redies, C., U. Lendahl, and R. D. McKay. 1991. Differentiation and heterogeneity in T-antigen immortalized precursor cell lines from mouse cerebellum. *J Neurosci Res* 30(4):601–15.
143. Lechner, M. S., and L. A. Laimins. 1991. Human epithelial cells immortalized by SV40 retain differentiation capabilities in an in vitro raft system and maintain viral DNA extrachromosomally. *Virology* 185(2):563–71.
144. Quaroni, A., and J. F. Beaulieu. 1997. Cell dynamics and differentiation of conditionally immortalized human intestinal epithelial cells. *Gastroenterology* 113(4):1198–213.
145. Bernard, O., H. H. Reid, and P. F. Bartlett. 1989. Role of the c-myc and the N-myc proto-oncogenes in the immortalization of neural precursors. *J Neurosci Res* 24(1):9–20.
146. Blasi, E., B. J. Mathieson, L. Varesio, J. L. Cleveland, P. A. Borchert, and U. R. Rapp. 1985. Selective immortalization of murine macrophages from fresh bone marrow by a raf/myc recombinant murine retrovirus. *Nature* 318(6047):667–70.

147. Rein, A., J. Keller, A. M. Schultz, K. L. Holmes, R. Medicus, and J. N. Ihle. 1985. Infection of immune mast cells by Harvey sarcoma virus: Immortalization without loss of requirement for interleukin-3. *Mol Cell Biol* 5(9):2257–64.
148. Pfeifer, A. M., R. T. Jones, P. E. Bowden, D. Mann, E. Spillare, S. A. Klein, B. F. Trump, and C. C. Harris. 1991. Human bronchial epithelial cells transformed by the c-raf-1 and c-myc protooncogenes induce multidifferentiated carcinomas in nude mice: A model for lung carcinogenesis. *Cancer Res* 51:3793–3801.
149. Fontemaggi, G., A. Gurtner, S. Strano, Y. Higashi, A. Sacchi, G. Piaggio, and G. Blandino. 2001. The transcriptional repressor ZEB regulates p73 expression at the crossroad between proliferation and differentiation. *Mol Cell Biol* 21(24):8461–70.
150. Jotte, R. M., and J. T. Holt. 1996. Myristylation of FBR v-fos dictates the differentiation pathways in malignant osteosarcoma. *J Cell Biol* 135(2):457–67.
151. Merlie, J. P., M. E. Buckingham, and R. G. Whalen. 1977. Molecular aspects of myogenesis. *Curr Top Dev Biol* 11:61–114.
152. Ricciardi-Castagnoli, P., and P. Paglia. 1992. New tools for investigating macrophage differentiation. *Res Immunol* 143(1):101–6.
153. Stenvers, K. L., M. L. Tursky, K. W. Harder, N. Kountouri, S. Amatayakul-Chantler, D. Grail, C. Small, R. A. Weinberg, A. M. Sizeland, and H. J. Zhu. 2003. Heart and liver defects and reduced transforming growth factor beta2 sensitivity in transforming growth factor beta type III receptor-deficient embryos. *Mol Cell Biol* 23(12):4371–85.
154. Ugai, H., H. O. Li, M. Komatsu, H. Tsutsui, J. Song, T. Shiga, E. Fearon, T. Murata, and K. K. Yokoyama. 2001. Interaction of Myc-associated zinc finger protein with DCC, the product of a tumor-suppressor gene, during the neural differentiation of P19 EC cells. *Biochem Biophys Res Commun* 286(5):1087–97.
155. Nakamura, R., T. Furuno, and M. Nakanishi. 2006. The plasma membrane shuttling of CAPRI is related to regulation of mast cell activation. *Biochem Biophys Res Commun* 347(1):363–8.
156. Swaminathan, G., and A. Y. Tsygankov. 2006. The Cbl family proteins: Ring leaders in regulation of cell signaling. *J Cell Physiol* 209(1):21–43.
157. da Paula, A. C., A. S. Ramalho, C. M. Farinha, J. Cheung, R. Maurisse, D. C. Gruenert, J. Ousingawat, K. Kunzelmann, and M. D. Amaral. 2005. Characterization of novel airway submucosal gland cell models for cystic fibrosis studies. *Cell Physiol Biochem* 15(6):251–62.
158. Schwartz, B., P. Vicart, C. Delouis, and D. Paulin. 1991. Mammalian cell lines can be efficiently established in vitro upon expression of the SV40 large T antigen driven by a promoter sequence derived from the human vimentin gene. *Biol Cell* 73(1):7–14.
159. Quissell, D. O., K. A. Barzen, D. C. Gruenert, R. S. Redman, J. M. Camden, and J. T. Turner. 1997. Development and characterization of SV40 immortalized rat submandibular acinar cell lines. *In Vitro Cell Dev Biol Anim* 33(3):164–73.
160. Djelloul, S., M. E. Forgue-Lafitte, B. Hermelin, M. Mareel, E. Bruyneel, A. Baldi, A. Giordano, E. Chastre, and C. Gespach. 1997. Enterocyte differentiation is compatible with SV40 large T expression and loss of p53 function in human colonic Caco-2 cells. Status of the pRb1 and pRb2 tumor suppressor gene products. *FEBS Lett* 406(3):234–42.
161. DenBesten, P. K., C. Gao, W. Li, C. H. Mathews, and D. C. Gruenert. 1999. Development and characterization of an SV40 immortalized porcine ameloblast-like cell line. *Eur J Oral Sci* 107(4):276–81.
162. Barasch, J., B. Kiss, A. Prince, L. Saiman, D. Gruenert, and Q. al-Awqatiah. 1991. Defective acidification of intracellular organelles in cystic fibrosis [see comments]. *Nature* 352:70–3.

163. Gruenert, D. C., M. J. Yezzi, L. Chin, and A. L. Cozens. 1991. Immortalized cell cultures of CF-tissues as a tool to study ion transport properties. *In* G. Döring, R. Greger, D. Kaiser and J. Schmidtko, editors. *Mukoviszidose 1991:Ergebnisse aus Forschung und Klinik*. Forschungsgemeinschaft Mukoviszidose mit Kali-Chemie Pharma GmbH, Hannover. pp. 52–64.
164. Menck, C. F., C. Madzak, G. Renault, A. Margot, and A. Sarasin. 1989. SV40-based shuttle viruses. *Mutat Res* 220(2–3):101–6.
165. Yanai, N., T. Satoh, S. Kyo, K. Abe, M. Suzuki, and M. Obinata. 1991. A tubule cell line established from transgenic mice harboring temperature-sensitive simian virus 40 large T-antigen gene. *Jpn J Cancer Res* 82(12):1344–8.
166. Wynford-Thomas, D., J. A. Bond, F. S. Wyllie, J. S. Burns, E. D. Williams, T. Jones, D. Sheer, and N. R. Lemoine. 1990. Conditional immortalization of human thyroid epithelial cells: A tool for analysis of oncogene action. *Mol Cell Biol* 10(10):5365–77.
167. Radna, R. L., Y. Caton, K. K. Jha, P. Kaplan, G. Li, F. Traganos, and H. L. Ozer. 1989. Growth of immortal simian virus 40 tsA-transformed human fibroblasts is temperature dependent. *Mol Cell Biol* 9(7):3093–6.
168. Gruenert, D. C., M. J. Yezzi, L. Chin, and A. L. Cozens. 1991. Characterization of normal and cystic fibrosis airway epithelial cells transformed with a temperature-sensitive SV40 plasmid. *Ped Pulmonol Suppl* 6:(Abstr) 137.
169. O'Hare, M. J., J. Bond, C. Clarke, Y. Takeuchi, A. J. Atherton, C. Berry, J. Moody, A. R. Silver, D. C. Davies, A. E. Alsop, A. M. Neville, and P. S. Jat. 2001. Conditional immortalization of freshly isolated human mammary fibroblasts and endothelial cells. *Proc Natl Acad Sci USA* 98(2):646–51.
170. Jat, P. S., and P. A. Sharp. 1989. Cell lines established by a temperature-sensitive simian virus 40 large T antigen are growth restricted at the non-permissive temperature. *Mol Cell Biol* 9:1672–81.
171. Ray, S., M. E. Anderson, and P. Tegtmeier. 1996. Differential interaction of temperature-sensitive simian virus 40 T antigens with tumor suppressors pRb and p53. *J Virol* 70(10):7224–7.
172. Tabuchi, Y., S. Ohta, Y. Arai, M. Kawahara, K. Ishibashi, N. Sugiyama, T. Horiuchi, M. Furusawa, M. Obinata, H. Fuse, N. Takeguchi, and S. Asano. 2000. Establishment and characterization of a colonic epithelial cell line MCE301 from transgenic mice harboring temperature-sensitive simian virus 40 large T-antigen gene. *Cell Struct Funct* 25(5):297–307.
173. Lechner, J. F. 1984. Interdependent regulation of epithelial cell replication by nutrients, hormones, growth factors, and cell density. *Federation Proc* 43:116–120.
174. Lechner, J. F., A. Haugen, I. A. McClendon, and A. M. Shamsuddin. 1984. Induction of squamous differentiation of normal human bronchial epithelial cells by small amounts of serum. *Differentiation* 25:229–237.
175. Azuma, M., T. Tamatani, Y. Kasai, and M. Sato. 1993. Immortalization of normal human salivary gland cells with duct-, myoepithelial-, acinar-, or squamous phenotype by transfection with SV40 ori- mutant deoxyribonucleic acid. *Lab Invest* 69(1):24–42.
176. Bartek, J., J. Bartkova, N. Kyprianou, E. N. Lalani, Z. Staskova, M. Shearer, S. Chang, and J. Taylor-Papadimitriou. 1991. Efficient immortalization of luminal epithelial cells from human mammary gland by introduction of simian virus 40 large tumor antigen with a recombinant retrovirus. *Proc Natl Acad Sci USA* 88(9):3520–4.
177. Harms, W., T. Rothamel, K. Miller, G. Harste, M. Grassmann, and A. Heim. 2001. Characterization of human myocardial fibroblasts immortalized by HPV16 E6–E7 genes. *Exp Cell Res* 268(2):252–61.

178. Imai, S., F. Saito, T. Ikeuchi, K. Segawa, and T. Takano. 1993. Escape from in vitro aging in SV40 large T antigen-transformed human diploid cells: A key event responsible for immortalization occurs during crisis. *Mech Ageing Dev* 69(1–2):149–58.
179. Kano, Y., and J. B. Little. 1989. Efficient immortalization by SV40 T DNA of skin fibroblasts from patients with Wilms' tumor associated with chromosome 11p deletion. *Mol Carcinog* 2(6):314–21.
180. Khoo, N. K., J. F. Bechberger, T. Shepherd, S. L. Bond, K. R. McCrae, G. S. Hamilton, and P. K. Lala. 1998. SV40 Tag transformation of the normal invasive trophoblast results in a premalignant phenotype. I. Mechanisms responsible for hyperinvasiveness and resistance to anti-invasive action of TGFbeta. *Int J Cancer* 77(3):429–39.
181. Muruganandam, A., L. M. Herx, R. Monette, J. P. Durkin, and D. B. Stanimirovic. 1997. Development of immortalized human cerebromicrovascular endothelial cell line as an in vitro model of the human blood-brain barrier. *Faseb J* 11(13):1187–97.
182. Yokoyama, M., Y. Nakao, X. Yang, Q. Sun, K. Tsutsumi, A. Pater, and M. M. Pater. 1995. Alterations in physical state and expression of human papillomavirus type 18 DNA following crisis and establishment of immortalized ectocervical cells. *Virus Res* 37(2):139–51.
183. Counter, C. M., W. C. Hahn, W. Wei, S. D. Caddle, R. L. Beijersbergen, P. M. Lansdorp, J. M. Sedivy, and R. A. Weinberg. 1998. Dissociation among in vitro telomerase activity, telomere maintenance, and cellular immortalization. *Proc Natl Acad Sci USA* 95(25):14723–8.
184. MacKenzie, K. L., S. Franco, C. May, M. Sadelain, and M. A. Moore. 2000. Mass cultured human fibroblasts overexpressing hTERT encounter a growth crisis following an extended period of proliferation. *Exp Cell Res* 259(2):336–50.
185. Russo, I., A. R. Silver, A. P. Cuthbert, D. K. Griffin, D. A. Trott, and R. F. Newbold. 1998. A telomere-independent senescence mechanism is the sole barrier to Syrian hamster cell immortalization. *Oncogene* 17(26):3417–26.
186. Zhu, J., H. Wang, J. M. Bishop, and E. H. Blackburn. 1999. Telomerase extends the lifespan of virus-transformed human cells without net telomere lengthening [see comments]. *Proc Natl Acad Sci USA* 96(7):3723–8.
187. Belge, G., B. Kazmierczak, K. Meyer-Bolte, S. Bartnitzke, and J. Bullerdiek. 1992. Expression of SV40 T-antigen in lipoma cells with a chromosomal translocation T(3;12) is not sufficient for direct immortalization. *Cell Biol Int Rep* 16(4):339–47.
188. Kazmierczak, B., B. Thode, S. Bartnitzke, J. Bullerdiek, and W. Schloot. 1992. Pleomorphic adenoma cells vary in their susceptibility to SV40 transformation depending on the initial karyotype. *Genes Chromosomes Cancer* 5(1):35–9.
189. Perrotti, D., V. Cesi, R. Trotta, C. Guerzoni, G. Santilli, K. Campbell, A. Iervolino, F. Condorelli, C. Gambacorti-Passerini, M. A. Caligiuri, and B. Calabretta. 2002. BCR-ABL suppresses C/EBPalpha expression through inhibitory action of hnRNP E2. *Nat Genet* 30(1):48–58.
190. Peterson, S. R., D. M. Gadbois, E. M. Bradbury, and P. M. Kraemer. 1995. Immortalization of human fibroblasts by SV40 large T antigen results in the reduction of cyclin D1 expression and subunit association with proliferating cell nuclear antigen and Waf1. *Cancer Res* 55(20):4651–7.

Binding-Uptake Studies and Cellular Targeting

Franz Gabor and Michael Wirth

Abstract Targeted drug delivery to diseased tissues offers profound advantages for therapy, such as increased efficacy and reduced side effects. The development of targeted drug delivery systems is driven by different design considerations, selection of appropriate cell culture models, and analytical tools for their detection. Targeting cells relies on the hardware encoding biological information. Whereas a practical utility of the genetic code has not been reported until now, that of the peptide code represented by antibody-based concepts entered clinical trials and some products are already on the market. Recently, utility of the sugar code also became apparent as a promising alternative.

Special emphasis is placed on the carbohydrate-mediated cell – target system interaction by describing hints and pitfalls of assays for cytoadhesion, specificity, cytoinvasion, and cytoevasion. In addition, basic considerations are presented to discriminate between active and passive uptake as well as to detect lysosomal accumulation. Finally, the pros and cons of two useful analytical techniques, namely, flow cytometry and confocal laser scanning microscopy, are described in detail.

Keywords: Cytoadhesion; Cytoinvasion; Lectin; Confocal laser scanning microscopy; Flow cytometry; Uptake

Abbreviations

BSA	Bovine serum albumin
CLSM	Confocal laser scanning microscopy
EDTA	Ethylenediamine tetraacetic acid
EGFR	Epidermal growth factor receptor
FITC	Fluorescein isothiocyanate
FS	Forward scatter
IgG	Immunoglobulin G
PBS	Phosphate-buffered saline
PLGA	Poly(D,L-lactide-co-glycolide)
RFI	Relative cell-associated fluorescence intensity
SS	Side scatter

TEER	Transepithelial electrical resistance
TEM	Transmission electron microscopy
WGA	Wheat germ agglutinin

27.1. Introduction

Inspired by the opera “Der Freischütz,” the concept of “magic bullets” for treatment of diseases was proposed by Paul Ehrlich at the beginning of the last century [1]. As a mastermind of chemotherapy he recognized, at an early stage, the potential of targeted drug delivery to increase the efficacy and to reduce the side effects of therapy by site-specific action of drugs. Exactly 100 years later, the era of genomics, proteomics, and glycomics has accelerated progress in this field, but the feasibility of drug targeting still requires highly concerted efforts.

Representing one of the three different types of hardware encoding biological information, genomics are investigated for therapeutic utility using nonviral and, with decreasing popularity, viral vectors to deliver oligonucleotides, ribozymes, or DNA sequences directly into the target cell population [2]. For targeted drug delivery, however, a genomic-based concept has not been reported so far. Referring to proteomics, a different strategy for cellular targeting exploits the information content of membrane proteins and their cell type-dependent expression. The possibility to elicit antibodies recognizing an epitope of 5–10 amino acids, the high specificity of interaction, and the large pool of at least 1.35×10^8 antibodies with different specificity fostered the concept of immuno-targeting. Particularly, the hybridoma technology and the discovery of monoclonal antibodies in 1975 yield virtually unlimited quantities of antibodies of uniform specificity [3]. Their refining by further advances in biotechnology boosted this promising and sometimes dually effective approach to targeted therapy [4]. Most frequently, a certain cell membrane protein not only functions as a common marker for a particular cell population but also acts as a transmembrane receptor with intrinsic activity on intracellular signaling. That way the targeting effect and the pharmacological effect are mediated by the same molecule. To date, 17 monoclonal antibodies have been approved by the Food and Drug Administration (FDA) and about 148 monoclonal antibodies are in the pipeline, expanding the world market from \$5.4 billion in 2002 to an estimated \$16.7 billion in 2008. In addition to the genetic and the peptide code, the sugar code has recently gained attention. It relies on the observation that cell–cell interactions and cell-routing is governed by oligosaccharide sequences [5]. The trafficking of information is accomplished by the interplay of two partners, an oligosaccharide and a carbohydrate-binding protein termed lectin. Since the cell membrane contains particular oligosaccharide moieties as a part of the glycocalyx, as well as lectins, either a particular oligosaccharide moiety or a certain lectin can act as a homing device for targeted drug delivery systems. Interestingly, Fuc α 1-2Gal β -terminated antigens are overexpressed in colon carcinoma cells of the rat and vice versa neoglycoconjugates containing this disaccharide specifically interact with these cells, whereas non-tumor tissue and liver shows weak staining. This suggests overexpression of Fuc α 1-2Gal β -R-binding lectins upon malignant transformation. Moreover, these neoglycoconjugate-targeted systems might escape the hepatic first-pass metabolism after peroral administration [6].

Finally, also low molecular weight ligands can act as targeting moieties being non-immunogenic and requiring far less complex coupling procedures, compared with the above-mentioned molecules which all comprise delicate structural features. Among the few low molecular weight ligands known, the vitamin folic acid is a very promising candidate targeter. The folate receptor is overexpressed in activated macrophages and also on a high number of tumors, including those of the brain, colon, lung, ovaries, testes, and kidneys. Nonmalignant tissues, however, generally use other uptake pathways for the vitamin. Advantageously, folate receptor targeting additionally opens a receptor-mediated pathway for uptake of drug delivery systems into the cell [7].

27.1.1. Design of Targeted Drug Delivery Systems

Biorecognition is the key mechanism for active targeting of drugs or drug delivery systems to diseased organs, tissues, or even certain cell types. Consequently, the specificity of the targeter, representing only one component of a targeted drug delivery system, predominantly determines the extent of accumulation at the desired location. The drug molecules, spacers, or drug reservoirs attached to the targeter can mediate nonspecific binding and overlay the target effect. A possible loss of drug delivery systems by interactions with nontarget sites will not only result in reduced pharmacological activity but also might cause undesired side effects.

To achieve a pharmacological effect, the targeter is coupled to drugs or a drug-containing reservoir. The advantages of the pro-drug approach representing a targeter decorated with drug molecules are its good water solubility and the rather unimpeded diffusion to the target site. In case of immuno-targeting, however, oversubstitution of immunoglobulin G (IgG) with more than ten drug molecules will result in a loss of binding specificity. Additionally, lipophilicity of the pro-drug increases with the degree of substitution and can result, in the worst case, in altered biodistribution and water insolubility. The main drawback of this design is that therapeutically relevant drug concentrations at the target site are hardly achieved, due to low accumulation of drug molecules. Consequently, the cargo of the targeter is increased by conjugating pharmacologically inactive macromolecules with multiple binding sites for drugs, such as albumin, dextran, carboxymethylcellulose and its derivatives, and polyacrylates. Moreover, colloidal carrier systems loaded with drug molecules, such as liposomes and nanoparticles, can be decorated with target moieties. Further parameters that influence the extent of cellular uptake in addition to the type of target molecule are surface charge, size, and hydrophilicity of the colloidal carrier [8].

The drug or drug reservoir and the targeter are connected either directly or by interposition of a spacer molecule. An appropriate spacer molecule exposes the combining site of the targeter so that any steric impediment of interaction with the target site is avoided and biorecognition is facilitated. Furthermore, the spacer molecule should not contain ester bonds, as the high esterase activity in the circulation will facilitate premature drug release from the conjugate. Third, the spacer can act as a predetermined breaking point for drug release. Amidase activity in lysosomes, for example, exceeds by far amidase activity of the blood. Thus, tetrapeptide spacers can add value to targeted pro-drugs, since the drug is not released until the intralysosomal compartment of the

target cell is reached. Alternatively, pH-sensitive spacers, such as *cis*-aconitic acid or hydrazone linkages, are exclusively cleaved intracellularly in acidic compartments, for example, the lysosomes or the trans-Golgi complex [9, 10].

27.1.2. Cell Culture Models

The chemical characterization of targeted drug delivery systems includes the drug content of the system, the drug/targeter ratio, the size, the surface charge, and the solubility. Elucidation of the integrity and functionality of the targeter, which might be strongly affected by the conjugation chemistry, requires biological assays. At early stages of development, cell cultures are usually preferred to whole animal studies. Not only ethical considerations but also easy handling, reproducible experimental conditions, and a lack of interindividual variability led to establishment of cell culture models in many labs. In spite of low industrial acceptance and lacking approval by legal authorities, the performance of a targeted drug delivery is more likely elucidated by scaling the system down to the cellular level. To get an overview on cell culture models, the reader is referred to Part II of this book. It is well worth to note, however, that cell lines of human origin should generally be preferred for the characterization of targeted delivery systems.

For bioanalytical purposes, tissue forming cell lines, such as the human epithelial cell line, Caco-2, can be employed at the single cell level or grown to confluent and polarized monolayers. The interpretation of the results, however, is significantly affected by the choice of experimental setup, since morphological and functional differentiation of cells is initiated by cell-cell and cell-matrix contacts. Full differentiation is a time-dependent process which also might affect the expression of receptor proteins for targeted drugs. Consequently, assays confirming complete differentiation are inevitable requirements. They can be based on functionality, such as the activity of brush border enzymes, the expression of certain integrins, or on ultrastructural morphology, like the formation of microvilli at the apical cell membrane. However, assays using cell monolayers are quite time-consuming, due to necessary cultivation time, and the number of replicates is restricted, due to the handling of an adherent layer. When single cells are harvested from monolayers by subcultivation, different agents are applied that break cell-cell and cell-matrix interactions. The most common procedure is the proteolytic cleavage of cell contacts by trypsin combined with calcium-depletion by Ethylenediamine tetraacetic acid (EDTA)-complexation. This procedure can negatively affect cellular membrane proteins that represent combining sites for the targeted drug delivery system. In addition, upon loss of cell contacts and hence, polarization, initially apically located membrane proteins are rapidly redistributed across the entire cell membrane. Nevertheless, the single cell level is a prerequisite for flow cytometry which represents one of the most advanced methods for characterization of the interplay between cells and target molecules.

27.1.3. Analytical Tools: Labeling and Detection of Targeted Drug Delivery Systems

Careful choice of the label and the conjugation chemistry is a key issue for detection and characterization of targeters. Among the quantitative methods, radiolabeling techniques are distinguished by their unrivaled sensitivity, but

they require special and cost-intensive equipment in addition to designated laboratories to fulfill safety issues. Consequently, fluorescence-based techniques have gained importance in recent years. Fluorescence relies on the emission of photons at higher wavelengths upon return of the electrons to their ground state, after excitation at lower wavelengths. The high selectivity of the method results from the fact that all other compounds in the matrix are unlikely emitting at the same wavelength. In addition, the detectability is usually about 0.1 ppb, but can increase up to several parts per trillion. Moreover, in some applications, fluorescence can be measured over 3–6 orders of magnitudes of concentration, without the need for sample dilution.

Not only for staining the Chicago River green on St. Patrick's Day but also for labeling of biological molecules, fluorescein is a popular choice. The excitation wavelength of the fluorophore, created by a planar multi-ring aromatic structure, closely matches the emission of an argon laser at 488 nm. Depending on the derivative chosen, the emission spectrum occurs between 518 and 525 nm. The quantum yield is about 0.75, meaning that 75% of the absorbed energy is emitted. However, its fluorescence intensity fades upon dissolution in buffers, exposition to light, and prolonged storage. Fluorescein has a pK_a at 6.4 and multiple ionization equilibria. This leads to pH-dependent absorption and emission over the range from pH 5 to 9. In environments below pH 7 its quantum yield is significantly reduced, which is important for detection of fluorescein-labeled targets in acidic cell compartments. Additionally, the fluorescence lifetimes of the protonated and deprotonated forms of fluorescein are ~ 3 and 4 ns, respectively, which allows for pH determination from nonintensity-based measurements. A wide range of pre-activated fluorescein derivatives is commercially available, but upon coupling of fluorescein to proteins, the quenching can increase up to 50%.

Replacing the oxygen atoms of fluorescein by nitrogen leads to rhodamine derivatives. Following excitation in the visible light from 400 to 500 nm, the emission occurs in the range of mid to high 500 nm, being strongly dependent on the particular derivative. Compared to fluorescein the quantum yield is only about 25%, but the fluorescence intensity is fading considerably slower. In contrast to the green fluorescence of fluorescein, rhodamine derivatives exhibit an orange to red luminescence. Thus, these two labels form an ideal pair for use in double staining techniques.

In practice, applications using high-intensity illuminations, such as confocal laser scanning microscopy (CLSM), can result in photobleaching. This irreversible destruction of the excited fluorophore is reduced by commercially available antifading reagents that inhibit the generation and diffusion of reactive oxygen species. Applying other techniques, photobleaching is avoided only by reducing the intensity of excitation light, which, in turn, decreases the detection sensitivity. Sensitivity might also be compromised by background signals. In some cases, the autofluorescence of cells, tissues, and biological fluids can be minimized only by probes that have an excitation wavelength above 500 nm. Finally, quenching can reduce the quantum yield without changing the fluorescence emission spectrum. Upon conjugation of the label to proteins the quench can derive not only from oversubstitution but also from charge transfer complexes with aromatic amino acid residues [11]. Moreover, the covalent binding of a fluorophore also induces a change in the protein that can influence the quantum yield and the affinity to the target site. Even

the binding to the target can induce some deformations of the fluorophore. Particularly, oxygen and heavy atoms are ubiquitous quenchers that act in a concentration-dependent manner.

For characterization of targeted drug delivery systems, the cargo can be labeled as well. In doing so the targeter and its binding characteristics are only affected by conjugation to the cargo and not additionally hampered by the fluorophore. Unfortunately, only a few drugs serve as appropriate labels. Doxorubicin, for example, as a compound of pro-drugs absorbs visible light and can be detected either by reading the absorbance at 468 nm or, with higher sensitivity, after argon laser excitation, by its emission at 575 nm [10]. In the case of targeted carrier systems, labeling can be simply performed by entrapment of both, marker molecules and drugs, in one step. In contrast to colloidal gold or fluorescent polystyrene nanoparticles drug delivery system interaction benefits from similar physical characteristics of the delivery system, such as hydrophobicity, surface charge, size distribution, density, and protein adsorption. To prevent any substantial leakage of the label during the experiment, the polymeric matrix can be prepared from a mixture of low amounts of prelabeled and high amounts of unlabeled polymer molecules [12]. This technique allows adjustment of the fluorophore content to the required detection limit and only marginally affects the physical properties of the poly(D,L-lactide-co-glycolide) (PLGA)-nanoparticles.

The fluorescent labels reported for investigation of intracellular uptake and distribution by CLSM comprise Nile red [13], Texas Red, and 6-coumarin [14]. Not only for fluorescence microscopy but also for transmission electron microscopy (TEM), the loading of markers proved to be useful. Osmium tetroxid as an electron dense marker and bovine serum albumin (BSA) as a model protein were entrapped in PLGA-nanoparticles to elucidate their uptake and intracellular distribution in human vascular smooth muscle cells [15].

27.2. The Cell–Target System Interaction

By chronological sequence, the interaction between targeted delivery systems and epithelial cells can roughly be divided into three different steps. Provided that the mucus represents a negligible barrier, in the case of peroral administration, the first step is the binding of the system to the cellular membrane, referred to as cytoadhesion. If the binding of the ligand leads to activation of transport mechanisms, the system is taken up into the cell, which is termed cytoinvasion. Finally, if no local pharmacological activity is desired, the system should escape the cell at the basal membrane to reach the circulation or the lymphatics, denoted by cytoevasion. To date, a number of analytical techniques are available to shed light on each single step of this cascade, some of which are described in more detail in Chap. 22 of this book.

27.2.1. Cytoadhesion Assays

Dependent on the type of cell line and the type of labeled ligand in use, the binding of the targeted system to the cell membrane can be investigated qualitatively by CLSM or TEM at the isolated cell level or in monolayer systems. To quantify the amount of cell-bound fluorescent-labeled system, flow

cytometry is best suited for single cell analysis, whereas microplate reading is the method of choice for cell monolayers. The results, however, are different. The membrane of isolated cells is better accessible and offers a higher number of potential specific and nonspecific binding sites, than the surface of tightly packed cells in a monolayer. In the latter case, the available membrane surface for cytoadhesion is restricted to the apical face of the cells. Another difference deriving from the measuring principle relates to quantification. Whereas calibration of flow cytometric assays is quite difficult, the establishment of a calibration curve using a microplate reader is straightforward.

Prior to interpreting the results of cytoadhesion assays, some characteristics of the receptor–ligand interaction need to be considered. The binding of any ligand to its corresponding receptor is independent from energy, but the translocation of the receptor–ligand complex requires energy. Consequently, the assays should be performed at 4°C to exclusively monitor cytoadhesion. Attention should be drawn to maintain this temperature in each step of the experiment by precooling of all solutions and the cells for at least 15 min in a refrigerator, as well as by using a cool pad during all pipetting maneuvers. Furthermore, the receptor–ligand interaction is distinguished by rapid ligand binding, high affinity, and high stability under physiological conditions. Approximately below pH values of 5 the ligand–receptor complex dissociates. Consequently, cytoadhesion should not vary considerably with time under physiological conditions at 4°C; otherwise this might be a hint toward nonspecific binding. Similarly, the dissociation of initially bound ligand followed by its appearance in the supernatant is another clue for contribution of nonspecific processes.

In spite of using fluorescent-labeled compounds, sometimes the detection limits turn out to be insufficient to measure the binding of targeters to their receptors. To overcome this limitation, the silver nanoparticle enhanced fluorescence technique has proven to be useful. It relies on the phenomenon that an electromagnetic near field is generated on the surface of silver nanoparticles upon illumination. The interaction of the near field with fluorophores results in a fluorescence enhancement zone of about 200 nm in width which allows discrimination from fluorophores in the supernatant without any separation step. The gain in fluorescence intensity increases with overlap of the absorption spectrum of silver colloid particles and the excitation or emission spectrum of the fluorophore [16]. In practice, silver colloid-coated microplates are grafted with different materials, generating surfaces to assess the binding process between targeters and their ligands. Known receptor proteins can be immobilized at the colloid surface. In doing so, the mean velocity of the biorecognitive process between labeled wheat germ agglutinin (WGA) as a targeter for lectin-mediated drug delivery systems and epidermal growth factor receptor (EGFR) was investigated. Moreover, inhibition studies with the corresponding complementary carbohydrate allowed determining the specificity, so that finally the oligosaccharide side chain of the receptor involved in the interaction was identified [17]. Additionally, artificial cell surfaces can be built up by fusion of membrane vesicles with a self-assembled monolayer, anchored at the silver colloid coating (Figure 27.1). For detailed characterization of cytoadhesion in terms of the receptor–lectin interplay and the influence of the degree of substitution of lectin pro-drugs, membrane vesicles prepared from Caco-2 cells proved to be useful [18]. Third, the surface of the silver

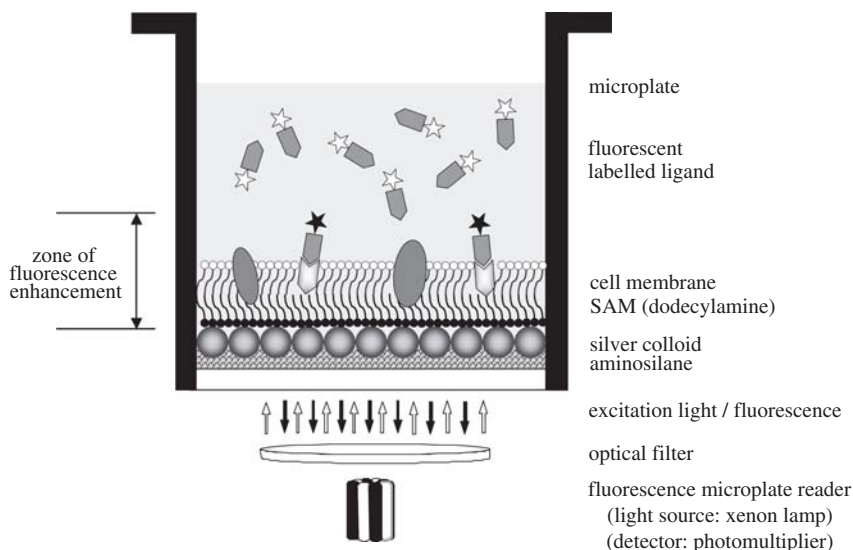


Figure 27.1 Principle of silver nanoparticle enhanced fluorescence applied to artificial cell surfaces.

colloid layer can be modified in a manner that the mucoadhesive properties of pharmaceutical excipients can be elucidated. At the optimum layer thickness, corresponding to 0.0025% pig gastric mucin, the signal intensity of fluorescently labeled mucoadhesive ligands was amplified up to ninefold, whereas the background signal was increased only twofold (unpublished data). All in all, this assay design allows end point determination of the binding rate, as well as real-time monitoring of the binding kinetics.

27.2.2. Specificity of Interaction

According to their literal sense, targeted drug delivery systems should act like cruise missiles that home in on only one target. In practice, however, such a high specificity of interaction is never reached because of the multifaceted biological environment of the body. Nevertheless, the reduction of dose in nontarget tissues, which usually provokes side effects, most likely yields high therapeutic benefits for the patient.

In general, an interaction can be termed specific, if it is inhibited by only one particular molecular structure. On the one hand, this inhibitor might be a soluble molecule representing the combining site of the targeter, such as an antigen or hapten in the case of immuno-targeting, or a well defined oligosaccharide, in the case of lectin-mediated targeting. On the other hand, another molecule, recognizing the target structure, but different to the targeter, might be applied as an inhibitor, for example, an antibody with similar specificity in the case of immuno-targeting. The principle of the experimental setup can rely either on competition or on displacement. A competitive assay comprises either the competition of the inhibitor with the cell-associated target for binding to the targeter or the competition of the inhibitor with the targeter for binding to the target at the cell membrane. If the target–targeter interaction is irreversible, the inhibitor and the targeter/target cell are added at the same time. In contrast,

a displacement protocol can be followed, when the target–targeter interaction is reversible. To obtain reliable results, the inhibitor should be added first to observe its displacement. The extent of both, competition and displacement, depends on the concentration of the inhibitor. At a fixed concentration of the labeled targeter, the binding of the targeter decreases with increasing concentration of the inhibitor. The results are usually indicated as IC_{50} – values representing the concentration of the inhibitor which inhibits 50% of the targeter from binding. Moreover, the contribution of the drug or the drug reservoir to nonspecific interactions can be estimated by comparing the IC_{50} of the targeter and that of the targeted drug delivery system.

Another way to describe specificity is the determination of the binding rate of labeled targeted systems to target cells and to nontarget cells, followed by comparison of the binding capacities. Using fluorescently labeled systems, this assay can be performed at the isolated cell level using flow cytometry, as well as at the monolayer level using fluorescent plate reading. As a prerequisite, the target cell type has to be known. For reliable results, target cells in addition to a wide array of different cell types, representing nontarget cells, highly sensitive lymphoblastic MOLT-4 cells (as a model of stem cells), and at least erythrocytes to represent the blood compartment, should be included in the assay [10]. Applying this technique on carrier systems, nonspecific interactions deriving from matrix–cell interactions that counteract target specificity can be elucidated, too.

Sometimes, the expression of the target moiety can be inhibited to identify the combining site of the targeter, which vice versa can be useful to examine the specificity of the interaction. In the case of targeting oligosaccharides which are present at the glycocalyx, enzymes that synthesize N-linked oligosaccharide chains or prevent prolongation of carbohydrate side chains can be inhibited [19]. When cells are pre-incubated with tunicamycin, which inhibits the *N*-acetyl-glycosyl-transferase at 0.5–10 $\mu\text{g/ml}$, the formation of N-linked carbohydrates is restricted. After addition of the labeled targeter and flow cytometric analysis, pretreated cells bound considerably lower amounts of WGA, compared with cells without treatment [20].

27.2.3. Binding Versus Uptake—Cytoinvasion Assays

Although confocal microscopic imaging of cells incubated with labeled targeted systems allow a rather clear decision about cytoinvasion, the quantification of cellular uptake is rather challenging, due to coincidence of cytoadhesion with cytoinvasion. The discrimination between both processes, however, is possible by taking into account some distinctive features of certain transport mechanisms.

Since active transport mechanisms require energy, the incubation temperature during the assay plays a crucial role. At 4°C, the fluidity of the cell membrane is reduced, the metabolism of the cell is downregulated, and energy-dependent transport processes are suppressed. Consequently, the amount of cell-associated target system refers mainly to the cytoadhesive fraction. In contrast, incubation at 37°C increases the fluidity of the cell membrane and the metabolic activity to an optimum, so both cytoadhesion and cytoinvasion occur at the same time. Thus, the uptake rate can be calculated from the difference in signal intensity measured upon incubation at both respective temperatures.

Provided that the cellular uptake of the fluorescently labeled targeted system results in only marginal shielding of the label by the cell membrane and the quantum yield of the label is independent from pH, the values acquired at 37°C will exceed those at 4°C, as observed in the case of rhodamine-labeling or doxorubicin-lectin pro-drugs (unpublished data). In contrast, the quantum yield of the fluorescein label is substantially quenched in an acidic environment. When fluorescein-labeled targeted systems are accumulated in acidic compartments of the cell, such as the lysosomes or the trans-Golgi complex, this pH dependency of the quantum yield will result in higher signal intensities at 4°C than at 37°C. Conclusively, the absence of a significant difference between incubation at both temperature levels can be an indication for passive transport.

Since the reloading of recycled receptors additionally exacerbates reliable interpretation of results from the assays as described above, implementation of a pulse–chase protocol can be of advantage. During the pulse phase, for example, incubation for 5 min at 4°C, the cell membrane is allowed to interact with the targeted system, followed by removal of excessive unbound ligand. Thus, a constant amount of labeled targeted system is bound to the cell membrane guaranteeing identical start conditions. This pulse phase is followed by the chase phase, wherein the cells are incubated at either 4°C or 37°C for different time intervals. These protocols proved to be useful for elucidating the characteristics of targeters, targeted pro-drugs, and targeted carrier systems. The cytoadhesive and cytoinvasive properties, as well as part of the intracellular trafficking of WGA as a targeter, were characterized using isolated cells and monolayers [21]. The usefulness of this targeter for intracellular protein delivery was assessed by soluble WGA–BSA, as well as WGA–IgG pro-drugs. Although the lectin facilitated uptake of these high molecular weight and membrane impermeable proteins into the cell, small amounts of both proteins were degraded by brush border hydrolases [22]. In addition, the cytoadhesive characteristics of WGA-grafted PLGA-microparticles enabled the uptake of the incorporated model drug. After exposure for 1 h, the entire payload was associated with the monolayer, as opposed to only 0.5% of the drug load in the case of BSA-grafted microparticles [23]. Moreover, the cytoadhesive and cytoinvasive characteristics of the lectin considerably enhanced the intracellular accumulation of PLGA-nanoparticles, as confirmed by assays with isolated cells and flow cytometric detection [24]. Interestingly, in the case of monolayer assays, the orientation of the cell layer and the recirculation of the floating targeted particles considerably influenced the binding and uptake rate of plain, as well as lectin-grafted nanoparticles. Upon horizontal orientation of the monolayer without particle movement, the overall cell association (i.e., binding and uptake) was higher than in the vertical system independent of the surface modification of the nanoparticles. Although the lectin-grafted nanoparticles exhibited highest cell association, their cell binding was only twice as high and their uptake was only three times higher than that of plain nanoparticles. Vertical orientation of the monolayer and circulation of the colloidal solution, however, strongly decreased the overall cell association, but the membrane binding of lectin-grafted nanoparticles was 10-fold and their uptake was 45-fold increased, compared with plain nanoparticles after an incubation of 3 h [12].

Another experimental setup to discriminate between binding and internalization of targeted systems relies on detection of the membrane-bound fraction by

a membrane-impermeable agent. As fluorescently labeled avidin neither binds to the cell membrane nor is it taken up into the cells, it only associates with biotinylated ligands at the cell membrane. Provided that excess biotinylated ligands are removed by washing and incubation with the labeled avidin is carried out at 4°C, the cell-associated fluorescence intensity refers to the cell-bound ligands exclusively. When this assay is performed at 4°C and 37°C, the uptake rate is obtained from the difference in cell-associated fluorescence intensity. From the results acquired at different time points, the kinetics of the interaction might be elucidated as well. However, it is pivotal to confirm that the ligand, once bound to the cell membrane, is not released again upon incubation at 37°C. This might be done by assaying the cell supernatant.

This experimental setup was applied for characterization of the interaction between WGA as a targeter and isolated Caco-2 cells, as well as monolayers. Accordingly, all the carbohydrate-combining sites accessible at the cell membrane were occupied within 10 min. This step was followed by internalization of 80% of membrane-bound lectin after 90 min in the case of isolated cells, and 240 min in the case of monolayers [25]. The principle of this assay design also works for characterization of the interaction between targeted nanoparticles and monolayers (unpublished data).

27.2.4. Cytoevasion

If localized pharmacological activity at the initially encountered epithelial barrier is not desired, the binding and uptake of the targeted system should be followed by leaving the cell and entering the circulation. The monitoring of cytoadhesion, cytoinvasion, and cytoevasion as referred to transcellular transport requires distinctive characteristics of the experimental setup. To imitate the polarity of the epithelial membrane and to gain access to the basolateral face the cells are cultivated on commercially available filter membranes, such as Transwell® systems, with different pore diameter and area. Provided sufficient tightness of the monolayer, as monitored by transepithelial electrical resistance (TEER) measurements, the amount of targeted system recovered from the basolateral compartment of the Transwell® corresponds to the absorbed fraction.

Using the Transwell® system, the transcellular transport of fluorescently labeled WGA was about 3% within the mean lifetime of enterocytes (3 days) corresponding to a tenfold improvement compared to dextrans of similar molecular weight [26]. According to preliminary results, the challenge of monitoring the transcellular transport of targeted colloidal drug delivery systems is to guarantee that the cell layer and not the cutoff diameter of the filter pores represents the main barrier to transcellular transport.

27.2.5. Active or Passive Uptake?

Transport across the cell membrane may occur via different routes. Some of these transport processes are energy dependent and therefore termed “active”; others are independent from energy, thus “passive.” Passive transport phenomena, for example, transcellular transport, are triggered by external driving forces, such as concentration differences, and do not require metabolic activity. However, generally, they are restricted to small lipophilic compounds. In contrast, active transport phenomena, such as active carrier-mediated transport or vesicular pathways, take course independent from external driving

forces. Internalization via active processes is in most cases saturable and substrate specific. Moreover, it also works against a concentration gradient and depends on metabolic energy. As already mentioned in Sect. 27.2.3, cellular metabolism is virtually inhibited by incubation at 4°C and promoted at 37°C. Hence, discrimination between active and passive uptake is possible. However, the underlying mechanisms are more precisely determined by affecting the cellular metabolism. For this purpose, sodium azide or 2-deoxyglucose are applied to inhibit the metabolic activity of cells. Sodium azide inhibits ATPase activity, resulting in a decrease of cellular ATP production capability [27]. In contrast, 2-deoxyglucose acts slightly different by depleting intracellular ATP stores [28]. In both cases, energy-dependent transport processes are impeded because of a lack of intracellular ATP. These inhibitors should be used with caution, since ATP depletion rapidly affects cellular integrity in general. Moreover, when using appropriate cell lines, such as Caco-2 cells, the uptake studies can be performed in presence and in absence of glucose. Upon involvement of energy-dependent mechanisms, significant differences in the amounts of drug taken up by the cells can be observed. In this regard, the cells should be pre-incubated with glucose-free medium prior to the experiments.

Besides by interfering with the general energy maintenance of the cell, impact of active transport during intracellular accumulation can also be investigated by direct inhibition of certain transport mechanisms. To detect contribution of Na⁺-dependent transport, the Na⁺/K⁺-ATPase, one of the primary active transport systems of the cell, can be inhibited by ouabain at ~10 μM. Higher amounts of the inhibitor may seriously impede with the viability of the cell. To obtain reliable results, the cells are pretreated with ouabain for 15 min prior to addition of the analyte. Usually, the inhibitory effect of ouabain lasts up to 45 min [29].

Furthermore, structural analogs can be applied to selectively block certain well-characterized transport processes to gain evidence of the involvement of a specific transporter. These experimental setups are favorable to analyze carrier-mediated uptake mechanisms. In doing so, the active uptake of targeted drug delivery systems relying on participation of transport systems, such as the bile acid transporter [30] or the intestinal peptide transporter PepT1 [31], were elucidated. In addition, selected carriers can be knocked down using siRNA technology.

27.2.6. Uptake and Intracellular Localization Within Acidic Compartments

In order to assess any uptake via the endosomal route followed by lysosomal enrichment of the drug delivery system, a particular assay design can be applied. A pH-sensitive fluorescence marker (e.g., fluorescein isothiocyanate, FITC) in combination with monensin is used to confirm the presence of the drug within acidic compartments of the cell. Fluorescein is a label with a reduced quantum yield at acidic pH and monensin, representing a carboxylic ionophore, triggers the exchange of protons for potassium ions, resulting in equilibration of the pH-gradient between the cytoplasm and acidic compartments of the cells.

To elucidate the accumulation of the drug within acidic compartments, it is recommended to adhere to a pulse–chase incubation protocol and to load the compound of interest to the cell surface at 4°C. That way, as discussed earlier in this chapter, solely binding to the cell surface occurs and any energy-dependent uptake is impeded. After removal of excessive analyte, the chase incubation should be performed at 37°C to monitor the uptake by the metabolically active cells. Provided that the fluorescein-labeled targeted system binds to the cell surface, followed by uptake into the cell and final accumulation within acidic compartments, the mean cell-associated fluorescence intensity decreases by time, during the chase incubation period [32]. However, this decrease might also be attributed to dissociation of initially membrane-bound targeted system, which results in appearance of the targeter in the supernatant. To unambiguously verify that the fluorescence quench is due to enrichment in acidic intracellular compartments, monensin is added to the same samples. Since monensin equilibrates the pH between acidic compartments and the cytosol, abolishing the quench of the fluorescein label, the potentially quenched fluorescence signal will be restored [25]. Because of the toxic potential of monensin, the concentration and the incubation time have to be adjusted to the particular cell type in preliminary experiments. Usually, the cells are treated with 20 μM monensin for 3–7 min at room temperature [29]. The difference of the cell-associated fluorescence intensity prior to and after monensin addition represents the quenched proportion of the labeled compound, which can be attributed to the drug located in acidic environment. As the quantum yield of fluorescein is reduced to about 10% at lysosomal pH, the fraction of the analyte entering the lysosomal pathway can be calculated [22].

During chase incubation at 4°C, no significant change of the cell-associated fluorescence intensity should be detected over time. Because of the reduced incubation temperature, the metabolism of the cells is minimized, resulting in an inhibition of active uptake processes. Upon subsequent addition of monensin, the fluorescence emission signals should not be altered as well. In doing so, any direct influence of monensin on the quantum yield of the fluorescein label can be excluded [25].

All in all, uptake studies with targeted systems carrying a pH-dependent fluorescent label in conjunction with monensin treatment at the end of the incubation period offer the possibility to discriminate between different intracellular trafficking pathways. At 37°C, an increasing fluorescence emission upon addition of monensin points toward accumulation of the targeted drug delivery system within acidic compartments of the cell, such as lysosomes.

27.3. Analytical Techniques

27.3.1. Flow Cytometry

27.3.1.1. Principles and Basic Considerations

In addition to the detection methods described hitherto, binding and uptake of targeted drug delivery systems can be determined by flow cytometric analysis. Similar to conventional fluorimetric techniques, flow cytometry

requires fluorescent labels to characterize the interaction between the analyte and the cell. However, flow cytometry is distinguished by rapid quantification of the association of targeted system with cells and concurrent analysis of a large number of cells. Thus, it is a powerful technique, also offering a comfortable statistical coverage of the results.

In general, flow cytometry is an optical analytical method to characterize cells or particles in suspension. Accordingly, a flow cytometer is simply described as a specialized fluorescence microscope equipped with a quantitative high-throughput detector system to measure various cellular parameters [33–35].

As flow cytometry is based on single cell analysis, a key component of the device is a proper fluidic system that provides individualization and correct arrangement of the cells during optical inspection. To obtain reliable results, the quality of the cell suspension is pivotal. This requires adequate handling of the cells, particularly, in terms of trypsination and resuspension during the entire assay, in order to actually analyze isolated single cells. For each individual cell, flow cytometry allows assessment of three different parameters: dimensions of the cell (e.g., volume, size, and diameter), granularity, and cell-associated fluorescence intensity, deriving from the amount of labeled analyte under investigation bound to or taken up by the cell. The flow cytometric evaluation of the cells occurs within a very short-time frame. The parameters of up to 100 cells can be analyzed per second. During flow cytometry, the cells are illuminated either by a conventional lamp or a laser, typically an argon ion laser (488 nm). The illuminating light beam is focused via prisms, mirrors, and several lenses to the middle of the flow chamber where the microscopic observation takes place. The detection optics of each flow cytometer collects the illuminating light scattered in the forward direction assessing the angle of the forward scattered light off the axis of the illuminating beam. This so-called “forward scatter” (FS) detector signal corresponds to the volume/size/diameter of the particular cell. Additionally, the light scattering perpendicular to the illumination beam, as well as the liquid stream, is examined. This side scatter (SS) and fluorescence-collection optics evaluates all light scattered by the cell to the side. The side scattering of the illuminating beam derives from the surface roughness or the granularity of the cells. The fluorescence detectors collect all light above the illumination wavelength emitted by fluorescent compounds associated with the cells under investigation, thus representing the quantitative aspects of flow cytometric analysis. State-of-the-art flow cytometers offer the possibility to analyze up to six different fluorescence emission signals simultaneously. The optical information gained during analysis is usually converted into electrical signals by photomultiplier tubes. After additional electronic amplification, the signals that exceed a specific adjustable trigger threshold are further processed by an analog-to-digital converter. The digitized signals are transmitted to a computer for data storage and evaluation. Usually, the signals of the forward scatter (FS) and side scatter (SS) detector are amplified linearly, whereas the cell-associated fluorescence intensity is monitored after logarithmic amplification over 4 decades. Thus, the scale is extended for weak signals and compressed for strong signals. In doing so, a single gain setting can be used throughout data acquisition, allowing direct comparison between various samples over a broad range of relative fluorescence intensities.

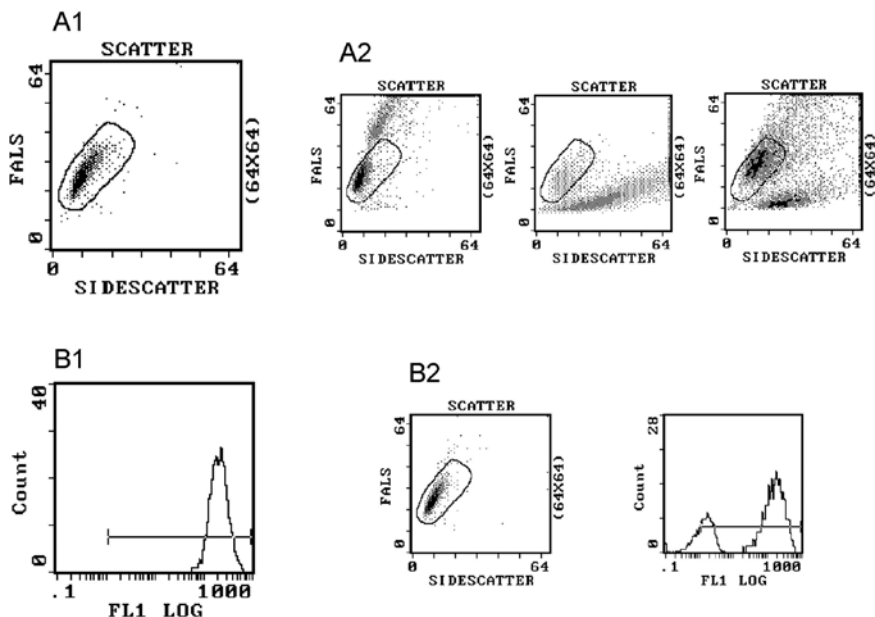


Figure 27.2 Selected histograms for evaluation of flow cytometric results.

27.3.1.2. Data Evaluation

For data evaluation, a multitude of data plots is available. The physical properties of a certain cell population are specified by a two-dimensional (2D) dot plot, where the FS signals are plotted versus the SS signals correlating to the size and granularity of the cells, respectively (Figure 27.2 A1). Within these histograms, each single cell is represented by a dot with specified size and granularity. Usually, all the cells are located within a narrow FS and SS range, indicating the homogeneity of the cell population. Hence, any anomalies can easily be detected. If there is a contamination with another cell type, an additional population will appear in the dot plot. If the isolated single cells agglomerate with the analyte during incubation, a second cell population will be observed at higher FS signals (Figure 27.2 A2). Moreover, any membrane blebbing, cell shrinkage, or fragmentation of cells can be identified, due to altered FS or SS values. An additional advantage of flow cytometry relies on the possibility to gate the cells of interest prior to further analysis. This so-called “gating” is achieved by setting up lower and upper thresholds for certain parameters, usually the FS and SS signals. In the histograms shown in Figure 27.2 the gating is indicated by the circle around the dots representing the cells. Consequently, only these preselected cells within the gate are analyzed in detail. That way, any nonspecifically stained particles (e.g., dead cells and debris) or cell agglomerates are excluded from the single cell analysis [36].

In contrast, one-dimensional (1D) histograms are used to illustrate the cell-associated fluorescence intensity deriving from the labeled targeted drug delivery system of interest (Figure 27.2 B1). Within these histograms, the relative cell-associated fluorescence intensity (RFI) is plotted versus the number of cells with a certain RFI value. Typically, a single peak is observed and the position of the peak corresponds to the cell-associated fluorescence intensity and thus the amount of labeled targeted system bound to or taken up by the

cell. Moreover, the shape of the peak offers additional information about the interaction between the analyte and the cell. A narrow single peak means that all the cells bind an equal amount of the substance under investigation. If there is a broad peak, the drug–cell association is rather inhomogeneous. Different binding characteristics of the same analyte to cells from a physically homogenous cell population can be elucidated only by flow cytometry. In this case, the 2D dot plot shows a narrow distribution of size and granularity, but the differences in binding characteristics are indicated in the fluorescence histogram by two or more peaks (Figure 27.2 B2).

Reliable statistical calculation of the data is performed by the cytometer's software, resulting in a simple evaluation of the association assays performed to characterize the interaction between targeted systems and the cells. The individual cell populations are usually described by the relative mean, either arithmetic or geometric, and the coefficient of variation of a particular parameter, as well as the number of cells within the respective population.

Flow cytometric analysis is widely used for the evaluation of binding and uptake of targeted drug delivery systems. The field of application comprises targeted pro-drug formulations [10, 22], delivery systems containing copolymers [37], nanoparticles [12, 24, 38], nanodevices based on dendrimer-drug conjugates [39], and polyethylenimine conjugates for targeted gene delivery [40]—just to name a few.

The principle of the experimental setup of the assays corresponds to the procedure described above. Individualization of the cells is achieved by trypsinization, either immediately prior to the experiment or after incubation with the compound under investigation. The benefit of freshly harvested cells results from the fact that there is no potential derogation of the binding between the analyte and the cell surface by subsequent trypsin treatment. However, the concentration of some membrane receptors may be reduced as compared to non-trypsinized cells. Anyway, an adequate dissociation step is necessary prior to flow cytometry to yield a homogeneous single cell suspension. Besides trypsination, gentle individualization can be obtained by nonenzymatic dissociation using EDTA (0.1–2% in PBS) or other specialized reagents (e.g., cell dissociation solution nonenzymatic, Sigma). These solutions are intended to preserve the structural and functional integrity of cells and their membrane proteins, but concurrently cell clumping might increase. Just before the flow cytometric analysis, the sample suspension, usually 50–200 μ l, is resuspended in 1 ml diluting reagent (e.g., CellPack™, particle-free PBS), in order to guarantee adequate analysis.

The amplification of the acquired fluorescence signals should be adjusted, so that the autofluorescence signal of unlabeled cells is located within the first decade of the usually 4-decade log range. Typically, between 3,000 and 7,000 cells of interest are accumulated for each analysis.

27.3.2. Intracellular Localization by Means of Confocal Laser Scanning Microscopy

Confocal laser scanning microscopy (CLSM) in conjunction with specific staining techniques is best suited to elucidate intracellular trafficking and localization. CLSM is a specific epifluorescence microscopical technique capable of optical cross-sectioning with a spatial resolution of 1 μ m and below [41, 42].

The main differences when compared to conventional fluorescence microscopes are based on several entities. A laser beam – usually an argon–krypton laser—is used for the illumination of the sample. The focused illuminating beam scans across the specimen by means of rotating mirrors, followed by a point-by-point signal collection which results in a raster sweep of the specimen at one particular focal plane. This is indicated by the term “laser scanning.”

The intrinsic characteristics of a confocal microscope are the pinholes inserted in the optical system. Usually, two pinholes are used, one in the illuminating beam and one in the detection beam. These pinholes eliminate all the light from “out-of-focus” planes. Thus, stray light is reduced, but sharpness and contrast are increased. The illumination pinhole provides for a point-like light source illumination exclusively within the focus plane. Consequently, only fluorescence-labeled analytes within this focal plane are excited. The second pinhole, the so-called “confocal pinhole,” is located immediately in front of the detectors. The term “confocal” indicates that the illuminating optics focuses in the same optical plane as the detection optics. The diameter of this detection pinhole is variable. That way, the thickness of the optical slice can be defined. For example, a small confocal pinhole setup results in an increased axial resolution and very thin optical cross-sections at the expense of sometimes rather weak fluorescence emission signal intensities. Thus, usually photomultiplier tubes are applied for signal transformation. Too large pinhole settings may result in a loss of confocality, leading to conventional microscopy. Finally, the image is generated pixel by pixel by an image processing program, which reconstructs the signals gained by the xy-scan pattern during light collection.

Using an optical bench with an adequate arrangement of several beam splitters and emission filters, different marker molecules featuring different emission wavelengths can be determined simultaneously, offering the possibility of proper colocalization. Because of the application of photomultiplier tubes for fluorescence detection, commonly an 8-bit grayscale image is generated. The observed pixel intensities within these images correlate to the relative intensity of the fluorescent light emitted by the respective structure of the labeled specimen. In the case of double or triple labeling, color can be added to the 8-bit grayscale images to discriminate between the different wavelength markers and highlight regions of interest. Moreover, different colors can be assigned to various pixel grayscale intensity ranges via color lookup tables, resulting in a pseudocolor image for enhanced image analysis.

In order to get an idea of the 3D specimen structure, a number of the already mentioned optical xy-sections are recorded concurrent with a slight refocusing of the microscope between the individual sections, resulting in a “stack” of multiple optical slices. These images can be digitized and reconstructed into a 3D object via computer technology. In addition to this stack recording, a so-called “z-scan” can be performed. In doing so, depth profiles in the xz-direction are recorded by the confocal microscope, resulting in a vertical scan instead of recording xy-images at a preset focus position.

In order to evaluate binding, uptake, and intracellular localization of targeted drugs via CLSM, nonfluorescent molecules of interest, as well as the appropriate structures of the specimen, have to be labeled with suitable fluorophores. This technique, however, requires a number of preparative steps, including fixation and permeabilization of the sample, staining and counterstaining, as

well as embedding prior to actual confocal microscopy. Some of these steps will be described below in more detail.

CLSM can generally be performed with cell monolayers, as well as with isolated single cells. Usually, the cells are incubated with the properly labeled compound of interest for an adequate period at 4°C or 37°C to investigate binding or binding/uptake. After this incubation step, the sample has to be prepared for CLSM. In order to retain the current status and to avoid any time-dependent alterations of the sample during staining and counterstaining, the specimen has to be fixed either by solvent or aldehyde fixation. In the case of aldehyde fixation (e.g., 2–4% paraformaldehyde in PBS), cellular morphology is conserved very well, because of cross-linking of proteins. However, fixation has to be followed by a separate permeabilization step using a suitable detergent (e.g., 0.1% Triton X-100 in PBS) in order to guarantee penetrable lipid membranes, particularly, in the case of immunofluorescent staining with antibodies. Solvent fixation is usually carried out with ice-cold methanol or acetone at –20°C. Thereby, denaturation, fixation, and even permeabilization of the specimen is achieved within one step, but sometimes structural changes, such as shrinkage of cells, may occur upon this fixation technique. Thus, rehydration of the sample in PBS or PBS/1% BSA before staining is very important.

Particular cellular structures can be stained either by direct conventional staining techniques using specifically interacting substances (e.g., fluorescence-labeled phalloidine for the actin skeleton) or by immunofluorescence histochemistry. Immunofluorescence staining techniques are usually performed as indirect methods using a site-specific unlabeled primary antibody, which in turn is detected by a secondary fluorescence-labeled antibody. Indirect immunofluorescence is preferred, due to its higher sensitivity, but it is also more economical, as a panel of primary antibodies originating from the same species can be visualized by only one secondary antibody. Moreover double- or triple-labeling is possible employing immunoglobulins from different species (e.g., mouse, rat, goat, or rabbit) or different isotypes/allotypes, which can be combined and detected selectively with type-specific secondary antibodies. In doing so, “multicolor” immunofluorescence is feasible, allowing analysis of two or more items in one sample as necessary for the evaluation of the intracellular localization of the compound under investigation. For better orientation within the specimen, counterstaining of the nucleus or other major cellular structures is commonly recommended. Typically, organelle-specific fluorescent dyes (e.g., propidium iodide, DAPI, or YOYO-1) are used.

After the staining procedure, the samples have to be mounted for CLSM, by embedding and covering with a coverslip. Nail polish may be used to seal the coverslip, if the embedding medium is not solidifying. However, to reduce photobleaching effects, the embedding medium should contain an antifade reagent. That way, the degradation process of the fluorophore due to the high intensity and focus of the laser beam is delayed, offering more convenient and longer microscopic inspection. For easy and safe handling, commercial embedding media that rapidly solidify (e.g., FluorSave™ Reagent and Calbiochem) are recommended.

When using isolated single cells, discrimination between binding and uptake is rather easily assessed by combining the confocal image with a usual transmission image. When the focus is set to the middle of the single cell,

a fluorescent ring encircling the cell can be observed in the case of merely surface-bound analyte. In contrast, localization of the compound within the cytosol, sometimes in a dot-like manner, points to uptake and (vesicular) intracellular enrichment.

In the case of cell monolayers, transmission images are not advisable. Thus, specific staining by, for example, immunofluorescence techniques is necessary in order to localize the drug delivery system within the specimen. A multitude of site-specific antibodies are commercially available, for staining the cellular structures of interest. Careful choice of the fluorescence labels for the analyte, as well as the cell staining, is of paramount importance to guarantee only minimal overlap of their excitation/emission wavelengths. To distinguish between cytoadhesion and cytoinvasion in general, staining of the cytosol or the cell membrane is required. For this purpose, a variety of dyes is available. Sometimes specific staining of cytoskeletal structures, however, seems to be more advisable, offering a detailed impression of the cellular dimensions. For instance, cytoplasmic actin filaments can be visualized via actin-reactive fluorescence-labeled phalloidine. Subsequent CLSM, including careful analysis of the images, offers the possibility to discriminate between solely surface-bound targeted systems and intracellularly accumulated ones.

An accurate localization of the drug delivery system within the cell including cellular trafficking, however, requires immunofluorescence staining techniques. As already mentioned above, almost all subcellular structures can be selectively stained by use of site-specific antibodies. That way, detailed colocalization analysis can be performed. Colocalization experiments via CLSM rely on the fact that two or more fluorescence emission signals overlap in the digital CLSM image, due to their close proximity within the sample. This effect is usually observed when fluorescent-labeled antibodies or dyes and the compound under investigation are located at identical spatial positions. Because of the high resolution of CLSM, conclusions about the colocalization of two differently labeled analytes within the pixel volume can be drawn. For (semi)quantitative evaluation, scatter plots of the distribution of the pixel intensities can be used. For that purpose an intensity value is assigned to each pixel of the image for the individual fluorescence emission signals at different wavelengths (e.g., red/green). All the pixels from both signals exceeding a certain threshold value indicate that both differently labeled structures/compounds most likely are present within the volume that corresponds to that pixel. Consequently, the extent of colocalization can be estimated from the position of the pixel populations in the 2D dot plot of the pixel values after defining certain threshold levels for both signals. However, diligent sample preparation and image acquisition is crucial in order to obtain reliable results. In particular, spectral bleed through or crossover of fluorescence emissions resulting in formation of artifacts is a fundamental problem that has to be considered. Such crossover most likely occurs when the intensities of both fluorescence signals are very different. However, careful selection of the staining and acquisition protocol followed by additional software correction should minimize these difficulties.

Elucidation of intracellular trafficking and localization by means of CLSM is widely spread in the field of targeted drug delivery systems. Thus, CLSM analysis was performed to determine uptake and intracellular distribution of potential targeters [25, 43], drug conjugates [44, 45], as well as nanoparticles

[12, 24]. A thorough overview on the topic of fluorescence imaging for drug delivery purposes is given by Watson et al. [46]. All in all, CLSM, particularly, in combination with immunofluorescence staining techniques, offers fascinating possibilities to discriminate between binding and uptake of drugs, as well as to localize internalized compounds in the subcellular range.

27.4. Concluding Remarks

The challenge in pharmaceutical research is to select and multiplex analytical techniques aligned with sophisticated cell biological background to advance our understanding of targeted drug delivery systems. The approaches described in this chapter attempt to subdivide the cell–target system interaction chronologically. Independent from the type of targeted system, cytoadhesion is a key for specific interaction and might be followed by cytoinvasion, which allows for different routes of intracellular trafficking, and finally cytoevasion. For elucidation of these single but interdependent steps, techniques relying on fluorescent labeling, such as flow cytometry, CLSM, and microplate reading, are presented. For a description in more detail, however, the arsenal of tools has to be extended to other fluorescence-based techniques, for example, fluorescence resonance energy transfer for monitoring protein–protein interactions, fluorescence recovery after photobleaching to monitor diffusion rates, or fluorescence correlation spectroscopy to elucidate diffusion dynamics.

Acknowledgments: Development of silver nanoparticle enhanced fluorescence technique was supported by the Austrian Science Fund (P-13513 MED). Another part of this paper and the work it concerns were generated in the context of the CellPROM project, funded by the European Community (NMP4-CT-2004–500039) under the 6th Framework Programme for Research and Technological Development in the thematic area of “Nanotechnologies and nano-sciences, knowledge-based multifunctional materials and new production processes and devices.” The contribution reflects the author’s views and the community is not liable for any use that may be made of the information contained therein.

References

1. Ehrlich, P., Collected works on immunity; Wiley, New York (1906).
2. Kataoka, K., Harashima, H., Gene delivery systems: Viral vs. non-viral vectors. *Adv Drug Deliv Rev* 52, 151 (2001).
3. Koehler, G., Milstein, C., Continuous cultures of fused cells secreting antibody of predefined specificity. *Nature* 256, 495–497 (1975).
4. Garnett, M.C., Targeted drug conjugates: Principles and progress. *Adv Drug Deliv Rev* 53, 171–216 (2001).
5. Yamazaki, N., Kojima, S., Bovin, N.V., Andrè, S., Gabius, S., Gabius, H.J., Endogenous lectins as targets for drug delivery. *Adv Drug Deliv Rev* 43, 225–244 (2000).
6. Minko, T., Drug targeting to the colon with lectins and neoglycoconjugates. *Adv Drug Deliv Rev* 56, 491–509 (2004).

7. Elnakat, H., Ratnam, M., Distribution, functionality and gene regulation of folate receptor isoforms: Implications in targeted delivery. *Adv Drug Deliv Rev* 56, 1067–1084 (2004).
8. Jung, T., Kamm, W., Breitenbach, A., Kaiserling, E., Xiao, J.X., Kissel, T., Biodegradable nanoparticles for oral delivery of peptides: Is there a role for polymers to affect mucosal uptake? *Eur J Pharm Biopharm* 50, 147–160 (2000).
9. Ulbrich, K., Suhr, V., Polymeric anticancer drugs with pH-controlled activation. *Adv Drug Deliv Rev* 56, 1023–1050 (2004).
10. Wirth, M., Fuchs, A., Wolf, M., Ertl, B., Gabor, F., Lectin-mediated drug targeting: Preparation, binding characteristics and antiproliferative activity of wheat germ agglutinin conjugated doxorubicin on Caco-2 cells. *Pharm Res* 15, 1031–1037 (1998).
11. Colucci, W.J., Tilstra, L., Sattler, M.C., Fronzeck, F.R., Barkley, M.D., Conformational studies of a constrained tryptophan derivative: Implications for the fluorescence quenching mechanism. *J Am Chem Soc* 11, 2 (1990).
12. Weissenboeck, A., Bogner, E., Wirth, M., Gabor, F., Binding and uptake of wheat germ agglutinin-decorated PLGA-nanospheres by Caco-2 monolayers. *Pharm Res* 21, 1919–1925 (2004).
13. Nguyen, C.A., Allémann, E., Schwach, G., Doelker, E., Gurny, R., Cell interaction studies of PLA-MePEG nanoparticles. *Int J Pharm* 254, 69–72 (2003).
14. Newman, K.D., Kwon, G.S., Miller, G.G., Chlumecky, V., Samuel, J., Cytoplasmic delivery of a macromolecular fluorescent probe by poly(D,L-lactic-co-glycolic acid) microspheres. *J Biomed Mater Res* 50, 591–597 (2000).
15. Panyam, J., Sahoo, S.K., Prabha, S., Bargar, T., Labhasetwar, V., Fluorescence and electron microscopy probes for cellular and tissue uptake of poly(D,L-lactide-co-glycolide) nanoparticles. *Int J Pharm* 262, 1–11 (2003).
16. Lobmaier, Ch., Hawa, G., Götzinger, M., Wirth, M., Pittner F., Gabor, F., Direct monitoring of molecular recognition processes using fluorescence enhancement at colloid coated microplates. *J Mol Recognit* 14, 1–8 (2001).
17. Lochner, N., Pittner, F., Wirth, M., Gabor, F., Wheat germ agglutinin binds to the epidermal growth factor-receptor of artificial Caco-2 membranes as detected by silver nanoparticle enhanced fluorescence. *Pharm Res* 20, 833–839 (2003).
18. Lochner, N., Wirth, M., Pittner, F., Gabor, F., Preparation, characterization and application of artificial Caco-2 cell surfaces in the silver nanoparticle enhanced fluorescence technique. *J Control Release* 89, 249–259 (2003).
19. Ausubel, I., Frederick, M. (eds.), *Current Protocols in Molecular Biology*, Unit 17.10 Inhibition of N-Linked Glycosylation, John Wiley & Sons (1993).
20. Gabor, F., Wirth, M., Jurkovich, B., Theyer, G., Walcher, G., Hamilton, G., Lectin-mediated bioadhesion: Proteolytic stability and binding-characteristics of wheat germ agglutinin and *Solanum tuberosum* lectin on Caco-2, HT-29 and human colonocytes. *J Control Release* 49, 27–37 (1997).
21. Gabor, F., Bogner, E., Weissenboeck, A., Wirth, M., The lectin-cell interaction and its implications to intestinal lectin-mediated drug delivery. *Adv Drug Deliv Rev* 56, 459–480 (2004).
22. Gabor, F., Schwarzbauer, A., Wirth, M., Lectin-mediated drug delivery: Binding and uptake of BSA-WGA conjugates using the Caco-2 model. *Int J Pharm* 237, 227–239 (2002).
23. Ertl, B., Heigl, F., Wirth, M., Gabor, F., Lectin-mediated Bioadhesion: Preparation, stability and Caco-2 binding of wheat germ agglutinin-functionalized poly(D,L-lactic-co-glycolic acid)-microspheres. *J Drug Target* 8, 173–184 (2000).
24. Weissenboeck, A., Wirth, M., Gabor, F., WGA-grafted PLGA-nanospheres: Preparation and association with Caco-2 single cells. *J Control Release* 99, 383–392 (2004).

25. Wirth, M., Kneuer, C., Lehr, C.M., Gabor, F., Lectin-mediated drug delivery: Discrimination between cytoadhesion and cytoinvasion and evidence for lysosomal accumulation of wheat germ agglutinin in the Caco-2 model. *J Drug Target* 10, 439–448 (2002).
26. Gabor, F., Wirth, M., Lectin-mediated drug delivery: Fundamentals and perspectives. *STP Pharm Sci* 13, 3–16 (2003).
27. Vasilyeva, E., Forgac, M., Interaction of the clathrin-coated vesicle V-ATPase with ADP and sodium azide. *J Biol Chem* 273, 23823–23829 (1988).
28. Unno, N., Menconi, M.J., Salzman, A.L., Smith, M., Hagen, S., Ge, Y., Ezzell, R.M., Fink, M.P., Hyperpermeability and ATP depletion induced by chronic hypoxia or glycolytic inhibition in Caco-2BBE monolayers. *Am J Physiol* 270, G1010–G1021 (1996).
29. Gabor, F., Klausegger, U., Wirth, M., The interaction between wheat germ agglutinin and other plant lectins with prostate cancer cells Du-145. *Int J Pharm* 221, 35–47 (2001).
30. Kagedahl, M., Swaan, P.W., Redemann, C.T., Tang, M., Craik, C.S., Szoka, F.C., Jr., Oie, S., Use of the intestinal bile acid transporter for the uptake of cholic acid conjugates with HIV-1 protease inhibitory activity. *Pharm Res* 14, 176–180 (1997).
31. Li, F., Hong, L., Mau, C.-I., Chan, R., Hendricks, T., Dvorak, C., Yee, C., Harris, J., Alfredson, T., Transport of Levovirin prodrugs in the human intestinal Caco-2 cell line. *J Pharm Sci* 95, 1318–1325 (2006).
32. Geisow, M.J., Fluorescein conjugates as indicators of subcellular pH. A critical evaluation. *Exp Cell Res* 150, 29–35 (1984).
33. Shapiro, H.M., *Practical Flow Cytometry*; Alan R. Liss, Inc., New York (1988).
34. Darzynkiewicz, Z., Crissman, H.A. (eds.), *Methods in Cell Biology: Flow Cytometry*, Vol. 33; Academic Press, New York (1990).
35. Radbruch, A., *Flow Cytometry and Cell Sorting*; Springer, Heidelberg (1992).
36. Sharpless, T., Traganos, F., Darzynkiewicz, Z., Melamed, M.R., Flow cytometry: Discrimination between single cells and cell aggregates by direct size measurement. *Acta Cytol* 19, 577–581 (1975).
37. David, A., Kopeckova, P., Rubinstein, A., Kopecek, J., Enhanced biorecognition and internalization of HPMA copolymers containing multiple or multivalent carbohydrate side-chains by human hepatocarcinoma cells. *Bioconjug Chem* 12, 890–899 (2001).
38. Yi, Y., Kim, J.H., Kang, H.W., Oh, H.S., Kim, S.W., Seo, M.H., A polymeric nanoparticle consisting of mPEG-PLA-toco and PLMA-COONa as a drug carrier: Improvements in cellular uptake and biodistribution. *Pharm Res* 22, 200–208 (2005).
39. Kolhe, P., Khandare, J., Pillai, O., Kannan, S., Lieh-Lai, M., Kannan, R.M., Preparation, cellular transport, and activity of polyamidoamine-based dendritic nanodevices with a high drug payload. *Biomaterials* 27, 660–669 (2006).
40. Merdan, T., Callahan, J., Petersen, H., Kunath, K., Bakowsky, U., Kopeckova, P., Kissel T., Kopecek, J., Pegylated polyethylenimine-Fab' antibody fragment conjugates for targeted gene delivery to human ovarian carcinoma cells. *Bioconjug Chem* 14, 989–996 (2003).
41. Pawley, J.B. (ed.), *Handbook of Biological Confocal Microscopy*, 2nd edn. Plenum Press, New York (1995).
42. Matsumoto, B., *Cell Biological Applications of Confocal Microscopy*; Academic Press, San Diego, CA (1993).
43. Wirth, M., Hamilton, G., Gabor, F., Lectin-mediated drug targeting: Binding and internalization of wheat germ agglutinin and Solanum tuberosum lectin by Caco-2 and Ht-29 cells. *J Drug Target* 6, 95–104 (1998).

44. Beyer, U., Rothen-Rutishauser, B., Unger, C., Wunderli-Allenspach, H., Kratz, F., Differences in the intracellular distribution of acid-sensitive doxorubicin-protein conjugates in comparison to free and liposomal formulated doxorubicin as shown by confocal microscopy. *Pharm Res* 18, 29–38 (2001).
45. Langer, M., Kratz, F., Rothen-Rutishauser, B., Wunderli-Allenspach, H., Beck-Sickinger, A.G., Novel peptide conjugates for tumor-specific chemotherapy. *J Med Chem* 44, 1341–1348 (2001).
46. Watson, P., Jones, A.T., Stephens, D.J., Intracellular trafficking pathways and drug delivery: Fluorescence imaging of living and fixed cells. *Adv Drug Deliv Rev* 57, 43–61 (2005).

Drug Permeability Studies in Regulatory Biowaiver Applications

Donna A. Volpe

Abstract The Biopharmaceutics Classification System is a drug development tool that estimates the contributions of solubility, dissolution, and intestinal permeability affecting drug absorption from solid oral products. A regulatory guidance proposes human, animal, and in vitro methods to determine the permeability class membership of a drug substance. Method suitability is a process to establish and validate cellular or tissue permeability assays for classification of drug substances. It consists of establishing an assay with comparison of experimental permeability to in vivo extent of absorption, defining reference standards and acceptance criteria, and classifying new drug substances. Literature examples with cells, intestinal tissue, and artificial membranes demonstrate the applicability and feasibility of method suitability for evaluating permeability models. An assay with established method suitability, standard compounds, and criteria for classifying drugs improves the reliability for such assays for regulatory applications.

Keywords: Biopharmaceutics Classification System; Biowaiver; Permeability; In vitro assays; Method suitability

Disclaimer: This chapter represents the personal opinion of the author and does not necessarily represent the views or policies of the FDA.

Abbreviations

BCS	Biopharmaceutics Classification System
f_a	Extent of absorption
FDA	Food and Drug Administration
FITC	Fluorescein isothiocyanate
HDS	Highest dose strength
HP	High permeability
HS	High solubility
IR	Immediate release
IS	Internal standard
IVIVC	In vivo–in vitro correlation
LS	Low solubility
LP	Low permeability

MDCK	Madin-Darby canine kidney
MRP	Multidrug resistance protein
PAMPA	Parallel artificial membrane permeation assay
P_{app}	Apparent permeability
P-gp	P-glycoprotein
TEER	Transepithelial electrical resistance
USP	United States Pharmacopeia

28.1. Biopharmaceutics Classification System

Drug absorption in the gastrointestinal tract is influenced by a variety of drug (e.g., solubility, pK_a , membrane permeability, partition coefficient), product (e.g., formulation, particle size, disintegration, dissolution rate), and physiological factors (e.g., motility patterns, volume and flow rate, regional differences, pH). The Biopharmaceutics Classification System (BCS) is a drug development tool for the estimation of the contributions of three major factors, solubility, dissolution, and intestinal permeability, affecting oral drug absorption from immediate release (IR) solid oral products. The system was developed to provide a scientific approach to predict in vivo drug product performance from in vitro assays of oral IR products by classifying drugs based on their dose-related solubility and intestinal permeability in combination with dissolution properties of the dosage form [1].

The solubility class boundary is based on the highest dose strength (HDS) of an IR product. Drug substances are regarded as highly soluble (HS) if the HDS is soluble in 250 ml or less aqueous media over pH range of 1.0 to 7.5. Low solubility (LS) drugs are soluble in more than 250 ml media over the same pH range [1]. This boundary value reflects the minimum fluid volume anticipated in stomach at the time of drug administration (typical glass of water) during a conventional fasting bioequivalence study [2]. The permeability class boundary is intended to identify drugs exhibiting complete absorption [1]. Class membership is documented when the drug is determined to be stable in the gastrointestinal tract and is based upon the extent of absorption (f_a) of an administered dose or intravenous (i.v.) reference dose. Highly permeable (HP) drugs have an f_a greater than 90%, whereas low permeability (LP) drugs have an f_a less than 90%. Drug substances are classified based upon their solubility and permeability characteristics, that is, class I (HS/HP), class II (LS/HP), class III (HS/LP), and class IV (LS/LP).

The dissolution category is based on the in vitro dissolution rate of an IR dosage form under specified test conditions and intended to demonstrate rapid in vivo dissolution in relation to gastric emptying in humans under fasting conditions. A drug product is considered to be rapidly dissolving when at least 85% of the labeled amount of drug substance dissolves within 30 min in 900 ml of three separate buffers (0.1 N HCl, pH 4.5 buffer, pH 6.8 buffer) [1].

In addition to efficacy and toxicity, biopharmaceutical properties of drugs play an important role in their discovery and development. Although the BCS was intended primarily for regulatory applications, it can assist in preclinical and clinical drug development processes. The use of in vitro data (e.g., solubility, permeability) may improve the quality of drug candidates and their selection by providing an estimate of human intestinal absorption in early discovery stages. The BCS provides clear and applicable rules for identifying

the rate-limiting step and predicating intestinal drug absorption based upon solubility and permeability [3]. In the later stages of development, it can assist in formulation approaches to improve oral bioavailability through the use of dissolution, solubility, and/or permeability enhancers.

28.2. Regulatory Application of the BCS

The classification of drug substances according to the BSC was applied to an Food and Drug Administration (FDA) guidance on IR solid oral dosage forms listing different dissolution documentation for class I, II, and III drugs [4]. A later guidance on dissolution utilized BCS classification as a basis for setting in vitro dissolution specifications and predicting the likelihood of in vitro–in vivo correlation (IVIVC) [5]. In 2000, the FDA applied the principles of the BCS to a regulatory guidance that recommends methods for classifying drug substance and products [6]. In this guidance, a biowaiver for clinical bioequivalence or bioavailability studies may be obtained for a class I drug substance whose drug product has rapid and similar dissolution. The guidance outlines specifications for solubility and dissolution experiments along with methods for intestinal permeability determinations. The BCS also appears in a food effect guidance which outlines important food effects on bioavailability that are less likely to occur with rapidly dissolving, IR products with BCS class I drug substances [7].

FDA's BCS guidance provides test specifications and acceptance criteria for conducting solubility, permeability, and dissolution studies for classification purposes [6]. The guidance outlines the criteria for biowaivers: high solubility (HS), high permeability (HP), rapid and similar dissolution, wide therapeutic window, excipients previously used in an FDA-approved IR solid dosage form, and stability in gastrointestinal tract (Figure 28.1) [1, 6].

Under the BCS approach [6], the equilibrium solubility of a drug substance is determined under physiological pH conditions. The pH-solubility profile of the test drug substance is determined at $37 \pm 1^\circ\text{C}$ in aqueous media in the range of pH 1.0–7.5. Concentrations of the drug substance in the pH conditions are determined using a validated stability-indicating assay that can distinguish the drug substance from its degradation products.

The permeability class of a drug substance can be determined by human, animal, or in vitro approaches. A drug substance is classified as HP when its f_a in humans is determined to be greater than 90% of an administered dose. Determining the f_a in humans does not account for the drug's degradation in the gastrointestinal fluid prior to intestinal membrane permeation. Therefore, stability in the gastrointestinal tract can be documented using human, animal or simulated gastric and intestinal fluids. Significant degradation (>5%) of a drug in such an assay, after measurement with a validated stability-indicating assay method, could suggest potential instability [6].

Dissolution testing is carried out in United States Pharmacopeia (USP) Apparatus I (100 rpm) or Apparatus II (50 rpm) utilizing 900 ml of the following dissolution media: (1) 0.1 N HCl or simulated gastric fluid USP without enzymes; (2) a pH 4.5 buffer; and (3) a pH 6.8 buffer or simulated intestinal fluid USP without enzymes. When 85% of the labeled amount of

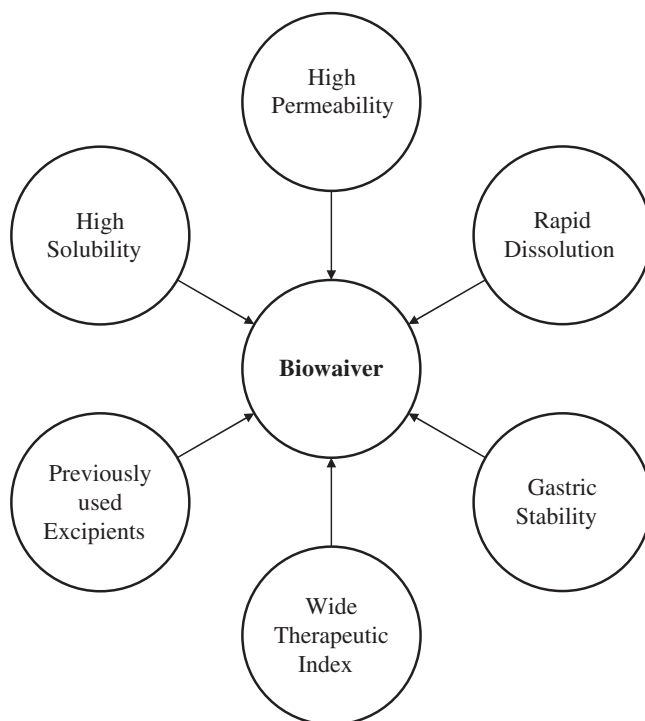


Figure 28.1 Requirements for a biowaiver of bioequivalence and bioavailability studies.

drug substance dissolves within 30 min in the three buffers, a drug product is considered to be rapidly dissolving [6].

Regulatory application of this guidance can occur in investigational and new drug applications for a waiver of bioequivalence studies following changes in formulation and/or method of manufacture (e.g., pivotal clinical trial *vs.* to-be-marketed formulation). Biowaivers for generic products in abbreviated new drug applications may be submitted if the test and reference products are highly soluble, highly permeable, and rapidly dissolving. Beyond drug applications, biowaivers for bioequivalence studies may be made for significant postapproval changes.

The Committee for Proprietary Medicinal Products [8] applied the BCS, with certain requirements, to dispense with bioequivalency tests if the active pharmaceutical ingredient is class I and the *in vitro* dissolution of the finished dosage form is fast [9]. An active substance is considered highly soluble if the amount contained in the HDS of an IR product is dissolved in 250 ml of each of three buffers within the range of pH 1–8 at 37°C (e.g., pH 1.0, 4.6, and 6.8). There should be linear and complete absorption, which indicates HP to reduce the possibility of an IR dosage form influencing the bioavailability [8]. The similarity of the dissolution profiles of the test and reference products is demonstrated in each of three buffers within the range of pH 1–8 at 37°C (e.g., pH 1.0, 4.6, and 6.8). If there is rapid dissolution of the product, where at least 85% of the active substance is dissolved within 15 min, no further comparison of the test and reference is required. Further requirements include that excipients be well established and have no interaction with the pharmacokinetics of the active substance and that the method of manufacture of finished product

in relation to physicochemical properties of the active substance is adequately addressed and documented [8].

28.3. Permeability Measurements

Unlike the straightforward methods for solubility, dissolution, and gastric stability, the BCS guidance recommends several methods to determine the permeability class membership of a drug substance (Table 28.1).

Pharmacokinetic mass balance studies in humans using unlabeled, stable isotopes, or a radiolabeled drug substance can be used to ascertain the f_a of the test drug. Oral bioavailability determinations using intravenous administration as a reference can also be used to classify a drug substance. Intestinal perfusion, based upon the difference between the solute concentration entering and leaving a specific region, offers a direct way to measure human intestinal permeability. The results of this perfusion method were utilized in the development of the BCS [10]. There was a good correlation between measured human effective permeability (P_{eff}) values and f_a in humans determined by pharmacokinetic studies for BCS classification [11].

Intestinal perfusion studies may be carried out in small animals (e.g., rat, rabbit) where permeability is calculated by analyzing drug concentration in the exiting solution from a cannulated intestinal segment after a single-pass perfusion. This is normalized for donor drug concentration, perfusion flow rate, and drug aqueous diffusion coefficient. Nonabsorbable or high molecular weight marker compounds are used to assess influence of intestinal water transport. Rat intestinal perfusion data can be utilized for the prediction of $\%f_a$ in humans for passively and actively transported drugs [12, 13]. It is a useful technique to classify compounds according to BCS with appropriate passively and actively absorbed reference compounds, demonstrating a relationship between rat intestinal P_{eff} and $\%f_a$ in humans [12, 13]. The perfusion method allows for the control of drug concentration, pH, osmolarity, intestinal region, and flow rate. The model integrates aspects of drug transport and metabolism in that all the physiological factors influencing drug passage are present.

The intestinal tissue flux assay mixes the advantages of an animal or human model that uses intestinal tissue with a higher throughput format to ascertain drug permeability potential. In a chamber, isolated intestinal segments are opened to form flat tissue sheets, stripped of musculature, and mounted in standard diffusion cells with buffer. A drug solution is applied to one side (mucosa or serosal) of the tissue, and the rate of drug absorption is determined by measuring the appearance or disappearance of the drug. A system is used

Table 28.1 Methods for Permeability Classification.

Human methods	Mass balance studies Absolute bioavailability studies In vivo intestinal perfusion
Animal methods	In vivo intestinal perfusion In situ intestinal perfusion
In vitro methods	Flux across excised human or animal tissue Transport through epithelial cell monolayers

to stir the buffers and oxygenate the tissues. Flux across tissue is defined as the rate of accumulation normalized for tissue surface area. The model allows for sink conditions, measurement of electrophysiological properties, directional fluxes, intestinal regional differences, and intestinal metabolism. Marker compounds can be added for continuous monitoring of tissue viability and integrity, reproducibility, and as references for classifying drug permeability. The tissue chamber flux method allows for drug transport at specific intestinal sites, investigating directional differences in permeability, and evaluation of drug metabolism during transport. This method retains the architecture of intestinal tissue and is of an intermediate level of complexity for permeability studies.

The Ussing chamber technique was optimized by Grass and Sweetana [14, 15] to measure the *in vitro* transport of passively absorbed compounds across rat, rabbit, and monkey mucosa by mounting sections of freshly excised intestine in specially designed side-by-side diffusion cells. Ungell et al. employed the tissue flux method with regional segments of rat intestine, proximal jejunum, ileum, and colon, in Ussing chambers to classify compounds as HP or LP according to the BCS [16]. Nejdors et al. compared the *in vitro* permeation of macromolecules in different species and various regions of gastrointestinal tract and found that results are difficult to interpret and sometimes conflicting [17]. Using human, rat, and pig intestinal segments they found that pig permeability data correlated fairly well with human to both rate and extent whereas it was more difficult to extrapolate permeability from the rat to human [17].

In the gut sac technique, animal intestinal segments are divided into 2–cm sacs by tying off each end. The sacs, with or without musculature, can be everted or not to measure directional drug transport into or out of the sacs. The sacs are placed in a vessel containing an oxygenated buffer and transport is measured with normalization for the sac size. The intestinal gut sac method is a relatively fast and inexpensive technique for measuring permeability that includes all intestinal cell types and mucus layer.

An experimental protocol with isolated frog intestinal sacs was utilized for the assessment of intestinal drug permeability with a series of 20 predominantly passively absorbed drugs [18]. The drugs completely absorbed in humans had apparent permeability (P_{app}) values greater than 1×10^{-6} cm/s, while drugs absorbed less than 90% had P_{app} values lower than 1×10^{-6} cm/s. It was concluded that a satisfactory permeability classification according to the BCS may be based on the P_{app} values determined by the frog intestinal permeability [18]. A noneverted rat intestinal sac system was validated and demonstrated for 11 model compounds with a good relationship between their permeability and the corresponding f_a [19].

Cell monolayers grown on permeable culture inserts form confluent monolayers with barrier properties and can be used for drug absorption experiments. The most well-known cell line for the *in vitro* determination of intestinal drug permeability is the human colon adenocarcinoma Caco-2 [20, 21]. The utility of the Caco-2 cell line is due to its spontaneous differentiation to enterocytes under conventional cell culture conditions upon reaching confluency on a porous membrane to resemble the intestinal epithelium. This cell model displays small intestinal carriers, brush borders, villous cell model, tight junctions, and high resistance [22]. Caco-2 cells express active transport systems, brush border enzymes, and phase I and II enzymes [22–24]. Permeability models

with the Caco-2 cell line provide a relatively fast, flexible, and simple method that can be used for mechanism transport studies and drug screening testing.

The Marbin-Darby canine kidney (MDCK) epithelial cell line has been used in permeability studies due to its faster growing time as compared to Caco-2 cells [25, 26]. The TC7 late passage clone of Caco-2 cells also spontaneously differentiates as its parent with a better array of P450 metabolizing enzyme and high resistance [27]. The TC-7 clone exhibits morphological characteristics similar to those of the parental Caco-2 cell line (apical brush border, microvilli, tight junctions, polarization) although it is more homogenous in terms of cell size [28]. TC7 cells express similar levels of sucrase isomaltase and other phase II enzymes as the human jejunum [28]. They express CYP3A, grow faster than Caco-2 cells, and need less glucose than Caco-2 cells.

The human colonic HT-29 cell line and its clones have goblet cell-like morphology and form a mucus layer [29, 30]. Collet et al. [30] described the HT29-18-C₁ line as being closer in permeability properties to small intestine as compared to Caco-2 cells. The HT29-18-C₁ cells must be induced to differentiate and provide a villous cell absorptive model, with tight junctions and small intestinal-like resistance at day 10 of culture [30]. The intestinal goblet cell line HT29-H secretes mucin on the apical surface of the confluent monolayer and form mucus layer on monolayer. It has lower transepithelial electrical resistance (TEER) values than Caco-2 but is more permeable to mannitol [29].

Other cell lines used in permeability studies include the T84 human colonic adenocarcinoma colonic crypt cell model. This line has a reduced carrier expression, secretes mucus, and has very high resistance [31, 32]. The IEC cell line is a rat fetal intestinal epithelium cell with higher permeabilities than Caco-2 cells [33]. LLC PK₁ is a pig kidney epithelial cell line with low expression of efflux systems, but expression systems for transport proteins [32]. 2/4/A1 cells are a conditionally immortalized rat fetal intestinal epithelium line with crypt cell-like morphology and temperature-sensitive differentiation [34]. They form differentiated monolayers with tight junctions, increased brush border enzymes when grown on extracellular matrices with laminin. Transport of drugs with LP in 2/4/A1 monolayers was comparable to that in the human jejunum and up to 300 times faster than that in Caco-2 monolayers. In contrast, the permeability of HP drugs was comparable in both cell lines [34].

As with all in vitro cell models, there are a number of advantages and limitations in their use as assay systems for evaluating the intestinal permeability of drug substances. Notable is that drug substances with very low aqueous solubility are difficult to assess in these systems as the cell monolayers may not be able to tolerate even moderate amounts of organic solvents that are used to solubilize the drug. Organic solvents can change the physical barrier of the cell monolayer and alter drug permeability [35]. Additionally, toxic drugs can adversely affect the monolayers, resulting in inaccurate permeability measures. Many factors affect the quality of cell monolayers and permeability values, including culture media, filter type, seeding density, cell passage number, monolayer age, and transport conditions [36, 37]. Different methodologies can affect cell morphology and uptake characteristics [38–40]. This results in difficulty to compare values obtained in different laboratories for the same drug [22]. Additionally, the cell systems do not consider regional differences in the gastrointestinal tract and may not have similar expression of active transporters and metabolic enzymes as the small intestine.

Table 28.2 IVIVC with Caco-2 Cell Permeability Assays.

P_{app} Range	Absorption	Reference
$>1 \times 10^{-6}$ cm/s	Completely absorbed in humans	[41]
0.1×10^{-6} to 1.0×10^{-6} cm/s	Absorbed to $>1\%$ but $<100\%$	
$\leq 1 \times 10^{-7}$ cm/s	Absorbed to $<1\%$	
$<1 \times 10^{-6}$ cm/s	Poorly (0–20%) absorbed	[42]
1×10^{-5} to 10×10^{-5} cm/s	Moderately (20–70%) absorbed	
$>10 \times 10^{-6}$ cm/s	Well (70–100%) absorbed	
$>10 \times 10^{-6}$ cm/s	$f_a > 90\%$	[43]
$<0.4 \times 10^{-6}$ cm/s	Very poor oral absorption	[44]
$>7 \times 10^{-6}$ cm/s	Excellent oral absorption	
$<0.2 \times 10^{-6}$ cm/s	Very poor absorption (BA $<1\%$)	[45]
0.2×10^{-6} to 2.0×10^{-6} cm/s	BA 1–90%	
$>2.0 \times 10^{-6}$ cm/s	Very good absorption (BA $>90\%$)	

BA, bioavailability.

However, cell permeability assays are screening tools studies which provide information at the cellular level on the absorption, metabolism, and transport of drug across intestinal epithelium. In some cases the cell lines are of human origin to eliminate interspecies differences and overall they minimize animal usage. A major advantage cell models bring to permeability assays is their IVIVC between human intestinal drug absorption and intestinal epithelial cell culture. Several authors have shown that drugs can be grouped into absorption levels based upon the experimental permeability values in a Caco-2 cell assay (Table 28.2). This also highlights the differences in the results among laboratories and that a single HP/LP boundary P_{app} value cannot be specified for all Caco-2 permeability assays.

28.4. Method Suitability

Due to the lack of standardized methodology in the preparation/culture, transport, and analysis phases of in vitro cell or tissue permeability assays utilized by researchers, the BCS guidance recommended the development of permeability models based on method suitability to classify drugs with the use of standard compounds [6]. The advantages of such a system are that it accounts for interlaboratory variability, allows for improvements in technology, and is applicable to a variety of intestinal tissues and epithelial cell lines [36]. Method suitability allows for a more generalized approach to standardize and validate a permeability model for classification purposes with a laboratory. It consists of establishing an assay with comparison of experimental P_{app} with in vivo f_a , defining reference standards and acceptance criteria, and classifying new drug substances [37]. Regulatory acceptance of in vitro permeability data by the FDA in context of the BCS guidance is based on method suitability where the goal is to classify drugs as low or high permeability.

In vitro cell or tissue permeability methods are regarded as being suitable for classifying passively transported drugs. For application of the BCS and biowaivers, an apparent passive transport mechanism can be assumed when one of the following conditions is satisfied [6]. A linear pharmacokinetic relationship between a relevant clinical dose range and bioavailability of a drug is demonstrated in humans. Alternatively, there can be a lack of dependence of the measured in vivo or in situ permeability in an animal model based upon initial drug concentration (e.g., 0.01, 0.1, and 1 times the HDS in 250 ml) in the perfusion fluid. Lastly, there can be no statistically significant difference in the rate of transport between the apical-to-basolateral and basolateral-to-apical direction for the drug concentrations selected using a suitable cell culture method that has been shown to express known efflux transporters (e.g., P-glycoprotein, [P-gp], multidrug resistance protein [MRP]).

To demonstrate the suitability of a permeability method intended for application of the BCS, a rank-order relationship between experimental permeability values and the extent of intestinal drug absorption in human should be established using a sufficient number of model drugs [6]. For in vivo intestinal perfusion studies in humans, six model drugs are recommended. For in vivo or in situ intestinal perfusion studies in animals and for in vitro cell culture methods, 20 model drugs are recommended. Depending on study variability, a sufficient number of subjects, animals, excised tissue samples, or cell monolayers are used in a study to provide a reliable estimate of drug permeability. This relationship should show a clear differentiation between drug substances of low and high intestinal permeability attributes [6].

Method suitability can be divided into (a) method development, (b) assay suitability, and (c) permeability classification. The first step is to establish the methodology to be used for the tissue or cell permeability assay. For in vitro intestinal tissue assays this would include the choice of animal model, intestinal segment (region), buffer composition and pH, oxygenation process, and sampling method. Development of cell culture models takes into account cell origin and restricted passage number, defined culturing protocol and media, filter type and size, specific transport conditions (i.e., buffer composition, pH, stirring, drug concentration, sampling method, time points), and P_{app} calculation.

The applicability of an in vitro assay to classify drug substances is verified by demonstrating a rank-order relationship between the extent of human absorption and experimental permeability values with 20 model drugs. The model drugs should represent ranges of 0–50%, 50–89%, and 90–100% absorption (f_a) and the results should clearly differentiate between HP and LP drugs. The model can also be characterized for the presence of functional active transporters (e.g., amino acids, di/tripeptides, monocarboxylic acids, nucleosides) and efflux mechanisms (e.g., P-gp, MRP).

After demonstrating the assay can accurately classify drug substances, it is not necessary to retest all the model drugs for subsequent studies on test drugs provided the identical study protocol intended to classify a drug substance is maintained [6]. Consistency is especially important for cell lines as they are not phenotypically stable, and culturing techniques can select for different cell populations. LP and HP model drugs should be used as reference standards for monitoring intralaboratory variation and to set acceptance criteria for that assay. In addition to these, markers of monolayer or tissue integrity are evaluated in each experiment for monitoring reproducibility. This can be in the

form of zero or LP paracellular markers (e.g., mannitol, dextran, polyethylene glycols, fluorescein) and/or measures of TEER. Reference standards run with each test drug may also include an HP and LP model drug along with a substrate of efflux (e.g., digoxin, rhodamine 123, cyclosporin A, vinblastine, sulforhodamine) and active transporters. From the original set of experiments, acceptance criteria can be set for the HP internal standard (IS), HP, LP and monolayer marker, TEER values, and efflux substrate that is to be met for every experiment where a test drug is classified. The use of reference and internal standards can improve the predictive ability of cellular and tissue absorption models [46, 47]. They allow for better estimations of intestinal permeability by normalizing against an IS, especially to rank order compounds [48].

Based upon the relationship of P_{app} to f_a , the HP-IS in close proximity to low/high class boundary is chosen to classify a test drug. If the permeability of a test drug is equal to or greater than the HP-IS, the test drug is classified as highly permeable. Conversely, if the permeability of the test drug is less than the HP-IS, the test drug is classified as LP.

Within our laboratory, a 21-day Caco-2 cell assay was evaluated using over 20 model drugs for its ability to classify drugs as high or low permeability drugs [49]. An HP standard (metoprolol) and a zero permeability monolayer marker (FITC-dextran) were examined throughout the study as reference standards. There was a rank-order relation between Caco-2 permeability values and f_a in humans for the model drugs, with clear segregation between low and high permeability drug substances (Figure 28.2). If the % f_a of a model drug was 90–100% (HP), then the experimental P_{app} was greater than 14.0×10^{-6} cm/s. Alternatively, for LP model drugs (% f_a 0–89%) the P_{app} value was less than 5.0×10^{-6} cm/s. Labetalol ($P_{app} = 14.96 \times 10^{-6}$ cm/s) fell at the LP/HP boundary (Figure 28.2) and can serve as a HP-IS to classify drugs within this laboratory. The presence of functional P-gp was verified in the Caco-2 cells by the difference in the bidirectional transport of rhodamine 123.

We then used this Caco-2 cell assay to categorize representative fluoroquinolone drug substance permeability [50]. The drugs demonstrated some concentration-dependent permeability indicative of active drug transport. Based upon comparison to labetalol, ciprofloxacin was classified as a LP drug, whereas levofloxacin, lomefloxacin, and ofloxacin were classified as HP drugs, which matched their human in vivo bioavailabilities. All four fluoroquinolone drugs were subject to efflux transport (ciprofloxacin > lomefloxacin > rhodamine 123 > levofloxacin > ofloxacin).

Other studies in the literature with a Caco-2 permeability assay have shown the ability to accurately predict the permeability class of passively absorbed drugs (Figure 28.3). Artursson and Karlsson [41], Grés et al. [28], Correll et al. [51], Nguyen et al. [52], and Jung et al. [53] all had good discrimination between LP and LP drugs with practolol, metoprolol, dexamethasone, metoprolol, and verapamil as the boundary drugs, respectively, that can be used as a HP-IS for classification purposes.

Regional permeability coefficients and BCS permeability class of 19 drugs with different physicochemical properties were determined using excised segments from three regions of rat intestine (jejunum, ileum, and colon) [16]. Passively absorbed drugs were divided into two groups, hydrophilic LP drugs had P_{app} values 0.9 – 8.3×10^{-6} cm/s ($\log D = -0.1$, pH 7.4) and hydrophobic

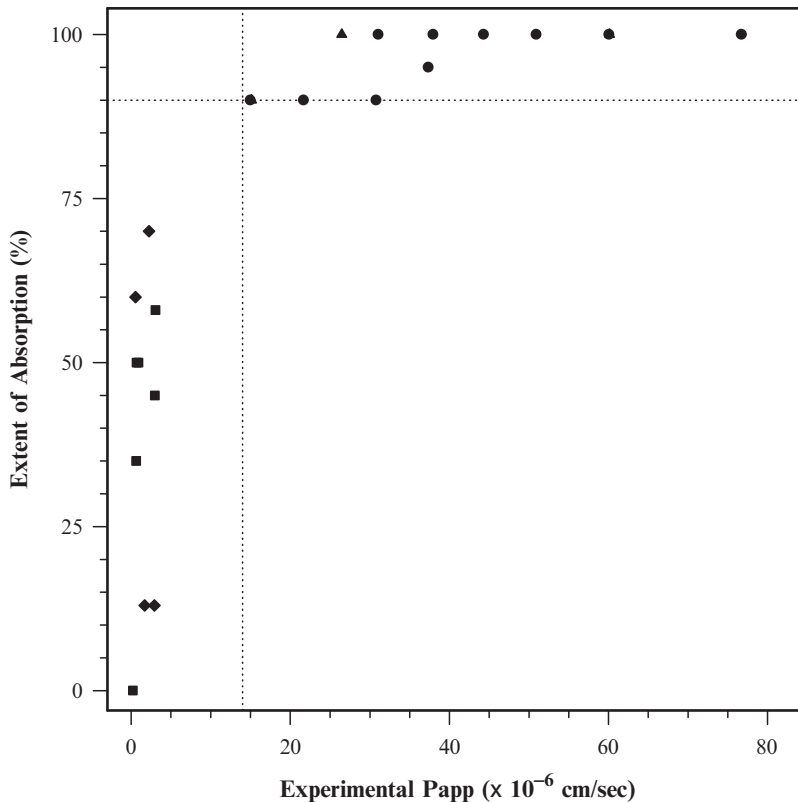


Figure 28.2 Method suitability of a Caco-2 permeability assay [49]. Horizontal line at 90% to classify as high or low permeability. Vertical line at low/high permeability boundary. (● Class I, ▲ Class II, ■ Class III, ◆ Class IV).

HP drugs had P_{app} values $11.4\text{--}100.3 \times 10^{-6}$ cm/s ($\log D = 0.07\text{--}2.4$, pH 7.4). An experimental protocol that isolated frog intestinal sacs was utilized for the assessment of 20 passively absorbed drugs' intestinal drug permeability in humans [18]. Drugs completely absorbed in humans had P_{app} values greater than 1×10^{-6} cm/s, while drugs absorbed <90% had P_{app} values lower than 1×10^{-6} cm/s. The frog intestinal sac method was generally able to classify the 20 model drugs as LP or HP [18].

A 7-day, 96-well Caco-2 permeability model was used to determine the permeability of 22 passively diffusing compounds and to classify them according to the BCS in a medium- to high-throughput mode [54]. The experimental permeability values with the Caco-2 cells correlated well to human in vivo permeability values [54]. A set of standard compounds belonging to the various BCS classes were used to assess the utility of the 96-well Caco-2 cells [55]. A validated 96-well Caco-2 cell system performed more efficiently for these investigators than the conventional 12- or 24-well systems while providing the same high-quality permeability screening data [56].

Solubility and permeability were measured by a high throughput solubility assay and parallel artificial membrane permeation assay (PAMPA), respectively [56]. The assays categorized 14 out of 18 drugs based on the BCS consistent with their known solubility and permeability characteristics [56].

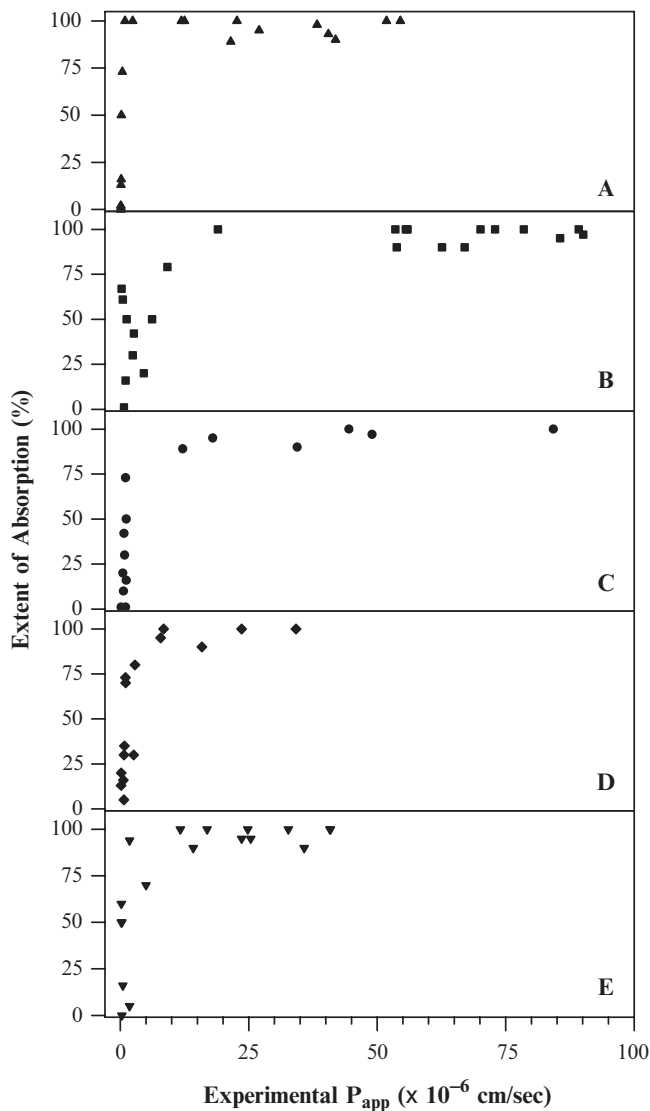


Figure 28.3 In vitro–in vivo correlations in the Caco-2 cell model. (A) Artursson and Karlsson [41], (B) Corell et al. [51], (C) Grés et al. [28], [D] Nguyen et al. [52], (E) Jung et al. [53].

The suitability and general applicability of an artificial membrane and PAMPA in vitro permeation methods were evaluated for their ability to predict drug absorption potential in comparison to Caco-2 cell literature data [57]. A linear correlation ($R^2 = 0.957$) was obtained between artificial membrane P_{app} and human absorption data, indicating the good predictive ability of the proposed method for HP compounds with greater differentiation of drugs with f_a below 50% [57].

28.5. Conclusions

The BCS guidance allows for the use of tissue and cell culture methods to classify a drug substance as high or low permeability [6]. The differences in laboratory methodologies for these assays suggest that a basic outline be

utilized for regulatory purposes that can be applied to a variety of intestinal tissue sources, epithelial cell types, and laboratory protocols. Therefore, the BCS guidance recommends the development of an *in vitro* permeability model based on method suitability to classify drugs with the use of reference standards. Method suitability is a process to establish and validate a cellular or tissue permeability assay for classification of drug substances. The advantages of such a system are that it accounts for interlaboratory variability, allows for improvements in technology, and is applicable to a variety of intestinal tissues and epithelial cell types [36]. Literature examples with cells [28, 41, 51–55], intestinal tissue [16, 18], and artificial membranes [56, 57] demonstrate the applicability and feasibility of method suitability for evaluating permeability models as outlined in the BCS guidance. An assay with established method suitability, standard compounds, and criteria for classifying drugs improves the reliability for such assays for regulatory applications.

References

1. Hussain AS, Lesko LJ, Lo KY, Shah VP, Volpe D, Williams RL (1999) The biopharmaceutics classification system: Highlights of the FDA's draft guidance. *Dissol Technol* 6:5–9.
2. Amidon GL, Lennernäs H, Shah VP, Crison JR (1995) A theoretical basis for a biopharmaceutical drug classification: The correlation of *in vitro* drug product dissolution and *in vivo* bioavailability. *Pharm Res* 12:413–420.
3. Lennernäs H, Abrahamsson B (2005) The use of biopharmaceutic classification of drugs in drug discovery and development: Current status and future extension. *J Pharm Pharmacol* 57:273–285.
4. Center for Drug Evaluation and Research, Food and Drug Administration (1995) Guidance for Industry. Immediate Release Solid Oral Dosage Forms: Scale-Up and Post-Approval Changes: Chemistry, Manufacturing and Controls, *In Vitro* Dissolution Testing, and *In Vivo* Bioequivalence Documentation.
5. Center for Drug Evaluation and Research, Food and Drug Administration (1997) Guidance for Industry. Dissolution Testing of Immediate Release Solid Oral Dosage Forms.
6. Center for Drug Evaluation and Research, Food and Drug Administration (2000) Guidance for Industry. Waiver of In Vivo Bioavailability and Bioequivalence Studies for Immediate Release Solid Oral Dosage Forms Based on a Biopharmaceutics Classification System.
7. Center for Drug Evaluation and Research, Food and Drug Administration (2000) Guidance for Industry. Food-Effect Bioavailability and Fed Bioequivalence Studies.
8. Committee for Proprietary Medicinal Products (2001) Note for Guidance on the Investigation of Bioavailability and Bioequivalence. CPMP/EWP/QWP/1401/98. The European Agency for the Evaluation of Medicinal Products, London.
9. Möller H (2002) The biopharmaceutical classification system (BCS) and its usage. *Drugs Made in Germany* 45:63–65.
10. Lennernäs H (1998) Human intestinal permeability. *J Pharm Sci* 87:403–410.
11. Lennernäs H (1997) Human jejunal effective permeability and its correlation with preclinical drug absorption models. *J Pharm Pharmacol* 49:627–638.
12. Stewart BH, Chan OH, Lu RH, Reyner EL, Schmid HL, Hamilton HW, Steinbaugh BA, Taylor MD (1995) Comparison of intestinal permeabilities determined in multiple *in vitro* and *in situ* models: Relationship to absorption in humans. *Pharm Res* 12: 693–699.

13. Fagerholm U, Johansson M, Lennernas H (1996) Comparison between permeability coefficients in rat and human jejunum. *Pharm Res* 13:1336–1342.
14. Grass GM, Sweetana SA (1988) *In vitro* measurement of gastrointestinal tissue permeability using a new diffusion cell. *Pharm Res* 5:372–376.
15. Grass GM, Sweetana SA (1989) A correlation of permeabilities for passively transported compounds in monkey and rat jejunum. *Pharm Res* 6:857–862.
16. Ungell AL, Nylander S, Bergstrand S, Sjoberg A, Lennernas H. (1998) Membrane transport of drugs in different regions of the intestinal tract of the rat. *J Pharm Sci* 87:360–366.
17. Nejdfor P, Ekelund M, Jeppsson B, Weström BR (2000) Mucosal *in vitro* permeability in the intestinal tract of the pig, the rat, and man: Species- and region-related differences. *Scand J Gastroenterol* 35:501–507.
18. Trapani G, Franco M, Trapani A, Lopodota A, Latrofa A, Gallucci E, Micelli S, Liso G (2004) Frog intestinal sac: A new *in vitro* method for the assessment of intestinal permeability. *J Pharm Sci* 93:2909–2919.
19. Ruan LP, Chen S, Yu BY, Zhu DN, Cordell GA, Qiu SX (2006) Prediction of human absorption of natural compounds by the non-everted rat intestinal sac model. *Eur J Med Chem* 41:605–610.
20. Hidalgo IJ, Raub TJ, Borchardt RT (1989) Characterization of the human colon carcinoma cell line (Caco-2) as a model system for intestinal epithelial permeability. *Gastroenterology* 96:736–749.
21. Artursson P (1991) Cell cultures as models for drug absorption across the intestinal mucosa. *Crit Rev Ther Drug Carrier Syst* 8:305–330.
22. Delie R, Rubas W (1997) A human colonic cell line sharing similarities with enterocytes as a model to examine oral absorption: Advantages and limitations of the Caco-2 model. *Crit Rev Ther Drug Carrier Syst* 14: 221–286.
23. Gan LSL, Thakker DR (1997) Applications of the Caco-2 model in the design and development of orally active drugs: Elucidation of biochemical and physical barriers posed by the intestinal epithelium. *Adv Drug Deliv Rev* 23:77–98.
24. Meunier V, Bourrie M, Berger Y, Fabre G (1995) The human intestinal epithelial cell line Caco-2; pharmacological and pharmacokinetic applications. *Cell Biol Toxicol* 11:187–194.
25. Irvine JD, Takahashi L, Lockhart K, Cheong J, Tolan JW, Selick HE, Grove JR (1999) MDCK (Madin-Darby canine kidney) cells: A tool for membrane permeability screening. *J Pharm Sci* 88:28–33.
26. Cho MJ, Thompson DP, Cramer CT, Vidmar TJ, Scieszka JF (1989) The Madin Darby canine kidney (MDCK) epithelial cell monolayer as a model cellular transport barrier. *Pharm Res* 6:71–77.
27. Caro I, Boulenc X, Rousset M, Meunier V, Bourrié M, Julian B, Joyeux H, Roques C, Berger Y, Zweibaum A, Fabre G (1995) Characterisation of a newly isolated Caco-2 clone (TC-7), as a model of transport processes and biotransformation of drugs. *Int J Pharm* 116:147–158.
28. Grés MC, Julian B, Bourrié M, Meunier V, Rogues C, Berger M, Boulenc X, Berger Y, Fabre G (1998) Correlation between oral drug absorption in humans and apparent drug permeability in TC-7 cells, a human epithelial intestinal cell line: Comparison with the parental Caco-2 cell line. *Pharm Res* 15: 726–733.
29. Wikman A, Karlsson J, Carlstedt I, Artursson P (1993) A drug absorption model based on the mucus layer producing human intestinal goblet cell line HT29-H. *Pharm Res* 10:843–852.
30. Collett A, Sims E, Walker D, He YL, Ayrton J, Rowland M, Warhurst G (1996) Comparison of HT29–18-C₁ and Caco-2 cell lines as models for studying intestinal paracellular drug absorption. *Pharm Res* 13:216–221.

31. Madara JL, Stafford J, Dharmasathaphorn K, Carlson S (1987) Structural analysis of a human intestinal epithelial cell line. *Gastroenterology* 92:1133–1145.
32. Thwaites DT, Hirst BH, Simmons NL (1993) Passive transepithelial absorption of thyrotropin-releasing hormone (TRH) via a paracellular route in cultured intestinal and renal epithelial cell lines. *Pharm Res* 10:674–681.
33. Duizer E, Penninks AH, Stenhuis WH, Groten JP (1997) Comparison of permeability characteristics of the human colonic Caco-2 and rat small intestine IEC-18 cell lines. *J Control Release* 49:39–49.
34. Tavelin S, Milovic V, Ocklind G, Olsson S, Artursson P (1999) A conditionally immortalized epithelial cell line for studies of intestinal drug transport. *J Pharmacol Exp Ther* 290:1212–1221.
35. Pauletti GM, Audus KL, Hidalgo IJ (1998) Effects of co-solvents on the physical barrier properties of Caco-2 cell monolayers. *Pharm Sci* 1(1): abstract 1182.
36. Volpe DA, Faustino PJ, Yu LX, Hussain AS (2001) Towards the standardization of an *in vitro* method of drug absorption. *Pharm Forum* 27:2916–2922.
37. Volpe DA, Möller H, Yu LX (2002) Regulatory acceptance of *in vitro* permeability studies in the context of the biopharmaceutics classification system. In: Lehr CM (ed.) *Cell Culture Models of Biological Barriers: In Vitro Test Systems for Drug Absorption and Delivery*. Taylor & Francis Publishing Group, London New York, pp. 130–139.
38. Hillgren KM, Kato A, Borchardt RT (1995) *In vitro* systems for studying intestinal drug absorption. *Med Res Rev* 15:83–109.
39. Hosoya KI, Kim HJ, Lee VHL (1996) Age-dependent expression of P-glycoprotein gp170 in Caco-2 cell monolayers. *Pharm Res* 13:885–890.
40. Audus KL, Bartel RL, Hidalgo IJ, Borchardt RT (1990) The use of cultured epithelial and endothelial cells for drug transport and metabolism studies. *Pharm Res* 7:435–451.
41. Artursson P, Karlsson J (1991) Correlation between oral drug absorption in humans and apparent drug permeability coefficients in human intestinal epithelial (Caco-2) cells. *Biochem Biophys Res Commun* 175:880–885.
42. Yee S (1997) *In vitro* permeability across Caco-2 cells (colonic) can predict *in vivo* (small intestinal) absorption in man—fact or myth. *Pharm Res* 14: 763–766.
43. Pade V, Stavchansky S (1997) Estimation of the relative contribution of the transcellular and paracellular pathway to the transport of passively absorbed drugs in the Caco-2 cell culture model. *Pharm Res* 14:1210–1215.
44. Yazdanian M, Glynn SL, Wright JL, Hawi A (1998) Correlating the partitioning and Caco-2 cell permeability of structurally diverse small molecular weight compounds. *Pharm Res* 15:1490–1494.
45. Biganzoli E, Cavenaghi LA, Rossi R, Brunati MC, Nolli ML (1999) Use of a Caco-2 cell culture model for the characterization of intestinal absorption of antibiotics. *Farmaco* 54:594–599.
46. Sulzbacher A, Jarosch A, Schüler R, Acerbi D, Ventura P, Puccini P, Woodcock BG (1998) Validation of a Caco-2 cells monolayer culture for drug transport studies. *Int J Clin Pharmacol Ther* 36:86–89.
47. Dowty ME, Dietsch CR (1997) Improved prediction of *in vivo* peroral absorption from *in vitro* intestinal permeability using an internal standard to control for intra- and inter-rat variability. *Pharm Res* 14:1792–1797.
48. Faustino PJ, Volpe DA, Knapton AD, Ellison CD, Hussain AS (1999) Value of an internal standard approach for determining internal permeability class membership of drugs. *AAPS PharmSci* 1(4): abstract.
49. Volpe DA, Faustino PJ, Ciavarella AB, Asafu-Adjaye EB, Ellison CD, Yu LX, Hussain AS (2007) Classification of drug permeability with a Caco-2 cell monolayer assay. *Clin Res Reg Affairs* 24:39–47.

50. Volpe DA (2004) Permeability classification of representative fluoroquinolones by a cell culture method. *AAPS PharmSci* 6(2): article 13.
51. Correll MA, Broward-Partin SM, Hansen DK, Behlow HW, Lewis MM, Rose JQ, Thompson TN (2000) Achievement of higher throughput in the Caco-2 absorption screen using a simplified experimental design. *AAPS PharmSci* 2(4): abstract.
52. Nguyen L, Dautrey S, Vo C, Sexton R, Morin PE, Ducharme, R. Proudlock (2001) Validation of a Caco-2 cell model for a higher throughput permeability assays. *AAPS PharmSci* 3(3): abstract.
53. Jung SJ, Choi SO, Um SY, Kim JI, Choo HY, Choi SY, Chung SY (2006) Prediction of the permeability of drugs through study on quantitative structure-permeability relationship. *J Pharm Biomed Anal* 41:469–475.
54. Alsenz J, Haenel E (2003) Development of a 7-day, 96-well Caco-2 permeability assay with high-throughput direct UV compound analysis. *Pharm Res* 20:1961–1969.
55. Marino AM, Yarde M, Patel H, Chong S, Balimane PV (2005) Validation of the 96 well Caco-2 cell culture model for high throughput permeability assessment of discovery compounds. *Int J Pharm* 297:235–241.
56. Obata K, Sugano K, Machida M, Aso Y (2004) Biopharmaceutics classification by high throughput solubility assay and PAMPA. *Drug Dev Ind Pharm* 30:181–185.
57. Corti G, Maestrelli F, Cirri M, Zerrouk N, Mura P (2006) Development and evaluation of an in vitro method for prediction of human drug absorption II. Demonstration of the method suitability. *Eur J Pharm Sci* 27:354–362.

Appendix Lab Protocols

The protocols to the respective chapter are available for
download from the following URL

<http://www.pharmacy.tcd.ie/protocols>

Index

A

- ABCA1*, 270
- ABCA3*, 270
- ABC transporters, 244, 270, 293, 406, 561, 570, 578
 - expression, 386
 - function and pharmacokinetic roles of, 568–569
 - structure and tissue distribution, 567–568
- Abraham's data set, 540
- Absorption constants (*K_a*), 492–494, 497–498, 503
- Absorption, distribution, metabolism and elimination (ADME), 578
- Absorption number (*A_n*), 495–496
- Absorption potential (AP), 491
- Absorption processes, 4
- Absorption scale factors, 497
- A549 cell line, 266–268
- Actin polymerization, 353
- Acyclovir oral bioavailability, 562
- [³H]Adenosine by retina, integration plot of initial uptake, 327
- Adenosine triphosphate (ATP), 123
- Adeno-SV40 hybrid virus, 620
- Ad5-induced ocular disease treatment, 313
- β -Adrenergic antagonist dihydroalprenolol, 374
- Advanced compartmental absorption and transit (ACAT) model, 497
- Aerosol inhalation, 141
- Aerosolised gene therapy, lung cancer treatment, 240
- Air-interfaced (AIC) culture method, 227, 242, 446–450
- Akaike Information Criterion (AIC), 467–469
- Alkane-water system, 513
- Alveolar epithelial type I (ATI) cells, 259
 - AEC damage in, 264
 - in alveoli, 260
 - apical plasma membrane of, 261
 - HTI56 protein in, 263
 - shape of, 260
 - T1 α in, 262
 - water permeability of, 262
- Alveolar epithelial type II (ATII) cells, 259
 - AQP-3 expression, 262
 - caveolin-1 expression, 262
 - characteristic, 268
 - dendritic cells (DC) movement, role in, 265
 - γ -aminobutyric acid receptor pi (GABRP) association, 263
 - localization of, 260
 - Na⁺ channels localization, 264
 - in rat and mouse, 271
 - shape of, 260, 261
- Alveolar epithelial cells
 - alveolus walls, 259
 - barrier properties of, 263
 - biopharmaceutical research, use in, 269–272
 - for chemokines, 265
 - of human, 259–261
 - primary models of, 268–269
 - surface area, 259
 - surfactant layer role, 261
- Alveolar macrophages, 140
- Alveolus
 - blood-air barrier function of, 263–265
 - gas exchange in, 271
 - solute carrier protein (SLC) expression, 270
 - wound repair of, 265–266
- Amidase activity, in lysosomes, 642
- Amino acid ester modification of drugs, 564
- Aminopeptidase M, 249
- Aminopeptidase N, 249
- Analytical techniques. *See also* Targeted drug delivery systems
 - confocal laser scanning microscopy, 655–659
 - flow cytometry, 652–655
 - principles, 652–653
- Angiotensin-converting enzyme (ACE), 185
- Animal buccal mucosa, for buccal absorption estimation, 172
- Animal tissues, availability of, 115
- Antiallergic drugs across, passage-cultured human nasal epithelial cell layer, 226
- API and bioavailability, 432
- APM. *See* Aminopeptidase M
- APN. *See* Aminopeptidase N

- Apocrine glands, 6
- Appendages route, 7–8
- Aquaporin-5 (AQP-5), 262
- Artificial Neural Networks (ANN), 474–476
- ASF. *See* Absorption scale factors
- Assembled tight junctions regulation by
extracellular ATP, 349
- Astra-type MSLI, 449
- Atenolol, mucosal-to-submucosal (m-s) value
of, 169–170, 173
- ATPase activity, 651
- ATP-binding cassette (ABC), 578
- ATP-binding cassette (ABC)-transporters, 243,
406
- ATP-dependent export pump, 402
- ATP-driven drug export pumps, 401
- ATR-FTIR. *See* Attenuated total reflectance
Fourier-transformation infrared
- Attenuated total reflectance
Fourier-transformation infrared, 10
- Autofluorescence, 644
- Automatic relevance determination (ARD)
approach, 538
- Automotility factor receptor (AMFR), 604
- Azidothymidine drug, 563
- B**
- Bacteriophage (T7, T3), 582
- Basement membrane, in buccal mucosa, 93
- Bauhinia purpurea, 261
- Beckett and Triggs, buccal absorption test of,
96
- Benzoic acid absorption, in nasal, 220
- BeWo cells as placental model, 376
- β -globin gene, 582
- Bifurcating airway model, 236
- Bile salt export pump, 568
- Biocoat technique, for Caco-2 cells, 198
- Biological activity
biosynthetic and metabolic, 6
skin absorption pathways
appendages route, 7–8
the *stratum corneum*, intercellular and
transcellular routes, 7
skin appendages, 6–7
- Biopharmaceutics Classification System
(BCS), 36, 45, 60, 62, 423, 666
method suitability, 672–676
permeability measurements, 669–672
regulatory application of, 667–669
- Biorecognition, active targeting of drugs,
642
- Biricodar (VX-710) inhibitor, 402
- β -lactam inhibitors, 19
- Blood-brain barrier
discovery of, 398
and drug delivery, 400–403
function study models, 405–410
partition coefficient, 514
and Silico methods, 512
structure and function of, 399–400
transport proteins expression at, 401
- Blood-retinal barrier (BRB) transport
methodology, 322–323
- Blood-to-retina influx transporters at inner
BRB, 332–334
- Bovine serum albumin (BSA), 192, 645
- Bovine Spongiform Encephalopathy (BSE),
117
- Bowman's layer, 286
- Brain capillary cells culturing and assaying,
409–410
- Brain capillary endothelial cell culture,
406–407
- Brain penetration lipophilicity using linear
regression (LR) method, 512
- Breast cancer resistance protein (BCRP), 143,
187, 244, 371, 383–386
associated ATPase activity, 385
expression, 376
expression in syncytiotrophoblast, 384
transfected K562 cells, 386
- Bronchial circulation, in lungs, 138
- Buccal cell cultures, 102–103
- Buccal mucosa
aminopeptidase activity, 94
assessment method to, 89
CYP activity in, 175
drug permeability assessment method, 95
drug permeation assessment, 168
enzymes existence in, 176
epithelial thickness and permeability
coefficient (P) for tritiated water, 98
of monkeys, 168
oral cavity
D glucose, 95
positive diffusion, 94
passive diffusion, 94
permeability barrier of
basement membrane, 93
chemical nature of, 92
location of, 91
metabolic barrier, 93
salivary film and mucus layer, 92
permeability enhancing, 99
porcine permeability, 172
structure and role of, 90, 91
- C**
- Caco-2 cell
model, 488, 490
monolayers, drug permeability in, 146
monolayer system
grown on Transwell filter insert, 420
and PAMPA, 426–427
permeability and human absorption of drugs
and excipients, 421
system model
absorption enhancers evaluation and
selection, 194

- assessment of drugs, 194–195
- Biocoat technique for, 198
- dissolution prediction, 195
- for drug permeability, 193
- growth, 198
- implementation of, 199
- for intestinal drug absorption study, 188
- limitations and drawbacks, 196–197
- prodrugs evaluation, 194
- screening of drugs, 193–194
- study of cytotoxicity, 195–196
- Caesium chloride centrifugation (CsCl), 581
- Caffeine, mucosal-to-submucosal (m-s) value of, 169–170, 173
- Calcium-mediated regulation of R_{TJ} for functional analysis, 352
- Ca^{2+} -mediated regulation model of occludin-based occlusion of tight junction, 348
- Camptothecin derivatives, anticancer substances, 382
- Capillary endothelial surface, in lungs, 138
- CAR. *See* Constitutive androstane receptor
- Carrier-mediated processes, transcellular route, 222
- Carrier-mediated transport systems
 - compounds absorbed by, 82
 - membrane permeability for, 82
 - Na^+/H^+ exchangers, 78, 81
 - probe substrates
 - L-carnitine and methotrexate, 83
- Caveolae
 - in alveolar wall, 260
 - pharmacology
 - action at, 692
 - cancer cell ablation, 606–607
 - caveolae-linked endocytosis, 603–604
 - caveolar mechanism of multidrug resistance, 605–606
 - caveolin-1 and caveolin-2, 602
 - caveolin expression, 604–605
 - drug delivery by caveolae-mediated endocytosis, 600, 602–603
 - enrichment of caveolin, 599
 - estradiol to endothelial cells affects signaling, 601
 - folate conjugates and therapeutics, 608
 - folate receptor, receptor clustering, and potocytosis, 607–608
 - isoforms of, 599
 - non-caveolae, clathrin-independent endocytosis, 603–604
 - two-stage fractionation procedure, 600
- Caveolae membrane (CM), 601
- Caveolin-1 expression, 262
- Caveolin-1, Src kinase oncogene, 605
- cDNA cloning kit, 582
- Cefazolin, ocular drug, 312
- Cell-associated fluorescence intensity, 652
- Cell–cell adhesion mechanisms, 238
- Cell–cell and cell–matrix interactions, 642–643
- Cell culture models, in vitro
 - air-interfaced (AIC) culture, 227
 - liquid-covered culture (LCC) method, 225
 - primary and passaged, 224
 - TEER and permeability relation ship of, 226
- Cell Culture models, targeted drug delivery, 643
- 4F2Cell surface antigen (4F2hc), 332
- Cell–target system interaction
 - active or passive uptake, 650–651
 - binding vs. uptake, cytoinvasion assays, 648–650
 - cytoadhesion assays, 645–647
 - cytoevasion, 650
 - specificity of interaction, 647–648
 - uptake and intracellular localization, acidic compartments, 651–652
- CEPI-17-CL 4, 294
- CFTR. *See* Cystic fibrosis transmembrane conductance regulator
- Charge, descriptor, 469
- Chemically based transfection systems, 623
- Chemical transfection reagents, 623
- Chicago River green, 643
- Chinese hamster ovary (CHO), 584
- Choriocarcinoma cell line JAr, 376
- Choriocarcinoma derived cell line (BeWo) for transcellular distribution of drugs study, 375
- Chronic obstructive pulmonary disease (COPD), 136, 239
- CIPSLINE database, 524–525
- Cisplatin, anticancer substances, 382
- Clark's data set, 522
- Claudin/Occludin model of regulation of R_{TJ} , 351
- Claudin proteins, 261, 347
- CNS-active drugs, 525
- CNT. *See* Concentrative nucleoside transporters
- Collagen matrix, 312
- Colonic epithelium
 - active in absorbing, 81
 - drug absorption barrier, 78
 - intestinal epithelium, 84
- Colon luminal environment, 79
- Colon-to-SI (small intestine) ratios, membrane permeability for, 84–86
- Committee for Proprietary Medicinal Products, 668
- Compartmental absorption and transit (CAT) models, 496–500
- Concentration-dependent adenosine uptake, 325
- Concentrative nucleoside transporters, 401

- Conducting airways, structure of, 236, 237
 Conductor-like Screening Model, 476
 Confocal laser scanning microscopy (CLSM), 655
 drug permeation pathways studies, 116
 Conjunctival disorders, 312–313
 Conjunctival short-circuit current, 315
 Conjunctival transport properties, model for
 conjunctival disease models, 317
 excised conjunctival tissues, 313–316
 primary culture models of conjunctival
 epithelial cell layers, 316–317
 Conjunctiva-scleral pathway, 310
 Conjunctiva tissues and ocular surface,
 308–309
 Constitutive androstane receptor, 382
 Corneal cell culture models
 primary corneal cell cultures, 290–291
 Cortical submembranous acto-myosin ring,
 353
 COSMO. *See* Conductor-like Screening Model
 Crohn's disease, 567
 Crosscarmellose-Na, calcium sequestering
 properties, 440
 CULTEX system, 446. *See also* Drug transport
 across
 Cultured nasal cell model, for drug transport,
 223
 Cyclosporine A (CsA), drug, 334
 CYP3A4, 173
 CYP3A, expression, 671
 CYP3A4, in human liver, 140
 CYP2C9, 173
 CYP2D6, 173
 CYP expression, cytochrome P450
 expression profiles of, 245, 246, 247
 Cystic fibrosis (CF), 239, 242
 airway, in vitro model
 autosomal recessive disease, 242
 epithelial cells, 242
 Cystic fibrosis transmembrane conductance
 regulator, 239, 308
 Cytoadhesion, 648
 Cytoevasion, 650
 Cytoinvasion, 648
 Cytokeratin filaments, 625
 Cytoplasmic tight junctional proteins, 344
 Cytosolic Ca²⁺ signaling, 349
 Czerenkov counts, 586
- D**
- 3-D cornea model, 296, 297
 Dehydroepiandrosterone sulfate, 385
 Dendritic cells (DC) movement, ATII cells role
 in, 265
 Descemet's membrane, 288
 Dexniguldipine (B8509–035) inhibitor, 402
 DHEAS. *See* Dehydroepiandrosterone sulfate
 Dimethyl sulfoxide (DMSO), in PAMPA, 192
 3-(4,5-Dimethylthiazol-2-yl)-2,5-diphenyl-2H-
 tetrazoliumbromid (MTT) cytotoxicity
 assay, 436
 Dioleoylphosphatidylcholine, 425
 Directional cloning systems, 582
 Discriminant function analysis (DFA) for
 blood–brain transport, 516
 Dissolution number (Dn), 496
 Dissolution testing, drug, 667
 Distal blood-air barrier constituents, lung,
 263
 Dithiothreitol (DTT), 622
 DMPC-water model, 541
 DOPC. *See* Dioleoylphosphatidylcholine
 Dose number (Do), 496
 Double-Sink PAMPA, 425
 Double-sink™, 191
 Doxorubicin, 645
 Doxorubicin-lectin pro-drugs, 649
 Drug absorption
 and food effects, 435
 of intestines, influencing factors, 183–184
 and metabolism, in ex vivo and in situ
 drug permeability techniques of,
 114–115
 experimental setup for nasal perfusion,
 115
 limitation of drug absorption and
 metabolism studies, 116–117
 living tissues, 114
 process
 gastrointestinal in situ models, perfusion
 techniques, 46–55
 gastrointestinal in vitro models, 36–45
 gastrointestinal in vivo models, 55–62
 in situ
 buccal mucosa, 89
 coadministration with protease inhibitors,
 119
 colon role in, 78
 tyrosine-linked drug, 117
 studies, 269–272
 in vivo
 absorption of thiamine, 95
 carrier-mediated systems, 95
 nicotine absorption, 97
 perfusion cells in, 96
 in plasma, 96, 97
 Drug candidate screening, 183
 Drug permeability, 665
 Drug permeation
 in buccal mucosa, 168, 172
 of hydrophilic compounds, 170
 Drugs testing, using animals tissues
 drawbacks, 284
 Drug substances, solubility and permeability,
 666
 Drug transporters, determination and
 classification of, 561

- Dry eye syndromes, 313
 Dry powder inhaler (DPI), 141
 DS-PAMPA. *See* Double-Sink PAMPA
 Dual expression plasmid, 594
 Dulbecco's modified Eagle's medium (DMEM), 623
- E**
 E-cadherin, 625
 Eccrine glands, 6
 ECVAM. *See* European Centre for the Validation of Alternative Methods
 Effective permeability coefficient (P_{eff}), 490, 494–496, 499, 503
 Efflux-mediated transport, in intestinal mucosa, 185
 Elacridar (GF 120918) inhibitor, 402
 Electron microscopy (EM), 603
 Electron-microscopy freeze-fracture technique, 343
 Electroporation, 623
 Enalapril (ACE inhibitor) drug, 565
 Endocytic processes, transcellular route, 222
 Endothelial nitric oxide synthase (eNOS), 354, 602
 Endothelin-1 (ET-1) effects on NBDL-CSA, 404
 ENT. *See* Equilibrative nucleoside transporters
 Epidermal growth factor receptor (EGFR), 646
 EpiOcular cell culture system, 293
 Epithelial permeability increment, of hydrophilic compounds, 140
 Epithelium, buccal mucosa, 90
 Equilibrative nucleoside transporters, 401
 ERK/MAPK (mitogen-activated protein kinase) cascades, 356
Erythrina cristagalli, 261
Escherichia coli, 588, 590
 Esterase activity, 642
 Estrogen modulation of paracellular permeability, 355
 Estrogen regulation of cortical myosin, 355–356
 Estrogen regulation of R_{TJ} , 349–350
 ET_B receptor antagonist, 404
 Ethanol, in PAMPA, 192
 Ethylenediamine tetraacetic acid (EDTA), 119, 120, 643
 Ethylene glycol tetraacetic acid (EGTA), 622
 European Centre for the Validation of Alternative Methods, 21
 Experimental models, for drug transport studies
 animal species choice, 65, 66
 animal suitability evaluation, 67, 68
 bioavailability
 large animal models and humans, 67
 predicted fraction absorbed, relation to, 66
 rat models and humans, 66, 67
 in situ vs. in vivo models, 64, 65
 Expressed sequence tags (EST), 585
 Expression systems, of drug transport proteins
 advantages and disadvantages in expression, 588, 589
 mammalian cell lines, use of, 595
 Extracellular matrix (ECM), 622
 Extracellular signal-regulated kinase (ERK)1/2 cascades, 350
 Ex vivo transporter gene expression levels at inner blood-retinal barrier, 330–332
 Eye, transcorneal drug absorption in, 289
 Eye medications, 284
- F**
 Farnesoid-X-receptor (FXR), 382
 Fasted state simulated intestinal fluid (FaSSIF), 432
 Fed state simulated intestinal fluid (FeSSIF), 432
 Fibrin-based sealants, 312
 Fick's diffusion law, 222
 Flavin monooxygenases (FMO), 245
 Floxuridine drug, 563
 Fluorescein, 643
 Fluorescein isothiocyanate (FITC), 101, 651
 for peptides compounds, 171
 Fluorescence emission, 652
 Flynn data set, permeability coefficients
 logarithms, 463
 Food and Drug Administration (FDA), 642, 667
 Forward scatter (FS), 653
 Four-descriptors model, 542
 Fraction dose absorbed (F_{abs}), 487–488, 491, 495–496, 499, 500, 501, 503, 505
 Franz-type diffusion cells, 97–99, 168, 169
 Fuc α 1-2Gal β -R-binding lectins, 641
 Fuc α 1-2Gal β -terminated antigens, 641
- G**
 γ -aminobutyric acid receptor pi subunit (GABRP), in ATII cells, 263
 Ganciclovir oral bioavailability, 562
 Ganglion cell layer, 323
 Ganglioside M1 (GM1), 603
 Gastrointestinal absorption, of drugs
 absorption extent
 effective permeability coefficient, use of, 44
 fundamental dimensionless groups, use of, 45
 Graetz number, 44
 effective permeability coefficient estimation
 mass balance model, 42, 43
 physicochemical properties, 42
 standardisation and validation criteria, 62, 63
 viability criteria, 64

- Gastrointestinal (GI) tract and drug absorption, 419
- Gastrointestinal in situ models
- anaesthetised large animal model, 55
 - isolated and vascularly perfused models
 - advantages, 54
 - experimental set-up, 53
 - mesenteric lymph duct cannulation model
 - current research studies, 55
 - experimental set-up, 54
 - perfusion techniques
 - advantages and limitations, 49
 - applications and modifications, 49–50
 - closed loop technique, 47
 - comparison of closed and open loop techniques, 48
 - single pass (open loop) technique, 48
 - venous sampling methods
 - advantages, 50
 - mesenteric cannulation and drainage, 51
 - permeability calculations, 52, 53
- Gastrointestinal in vitro models
- absorption potential (AP) model, 39
 - aqueous pores and lipoidal pathway, 37, 38
 - effective permeability coefficient, 41
 - factors influencing, 36, 37
 - general (dispersion) model, 40, 41
 - passive absorption model, 38, 39
 - pH partition hypothesis, 37
 - polar surface area (PSA) based model, 39, 40
 - quasi-equilibrium models, 40
- Gastrointestinal in vivo models
- cannulated conscious large animal model
 - advantages and limitations, 59
 - experimental set-up, 57
 - pharmacokinetics of verapamil studies, 58
 - variations of the model, 58
 - cannulated conscious rat models
 - absolute bioavailability and hepatic extraction ratio, 57
 - experimental set-up, 55, 56
 - single pass vs. isolated loops model, 56
 - Loc-I-Gut technique
 - animal models, 59
 - applications, 61, 62
 - human model, device description, 60
 - validity of results, 60, 61
- Gastrointestinal Transit Absorption (GITA) model, 498–499
- GastroPlus, 501, 503
- absorption simulation software package, 497–498
- GCL. *See* Ganglion cell layer
- Gemcitabine drug, 563
- GeneRacer, 587, 588
- General regression neural network, 540
- Gentamicin, ocular drug, 312
- Glutamic acid transporter, 593
- γ -glutamyl transpeptidase, 374
- P-Glycoprotein
 - transcription modulation, 404
- Glycosyl phosphatidylinositol (GPI)-anchored protein, 603
- GRNN. *See* General regression neural network
- Guanidinium isothiocyanate method, RNA preparation, 581
- Guanosine triphosphate (GTP), 602
- H**
- Hank's balanced salt solution (HBSS), 436
- HCE-T cells, 292–293
- Helix pomatia*, 262
- Heparin infusion, for thrombosis prevention, 147
- HEPES-buffered Ringer's solution, 328
- Heterologous expression systems, 588. *See also* Expression systems, of drug transport proteins
- bacterial expression systems, 590–591
 - cell-free expression systems, 588–590
 - insect cell lines, 593
 - mammalian cell lines, 593
 - expression of multiple transport proteins, 595–596
 - expression vectors, 594
 - non-polarised and polarised cell lines, 594–595
 - Xenopus oocytes*, 592–593
 - yeast expression systems, 591–592
- HGNC. *See* Human Gene Nomenclature Committee
- High-activity promoters (PMA1, PDR5), 591
- Highest dose strength (HDS), 666
- Highly soluble (HS), 666
- High Throughput Screening (HTS), 487
- HIV-1 nucleoside reverse transcriptase inhibitors, 384
- Horseradish peroxidase, in tissue, 91
- Human Ad mutants, 313
- Human alveolar epithelial cells (hAEPs), 267
- Human alveolar epithelium, 259–261
- Human chorionic gonadotropin (hCG), 374
- Human cornea
 - corneal endothelium role, 288
 - corneal epithelium, 286
 - layers in, 286
 - Na⁺-K⁺-ATPase in, 288
 - ocular biodefense system, 285
 - tear film, 286
 - tight junction complex, 287
- Human Gene Nomenclature Committee, 561
- Human immunodeficiency virus (HIV), blood-borne diseases, 240
- Human papilloma virus (HPV), 620
- Human placenta, 369
- Human placental lactogen (hPL), 374
- Human respiratory system, 137

- Human telomerase reverse transcriptase cDNA (hTERT), 621
- Human vaginal-cervical epithelia, 340
- Human vaginal-ectocervical epithelial cells, ion transporters in, 343
- Hydrogen Bond Donors (HBD), 480, 523, 534
- I**
- IC50 values, 580, 647
- iDEA database, structurally diverse compounds, 488, 498, 501, 503
- Idiopathic renal hypouricemia (URAT1), 566–567
- Iganidipine, Ca²⁺ antagonist, 310
- ILM. *See* Inner limiting membrane
- Immortalization, epithelial cells in primary culture, 616
- human epithelial cells as model, 619
 - spontaneous transformation, 619–620
 - transformation *vs.* immortalization, 618
 - transformed and immortalized cell systems, generation of, 621
 - characterization of transformed/immortalized cells, 625–626
 - primary cultures, 621–623
 - transfection and isolation of transformants, 623–625
 - viral and oncogene transformation, 620–621
- Immunoglobulin G (IgG), 642
- INL. *See* Inner nuclear layer
- Inner blood-retinal barrier, mechanism of drug transport
 - blood-to-retina influx transport, 332–334
 - retina-to-blood efflux transport, 334
- Inner blood-retinal barrier model, 324–326
- Inner BRB, representative transporters and transport processes, 333
- Inner limiting membrane, 323
- Inner nuclear layer, 323
- Inner plexiform layer, 323
- Integration plot analysis, 326–327
- Integrins, 643
- Intellipharm PK, computer program, 492–494
- Intercellular adhesion molecule-1 (ICAM-1), 261, 262
- Intercellular domain organization, 90–91
- internal ribosome entry site (pIRES), plasmid, 594
- Interstitial fluid, drainage pathway for, 139
- Intestinal drug absorption
 - influencing factors, 183–184
 - models strengths and weaknesses, study, 188
- Intestinal epithelial cells, drug transporters, 187, 570
- Intestinal mucosa, barrier in drug absorption
 - biochemical barrier function, 185–187
 - physical barrier function, 184–185
- Intestinal mucosa layers, 184
- Intestinal peptide transporter PepT1, 651
- Intestinal perfusion studies, drug, 669
- In vitro–in vivo correlation (IVIVC), 667
- In vitro penetration
 - stratum corneum
 - assessment of drug levels in, 16–17
 - Saarbrücken penetration model, 17
 - stratum corneum depth determination
 - optical spectroscopy, use of, 18
 - removed tissue weight, use of, 18
 - tape-strip number, use of, 17–18
- In vitro permeation studies
 - acceptor solutions, 13
 - animal skin membranes
 - amphiphilic composite membranes, 16
 - nonskin membranes, 15
 - suitability for research, 15
 - dosage and temperature control, 12–13
 - human skin membranes
 - harvesting different areas, 14–15
 - human epidermis equivalent reconstruction, 15
 - preparation, 13–14
 - supply and source, 13
 - standardization and regularization, 12
- In vitro studies
 - buccal epithelial cell cultures, 172–176
 - buccal tissue isolation, 168
 - acyclovir delivery, 171
 - intestinal absorption study, 187
 - intestinal metabolism assessment, 204–205
- In vitro techniques, information sources, 4
- In vivo animal models, 144
- In vivo blood-to-retina influx transport
 - integration plot analysis, 326–327
 - retinal uptake index method, 327–328
- In vivo methods, buccal mucosa
 - animal models, 97
 - barrier nature of biological tissue, 97
 - buccal absorption test, 96
 - donor and receptor chambers, 99
 - flow-through diffusion cells, 98–99
 - Franz-type diffusion cells, 98
 - liquid and air mucosa interphase comparison of, 117
- Modified Ussing chambers
 - donor and receptor chambers, 99
 - representation drug in receptor chamber, 100
- perfusion cells, 96
- permeability models, 97
- In vivo skin absorption
 - comparison to in vitro absorption, 8
 - dermal microdialysis technique, 10
 - advantages and current studies, 11
 - relative recovery calculation, 11

- In vivo skin absorption (*cont.*)
 dermatopharmacokinetic approach
 recovery studies vs. mass balance studies, 9
 taping and ATR-FTIR studies, 10
 pharmacodynamic response study, 9
- In vivo vitreous/retina-to-blood efflux
 transport, 328–330
- Iontophoresis in ocular drug delivery, 312
- IPL. *See* Inner plexiform layer; Isolated perfused lung
- Iris-lens barrier, 312
- Isolated cerebral capillaries, 406
- Isolated perfused lung, 136
 administration of drugs, 150–151
 advantages, 145, 146
 design of experiments, 145
 developments, 154–155
 drawbacks, 145
 drugs absorption study through
 active transport mechanisms evaluation, 153
 disposition and absorption, 152–153
 lung permeability, 151–152
 in vitro-in vivo correlation, 153–154
 evolution of, 146
 experimental set-up for
 apparatus and maintenance conditions, 148–149
 procedures for surgery, 147–148
 selection of species, 150
 viable preparation, 149–150
 oedema formation in, 150
 preparation principles, 146–147
 use of, 144
- Isopropylbeta-D-thiogalactopyranoside (IPTG), 590
- J**
- JAM. *See* Junctional adherence molecules
- Junctional adherence molecules, 344
- K**
- Karyotype, transformed/immortalized cells, 626
- Keratoconjunctivitis sicca, 313
- Kidney-specific human MATE2 (MATE2-K), 567
- k*-nearest-neighbor (*k*NN) models, 474, 476
- Krebs Ringer buffer (KRB), 436
- L**
- Lactate dehydrogenase (LDH), 121
- Lactoferrin and lysozyme, antibacterial substances, 239
- LADME model, 431–432
- Lamina muscularis mucosa, 184
- Lamina propria, 184, 237
- Laniquidar (R101–9333) P-glycoprotein blockers, 403
- L-2 cells, in AII cells of rat lungs, 268
- LC/MS method, for PAMPA determination, 191
- Leukotriene B4 measurement, in athletes, 140
- Levovirin drug, 563
- Ligand-activated nuclear receptor, 404–405
- Linear free energy relation (LFER) models, 525
- Linear Solvation Energy Relationship (LSER), 467
- Lipophilic compounds, unstirred water layer (UWL) in, 192
- Liquid-covered culture (LCC), 225, 241, 242, 445, 446
- LLC-PK1 cells, 200
- Log-linear model, for pulmonary drug absorption prediction, 146
- Low permeability (LP), 666
- Low solubility (LS), 666
- Lung airways
 barrier function, 238
 BEAS-2B cell line, 242
 drug absorption, 243
 epithelial cells, 241
 mucociliary clearance, 239
 primary cell cultures of, 240
 protective mediators
 secretion of, 239
 structure of, 236
- Lung resistance protein (LRP), 244
- Lung, respiratory drug delivery through
 absorption of drugs, 142–143
 models selection for, 143–146
 distal blood-air barrier of, 138–139
 drug administration in, 150
 particle deposition, 141
 preclinical studies dosing, 141–142
 low proteolytic activity, 274
 non-absorption clearance
 CYP3A4, in human liver, 140
 mucociliary clearance, 139–140
 pathophysiological and physiological changes, 140–141
 respiratory mucosa, 138–139
 structure and function of, 137–138
 ventilation mechanism, 148
- Lycopersicon esculentum*, 261
- Lymphoblastic MOLT-4 cells, 647
- M**
- Maclura pomifera*, 262
- Macroscopic mass balance models, 494–495
- Madin-Darby canine kidney cells, 199, 424, 592, 603, 671
- Marathon cDNA, 585
- MATE (SLC47)
 function and pharmacokinetic roles, 567
 structure and tissue distribution, 567
- Maximum Absorbable Dose (MAD), 494, 500

- MCT. *See* Monocarboxylate transporter
- MDCK. *See* Madin-Darby canine kidney cells
- MDCKII cells, signal transduction pathways, 383
- Melting temperature (T_m), 585, 587
- Membrane-Interaction (MI)-QSAR approach, 541
- Metabolic barrier, in buccal mucosa, 93
- Michaelis-Menten (K_m) constant, 326
- Microcapillary endothelial cells, 260
- Microdialysis study, 328–330
- Microinjection, 623
- Microscopic mass balance models, 495–496
- Microvillous border membrane and basal membrane vesicles, 373–374
- MI-QSAR models, 532
- Mitoxantrone drug, 384
- Mitragotri model, 473
- Miyazaki's method, 441
- MK571 inhibitor, 244
- MLR-based BBB permeability model, 540
- MLR-based model 65, 535
- mMESSAGE mMACHINE kit, 583
- Modified Ussing chamber
- active ion transport, 240
 - advantage of, 100
 - drug migration of, 117
 - drug permeability technique, 114, 116
 - rabbit nasal mucosa, 122
- Molar Refractivity (MR), 467, 480
- Molecular Volume (MV), 465, 468, 535
- Molecular weight (MW), 533, 583
- MolSurf technology, 518
- Monocarboxylate transporter, 343
- Monocarboxylate transporter 1 (MCT1), 332
- Monolayer cell models for estimating permeability and transcellular flux, 419
- Monolayer integrity assessment, 193
- Mouse lung epithelium (MLE) cells, 268
- MRP. *See* Multidrug resistance-associated protein
- MRP2 expression, 382
- MRP5 inhibitor, 383
- MRP1, 190-kDa protein, 244, 381
- Mucosal epithelium
- drug permeability, 113
 - role in, 113
- Mucosal pellicle, as barrier, 92
- Multidrug and toxin extrusion (MATE) family, 567
- Multidrug resistance associated proteins (MRP), 143, 332, 401, 580, 673
- Multidrug resistance protein 1 (MDR1), 578
- Multidrug resistant transporters of placenta
- MDR1/P-glycoprotein (ABCB1), 376–380
 - MRP1/ABCC1, 380–381
 - MRP2/ABCC2, 382
 - MRP3/ABCC3, 382–383
- MRP5/ABCC5, 383
- Multilayer feedforward neural network (MLFN) method, 540
- Multiple linear regression (MLR), 512
- Muscularis mucosa*, 237
- N**
- Na^+ Absorption from conjunctival mucosa, 308
- Na^+ -dependent transport, 651
- Nails composition, 7
- Na^+/K^+ -ATPase, 262, 593, 651
- Nasal cavity, in human and animals
- enhancers, 221
 - mucosa
 - physiology of, 219
 - mucosal cavity and epithelial cells
 - metabolic enzymes, 220
 - nasally administered drugs
 - physicochemical characteristics of, 220
 - physiological factors
 - mucociliary clearance, 219
 - structure of, 218
- Nasal drug absorption
- correlation, in vitro model, 127–128
 - and drug delivery, in vitro models
 - ethical limitations, 217
 - peptides and proteins, 216
 - for treating nasal allergy, 217
 - and drug delivery studies, ex vivo models
 - drug absorption enhancement strategies,
 - optimisation of, 126
 - drug metabolism studies, 125–126
 - irritation and tolerance, 127
 - permeability studies and drug characterization, 121
 - specific applications of, 121
 - and drug delivery studies, in situ
 - advantage of, 113
 - application of, 117–118
 - drug absorption enhancement strategies,
 - optimization of, 119
 - factors affecting drug absorption, in vivo, 114
 - metabolism studies, 118
 - permeability studies, 117
 - factors affecting pharmacokinetics of, 129
 - mucosal enzymes interactions of, 116
 - overestimation of, 117
 - perfusion volume effects on, 120
- Nasal drug transport studies
- animal models, in vivo, 223
 - cell culture models, 224
 - in transport and metabolism studies, 225
 - for drug absorption, 223
 - excised nasal models, in vivo, 224
 - liquid-covered culture (LCC) model, 225

- Nasal epithelium
 aminopeptidases, 119
 apparent permeability coefficients (P_{app}) of, 122
 barrier
 paracellular routes, 222
 transcellular route of, 221
 transport route of, 221
 drug-metabolizing enzymes, 125
 drug transport across, 219
 flow rate of, 219
 perfusion of, 121
 permeability and drug absorption, 124, 216
 physiology of, 219
 RPMI 2650, human cell line, 224
 toxicity enhancing, 121
 transport of TP4, 126
- Nasal perfusion studies, experimental set up, in situ, 114, 115
- NBD-CSA. *See* Nitrobenzoxadiazol-cyclosporine
- Nerve fiber layer, 323
- New chemical entities (NCEs), 418
- NFL. *See* Nerve fiber layer
- Nipradilol, β -blocker, 310
- Nitric oxide synthase (NOS) inhibitors, 312
- Nitrobenzoxadiazol-cyclosporine, 404
- NMMIIB MgATPase activity, 356
- Non-muscle myosin II isoforms, 354
- Non steady-state solutions
 and morphological models, 477–478
- Normal Human Bronchial Epithelium (NHBE), 244
- Noyes-Whitney equation for dissolution
 rate for poorly soluble compounds, 504
- Nucleofection, 624
- O**
- OAT. *See* Organic anion transporters
- OATP. *See* Organic anion transporting polypeptides
- Oatp (rodents)/OATP (human) isoforms, 563
- OATP (SLCO)
 function and pharmacokinetic roles of, 565
 structure and tissue distribution, 563–564
- OCCL, indicator variable, 480
- Occludin protein, 261, 347–348, 350
- OCT. *See* Organic cation transporters
- OCT2-mediated creatinine secretion, 566
- Ocular Ad infection, 313
- Ocular drug delivery, 284
- Oedema formation, in IPL, 150
- Olfactory region, in nasal cavity, 218
- Oligo dT primer, 582
- OLM. *See* Outer limiting membrane
- Oncogenes, 620
- ONL. *See* Outer nuclear layer
- OPL. *See* Outer plexiform layer
- Oral drug absorption
 physiologically-based models
 compartmental absorption and transit, 496–500
 general considerations of, 491–492
 mass balance, 494–496
 mixing tank, 492–494
 use and validation of, 500–505
 process of, 488–491
- Oral drug administration
 bioavailability, 35
 drug absorption process, 35, 36
 drug delivery models
 estimation of drug absorption, 36
 rate-limiting processes, 36
 drug design focus, 35
- Oral mucosa
 antibacterial agents in, 95
 carrier-mediated transport system, 94
 D-glucose absorption, 95
 passive diffusion, drug transfer mechanism, 94
- Organic anion transporters (OAT), 401, 578, 580
- Organic anion transporting polypeptides (OATP), 329, 401, 578, 580
- Organic cation transporters (OCT), 271, 401, 580
- Outer limiting membrane, 323
- Outer nuclear layer, 323
- Outer plexiform layer, 323
- P**
- PAMPA. *See* Parallel artificial membrane permeation assay
- Paracellular permeability regulation, 345–346
- Paracellular transport, 341
- Paracellular transport across secretory epithelia regulation, 344–345
- Parallel artificial membrane permeation assay (PAMPA), 419, 425–426, 675–677
 alkane-water partition coefficients
 measurement, 190
 applications, 187, 191
 evolution of, 187, 189
 initial experiments, 189
 lipid composition effect on, 190
 optimization of, 191–192
 pH conditions and cosolvents influence, 190
- Passive diffusion
 active/carrier-mediated transport
 mechanisms, 115–116
 drug transfer mechanism, 94
- PBEC. *See* Porcine brain microvessel endothelial cells
- PCA. *See* Principal Component Analysis
- P450 enzymes, 299
- PEPT (SLC15)
 function and pharmacokinetic roles of, 561–563

- structure and tissue distribution, 561
 - Perfused placental model, 371–372
 - Perfused skin models
 - benefits, 11
 - specimens used, 12
 - Perfusion experiment, 80
 - Permeability
 - apparent permeability (*P*_{app}) values, 670
 - Caco-2 model, 675
 - class of drug substance, determination, 667
 - IVIVC with Caco-2 cell assays, 672
 - methods for classification, 669
 - regional permeability coefficients and BCS
 - permeability class, drugs, 674
 - and solubility measurement, 675
 - Permeability barrier
 - chemical nature of, 92
 - location of, 91
 - P-glycoprotein (P-gp), 187, 402, 404, 578, 593, 673
 - P-gp inhibitor verapamil, 383
 - Pharmacokinetic, mass balance studies, 669
 - pH-dependent fluorescent label, 652
 - Pheochromocytoma (PC-12), 602
 - Phosphate buffered saline (PBS), 622
 - Photobleaching, 644
 - Photoreceptor outer segments, 323
 - Pink eye, inflammation of conjunctiva, 312
 - PK-Map and PK-Sim, *in silico* simulation
 - software packages, 500
 - Placental perfusion model, 372
 - Placental transport mechanisms, 370–371
 - Plasma concentrations and salivary concentrations, 97
 - Platelet-endothelial cell adhesion molecule-1, 330
 - Poly(D,L-lactide-co-glycolide) (PLGA)-nanoparticles, 645, 649
 - Polyethylene glycol (PEG), 608
 - Polymerase chain reaction (PCR), 585
 - Polyoma virus, 620
 - Polyvinylpyrrolidone (PVP), 622
 - Population doublings (PD), 618
 - Porcine brain capillary endothelial cells
 - isolation, 408
 - Porcine brain microvessel endothelial cells, 407
 - Porcine buccal mucosa, 172
 - POS. *See* Photoreceptor outer segments
 - Post-translational modifications, 590
 - Potts and Guy model, 465–466
 - Pravastatin drug, 565
 - Pressurised metered dose inhaler (pMDI), 141
 - Primary rabbit conjunctival epithelial cell
 - layers, steps for preparation and maintenance, 316
 - Primary systemic carnitine deficiency, 566
 - Principal Components Analysis (PCA), 469, 516
 - Prodrugs evaluation, in Caco-2 cells, 194
 - Prostaglandin, 602
 - Proteinase K digestion, 583
 - Protein kinase C (PKC) α , 602
 - Protein–ligand interaction, 588
 - Proteolytic degradation, in alveolar airspaces, 264
 - pSVori, plasmids, 620
 - Pugh and Hadgraft linear models, 466–467
 - Pulmonary aerosol formulations, permeability assessment, 443–444
 - Pulmonary circulation, in lungs, 138
 - Pulmonary delivery, for analgesic drugs, 136
- Q**
- QSPR models, 541
 - development of, 463–464
 - early, 464–471
 - multiple barriers and pathways, 471–473
 - recent empirical, 473–477
 - Quantitative Structure Activity (property) Relation (QSA(P)R), 488
 - Quantitative Structure Permeability Relationship (QSPR) models, 463–464, 473, 541
- R**
- Rabbit conjunctival epithelial cells (RCEC), 312
 - Rabbit corneal epithelial cell line, 291–292
 - RAGE. *See* Receptor for advanced glycation end products
 - Randic's topological properties of molecules, 540
 - Rapid transport protein modulation, 403–404
 - Rat colon model, *in situ*
 - for absorption evaluation, 79–80
 - carrier-mediated transport
 - compounds absorbed by, 82
 - membrane permeability for, 82
 - Na⁺/H⁺ exchangers, 81
 - probe substrates, 83
 - cross section of, 79
 - luminal surface of, 79
 - membrane
 - permeability characteristics of, 81
 - passive transport in, 84
 - perfusion experiment in
 - parameters, 80
 - riboflavin (vitamin B2), 81
 - saturable transport in, 82
 - unsaturable transport in, 83
 - Rat model, of endotoxin-induced uveitis, 312
 - Rat perfusion models, tool to nasal mucosal, 118
 - Rat retinal vascular endothelial cells, 331
 - Receptor for advanced glycation end products, 262

- Resistance genes genes for G418, 596
- Respiratory drug delivery
 drug inhalation
 absorption of drug, 142–146
 administration of drug, 141–142
 human respiratory tract structure, 137
 illustration of, 139
 inhaled route usage, 136
 insulin inhalation, 136
 non-adsorption clearance, 139–140
 pathophysiological and physiological changes, 140–141
 respiratory mucosa, 138–139
 structure and function, 137–138
- Retardation Coefficient (RC), 469
- Retinal influx clearance, $K_{in,retina}$, 326
- Retinal pigment epithelium (RPE), 322–323
- Retinal uptake index (RUI) method, 322, 327–328
- Retina tissue, 322
- Retina-to-blood efflux transport, 334
- Reverse transcription, 586
- Rheumatoid arthritis, 567
- Rho-associated coiled coil-forming protein kinase (RhoA-p160ROCK), 350
- Rhodamine, 643
- Ricinus communis*, 261
- Riviere and Brooks model, 480
- R_{LIS} regulation, 352
 actin polymerization modulation and, 354–355
 estrogen on paracellular permeability composite effects of, 356–357
 estrogen regulation of, 353–354
 and estrogen regulation of actin polymerization, 354
 and estrogen regulation of cortical myosin, 355–356
- Robinson model, 473
- Roche in-house program, MOLOC, 513
- Root-mean-square (RMS) error, 475–476
- RPMI 2650, human nasal epithelial cell, 224
- R_{TJ} , regulation
 assembled tight junctions regulation by extracellular ATP, 349
 C_{ao} role of, 346–349
 claudin/occludin model of regulation of, 351–352
 estrogen regulation of, 349–350
 and tight junctional disassembly, 350–351
- RVEC. *See* Rat retinal vascular endothelial cells
- S**
- Saccharomyces cerevisiae*, 591
- Salivary film and mucus layer, in buccal mucosa, 92
- Salmonella typhimurium* (SP6), 580
- Sambucus nigra*, 262
- Scaled particle theory, 471
- Schizosaccharomyces pombe*, 591
- Sf9, Sf21 (*Spodoptera frugiperda*), 593
- Short-chain fatty acid (SCFA), 77, 78
- Side scatter (SS), 654
- Silver nanoparticle enhanced fluorescence, 647
- Simian virus 40 (SV40), 620
- siRNA technology, 651
- Skin
 anatomical structure
 dermis, 5–6
 epidermis, 5
 subcutis or subcutaneous fatty tissue, 6
 invasion test strategies
 perfused skin models, 11–12
 in vitro penetration, 16–18
 in vitro permeation, 12–16
 in vivo skin absorption, 9–11
 toxicity testing
 irritation and corrosion, 21–22
 phototoxicity of skin, 23–24
 sensitization of skin, Buehler test, 20
 sensitization of skin, guinea pig maximization test (GPMT), 19
 sensitization of skin, local lymph node assay (LLNA), 20–21
- SLC-transporters, 244, 259, 270, 560–562, 580
- Small intestine (SI), in rat
 comparison by rat colon, 79
 compound absorption in, 82, 83
 drug concentration in, 80
 drugs from, 77
 hydrophilic compounds absorption by passive transport in, 84–85
 length of, 79
 membrane permeabilities of, 82
 peptide drugs in, 77
- Smooth endoplasmic reticulum (SER), 604
- SNARE-dependent exocytosis, 351
- Sodium-dependent VC transporters (SVCT), 271
- Sodium dodecyl sulphate (SDS), 579
- Sodium/glucose co-transporter, 580
- Sodium taurodihydrofusidate (STDHF), 126
- Solid drugs delivery and intestinal permeability, 431–435
- Sphingomyelin, in intestinal membrane, 190
- Spontaneous transformation, 619–620
- SP6 promoter upstream, 582
- Statens Seruminstitut Rabbit Cornea (SIRC), 292
- Stein's hydrogen-bonding number, 540
- Stokes-Einstein radius, for hydrophilic molecules, 264
- Stratum corneum, and transport pathways, 7

- Structural thinking experimental learning
laboratory with animation (STELLA),
498
- Sub-conjunctival ocular drug delivery,
310–312
- Suramin, urea derivative, 607
- SUR1 and SUR2 (sulfonylurea receptors),
568
- Syncytiotrophoblast (placental barrier)
anatomical arrangement, 370
- T**
- T1 α , for mammalian ATI cells, 262
- Targeted drug delivery systems
analytical tools, labeling and detection of,
643–645
design, 642
- Target–targeter interaction, 647
- Tariquidar (XR9576) P-glycoprotein blockers,
403
- Taxol drug, 403
- TEER. *See* Transepithelial electrical resistance
- Ticarcillin, ocular drug, 312
- Tight junction modulating (TJM), 223
- Tight junctions (TJ), 341
- Topical drug delivery, implications of data, 357
- Topological polar surface area (TPSA), 522
- Topological substructural molecular design
approach (TOPS-MODE), 539
- Topotecan drug, 384
- T7 polymerase, 590
- Tracheo-bronchial airways lining, 138
- Tracheo-bronchial epithelium, in vitro model
active transport mechanisms in, 243
BEAS-2B cell line, 242
and bronchiolar epithelia, 237
cell lines, 241
distinct cell types of, human, 238
drug delivery to, 239
drug metabolism studies, 245
integrity of, 238
interface formation, 237
P450 enzymes in, 246
phase II enzymes in, 247
expression profiles of, 248
primary cell cultures of, 240
region of lung, 236
in vitro–in vivo correlation, 245
- Tracheo-bronchial mucosa and cell cultures
expression of peptidases and proteinases in,
248
metabolic activity in, 249
phase II enzymes expression of, 247
- Transcellular passive diffusion, transcellular
route, 222
- Trans-conjunctival ocular drug delivery,
310–312
- Transcorneal iontophoresis, 312
- Transcytosis, in intestinal epithelium, 185
- Transdermal absorption
data analysis, 461–478
diffusion equation, 461
pharmacokinetic models, 478
skin barrier, 460–461
- Transepithelial electrical resistance, 193, 196,
225, 240, 242, 315, 420, 650, 674
- Transepithelial fluid transport by
Ussing-Zerahn model, 341–344
- Transepithelial hydrostatic gradients, 345
- Transepithelial transport from subluminal
compartment, 341
- Transfection, 585, 593, 623
- Transformation of fibroblasts, 620
- Transformed cells, characterization, 625
- Transforming growth factor- β (TGF- β),
622
- Transforming transgene, expression, 625
- Transit function (T_{ST}), 499
- Translation initiation codon (ATG), 591
- Transmission electron microscopy (TEM),
645
- Transporters, cloning and functional
heterologous expression
cloning techniques
cDNA library for a drug carrier, screening
of, 583–584
cDNA synthesis, 582
controls, 584
mRNA preparation, size fractionation,
581–582
transcription, in vitro, 582–583
Xenopus laevis oocytes, for cloning of
drug carrier, 580–581
complementation cloning strategies,
584–585
homology cloning, 585
RACE-PCR, 585–588
- Transwell systems, 420, 432, 445, 594, 650
- TR146 cell culture, for drug transport
assessment, 172
- TR-iBRB cells, 326
- Tricellulin protein, 261
- Tris/EDTA (TE) buffer, 581
- Trophoblast cell cultures, 374
- Trophoblast tissue preparations, 372–373
- Trypsin-containing cell suspension, 622
- Tunicamycin, inhibition of
N-acetyl-glycosyl-transferase, 648
- Tween 80, 187
- U**
- United States Pharmacopeia (USP), 667
- Unstirred water layer (UWL), in PAMPA,
192
- Ussing Chambers Technique, 201–204,
313–314
- Ussing-Zerahn model of transepithelial fluid
transport, 341–344

V

- Vaginal dryness, postmenopausal women, 354–355
- Valacyclovir oral bioavailability, 562
- Valsartan drug, 565
- Valspodar (PSC-833) inhibitor, 402
- Variable Selection and Modeling method, 541
- Variables influencing drug permeation and penetration, 479–480
- Vector pSP64T, 582
- Villous preparations, 373
- Vinblastine, anticancer substances, 382
- Volsurf program, 522
- VSMP. *See* Variable Selection and Modeling method

W

- Western blot analysis, 95, 271, 380
- WGA-grafted PLGA-microparticles, 649
- WGA-IgG pro-drugs, 649
- Wheat germ agglutinin (WGA), 646

X

- Xenobiotics
 - biological effects of, 246
 - biotransformation reactions, 245
 - metabolism of, 185, 246, 274

Y

- Young's data set, 516–517

Z

- Zonula occludens (ZO) protein, 261
- Zosuquidar (LY335-979) P-glycoprotein blockers, 403